ARBITRATION UNDER ANNEX VII OF THE UNITED NATIONS CONVENTION ON THE LAW OF THE SEA

PEOPLE'S REPUBLIC OF BANGLADESH

V.

REPUBLIC OF INDIA

MEMORIAL OF BANGLADESH

VOLUME IV
ANNEXES

31 MAY 2011

ARBITRATION UNDER ANNEX VII OF THE UNITED NATIONS CONVENTION ON THE LAW OF THE SEA

PEOPLE'S REPUBLIC OF BANGLADESH

V.

REPUBLIC OF INDIA

MEMORIAL OF BANGLADESH

VOLUME IV
ANNEXES

---

31 MAY 2011

VOLUME IV
TABLE OF CONTENTS

SCIENTIFIC ARTICLES AND MANUSCRIPTS

Annex B66 M. Alam et al., "An Overview of the Sedimentary Geology of the Bengal Basin in Relation to the Regional Tectonic Framework and Basin-fill History", *Sedimentary Geology*, Vol. 155, No. 3-4 (2003)

Annex B67 Nanna Roos et al., "Small Indigenous Fish Species in Bangladesh: Contribution to Vitamin A, Calcium and Iron Intakes, Animal Source Foods to Improve Micronutrient Nutrition and Human Function in Developing Countries", *Journal of Nutrition*, Vol. 133, No. 11 (2003)

Annex B68 T. Pal et al, "Geodynamic evolution of the outer-arc-forearc belt in the Andaman Islands, the central part of the Burma-Java subduction complex", *Geological Magazine,* Vol. 140, No. 3 (2003)

Annex B69 A. Uddin & N. Lundberg, "Miocene Sedimentation and Subsidence During Continent–Continent Collision, Bengal Basin, Bangladesh", *Sedimentary Geology*, Vol. 164, No. 1-2 (2004)

Annex B70 C. Nielsen et al., "From Partial to Full Strain Partitioning Along the Indo-Burmese Hyper-oblique Subduction", *Marine Geology*, Vol. 209 (2004)

Annex B71 S. Kuehl et al., "The Ganges-Brahmaputra Delta", in *River Deltas--Concepts, Models, and Examples* (L. Giosan & J. Bhattachar eds., 2005)

Annex B72 Joseph R. Curray, "Tectonics and history of the Andaman Sea region", *Journal of Asian Earth Sciences,* Vol. 25, No. 1 (2005)

Annex B73 C. Subrahmanyam & S. Chand, "Evolution of the Passive Continental Margins of India—A Geophysical Appraisal", *Gondwana Research*, Vol. 10, No. 1-2 (2006)

Annex B74 M. S. Steckler et al., "Collision of the Ganges-Brahmaputra Delta with the Burma Arc: Implications for Earthquake Hazard", *Earth and Planetary Science Letters*, Vol. 273 (2008)

Annex B75 A. Mukherjee et al., "Geologic, Geomorphic and Hydrologic Framework and Evolution of the Bengal Basin, India and Bangladesh", *Journal of Asian Earth Sciences*, Vol. 34, No. 3 (2009)

Annex B76 T. Islam and Richard E. Peterson, "Climatology of landfalling tropical cyclones in Bangladesh 1877-2003", *Natural Hazards,* Vol. 48, No. 1 (2009), at pp. 115-16.

Annex B77 Rodman E. Snead, "Bangladesh", in *Encyclopedia of the World's Coastal Landforms* (Eric C.F. Bird ed., 2010)

Annex B78 Susmita Dasgupta et al., "Vulnerability of Bangladesh to Cyclones in a Changing Climate: Potential Damages and Adaptation Cost", World Bank Policy Research Working Paper No. 5280 (April 2010)

Annex B79 Katherine J. Houghton et al., "Maritime boundaries in a rising sea", *Nature Geoscience*, Vol. 3, No. 12 (2010)

Annex B80 S. T. Sinha et al., "The Crustal Architecture and Continental Break Up of East India Passive Margin: An Integrated Study of Deep Reflection Seismic Interpretation and Gravity Modelling", *Search and Discovery,* Article #40611 (10 October 2010) (available at <http://www.searchanddiscovery.com/documents/2010/40611sinha/ndx_sinha.pdf>)

Annex B52

Joseph R. Curray, "The Bay of Bengal: Tectonics, Stratigraphy and History of Formation" (26 May 2011).

THE BAY OF BENGAL: TECTONICS, STRATIGRAPHY AND HISTORY OF FORMATION

Joseph R. Curray
Scripps Institution of Oceanography
La Jolla, CA 92037
jcurray@ucsd.edu

INTRODUCTION

The Bay of Bengal is the northeastern lobe of the Indian Ocean (Figs. 1 and 2), surrounded by Sri Lanka (SL), India (I), Bangladesh (B), Myanmar (M), the Andaman and Nicobar Islands (A) and Sumatra (S). It was formed during the process of collision of the Indian subcontinent with the southern margin of Asia. This collision, commencing in middle Paleocene time (about 60 million years ago) and continuing to the present day, has created the indentation in Asia in which India lies today (Fig. 2).

The Bengal Basin (B), which includes Bangladesh, lies in the corner between continental India on the west and continental Asia on the east. Geologically, the edge of Indian continental crust, generally considered to be "granitic", is believed to extend northeasterly from offshore of the eastern Indian continental margin through the center of the basin, so part of the Bengal Basin is underlain by oceanic crust, made up of basalt-type lava. The Fold Belt in the eastern part of the Basin is part of the northern continuation of the Sunda Arc Subduction Zone, which lies offshore from Java (J), Sumatra (S) and the Andaman and Nicobar Islands (A). This subduction zone, in which the Indian tectonic plate is passing under the Asian tectonic plate, passes onshore in southwestern Myanmar. Thus India and Bangladesh are on the Indian tectonic plate, while Myanmar and the Andaman and Nicobar Islands are on the Asian tectonic plate, or what subsequently became the "Burma Plate". The suture between the plates is the subduction zone. When subduction occurs, the upper layers of the lower plate, mainly sediments, are scraped off by the edge of the upper plate and piled up on the edge of the upper plate as a folded and faulted complex of sediments and other rocks known as an "accretionary prism". The Andaman-Nicobar Ridge (including the Andaman and Nicobar Islands), the Indo-Burman Ranges and the outer-arc ridge offshore from Sumatra and Java all form part of this long continuous accretionary prism.

The entire Bay of Bengal beyond the foot of the continental slope is floored by the Bengal Fan, the largest submarine fan in the world. Bangladesh occupies most of the Bengal Basin, which contains the Bengal Delta (sometimes called the Ganges-Brahmaputra Delta), the largest delta in the world. The sedimentary fill in the Bengal Fan and the Bengal Delta have been derived from erosion of the Himalayas and Tibetan Plateau since Eocene time, between about 43 and 55 Ma (million years ago).

"Depositional system" is a concept in geology, usually associated with sedimentary environments. The Bengal Basin and the Bay of Bengal together constitute the Bengal Depositional System. This single integrated depositional system represents a continuum of smaller sedimentary environments, all created during the collision of India with Asia. The sedimentary fill has been derived from the same immense source of sediments, the uplifting and eroding Himalayan Mountains and the Tibetan Plateau. These environments extend from the river-deposited sediments of Bangladesh, through the sediments of the Bengal Delta, to the continental shelf and slope deposits off the Bengal Delta, and finally to the submarine Bengal Fan. The margins of this depositional system are the foot of the continental slope off peninsular India on the west and the axis of the Sunda Trench off the accretionary prism on the east. The volume of sediments coming into the Bengal Depositional System from the confluent Ganges and Brahmaputra Rivers is immense, by far the world's largest river contribution to the oceans.

Myanmar and the Andaman Sea are part of a different system, the Myanmar-Andaman Depositional System. Its origin and hence its geology are very different. This depositional system originated by extension and elongation of a fault located behind and parallel to the trench and accretionary prism of the Sunda Plate margin. As subduction of the Indian Plate proceeded, the subduction zone rotated clockwise and a series of basins opened with north-south elongation caused by continuing motion along this fault trend parallel to the subduction zone, accompanied by extension perpendicular to the trend of the subduction zone. Volcanism behind the subduction zone has occurred throughout the western part of this depositional system.

In the following sections of this report, I will discuss the common origin of the Bengal Basin and the Bay of Bengal and the stratigraphy of the Bay of Bengal region, and I will contrast it with the Myanmar-Andaman Depositional System. I will also discuss the nature of the sedimentary section in the Bay of Bengal adjacent to the eastern continental margin of India.

EVOLUTION OF THE BENGAL BASIN AND THE BAY OF BENGAL

The Indian subcontinent separated from the Gondwana super-continent (Fig. 3) between about 120 and 136 Ma (million years ago). India at that time included both the India we see today and an extension of India believed to have passed beneath the Asia plate in the subduction zone. Together, they have been called "Greater India". The motion of India toward Asia was at times very rapid, over 100 mm/yr (Fig. 4). By about 70 Ma (Fig 5) the Indian subcontinent lay in mid-ocean, forming the new Indian Ocean in its wake and closing the old Tethys Sea in front of it. During this period, sediment shed from continental India contributed to its margin.

When India first contacted the subduction zone about 59 Ma in what has been called the "soft collision" (Fig. 6), the rate of convergence decreased (Fig. 4),

and it started pushing into whatever lay offshore from Asia proper, probably part of present day Tibet, the Lhasa block (L, Fig. 6). The soft collision event closed any marginal seas that may have existed and started the clockwise rotation of the subduction zone. The subduction zone bordering southern Asia initially probably trended about 120°- 300° (Fig. 2). A proto Bengal Basin and a proto Bay of Bengal were formed. Sediment from erosion of the collision zone was probably carried to the southeast in the axis of the subduction zone trench (Fig. 6). Deposition started in the Bengal Basin as shales, sandstone and coal.

The "hard collision" (Fig. 4) occurred about 43 Ma when India started pushing its way into Asia (Fig. 7), creating the indentation in Asia in which India lies today (Fig. 2). The rate of convergence decreased again. Uplift started in the Himalayas and the Tibetan Plateau. Deposition had started in the Bay of Bengal with the early deposits of the Bengal Fan (Fig. 7). Only relatively minor amounts of sediment were shed eastward from continental India compared to the flood of sediment coming from the Himalayas and Tibet. Erosion products from Sumatra and the Burma Block, which was the continental part of present-day Myanmar, were trapped in the forearc basins and the trench of the Sunda Arc subduction zone. By Early Miocene (21 Ma)(Fig. 8), the Himalayas and Tibet had been uplifted and India had penetrated deeply into Asia (Fig. 2). The Bengal Fan was prograding rapidly seaward, the Bengal Basin had been filled, and the shoreline was also rapidly building seaward. Rotation of the Sunda Arc had progressed almost as far as it is today (Fig. 9).

At the present time (Fig. 9) erosion rates are high in the Himalayas and the Tibetan Plateau, and a huge sediment volume is carried by the confluent Ganges and Brahmaputra Rivers for deposition in the Bengal Basin, continuing to advance the shoreline. The sediment that escapes deposition behind the shoreline is carried to the geologic shelf and some of it is swept into the Swatch-of-No-Ground submarine canyon incised into the shelf (Figs. 1 and 15). Still only relatively minor amounts of sediment are shed from continental India and Myanmar into the Bay of Bengal, as compared with the load of the confluent Ganges and Brahmaputra Rivers. The major rivers of Myanmar drain into the Andaman Sea behind the Andaman-Nicobar Ridge and islands. Erosion products from the Andaman and Nicobar Islands, Sumatra and Java are minor and are caught in the forearc basins behind the outer islands and accretionary prism ridge on the Andaman Sea side of the Andaman-Nicobar Ridge (Fig. 9).

The creation of the Myanmar-Andaman Depositional System, in contrast, was started about 30 Ma by extension both parallel and perpendicular to the Sunda Subduction Zone. The Irrawaddy River, the principal source of sediments to the Andaman Sea today, has drainage entirely within Myanmar, although it has been speculated that prior to about 5 to 10 Ma, it may have drained from the Tibetan Plateau. In contrast with most of Bangladesh, the Andaman and Nicobar Islands, as well as the Indo-Burman Ranges, are hilly and mountainous.

TECTONIC FEATURES

The important tectonic features of the Bay of Bengal region are shown in Figure 9. These include two submarine ridges, the 85° E Ridge and the Ninetyeast Ridge (NER), running approximately N-S in the Fan. Both of these are believed to have been formed as traces of volcanic hot spots, but they are not important for consideration in this report. The Sunda subduction zone in the Sunda trench is important, as the boundary between the Indian tectonic plate on the west and the Burma plate on the east. This subduction zone is a part of the original subduction zone lying off the margin of the Asian continent at the time of breakup of the eastern half of Gondwanaland (Fig. 2) and our collision scenario (Fig. 6 and on). The Sunda Arc was pushed inland and bent as India pushed its way into Asia. This arc takes a sharp bend at the Eastern Himalayan Syntaxis (EHS, Figs. 2 and 9), and thence continues to the west through the Himalayas as the plate edge between the Indian plate and the Tibetan or Asian plate in the north. Another bend occurs on the western end of the Indian indentation at the Western Himalayan Syntaxis (WHS, Fig.2), but that is not a consideration in this report.

The Sunda Trench lies offshore from the accretionary prism, the accumulation of sediment and rock scraped off the descending Indian plate, and lying on the edge of the overriding Burma plate. That is not a part of the Bengal Depositional System, which lies offshore and to the west of the subduction zone. The surface trace of the subduction zone is in approximately the bottom of the trench. It runs ashore in Myanmar and continues around to the EHS. Most investigators have correlated the main subduction zone fault with the Kaladan Fault in Myanmar, Bangladesh and India, but the actual subduction zone splays into several sub-parallel underthrust faults in this complex Fold Belt and the Indo-Burman Ranges. In any case, this system of faults and the associated folds mark the eastern margin of the Bengal Depositional System.

This fault and the surface trace of the subduction zone delineate the boundary between the Indian Plate and the Burma Plate. They also separate the Indo-Burman Ranges of Myanmar from the Chittagong Fold Belt of Bangladesh. Most of the rocks that have been dated in this part of the Indo-Burman Ranges, located in Myanmar's Rakhine State, are older than about 40 million years (my) in age. They have been shown to have a source of arc-type rocks, such as the volcanic part of the Sunda Arc behind the subduction zone in both Myanmar and the Andaman Sea. The rocks in the Bangladesh Fold Belt, in contrast, are younger than about 40 my and show strong evidence of a source in the Himalayas and Tibet. The uplift of Tibet and the Himalayas started with the "Hard Collision" about 43 Ma.

The Andaman and Nicobar Islands are the top of the accretionary prism, the Andaman-Nicobar Ridge. They are composed of a *mélange* of ophiolites (pieces of deep ocean seafloor and crust, with some of the deep ocean sediments which overlie the seafloor), Bengal Fan sediments and some sediments from

basins which lay on and behind the ridge. These rocks were scraped off the descending Indian Plate and mixed together at the subduction zone, while most of the oceanic crust and the underlying mantle were carried downward to several hundred kilometers.

THE BENGAL DEPOSITIONAL SYSTEM

The Bengal Depositional System is the past, present and potential future surface for the deposition of sediments introduced into the Bengal Basin, primarily from the Ganges and Brahmaputra Rivers. Comprising the Bengal Basin and Bengal Fan, this system includes the complete range of depositional environments, from river and lake deposits, through the delta, continental shelf and slope to a submarine canyon and submarine fan. These environments are all a continuum and part of the complete depositional system. The entire system has prograded, or built seaward to the south, as the flood of sediment has come in from the Himalayas and Tibet.

The most proximal part of this depositional system is the topset beds of the Bengal Delta (Fig. 10). Even in the Quaternary deposits (younger than 2.6 my), progradation, or building the shoreline seaward, can be seen, with the Pleistocene (ice age) deposits in the north and the Holocene (recent) deposits becoming progressively younger in a seaward direction. This progradation is due in part to the complications of Quaternary fluctuations of sea level, from low glacial stands of sea level to higher interglacial stands. The complications of a huge delta can be seen in the eastward migration of the confluent Ganges-Brahmaputra River mouth, from G1, to G2, to G3, to GB1, the present mouth. Erosion of the delta front shoreline is occurring in the western part of the delta, and active deposition and progradation are occurring in the east because that is where the confluent Ganges and Brahmaputra Rivers now discharge.

The Tertiary and Quaternary (65 my to present) or older seaward progradation of the shelf edge can be seen in Figure 11 extending across the Bengal Delta from NW to SE, with a Paleocene-Eocene shelf edge (about 55 Ma), prograding to middle Eocene (about 45 Ma) and to upper Miocene (10 Ma). The present shelf edge is off the diagram farther to the south and southeast. It also shows how the geologic continental shelf has prograded from overlying continental crust to oceanic crust. The first sediments deposited on this oceanic crust are believed to be proximal sediments of the Bengal Fan lying offshore from what at the time were the shelf and delta. The delta and shelf then prograded across the top of these early fan sediments. Figure 12 show diagrammatically how the Bengal Fan has also subsequently prograded.

The edge of the geologic continental shelf is located at a depth of about 150 meters in the Bay of Bengal; the base of the continental slope is about 1400 to 3300 meters. The fan is divided into three parts, upper, middle and lower as a function of dominant sedimentary transport processes and morphology. The upper fan is about 1400 to 2250 meters; the middle fan is at about 2250 to 2900

meters; and the lower fan is about 2900 to the distal end of the fan at about 5000 meters.

Distribution of sediments in the Bay of Bengal occurs by turbidity currents through the submarine canyon, Swatch-of-No-Ground (Fig. 1 and 15), which feeds into a turbidity current channel system on the surface of the Bengal Fan. Turbidity currents are turbulent mixtures of sediment and water. They are generally formed by submarine slumping of rapidly deposited and uncompacted sediment on a slope or in the head of a submarine canyon (Fig. 13). The sediment that has slumped mixes with seawater and a turbidity current is formed. Turbidity currents are believed to flow at high velocities, perhaps as rapidly as 10 m/sec, and can flow for many kilometers in channels with only a very low gradient. The gradient of the lower Bengal Fan is less than 1 m/km for over 1500 km.

The parts of a turbidity current are illustrated in Figure 14. Large turbidity currents fill channels bank to bank, and some of the fine sediment carried in the body and head may spill out over the banks to be deposited on the surface of the fan. Some sand, probably carried at the bottom of the flow, may be deposited within the channel, but most of the sand is believed to stay with the flow until the velocity drops and the current ceases to flow.

There is normally only one active channel on the fan at any time, but channels can migrate and/or become abandoned when a new channel forms. Thus the surface of the fan is covered by many abandoned channels (Fig. 15) with the one active channel shown in red. Channel migration occurs mainly through channel breakthrough in the upper fan. Similarly, submarine canyon change can occur on the continental shelf as the river mouth migrates back and forth in the delta.

A complication of the Quaternary period has been the sea level fluctuations associated with the formation and melting of glaciers. The depositional processes are quite different between a glacial period and an inter-glacial period, as shown in Figures 16 and 17. Figure 16, low sea level stands or a glacial period, would more nearly resemble normal, pre-Quaternary processes because the confluent Ganges and Brahmaputra very likely discharged its sediment directly into the submarine canyon. The sizes of the channels in the upper fan were adjusted to the average size of turbidity currents and were filled completely and were sometimes overtopped during the passage of a large turbidity current. Today, having recovered from a glacial period, the rivers do not flow directly to the submarine canyon head. Instead, the sediment load of the confluent Ganges and Brahmaputra Rivers is deposited in the delta front and on the continental shelf. Some of the sediment on the shelf is swept into the Swatch-of-no-Ground canyon, and small turbidity currents are formed. These smaller turbidity currents probably flow only to about the middle fan, and the final sediments of the flow are deposited there.

STRATIGRAPHY OF THE BENGAL BASIN AND THE BENGAL FAN

Stratigraphy is the branch of geology that studies the classification, correlation, age and interpretation of stratified rocks.

The sediment section in the Bay of Bengal is extremely thick, one of the thickest known sections in the world today. It is shown in seismic reflection and refraction measurements to exceed 20 km in thickness beneath the shelf at the juncture between the Bengal Basin and the Bengal Fan (Fig. 18). Isopachs (contours of sediment thickness) are shown in kilometers. To date, no drilling has been conducted in the Bengal Fan deep enough to establish the older stratigraphy. Thus far, core samples have been obtained only to Middle Miocene (17 Ma). By tracing unconformities in seismic reflection records from drilling on the Ninetyeast Ridge, a unified stratigraphy has been postulated for the entire Bay of Bengal. Two major units can be defined, separated by a major unconformity or hiatus in deposition postulated from this correlation to be late Paleocene to early Eocene, about 55 my old.

The older unit (Fig. 19) is pre-Eocene, interpreted as continental rise deposits shed off India. The younger unit (Fig. 20), post-Paleocene, younger than about 55 my, is interpreted as the Bengal Fan itself, deposited by the flood of sediments shed off the rising Himalayas and Tibetan Plateau, and transported to the Bay of Bengal today by the confluent Ganges and Brahmaputra Rivers. A longitudinal section from the Bengal Basin down the length of the Bengal Fan is illustrated in Fig. 21, with the unconformity designated "P". Seismic velocities are shown in km/sec.

The sedimentary section is continuous from the onshore Bengal Basin, across the continental shelf and slope and into the Bengal Fan, as shown in Figure 11. The stratigraphic rock units are continuous, but the facies, or nature of the rocks, changes with the transition from subaerial, to shallow marine, to deep marine deposition. The same sedimentary materials deposited by different sedimentary processes in different environments, shallow water vs. deep water, will become different rocks with different characteristics.

THE EASTERN MARGIN OF CONTINENTAL INDIA

The eastern continental margin of India is a typical "passive continental margin", i.e., it lies in the interior of a tectonic plate and not at a plate margin, such as a subduction zone. A seismic section (Fig. 22), located offshore from the Krishna-Godavari Delta on the NE-SW trending part of the margin, shows the continental rocks of India faulted and thinned by the rifting process which occurred during the Cretaceous (about 136 to 120 Ma). Farther offshore oceanic basement and crust can be observed or interpreted.

A line drawing of a seismic reflection record off the Cauvery Basin region of the margin is shown in Figure 23. The depth at the edge of the geomorphic continental shelf is about 150 meters; the base of the continental slope here is at

about 3300 meters. The "P" horizon at about the Paleocene-Eocene boundary (about 55 my) is shown, as are a late Miocene horizon (M, about 7 my) and the base of the Quaternary (Q, about 2.6 my). The Pre-Eocene sediments (below the P horizon), interpreted as a continental rise formed prior to India's collision with Asia, lie at the base of the continental slope and thin seaward. Sediments of the Bengal Fan, which began to form mainly after the hard collision, overlie the P horizon and abut against the slope. Here the margin of the Bengal Depositional System is the point of abutment of the fan section (younger than P).

As stated, the volume of sediments introduced into the Bengal Depositional System is immense, by far the greatest volume of river-borne sediments contributed to the oceans today. Estimates and measurements vary, but it is believed to exceed by more than a factor of ten all of the sediments of the rivers on the east coast of peninsular India.

THE MYANMAR-ANDAMAN DEPOSITIONAL SYSTEM

In contrast to the Bengal Depositional System on the Indian tectonic plate, the Myanmar-Andaman Depositional system (Fig. 24) lies on and eastward of the Burma tectonic plate. Initially, in the early stages of the India-Asia collision, the Burma plate did not exist. As rotation of the Sunda Subduction Zone occurred after the collision process had commenced, a "sliver fault" was formed behind and parallel to the subduction zone. This formed the edge of the Burma plate, and now extends from the Sumatra Fault System (Fig. 9, SFS) longitudinally bisecting Sumatra, through the center of the Andaman Sea and into the Sagaing Fault in Myanmar (Fig. 9, SF).

The depositional system derives its sediment almost entirely from within Myanmar. Transport of this sediment into the basins of the Andaman Sea is accomplished mainly by the Irrawaddy and Salween Rivers.

The boundary between these Bengal and Myanmar-Andaman depositional systems is the subduction zone, previously described. The accretionary prism of the subduction zone lies on the margin of the Burma plate. The plate boundary is the surface trace of the subduction zone in the axis of the trench off the Andaman and Nicobar Islands at about 13°N (shown by the arrow in Figure 25). Sedimentary layers of the Bengal Fan are compressed against the landward wall of the trench, uplifted as folds and accreted to that landward wall to become a part of the accretionary prism. The accretionary prism, although obviously composed here of Bengal Fan sediment, is not a part of the Bengal Depositional System, because it lies on the margin of the Burma Plate, not on the surface of any part of the Bengal Depositional System.

SUMMARY

The Bengal Basin and Bay of Bengal have been created during the continuing collision of India with southern Asia starting about 59 Ma. The huge

sediment load from erosion in the uplifting Himalayas and Tibet has fed these regions, which evolved into a single Bengal Deposition System, extending from the topset beds of the Bengal Delta, across the continental shelf and slope, through the Swatch-of-no-Ground submarine canyon to a vast fan valley system extending the length of the Bengal Fan. These different individual environments are related by common origin, common sediment source and inter-related processes of sediment transportation and deposition. These elements represent an offshore continuation of the geological processes and depositional environments of the land territory of Bangladesh into the Bay of Bengal.

The margins of this system are the continental margin of India on the west and the Sunda Subduction Zone plate edge on the east. Peninsular India is not a part of the Bengal Depositional System, nor are the rivers of the eastern margin of India. The western margin of the Bengal Depositional System is where the sediments of the Bengal Fan abut the lower continental slope of eastern India.

Myanmar and the Andaman and Nicobar Islands lie on a different tectonic plate, and are separated from the Bengal Depositional System by a subduction zone and accretionary prism plate edge. The approximate present day boundaries of these two depositional systems are illustrated in Figure 22, along with the Sunda Arc subduction zone plate edge that separates the two systems.

Joseph R. Curray — 26 May 2011

Joseph R. Curray — Date

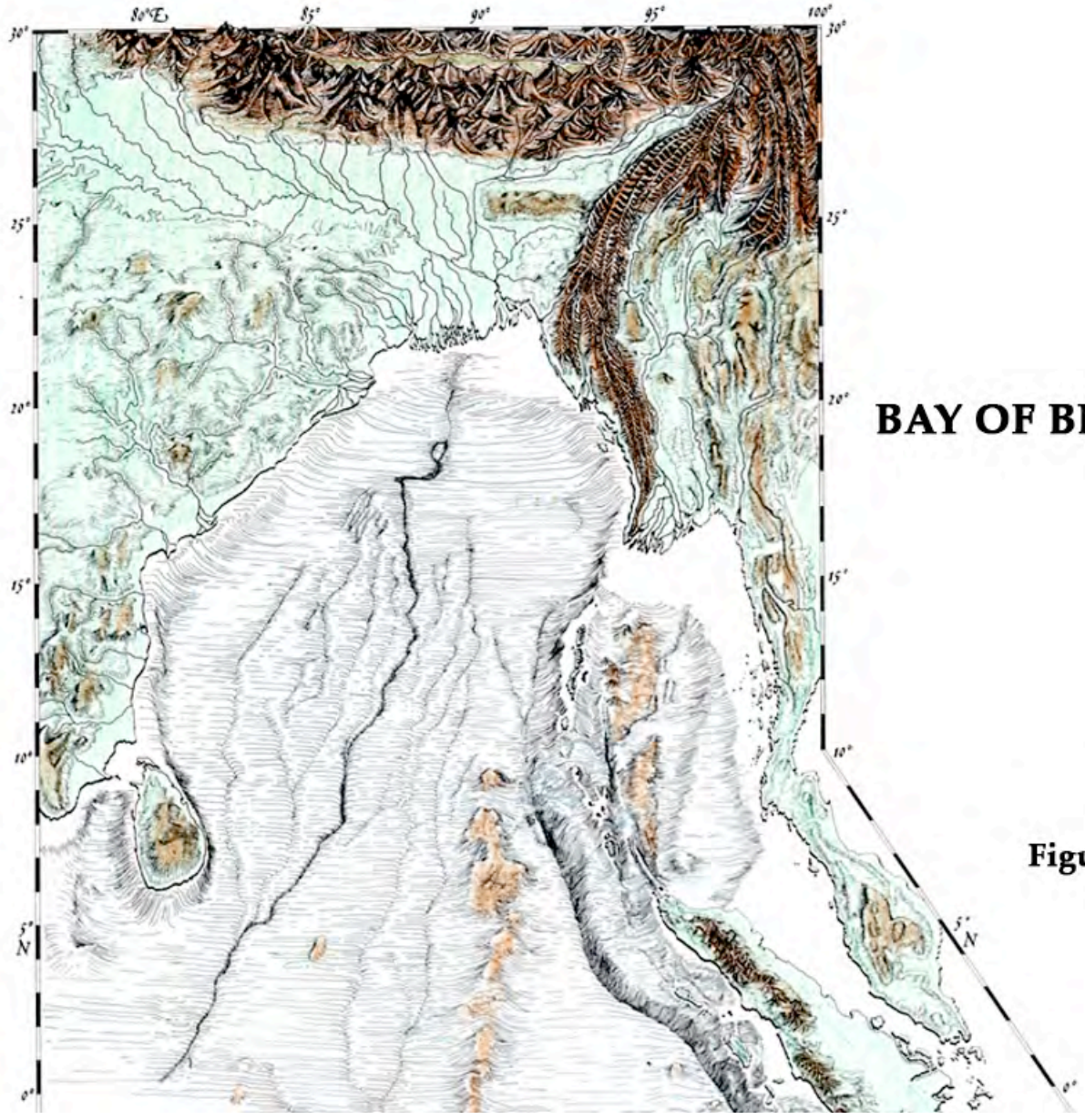

Figure 1

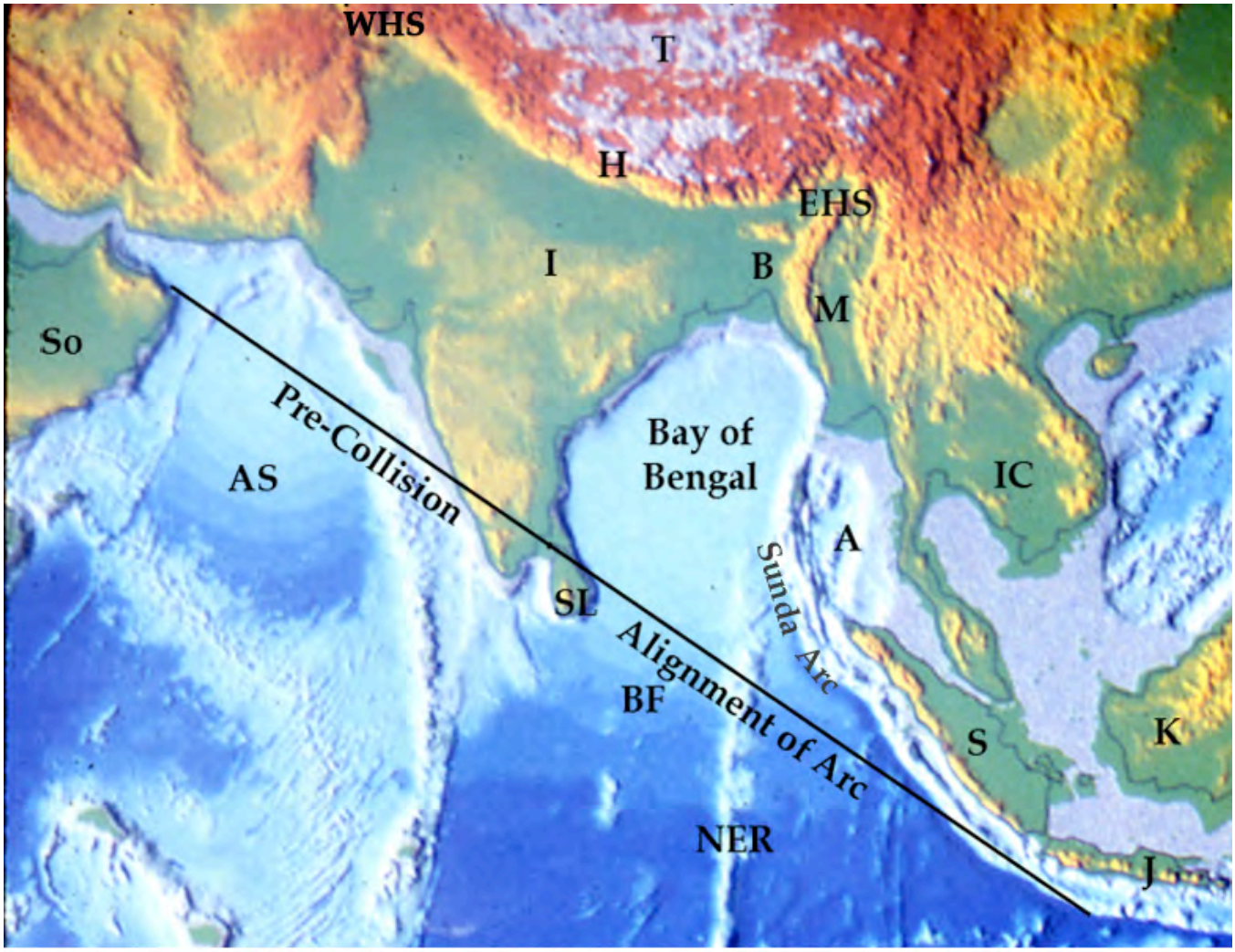
WHS
T
H
EHS
I
B
M
So
Pre-Collision
Bay of
Bengal
IC
AS
A
Sunda Arc
SL
Alignment of Arc
BF
S
K
NER
J

Figure 2.

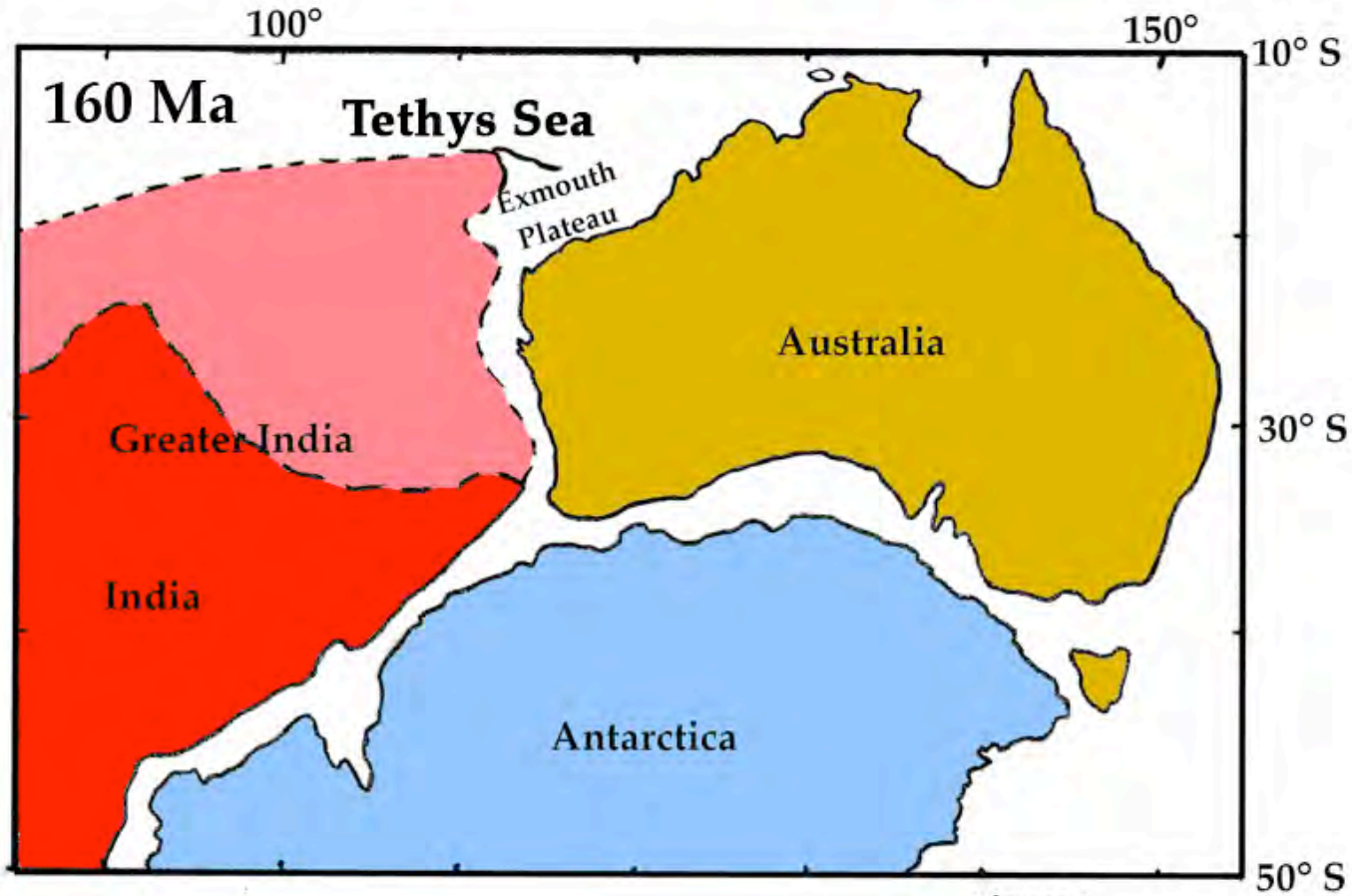
100°
150°
10° S
160 Ma
Tethys Sea
Exmouth
Plateau
Australia
Greater India
India
Antarctica
30° S
50° S

Figure 3

Convergence between India and Asia

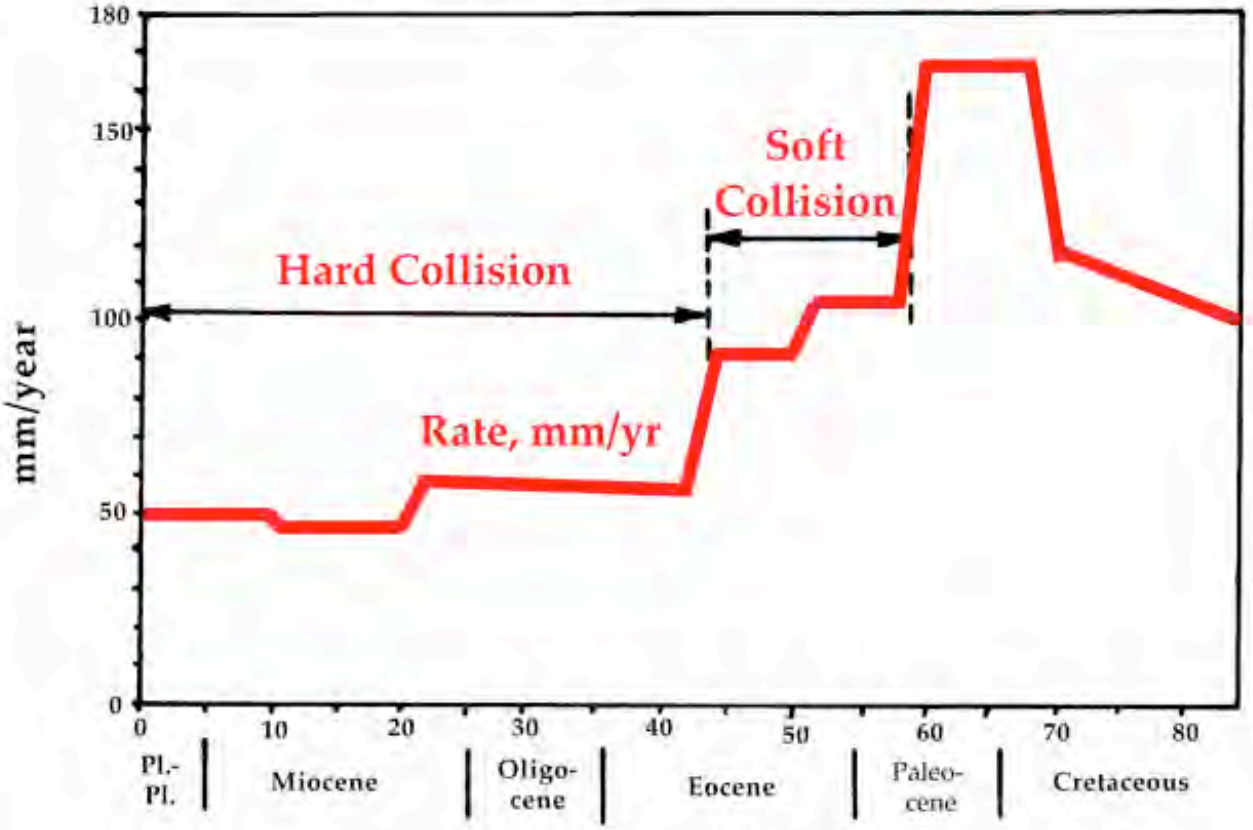

Figure 4

After Lee and Lawver, 1995

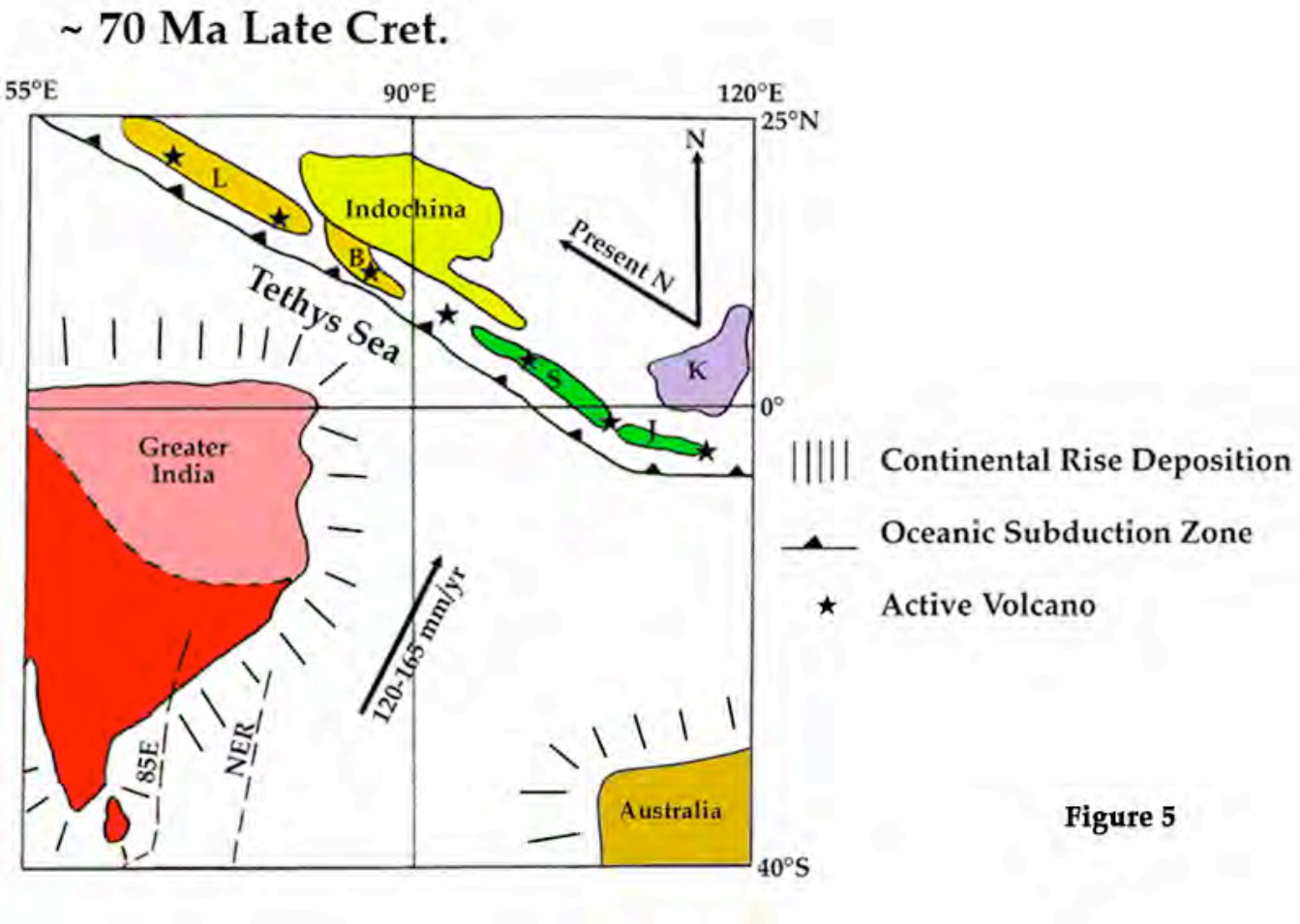
~ 70 Ma Late Cret.
55°E
90°E
120°E
25°N
0°
40°S
N
Present N
L
B
Indochina
Tethys Sea
K
J
Greater India
120-165 mm/yr
85E
NER
Australia
Continental Rise Deposition
Oceanic Subduction Zone
Active Volcano

Figure 5

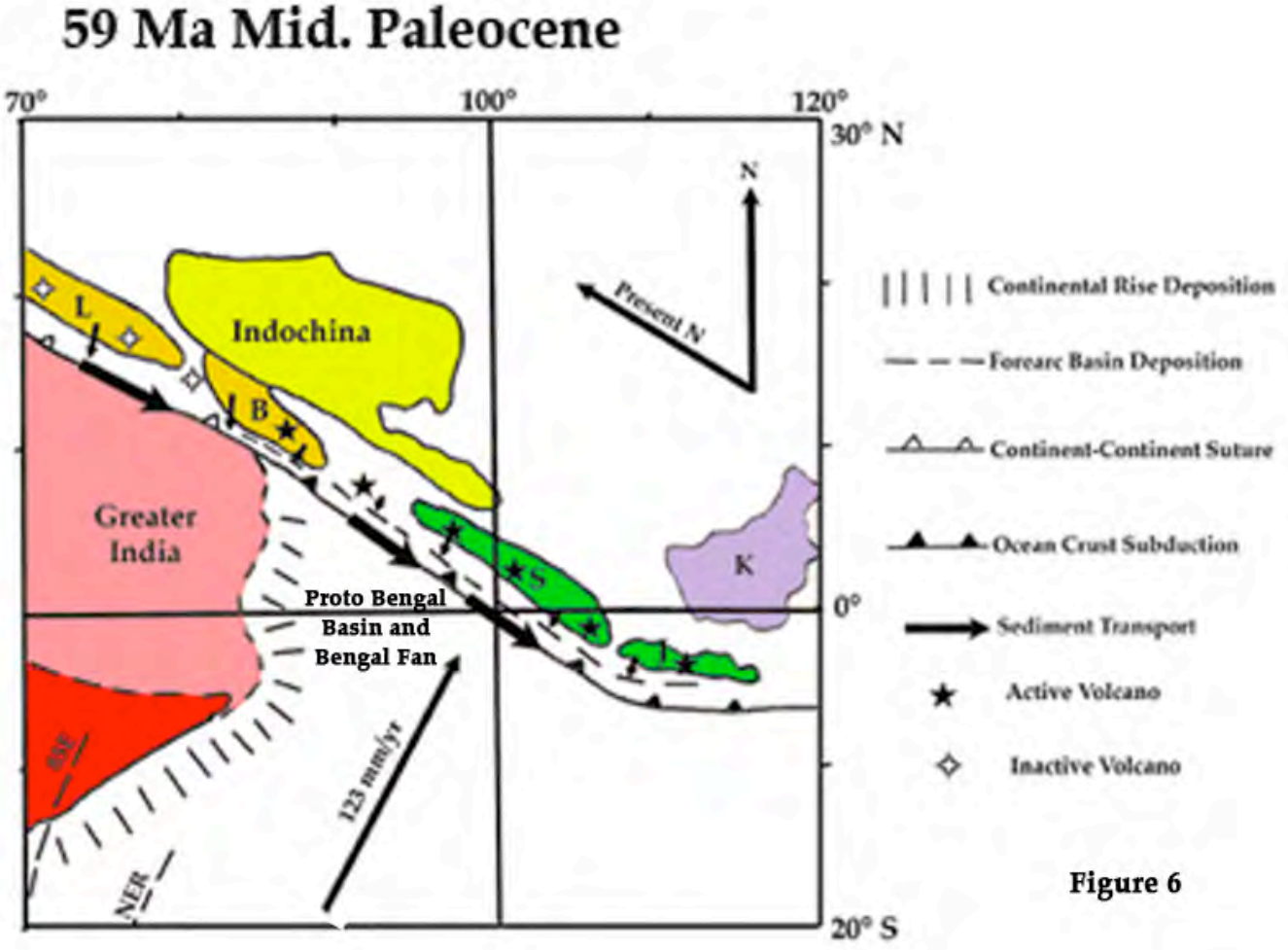
59 Ma Mid. Paleocene
70°
100°
120°
30° N
0°
20° S
N
Present N
L
Indochina
B
Greater India
S
K
Proto Bengal Basin and Bengal Fan
123 mm/yr
BSF
NER
Continental Rise Deposition
Forearc Basin Deposition
Continent-Continent Suture
Ocean Crust Subduction
Sediment Transport
Active Volcano
Inactive Volcano

Figure 6

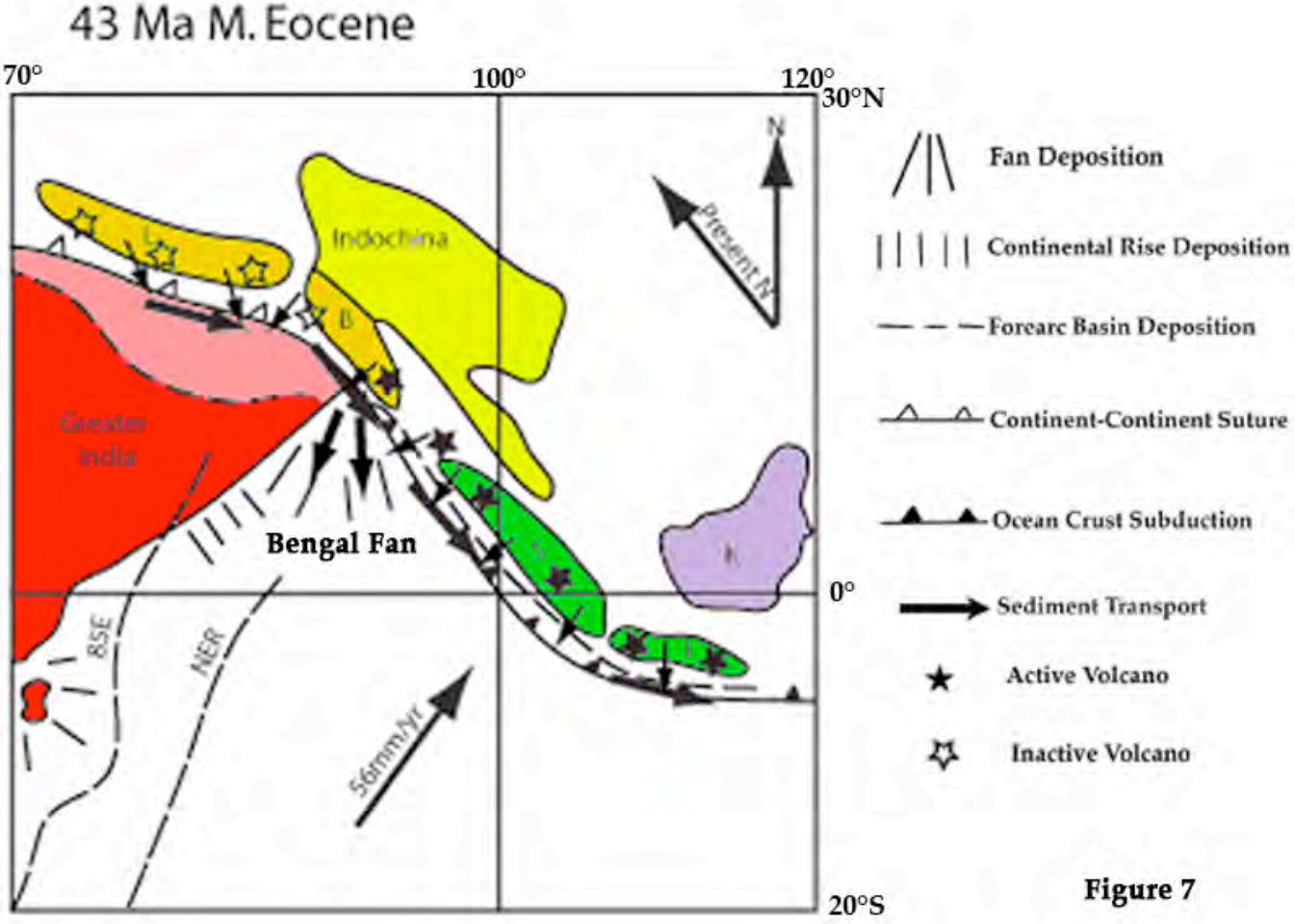
43 Ma M. Eocene
70°
100°
120°
30°N
0°
20°S
N
Present N
Indochina
Greater India
Bengal Fan
BSE
NER
56mm/yr
Fan Deposition
Continental Rise Deposition
Forearc Basin Deposition
Continent-Continent Suture
Ocean Crust Subduction
Sediment Transport
Active Volcano
Inactive Volcano

Figure 7

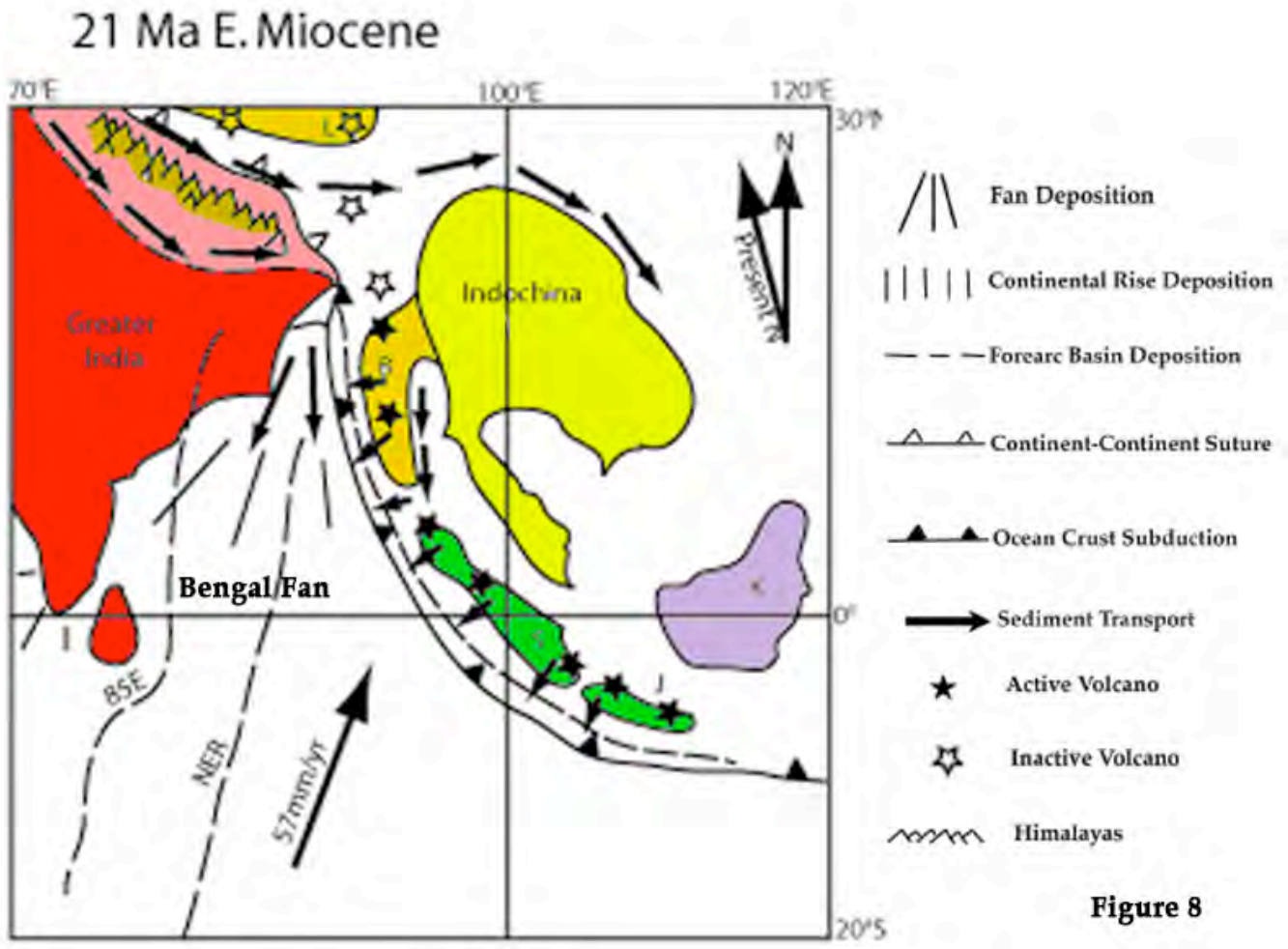
21 Ma E. Miocene
70°E
100°E
120°E
30°N
0°
20°S
N
Present
Greater India
Indochina
Bengal Fan
85E
NER
57mm/yr
Fan Deposition
Continental Rise Deposition
Forearc Basin Deposition
Continent-Continent Suture
Ocean Crust Subduction
Sediment Transport
Active Volcano
Inactive Volcano
Himalayas

Figure 8

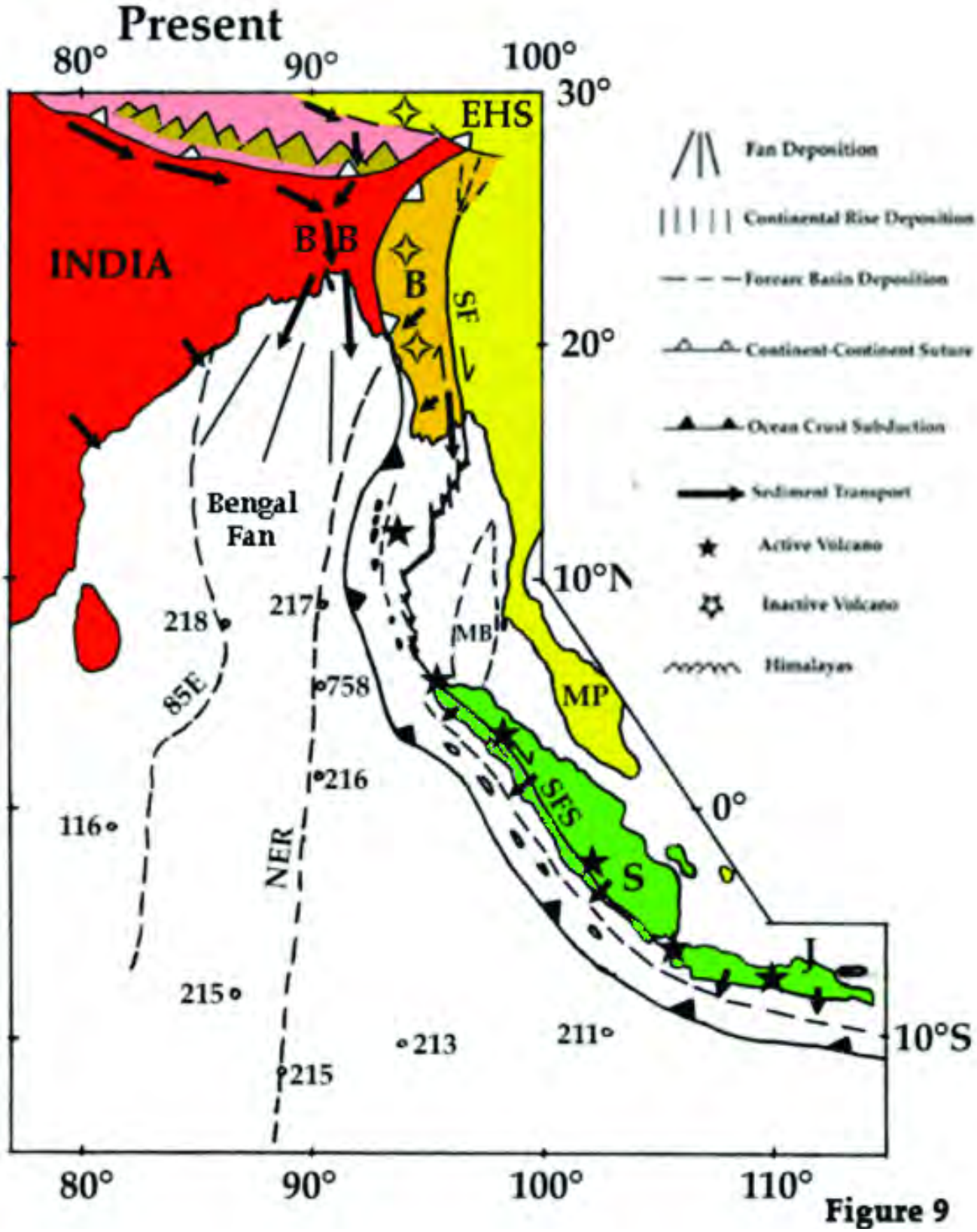
Present
80°
90°
100°
30°
20°
10°N
0°
10°S
110°
EHS
INDIA
B
B
B
SF
Bengal
Fan
218
217
758
216
215
213
211
85E
NER
MB
MP
SES
S
I
Fan Deposition
Continental Rise Deposition
Forearc Basin Deposition
Continent-Continent Suture
Ocean Crust Subduction
Sediment Transport
Active Volcano
Inactive Volcano
Himalayas

Figure 9

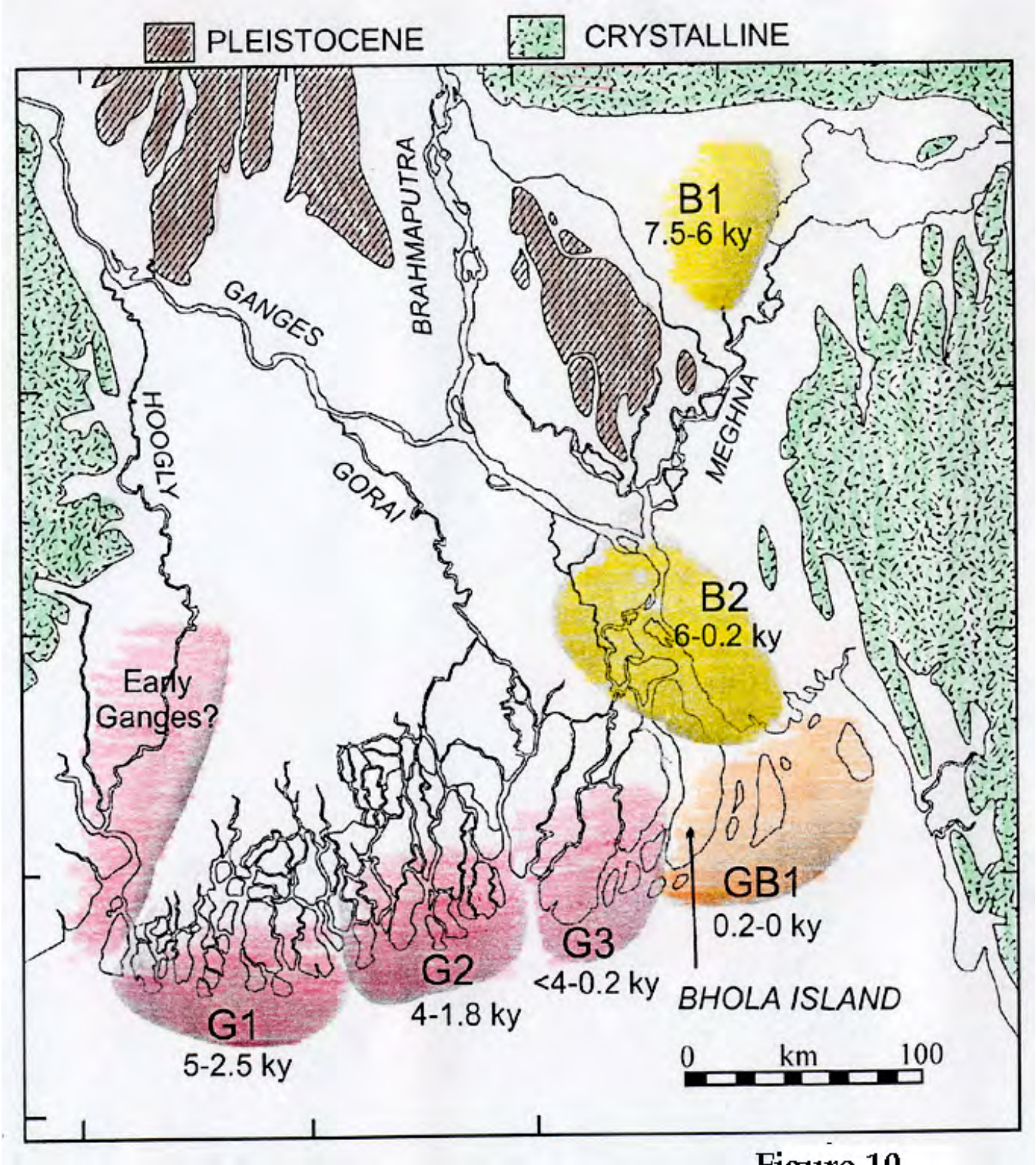
PLEISTOCENE
CRYSTALLINE
BRAHMAPUTRA
GANGES
HOOGLY
GORAI
MEGHNA
B1
7.5-6 ky
B2
6-0.2 ky
Early
Ganges?
G1
5-2.5 ky
G2
4-1.8 ky
G3
<4-0.2 ky
GB1
0.2-0 ky
BHOLA ISLAND
0
km
100

Figure 10

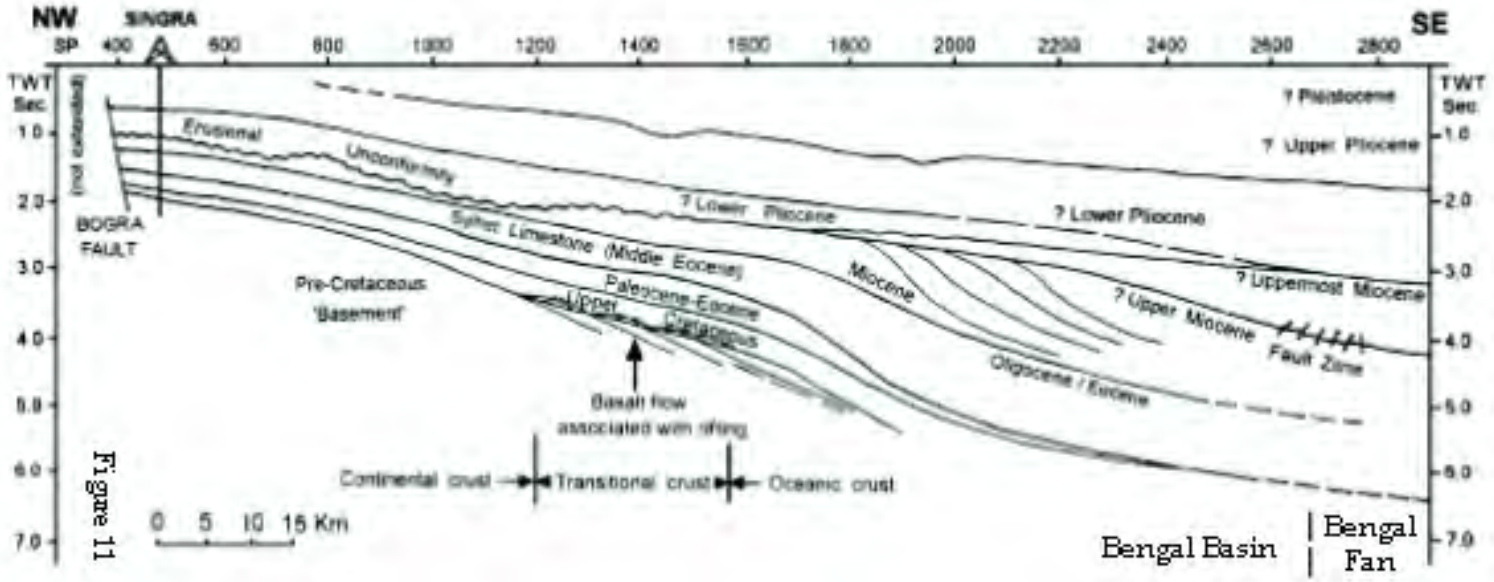
NW
SE
SP
400
500
600
800
1000
1200
1400
1600
1800
2000
2200
2400
2600
2800
TWT Sec.
1.0
2.0
3.0
4.0
5.0
6.0
7.0
BOGRA FAULT
Erosional Unconformity
? Pleistocene
? Upper Pliocene
? Lower Pliocene
? Lower Pliocene
? Uppermost Miocene
? Upper Miocene
Fault Zone
Miocene
Oligocene / Eocene
Sylhet Limestone (Middle Eocene)
Paleocene-Eocene
Upper Cretaceous
Pre-Cretaceous 'Basement'
Basalt flow associated with rifting
Continental crust
Transitional crust
Oceanic crust
0 5 10 15 Km
Bengal Basin
Bengal Fan

Figure 11

Fan Progradation

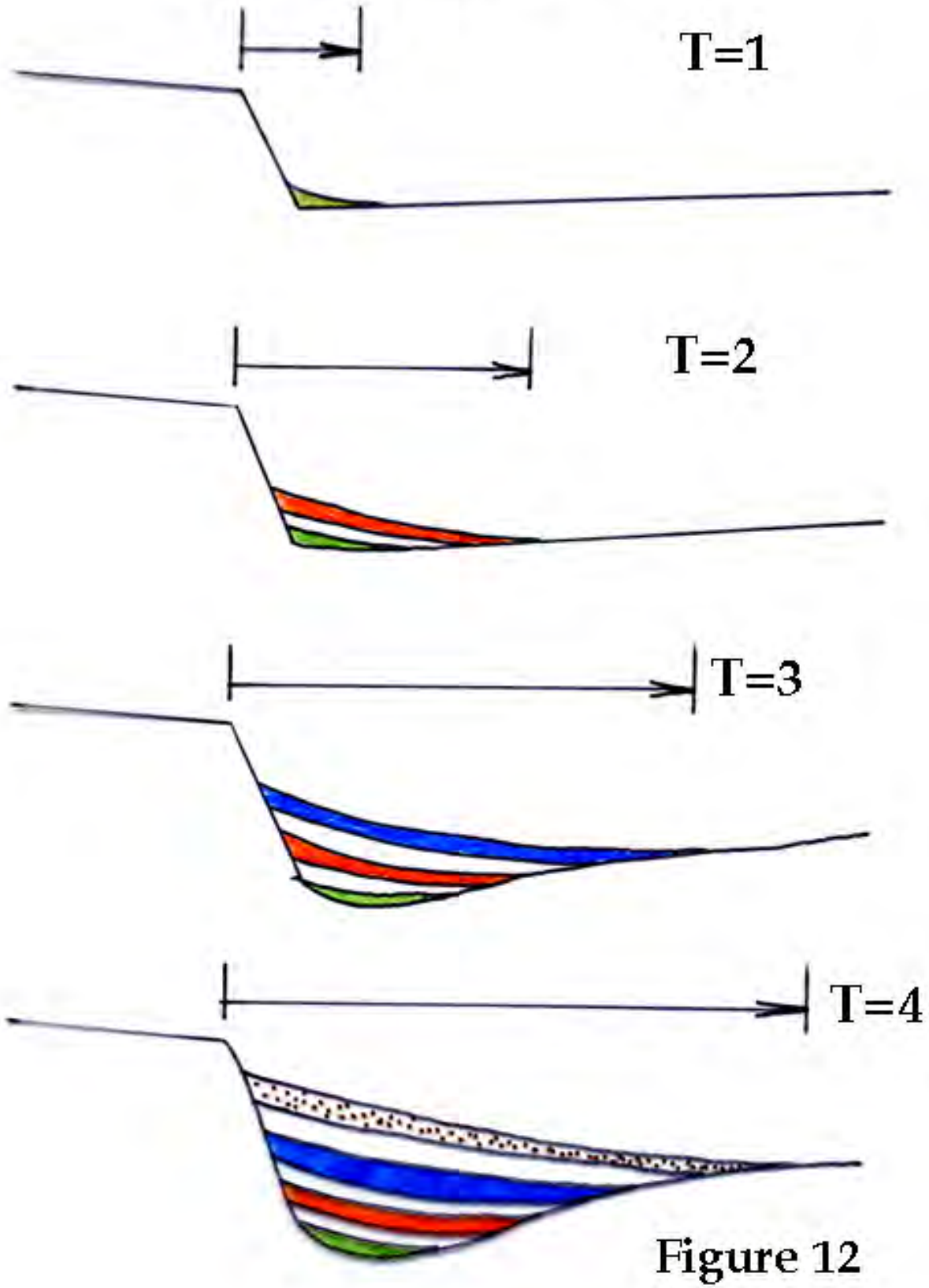

Figure 12

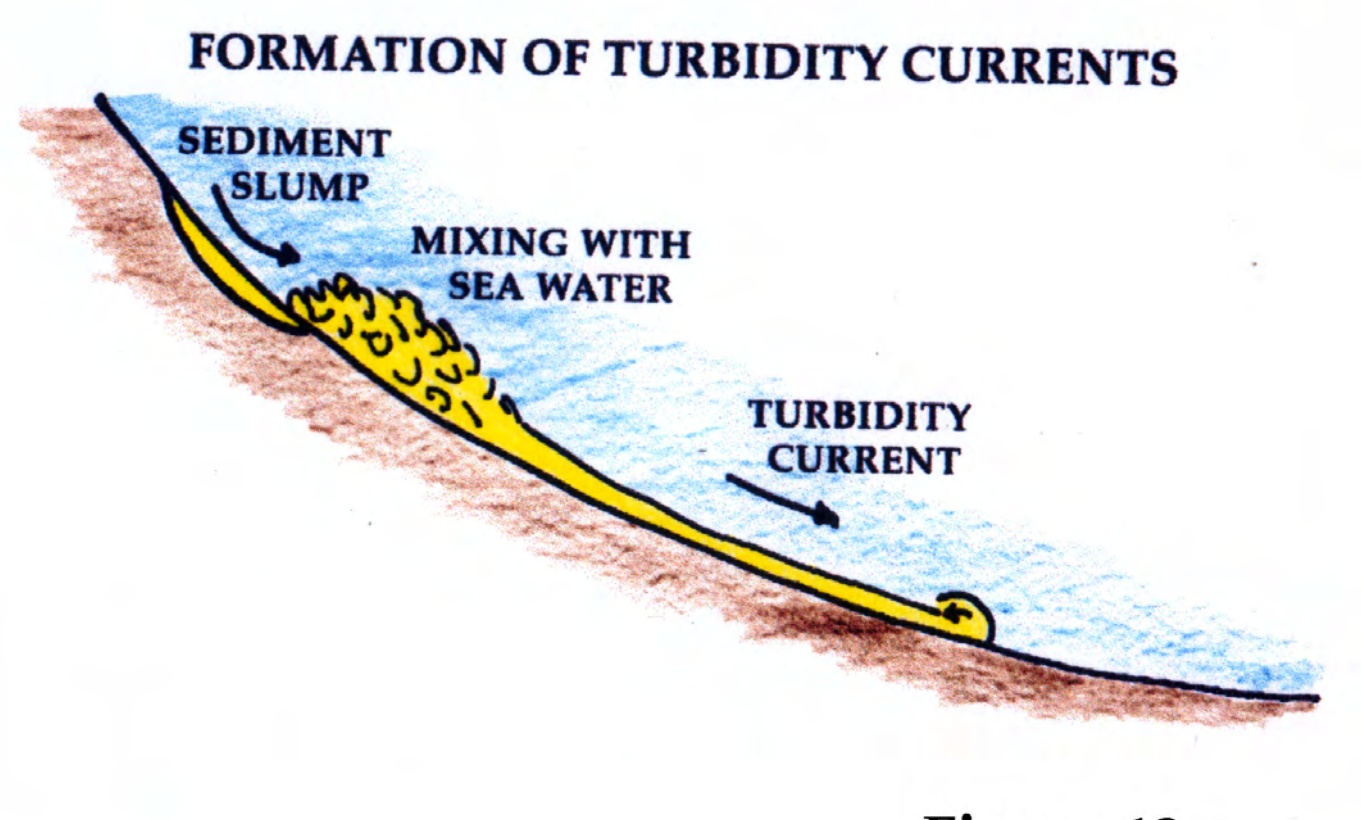
FORMATION OF TURBIDITY CURRENTS
SEDIMENT SLUMP
MIXING WITH SEA WATER
TURBIDITY CURRENT

Figure 13

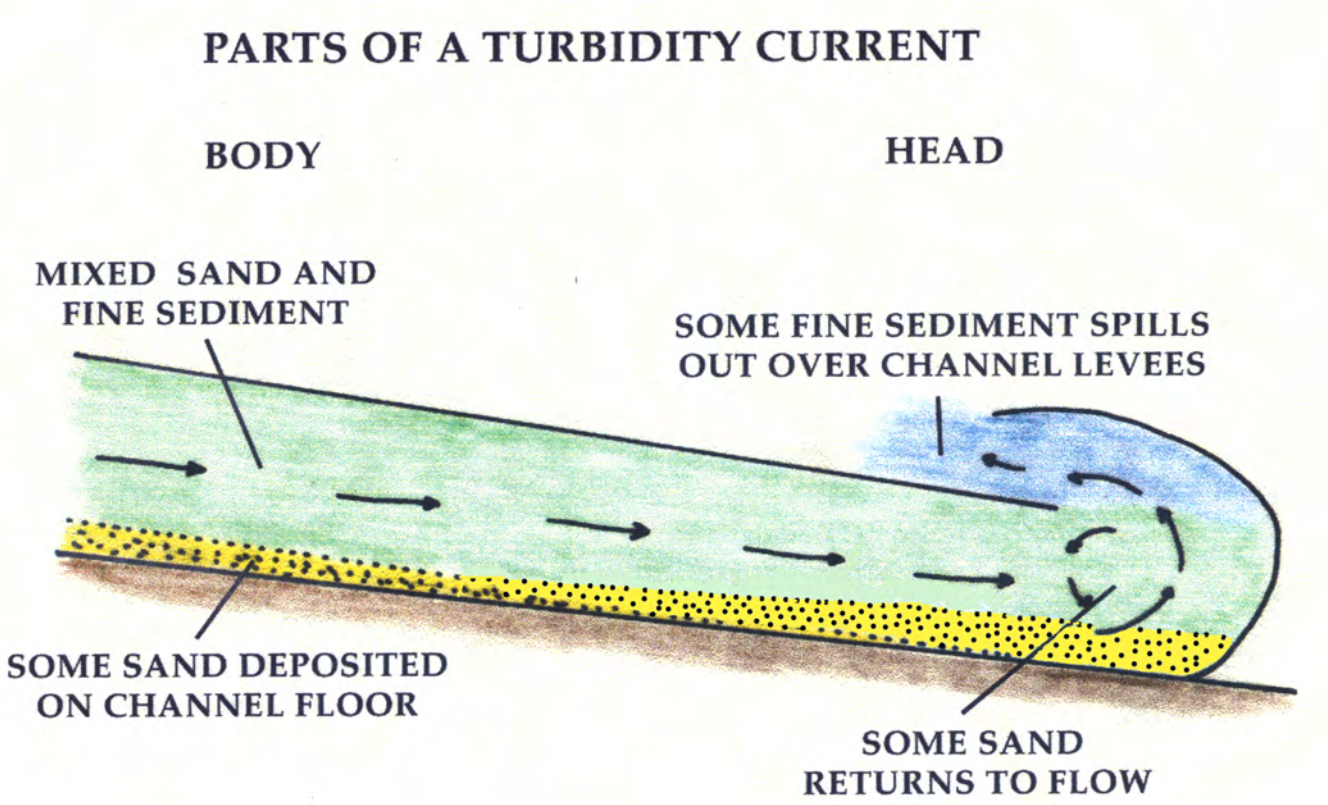
PARTS OF A TURBIDITY CURRENT
BODY
HEAD
MIXED SAND AND FINE SEDIMENT
SOME FINE SEDIMENT SPILLS OUT OVER CHANNEL LEVEES
SOME SAND DEPOSITED ON CHANNEL FLOOR
SOME SAND RETURNS TO FLOW
MOST OF SAND CONTINUES TO END OF FLOW

Figure 14

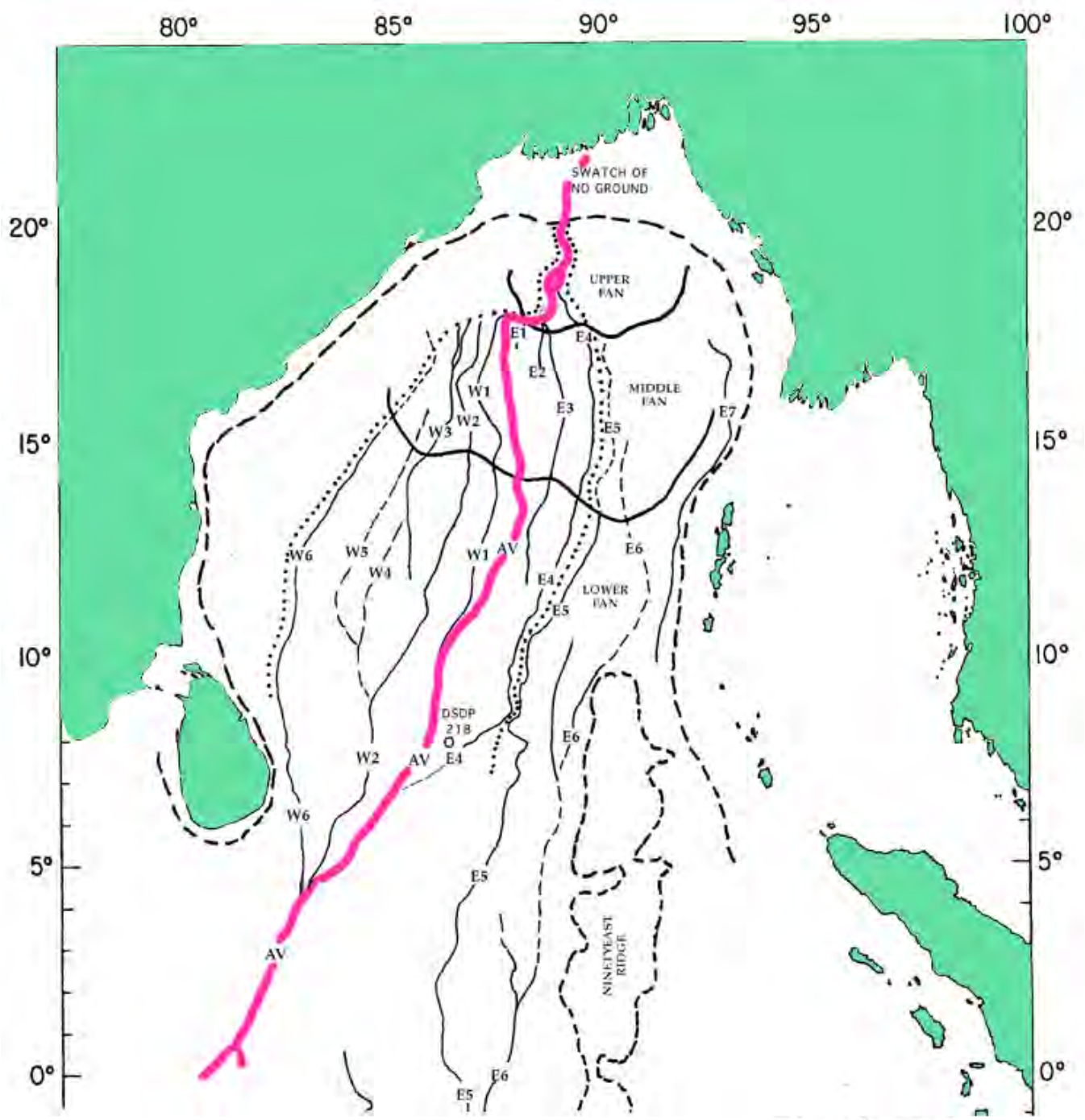
80°
85°
90°
95°
100°
20°
15°
10°
5°
0°
SWATCH OF NO GROUND
UPPER FAN
MIDDLE FAN
LOWER FAN
E1
E2
E3
E4
E5
E6
E7
W1
W2
W3
W4
W5
W6
AV
DSDP 218
NINETYEAST RIDGE

Figure 15

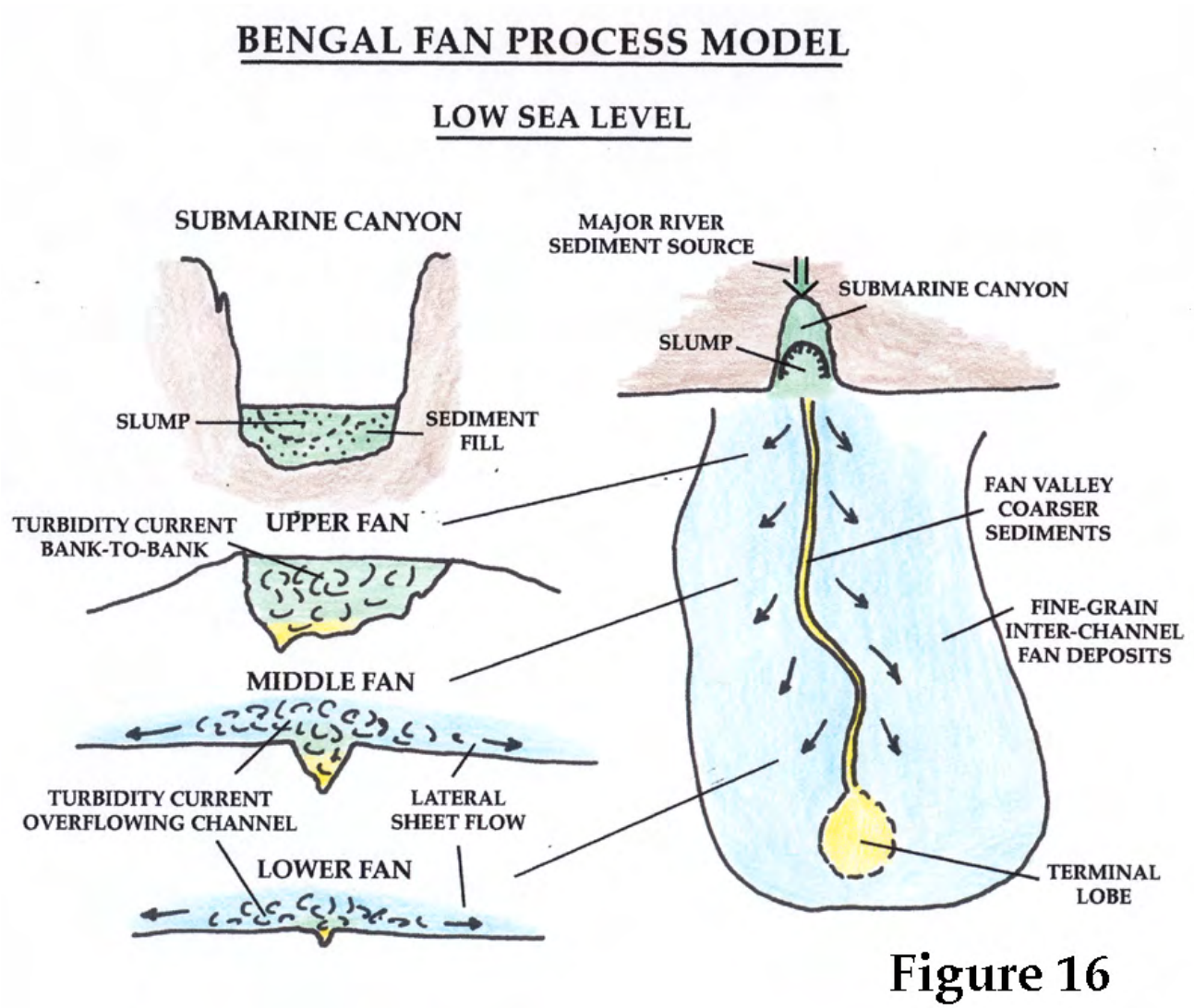
BENGAL FAN PROCESS MODEL
LOW SEA LEVEL
SUBMARINE CANYON
SLUMP
SEDIMENT FILL
TURBIDITY CURRENT BANK-TO-BANK
UPPER FAN
MIDDLE FAN
TURBIDITY CURRENT OVERFLOWING CHANNEL
LATERAL SHEET FLOW
LOWER FAN
MAJOR RIVER SEDIMENT SOURCE
SUBMARINE CANYON
SLUMP
FAN VALLEY COARSER SEDIMENTS
FINE-GRAIN INTER-CHANNEL FAN DEPOSITS
TERMINAL LOBE

Figure 16

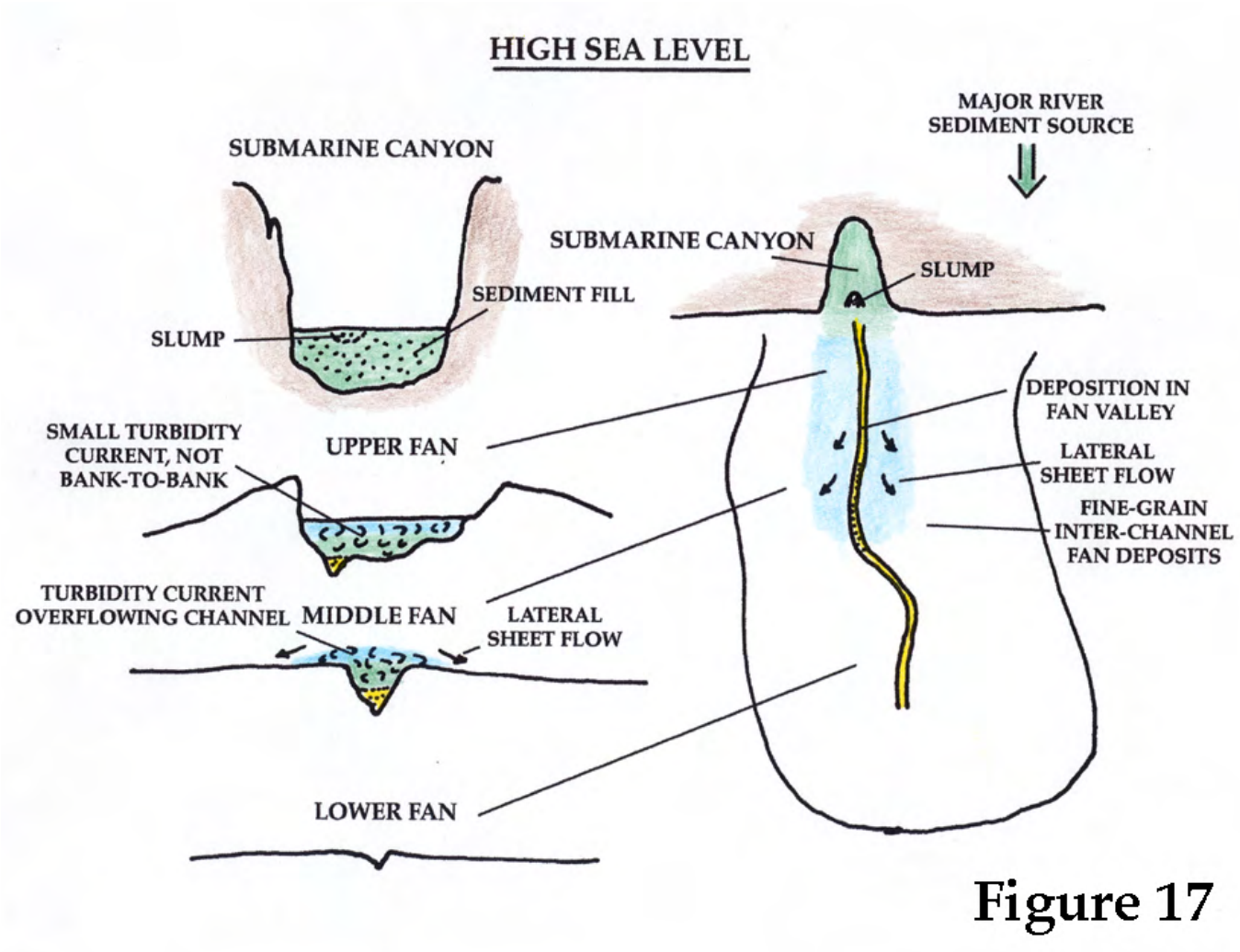
HIGH SEA LEVEL
MAJOR RIVER
SEDIMENT SOURCE
SUBMARINE CANYON
SUBMARINE CANYON
SLUMP
SEDIMENT FILL
SLUMP
DEPOSITION IN
FAN VALLEY
SMALL TURBIDITY
CURRENT, NOT
BANK-TO-BANK
UPPER FAN
LATERAL
SHEET FLOW
FINE-GRAIN
INTER-CHANNEL
FAN DEPOSITS
TURBIDITY CURRENT
OVERFLOWING CHANNEL
MIDDLE FAN
LATERAL
SHEET FLOW
LOWER FAN

Figure 17

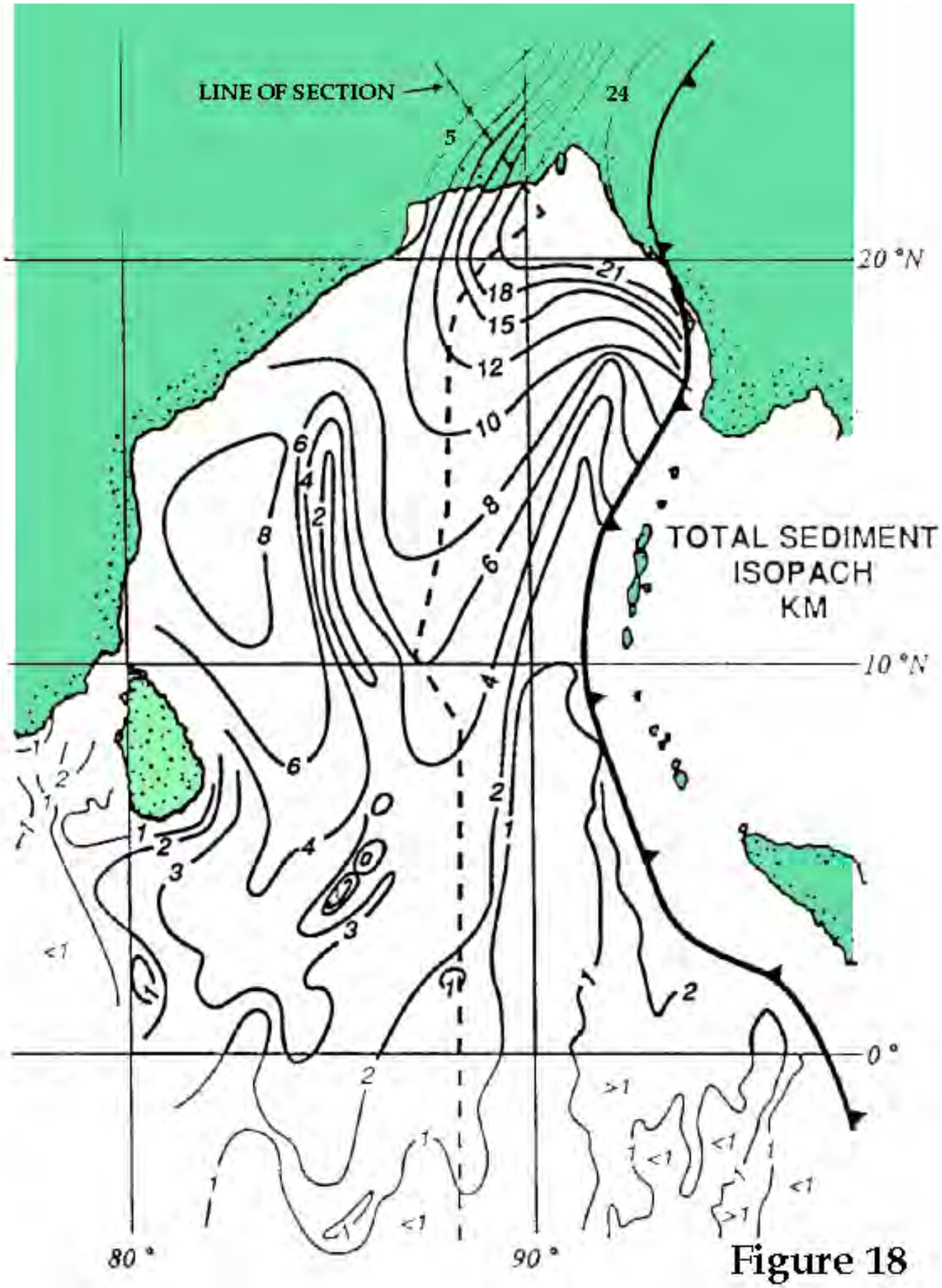
LINE OF SECTION
5
24
20 °N
21
18
15
12
10
8
6
4
2
TOTAL SEDIMENT
ISOPACH
KM
10 °N
0
1
2
3
<1
>1
0 °
80 °
90 °

Figure 18

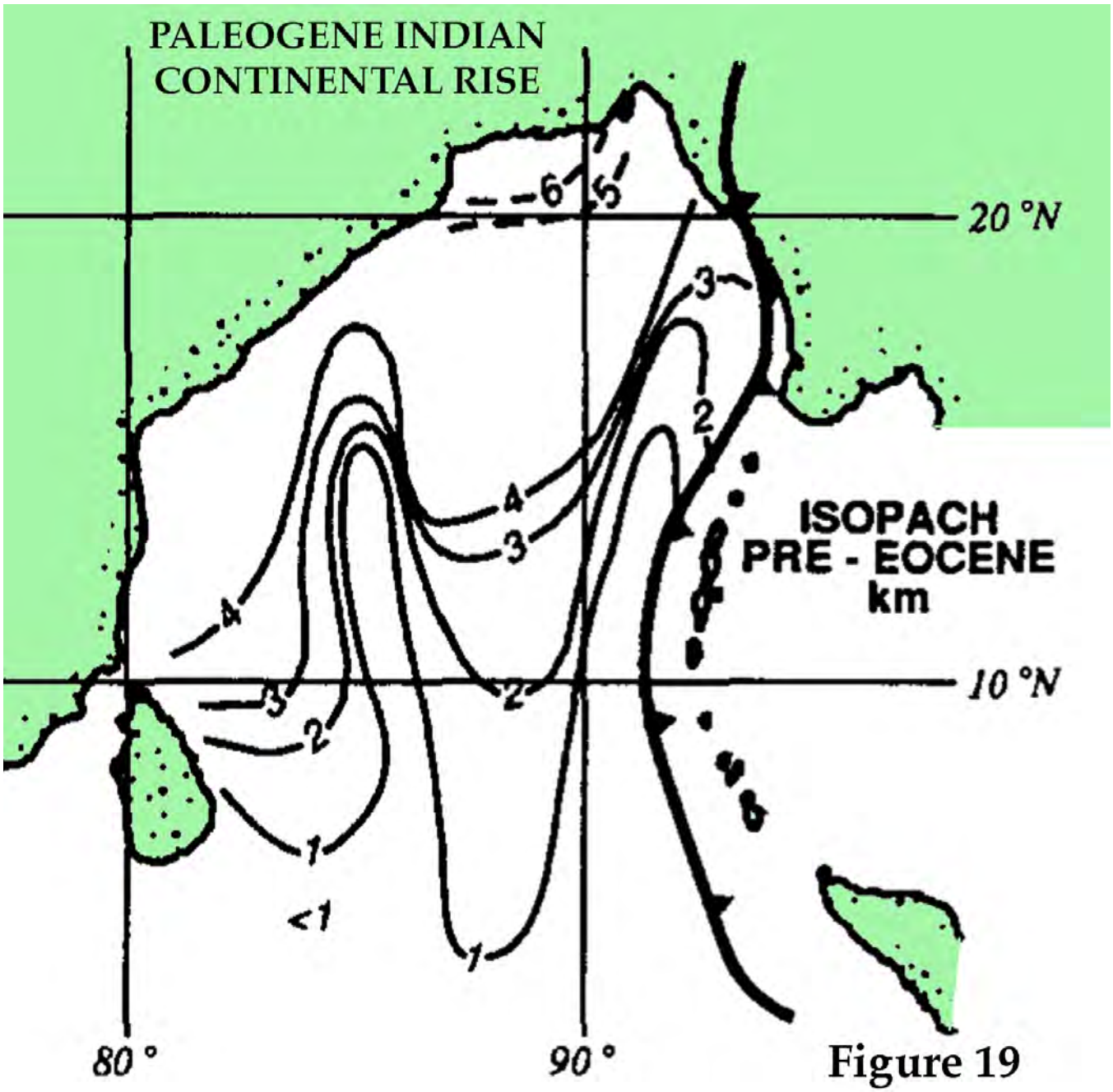
PALEOGENE INDIAN
CONTINENTAL RISE
20 °N
10 °N
80 °
90 °
ISOPACH
PRE - EOCENE
km
6
5
3
2
4
3
4
3
2
2
1
<1
1

Figure 19

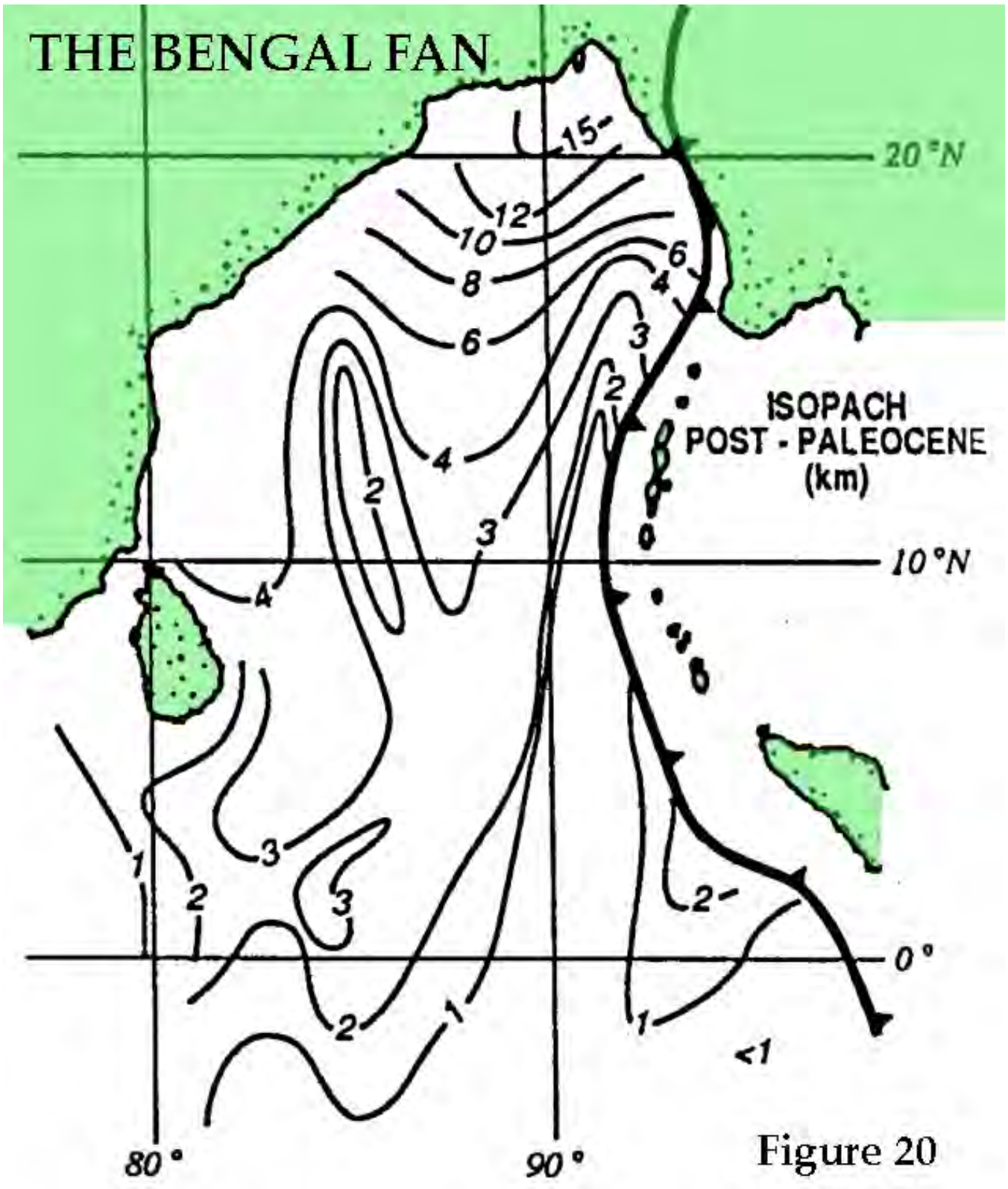
THE BENGAL FAN
ISOPACH
POST - PALEOCENE
(km)
20 °N
10 °N
0 °
80 °
90 °
15
12
10
8
6
4
3
2
1
0
<1

Figure 20

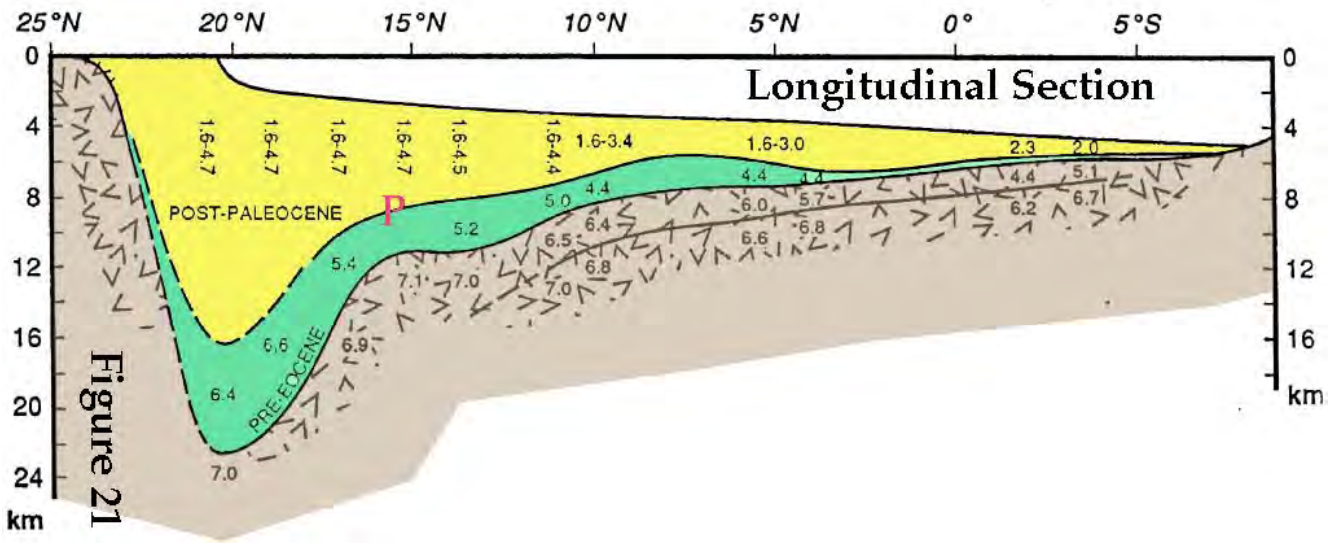
25°N
20°N
15°N
10°N
5°N
0°
5°S
Longitudinal Section
POST-PALEOCENE
PRE-EOCENE
P
1.6-4.7
1.6-4.5
1.6-4.4
1.6-3.4
1.6-3.0
2.3
2.0
4.4
5.1
6.0
5.7
6.2
6.7
5.0
4.4
6.4
5.2
6.5
6.8
6.6
5.4
7.1
7.0
6.8
6.6
6.9
6.4
7.0
0
4
8
12
16
20
24
km

Figure 21

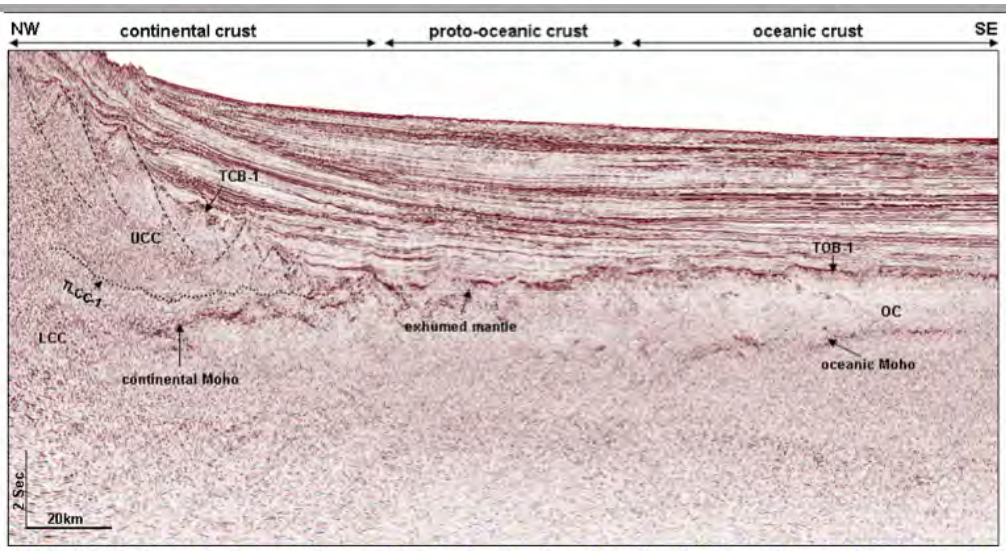

Figure 22

Profile GXT-1000 through the southern Krishna basin showing distribution of crustal types including thinned upper continental crust (UCC), thinned lower continental crust (LCC), proto-oceanic crust (exhumed mantle), and oceanic crust (OC), mapped as based on seismic signatures. Note the break-up initiated by normal faulting.

The continental Moho uprising towards NW is seismically very well imaged

Towards SE, the more organized layered normal oceanic crust with a prominent Moho resolution (oceanic Moho) can be observed. The top oceanic basement (TOB-1) is relatively flat and tectonically undisturbed

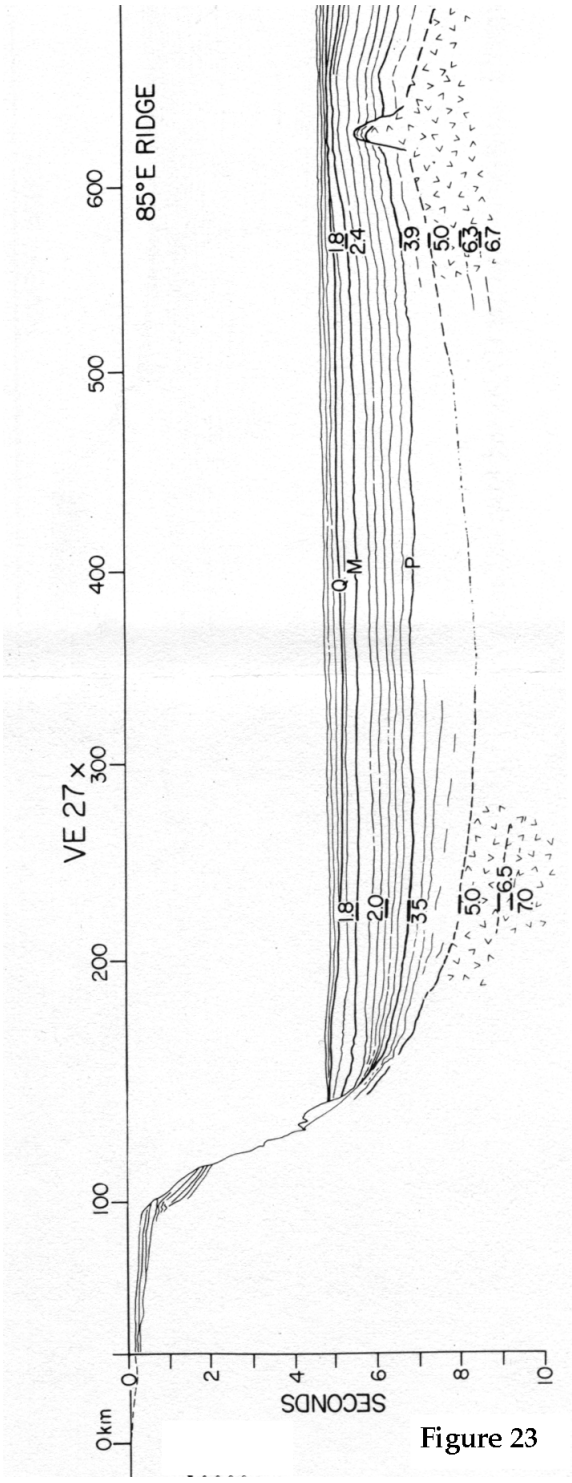
85°E RIDGE
VE 27 x
0km
SECONDS
Q
M
P
1.8
2.4
3.9
5.0
6.3
6.7
1.8
2.0
3.5
5.0
6.5
7.0

Figure 23

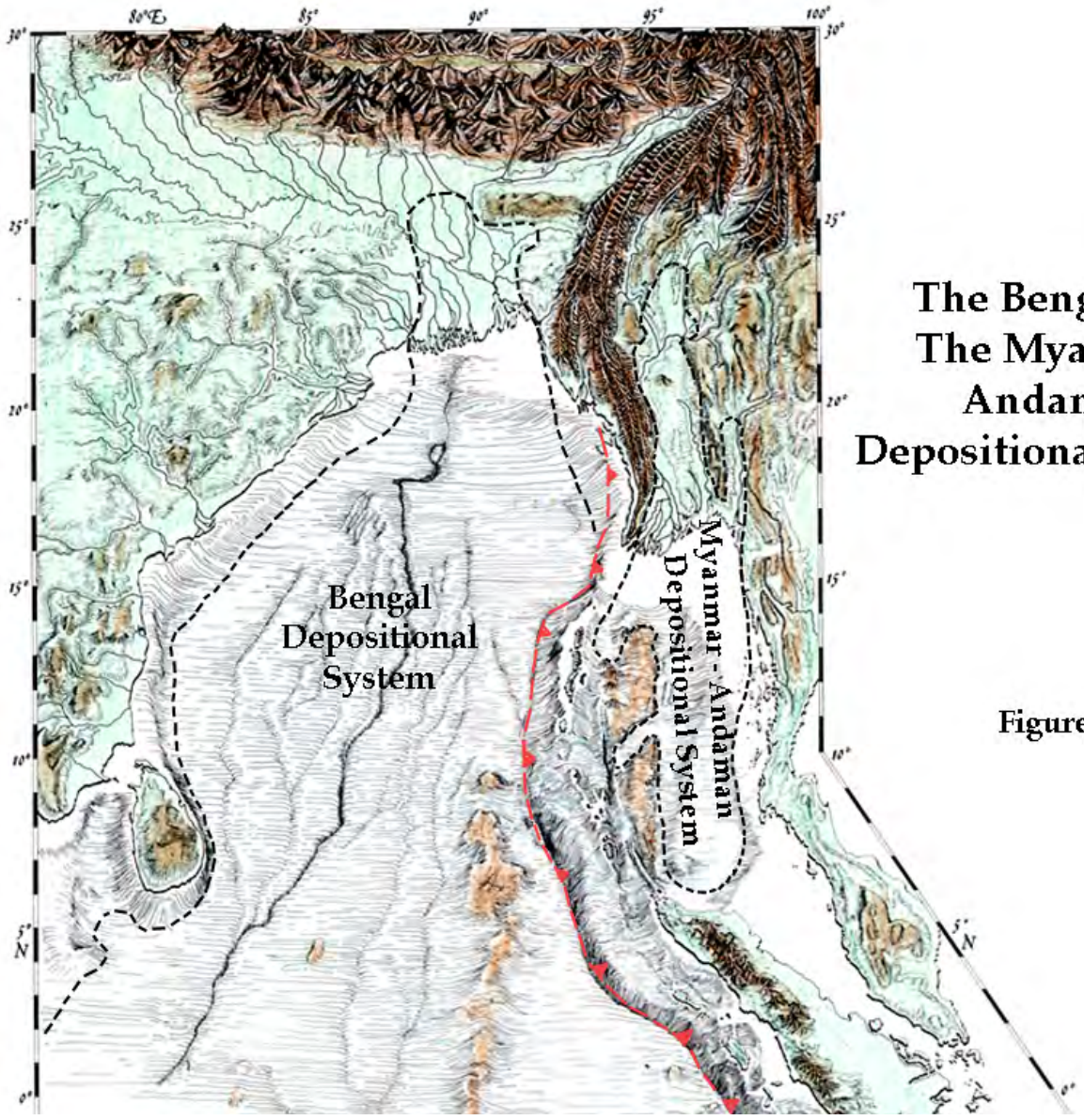

The Bengal and The Myanmar - Andaman Depositional Systems

Figure 24

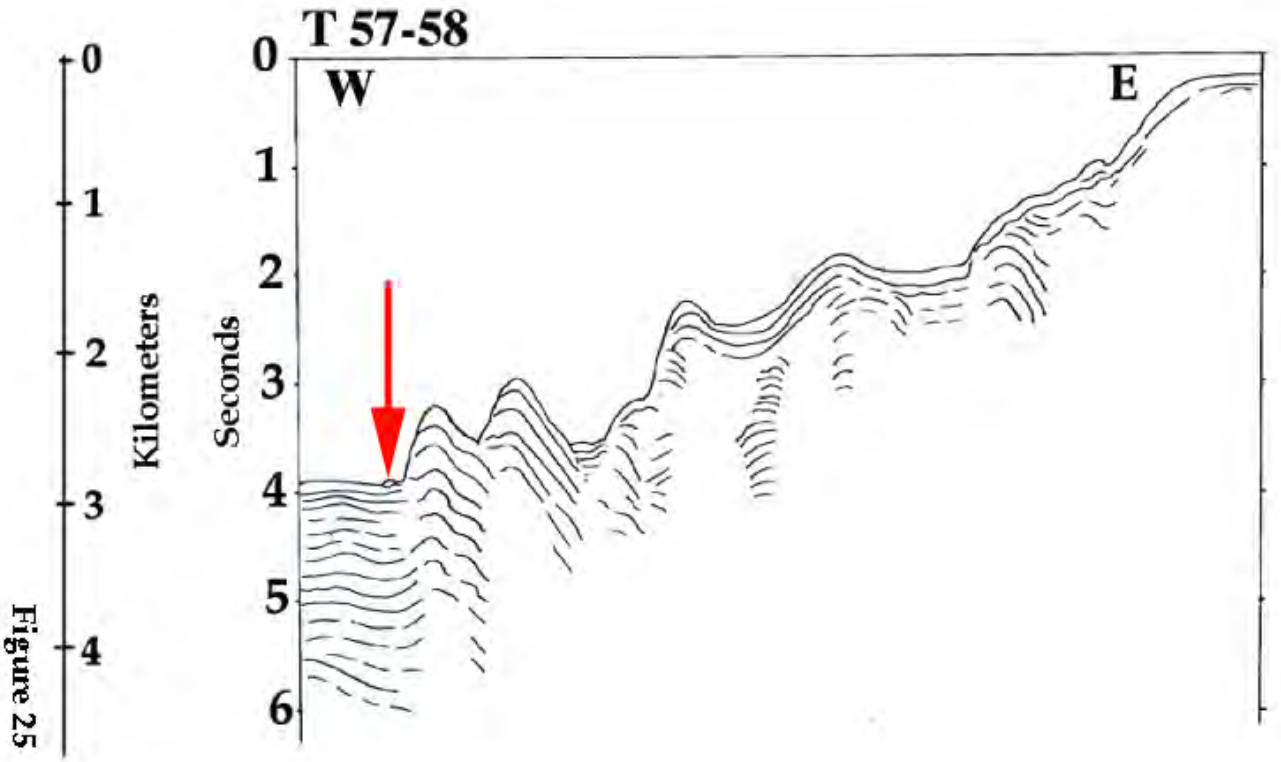

Figure 25

APPENDIX 1 TO ANNEX B52

Biographical Information of Dr.Joseph R. Curray

BIOGRAPHICAL INFORMATION

JOSEPH R. CURRAY

Born 19 January 1927, Cedar Rapids, Iowa.

Education

B.S. (Geology) The California Institute of Technology, June 1949.
M.S. (Mineralogy) The Pennsylvania State University, June 1951.
Ph.D. (Oceanography) Scripps Institution of Oceanography, University of California, January 1959.

Experience

U.S. Navy, 1945-1946.
Instructor in Geology and Mineralogy, The Pennsylvania State University,1950-1951.
Research Geologist, The Carter Oil Co. Research Lab., Tulsa, Oklahoma, 1951-53.
Scripps Institution of Oceanography, University of California at San Diego.
Graduate student to Professor of Geology and Research Geologist, 1953-1991.
Chairman of Graduate Department, 1973, 1974, 1975.
Chairman of Geological Research Division, 1976, 1977, 1978.
Chairman SIO Faculty, 1983-1984.
Present position, since October 1991: Professor of Geology, Emeritus.
Director of Nekton, Inc., 1957-1986; Chairman of the Board: 1983-1986.
Visiting Professor: Universities of Texas, Colorado, Kuwait and Stanford.

Fields of Research

Geology of continental margins: sediments, structure, tectonics, and geological history.
Specialize in sediments, structure, tectonics and geological history of NE Indian Ocean and SE Asia since 1968: Bengal submarine fan, Andaman Sea, Bay of Bengal, and continental margins of Sri Lanka, India, Bangladesh, Myanmar, Thailand, Malaysia, Sumatra and Java.
Previous fields of research: quantitative sedimentology; Quaternary sea level changes; coastal sedimentary environments; continental shelves of the Gulf Coast and the rest of the US; formation of the Gulf of California; San Andreas Fault; coral reefs and atolls of Micronesia and Panama; continental margins of California, western Mexico, eastern US, western Europe, NW South America, western Florida, NW Australia, etc.
Work at sea on about a dozen ships of the SIO fleet and several dozen other vessels of other nations, institutions and organizations, including Deep Sea Drilling Project's Glomar Challenger.

Publications

See attached: over 200 total, including 108 scientific research papers and books edited.

Honors

Francis P. Shepard Medal for Excellence in Marine Geology for 1970 by Society of Economic Paleontologists and Mineralogists.
Fellow, Geological Society of America.
Fellow, Geological Society of London.
Fellow, American Association for the Advancement of Science.
Centennial Fellow of the College of Earth & Mineral Sciences, The Pennsylvania State University, 1996.
Annual Report of the Scripps Institution of Oceanography, Fiscal 1995, dedicated to JRC.

Other Activities

Chairman and Advisor, about 12 SIO PhDs.
Invited lecturer, many universities and national and international meetings and organizations.
Member, American Association of Petroleum Geologists, American Geophysical Union, Society of Sedimentary Geologists.
Trustee, Foundation for Ocean Research, 1971-1987.
Founder, La Jolla Hash House Harriers, 1978.
Registered Geologist, State of California.

JOIDES (Joint Oceanographic Institution for Deep Earth Sampling), Member Gulf of Mexico Panel.
IPOD (International Program for Ocean Drilling):
Passive Continental Margin Panel, 1974-1980; Chairman 1974-1978.
Safety Panel 1975-1978.
ODP (Ocean Drilling Program)
Indian Ocean Regional Panel, Chairman 1983-1985; Member until 1987.
INQUA (International Quaternary Association), Holocene Subcommission for N. America and Greenland, 1972-1973.
AAPG (American Association of Petroleum Geologists):
Member Marine Geology Committee 1971-1982, 1984-1987
Member Research Committee, 1979-1981
Chairman Jules Braunstein Poster Awards Committee, National Meeting 1996.
GSA (Geological Society of America):
National Representative 1973-1975; Subcommittee for Honorary Fellows, 1980, Chairman 1981.
SEPM (Society for Sedimentary Geology), Councilor, 1973-1975
Advisor for Oceanography program, King Abdul Aziz University, Jeddah, Saudi Arabia, 1976.
Member Ad Hoc Panel to Investigate the Geological and Geophysical Research Needs and Problems of Continental Margins, Ocean Sciences Board, NRC, 1976-1979.
Member U. S. Geodynamics Committee, Plate Margins Groups, Working Group C, 1978-1980.
UNOLS (University National Ocean Laboratories): Member Advisory Council 1981-1983;UNOLS Vice Chairman 1983-1984; Member Submersible Science Study, 1979-1980, 1987-1990.
Editor of MARINE GEOLOGY 1963-1966, Editorial Board 1963-1995.
Editorial Board GEOMARINE LETTERS, 1980-1993.
Editorial Board, SEDIMENTOLOGY, 1972-1975.
Editorial Board BOLLETTINO DI OCEANOLOGIA, 1983-present.
Advisor, National Aquatic Resources Agency, Sri Lanka, December 1982-February 1983.
Consultant, Chulalonghorn Univ., Bangkok, Thailand (UNDP/UNESCO), Dec. 1983-Feb. 1984.
Coordinator, SEATAR (Studies in East Asian Tectonics and Resources) Transect Project 1985-1987 (UNDP/UNESCO).
U. S. Representative, IOMAC (Indian Ocean Marine Affairs Cooperation, IOC/UNESCO) Workshops, Indian Ocean, Colombo, Sri Lanka, 1985 and 1993; Karachi, Pakistan, 1988.
Meet the Scientist Lecturer, American Geological Institute, 1963-1964.
Symposium Convener, International Geological Congress, Washington, DC, 1989.
Chief Technical Advisor, UNDP Project, Republic of Korea, "Strengthening of KORDI's Deep Sea Research Capability, Korean Ocean Research and Development Institute, 1989 -1991.
San Diego Underwater Park Advisory Board 1982-1983.
National Academy of Science US/Indonesia Marine Science Exchange Lecturer, 1982.
Member UNESCO Study Tour-cum-seminar for Quaternary Geology Research Institutes in Peoples' Republic of China, 1982.
UCSD Academic Senate various committees, including:
Chairman, Committee for Privilege and Tenure, 1987-1990.
Chairman, Committee for Community Environment , 1980-1981.
Program Review Committee, 1972-1975.
Panel for Resolution of Sexual Harassment Charges, 1991-1995.
Administrative Council, 1988-1990.
SIO, various committees: Budget Committee (Chairman), Committee on Committees (Chairman), Scripps Industrial Associates (Chairman), Director's Space Advisory Committee (Chairman), Geological Data Center (Chairman), Specialist Review Panel, Academic Administrator Review Panel, Aquarium Museum Committee, Marine Sciences Physical Planning Committee, Chairman SIO Faculty 1983-1984, etc.

Indian Ocean and Asian Experience

Chief scientist or co-chief scientists on oceanographic research vessels working in the Bay of Bengal, Andaman Sea and off southwest Sumatra and Java in 1968, 1971, 1973, 1975, 1977 and 1986.
National Academy of Science US/Indonesia Marine Science Exchange Lecturer, 1982.
Member UNESCO Study Tour-cum-seminar for Quaternary Geology Research Institutes in Peoples' Republic of China, 1982.

Advisor, National Aquatic Resources Agency, Sri Lanka, December 1982-February 1983.
Consultant, Chulalonghorn Univ., Bangkok, Thailand (UNDP/UNESCO), Dec. 1983-Feb. 1984.
ODP (Ocean Drilling Program)
Indian Ocean Regional Panel, Chairman 1983-1985; Member to 1987.
Coordinator, SEATAR (Studies in East Asian Tectonics and Resources) Transect Project 1985-1987 (UNDP/UNESCO).
U. S. Representative, IOMAC (Indian Ocean Marine Affairs Commission, IOC/UNESCO) Workshops, Indian Ocean, Colombo, Sri Lanka, 1985 and 1993; Karachi, Pakistan, 1988.
Chief Technical Advisor, UNDP Project, Republic of Korea, "Strengthening of KORDI's Deep Sea Research Capability, Korean Ocean Research and Development Institute, 1989 -1991.
Author or co-author of about 40 papers in scientific journals on the northeastern Indian Ocean and Southeast Asia.

APPENDIX 2 TO ANNEX B52

Publications of Dr.Joseph R.Curray

Publications of Joseph R. Curray

Research Papers

1. Curray, J. R. and Griffiths, J. C., 1955, Sphericity and roundness of quartz grains in sediments. Bull. Geol. Soc. Amer., v. 66, 1075-1096.

2. Curray, J. R., 1956, The analysis of two-dimensional orientation data. Jour. Geol., v. 64, 117-131.

3. Parker, R. H. and Curray, J. R., 1956, Fauna and bathymetry of banks on the continental shelf, northwest Gulf of Mexico. Bull. Amer. Assoc. Petrol. Geol., v. 40, 2428-2439.

4. Curray, J. R., 1956, Dimensional grain orientation studies of Recent coastal sands. Bull. Amer. Assoc. Petrol. Geol., v. 40, 2440-2456.

5. Lankford, R. R. and Curray, J. R., 1957, Mid-Tertiary rock outcrop on continental shelf, northwest Gulf of Mexico. Bull. Amer. Assoc. Petrol. Geol., v. 41, 2113-2117.

6. Curray, J. R. and Shepard, F. P., 1959, Sea-level rise along the Texas coast. Interntl. Oceanogr. Congr. Preprints, Amer. Assoc. Adv. Sci., Washington, D. C., 609-610.

7. Curray, J. R., 1960, Sediments and history of the Holocene Transgression, continental shelf, northwest Gulf of Mexico: in Shepard et al. (Eds.), Recent Sediments, Northwest Gulf of Mexico, A.A.P.G., 221-266.

8. Van Andel, Tj. H. and Curray, J. R., 1960, Regional aspects of modern sedimentation in northern Gulf of Mexico and similar basins, and paleogeographic significance: in Shepard, F. P. et al. (Eds.), Recent Sediments, Northwest Gulf of Mexico, A.A.P.G., 345-364.

9. Curray, J. R., 1961, Late Quaternary sea level: a discussion. Bull. Geol. Soc. Amer., v. 72, 1707-1712.

10. van Andel, Tj. H., Curray, J. R., and Veevers, J. J., 1961, Recent carbonate sediments of the Sahul Shelf -- Northwestern Australia. Proc. Coastal and Shallow Water Res. Conf., 1961, Pub. by N.S.F. and O.N.R., 564-567.

11. Curray, J. R., 1961, Continental shelf-coastal plain of northwest mainland Mexico. Proc. 1st Natl. Shallow Water Conf., Oct. 1961, Pub. by NSF and ONR, 533-536.

12. Curray, J. R., 1961, Tracing sediment masses by grain size modes. Rept. of 21st Session Interntl. Geol. Congr., Norway, 1960, Part 23, Interntl. Assoc. Sedimentol., 119-130.

13. Curray, J. R., 1960, Bibliographie de travaux Americains recents, 3. Fabric and packing analysis, 83-85: in Siever, R. (Ed.), Section Etats-Unis, Assoc. Internatl. Sedimentol., 5th World Petrol. Congr., N. Y., 1959 (publ. Edits. Technip, Paris).

14. Moore, D. G. and Curray, J. R., 1963, Structural framework of continental terrace, northwest Gulf of Mexico. Jour. Geophys. Res., v. 68, 1725-1747.

15. Curray, J. R. and Moore, D. G., 1963, Facies delineation by acoustic reflection: northern Gulf of Mexico. Sedimentology, v. 2, 130-148.

16. Moore, D. G. and Curray, J. R., 1963, Sedimentary framework of continental terrace off Norfolk, Virginia and Newport, Rhode Island. Bull. Amer. Assoc. Petrol. Geol., v. 47, 2051-2054.

17. Bouma, A. H. and Curray, J. R., 1964, Editorial. Marine Geol., v. 1, 1-3.

18. Curray, J. R., 1964, Transgressions and regressions: in Papers in Marine Geology (Shepard Commemorative Volume), Macmillan, N. Y., 175-203.

19. Curray, J. R. and Moore, D. G., 1964, Holocene regressive littoral sand, Costa de Nayarit, Mexico: in van Straaten, L. M. J. U. (Ed.), Deltaic and Shallow Marine Deposits, Elsevier, Amsterdam, 76-82.

20. Moore, D. G. and Curray, J. R., 1964, Sedimentary framework of the drowned Pleistocene delta of Rio Grande de Santiago, Nayarit, Mexico: in van Straaten, L. M. J. U. (Ed.), Deltaic and Shallow Marine Deposits, Elsevier, Amsterdam, 275-281.

21. Curray, J. R. and Moore, D. G., 1964, Pleistocene deltaic progradation of continental terrace, Costa de Nayarit, Mexico: in van Andel, Tj. H. and Shor, G. G., Jr. (Eds.), Marine Geology of the Gulf of California, A.A.P.G., Tulsa, OK, 193-215.

22. Shepard, F. P., Curray, J. R., Inman, D. L., Murray, E. A., Winterer, E. L., and Dill, R. F., 1964, Submarine geology by diving saucer. Science, v. 145, no. 3636, 1042-1046.

23. Moore, D. G. and Curray, J. R., 1964, Wave-base, marine profile of equilibrium, and wave-built terraces: discussion. Bull. Geol. Soc. Amer., v. 75, 1267-1274.

24. Curray, J. R., 1965, Structure of the continental margin off central California. Trans. N. Y. Acad. Sci., Ser. 11, v. 27, 794-801.

25. Curray, J. R., 1965, Late Quaternary history, continental shelves of the United States: in Wright, H. E., Jr. and Frey, D. G. (Eds.), The Quaternary of the United States, Princeton Univ. Press, 723-735.

26. Curray, J. R. and Moore, D. G., 1963, Sedimentos e historia de la Costa de Nayarit, Mexico. Bol. Soc. Geol. Mexicana, T. 26, no. 2, 107-116.

27. Curray, J. R., Moore, D. G., Belderson, R. H., and Stride, A. H., 1966, Continental margin of western Europe: slope progradation and erosion. Science, v. 154, 265-266.

28. Curray, J. R., 1966, Geologic structure on the continental margin, from subbottom profiles, northern and central California: in Bailey, E. H. (Ed.), Geology of Northern California, Div. Mines and Geol. Bull., v. 190, 337-342.

29. Curray, J. R., 1966, Continental terrace: in Fairbridge, R. W. (Ed.), The Encyclopedia of Oceanography. Encycl. Earth Sci. Ser., v. 1, Reinhold, N. Y., 207-214.

30. Curray, J. R. and Nason, R. D., 1967, San Andreas Fault north of Point Arena, California. Bull. Geol. Soc. Amer., v. 78, 413-418.

31. Stride, A. H., Belderson, R. H., Curray, J. R., and Moore, D. G., 1967, Geophysical evidence on the origin of the Faeroe Bank Channel. 1. Continuous reflection profiles. Deep-Sea Res., v. 14, 1-6.

32. Shepard, F. P., Curray, J. R., Newman, W. A., Bloom, A. L., Newell, N. D., Tracey, J. I., Jr., and Veeh, H. H., 1967, Holocene changes in sea level: evidence in Micronesia. Science, v. 157, no. 3788, 542-544.

33. Curray, J. R., 1967, Morphology of Pre-Quaternary continental terraces. Proc. VII Interntl. Sedimentol. Congr., Reading-Edinburgh, 2 pp.

34. Shepard, F. P. and Curray, J. R., 1967, Carbon-14 determination of sea level changes in stable areas: in Progress in Oceanography, Vol. 4, The Quaternary History of the Ocean Basins, Pergamon Press, Oxford, 283-291.

35. Normark, W. R. and Curray, J. R., 1968, Geology and structure of the tip of Baja California, Mexico. Bull. Geol. Soc. Amer., v. 79, 1589-1600.

36. Winterer, E. L., Curray, J. R., and Peterson, M.N.A., 1968, Geologic history of the intersection of the Pioneer Fracture Zone with the Delgada Deep-Sea Fan, northeast Pacific. Deep-Sea Res., v. 15, 509-520.

37. Stride, A. H., Curray, J. R., Moore, D. G., and Belderson, R. H., 1969, Marine geology of the Atlantic continental margin of Europe. Phil. Trans. Roy. Soc., Ser. A, v. 264, 31-75.

38. Curray, J. R., 1969, Shore zone sand bodies: barriers, cheniers, and beach ridges: in Stanley, D. J. (Ed.), The New Concepts of Continental Margin Sedimentation. Amer. Geol. Inst. Lecture 2, 18 pp.

39. Curray, J. R., 1969, Estuaries, lagoons, tidal flats, and estuaries: in Stanley, D. J. (Ed.), The New Concepts of Continental Margin Sedimentation. Amer. Geol. Inst. Lecture 3, 30 pp.

40. Curray, J. R., 1969, History of continental shelves: in Stanley, D. J. (Ed.), The New Concepts of Continental Margin Sedimentation. Amer. Geol. Inst. Lecture 6, 18 pp.

41. Curray, J. R., 1969, Shallow structure of the continental margin: in Stanley, D. J. (Ed.), The New Concepts of Continental Margin Sedimentation. Amer. Geol. Inst. Lecture 12, 22 pp.

42. Curray, J. R., Emmel, F. J., and Crampton, P. J., 1969, Holocene history of a strand plain lagoonal coast, Nayarit, Mexico: in Ayala-Castenares, A. and Phleger, F. B (Eds.), Lagunas Costeras, Un Simposio, Univ. Nac. Auton. de Mexico, 63-100.

43. Curray, J. R., Shepard, F. P., and Veeh, H. H., 1970, Late Quaternary sea level studies in Micronesia: Carmarsel Expedition. Geol. Soc. Amer. Bull., v. 81, 1865-1880.

44. Swift, D.J.P., Stanley, D. J., and Curray, J. R., 1971, Relict sediments on continental shelves: a reconsideration. Jour. Geol., v. 79, 322-346.

45. Curray, J. R. and Moore, D. G., 1971, Growth of the Bengal Deep-Sea Fan and denudation in the Himalayas. Bull. Geol. Soc. Amer., v. 82, 563-572.

46. Moore, D. G. and Curray, J. R., 1971, On the planning of cruise tracks with string. Marine Geology, v. 10, M9-M10.

47. Curray, J. R., 1970, Quaternary influence, coast and continental shelf of western U.S.A. and Mexico: in Guilcher, A. (Ed.), Quaternaria, Vol. XII, Symposium on the Evolution of Shorelines and Continental Shelves in their Mutual Relations During the Quaternary, Paris, 19-34.

48. Silver, E. A., Curray, J. R., and Cooper, A. K., 1971, Tectonic development of the continental margin off central California: in Lipps, J. H. and Moore, E. M. (Eds.), Geologic Guide to the Northern Coast Ranges, Point Reyes Region, California, Geol. Soc. Sacramento, 1-10.

49. Moore, D. G., Curray, J. R., Raitt, R. W., and Emmel, F. J., 1974, Stratigraphic-seismic section correlations and implications to Bengal Fan history: in von der Borch, C. C., Sclater, J. G. et al. (Eds.), Init. Repts. of the Deep Sea Drilling Project, Vol. XXII, Washington, DC, U. S. Govt. Print. Off., 403-412.

50. Moore, D. G. and Curray, J. R., 1974, Mid-plate continental margin geosynclines: growth processes and Quaternary modifications: in Dott, R. H. (Ed.), Modern and Ancient Geosynclinal Sedimentation, S.E.P.M., Tulsa, 26-35.

51. Hamilton, E. L., Moore, D. G., Buffington, E. C., Sherrer, P. L., and Curray, J. R., 1974, Sediment velocities from sonobuoys: Bay of Bengal, Bering Sea, Japan Sea, and North Pacific. Jour. Geophys. Res., v. 79, 2653-2668.

52. Curray, J. R. and Moore, D. G., 1974, Sedimentary and tectonic processes in the Bengal Deep-Sea Fan and Geosyncline: in Burk, C. A. and Drake, C. L. (Eds.), Continental Margins, Springer-Verlag, N. Y., 617-627.

53. Curray, J. R., 1975, Marine sediments, geosynclines, and orogeny: in Judson, S. and Fischer, A. G. (Eds.), Petroleum and Global Tectonics, Princeton Univ. Press, Princeton, N. J., 157-222.

54. Curray, J. R., 1976, Passive ocean margins. Geotimes, v. 21, no. 2, 26-27.

55. Moore, D. G., Curray, J. R., and Emmel, F. J., 1976, Large submarine slide (olistostrome) associated with Sunda Arc subduction zone, northeast Indian Ocean. Marine Geology, v. 21, 211-226.

56. Kolla, V., Moore, D. G., and Curray, J. R., 1976, Recent bottom-current activity in the deep western Bay of Bengal. Marine Geology, v. 21, 255-270.

57. Audley-Charles, M. G., Curray, J. R., and Evans, G., 1977, Location of major deltas. Geology, v. 5, no. 6, 341-344.

58. Curray, J. R., 1977, Modes of emplacement of prospective hydrocarbon reservoir rocks of outer continental marine environments. A.A.P.G. Short Course, Geology of Continental Margins, June 1977, Washington, DC, E-1 - E-14.

59. Curray, J. R., Shor, G. G., Jr., Raitt, R. W., and Henry, M., 1977, Seismic refraction and reflection studies of crustal structure of the eastern Sunda and western Banda Arcs. Jour. Geophys. Res., v. 82, no. 17, 2479-2489.

60. Hamilton, E. L., Bachman, R. T., Curray, J. R., and Moore, D. G., 1977, Sediment velocities from sonobuoys: Bengal Fan, Sunda Trench, Andaman Basin, and Nicobar Fan. Jour. Geophys. Res., 3003-3012.

61. Audley-Charles, M. G., Curray, J. R., and Evans, G., 1979, Significance and origin of big rivers: a discussion. Jour. Geol., v. 87, 122-123.

62. Curray, J. R., Moore, D. G., Lawver, L. A., Emmel, F. J., Raitt, R. W., Henry, M., and Kieckhefer, 1979, Tectonics of the Andaman Sea and Burma: in Watkins, J., Montadert, L., and Dickerson, P. W. (Eds.), Geological and Geophysical Investigations of Continental Margins. Amer. Assoc. Petrol. Geol. Memoir 29, 189-198.

63. Moore, D. G., Lawver, L. A., and Curray, J. R., 1977, Tectonics and geological history of the Gulf of California: in CIBCASIO Trans., Vol. III, Centros de Investigacion de Baja California and Scripps Inst. of Oceanog., 3rd Meet., La Jolla, CA, Oct. 1977, 64-75.

64. Curray, J. R., Moore, D. G., et al. (Shipboard Scientific Party), 1979, Leg 64 seeks evidence on development of basins -- in the Gulf of California. Geotimes, July 1979, 18-20.

65. Curray, J. R., 1980, The IPOD programme on passive continental margins: in The Evolution of Passive Continental Margins in the Light of Recent Deep Drilling Results, Roy. Soc. London Discussion, 19 and 20 Oct. 1977, London, 17-33.

66. Schrader, H., Kelts, K., Curray, J. R., Moore, D. G., et al. (Shipboard Scientific Party), 1980, Laminated diatomaceous sediments from the Guaymas Basin slope (central Gulf of California): an over 250,000-year climate record. Science, v. 207, no. 4436, 1207-1209.

67. Karig, D. E., Lawrence, M. B., Moore, G. F., and Curray, J. R., 1980, Structural framework of the fore-arc basin, NW Sumatra. J. Geol. Soc. London, v. 137, 77-91.

68. Kieckhefer, R. M., Shor, G. G., Curray, J. R., Sugiarta, W., and Hehuwat, F., 1980, Seismic refraction studies of the Sunda Trench and Forearc Basin. Jour. Geophys. Res., v. 85, no. B2, 863-889.

69. Moore, G. F. and Curray, J. R., 1980, Structure of the Sunda Trench lower slope off Sumatra from multichannel seismic reflection data. Marine Geophys. Res., v. 4, 319-340.

70. Einsele, G., Gieskes, J. M., Curray, J. R., Moore, D. G., et al. (Shipboard Scientific Party, DSDP Leg 64), 1980, Intrusion of basaltic sills into highly porous sediments, and resulting hydrothermal activity. Nature, v. 283, no. 5746, 441-445.

71. Moore, G. F., Curray, J. R., Moore, D. G., and Karig, D. E., 1980, Variations in deformation along the Sunda forearc, eastern Indian Ocean: in Hayes, D. E. (Ed.), The Tectonic and Geologic Evolution of Southeast Asian Seas and Islands, Amer. Geophys. Union Geophys. Monograph 23, 145-160.

72. Karig, D. E., Moore, G. F., Curray, J. R., and Lawrence, M. B., 1980, Morphology and shallow structure of the lower trench slope off Nias Island, Sunda Arc: in Hayes, D. E. (Ed.), The Tectonic and Geologic Evolution of Southeast Asian Seas and Islands, Amer. Geophys. Union Geophys. Monograph 23, 179-208.

73. Curray, J. R. and Emmel, F. J., 1981, Demise of the Diamantina Dent. Marine Geol., v. 40, M69-M72.

74. Emmel, F. J. and Curray, J. R., 1981, Channel piracy on the lower Bengal Fan. Geo-Marine Letters, v. 1, 123-127.

75. Emmel, F. J. and Curray, J. R., 1981, Dynamic events near the upper and midfan boundary of the Bengal Fan. Geo-Marine Lett., v. 1, 201-205.

76. Moore, G. F., Curray, J. R., and Emmel, F. J., 1982, Sedimentation in the Sunda Trench and forearc region. Trench-Forearc Geology, Geol. Soc. London Spec. Pub. 10, 245-257.

77. Emmel, F. J. and Curray, J. R., 1982, Submerged late Pleistocene delta and other features related to sea level changes in the Malacca Strait. Marine Geol., v. 47, 197-216.

78. Liu, C.-S., Sandwell, D. T., and Curray, J. R., 1982, The negative gravity field over the 85°E Ridge. Jour. Geophys. Res., v. 87, 7673-7686.

79. Curray, J. R., Emmel, F. J., Moore, D. G., and Raitt, R. W., 1982, Structure, tectonics, and geological history of the northeastern Indian Ocean: in Nairn, A. E. and Stehli, F. G. (Eds.), The Ocean Basins and Margins, Vol. 6, Plenum Pub. Corp., 399-450.

80. Moore, D. G. and Curray, J. R., 1982, Objectives of drilling on young passive continental margins: application to the Gulf of California. in Curray, J. R., Moore, D. G., et al. (Eds.), Initial Reports of the Deep Sea Drilling Project, Vol. 64, U. S. Govt. Print. Off., Washington, DC, 5-26.

81. Shipboard Scientific Party, 1982, Baja California passive margin transect: Sites 474, 475, and 476. Ibid., 35-210.

82. Shipboard Scientific Party, 1982, Guaymas Basin: Sites 477, 478, and 481. Ibid., 211-415.

83. Shipboard Scientific Party, 1982, Guaymas Basin Slope: Sites 479 and 480. Ibid., 417-504.

84. Moore, D. G., Curray, J. R., and Einsele, G., 1982, Salado-Vinorama submarine slide and turbidity current off the southeast tip of Baja California. Ibid., 1071-1082.

85. Curray, J. R., Moore, D. G., Kelts, K., and Einsele, G., 1982, Tectonics and geological history of the passive continental margin at the tip of Baja California. Ibid., 1089-1116.

86. Moore, D. G. and Curray, J. R., 1982, Geologic and Tectonic History of the Gulf of California. Ibid., 1279-1294.

87. Bachman, R. T., Hamilton, E. L., and Curray, J. R., 1983, Sediment sound velocities from sonobuoys: Sunda Trench and forearc basins, Nicobar and central Bengal Fans, and Andaman Sea basins. J. Geophys. Res., v. 88, no. B11, 9341-9346.

88. Liu, C.-S., Curray, J. R., and McDonald, J. M., 1983, New constraints on the tectonic evolution of the eastern Indian Ocean. Earth Planet. Sci. Lett., v. 65, 331-342.

89. Curray, J. R. and Moore, D. G., 1984, Geologic history of the mouth of the Gulf of California: in Crouch, J. K. and Bachman, S. B. (Eds.), Tectonics and Sedimentation Along the California Margin, Pac. Sect. S.E.P.M., Vol. 38, 17-36.

90. Emmel, F. J. and Curray, J. R., 1984, The Bengal Submarine Fan, Northeastern Indian Ocean. Geo-Marine Letters, v. 3, 119-124.

    reprinted in 1985 as: Bengal Fan, Indian Ocean: in Bouma, A.H., Barnes, N.E., and Normark, W.R. (Eds.), Submarine Fans and Related Turbidite Sequences, Chapter 16, 107-112.

91. Paull, C.K., Hecker, B., Commeau, R., Freeman-Lynde, R.P., Neumann, C., Corso, W.P., Golubic, S., Hook, J.E., Sikes, E., and Curray, J., 1984, Biological Communities at the Florida Escarpment Resemble Hydrothermal Vent Taxa. Science, v. 226, 965-967.

92. Curray, J.R., Prell, W.L., Weissel, J.K., 1984, Report of the NSF-ORD workshop on future scientific drilling in the Indian Ocean, 22-50.

93. Hoyt, C.L., Kennedy, M.P., and Curray, J.R., 1986, Mineral Resources, in E.D. Goldberg, Editor, The Oceans and The Economy of San Diego, published by San Diego Oceans Foundation, in honor of the 25th Anniversary of the University of California, San Diego, pp. 7-15.

94. Curray, J.R., 1984, Sri Lanka: is it a mid-plate platelet?, Journal of NARA, v.31, p. 30-50.

95. Curray, J.R. and T. Munasinghe, 1989, Timing of intraplate deformation, northeastern Indian Ocean, Earth and Planetary Science Letters, v.94, pp. 71-77

96. Curray, J.R., 1989, The Sunda Arc: a model for oblique plate convergence, Netherlands Journal of Sea Research, v.24, pp 131-140.

97. Paull, C.K., F.N. Spiess, J.R. Curray, and D. C. Twitchell, 1990, Origin of Florida Canyon and the role of spring sapping on the formation of submarine box canyons, Geol. Soc. of America Bull., v.102, pp 502-511

98. Paull, C.K., Commeau, R.F., Curray, J.R., and Neumann, A.C., 1991, Seabed measurements of modern corrosion rates on the Florida Escarpment: Geo-Marine Letters, v. 11-16, p. 16-22.

99. Curray, J.R., 1991, Geological history of the Bengal Geosyncline: Jour. Assoc. Expl. Geophys, v. XII, p. 209-219.

100. Brune, J.N., Curray, J.R., Dorman, L.M., and Raitt, R.W, 1991, Super-thick sedimentary Basin, Bay of Bengal, Jour. Assoc. Expl. Geophys, v. XII, p. 123-129.

101. Curray, J.R., 1991, Possible greenschist metamorphism at the base of a 22 km sediment section, Bay of Bengal, Geology v. 19, p. 1097-1100.

102. Curray, J. R. and Munasinghe, T., 1991, Origin of the Rajmahal Traps and the 85°E Ridge: Preliminary reconstruction of the trace of the Crozet hotspot: Geology, v. 19, p. 1237-1240.

103. Brune, J.N., Curray, J.R., Dorman, L.M., and Raitt, R.W, 1992, A proposed super-thick sedimentary Basin, Bay of Bengal, Geophysical Research Letters, v. 19, p. 565-568.

104. Paull, C.K., Twichell, D.C., Spiess, F.N., and Curray, J.R., 1991, Morphological development of the Florida Escarpment: observations on the generation of time transgressive unconformities in carbonate terrains: Marine Geology v. 101, p. 181-201.

105. Liu, C.S., Shor, G.G. Jr., and Curray, J.R., 1991, Velocity structure and nature of the forearc basin off west Sumatra from expanding spread experiments: Acta Oceanograp hica Taiwanica, v. 27, p. 21-39.

106. Curray, J.R., et al., 1982, Initial Reports, Deep Sea Drilling Project, Leg 64, The Gulf of California: Washington D.C., U.S. Govt. Printing Office, Parts 1 and 2, 1313 pp.

107. Curray, J.R., 1994, Sediment volume and mass beneath the Bay of Bengal: Earth and Planetary Science Letters, v. 125, p. 371-383.

108. Curray, J.R., 1996, Origin of beach ridges: Comment on Tanner, W.F., 1995, Origin of beach ridges and swales. Marine Geology, v. 129, pp. 149-161, Marine Geology, v. 136, pp. 121-125.

109. Curray, J.R. and Wijayananda, N.P., 2000, conversion of seismic reflection travel times to depth, Bay of Bengal, Jour. of the Geol. Soc. of Sri Lanka, v. 9, pp. 63-65 .

110. Alam, M. Mustafa and Curray, J.R. (Guest Editors), 2003, Sedimentary Geology of the Bengal basin, Bangladesh, in Relation to the Asia-Greater India Collision and the Evolution of the Eastern Bay of Bengal, Special Issue, Sedimentary Geology, v. 155, pp. 175-424.

111. Alam, Mahmood, Alam, M.Mustafa, Curray, J.R., Chowdhury, M. Lutfar Rahman and Gani, M. Royhan, 2003, An overview of the sedimentary geology of the Bengal Basin in relation to the regional tectonic framework and basin-fill history, in Alam and Curray (Editors), see #110 above. Sedimentary Geology, v. 155, pp. 179-208.

112. Curray, J.R., Emmel, F.J. and Moore, D.G., 2003, The Bengal Fan: geometry, stratigraphy, history and processes, Marine and Petroleum Geology, v. 19, pp. 1191-1223.

113. Curray, J.R., 2005, Tectonics and history of the Andaman Sea region, Journal of Asian Earth Sciences, v. 25, pp. 187-232.

114. Curray, J. R. and Allen, Ruth, 2008, Evolution, paleogeography and sediment provenance, Bay of Bengal region, Indian Ocean, in Gupta, Harsh and Fareeduddin (Editors), Golden Jubilee Memoir of the Geological Society of India, No. 66, Bangalore, India, pp. 487-520.

Publications of Joseph R. Curray

Short Contributions

1. Parker, R. H. and Curray, J. R., 1955, Macrofauna and bathymetry of calcareous banks on the continental shelf of the northern Gulf of Mexico. Bull. Geol. Soc. Amer., v. 66, 1604-1605 (abstract).

2. Shepard, F. P. and Curray, J. R., 1955, Post-glacial continental shelf sedimentation, Northwest Gulf of Mexico. Bull. Geol. Soc. Amer., v. 66, 1615-1616 (abstract).

3. Curray, J. R., 1956, Grain orientation studies of Recent sands. Jour. Sed. Petrol., v. 26, 177, in S.E.P.M. Symposium, "Directional Properties of Sedimentary Rocks", Chicago, 1956 (abstract).

4. Curray, J. R., 1957, Sediments of the continental shelf of the northwest Gulf of Mexico. Abst. Program 42nd Ann. Mtg., Amer. Assoc. Petrol. Geol., p. 12. Reprinted in Oil and Gas Jour., v. 55 (13), 186, April 1957.

5. Curray, J. R., 1959, Coastal Plain - Continental Shelf Studies: in Study of Recent Sediments and their Environments in the Gulf of California. Univ. of Calif. Inst. of Marine Resources 4th Quarterly Report, 1958-1959, 9-12.

6. Curray, J. R. and Moore, D. G., 1962, Shallow structure and stratigraphy along acoustic reflection and coring traverses, Breton, Chandeleur, and Mississippi Sounds, northern Gulf of Mexico. Geol. Soc. Amer. Abstr. with Prog., 134 (abstract).

7. Moore, D. G. and Curray, J. R., 1963, Sedimentary framework of continental margins. Amer. Assoc. Petrol. Geol. Abstract, 364.

8. Shor, G. G., Curray, J. R., and Moore, D. G., 1963, Reflection profiling off California. Amer. Geophys. Union, v. 44, no. 1, 62 (abstract).

9. Curray, J. R., 1964, Shallow structure, continental terrace, northern and central California. Geol. Soc. Amer. Abstr. with Prog., 38 (abstract).

10. Curray, J. R. and Shepard, F. P., 1964, Book Review of "Sharks and Survival" by Perry W. Gilbert. Marine Geol., v. 2, 171-172.

11. Winterer, E. L., Curray, J. R., and Peterson, M. N. A., 1966, Geologic history of an intersecting oceanic fracture zone and deep-sea fan, northeast Pacific. Abstr. Proc. 2nd Interntl. Oceanogr. Congr., Moscow, 1966, Nauka, Moscow, 395-396 (abstract).

12. Curray, J. R., Moore, D. G., Stride, A. H., and Belderson, R. H., 1966, Slope progradation and subsequent erosion, continental margin, western Europe. Abstr. Proc. 2nd Interntl. Oceanogr. Congr., Moscow, 90 (abstract).

13. Shepard, F. P., Curray, J. R., Inman, D. L., Murray, E. A., Winterer, E. L., and Dill, R. F., 1964, Saucer dives in La Jolla submarine canyons of La Jolla, California. Geol. Soc. Amer. Spec. Paper 82, 182-183 (abstract).

14. Normark, W. R. and Curray, J. R., 1968, Marine geology and structure of the tip of Baja California, Mexico. Geol. Soc. Amer. Spec. Paper 115, 167 (abstract).

15. Shepard, F. P., Curray, J. R., and Newman, W. A., 1968, Lagoonal topography of Caroline and Marshall Islands. Geol. Soc. Amer. Spac. Paper 115, 202 (abstract).

16. Newman, W. A., Veeh, H. H., and Curray, J. R., 1968, Shallow submarine terraces of Micronesian Oceanic Reefs. Geol. Soc. Amer. Spec. Paper 115, 163 (abstract).

17. Curray, J. R., Bloom, A. L., Newman, W. A., Newell, N. D., Shepard, F. P., Tracey, J. I., and Veeh, H. H., 1968, Late Holocene sea-level fluctuations in Micronesia. Geol. Soc. Amer. Spec. Paper 115, 40-41 (abstract).

18. Curray, J. R., 1967, Sediments and history of a strand-plain, lagoonal coast. Interntl. Symp. Coastal Lagoons, Mexico City, 28-29 (abstract).

19. Curray, J. R. and Moore, D. G., 1969, The Bengal Deep-Sea Fan. Geol. Soc. Amer. Spec. Paper 121, 67 (abstract).

20. Curray, J. R. and Newman, W. A., 1969, Holocene history of atolls and reefs. Prog. Western Soc. of Naturalists Ann. Meeting, 11-12 (abstract).

21. Normark, W. R., Allison, E. C., and Curray, J. R., 1970, The geology of the Pacific continental margin of the peninsula of Baja California. Geol. Soc. Amer. Ann. Meet., 1969, Abstr. with Prog., 163 (abstract).

22. Moore, D. G., Curray, J. R., and Winterer, E. L., 1970, Denudation rates in the Himalayas and New Guinea as deduced from marine sediments in the Bengal Fan and Coral Sea. Geol. Soc. Amer. Cordilleran Sect. Meet., Hayward, CA, Abstr. with Prog., 120 (abstract).

23. Vernon, J. W., Slater, R. A., Buffington, E. C., Curray, J. R., Moore, D. G., Dill, R. F., and Huckabay, W. B., 1971, A memoriam to L. A. Headlee. Bull. Amer. Assoc. Petrol. Geol., v. 55, 132-133.

24. Curray, J. R. and Silver, E., 1971, Structure of the continental margin and distribution of basement rock types off Central California. Geol. Soc. Amer. Abstr. with Prog., v. 3, no. 2, 106-107 (abstract).

25. Curray, J. R., Emmel, F. J., Moore, D. G., and Normark, W. R., 1971, Migrating mega-channels and sediment distribution, Bengal Deep-Sea Fan. Proc. VIII Interntl. Sedimentol. Congr., 19 (abstract).

26. Moore, D. G., Curray, J. R., and Raitt, R. W., 1971, Structure and history of the Bengal Deep-Sea Fan and Geosyncline, Indian Ocean. Proc. VIII Interntl. Sedimentol. Congr., 69 (abstract).

27. Curray, J. R. and Moore, D. G., 1972, Cenozoic mid-plate continental terraces: modern miogeosynclines. Abstr. Vol., Conf. on Modern and Ancient Geosynclinal Sedimentation, Nov. 1972, Madison, Wisc., 10-11 (abstract).

28. Curray, J. R. and Shepard, F. P., 1972, Some major problems of Holocene sea levels. Abstr., AMQUA 2nd Nat. Conf., Dec. 1972, Miami, FL, 16-18 (abstract).

29. Curray, J. R., 1973, Equilibrium, relict, palimpsest, and pseudo-equilibrium shelf sediments. Relations Sedimentaires Entre Estuaires et Plateaux Continentaux, Bordeaux, July 1973, 18 (abstract).

30. Moore, D. G. and Curray, J. R., 1974, Marine geology of the northeast Indian Ocean and relationships to associated plate edge structure. Abstr. and Proc. of 2nd Interntl. Conf. on Geophysics of the Earth and the Oceans, Sydney, Jan. 1973, Geoexploration, v. 12, 205-206 (abstract).

31. Curray, J. R. and Moore, D. G., 1973, The Bengal Geosyncline and Gondwanaland. Abstr. Vol., 3rd Interntl. Gondwana Symp., Canberra, Aug. 1973 (abstract).

32. Curray, J. R. and Moore, D. G., 1974, Sedimentary and tectonic processes in the Bengal Deep-Sea Fan and Geosyncline. Ann. Meet. Abstr., Amer. Assoc. Petrol. Geol., San Antonio, TX, April 1974, 22 (abstract).

33. Kolla, V., Moore, D. G., Curray, J. R., and Yount, J. C., 1975, Bottom current activity in the deep western Bay of Bengal. Geol. Soc. Amer. Abstr. with Prog., Ann. Meet., Salt Lake City, Oct. 1975, 1151 (abstract).

34. Henry, M., Raitt, R. W., Curray, J. R., and Moore, D. G., 1975, Delay-time function analysis of multiple sonobuoy refraction lines in the Andaman Sea. EOS, v. 56, no. 12, 1063, Abstr. A.G.U. Meet., San Francisco, Dec. 1975 (abstract).

35. Lawver, L. A., Curray, J. R., and Moore, D. G., 1975, Magnetics in the Andaman Sea and the effect of high sedimentation rates. EOS, v. 56, no. 12, 1064, Abstr. A.G.U. Meet., San Francisco, Dec. 1975 (abstract).

36. Lawver, L. A., Curray, J. R., and Moore, D. G., 1976, Tectonics of the Andaman Sea. EOS, v. 57, no. 4, 333-334, Abstr. Ann. Meet. A.G.U., Washington, DC, Apr. 1976 (abstract).

37. Moore, D. G., Curray, J. R., and Emmel, F. J., 1976, Dynamic processes of upper Bengal Fan and Swatch-of-No-Ground, northeast Indian Ocean. Bull. Amer. Assoc. Petrol. Geol., v. 60, no. 4, 699, Abstr. A.A.P.G.-S.E.P.M. Meet., New Orleans, May 1976 (abstract).

38. Curray, J. R. and Moore, D. G., 1976, The Bengal Geosyncline: a complex of sedimentary basins. Abstr. Vol., Symp. on Sedimentary Basins, Durham, April 1976 (abstract).

39. Curray, J. R., 1977, Modes of emplacement of prospective hydrocarbon reservoir rocks of outer continental margin environments. Bull. Amer. Assoc. Petrol. Geol., v. 61, no. 5, 778 (abstract).

40. Karig, D. E., Moore, G. F., Suparka, S., and Curray, J. R., 1977, Aspects of continental margin development west of Sumatra. Geol. Soc. Amer. Abstr. with Prog., v. 9, no. 7, 1044 (abstract).

41. Curray, J. R., 1977, Henry William Menard (A Citation for the Francis P. Shepard Medal). Jour. Sed. Pet., v. 47, 1647-1648.

42. Moore, G. F., Curray, J. R., and Moore, D. G., 1978, Variation in subduction deformation along the Sunda Arc, eastern Indian Ocean. EOS, v. 59, 1184 (abstract).

43. Kieckhefer, R. M., Shor, G. G., Jr., and Curray, J. R., 1978, Seismic refraction studies of the Sunda Trench and Forearc Basin. EOS, v. 59, 1184 (abstract).

44. Curray, J. R., 1977, Fred B Phleger - Retirement Remarks. SIO Contributions, v. 47, pt. 2, 1613-1615.

45. Curray, J. R., 1979, Citation for Sorby Medallist Francis P. Shepard. Sedimentology, v. 26, 160-163.

46. Curray, J. R. et al. (Shipboard Scientific Party), 1979, Deep Sea Drilling Project, Leg 64, in the Gulf of California -- a new ocean basin. Fourth Latin Amer. Geol. Congr., 1979 (abstract).

47. Moore, D. G. and Curray, J. R., 1979, Deep Sea Drilling in the Gulf of California -- a new ocean basin. Geol. Soc. Amer. Abstr. with Prog., 1979 Ann. Meet., San Diego, CA, 482 (abstract).

48. Moore, G. F. and Curray, J. R., 1979, Structure of the Sunda Trench slope from multichannel seismic data. Geol. Soc. Amer. Abstr. with Prog., 1979 Ann. Meet., San Diego, CA, 482 (abstract).

49. Schrader, H., Curray, J. R., et al. (Shipboard Scientific Party), 1979, Successful recovery of a 152-meters hydraulic piston core section on the Guaymas Slope, DSDP-IPOD Leg 64, Site 480. Geol. Soc. Amer. Abstr. with Prog., 1979 Ann. Meet., San Diego, CA, 512 (abstract).

50. Curray, J. R., Moore, D. G., and Emmel, F. J., 1979, The northern end and geologic history of the Ninetyeast Ridge. Geol. Soc. Amer. Abstr. with Prog., 1979 Ann. Meet., San Diego, CA, 408 (abstract).

51. Curray, J. R., 1979, Eastern Indian outer continental margin and its relationship to the Bay of Bengal. Proc. I.U.G.G., Canberra, Dec. 1979, Symp. "Continental Margins of the Indian Ocean" (abstract).

52. Curray, J. R., 1980, The origin and tectonic conversions of continental margins. Proc. A.A.A.S. Ann. Meet., San Francisco, Jan. 1980, Symposium "New Horizons for Marine Geosciences" (abstract).

53. Curray, J. R., Moore, G. F., Moore, D. G., Kieckhefer, R. M., Emmel, F. J., and Shor, G. G., 1981, Trends and variations around the Sunda Arc. Abstr., Hedberg Conf. on Continental Margins, Galveston, TX, 11-16 Jan. 1981, 19-20 (abstract).

54. Kelts, K., Einsele, G., and Curray, J., 1981, Controls on diatomaceous lithofacies in obliquely-rifted marginal basin: Gulf of California. Bull. Amer. Assoc. Petrol. Geol., v. 65, 945 (abstract).

55. Moore, G. F. and Curray, J. R., 1981, Characteristics of Sunda subduction zone. Bull. Amer. Assoc. Petrol. Geol., v. 65, 959-960 (abstract).

56. Liu, C. S., Sandwell, D. T., and Curray, J. R., 1981, Regional compensation of a sediment-covered ridge in the Bay of Bengal. EOS, v. 62, no. 17, 391 (abstract).

57. Lawver, L. A. and Curray, J. R., 1981, Evolution of the Andaman Sea. EOS, v. 62, no. 45, 1044.

58. Curray, J. R., Emmel, F. J., Moore, G. F., Moore, D. G., and Kieckhefer, R. M., 1981, Sediment budget and accretionary prism volume variations around the Sunda Arc. Proc. Symp. on Convergence and Subduction, College Station, TX, Apr. 1981 (abstract).

59. Moore, D. G. and Curray, J. R., 1982, Opening of the Gulf of California by a single two-phase process. Geol. Soc. Amer. Abstr. with Prog., Cordilleran Sec., Anaheim, CA, 217 (abstract).

60. Sandwell, D. T., Liu, C.-S., and Curray, J. R., 1982, The negative gravity field over the 85° Ridge. EOS, v. 63, no. 18, 426 (abstract).

61. Liu, C.-S., McDonald, J. M., and Curray, J. R., 1982, A fossil spreading ridge in the northwestern Wharton Basin. EOS, v. 63, no. 18, 448 (abstract).

62. Curray, J. R. and Lawver, L. A., 1982, The Andaman Sea -- a ripoff type of backarc basin. Proc. Geodynamics of Back-arc Regions Symposium, Texas A&M Univ., 29-30 Apr. 1982 (abstract).

63. Moore, G. F. and Curray, J. R., 1982, Structure of the Sunda Trench slope south of Java. EOS, v. 63, 1115 (abstract).

64. Kelts, K., Curray, J. R., and Moore, D. G., 1982, Introduction and explanatory notes: in Curray, J. R., Moore, D. G., et al. (Eds.), Initial Reports of the Deep Sea Drilling Project, Vol. 64, U. S. Govt. Print. Off., Washington, DC, 5-26.

65. Curray, J. R., Moore, D. G., Smith, S. M., and Chase, T. E., 1982, Underway geophysical data from Deep Sea Drilling Project Leg 64: navigation, bathymetry, magnetics, and seismic profiles. Ibid., 505-507.

66. Curray, J. R. and Moore, D. G., 1982, Introduction to the Baja California passive margin transect symposium. Ibid., 1067-1069.

67. Curray, J. R. and Moore, D. G., 1982, Introduction to the Guaymas Basin and hydrothermal symposium. Ibid., 1119-1121.

68. Curray, J. R. and Moore, D. G., 1982, Introduction to the Guaymas Slope and laminated diatomite symposium. Ibid., 1179-1181.

69. Curray, J.R., 1985, Bathymetry and Physiography of the Northeastern Indian Ocean, National Geographic Society Research Reports, v. 21, 101-107.

70. Paull, C.K., Curray, J., Hecker, B., Freeman-Lynde, R.P., Newmann, C., Sykes, E., Corso, W.P., Golubic, S., and Hook, J.E., 1984, Vent-type communities, discovered at the Florida Escarpment, EOS v.65, p. 8.

71. Florida Escarpment Cruise Participants, 1984, The seep find at the Florida Escarpment, OCEANUS, vol 27, No. 3, pp. 32-33.

72. Munasinghe, Tissa, and J. R. Curray, 1986, Tectonic evolution of the continental margins of Sri Lanka, EOS, v. 67, pp. 1192-1193.

73. Curray, Joseph R., Winterer, Edward L., and Inman, Douglas L., 1988, Memorial to Francis Parker Shepard, Geological Soc. America. Memorial Vol 18, pp 1-5

74. Paull, C.K., F.N. Spiess, J.R. Curray, and D. Twitchell, 1987, Enigmatic submarine box canyons: Florida Escarpment, EOS v. 68, p. 1316

75. Curray, J.R., 1987, Variations around the Sunda Arc, Bull. Amer. Assoc. Petroleum Geol., v. 71, p.545.

76. Curray, J.R., 1987, The Sunda Arc: a model for oblique plate convergence, in General Information, Programs and Abstracts, International Symposium on the Results of SNELLIUS II Expedition, Jakarta, Indonesia, 23-28 Nov. 1987, sponsored by Indonesian Institute of Sciences and Nederlands Raad Voor Zeeonderzoek, p. 35

77. Paull, C.K., F.N. Spiess, J.R. Curray, and D. Twitchell, 1988, Morphology of Florida Escarpment Chemosynthetic Brine Seep Community Sites: Deep-Tow, Seabeam, and GLORIA surveys, Bull. Amer. Assoc. Petroleum Geol., v. 72, p 233.

78. Curray, J.R., 1988, Tectonics of the northeastern Indian Ocean: current ideas and important problems for cooperative research, Proc. Vol. and Report, First Meeting of Experts on Off-shore Prospecting for Mineral Resources in the Indian Ocean, Karachi, Pakistan, 11-14 July 1988, Indian Ocean Marine Affairs Co-Operation, 8 pp.

79. Curray, J.R., 1987, Gulf of California, McGraw-Hill Encyclopedia of Science and Technology, v.8, pp.260-261

80. Liu, C-S, J.R. Curray, and G.G. Shor, Jr., 1988, Structure and nature of the forearc basin off west central Sumatra, EOS, v.69, p.1443-1444.
Also, 1989, EOS v.70, p.603.

81. Munasinghe, Tissa, and J.R. Curray, 1986, Sediment deformation at the southern continental margin of Sri Lanka: evidence for initiation of small scale subduction, Abstracts of Papers, International Kaiko Conference on Subduction ones, 10-15 Nov. 1986, Tokyo and Shimizu, p.95-96.

82. Curray, J.R., 1989, The India-Asia collision and history of the Bengal Fan, Program and Abstracts, M.T. Halbouty Continental Margins Conference, Galveston, TX, 5-9 Feb. 1989.

83. Curray, J.R., 1989, The Andaman Sea, an oblique convergence extensional basin: Proc.28th International Geological Congress, Washington D.C., p.1-352.

84. Brune, J., J.R. Curray, L. Dorman and R. Raitt, 1990, Super-thick sedimentary basin, Bay of Bengal, EOS, v. 71, p. 1444.

85. Munasinghe, T., L. Dorman and J.R. Curray, 1990, A three-dimensional gravity study over the southern continental margin of Sri Lanka, EOS, v. 71, p. 1644.

86. Curray, J.R., 1990, Geological history of the Bengal Geosyncline, in Proc. Seismotectonics of Indian Sub-Continent, Dehra Dun, India, Dec. 1990.

87. Curray, J.R., 1991, Tectonics of oblique convergence, with examples from the western Sunda Arc, Proc. Seminar, Geophysical Technology Trend in the nineties, Jakarta, Indonesia, April 1991.

88. Curray, J.R., 1991, Postcollision sediments in the Bay of Bengal: EOS, v. 72, p. 250.

89. Curray, J.R., 1992, Reply to Comment on "Possible greenschist metamorphism at the base of a 22-km sedimentary section, Bay of Bengal", by Acharyya, S.K.: Geology, v. 20, p. 956-957.

90. Curray, J.R. and Munasinghe, T., 1992, Reply to Comment on "Origin of the Rajmahal Traps and the 85°E Ridge: Preliminary reconstructions of the trace of the Crozet hotspot", by Kent, R.W., Storey, M., Saunders, A.D., Ghose, N.C. and Kempton, P.D.: Geology, v. 20, p. 958-959.

91. Munasinghe, T., Dorman, L.M., and Curray, J.R., 1992, An Alternative Procedure to Utilize the Werner-Deconvolution Method to Estimate the Depth to Magnetic Bodies in Sedimentary Basins: EOS, v. 73, p. 137.

92. Curray, J.R., Moore, D.G., Kelts, K., and Einsele, G., 1982, Bathymetry of the region of the tip of Baja California, in Curray, J.R., Moore, D.G., et al, Init. Repts. DSDP, 64, Pt. 2: Washington (U.S. Govt. Printing Office), Backpocket Foldout.

93. Curray, J.R., 1978, Tectonic setting of the Central Sumatra Transect: Relationship to the Andaman Sea, Abstract. Riset-LIPI, Special Issue: CCOP/SEATAR workshop on the Sumatra Transect. Parapat, Indonesia.

94. Berger, W.H., Curray, J.R., and Herbert, T.D., 1994, Fred B Phleger, 1909-1993, Professor of Oceanography, Emeritus, In Memoriam, University of California, p. 201-204.

95. Curray, J. R.: 1999, A new look at present tectonics and opening history of the Andaman Sea, Program Annual Meeting, San Antonio, TX, April 1999.

96. Buffington, E.C., Curray, J.R., and Moore, D.G.: Memorial to Edwin Lee Hamilton, 1914-1998, Geological Society of America Memorial Vol. 29.

97. Emery, K.O., R.S. Dietz, G.G. Kuhn, R.E. Stevenson and J. R. Curray: Memorial to Francis Parker Shepard (1997-1985), Bull. AAPG, v. 70, pp. 331-333.

98. Curray, J.R.,2001, Wolfgang Berger: Citation: Francis P. Shepard Medalist For Excellence in Marine Geology. J. Sedimentary Research, v. 71, pp 1034-1035.

99. Curray, J.R., 2001, Francis. Parker Shepard, 1897-1985, Rock Star Series, GSA Today, December 2001, pp. 20-21.

100. Curray, J.R., 2003, Francis Parker Shepard, 189701985. In Fisher, R.L., Goldberg, E.D. and Cox, C.S. (Editors), Coming of Age, Scripps Institution of Oceanography, A Centennial Volume, 1903-2003. Scripps Institution of Oceanography, La Jolla, CA, pp. 157-167.

101. Alam, M.. Mustafa and Curray, J.R., 2003, Editorial, the curtain goes up on a sedimentary basin in south-central Asia: unveiling the sedimentary geology of

the Bengal Basin of Bangladesh, In Alam and Curray, Editors, see # 110, research publications, pp. 175-178.

102. Curray, J.R., 2002, Tectonics and history of the Andaman Sea region, (abstract), Chapman Conference on Continent-Ocean Interactions within the East Asian Marginal Seas, American Geophysical Union, San Diego, CA, 11-14 Nov. 2002.

103. Curray, J.R., 2003, Retrospectives of KORDI, 30 Years with Ocean, KORDI, Korean Ocean Research & Development Institute, South Korea, 2 pp.

104. Curray, J.R., 2005, Tectonics of the Andaman Sea region, (abstract), AGU Annual Meeting Program, EOS, T41B-1312, poster session.

105. Curray, J.R., 2006, Evolution of the western Sunda Arc, (abstract), AGU Annual Meeting Program, EOS, U44A-01.

106. McNeil, L., Ilenstock, T., Tappin, D, Curray, J., Forearc morphology and thrust vergence, AGU Annual Meeting Program, EOS, U44A-07.

107. Curray, J.R. and Allen, Ruth, 2008, The India-Asia collision: formation and sediment provenance of the Bay of Bengal, Program Golden Jubilee Geological Society of India, Bangalore, India, October 2008.

Annex B53

Joseph R. Curray, "Sediment Volume and Mass beneath the Bay of Bengal", *Earth and Planetary Science Letters*, No. 125 (1994)

ELSEVIER

Earth and Planetary Science Letters 125 (1994) 371–383

EPSL

Sediment volume and mass beneath the Bay of Bengal

Joseph R. Curray

Scripps Institution of Oceanography, University of California, San Diego, La Jolla, CA 92093-0215, USA

Received 10 December 1993; revision accepted 3 May 1994

Abstract

Rates of sediment accumulation and the amount of sedimentary fill in depocenters lying downstream of erosion in the Himalayas and Tibet can provide some insight into tectonics and geological history. The objective of this paper is to put on record the best estimates which are possible with existing data of the volume and mass of sediments, sedimentary rock and metasedimentary rock beneath the sea floor of the Bay of Bengal.

The sedimentary section in the Bay of Bengal is divided into two parts: (1) Eocene through Holocene, sediments and sedimentary rocks which post-date the initial India–Asia collision: volume = 12.5×10^6 km^3; mass = 2.88×10^{16} t; this is most of the Bengal Fan, including its eastern lobe, the Nicobar Fan, plus some of the outer Bengal Delta; (2) Early Cretaceous through Paleocene, pre-collision sedimentary and metasedimentary rocks: volume = 4.36×10^6 km^3; mass = 1.13 to 1.18×10^{16} t; these are interpreted as continental rise and pelagic deposits.

1. Introduction and statement of the problem

A surge of interest has occurred during the past decade in the history of the collision between India and Asia, the uplift of Tibet and the Himalayas and the volume and mass of erosional products shed into downstream depocenters. Various estimates have been made and limits have been published on many of the parameters of this problem, such as: the size and extent of Greater India; the time of first contact between India and a subduction zone off southern Asia; the time of first hard continent to continent collision; amount of convergence; lateral tectonic extrusion; rotation of parts of Asia; the time and rate of uplift of Tibet and the Himalayas; and the amount of erosion off the uplifting regions. To provide indirect aid in evaluating some of these parameters, estimates have been made of the volume and mass of sediments shed off Tibet and the Himalayas into depocenters lying downstream [e.g., 1–9]. The greatest volume of these sediments is in the Siwaliks in India, in the Ganges alluvium, in the Bengal Basin, as the Bengal Delta, and in the Bay of Bengal, as the Bengal Fan [7].

The primary objective of this paper is to replace earlier estimates of the volume and mass of sediments and sedimentary rock lying beneath the sea floor of the Bay of Bengal with the most recent and best estimates possible with the data currently available. This paper reports only on the volume and mass of sediments beneath the deep Bay of Bengal and does not include estimates of the many other depocenters, including the Bengal Basin on land, the sedimentary basins

[MK]

SSDI 0012-821X(94)00099-K

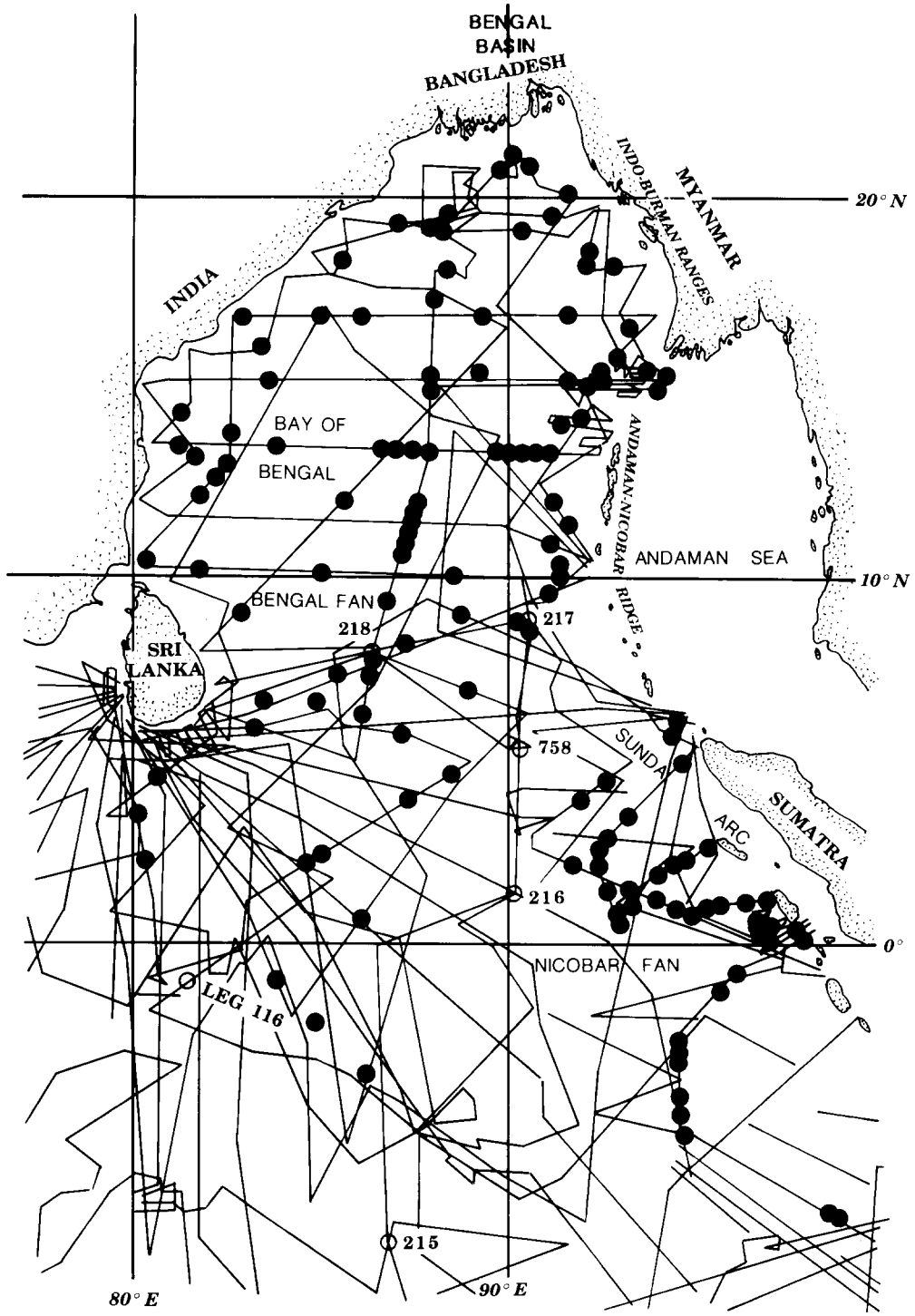

Fig. 1. Data base of seismic reflection tracks and DSDP and ODP drilling data used in this study. All track lines have bathymetry and seismic reflection data and most have gravity and magnetic data. Dots = seismic wide angle reflection and/or refraction stations, as explained in the text. Some stations represent multiple sonobuoys.

of the eastern Indian continental margin, and the sediments from the Bay of Bengal which have passed into the Sunda accretionary prism.

Neither the data nor the interpretations presented here are definitive. The data are not current, state-of-the-art, and other interpretations are possible; however, my best interpretations possible at this time are presented here. If I do not document them now, other investigators will continue to use obsolete numbers and interpretations, or will continue to reinterpret those earlier conclusions and interpretations without examining the data.

2. Data base

The data base in the Bay of Bengal available for this study is shown in Fig. 1, excluding data from the Andaman Sea, the Sunda accretionary prism and the Sumatra fore-arc region. Most of these ship tracks are from expeditions of the Scripps Institution of Oceanography, but they also include some tracks run by ships of the Lamont-Doherty Geological Observatory, the Deep Sea Drilling Project and the U.S. Naval Oceanographic Office. All tracks shown include seismic reflection data. Most are airgun or high power sparker, analog or digital, single-channel data, but about 1000 km have 21-channel, digital data. In addition, the survey net includes about 225 sonobuoy airgun or sparker wide angle reflection and/or refraction runs, of which about 140 also included shooting with explosives. Three recording and telemetering anchored buoy, reversed, seismic refraction stations were run using explosives in the central and northern Bay of Bengal. Drilling sites of DSDP Leg 22 [10], ODP Leg 116 [11] and ODP Leg 121 [12] are shown. Results from hydrocarbon exploration and seismic surveys in Bangladesh were used to extend coverage for the isopach maps (Fig. 2) into the Bengal Basin [13,14] but those sediments and rocks are not included in the calculations of volume and mass. All data collected during cruises organized by the Scripps Institution of Oceanography are on file in the Geological Data Center of the Institution.

3. Seismic stratigraphy and geological history

The seismic stratigraphic subdivisions and geological history on which this study is based have been published previously [1,15–18]. Simply and concisely, the scenario is that the sedimentary section can be subdivided by a regional unconformity, marking a hiatus starting in the early Eocene (ca. 55 My), which can be traced through parts of the seismic network. This horizon appears to correlate with some part of the collision history of India with southern Asia. Sediments deposited prior to this time are interpreted as continental rise and pelagic deposits surrounding the isolated continent of India. Following initial collision, a proto-Bay of Bengal was created and the sediments came from a closer point source lying to the north. Following this scenario, initial deposition of the proximal northern part of the Bengal Fan was in the early Eocene and the fan has prograded since that time.

An alternative interpretation by Cochran [19] of the time of initiation of Bengal Fan deposition as Early Miocene has gained considerable popularity recently, partly because of observations which document accelerated uplift of parts of the Himalayas and Tibet in the Early Miocene [e.g., 2,20]. Cochran actually states [19, p. 405] that "Fan sedimentation in the northern Bay of Bengal....would have begun prior to the Miocene", but most of his readers seem to have missed that point, and, as will be shown in the Discussion section, have concluded that the fan sedimentation, in fact, started in the Early Miocene. Such a conclusion cannot be substantiated from the DSDP or ODP drilling in the fan because the base of the fan was not reached.

The oldest sediments which have as yet been sampled are Early Miocene (ca. 17 My), at the ODP Leg 116 sites, located more than 2500 km from the present apex of the fan. A step in velocity in one of six sonobuoy wide angle reflection records in the area has been suggested as possibly the base of the fan, at a depth of 1100 m, in a total sediment column of about 2 km [19,21]. However, no change is apparent at that depth in seismic reflection records [11], which would suggest an unconformity, such as a transition from

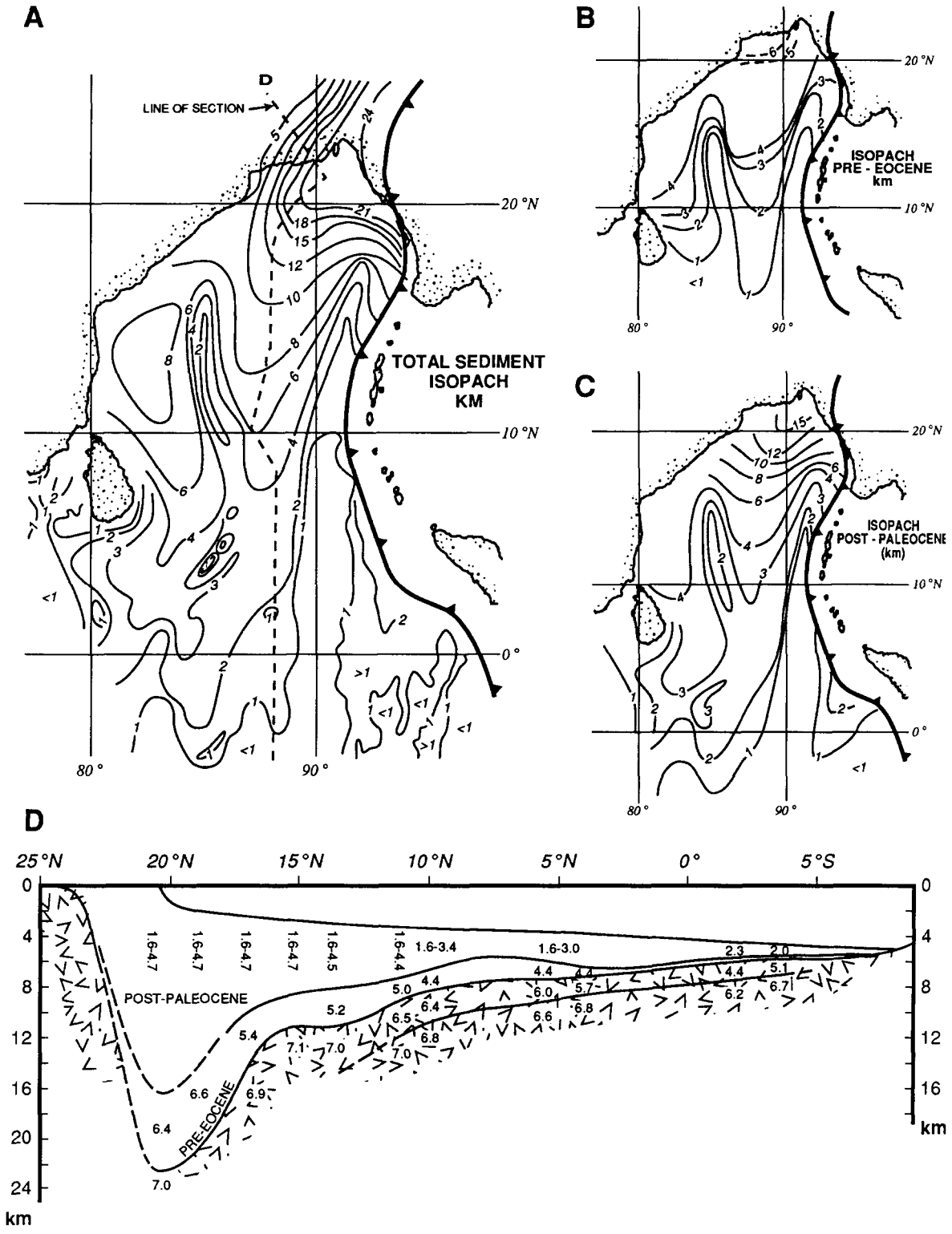
A
D
LINE OF SECTION
TOTAL SEDIMENT
ISOPACH
KM
20 °N
10 °N
0 °
80 °
90 °
B
ISOPACH
PRE - EOCENE
km
C
ISOPACH
POST - PALEOCENE
(km)
D
25 °N
20 °N
15 °N
10 °N
5 °N
0 °
5 °S
POST-PALEOCENE
PRE-EOCENE
km

stratified turbidites to less stratified, more nearly transparent pelagic sediments. Cochran [19, p. 404] uses an average rate of accumulation of Middle and Lower Miocene sediments in Hole 718 to demonstrate that the age of that horizon is about 20 My. The actual rate of accumulation of the oldest, well-dated sediments recovered on ODP Leg 116, at the bottom of Hole 718, at 11–16 My, is about 26 m/My [21, Fig. 9]. While it can be argued that the kinks in the curve of sediment accumulation can be explained as "artifacts resulting from the sparse fossil assemblage" [19, p. 403], the conclusion was that "prior to 11 m.y. ago sediment accumulated more slowly" [22, p. 186]. The rate of 26 m/My yields an age at that horizon of about 28 My, or late Oligocene. Furthermore, the isopachs in this present study suggest that the base of the fan is just above the oceanic second layer, at a depth of about 2 km, rather than at the 1100 m level.

Lower rates of accumulation might reasonably be expected for the most distal parts of a prograding fan, making the extrapolation of age of the oldest turbidites even older. Mid-Oligocene is approximately the age one would expect for progradation of the fan to this distal site since the early Eocene. Even if it can be demonstrated that fan initiation occurred in the Early Miocene at the Leg 116 sites, this has no bearing on the time of initiation of deposition in the upper and middle parts of the fan. Furthermore, seismic records do not show a reflecting or refracting horizon of Early Miocene age which could reasonably be attributed to initiation of fan deposition.

The Eocene unconformity is interpreted as a hiatus which began in the early Eocene. It is of variable duration: of short duration near the apex of the fan and of long duration far from the apex. As a fan progrades, pelagic sediments are overlain by the most distal turbidites, which are, in turn, overlain by the main turbidites of the fan. At the extreme distal end of the Bengal/Nicobar Fan, the hiatus appears to have been from the early Eocene to Late Miocene at DSDP Site 215 (Fig. 1) [10] and from some time after the Maastrichtian until the Pliocene at DSDP Site 211, located at about 10°S and 103°E [10].

Eocene initiation of Bengal Fan deposition is suggested in the geology of Bangladesh, in the Indo–Burman Ranges of India and Myanmar and on the Andaman–Nicobar Ridge (Fig. 1). Hydrocarbon exploration work on and offshore from southeastern Bangladesh [e.g., 13,14,23] shows total sediment thicknesses, calculated from gravity data, of greater than 20 km, with Eocene and Oligocene Disang Series deep-water shales and turbidites over oceanic crust. These are, in turn, overlain by the Neogene prograding deposits of the Bengal Delta, of the Ganges, Brahmaputra (Jamuna), Meghna and their ancestral rivers. Some of these rocks have been mildly metamorphosed and uplifted into the accretionary prism in the Indo–Burman Ranges, and are there described in various flysch formations, only sparsely fossiliferous, but usually correlated with the Disang Series [e.g. 24–26]. Similar turbidites, the Andaman Flysch or Port Blair Formation, are found in the Andaman and Nicobar Islands, again usually believed to be Eocene and Oligocene [e.g. 26–28]. Our interpretation [1,15–18] has been that these Eocene and Oligocene turbidites represent parts of the early Bengal Fan, some of which have been incorporated into the Sunda Arc accretionary complex.

The sedimentary section in the Bay of Bengal can, therefore, by this interpretation, be subdivided by the lower Eocene horizon into a post-collision, post-Paleocene, younger section, and a

Fig. 2. Isopach maps and section (in km). (a) Total sediment, sedimentary rock and metasedimentary rock to oceanic second layer, as interpreted from seismic reflection and refraction data. (b) Pre-Eocene, or pre-collision, sedimentary and metasedimentary rock. (c) Post-Paleocene, or post-collision, sediment and sedimentary rock. (d) Simplified longitudinal section along line shown in (a) passing northward into the Bengal Basin and Bengal delta. Velocities shown are averaged from the layer solutions of many seismic refraction stations, and are therefore horizontal velocities at the tops of their respective units. The Eocene unconformity lies between the younger and older units. Modified from [18] by use of total sediment isopachs in the Bengal Basin from [14].

pre-collision, pre-Eocene, older part. The younger unit is primarily Bengal Fan, which was started during the Eocene. The rate of sediment supply and progradation may well have accelerated in the Early Miocene [29], although this hypothesis cannot yet be proven.

4. Isopach maps

Three isopach maps and a simplified longitudinal section are presented: Fig. 2a is total sediment, sea floor to oceanic second layer; Fig. 2b is pre-collision rocks, from what is interpreted as the lower Eocene unconformity to oceanic second layer; Fig. 2c is post-collision sediments and sedimentary rocks, from the sea floor to the Eocene unconformity; and Fig. 2d is a simplified longitudinal section along the line in Fig. 2a. The velocities shown in Fig. 2d are each averaged from several seismic refraction layer solutions and therefore represent horizontal velocities at the tops of their respective units. The total sediment isopachs in the Bengal Basin were adapted from [14] and differ slightly from the previous interpretations in [18].

Basement, or oceanic second layer, is visible in seismic reflection records where the section is thin, but cannot be observed in reflection records where the section is thicker. In those areas, mainly the northern and western side of the Bay of Bengal, the isopachs are based on the network of seismic refraction stations run on the Scripps cruises, mainly in collaboration with Professor R.W. Raitt [17]. Similar difficulties were encountered in correlating the lower Eocene unconformity from DSDP and ODP drilling sites on the Ninetyeast Ridge and, as explained in [18], part of the correlation in the deep part of the Bay of Bengal was through the network of seismic refraction stations.

The maximum measured thickness of post-collision sediments is 16.5 km, beneath the Bangladesh shelf (Fig. 2d). The upper, or Neogene part of this, is interpreted as being part of the Bengal Delta, while the lower, or Paleogene part, is believed to be Bengal Fan. The 6.1 km of material lying below this is interpreted as

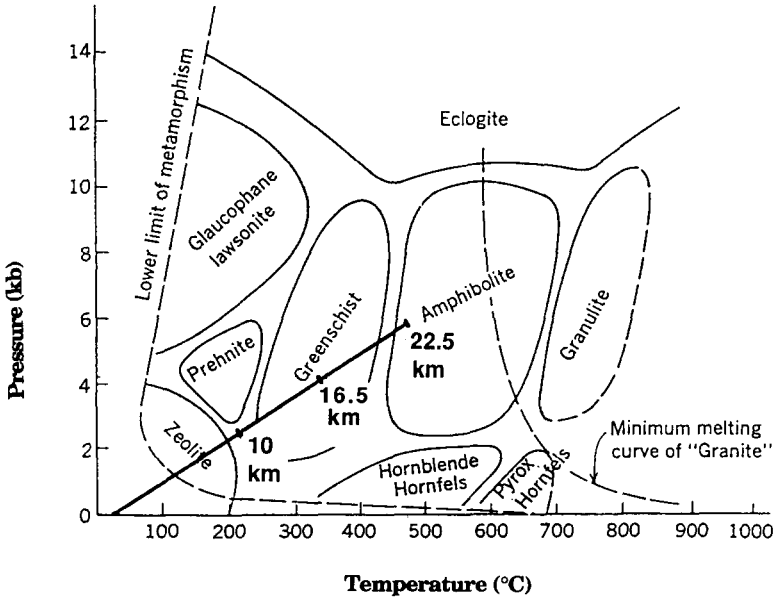

Fig. 3. Pressure–temperature plot of metamorphic facies, from Verhoogen et al. [32], with extrapolated pressures and temperatures to depths of seismic refraction station on Bangladesh shelf in Fig. 2d.

metasediment [14,18,29–31], because extrapolation of pressure and thermal gradients [18] suggests that, where the older unit is deeper than about 12 km beneath the sea floor, it is within the pressure and temperature field of greenschist facies metamorphism (Fig. 3) [32]. Kingston [14] was apparently the first to suggest load metamorphism of the deeper parts of this section. The measured seismic velocities and corresponding estimates of density are compatible with this interpretation and with isostatic calculations.

5. Conversion to volume and mass

The post-collision and pre-collision isopach maps were converted to volume by interpolating thicknesses at the intersections of a 100 km grid, centered on the Equator and 90°E longitude, superimposed over the isopach maps. The limits of the grid coincide with the limits of the isopach maps, except that the Bengal Basin on land in Bangladesh is not included. Also not included are the sedimentary basins along the eastern shelf and slope of India and the accretionary prism of the Sunda subduction zone. The resulting volumes are 12.5×10^6 km^3 for the post-collision sediments and sedimentary rocks, summed from 399 points, and 4.36×10^6 km^3 for the pre-collision rocks, summed from 192 points.

The post-collision sediment thickness and volume were converted to mass by the mean curve of sediment density versus depth, published by Kinsman [33, Fig. 6], as shown here in the lower line in Fig. 4. With burial, sedimentary rock densities approach an asymptote, a grain density of about 2.7 g/cm^3. A mean density was calculated from this relationship for the interpolated sedimentary thickness for each of the 399 data points and a total mass was calculated: 2.88×10^{16} t.

Estimating appropriate densities for the pre-collision rocks, which are presumed to have been

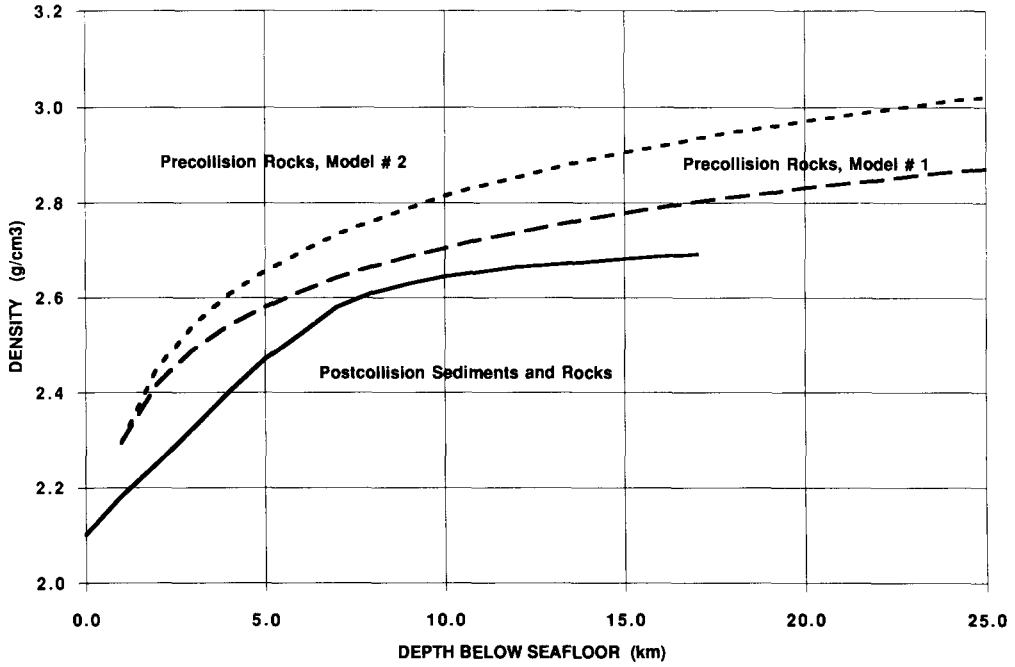

Fig. 4. Relationship of density to depth below sea floor: lower curve of buried sediments and sedimentary rock from [33]. Middle curve, Model #1, calculated by extrapolation of the densities of sedimentary rock with burial, from [34]. Upper curve, Model #2, calculations of densities of metasedimentary rocks by assumption of density appropriate for compressional wave velocities, from data in [35], as discussed in text.

metamorphosed with greater age and burial, was more difficult. The only direct information we have on these rocks is their compressional wave velocities and depths of burial (Fig. 5), which show an apparent exponential relationship. Two possible ways of estimating densities from these velocities will be utilized: first, by a minimum, very conservative method, extrapolation of the known relationship between velocity and density in deeply buried sedimentary rocks; and second, by probably a more realistic method, calculation of the density gradient appropriate for the velocities for known metasedimentary rocks.

Nafe and Drake [34, Fig. 4] show the increase in velocity of sediments and sedimentary rocks with increasing density (Fig. 6). This relationship is linear above a density of about 2.3 g/cm^3 (velocity $\sim$ 3.5 km/s) to a maximum density of about 2.85 g/cm^3 (velocity = 7.0 km/s). The relationship presumably applies only to burial depths of less than about 10 km [34, Fig. 8], near the depth at which metamorphism from zeolite facies to greenschist facies rocks can be expected (Fig. 3) [32]. As a simple approach, by combining the trend line of the Nafe and Drake relationship in Fig. 6 (velocity versus density) with the trend line of Fig. 5 (burial depth versus velocity), the middle curve (Model #1) of Fig. 4 is derived as a minimum value for densities corresponding to depths of burial. The density read from this relationship for each point at the top of the pre-collision unit was used for the entire unit underlying it, to give the minimum (Model #1) estimate of mass for the pre-collision rocks: 1.13×10^{16} t.

The alternative and probably better way of estimating density for the older, presumably metamorphosed, sedimentary rocks is to assume a density appropriate for a metasedimentary rock corresponding to an observed velocity, and to calculate a density gradient. Christensen [35] lists compressional wave velocities and densities in metamorphic rocks as a function of pressure. From the data in his compilation, it appears that, at a pressure of 6 kbar, a density of 3.0 g/cm^3 is appropriate for schist with a velocity of 7.0 km/s. This corresponds to the measured velocity at the base of the presumed metasediments at 22.6 km (Fig. 2d). An exponential gradient was calculated

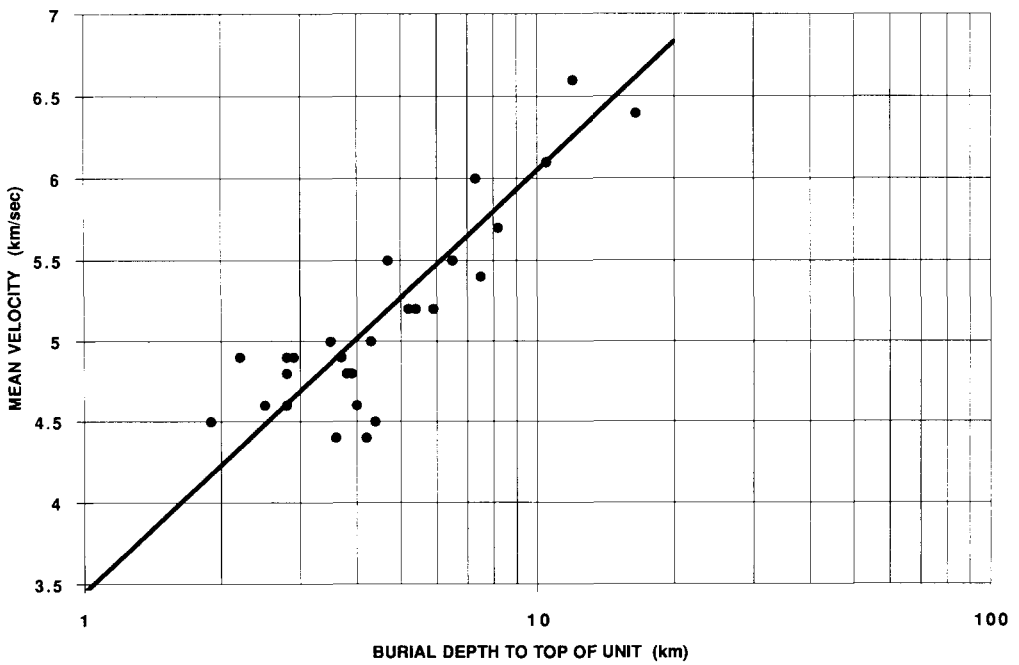

Fig. 5. Relationship of compressional wave velocities to depth of burial of older unit, interpreted as pre-collision rocks, from seismic data in data base, Fig. 1. Least-squares trend line is slightly weighted in favor of deeper data.

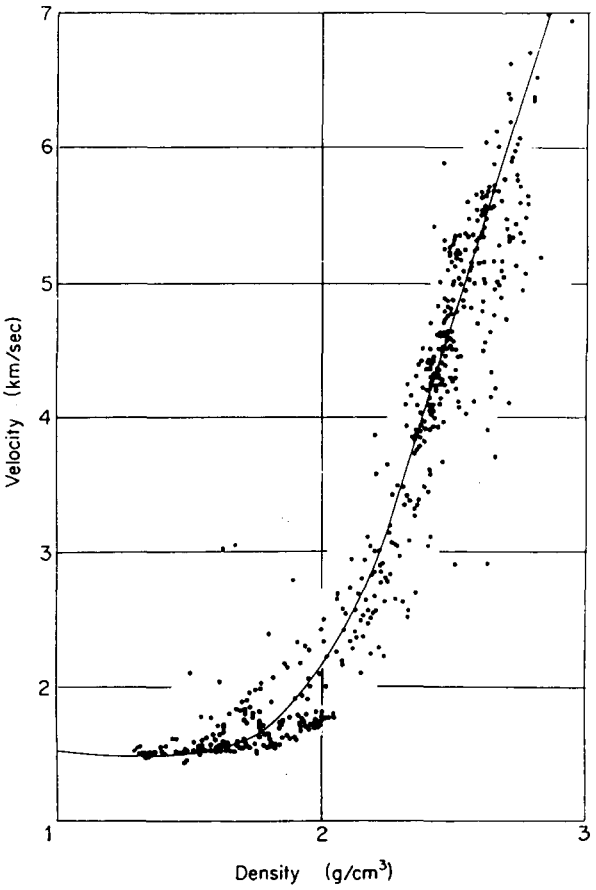

Fig. 6. Compressional wave velocity as a function of density of deeply buried sediments, from Nafe and Drake [34]. As explained in text, this relationship is probably not valid for burial greater than about 8–10 km.

to these values, shown in the upper line, Model #2, Fig. 3. This, for example, gives a density of 2.93 g/cm^3 at a depth of 16.5 km, the top of the older (metasedimentary) unit, where the trend line velocity in Fig. 5 is 6.61 km/s.

Schists display a high degree of velocity anisotropy, with velocities parallel to the schistosity as much as 25% higher than velocities perpendicular to the schistosity [36]. Christensen does not specify whether the velocities he reports for schists are parallel or perpendicular; that is, maximum or minimum, but it appears that they are maximum velocities which would correspond to the horizontal seismic refraction velocities used in Fig. 2d. Brune et al. [31] have recently observed strong anisotropy in surface wave data in the deep section beneath the Bay of Bengal, adding further credence to the interpretation of burial metamorphism of the lower part of the section.

A mean density was calculated from this gradient (Model #2, Fig. 4) for each of the 192 estimates of thickness of the buried unit, and the results were summed to give a mass of 1.18×10^{16} t. This is probably a more realistic estimate than Model #1, although the difference is not significant considering the probable errors in the estimates.

6. Discussion and implications

Kinsman [33] had earlier suggested, on the basis of isostatic considerations, that a maximum of about 17 km of sediments could accumulate to sea level over 100 My old oceanic crust. This was based on his estimates of maximum density of sediments under deep burial approaching a grain density of about 2.7 g/cm^3. If we now accept the possibility of burial metamorphism with age and deep burial yielding higher densities, a greater accumulation is possible, as we appear to have here at the northern end of the Bay of Bengal.

Table 1 shows an extension of Kinsman's calculations. The first pair of columns, following

Table 1
Isostasy calculations

	NO SEDIMENT		"MAXIMUM SEDIMENT"		OVER METASEDS	
	Th	ρ	Th	ρ	Th	ρ
WATER	5.7	1.0	0.1	1.0	0.1	1.0
SEDIMENT	0.0	-	16.5	2.53	16.5	2.53
METASEDS	0.0	-	0.0	-	6.1	2.97
CRUST	5.0	2.9	6.1	2.9	5.0	3.02
MANTLE	89.3	3.3	77.3	3.3	72.3	3.3
Σ ρ x Th	314.9		314.6		313.7	

Th = thickness (km); ρ = density (g/cm^3).

Kinsman [33], is based on 100 My old oceanic crust without any sediment cover. The second pair of columns is Kinsman's theoretical maximum, interpreting the refraction data as indicating a total of 16.5 km of sediments and sedimentary rocks beneath the Bangladesh shelf, and interpreting the underlying 6.1 km unit as oceanic second layer. This was our original interpretation of our seismic data [15–17]. The third pair of columns represents the interpretation used in this paper, that the underlying unit is metasediment with the densities derived in Model #2. The density of the underlying oceanic second layer (crust) is also estimated from the Model #2 density curve (Fig. 4, upper curve). The Table suggests that isostatic balance is possible with the densities which are assumed here.

In summary, the section beneath the Bay of Bengal is divided into two parts:

(1) Eocene through Holocene; post India–Asia collision sediments and sedimentary rocks: volume = 12.5×10^6 km^3; mass = 2.88×10^{16} t. Most of this unit is Bengal Fan.

(2) Early Cretaceous through Paleocene; pre-collision sedimentary and metasedimentary rocks: volume = 4.36×10^6 km^3; mass = $1.13–1.18 \times 10^{16}$ t. This unit is interpreted as being continental rise and pelagic sediments.

These numbers should be considered minimal because they include only the areas covered by isopachs in Fig. 2b,c. Excluded are the sedimentary basins beneath the eastern Indian shelf and slope, the Bengal Basin on land, the Sunda Arc accretionary prism, and the distal parts of the Bengal and Nicobar Fans beyond the data base and isopachs. The most important of these omissions is the accretionary prism extending around the Sunda Arc (Fig. 1), from the Indo–Burman Ranges in Myanmar to the outer arc ridge off Java, one of the largest in the world. No estimate is feasible at present of the amount of sedimentary material in the accretionary prism or the amount which may have been subducted.

The other serious omission is the Bengal Basin, a lower part of which is Bengal Fan. Our northernmost refraction station on the Bangladesh shelf (Fig. 2d) shows the greatest thickness measured with our seismic work and this thick section may continue beneath the shoreline of southeastern Bangladesh (Fig. 2a), as suggested by Kingston [14]. The margin of our data base and calculations, therefore, occurs where the section is thickest. Inclusion of the Bengal Basin would make these figures much more useful. Volume or mass comparisons with erosion in the source areas should, therefore, include a separate estimate for the Bengal Basin.

The volume estimates which have been used in the recent literature are of the post-collision part of the sedimentary section, which is mainly Bengal Fan. There have been attempts to relate volume or mass of these sediments to total amount and timing of uplift and erosion in the source areas [2,3,5,7,9], rates of denudation in the source area [6] and rates of deposition as controls on fan development [8]. Unfortunately, most of these papers have drawn their data from the first preliminary paper on the Bengal Fan [1] published before DSDP and ODP drilling on the fan or on the northern Ninetyeast Ridge. The age assignments in that paper were a 'working hypothesis' [1, p. 568], based on prevailing opinions on the time of orogeny in the Himalayas; and the longitudinal section was a 'hypothetical section' [1, Fig. 5]. That seismic stratigraphic study delineated three sedimentary units, 'W', 'Y' and 'O', respectively in order of age, separated by two regional unconformities. The 'W' and 'Y' units were believed to constitute the Bengal Fan, and the 'O' unit was interpreted as a pre-fan continental rise. Ages of the unconformities were not known until DSDP Leg 22 drilling in 1972, and the 1971 'working hypothesis' age assumptions were wrong. The DSDP drilling established the age of the younger unconformity as uppermost Miocene and the older one as lower Eocene [10,16], and later ODP drilling further confirmed these ages [11,12,37]. To confuse the situation further, subsequent acquisition and interpretation of much more seismic data greatly improved these correlations and we revised our interpretation of the data, increasing the thickness of the fan section and allowing for the probability of burial metamorphism of the deeply buried older sediments [18,30 and this paper]. As a part of this present study, a serious attempt has been made

to repeat the subdivision of the fan into the 'W' and 'Y' units by correlation of the uppermost Miocene unconformity, ca. 7 My; that is, the time of onset of the present phase of intraplate deformation [10,11,16,37]. This effort has for now been abandoned as subject to too much uncertainty, especially in the northern Bay of Bengal, far from where the unconformity has been sampled by drilling.

In retrospect, it is perhaps unfortunate that we published those first preliminary interpretations, even though we published revised interpretations [15,16] very soon after collection of additional seismic data and after the DSDP Leg 22 drilling. These revisions included the new age correlations and isopach maps of both pre-collision (pre-fan) and post-collision (fan) sediments as interpreted at that time. Despite these published revisions, many authors have chosen to use those early interpretations and have reassigned the preliminary age assumptions to suit their own prejudices on time of initiation of the Bengal Fan. The correlations and volume estimates published in 1971, 1974 and 1982 [1,15–17] should now be rejected in favor of the estimates and correlations published in 1991 and 1992 [18,30] and in this paper. Fortuitously, the estimate of total volume of 'W' plus 'Y' sedimentary units in the 1971 paper [1] (10.1×10^6 km^3) is close to the present estimate for the sediment volume of the Bengal Fan: 12.5×10^6 km^3. The estimate by Barnes and Normark [38] of the volume of Bengal Fan sediments (4×10^6 km^3) is about one third of the present estimate, but they do not explain how they derived this independent estimate.

Copeland and Harrison [2] used a volume estimate they made from several combined sources [1,16,39], which is too high. LePichon et al. [3] wisely calculated a volume from the small-scale published total sediment isopach map [18], which agrees precisely with the laboriously derived estimate published in this paper. Corrigan and Crowley [5] used the estimate directly from the 1971 paper [1], which, as mentioned previously, is fortuitously close to the estimate in this paper. Lyon-Caen and Molnar [9] also used our original estimate [1], to which they added an estimate for the Ganga Basin. Johnson [7] used the numbers from the present study, conveyed by personal communication.

Einsele [6] used the 1971 numbers, including the subdivision between the 'W' and 'Y' units. He reassigned ages as interpreted from the ODP drilling to estimate rates of denudation in the high mountain source areas for two periods of time: (1) from the initiation of Bengal Fan deposition (assumed to be 20 My) to onset of intraplate deformation (the Miocene unconformity between units 'W' and 'Y', or about 7.7 My); and (2) from the Miocene unconformity to the present. In view of the contention in this paper that initiation of Bengal Fan deposition started in the Eocene, and in view of the failure in the present study to correlate the Miocene unconformity into the northern Bay of Bengal satisfactorily, the apparent change in denudation rate which Einsele observed may not be significant.

Wetzel [8] was also an unfortunate victim of using obsolete numbers. He used the ratio between the volumes of 'W' and 'Y' sediments from [1], the low volume estimate for the fan of Barnes and Normark [38] and he assumed that the Bengal Fan started at 21 Ma. He used this low estimate of volume because he defined 'fan' in a very restrictive manner, with some assumptions of the underlying geometry of the fan. He also assumed that the entire Bengal Basin and the Bangladesh shelf and slope are comprised of deltaic sediments, in contrast to the interpretation used in this paper that most of the Paleogene part of the Bengal Basin southeast of the 'hinge zone' [e.g. 13,14,23] is Bengal Fan, especially where it apparently overlies oceanic crust. His objective was to establish deposition rates for two periods of time on the Bengal Fan, and he concluded that climatic influences on rates of deposition on the fan are not significant over a long term. Some of Wetzel's relationships between rates of deposition and fan geometry may require revision.

Finally, a plea to compare sediment and rock quantities in terms of mass, rather than volumes, just as present river discharge rates are reported in terms of mass. Some very imprecise methods have been used to 'decompact' sediment volumes or to convert to 'dry' volumes by assumption of

round number densities in order to compare hard rocks with sediments of varying ages. The densities of rocks eroded from high mountains are reasonably well known and velocity information on sediments and sedimentary rocks in sedimentary basins provides rather precise information on densities. Better, more precise comparisons should be possible using mass.

Acknowledgments

This study and manuscript have benefited from comments and suggestions by Jim Cochran, Gerhard Einsele, Michael Johnson, Peter Molnar, Matt Salisbury and Andreas Wetzel, although these advisors do not necessarily agree with the conclusions of the paper, which are my own responsibility.

References

[1] J.R. Curray and D.G. Moore, Growth of the Bengal deep-sea fan and denudation in the Himalayas, Geol. Soc. Am. Bull. 82, 563–572, 1971.

[2] P. Copeland and T.M. Harrison, Episodic rapid uplift in the Himalaya revealed by $^{40}Ar/^{39}Ar$ analysis of detrital K-feldspar and muscovite, Bengal fan, Geology 18, 354–357, 1990.

[3] X. LePichon, M. Fournier and L. Jolivet, Kinematics, shortening, and extrusion in the India–Eurasia collision, Tectonics 11, 1085–1098, 1992.

[4] D.W. Burbank, Causes of recent Himalayan uplift deduced from deposited patterns in the Ganges basin, Nature 357, 680–683, 1992.

[5] J.D. Corrigan and K.D. Crowley, Unroofing of the Himalayas: a view from apatite fission-track analysis of Bengal fan sediments, Geophys. Res. Lett. 19, 2345–2348, 1992.

[6] G. Einsele, Sedimentary Basins — Evolution, Facies, and Sediment Budget, 628 pp., Springer, Berlin, 1992.

[7] M. Johnson, Volume balance of erosional loss and sediment deposition related to Himalayan uplifts, J. Geol. Soc. London 151, 217–220, 1994.

[8] A. Wetzel, The transfer of river load to deep-sea fans: a quantitative approach, Am. Assoc. Pet. Geol. Bull. 77, 1679–1692, 1993.

[9] H. Lyon-Caen and P. Molnar, Constraints on the structure of the Himalaya from an analysis of gravity anomalies and a flexural model of the lithosphere, J. Geophys. Res. 88, 8171–8191, 1983.

[10] C.C. Von der Borch, J.C. Sclater, et al., Init. Rep. Deep Sea Drill. Proj. 22, 890 pp., 1974.

[11] J.R. Cochran, D.A.V. Stow, et al., Proc. Ocean Drill. Prog., Sci. Results 116, 445 pp., 1990.

[12] J.W. Pierce, J.K. Weissel, et al., Proc. Ocean Drill. Prog., Sci. Results 121, 990 pp., 1991.

[13] F.M. Mirhamidov and M.A. Mannan, Nature of the gravity field and its relation with the geotectonics of Bangladesh, Petrobangla Rep., 51 pp., Dhaka, 1981.

[14] J. Kingston, Undiscovered petroleum resources of south Asia, US Geol. Surv. Open File Rep. 84, 96 pp., 1984.

[15] J.R. Curray and D.G. Moore, Sedimentary and tectonic processes in the Bengal deep-sea fan and geosyncline, in Continental Margins, C.A. Burk and C.L. Drake, eds., pp. 617–627, Springer, New York, 1974.

[16] D.G. Moore, J.R. Curray, R.W. Raitt and F.J. Emmel, Stratigraphic–seismic section correlations and implications to Bengal Fan history, Init. Rep. Deep Sea Drill. Proj. 22, 403–412, 1974.

[17] J.R. Curray, F.J. Emmel, D.G. Moore and R.W. Raitt, Structure, tectonics, and geological history of the northeastern Indian Ocean, in: Ocean Basins and Margins, Vol. 6, A.E.M. Nairn and F.G. Stehli, eds., pp. 399–450, Plenum, New York, 1982.

[18] J.R. Curray, Possible greenschist metamorphism at the base of a 22-km sedimentary section, Bay of Bengal, Geology 19, 1097–1100, 1991. Comment by S.K. Acharya and Reply by J.R. Curray, Geology 20, 955–957, 1992.

[19] J.R. Cochran, Himalayan uplift, sea level, and the record of Bengal Fan sedimentation at the ODP Leg 116 sites, Proc. Ocean Drilling Prog., Sci. Results 116, 397–414, 1990.

[20] R.B. Sorkhabi and E. Stump, Rise of the Himalaya: a geochronologic approach, GSA Today 3, 86, 88–92, 1993.

[21] J.M. Bull and R.A. Scrutton, Sediment velocities and deep structure from wide-angle reflection data around Leg 116 sites, Proc. Ocean Drill. Prog., Sci. Results 116, 311–316, 1990.

[22] S. Gartner, Neogene calcareous nannofossil biostratigraphy, Leg 116 (Central Indian Ocean), Proc. Ocean Drill. Prog., Sci. Results 116, 165–187, 1990.

[23] D.D. Paul and H.M. Lian, Offshore Tertiary basins of southeast Asia, Bay of Bengal to South China Sea, 9th World Petroleum Congr., Vol. 3, pp. 107–121, Tokyo, 1975.

[24] R.O. Brunnschweiler, On the geology of the Indoburman Ranges (Arakan coast and Yoma, Chin hills, Naga hills), Geol. Soc. Aust. 13, 137–194, 1966.

[25] F. Bender, Geology of Burma, 293 pp., Bornträger, Berlin, 1983.

[26] S.K. Acharya, K.K. Ray and S. Sengupta, The Naga Hills and Andaman ophiolite; their setting, nature and collisional history, in: Geology and Geodynamic Evolution of the Himalayan Collision Zone, K.K. Sharma, ed., Phys. Chem. Earth 18, 293–315, 1991.

[27] C. Karanakaran, K.K. Ray, C.R. Sen, S.S. Saha and S.K.

Annex B54

Tung-Yi Lee & Lawrence A. Lawver, "Cenozoic Plate Reconstruction of Southeast Asia", *Tectonophysics*, Vol. 251 (1995)

ELSEVIER

Tectonophysics 251 (1995) 85–138

TECTONOPHYSICS

Cenozoic plate reconstruction of Southeast Asia

Tung-Yi Lee [a], Lawrence A. Lawver [b]

[a] *Department of Earth Sciences, National Taiwan Normal University, Taipei 117, Taiwan*
[b] *Institute for Geophysics, The University of Texas at Austin, Austin, TX 78759, USA*

Received 21 March 1994; accepted 21 February 1995

Abstract

The India–Eurasia collision alone set up a series of chain reactions and caused the formation and destruction of sedimentary basins within the domain of the collision belt. Changes in the rate and angle of convergence between the India and Eurasia plates reflect different stages of tectonic development in Southeast Asia. For example, extrusion of the Indochina block induced the consumption of the pre-existing proto-South China Sea along northeastern Kalimantan and led to the eventual opening of the South China Sea along the South China margin. Subsequent motions of the Sino-Burma–Thailand, Malay Peninsula, Sumatra, and Kalimantan blocks have produced a succession of basins stretching from north Sumatra to central Thailand and on to the Natuna area.

We present reconstructions of the Southeast Asia region at 60 Ma, 50 Ma, 40 Ma, 30 Ma, 20 Ma, 15 Ma, 10 Ma, and 5 Ma. It is clear, from the reconstructions, that the impact between Greater India and Southeast Asia took place in the northwestern part of Southeast Asia. The duration for the impact was probably from the Middle Eocene to Early Miocene. This timing is in good agreement with the dating of the main Red River Fault motion (Wu et al., 1989; Schärer et al., 1990). Since the impact between Greater India and Southeast Asia was basically west of the Burma block, there is no reason to assume that the Sumatra, Malay Peninsula, and Kalimantan should extrude to the southeast first along the left-laterally displaced Mae Ping and Three Pagodas fault zones as suggested by Peltzer and Tapponnier (1988). If the opening of the central Thailand basins, the Gulf of Thailand, and the Malay Basin are taken into consideration, a dextral megashear zone is required to compensate the relative motion between Indochina and the Malay Peninsula. This dextral megashear zone might even extend into western Kalimantan and serve as a boundary between the Indochina block and Kalimantan.

1. Introduction

Tertiary deformation of Southeast Asia is the result of the India–Eurasia continental collision (Tapponnier et al., 1982, 1986; Daly et al., 1987, 1991; Dewey et al., 1989; Rangin et al., 1990). Among the many tectonic models for the Tertiary evolution of East Asia, the propagating extrusion model proposed by Tapponnier et al. (1982) is the most widely accepted one. The propagating extrusion model (Tapponnier et al., 1982) uses a free boundary to the south and east of the Indochina block and assumes that Indochina can rotate freely. A truly free boundary south of the Indochina block would have resulted in seafloor spreading in the South China Sea Basin that would still be active. It would not have produced a reversal of the sense of displacement along the Red River Fault since the Indochina block would be free to continue its rotation and extrusion. In a later paper, Peltzer and Tapponnier (1988)

SSDI 0040-1951(95)00023-2

Table 1
Data sources used to prepare Fig. 1, present-day tectonic map of the Southeast Asia region

Data type	Area	Reference
Coastline and bathymetric contours	Southeast Asia	GEBCO (1981), charts 5 · 05, 5 · 06, 5 · 09, and 5 · 10
	East Asia	Letouzey and Sage (1988)
	South China Sea	Bao (1987)
	Indonesia	Hamilton (1979)
Structural elements	East Asia	Letouzey and Sage (1988)
	Andaman Sea	Curray et al. (1979)
	Indonesia	Hamilton (1979)
	Philippines	Bischke et al. (1990)
Marine magnetic anomalies	Northwest Pacific	Nakanishi et al. (1989)
	Indian Ocean	Royer and Chang (1991)
	Western Philippine Sea	Shih (1980)
		Hilde and Lee (1984)
	Shikoku Basin	Chamot-Rooke et al. (1987)
	Parece Vela Basin	Mrozowski and Hayes (1979)
	Celebes Basin	Weissel (1980)
	South China Sea	Taylor and Hayes (1980, 1983)
	Caroline Basin	Bracey (1975, 1983)
	Bismarck Basin	Taylor (1979)
	Woodlark Basin	Weissel et al. (1982)
	Coral Sea	Weissel and Watts (1979)
Sedimentary basin	Southeast Asia	St. John (1984)

presented a tentative reconstruction of horizontal displacements of large continental blocks in Southeast Asia (Peltzer and Tapponnier, 1988, fig. 13). In their reconstruction, from 45 to 35 Ma the convergence between India and Eurasia was more toward Malay Peninsula, Sumatra, and Kalimantan. Therefore, the southeastward extrusion of these blocks was activated along the Mae Ping and Three Pagodas fault zones. From 35 to 15 Ma, the convergence was more toward the western part of the Sino-Burma–Thailand and Burma blocks than to Malay and Sumatra. The major extrusion switched to the Indochina and Sino-Burma–Thailand blocks and the Red River Fault became the main active left-lateral plate boundary. From 15 Ma and on, the collision has been mainly in the Tibetan area and the active extrusion moved further to the north to the South China block. (For geographic locations and tectonic features, please refer to Fig. 1 and Table 1.) The major problems for their reconstructions are the constraints for the size and shape of Greater India and the relative positions of Greater India with respect to the Eurasia through time. In this study, we try to better define the outline of pre-collision Greater India (especially the northeastern margin) and also examine the rate and angle of convergence between the India and Eurasia plates to determine collisional processes and the effects of Tertiary deformation in Southeast Asia.

The tectonic blocks in this region are treated as rigid bodies, and they are rotated as if they were on a globe by using a 3-D computer graphics system. The advantages of a quantitative approach are space accommodation and plate orientation. Since plate boundaries can be defined, "space" problems (overlap or gaps) must be addressed in all plausible tectonic scenarios. Any changes in the orientation

Fig. 1. Present-day tectonic map of the Southeast Asia region. For a complete list of information used in compiling this map, please refer to Table 1.

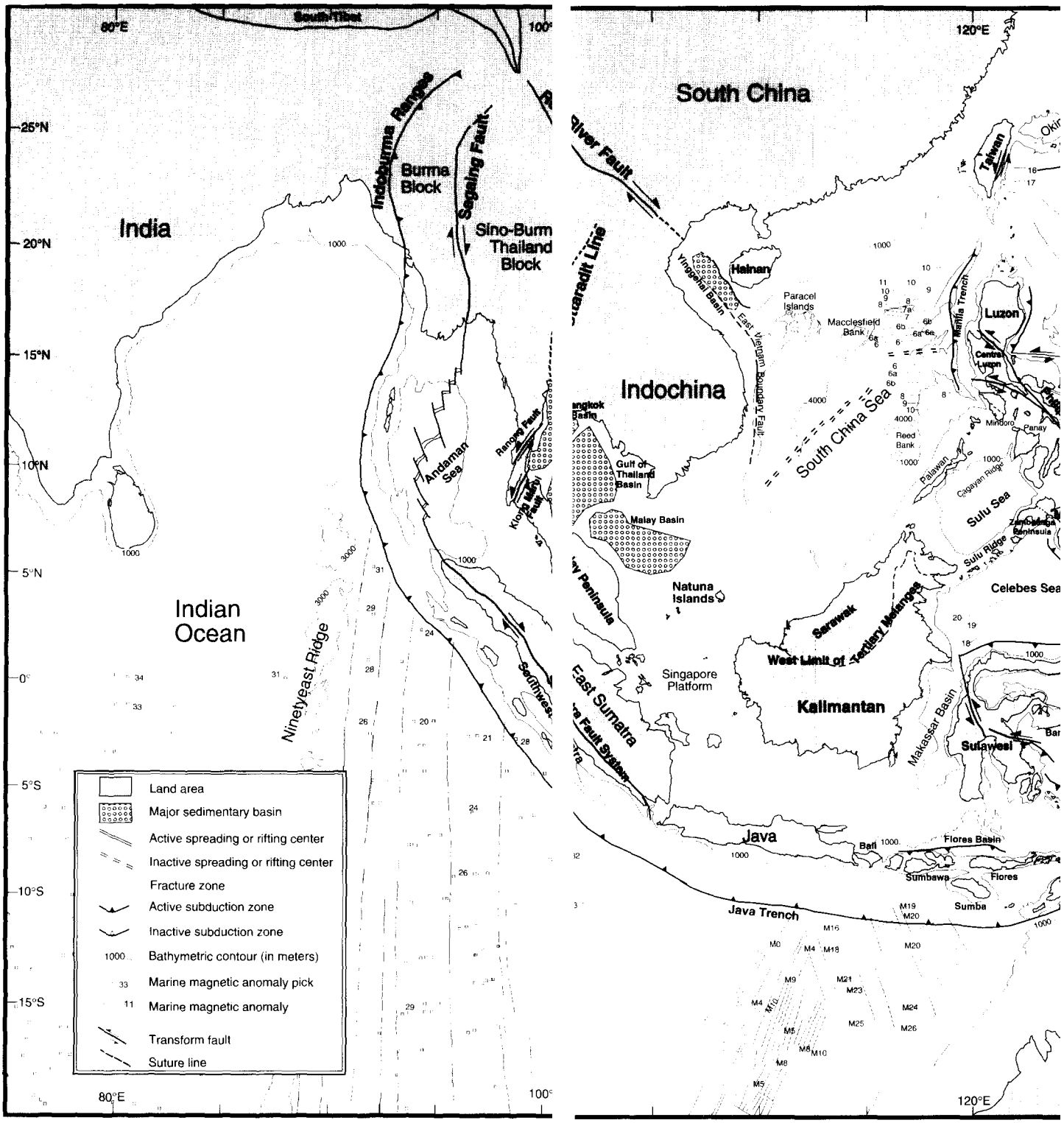
India
Indochina
South China
Indian Ocean
Burma Block
Sino-Burm Thailand Block
Indoburma Ranges
Sagaing Fault
Andaman Sea
Ninetyeast Ridge
Gulf of Thailand Basin
Malay Basin
Natuna Islands
Singapore Platform
Kalimantan
Sarawak
West Limit of Tertiary Melanges
East Sumatra Fault System
Java
Java Trench
Sulawesi
Makassar Basin
Celebes Sea
Sulu Sea
Sulu Ridge
Palawan
Cagayan Ridge
Luzon
Mindoro
Panay
Reed Bank
Macclesfield Bank
Paracel Islands
Hainan
Taiwan
Manila Trench
South China Sea
East Vietnam Boundary Fault
Red River Fault
Flores Basin
Flores
Sumbawa
Sumba
Bali
Land area
Major sedimentary basin
Active spreading or rifting center
Inactive spreading or rifting center
Fracture zone
Active subduction zone
Inactive subduction zone
Bathymetric contour (in meters)
Marine magnetic anomaly pick
Marine magnetic anomaly
Transform fault
Suture line
80°E
100°
120°E
25°N
20°N
15°N
10°N
5°N
0°
5°S
10°S
15°S

pp. 87–90

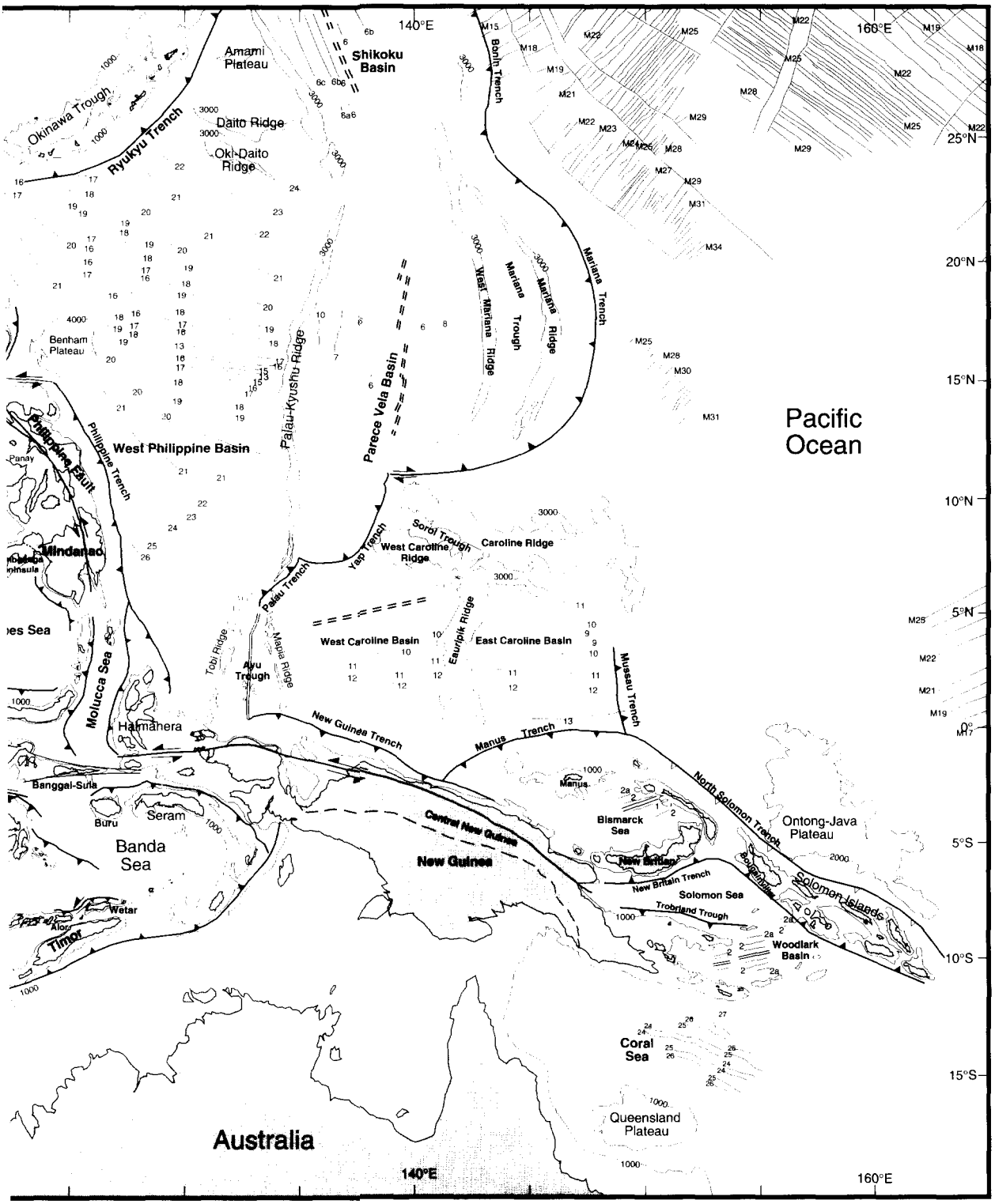
140°E
160°E
25°N
20°N
15°N
10°N
5°N
0°
5°S
10°S
15°S
Amami Plateau
Shikoku Basin
Okinawa Trough
Ryukyu Trench
Daito Ridge
Oki-Daito Ridge
Bonin Trench
Mariana Trench
West Mariana Ridge
Mariana Trough
Mariana Ridge
Parece Vela Basin
Palau-Kyushu Ridge
Benham Plateau
Philippine Fault
Philippine Trench
West Philippine Basin
Pacific Ocean
Mindanao
Yap Trench
Sorol Trough
West Caroline Ridge
Caroline Ridge
Palau Trench
West Caroline Basin
East Caroline Basin
Eauripik Ridge
Tobi Ridge
Ayu Trough
Mapia Ridge
Molucca Sea
Halmahera
New Guinea Trench
Manus Trench
Mussau Trench
North Solomon Trench
Banggai-Sula
Buru
Seram
Banda Sea
Central New Guinea
New Guinea
Bismarck Sea
Manus
New Britain
New Britain Trench
Ontong-Java Plateau
Solomon Sea
Trobriand Trough
Solomon Islands
Woodlark Basin
Wetar
Timor
Coral Sea
Queensland Plateau
Australia

and direction of one plate may affect the orientation, rate of motion, or direction of neighboring plates. For instance, it is unlikely that an isolated plate could have undergone rotation without interacting with adjacent and conjugate plates. Consequently, plate motions are best considered on a regional rather than a local scale. In a quantitative approach, finite rotation poles (Euler poles) can be derived from the reconstructions interactively on the 3-D computer graphics system, and it is possible to estimate the rate and amount of rotations. This quantitative information can be compared with the present-day values derived from other methods (e.g. from earthquake slip vectors). The resulting rotation poles are then taken to calculate the reconstructed positions of individual tectonic blocks. These paleo-positions are plotted by using the Macerator Projection to create different time slices.

2. Size and shape of pre-collision Greater India

In this study, the size and shape of Greater India is taken from the fit between India and Australia at 160 Ma from the reconstruction of the Indian Ocean (Fig. 2; Royer and Sandwell, 1989). The Shillong Plateau, which is a Precambrian outcrop, marks the eastern limit of the Indian Shield (Royer and Sandwell, 1989). The northeastern margin of Greater India is fairly well constrained by the continental margin of western Australia. The maximum possible northeastern extent for Greater India would run all the way to the Exmouth Plateau. Although it is impossible to constrain the northwestern extension of Greater India from the fit between India and Australia, the northeastern limit (the future contact with Southeast Asia) of Greater India is reconstructed with good confidence. The maximum size of Greater

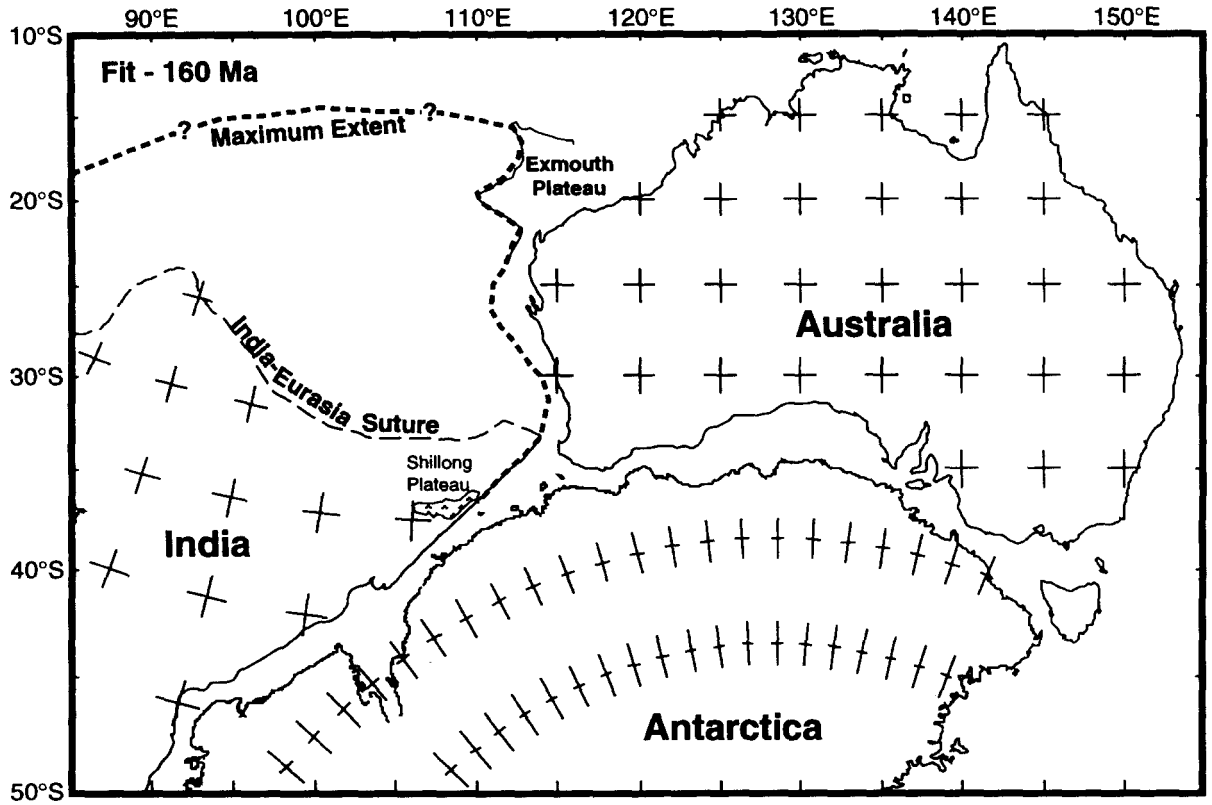

Fig. 2. New fit of the margins of India, Australia and Antarctica based on the interpretation of the deflection of the vertical chart (modified from Royer and Sandwell, 1989). The Shillong Plateau is a Precambrian outcrop that marks the eastern limit of the Indian Shield. The heavy dashed lines represent the possible extent of Greater India. Crosses are five-degree grid marks.

India is used in this study to show the possible plate interaction with Southeast Asia.

3. Rate and angle of convergence between the India and Eurasia plates

As for the relative motion between the India and Eurasia plates, there is no direct measure available for the calculation of India–Eurasia motion. The following loop was used to calculate the relative motion between India and Eurasia; from India to an absolute framework (Müller et al., 1992), absolute framework to North America (Müller et al., 1992), and North America to Eurasia (Müller and Roest, 1992). The resulting Euler poles of India–Eurasia relative motion are shown in Table 2. These poles are quite different from those published previously (e.g. the poles by Patriat and Achache, 1984) because they were derived from hotspot frameworks and the deformation in the Central Indian Basin (Royer and Chang, 1991; Müller et al., 1992) was also taken into consideration. Therefore, they may better describe the relative motion between the India and Eurasia plates. Calculated rates and angles of convergence between the India and Eurasia plates are shown in Fig. 3.

Fig. 3 demonstrates that there are several different stages of collision. Up to Early Paleocene time, the convergence rate was as high as 170 mm/yr, and the convergence direction was generally NE–SW. After the early Late Paleocene (~ 58 Ma), the convergence rate dropped to about 110 mm/yr although the direction remained essentially the same. During the late Middle Eocene (~ 44 Ma) the convergence rate dropped to about 60 mm/yr. The convergence direction remained roughly the same until the earliest Oligocene (~ 36 Ma) when it changed to a more northerly direction. In the middle Early Miocene (~ 21 Ma) the convergence rate dropped again to about 45 mm/yr, and the direction shifted about 5° E. Finally, a minor change occurred at the beginning of the Late Miocene (~ 10 Ma) when convergence sped up to around 50 mm/yr and returned to a northerly trend.

The first drop in the convergence rate is interpreted as the "soft collision" between the India and Eurasia continental margins. This Late Paleocene collision is confirmed in the results of ODP Leg 121 (Klootwijk et al., 1992). The subsequent "hard" continent–continent collision began when the convergence rate dropped to about 60 mm/yr in the Middle Eocene. The change in the convergence direction to N at the beginning of the Oligocene was probably caused by the additional collision of the Greater India plate with the Indochina plate as well as the Eurasia plate.

4. Plate reconstruction

4.1. Rotation poles

One of the constraints on the finite rotation poles for this region are the marine magnetic anomalies that have been identified in the Western Philippine

Table 2
Euler poles of India–Eurasia relative motion since 84 Ma

Age (Ma)	Anomaly	Latitude (°N)	Longitude (°E)	Angle[a] (°)
10.5	A5	23.8	23.2	−5.36
20.5	A6	27.2	14.6	−9.51
35.5	A13	23.8	25.3	−19.43
42.7	A18	25.5	24.5	−23.48
50.3	A21	25.0	20.0	−29.61
58.6	A25	23.7	15.5	−37.24
68.5	A31	20.7	11.8	−52.00
73.6	A33y	22.4	10.1	−57.02
80.2	A33o	24.2	8.6	−63.08
84.0	A34	23.6	9.5	−67.07

[a] + = counterclockwise.

Sea (Shih, 1980; Hilde and Lee, 1984), the Shikoku Basin (Chamot-Rooke et al., 1987), the Parece Vela Basin (Mrozowski and Hayes, 1979), the Celebes Basin (Weissel, 1980), the South China Sea Basin (Taylor and Hayes, 1980, 1983), the Caroline Basin (Bracey, 1975, 1983), the Bismarck Basin (Taylor, 1979), the Woodlark Basin (Weissel et al., 1982), and the Coral Sea (Weissel and Watts, 1979). The opening history of these basins can be determined with reasonable accuracy by matching identified marine magnetic anomalies from opposite sides of the same seafloor spreading center. A second constraint is paleomagnetic data (e.g. Haile et al., 1977; Haile, 1979a, b; Jarrard and Sasajima, 1980; Otofuji et al., 1981; McCabe et al., 1987; Lumadyo et al., 1990, 1993), which provide some paleo-latitude information for the various blocks and the previous orientation of some of the blocks. A third constraint is the positions of the Indian and Australian plates, which are well established from published information (e.g. Royer et al., 1988; Royer and Sandwell, 1989; Müller et al., 1992). One can calculate the relative positions of these two major plates with respect to the "fixed" East Asia to determine the major plate motions. Fourth, convergence rates between the Philippine Sea plate and the Eurasian Plate have been published and range from 1.0–1.1°/Ma (Seno et al., 1987, 1993) to 1.6°/Ma (Ranken et al., 1984). These convergence rates can be used to constrain the angular velocity between certain blocks. Finally, "rigid" plate tectonics requires that certain changes in relative plate positions be accompanied by creation and/or destruction of material. Plate interactions consist of either translation, creation of new crust

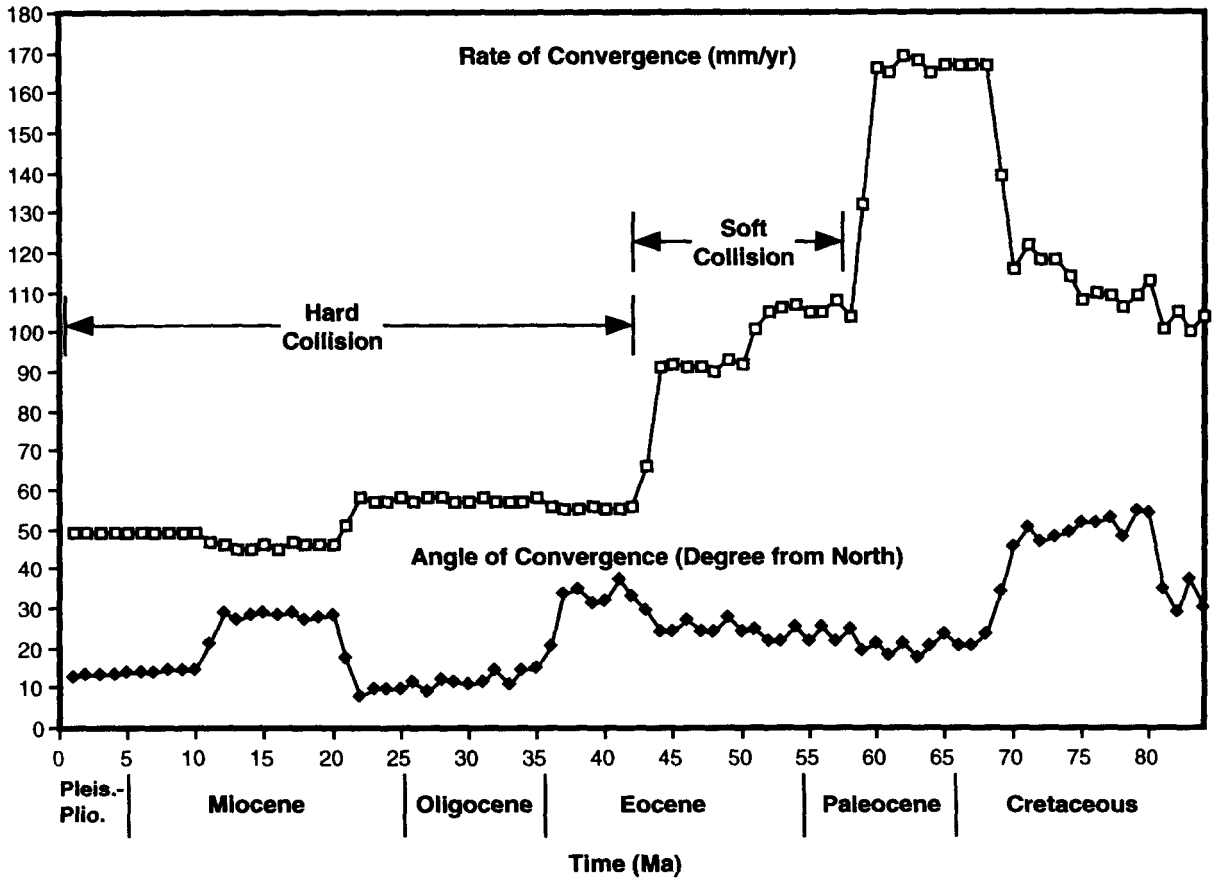

Fig. 3. Rate and angle of convergence between India and Eurasia plates from 84 Ma to present.

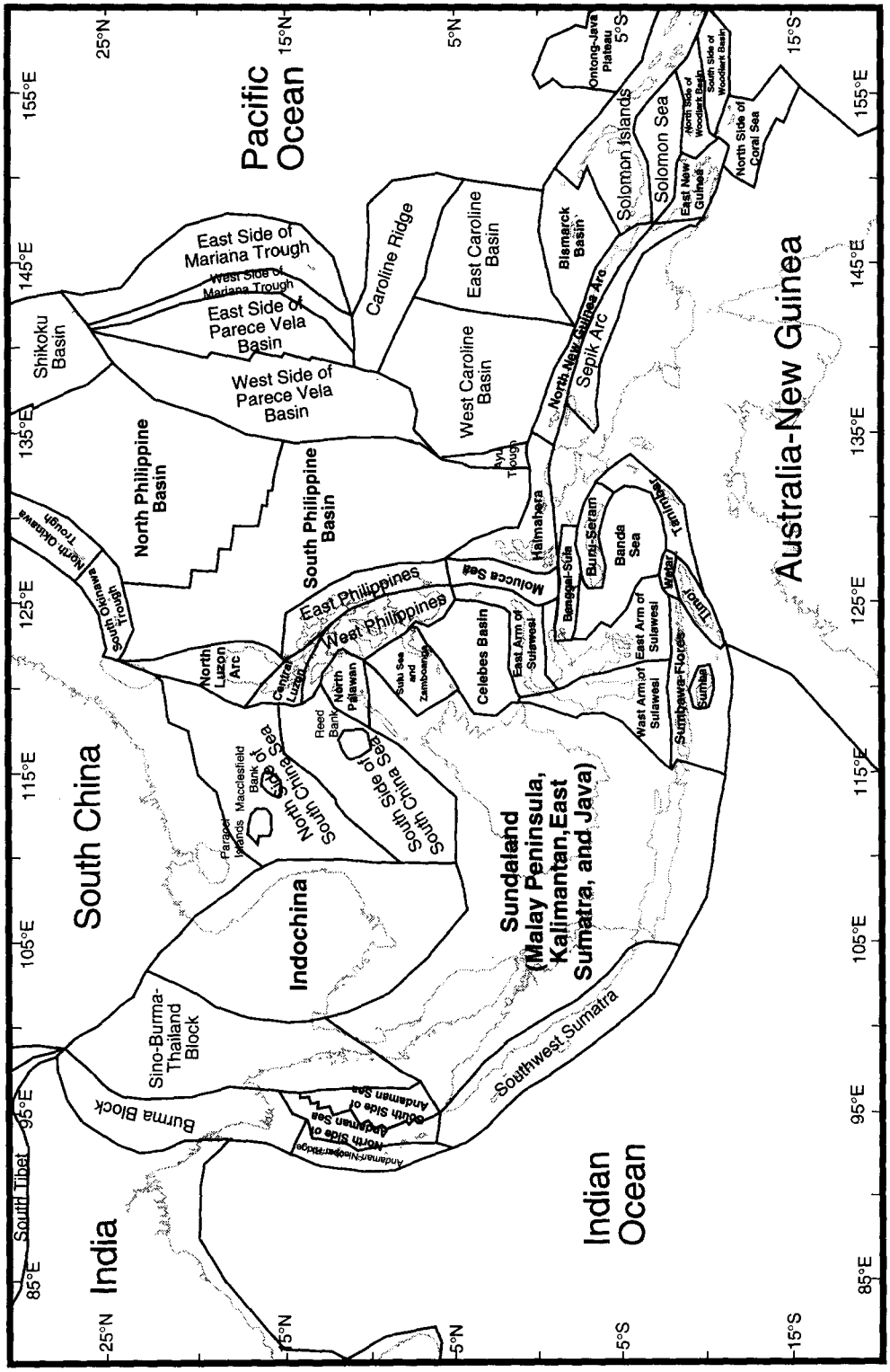

Fig. 4. Schematic configuration of major tectonic elements in Southeast Asia. Gray lines are coastlines.

(e.g. basin formation), or destruction of crust (e.g. subduction or continental collision) along plate boundaries. Both creation and destruction of material must be accommodated somewhere to conserve total surface area.

To derive finite rotation poles, it is adequate to assume that eastern Asia has remained stable since the Late Cretaceous (Lee et al., 1987) and has remained fixed with respect to a global framework. As a consequence, in our reconstructions, all the plates are reconstructed with respect to East Asia. The major tectonic blocks in this study are shown in their present-day locations in Fig. 4. Fig. 5 shows the flowline of a point on the Reed Bank, at present at 11.5°N and 117°E, with respect to a fixed East Asia, based on the constraints mentioned above. Working backwards in time, the central and southwestern portions of the South China Sea are closed with a 8.1° counterclockwise rotation with respect to the South China block about a pole at 5.3°N, 109.4°E. This rotation closes the NW–SE opening of the central and southwest portions of the South China Sea Basin. Next, by matching E–W-trending marine magnetic anomalies on both sides of the basin, it is apparent that the basin closed in a stepwise fashion. Since there is not an Anomaly 7 on the south side of

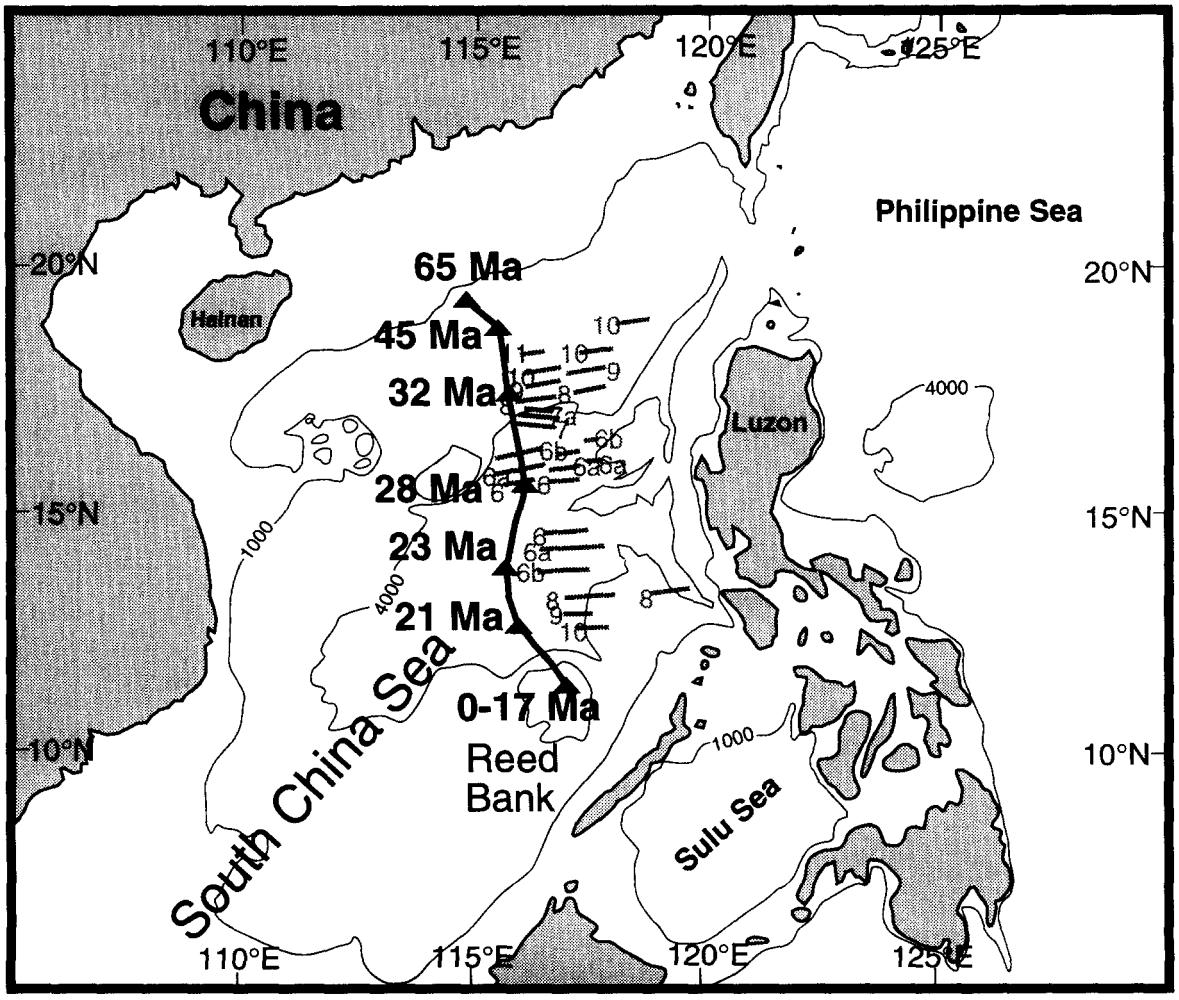

Fig. 5. Flowline of a point on Reed Bank (11.5°N, 117°E) with respect to the South China Block. Light lines are bathymetric contours (in m). Gray lines are marine magnetic anomalies from Taylor and Hayes (1983).

Table 3
Finite reconstruction poles for major tectonic blocks in the Southeast Asia region during the Cenozoic

Anomaly	Age [a]	Latitude	Longitude	Angle	
			South Tibet to South China		
6	20.5	−57.4	−176.8	1.4	
	60.0	−49.5	172.3	17.4	
Reed Bank / North Palawan and south part of South China Sea Basin to South China					
5d	17.0	0.0	0.0	0.0	Collision at Palawan
6	20.5	5.3	109.4	8.1	Opening in NW–SE direction
6A	21.7	5.4	107.3	10.0	
6B	23.0	5.8	103.8	10.9	
8	27.7	−5.3	53.0	4.7	
9	29.2	5.4	85.2	9.2	
10	30.3	5.4	84.3	10.0	
11	32.1	6.4	86.2	11.8	
	45.0	6.9	84.7	14.1	N–S rifting
	65.0	6.3	87.2	16.3	NW–SE rifting
			Macclesfield Bank to South China		
6	20.5	0.0	0.0	0.0	
11	32.1	8.1	96.9	4.9	
	45.0	11.5	105.1	13.8	
			Paracel Islands to South China		
6	20.5	0.0	0.0	0.0	
11	32.1	2.8	107.6	1.8	
	65.0	2.8	107.6	4.8	
			South Ryukyu Islands to South China		
	10.0	24.7	121.7	19.0	Opening of the South Okinawa Trough [b]
			North Philippine Sea to South Philippine Sea		
	35.0	0.0	0.0	0.0	
15	37.7	9.4	−97.6	0.83	
16	39.9	21.5	167.8	2.11	
17	41.1	17.9	174.7	2.81	
18	42.7	14.9	105.5	−6.96	
19	44.1	16.2	107.1	−11.80	
20	46.2	1.2	−171.9	7.16	
21	50.3	13.1	51.0	−9.58	
22	52.6	20.8	71.2	−13.77	
23	54.7	23.0	80.4	−17.61	
24	56.1	22.0	92.1	−24.29	
			South Philippine Sea to West Philippines		
	10.2	24.66	−93.68	9.20	
			Mapia Ridge to South Philippine Sea		
	10.0	7.0	133.0	−20.0	opening of the Ayu Trough
			East Parece Vela to West Parece Vela		
	17.0	0.0	0.0	0.0	
6	20.5	30.5	138.1	−11.9	
8	27.7	30.5	138.1	−20.9	
10	30.3	30.5	138.1	−28.8	
			West Philippines to South China		
	10.2	0.0	0.0	0.0	Collision with North Palawan at Panay and Mindoro, also collision with the Sulu Ridge at Mindanao
11	32.1	35.8	148.0	33.2	
			East Philippines to West Philippines		
	10.2	21.1	132.6	3.2	left-lateral movement along the main Philippine Fault

Table 3 (continued)

Anomaly	Age [a]	Latitude	Longitude	Angle	
			Central Luzon to West Philippines		
	5.0	7.9	119.3	−6.4	Collision with Eurasia at eastern Taiwan
	10.2	7.9	119.3	−25.0	Left-lateral movement along the Sibuyan Sea branch of the Philippine Fault
			North Luzon Arc to Central Luzon		
	10.2	5.3	112.9	−2.0	Left-lateral movement along the northern branch of the Philipine Fault
			Indochina to South China		
	15.0	16.7	103.2	−0.9	Changed to right-lateral movement along the Red River Fault
6	20.5	16.7	103.9	−0.9	
8	27.7	9.4	95.8	7.8	
11	32.1	8.3	93.4	11.9	Opening of the South China Sea
	44.0	8.7	93.9	15.7	Left-lateral movement along the Red River Fault
			Sino-Burma–Thailand Block to Indochina		
	10.2	26.9	96.4	0.6	
6	20.5	26.9	96.4	0.7	
11	32.1	26.9	96.4	3.6	Opening of the South China Sea
	44.0	26.9	96.4	4.2	Rifting in central Thailand to Gulf of Thailand
			Burma Block to Sino-Burma–Thailand Block		
	10.8	17.5	137.9	5.0	spreading in the Andaman Sea
	15.0	1.8	26.8	−6.0	rifting in the Mergui Basin–Andaman Sea
Malay Peninsula / East Sumatra / Natuna / Kalimantan (and South Palawan) to Sino-Burma–Thailand block					
	10.2	−28.7	130.3	0.1	
6	20.5	−17.5	122.6	0.2	Left-lateral movement along the Ranong Fault
11	32.1	−8.6	−78.7	15.3	Opening of the Gulf of Thailand and Malay Basin
	44.0	−7.7	−76.8	17.8	Right-lateral movement along the Ranong Fault
			Southwest Sumatra to East Sumatra		
	13.0	15.8	129.1	2.1	Right-lateral movement along the central Sumatra Fault associated with the opening of the Sunda Strait
			Zamboanga Peninsula / Sulu Ridge to Kalimantan		
	10.2	0.0	0.0	0.0	
	12.5	−19.2	−51.1	2.8	Collision with Mindanao
	16.0	−2.2	109.1	7.1	Opening of the Sulu Sea
			West Sulawesi to Kalimantan		
	17,0	0.0	0.0	0.0	
	50.0	2.1	120.9	−21.2	Opening of the Makassar Strait
			North Sulawesi to West Sulawesi		
	10.2	6.3	142.4	5.3	
	25.0	0.6	125.7	45.7	
18	42.7	−0.5	123.6	55.9	
20	46.2	−0.5	123.1	64.2	Opening of the Celebes Sea
	65.0	−0.5	121.9	101.2	Clockwise rotation of North Arm of Sulawesi
			East Sulawesi to West Sulawesi		
	10.2	12.1	154.8	3.4	Collision with West Sulawesi
	20.0	11.2	142.6	10.5	
	25.0	16.5	177.3	13.8	
			Sula–Banggai to East Sulawesi		
	5.0	1.43	−57.04	20.71	
	10.0	1.43	−57.71	35.42	Collision with Sulawesi
			Sula–Banggai to Papua New Guinea		
	10.0	2.79	−48.0	32.49	Switchover to East Sulawesi

Table 3 (continued)

Anomaly	Age [a]	Latitude	Longitude	Angle	
	15.0	7.74	−43.8	30.19	
	20.0	14.25	−47.23	31.4	
	25.0	30.77	−46.61	19.5	
	Sumba to Flores–Alor Islands				
	10.0	1.16	119.62	24.06	Opening of the Savu Basin
	Sumba to West Sulawesi				
	10.0	0.7	120.0	25.03	Switchover to West Sulawesi
	15.0	0.7	120.0	25.03	
	20.0	−0.73	110.7	6.00	
	25.0	−8.76	107.29	10.10	Opening of the Flores Basin
	West Halmahera Block to West Philippines				
	10.2	23.13	−100.98	9.66	
	East Halmahera Block to West Hamahera Block				
	3.0	−22.85	142.05	−1.09	
	5.2	−26.37	125.75	−2.40	Eastward subduction
	Seram–Buru to Papua New Guinea				
	10.2	−3.0	129.41	−74.0	
	25.0	−3.0	128.97	−98.0	Counterclockwise rotation
Southwest Caroline Basin to West Caroline–Eauripik Ridge					
9	29.2	0.0	0.0	0.0	
10	30.3	−8.9	97.7	2.7	
12	32.9	−8.9	97.7	4.98	Opening of the West Caroline Basin
Northeast Caroline Basin to Southeast Caroline Basin					
9	29.2	−10.5	59.7	−0.45	
10	30.3	−10.5	59.7	−1.30	
11	32.1	−10.5	59.7	−3.08	
12	32.9	−10.5	59.7	−4.7	
13	35.9	−10.5	59.7	−5.9	Opening of the East Caroline Basin
	West Caroline–Eauripik Ridge to Caroline Ridge				
	10.2	5.0	146.4	−5.9	Opening of the Sorol Trough
	Bonin ridge to Amami Plateau				
	14.0	0.0	0.0	0.0	
6B	23.0	46.46	122.93	−6.98	
6C	24.2	60.43	118.81	−6.29	Opening of the Shikoku Basin
	North New Guinea to Central New Guinea				
	5.0	35.19	149.50	3.99	
	10.0	34.32	152.54	8.36	Collision with Central New Guinea
North New Guinea to West Caroline–Eauripik Ridge					
	10.0	1.75	145.58	18.01	Switchover to Central New Guinea
Central New Guinea to Papua New Guinea–Australia					
	20.0	0.0	0.0	0.0	Suturing to Papua New Guinea
	25.0	−2.56	136.73	12.94	Collision with Papua New Guinea
	30.0	14.45	136.15	10.26	
	65.0	80.7	162.21	34.67	
	New Guinea–Australia to South China				
	5.0	−12.7	−139.2	3.38	
	10.0	−12.8	−139.1	6.78	
	20.0	−14.6	−142.3	12.75	
	25.0	−15.7	−143.2	16.11	
	30.0	−16.3	−143.7	19.52	
	35.0	−16.7	−144.1	22.94	
	40.0	−19.0	−145.8	25.52	
	45.0	−19.4	−145.7	27.59	
	50.0	−18.8	−144.7	28.59	

Table 3 (continued)

Anomaly	Age [a]	Latitude	Longitude	Angle	
	55.0	−19.6	−144.3	29.29	
	60.0	−18.9	−143.2	29.59	
	65.0	−19.7	−141.2	30.01	
	North Woodlark Basin to North Coral Sea				
2	1.9	−16.2	73.5	−0.97	
2A	3.2	−16.2	73.5	−1.45	
3	4.8	−16.2	73.5	−1.51	Opening of the Woodlark Basin
	North Coral Sea to Australian Craton				
	55.0	0.0	0.0	0.0	
24	56.1	6.5	113.85	−0.36	
25	59.2	6.5	113.9	−2.6	
27	63.5	6.5	113.9	−3.6	Opening of the Coral Sea
	Ontong–Java Plateau to South China				
	8.0	37.63	−153.35	9.2	Collision with the Solomon Arc
	25.0	70.71	−95.63	38.12	
	48.0	65.68	−72.48	48.74	
	65.0	60.7	−82.32	33.6	
East Papuan Composite Terrane to Papua New Guinea–Australia					
	15.0	−14.96	143.56	2.47	Collision with Papua New Guinea
East Papuan Composite Terrane to South Bismarck Basin					
	15.0	−61.44	−34.29	12.09	Switchover to Papua New Guinea
	25.0	−61.44	−34.29	12.09	
	40.0	−10.35	145.02	16.50	Opening of the Solomon Sea
	North Bismarck Basin to South Bismarck Basin				
2	1.9	−64.47	33.02	−1.84	
2A	3.2	−64.47	33.02	−3.23	Opening of the Bismarck Basin

[a] Ages in Ma.[b] Pole and amount of rotation from Miki et al. (1990).

the South China Sea Basin, we must assume that the WNW–ESE-trending Anomaly 7 on the north side of the basin accurately indicates that a NNE–SSW direction of opening occurred at the time Anomaly 7 was produced. Prior to the complete restoration of the South China Sea Basin, i.e. Anomaly 11, Reed Bank was assumed to have moved in a N–S direction from the Middle Eocene to Anomaly 11 time. Prior to the Middle Eocene it moved in a NW–SE direction from the time it first stretched from the South China margin at the end of the Cretaceous (Holloway, 1982). (Please see Table 3 for a complete listing of all the finite rotation poles derived from this study.)

All the derived finite rotation poles are kept in a "rotation file", which is ready to import to the reconstruction program for calculation. The basic architecture of a rotation file would have a tree-like structure with relative rotations between each pair of plates. Fig. 6 shows the "rotation tree" for Southeast Asia prior to the Late Miocene. For instance, seafloor spreading in the West Philippine Basin (Shih, 1980; Hilde and Lee, 1984) resulted in motion of the North Philippine Basin plate with respect to the South Philippine Basin plate between 56.1 and 32.9 Ma. Prior to 10.2 Ma, the South Philippine Basin plate was fixed to the West Philippine Archipelago plate. There was no relative motion between the South Philippine Basin plate and the West Philippine Archipelago plate until the South Philippine Basin plate began to be subducted beneath the West Philippine Archipelago plate during the Late Miocene (McCabe and Cole, 1989). The South China Platform is fixed for all of the Cenozoic and seems to be representative of the whole of eastern Asia. Fig. 7 shows the changes in the "rotation tree" for Southeast Asia from the Late Miocene to present. The effect of the collision of the Philippine Islands with

the South China Sea block (Sarewitz and Karig, 1986; Marchadier and Rangin, 1990; Bird et al., 1993) is indicated by a change in the rotation parameters for the West Philippine Archipelago plate. The West Philippine Archipelago changes from direct motion with respect to South China Platform, as the result of subduction along the South China Platform margin, to being attached to the North Palawan block. The North Palawan block, which had been moving with respect to the South China Platform because of seafloor spreading in the South China Sea, is attached to the South China Sea blocks, which in turn are fixed to the continental South China Platform or our fixed eastern Asia. Seafloor spreading ceased in the South China Sea around 17 Ma (Taylor and Hayes, 1980, 1983; Briais et al., 1993). By the time that the West Philippine Archipelago was attached to the North Palawan block at 10.2 Ma, it is in essence fixed to stable East Asia. The Indochina block moves with respect to South China, but only from 44 to 20.5 Ma in a left-lateral sense, and then it moved in a right-lateral sense from 15 Ma to present. The Sino-Burma–Thailand block is moving with respect to the Indochina block from 44 Ma to present to account for the opening of sedimentary basins in central Thailand.

Certain events changed the relationships of our rotation tree. The most significant event was the arc–continent collision between the Philippine arc and the North Palawan micro-continental block at Mindoro and Panay islands during the Middle–Late Miocene (Holloway, 1982; Uyeda and McCabe, 1983). The arc–continent collision precipitated the reversal from the eastward dipping subduction be-

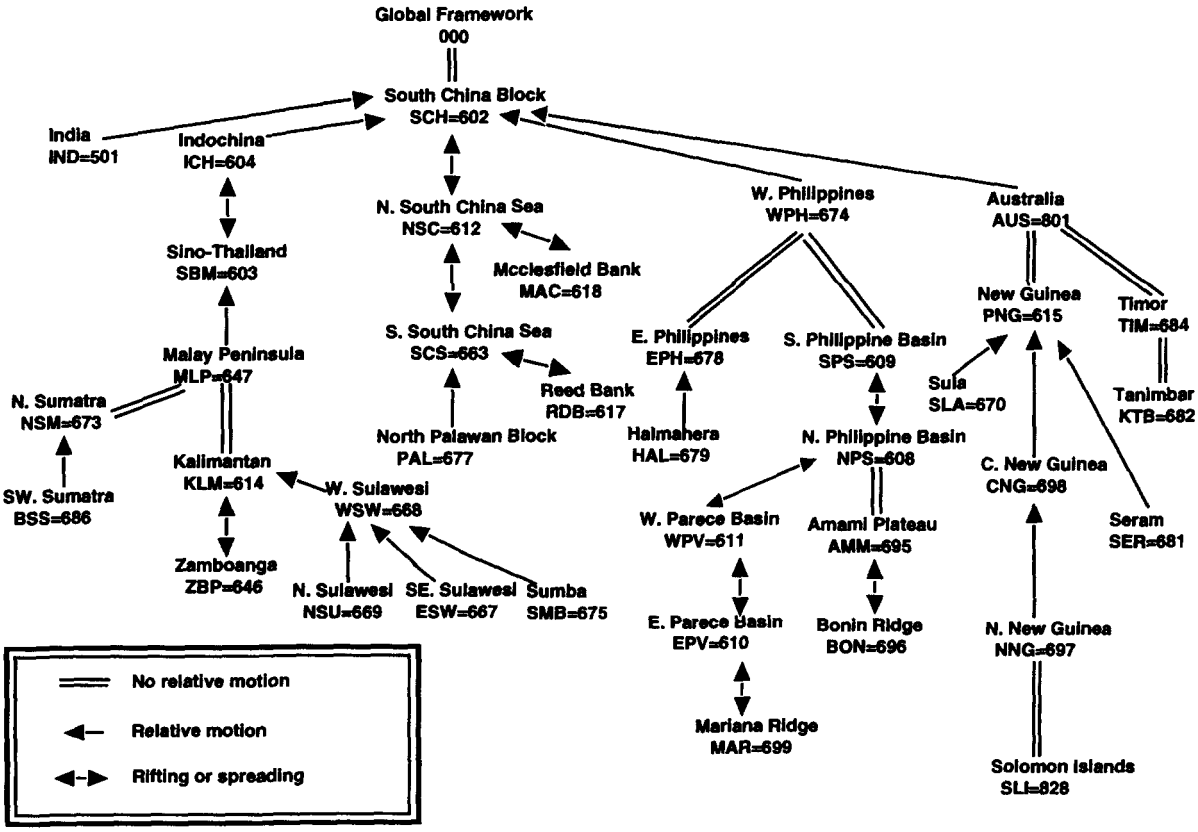

Fig. 6. Rotation tree for the major tectonic blocks in Southeast Asia before the Late Miocene.

neath the Philippine Archipelago (Uyeda and McCabe, 1983) to the present westward subduction along the Philippine Trench. After the collision, the Philippine Sea basins no longer moved with the West Philippines. Instead they moved with respect to East Asia as evidenced by subduction along westward dipping Philippine Trench. The West Philippines are attached to the North Palawan block, which is assumed fixed to Kalimantan after colliding with South Palawan–Kalimantan in the Middle Miocene (Holloway, 1982). Movement of the East Philippine Archipelago plate with respect to the West Philippine Archipelago plate continues along the Philippine Fault. In the mean time, collision of the Sulu Ridge–Zamboanga Peninsula with the West Philippines at the island of Mindanao has changed the configuration of part of the rotation tree. The Zamboanga Peninsula, which had moved with respect to Kalimantan as the Sulu Sea opened between 19 and 15 Ma (Rangin and Silver, 1991), became part of the West Philippine Archipelago since the Late Miocene.

The reconstructions presented here use a Mercator projection with a window from 30°N to 35°S and from 70°E to 170°E. The South China block is used as a reference frame fixed in its present-day position.

4.2. Paleocene reconstruction (60 Ma; Fig. 8)

Indochina is presumed to have been about 500 km NW of its present-day position, based on left-lateral strike-slip motion along the Red River Fault (Tapponnier et al., 1990). Limited paleomagnetic data from Indochina suggest a clockwise rotation about 20–30° for Indochina since the Late Cretaceous (Jarrard and Sasajima, 1980; Achache et al., 1983; Maranate and Vella, 1986; Yan and Courtillot, 1989). A counterclockwise rotation of the East Vietnam boundary fault of 18° restores it with the offshore

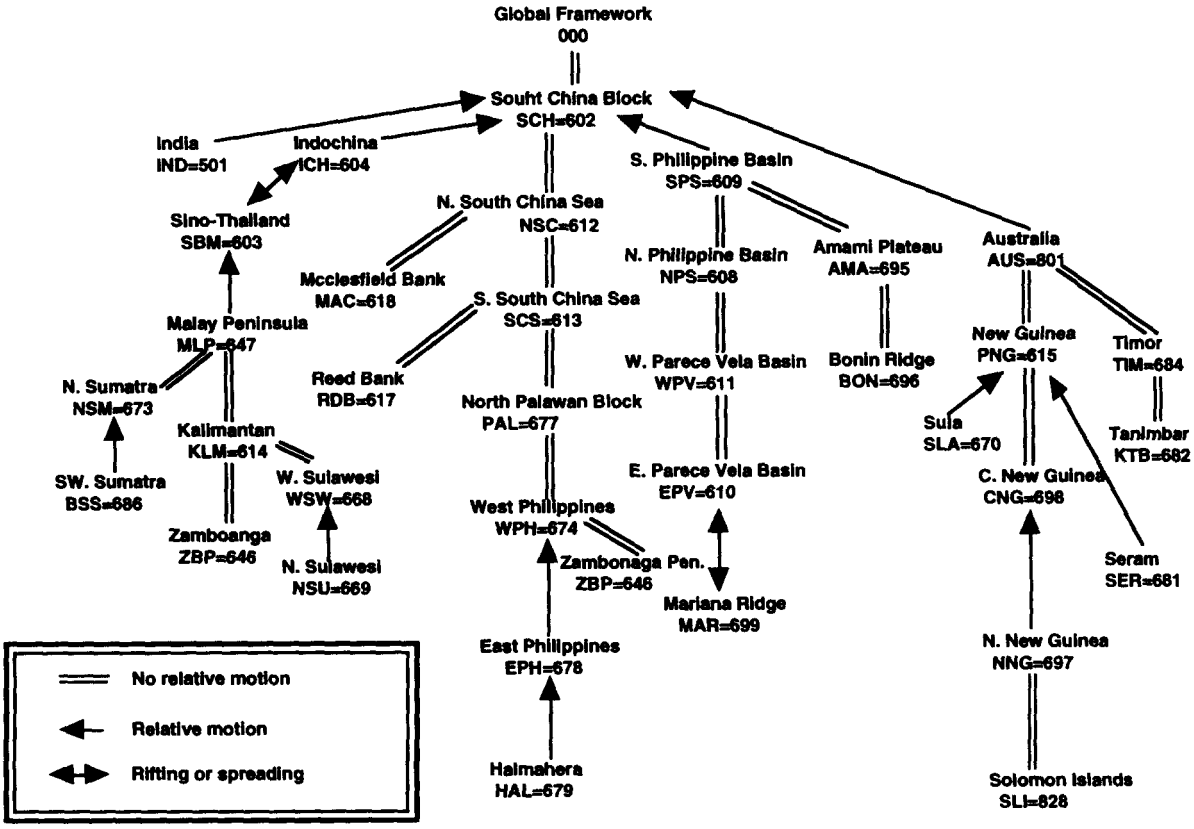

Fig. 7. Rotation tree for the major tectonic blocks in Southeast Asia after the Late Miocene.

extension of the Red River Fault. Such a rotation agrees well with the paleomagnetic data for Indochina. East of the Indochina block, the Mesozoic South China continental margin between southwestern Taiwan and Hainan Island consisted of a number of future micro-continents. These included the North Palawan block with parts of Panay and Mindoro, Reed Bank, Macclesfield Bank, and Paracel Islands. Since the Late Cretaceous, these microcontinents have rifted away from the South China margin (Holloway, 1982).

West of Indochina, the Burma block has been restored to its position prior to the opening of the Mergui Basin and the Andaman Sea. The right-lateral Sagaing Fault is assumed to delineate plate motion of the Burma block with respect to the Sino-Burma–Thailand block (Curray et al., 1979; Curray, 1989; Dewey et al., 1989). Central Thailand is shown with a slight overlap to compensate for the subsequent development of the Cenozoic sedimentary basins in central Thailand and the northern Gulf of Thailand. The Sino-Burma–Thailand block rotated clockwise with respect to Indochina (Khorat Plateau) as a result of Neogene E–W extension in these basins (McCabe et al., 1988). There appears to have been greater opening in the south in the Bangkok Basin region than farther north (McCabe et al., 1988). South of the Indochina block, the Gulf of Thailand and the Malay Basin opened by motion of the Malay Peninsula southward along the Ranong Fault.

Results from paleomagnetic studies of Kalimantan have been reported from Indonesian Kalimantan and Sarawak (Haile et al., 1977; Haile, 1979a) and from Sabah (Schmidtke et al., 1990). Haile et al. (1977) reported paleomagnetic data from the Late Cretaceous basement rock of western Kalimantan. Their study suggested a 50° counterclockwise rotation with no latitudinal change for the western portion of Kalimantan since the Cretaceous. The Late Cretaceous paleomagnetic pole for Kalimantan is in good agreement with that of the Malay Peninsula (McElhinney et al., 1974), and thus, suggests that there has been little or no differential movement between Kalimantan and the Malay Peninsula since the Cretaceous. Paleomagnetic data from Oligocene/Miocene red beds on Sarawak were reported by Haile (1979a). The results from these red beds are indistinguishable from the present-day magnetic field, which suggests that any counterclockwise rotation of Kalimantan was completed by the late Tertiary. Although the Late Cretaceous data and the limited Tertiary data from Kalimantan suggest that the island has behaved as a single tectonic unit and has undergone a 50° counterclockwise rotation, the northern portion of the island is composed of numerous ophiolitic fragments (Hutchison, 1975). Hamilton (1979) has suggested that these fragments are Cretaceous and Tertiary melange belts. A large counterclockwise rotation of western Kalimantan with respect to a stable East Asia sometime during the Cretaceous or Cenozoic was recently re-affirmed by new data from Schmidtke et al. (1990). Their data imply up to 108° of counterclockwise rotation of Kalimantan with respect to Eurasia. If the lithologic boundary defined by Hamilton (1979) for the southeast limit of Cretaceous continental crust for Java and Kalimantan is accepted, then the 108° counterclockwise rotation of Kalimantan around an arbitrary pole of rotation (the center of Kalimantan will have the minimum vertical and horizontal displacements for the island) will bring the northwestern melange belt to the east, facing the present-day Celebes Sea and the island of Sulawesi. Structural mapping of the Sunda Shelf basement (Ben-Avraham and Emery, 1973) indicates that with the possible exception of the very minor Billiton Depression, the continental margin of western Kalimantan is directly connected to the "Singapore Platform" and therefore, was probably connected to the Malay Peninsula. There is no major structural or physiographic break between western Kalimantan and the Singapore Platform (Fig. 1). It is, therefore, inconceivable that Kalimantan has rotated as a solitary block because such a rotation would have resulted in a major reorganization of the other structural elements in this area. If the 108° counterclockwise rotation of Kalimantan did occur sometime during the Cretaceous or Cenozoic, there should exist evidence of large strike-slip motion and compressional features in the Natuna area, the Tin islands, and in the Java Sea (especially in the northwestern portion of the Java Sea). Structural studies using the reflection seismic sections from the Sunda Basin in the Java Sea show only extensional features such as block faults and listric normal faults (Fainstein and Pramono, 1986). Other published information suggests that extensional tectonics dominate this

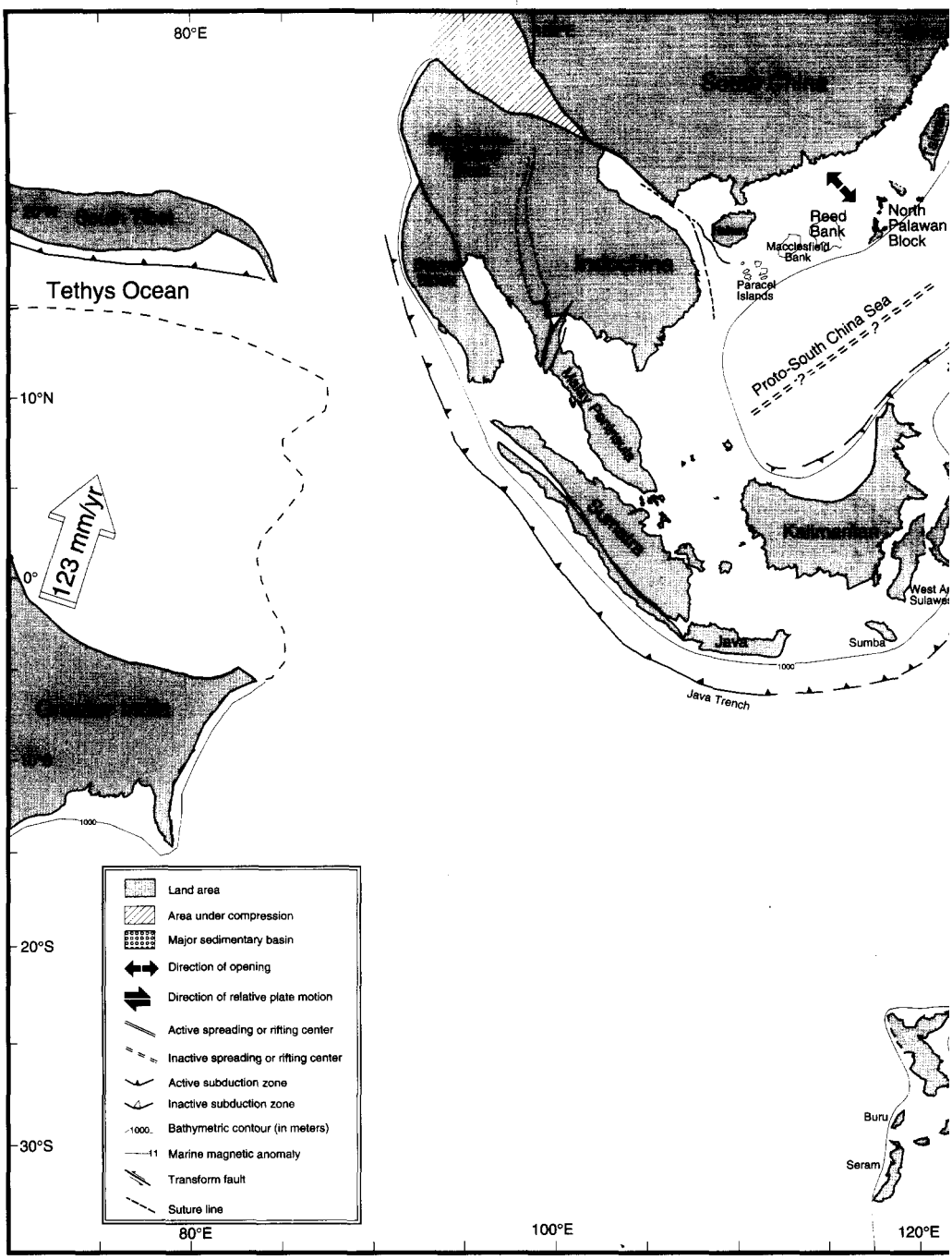

Fig. 8. Paleocene (60 Ma) plate reconstruction of Southeast Asia. Open arrows and numbers indicate convergence rat respect to the South China Block.

pp. 103–104

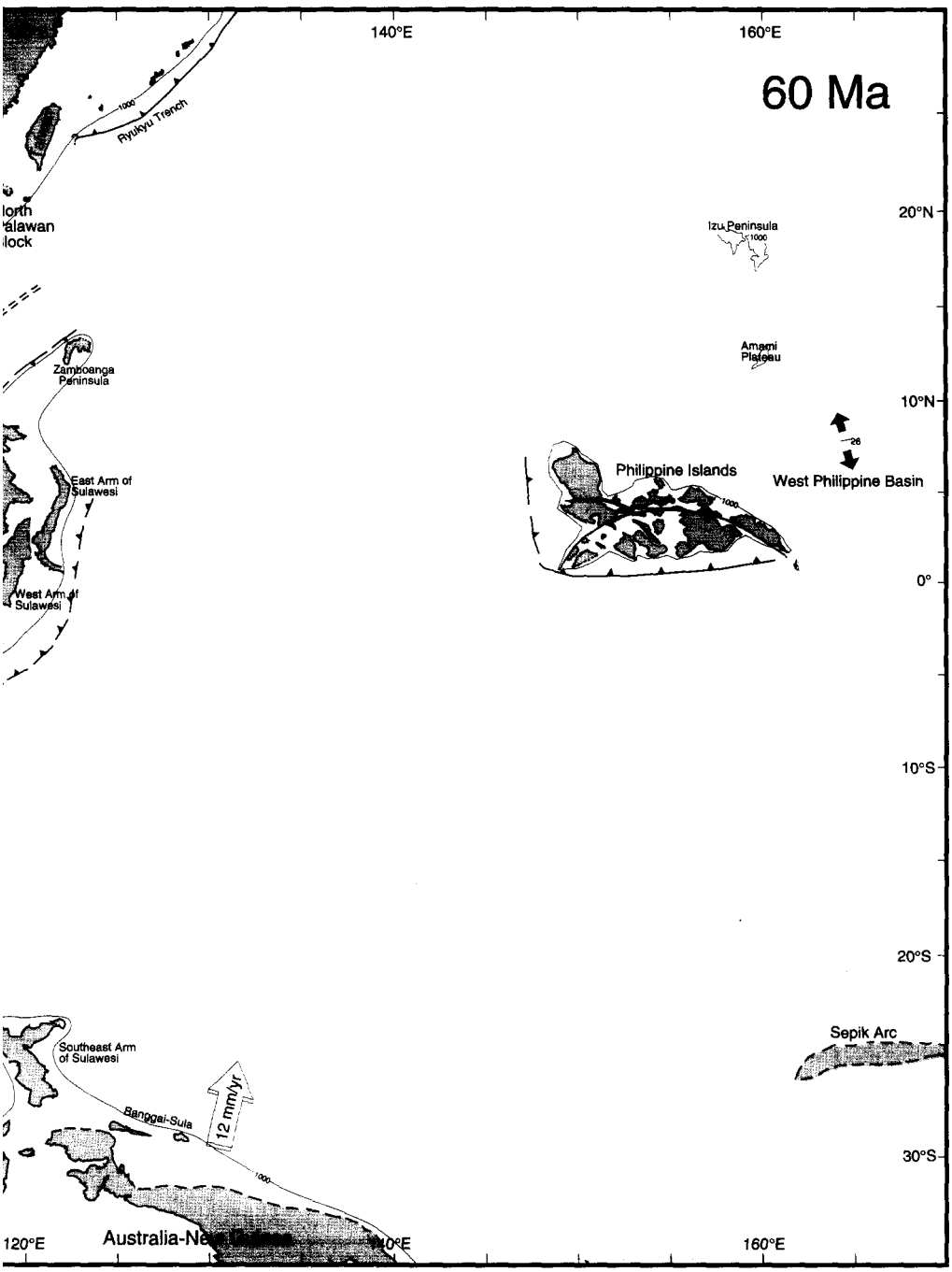

ıce rates of major plates with

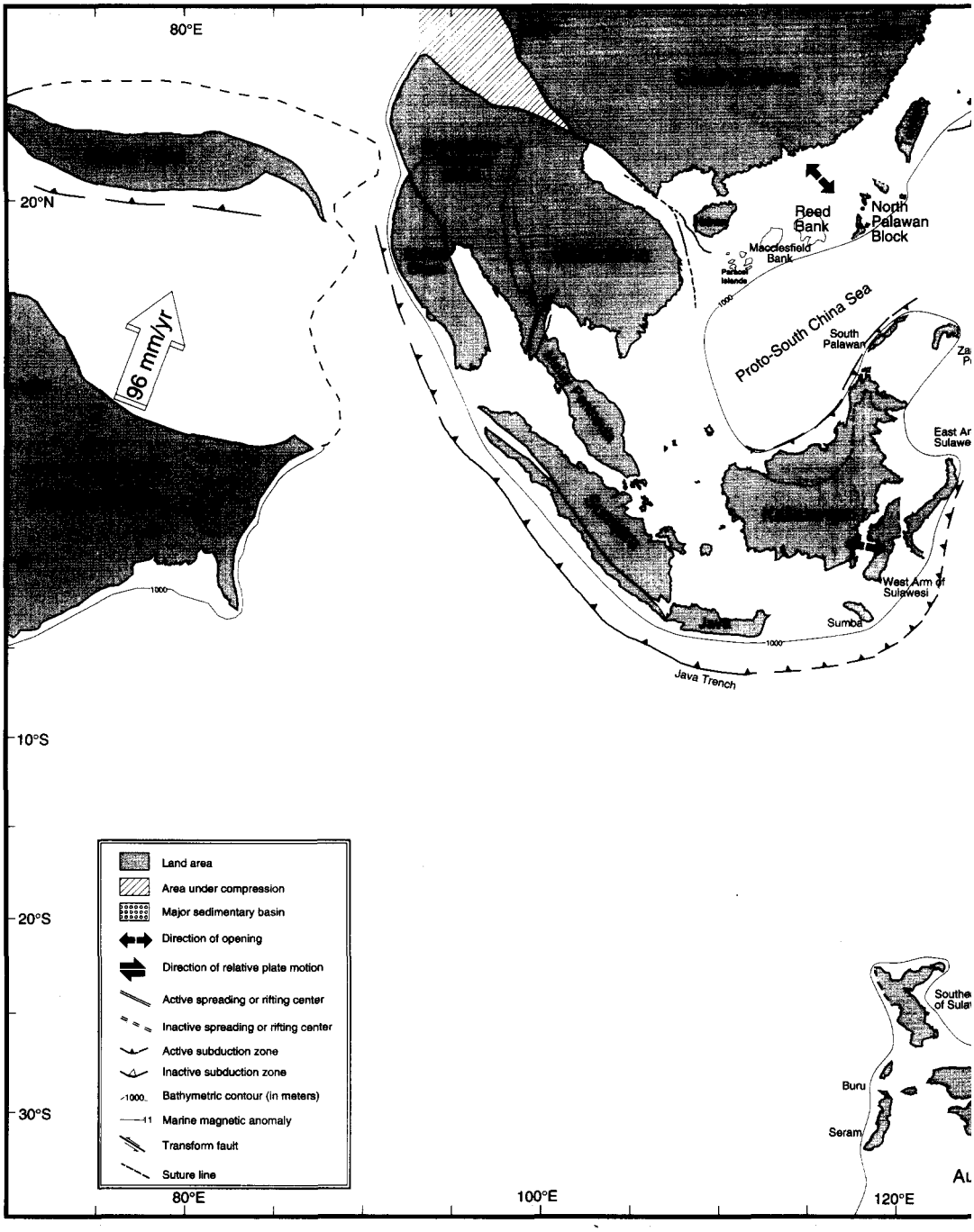

Fig. 9. Early Eocene (50 Ma) plate reconstruction of Southeast Asia. Open arrows and numbers indicate convergence rate with respect to the South China Block.

vergence rates of major plates

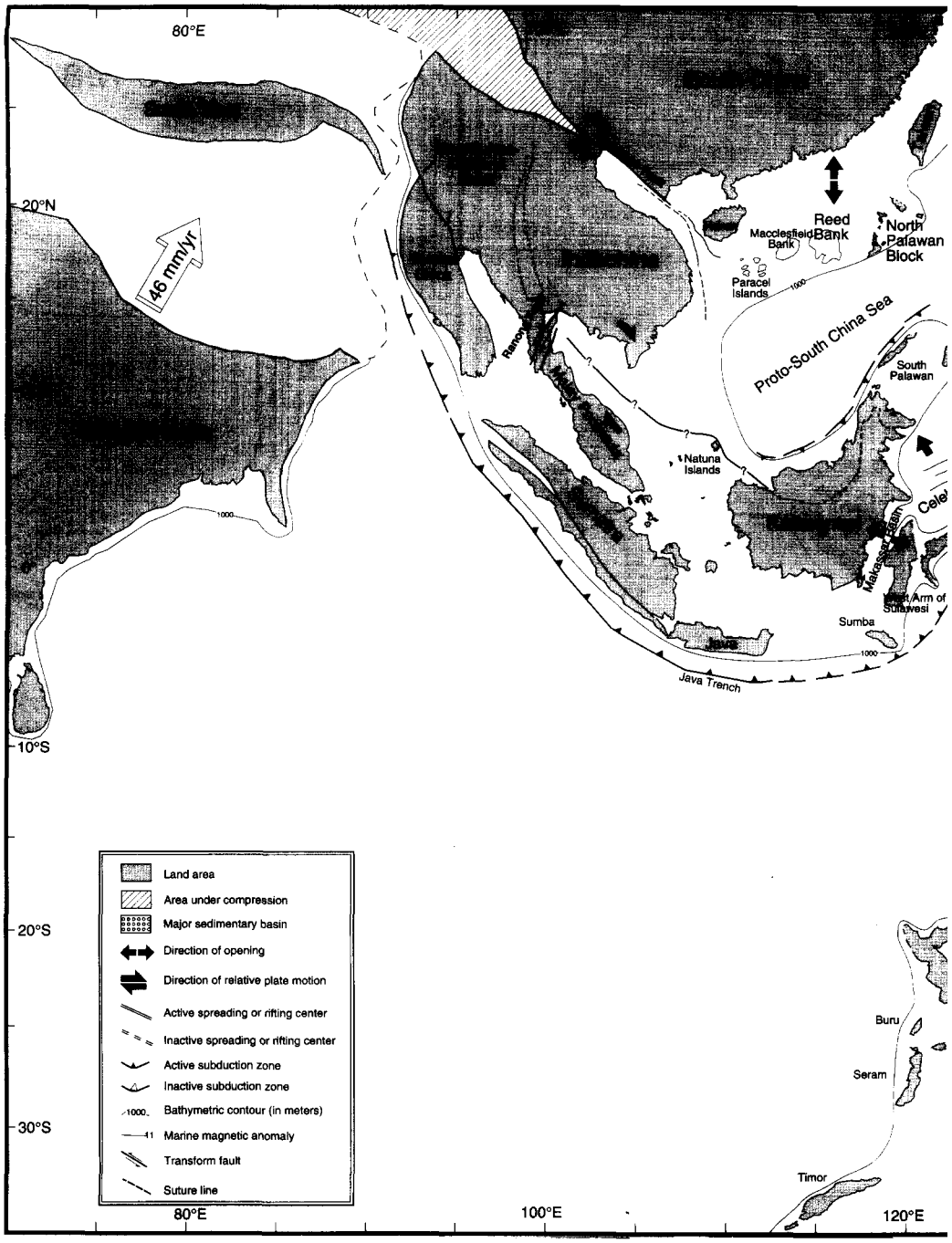

Fig. 10. Middle Eocene (40 Ma) plate reconstruction of Southeast Asia. Open arrows and numbers indicate converg plates with respect to the South China Block.

pp. 107–108

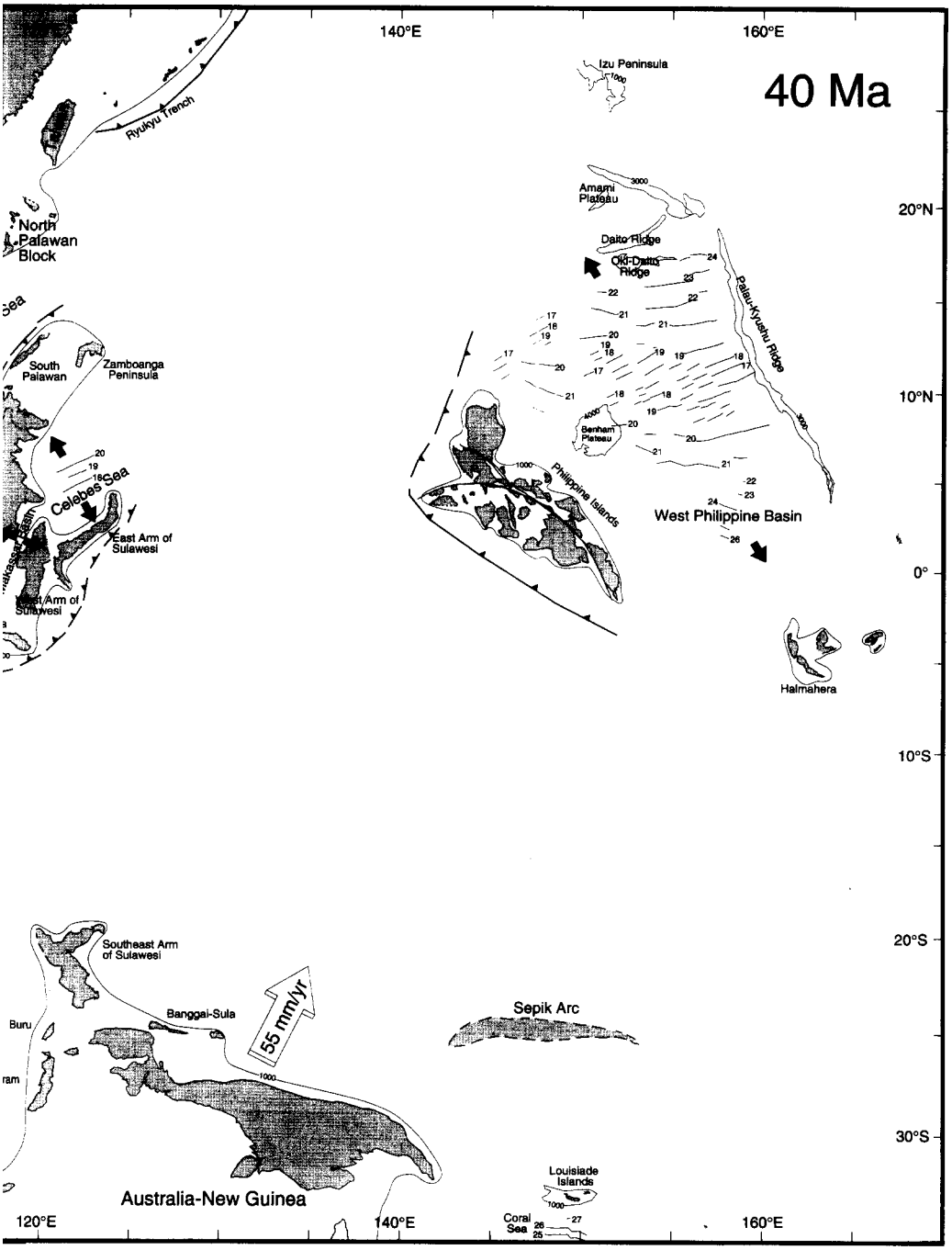

te convergence rates of major

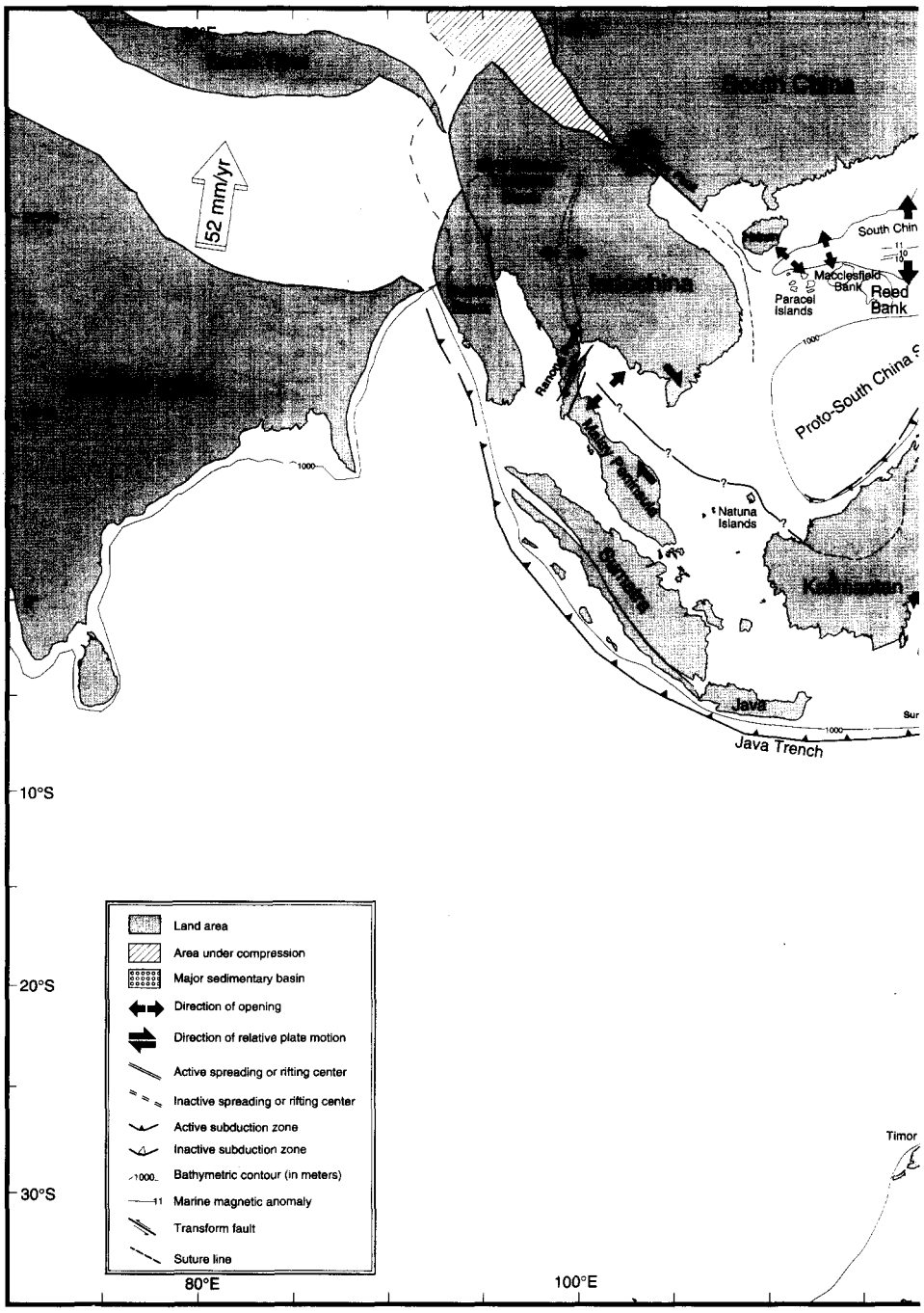

Fig. 11. Oligocene (30 Ma) plate reconstruction of Southeast Asia. Open arrows and numbers indicate con with respect to the South China Block.

vergence rates of major plates

region (Ponto et al., 1988). Another recent paleomagnetic study of the stable western part of Kalimantan (Lumadyo et al., 1990, 1993) indicates that the stable part of Kalimantan has not been rotated at least since the Eocene. This finding agrees with the observed geology. The data of Lumadyo et al. (1990, 1993) do not directly contradict the other published paleomagnetic data because their measured rotation (Haile, 1979a; Schmidtke et al., 1990) could have occurred in the Cretaceous. After due consideration, in this study, Kalimantan has been fixed with the Malay Peninsula for the Cenozoic reconstructions. Such a restriction severely limits the amount of Tertiary rotation that Kalimantan could have undergone. This serves as an additional constraint for the orientation of these blocks. Southwest Sumatra was restored to its position prior to any movement along the Sumatra Fault System (Huchon and Le Pichon, 1984).

With the restoration of Indochina, the Malay Peninsula, and Kalimantan, a "gap" is still left between the South China block and northern Kalimantan. We assume that this area was occupied by a proto-South China Sea as suggested by Holloway (1982) and Parker and Gealey (1985). The Cenozoic rifting along the South China margin resulted in this proto-South China Sea being consumed under northern Kalimantan and Palawan (Williams et al., 1988).

East of Kalimantan, the Zamboanga Peninsula and the Sulu Ridge are assumed to have been against the Cagayan Ridge prior to the opening of the Sulu Sea Basin (Rangin, 1989). West Sulawesi was originally next to Kalimantan prior to seafloor spreading in the Makassar Strait. The north arm of Sulawesi may have originally been oriented N–S (Otofuji et al., 1981) adjacent to Kalimantan and west Sulawesi prior to its being rotated clockwise with the opening of the Celebes Sea Basin. Recent paleomagnetic results by Surmont et al. (1994) suggest the existence of a post-Miocene clockwise rotation of about 20–25° of the western part of the north arm. If this is correct, combined with the roughly E–W-trending magnetic anomalies (Anomalies 18–20) in the Celebes Sea (Weissel, 1980), it is highly possible that most of the rotation of the north arm might have taken place prior to the seafloor spreading in the Celebes Sea during the Middle Eocene. West Sulawesi, north Sulawesi and the Sulu Ridge probably formed a continuous magmatic arc as a result of northward subduction of the Pacific/Australian Plate.

In the Paleocene, the Philippine Archipelago was located near the equator (McCabe et al., 1987), and it was oriented roughly E–W based on paleomagnetic data and convergence rates and directions (Seno et al., 1987; Ranken et al., 1984). The paleogeography of the Philippine Archipelago was deduced by restoration of offset geological features, including forearc basins, ophiolite belts, and volcanic belts, as well as offset long-wavelength geophysical anomalies including regional Bouguer, free-air and magnetic anomalies (Bischke et al., 1990, figs. 13 and 14). These diverse features suggest a 200–300 km left-lateral offset along the Philippine Fault since the Middle Miocene. The Philippine Basin began to open (Fig. 7) at Anomaly 26 time (Late Paleocene; Hilde and Lee, 1984). This implies that the Eocene-aged Oki–Daito and Daito Ridges were probably formed close to the Philippine Archipelago. Lewis et al. (1982) suggested that the formation of the Philippine Basin was related to northward subduction along the Philippine Archipelago. Along the northern margin of Australia–New Guinea, Seram and Buru can be reconstructed by rotating them 90° into positions along the western margin of the Vogelkop of Irian Jaya (the Indonesian side of the island of New Guinea). This fit is suggested by paleomagnetic data from Haile (1979b) and by stratigraphic similarities between this continental fragment and the Australian continent (Pigram and Panggabean, 1984). The recognition of a Jurassic rift–drift sequence on the Banggai–Sula microcontinent indicates that it may have originally come from that part of the northern margin of the Australian continent now found in central New Guinea (Pigram and Panggabean, 1984). Even though the former position of this microcontinent is not constrained, it is reasonable to place it on the northern margin of the Australian–New Guinea continent north of Irian Jaya. Audley-Charles et al. (1988) pointed out that the southeast arm of Sulawesi should also have come from the northern margin of the Australian–New Guinea continent, but again, there are no constraints on its exact position. It is possible that Banggai–Sula has been in its present position adjacent to east Sulawesi since the Triassic (Pigram and Panggabean, 1984). Therefore, the east arm of Sulawesi is also reconstructed to the

northern margin of the Australian–New Guinea continent next to the Banggai–Sula microcontinent. As to the position of the Sepik composite terrane, due to the structural complexity of the western Pacific margin and the lack of any paleomagnetic data in this region, it is impossible at this stage to constrain its position. In this reconstruction, it is placed along the southwestern margin of the Pacific Plate. The Sepik Arc might have occupied a position similar to that of the present-day South Banda Arc, a feature which may be accreted to the Australian margin in the near geologic future (Pigram and Davies, 1987).

4.3. Early Eocene reconstruction (50 Ma; Fig. 9)

The collision between Greater India and south Tibet has closed the Tethys Ocean. NW–SE-oriented rifting along the South China margin has initiated the opening of the Pearl River Mouth Basin. Hamilton (1979) suggested that the west arm of Sulawesi began to rift from Kalimantan after the Oligocene when the Makassar Basin opened. Situmorang (1982a, b) used well records and multichannel seismic reflection profiles to determine that rifting in the Makassar Basin actually began in early Middle Eocene (or possibly earlier) but that rifting ceased by the end of the Early Miocene.

4.4. Middle Eocene reconstruction (40 Ma; Fig. 10)

Eocene rifting and stretching continued to occur along most of the south-facing continental margin of the South China Platform. From the Late Cretaceous to the Eocene, NE–SW-trending grabens developed and eventually formed the Pearl River Mouth Basin (Feng and Zhang, 1986; Chen et al., 1987; Ru, 1988; Yu, 1988). Between 44 and 20 Ma, collision between Greater India and Eurasia resulted in Indochina moving southeastward with respect to the South China block along the left-lateral Red River Fault (Wu et al., 1989; Tapponnier et al., 1990). This Middle Eocene event may have been recorded in eastern Sarawak (Bènard et al., 1990) with the emplacement of the Eocene melanges along the Lupar Line, where reworked Late Cretaceous–Early Eocene nannoplankton are encountered in Late Eocene sediments (Bènard et al., 1990). A 130° schistosity in Sarawak was developed during this same event. According to Hamilton (1979) and Holloway (1982), southward directed subduction along the northern margin of Kalimantan resulted in crustal accretion along northwest Kalimantan and along the South Palawan Arc. It also resulted in a reduction in the size of the proto-South China Sea. The southeastward movement of the Indochina block may also have initiated the development of the Yinggehai, Beibu Gulf, and Southwest Hainan Basins on the South China margin. The Malay Peninsula, Sumatra, and Kalimantan also moved southeastward with Indochina during the Middle Eocene. The stretching direction along the South China margin might have changed from NW–SE to N–S as recorded by changes in fault patterns in this area.

Middle Eocene rifting in the Makassar Basin (Situmorang, 1982a, b) is in good agreement with the age of the Celebes Sea Basin (Weissel, 1980; Silver et al., 1991). This coincidence in time might indicate a major rift–drift event from eastern Kalimantan to the southern Sulu Ridge caused by prolonged northwestward subduction. Northwestward subduction opened the Celebes Sea Basin in the Eocene and resulted in the the north arm of Sulawesi rotating clockwise away from northeastern Kalimantan. The opening of the Celebes Sea may have continued into the Oligocene (or even Miocene) after the clockwise rotation of the north arm of Sulawesi (Otofuji et al., 1981).

Based on stratigraphic observations, Hall (1987) suggested that the Halmahera Basement complex and the basement of east Mindanao were part of an arc and forearc of Late Cretaceous–Early Tertiary age. Together they formed part of a single plate from the Late Eocene to Early Oligocene. The subducted Molucca Sea Plate has been restored using the Benioff zone identified by Cardwell and Isacks (1981). The movements along the Philippine and Sorong Faults have been taken into consideration to place present-day Halmahera to the southeast of the East Philippines. The position of Halmahera during the Eocene implies that it formerly occupied a position on the margin of the Philippine Sea Plate (Fig. 10). Along the northern margin of Australia–New Guinea, Timor is assumed to have been basically in its present-day position with respect to Australia as part of its outer continental margin.

4.5. Oligocene reconstruction (30 Ma; Fig. 11)

N–S spreading in the present-day South China Sea started with renewed extension along the South China continental margin (Taylor and Hayes, 1980, 1983; Holloway, 1982). A major unconformable surface, associated with seafloor spreading in the South China Sea Basin, can be identified across the South China block's southern margin (Holloway, 1982). Seafloor spreading in the South China Sea separated the North Palawan–Reed Bank–Macclesfield Bank–Paracel Islands microcontinents from the continental South China block. The motions of these microcontinental blocks were not all the same. North Palawan and Reed Bank followed the N–S opening of the South China Sea and moved in the same general direction. On the other hand, the major fault trends in the area between southwestern Hainan Island and the Paracel Islands is NE–SW (Liu and Yang, 1988), while the faults between Macclesfield Bank and the South China block are nearly E–W in direction. The Paracel Islands seem to have moved in a NW–SE direction, and the net direction of motion for the Macclesfield Bank was NNW–SSE (see Table 3 for pole locations). As the present-day South China Sea Basin grew, the proto-South China Sea was subducted along the northern margin of Kalimantan as evidenced by the Paleogene melange belt in northwestern Kalimantan (Hamilton, 1979). It was also consumed to the east by the northwestward migration of the Philippine Archipelago at the proto-Manila Trench.

The collision of India with Eurasia seems to have produced a greater extrusion of Indochina than of either the Sino-Burma–Thailand block or the Burma block. This led to the opening of a series of sedimentary basins in central Thailand, in the Gulf of Thailand, and in the Mergui Basin. Apparently there was greater relative motion in the south than in the north, implying that the pole of rotation for the opening is located to the north, possibly near the edge of the South China block (McCabe et al., 1987).

During the Oligocene, island arcs in the Pacific region moved to the WNW and began to accrete to the northern margin of the northward moving Australia–New Guinea continental block (Daly et al., 1987). The first terrane to dock against the northern Australia–New Guinea margin was the Sepik Arc (Pigram and Davies, 1987) in the Late Oligocene (prior to 25 Ma). This collision event probably extended west into Irian Jaya, based on the time of development of the foreland basin (Pigram and Davies, 1987). Upon collision, left-lateral strike-slip motion has translated the micro-plates westward along the northern continental margin of New Guinea.

Spreading in the West Philippine Basin stopped at Anomaly 13 (36 Ma, beginning of the Oligocene; Hilde and Lee, 1984). Seafloor spreading shifted to the east into the Parece Vela Basin. A W-dipping subduction zone east of the Palau–Kyushu Ridge existed in the Early Oligocene. The Palau–Kyushu volcanic arc split at about 30 Ma (Anomaly 10, beginning of the Late Oligocene) and E–W interarc spreading was initiated between the Palau–Kyushu Ridge and the West Mariana Ridge (Fig. 11; Mrozowski and Hayes, 1979).

4.6. Early Miocene reconstruction (20 Ma; Fig. 12)

Spreading in the South China Sea underwent a major change from N–S spreading to NW–SE spreading at about 21 Ma (Pautot et al., 1986). The change in the spreading direction in the South China Sea may have resulted from a ridge jump or by the initiation of oblique spreading (Hayes, 1988; Taylor and Rangin, 1988). The proto-South China Sea had been nearly consumed by this time. Left-lateral movement along the Red River Fault has been dated at approximately 23 Ma (Schärer et al., 1990; Tapponnier et al., 1990), although the motion had apparently stopped by 20 Ma (Wu et al., 1989). Compressive forces began to dominate in the West Natuna Basin (Wirojudo and Wongsosantiko, 1985) where previously only tensional forces had existed. This change caused reverse movement on pre-existing normal faults and the corresponding uplift of areas that previously were half grabens. This compressive event may have marked the end of the extrusion of the Indochina block (Wirojudo and Wongsosantiko, 1985). From Fig. 11, it is very clear that at this time the western side of the South China Sea Basin was in close contact with rigid continental blocks. The rigidity of the South China block, the Indochina block, and the Sundaland block left little room for the South China Sea Basin to expand in a N–S direction.

In contrast, the eastern border of the South China Sea Basin was still a free boundary. To the southeast, the proto-South China Sea was still being consumed along southern Palawan to northern Kalimantan. At this time, there was a switch of the opening direction from roughly N–S to NW–SE with a consequent clockwise rotation of the south side of South China Sea Basin (including Reed Bank and North Palawan) with respect to South China. The pole for this rotation was close to the southwestern tip of South China Sea Basin (5.3°N, 109.4°E; Table 3).

By the Early Miocene, the Malay Peninsula had almost reached its present-day position, but the North Sumatra Basin and central Thailand basins were still undergoing extension (McCabe et al., 1988). One result of the opening of these basins was a change from right-lateral to left-lateral movement along the Ranong Fault. Detailed subsea mapping by Polachan et al. (1991) revealed a 4–6 km left-lateral offset of the Ranong Ridge (a subsea basement ridge), offset of topographic features on the seafloor, and the development of S-shaped pull-apart basins in the Gulf of Thailand (Polachan et al., 1991, figs. 26 and 27). This evidence supports the idea of a change in motion along the Ranong Fault zone. Rifting in the Makassar Strait stopped at the end of the Early Miocene (Situmorang, 1982a, b), possibly caused by the collision of east Sulawesi with west Sulawesi. The north arm of Sulawesi was nearly in its present-day orientation by the end of the Early Miocene. Southeastward migration of the island of Sumba opened up the Flores Basin. This rifting event and the creation of a volcanic arc south of Kalimantan are assumed to have been caused by northward subduction along the Java Trench.

Continued subduction along the western side of the Philippine Archipelago resulted in a northward extension of the Luzon Arc, that included the East Taiwan Act (Fig. 12) and an additional volcanic arc between Luzon and east Taiwan (Ho, 1986; Richard et al., 1986; Suppe, 1981). The collision between the Sepik Arc and New Guinea at the beginning of Miocene (Pigram and Davies, 1987) induced strike-slip motion along the northern continental margin of the Australia–New Guinea plate, caused east Sulawesi to move west-northwestward, and initiated counterclockwise rotation of the Seram–Buru microcontinent towards its present-day position.

Seafloor spreading in the Parece Vela and Shikoku Basins migrated the Mariana–Bonin Trenches eastward with respect to the Palau–Kyushu Ridge. With the approach of the Caroline plate, the collision between the Caroline Ridge and the Mariana Arc occurred around the Late Oligocene–Early Miocene (McCabe and Uyeda, 1983). A continuous subduction belt along the southern boundary of the Philippine–Caroline plate extended from the West Philippines to the East New Guinea Composite Terrane (Fig. 12). The only remnant of trapped oceanic crust between this subduction belt and the Celebes Sea Basin is probably the present-day Molucca Sea. Another piece of trapped oceanic plate is the one between the North New Guinea–Solomon Arc and the East New Guinea Composite Terrane. This oceanic plate is probably the Solomon Sea plate created by the Late Oligocene spreading between the North New Guinea–Solomon Arc and the East New Guinea Composite Terrane (Honza et al., 1987).

4.7. Middle Miocene reconstruction (15 Ma; Fig. 13)

The collision of the North Palawan block with Kalimantan at about 17 Ma hindered Cenozoic seafloor spreading in the South China Sea (Holloway, 1982; Taylor and Hayes, 1983). From mid-Middle Miocene, the Red River Fault began to change to right-lateral motion from its previous left-lateral motion (Wang et al., 1989). This reversal caused some local unconformities and high-angle reverse faults. According to Tapponnier et al. (1982), the reversal of motion on the Red River Fault may have been caused by an increase in extrusion rate of the South China block relative to the Indochina block. This may have resulted from increased compression between the Indochina block and the "rigid" Sundaland continental block. The southwestward motion of Indochina was blocked by Sundaland, and Sundaland in turn was beginning to undergo collision with the advance pieces of the Australian continent.

Collision of the east Sulawesi with west Sulawesi is evidenced by the Middle Miocene blueschist zone on central Sulawesi (Audley-Charles et al., 1988). This collision isolated the Banda Sea and may have produced an even greater rotation of the north arm of Sulawesi. The Sulu Basin opened in the Early Miocene as a result of subduction along the north-

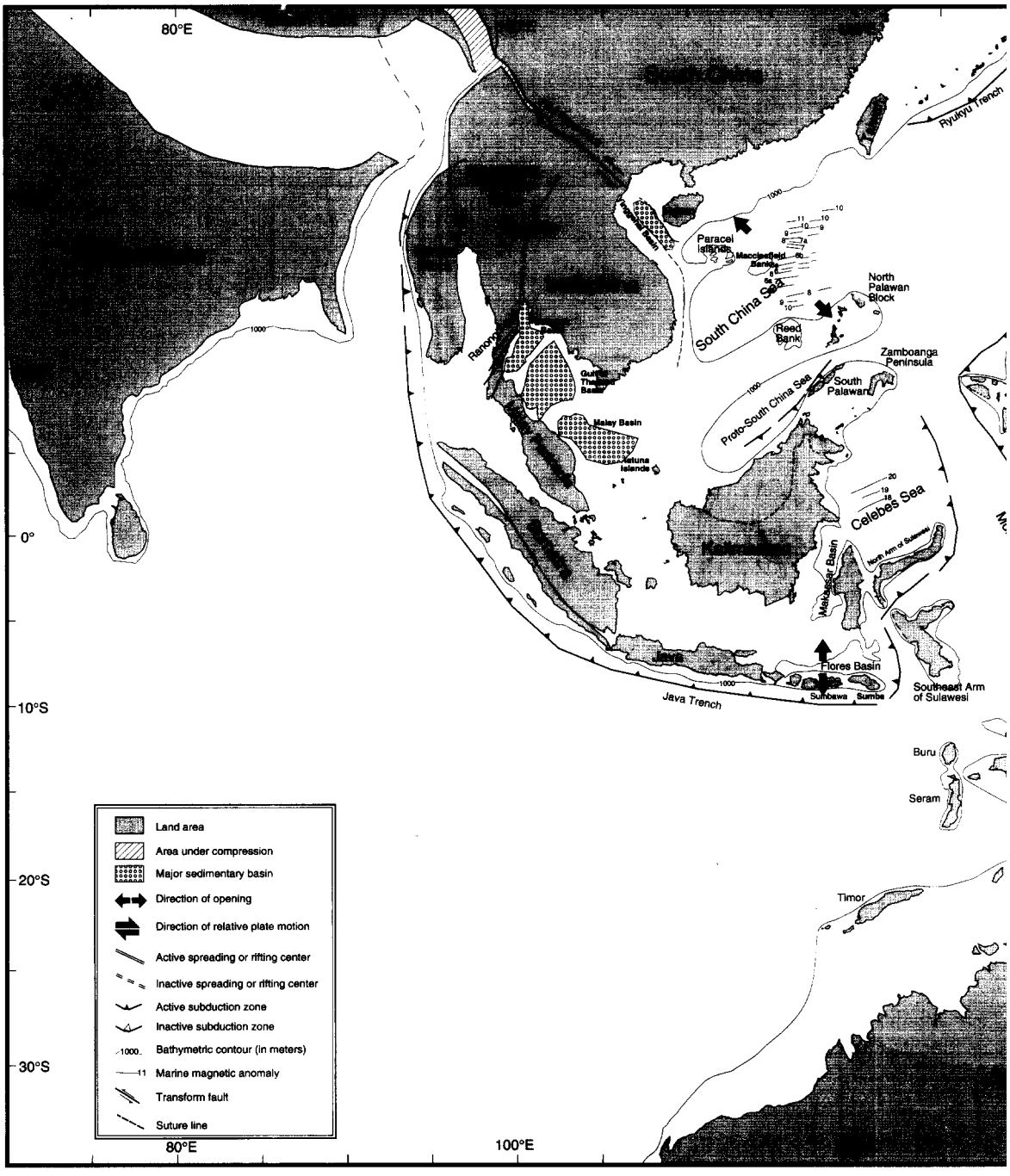

Fig. 12. Early Miocene (20 Ma) plate reconstruction of Southeast Asia. Open arrows and numbers indicate convergence rates of major with respect to the South China Block.

pp. 115–116

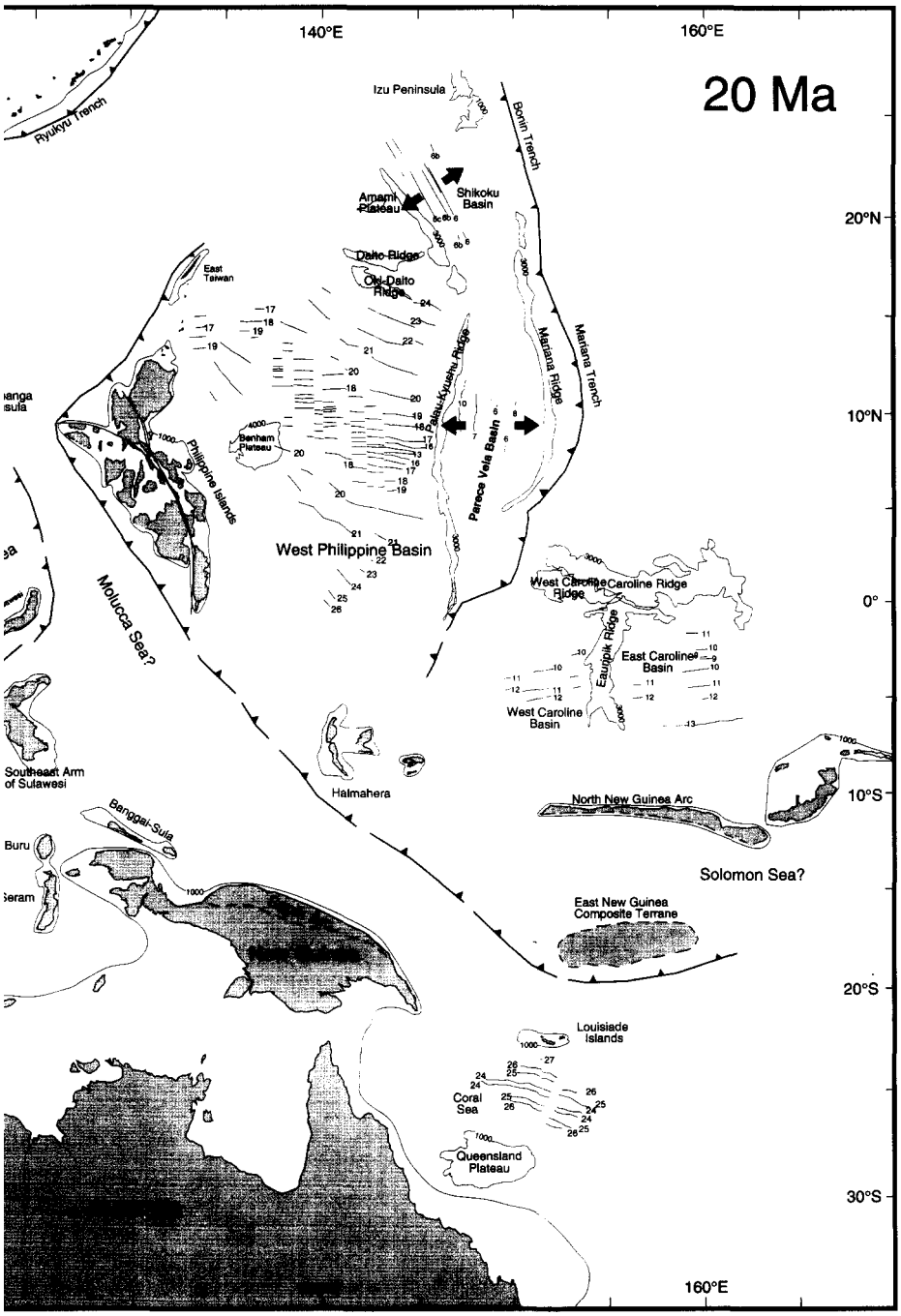

tes of major plates

pp. 117–118 T.-Y. Lee, L.A. Lawver / Tectonophysics 251 (1995) 85–138

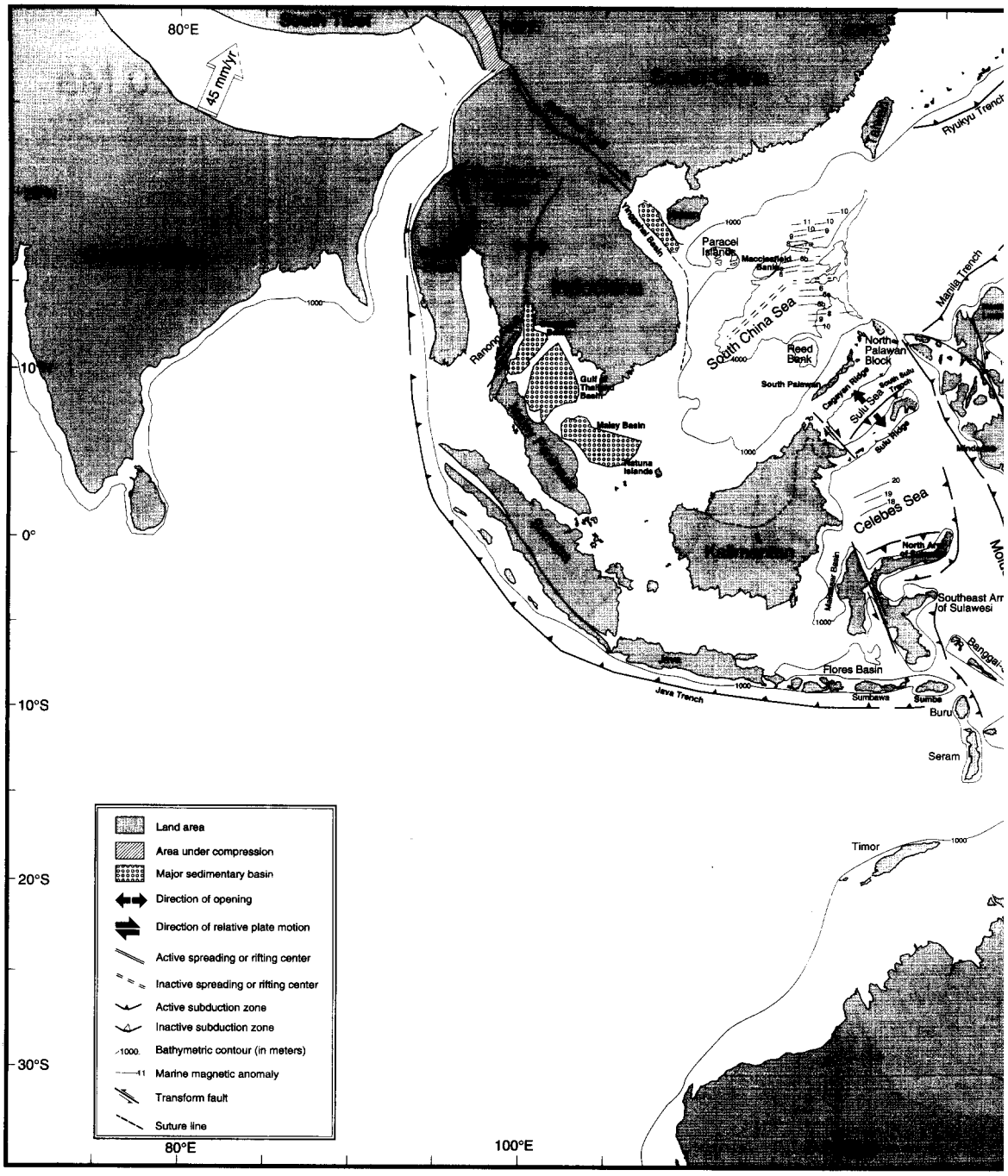

Fig. 13. Middle Miocene (15 Ma) plate reconstruction of Southeast Asia. Open arrows and numbers indicate convergence rates of plates with respect to the South China Block.

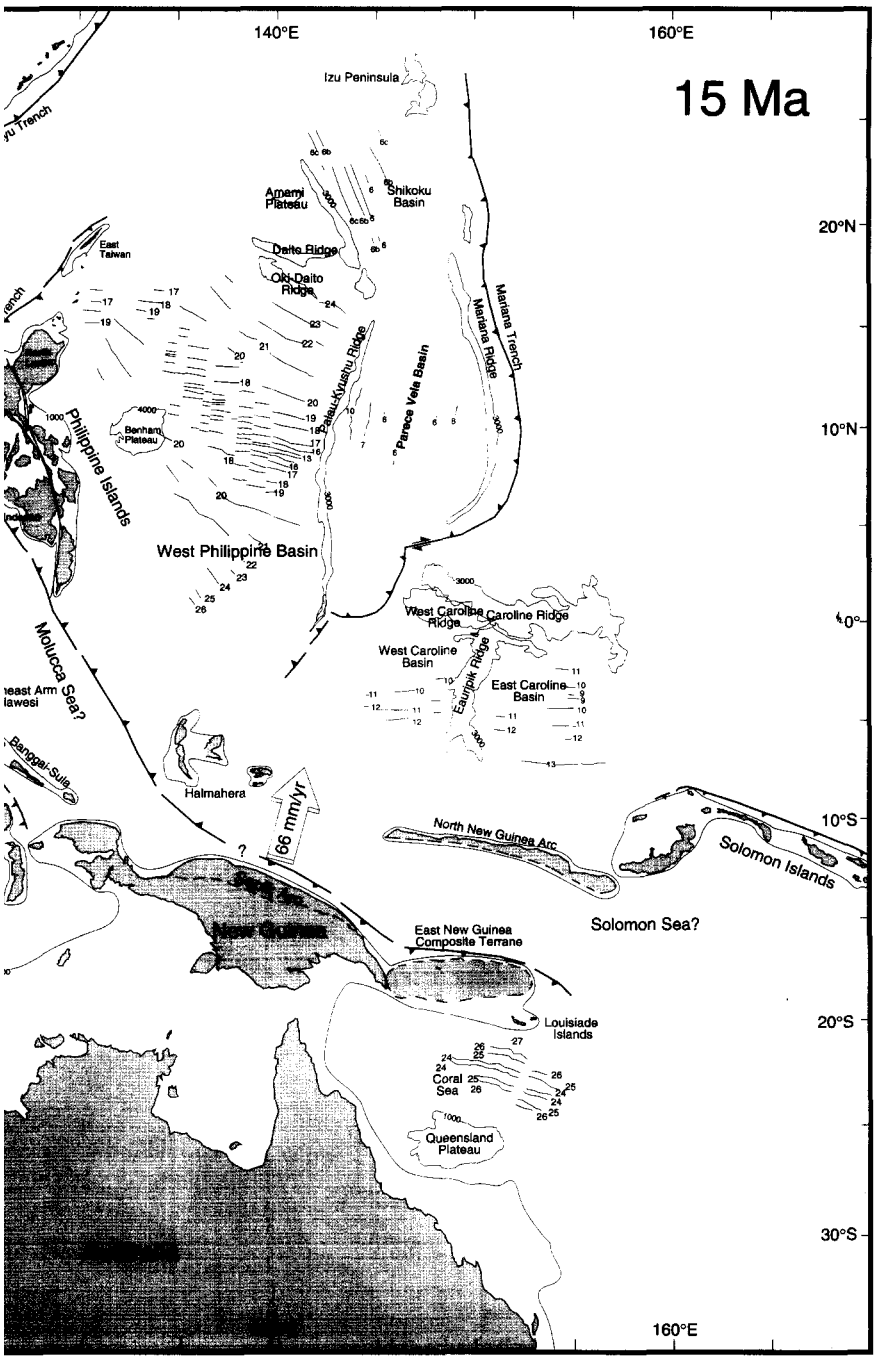
140°E
160°E
15 Ma
Izu Peninsula
Amami Plateau
Shikoku Basin
East Taiwan
Daito Ridge
Oki-Daito Ridge
Mariana Trench
Mariana Ridge
Palau-Kyushu Ridge
Parece Vela Basin
20°N
10°N
0°
Philippine Islands
Benham Plateau
West Philippine Basin
West Caroline Ridge
Caroline Ridge
West Caroline Basin
East Caroline Basin
Eauripik Ridge
Moluccas Sea?
Halmahera
66 mm/yr
North New Guinea Arc
Solomon Islands
10°S
Solomon Sea?
East New Guinea Composite Terrane
Louisiade Islands
20°S
Coral Sea
Queensland Plateau
30°S
160°E

tes of major

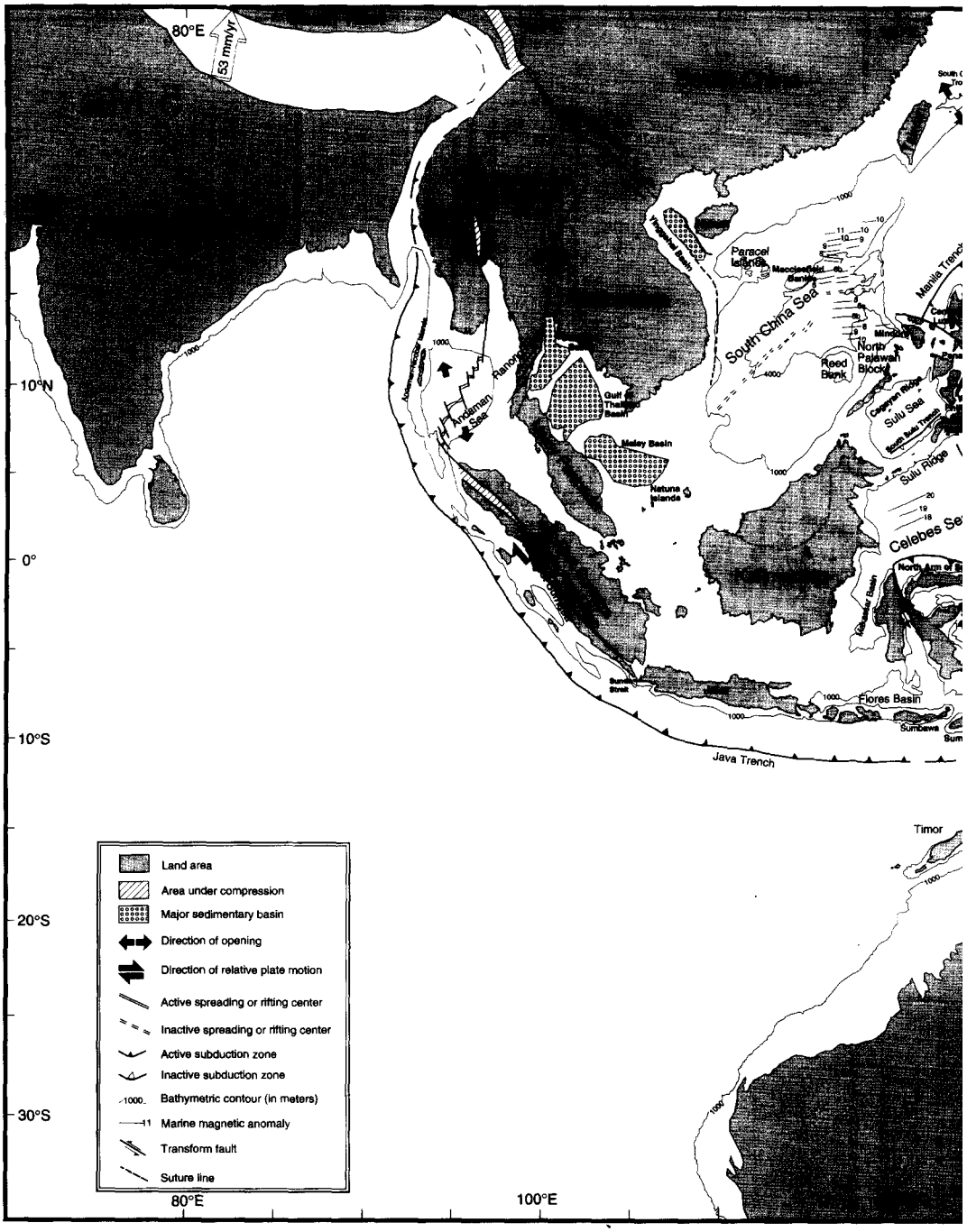

Fig. 14. Late Miocene (10 Ma) plate reconstruction of Southeast Asia. Open arrows and numbers indicate convergence rate
with respect to the South China Block.

pp. 119–120

ates of major plates

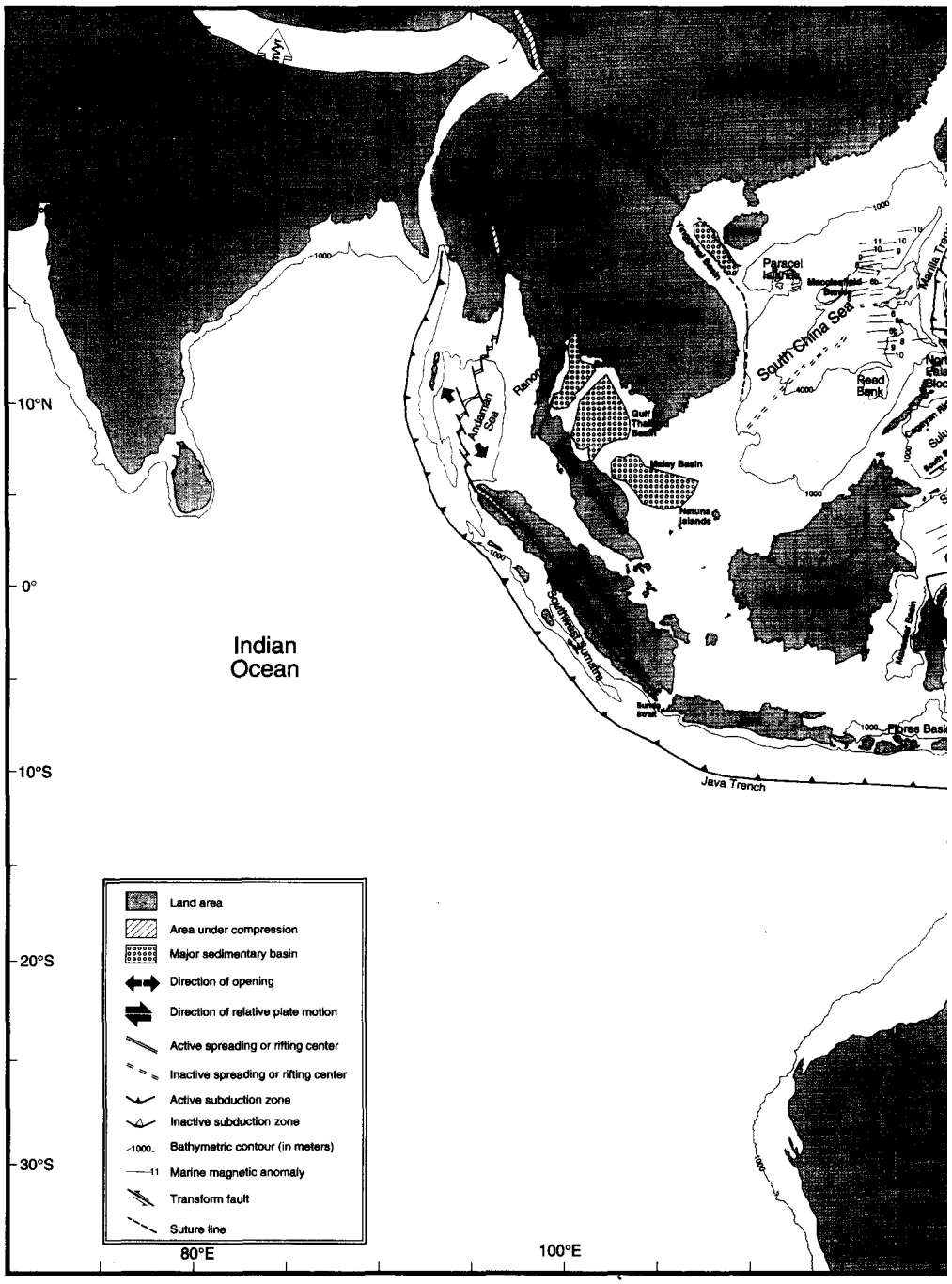

Fig. 15. Pliocene (5 Ma) plate reconstruction of Southeast Asia. Open arrows and nunbers indicate convergence respect to the South China Block.

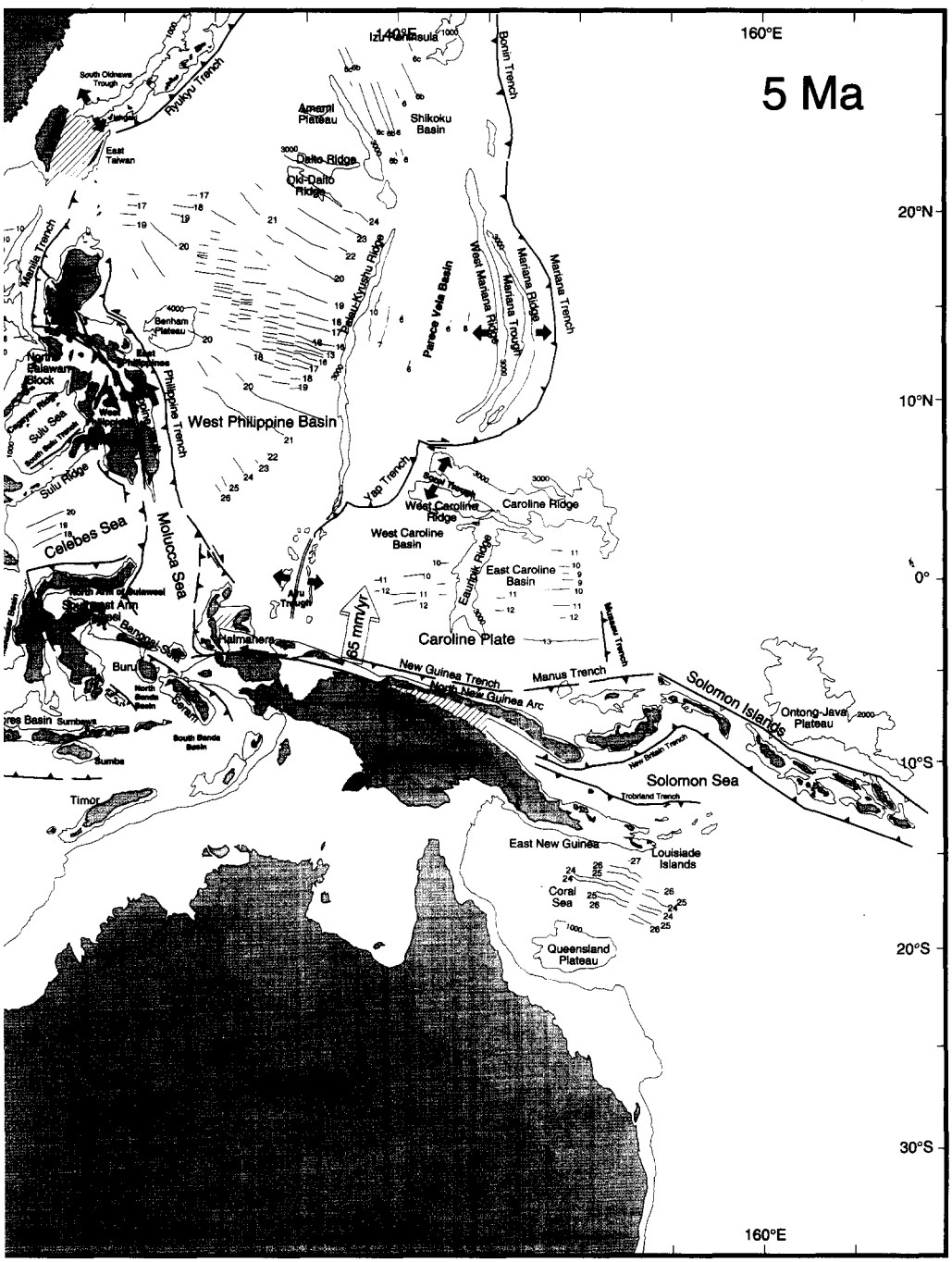

ence rates of major plates with

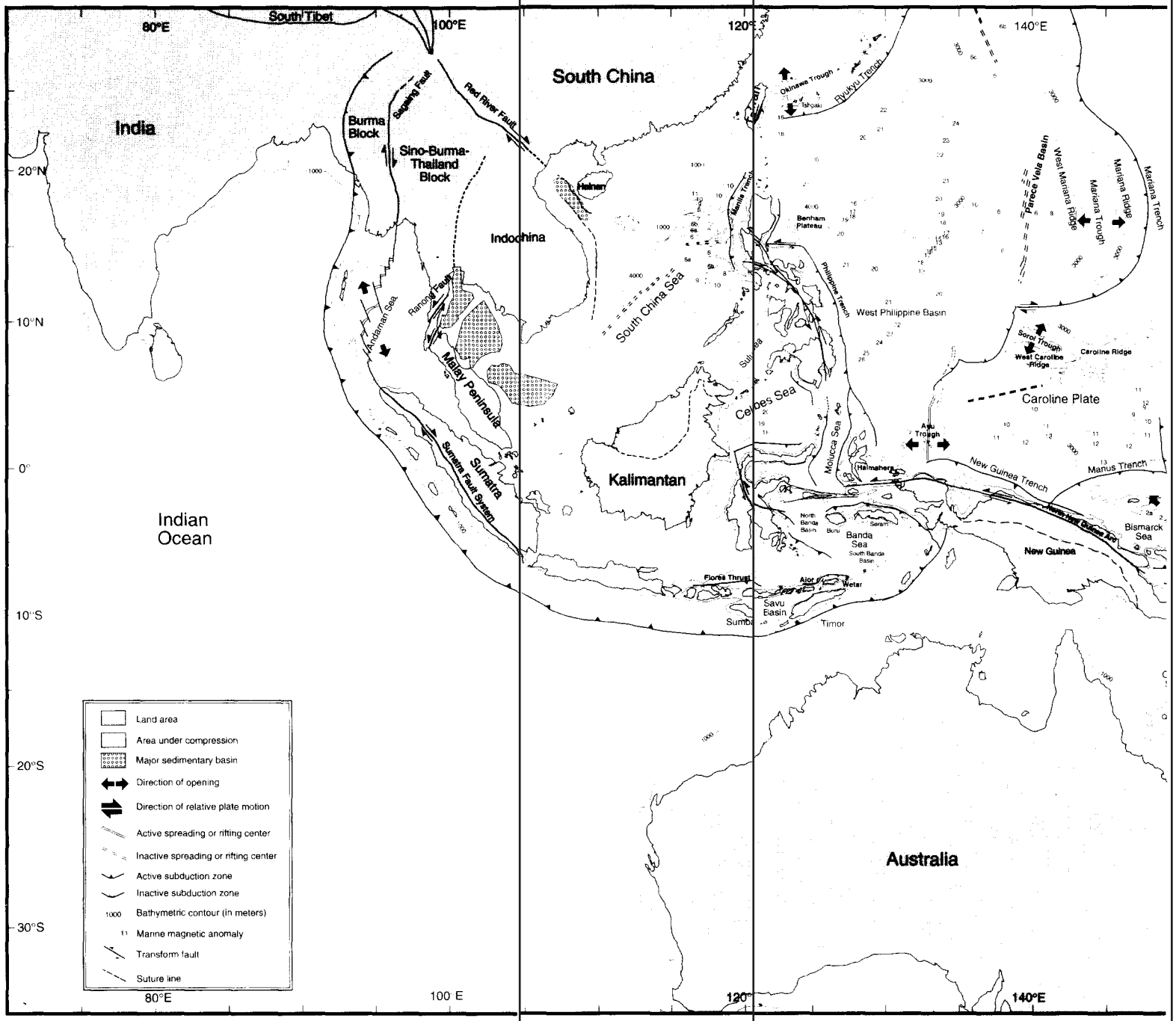

Fig. 16. Present-day (0 Ma) plate tectonics of Southeast Asia.

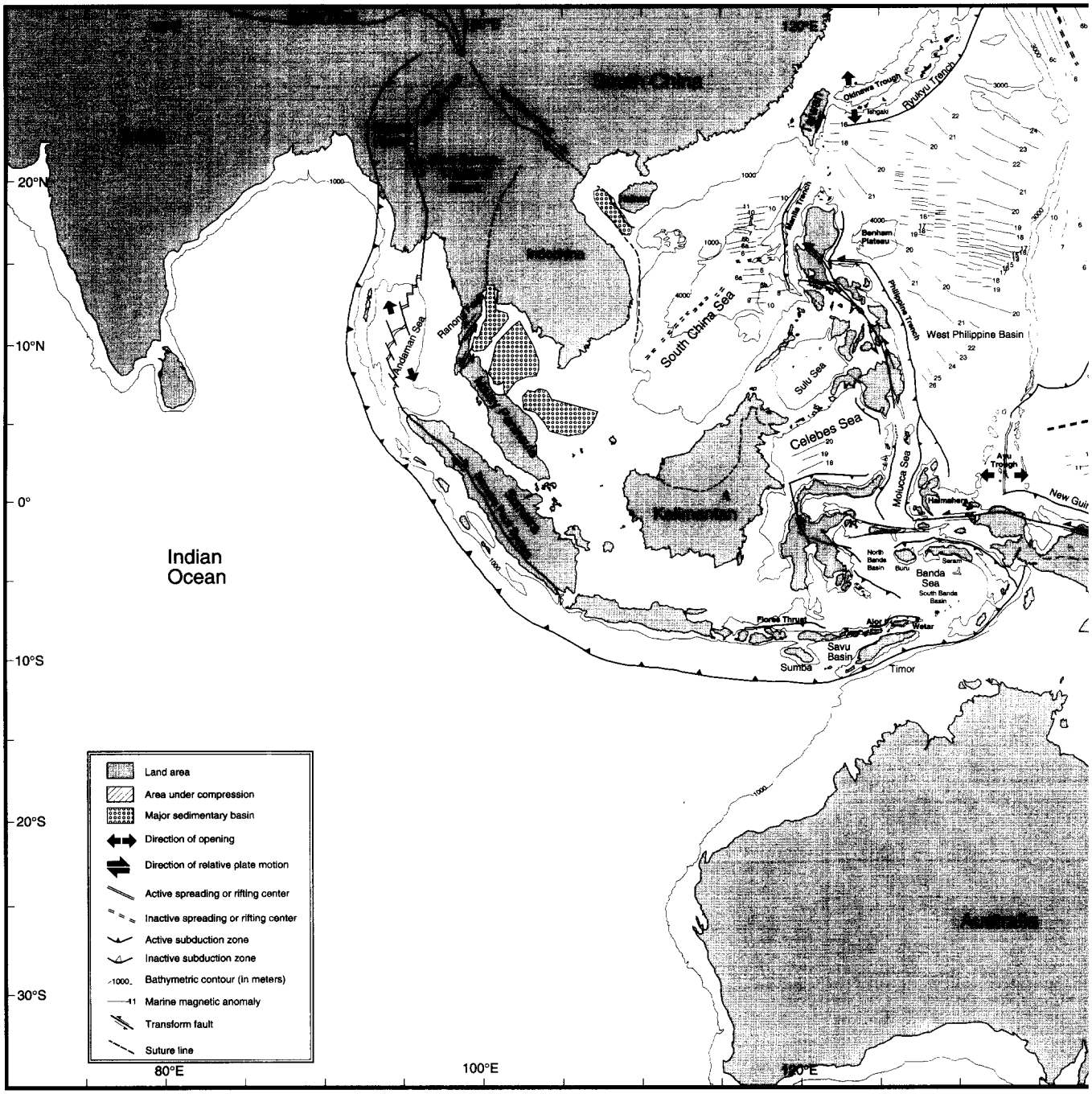

Fig. 16. Present-day (0 Ma) plate tectonics of Southeast Asia.

eastern margin of Kalimantan (Rangin and Silver, 1991). It is not clear whether Sulu Basin seafloor spreading resulted from southward subduction of proto-South China Sea crust at the Cagayan Ridge, or whether northwestward subduction of oceanic crust between the Philippine Archipelago and Sulu Ridge produced the Sulu sea as a back-arc basin. The collision between the North Palawan block and Kalimantan might also have terminated the opening of the Sulu Sea Basin in the Middle Miocene. Northward motion of Sulawesi, the Celebes Basin, and the Sulu Ridge may have initiated southwestward subduction of the Sulu Basin beneath the South Sulu Trench about 15 Ma (Rangin and Silver, 1991).

Seafloor spreading continued in the northern Parece Vela Basin, after the collision between the Caroline Ridge and Mariana Arc, until the Middle Miocene. This collision bent part of the Mariana Arc and converted the trench system into a right-lateral transform fault (McCabe and Uyeda, 1983). Docking of the East New Guinea Composite Terrane to the New Guinea–Australia continental margin at about 15 Ma (Pigram and Davies, 1987) probably shut off subduction to the south of the terrane. It is conceivable that the docking of the East New Guinea Composite Terrane led to the initiation of a new southward-dipping subduction belt north of the New Guinea–Australia continental margin resulting in an inversion of subduction polarity. This subduction zone consumed the Solomon Sea plate between the New Guinea–Australia continental margin and the North New Guinea Arc and brought the North New Guinea Arc into collision with New Guinea in the Late Miocene.

4.8. Late Miocene reconstruction (10 Ma; Fig. 14)

The collisions of the North Palawan block with first, the West Philippine Archipelago near Mindoro and Panay in the Late Miocene, and later the Sulu Ridge with the West Philippines at the Zamboanga Peninsula at the end of the Middle Miocene (Mitchell et al., 1986), resulted in decoupling of the Philippine Sea Plate from the Philippine Archipelago (McCabe and Cole, 1989). The collision resulted in a cessation of eastward subduction in the Manila Trench from Mindoro south to Panay and resulted in a polarity reversal of the subduction. Westward subduction was initiated along the east side of the Philippine Archipelago at the Philippine Trench (Uyeda and McCabe, 1983). This trench system probably extended all the way to northern Halmahera (Fig. 13). After the second collision, the West Philippine Archipelago was essentially attached to the South China block through Sundaland. The left-lateral Philippine Fault, including the Sibuyan branch as defined by Bischke et al. (1990), initiated motion between the East Philippines and the West Philippines blocks much as the Sumatran Fault System offsets the trenchward sliver of Southwest Sumatra from the remainder of Sumatra (Allen, 1962). In both cases the offset on the strike-slip fault resulted from oblique subduction. Motion along the Sumatran Fault System began at about 13 Ma (Huchon and Le Pichon, 1984), and it may be partially responsible for the observed crustal shortening (Hamilton, 1979) in northwest Sumatra. The opening of the Sunda Strait is also a result of the northwestward movement of the Southwest Sumatra block (Huchon and Le Pichon, 1984).

Collisions in the West Philippines also terminated the subduction belt west of the Molucca Sea between Mindanao and North Sulawesi. Halmahera is trapped between two subduction zones with both the Molucca and West Philippine sea plates subducting beneath it.

Identifiable Middle Miocene marine magnetic anomalies are found in the Central Andaman Sea (Curray et al., 1979). As Greater India continued its northward path, it seems to have ripped open the Andaman Sea as it moved northward. Initial northward motion did not involve the Sumatran Fault System but simply crossed the continental margin near 95°E. The Andaman and Nicobar islands formed as the Andaman Sea opened and the outer arc overrode the Indian plate. The rotation and northward movement of the north arm of Sulawesi may have resulted in the southward subduction of the Celebes Sea along the North Sulawesi Trench.

Subduction at the Ryukyu Trench produced active rifting in the Okinawa Trough northwest of the Ryukyu Trench in the Late Miocene (Letouzey and Kimura, 1985, Miki et al., 1990). The North New Guinea Arc collided with the northern New Guinea–Australia continental margin in early Late Miocene (Pigram and Davies, 1987). Post collision lateral translation caused the Banggai–Sula micro-

continent to collide with east Sulawesi (Hamilton, 1979). Collision of the Ontong–Java Plateau with the Solomon Islands led to the demise of the subduction belt north of the islands (Honza et al., 1987). This collision probably led to the subsequent development of the northerly dipping New Britain Trench south of the Solomon Islands in the Late Miocene–Pliocene.

4.9. Pliocene reconstruction (5 Ma; Fig. 15)

The Philippine Sea Plate has been consumed at both the Ryukyu and Philippine trenches. During the last few million years, subduction along the northern Manila Trench put the North Luzon Arc in collision with the East Asia continental margin at Taiwan (Suppe, 1981). Based on analysis of east Taiwanese geology, Teng (1990) indicated that the collision between the Luzon Arc and the East Asia continent began at 5 Ma. An estimated 200–300 km of crustal shortening in northern Taiwan has been attributed to the collision (Suppe, 1981). Prior to the opening of the South Okinawa Trough, the East Asia continental margin trended about 50° from southern Taiwan to the western tip of the Ryukyu Trench (Fig. 12). If the northern part of the North Luzon Arc extended to east Taiwan at 5 Ma, then the motion along the Philippine Fault can be estimated during this time. From the time of the collision of the Philippine Archipelago with the North Palawan block at the beginning of Late Miocene, which activated motion along the Philippine Fault, until 5 Ma when the North Luzon Arc collided with the South China block, the rate of motion along the Philippine Fault was ~ 41 mm/yr. After the collision, the calculated translation along the Philippine Fault slowed to ~ 21 mm/yr based on the total possible distance that the North Luzon Arc could have traveled before it collided with Taiwan. This estimation is compatible with the prediction of 20–25 mm/yr by Barrier et al. (1991). Even with the collision at Taiwan, subduction at the Ryukyu Trench to the northeast continued, resulting in continuous backarc spreading in the Okinawa Trough (Letouzey and Kimura, 1985).

The Molucca Sea Plate moved to the north along with the West Philippines. This northward movement was compensated by the northward movement of the New Guinea–Australia Plate and the subduction of the Molucca Sea Plate beneath the Halmahera. Therefore, the trench system northeast of the Halmahera would have a large right-lateral strike-slip component. It is reasonable to assume that the opening of the Ayu Trough is partially due to the need for space created by the northwestward motion of Halmahera. East of the Ayu Trough, because of the collision between the North New Guinea Arc and the northern New Guinea–Australia continental margin, new trench systems were initiated in response to the continued convergence between the Eurasia–Philippine Sea plates and the New Guinea–Australia Plate. With active subduction south of the Caroline Plate beneath the New Guinea and Manus trenches and east beneath the Mussau Trench, the major part of the Caroline Plate (West Caroline Ridge, West Caroline Basin, East Caroline Basin, and Eauripik Ridge) has undergone a counterclockwise rotation. This rotation was necessary to pull apart the Sorol Trough between the Caroline Ridge and the West Caroline Ridge and the Ayu Trough west of the Caroline Plate.

In the reconstructions for the Mariana Ridges (Figs. 14 and 15), it is impossible to fully close the Mariana Basin by applying a finite rotation of the Mariana Ridge with respect to the West Mariana Ridge. There are two possibilities to explain that. First of all, the basin has a differential spreading history (i.e. faster in the center and slower at both ends). Or, as suggested by McCabe and Uyeda (1983), a collision of the Caroline Ridge with the proto-Mariana Yap Arc during the Late Oligocene produced the bending of the ridges. The latter explanation is supported by both paleomagnetic data and other geological and geophysical data from the region (McCabe, 1984), and it can be demonstrated from the reconstructions. A right-lateral transform developed at the southern end of the Mariana Trench (McCabe and Uyeda, 1983). This transform served as a nucleus for the development of spreading in the Mariana Trough.

4.10. Present (0 Ma; Fig. 16)

NW–SE opening of the Andaman Sea Basin continues to the present and at least 100 km of right-lateral motion along the Sumatran Fault System has occurred. Collision of the North Luzon Arc with the

Eurasia continental margin at Taiwan has since converted the suture zone, the Longitudinal Valley, into a left-lateral transform belt. The approach of the Benham Plateau to the Philippine Trench may have clogged the subduction zone and converted the segment east of Central Luzon into a left-lateral transform system similar to the one at the southern Mariana Trench (McCabe and Uyeda, 1983). Collision of the northwestern Australian passive continental margin with the Banda Arc generated the Timor allochthon described by Audley-Charles et al. (1988). Burke and Rutherford (1987) have suggested that the island of Sumba slid away from Timor to open up the Savu Basin as a result of the collision (Fig. 16). This collision possibly also offset the island of Wetar from the Alor to the west along a left-lateral strike-slip fault and produced the back arc thrust belts from Alor to Wetar (Breen et al., 1989).

The collision of the Ontong–Java Plateau with the Solomon Islands effectively blocked further subduction at the North Solomon Trench system (Honza et al., 1987). Subduction of the Solomon Sea Plate to the north along the New Britain Trench, subduction of Caroline Plate to the south along the Manus Trench, and the left-lateral strike-slip motion between the North New Guinea Arc and the northern New Guinea–Australia continental margin have probably all contributed to producing seafloor spreading in the Bismarck Basin since 3.5 Ma (Taylor, 1979; Weissel et al., 1982; Honza et al., 1987). Southward subduction of the Solomon Sea Plate beneath the Tribiand Arc is possibly responsible for the seafloor spreading in the Woodlark Basin since the Pliocene (Honza et al., 1987). The eastern part of the Woodlark Basin is being subducted at a high rate (> 100 mm/yr) beneath the Solomon Islands during the opening of the basin (Weissel et al., 1982).

5. Discussion

From the plate reconstructions of Southeast Asia, it is clear that collision tectonics plays an important role in the shaping of the present-day plate configuration in this area. A prominent example is the collision of India with Eurasia which resulted in Indochina being extruded to the southeast along the Red River Fault. This motion resulted in the consumption of the pre-existing proto-South China Sea along northeastern Kalimantan and led to the eventual opening of the South China Sea along the South China margin. Subsequent motion of the Sino-Burma–Thailand, Malay Peninsula, Sumatra, and Kalimantan blocks has produced a series of basins stretching from North Sumatra to central Thailand and on to the Natuna area. Arc–continent collisions at Palawan and Mindoro/Panay during the late Early Miocene stopped seafloor spreading in the South China Sea. Still, there are several problems concerning the opening of the marginal basins, change in slip senses of major faults, and modification of the propagating extrusion model need to be addressed.

5.1. Opening of the marginal basins

5.1.1. Sulu Basin

Lee and McCabe (1986) proposed that the Sulu Sea Basin formed between Anomaly 20 (46 Ma) and Anomaly 17 (41 Ma) time. Their age for the Sulu Basin has been used in the reconstructions presented by Daly et al. (1987), McCabe and Cole (1989), and Hutchison (1989a, b). The north end of Palawan Island is a continental fragment rifted off the South China margin with opening of the present-day South China Sea. The Cagayan Ridge has arc-like affinities which suggest that it may have been the magmatic arc that resulted from the southeastward subduction of the proto-South China Sea. This subduction of the proto-South China Sea caused the Sulu Basin to open as a back-arc basin behind the Cagayan Ridge during the Early Miocene. Opening of the Sulu Basin caused the southeastward migration of the Zamboanga Peninsula and the Sulu Ridge, which in turn collided with the northwestward migrating West Philippine Archipelago at Mindanao Island in the Middle Miocene. Recent ODP drilling in the Sulu Sea region (Rangin and Silver, 1991) supports this scenario and also helps to explain the Middle Miocene collision at Mindanao, which was first suggested by Mitchell et al. (1986).

5.1.2. Celebes Basin

Lee and McCabe (1986) proposed that the Celebes Basin formed between Anomaly 33 (73 Ma, beginning of the Maastrichtian) and Anomaly 30 (67 Ma,

end of the Maastrichtian) time. This age for the Celebes Sea was used in the reconstructions mentioned earlier (Daly et al., 1987; Hutchison, 1989b; McCabe and Cole, 1989). Rotation of the north arm of Sulawesi based on the paleomagnetic measurements of Otofuji et al. (1981) suggests that the Celebes Sea originated as a back-arc basin between the Eocene and Early Miocene. The reconstructions suggest that the volcanic arc systems that surround the Celebes Sea have been established since the Late Miocene (Fig. 14). Recent ODP drilling in the Celebes Sea (ODP Site 767) concluded that the Celebes Sea formed in the Middle Eocene under open-ocean conditions. Paleomagnetic evidence from the drilling apparently limits any latitudinal change of the Celebes Basin to less than 15° (Rangin and Silver, 1991). This interpretation matches with the reconstructions presented here.

5.1.3. Banda Sea

The origin of the deep, flat-lying South Banda Basin (between the Banda Ridge and the East Banda Arc to the south) is very different from that of the North Banda Basin (between east Sulawesi and Buru). The South Banda Basin may be a trapped piece of oceanic crust that was originally formed as part of the Indian or Australian plates (Figs. 14 and 15). Bowin et al. (1980) noted long wavelength, N60–70°E-trending magnetic anomalies in the South Banda Basin and inferred their correlation with the Cretaceous anomalies in the Wharton Basin of the eastern Indian Ocean. The age-vs.-depth relationship of the deep, flat-lying South Banda Basin also suggests a Late Cretaceous age. The North Banda Basin was part of the Molucca Sea Plate, but later it was cut off from the Molucca Sea by the collision between the Banggai–Sula microcontinent and East Sulawesi in Late Miocene (Hamilton, 1979, figs. 28 and 29). Bowin et al. (1980) suggested that the North Banda Basin is much younger, based on the roughness of the basement topography as well as the heat flow. The North Banda Basin may have opened in the Miocene as the result of collision of eastern Sulawesi with western Sulawesi. It is possible that southward subduction (Hamilton, 1979) beneath Seram and Buru has resulted in present-day back-arc basin formation on the north edge of the older South Banda Sea Basin. Bowin et al. (1980) found evidence from heat-flow data which supported the idea of present-day extension in the northern part of the Banda Sea Basin south of Seram and Buru.

5.1.4. West Philippine Basin

There are two major models for the origin of the West Philippine Basin. Uyeda and Ben-Avraham (1972), Hilde et al. (1977), and Hilde and Lee (1984) all favored the origin of the Philippine Sea Basin as a trapped seafloor, isolated from the Pacific–Kula system when the Pacific Plate motion changed from NW to WNW at about 43 Ma (Engebretson et al., 1984, 1985). If the Philippine Basin is trapped oceanic seafloor, then the NW–SE-trending abandoned spreading center may have been the connection between the India–Antarctica spreading center in the Wharton Basin, which is known to have large N–S offset transform faults, and the Kula–Pacific spreading center in the North Pacific. This implies that the Kula and Indian plates may have been moved as a single plate during the Early Cenozoic. If the India–Antarctica spreading center was connected to the Kula–Pacifc spreading center, then the collision of India with Eurasia may have contributed to the change in Pacific Plate motion at 43 Ma. The original NNW–SSE-trending transform faults became the sites of westward subduction with the change in the Pacific Plate motion at 43 Ma.

In contrast, Lewis et al. (1982) suggested that the Philippine Basin resulted from back-arc spreading. According to them, the associated volcanic arcs and accretionary wedges can be found in east Mindanao, Samar, and also on Luzon Island. The Daito and Oki–Daito Ridges southeast of the Japan Islands were interpreted by Lewis et al. (1982) to be remnant arcs, originally adjacent to the East Mindanao–Samar Arc. The paleomagnetic results for this region suggest a clockwise rotation of the Philippine Archipelago and the West Philippine Basin and an equatorial origin for the Philippine Archipelago (Shih, 1980; Jarrard and Sasajima, 1980). Therefore, Lewis et al. (1982) suggested that of the two models, a back-arc basin origin for the Philippine Basin is more probable. The calculated average convergence rate from the reconstruction for the West Philippine Basin with respect to East Asia for the past 60 Ma is 1.3°/Ma. This value agrees well with the calculations for the present-day kinematics between the

Philippine Sea Plate and the Eurasian Plate of Seno et al. (1987, 1993) - 1.0–1.1°/Ma - and Ranken et al. (1984) - 1.6°/Ma. Compared to the Paleocene–Early Eocene reconstructions (Figs. 8 and 9), the marine magnetic anomalies in the West Philippine Basin are perpendicular to the convergent direction between the Indo-Australia plate and the Philippine Archipelago. It is reasonable to assume that the West Philippine Basin originated as a back-arc basin behind the Philippine Islands in the Paleocene and since moved with the Philippine Islands until the Late Miocene collisions in the West Philippines (Mindoro/Panay and Mindanao) separated the motion between the West Philippine Basin and the Philippine Archipelago.

5.1.5. Proto-South China Sea

The reconstruction suggest that there had to be an older oceanic plate between the Palawan are and the present-day South China Sea between the Paleocene and Early Miocene (Figs. 8–12). We propose that this "space" was occupied by the "proto-South China Sea". Although some of the paleomagnetic data indicate a counterclockwise rotation of Kalimantan (Haile et al., 1977; Haile, 1979a; Schmidtke et al., 1990), the collision–extrusion model of Tapponnier et al. (1982) predicts a clockwise rotation of Kalimantan as a result of the opening of the South China Sea along the Red River Fault. As discussed earlier, recent paleomagnetic results of Lumadyo et al. (1990, 1993), which fix Kalimantan in its present-day orientation and preserve the proto-South China Sea, make it possible to avoid inconsistencies as demonstrated in the reconstructions. The proto-South China Sea would have been oriented in a NE–SW direction with possible opening in the NW–SE direction. It existed from about Late Cretaceous/Paleocene to Early Miocene, but subduction along the northwestern margin of Kalimantan and Palawan consumed the last of this ocean basin (Ludwig et al., 1979; Ben-Avraham and Emery, 1973).

5.1.6. Solomon Sea

The age estimation of the solomon Sea Basin has been refined by the new magnetic, heat-flow, and water-depth data published by Joshima and Honza (1987) and Joshima et al. (1987). Their data indicated essentially an Oligocene age for the Solomon Sea Basin. This age estimation is adopted in the reconstructions. It is possible to infer further that the opening of the Solomon Sea Basin resulted from spreading between the North New Guinea Arc and the East New Guinea Composite Terrane northwest of the New Guinea–Australia continental margin. Later, the basin was brought into contact with the New Guinea–Australia continental margin by subduction of the southeastern extension of the Molucca Sea Plate (Fig. 12).

5.2. Complexities of the Philippine Archipelago

In our reconstructions, the Philippine Arc was treated as a single unit since the Paleocene (except for East Mindoro and Zamboanga Peninsula), and the subduction system on the western side of the West Philippine Archipelago was considered to be a consistent plate boundary through time (Uyeda and McCabe, 1983). There is evidence to suggest a Cretaceous–Paleocene volcanic arc on Luzon Island (Blace et al., 1980; Karig, 1983), and also on the islands of Cebu, Marinduque, Samar, and East Mindanao (McCabe et al., 1985; Mitchell et al., 1986). The evdience implies that some form of consumptive plate boundary has existed in this region since the Cretaceous. There are also structural and stratigraphic studies to support an arc–arc collision which took place on eastern Mindanao in the middle Tertiary (Mitchell et al., 1986; Hawkins et al., 1985, Lewis et al., 1982). All the paleomagnetic measurements taken from the Philippines were from the central and northern parts of the archipelago. The paleomagnetic results show great discrepancies, which can be interpreted as either the Luzon block and the Philippines rotating counterclockwise (Fuller et al., 1983, 1989) or the Philippines rotating clockwise (McCabe et al., 1987). The situation is further complicated by block rotations along a megashear zone, the Philippine fault, as well as disruptions in the collision belts, e.g. the North Palawan and Mindoro arc–continent collision belt. Based on the paleomagnetic data discussed earlier, the Philippine Archipelago was constrained to rotate with the Philippine Sea plate prior to the Late Miocene. Although this assumption works well with the reconstructions, it is important to bear in mind both the possibility that separate motion occurred between the

Philippine Sea Plate and the Philippine Archipelago and that accretions of terranes to the Philippines may have distorted the paleomagnetic measurements.

5.3. Different slip senses of major faults

At least two transform faults, the Red River and the Ranong, have changed direction of their strike-slip motion during the Cenozoic. Change in slip direction during subsequent tectonic events (orogenies) may be a common geological occurrence according to Muehlberger (1986). The reversal of displacement along the Red River Fault is related to the slower southeastward extrusion rate of the Indochina/Sino-Burma–Thailand blocks compared to that of the South China block during the Middle Miocene.

A change in slip direction along the Ranong Fault explains the discrepancy between the 200 km of right-lateral displacement of an Upper Mesozoic structural belt that crosses the fault (Peltzer and Tapponnier, 1988, fig. 33), and the 4–6 km of left-lateral displacement found by the mapping of subsea structural features by Polachan et al. (1991). The need for the reversal in the slip direction was caused by differential rates of motion between the Sino-Burma–Thailand block and the Malay Peninsula. Observed right-lateral motion is related to the main stage for opening of the Gulf of Thailand and the Malay Basin, and later left-lateral motion is related to the opening of the central Thailand basins.

Certain structural events can be used to date the change in slip sense. In the case of the Red River Fault, it is marked by local unoconformities and high-angle reverse faults, as reported by Wang et al. (1989) from the Pearl River Mouth Basin. The exact timing of reversal of the Ranong Fault is less well constrained, but it probably occurred in the Early Miocene.

5.4. Propagating extrusion model

From our previous discussin, clearly some modifications to the propagating extrusion model are required. These might include:

(1) A "rigid" Sunda Shelf: the Sunda Shelf (Malay Peninsula, Sumatra, and Kalimantan; Fig. 1) is considered to be a rigid plate so the boundary conditions for this margin need to be reevaluated.

(2) Amount of rotation for Indochina: Indochina has apparently rotated about 18° since the Paleocene. This is in good agreement with the paleomagnetic results in this region (Jarrard and Sasajima, 1980; Achache et al., 1983; Maranate and Vella, 1986; Yan and Courtillot, 1989). A greater rotation requires crustal shortening between East Vietnam and West Hainan Island (Figs. 8–10).

(3) A dextral megashear zone in the Gulf of Thailand: if the opening of the central Thailand basins, the Gulf of Thailand, and the Malay Basin are taken into consideration, a dextral megashear zone is required to compensate the relative motion between Indochina and the Malay Peninsula (Figs. 10–12). Since the impact between Greater India and Southeast Asia was basically west of the Burma block, there is no reason to assume that Sumatra, the Malay Peninsula, and Kalimantan should extrude to the southeast first along the left-laterally displaced Mae Ping and Three Pagodas fault zones as suggested by Peltzer and Tapponnier (1988). Therefore, this megashear zone should have right-lateral displacement and can be represented by a series of NW–SE-trending strike-slip faults, e.g. Mae Ping and Three Pagodas fault zones. Furthermore, recent structural mapping in the Central Thailand did indicate possible transtensional dextral shear in a series of pull-apart basins (Polachan et al., 1991). This dextral megashear zone might even extend into western Kalimantan and serve as a boundary between the Indochina block and Kalimantan. The exact extension of this megashear zone is still open to question.

6. Correlation with India–Eurasia collision

Comparing Fig. 10, Fig. 11, and Fig. 12, the Greater India plate only had minimal contact with the Sino-Burma–Thailand and Indochina blocks at

Fig. 17. Flowline of a moving point (30°N, 80°E) on the Indian Continent with respect to Eurasia from 84 Ma to present.

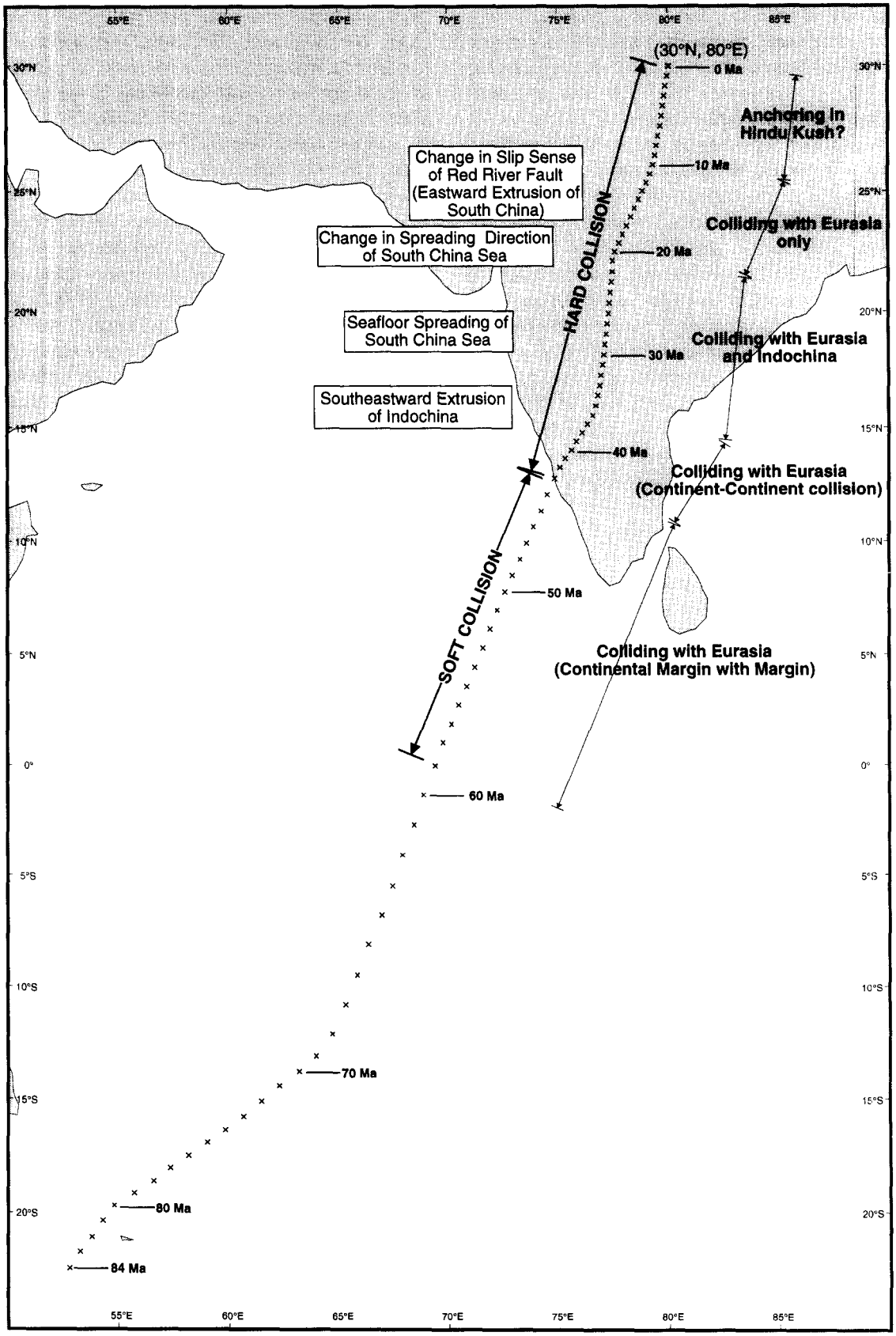
(30°N, 80°E)
0 Ma
10 Ma
20 Ma
30 Ma
40 Ma
50 Ma
60 Ma
70 Ma
80 Ma
84 Ma
HARD COLLISION
SOFT COLLISION
Change in Slip Sense of Red River Fault (Eastward Extrusion of South China)
Change in Spreading Direction of South China Sea
Seafloor Spreading of South China Sea
Southeastward Extrusion of Indochina
Anchoring in Hindu Kush?
Colliding with Eurasia only
Colliding with Eurasia and Indochina
Colliding with Eurasia (Continent-Continent collision)
Colliding with Eurasia (Continental Margin with Margin)
55°E
60°E
65°E
70°E
75°E
80°E
85°E
30°N
25°N
20°N
15°N
10°N
5°N
0°
5°S
10°S
15°S
20°S

40 Ma. By 30 Ma, a considerable portion of the Greater India plate had been brought into contact with the Sino-Burma–Thailand and Indochina blocks (Fig. 11). At that time, there was also a major episode of southeastward extrusion of Indochina as well as seafloor spreading in the South China Sea. The minor reduction in the convergence rate and the deflection of the convergence direction to the east in the Early Miocene coincided with a change in spreading direction in the South China Sea from N–S to NW–SE. The change may indicate that the Greater India plate was no longer in contact with the Sino-Burma–Thailand and Indochina blocks so there was a termination of southeastward extrusion of the Indochina block in the Early Miocene (Fig. 11). At the same time, northward directed collision between the Greater India and Eurasia plates probably caused the South China block to extrude to the east faster than the Indochina block. Consequently, the slip sense reversed along the Red River Fault (Figs. 13 and 14). The final stage of northerly motion of the Greater India plate can be explained as lithospheric anchoring of the Greater India plate at the Hindu Kush which caused a deflection of motion to the north. These tectonic events and the flowline of the Greater India plate are summarized in Fig. 17.

7. Summary

The India–Eurasia collision alone set up a series of chain reactions and caused the formation and destruction of sedimentary basins within the domain of the collision belt. Changes in the rate and angle of convergence between the India and Eurasia plates (Fig. 3) reflect different stages of tectonic development in Southeast Asia (Fig. 17). For example, extrusion of the Indochina block induced the consumption of the pre-existing proto-South China Sea along northeastern Kalimantan and led to the eventual opening of the South China Sea along the South China margin. Subsequent motions of the Sino-Burma–Thailand, Malay Peninsula, Sumatra, and Kalimantan blocks have produced a succession of basins stretching from North Sumatra to central Thailand and on the Natuna area (Figs. 10–12).

It is clear from the reconstructions (Figs. 10–12) that the impact between Greater India and Southeast Asia took place in the northwestern part of Southeast Asia. The duration for the impact was probably from the Middle Eocene to Early Miocene. This timing is in good agreement with the dating of the main Red River motion (Wu et al., 1989; Schärer et al., 1990). Since the impact between Greater India and Southeast Asia was basically west of the Burma block, there is no reason to assume that the Sumatra, the Malay Peninsula, and Kalimantan should extrude to the southeast first along the left-laterally displaced Mae Ping and Three Pagodas fault zones as suggested by Peltzer and Tapponnier (1988). If the opening of the central Thailand basins, the Gulf of Thailand, and the Malay Basin are taken into consideration, a dextral megashear zone is required to compensate the relative motion between Indochina and the Malay Peninsula (Figs. 10–13). This dextral megashear zone might even extend into western Kalimantan and serve as a boundary between the Indochina block and Kalimantan. The exact extension of this megashear zone is still open to question.

Acknowledgements

We thank I. Norton, C. Rangin, T. Hilde, and one anonymous reviewer for their critical reviews and comments. This study was partially supported by the PLATES Project at the Institute for Geophysics, University of Texas at Austin. The plate reconstruction of the Taiwan area was supported by the National Council (ROC) grant NSC84-2111-M-003-008GC to the first author.

References

Achache, J., Courtillot, V. and Besse, J., 1983. Paelomagnetic constraints on the Late Cretaceous and Cenozoic tectonics of southeastern Asia. Earth Planet. Sci. Lett., 63: 123–136.

Allen, C.R., 1962. Circum-Pacific faulting in the Philippines–Taiwan region. J. Geophys. Res., 67: 4795–4812.

Audley-Charles, M.G., Ballantyne, P.D. and Hall, R., 1988. Mesozoic–Cenozoic rift–drift sequence of Asian fragments from Gondwanaland. Tectonophysics, 155: 317–330.

Bao, C., 1987. Map of topography 1:2000000, Atlas of Geology and Geophysics of South China Sea. Map Publ. House Guangdong Province, Guangzhou.

Barrier, E., Huchon, P. and Aurelio, M., 1991. Philipine fault: A key for Philippine kinematics. Geology, 19: 32–35.

Ben-Avraham, Z. and Emery, K.O., 1973. Structural framework of Sunda Shelf. Am. Assoc. Pet. Geol. Bull., 57: 2323–2366.

Bènard, F., Muller, C., Letouzey, J., Rangin, C. and Tahir, S., 1990. Evidence of multiphase deformation in the Rajang–Crocher Range (northern Borneo) from Landsat imagery interpretation: Geodynamic implications. Tectonophysics, 183: 321–339.

Bird, P.R., Quinton, N.A., Beeson, M.N. and Bristow, C., 1993. Mindoro: A rifted microcontinent in collision with the Philippines volcanic are; basin evolution and hydrocarbon potential. J. Southeast Asian Earth Sci., 8: 449–468.

Bischke, R.E., Suppe, J. and Del Pilar, R., 1990. A new branch of the Philippine fault system as observed from aeromagnetic and seismic data. Tectonophysics, 183: 243–264.

Blace, G.R., Encina, R.Y., Momongan, A. and Lara, E., 1980. Geology of the Baguio district and its implication on the tectonic development of the Luzon Central Cordillera. Geol. Paleontol. Southeast Asia, 21: 265–287.

Bowin, C., Purdy, G.M., Johnston, C., Shor, G., Lawver, L.A., Hartono, H.M.S. and Jezek, P., 1980. Arc–continent collision in Banda Sea region. Am. Assoc. Pet. Geol. Bull., 64: 868–915.

Bracey, D.R., 1975. Reconnaissance geophysical survey of the Caroline Basin. Geol. Soc. Am. Bull., 86: 775–784.

Bracey, D.R., 1983. Geophysical and tectonic development of the Caroline Basin. US Naval Oceanogr. Off. Techn. Rep., TR-283, 82 pp.

Breen, N.A., Silver, E.A. and Roof, S., 1989. The Wetar back arc thrust belt, eastern Indonesia: The effect of accretion against an irregularly shaped arc. Tectonics, 8: 85–89.

Briais, A., Patriat, P. and Tapponnier, P., 1993. Updated interpretation of magnetic anomalies and seafloor spreading stages in the South China Sea: Implications for the Tertiary tectonics of Southeast Asia. J. Geophys. Res., 98: 6299–6328.

Burke, K. and Rutherford, E., 1987. Sumba as a sideways slipping sliver (unpubl. ms.).

Cardwell, R.K. and Isacks, B.L., 1981. A review of the configuration of the lithosphere subducted beneath the eastern Indonesian and Philippine Islands. In: A.J. Barber and S. Wiryosujono (Editors), The Geology and Tectonics of Eastern Indonesia. Geol. Res. Dev. Cent., Bandung, pp. 31–47.

Chamot-Rooke, N., Renard, V. and Le Pichon, X., 1987. Magnetic anomalies in the Shikoku Basin: A new interpretation. Earth Planet. Sci. Lett., 83: 214–228.

Chen, S., Li, Z. and Zou, Y., 1987. Major oil accumulation characteristics and exploration direction in the Pearl River Mouth Basin. China Oil, 17–23.

Curray, J.R., 1989. The Sundac Arc: A model for oblique plate convergence. Neth. J. Sea Res., 24: 131–140.

Curray, J.R., Moore, D.G., Lawver, L.A., Emmel, F.J., Raitt, R.W., Henry, M. and Kieckhefer, R., 1979. Tectonics of the Andaman Sea and Burma. In: J.S. Watkins, J. Montadert and P.W. Dickerson (Editors), Geological and Geophyscial Investigations of Continental Margins. Am. Assoc. Pet. Geol. Mem., 29: 189–198.

Daly, M.C., Hooper, B.G.D. and Smit, D.G., 1987. Tertiary plate tectonics and basin evolution in Indonesia. Proc. Indones. Pet. Assoc. 16th Annu. Conv., pp. 399–428.

Daly, M.C., Cooper, M.A., Wilson, I., Smith, D.G. and Hooper, B.G.D., 1991. Cenozoic plate tectonics and basin evolution in Indonesia. Mar. Pet. Geol., 8: 2–21.

Dewey, J.F., Cande, S. and Pitman III, W.C., 1989. Tectonic evolution of the India/Eurasia collision zone. Eclogae Geol. Helv., 82: 717–734.

Engebretson, D.C., Cox, A. and Gordon, R.G., 1984. Relative motions between oceanic plates of the Pacific Basin. J. Geophys. Res., 89: 10,291–10,310.

Engebretson, D.C., Cox, A. and Gordon, R.G., 1985. Relative motions between oceanic and continental plates in the Pacific Basin. Geol. Soc. Am. Spec. Pap., 206, 59 pp.

Fainstein, R. and Pramono, H., 1986. Structure and stratigraphy of Avs Field, Java Sea. Indones. Pet. Assoc. 15th Annu. Conv., pp. 19–45.

Feng, Z. and Zhang, W., 1986. Tectonic evolution of Zhujiangkou (Pearl-River-Mouth) basin and origin of South China Sea. In: J. Huang (Editor), Symposium on Mesozoic and Cenozoic Geology in Connection of the 60th Anniversary of the Geological Society of China, pp. 283–296.

Fuller, M., McCabe, R., Williams, I.S., Almasco, J., Encina, R.Y., Zanoria, A.S. and Wolfe, J.A., 1983. Paleomagnetism of Luzon. In: D.E. Hayes (Editor), The Tectonic and Geologic Evolution of Southeast Asian Seas and Islands, 2. Am. Geophys. Union, Washington, DC, pp. 79–94.

Fuller, M., Haston, R. and Almasco, J., 1989. Paleomagnetism of the Zambales ophiolite, Luzon, northern Philippines. Tectonophysics, 168: 171–203.

GEBCO, 1981. General Bathymetric Chart of the Oceans. Can. Hydrogr. Serv., Ottawa.

Haile, N.S., 1979a. Rotation of Borneo microplate completed by Miocene: Paleomagnetic evidence. Warta Geol., 5: 19–22.

Haile, N.S., 1979b. Paleomagnetic evidence for the rotation of Seram, Indonesia. In: S. Uyeda, R.W. Murphy and K. Kobayashi (Editors), Geodynamics of the Western Pacific. Cent. Acad. Publ. Jpn., Tokyo, pp. 191–198.

Haile, N.S., McElhinny, M.W. and McDougall, I., 1977. Paleomagnetic data and radiometric ages from the Cretaceous of west kalimantan (Borneo), and their significance in interpreting regional structure. J. Geol. Soc. London, 133: 133–144.

Hall, R., 1987. Plate boundary evolution in the Halmahera region, Indonesia. Tectonophysics, 144: 337–352.

Hamilton, W., 1979. Tectonics of the Indonesian region. US Geol. Surv. Prof. Pap., 1078, 345 pp.

Hawkins, J.W., Moore, G.F., Villamor, R., Evans, C. and Wright, E., 1985. Geology of the composite terranes of east and central Mindanao. In: D.G. Howell (Editor), Tectonostratigraphic Terranes of the Circum-Pacific Region. Circum-Pac. Counc. Energy Miner. Resour., Houston, TX, pp. 437–463.

Hayes, D.E., 1988. The tectonic evolution of the South China Sea region. 1988 DELP Tokyo Int. Symp.: Tectonics of Eastern Asia and Western Pacific Continental Margin, pp. 68–69.

Hilde, T.W.C. and Lee, C.S., 1984. Origin and evolution of the West Philippine Basin: A new interpretation. Tectonophysics, 102: 85–104.

Hilde, T.W.C., Uyeda, S. and Kroenke, L., 1977. Evolution of the western Pacific and its margin. Tectonophysics, 38: 145–165.

Ho, C.S., 1986. A synthesis of the geologic evolution of Taiwan. Tectonophysics, 125: 1–16.

Holloway, N.H., 1982. North Palawan block, Philippines-its relation to Asian mainland and role in evolution of South China Sea. Am. Assoc. Pet. Geol. Bull., 66: 1355–1383.

Honza, E., Davies, H.L., Keene, J.B. and Tiffin, D.L., 1987. Plate boundaries and evolution of the Solomon Sea region. Geo-Mar. Lett., 7: 161–168.

Huchon, P. and Le Pichon, X., 1984. Sunda Strait and Central Sumatra Fault. Geology, 12: 668–672.

Hutchison, C.S., 1975. Ophiolites in Southeast Asia. Geol. Soc. Am. Bull., 86: 61–86.

Hutchison, C.S., 1989a. Displaced terranes of the Southwest Pacific. In: Z. Ben-Avraham (Editor), The Evolution of the Pacific Ocean Margins. Oxford Univ. Press, New York, NY, pp. 161–175.

Hutchison, C.S., 1989b. Geological Evolution of South-east Asia. Clarendon, Oxford, 368 pp.

Jarrard, R.D. and Sasajima, S., 1980. Paleomagnetic synthesis for Southeast Asia: Constraints on plate motions. In: D.E. Hayes (Editor), The Tectonic and Geologic Evolution of Southeast Asian Seas and Islands. Am. Geophys. Union, Washington, DC, pp. 293–316.

Karig, D.E., 1983. Temporal relationships between back arc basin formation and arc volcanism with special reference to the Philippine Sea. In: D.E. Hayes (Editor), The Tectonic and Geologic Evolution of Southeast Asian Seas and Islands, 2. Am. Geophys. Union, Washington, DC, pp. 318–325.

Klootwijk, C.T., Gee, J.S., Peirce, J.W., Smith, G.M. and McFadden, P.L., 1992. An early India–Asia contact: Paleomagnetic constraints from Ninetyeast Ridge, ODP Leg 121. Geology, 20: 395–398.

Lee, C.S. and McCabe, R., 196. The Banda–Celebes–Sulu basin: A trapped piece of Cretaceous–Eocene Oceanic crust? Nature, 322: 51–54.

Lee, G., Besse, J., Courtillot, V. and Montigny, R., 1987. Eastern Asia in the Cretaceous: New paleomagnetic data from South Korea and a new look at Chinese and Japanese data. J. Geophys. Res., 92: 3580–3596.

Letouzey, J. and Kimura, M., 1985. Okinawa Trough genesis: Structure and evolution of a backarc basin developed in a continent. Mar. Pet. Geol., 2: 111–130.

Letouzey, J. and Sage, L., 1988. Geological and Structural Map of Eastern Asia. Am. Assoc. Pet. Geol., Tulsa, OK.

Lewis, S.D., Mrozowski, C.L. and Hayes, D.E., 1982. The origin of the West Philippine Basin by inter-arc spreading. In: G.R. Brace and A.S. Zanoria (Editors), Geology and Tectonics of the Luzon–Marianas Region. SEATAR Workshop Luzon–Marianas Transect, Manila 1981, pp. 31–51.

Liu, Z. and Yang, S., 1988. The Tectonics of the South China Sea and Spreading of the Continental Margins. South China Sea Inst. Oceanol. Acad. Sin., Beijing, 398 pp. (in Chinese).

Ludwig, W.J., Kumar, N. and Houtz, R.E., 1979. Profiler-Sonobuoy measurements in the South China Sea Basin. J. Geophys. Res., 4: 3505–3518.

Lumadyo, E., McCabe, R., Harder, S., Merill, D. and Lee, T., 1990. Borneo: A stable portion of the Eurasian margin since the Eocene. EOS Trans. Am. Geophys. Union, 71: 1642.

Lumadyo, E., McCabe, R., Harder, S. and Lee. T., 1993. Borneo: A stable portion of the Eurasian margin since the Eocene. J. Southeast Asian Earth Sci., 8: 225–231.

Maranate, s. and Vella, P., 1986. Paleomagnetism of the Khorat Group, Mesozoic, northeast Thailand. J. Southeast Asian Earth Sci. Res., 1: 23–31.

Marchadier, Y. and Rangin, C., 1990. Polyphase tectonics at the southern tip of the Manila trench, Mindoro–Tablas Islands, Philippines. Tectonophysics, 183: 273–287.

McCabe, R.E., 1984. Implications of paleomagnetic data on the collision related bending of island arcs. Tectonics, 3: 409–428.

McCabe, R. and Cole, J., 1989. Speculations on the Late Mesozoic and Cenozoic evolution of the Southeast Asian margin. In: Z. Ben-Avraham (Editor), The Evolution of the Pacific Ocean Margins. Oxford Univ. Press, New York, NY, pp. 143–160.

McCabe, R. and Uyeda, S., 1983. Hypothetical model for the bending of the Mariana Arc. In: D.E. Hayes (Editor), The Tectonic and Geologic Evolution of Southeast Asian Seas and Islands, 2. Am. Geophys. Union, Washington, DC, pp. 281–293.

McCabe, R.E., Almasco, J.N. and Yumul, G., 1985. Terrances of the central Philippines. In: D.G. Howell (Editor), Tectonostratigraphic Terranes of the Circum-Pacific Region. Circum-Pac. Counc. Energy Miner. Resour., Houston, TX, pp. 421–435.

McCabe, R., Kikawa, E., Cole, J.T., Malicse, A.J., Baldauf, P.E., Yumul, J. and Almasco, J., 1987. Paleomagnetic results from Luzon and the central Philippines. J. Geophys. Res., 92: 555–580.

McCabe, R.E., Celaya, M., Cole, J., Han, H.-C., Ohnstad, T., Paijitprapapon, V. and Thitipawarn, V., 1988. Extension tectonics: The Neogene opening of the north–south trending basins of Central Thailand. J. Geophys. Res., 93: 11,899–11,910.

Miki, M., Matsuda, T. and Otofuji, Y., 1990. Opening of the Okinawa Trough: Paleomagnetic evidence from the South Ryukyu Arc. Tectonophysics, 175: 335–347.

Mitchell, A.H.G. Hernandez, F. and Dela Cruz, A.P., 1986. Cenozoic evolution of the Philippine Archipelago. J. Southeast Asian Earth Sci., 1: 3–22.

Mrozowski, C.L. and Hayes, D.E., 1979. The evolution of the Parece Vela Basin, eastern Philippine Sea. Earth Planet. Sci. Lett., 46: 49–67.

Muehlberger, W.R., 1986. Different slip senses of major faults during different orogenies: The rules? 6th Int. Conf. Basement Tectonics. Int. Basement Tectonics Assoc., pp. 76–81.

Müller, R.D. and Roest, W.R., 1992. Fracture zones in the North Atlantic from combined Geosat and Seasat data. J. Geophys. Res., 97: 3337–3350.

Müller, R.D., Royer, J.-Y. and Lawyer, L.A., 1992. Revised plate motions relative to the hotspots from combined Atlantic and Indian Ocean Hotspot tracks. Geology, in press.

Nakanishi, M., Tamaki, K. and Kobayashi, K., 1989. Mesozoic

magnetic anomaly lineations and seafloor spreading history of the Northwestern Pacific. J. Geophys. Res., 94: 15,437–15,462.

Otofuji, Y. Sasajima, S., Nishimura, S., Dharma, A. and Hehuwat, F., 1981. Paleomagnetic evidence for clockwise rotation of the northern arm of Sulawesi, Indonesia. Earth Planet. Sci. Lett., 54: 272–280.

Parker, E.K. and Gealey, W.K., 1985. Plate tectonic evolution of the western Pacific–Indian Ocean region. Energy, 10: 249–261.

Patriat, P. and Achache, J., 1984. India–Eurasia collision chronology has implications for driving mechanism of plates. Nature, 311: 615–621.

Pautot, G., Rangin, C., Briais, A., Tapponnier, P., Beuzart, P., Lericolais, G., Mathieu, X., Wu, J., Han, S., Li, H., Lu, Y. and Zhao, J., 1986. Spreading direction in the central South China Sea. Nature, 321: 150–154.

Peltzer, G. and Tapponnier, P., 1988. Formation and evolution of strike-slip faults, rifts, and basins during the India–Asia collision: An experimental approach. J. Geophys. Res., 93: 15,085–15,117.

Pigram, C.J. and Davies, H.L., 1987. Terranes and the accretion history of the New Guinea orogen. J. Aust. Geol. Geophys. Bur. Miner. Resour., 10: 193–211.

Pigram, C.J. and Panggabean, H., 1984. Rifting of the northern margin of the Australian continent and the origin of some microcontinents in eastern Indonesia. Tectonophysics, 107: 331–353.

Polachan, S., Pradidtan, S., Tongtaow, C., Janmaha, S., Intarawijitr, K. and Sangsuwan, C., 1991. Development of Cenozoic basins in Thailand. Mar. Pet. Geol., 8: 84–97.

Ponto, C.V., Wu, C.H., Pranoto. A. and Stinson, W.H., 1988. Improved interpretation of the Talang Akar depositional environment as an aid to hydrocarbon exploration in the ARII offshore Northwest Java Contract area. Proc. Indones. Pet. Assoc. 16th Annu. Conv., pp. 397–422.

Rangin, C., 1989. The Sulu Sea, a back-arc basin setting within a Neogene collision zone. Tectonophysics, 161: 119–141.

Rangin, C. and Silver, E.A., 1991. Neogene tectonic evolution of the Celebes–Sulu basins: New insights from Leg 124 drilling. Proc. ODP Sci. Results, 124: 51–63.

Rangin, C., Jolivet, L., Pubellier, M. and Group, T.P.W., 1990. A simple model for the tectonic evolution of Southeast Asia and Indonesia region for the past 43 m.y. Bull. Soc. Gèol. Fr., 8: 889–905.

Ranken, B., Cardwell, R.K. and Karig, D.E., 1984. Kinematics of the Philippine Sea plate. Tectonics, 3: 555–575.

Richard, M., Bellon, H., Maury, R.C., Barrier, E. and Juang, W.-S., 1986. Miocene to recent calc-alkalic volcanism in eastern Taiwan: K–Ar ages and petrography. Tectonophysics, 125: 87–102.

Royer, J.-Y. and Chang, T., 1991. Evidence for relative motions between the Indian and Australian plates during the last 20 m.y. from plate tectonic reconstructions: Implications for the deformation of the Indo-Australian plate. J. Geophys. Res., 96: 11,779–11,802.

Royer, J.-Y. and Sandwell, D.T., 1989. Evolution of the Eastern Indian Ocean since the Late Cretaceous: Constraints from Geosat altimetry. J. Geophys. Res., 94: 13,755–13,782.

Ru, K., 1988. The development of superimposed basins on the northern margin of the South China Sea and its tectonic significance. Oil Gas Geol., 9: 22–31 (in Chinese with English abstract).

Sarewitz, D.R. and Karig, D.E., 1986. Geologic evolution of western Mindoro Island and Mindoro suture zone, Philippines. J. of Southeast Asian Earth Sci., 1: 117–141.

Schärer, U., Tapponnier, P., Lacassin, R., Leloup, P.H., Zhong, D. and Ji, S., 1990. Intraplate tectonics in Asia: A precise age for large-scale Miocene movement along the Ailao Shan–Red River shear zone, China. Earth Planet. Sci. Lett., 97: 65–77.

Schmidtke, E., Fuller, M. and Haston, R., 1990. Paleomagnetic data from Sarawak, Malaysian Borneo, and the Late Mesozoic and Cenozoic tectonics of Sundaland. Tectonics, 9: 123–140.

Seno, T., Maruyama, S., Stein S., Woods, D.F., Demets, D., Argus, D. and Gordon, R., 1987. Redetermination of the Philippine Sea Plate motion. EOS Trans. Am. Geophys. Union, 68: 1474.

Seno, T., Stein, S. and Gripp, A.E., 1993. A model for the motion of the Philippine Sea Plate consistent with NUVEL-1 and geologic data. J. Geophys. Res., 98: 17,941–17,948.

Shih, T.C., 1980. Marine magnetic anomalies from the western Philippine Sea: Implications for the evolution of marginal basins. In: D.E. Hayes (Editor), The Tectonic and Geologic Evolution of Southeast Asian Seas and Islands. Am. Geophys. Union, Washington, DC, pp. 49–75.

Silver, E.A., Rangin, C., Von Breymann, M.T., et al., 1991. Proc. ODP Sci. Results, 124.

Situmorang, B., 1982a. Formation, evolution, and hydrocarbon prospect of the Makassar Basin, Indonesia. In: S.T. Watson (Editor), Trans. 3rd Circum-Pacific Energy and Mineral Resources Conference. Am. Assoc. Pet. Geol., Tulsa, OK, pp. 227–231.

Situmorang, B., 1982b. The formation of the Makassar Basin as determined from subsidence curves. Proc. Indones. Pet. Assoc. 11th Annu. Conv., pp. 83–107.

St. John, B., 1984. Sedimentary Provinces of the World - Hydrocarbon Productive and Nonproductive. Williams&Heinz, Capitol Heights, MD.

Suppe, J., 1981. Mechanics of mountain building and metamorphism in Taiwan. Geol. Soc. China Mem., 4: 67–89.

Surmont, J., Laj, C., Kissel, C., Rangin, C., Bellon, H. and Priadi, B., 1994. New paleomagnetic constraints on the Cenozoic tectonic evolution of the North Arm of Sulawesi, Indonesia. Earth Planet. Sci. Lett., 121: 629–638.

Tapponnier, P., Peltzer, G., Le Dain, A.Y. and Armijo, R., 1982. Propagating extrusion tectonics in Asia: New insights from simple experiments with plasticine. Geology, 10: 611–616.

Tapponnier, P., Peltzer, G. and Armijo, R., 1986. On the mechanics of the collision between India and Asia. In: M.P. Coward and A.C. Ries (Editors), Collision Tectonics. Blackwell, Oxford, pp. 115–157.

Tapponnier, P., Lacassin, R., Leloup, P.H., Schärer, U., Zhou, D., Wu, H., Liu, X., Ji., S., Zhang, L. and Zhong, J., 1990. The Ailao Shan/Red River metamorphic belt: Tertiary left-lateral

shear between Indochina and South China. Nature, 343: 431–437.

Taylor, B., 1979. Bismarck Sea: Evolution of a back-arc basin. Geology, 7: 171–174.

Taylor, B. and Hayes, D.E., 1980. The tectonic evolution of the South China Basin. In: D.E. Hayes (Editor), The Tectonic and Geologic Evolution of Southeast Asian Seas and Islands, 1. Am. Geophys. Union, Washington, DC, pp. 89–104.

Taylor, B. and Hayes, D.E., 1983. Origin and history of the South China Sea Basin. In: D.E. Hayes (Editor), The Tectonic and Geologic Evolution of Southeast Asian Seas and Islands, 2. Am. Geophys. Union, Washington, DC, pp. 23–56.

Taylor, B. and Rangin, C., 1988. Tertiary right-lateral pull-apart basins along the Asian–Pacific margin: Constraints on the propogating extrusion model of Indo-Asian tectonics. Int. Symp. Geodynamic Evolution of Eastern Eurasian Margin, September 13–20, Paris, p. 100.

Teng, L.S., 1990. Geotectonic evolution of Late Cenozoic arc–continental collision in Taiwan. Tectonophysics, 183: 57–26.

Uyeda, S. and Ben-Avraham, Z., 1972. Origin and development of the Philippine Sea. Nature, 240: 176–178.

Uyeda, S. and McCabe, R., 1983. A Possible mechanism of episodic spreading of the Philippine Sea. In: M. Hashimoto and S. Uyeda (Editors), Accretion Tectonics in the Circum-Pacific Pacific Regions. Terra, Tokyo, pp. 291–306.

Wang, X., Yan, J. and Lin, J., 1989. The inverted structure and its significance in petroleum geology. Earth Sci. J. China Univ. Geosci., 14: 101–108 (in Chinese with English abstract).

Weissel, J.K., 1980. Evidence for Eocene oceanic crust in the Celebes Basin. In: D.E. Hayes (Editor), The Tectonic and Geologic Evolution of Southeast Asian Seas and Islands, 1. Am. Geophys. Union, Washington, DC, pp. 37–48.

Weissel, J.K. and Watts, A.B., 1979. Tectonic evolution of the Coral Sea Basin. J. Geophys. Res., 84: 4572–4582.

Weissel, J.K., Taylor, B. and Karner, G.D., 1982. The opening of the Woodlark Basin, subduction of the Woodlark spreading system, and the evolution of northern Melanesia since mid-Pliocene time. Tectonophysics, 87: 253–277.

Williams, P.R., Johnston, C.R., Almond, R.A. and Simamora, W.H., 1988. Late Cretaceous to Early Tertiary structural elements of West Kalimantan. Tectonophysics, 148: 279–297.

Wirojudo, G.T. and Wongsosantiko, A., 1985. Tertiary tectonic evolution and related hydrocarbon potential in the Natuna area. Energy, 10: 433–455.

Wu, H., Zhang, L. and Ji, S., 1989. The Red River–Ailaoshan fault zone–Himalayan large sinistral strike-slip intracontinental shear zone. Sci. Geol. Sin., 1–8 (in Chinese with English abstract).

Yan, C. and Courtillot, V., 1989. Widespread Cenozic (?) remagmetization in Thailand and its implications for India–Asia Collision. Earth Planet. Sci. Lett., 93: 113–122.

Yu, H.-S., 1988. Comparative structure and stratigraphy of the Tertiary basins off the southeastern China coast. Proc. 2nd Taiwan Symp. Geophysics, pp. 350–354.

Annex B55

G. Einsele et al., "The Himalaya-Bengal Fan Denudation-Accumulation System during the Past 20 Ma", *The Journal of Geology*, Vol. 104, No. 2 (1996)

The Himalaya–Bengal Fan Denudation-Accumulation System during the Past 20 Ma[1]

Gerhard Einsele, Lothar Ratschbacher,[2] Andreas Wetzel[3]
Geologisches Institut, Universität, D-72076 Tübingen, Germany

ABSTRACT

Mass balances for both denudation in the Himalayas and sediment accumulation in the Subhimalayan basins, including the Bengal deep-sea fan but excluding the Indus fan, yield 7.1 × 10^6 km^3 and 7.4 × 10^6 km^3 (s ± 20%, rock of 2.75 g/cm^3 density), respectively, for the past 20 million years. Coarsening and increased sediment accumulation rates in the foreland basin and in the Bengal foredeep indicate accentuated tectonic activity and unroofing in the Himalayas since that time. The sediment volume includes ≥1 × 10^6 km^3 of Neogene Bengal fan sediment that was lost via the Nicobar fan to the Sunda accretionary wedge. In addition, the Indian peninsular rivers contributed about c. 0.6 × 10^6 km^3 of solid load to the basins. Average denudation during the past 20 m.y., as derived from geothermobarometric data and restored cross sections, occurred most rapidly along the High Himalayan crystalline chain (vertical unroofing c. 1000 m/m.y.; northward lateral retreat of southern Himalayan slope, exposed to monsoonal rain, ≤3.5 km/m.y.) and much slower in the Tethyan sedimentary zone to the north (average 150 m/m.y.). The solute loads of the modern Himalayan rivers indicate a mean chemical denudation rate of 17 m/m.y. The distinct decrease in sediment accumulation on the outer Bengal fan between about 7 and 1 Ma (in contrast to the Indus fan) is probably caused by exogenic factors rather than by a significant decline in tectonic activity. Pre-20 Ma sediments in the Subhimalayan basins were derived mainly from the southern margin of the Tibet plateau or from sources outside the study area.

Introduction

Increasing information about the evolution of the Himalayas and correlated sedimentary basins, its effects on regional and global climate (e.g., Kootwijk et al. 1992; Raymo and Ruddiman 1992; Molnar et al. 1993), and sea water chemistry (e.g., Hodell et al. 1991; but also see Rea 1992) encouraged us to attempt a quantification of both denudation and sediment accumulation for this most spectacular geological system of the modern world. Apart from basic insights into mountain building, this system demonstrates a huge exogenic cycle, in which the sediment fill of a number of basins is directly linked to an evolving orogenic belt. Besides yielding quantitative estimates, an important outcome of such a mass balance is the recognition of uncertainties and gaps in the knowledge of the areas in question.

Earlier studies related the volume of the Bengal fan to the solid load of the rivers Ganges and Brahmaputra and derived denudation rates for the Himalayas from the sediment volume (e.g., Curray and Moore 1971 and Curray et al. 1982 both cited *in* Curray 1994; Einsele 1992, p. 373–376). Le Pichon et al. (1992), Brookfield (1993), and Johnson (1994) considered the total area of Indian-Asian collision since about 55 Ma and included both the Bengal and Indus deep-sea fans as sites of most distal sediment accumulation.

We feel that the investigation of a more limited area for a shorter time period (the past 20 m.y.) can be carried out with more confidence. We therefore chose the Himalayan Range between the western and eastern syntaxes (drained by the Brahmaputra, Ganges, and Indus rivers) as the principal denudation area and a basin chain with the Bengal fan as the most distal repository of river sediment (figure 1*b*, and *d*). The reasons for this choice are as fol-

[1] Manuscript received March 3, 1994; accepted September 8, 1995.

[2] Present address: Geophysics Department, Stanford University, Stanford, CA 94305-2215, USA.
[3] Geologisches Institut der Universität, CH-4056 Basel, Switzerland.

[The Journal of Geology, 1996, volume 104, p. 163–184] 0022-1376/10402-0006$01.00

lows: (1) The pre-Miocene tectonic evolution of the Himalayas and the Tibet plateau is still poorly known and controversial (see below). (2) Less data on denudation are available for the exhumation of the tectonically complex Sulaiman Ranges and other mountain chains of western Pakistan than for the main Himalayan orogen. (3) It is problematic to define the paleo-drainage system of the pre-Miocene Himalayan rivers. (4) The areal distribution and volume of pre-Miocene sediments, a considerable part of which is incorporated into the accretionary wedges of the Indoburman ranges and the Sunda arc system, are more difficult to evaluate than the younger deposits (also see Brookfield 1993). (5) The sediment volumes of the Indus foredeep, the Indus delta, and the Indus deep-sea fan are difficult to asses. A portion of the northwestern paleo-Indus fan may have been subducted northward and incorporated into the Makran accretionary wedge (present rate of subduction c. 5 cm/yr—figure 1*a*; Farhoudi and Karig 1977). In addition, a large proportion of the Indus river load does not reach the deep-sea fan but is either dropped on land (Meade 1992) or transported along the coastline far to the southeast (Hovius 1993). The Bengal deep-sea fan (c. 3000 km in length, max. width of 1000 km) is considerably larger and better known than the Indus fan.

Note. Because of space limits, some relevant points in the context of this paper could not be discussed. Part of the data documentation (tables, I, II, and III) is deposited in The Journal of Geology Data Depository and referred to in the text as, e.g., table I (file). This material will be sent to anybody free of charge, either by the journal office or by the authors. The list of references was reduced by referring to previous publications with extensive bibliography (e.g., Burg et al. 1987 *in* Einsele et al. 1994). The reference list with full citations is also available from *The Journal of Geology* free of charge.

Structure and Evolution of the Himalayan-Tibetan Denudation Area

Present-Day Morphotectonic Zones. From north to south the denudation area of the Himalayan orogen is subdivided into the following morphotectonic belts (figure 2), which are bound by major, generally north-dipping thrust faults: (1) the Tibet plateau with the roots of the Cretaceous-Eocene magmatic arc of the Gangdese belt along the southern margin of the Lhasa block; (2) the Indus-Yarlung suture zone (IYS), including the ophiolite belt, the Mesozoic to Eocene mostly deep-water sedimentary rocks of the accretionary wedge, the late Cretaceous to Eocene sedimentary rocks of the Xigaze forearc basin, and the Oligocene to Miocene molasse-type, intermontane Indus-Kailas-Qiuwu-Liuqu continental deposits; (3) the Tibetan sedimentary series (also referred to as the "Tethyan sediments" or the "Tethys Himalaya") with Proterozoic/Cambrian to Permian sedimentary rocks of a Gondwanan epicontinental sea and Mesozoic to Eocene sedimentary rocks of the former northern Indian passive margin; (4) the Higher Himalaya crystalline basement rocks; (5) the Lesser Himalaya series with metamorphic and sedimentary rocks of Precambrian to Eocene age; (6) the Subhimalaya with the Siwalik molasse of middle Miocene to Pleistocene age; (7) the modern fluvial plain of the Indus and Ganges-Brahmaputra rivers.

Plate-Tectonic Evolution. Continental collision between India and Asia began at the northwestern edge of India between 65 and 55 Ma and was completed in the eastern Himalaya at about 45 Ma (e.g., Klootwijk et al. 1992; Le Pichon et al. 1992). Since that time total convergence between India and Asia (Kazakhstan block, Mongolia block) amounted to ≥2180 km at the western syntaxis and ≥2860 km at the eastern syntaxis (Le Pichon et al. 1992). These authors assume that part of this convergence was accommodated by crustal shortening with the transfer of lower crust to the mantle within Tibet and that another part was absorbed by lateral continental escape. Most of the total shortening has occurred north of the Himalayas, i.e., between the Lhasa and Tarim blocks and along the Tien Shan. Shortening in the Himalayas and southern Tibet only, i.e., between the Indus-Yarlung suture (IYS) and the present-day Main Frontal Thrust (MFT), amounts to 470 to 550 km (e.g., Schelling 1992; Ratschbacher et al. 1994; Srivastava and Mitra 1994). Most of this crustal

Figure 1. (*a*) Overview of the Bengal and Indus deep-sea fans and locations of DSDP and ODP drilling sites cited in text. (*b*) Major modern drainage systems of the Himalayas and India (Rao 1979); oversteepened river gradients in the Himalayas after Seeber and Gornitz (1983), simplified. (*c*) Isopachs (in kilometers) of post-Paleocene (post-collision) sediments of the Bengal and Nicobar fans (after Curray 1994). Note reduced sediment thicknesses along 85-East Ridge (indicated in *d*) and eastward subduction of Nicobar fan along Sunda arc-trench system. (*d*) Areal extent, subdivision, and bathymetry of the Bengal fan (contour lines in meters; after Emmel and Curray (1984). Note loss of Nicobar fan sediments along the subduction zone of the Sunda arc.

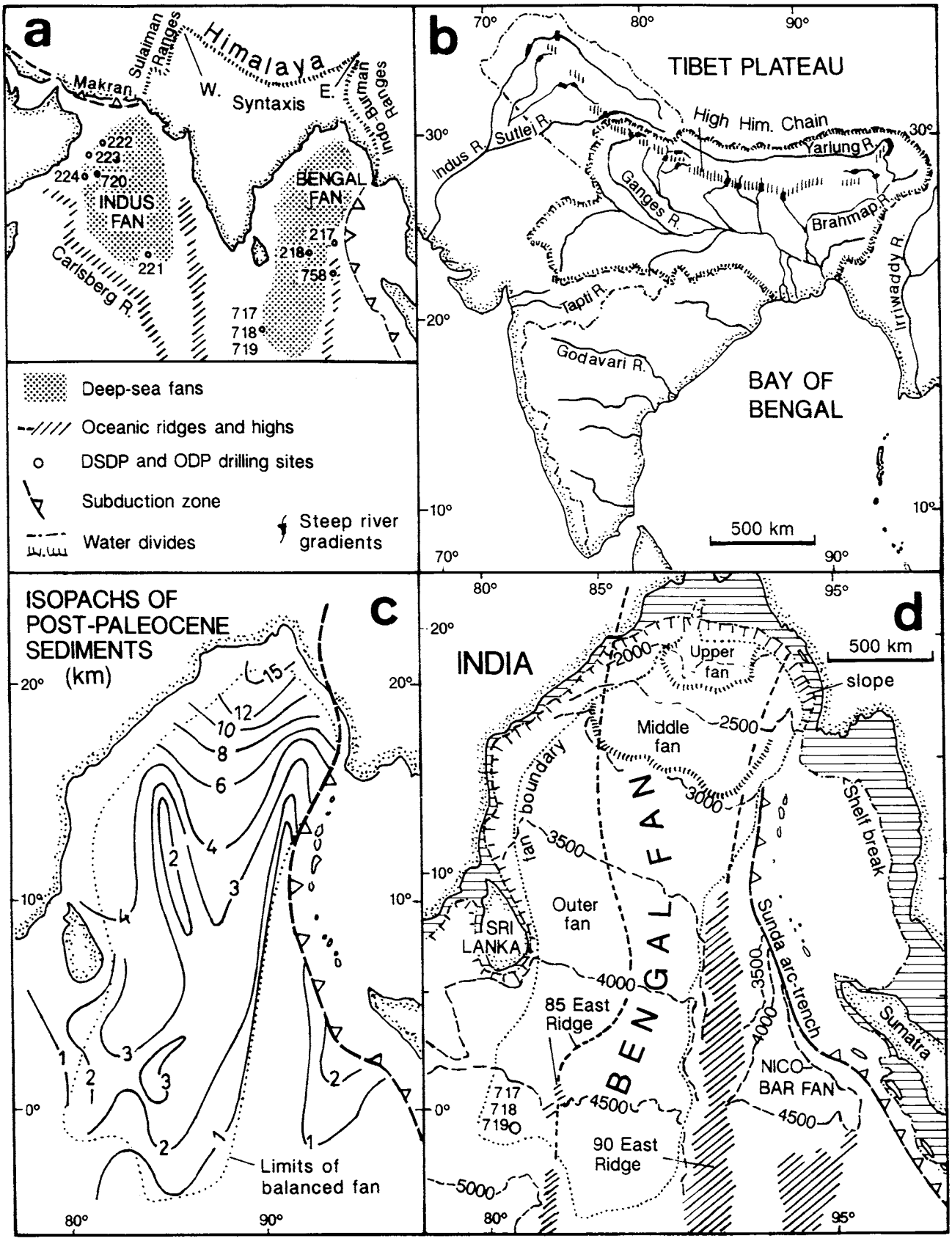
a
Himalaya
Sulaiman Ranges
Makran
W. Syntaxis
E.
Indo-Burman Ranges
222
223
224
720
INDUS FAN
221
Carlsberg R.
BENGAL FAN
217
218
758
717
718
719
b
TIBET PLATEAU
70°
80°
90°
30°
20°
10°
Indus R.
Sutlej R.
High Him. Chain
Yarlung R.
Ganges R.
Brahmap. R.
Irrawaddy R.
Tapti R.
Godavari R.
BAY OF BENGAL
500 km
Deep-sea fans
Oceanic ridges and highs
DSDP and ODP drilling sites
Subduction zone
Water divides
Steep river gradients
c
ISOPACHS OF POST-PALEOCENE SEDIMENTS (km)
15
12
10
8
6
4
3
2
1
Limits of balanced fan
80°
85°
95°
d
INDIA
500 km
2000
Upper fan
slope
Middle fan
2500
3000
3500
4000
4500
5000
fan boundary
Outer fan
SRI LANKA
BENGAL FAN
Shelf break
Sunda arc-trench
3500
Sumatra
85 East Ridge
90 East Ridge
NICO BAR FAN
717
718
719

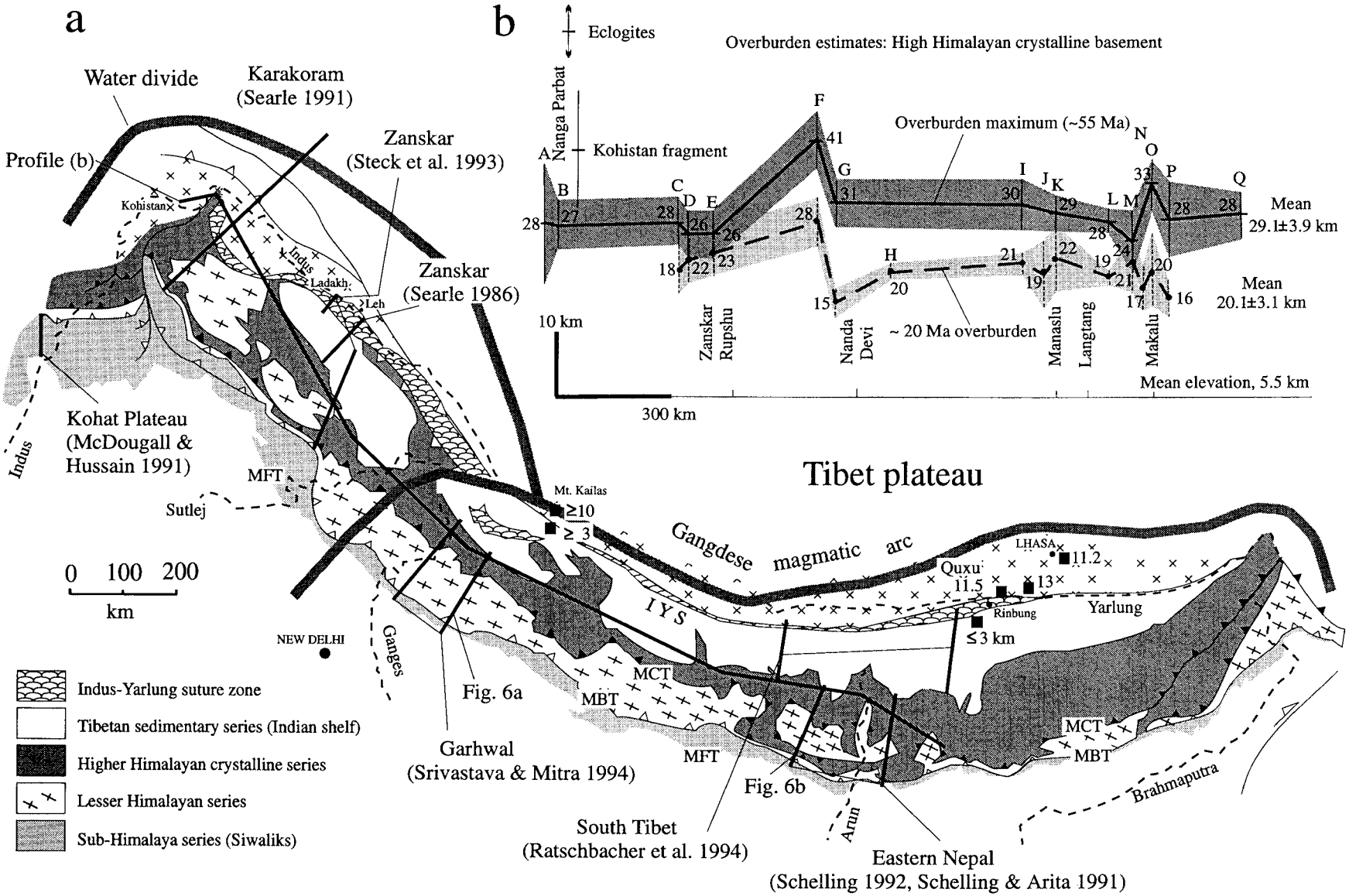
a
b
Water divide
Karakoram
(Searle 1991)
Zanskar
(Steck et al. 1993)
Profile (b)
Kohistan
Indus
Ladakh
Leh
Zanskar
(Searle 1986)
Kohat Plateau
(McDougall &
Hussain 1991)
Indus
MFT
Sutlej
0 100 200
km
NEW DELHI
Ganges
Mt. Kailas
≥10
≥ 3
Gangdese magmatic arc
IYS
LHASA
11.2
Quxu
11.5
13
Rinbung
≤3 km
Yarlung
Tibet plateau
MCT
MBT
MFT
Fig. 6a
Fig. 6b
Garhwal
(Srivastava & Mitra 1994)
South Tibet
(Ratschbacher et al. 1994)
Arun
Brahmaputra
Eastern Nepal
(Schelling 1992, Schelling & Arita 1991)
Indus-Yarlung suture zone
Tibetan sedimentary series (Indian shelf)
Higher Himalayan crystalline series
Lesser Himalayan series
Sub-Himalaya series (Siwaliks)
Eclogites
Overburden estimates: High Himalayan crystalline basement
Nanga Parbat
Kohistan fragment
Overburden maximum (~55 Ma)
Mean
29.1±3.9 km
Mean
20.1±3.1 km
10 km
300 km
Zanskar
Rupshu
Nanda
Devi
~ 20 Ma overburden
Manaslu
Langtang
Makalu
Mean elevation, 5.5 km

shortening occurred in the Neogene, when lateral continental escape had slowed and continued convergence was mainly translated into crustal thickening and uplift in the Himalaya (e.g., LeFort 1989 *in* Ratschbacher et al. 1994; Harrison et al. 1992).

The Rise of Southern Tibet (Gangdese Belt). The Gangdese batholith rose significantly since about 35 Ma (e.g., Yin et al. 1994). Intracontinental, south-directed thrusting along the Gangdese Thrust System (GTS) began at 27 Ma and lasted until about 22 Ma. The displacement along the north-dipping GTS is thought to be 46 ± 9 km in eastern south Tibet and thus must have caused significant rock uplift along the Gangdese belt. The uplift history of the entire Tibet plateau farther north does not significantly affect our mass balance because this area is beyond the drainage system of the Himalayan rivers, and denudation here operated slowly due to the increasing aridity of the climate.

Structural Evolution and Rise of the Himalayas. South-directed stacking along the main thrust systems commenced later in the Himalayas than in southern Tibet, and the activity along these systems successively migrated from north to south (figure 3). In the middle section of the mountain range (through Nepal), the Main Central Thrust (MCT), which produced the High Himalayan crystalline chain, was most active between 22 and 18 Ma (e.g., Hodges et al. 1992; Yin et al. 1994). The Main Boundary Thrust (MBT) and Main Frontal Thrust (MFT) systems developed later, but both the periods of thrusting and the amounts of displacement vary along strike of the orogen. To the north of the present-day High Himalayan chain, the Tethyan zone was affected by normal faulting along the North Himalayan Normal Fault zone (the NHNF of, e.g., Pêcher 1991 *in* Ratschbacher et al. 1994, or the South Tibetan Detachment System [STDS] of Burchfiel et al. 1992) and backthrusting (figure 3*b*; Ratschbacher et al. 1994; Yin et al. 1994). Movement along the faults in the Himalayas occurred subsequent to the formation of the GTS. The NHNF developed more or less coeval with the MCT, whereas backthrusting operated somewhat later. These processes concentrated exhumation to the zone of the High Himalayan crystalline chain and caused relatively limited denudation in the zone of the Tethyan sediments; however the Kangmar Fault System locally exposed crystalline basement rocks and led to leucogranite intrusions within the Tethyan zone in southern Tibet (figure 3; e.g., Chen et al. 1990). There, an about 20 km thick rock sequence must have been denudated by erosion and/or tectonic unroofing.

It is likely that both surface uplift and denudation (or unroofing; for definitions see England and Molnar 1990) intensified shortly after the onset of large-scale thrusting along the MCT during the Early Miocene and during the Late Miocene when thrusting along the MBT commenced (see also Harrison et al. 1992). Younger, up to Recent, thrusting is concentrated along the MFT, which affected and partially uplifted Pliocene and early Pleistocene sediments of the Upper Siwalik Group (e.g., Burbank and Johnson 1983 *in* France-Lanord et al. 1993).

Tertiary Sediments as Records of Tectonic Evolution. After closure of the Neo-Tethys, marine sedimentation persisted within remnant basins of limited extent along and south of the IYS up to the Eocene (e.g., Gaetani and Garzanti 1991 *in* Einsele et al. 1994; Liu and Einsele (1994). During the Late Eocene and Oligocene elongate depressions within the embryonic orogen were filled with predominantly fluvial, molasse-type sediments of the Indus-Kailas-Qiuwu basins south of the Gangdese belt and the Liuqu conglomerate deposits along the IYS (e.g., Garzanti and Van Haver 1988; Searle et al. 1990 both *in* Einsele et al. 1994). These intramontane basins mainly accumulated coarse-grained sediments at least 4 km thick and derived from local sources, i.e., from the Gangdese magmatic arc and the accretionary wedge of the former

Figure 2. (*a*) Tectonostratigraphic map of the Himalayas and southern Tibet modified from Brunel and Kienast (1986), with drainage divides and cross sections used for estimation of denudation areas (see text). Numbers along the central and eastern Gangdese belt refer to overburden (in kilometers) denudated (data from Copeland et al. 1987 *in* Ratschbacher et al. 1994; Harrison et al. 1993; Ratschbacher et al. 1994). (*b*) Overburden estimates based on geothermobarometric data for the High Himalayan crystalline basement between the Nanga Parbat und Darjeeling (along E-W line in [*a*]) and subdivision in overburden denudated since ~55 Ma (time of India-Asia collision) and ~20 Ma (time of major thrusting along the Himalayas) using published radiometric data: A: Treloar et al. (1989); B: Chamberlain et al. (1989); C: Staeubli (1989); D: Pognante et al. (1993); E: Pognante and Lombardo (1989); F: Metcalfe (1993); G: Hodges and Silverberg (1988); H: Valdiya (1988); I: LeFort et al. (1986); J: Hodges et al. (1988*a*, 1988*b*); K: Pêcher (1989); L: Hodges et al. (1993); M: Hubbard (1989); N: Hodges et al. (1992); O: Pognante and Benna (1993); P: Brunel and Kienast (1986); Q: Mohan et al. 1989).

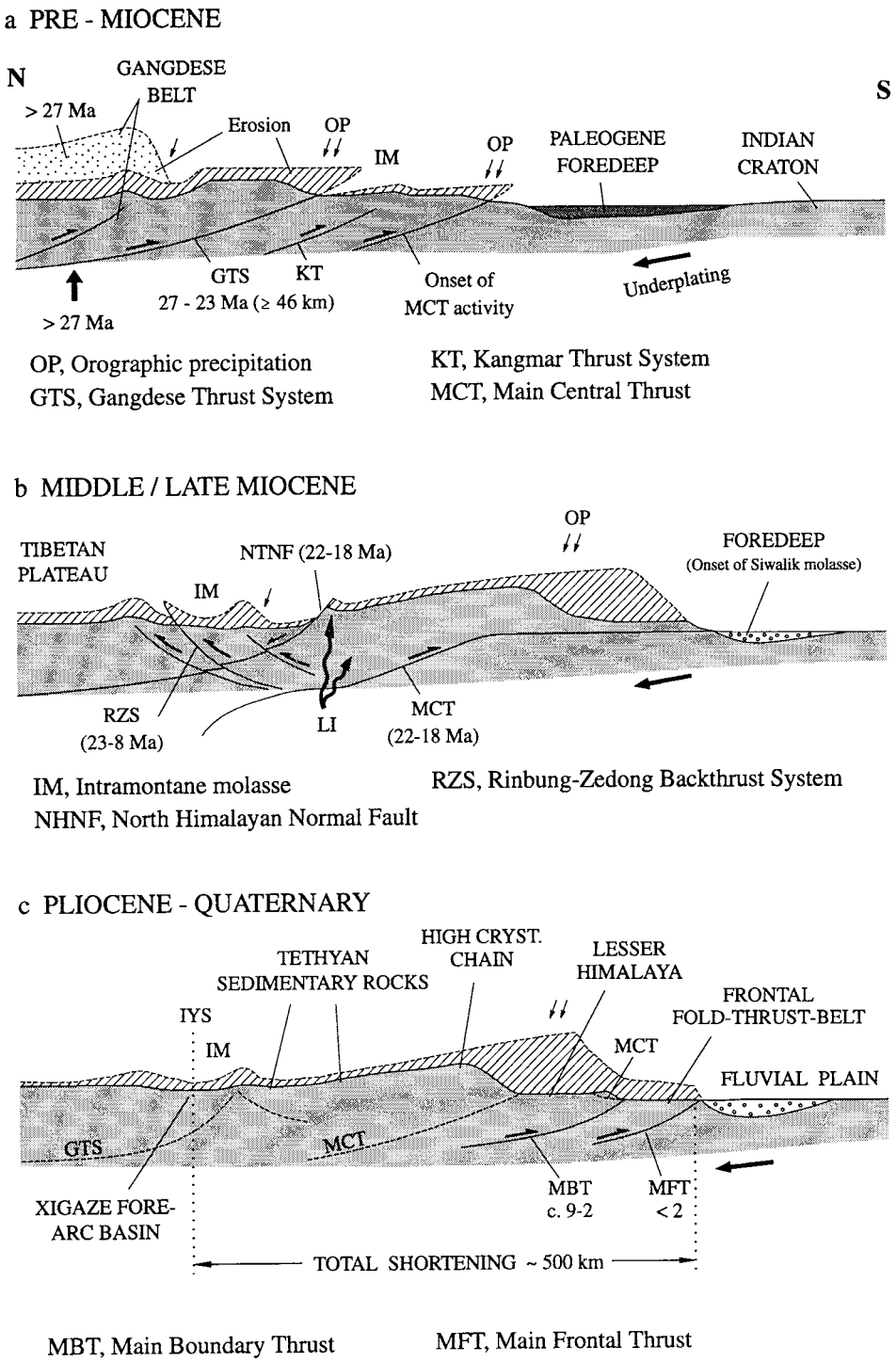

Figure 3. Conceptual models of three stages (*a–c*) of structural and erosional evolution of the Himalayan orogen (cross section through Nepal, not to scale). Underplating of Indian continental crust caused pre-Miocene rock uplift and exhumation of the Gangdese belt and southern Tibet and southward overthrusting of this zone along the Gangdese Thrust System accompanied by further denudation. Overthrusting migrated successively southward generating the Main Central Thrust, the Main Boundary Thrust, and finally the Main or Himalayan Frontal Thrust. Numbers signify periods of thrusting in Ma; note that thrust activities may have varied along strike. Backthrusting, most active during the Early Miocene, was concentrated along the Indus-Yarlung suture zone, e.g. along the Rinbung-Zedong Thrust System. Most intense denudation and exhumation occurred at the fronts of thrust sheets where zones of high orographic precipitation developed. (Based on Yin et al. 1994; Masek et al. 1994; Ratschbacher et al. 1994).

Indus-Yarlung subduction zone. Later on a portion of these basin fills was eroded and redeposited farther south.

The pre-Miocene sediments of the Subhimalayan foredeep document an evolution from shallow-marine to deltaic-fluvial (meandering) deposition, semi-arid climate (red beds, caliche, some evaporites), and a provenance from distal northern areas undergoing limited unroofing (McDougall et al. 1993; Najman et al. 1993; Reimann 1993; Critelli and Garzanti 1994). They normally are much thinner than the Neogene sediments of the Siwalik Group (e.g., 0.5 to 1 km vs. 3 to >5 km). It should be noted, however, that the pre-Miocene sediments mainly represent deposits of the outer, cratonward part of the southward-migrating foreland basin. In any case, both the evolution of the Subhimalayan foredeep and the fact that substantial amounts of pre-Miocene sediments were incorporated into the Bengal fan, the Nicobar fan, the Indoburman ranges, and into the Sunda arc system (e.g., Curray 1994 and below) indicate that effective sediment sources existed in pre-Miocene times. One of these must have been the Gangdese belt of southern Tibet.

Around the Paleogene/Neogene boundary the sediments of the Subhimalayan foredeep document both an increase in relief and a change to a more humid climate. In northern India and Nepal the fluvial molasse gradually became sand-dominated, grey, and rich in plant and wood fragments (Kumar et al. 1991; Najman et al. 1993). The earlier meandering systems were replaced by braided systems with channel fills containing metamorphic lithic fragments from the rising Himalayan chain. This is in accordance with the evolution of the MCT, which may have reached its maximum activity around 20 Ma (e.g., Hodges et al. 1992). Due to continued overthrusting, the sediments of the Siwalik Group tend to coarsen upward. In Nepal, northern India, and Bangladesh, the upper part of the Siwalik Group is rich in conglomerates (e.g., Kumar et al. 1991; Reimann 1993).

Evolution of Drainage Systems and Topography in the Himalayas

About two-thirds of the modern major rivers of the Himalayas originate north of the highest Himalayan mountain chain. They mainly drain, in their upper reaches, the Tethyan sedimentary series and the Gangdese belt (figure 1*b*). Some of these trans-Himalayan rivers, such as the Indus and Yarlung-Brahmaputra, evolved parallel to the strike of the rising orogenic belt before they turned south to cross the mountain range. Other rivers, including most of the tributaries of the Ganges drainage system, cross the Himalayas from north to south. Almost all form deep gorges with steep gradients along their course through the high mountain ranges. Several authors (e.g., Seeber and Gornitz 1983) have therefore assumed that these rivers are antecedent, i.e., that they predate thrusting and surface uplift in the Himalayas. Whether this is true for their entire evolution, and to which degree the rivers and gorges reflect the younger structural history of the High Himalayan chain, is poorly known. In any case, once the rivers had incised deep valleys they tended to maintain their courses as well as their drainage divides. A substantial shift of the drainage divide between the Yarlung and Indus rivers in the Himalayas is unlikely, although some minor changes in river courses due to glaciation and strike-slip movements cannot be excluded (e.g., Brookfield 1993).

The river gradients decrease close to the outcrop trace of the MCT. As the crest of the High Himalayas coincides with a belt of thrust earthquakes (e.g., Ni and Barazangi 1984 *in* Molnar et al. 1993), the high topography and the steep river gradients may reflect movement of the Himalayan thrust systems across a ramp structure within the basal decollement. In contrast, Masek et al. (1994) interpreted the topography of the present-day Himalayas as largely determined by erosion and northward retreat of the steep southern slope of the mountain range (figure 3). Particularly high rates of orographically induced precipitation (≥2000 mm/yr) on the lower slope and the resulting removal of rock detritus have maintained a steep frontal slope. High peaks at the plateau edge and deep canyon incision across the plateau margin mainly reflect isostatic uplift as a result of rapid erosional unloading (e.g., England and Molnar 1990; Montgomery 1994). These processes may have been promoted by highly effective glacial erosion.

During the early stages of mountain building, tectonic mass influx along the GTS (since about 27 Ma) and the MCT (since about 22 Ma) probably exceeded erosion and thus caused southward advance and increased elevation of an earlier Gangdese mountain front and a younger High Himalayan mountain front (figure 3). In the later Neogene, erosion-controlled retreat of the mountain front (efflux of material) may have operated faster than tectonic mass influx (Masek et al. 1994).

Even in pre-Miocene times, a N–S-oriented transverse drainage system must have existed, because the Indian ocean acted as the closest base

level. This is documented by terrigenous sediments from northern sources in the Himalayan foredeep and other basins since the Eocene. The Eocene to Miocene molasse-type basin fills along the IYS indicate that the Gangdese magmatic arc (active between 110 and 40 Ma) must have formed a major drainage divide between northward- and southward-flowing river systems that persisted up to the present.

The younger history of the rivers Indus and Ganges in the Subhimalayan foredeep and the present-day alluvial plain is not clear. From paleocurrent measurements in the northwestern Himalayan foreland, Burbank and Beck (1991 *in* Burbank 1992) inferred that the upper drainage system of the Indus river formed part of the Gangetic system during a certian period in the Miocene and therefore transported its surplus of sediment to the southeast. Later, in the Pliocene, continued sediment aggradation in the foredeep and progradation of large alluvial fans established the modern drainage divide between the Indus and Ganges rivers. Although this change in drainage pattern is not accurately dated (Khan and Opdyke 1993; Willis 1993), we here assume that the Himalayan tributaries of the Indus river fed solid load into the Ganges river up to about 5 Ma, i.e., during about three-fourths of the time period in our study.

Volume of Eroded Rocks in the Himalayas

For our mass balances, we refer to the drainage areas of the modern rivers Ganges and Yarlung/Brahmaputra (in total 1.62×10^6 km^2, in the Himalayas about 0.62×10^6 km^2) and, in addition, the upper reaches of the Indus river in the Himalayas (0.43×10^6 km^2) for three-fourths of the time considered.

General Aspects and Methods. Buried rocks can be exhumed either by erosion or "tectonic unroofing." Both processes have been active in the Himalayas and southern Tibet (e.g., Burchfiel et al. 1992; Masek et al. 1994). For this paper, however, only erosion is relevant. We used several different data sets to constrain exhumation (or unroofing) in the Himalayas:

a) Published balanced cross sections normal to the strike of the orogenic belt were utilized to determine the pre-deformational erosion level and to calculate the area denudated above the present topography. The cross-sectional areas were estimated from both the reconstructed deformed and the restored (pre-deformation) sections. Figure 4*a* shows a simplified version of the deformed Pindari section of Srivastava and Mitra (1994). We reconstructed the pre-erosion level above the present-day land surface, assuming average thicknesses for the eroded rock formations as determined by various authors in the foreland portion of the thrust belt, along strike, or in areas of strong relief. We assumed minimum thicknesses for the Precambrian-Cambrian formations and a northward thinning of the Cambrian strata.

b) To assess independently the amount of eroded overburden, we used the reconstructed deformed sections and projected the available overburden estimates given by geothermobarometry of metamorphic and igneous rocks into the line of the sections (figure 4*b*). The thermometric data of post-collisional metamorphism were converted into overburden by using a geothermal gradient of 35°C/km. As far as deviations from this mean value occur along strike, these were taken into account, considering the discussions by the authors of the P-T data. To calculate the thicknesses of removed rocks from barometry, typical rock densities of the gneisses of the High Himalayas (2.7–2.8 g/cm^3) were used. The barometric data yield total amounts of vertical denudation since the onset of mountain building (figure 4*a* and *c*). In both sections the pre-erosion level, as inferred from the reconstructed stratigraphic pile, and overburden, as obtained from the P-T data, coincide within the errors inherited in geothermobarometry ($\pm 10\%$).

c) To determine the cross-sectional areas denudated in the western Himalayas and the Karakoram, we relied on published estimates of maximum overburden both from stratigraphic thicknesses and metamorphic isograds.

Eroded Rock Volumes in the Zones of Deformed India (between IYS and MFT). This zone is subdivided from west to east into five segments. The Gangdese belt north of this zone is referred to as segment 6. The following summary (table 1) presents the principal results only; for detailed data sets see table I (file).

1) Western Himalaya, western syntaxis and Karakoram. We used this section of Searle (1991) across K2 and western Kashmir, which shows a cumulative overburden estimate based on a wealth of thermobarometric data, probably the most extensive mapping of isograds from any region of the Himalayas. However, as for the Zanskar section, this cross section is relatively schematic and therefore does not provide very accurate data. Denudation south of the MBT is derived from a balanced section west of the western syntaxis (Kohat plateau; McDougall et al. 1993). For the volume calculation we applied the cross-sectional area estimates 425 km along strike, i.e., from the northwestern tributaries of the Indus river to western

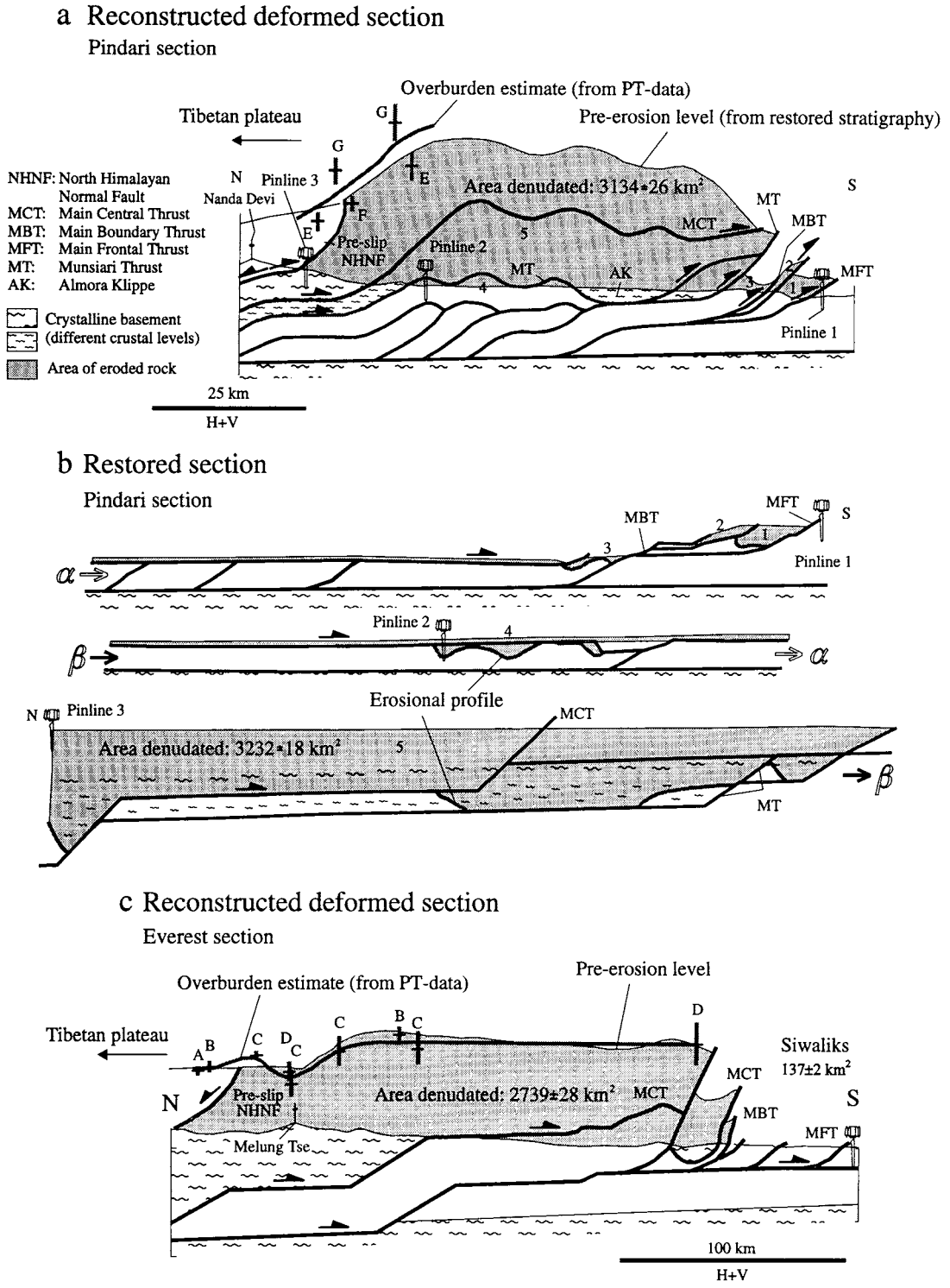

Figure 4. Published cross sections (for locations, see figure 2) with estimates of the pre-deformational erosion level and area denudated (shaded). Area estimates were obtained from both the reconstructed deformed and the restored sections (*a,b*). Simplified versions of both the deformed and restored Pindari section of Srivastava and Mitra (1994) and *c*) the Everest section of Schelling (1992) with reconstructed pre-erosion levels. See text for explanation. Geothermobarometric data from: A: Hodges et al. (1992); B: Hodges et al. (1993); C: Hubbard (1989); D: Brunel and Kienast (1986); E: Hodges and Silverberg (1988); F: Valdija (1988); G: Metcalfe (1993).

Table 1. Summary of Eroded Rock Volumes in Different Segments of the Himalayan Orogen and Error Estimates

Time Period (Ma)	Region	No. of segment	Eroded rock volumes [$\times 10^6$ km^3]
55	Himalayas and	1	.433 ± .003[a]
	Karakoram,	2	.50 ± .004
	south of IYS	3	3.30 ± .17
		4 + 5	3.97 ± .21
55	Total	1 – 6	8.2 ± .4
55	Gangdese belt	6	1.49 ± .14
55	Total	1 – 6	9.69 ± .54
20[b]	Total	1 – 5	6.69 ± .37
20[c]	Gangdese belt	6	.75 ± .07
20	Total	1 – 6	7.44 ± .44
55	Indus-Sutlej catchment		1.94[d] ± .07
5[e]	Sediment loss to Indus accumulation system		.176[f] .3[g]

[a] Does not include error due to extrapolation of cross sectional area along strike.
[b] 69% of value for 55 Ma.
[c] 50% of value for 55 Ma.
[d] Total volume (55 Ma) of eroded rock from the Indus-Sutlej drainage system.
[e] After capture of the upper reaches of the Paleo-Ganges river by the Indus river c. 5 Ma (see text).
[f] 9.1% of value for 55 Ma, corresponding to sediment loss to the modern Indus depositional system (minimum value).
[g] Value taken for ultimate mass balance (see text).

Zanskar. The estimate of the eroded rock volume in this section (table 1) gives a minimum value, because it crosses the Himalaya where it is comparatively narrow.

2) Zanskar. We used the composite section of Steck et al. (1993) across eastern Zanskar and Lahul, where the maximum overburden was estimated from stratigraphic thicknesses and metamorphic isograds. This section is relatively schematic and, in parts, oblique to strike. Furthermore, it crosses dextral shear zones along which rock material moved across the plane of section. The eroded cross section area is applied to a length of 225 km along strike (table 1). As this section crosses the Himalayan belt where it is particularly wide and because it is oblique to strike in some stretches, the calculated rock volume probably overestimates the actual volume. We partly compensate this by not taking into account the volume of sediment eroded from the zone south of the MBT.

3) Garhwal-Zanskar. For the central Himalayas we used the two balanced sections of Srivastava and Mitra (1994). We delimited the area of eroded rocks from these sections in the north by the preslip trace of the NHNF, for which we assume a listric shape cutting up from a 10° dip at the basement-cover interface to a 60° dip at the surface. The overburden calculated from P-T data exceeds somewhat the maximum erosion level given by the reconstructed deformed section (see figure 6*a*). However, this is mostly due to Metcalfe's (1993) data, whose estimates are the highest along the entire Himalayas; without these data both levels, determined with independent data sets, coincide within the errors of the P-T estimates. The two sections, 100 km apart along strike and crossing a similar overall structural geometry, allow us to estimate the error caused by extrapolating along strike (table 1). To obtain the total cross-sectional area between the MFT and the IYS, we added the area obtained from Searle's (1986 *in* Searle 1991) balanced section across the Tethyan shelf sediments in Zanskar (following Srivastava and Mitra). From both sections, the average area of erosion was taken for a length of 900 km along strike (from Zanskar to Kathmandu).

4) and (5) Everest and Jannu. The balanced sections of Schelling (1992) and Schelling and Arita (1991) were combined with those of Ratschbacher et al. (1994) to obtain cross-sectional denudation areas between the MFT and the IYS (see figure 5 in Ratschbacher et al. 1994). Total eroded areas from both sections (about 160 km apart) correspond to within 3%, although marked differences exist in the areas eroded from the Siwaliks along strike (table I, file). The average cross-sectional area denudated from the Himalayas (~2900 km^2 from MFT to NHNF) is taken as representative for a length of 1125 km along strike from Kathmandu to the eastern tributaries of the Brahmaputra.

Finally, tectonic exhumation along the NHNF north of the MCT (figure 3) has to be discussed. We follow the argument of Masek et al. (1994) that erosion has almost entirely dominated exhumation since the end of slip along the MCT and the NHNF (~18 Ma, e.g., Hodges et al. 1992). For the cross-sectional area calculations from balanced sections, we allowed ~6 km of unroofing along a listric normal fault with a displacement of ~35 km (Burchfiel et al. 1992, Mt. Everest area). For the total area calculated along these sections, however, tectonic unroofing is not a major factor.

6) The Gangdese belt. Only a few geothermobarometric data and no balanced sections are available from this region. The former indicate that denudation in the drainage system of the Indus river in the Karakoram north of the IYS has reached up to 25 km (e.g., Kohistan complex, figure 2; for geographic reference see Searle 1991). From Ladakh to

east of Mt. Kailas the width of the plutonic belt decreases substantially. About 10 km of rocks have been denuded from the Gangdese plutons in the Mt. Kailas area (Harrison et al. 1993). Most of the Gangdese belt between Mt. Kailas and Quxu (southwest of Lhasa) has not been exhumed to the plutonic level. For the eastern segment, from Quxu to the eastern syntaxis, the few geobarometric data (e.g., Quxu pluton, Copeland et al. 1987 *in* Einsele et al. 1994; figure 2), the greenschist-facies metamorphism of the Gangdese basement (Burg et al. 1983 *in* Einsele et al. 1994; Ratschbacher et al. 1992 *in* Ratschbacher et al. 1994), and the observation that the magmatic arc has been denudated mostly to its plutonic level indicate an average exhumation of $\leq$15 km.

For the central and eastern stretches of the Gangdese belt, we employed Rowley's (1995) approach to estimate erosion from the front of a thrust sheet, thus modeling erosion from the leading edge of the GTS (figure 3). We assumed syn-kinematic denudation, an initial elevation of the land surface of 1 km (insensitive for the obtained results), and a 25–35° N-dipping GTS (corresponding to the values of Yin et al. [1994] in eastern South Tibet). Furthermore, a maximum of 5–15 km of vertical denudation of the hanging-wall block (10 km for the Mt. Kailas area, i.e., from Leh to Gyêdar Tso, 5 km for the central Gangdese belt, i.e., from Gyêsar Tso to Rinbung, and 15 km for the stretch from Rinbung to the eastern syntaxis) is taken into account. For the area calculations, we evaluated the dip of the thrust and the amount of vertical denudation; this resulted in slip values between 10 and 36 km.

Total Rock Volume Eroded and Error Estimation. The total rock volume eroded in the Himalayas and Karakoram (between IYS and MFT) since continental collision is 8.2×10^6 km^3 (table 1): adding erosion in southern Tibet and along the Gangdese belt (north of IYS) yields 9.7×10^6 km^3.

A major source of error is the difference in the definition of cross-sectional areas of denuded rocks above the present-day erosion surface. For the two sections across the western Himalayas (Karakoram and Zanskar sections) these errors are at least as large as the errors in the P-T data used to construct the overburden, which are usually 10% of the individual estimate. Together with the minor inaccuracies in plotting, scaling, and digitizing, we expect that the area calculations are off by 10–15%. For the central and eastern Himalayas we separately calculated areas for the restored and the reconstructed deformed sections and obtained deviations of ~10% between the minimum and maximum values. A further error is introduced by the along-strike extrapolation of specific cross-sectional areas. We chose those distances on geological arguments, particularly taking into account the width of the exposed tectonostratigraphic units. We believe that this error is on the order of 10%. In total, a 10–20% deviation of the true volume from the calculated average is possible. For the Gangdese belt (the stretches where we used Rowley's [1995] method for area calculations), we estimated errors by varying the dip of the thrust plane from 25 to 35°, which yields a deviation of ~30%.

Partitioning of Rock Volumes Eroded Prior to and After 20 Ma. In figure 2*b* we distinguished between total (cumulative) overburden and overburden at 20 Ma. Overburden estimates are plotted above an elevation of 5.5 km (average present-day elevation of the Himalayas) along strike of the High Himalayan crystalline basement from the western syntaxis to the Darjeeling area in Sikkim. Most geothermobarometric data have been reported for this zone. We distinguished between peak pressure values at different localities along strike and overburden estimates from pressures accompanying peak temperatures. The level of peak pressure overburden is taken to represent total overburden. By contrast, peak temperatures are thought to be coeval with leucogranite emplacement, dated precisely in the Manaslu area (23 Ma, Harrison et al. 1995), and somewhat younger elsewhere (e.g., Schärer et al. 1986 *in* Harrison et al. 1993). Cooling of the High Himalayan crystalline basement between 20–15 Ma, as given by ^{40}Ar/^{39}Ar thermochronology (e.g., Hubbard and Harrison 1989 *in* Harrison et al. 1993; Copeland et al. 1991 *in* Harrison et al. 1993), supports the assumption that the pressure at peak temperature approximates the overburden at ~20 Ma. Note that the overburden estimates are quite uniform along strike, with the exception of the values given by Metcalfe (1993; see discussion above). Taking mean values (figure 2*b*) and assuming they represent either total denudation (since 55 Ma) or denudation since ~20 Ma, about 31% of the Himalayas south of the IYS have been denudated between collision and ~20 Ma, and 69% thereafter; thus the volume denudated in the Himalayas south of the IYS since ~20 Ma is about 6.7×10^6 km^3.

Most of the denudation along the Gangdese belt should have occurred prior to 20 Ma, as indicated by the continental molasse deposits of the Indus-Kailas-Qiuwu formations along the IYS. These coarse-grained sediments are of Eocene to Miocene age, several kilometers thick, and were predominantly derived from the Gangdese magmatic arc.

Part of this material should be included in the mass balance because, due to the relief created during backthrusting, it was later eroded and redeposited farther south. For the mass balance, we assumed that a maximum of 50% (0.75×10^6 km^3) of the total denudation along the Gangdese belt was post-20 Ma. The cumulative volume of rocks denudated from the Himalayas, southern Tibet, and the Gangdese belt since ~20 Ma is thus about 7.4×10^6 km^3 (table 1).

Dissolved Loads of Himalayan Rivers. This material is included in the above mass balances of erosion. At present, the solute loads of the rivers Brahmaputra, Ganges, and Indus make up 5–10% of their total river loads. About 40% of these solute loads are derived from the atmosphere (mainly HCO_3^- and Cl^-) and therefore not relevant for denudation. Taking this into account, average chemical denudation in the drainage areas of these rivers today amounts to 16 to 18 m/m.y. (Summerfield and Hulton 1994; see also Einsele 1992, p. 355–357). This is 2.6%, 5.7%, and 11.5%, respectively, of the present-day total denudation rates in these regions and corresponds to a total geogenic solute load of 0.36×10^6 km^3 for the Himalayan drainage area of 1.05×10^6 km^2 of these rivers. Part of this load, mainly calcium carbonate (calcium constitutes about 40% by weight of the dissolved geogenic river load), was left behind on fluvial plains (e.g., as caliche) and as skeletal carbonate in the marine basins. This part of the dissolved river load is included in the sediment volumes estimated for the various basins. The remainder of the dissolved constituents (about 0.2×10^6 km^3) may have drifted beyond the limits of the Bengal fan.

Rock Volume Eroded by Rivers from Peninsular India

A small portion of the Gangetic river load in the basins listed below is derived from hilly and mountainous areas of the Indian peninsula to the south of the main river. We estimate that about 0.35×10^6 km^2 of this southern tributary system was subjected to significant denudation. Its elevation is mostly between 200 and 500 m, and its rocks are exposed to subtropical to tropical monsoon climate. Taking into account the measured modern suspended loads of Indian and other, comparable, rivers (sediment yields on the order of 100 t/km^2/a; Milliman and Meade 1983; Einsele 1992, p. 357–361), the mechanically eroded rock volume during the last 20 Ma amounts to 0.22×10^6 km^3 (100 t/km^2/a $\times$ 0.35×10^6 km^2 $\times$ 20 m.y., divided by rock density of 2.75 t/m^3; subject to at least ± 10% error as values in table 2). In comparison to the

Table 2. Sediment Volumes of post-20 Ma Sediments in Various Basins fed by the Ganges-Brahmaputra River System

Basin	Extensions [km] N-S	Extensions [km] E-W	Average thickness [km]	Sediment volume [$\times 10^6$ km^3] Wet	Sediment volume [$\times 10^6$ km^3] Dry[a]	Conversion factor (mean)
Ganges foredeep[b]	250 (170–330)	2400	2.8 (0 to 7)	1.5 ± .2	1.19	.79
Bengal foredeep[c]	330	550	6.5 ± .5	1.0 ± .1	.88	.88
Delta (subaerial)[c]	110	550	10 ± 2	.5 ± .1	.45	.9
Prodelta (shelf)[c]	110	700 (550–800)	10 ± 2	.7 ± .15	.63	.9
Bengal fan (south of 20° N)	3100	800–1000	10 to 0	(5.2)[d] 4.8[e] ± 1	(4.2)[d] 3.9[e]	.81 .81
Total				8.5 ± .65	7.05 ± .65	

[a] Converted to rock of 2.75 g/cm^3 bulk density. The mean conversion factor for Bengal fan sediments of bulk densities from 1.2 to 2.65 g/cm^3 is about 0.81, based on Curray and Moore (1971) and Curray (1994). Those for the other basins vary between 0.79 and 0.90 according to the thicknesses of post-20 Ma sediments. After Perrier and Quiblier (1974) and Smosna (1989) it was assumed that young sequences of immature sandstones and mudstones of 1, 2, 3, 4, 5 and 7 km thickness require conversion factors of 0.67, 0.74, 0.79, 0.83, 0.85, and 0.9, respectively.

[b] Planimetry of isopach map of Burbank (1992), value includes minor proportion of Paleogene.

[c] Basin shape factor 0.85 (see text).

[d] Volume estimate from fan geometry and shape factor after Wetzel (1993), thickening of upper fan due to isostatic response of the crust under the sediment load included. This value is not used for summing up total sediment volume.

[e] Planimetry of isopach map (Curray 1991, 1994) for post-collision sediments (figure 1c) and assuming 65% of volume is post-20 Ma (minimum value because areas outside the 1 km isopach are not considered).

larger regions discussed below, chemical denudation may have been on the order of 0.1×10^6 km^3.

The major part of peninsular India to the south of the Ganges river catchment is drained by eastbound rivers entering the Bay of Bengal and the Indian ocean (figure 1*b*). The sediment yield of these rivers (Mahanadi, Godavari, Krishna, Cauvery) ranges from 10 to 60 t/km^2/a and is therefore less than one-tenth that of the Himalayan rivers (Subramian 1985). Assuming an average of 50 t/km^2/a for the total drainage area of about 1×10^6 km^2, we obtain an eroded rock volume of approximately 18.2×10^6 m^3/a (bulk density 2.75 g/cm^3). Because neither climate nor relief of this region seems to have changed drastically during the past 20 Ma, we extrapolate the modern river load to 20 Ma, which yields 0.36×10^6 km^3 eroded rocks. This value may be subject to considerable error (±50%) but does not significantly affect our mass balances. The major part of the peninsular solid river load is probably deposited in deltas and distributed on the eastern shelf and continental rise of India; therefore the contribution of the Indian peninsula to the Bengal fan sediment may be on the order of $\leq 0.2 \times 10^6$ km^3.

The dissolved river load from the Indian peninsula south of the Ganges drainage (75 ± 15 t/km^2/a or 27.3 m^3/km^2/a) is higher than their suspended load; related to unit area, it makes up about 60% of the dissolved load of the Himalayan rivers (Subramian 1985). Subtracting the atmogenic constituents HCO_3^- and Cl^- (in total about 50%), we get (for an area of 1×10^6 km^2 and a time period of 20 m.y.) a mass transfer of approximately 0.27×10^6 km^3 to the Bay of Bengal and Indian ocean. Because most of the dissolved carbonate of these rivers was biologically precipitated in coastal and shallow waters, the contribution of the residual solute river load to the Bengal fan sediment was low and is here neglected. In summary, the proportion of dissolved material lost to the ocean is relatively small (<3%) compared to total denudation in the high mountain region.

Sediment Accumulation

The sediments in the Subhimalayan foredeep and in other basins downstream of the Ganges and Brahmaputra record either a gradual or abrupt change in their facies from pre-Miocene to Early/Middle Miocene times (since about 20 Ma). This change is obvious in the oversupplied Subhimalayan foredeep (with the onset of the fluvial Siwalik molasse), but it has also been observed in more distal basins, such as in the shallow-marine Bengal basin fill of Bangladesh (BOGMC 1988) and in sediment cores from ODP Site 758 on the northern Ninetyeast Ridge (Klootwijk et al. 1992).

Subhimalayan Foredeep (Ganges and Upper Indus Foreland Basins). Burbank's (1992) isopach map shows that the foreland basin fill consists mainly of Siwalik Group sediments. We determined the areal extents and sediment volumes of the zones of different sediment thicknesses along strike of the orogen from the foot of the Sulaiman range to the eastern end of the foredeep where the Brahmaputra river crosses the Himalaya (table III, file). This zone contains a total post-collision sediment volume of 1.15×10^6 km^3. In addition, we used five balanced sections across the frontal thrust system of the Himalayas to estimate Siwalik sediments buried below thrust sheets; this yielded a volume of 0.34×10^6 km^3 (table III, file). Taking into account that the value from the isopach map includes a minor proportion of pre-20 Ma sediment and that the value for overthrust Neogene strata may be underestimated, the total post-20 Ma sediment of the foredeep is 1.5×10^6 km^3 with an error of about 15%.

Bengal Basin, Subaerial Delta, and Prodelta in the Bay of Bengal. This chain of basin fills was essentially formed by the seaward prograding deltas of the Ganges and Brahmaputra and is therefore genetically related. The artificial separation of this basin chain into different parts is here necessary for the evaluation of the post-20 Ma sediments. The Bengal basin in Bangladesh (figures 5 and 6*a*) represents a remnant basin or foredeep that evolved by eastward underthrusting of the Indian plate beneath the accretionary wedge of the Indoburman ranges (Hutchinson 1989, p. 221–224). The crust beneath the basin fill on land is transitional to oceanic (BOGMC 1988), whereas farther south in the Bay of Bengal, it is oceanic. Here, the prodelta sediments reach an abnormal thickness in the "Swatch-of-No-Ground" (Curry 1991 *in* Curray 1994). By the end of the Oligocene, the Bengal foredeep and the Burman basins in the east were separated by an emerging island arc causing westward movement of the depocenter of the Bengal foredeep (Reimann 1993, p. 91). Thus, Neogene sediment accumulation was restricted mainly to the narrowing Bengal basin, whereas the accretionary wedge of the Indoburman ranges of eastern India and Burma predominantly contains pre-Miocene sediments.

The Mesozoic-Cenozoic sediments of the Bengal basin, on top of Precambrian basement and strata of the Gondwana Super Group, consist of proto-

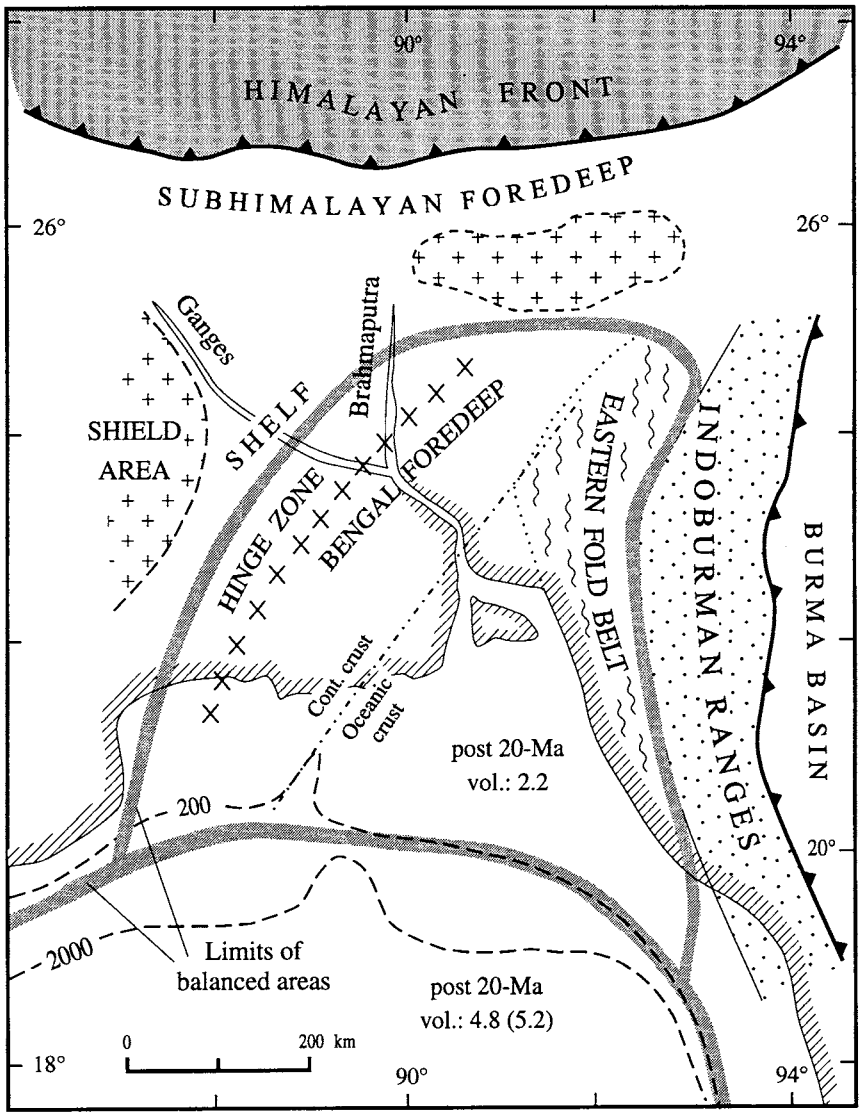

Figure 5. Simplified geotectonic setting of Bengal basin (foredeep) including the present-day subaerial delta and prodelta of the rivers Ganges and Brahmaputra, bound in the south by latitude 20°N (after BOGCM 1988; Alam 1989; Hutchinson 1989; Reimann 1993). The volume of post-20 Ma porous sediment within the marked limits is given in $\times 10^6$ km^3. See text, figure 6*a* and table 2 for further explanation. Note boundary between thinned continental crust and oceanic crust. The Indoburman ranges predominantly contain pre-Miocene sediments.

Bengal fan deposits overlain by a seaward prograding prodelta complex of Eocene to Oligocene age (e.g., Alam 1989; Lindsay et al. 1991 *in* France-Lanord et al. 1993; Reimann 1993). The base of the Neogene Siwalik molasse (Surma Group) froms a distinct seismostratigraphic boundary (BOGMC 1988) and may reflect the onset of a paleo-Ganges drainage system (Reimann 1993, p. 94). Based on drillholes, the Neogene sediments in the basin center and farther east within the eastern fold belt range from 3 to more than 6 km in thickness and make up about 65% of the total Tertiary. However, stratigraphic control for the position of the Oligocene/Miocene boundary is generally poor. Toward the western flank of the foredeep and shelf, the Neogene strata (about 70% of the total Tertiary) thin (figure 6*a*). From northeast to southwest, along strike of the foredeep, Neogene sediment increases from a few kilometers to about 10 km at the coastline of Bangladesh (below the present-day delta, figure 6*b*), if about 50% of the total Cretaceous and Tertiary basin fill of 20 km is post-Oligocene.

The Bengal foredeep was subdivided into two segments, A and B (figure 6*a*), because it narrows toward the northwest, and Neogene sediment thicknesses increase southward. The sediment thicknesses from the basin center to the eastern fold belt were assumed to be constant and equal to an average value in drillholes (BOGMC 1988; Reimann 1993). The asymmetric shape of the cross-sections is taken into account by the "shape factor" of 0.825. This means that the area of a cross section is $0.825 \times W \times Th$, where W is the width of the basin and Th is the mean sediment thickness in the basin center. The Neogene sediment volume of the Bengal foredeep obtained by this method is 1.0×10^6 km^3 (table 2).

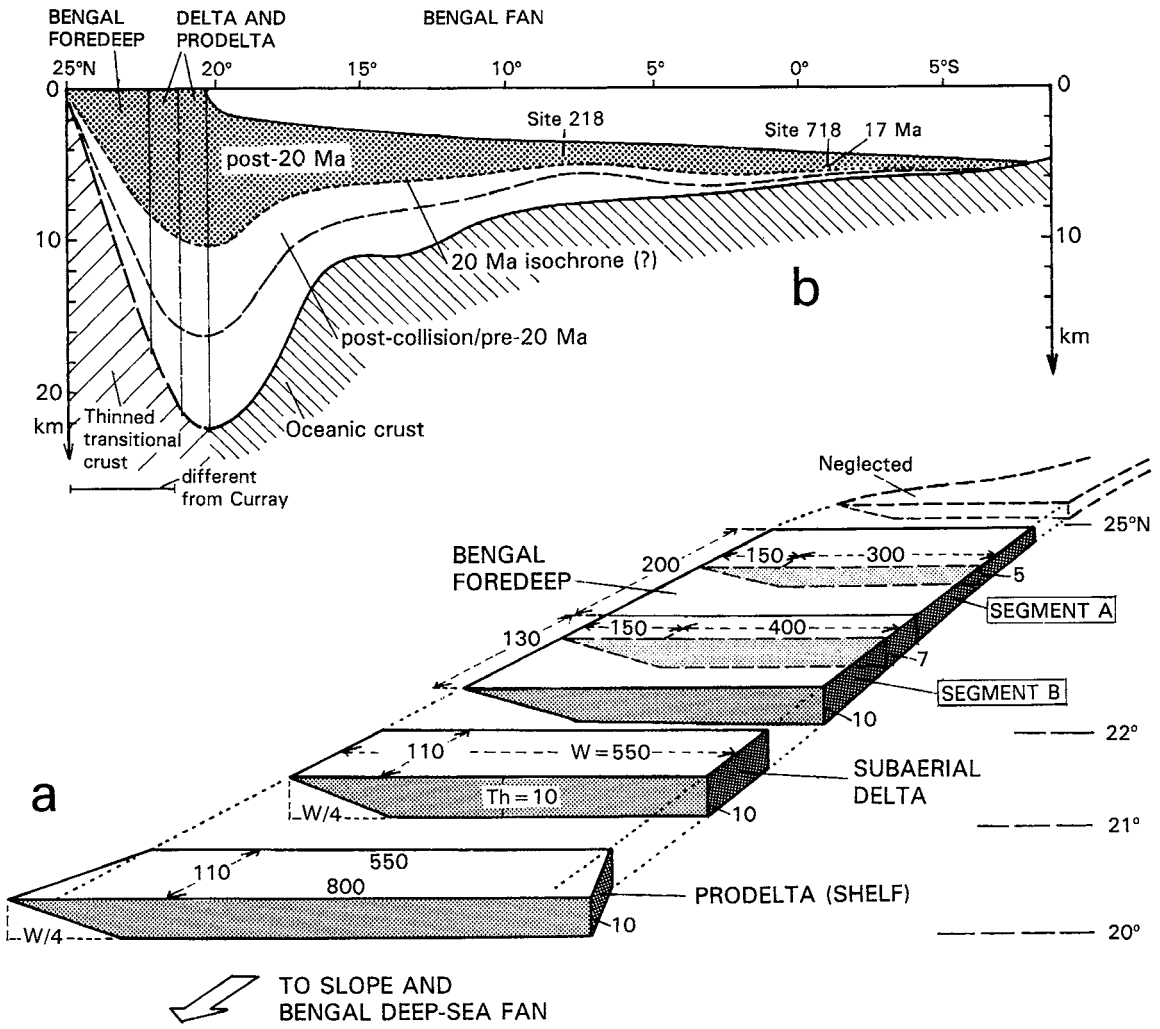

Figure 6. (a) Simplified geometries of the Neogene basin fills (cf. figure 5) of the Bengal foredeep and the modern subaerial delta and prodelta of the rivers Ganges and Brahmaputra. Hatched cross sections are taken as representative of individual basin segments. Numbers signify kilometers. See text for discussion on the basin shapes and sediment thicknesses used to calculate sediment volumes (table 2). Note that the prodelta widens southward and its sediment surface drops below sea level. (*b*) Longitudinal section through Bengal fan and foredeep with boundary between pre-Eocene (pre-collision) and post-Eocene (post-collision) sediments (based on Curray 1994, but modified to the north of 20°N because our line of section is almost parallel to the strike of the foredeep). The 20 Ma isochrone is based on information from the Bengal foredeep. The mass balance for the present-day Bengal fan comprises post-20 Ma sediment south of about 20°N (table 2).

The geometries of the subaerial delta and prodelta are also assumed to be asymmetric in E-W cross sections (shape factor 0.825), because they are bound in the east by a fault zone (figure 6*a*). However, the base of the Miocene is difficult to assess, because no drill hole has reached its depth. Offshore drillholes (ARCO A-1 and BINA 2) in the prodelta region ended in the upper Miocene at a depth of approximately 4.5 km below the sea floor (Reimann 1993). Some information can be gained from N-trending seismic lines (BOGMC 1988; Curray 1994; Reimann 1993). The depth to basement (break-up unconformity) below the present delta front is 20 to 22 km (Curray 1994; Reimann 1993). Post-Paleocene sediments are up to about 16 km thick (figure 1*c*). Taking into account the information from the Bengal foredeep as well as the length of the Oligocene (25 m.y.) and the subsequent increase in sedimentation rate since about 20 Ma, we assume that post-collision Eocene and Oligocene strata make up not more than about 35% of the total post-collision sediment thickness. Thus we obtain a thickness of about 10 km for post-20 Ma sediments (figure 6*b*) for the delta and prodelta segments. This corresponds to ~50% of the total Cretaceous/Cenozoic sediment thickness present

on thinned continental or oceanic crust. Based on these estimations, the Neogene sediments of the Bengal foredeep, the delta, and prodelta to the north of 20°N have a total volume of 2.2×10^6 km^3 (table 2). This is almost the same value obtained by planimetry of Curray's isopachs for post-collision sediment in this area (3.1×10^6 km^3), assuming that 65% of this volume (2.0×10^6 km^3) is post-20 Ma.

Bengal Deep-sea Fan. The sediments in the Bay of Bengal and in the Indian ocean principally consist of two units separated by a more or less distinct regional unconformity of Early Eocene age (figure 6*b*, Curray 1994). The lower pre-Eocene unit is thought to represent pre-collision sediments of the continental rise surrounding India and pelagic deposits. The upper unit is interpreted as the post-collision turbidite section of the Bengal fan shed by a point source from the north. Drilling to the Eocene unconformity, however, was not yet possible; thus neither the onset of post-collision proximal Bengal fan sedimentation nor the nature and areal extent of the unconformity are clear. In the distal fan region only (ODP-Leg 116, Sites 717 and 718, figures 1*d* and 6*b*), a major portion of the fan sediments (961 m maximum), consisting predominantly of mud turbidites, was drilled. The oldest sediment age at Site 718 is 17 Ma (Early Miocene); the base of the fan was not drilled. Seismic lines and the downhole trend in sedimentation rate point to a fan base age of approximately 20 Ma, but an older fan base (Curray 1994) is also possible. Either the fan slowly prograded from north to south since the Eocene onset of mountain building in the Himalayas (as assumed by Curray 1994), or deposition of the major part of the outer Bengal fan commenced as late as about 20 Ma (e.g., Cochran 1990 *in* Harrison et al. 1993). It appears that an early stage of fan deposition with shorter transport distance was followed by intensified, long-distance fan deposition since the Miocene. Increased sediment influx in combination with a high tidal range and sea-level changes may have generated larger sediment gravity flows and turbidity currents. In any case, upbuilding of the present-day distal Bengal fan already began in the Early Miocene. The fan did not significantly prograde since that time.

To determine the sediment volume of the Bengal fan, we used Curray's isopach map (figure 1*c*) for post-Paleocene Bengal fan deposits. In contrast to Curray's volume calculation, we considered the present-day fan configuration south of 20°N latitude only (figure 6*b*). Similar to the basin fills upstream, we took 65% of Curray's post-Paleocene sediment thickness at the head of the fan as Neogene (post-20 Ma). However, a distinct change in lithology, as described above from the sediment-filled basins, has not been observed on the existing seismic lines. Although the lower fan may almost entirely consist of post-20 Ma fan material, we assumed that 65% of the entire post-collision fan volume of 7.4×10^6 km^3 to the south of 20°N is post-20 Ma (table 2). Areas outside of Curray's 1-km isopach along the lower fan were neglected because the present-day lower end of the morphologically expressed fan approximately coincides with the 1 km isopach in Curray's map (figure 1*c,d*). The Nicobar fan as shown on the isopach map is included in the calculation. In this way we found a post-20 Ma fan volume of 4.8×10^6 km^3.

Summing up the post-20 Ma (Miocene through Holocene) sediment volumes of both the Bengal fan (south of 20°N) and the basin segments to the north of 20°N, we got 7.0×10^6 km^3 (wet sediment). This is 56% of Curray's volume of 12.5×10^6 km^3 for post-collision Eocene through Holocene sediments which includes "part of the outer Bengal delta" (Curray 1994).

Sediment Lost to the Indus Accumulation System and the Sunda Arc

The Indus river system in the northwestern Himalayas and Karakoram drained toward the Gulf of Bengal up to about 5 Ma; thereafter, it took its present course toward the Arabian Sea. Consequently, we have to subtract the volume of rocks eroded within the Indus–Sutlej drainage system during the past 5 m.y. from our mass balance (table I, file). For this estimate we calculated cumulative erosional volumes (1) north of the IYS using Searle's (1991) Karakoram section (segment 6); (2) in the western central Gangdese belt (Leh to Mt. Kailas area, ~480 km along strike) based on our previous estimate using Rowley's (1995) technique (segment 6); and (3) south of the IYS, based on Searle's (1991) and Steck et al.'s (1993) western Himalaya sections (segments 1 and 2) that cover the area of the drainage systems of Indus and Sutlej. In this way, the total erosional volume for the past 55 Ma was 1.94×10^6 km^3. Because a partition of this amount into a pre-20 Ma and post-20 Ma value is problematic in this area, we calculated 9.1% (corresponding to 5 Ma) from the total rock volume eroded as a minimum value (0.18×10^6 km^3; table 1). This value is definitely too low (see section on partitioning of rock volume); therefore we took 0.3×10^6 km^3 as a more realistic estimate for sediment loss to the modern Indus depositional system.

The major part of the sediments of the present-

day Nicobar fan originated from the Himalayas because detritus from eastern land masses (Burma and Indonesia) were largely trapped by backarc, forearc, and slope basins of the Sunda arc-trench system (figure 1; Curray et al. 1982 *in* Curray 1994). In addition, a significant portion of the Himalaya-derived material of the Nicobar fan was subducted along the Sunda trench (Curray et al. 1982 and Moore et al. 1982 both *in* Curray 1994). Convergence at this plate boundary was highly oblique with a northward-increasing right-lateral strike-slip component (e.g., Dewey et al. 1989 *in* Le Pichon et al. 1992; Hutchinson 1989, p. 41). Nevertheless, a large accretionary prism has built up, particularly in the north. From cross sections of the Andaman Islands and Nias Island (off Sumatra), based on seismic lines and drill holes (Moore et al. 1982 and Curray et al. 1982, both *in* Curray 1994), we inferred that one-fourth to one-third of the presently incoming Nicobar fan sediment is pre-Miocene; hence about 1.26×10^6 km^3 of post-Oligocene sediment has been incorporated in the accretionary wedge along the Sunda trench from 20°N to 3°S. Converted to dry solid rock of 2.75 g/cm^3, this may yield about 1.1×10^6 km^3. The Indo-Burman ranges to the east of the Kaladan fault represent an accretionary prism predominantly of Triassic to Oligocene rocks (BOGMC 1988).

Results of the Mass Balances for Denudation and Sediment Accumulation

The results of the mass balances for rocks eroded and sediments accumulated during the past 20 m.y. are summarized in figure 7 (rounded values). Volumes of differently compacted sediments in the various basins were transformed into volumes of solid rock of a bulk density of 2.75 g/cm^3 (table 2); this is the average density assumed for the eroded rock sequences in the Himalayas as well as those of peninsular India.

The total eroded rock volume in the Himalayas ($A = 7.4 \times 10^6$ km^3) and peninsular India (C + D in figure 7, including chemical denudation), minus sediment loss both to the Indus system (B) south of the Subhimalayan foredeep and to the eastern Indian shelf/slope (E) is 7.8×10^6 km^3. The total sediment volume (converted to dry solid rock) accumulated in the various basins, plus sediment loss (G in figure 7) to the Sunda arc (taking a minimum of 1×10^6 km^3), is c. 8.1×10^6 km^3.

To compare erosion in the Himalayas and sediment derived from the Himalayas only, the values are as follows (figure 7):

—Eroded rocks: (A–B) = c. 7.1×10^6 km^3 (= 1.95×10^{16} metric tons).
—Sediments: (total from above–C–F) = c. 7.4×10^6 km^3 (= $2.04\ 10^{16}$ metric tons).

Dissolved matter that may have escaped to the ocean beyond the Bengal fan is of minor importance and not considered in the above calculation.

Discussion and Conclusions

Mass Balances. The Himalayas appear to be better suited than many other mountain ranges (e.g., the Alps) for a mass balance of eroded rocks and accumulated sediments. The modern High Himalayan chain and the southern margin of the Tibet plateau represent a divide separating a region of

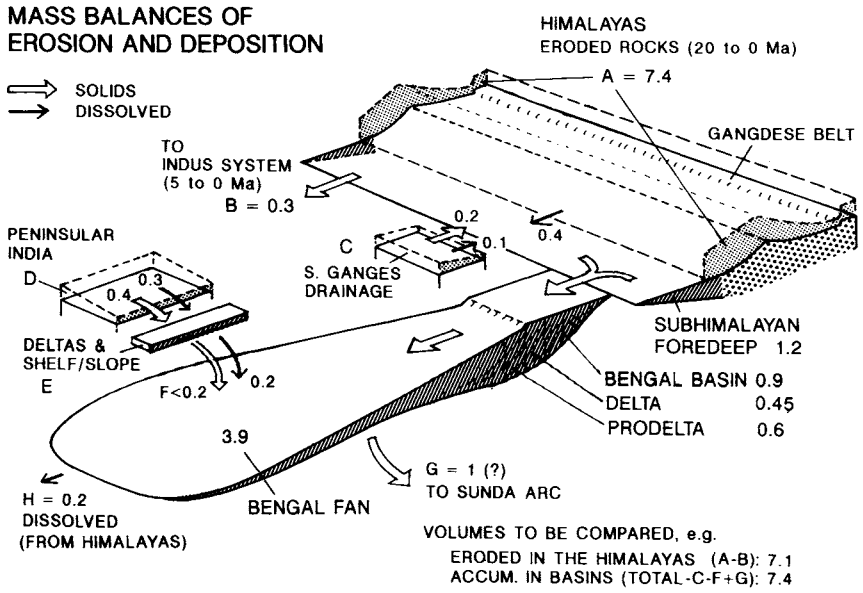

Figure 7. Eroded rock volumes from the Himalayas, southern Tibet, and the Indian subcontinent as well as accumulated sediment volumes from the Subhimalayan foredeep to the Bengal deep-sea fan (and Sunda arc) during the past 20 m.y. (not to scale; numbers indicate 10^6 km^3 rocks of 2.75 g/cm^3 mean density, all values rounded). Total values of mass balances to be compared are at bottom of figure.

moist monsoonal climate in the south (with high rates of erosion) from one of arid climate in the north (with very limited erosion). South of this divide, all weathering products are transported to the Indo-Gangetic foreland basin, the Bengal foredeep, and ultimately to large deep-sea fans. Because this scenario cannot be traced very far back into geological history, we chose a shorter time period (20 instead of 55 m.y.) and a smaller study area than previous authors. For the denudation area of the Himalayas from the western to the eastern syntaxis more data for rock exhumation are available than for neighboring regions. Whether and to what degree the ancestral Himalayan rivers were antecendent or whether individual rivers changed their courses or captured one another within the entire drainage system is not relevant here. The tectonic nature and geometry of the sedimentary basins accumulating detritus from the Himalayas is largely known, including the extent and thickness of the Bengal fan. However, two serious problems arose from the choice of the 20 Ma isochrone as the base of our study: (1) the distinction of pre- and post-20 Ma erosion and (2) the identification of the Oligocene/Miocene boundary (the c. 20 Ma isochrone) in the basin fills, particularly in the Bengal deep-sea fan.

The errors in the mass balances introduced by this uncertainty as well as by incomplete knowledge and dating of the orogenic system (including part of the Sunda accretionary wedge) are difficult to assess. Smaller errors (1 to 5%) due to inaccuracies in the methods and inherent in the overburden estimates (around 10%) are in tables 1 and 2 as well as I and III (file). A reliable estimate of the total error as not possible, but we believe that the true rock volumes do not deviate by more than about ±10–20% from the obtained values. In any case, the values for the eroded and accumulated rock volumes, independently determined for the Himalayan-Bengal fan denudation-accumulation system for the last 20 m.y., are surprisingly close.

Denudation Rates in the Himalayas. Denudation rates normally describe the average vertical lowering of the land surface and do not specificly take into account lateral slope retreat. However, at the margins of plateaus, for example generated by thrusting in orogenic belts, lateral slope retreat may operate faster than vertical lowering (e.g., Masek et al. 1994). The southern slope of the High Himalayan chain is exposed to heavy monsoonal rain (up to more than 2000 mm/a) and retreated at a rate of c. 3.5 km/Ma during the past 20 m.y. (figures 4*a,c*) and 8). Average vertical denudation rates as inferred from restored cross sections are

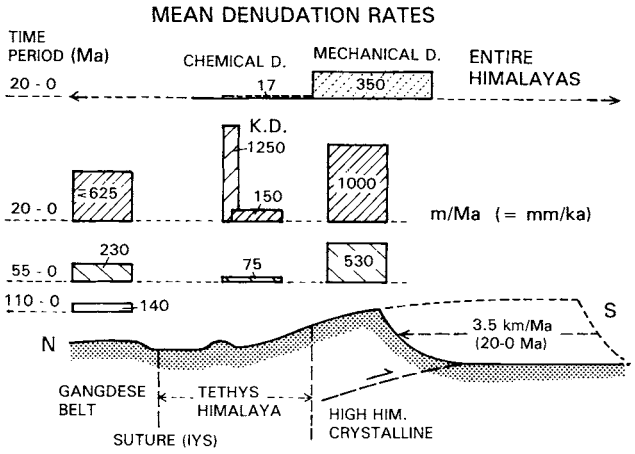

Figure 8. Average denudation rates (m/m.y.) for various zones and time periods (Ma) in the Himalayas. K.D., Kangmar dome.

considerably smaller (figure 8 and table II, file) and vary significantly with the time period considered as well as from region to region. Denudation clearly operated faster in the post-20 Ma period (e.g., 1000 m/m.y. in the High Himalayan crystalline chain, 150 m/m.y. in the Tethyan sedimentary zone). An exception within the Tethyan zone is the Kangmar basement dome; rapid exhumation (up to 1250 m/m.y.; Maluski et al. 1988 *in* Molnar et al. 1993). Post-20 Ma denudation along the southern margin of the Tibet plateau (Gangdese belt) varied significantly along strike and may have reached an average value of some hundred meters per million years (figure 8). Normal faulting has reduced denudation in the Tethyan sedimentary zone where Paleozoic to Paleogene sediments are preserved at the land surface. The denudation rate calculated from the total (dry) sediment volume (7.4×10^6 km^3) accumulated in the Subhimalayan basins (sediment budget method) only yields an average value of approximately 350 m/m.y. for the entire Himalayan drainage area of 1.05×10^6 km^2 and the past 20 m.y.

The composition of Bengal fan sediments reflects the marked regional differences in denudation rates. Both the coarser-grain fractions with their isotopic characteristics and the illite-chlorite-rich clay association display the signature of the metamorphic source rocks (France-Lanord et al. 1993) and confirm that the High Himalayan crystalline series were the principal denudation area since at least 17 Ma. The sediment contributions from the Lesser Himalayas and the Tibetan sedimentary series are thought to be <20% of the total rock volume eroded.

Sedimentation Rates as Records of Tectonic Activity in the Himalayas. Several authors have postulated specific tectonic events in the evolution of the Himalayan orogen (e.g., Klootwijk et al. 1992; Rea 1992; Sorkhabi and Stump 1993). The onset of the fluvial Siwalik molasse deposition and a distinct facies change in the shallow-marine Bengal foredeep in the Early/Middle Miocene evidently record a phase of increased tectonic activity in the Himalayan orogen. An advanced state of unroofing in the Himalayas since that time is also testified to by studies on detrital minerals from the molasse foredeep and outer Bengal fan (e.g., Cerveny et al. 1989; Copeland and Harrison 1990 *in* Harrison et al. 1993). Later on (since ~8 Ma), the relationship between tectonics and sedimentation is less clear. There is a tendency to continued coarsening-upward of the Siwalik molasse (e.g., Kumar et al. 1991), but it is accompanied by decreasing accumulation rates (Burbank et al. 1993). Whereas the increasing proportion of conglomerates in the Upper Siwaliks is either associated with the approaching front of the mountain range or accelerated uplift driven by erosional unloading (Burbank 1992), the reduced accumulation rate may result from the fact that the still subsiding, but sediment-filled foreland basin and its river gradients did not allow unlimited sediment aggradation.

Cumulative curves for Bengal fan aggradation (decompacted sediments) at the distal ODP Sites 717C and 718C show decreasing sediment accumulation since about 7 Ma (Burbank et al. 1993). Similarly, mass accumulation rates for these sites display, after an earlier peak, reduced sediment influx since that time (Rea 1992). The average accumulation rates (30 to 40 m/m.y. including DSDP Site 218 on the central fan) are comparatively low apart from short periods with high rates of up to more than 100 m/m.y. We cannot further discuss this problem here. In any case, all three sites display an overall decrease in sediment accumulation with rates (3 to 8 m/m.y.) as low as those for pure pelagic or hemipelagic sedimentation between 1 and 5 Ma. This contrasts with locally increased accumulation rates on the Indus fan (Rea 1992), which may result from the enlarged drainage system of the Indus river since late Miocene to Pliocene time.

The distinct decrease in sediment accumulation on the Bengal fan over several million years probably was controlled by exogenic factors rather than by slowing tectonic activity. (1) Mechanical denudation in the mountain ranges may have declined as a result of increasing slope stabilization from dense plant cover (Burbank et al. 1993) under intensified monsoonal climate (e.g., Kroon et al. 1991 *in* Harrison et al. 1993). The change from the previous illite-chlorite-dominated clay assemblage to a smectite-kaolinite association from 7 to 0.8 Ma may be climate-controlled (France-Lanord et al. 1993). (2) Reduced deposition on the outer Bengal fan may have been caused by a change in the capacity of the mass transport system feeding the deep-sea fan. Reduced river floods, finer-grained solid river loads, and smaller, but more frequent slope failures in the delta region could have led to suspension currents of shorter travel distance and therefore to enhanced deposition on the upper and middle fan at the expense of the outer fan. Such a situation may also have existed during the early phases of fan deposition, for example during the Eocene.

During the middle and late Pleistocene (the past 0.8 to 1 m.y.) all three Bengal fan DSDP/ODP-drilling sites exhibit a distinct pulse of sediment accumulation. This probably resulted from increased mechanical denudation (glacial and periglacial processes) in the source area and high-frequency, high-amplitude (since 0.8 Ma in excess of 100 m) sea-level changes (Cochran 1993). The latter may have affected even the shelf break and thus triggered large-scale removal of older deltaic and shelf sediments and their redeposition in deeper water.

In conclusion, we believe that the denudation-sediment accumulation system of the Himalayas probably was not far from a dynamic equilibrium in the sense of England and Molnar (1990) and Burbank (1992) during the past 20 m.y. Since that time the high and differentiated relief of the denudation area appears to have more or less persisted. A further discussion on the interplay between surface uplift, relief, regional and global climate is beyond the scope of this paper.

ACKNOWLEDGMENTS

This contribution was inspired by our field work in Tibet and the participation of A. W. in ODP-Leg 116. Both projects and L. R.'s work at Stanford were funded by Deutsche Forschungsgemeinschaft. We thank Ed Sobel and Manfred Strecker for pre-submission reviews and Joe R. Curray and an anonymous reviewer for their comments to the first version of this paper. In particular the constructive advice of J. R. Curray and recommendations by A. T. Anderson, Jr., were most useful for the revision of the manuscript. Jörg Pfänder assisted with drawing and electronic trans-Atlantic communication.

REFERENCES CITED

Alam, M., 1989, Geology and depositional history of Cenozoic sediments of the Bengal Basin of Bangladesh: Palaeogeog. Palaeoclimatol. Palaeoecol., v. 69, p. 125–139.

BOGMC (Bangladesh Oil Gas and Mineral Corporation), 1988, Exploration opportunities in Bangladesh: BOGMC, Dakha, 40 p.

Brookfield, M. E., 1993, Miocene to Holocene uplift and sedimentation in the northwestern Himalaya and adjacent areas, *in* Shroder, J. F., Jr., ed., Himalaya to the Sea—Geology, Geomorphology and the Quaternary: Routledge, London and New York, p. 43–75.

Brunel, M., and Kienast, J.-R., 1986, Etude petrostructurale des chevauchements ductiles himalayens sur la transversale de l'Everest–Makalu (Nepal oriental): Can. Jour. Earth Sci., v. 23, p. 1117–1137.

Burbank, D. W., 1992, Causes of recent Himalayan uplift deduced from deposited patterns in the Ganges basin: Nature, v. 357, p. 680–683.

———; Derry, L. A.; and France-Lanord, C., 1993, Reduced Himalayan sediment production 8 Myr ago despite an intensified monsoon: Nature, v. 364, p. 48–50.

Burchfiel, B. T.; Chen, Z.; Hodges, K. V.; Liu, Y.; Royden, L. H.; Deng, C.; and Xu, J., 1992, The South Tibetan detachment system, Himalayan Orogen: Extension contemporaneous with and parallel to shortening in a collisional mountain belt: Geol. Soc. America Spec. Paper 269, 41 p.

Cerveny, P. F.; Johnson, N. M.; Tahirkheli, R. A. K.; and Boni, N. R., 1989, Tectonic and geomorphic implications of Siwalik Group heavy minerals, Potwar Plateau, Pakistan: Geol. Soc. America Spec. Paper 132, p. 129–136.

Chen, Z.; Liu, Y.; Hodges, K. V.; Burchfiel, B. C.; Royden, L. H.; and Deng, C., 1990, The Kangmar dome: A metamorphic core complex in southern Xizang (Tibet): Science, v. 250, p. 1552–1556.

Chamberlain, C. P.; Zeitler, P. K.; and Jan, M. Q., 1989, The dynamics of the suture between the Kohistan island arc and the Indian plate in the Himalaya of Pakistan: Jour. Meta. Geol., v. 7, p. 135–149.

Cochran, J. R., 1993, Two-phase uplift of Higher Himalayas since 17 Ma: Comment: Geology, v. 21, p. 378–379.

Critelli, S., and Garzanti, E., 1994, Provenance of Lower Tertiary Murree redbeds (Hazara-Kashmir syntaxis, Pakistan) and initial rising of the Himalayas: Sed. Geol., v. 89, p. 265–284.

Curray, J. R., 1994, Sediment volume and mass beneath the Bay of Bengal: Earth Planet. Sci. Lett., v. 125, p. 371–383.

Einsele, G., 1992, Sedimentary basins: Evolution, Facies, and Sediment Budget: Berlin, Springer-Verlag, 628 p.

———; Liu, B.; Dürr, S.; Frisch, W.; Liu, G.; Luterbacher, H. P.; Ratschbacher, L.; Ricken, W.; Wendt, J.; Wetzel, A.; Yu, G.; and Zheng, H., 1994, The Xigaze forearc basin: Evolution and facies architecture (Cretaceous, Tibet): Sed. Geol., v. 90, p. 1–32.

Emmel, F. J., and Curray, J. R., 1984, The Bengal submarine fan, northern Indian Ocean: Geo-Marine Letters, v. 3, p. 119–124.

England, P., and Molnar, P., 1990, Surface uplift, uplift of rocks, and exhumation of rocks: Geology, v. 18, p. 1173–1177.

Farhoudi, G., and Karig, D. E., 1977, Makran of Iran and Pakistan as an active arc system: Geology, v. 5, p. 664–668.

France-Lanord, C.; Derry, L.; and Michard, A., 1993, Evolution of the Himalaya since Miocene time: Isotopic and sedimentological evidence from Bengal fan, *in* Treloar, P. J., and Searle, M. P., eds., Himalayan tectonics: Geol. Soc. London Spec. Pub. 74, p. 603–621.

Harrison, T. M.; Copeland, P.; Hall, S. A.; Quade, J.; Burner, S.; Ojha, T. P.; and Kidd, W. S. F., 1993, Isotopic preservation of Himalayan/Tibetan uplift, denudation, and climatic histories of two molasse deposits: Jour. Geology, v. 101, p. 157–175.

———; ———; Kidd, W. S. F.; and An, Y., 1992, Raising Tibet: Science, v. 255, p. 1663–1670.

———; McKeegan, K. D.; and Le Fort, P., 1995, Identification of inherited monazite in the Manaslu leucrogranite by $^{208}Pb/^{232}Th$ ion microprobe dating: Geology, in press.

Hodell, D. A.; Mueller, P. A.; and Garrido, J. R., 1991, Variations in the strontium isotopic composition of seawater during the Neogene: Geology, v. 19, p. 24–27.

Hodges, K. V.; Burchfiel, B. C.; Royden, L. H.; Chen, Z.; and Liu, Y., 1993, The metamorphic signature of contemporaneous extension and shortening in the central Himalayan orogen: Data from the Nyalam transect, southern Tibet: Jour. Meta. Geol., v. 11, p. 721–737.

———; Hubbard, M. S.; and Silverberg, D. S., 1988*a*, Metamorphic constraints on the thermal evolution of the central Himalayan orogen: Royal Soc. (London) Philos. Trans., v. 326A, p. 257–280.

———; Lefort, P.; and Pêcher, A., 1988*b*, Possible thermal buffering by crustal anatexis in collisional orogens: Thermobarometric evidence from the Nepalese Himalaya: Geology, v. 16, p. 707–710.

———; Parrish, R.; Housh, T.; Lux, D.; Burchfiel, B. C.; Royden, L. H.; and Chen, Z., 1992, Simultaneous Miocene extension and shortening in the Himalayan orogen: Science, v. 258, p. 1466–1470.

———, and Silverberg, D. S., 1988, Thermal evolution of the Greater Himalaya, Garhwal, India: Tectonics, v. 7, p. 583–600.

Hovius, N., 1993, Sediment flux from source to basin: a global overview using new database: Terra Abstracts 6 (Supplement 1), p. 169.

Hubbard, M. S., 1989, Thermobarometric constraints on the thermal history of the Main Thrust zone and Ti-

betan slab, eastern Nepal Himalaya: Jour. Metamor. Geol. v. 7, p. 19–30.

Hutchinson, C. S., 1989, Geological Evolution of South-East Asia (Oxford Mon. Geol. Geophys. 13): Oxford, Clarendon Press, 368 p.

Johnson, M. R. W., 1994, Volume balance of erosional loss and sediment deposition related to Himalayan uplifts: Jour. Geol. Soc., London, v. 151, p. 217–220.

Khan, M. J., and Opdyke, N. D., 1993, Position of the Paleoindus as revealed by the magnetic stratigraphy of the Shinghar and Surghar ranges, Pakistan, *in* Shroder, J. F., Jr., ed., Himalaya to Sea—Geology, Geomorphology and the Quarternary: London and New York, Routledge, p. 198–212.

Klootwijk, C. T., Gee, J. S.; Peirce, J. W.; and Smith, G. M., 1992, Neogene evolution of the Himalayan-Tibetan region: Constraints from ODP Site 758, northern Ninetyeast Ridge; bearing on climatic change: Palaeogeog. Palaeoclimatol. Palaeoecol., v. 95, p. 95–110.

Kumar, R.; Ghosh, S. K.; Virdi, N. S .; and Phadtare, N. R., 1991, The Siwalik Foreland Basin (Dehra Dun-Nahan sector) Excursion Guide: Wadia Inst. Himalayan Geol. Spec. Pub. 1, 61 p.

LeFort, P.; Pêcher, A.; and Upreti, B. N., 1986, A section through the Tibetan slab in central Nepal (Kali Gandaki valley): mineral chemistry and thermobarometry of the Main Central Thrust Zone, *in* LeFort, P.; Colchen, C.; and Montenat, C., eds., Sciences de la Terre Mem. 47, p. 211–228.

Le Pichon, X.; Fournier, M.; and Jolivet, L., 1992, Kinematics, topography, shortening, and extrusion in the India-Eurasia collision: Tectonics, v. 6, p. 1085–1098.

Liu, G., and Einsele, G., 1994, Sedimentary history of the Tethyan basin in the Tibetan Himalayas: Geol. Rundschau, v. 83, p. 32–61.

Masek, J. G.; Isacks, B. L.; Gubbels, T. L.; and Fielding, E. J., 1994, Erosion and tectonics at the margins of continental plateaus: Jour. Geophys. Res., v. 99, p. 13,941–13,956.

McDougall, J. W.; Huassain, A.; and Yeats, R. S., 1993, The Main Boundary Thrust and propagation of deformation into the foreland fold-and-thrust belt in northern Pakistan near the Indus River, *in* Treloar, J. P., and Searle, M. P., eds., Himalayan tectonics: Geol. Soc. London Spec. Pub. 74, p. 581–588.

Meade, R. H., 1992, River-sediment inputs to major deltas, *in* Milliman, J. D., and Sabhasri, S., eds., Sea-Level Rise and Coastal Subsidence: Problems and Strategies (SCOPE Series): New York, Wiley.

Metcalfe, R. P., 1993, Pressure, temperature, and time constraints on metamorphism across the in Central Thrust zone and High Himalayan Slab in the Garhwal Himalaya, *in* Treloar, P. J., and Searle, M. P., eds., Himalayan tectonics: Geol. Soc. London Spec. Pub. 74, p. 485–509.

Milliman, J. D., and Meade, R. J., 1983, World-wide delivery of river sediment to the oceans: Jour. Geology, v. 91, p. 1–21.

Mohan, A.; Windley, B. F.; and Searle, M. P., 1989, Geothermobarometry and development of inverted metamorphism in the Darjeeling-Sikkim region of the eastern Himalaya: Jour. Metamorph. Geol., v. 7, p. 95–110.

Molnar, P.; England, P.; and Martinod, J., 1993, Mantle dynamics, uplift of the Tibetan plateau, and the Indian monsoon: Rev. Geophys., v. 31, p. 357–396.

Montgomery, D. R., 1994, Valley incision and the uplift of mountain peaks: Jour. Geophys. Res., v. 99, p. 13,913–13,921.

Najman, Y.; Clift, P.; Johnson, M. R. W.; and Robertson, A. H. F., 1993, Early stages of foreland basin evolution in the Lesser Himalayas, *in* Treloar, J. P., and Searle, M. P., eds., Himalayan tectonics: Geol. Soc. Spec. Pub. 74, p. 541–558.

Pêcher, A., 1989, The metamorphism in the Central Himalaya: Jour. Metamor. Geol., v. 7, p. 31–41.

Perrier, R., and Quiblier, J., 1974, Thickness changes in sedimentary layers during compaction history: methods for quantitative evaluation: Am. Assoc. Petrol. Geol. Bull., v. 58, p. 507–520.

Pognante, U., and Benna, P., 1993, Metamorphic zonation, migmatization, and leucogranites along the Everest transect of eastern Nepal and Tibet: Record of an exhumation history, *in* Treloar, P. J., and Searle, M. P., eds., Himalayan Tectonics: Geol. Soc. London Spec. Pub. 74, p. 323–340.

———; ———; and LeFort, P., 1993, High-pressure metamorphism in the High Himalayan Crystallines of the Stak Valley, northeastern Nanga-Parbat, Haramosh syntaxis, Pakistan Himalaya, *in* Treloar, P. J., and Searle, M. P., eds., Himalayan Tectonics: Geol. Soc. London Spec. Pub. 74, p. 161–172.

———, and Lombardo, B., 1989, Metamorphic evolution of the High Himalayan Crystallines in SE Zanskar, India: Jour. Meta. Geol., v. 7, p. 9–17.

Rao, K. L., 1979, India's water wealth: Its assessment, uses, and projections: New Delhi, Orient Longman, 267 p.

Ratschbacher, L.; Frisch, W.; Liu, G.; and Chen, C., 1994, Distributed deformation in southern and western Tibet during and after the India-Asia collision: Jour. Geophys. Res., v. 99, p. 19,917–19,945.

Raymo, M. E., and Ruddiman, W. F., 1992, Tectonic forcing of Cenozoic climate: Nature, v. 359, p. 117–122.

Rea, D. K., 1992, Delivery of Himalayan sediment to the northern Indian Ocean and its relation to global climate, sea level, uplift, and seawater strontium, *in* Duncan, R. A.; Rea, D. K.; et al. eds., Synthesis of results from scientific drilling in the Indian ocean: Am. Geophys. Union, Geophys. Mon. 70, p. 387–402.

Reimann, K.-U., 1993, Geology of Bangladesh: Beitr. zur Regionalen Geologie der Erde, Bd. 20, Berlin and Stuttgart, Bornträger, 160 p.

Rowley, D. B., 1995, A simple geometric model for the syn-kinematic erosional denudation of thrust fronts: Earth Planet. Sci. Lett., v. 129, p. 203–216.

Schelling, D., 1992, The tectonostratigraphy and structure of the eastern Nepal Himalaya: Tectonics, v. 11, p. 925–943.

———, and Arita, K., 1991, Thrust tectonics, crustal shortening, and the structure of the Far-Eastern Nepal Himalaya: Tectonics, v. 10, p. 851–862.

Searle, M. P., 1991, Geology and Tectonics of the Karakoram Mountains: Chichester, Wiley, 358 p.

Seeber, L., and Gornitz, V., 1983, River profiles along the Himalayan arc as indicators of active tectonics: Tectonophysics, v. 92, p. 335–367.

Smosna, R., 1989, Compaction law for Cretaceous sandstones of Alaska's north slope: Jour. Sediment. Petrol., v. 59, p. 572–584.

Sorkhabi, R. B., and Stump, E., 1993, Rise of the Himalaya: a geochronologic approach: GSA Today v. 3, n. 4, p. 85 and 88–92.

Srivastava, P., and Mitra, G., 1994, Thrust geometries and deep structure of the outer and lesser Himalaya, Kumaon, and Garhwal (India): Implications for evolution of the Himalayan fold-and-thrust belt: Tectonics, v. 13, p. 89–109.

Staeubli, A., 1989, Polyphase metamorphism and the development of the Main Central Thrust: Jour. Meta. Geol., v. 7, p. 73–93.

Steck, A.; Spring, L.; Vannay, J.-C.; Masson, H.; Bucher, H.; Stutz, E.; Marchant, R.; and Tieche, J.-L., 1993, The tectonic evolution of the Northwestern Himalaya in eastern Ladakh and Lahul, India, *in* Treloar, P. J., and Searle, M. P., eds., Himalayan tectonics: Geol. Soc. London Spec. Pub. 74, p. 265–276.

Subramian, V., 1985, Geochemistry of river basins in the Indian subcontinent, part I: Water chemistry, chemical erosion, and water-mineral equilibria: Mitt. Geol.-Paläont. Inst. Univ. Hamburg, H. 58, p. 495–512.

Summerfield, M. A., and Hulton, N. J., 1994, Natural controls of fluvial denudation rates in major world drainage basins: Jour. Geophys. Res., v. 99, p. 13,871–13,883.

Treloar, P. J.; Rex, D. C.; Guise, P. G.; Coward, M. P.; Searle, M. P.; Windley, B. F.; Petterson, M. G.; Jan, M. Q.; and Luff, I. W., 1989, K-Ar and Ar-Ar geochronology of the Himalayan collision in NW Pakistan: Constraints on the timing of suturing, deformation, metamorphism, and uplift: Tectonics, v. 8, p. 881–910.

Valdiya, K. S., 1988, Tectonics and evolution of the central sector of the Himalaya: Philos. Trans. Royal Soc. London, v. A326, p. 151–175.

Wetzel, A., 1993, The transfer of river load to deep-sea fans: A quantitative approach: Am. Assoc. Petrol. Geol. Bull., v. 77, p. 1679–1692.

Willis, B., 1993, Evolution and Miocene fluvial systems in the Himalayan foredeep through a two kilometer-thick succession in northern Pakistan: Sed. Geol., v. 88, p. 77–121.

Yin, A.; Harrison, T. M.; Ryerson, F. J.; Wenji, C.; Kidd, W. S. F.; and Copeland, P., 1994, Tertiary structural evolution of the Gandese thrust system, southeastern Tibet: Jour. Geophys. Res., v. 99, p. 18,175–18,201.

Annex B56

R. Bilham et al., "GPS Measurements of Present-day Convergence Across the Nepal Himalaya", *Nature*, Vol. 386 (6 March 1997)

for by degassing of CO_2 to the atmosphere and by downward flux of sinking particles. Estimates of the partitioning between these latter two processes can be made using the downward flux of organic nitrogen as a measure of the downward export of organic carbon. In order to estimate downward flux of nitrogen, and because concurrent measurements of TOC, DIC and TON near the Equator were few, we first estimated the amount of nitrogen that accumulated in the suspended organic fraction. TON concentrations were estimated from TOC concentrations measured during the OACES program by assuming a C:N atomic ratio of 12 for total organic matter, a value reported for the surface layer along 110° W (ref. 10). Measured DIC concentrations were then plotted against estimated concentrations of total nitrogen (TIN plus estimated TON; Fig. 2c; s.e. of slope, 0.57). A decrease in total nitrogen of 8 μM corresponded to a 99.4 $\mu mol\,kg^{-1}$ decrease in DIC concentrations. The organic carbon removed to depth with the nitrogen was estimated using a C:N atomic ratio for sinking particles of 6.6. The downward flux of organic carbon represented 52.8 $\mu mol\,kg^{-1}$ (53%) of the total DIC drawdown of 99.4 $\mu mol\,kg^{-1}$. This analysis indicates that <6% and 53% of DIC depletion occurred owing to the production of TOC (with the potential for horizontal export by advection from upwelling system) and downward flux of sinking particles, respectively. Mass balance requires that the remaining 41% of inorganic carbon loss take place by degassing of CO_2 to the atmosphere.

TOC production and accumulation in the surface layer accounted for ~10% of the net community production (sum of TOC accumulation and downward flux of sinking particles) of carbon, compared to approximately 27% for nitrogen. If these data sets were directly comparable, we would expect the fractional accumulation of organic carbon in the surface layer to be greater than that for organic nitrogen. This follows from the high C:N ratio of the material. Such an inconsistency suggests that a direct comparison of the data sets is not warranted, perhaps due to analytical uncertainties and natural variability in the equatorial system.

Sensitivity analysis for the C:N ratios for sinking particles demonstrates that the proportion of C found in the TOC pool remains the same, while the contributions of export by degassing and sinking particles varies. By assuming a higher C:N ratio for sinking particles of 9, this contribution to export increases to 72%.

Assessing the fate of carbon fixed by new production is critical for determining the role of the biological pump in the long-term removal of carbon from the surface ocean. Sinking particles can remove organic carbon to below the main thermocline, thereby sequestering the carbon for periods approaching the timescale of oceanic turnover (10^2–10^4 years). Horizontal export of organic matter from the upwelling regions in the equatorial Pacific Ocean results in negligible removal of carbon from the surface ocean, leaving it available for export to the atmosphere on short timescales. The results presented here demonstrate that vertical processes (carbon transfer by degassing to the atmosphere and by downward flux of biogenic particles to the deep ocean) predominate in the export of carbon from this globally important region. □

Received 20 June 1996; accepted 13 January 1997.

1. Murray, J. W., Barber, R. T., Roman, M. R., Bacon, M. P. & Feely, R. A. *Science* **266,** 58–65 (1994).
2. Feely, R. A. *et al. J. Geophys. Res.* **92,** 6545–6558 (1987).
3. Francey, R. J. *et al. Nature* **373,** 326–330 (1995).
4. Wong, C. S., Chan, Y. H., Page, J. S., Smith, G. E. & Bellegay, R. D. *Tellus* **45,** 64–79 (1993).
5. Tans, P. P., Fung, I. Y. & Takahashi, T. *Science* **247,** 1431–1438 (1990).
6. Chavez, F. P. & Barber, R. T. *Deep-Sea Res.* **34,** 1229–1243 (1987).
7. Feely, R. A. *et al. Deep-Sea Res. II* **42,** 365–386 (1995).
8. Peltzer, E. T. & Hayward, N. A. *Deep-Sea Res. II* **43,** 1155–1180 (1996).
9. Libby, P. S. & Wheeler, P. A. *Deep-Sea Res. I* (in the press).
10. Hansell, D. A. & Waterhouse, T. Y. *Deep-Sea Res. I* (in the press).
11. Lamb, M. F. *et al. Data Rep. ERL PMEL-56* (NOAA, Seattle, WA, 1995).
12. Lukas, R. & Lundstrom, E. *J. Geophys. Res.* **96,** 3343–3357 (1991).
13. Wanninkhof, R. *et al. Deep-Sea Res. II* **42,** 387–409 (1995).
14. Redfield, A. C., Ketchum, B. H. & Richards, F. A. in *The Sea* Vol. 2 (ed. Hill, M. N.) 26–77 (Wiley, New York, 1963).

Acknowledgements. We thank R. Feely, M. Roberts, E. Peltzer, S. Libby and P. Wheeler for their analytical work, and whose data we used in the analysis. Comments from R. Murnane were appreciated.

Correspondence should be addressed to D.A.H. (e-mail: dennis@bbsr.edu).

GPS measurements of present-day convergence across the Nepal Himalaya

Roger Bilham*, Kristine Larson†, Jeffrey Freymueller‡ & Project Idylhim members§

* *CIRES and Department of Geological Sciences, University of Colorado, Boulder, Colorado 80309, USA*
† *Department of Aerospace Engineering Sciences, University of Colorado, Boulder, Colorado 80309, USA*
‡ *Geophysical Institute, University of Alaska, Fairbanks, Alaska 99775, USA*

The high elevations of the Himalaya and Tibet result from the continuing collision between India and Asia, which started more than 60 million years ago[1–4]. From geological and seismic studies of the slip rate of faults in Asia[5], it is believed that approximately one-third of the present-day convergence rate between India and Asia (58 ± 4 mm yr^{-1}) is responsible for the shortening, uplift and moderate seismicity of the Himalaya. Great earthquakes also occur infrequently in this region, releasing in minutes the elastic strain accumulated near the boundary zone over several centuries, and accounting for most of the advance of the Himalaya over the plains of India. The recurrence time for these great earthquakes is determined by the rate of slip of India beneath Tibet, which has hitherto been estimated indirectly from global plate motions[6], from the slip rates of faults in Asia[7,8], from seismic productivity[9], and from the advance of sediments on the northern Ganges plain[10]. Here we report geodetic measurements, using the Global Positioning System (GPS), of the rate of contraction across the Himalaya, which we find to be 17.52 ± 2 mm yr^{-1}. From the form of the deformation field, we estimate the rate of slip of India beneath Tibet to be 20.5 ± 2 mm yr^{-1}. Strain sufficient to drive one or more great Himalayan earthquakes, with slip similar to that accompanying the magnitude 8.1 Bihar/Nepal 1934 earthquake, may currently be available in western Nepal.

In March 1991 we used Global Positioning System (GPS) geodesy to measure the relative positions of 24 points in India, Nepal and Tibet. Some of these points were remeasured in 1992[11] and in 1995, and additional points were installed in November 1995 in collaborative programmes between US, Nepalese, Indian, Chinese and French teams. Data were obtained in five 8-h sessions in 1991 and 1992 and for three to five consecutive 24-h sessions in 1995. We occupied a central point near Kathmandu (NAGA) continuously during each survey relative to which all positions are referred. The data from all surveys were analysed with the GIPSY software[12], using an estimation strategy summarized in ref. 13, and orbital data from the global tracking network using a geodetic reference frame defined by ITRF94 (ref. 14).

For 20 points common to the 1994 and 1991 surveys the mean formal uncertainty in northward velocities relative to NAGA is ±1.1 mm yr^{-1}, and ±1.8 mm yr^{-1} for eastward components, considerably smaller than previous GPS measurements in the Himalaya[15]. The maximum observed convergence velocity between northern India and southern Tibet is 18.2 ± 2 mm yr^{-1} at 13° ± 4°. Mean velocity uncertainties relative to Bangalore, southern India (the nearest permanent site), are ±1.9 mm yr^{-1} north and ±2.3 mm yr^{-1} east (Fig. 1). In southern Nepal, convergence velocities

§ F. Jouanne (Univ. Savoie, Chambiry, France), P. Le Fort, P. Leturmy & J. L. Mugnier (LGCA-CNRS, UJF, Grenoble, France), J. F. Gamond, J. P. Glot & J. Martinod, (LGIT-CNRS, UJF, Grenoble, France), N. L. Chaudury, G. R. Chitrakar, U. P. Gautam, B. P. Koirala, M. R. Pandey, R. Ranabhat, S. N. Sapkota, P. L. Shrestha, M. C. Thakuri, U. R. Timilsina & D. R. Tiwari (Dept Mines and Geology, Kathmandu, Nepal), G. Vidal (ENS Lyon, France), C. Vigny (ENS Paris, France), A. Galy (CRPG-CNRS, Nancy, France), B. de Voogd (Univ. Pau, France).

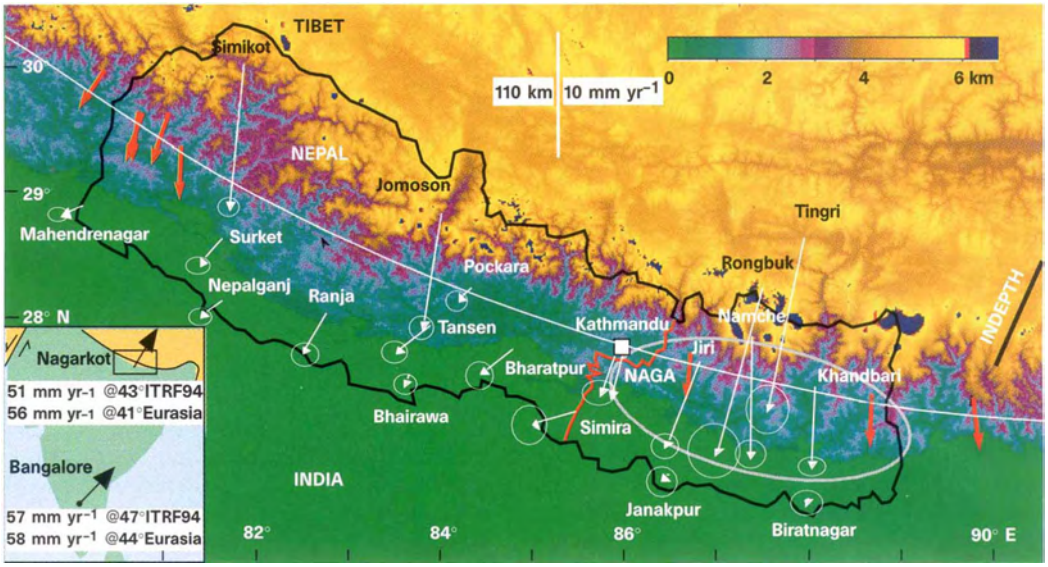

Figure 1 Himalayan GPS velocity vectors (white lines with arrowheads) 1991–95 relative to Bangalore. The levelling line (see text; red) passes near Nagarkot (white square, NAGA, to which GPS processing was referenced) and the western edge of the inferred rupture of the 1934 earthquake (large ellipse). White line, small-circle approximation for the Himalayan arc; black line, INDEPTH seismic profile[26]; red arrows, slip vectors for moderate earthquakes[15] since 1960. Inset, location map showing Bangalore and Nagarkot vectors[18,19] for ITRF94 and for a no-net-rotation frame for Eurasia fixed with uncertainties of 4 mm in scale and 5° in azimuth. Error ellipses are one standard deviation; the colour scale indicates elevation in kilometres.

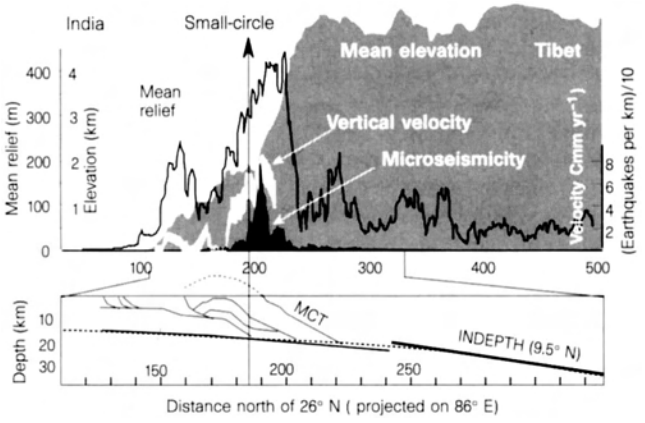

Figure 2 Top, levelling data (white envelope), seismic data[28] (black envelope), mean elevation data (shaded) and topographic relief (0.05° digital terrain data) at 86° ± 1° E. The high peaks of the Himalaya are found close to the edge of the Tibetan plateau, 20–30 km north of the region of maximum relief. A small-circle fit to maximum Himalayan stream gradients and moderate seismicity[24] intersects the section near maximum downslope tilts (2.5 μrad yr⁻¹) in the vertical velocity field. Bottom, a typical geological section for eastern Nepal[25] (MCT, Main Central Thrust) and the estimated dip of the upper surface of the Indian plate from the INDEPTH seismic profile[26] (see Fig. 1), using the small-circle approximation for the Himalayan arc to project at 86° E. Dashed line, polynomial fit used to approximate flexure of the Indian plate used in Fig. 3.

are low but approximately arc-normal. In contrast, the mean convergence velocity for points on the southern margin of the Tibetan plateau is apparently directed at the approaching Indian plate (17° ± 4°), arc-normal in eastern Nepal but trending 22° east of arc-normal in western Nepal, not significantly different from the slip vectors of published focal mechanisms for nearby thrust earthquakes[16]. Focal mechanisms for moderate earthquakes along the Himalayan arc approximate arc-normal slip which, if India is assumed rigid, requires ~N100° E extension of the southern Tibetan plateau at a rate approximating the rate at which India collides with Tibet[17–19]. Thus if extension occurs steadily, Simikot and Tingri should recede from each other at ~7 ± 2 mm yr^{-1}. That these points currently converge at 3 ± 3 mm yr^{-1} requires episodic and/or heterogeneous east–west extension of southern Tibet.

GPS data from NAGA and Bangalore were used recently to confirm[20] the NUVEL1 hypothesis that India rotates anticlockwise relative to the Australia plate[6]. The data we have since collected at Bangalore confirm NUVEL1 motions in southern India, but it is clear that NAGA, which approaches Bangalore at 5.0 ± 1.5 mm yr^{-1}, is within the deforming zone between India and Eurasia, consistent with earlier findings that minor deformation occurs in the Lesser Himalaya[21]. The eastward motion of our points in Nepal and south central Tibet relative to Eurasia, assuming no net rotation of India and Eurasia, is 25 ± 5 mm yr^{-1}.

Because we may have incompletely sampled deformation in southern Tibet, our GPS data do not provide an upper bound to the rate at which India slips beneath Tibet. But, if we assume that the slip of India beneath Tibet can be approximated by slip on a subsurface dislocation (a mathematically convenient but by no means unique explanation for surface deformation), a strong constraint occurs because the maximum uplift rate in the vertical velocity field, and the maximum gradient in the horizontal velocity field, overlie the tip of an active subsurface dislocation[22,23]. Moreover, if the dip of the dislocation is shallow (<15°) the horizontal deformation field is approximately antisymmetric about the tip of this dislocation, permitting data from the south of the dislocation to yield approximate constrains on deformation to its north.

Vertical uncertainties in the GPS data are large (>5 mm yr^{-1}), partly due to uncertainties in the phase centres of some of the antennas used, and these data are inadequate to constrain models of subsurface deformation. Recent spirit-levelling data (Fig. 2) obtained by the Nepalese Survey Department (1977–95), however, confirm a previously identified 40-km wavelength region of uplift in northern Nepal rising at a peak rate of 7 ± 3 mm yr^{-1} relative to the

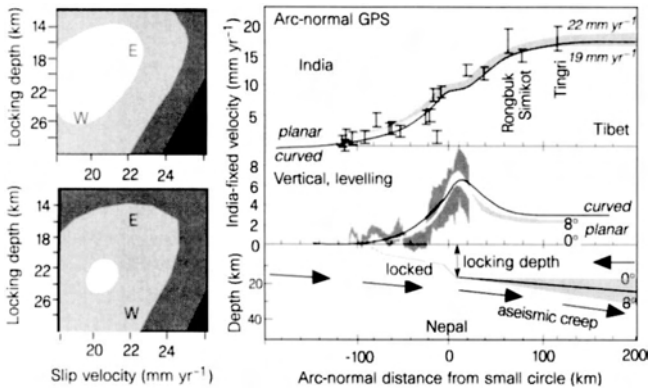

Figure 3 Right, surface deformation resulting from subsurface creep on planar and curved dislocations compared to GPS horizontal velocities and levelling data. Left, shaded regions correspond to 68%, 90% and 99% confidence intervals that satisfy synthetic and observed deformation for a planar dislocation dipping 4° northwards (upper left) and for a curved dislocation (lower left) steepening from 3° northwards at the locking depth to 9° northwards beneath southern Tibet. A deeper locking depth in western Nepal (W) than in eastern Nepal (E) is indicated by the GPS data (68% confidence open ellipses, left) if constraints from the vertical data are ignored.

Indian border. Interestingly, the location of peak uplift corresponds to a maximum in arc-normal Himalayan relief (Fig. 2). The central segment of the Himalayan arc follows a 1,696-km-radius small-circle defined by a belt of moderate Himalayan earthquakes and maximum river gradients[24] which intersects the levelling line ~15 km south of this peak uplift. The similarity in wavelength of the mean arc-normal relief and vertical deformation field, and the correspondence between maximum southward tilt (2.5 μrad yr^{-1}) and maximum stream gradients, suggests that the deformation field we observe is not a transient feature of Himalayan uplift as we might suspect from the brief 18-yr duration of these interseismic measurements. One of several mechanisms that could account for the observed coincidence is that the region may be repeatedly taken close to its elastic limit, with average uplift equal to half its pre-seismic peak value of 2–5 m (assuming 7 ± 3 mm yr^{-1} for, say, 300–500 yr). If a fraction of this uplift were non-recoverable inelastic deformation, permanent uplift of the region would mimic the form of the interseismic deformation field.

To reconcile the levelling data with the GPS data we projected both onto a cross-section parallel to the mean convergence direction at 86° E, using the above small-circle approximation to correct for the curvature of the Himalaya (Fig. 1). The projected horizontal and vertical deformation data were then compared to the surface deformation accompanying slip on a planar dislocation (the simplest of possible slip geometries) locked below, and south of, the region of maximum uplift. A dislocation dipping at $4° \pm 4°$ to the north best fits the data with a slip rate of 20.5 ± 2 mm yr^{-1} and a locking depth of 20 ± 4 km (Fig. 3). When the vertical deformation data are ignored, independent best fits to the GPS data from eastern Nepal favour slip at 22 ± 3 mm yr^{-1} starting at 17 ± 4 km depth dipping to the north at $4° \pm 4°$, but the data from western Nepal require deeper locking depths (24 ± 4 km). Whereas slip on a curved dislocation surface dipping increasingly to the north (approximating the flexure of a descending Indian plate) is permitted by the data, we can exclude the possibility of active creep on dislocations at 10–20 km depths dipping to the north at 10°–30°, on which moderate seismicity has been observed in the past century. Satisfactory models for a curved dislocation have a slip velocity of 20.5 ± 1 mm yr^{-1} and starting dip of $4° \pm 2°$ to the north (compare ref. 25) at a locking depth of 21 ± 2 km, and increase smoothly in dip to 9° northward at a distance of 150 km north of the locking depth (compare ref. 26).

More complex geometries and slip distributions, such as those as have been proposed to explain the vertical velocity data[21] cannot be constrained uniquely by our sparse horizontal GPS data, although we can exclude significant creep on surfaces dipping more than 9° northward. Moreover, convergence south of the Himalayan boundary thrusts in western Nepal (Fig. 1) and its absence in eastern Nepal reveals that deformation is not identical in both regions, indicating spatial and/or temporal variations in the convergence process. Synforms and antiforms with wavelengths of less than 100 km imply along-arc heterogeneity[25,27], but microseismic data in the Himalaya that might assist our identification of active subsurface geometries are insufficiently detailed except for the region near Kathmandu[28]. A deep focus magnitude $M = 6.5$ earthquake occurred in 1988 in southeastern Nepal[29,30] near the southern rupture limit of the great 1934 Bihar/Nepal earthquake. Although this event was too small to produce regionally significant surface deformation, viscoelastic relaxation of the region following the 1934 earthquake may partly be responsible for this event, and for observed differences in deformation style in eastern and western Nepal. Numerical estimates of viscous processes are hindered by incomplete information on the 1934 rupture geometry and slip distribution[31].

The locking depth, an arc-parallel line in our two-dimensional model for sub-Tibetan slip, may correspond to the northern limit of rupture during the great 1934 Bihar/Nepal event. Assuming that rupture does not propagate south of the main frontal thrusts of the southern Himalaya[32], or significantly north of this locking depth, the down-dip width of the 1934 rupture zone is estimated to be less than 90 km. This is 20% shorter than previous estimates, requiring estimates of co-seismic slip and renewal time based on seismic energy release from these events to be increased accordingly. In western Nepal there have been no recent great earthquakes for 200 years and perhaps for much longer. Earthquakes in 1803 (Uttarkashi) and 1833 (Nepal) have been assigned maximum magnitudes of $M = 7.7 \pm 0.2$ based on available historical data[9,33]. Magnitude estimates for earlier events are unavailable, although from readings of colonial and Indian archives it is considered unlikely that a $M > 8$ event beneath the Kumaun Himalaya or western Nepal would have escaped mention in the past 350 years. Hence, one or more great earthquakes in western Nepal, if they occurred today, would release >6 m (refs 33, 34) of co-seismic displacement, similar to other $M > 8$ Himalayan events that have occurred in the past 100 years. □

Received 31 July 1996; accepted 23 January 1997.

1. Molnar, P. *Annu. Rev. Earth Planet. Sci.* **12,** 489–518 (1984).
2. Molnar, P. *J. Himalayan Geol.* **1,** 131–154 (1990).
3. Harrison, M. T., Copeland, P., Kidd, W. S. F. & Yin, A. *Science* **255,** 1663–1670 (1992).
4. Ni, J. F. *Proc. Ind. Acad. Sci. (Earth Planet. Sci.)* **98,** 71–89 (1989).
5. Molnar, P. & Tapponier, P. *Science* **189,** 149–426 (1975).
6. DeMets, C., Gordon, R., Argus, D. & Stein, S. *Geophys. J. Int.* **101,** 425–478 (1990).
7. Molnar, P. & Tapponier, P. *J. Geophys. Res.* **83,** 5361–5375 (1978).
8. Avouac, J.-P. & Tapponier, P. *Geophys. Res. Lett.* **20,** 895–898 (1993).
9. Molnar, P. & Deng, Q. *J. Geophys. Res.* **89,** 6203–6228 (1984).
10. Lyon Caen, H. & Molnar, P. *Tectonics* **4,** 513–518 (1985).
11. Jackson, M. & Bilham, R. *Geophys. Res. Lett.* **21,** 1169–1172 (1994).
12. Lichten, S. M. & Border, J. S. *J. Geophys. Res.* **92,** 12751–12762 (1987).
13. Larson, K. M. & Freymueller, J. *Geophys. Res. Lett.* **22,** 37–40 (1995).
14. Boucher, C., Altamimi, Z., Feissel, M. & Sillard, P. *Results and Analysis of the ITRF94 (IERS Tech. Note 20* IERS Central Bureau, Observatoire de Paris, 1996).
15. Anzidei, M. *Terra Nova* **6,** 82–89 (1994).
16. Molnar, P. & Lyon Caen, H. *Geophys. J. Int.* **99,** 123–153 (1989).
17. Armijo, R., Tapponier, P., Mercier, J. L. & Tonglin, H. *J. Geophys. Res.* **91,** 13803–13872 (1986).
18. England, P. C. & Houseman, G. A. *J. Geophys. Res.* **91,** 3664–3676 (1986).
19. Molnar, P. & Tapponier, P. *Geology* **5,** 212 (1977).
20. Freymueller, J. *et al. Geophys. Res. Lett.* **23,** 3107–3110 (1996).
21. Jackson, M. & Bilham, R. *J. Geophys. Res.* **99,** 13897–13912 (1994).
22. Savage, J. C. *J. Geophys. Res.* **88,** 4984–4996 (1983).
23. Okada, Y. *Bull. Seism. Soc. Am.* **75,** 1135–1154 (1985).
24. Seeber, L. & Gornitz, V. *Tectonophysics* **92,** 335–367 (1983).
25. Schelling, D. *Tectonics* **11,** 925–943 (1992).
26. Makovsky, Y., Klemperer, S. L., Liyan, H., Deyuan, L. & Project INDEPTH team *Tectonics* **15,** 997–1005 (1996).
27. Johnson, M. R. W. *Tectonophysics* **239,** 139–147 (1994).
28. Pandey, M. R. *et al. Geophys. Res. Lett.* **22,** 751–754 (1995).
29. Pandey, M. R. & Nicolas, M. (Rep. 2, Dept. Mines and Geology, HMG Nepal, Kathmandu, 1988).

30. Banerjee, S. N. & Chakravarti, P. (eds) *Bihar-Nepal Earthquake 20 August 1988* (Spec. Publ. 31, Geol. Surv. India, Calcutta, 1993).
31. Yu, Tingto thesis, Univ. Colorado (1995).
32. Bilham, R., Bodin, P. & Jackson, M. *J. Nepal. Geol. Soc.* **11**, 73–88 (1995).
33. Khatri, K. N. *Tectonophysics* **138**, 79–92 (1987).
34. Molnar, P. *Ann. Geophys.* **5**, 663–670 (1987).

Acknowledgements. We thank the Survey Department and the Ministry of Mines and Geology, HMG, Nepal, for their participation in the 1991 and 1995 measurements and for their generous contributions of new data. M. Jackson, B. Washburn and P. Molnar made substantial contributions to the initial GPS network. W. Wang, P. Bodin and F. Sigmundsson gathered GPS data in Tibet, and V. Gaur, J. Paul and S. Jade contributed data from India. R. Bürgmann, F. Blume, D. Shelling, P. Molnar, J-P. Avouac and T. Herring provided insights into modelling and interpretation. This work was supported by the US NSF; we thank Trimble Navigation Solarex Corp. and Campbell Scientific Inc. for donations of equipment.

Correspondence should be addressed to R.G.B. (e-mail: bilham@stripe.Colorado.edu).

Confined subsurface microbial communities in Cretaceous rock

Lee R. Krumholz*, James P. McKinley†, Glenn A. Ulrich* & Joseph M. Suflita*

* *Department of Botany and Microbiology, University of Oklahoma, 770 Van Vleet Oval, Norman, Oklahoma 73019, USA*
† *Pacific Northwest National Laboratory, Richland, Washington 99352, USA*

Deep subsurface microbial communities[1] are believed to be supported by organic matter that was either deposited with the formation sediments or which migrated from the surface along groundwater flowpaths. Investigation has therefore focused on the existence of microorganisms in recently deposited or highly permeable sediments[2,3]. Fewer reports have focused on consolidated rocks[4–7]. These findings have often been limited by inadequate tracer methodology or non-sterile sampling techniques. Here we present evidence for the presence of spatially discrete microbial communities in Cretaceous rocks and advance a mechanism for the long-term survival of these subterranean communities. Samples were collected using aseptic methods and sensitive tracers[8]. Our results indicate that the main energy source for these communities is organic material trapped within shales. Microbial activity in shales appears to be greatly reduced, presumably because of their restrictive pore size[9]. However, organic material or its fermentation products could diffuse into adjacent, more permeable sandstones, where microbial activity was much more abundant. This process resulted in the presence of microbial communities at sandstone–shale interfaces. These microorganisms presumably ferment organic matter and carry out sulphate reduction and acetogenesis.

Alternating members of the Cretaceous Mancos (shale) and Dakota (sandstone) formations were drilled and sampled adjacent to Cerro Negro, a volcanic neck in central New Mexico near the village of Seboyeta. Core samples were collected into lexan liners using aqueous and particulate tracers for detection of potential contaminants[9]. The sampled strata represented relatively minor transgressive and regressive episodes within an overall transgressive sequence[10]. Sandstone members represented near-shore (shore face or near-shore bar) depositional environments; shale members represented adjacent, deeper and less energetic, near-shore ('toe-of-slope') environments.

A regional analysis of groundwater composition and hydrology using water from existing wells was conducted in parallel with this work (refs 9, 11, and J.P.McK., unpublished results). Recharge occurred on an upland mesa 10 km to the west and 425 m higher than the sampled well, where the water table was at a depth of 69 m. Cerro Negro groundwaters were sampled by setting downhole packers across sandstone units (shales were non-transmissive and would not yield water) and removing water to the surface using gas-driven Teflon bladder pumps. Dissolved oxygen was below detection (0.2 mg l^{-1}) for three sampled sandstone units, and sulphate and sulphide were present at 80–370 mg l^{-1} and 8–14 mg l^{-1}, respectively. The sandstones and shales contained 0.1–2 wt% sulphide minerals (mainly pyrite). Analysis of isotope data for Paguate and Cubero sandstone aquifers indicated an age for these groundwaters of 20,000–30,000 years. Moreover, relatively low levels of Fe(III) were detected in the sediments (data not shown), and the

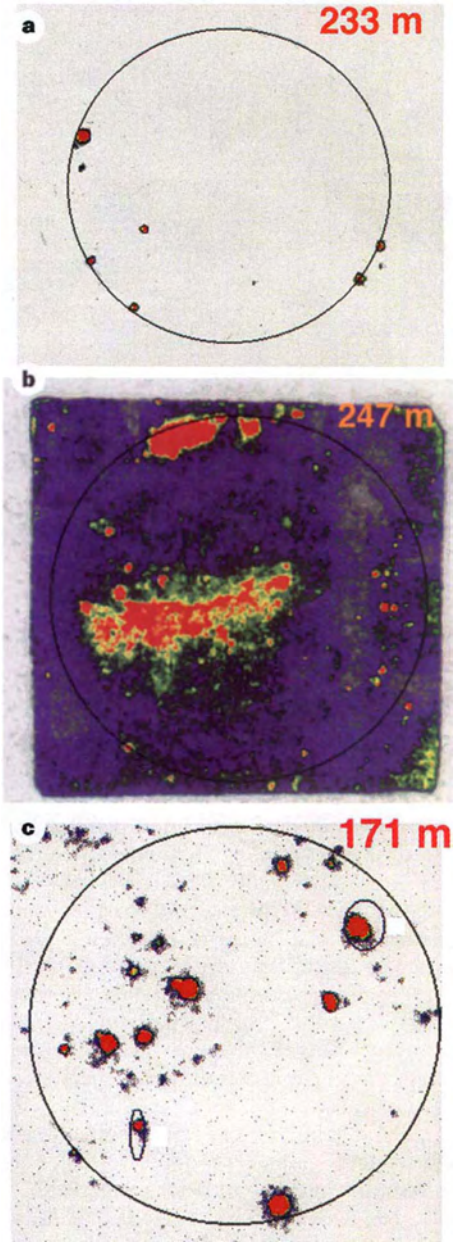

Figure 1 Radioisotope images of sulphate-reduction activity on the freshly exposed face of rock cores obtained from different depths at the Cerro Negro, New Mexico, exploratory drilling site. These images allow for localization of sulphate-reducing activity on a two-dimensional scale. **a**, 233-m core showing microbial contamination of the exterior surface, **b**, 247-m core showing generally high levels throughout, with maximal activity in the centre region. **c**, 171-m core showing patchy distribution of microbial activity. The interior (circled) represents the contact area of the cylindrical core with the foil. The level of radioactivity at that location on the foils is represented in colour (red > yellow > green > blue), although the scale is different for each foil. Small outlined areas in the 171-m core represent points of reference and not necessarily microbial activity.

Annex B57

S. Kuehl et al., "Subaqueous Delta of the Ganges-Brahmaputra River System", *Marine Geology*, Vol. 144, No. 1 (1997)

ELSEVIER

Marine Geology 144 (1997) 81–96

MARINE GEOLOGY
INTERNATIONAL JOURNAL OF MARINE GEOLOGY, GEOCHEMISTRY AND GEOPHYSICS

Subaqueous delta of the Ganges–Brahmaputra river system

Steven A. Kuehl [a,*], Beth M. Levy [a], Willard S. Moore [b], Mead A. Allison [c]

[a] *Virginia Institute of Marine Science, College of William and Mary, Gloucester Point, VA 23062, USA*
[b] *Department of Geological Sciences, University of South Carolina, Columbia, SC 29208, USA*
[c] *Department of Oceanography, Texas A&M University, 5007 Avenue U, Galveston, TX 77551, USA*

Received 19 July 1996; accepted 16 June 1997

Abstract

The Ganges–Brahmaputra is among the world's three largest river systems in terms of sediment load, but, until now, no high-resolution seismic data have been obtained to document the nature of the sediment deposit seaward of the rivers' mouths. The other two (Amazon, Huanghe) discharge into energetic coastal environments and form subaqueous deltas with characteristic clinoform stratigraphy. High-resolution seismic reflection profiles of the Bengal shelf reveal similar stratigraphy: topset beds dip gently (0.036°) and diverge offshore; more steeply dipping foreset beds (0.190°) converge farther seaward; and relatively thin, gently dipping bottomset beds (0.022°) extend across the outer shelf, overlying an erosional surface presumed to be of Late Pleistocene age. Sediment accumulation rates are highest in the foreset region (≥5 cm/year) and reduced in the bottomset region (<0.3 cm/year), corroborating the relative thickening and thinning of strata observed in seismic profiles. Taken together, these data indicate a subaqueous delta is actively prograding across the Bengal shelf. Volume estimates for the Holocene subaqueous delta reveal that about one third of the total load of the Ganges–Brahmaputra has accumulated on the shelf. The remainder is likely partitioned between the river floodplain/delta plain and off-shelf transport via the submarine canyon, Swatch of No Ground. The canyon incises the shelf in the area of highest sedimentation rates (foreset), and growth faults and slumping of modern sediments near the head of the canyon support the idea that significant off-shelf transport of sediments to the Bengal Fan is occurring. © 1997 Elsevier Science B.V.

Keywords: delta; shelf sedimentation; seismic reflection profiling; sediment budget; Bay of Bengal; Ganges River; Brahmaputra River

1. Introduction

Modern river deltas have a range of characteristic morphologies that, to a first approximation, are controlled by the fluvial, tidal, and wave regime (Wright and Coleman, 1973). Deltas with extensive subaerial expression, such as the Mississippi delta, commonly are found in quiescent seas or protected locations such as fjords and embayments. Rivers entering energetic marine environments display a variety of morphologies. For example, the Columbia River (Northwest coast, U.S.A.) has no subaerial delta, rather, accumulation occurs as a mid-shelf mud deposit (Wright and Nittrouer, 1995). Rivers with sediment loads comparable to the Ganges–Brahmaputra, such as the Amazon and Huanghe, exhibit predominant

* Corresponding author. Fax: +1 (804) 684 7250; e-mail: kuehl@vims.edu

PII S0025-3227(97)00075-3

or partial subaqueous growth of their deltas, respectively (Nittrouer et al., 1986; Prior et al., 1986; Alexander et al., 1991). Even though the sediment discharge of the Amazon is sufficient to produce a sizable subaqueous delta (clinoform) on the shelf, large shear stresses, generated primarily by tides, appear to prevent or limit significant subaerial growth in the vicinity of the river's mouth (Kuehl et al., 1986; Geyer et al., 1996). For the Huanghe, about 10–15% of the sediment discharge accumulates south of the Shangdong Peninsula as a subaqueous delta (Alexander et al., 1991), with much of the remaining discharge contributing to rapid subaerial growth. This dual-mode progradation of the delta reflects the phasing of river discharge and energy conditions in the Gulf of Bohai; high discharge occurs during low-energy conditions resulting in deposition near the mouth and significant subaerial growth (Wright and Nittrouer, 1995).

Although the combined sediment discharge of the Ganges–Brahmaputra river system is among the world's largest and its delta plain among the world's most densely populated, little is known regarding the Holocene evolution of the delta or the processes and patterns of recent deltaic sedimentation. Based on examination of nautical charts dating back some 200 years, Coleman (1969) suggested that no significant seaward progradation of the shoreline had occurred and that sediments discharged to the coastal ocean therefore escaped to the deep sea through the Swatch of No Ground, a major submarine canyon feeding the immense Bengal Fan. A recent critical examination of a more extensive set of historical charts, however, has provided evidence for some recent growth of the subaerial delta, but with progradation occurring in a lateral (west to east) fashion (Allison, 1997). Preliminary study of the continental shelf seaward of the rivers' mouths revealed significant sediment accumulation, leading to the suggestion that the observed clinoform-like morphology reflects the presence of an active subaqueous delta (Kuehl et al., 1989). However, until now, no seismic data have been obtained to document the stratigraphic nature of this feature. Here we report the results of the first high-resolution seismic reflection study conducted on the Bengal shelf seaward of the Ganges–Brahmaputra river system. In addition, sediment cores collected from the shelf are used to examine the distribution of recent accumulation rates in relation to seismic observations. The objectives are to examine the idea that a major component of the Ganges–Brahmaputra delta occurs on the shelf as a subaqueous clinoform and to evaluate the role of the Swatch of No Ground as a potential conduit for bypassing modern river sediments to the Bengal Fan.

2. Background

2.1. River characteristics and Holocene stratigraphy of the delta

The Ganges, Brahmaputra and Meghna rivers have occupied and abandoned numerous courses during the Quaternary and have deposited a large, flat, low-lying alluvial/delta plain encompassing most of the country of Bangladesh (Coleman, 1969). The Ganges drains the south slopes of the Himalayan mountains whereas the Brahmaputra mostly drains the north slopes, with estimated suspended sediment loads of 520×10^6 t/year and 540×10^6 t/year, respectively (Milliman and Syvitski, 1992). The Meghna River drains northeastern Bangladesh but has a negligible impact on the combined load of the system, contributing only about 1% of the total sediment discharge (Coleman, 1969). Combined monthly sediment and water discharge reaches a maximum in August during the southwest monsoon, with minimal levels (an order of magnitude less than peak rates) in January–March. Suspended sediments of the Ganges–Brahmaputra are coarse relative to other large river systems; at the confluence of the Ganges and Brahmaputra about 40% is sand (mostly fine–very fine) and 60% silt–clay (Barua et al., 1998).

Umitsu (1985, 1987, 1993) divided the landforms of the Bengal Basin into two geomorphological units: Pleistocene terrace uplands and recent alluvial lowlands (Fig. 1). The Pleistocene terraces are found in the marginal and interior portions of the Basin. In the north the uplands are known as the Barind Tract, and as the Madhupur Terrace

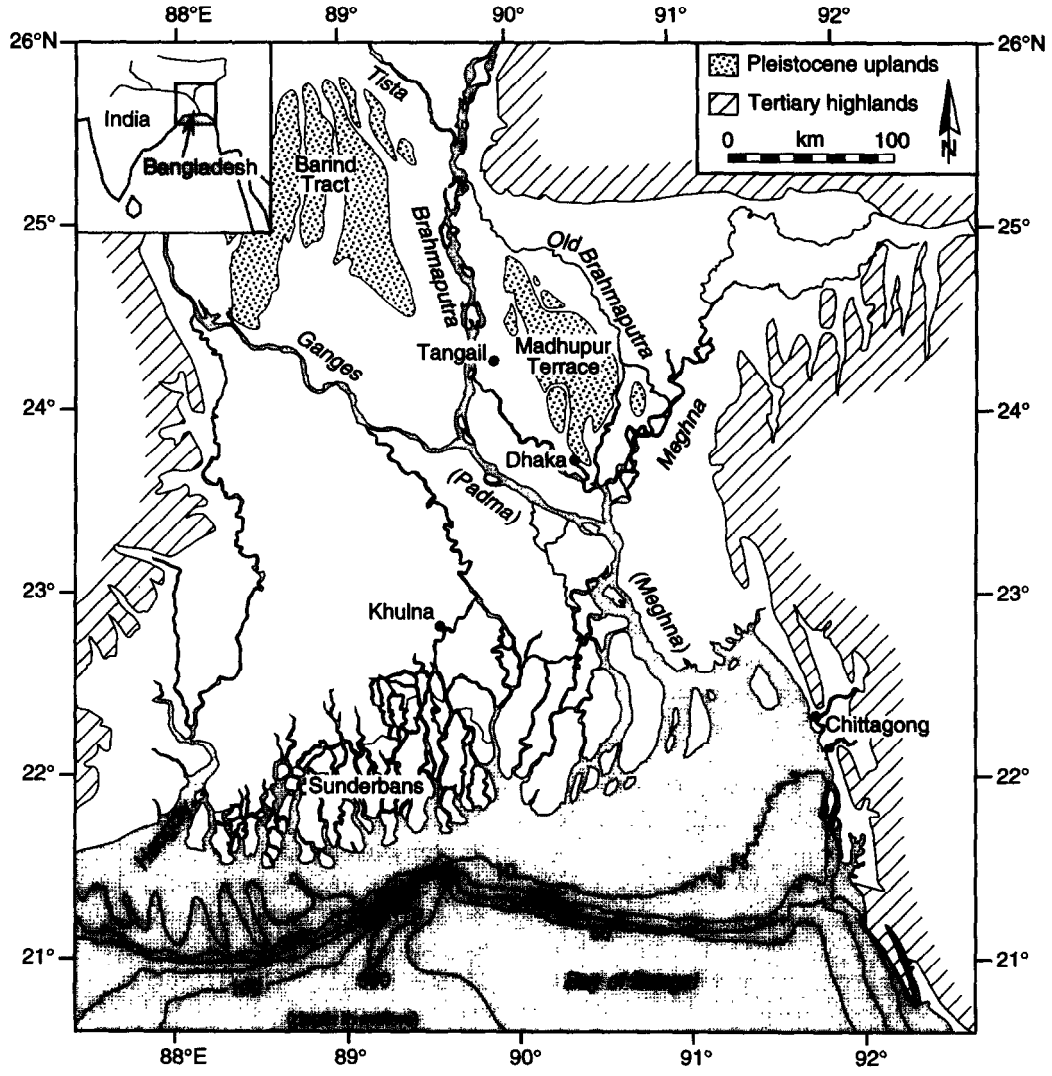

Fig. 1. Physiographic map of the Ganges–Brahmaputra delta.

in the central region. Alluvial lowlands are distributed widely over the Bengal Basin with characteristic levees, point bars and channel bars, as well as lower landform units such as swamps, marshes and former river channels. Sediments consist mainly of sand, silt, and clay layers with peat layers recognized in several places. The elevation of the lowlands typically is <15 m above sea level and most of the southern region is <3 m above sea level.

Five stratigraphic units characterize the evolution of the Ganges–Brahmaputra delta since the last glacial maximum (Umitsu, 1993). The *lowest unit* dates from the last glacial maximum and consists of sandy gravels deposited by the rivers down cutting older surfaces. Radiocarbon dating and similarities in sediment facies and grain size of the *lower* unit near Khulna City with that of the present Brahmaputra River flood plain suggest that this unit represents the flood plain about 12,000 years before present. The *middle unit* is composed of fine deltaic sediments deposited during the transgression. Peat layers are found in the Sylhet Basin in the lower horizon of the unit,

indicating the presence of marshes during this period. The lower portion of the *upper unit* (mid-Holocene) is comprised of silt and clay in the inland region of Tangail; however, near the more coastal region of Khulna, the sediments exhibit a strong marine influence. Umitsu (1993) proposed that the coastline at that time retreated slightly north of the present Khulna City. The upper portions of the *upper unit* become coarser, with peat in places, suggesting that the coastline prograded during this time as broad marshy peat lands covered the central Ganges–Brahmaputra delta. During the late Holocene the rate of sea-level rise decreased, allowing fine silts and clays with intermittent peat layers to be deposited, here called the *uppermost unit*.

2.2. Oceanography of the Bay of Bengal

The Ganges–Brahmaputra river system discharges into an energetic marine environment characterized by strong tidal currents, moderate wave activity, seasonal monsoons and frequent cyclones. The mixing and subsequent spreading of the fresh water greatly affects the oceanography of the coastal waters. In addition to perennial discharge from the Ganges and Brahmaputra, seasonal discharges are introduced into the Western Bay from India via the Godavari, Krishna and Cauvery rivers (Suryanarayana et al., 1992). The advection and mixing of these fresh waters (about 2300 km^3/year) with the coastal ocean is controlled by external and internal forcing from wind and thermohaline conditions (Suryanarayana et al., 1992).

Seasonal low-pressure areas over the Persian Gulf during the summer and high pressure over the Tibetan Plateau during the winter create monsoonal winds, from the southwest in summer and from the northeast in winter (Murty et al., 1992). Changing monsoonal winds affect surface water flow in the open Bay of Bengal (Wyrtki, 1973). The spring is characterized by clockwise rotation, with the fastest flow close to the central Indian continental shelf, where it can reach 1.5–2.5 m/s. The autumn is characterized by counterclockwise movement with lower speeds in the eastern and central regions of the bay as opposed to the western region. Spring winds, combined with the Coriolis effect, result in the movement of surface water away from the east Indian coast with deeper water upwelling, causing the isopycnals to tilt upward towards the Indian coast. In the autumn, the reverse occurs as water is piled up in the western part of the bay and the isopycnals tilt down toward the east Indian coast. Resulting seasonal changes in sea level exceed 1 m for the northeast coast at Chittagong and along southeast Bangladesh, the largest on record (Murty et al., 1992). Observations and modeling of the fresh water emanating from the Ganges–Brahmaputra rivers' mouths indicate that during the period of maximum sediment and water discharge (June–September), the plume trajectory is along the coast toward the west (Shetye et al., 1996).

Tides in the coastal waters off Bangladesh primarily are semi-diurnal. The combined effects of Coriolis acceleration and the funnel shape of the bay produce an area of increased tidal amplitude along the eastern coast, typically about 4 m, decreasing to less than 2 m for the western portion of Bangladesh. For a small area between Hatia and Sandwip channels amplitudes of up to 6 m (Barua et al., 1994) and velocities exceeding 300 cm/s (Coleman, 1969) are observed.

Cyclones are common in the Bay of Bengal, and about 16% of cyclonic storms developing in the bay strike the Bangladesh coast (Mooley and Mohile, 1983). The frequency distribution of cyclone activity is distinctly bi-modal with peak activities in May and October, corresponding to the transition periods between the northeast and southwest monsoons.

2.3. Sediment dispersal on the Bengal shelf

Few published studies have addressed recent sediment dispersal on the Bengal shelf. Barua et al. (1994) show that the magnitude and distribution of suspended sediments during the low-discharge period are primarily a function of tidal energy in the nearshore region (<15 m water depth). Sediments which are ≤ 125 μm (fine sand to clay) are continuously transported in suspension, except for brief periods during slack water. Based on mineralogical investigation of surficial sediments,

Segall and Kuehl (1992) suggest that only during high-discharge periods (May–October) are significant amounts of sediment transported seaward of the 20-m isobath. Seabed textural and geochronological data reveal a westward fining along the mid-shelf area with a corresponding increase in sediment accumulation rates, suggesting westward transport along the shelf toward the Swatch of No Ground (Kuehl et al., 1989).

3. Methods

3.1. Field methods and seismic interpretation

A total of 450 km of GeoPulse® multifrequency seismic reflection data were obtained during a 1991 survey of the Bengal shelf along eight transects (Fig. 2), with maximum seabed penetration in excess of 100 m and vertical resolution of ~0.5 m. Seabed sampling retrieved nine kasten cores (3-m maximum length) and eleven grab samples. Sediment cores were subsampled by taking centimeter-thick sections, typically at 5- or 10-cm intervals, which were homogenized and bagged for sedimentological and geochemical analyses. A wood fragment recovered from the kasten-core nosepiece at Station 1 (~1.4 m depth in seabed) was saved for radiocarbon dating.

Navigation data from the 1991 cruise was converted from local Decca coordinates to latitude and longitude. Using a 3-point moving average, horizontal distances (in km) were determined along transects between each time mark, typically every 15 min. Vertical scales were calculated based on the recorder setting, assuming a velocity of 1500 m/s. The seismic profiles were collected in analog format using an EPC® graphic recorder, and key sections were digitally scanned at 400 dpi resolution. Scanned sections were cleaned, scaled, and mosaicked using Intergraph Microstation® and IRASB® vector/raster processing software.

3.2. Laboratory methods

Analyses of short-lived radioisotopes were performed using gamma spectroscopy. ^{210}Pb and ^{137}Cs activities were determined by direct measure-

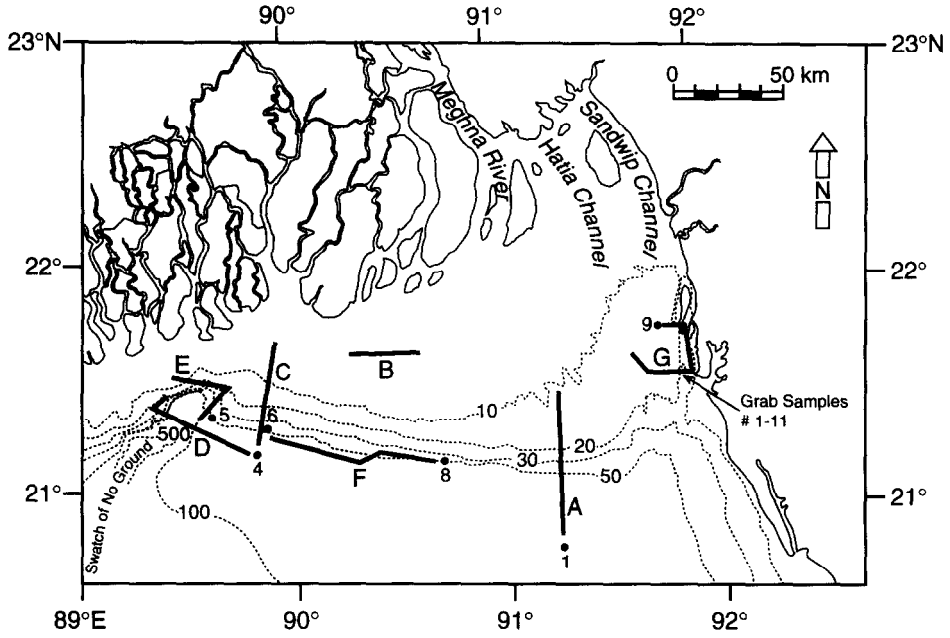

Fig. 2. Bathymetric chart of the Bengal shelf showing coring station locations (numbers) and seismic transects (letters). A major submarine canyon, 'Swatch of No Ground', incises the shelf along the western side of the study area.

ment of their characteristic gamma-ray emissions, whereas ^{226}Ra activities were determined indirectly through measurement of its short-lived daughters. Samples were packed in petri dishes (6.5 cm diameter by 2.25 cm), sealed to prevent loss of ^{222}Rn (an intermediate daughter between ^{226}Ra and its measured daughters, ^{214}Pb and ^{214}Bi) and to allow for ingrowth before counting. Self absorption corrections for ^{210}Pb were made using the methods of Cutshall et al. (1983).

Radiocarbon analysis was performed on the wood sample using the benzene synthesis and liquid scintillation counting method similar to that described by Polach and Stipp (1967).

Textural analyses were performed by wet sieving samples through a 63 μm sieve to separate the sand and mud (clay and silt) fractions. Sand was sieved at 1/2 ϕ intervals, and detailed analysis of the mud fraction was performed using a Sedigraph® model 5100 ET X-ray digital settling analyzer. Results of Sedigraph® and sieve analyses were combined to calculate grain-size and sorting statistics.

4. Results

4.1. Seismic profiles

The GeoPulse® records reveal clinoform stratigraphy for the sediment wedge off the Ganges–Brahmaputra rivers' mouths (Fig. 3). The clinoform thickness exceeds 60 m on the middle shelf, thinning to <10 m at the seaward limit of the profiling. Five regions of the shelf have been delineated based on regional variations in acoustic character of the seabed and are described below.

4.1.1. Nearshore (5–15 m)

Seismic profiles from the nearshore region of the Bengal shelf reveal a highly reflective sediment surface with limited acoustic penetration (<25 m) and few distinct subsurface reflectors (Fig. 4), characteristic of high sand content. In the northeastern section of the bay, along the Chittagong coast, asymmetrical sand waves ranging in height from 3 to 5 m (Fig. 5) are present in the channel (Fig. 2) which presumably is related to the struc-

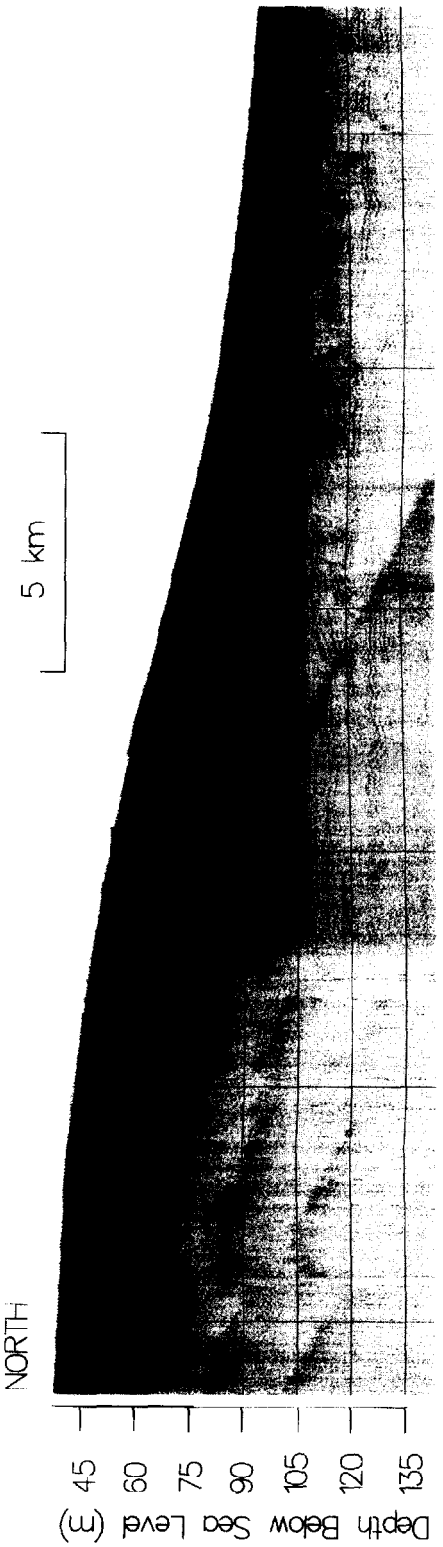

Fig. 3. GeoPulse® record from transect A showing clinoform stratigraphy for the Holocene sediment wedge on the Bengal shelf. The modern subaqueous delta is prograding over Pleistocene strata which are seen as irregular reflectors underneath bottomset beds of the clinoform below about 100 m. Subsurface foreset beds between about 60 to 75 m (northern portion of profile) display zones of acoustically transparent sediment which may result from mass movement (cf. Fig. 7).

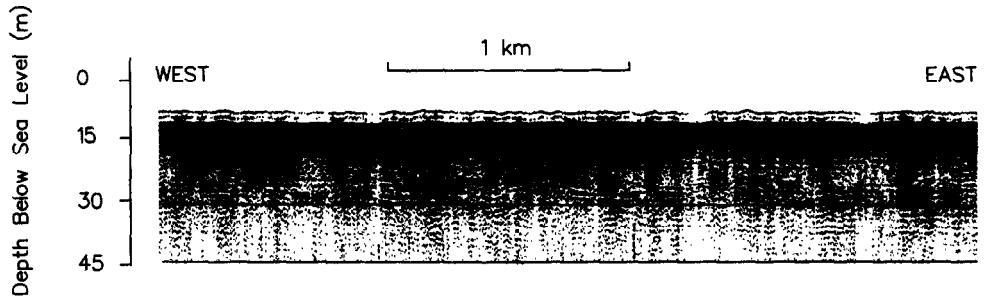

Fig. 4. GeoPulse® record from the near-shore (transect *B*) revealing poor acoustic penetration, probably a result of the high abundance of sand in this region. The thin (2–3 m) surface unit may represent a veneer of mud (probably ephemeral) overlying sand typical of the inner topset region.

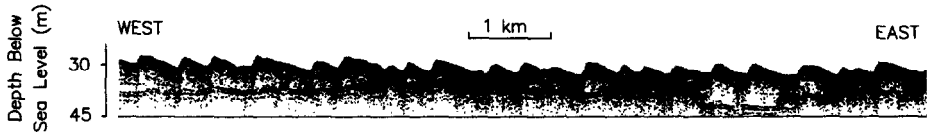

Fig. 5. GeoPulse® record from the eastern region of the study area (transect *G*) showing asymmetrical sand waves indicating transport toward the west. Grab samples from this area reveal clean medium sand.

tural troughs of the adjacent Chittagong hill tracts. The sand waves appear to be more widely spaced toward the west, in the direction of the lee face. Very shallow (<15 m) acoustic penetration was achieved in this area and field descriptions of surficial grab samples indicate a well-sorted medium sand.

4.1.2. Inner shelf (15–30 m)

Closely spaced acoustic reflectors (<2–3 m spacing) are present in the shallow seabed (upper 15 m) for much of the inner-shelf region. These reflectors are underlain by an irregular erosional surface in transects A and C that has an areal extent of at least 720 km^2. The erosional surface displays cut and fill features perhaps associated with subaqueous distributary channels (Fig. 6).

The inner shelf dips gradually seaward in this region, with an average gradient of 0.036°. No significant change in this gradient is observed from east to west. Farther seaward, in water depths of ~30 m, greater than 30 m of subbottom penetration is achieved and previously-parallel reflectors begin to diverge (Fig. 3). The spacing between reflectors increases from <2–3 to ~5 m with distance from shore.

4.1.3. Middle shelf (30–60 m)

Densely spaced reflectors (3–5 m spacing) are observed in the middle-shelf region where typical acoustic penetration between 30 and 45 m is achieved. The beds begin to converge seaward in water depths of about 60 m (Fig. 3), where reflector spacing is reduced to <2–3 m. Individual beds

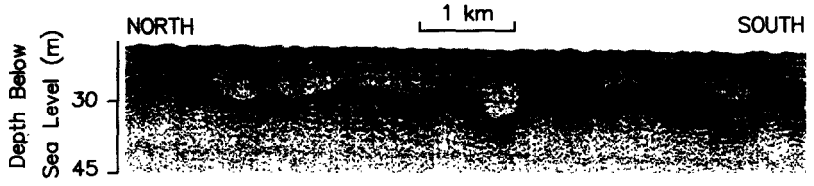

Fig. 6. GeoPulse® record from the inner shelf (transect *C*) revealing an erosional surface beneath thin topset beds. The cut and fill features could reflect migration of subaqueous distributary channels.

are difficult to discern in the seaward portion of the middle shelf and irregular, erosional surfaces can be seen below the stratified sediments. The gradient of the sediment wedge over the middle shelf averages 0.19°. This gradient appears to be uniform from the eastern transect to the Swatch of No Ground.

Two distinct acoustically transparent layers, about 3–5 m thick, are observed both from shore perpendicular and shore parallel transects. Located at depths of ~10 and ~20 m below the sediment surface, the layers are roughly parallel to one another and to the seabed surface (Fig. 7). The acoustically transparent layers pinch out in water depths of about 80 m on the outer shelf. Based on the seismic data, the layers appear to have an areal extent of ~1500 km^2, extending at least 12 km north–south and 127 km east–west.

4.1.4. *Outer shelf (60–>80 m)*

Profiles from the outer-shelf region reveal closely spaced (<2–3 m spacing), parallel acoustic reflectors extending to water depths of at least 80 m, the seaward extent of the seismic lines. The seafloor gradient in this area is very gentle, 0.022°. An erosional contact is seen below the shallow strata relatively close to the seabed surface (within ~10 m). The erosional contact is uneven and displays varying relief, with distinct cut-and-fill features (Fig. 8). Strata underlying this reflector are discontinuous with indistinct bedding.

4.1.5. *Swatch of No Ground*

Profiles near the Swatch of No Ground (Figs. 9 and 10) reveal increased acoustic penetration relative to the eastern and nearshore shelf regions of similar water depths. On the western side of the canyon, a well-stratified seabed is observed, containing distinct, parallel, and continuous acoustic reflectors with typical spacing of 3–5 m between beds. On the eastern side of the canyon, beds are also densely spaced but are more irregular in nature than their western counterparts.

Abundant growth faults and slumps are found on the eastern flanks of the canyon. Slumps with rotational movement to the west are observed along the margin of the canyon (Fig. 9). An east–west trending gully feeds into the canyon with growth faults along the south side dipping steeply into the canyon (Fig. 10). Near the canyon head, strata become more irregular and often are chaotic, with discontinuous and truncated beds. Profiles of the canyon floor near its head show irregular strata with few discernible beds and an uneven sediment surface.

4.2. *Sediment accumulation rates*

Sediment accumulation rates were estimated primarily using ^{137}Cs and, in one instance, corroborated by ^{210}Pb geochronology. In most cases, ^{210}Pb profiles could not be modeled as steady-state accumulation because activities fluctuate markedly down core, in part a result of grain-size variations (Kuehl et al., 1989). In these cases, the penetration depths of ^{137}Cs were used to provide a first-order estimate (Table 1). As ^{137}Cs has been present worldwide in measurable quantities since about 1954, the depth to which ^{137}Cs is observed in the cores divided by the number of years since introduction (in this case 37 years) provides a rough estimate of the sediment accumulation rate. A

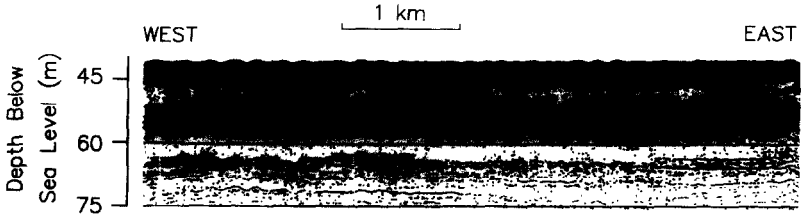

Fig. 7. GeoPulse® record from the foreset beds (transect *F*) showing two distinct acoustically transparent beds at about 48 m and 62 m. The ~5-m thick transparent beds extend at least 100 km along the foreset region and probably represent large-scale mass movement, perhaps triggered by cyclones or earthquake activity common to the area.

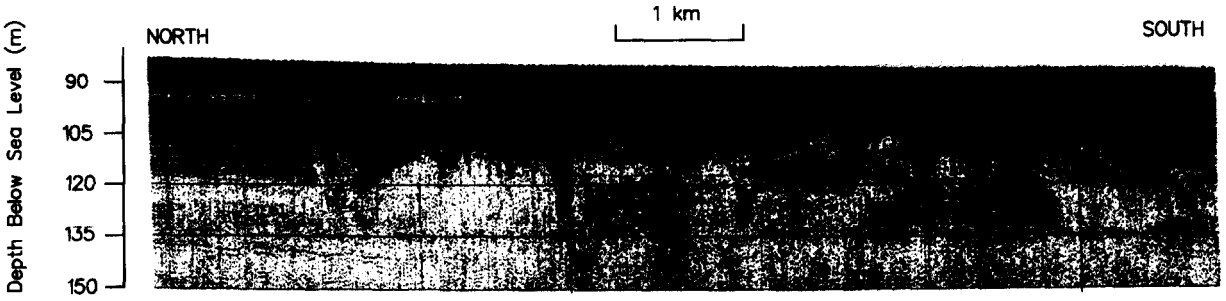

Fig. 8. GeoPulse® record from the seaward portion of transect *C*, showing thin parallel bottomset beds overlying Pleistocene strata below about 100 m. Cut and fill features are evident in the Pleistocene strata suggesting former channels or gullies.

potential problem with this approach is the effect of seabed mixing (physical or biological) on ^{137}Cs profiles, which would increase penetration depths and lead to an overestimate of sediment accumulation rate. Areas most susceptible to this effect would be those experiencing low accumulation rate ($< \sim 1$ cm/year) and/or deep intense mixing. Previous studies have shown that physical sedimentary structures dominate the inner and middle shelf area (Segall and Kuehl, 1994), indicating that biological mixing is unlikely to affect ^{137}Cs penetration depths in these areas. Deep physical mixing, such as that observed for the Amazon delta (Kuehl et al., 1995), would most likely be a problem in shallow water depths ($< \sim 20$ m) where the effects of waves and tides are most pronounced. Most of the cores examined for this study were collected in water depths >20 m (Fig. 2). Using ^{137}Cs penetration depth as a first-order estimate, a sediment accumulation rate of 1.8 cm/year is obtained for a core collected in a shallow trough in the eastern part of the inner shelf (Station 9). This rate could represent a minimum because ^{137}Cs is present throughout the core, thus the actual first appearance of ^{137}Cs in the seabed may be deeper. Kasten cores could not be obtained from the nearshore region because of the presence of sands, which hinders gravity coring. For the middle-shelf area, sediment accumulation rates were 1.1 cm/year (Station 6) and 0.6 cm/year (Station 4). The highest sedimentation rates are found in the area surrounding the Swatch of No Ground. Station 5 revealed a minimum rate of 5.2 cm/year, based on the presence of ^{137}Cs throughout the core. For the outer shelf Station 1, sediment accumulation rates were derived using both ^{137}Cs and ^{210}Pb profiles, with a maximum rate of 0.3 cm/year. Although some evidence of bioturbation was noted at this station (indicating the reported rate may be a maximum), the accumulation rate was the lowest measured in this study. Radiocarbon dating of a wood fragment collected from the nosepiece at Station 1 gave an age of $10{,}000 \pm 240$ year.

4.3. Grain-size analysis

Textural analyses were performed on samples from six cores (Table 2). Cores from the western middle shelf (Stations 4, 5 and 6) are very fine-grained, with down-core average means of 8.5 ϕ for Stations 4 and 5, as compared with an average mean of 7.0 ϕ for Station 8 on the central middle shelf. The cores from the outer shelf (Station 1) and from the shallow trough in the eastern inner shelf (Station 9) have intermediate average means of 7.9 ϕ and 7.6 ϕ, respectively.

5. Discussion

5.1. Subaqueous delta

A distinctive morphology can be seen in the sediment wedge prograding southward and westward from the rivers' mouths on the inner Bengal shelf (Fig. 11). The seismic profiles reveal the gently sloping topset, more steeply dipping foreset, and gently sloping bottomset stratigraphy characteristic of subaqueous deltas (Fig. 3). On the inner

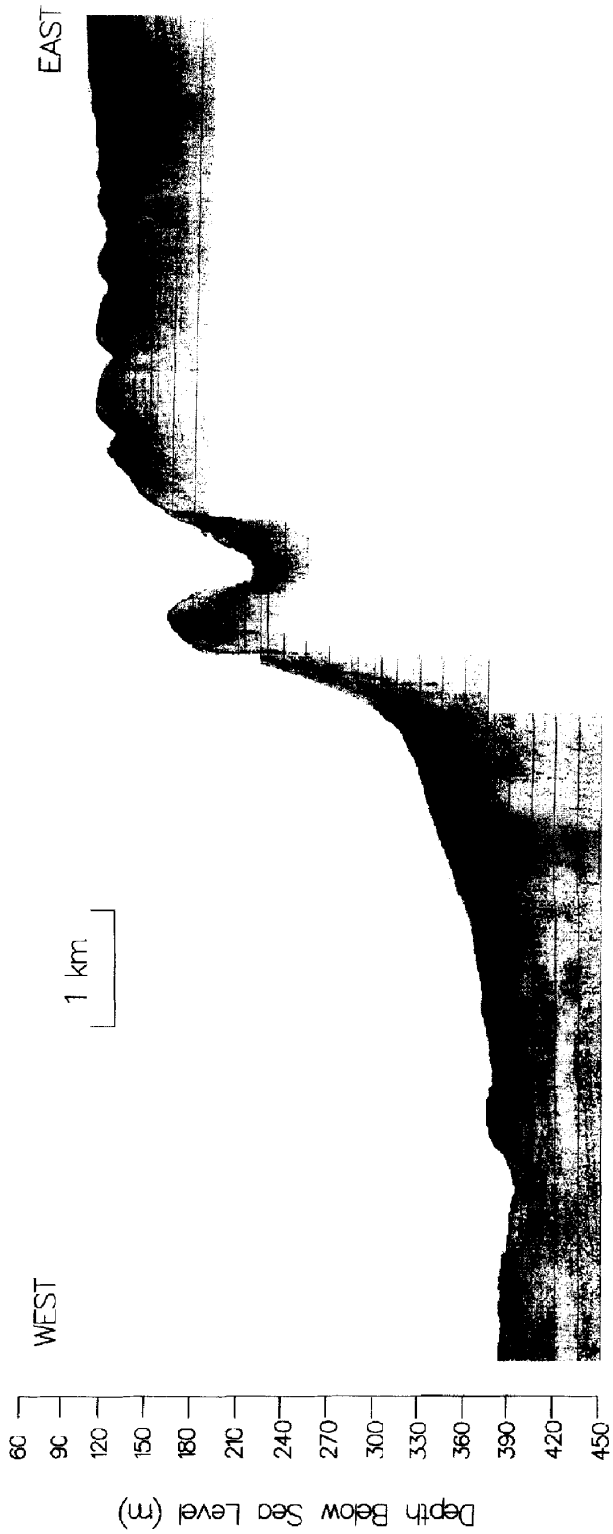

Fig. 9. GeoPulse® record from the head of the submarine canyon, Swatch of No Ground (east–west leg of transect *E*). A series of four large (~0.5 km) slump blocks are seen at the edge of the shelf. Reflectors within the slump blocks dip east, back towards the shelf. Below the shelf edge the profile crosses a deep (~60 m) gully before falling off to the canyon floor. A hummocky sediment surface on the canyon floor suggests mass movement of sediment from the shelf into the canyon.

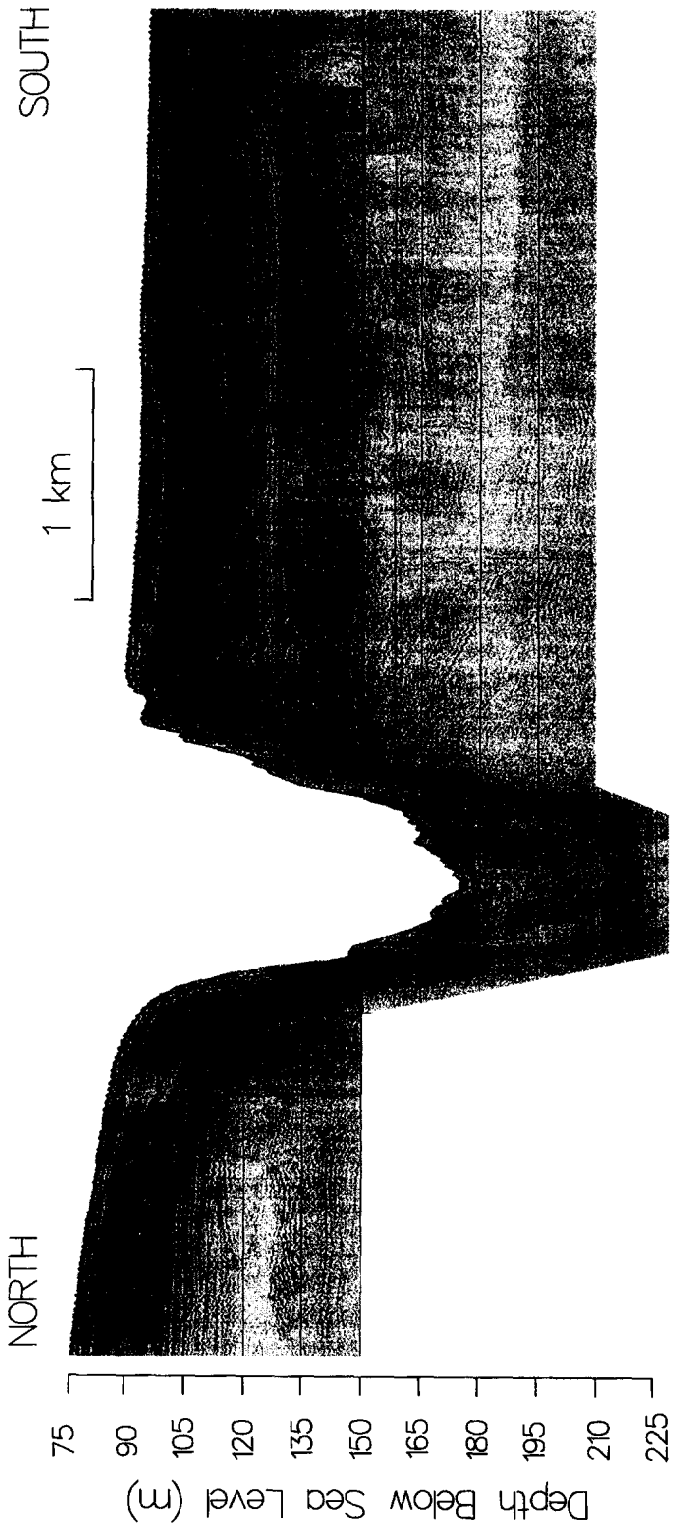

Fig. 10. GeoPulse® record across a gully on the eastern side of the Swatch of No Ground (northeast–southwest leg of transect *E*). A series of growth faults is present along the south edge with shear planes dipping down into the gully with decreasing angles towards the south. Deep subbottom acoustic penetration (> 100 m), along with the growth faults and deformed strata at depth, suggest rapid accumulation of fine-grained sediment. The hummocky sediment surface of the gully floor suggest mass movement into the gully/canyon system.

Table 1
^{137}Cs-based accumulation rates

Station Nr.	Core length (cm)	^{137}Cs penetration (cm)	Accumulation rate (cm/year)
1	81	11	0.3
4	151	21	0.6
5	191	191	>5.2
6	50	40	1.1
9	66	66	>1.8

shelf, in water depths of about 15–25 m, reflectors are nearly parallel and slope gently seaward. This trend gives way to divergent beds at the seaward edge of the topset region, evidenced by increased spacing between reflectors, indicating increased sedimentation rates. At depths of ~30 m the seafloor gradient increases abruptly (from 0.036° to 0.19°) and reflectors converge seaward across the foreset region. In the bottomset region (>60 m water depth) near-surface reflectors once again take on a semi-parallel appearance with strata that are closely spaced and thin. A hiatal surface is seen below the bottomset beds with evidence of uneven truncated beds and relict channels. A wood fragment from the core catcher at Station 1 was radiocarbon dated at ~10,000 years, suggesting that the underlying surface is most likely Pleistocene in age. Sediment accumulation rates obtained from this study indicate that the subaqueous delta is an active feature. High accumulation rates are observed for the thickest (foreset) part of the clinoform, ranging from about 1–>5 cm/year, and rates decrease to <0.3 cm/year in the bottomset region. Although accumulation rates were not determined for the nearshore topset region, the abundance of coarse (sandy) sediment indicates bypassing of fine-grained sediment to the middle and outer-shelf areas.

5.2. *Shelf sediment dispersal*

Textural and acoustical characteristics of the seabed provide clues to patterns of shelf sediment dispersal. In the nearshore region, poor acoustic penetration (0–25 m) and our inability to collect long gravity cores suggest a sandy seabed. Along the eastern margin, near Chittagong, sand waves are observed and field descriptions of grab samples from this area reveal a clean medium sand. The sand waves have considerable relief (3–5 m), implying a high-energy environment. The orienta-

Table 2
Grain-size data

Sample	Mean depth (cm)	Mean grain size (ϕ)	Average mean for core	Sorting
Core 1				
A911-0	1.0	6.9	7.9	3.5
A911-20	21.0	8.1		2.4
A911-30	31.0	6.5		4.0
A911-80	81.0	7.6		2.4
A911-100	101.0	8.7		2.6
A911-140	141.0	9.5		2.6
Core 4				
A914-8	9.0	6.9	8.5	2.1
A914-15	16.0	9.8		1.8
A914-25	26.0	8.4		2.5
A914-55	56.0	8.2		2.2
A914-65	66.0	8.4		2.1
A914-90	91.0	8.3		2.5
A914-140	141.0	9.1		2.3
A914-160	161.0	8.8		2.4
A914-200	210.0	8.2		2.7
Core 5				
A915-0	1.0	8.7	8.5	2.0
A915-20	21.0	9.4		2.2
A915-25	26.0	7.4		2.4
A915-40	41.0	8.1		2.3
A915-75	76.0	8.7		2.1
A915-100	101.0	9.0		2.1
A915-130	131.0	8.0		1.7
A915-140	141.0	8.7		2.2
Core 6				
A916-0	1.0	7.9	7.9	2.4
Core 8				
A918-0	1.0	7.0	7.0	1.9
A918-8	9.0	7.0		2.4
A918-15	16.0	6.9		2.3
A918-25	26.0	6.9		2.3
Core 9				
A919-0	1.0	8.6	7.6	3.3
A919-2	3.0	7.4		2.1
A919-10	11.0	9.0		0.7
A919-15	16.0	8.4		1.2
A919-45	46.0	5.6		2.6
A919-50	51.0	6.7		2.7

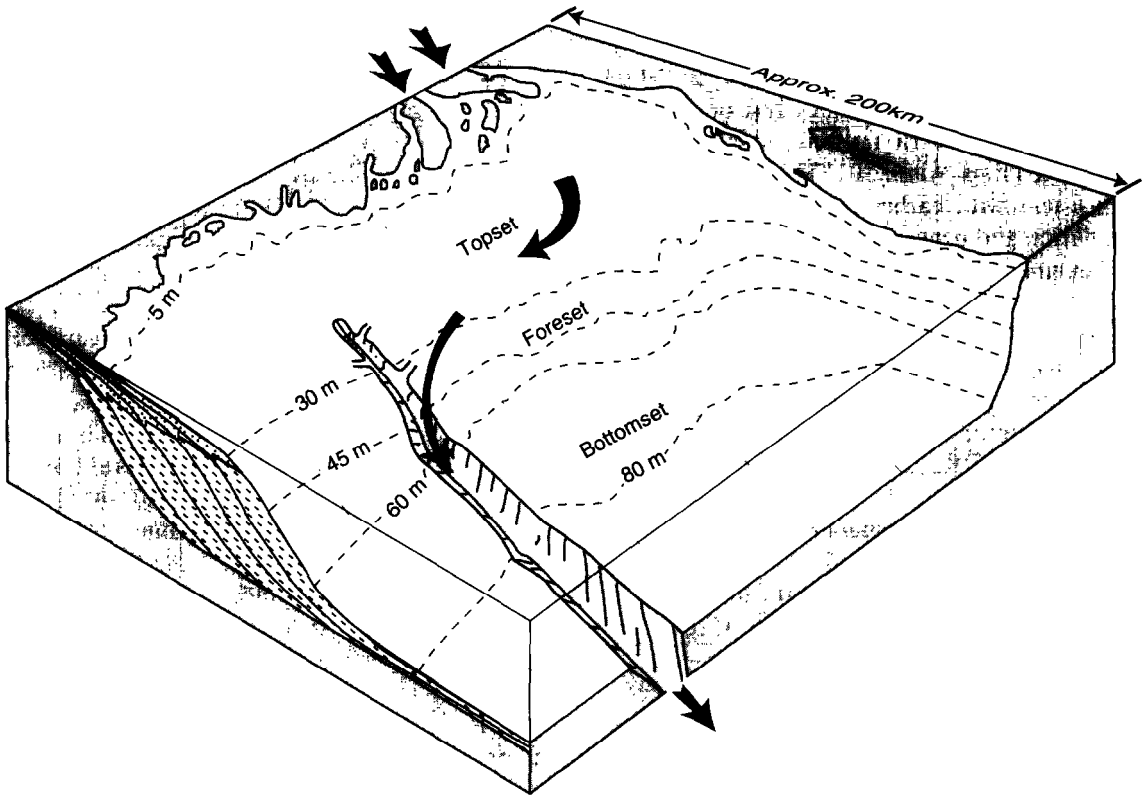

Fig. 11. Cartoon illustrating features of the subaqueous delta on the Bengal shelf seaward of the Ganges–Brahmaputra river system. The clinoform is characterized by relatively coarse-grained (sand) topset beds and fine-grained (mud) foreset and bottomset beds. Evidence from a variety of sources indicates that a significant fraction of sediment discharged to the shelf is transported seaward and westward along the shelf, and escapes to the deep sea through the Swatch of No Ground.

tion of lee and stoss sides of the sand waves indicates east to west flow direction (Fig. 5). These features disappear toward the west, and acoustic penetration gradually increases as the sediment becomes finer. Along the middle shelf, textural analyses suggest a fining trend westward from Station 8 (7.0 ϕ) toward Station 6 (7.9 ϕ) and 5 (8.5 ϕ), near the Swatch of No Ground. Surface grain-size distributions from grab samples demonstrate a similar pattern of westward fining (Kuehl et al., 1989). The highest acoustic penetration is observed near the canyon (>100 m) indicating thick deposits of fine-grained sediments.

The evidence above indicates southward and westward transport of fine-grained sediments from the rivers' mouths toward the Swatch of No Ground. Energetic waves and currents at times of maximum sediment discharge likely prevent rapid accumulation of fine-grained sediments near shore. Westward sediment transport is evidenced by fining towards the west, sand wave orientation, and increased sedimentation rates near the Swatch of No Ground. This seabed evidence is corroborated by physical oceanographic observations and modeling which indicates westward extension of the river plume during the southwest monsoon (Shetye et al., 1996).

The Swatch of No Ground appears to divert the westward dispersal of sediments from the shelf into the canyon. This is supported by clay mineralogical studies which show a depletion of chlorite on the western side of the canyon, indicating that transport of chlorite-rich Brahmaputra sediment is interrupted by the canyon (Segall and Kuehl, 1992). The Swatch of No Ground incises the middle shelf in the western foreset region, the

area of highest measured sedimentation rates (>5 cm/year). Evidence of mass movement is common in areas surrounding the canyon. High rates of sediment loading are one cause of sediment failures such as growth faulting, slumping, and mud flowage (Figs. 9 and 10). These observations are consistent with earlier studies showing rapid accumulation and penecontemporaneous deformation of sediment fabric in the vicinity of the canyon (Kuehl et al., 1989, 1991). The existence of growth faults and slumps directed into the canyon, coupled with the irregular, thick sequences of sediment found at the bottom of the canyon, is dramatic evidence that some sediment is bypassing the shelf via the Swatch of No Ground, presumably to the Bengal Fan.

Evidence of mass movement is also observed in the relatively steep foreset region of the subaqueous delta where two distinct, acoustically transparent layers are observed from the GeoPulse™ profiles (Fig. 7). The transparent layers extend from the outer topset to inner bottomset beds, following the gradient of the subaqueous delta, and have an areal extent of ~1500 km^2. One possible explanation for these features is that they represent large-scale mud flows similar to those observed off the Mississippi River (Wright and Coleman, 1974). The widespread nature of these features suggests large-magnitude external forcing for failure. Such forcing could be accomplished by cyclones or earthquake activity common in the study area.

5.3. Volume of Holocene sediment wedge

In order to examine the significance of subaqueous deltaic progradation for the Ganges–Brahmaputra system since the maximum Holocene transgression, a first-order estimate was made of the volume of the sediment wedge forming on the inner shelf. Areal boundaries were delineated primarily based on seismic data from this study, stratigraphic analysis and interpretation of Umitsu (1993), and geographic information. Extrapolation of Umitsu's bore-hole data to the offshore enables estimates for the thickness of subaerial and subaqueous components of Holocene sediments deposited seaward of the maximum transgressive shoreline.

The Khulna region is considered the northernmost extent of the Ganges–Brahmaputra delta shoreline during the Holocene (Umitsu, 1993). Two fossil molluscs, *Corbiculidae geloina* and *Neritiolae neritina*, found at a depth of 16 m suggest that this was once a tidal environment. Radiocarbon dating of wood fragments found in the core at a depth of 16 m below sea level reveal an approximate age of 7000 ^{14}C years before present (Umitsu, 1993). The 7000-year shoreline is extrapolated laterally from Khulna for the volume estimates. In the east, the mountainous Chittagong hill tract provides a natural boundary. A southern boundary is provided by the 80-m isobath; bottomset beds are thin at this water depth and immediately overly the Pleistocene surface. The western boundary is taken to be the Hooghly River, just to the west of the Swatch of No Ground, which was a major outlet for the Ganges River in recorded history. Bathymetric and topographic data were used to constrain the upper surface, and the lower surface was taken as a plane extrapolated landward from the ~80-m isobath. All depth/elevation and position information was processed using Surfer™ to calculate the volumes for the marine (1.97×10^{12} m^3) and terrestrial (0.26×10^{12} m^3) sediment accumulation seaward of the Holocene maximum transgression.

Based on the estimated annual sediment load of 1060×10^6 t/year (Milliman and Syvitski, 1992), the volume of marine material on the shelf (integrated over 7000 years and assuming a dry bulk density of 1.1 g cm^{-3}) represents about 31% of the rivers' input. The corresponding terrestrial portion is about 4.2%. Error of these budget estimates likely is large as they are based on modern sediment discharge figures that may not be representative of the entire late Holocene. For example, anthropogenic activities can have significant effects on sediment discharge; farming can increase load whereas river-control structures, such as dams, can reduce the load through trapping. Uncertainty in the chronology taken from Umitsu (1993) contributes further to the potential error of this estimate. Most importantly, the boundaries were based on sedimentary facies and geographical features and

are, as such, arbitrary to some degree. Despite these uncertainties, the subaqueous delta off the Ganges–Brahmaputra clearly represents a significant component of the late Holocene delta.

In comparing the integrated discharge values to the volume of the subaqueous delta, an important consideration is that river discharge measurements are taken some distance upstream of the shoreline and may not reflect the amount supplied to the coastal ocean. Floodplain sedimentation appears to be a significant factor, accounting for a loss of 10–40% of the measured discharge for the Mississippi, Amazon and Changjiang rivers (Kesel et al., 1992; Nittrouer et al., 1995; Xiqing, 1996). For the Ganges–Brahmaputra system, estimates of floodplain sequestering range as high as 80% of the discharge, although these estimates are based on a limited data set (Milliman and Syvitski, 1992). Because floodplain accommodation could significantly reduce the rivers' input to the shelf, the proportion of sediment accumulation represented by the subaqueous delta could easily exceed the above estimate of 31%. A recent study of floodplain sedimentation rates for a 110 km reach of the Brahmaputra left bank estimates the removal of about 5% of the river's load (Allison et al., 1998); however, extrapolation of this figure to the rest of the floodplain and delta plain is problematic as considerable regional variation in floodplain sedimentation rates in this dynamic and tectonically complex region seems likely. More detailed study is needed to ascertain the role of the floodplain sedimentation in the overall budget.

6. Conclusions

(1) Seismic reflection profiles of the sediment wedge seaward of the Ganges–Brahmaputra river system reveal clinoform stratigraphy characteristic of a subaqueous delta. Sediment accumulation rates are highest in the foreset region (1–>5 cm/year) and decrease in the bottomset region (<0.3 cm/year), an observation consistent with an actively prograding clinoform.

(2) Seabed evidence suggests that the dominant transport of fine-grained sediment on the Bengal shelf is to the south and west. Sediments fine seaward and westward, with the thickest accumulation of mud near the submarine canyon, Swatch of No Ground, which incises the western shelf. Sand waves found near the eastern coast of Chittagong are oriented with their lee side facing west, also indicating westward transport.

(3) Slumps, growth faults and evidence of mass movement coupled with high sedimentation rates near the Swatch of No Ground provide dramatic evidence that modern sediment is being channeled off-shelf through the submarine canyon to the Bengal Fan.

(4) Sediment volume estimates reveal that the Holocene subaqueous delta accommodates about 30% of the rivers' load, indicating that subaqueous deltaic progradation is an important sink for the rivers' sediment. The remainder is partitioned between the floodplain/delta plain and deep sea, but the relative importance of these sinks is not known.

Acknowledgements

The authors would like to thank the Netherlands sponsored Land Reclamation Project for their logistical support during the field work. Financial support was provided by the National Science Foundation grants OCE-9019472 and OCE-9322254. Charles A. Nittrouer generously provided access to his GeoPulse® system used in the field study. Steven L. Goodbred drafted Fig. 1. This paper forms contribution No. 2069 from the Virginia Institute of Marine Science, College of William and Mary.

References

Alexander, C.R., DeMaster, D.J., Nittrouer, C.A., 1991. Sediment accumulation in a modern epicontinental-shelf setting: The Yellow Sea. Mar. Geol. 98, 51–72.

Allison, M.A., 1997. Historical changes in the Ganges–Brahmaputra delta front. J. Coastal Res., in press.

Allison, M.A., Kuehl, S.A., Martin, T., 1998. The importance of floodplain sedimentation for river sediment budgets and terrigenous input to the oceans: Insights from the Brahmaputra–Jamuna River. Geology, submitted.

Barua, D.K., Kuehl, S.A., Miller, R.L., Moore, W.S., 1994.

Suspended sediment distribution and residual transport in the coastal ocean off of the Ganges–Brahmaputra river mouth. Mar. Geol. 120, 41–61.

Barua, D.K., Martin, T.C., Hasan, A., Mahmood, S., Kuehl, S.A., 1998. Suspended sediment transport through the Ganges–Brahmaputra fluvial system: Implications for floodplain sedimentation and sediment delivery to the ocean. Sediment. Geol., submitted.

Coleman, J.M., 1969. Brahmaputra River: Channel processes and sedimentation. Sediment. Geol. 3, 129–239.

Cutshall, N.H., Larsen, I.L., Olsen, C.R., 1983. Direct analysis of ^{210}Pb in sediment samples: Self-absorption correction. Nucl. Instrum. Methods 206, 309–312.

Geyer, W.R., Beardsley, R.C., Lentz, S.J., Candela, J., Limeburner, R., Johns, W.E., Castro, B.M., Soares, I.D., 1996. Phys. Oceanogr. Amazon Shelf 16, 575–616.

Kesel, R.H., Yodis, E.G., McCraw, D.J., 1992. An approximation of the sediment budget of the lower Mississippi river prior to major human modification. Earth Surf. Process. Landf. 17, 711–722.

Kuehl, S.A., DeMaster, D.J., Nittrouer, C.A., 1986. Nature of sediment accumulation on the Amazon continental shelf. Cont. Shelf Res. 6, 209–225.

Kuehl, S.A., Hariu, T.M., Moore, W.S., 1989. Shelf sedimentation off the Ganges–Brahmaputra river system: Evidence for sediment bypassing to the Bengal fan. Geology 17, 1132–1135.

Kuehl, S.A., Hariu, T.M., Sanford, M.W., Nittrouer, C.A., DeMaster, D.J., 1991. Millimeter-scale sedimentary structure of fine-grained sediments: Examples from continental margin environments. In: Bennett, R.H., Bryant, W.R., Hulbert, M.H. (Eds.), Microstructure of Fine-Grained Sediments. Springer, New York, pp. 33–45.

Kuehl, S.A., Pacioni, T.D., Rine, J.M., 1995. Seabed dynamics of the inner Amazon shelf: temporal and spatial variability of surficial strata. Mar. Geol. 125, 283–302.

Milliman, J.D., Syvitski, J.P.M., 1992. Geomorphic/tectonic control of sediment discharge to the ocean: The importance of small mountainous rivers. J. Geol. 100, 525–544.

Mooley, D.A., Mohile, C.M., 1983. A study of cyclonic storms on the different sections of the coast around the Bay of Bengal. Mausam (India) 43, 139–152.

Murty, V.S.N., Sarma, Y.V.B., Rao, D.P., Murty, C.S., 1992. Water characteristics, mixing and circulation in the bay of Bengal during southwest monsoon. J. Mar. Res. 50, 207–228.

Nittrouer, C.A., Kuehl, S.A., DeMaster, D.J., Kowsmann, R.O., 1986. The deltaic nature of Amazon shelf sedimentation. Geol. Soc. Am. Bull. 97, 444–458.

Nittrouer, C.A., Kuehl, S.A., Sternberg, R.W., Figueiredo, A.G., Faria, L.E.C., 1995. An introduction to the geological significance of sediment transport and accumulation on the Amazon continental shelf. Mar. Geol. 125, 177–192.

Polach, H.A., Stipp, J.J., 1967. Improved synthesis technique for methane and benzene radiocarbon dating. Int. J. Appl. Radiat. Isot. 18, 359–364.

Prior, D.B., Yang, Z.S., Bornhold, B.D., Geller, G.H., Lin, Z.H., Wiseman Jr., W.J., Wright, L.D., Lin, T.C., 1986. The subaqueous delta of the modern Huanghe (Yellow River). Geo-Mar. Lett. 6, 67–75.

Segall, M.P., Kuehl, S.A., 1992. Sedimentary processes on the Bengal shelf as revealed by clay-size mineralogy. Cont. Shelf Res. 12, 517–541.

Segall, M.P., Kuehl, S.A., 1994. Sedimentary structures on the Bengal shelf: a multi-scale approach to sedimentary fabric interpretation. Sediment. Geol. 93, 165–180.

Shetye, S.R., Gouveia, A.D., Shankar, D., Shenoi, S.S.C., Vinayachandran, P.N., Sundar, D., Michael, G.S., Nampoothiri, G., 1996. Hydrography and circulation in the western Bay of Bengal during the northeast monsoon. J. Geophys. Res. 101, 14011–14026.

Suryanarayana, A., Murty, C.S., Rao, D.P., 1992. Characteristics of coastal waters of the western bay of Bengal during different monsoon seasons. Austr. J. Freshwater Res. 43, 1517–1533.

Umitsu, M., 1985. Natural levees and landform evolution in the Bengal lowland. Geogr. Rev. Jpn. 58, 149–164.

Umitsu, M., 1987. Late Quaternary sedimentary environment and landform evolution in the Bengal lowland. Geogr. Rev. Jpn. 60, 164–178.

Umitsu, M., 1993. Late Quaternary sedimentary environments and landforms in the Ganges delta. Sediment. Geol. 83, 177–186.

Wright, L.D., Coleman, J.M., 1973. Variations in morphology of major deltas as functions of ocean wave and river discharge regimes. Bull. AAPG 57, 370–398.

Wright, L.D., Coleman, J.M., 1974. Mississippi River mouth processes: Effluent dynamics and morphologic development. J. Geol. 82, 751–778.

Wright, L.D., Nittrouer, C.A., 1995. Dispersal of river sediments in coastal seas: Six contrasting cases. Estuaries 18, 494–508.

Wyrtki, K., 1973. Physical oceanography of the Indian Ocean. In: Zeitzschel, B. (Ed.), Ecology Studies, The Biology of the Indian Ocean. Springer, New York, pp. 18–36.

Xiqing, C., 1996. An integrated study of sediment discharge from the Changjiang River, China, and the delta development since the mid-Holocene. J. Coastal Res. 12, 26–37.

Annex B58

D. Rao et al., "Crustal Evolution and Sedimentation History of the Bay of Bengal Since the Cretaceous", *Journal of Geophysical Research*, Vol. 102, No. B8 (1997)

JOURNAL OF GEOPHYSICAL RESEARCH, VOL. 102, NO. B8, PAGES 17,747–17,768, AUGUST 10, 1997

Crustal evolution and sedimentation history of the Bay of Bengal since the Cretaceous

D. Gopala Rao and K. S. Krishna

Geological Oceanography Division, National Institute of Oceanography
Dona Paula, Goa, India

D. Sar

Keshava Deva Malaviya Institute of Petroleum Exploration
Oil and Natural Gas Corporation Limited, Dehra Dun, India

Abstract. Multichannel seismic reflection, gravity, magnetic, and bathymetric investigations were made along five latitudinal profiles from the eastern shelf of India to the Andaman shelf and four NW-SE profiles in the Western Basin off Madras (seismics on three latitudinal profiles) in the Bay of Bengal. The trend of the fracture zones, the locations of the magnetic chron 34, and the Cretaceous Magnetic Quiet Zone suggest that Greater India separated from Antarctica after a period of transform motion in the early Cretaceous, that is, about polarity chron M0 (120 Ma) and drifted northwestward. Negative gravity anomalies are associated with basement rises including the 85°E Ridge between the continental margin of India and the Ninetyeast Ridge. Magnetic reversals and northward trend of the 85°E Ridge support a hotspot origin of the ridge and its emplacement most likely after the Cretaceous quiet period. Juxtaposition of high-amplitude hyperbolic reflections, down-faulted continental blocks buried under thick sediments, and associated gravity and magnetic anomalies mark the boundary between continental and oceanic rocks at the foot of continental slope, about 80 km seaward of the present continental shelf edge. Eight seismic sequences, as thick as 8.5 km, overlie the early Cretaceous oceanic basement and include four unconformities (lower Eocene, upper Oligocene, upper Miocene, and upper Pleistocene) which have been correlated to the major geologic/tectonic events. We also interpret the late Cretaceous/early Tertiary features on the eastern flank of the buried 85°E Ridge as carbonate reefs. The observation of steep subduction of older (cold) Indian plate beneath the Burmese plate near the Andaman Islands suggests the Sunda Arc in this region as low to intermediate stress subduction zone.

Introduction

About a billion tonnes/yr of continental sediments are discharged by the Ganges and Brahmaputra Rivers into the Bay of Bengal [*Subrahmanian*, 1993] and reach as far as 8°S, that is, about 3000 km away from the Ganges mouth [*Curray et al.*, 1982; *Nath et al.*, 1992]. They constitute the largest fan system on Earth and rest on early Cretaceous oceanic basement. The sediments record the imprints of geologic/tectonic events such as the plate collision between India and Eurasia, the Himalayan orogeny and paleo-oceanographic conditions.

This paper presents the results of deep seismic reflection, gravity, and magnetic investigations with the aim of understanding the nature and time span of deposition of sediments and the physical and geological processes influencing their deposition. The time of opening of the Bay of Bengal is discussed together with the origin of the morphotectonic features of the basement, especially the 85°E Ridge.

Tectonics and Sediments

Breakup of eastern Gondwanaland in the early Cretaceous followed by seafloor spreading, generated the oceanic lithosphere underlying the present Bay of Bengal [*Peirce*, 1978; *Norton and Sclater*, 1979; *Curray et al.*, 1982]. Consequently, Greater India drifted in a NNW to NW direction. The ocean floor in the Bay of Bengal was cut by N6°W trending fracture zones [*Ramana et al.*, 1994b]. Collision between India and Eurasia occurred in the lower Eocene, beginning around 53 Ma [*Norton and Sclater*, 1979; *Patriat and Achache*, 1984; *Patriat and Sègoufin*, 1988; *Molnar et al.*, 1988; *Klootwijk et al.*, 1992]. Major uplift and erosion of the Himalayas resulted in rapid deposition of sediments into the Bay of Bengal [*Gansser*, 1981]. The Ninetyeast Ridge and the 85°E Ridge in the Bay of Bengal divide the sedimentary fan into two basins: the Western Basin between eastern margin of India and the 85°E Ridge and the Central Basin between the ridges [*Rao and Bhaskara Rao*, 1986]. *Curray* [1991, 1994] estimated the sediments as thick as 22 km at the head of the Bay of Bengal and volume about 17 x 10^6 km^3. *Gopala Rao et al.* [1994] reported a sediment thickness of about 6.7 km above oceanic basement along 13°N. *Liu et al.* [1982] reported a negative free-air gravity anomaly associated with the 85°E Ridge.

Deep Sea Drilling Project (DSDP) Leg 22 and Ocean Drilling Program (ODP) Legs 116 and 121 investigations in the distal Bengal Fan and on the Ninetyeast Ridge revealed (1) gray silt to mud turbidites and biogenic horizons of Miocene to Recent [*Stow et al.*, 1990], (2) shallow water carbonates [*Von der Borch et al.*, 1974; *Peirce et al.*, 1989], (3) the precollision and postcollision sediments separated by the lower Eocene unconformity "P" [*Curray et al.*, 1982], and (4) unconformities of upper Miocene "A" and upper Pleistocene "B" [*Cochran*, 1990]. Unconformity "A" marks the time of intense deformation in the Central Indian Ocean and Himalayan

Paper number 96JB01339.
0148-0227/97/96JB-01339$09.00

orogeny [*Moore et al.*, 1974; *Weissel et al.*, 1980; *Geller et al.*, 1983; *Bull and Scrutton*, 1992]. Lowered sea levels are also reported during the upper Oligocene, upper Miocene and upper Pleistocene [*Haq et al.*, 1987]. Relatively low sedimentation since the end of Miocene is related to heavy continental vegetation due to intense monsoon [*Douglas et al.*, 1993].

Data Acquisition and Processing

Multichannel seismic reflection (3500 line km), gravity (6575 line km), magnetic (9750 line km), and bathymetric (9750 line km) data along five E-W profiles from the eastern margin of India to Andaman-Nicobar Islands, four NW-SE profiles in the Western Basin off Madras, and one short NNW-SSE profile on the Andaman shelf in the Bay of Bengal were collected aboard the ORV *Sagar Kanya* and M/V *Sagar Sandhani*. Seismic profiles are along latitudes of around 12°59'N (SK 31-2), 13°01'N (MAN-03) and 14°38'N (MAN-01) (Figure 1).

An Integrated Navigation System (Magnavox 1107) and Global Positioning System were used for position fixing during the surveys. Seismic reflection data were acquired with a DFS V (Seg B format) system. A Geometrics G 801 and G 886 proton precession magne-

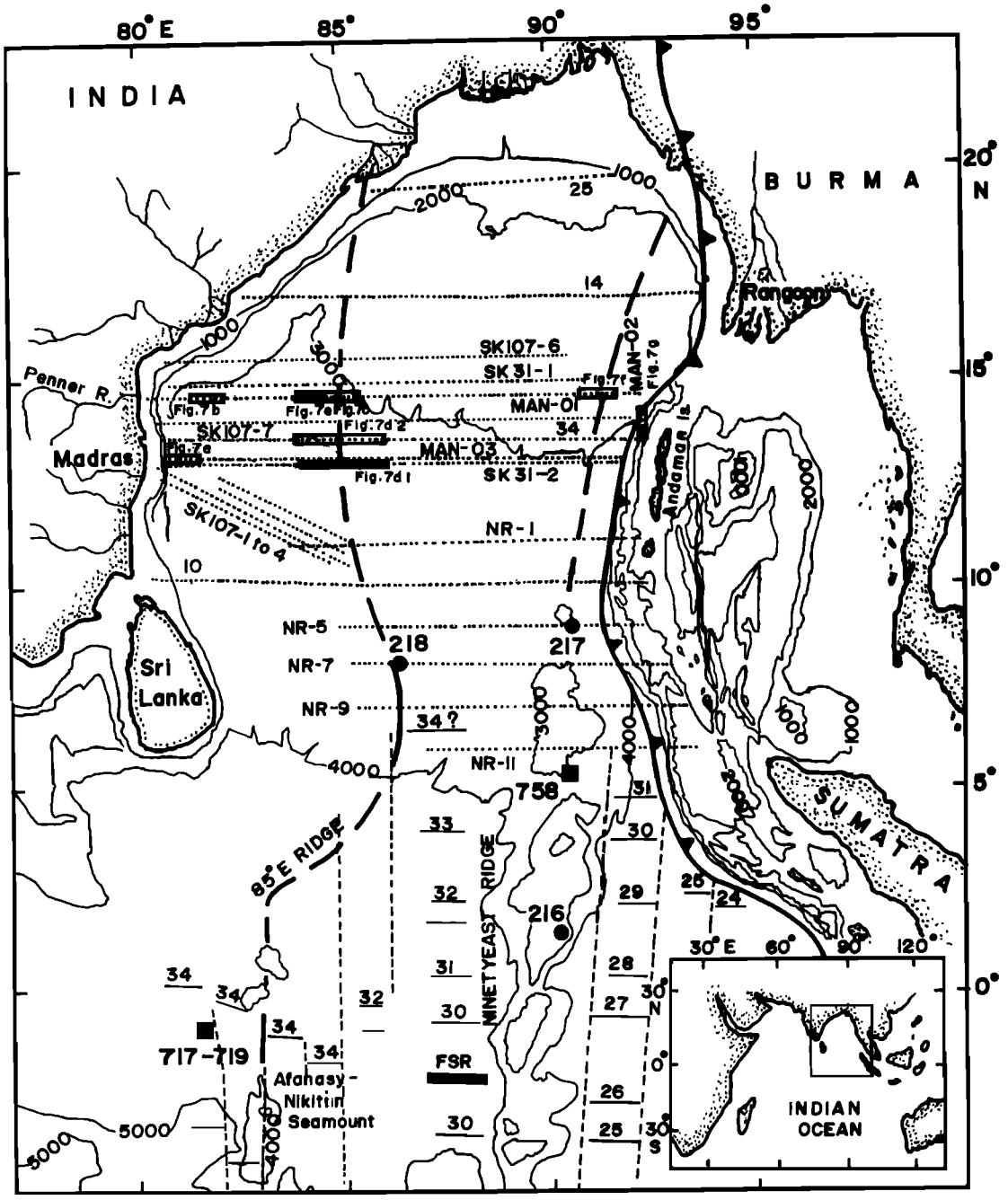

Figure 1. Tectonic map of the northeast Indian Ocean. Dotted lines show profiles of geophysical data generated in different cruises (the profiles MAN-01, MAN-02, MAN-03, SK31-1, SK31-2, and SK107-1 to 4, 6 and 7 are from the present studies and the rest are published by *Rao and Bhaskara Rao*, [1986]; *Rao et al.*, [1987] and *Ramana et al.*, [1994a]. Thick dashed lines show the continuous 85°E Ridge and the Ninetyeast Ridge [*Curray and Munasinghe*, 1991]. Magnetic lineations (short lines with numbers), fracture zones (dashed lines) and fossil spreading ridge (FSR) segments are from *Royer et al.* [1991]. Solid triangles along thick line represent the Sunda Subduction Zone. Solid circles and squares are locations of DSDP and ODP Sites, respectively.

tometers were used to record the total field magnetic data, which were reduced to anomaly values by substracting the International Geomagnetic Reference Field [*International Association of Geomagnetism and Aeronomy Division, Working group* 1, 1986]. Figure 3a shows a plot of magnetic anomalies along several ship tracks including published data used in this study. The gravity data were obtained with KSS-30 and 31 Bodenseewerk Sea Gravimeters with reference base system IGSN-71. Then free-air gravity anomalies were calculated by applying the Eotvös correction and normal gravity (with reference ellipsoid GRS 67) at the observation positions. Figure 4a presents free-air gravity anomalies along profiles together with published data. Bathymetric observations were made using Honeywell Elac narrow beam echosounder system.

The field parameters used for acquisition of seismic reflection data on both vessels were different. A 24-channel seismic streamer with 32 hydrophones per group spaced at 25 m, and a D- type array of seven air guns with a total capacity of 7.98 L and shot firing at every 50 m, were used aboard ORV *Sagar Kanya* for acquisition of data on profile SK 31-2. The six fold coverage was recorded for a length of 12 s using 4-ms sampling interval. A standard processing (GECO) package was used at National Institute of Oceanography, Goa, to obtain stack sections. Profiles MAN-01, 02, and 03 were acquired aboard M/V *Sagar Sandhani* with 96-channel seismic streamer with 32 hydrophones per group spaced at 25 m, and using two D-type array of nine air guns with a total capacity of 31.25 L and with shot firing at every 50 m. The 24-fold coverage was recorded for a length of 10 s using 2-ms sampling interval. Standard processing was performed at Interra Exploration Company (India) Pvt. Ltd., Bombay, to obtain the stack sections.

Results

Seismic Reflection

The seafloor topography ranges from 116 to 3150 m water depth and varies significantly on the margins and in levee channels in contrast to a more even bathymetry in the basins. The seafloor along the eastern continental margin of India is characterized by abrupt seaward deepening with two steplike structures (Figures 2 and 7a). The first step at the shelf edge (SP. 23200 on MAN- 03) is controlled by vertical faults against which the seafloor deepens abruptly to the east by about 2.3 km. The second step with 0.7 km down throw is in the middle slope (SP. 22775 on MAN- 03; 1800 on SK 31-2) and is also caused by near vertical faults. Another buried steplike structure with a very steep eastern flank occur at 8.1 s depth (Figure 7a; SP 22300-22280).

The seafloor near the Sunda Arc and Andaman shelf abruptly becomes shallower with a series of minor steplike structures. At the steps (Figure 7g, SP 640 and Figure 2, SP 23050 on SK 31-2) the seafloor rises abruptly by 0.45 to 0.9 km. A further rise in seafloor by about 0.38 to 0.6 km occurs at the Andaman shelf edge.

Eight seismic sequences, H1 to H8 of total maximum thickness of about 5.0 s two-way travel time (TWT) are identified by the reflection character and pattern (Table 1) displayed on the seismic sections. Three interpreted seismic sections and magnetic and free-air anomalies are shown in Figure 2. In this paper the term "seismic sequence" is being used in a general sense and different from Exxon type. The sequences are bounded by major widespread seismic reflectors, but only some of these reflectors are produced by recognized unconformities. In addition, some of these sequences are observed to contain internal unconformities, such as cut-and-fill structures. The sequences, H1 to H6 consist of high-amplitude pattern and acoustically transparent character, which are parallel and have a maximum thickness of 3.1 s. These are often interrupted by levee channel complexes and turbidite sequences (Figures 7a, 7b, and 7e). Abrupt dissection of the seafloor and underlying reflectors occurs in areas of the channels in the Western and Central Basins. The maximum width and depth of the channels are 8.0 km and 0.1 km, respectively.

The transparent character of sequences H4, H7 (lower part) and H8 (upper part) (Table 1) are interpreted to be fine-grained sediments, which were perhaps deposited by pulses of weak turbidity currents and/or hemipelagic to clastic facies. This characteristic reflection of turbidites also occurs at about 6.7 s depth in the Western Basin within the H6 sequence (Figure 2, SP 520-920 on MAN-01).

The underlying hyperbolic reflectors indicate oceanic basement at a depth ranging from 4.6 to 8.4 s TWT within the basins. Earlier studies [*Curray and Munasinghe*, 1991; *Gopala Rao et al.*, 1994; *Ramana et al.*, 1994b) identified the early Cretaceous oceanic basement in the region. The basement configuration in the Western and Central Basins indicates regional tilt toward west. This tilt may indicate that the basaltic oceanic crust toward west has undergone the effect of subsidence due to plate cooling and sediment load for longer time. The basement consists of several morphotectonic features (Figures 2, 7b, 7c, 7d, 7e, and 7f) including pairs of basement rises separated by depressions, the 85°E Ridge, and the Ninetyeast Ridge. In addition, we have noticed isolated, small relief basement rises and troughs, and lens/mound/sigmoidal shaped structures resting on the flanks of the ridges/rises (Figure 2).

Two sediment-filled grabens bounded by near vertical faults exist on the Ninetyeast Ridge (Figure 7f) and on midslope of eastern margin (off Madras coast) of India (Figure 7a). The Ninetyeast Ridge is broken into two rises separated by a graben of about 25 km wide and 1.0 s deep. This may indicate enechlon structural style of the Ninetyeast Ridge and continues at least this far north (14°40' N latitude). The other graben (Figure 7a) has 10-12 km width and 1.2 s deep and contains internal seismic reflectors that steeply deepen toward its axis.

The sequences, H4 to H8, pinch out against the Ninetyeast Ridge, whereas only sequence H8 pinches out on the 85°E Ridge and some of basement rises. Drape structures are seen on the 85°E Ridge and the prominent basement rises extend to sequence H3. The 85°E Ridge is about 100 km wide with a very steep rise of about 1.7 s TWT on its west side (Figures 7c, 7d, and 7e) and is overlain by seismic sequences H1 to H6. The broader Ninetyeast Ridge is approximately 200 km wide and has a secondary rise of about 45-70 km width and 1.3 to 1.7 s relief to the east (Figure 2; MAN-03 and SK31-2).

At several places deep crustal reflections occur below the Cretaceous basement. A prominent high-amplitude and low- frequency reflector occurs at 9.55 - 9.9 s which apparently deepens westward in the Central Basin (Figure 7e). At the Sunda Arc and Andaman shelf, the deeper reflections reveal the present and past toe of the accretionary complexes separated by a basin filled with drape sediments, the deformation front, and numerous thrust faults separating the uplifted and down-faulted crustal blocks (Figure 7g). The sediments and the oceanic basement are deformed between the Ninetyeast Ridge and the Andaman shelf.

Magnetics

The regional magnetic anomaly profiles (Figure 3a) reveal prominent trends of N-NNW along 85°E, NNE-SSW to the east of the Ninetyeast Ridge, and distinct magnetic anomalies south of 10°N between 86°E and 89°E longitudes. The NNE-SSW trending anomalies occur in the Sunda Arc region.

The closely spaced NW-SE profiles (Figure 3a, SK 107-1 to 4) reveal clear magnetic smooth zone except the anomaly on the shelf and between 83°E and 84°E. Similar anomalies are also seen (MAN-03, 34, RVG-4 in Figure 3a) in immediate east of the 85°E Ridge.

Table 1. Summary of Seismic Sequences Stratigraphy in the Bay of Bengal

Seismic Sequences	Lithology Units Following ODP (Leg 116) Results	Possible Unconfirmities (At Tops)	Regional/Global Geological and Tectonic Event	Inferred Ages	Average Interval Velocity (km/s)	Likely Lithology	Reflection Pattern	
							Western Basin	Central Basin
H1	Units I & II	—	regression in sea level	upper Pleistocene Recent	1.7-1.8	gray silt and mud turbidites	acoustically transparent to high-amplitude continuous parallel reflectors often intercepted by cut and fill type of reflections (levee channels complexes).	mostly high-amplitude continuous parallel reflectors often intercepted by the levee channels complexes
H2	Units III&IV	upper Pleistocene (B)	transgression in sea level	upper Pliocene to upper Pleistocene	1.9-1.95	mud turbidites	high-amplitude continuous parallel to discontinuous reflectors less frequently intercepted by the levee channels complexes.	high-amplitude continuous parallel to discontinuous reflectors less frequently intercepted by the levee channels complexes
H3	Unit VA	upper Miocene (A)	onset of intraplate deformation in the CIB and erosionof Himalayas	upper Miocene	2.2-2.3	gray silt and mud turbidites	high-amplitude .continuous parallel to discrete reflectors with levee channels complexes and high sediment flux	high-amplitude continuous parallel to discrete reflectors with levee channels complexes
H4	—	—	—	middle Miocene	3.0	clay silt and mud turbidites	coustically transparent to continuous parallel to discrete reflectors. transparent reflectors occur on the western flank of the basin and the 85°E Ridge	acoustically transparent to low-amplitude discontinuous parallel reflectors occur on the western flank of Ninetyeast Ridge and sparsely in the basin
H5	—	—	—	lower later half of lower Miocene	3.25-3.55	gray silt and mud turbidites	high-amplitude continuous parallel to discrete reflectors with occasional levee channels complexes	high-amplitude continuous parallel to discrete reflectors with occasional levee channels complexes
H6	—	—	globalsea level regression	first half of lower Miocene	3.52-4.1	hemipelagic and organic rich turbidites	high-amplitude oblique discrete reflections down lap the parallel reflections	Alternate bands of high-amplitude discontinuous parallel and transparent reflectors
H7	—	upper Oligocene	transgressed sealevel	lower Eocenecene - upper Oligocene	4.15-4.5	mostly pelagic(?)	acoustically transparent (lower part) to low-amplitude continuous parallel reflectors are present on the eastern flank of the basin (i.e. 85°E Ridge)	acoustically transparent (lower part) low-amplitude continuous parallel reflectors are present on the flanks of the basin i.e. eastern flank of the 85°E Ridge and western flank of Ninetyeast Ridge
H8	—	lower Eocene (P)	India and Eurasia collision	late Cretaceous/ Paleocene lower Eocene	4.55-4.85	siliciclastic (?)	acoustically transparent (lower part) to low-amplitude continuous parallel reflectors are present on the eastern flank of the basin (i.e. 85°E Ridge)	acoustically transparent (lower part) low-amplitude continuous parallel reflectors are present on the flanks of the basin i.e. eastern flank of the 85°E Ridge and western flank of Ninetyeast Ridge
Basement	—	—	—	early Cretaceous oceanic basement	6.4-8.0	crystalline rocks	high-amplitude hyperbolic reflectors overlie the deep internal reflectors. low frequency and high-amplitude reflector (from irregular source) occur at 9.5 s to 9.9 s depth	high-amplitude hyperbolic reflectors. strong internal reflectors steeply deepen to east, further east reflectors are of a classic accretionary sediment wedge and subducting Indian plate

Average interval velocities assigned to individual seismic sequences are from *Curray et al.* (1982).

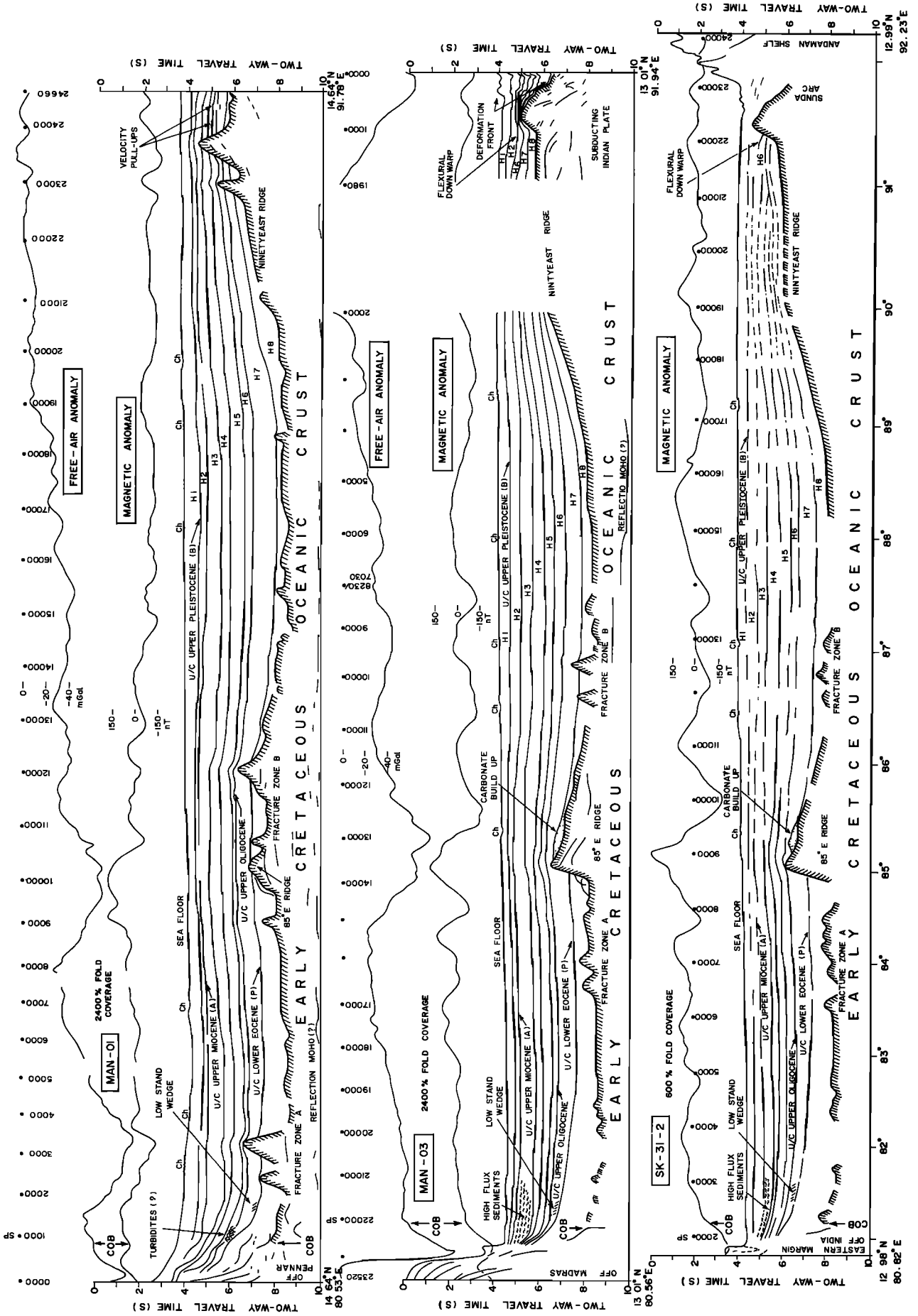

Figure 2. Stacked line diagrams of interpreted crustal structure from three regional seismic profiles along with free-air gravity and magnetic anomaly data.

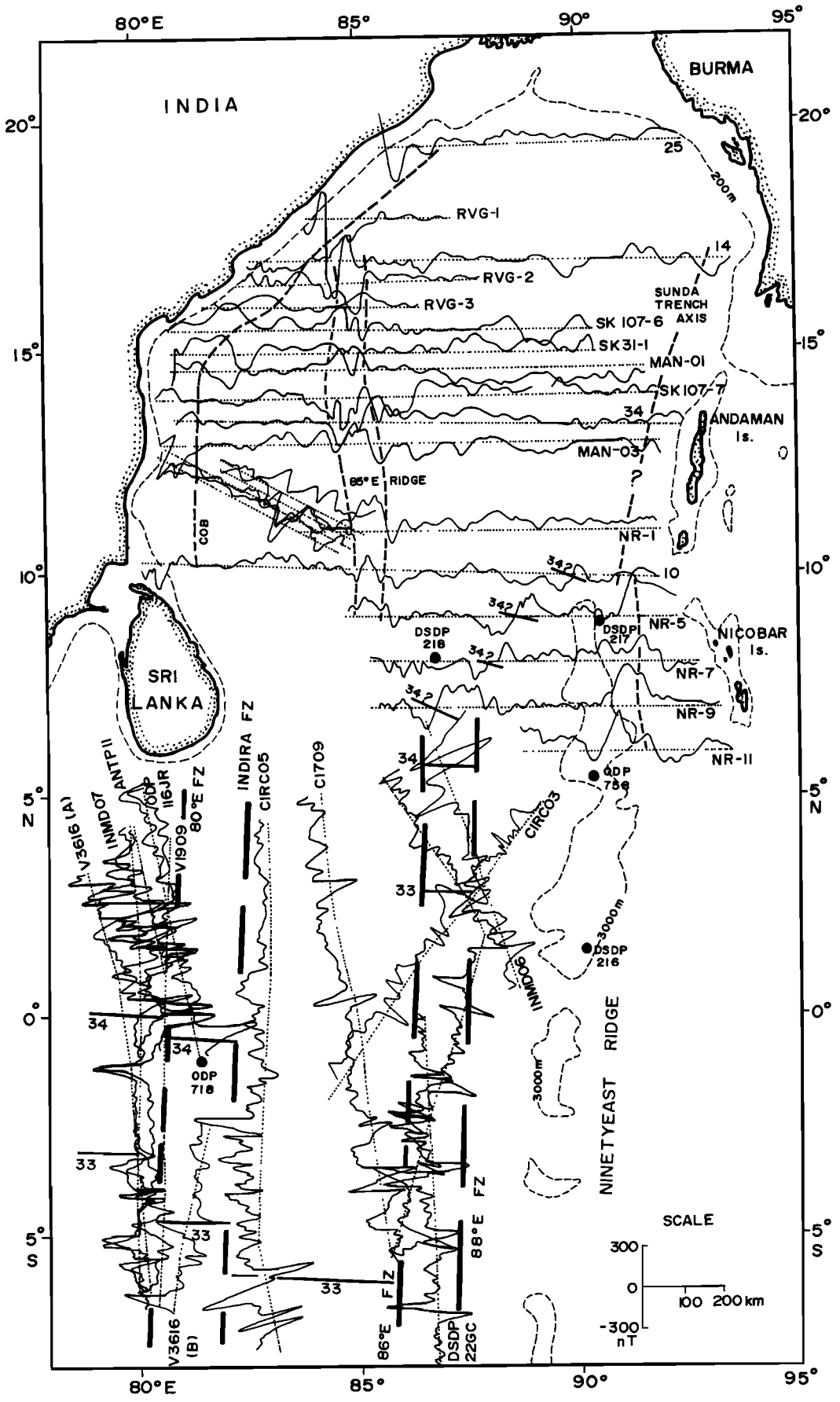

Figure 3a. Magnetic anomaly map of the Bay of Bengal. Magnetic anomalies are plotted perpendicular to the ship tracks. Profiles designated with NR, RVG, and only numbering are after *Ramana et al.* [1994a], *Rao et al.* [1987], and *Rao and Bhaskara Rao* [1986], respectively.

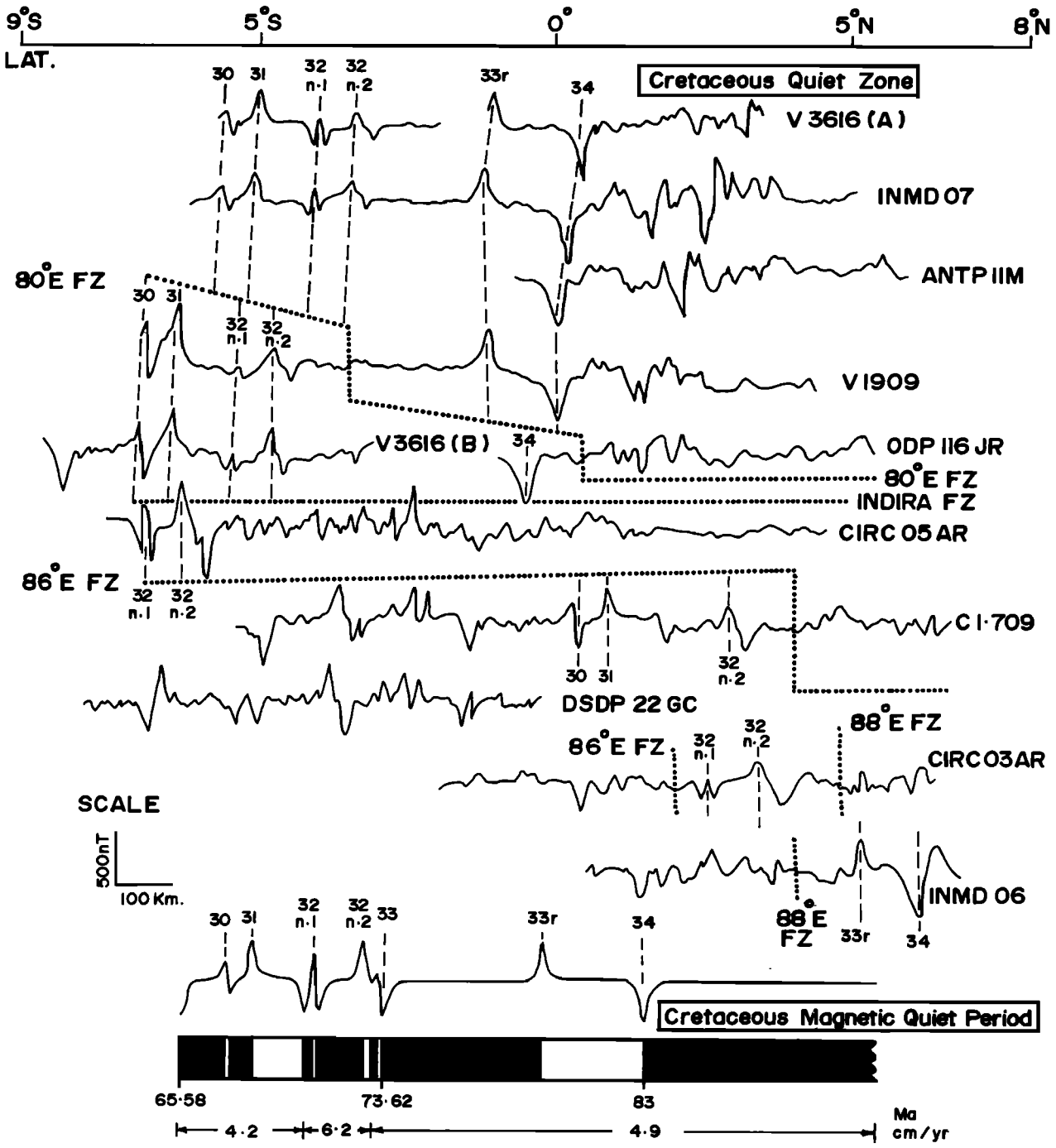

Figure 3b. Observed magnetic anomalies in the distal Bengal Fan and their correlations to synthetic model. Cretaceous Quiet Zone and magnetic lineations 34 and younger ones are shown. The polarity timescale of *Cande and Kent* [1995] was used for assigning the age of magnetic anomalies. For generating the synthetic magnetic anomaly model, the seafloor is divided into 500 m thick normally (solid) and reversely (open) magnetized blocks with a magnetization of 0.01 A/m. The synthetic profile is generated normal to the ridge striking east-west and with a paleolatitude of 40°S. Half spreading rates varying from 4.2 to 6.2 cm/yr, in north-south direction, are used in the calculations.

They are not found on profiles SK 31-1, SK 107-6, RVG-3, and MAN- 01 (Figure 3a). The anomalies near the 85°E Ridge appear to be localized and associated with magmatism and/or basement undulations. The rest of the area is mostly devoid of significant and correlatable anomalies. The N-NNW trending anomalies consist of positive and negative magnetic anomalies (about 400 nT amplitude and 100 km wide) and are associated with the 85°E Ridge (Figure 3a). It is apparent from the magnetic and free-air gravity anomalies (also seen in unprocessed seismic records by the authors) along profile SK 107-6 that the ridge is less wide, suggesting less supply of magma at the time of formation.

The published north-south profiles in the distal Bengal Fan are compared to the synthetic model to establish the anomaly 34 and younger ones (Figure 3b). The magnetic lineations 31 through 34 are dislocated at places indicating existence of four fracture zones (FZ) namely, 80°E FZ, Indira FZ, 86°E FZ, and 88°E FZ. Anomaly 34 on INMD 07 profile (Figure 3a) lies at 6°N and helps to identify the same on east-west profiles 10 and NR-1, 5,7 and 9. The anomaly

34 is left laterally displaced by nearly north- south fracture zones. It is in good agreement in spatial relation with the anomalies 33 and 32 identified by *Royer et al.* [1991].

Royer et al. [1991] reported magnetic anomaly 33 at 4°N, 87°E and 34 at 6°30'N, 87°E (Figure 1). In contrast, Ramana et al. (1994a, b) interpreted Mesozoic lineation M0 at 7°N, 87°E and 7°30'N, 87°30'E. It implies that the anomalies 34 and M0 are separated by only 55 km. This distance is too short to account for the oceanic crust generated during 36 m.y. (between anomalies 34 and M0) with an average plate velocity of about 3 cm/yr. Hence we feel that there is a disagreement between the results [*Royer et al.*, 1991; *Ramana et al.*, 1994a,b].

Gravity

The regional free-air gravity anomaly profiles (Figure 4a) reveal prominent trends of N-NNW along 85°E, N-NNE along 90°E, NNE-SSW on east of the Ninetyeast Ridge and NE-SW along the margin of the east coast of India. The closely spaced profiles in Western Basin show NE-SW trending free-air gravity low, about 60 km wide and 20 mGal in amplitude. It is localized and associated with magnetic anomalies. Apart from these, some isolated gravity lows are also present. The general westward decrease in the free-air anomaly along profiles seems to be associated with regional tilt of the basement to the west. The N-NNW trending negative anomalies are broad, about 200 km wide and are associated with the 85°E Ridge. The N-NNE trending anomalies are broad, about 200 km wide and are associated with the Ninetyeast Ridge. The trends of the ridges in the study area are close to the regional north-south trends of the ridges. NNE-SSW trending anomalies with about 65 mGal troughs occur in the Sunda Arc region. In addition, basement rises to the west of the Ninetyeast Ridge are associated with negative free-air anomalies (SP. 2000-4000, SP. 11500-13000 and SP. 15000-16000 on MAN-01, and SP. 15500-17000 and SP. 8250-11000 on

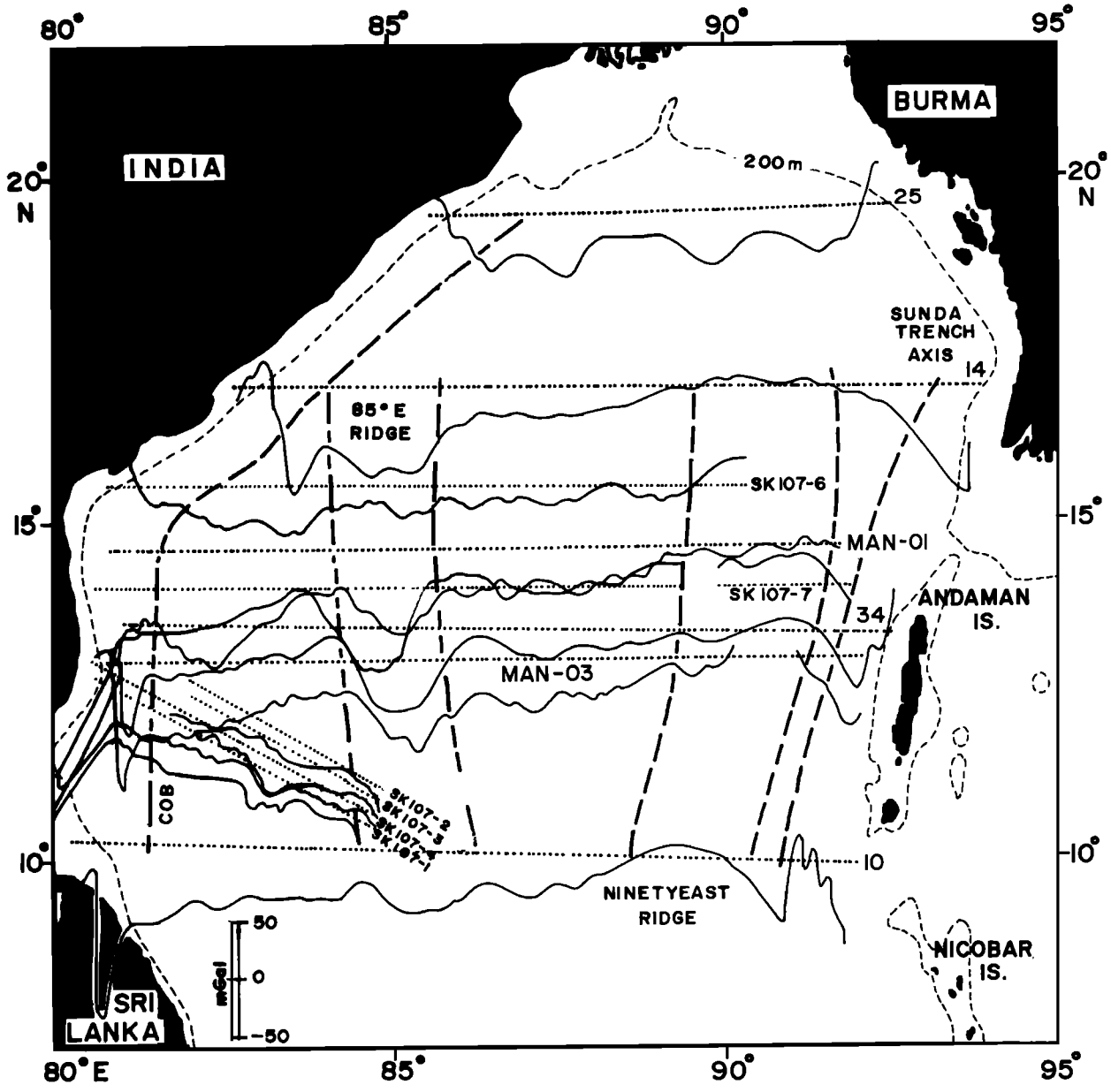

Figure 4a. Free-air anomaly map of the Bay of Bengal. Free-air anomalies are plotted perpendicular to the ship tracks. The profiles designated with other than MAN and SK107 are after *Rao and Bhaskara Rao* [1986].

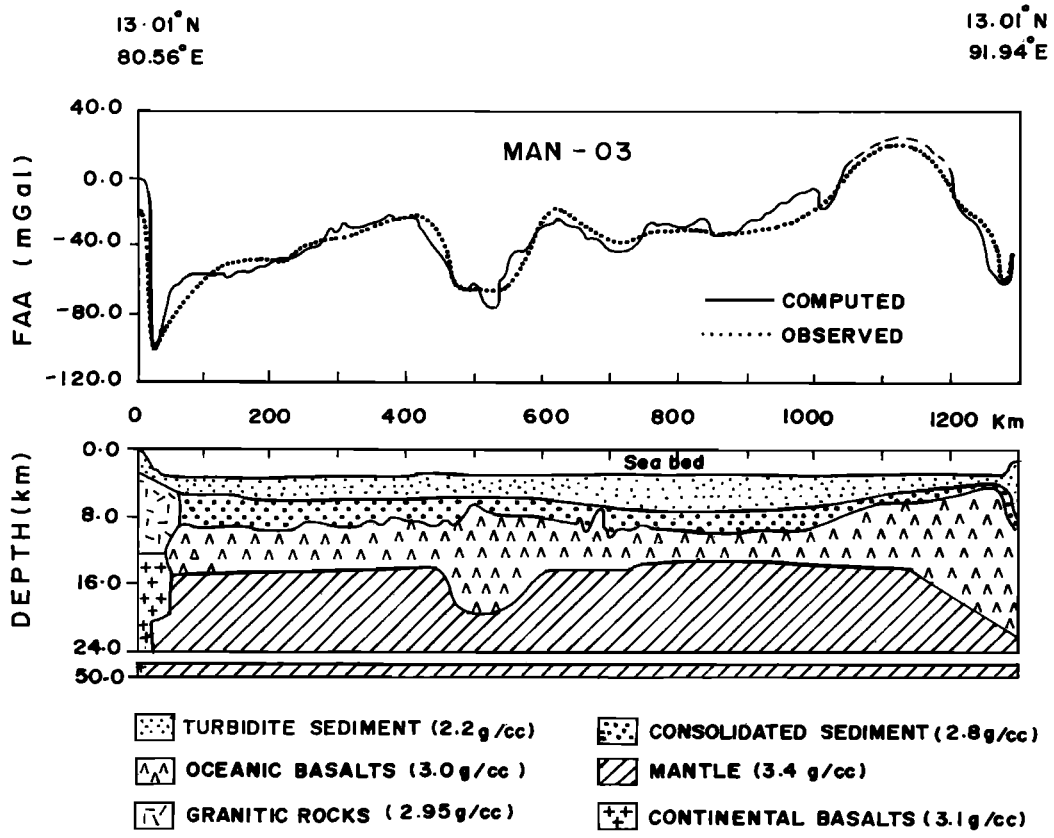

Figure 4b. Two-dimensional gravity modeling and interpreted crustal structure along MAN-03. Sedimentary layers and basaltic layer (top) are taken from the seismic results of the same profile. The TWT of the layers are converted into depth (kilometers) after considering seismic refraction results [*Curray et al.*, 1982] surrounding the profile.

MAN-03 in Figure 2), whereas the Ninetyeast Ridge and basement rises to its east are associated with positive free-air anomalies. Two-dimensional model studies of the free-air gravity anomalies of profile MAN-03 reveal crustal structure and lateral density variations (Figure 4b). It indicates continental rocks extending seaward up to 75 km from the shelf edge and low-density root below the 85°E Ridge. In contrast, previous crustal models not constrained by seismic results in this region [*Mukhopadhyay and Krishna*, 1991] had interpreted possible presence of continental rocks seaward up to 200 km from the shelf edge.

Seismic Stratigraphy and Lithology of Sediments

The seismic sequences H1 to H8 in the Western and Central Basins of the study area (Figure 2) consist of approximately 8.5 km precollisional and postcollisional sediments of India and Eurasia (Table 2). Precollision sediments in the Western Basin and postcollision sediments in the Central Basin are relatively thick, suggesting the high flow of sediment flux from the Indian land mass to the Western Basin and silty/sand mud turbidites from the Ganges and Brahmaputra Rivers to the Central Basin. The pre- collisional sediments are very thin over the ridges. The chronology of the sediments and their unconformities are interpreted based on comparison with the litho-stratigraphic results of ODP Leg 116 Sites (Figure 6), which are about 1500 km southward from the study area; however, there is no north-south transect available which allows direct correlation between the ODP Leg 116 Sites and the study area.

Oceanic basement occurs at 8.5 to 8.7 s TWT in the axial parts of the basins. The top of sequence H8 occurs at 5.0 - 8.0 s. The sequence termination with several onlaping reflectors is interpreted as unconformity. *Moore et al.* [1974] interpreted their lowermost sequence boundary, which is the base of sequence H6 in our study, as lower Eocene unconformity "P" (their data did not image the oceanic basement). Wedgelike structures occur within the sediments of sequence H7 (Figures 2 and 7a). The wedges were developed during lowered sea levels, perhaps the major regression of the Oligocene period [*Haq et al.*, 1987]. The top of the wedges (base of sequence H6) marks an unconformity, as Moore et al. [1974] have observed, but we suggest a much younger age is possible.

Table 2. Sediment Thicknesses of Precollision and postcollision of India and Eurasia and Depth to the Cretaceous Basement Between 13° and 14° 38' N

S. No.	Location	Precollision Sediments, km		Postcollision Sediments, km		Maximum Depth From Seafloor to the Cretaceous Oceanic Basement, km
		Maximum	Minimum	Maximum	Minimum	
1	Western Basin	3.0	0.1	4.8	3.2	7.5
2	Central Basin	2.4	0.1	6.6	4.7	8.5
3	85°E Ridge	–	–	4.1	3.1	4.1
4	Ninetyeast Ridge	1.0	0.1	3.2	0.8	4.0

Sequence H3 is the thickest succession with high sediment influx among the postcollision sedimentary layers along the continental rise/slope of the east coast of India (Figures 2 and 7a). The upper surface has several onlapping reflectors indicating a major unconformity. ODP Sites 717 to 719 contain a major unconformity "A" at end of Miocene (8 to 7 Ma) in the distal fan area (Figure 6) [*Cochran*, 1990]. We infer the top of sequence H3 to be this upper Miocene unconformity. The onset of intraplate deformation in the Central Indian Basin [*Moore et al.*, 1974; *Weissel et al.*, 1980; *Geller et al.*, 1983; *Bull and Scrutton*, 1992] may coincide with this upper Miocene unconformity. Between the identified "Oligocene" (top of H7) and upper Miocene (top of H3 or "A") unconformities, we interpolate Middle and lower Miocene ages for sequences H4 through H6 (Table 1). The middle Miocene is relatively thin at ODP Site 718, and we tentatively assign sequence H4 to this middle Miocene unit and lower Miocene age to sequences H5 and H6.

Sequence H2 is relatively thin, and its top is overlain by onlapping reflectors. ODP Sites 717 to 719 investigations identified an upper Pleistocene unconformity "B" (Figure 6). The top of sequence H2 is assumed to be this upper Pleistocene unconformity, which developed as a result of reduced sediment input to the basins. The thin sequence H2 confirms that the sediment input to the basins were drastically reduced soon after the upper Miocene high influx of sediments.

Sequences H1 to H8 sediments in the Bay of Bengal are thus interpreted as mid-Cretaceous through Cenozoic clastic/turbidites and hemipelagic sediments overlying the early Cretaceous oceanic basement. The Miocene to Recent sediments are gray silty clays at ODP Sites 717 to 719 [*Stow et al.*, 1990] and sandy turbidites at DSDP Site 218 [*Curray and Moore*, 1971]. Therefore we interpret the sequence H3 through H1 to be of upper Miocene to Recent silty/sand mud turbidites. These clastics were derived from the Himalayas and transported into the Bay of Bengal. Sequence H8 is interpreted as precollision clastics. The sequence H7 sediments are postcollision clastics and hemi-pelagics of Eocene-Oligocene age.

The early Cretaceous Fracture Zones

Prominent high-amplitude hyperbolic reflections at varied depths (4.6 to 8.4 s) are identified on profiles MAN-01, 03, and SK 31-2. These are interpreted as oceanic basement with rises and depressions. Pairs of basement rises with intervening depressions occur at 6.2 s - 8.2 s TWT. The relief of the rises varies between 0.8 and 1.2 s. They are reflected in gravity and magnetic anomalies (Figure 2). The pairs of raises are correlated on the profiles by considering their morphology, gravity, and magnetic signatures and the direction of early plate motion between Indian and Antarctica. They lie between 82°E and 84°E, and 85°E and 87°E, and trend approximately N-W (Figure 5). This trend is oblique to the northward trends of the 85°E Ridge and Ninetyeast Ridge.

The direction of seafloor spreading was toward the present northwest during the separation of Greater India from Antarctica [*Norton and Sclater*, 1979; *Curray et al.*, 1982; *Ramana et al.*, 1994b]; therefore we interpret these northwest trending pairs of rises to be fracture zones. Paleocene/lower Oligocene to Recent sediments with thickness of about 2.6 s to 3.5 s rest on them. The sequence H8 pinches out against the rises of the fracture zone (Figures 2 and 7b). The depressions between rises are filled with sediment of sequence H8 and subsequent ones.

Carbonate Reefs

The 85°E Ridge is covered by post upper Oligocene (H6 to H1) sediments (Figures 2, 7c, and 7d). The reflections on its shallow dipping eastern flank are much less hyperbolic in character and form lens- or mound-shaped structures of about 50 km wide and 0.8 km thick. Within these structures, the reflections have a sigmoidal pattern and transparent to semitransparent character (Figure 7d). There is an inversion (2.2 to 2.9 km/s) in the interval velocity structure at the depth along the eastern flank of the 85°E Ridge. The lens-shaped transparent reflections, sigmoidal pattern, and pinch-out structure with low velocity that are along the flanks and atop of the 85°E Ridge are interpreted as carbonate reefs. The reefs might have developed over the 85°E Ridge when it was in shallow water depths with low sedimentation rates during the late Cretaceous/early Tertiary. Shallow water carbonates are also reported on the Ninetyeast Ridge [*Von der Borch et al.*, 1974; *Peirce et al.*, 1989] and the Chagos-Laccadive Ridges [*Shipboard Scientific Party*, 1988], which lends credence to our interpretation.

Continent - Ocean Boundary Along the Eastern Continental Margin of India

The seafloor of the continental shelf (off Madras) is down faulted in two steps by about 2.3 and 0.7 km (Figures 2 and 7a). The steplike structure at 8.1 s depth with very steep eastern flank is buried below about 3.85 s thick sediments of sequences H8 to H1. A negative free-air anomaly of about -105 mGal is centered at the outer shelf edge near the first steplike structure. On the west of second step, subsurface reflectors steeply deepen to about 6.0 s. The early Cretaceous oceanic basement abruptly ends against the eastern flank of the buried step. At this buried step, the high-amplitude negative free-air anomaly of the continental slope region changes to the low-amplitude, westward tilted regional anomaly (Figure 2). Such changes in gravity and magnetic anomalies generally occurs at the contact of the step faulted continental blocks and the oceanic crust [*Srivastava*, 1978; *Srivastava et al.*, 1988]. Gravity model studies also are consistent with a sharp contact between continental and oceanic crust (Figure 4b). Therefore we assign the Continent Ocean Boundary (COB) at these changes in potential field data. The COB

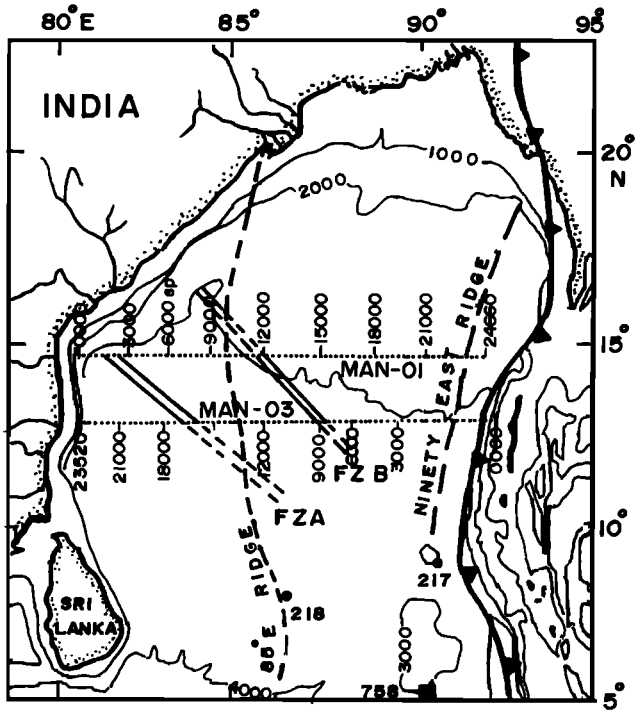

Figure 5. Trends of early Cretaceous fracture zones.

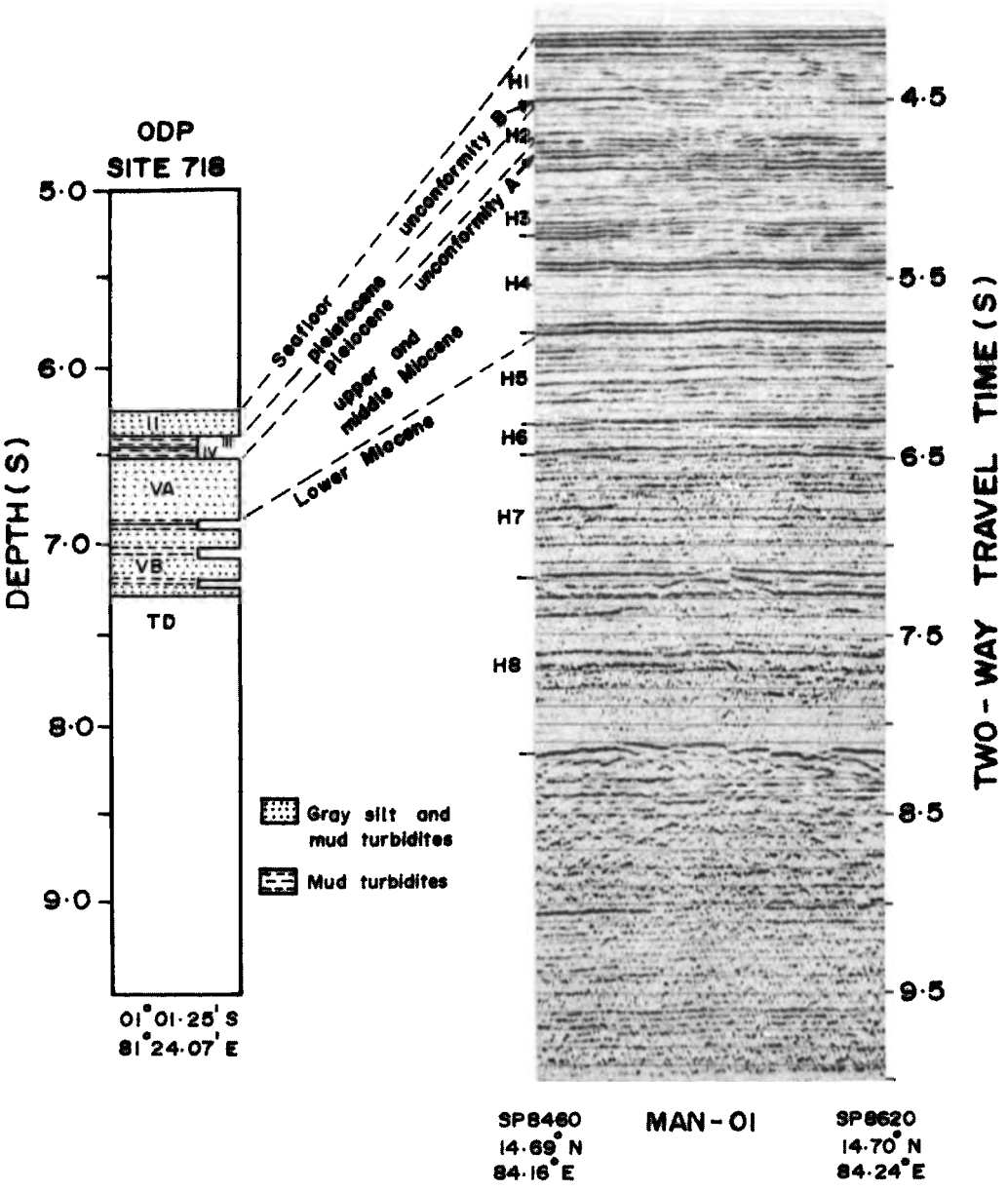

Figure 6. Correlation between the seismic sequence in the study area and ODP Leg 116 data.

has been identified on the several east-west profiles and mapped along the margin (Figure 4a). The identified COB lies close to the foot of the continental slope that is, about 70-80 km from the shelf edge. *Murthy et al.* [1993] inferred a COB from magnetic data to occur at the foot of the continental slope between Madras (13°N) and Kakinada (17°N). However, our integrated studies of the geophysical data would place the COB at about 70-80 km seaward of the shelf edge, that is, at about 50 km away from the foot of the slope.

Tectonic and Sedimentation History

In the study area, sediments of about 8.5 km maximum thickness overlie the early Cretaceous basaltic oceanic crust. The oceanic basement includes morphotectonic features such as fracture zones, aseismic ridges, sediment-filled grabens, basement rises and carbonate reefs. The features other than the 85°E Ridge, the Ninetyeast Ridge, and carbonate reefs were mostly developed during the time of early spreading (younger than anomaly M0 time) between Greater India and Antarctica. The results of the Ocean Drilling Program Leg 121 [*Weis et al.*, 1991; *Royer et al.*, 1991] confirmed the hotspot (Kerguelen) origin for the Ninetyeast Ridge. The nature of the 85°E Ridge consistent with the geophysical anomalies remains uncertain.

Breakup of India from Antarctica

The location of major magnetic anomaly 34 identified by *Royer et al.* [1991] and from our studies (Figures 3a and 3b), absence of prominent correlatable magnetic anomaly lineations (Figure 3a), and NW-SE trending fracture zones (Figure 5) in the Bay of Bengal indicate that oceanic crust was formed during the Cretaceous magnetic quiet period, 120-84 Ma. Crust of Cretaceous quiet period age spans more than 8° in NW-SE direction south of Sri Lanka [*Merrill et al.*, 1989], 14° in NW-SE direction off the northwest Australia [*Veevers and Li*, 1991] and 12° in NE-SW direction off southeast coast of Africa [*Royer et al.*, 1989]. Based on these spatial separations between anomalies 34 and M0, one expects anomaly M0 close

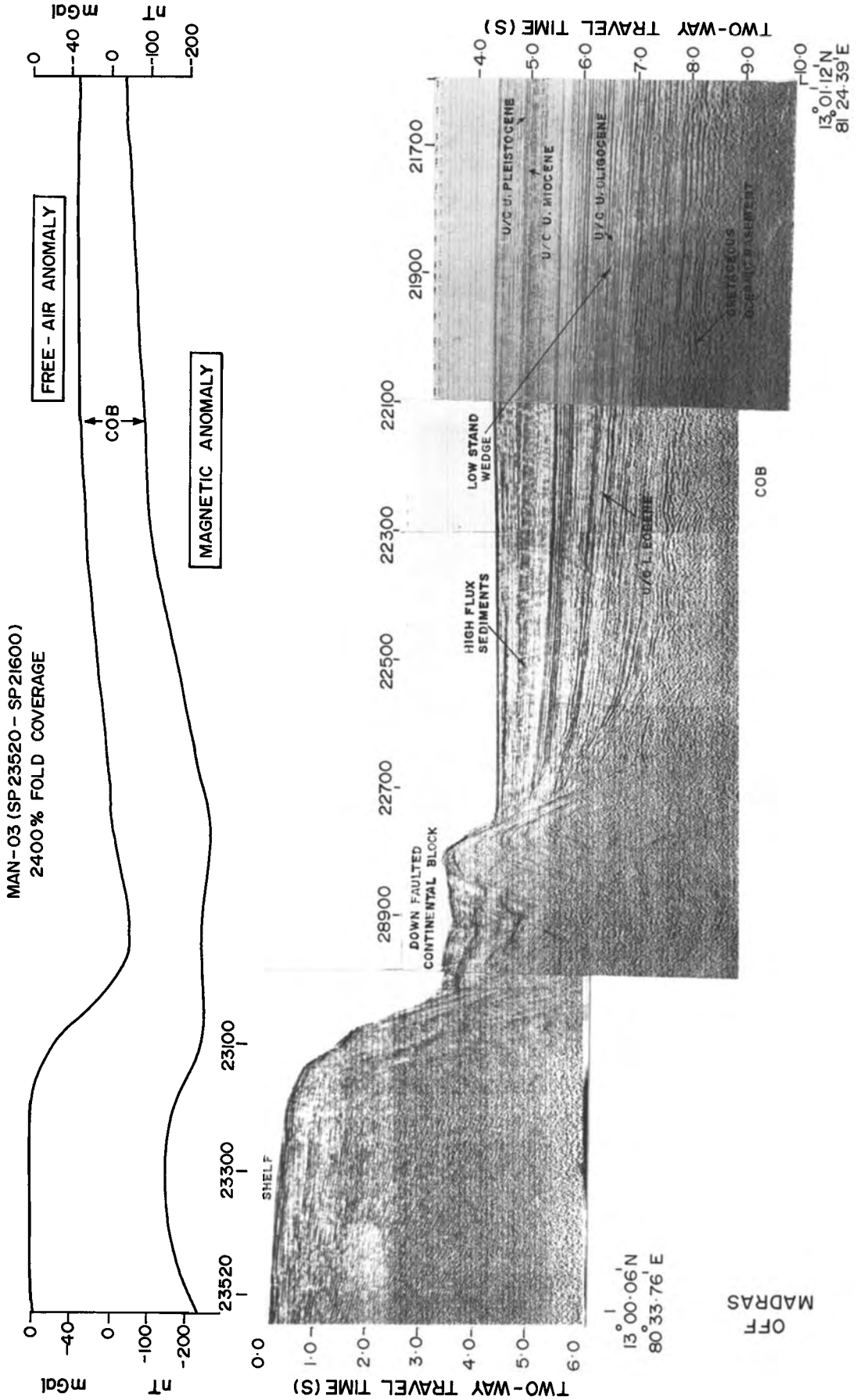

Figure 7a. Multichannel seismic record and free-air gravity and magnetic anomalies across the eastern continental margin of India (off Madras) show the down-faulted continental blocks, the Continent Ocean Boundary (COB), and stratigraphic unconformities.

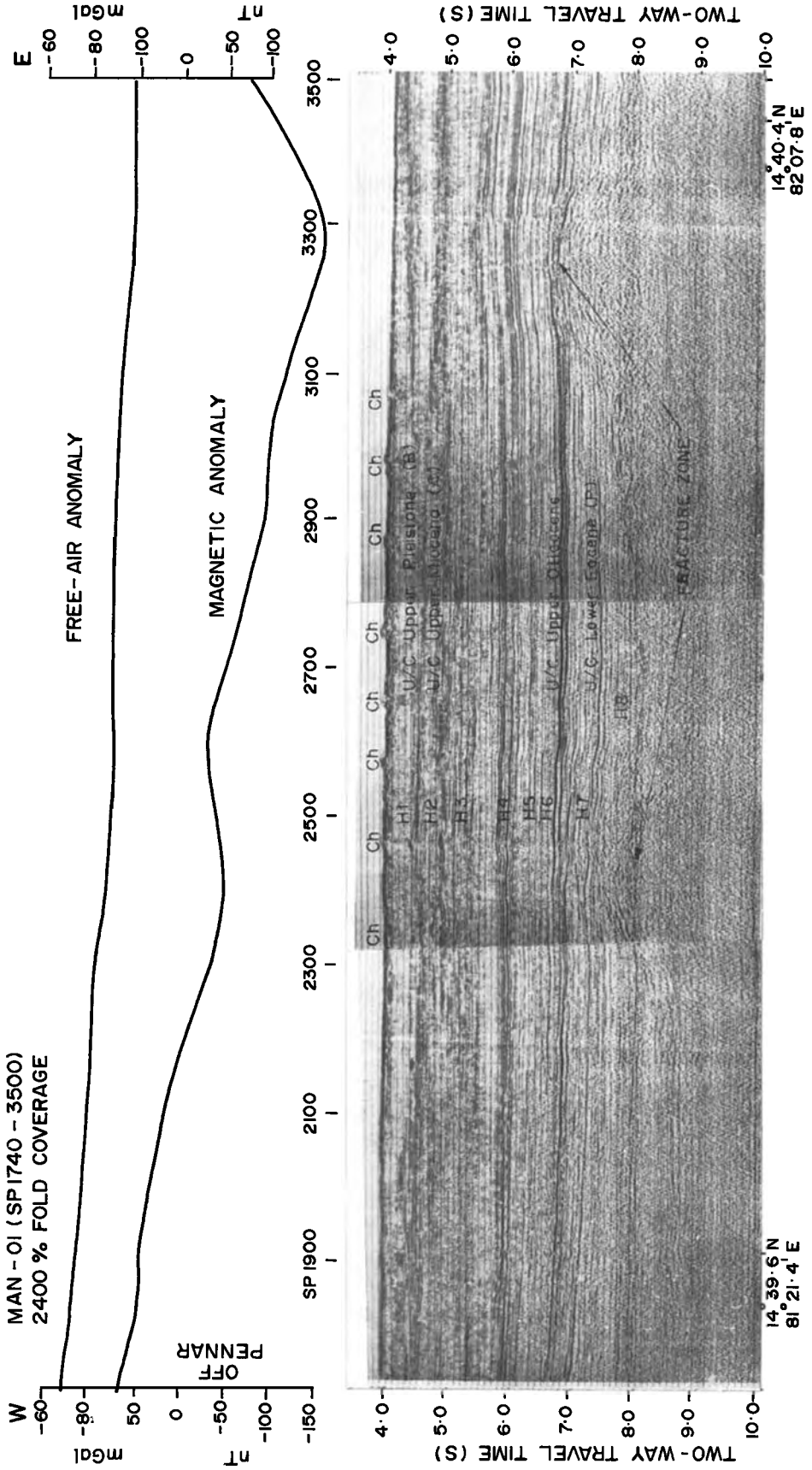

Figure 7b. Multichannel seismic record and free-air gravity and magnetic anomalies in the Western Basin (off Pennar) depict the transverse ridges separated by trough (fracture zone), seismic sequences H1 to H8, and associated unconformities.

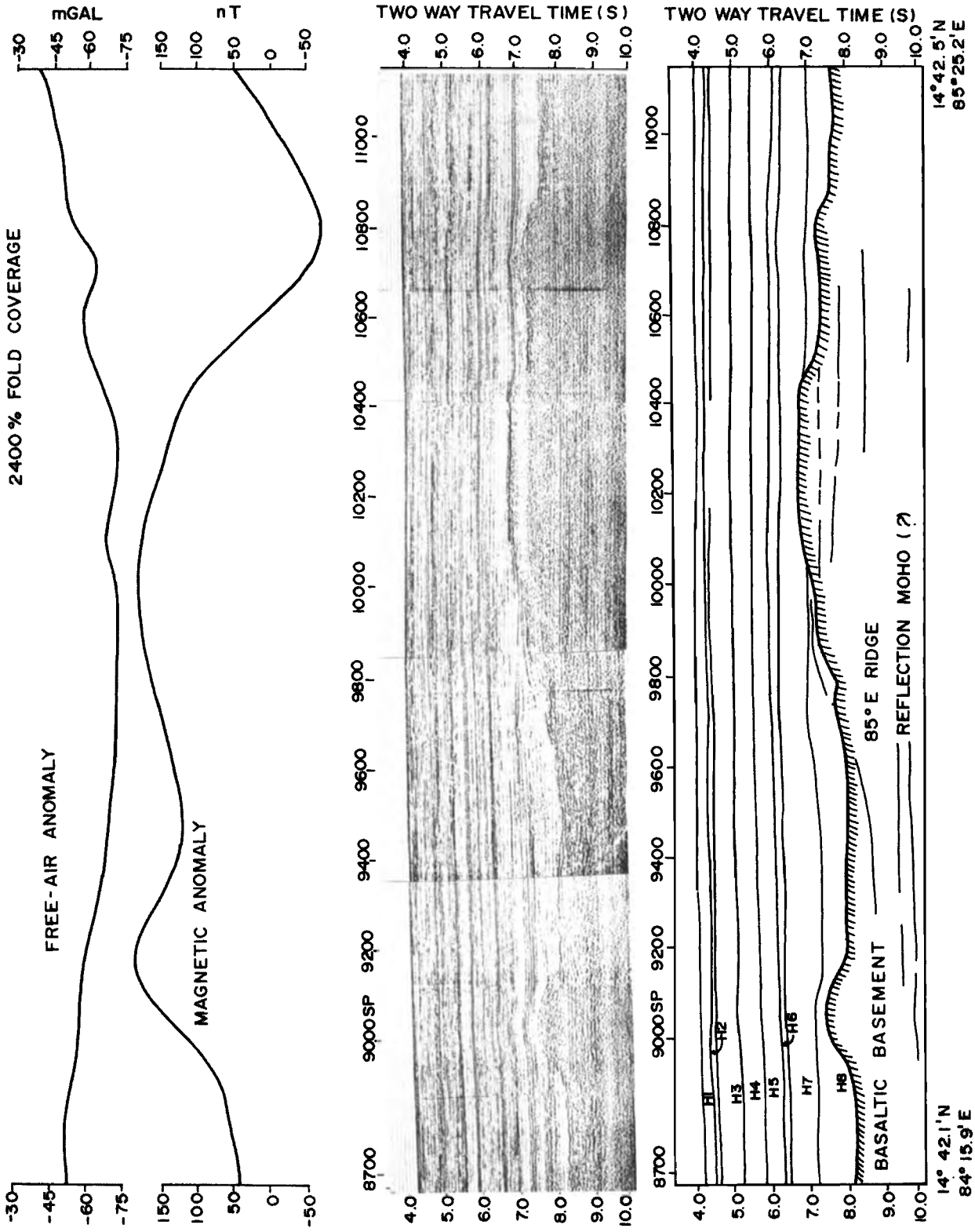

Figure 7c. Multichannel seismic record and free-air gravity and magnetic anomalies of the 85°E Ridge on MAN-01.

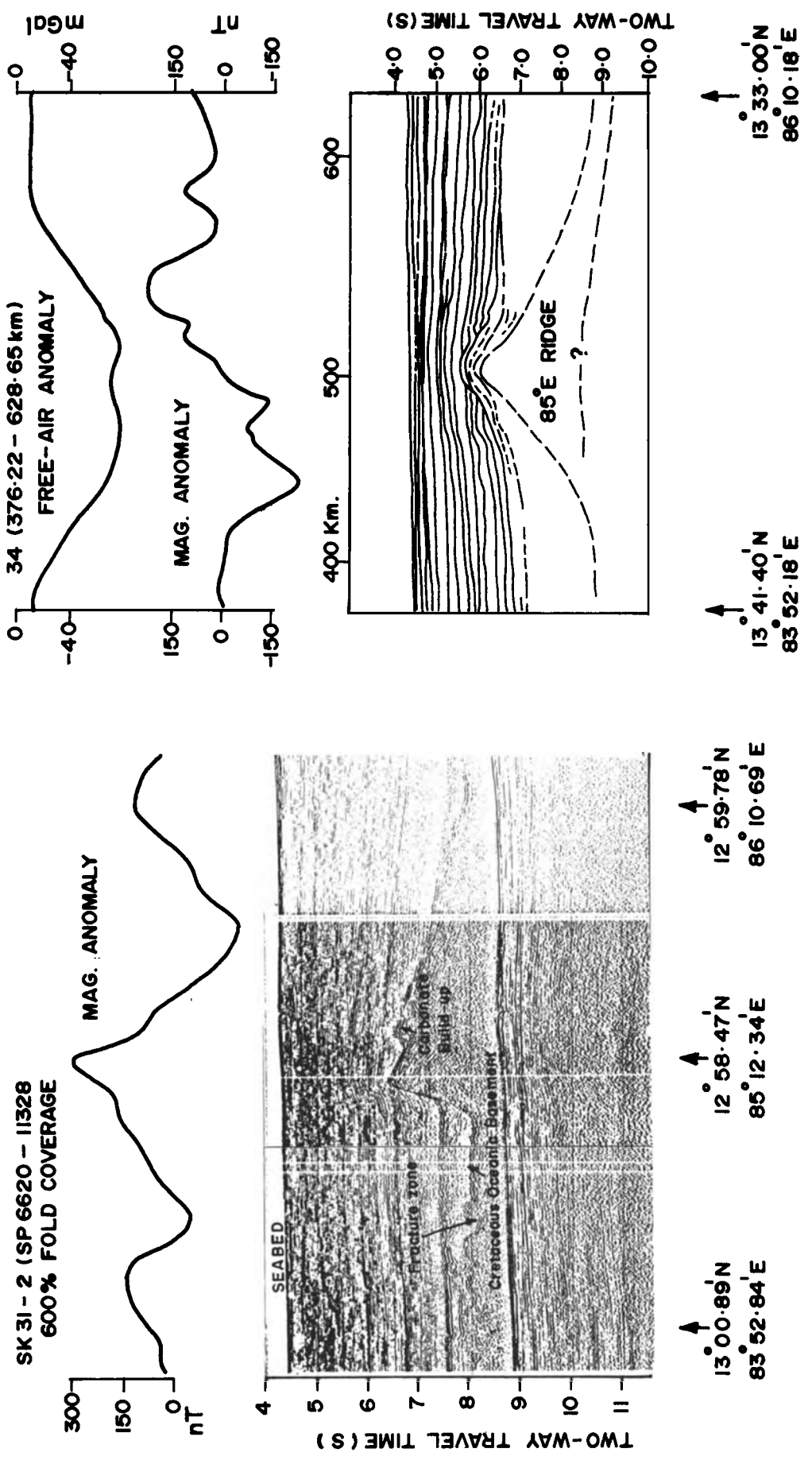

Figure 7d. (Left) Multichannel seismic record and magnetic anomaly across the 85°E Ridge on SK-31-2 depict seismic structure of the ridge, carbonate build up, fracture zone, etc. (Right) Line diagram of interpreted seismic section (J. R. Curray personnel communication, 1994) and free-air and magnetic anomalies [*Rao and Bhaskara Rao*, 1986] across the 85°E Ridge on profile 34 depict seismic structure of the ridge, and stratigraphic unconformities.

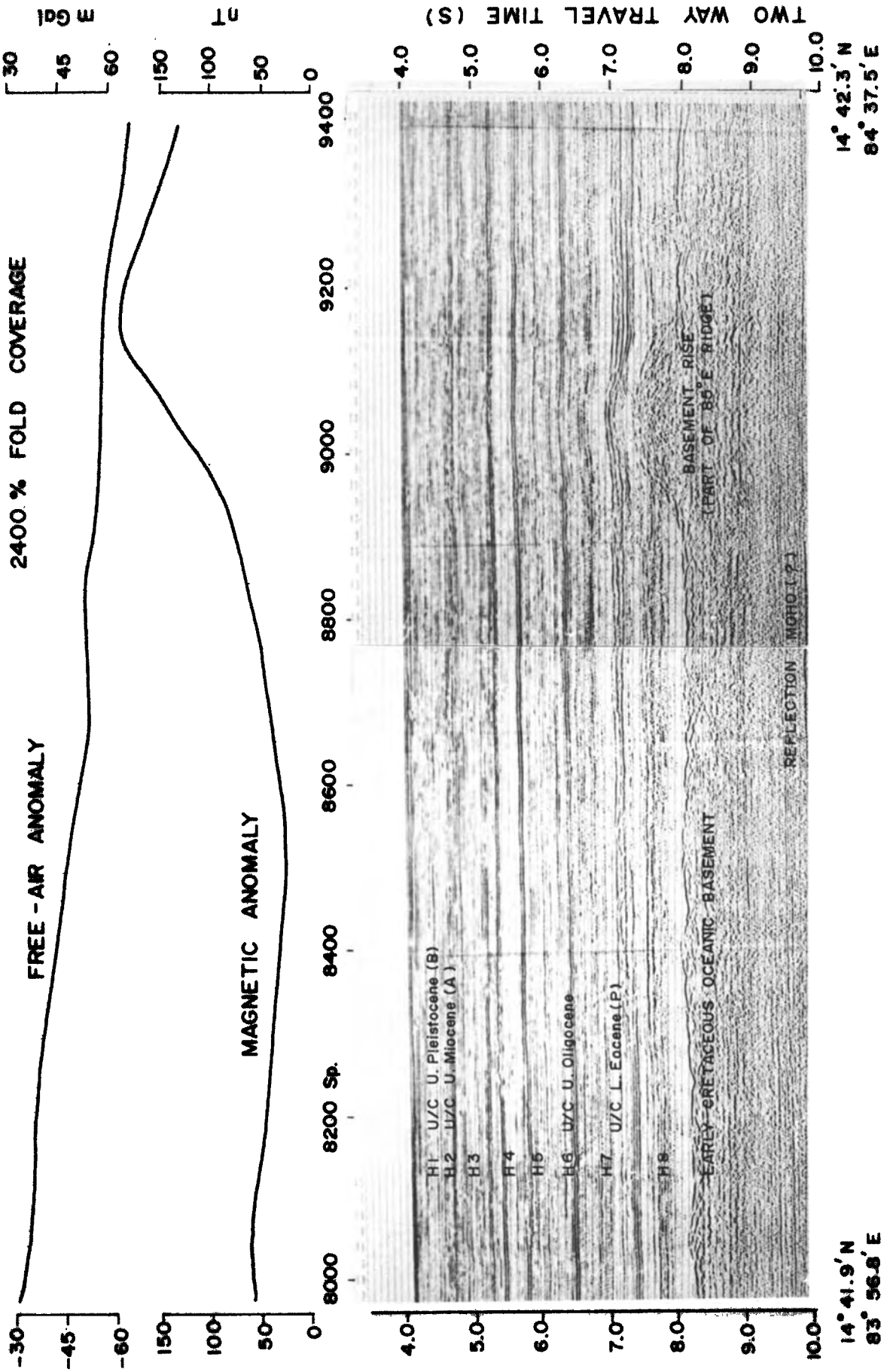

Figure 7e. Multichannel seismic record and free-air gravity and magnetic anomalies show the early Cretaceous oceanic basement and part of the 85°E Ridge.

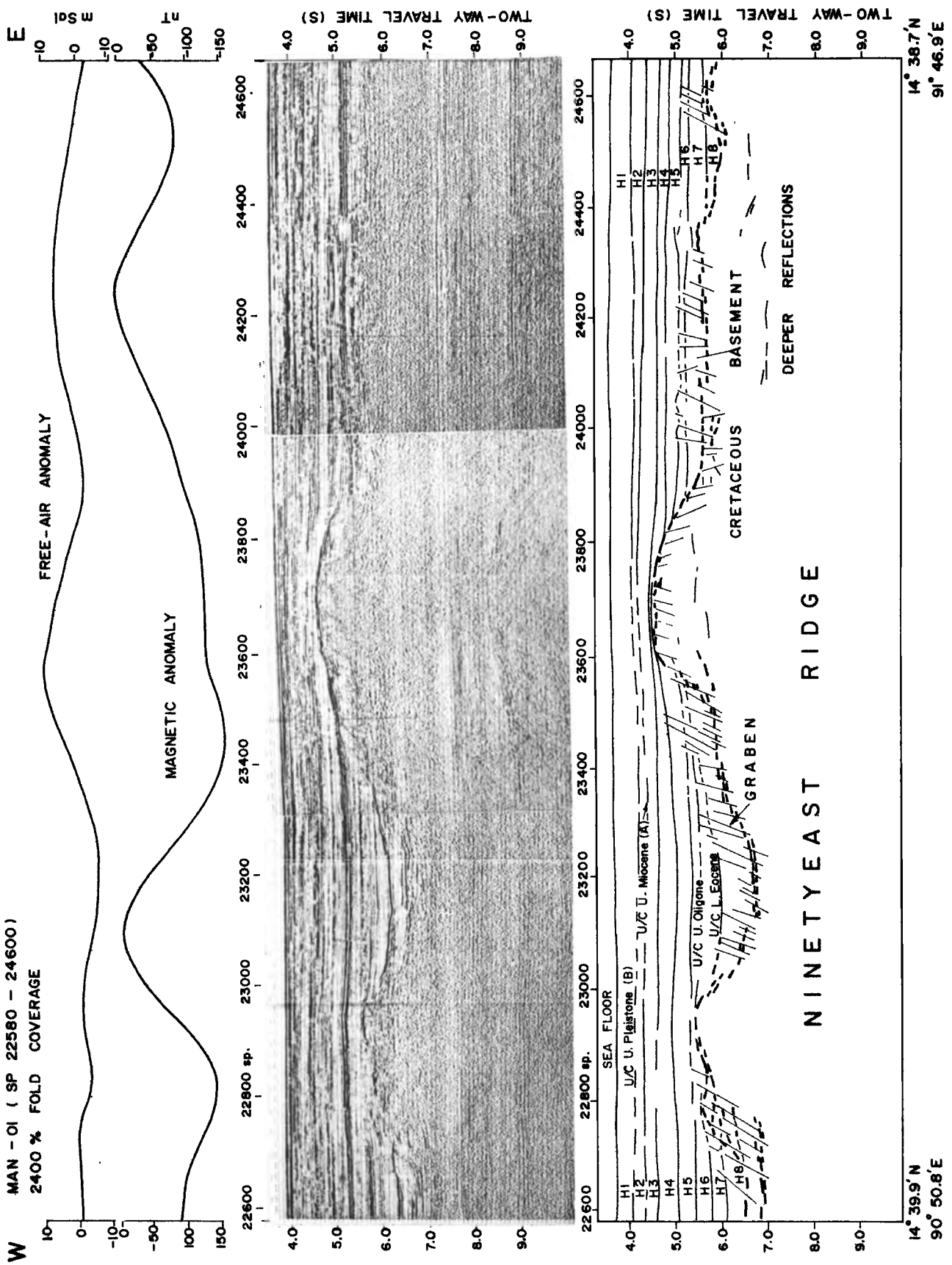

Figure 7f. Multichannel seismic record and free-air gravity and magnetic anomalies depict a broad bulge of the Ninetyeast Ridge and two basement rises with a graben in between on summit of the ridge.

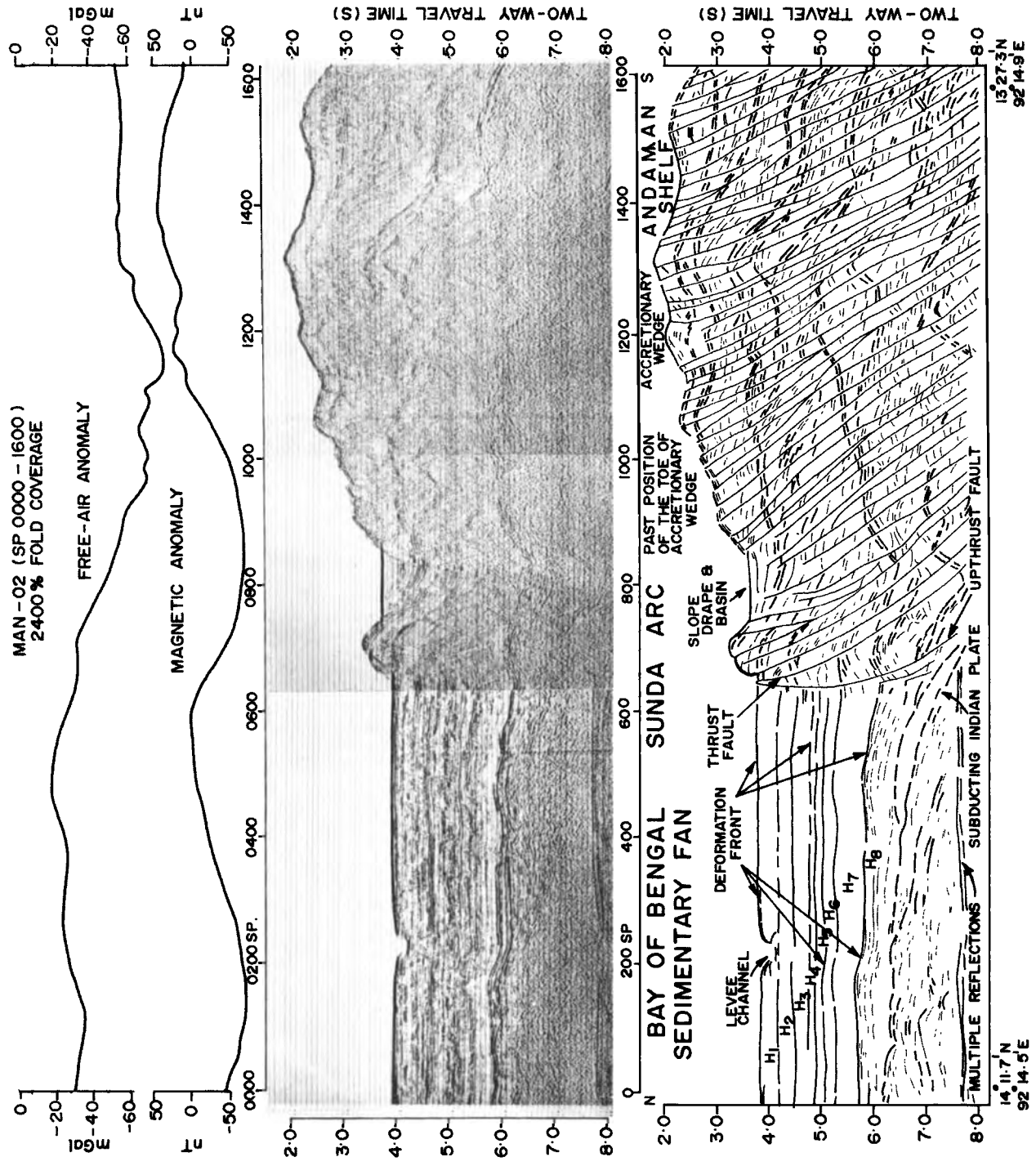

Figure 7g. Multichannel seismic record and its interpreted line diagram and free-air and magnetic anomalies across the Sunda subduction zone depict the typical crustal features of a convergent plate boundary.

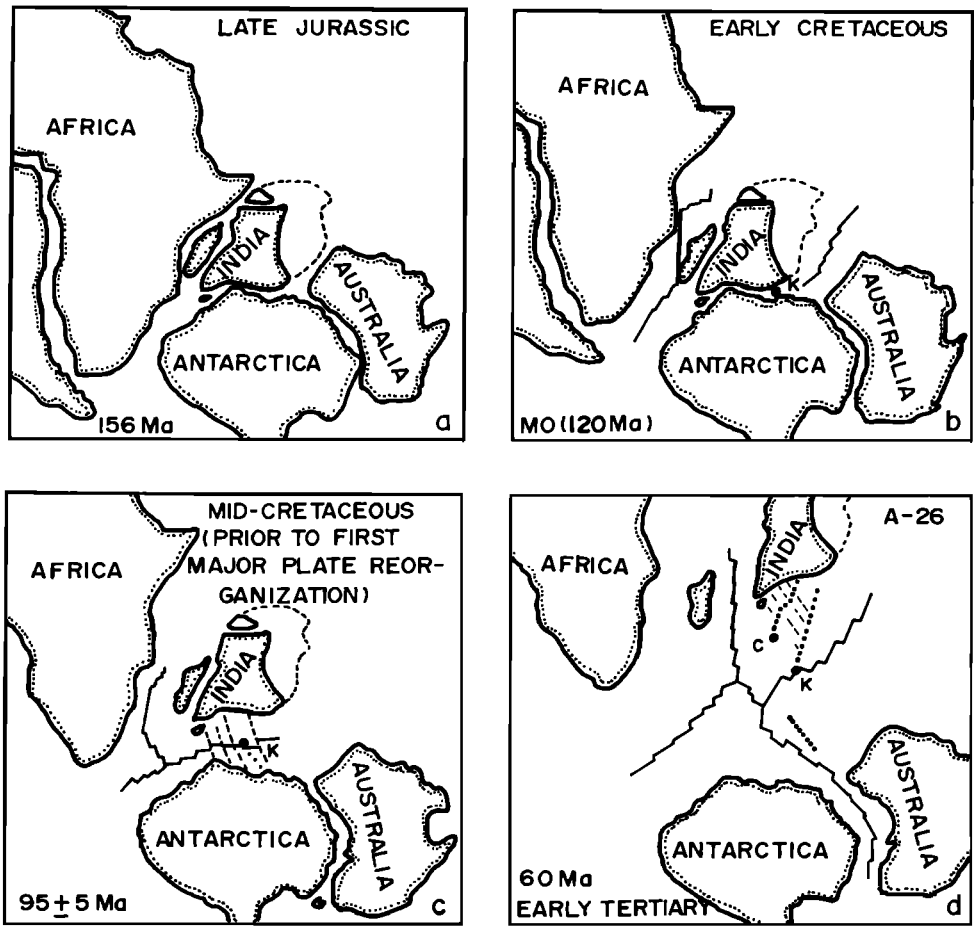

Figure 8. Schematic plate reconstructions for ages of 156, 118, 95±5, and 60 Ma. (a) Reconstruction for age 156 Ma shows earliest spreading between the Australia and northeast of Greater India, and (b) reconstruction for age 118 Ma shows the initial breakup of the eastern Gondwanaland and location of the Kerguelen (K) hotspot. (c) Reconstruction for age 95±5 Ma shows the NW-SE trending early Cretaceous fracture zones and location of the Kerguelen (K) hotspot on the Australia-Antarctica plate. (d) Reconstruction for age 60 Ma shows traces (thick dotted lines) and locations of the Crozet (C) and Kerguelen (K) hotspots on Indian plate.

to the identified COB on the eastern margin of India. Thus the majority of the Bay of Bengal crust must have formed during the Cretaceous quiet period. The magnetic anomalies associated with the 85°E Ridge may indicate later volcanic emplacement over oceanic crust that formed during the Cretaceous quiet period. Therefore we propose initiation of seafloor spreading between Greater India and Antarctica around M0, 120 Ma (Figure 8b) following the Mesozoic timescale of *Gradstein et al.* [1994], and its breakup was probably synchronous with eruption of Rajmahal Traps (oldest volcanic rocks are 118 Ma with normal magnetization) of northeast India. Earlier, at about 156 Ma, the Thakkhola region of north-central Nepal had separated from the Exmouth Plateau margin of northwest Australia during the breakup of eastern Gondwanaland, thereby initiating seafloor spreading in the incipient Indian Ocean [*Gradstein and Vonrad*, 1991] (Figure 8a).

Earlier workers have speculated that breakup of India from Antarctica occurred at M11 [*Curray et al.*, 1982] or at M4 [*Curray and Munasinghe*, 1991]. A magnetic quiet zone was reported in the Western Basin off the Madras coast [*Murthy et al.*, 1993; *Subrahmanyam et al.*, 1996]. *Banerjee et al.* [1995] reported Barremian (116 Ma) or younger oceanic crust beneath the Bay of Bengal along 14°N between 81°E and 93°E based on ages of marine basal sediments and basic lavas. *Ramana et al.* [1994b] proposed the breakup at anomaly M11. Earlier speculations on breakup of India from Antarctica by *Curray et al.* [1982] and by *Curray and Munasinghe* [1991], and the presence of Mesozoic lineations on the northwest Australian margin [*Larson et al.*, 1978; *Fullerton et al.*, 1989] led *Ramana et al.* [1994b] to propose early Cretaceous M-sequence lineations in the Bay of Bengal. However, these M- sequence anomaly assignments required fracture zones between every two profiles, high spreading rates (3.4 to 10 cm/yr) in comparison to Mesozoic anomalies of Australian and African margins, and a narrow stretch of 55 km encompassing the 36 m.y. duration of the Cretaceous Magnetic Quiet Zone. These problems drew the attention to the need for reexamining the interpreted timing of breakup of India from Antarctica. Based on the new data in this study, we propose the breakup of India from Antarctica at M0 time, that is, 120 Ma. This conclusion needs validation with age determinations of the oceanic rocks in the study area.

Continental Margin Formation

The steps and the intervening sediment (deformed) filled grabens of the eastern continental margin of India mark a horst and graben structural style. The potential field data indicate that the crustal features are parallel to the margin. The several steplike structures

bounded by near vertical faults and seaward downthrown blocks reveal extension-subsidence related tectonics. Our interpreted COB is close to the foot of the slope (Figure 7a). The abrupt termination of early Cretaceous oceanic basement close to the eastern margin of India may indicate rift-transform margin following the model suggested by *Mascle and Blarez* [1987]. *Powell et al.* [1988] also proposed strike-slip motion along a dextral transform fault between the southern half of the eastern margin of India and the Kron Prins Olav Kyst margin of Antarctica. The structural style suggests initial breakup, rapid subsidence, and extensional strain deformation was probably followed the strike-slip motion. Detailed investigations are suggested for identification of further evidences such as folds, parallel ridges, etc., to further substantiate the transform motion along the eastern margin of India.

Formation of the 85°E Ridge

All the basement rises, including the 85°E Ridge in the area west of the Ninetyeast Ridge and to the north of the Afanasy Nikitin seamounts are associated with negative free-air anomalies. In contrast the Afanasy Nikitin seamounts are associated with positive free-air gravity anomalies [*Paul et al.*, 1990]. Negative free-air anomalies can be caused by low density, tectonic origin, or over compensation below the features. *Liu et al.* [1982] explain the negative free-air anomaly in terms of a low-density root below the ridge. It is possible that the fracture zones, 85°E Ridge and other basement rises are (1) low density volcanic material constructs, (2) altered low-density crust as a result of petrological changes controlled by tectonics and hydrothermal processes, or (3) low-density mantle. Petrological alteration might be widespread through all areas of the ancient Cretaceous crust. Thus the negative gravity effect is not a constraint while proposing the hotspot origin of the 85°E Ridge. The observations on the 85°E Ridge, such as near northward trend and anomalies with different polarities (Figures 3a and 7d) which clearly indicate the presence of magnetic reversals providing clues for critical assessment and to favor the hotspot formation of the enigmatic ridge. The magnetic expression of the 85°E Ridge suggests that its age is younger than the Cretaceous quiet period (Figures 8c and 8d). However, it was formed prior to deposition of upper Oligocene sediments.

Four hypotheses have been proposed to explain the formation of the 85°E Ridge, although none offer a satisfactory explanation for all its geophysical anomalies, particularly its negative gravity field. *Curray and Munasinghe* [1991] and *Müller et al.* [1993] attributed its origin to the Crozet hotspot. *Kent et al.* [1992] proposed the ridge as northward continuation of 86°E FZ, which was negated by *Curray and Munasinghe* [1992] based on the contrasting geophysical anomalies and structure between the 85°E Ridge and the 86°E FZ. Further, the first major plate reorganization (at 95±5 Ma) limits the older part of the 86°E FZ at around 6°N in lower Bengal Fan. Prior to the first major plate reorganization, fracture zones (early Cretaceous age) in the Bay of Bengal have a NW-SE trend. *Chaubey et al.* [1991] suggested that the ridge was formed as a result of volcanism along a weak zone for a short span of time in the late Cretaceous during the reorganization of Indian and Australian plates. *Mishra* [1991] opined that the ridge is an abandoned spreading center.

Müller et al. [1993] proposed a major ridge jump to the north between chrons 31 and 25 to explain the absence of the 85°E Ridge continuation further south. Such a major ridge jump would transfer a portion of the Indian plate to the Antarctica plate. Consequently, one expects some missing lineations in the Central Indian Basin and duplication of those lineations in the Crozet Basin. But magnetic lineation maps [*Royer et al.*, 1989; *Krishna et al.*, 1995] show anomalies 1 to 34 without interruption in both the Central Indian Basin and the Crozet Basin, and therefore do not support a northward ridge jump. Instead, southward ridge jumps were interpreted between chrons 30 and 19 to the east of the 86E FZ [*Royer et al.*, 1991; *Krishna et al.*, 1995]. Hence we feel that a major ridge jump may not have occurred and that hotspot activity continued on the Indian plate. This leads us to suspect that the Crozet Plateau is a continuation of the 85°E Ridge. In our opinion the hotspot might have started its volcanism near the eastern margin of India at around 84 Ma. Then its activity was ceased after formation of the 85°E Ridge and the Afanasy Nikitin seamounts. The above discussion raises the question whether the hotspot activity ceased at the Afanasy Nikitin seamounts or presently lies at the Conrad Rise/Crozet Plateau. This hypothesis needs further substantiation with detailed geophysical investigations.

Indian Plate Subduction

The deformed sediments and basement, the eastward dipping lower crust reflectors, and the negative free-air gravity anomalies to the east of the Ninetyeast Ridge mark subduction of the Indian plate into the Sunda Arc. Further, the observed deformation front, the steep upthrust and listric faults, and the upthrust crustal blocks, slope drape basin between the upthrust crustal blocks, and the past and present toe positions of the accretionary sediment complex between the Ninetyeast Ridge and the Andaman shelf are explicit expressions of the ongoing tectonics and subduction of the Indian plate into the Sunda Arc (Figure 7g). We estimated the dip of the ongoing Indian lithospheric slab at the Sunda Arc as 30°-40° by considering the thickness of slab 70-100 km and horizontal distance of 120 km. The oceanic crust of the Indian plate is subducting steeply beneath oceanic crust of the Burmese plate with limited growth of an accretionary wedge, a well-developed back arc basin of the Andaman Sea and relatively few large magnitude (5.0) earthquakes [*Singh*, 1988]; therefore we suggest this portion of Sunda Arc as low to intermediate stress subduction zone similar to the Mariana Arc [*Hutchinson*, 1992] in the Pacific Ocean.

Sedimentary Layers and Unconformities

The early Cretaceous oceanic basement is overlain by Mesozoic and Cenozoic clastic/turbidite, hemipelagic sediments. The sediments, most likely, represent the upper Pleistocene to Recent (H1), Pliocene to upper Pleistocene (H2), upper Miocene (H3), Middle Miocene (H4), upper half of lower Miocene (H5), lower half of lower Miocene (H6), lower Eocene to upper Oligocene (H7), and late Cretaceous to Paleocene (H8), respectively. The sequence boundaries of the lower Eocene (collision of India with Eurasia and final closing of the Tethys Sea), upper Oligocene (Oligocene lowered global sea level), upper Miocene (Himalayan orogeny, onset of intraplate deformation and eustatic sea level changes) and upper Pleistocene (lowered sea levels) mark the major unconformities developed during the geological events. *Cochran* [1990] reported turbidite sedimentation only since the lower Miocene. But the seismic character of our profiles suggest the occurrence of turbidites since the Oligocene. The undistorted parallel layering of sequences H1 to H8 indicates that deformation, such as that reported in the Central Indian Basin [*Bull and Scrutton*, 1992] is absent in our area of seismic studies.

Summary and Conclusions

The study of multichannel deep seismic reflection, gravity, magnetic and bathymetric data in the Bay of Bengal has yielded the following significant results.

1. The Cretaceous basement in the Bay of Bengal is characterized by approximately NW trending fracture zones, the N-NNW oriented 85°E Ridge and the N-NNE oriented Ninetyeast Ridge. The trend of fracture zones and the lack of linear magnetic anomalies reveal that the Bay of Bengal formed during the Cretaceous quiet period as Greater India drifted in NW-SE direction from Antarctica. These paleofracture zones intersect the 85°E Ridge. The near north-south trend and magnetic reversals of the 85°E Ridge and overburden of lower Tertiary sediments suggest that the ridge might have formed at a later time to the fracture zones formation, that is, after the Cretaceous quiet period.

2. Schematic plate reconstruction models for the late Jurassic, early Cretaceous, mid-Cretaceous and early Tertiary (Figures 8a to 8d) are proposed to depict the breakup of eastern Gondwanaland (156 Ma) and separation of Greater India from Antarctica about M0 (118 Ma), formation of fracture zones during the Cretaceous seafloor spreading process, and hotspot origin of the 85°E Ridge.

3. The landward deepening oceanic basement, the presence of 3 to 4 km down-faulted continental blocks along the eastern margin of India, and the distinct marginal free-air gravity anomalies place the continent-ocean boundary close to the present continental slope region.

4. "Mounded" seismic features interpreted as carbonate platforms, about 50 km wide and 0.8 km thick, are identified on the eastern flank of the 85°E Ridge. The occurrence of thick carbonates indicates environmental and oceanographic conditions favorable for their growth. These carbonate structures adjacent to hemipelagic sediments are potential reservoir rocks for hydrocarbons.

5. The older Indian plate is steeply subducting beneath oceanic crust of the Burmese plate, thereby, the portion of the Sunda Arc can be suggested as low to intermediate stress subduction zone.

6. In our transects, the total sediment thickness reaches a maximum of 8.5 km. Thick precollisional sediments in the Western Basin and postcollisional sediments in the Central Basin are interpreted. Prominent seismic sequences H1 to H8 sediments of U-Pleistocene to Recent, U-Pliocene to U-Pleistocene, U- Miocene, M-Miocene, upper half of L-Miocene, lower half of L- Miocene, L-Eocene to U-Oligocene, and U-Cretaceous to Paleocene overlie the early Cretaceous oceanic basement. Four major unconformities are identified at the bases of H7, H6, H2 and H1 as L-Eocene, U-Oligocene, U-Miocene and U-Pleistocene, respectively. They were developed by major geological events: collision of Greater India with Eurasia; lowered sea levels of Oligocene; onset of intraplate deformation, built-up and erosion of Himalayas; and lowered sea levels of Pleistocene epoch, respectively.

Acknowledgements. We are grateful to V. K. Gaur, Distinguished Scientist and former Secretary, Department of Ocean Development, New Delhi, for promoting us for the collaborative study between the NIO and KDMIPE, Oil and Natural Gas Corporation Limited. G.P.S Murty and K. Srinivas helped in computation of Gravity model and preparation of magnetic anomaly map from NGDC data. We thank the reviewers James G. Ogg, John W. Peirce, and T. Munasinghe for their constructive comments and suggestions. We are thankful to William J. Hinze, senior editor for the encouragment. A.Y. Mahale prepared camera ready version of the manuscript. NIO Contribution No. 2494.

References

Banerjee, B., B.J. Sengupta, and P.K. Banerjee, Signals of Barremian (116 Ma) or younger oceanic crust beneath the Bay of Bengal along 14°N latitude between 81°E and 93°E, *Mar Geol.*, **128**, 17-23, 1995.

Bull, J.M., and R.A. Scrutton, Seismic reflection images of intraplate deformation, central Indian Ocean, and their tectonic significance, *J Geol. Soc London*, **149**, 955-966, 1992.

Cande, S.C., and D.V. Kent, Revised calibration of the geomagnetic polarity time scale for the late Cretaceous and Cenozoic, *J Geophys Res*, **100**, 6093-6095, 1995.

Chaubey, A.K., M.V. Ramana, K.V.L.N.S. Sarma, K.S. Krishna, G.P.S. Murty, V. Subrahmanyam, G.S. Mittal, and R.K. Drolia, Marine geophysical studies over the 85°E Ridge, Bay of Bengal, in First International Seminar and Exhibition on "Exploration Geophysics in Nineteen Nineties", Hyderabad, India, *Extended Abstracts (AEG Publ)*, pp. 508-515, 1991.

Cochran, J.R., Himalayan uplift, sea level, and the record of Bengal Fan sedimentation at the ODP Leg 116 Sites, *Proc Ocean Drilling Program Sci. Results*, **116**, 397-414, 1990.

Curray, J.R., Possible greenschist metamorphism at the base of a 22-km sedimentary section, Bay of Bengal, *Geology*, **19**, 1097-1100, 1991.

Curray, J.R., Sediment volume and mass beneath the Bay of Bengal, *Earth Planet Sci Lett*, **125**, 371-383, 1994.

Curray, J.R., F.J. Emmel, D.G. Moore, and W.R. Russel, Structure, tectonics and geological history of the northeastern Indian Ocean, in *The Ocean Basins and Margins*, vol. 6, **The Indian Ocean**, edited by A.E. Nairn and F.G. Stehli, pp. 399-450, Plenum, New York, 1982

Curray, J.R., and T. Munasinghe, Origin of the Rajmahal Traps and the 85°E Ridge: Preliminary reconstructions of the trace of the Crozet hotspot, *Geology*, **19**, 1237-1240, 1991.

Curray, J.R., and T. Munasinghe, Comment and reply on "Origin of the Rajmahal Traps and the 85°E Ridge: Preliminary reconstructions of the trace of the Crozet hotspot", *Geology*, **20**, 957-959, 1992.

Curray, J.R., and D.G. Moore, Growth of the Bengal deep-sea Fan and denudation in the Himalayas, *Geol Soc. Am. Bull.*, **82**, 563-572, 1971.

Douglas, W.B., A.D Louis, and F.L. Christian, Reduced Himalayan sediment production 8 Myr ago despite an intensified monsoon, *Nature*, **364**, 48-50, 1993.

Fullerton, L.G., W.W. Sager, and P.W. Handschumacher, late Jurassic-early Cretaceous evolution of the eastern Indian Ocean adjacent to northwest Australia, *J Geophys. Res*, **94**, 1937-2953, 1989.

Gansser, A., The geodynamic history of the Himalayan, in **Zagros, Hindu Kush, Himalayan Geodynamic Evolution**, *Geodyn Ser.*, vol. 3, edited by H.K. Gupta and F.M. Delany, pp. 111-121, AGU, Washington, D.C., 1981.

Geller, C.A., J.K. Weissel, and R.N. Anderson, Heat transfer and intraplate deformation in the Central Indian Ocean, *J Geophys. Res.*, **88**, 1018-1032, 1983.

Gopala Rao, D., et al., Analysis of multichannel seismic reflection and magnetic data along 13°N latitude across the Bay of Bengal, *Mar Geophys Res.*, **16**, 225-236, 1994.

Gradstein, F.M., P.F. Agterberg, J.G. Ogg, J. Hardenbol, P.A. Veen, J. Thierry, and Z. Huang, A Mesozoic time scale, *J Geophys Res.*, **99**, 24,051-24,074, 1994.

Gradstein, F.M., and U. Vonrad, Stratigraphic evolution of Mesozoic continental margin and oceanic sequences: Northwest Australia and northern Himalayas, *Mar Geol*, **102**, 131-174, 1991.

Haq, B.U., J. Hardenbol, and P.R. Vail, Chronology of fluctuating sea levels since the Triassic, *Science*, **235**, 1156- 1167, 1987.

Hutchinson, D.R., Continental margins - Windows into Earth's history, *Oceanus*, **35**, 34-44, 1992.

International Association of Geomagnetism and Aeronomy Division 1, Working group 1, International Geomagnetic reference field Revision 1985, *Eos Trans. AGU*, **67**, 523-524, 1986.

Kent, R.W., M. Storey, A.D. Saunders, N.C. Ghose, and P.D. Kempton, Comment and reply on "Origin of the Rajmahal Traps and the 85°E Ridge: Preliminary reconstructions of the trace of the Crozet hotspot", *Geology*, **20**, 957-959, 1992.

Klootwijk, C.T., J.S. Gee, J.W. Peirce, G.M. Smith, and P.L. McFadden, An early India-Asia contact: Paleomagnetic constraints from Ninetyeast Ridge, ODP Leg 121, *Geology*, **20**, 395-398, 1992.

Krishna, K.S., D. Gopala Rao, M.V. Ramana, V. Subrahmanyam, K.V.L.N.S. Sarma, A.I. Pilipenko, V.S. Shcherbakov, and I.V. Radhakrishna Murthy, Tectonic model for the evolution of oceanic crust in the northeastern Indian Ocean from the late Cretaceous to the early Tertiary, *J. Geophys. Res*, **100**, 20,011-20,024, 1995.

Larson, R.L., G.B. Carpenter, and J.B. Diebold, A geophysical study of the Wharton Basin near the Investigator Fracture Zone, *J. Geophys Res.*, **83**, 773-782, 1978.

Liu, C.S., D.T. Sandwell, and J.R. Curray, The negative gravity field over the 85°E Ridge, *J Geophys. Res*, **87**, 7673-7686, 1982.

Mascle, J., and E. Blarez, Evidence for transform margin evolution from the Ivory coast - Ghana continental margin, *Nature*, **36**, 378-381, 1987.

Merrill, D.L., and Shipboard Scientific Party, Underway Geophysics, *Proc Ocean Drill. Program Initial Rep*, **116**: 29-42, 1989.

Mishra, D.C., Magnetic crust in the Bay of Bengal, *Mar. Geol*, **99**, 257-261, 1991.

Molnar, P., F. Pardo-Casas, and J. Stock, The Cenozoic and late Cretaceous evolution of the Indian Ocean Basin: Uncertainties in the reconstructed positions of the Indian, African and Antarctica plates, *Basin Res*., **1**, 23-40, 1988.

Moore, D.G., J.R. Curray, R.W. Raitt, and F.J. Emmel, Stratigraphic-seismic section correlations and implications to Bengal Fan history, *Initial Rep. Deep Sea Drill. Proj.*, **22**, 403-412, 1974.

Mukhopadhyay, M., and M.R. Krishna, Gravity field and deep structure of the Bengal Fan and its surrounding continental margins, northeast Indian Ocean, *Tectonophysics*, **186**, 365-386, 1991.

Müller, R.D., J.-Y. Royer, and L.A. Lawver, Revised plate motions relative to the hotspots from combined Atlantic and Indian Ocean hotspot tracks, *Geology*, **21**, 275-278, 1993.

Murthy, K.S.R., T.C.S. Rao, A.S. Subrahmanyam, M.M. Malleswara Rao, and S. Lakshminarayana, Structural lineaments from the magnetic anomaly maps of the eastern continental margin of India (ECMI) and NW Bengal Fan, *Mar Geol*., **114**, 171-183, 1993.

Nath, B.N., I. Roelandts, M. Sudhakar, and W.L., Pluger, Rare earth element patterns of the Central Indian Basin sediments related to their lithology, *Geophys Res Lett* **19**, 1197-1200, 1992.

Norton, I.O., and J.G. Sclater, A model for the evolution of the Indian Ocean and the breakup of Gondwanaland, *J. Geophys. Res*., **84**, 6803-6830, 1979.

Patriat, P., and J. Achache, India - Eurasia collision chronology has implications for crustal shortening and driving mechanism for plates, *Nature*, **311**, 615-621, 1984.

Patriat, P., and J. Ségoufin, Reconstruction of the Central Indian Ocean, *Tectonophysics*, **155**, 211-234, 1988.

Paul, J., R.N. Singh, C. Subrahmanyam, and R.K. Drolia, Emplacement of Afanasy Nikitin seamount based on transfer function analysis of gravity and bathymetric data, *Earth Planet. Sci. Lett.*, **96**, 419-426, 1990.

Peirce, J.W., The northward motion of India since the late Cretaceous, *Geophys. J. R. Astron. Soc.*, **52**, 277-311, 1978.

Peirce, J., et al., *Proc. Ocean Drill. Program Initial Rep*., vol. 121, Ocean Drilling Program, College Station, Tex., 1989.

Powell, C.M., S.R. Roots, and J.J. Veevers, Pre-breakup continental extension in east Gondwanaland and the early opening of the eastern Indian Ocean, *Tectonophysics*, **155**, 261-283, 1988.

Ramana, M.V., V. Subrahmanyam, K.S. Krishna, A.K. Chaubey, K.V.L.N.S. Sarma, G.P.S. Murty, G.S. Mittal, and R.K. Drolia, Magnetic studies in the northern Bay of Bengal, *Mar Geophys Res.*, **16**, 237-242, 1994a.

Ramana, M.V., et al., Mesozoic anomalies in the Bay of Bengal, *Earth Planet Sci. Lett.*, **121**, 469-475, 1994b.

Rao, T.C.S., and V. Bhaskara Rao, Some structural features of Bay of Bengal, *Tectonophysics*, **124**, 141-153, 1986.

Rao, T.C.S., S. Lakshminarayana, and K.V.L.N.S. Sarma, Magnetic anomalies in Central Bengal Fan, *Indian J. Mar. Sci*., **16**, 15-18, 1987.

Royer, J.-Y., J.G. Sclater, and D.T. Sandwell, A preliminary tectonic fabric chart of the Indian Ocean, *Proc Indian Acad Sci. (Earth Planet Sci.)*, **98**, 7-24, 1989.

Royer, J.-Y., J.W. Peirce, and J.K. Weissel, Tectonic constraints on the hot-spot formation of Ninetyeast Ridge, in: *Proc Ocean Drill. Program Sci. Results*, **121**, 763-776, 1991.

Shipboard Scientific Party, Site 715, In Backman, J., R.A. Duncan et al., *Proc. Ocean Drill. Program Initial Rep.*, **115**, 917-1003, 1988.

Singh, D.D. Strain deformation in the northern Indian Ocean, *Mar. Geol.*, **79**, 105-118, 1988.

Srivastava, S.P., Evolution of the Labrador Sea and its bearing on the early evolution of the North Atlantic, *Geophys. J R. Astron. Soc.*, **52**, 313-357, 1978.

Srivastava, S.P., J. Verhoef, and R. Macnab, Results from a detailed aeromagnetic survey across the northeast Newfoundland margin, part 1: spreading anomalies and relationship between magnetic anomalies and the ocean-continent boundary, *Mar. Pet. Geol.*, **5**, 306-323, 1988.

Stow, D.A.V., K. Amano, P.S. Balson, G.W. Brass, J. Crrigan, C.V. Raman, J.-J. Tiercelin, M. Townsend, and N.P. Wijayananda, Sediment facies and processes on the distal Bengal Fan, Leg 116, *Proc. Ocean Drill. Program Sci. Results*, **116**, 377-396, 1990.

Subrahmanian, V., Sediment load of Indian rivers, *Curr Sci.*, **64**, 928-930, 1993.

Subrahmanyam, A.S., K.S.R. Murthy, S. Lakshminarayana, M.M. Malleswara Rao, K. Venkateswarulu, and T.C.S. Rao, Magnetic expression of some mega lineaments and Cretaceous Quiet Zone in Bay of Bengal, *Geo-Mar Lett.*, in press, 1996.

Veevers, J.J., and Z.X. Li, Review of seafloor spreading around Australia, II, Marine magnetic anomaly modelling, *Aust. J. Earth Sci*., **38**, 391-408, 1991.

Von der Borch, C.C., et al., Site 214, *Initial Rep. Deep Sea Drill Proj.*, **22**, 119-191, 1974.

Weis, D., F.A. Frey, A. Saunders, I. Gibson, and Leg 121 Scientific Shipboard Party, Ninetyeast Ridge (Indian Ocean): A 5000 km record of a Duple mantle plume, *Geology*, **19**, 99-102, 1991.

Weissel, J.K., R.N. Anderson, and C.A. Geller, Deformation of the Indo-Australian plate, *Nature*, **287**, 284-291, 1980.

D. Gopala Rao and K.S. Krishna, Geological Oceanography Division, National Institute of Oceanography, Dona Paula, Goa 403004, India. (e-mail: gopalrao@bcgoa.ernet.in / gopalrao@csnio.ren.nic.in; krishna@bcgoa.ernet.in / krishna@csnio.ren.nic.in)

D. Sar, Keshava Deva Malaviya Institute of Petroleum Exploration, Oil and Natural Gas Corporation Limited, 9 Kaulagarh Road, Dehra Dun 248195 (U.P.), India.

(Received October 27, 1994; revised February 23, 1996;
accepted April 29, 1996.)

Annex B59

G. S. Roonwal et al., "Mineralogy and Geochemistry of Surface Sediments from the Bengal Fan, Indian Ocean", *Journal of Asian Earth Sciences*, Vol. 15, No. 1 (1997)

Pergamon

Journal of Asian Earth Sciences, Vol. 15, No. 1, pp. 33–41, 1997

Printed in Great Britain

PII: S0743-9547(96)00078-5

1367-9120/97 $17.00 + 0.00

Mineralogy and geochemistry of surface sediments from the Bengal Fan, Indian Ocean

G. S. Roonwal, G. P. Glasby and R. Chugh

Centre of Georesources, University of Delhi South Campus, Benito Juarez Road, New Delhi-110021, India

(*Received* 4 *August* 1995; *accepted for publication* 29 *October* 1996)

Abstract—The mineralogy and composition of 75 sediment samples from the Bengal Fan, Andaman Sea and the eastern flanks of the upper Nicobar Fan have been determined. Sediments from the Upper and Middle Bengal Fan are mainly terrigenous and derived from the Ganges–Brahmaputra river system, whereas sediments from the Andaman Sea and the eastern flank of the upper Nicobar Fan vary from terrigenous to largely biogenic. For the terrigenous sediments, the continental influence is illustrated by the distribution of the major elements (excluding Ca) which decrease away from the source. The Ti/Al and Fe/Al ratios of the sediments are higher in samples from the east coast of India than from the fans, indicating the influence of material from the Deccan basalts as well as from mafic rocks of the Indian Peninsula. In the clay mineral fraction of Upper Bengal Fan sediments, illite and chlorite are the dominant constituents, with minor amounts of smectite and traces of kaolinite. Illite is mainly a weathering product of lithic material from the Himalaya and is transported by the Ganges–Brahmaputra river system. Smectite is the dominant constituent of the sediments adjacent to the Indian Peninsula. © 1997 Elsevier Science Ltd

Introduction

The Bengal Fan, together with its eastern lobe, the Nicobar Fan, is the world's largest submarine fan (Stow *et al.*, 1989). It is 2800–3000 km long and 830–1430 km wide, with an area of $2.8–3.0 \times 10^6$ km^2 (Anon, 1992). It is bounded by the Indian continental slope to the west, the Ninetyeast Ridge to the east and the Swatch of No Ground to the north. The Bengal Fan is separated from the Nicobar Fan by the Ninetyeast Ridge, although both are part of the same sediment dispersal system (Fig. 1). The sediment thickness in the fan exceeds 16 km in the north, and it is only on some topographic highs that basement can be observed on seismic profiles. The fan is fed mainly by the Ganges–Brahmaputra river system, which discharges 2.2×10^9 tonnes of sediment into the ocean, the highest discharge rate of any river in the world (Lisitizin, 1972; Chester and Aston, 1976; Subramaniam, 1980; Kolla and Kidd, 1982; Milliman and Meade, 1983). These two rivers drain the northern and southern slopes of the Himalaya. The Swatch of No Ground appears to be conduit for the transport of shelf sediments to the Bengal Fan (Kuehl *et al.*, 1989). In addition, many Peninsular rivers such as the Mahanadi, Krishna and Godavari contribute to the sediment input. Schematic maps of the fan, including sediment paths into the Bay of Bengal, are given by Kolla and Kidd (1982), Stow *et al.* (1989, 1990) and Amano and Taira (1992).

The high rate of sediment discharge into the Bengal Fan results from the following factors:

- the mature nature of the Ganges–Brahmaputra river system;
- the influence of the north Indian monsoon;
- successive capturing of tributaries of the Ganges–Brahmaputra river system, which has increased the amount of sediment reaching the Bay of Bengal; and
- Himalayan uplift with the resultant increase in monsoonal precipitation and increased rate of denudation of the landmass.

During periods of lowered sea level, a much larger proportion of the sediment load of the inflowing rivers was introduced directly into the canyon system of the fan (Curray *et al.*, 1982). At present, the most active turbidite channel lies immediately east of the buried extension of 85 E Ridge and passes from the shelf into the abyssal zone via the Swatch of No Ground.

The most prominent feature in the Bay of Bengal is Ninetyeast Ridge, which represents a hot spot trace resulting from the northward migration of India (Schmitz, 1987a; Duncan, 1990; Royer *et al.*, 1991; Class *et al.*, 1993; Ramana *et al.*, 1994; Mukhopadhyay and Krishna, 1995). It is almost 4000 km long and extends from 31 S to about 10° N, where it is buried by fan sediments.

Two major unconformities can be traced over most of the fan. The upper unconformity is Upper Miocene. The lower unconformity coincides with the Paleocene/Middle Eocene boundary. Curray and Moore (1971) have subdivided the fan into three major stratigraphic units: younger and older fan sections overlying older sedimentary and basement rocks (Fig. 2). Maps showing the positions of the upper, middle and lower fans have been presented in Kolla and Kidd (1982) and Stow *et al.* (1989, 1990).

The surface sediments in the Bay of Bengal are mainly terrigenous. The terrigenous component extends to at least 8 S (Kolla and Kidd, 1982; Roonwal, 1986; Nath *et al.*, 1989). However, calcareous sediments occur near the Ninetyeast Ridge where the $CaCO_3$ content reaches 75% (Kolla *et al.*, 1976).

Summaries of the nature and sediments of the Bengal Fan have been presented by Curray and Moore (1971,

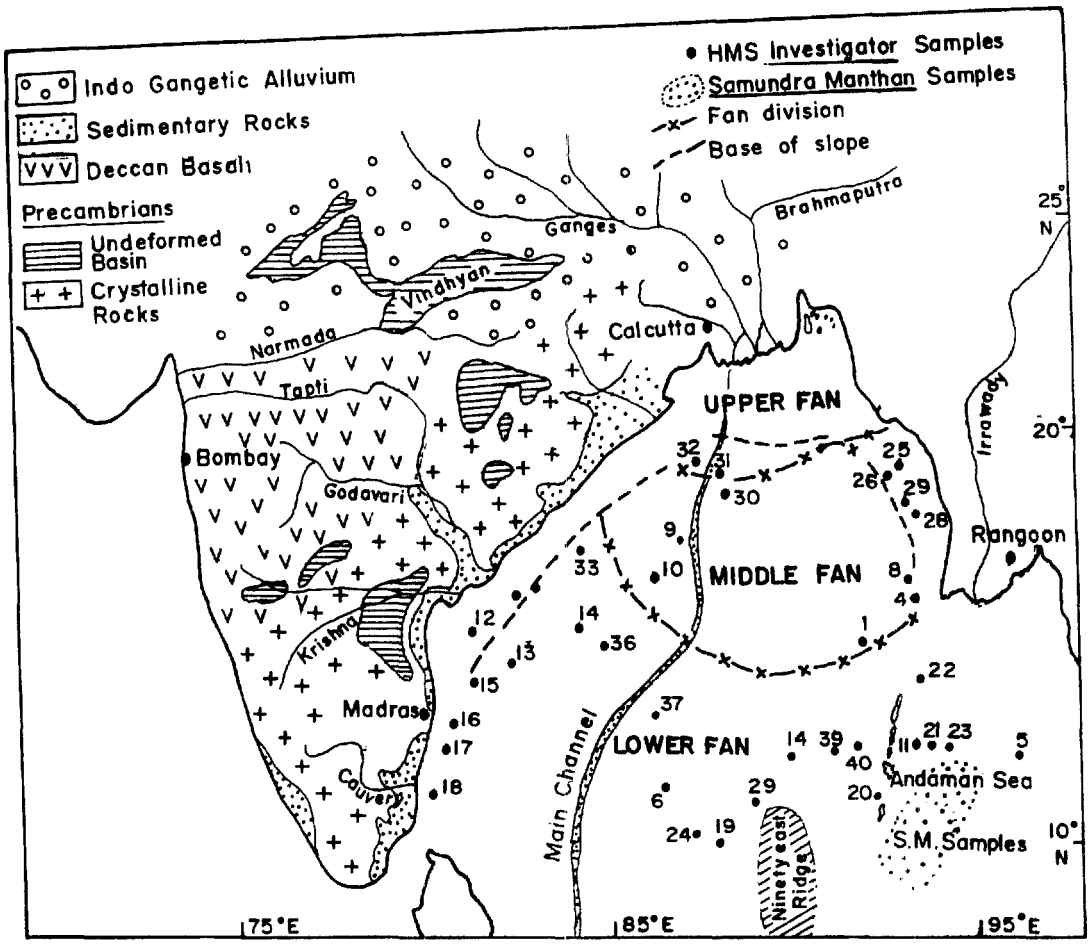

Fig. 1. Schematic map showing the position of the Bengal Fans, together with individual positions of HMS *Investigator* samples and the area from which RV *Samundra Manthan* samples were collected.

1974), Naini and Leyden (1973), Kolla *et al.* (1976), Ingersoll and Suczek (1979), Curray *et al.* (1982), Kolla and Kidd (1982), Emmel and Curray (1984), Roonwal (1986), Schmitz (1987a, b), Bouquillon *et al.* (1989, 1990), Stow *et al.* (1989, 1990), Copeland and Harrison (1990), Yokoyama *et al.* (1990), Cronan and Wijayananda (1991), Curray (1991, 1994), Chauhan *et al.* (1992), Anon. (1992), Dia *et al.* (1992), Wetzel and Balson (1992), Borole (1993), Debrabant *et al.* (1993), Levchenko *et al.* (1993), Suresh (1993), France-Lanord and Derry (1994), Rao *et al.* (1993), Wijayananda and Cronan (1994) and Crowley (in press). Similar descriptions have been made of the western part of the Bay of Bengal (Mallik, 1976), the Andaman Sea (Rodolfo, 1969; Curray *et al.*, 1982; Anon., 1992) and the Nicobar Fan (Bowles *et al.*, 1978; Curray *et al.*, 1982).

Newer information has been presented on sediments collected during ODP leg 116 (Stow *et al.*, 1989, 1990; Aoki *et al.*, 1991; Amano and Taira, 1992; Ormond *et al.*, 1995; Crowley, in press), the chemistry of the waters, bed load and organic matter content of the Ganges–Brahamputra river system (Naidu *et al.*, 1985; Subramaniam, 1985; Subramaniam *et al.*, 1985, 1988; Sarin *et al.*, 1989, 1990, 1992a, b; Krishnaswami *et al.*, 1992; Kumar *et al.*, 1992; Reetsma *et al.*, 1993), particulate fluxes in the Bay of Bengal (Ittekkot *et al.*, 1985, 1991, 1992), heavy metals in the Cauvery estuary (Subramaniam *et al.*, 1989) and circulation in the Bay of Bengal (Suryanarayana *et al.*, 1993). The data of Amano and Taira (1992) indicate that the provenance of sediments younger than 0.9 Ma is the higher Himalaya where a large peridotite body was thrust up over the Tethys Himalaya. The relationship between the uplift of the Himalaya and the input of sediment into the Bay of Bengal is becoming better known (Sharma, 1984; Klootwijk *et al.*, 1991; Verma, 1991; Hovan and Rea, 1992; Rea, 1992; France-Lanord *et al.*, 1993; Curray,

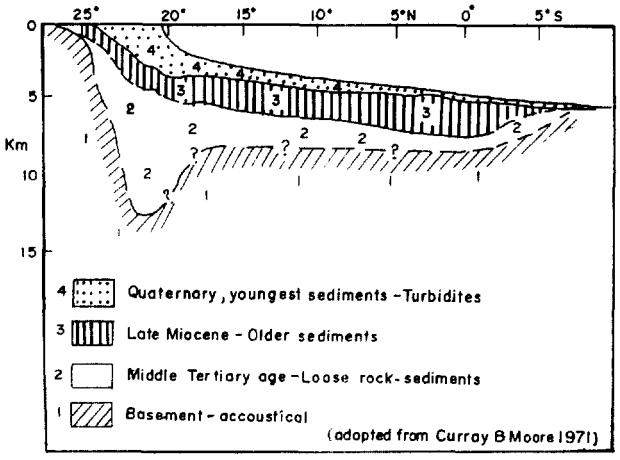

Fig. 2. Schematic map showing stratigraphy of the Bengal Fan (adapted from Curray and Moore, 1971).

Table 1. Locations of sediments samples from the Bay of Bengal and Andaman Sea

Fan Zone	Location no.	Total
HMS *Investigator* samples		
Upper Fan	32, 31, 30	3
Middle Fan	9, 3, 2, 10, 41, 8, 1	7
Lower Fan		
(a) Ninetyeast ridge area	37, 38, 4, 29, 6, 24	6
(b) Andaman Sea	39, 40, 20, 5, 11, 21, 23, 22	9
(c) Along continental margin of the Indian Peninsula	33, 35, 14, 36, 34, 12, 13, 15, 17, 18	10
(d) Along Myanmar coast	25, 26, 27, 28, 7	5
RV *Samundra Manthan* samples		
(e) Andaman Sea		
Samundra Manthan (SM28)		28
(f) Eastern flanks of Nicobar Fan		
Samundra Manthan (SM30)		7
Total		75

1994; Johnson, 1994; Derry and France-Lanord, 1996; Einsele *et al.*, 1996). The data of Ittekkot *et al.* (1985, 1991, 1992) show that 80% of the annual discharge of water from the Ganges takes place between July and November during the S.W. monsoon. Particles introduced into the northern Bay of Bengal are dominantly lithogenous (54%). Opal, lithogenic and organic fluxes to the sea floor decrease and carbonate fluxes increase from north to south. Present day sedimentation rates of the Bengal Fan are estimated to have been greater than 0.32 mm/yr over the last 50 Ma (Curray, 1991). In spite of high sedimentation rates, manganese micronodules have been recorded in the upper 0.5 m of these sediments (Chauhan *et al.*, 1994).

Clay mineralogy has been used to differentiate the source of terrigenous sediments. Bengal Fan sediments are formed from material of the Ganges–Brahmaputra system and the Deccan provinces, as shown by Venkatarathnam and Biscaye (1973), Kolla *et al.* (1976), Brass and Ramana (1990); Aoki *et al.* (1991), Wijayananda and Cronan (1994) and Crowley (in press). The Ganges province material is rich in illite and chlorite, which are supplied by the Himalayan rivers, whereas the Deccan province material is rich in smectite derived from the Deccan basalts and transported by Peninsular rivers. The clays of the Middle Fan sediment contain 81% illite, 8% chlorite and 6% kaolinite, indicating that material from the Godavari and Krishna Rivers (on the Indian Peninsula) does not reach the middle fan (Anon., 1992). This is to be expected, since higher regions such as the High Himalaya undergo the most rapid erosion (Yokoyama *et al.*, 1990). The clay content of the suspended material of the Godavari and Krishna rivers contains up to 81% smectite, whereas the Ganges–Brahmaputra river system contains 72% illite and 28% chlorite. Ar^{40}/Ar^{39} dating of detrital feldspar and muscovite from the sediments of the Bengal Fan has shown that a significant proportion of these sediments is first-cycle detritus from the Himalaya (Copeland and Harrison, 1990).

Mineralogical studies of sediments from ODP Leg 116 have shown that the input of Himalayan material to the Bengal Fan is dominant, with a lesser contribution from the continental margin of the Indian sub-continent, probably derived from the Deccan Traps (Bouquillon *et al.*, 1990; Brass and Ramana, 1990; Crowley, in press). Einsele *et al.* (1996) were able to calculate that the Peninsular rivers have contributed somewhat less than 3% of the materials supplied to the Bengal Fan, whereas France-Lanord *et al.* (1993) ruled out such contribution based on isotopic evidence. The source of material to the fan appears to have varied through geological time as a result of changes in the uplift and erosion rates of Himalaya and eustatic sea level as well as switching of the main channels suppling sediments to the fan from the Brahmaputra (Crowley, in press). A map showing the main source of sediment to the Bengal Fan has been presented by Stow *et al.* (1990, Fig. 14).

Material and methods

The present study was carried out on surface sediments from 40 locations in the Bengal Fan (Fig. 1 and Table 1). These constitute the upper part of Unit I (topmost 2–6 m of clay and mud turbidites) as defined by Stow *et al.* (1989) and were supplied by the British Museum, London. These are mainly grab samples collected by HMS *Investigator* between 1889 and 1910. In addition, 35 samples from the Andaman Sea and eastern flank of the Nicobar Fan were analysed for comparison. These were collected during two cruises (SM28 and SM30) of RV *Samundra Manthan* in 1986. The first cruise was in the Andaman Sea and the second to the southwest of the Andaman Islands. The two cruises covered about 16,420 km^2 and 7860 km^2, respectively. Sediments from *Samundra Manthan* (SM28) are generally fine grained, silty clays containing foraminifera and clastic sand. *Samundra Manthan* (SM30) samples are dominantly calcareous ooze admixed with olive gray to greenish clays. A fuller account of sediments from the Andaman Sea and Upper Nicobar Fan will be presented elsewhere (Roonwal *et al.*, in press).

X-ray diffraction of bulk samples and the separated clay fractions as well as bulk geochemical analyses were carried out on these samples. The sediments can be differentiated into two groups: those of the upper and middle Bengal Fan are mainly terrigenous, whereas those from the Andaman Sea and eastern flank of the Nicobar Fan vary from terrigenous to largely biogenic.

For bulk mineralogical studies, pressed powder mounts were used, whereas, for clay mineralogical studies, the sediments were wet-stirred and the clay

fraction separated and pipetted onto glass slides and allowed to dry at room temperature (Biscaye, 1965). Smectite, illite, chlorite and kaolinite were determined at 14, 10 and 7A°, quartz and feldspar at 3.34 and 3.26A and calcite and dolomite at 3.03 and 2.88A, respectively.

Mineralogy

From the bulk mineralogical determinations, the concentrations of quartz and feldspar were estimated (Fig. 3). Quartz forms the major component in samples from the upper and middle Bengal Fan, and from SM28 locations in the Andaman Sea. Samples from SM30 from the eastern flank of the Nicobar Fan have calcite

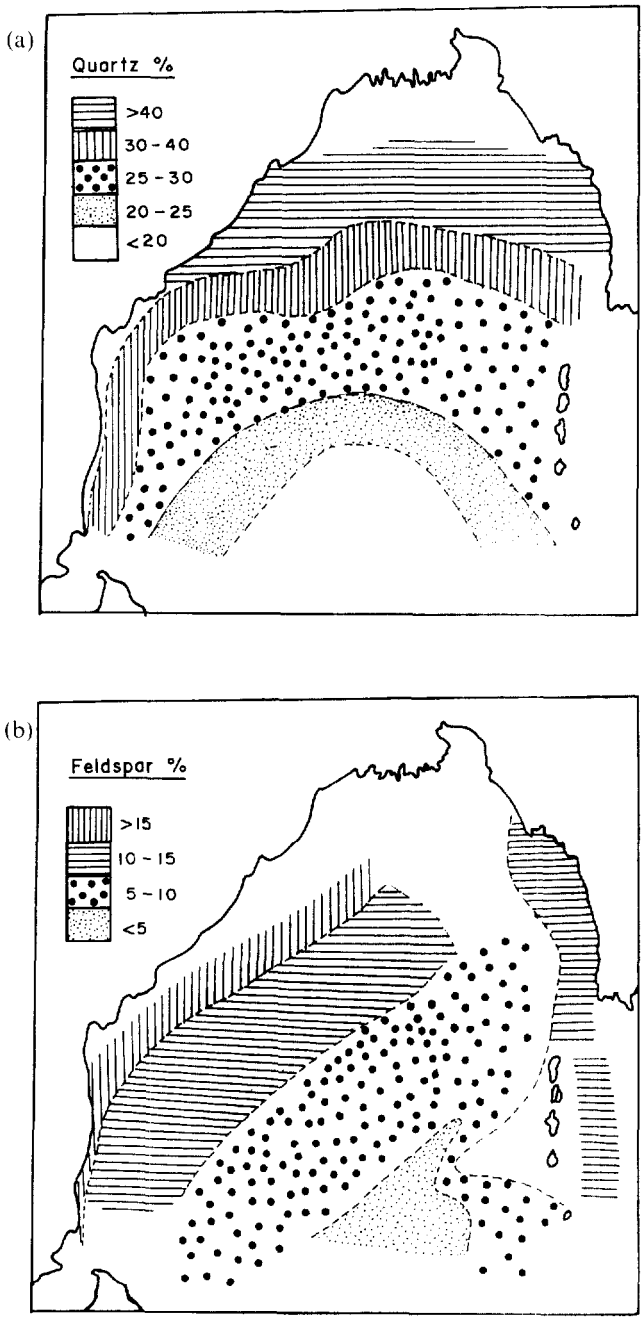

Fig. 3. Schematic maps showing distribution of (a) quartz and (b) feldspar in the Bengal Fan sediments

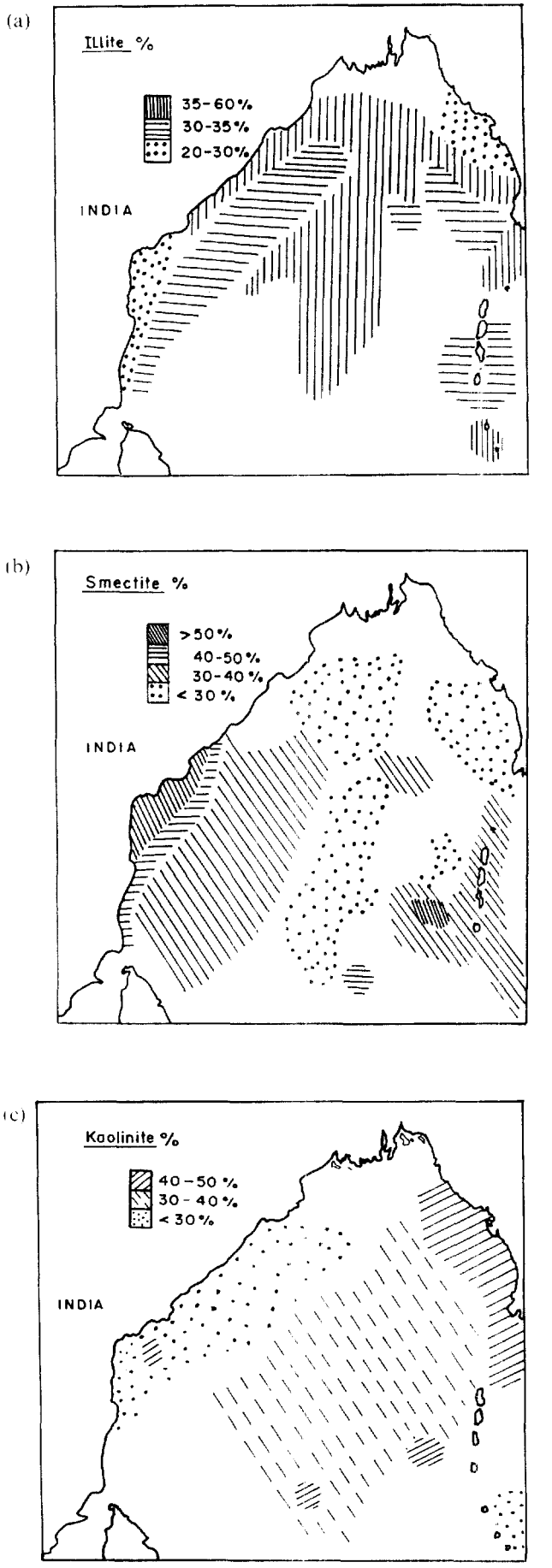

Fig. 4. Schematic maps showing the distribution of (a) illite, (b) kaolinite and (c) smectite (montmorillonite) in the Bengal Fan sediments.

as the major component, with quartz, muscovite, illite, smectite, chlorite, and sometimes mixed-layer clays and feldspar present in subordinate amounts. Gypsum and aragonite were found as traces in most samples. The highest percentage of quartz is found adjacent to the Indian Peninsula and, in particular, adjacent to the Ganges–Brahmaputra mouth, where it exceeds 40%. From there, it decreases to less than 20% near the equator. Analysis of suspended river material confirms this trend, with Ganges–Brahmaputra material containing 11 to 16.7% quartz, whereas Cauvery river material contains only 4.9% (Subramaniam, 1980).

Carbonate is present in the highest abundance in sediments above the Carbonate Compensation Depth (CCD) from the eastern flank of Nicobar Fan (adjacent to Ninetyeast Ridge) where inputs of terrigenous sediments are the lowest. In this area, the CCD is deeper than 5000 m (Kolla and Kidd, 1982) and the $CaCO_3$ content of the sediments reaches a maximum of 61.6%. There is a systematic decrease in the calcite towards the shelf area where the calcite content averages 15%. The distribution of clay minerals in the Indian Ocean has been reported by Venkatarathnam and Biscaye (1973), Windom (1976), Kolla and Kidd (1982) and Roonwal and Srivastava (1991). The principal clay minerals found in the study are illite, smectite, subordinate chlorite and kaolinite. Trends of their distribution are shown in Fig. 4.

Illite is predominant in the northern part of the Bay of Bengal. It originates from source rocks and soils of the catchment areas of the Ganges river and dominates the plains of northern India. It is the main constituent of the monsoonal Ganges river silt. The decrease of illite away from the mouth shows this river to be the main source of illite in the sediments. Data on these river silts show a high quantity of illite (37%), smaller quantities of kaolinite and chlorite and only traces of smectite.

Chlorite group minerals occur in both sedimentary and metamorphic rocks, such as phyllite, mica schists and also with magmatic rocks. Chlorite is also a weathering product of the ferro-magnesian silicates. The Himalaya contains all these rock. Chlorite is therefore derived principally from Himalayan rocks.

Kaolinite is derived from laterite soils formed from weathering of khondalites, granites and gneisses, along the Bengal, Orissa and Andhra Pradesh coasts. The pre-monsoonal silt is high in kaolinite, and its abundance indicates subaerial enrichment of alumina.

Smectite is formed as a sub-tropical weathering product of basalts of the Deccan Traps, the Cuddapah, Rajmahal and Simlipal, Dalma-Dhanjori and other bodies. The suspended loads of rivers draining these regions have high smectite contents.

Geochemistry

Sediment samples were analysed for 19 elements by ICP-AES in the case of HMS *Investigator* samples and for 34 elements by XRF in the case of the Andaman Sea sediments. Average compositional data are presented in Table 2. The aim was to prepare schematic geochemical maps of the Bengal Fan sediments, to determine the degree and extent of continental influence on the sediments and to establish the inter-relationships between the various elements.

Table 2. Average chemical composition of Bengal Fan and Andaman Sea sediments (major elements analyses in weight % and trace elements in ppm)

	Al_2O_3	TiO_2	FeO	MgO	CaO	Na_2O	K_2O	MnO	P_2O_5	Co	Cu	Pb	Ni	V	Zn	Ba	Mo	Sr	Cr
Bengal Fan																			
HMS *Investigator* samples																			
Upper Fan ($n = 3$)	9.51	0.62	7.12	2.98	1.64	2.43	3.32	0.23	0.32	43	75	312	99	146	194	533	96	112	157
Middle Fan ($n = 7$)	7.40	0.48	5.37	2.82	5.79	2.45	2.66	0.33	0.26	45	105	312	154	141	213	630	116	220	167
Lower Fan ($n = 30$)																			
(a) North of Ninetyeast ($n = 6$)	4.45	0.24	4.39	1.55	24.20	2.05	1.43	0.29	0.20	35	87	217	138	87	192	952	88	684	258
(b) Andaman Sea ($n = 9$)	8.30	0.36	5.94	3.30	27.71	3.34	2.19	1.40	0.22	29	67	221	122	107	146	446	80	586	212
(c) Continental margin of India ($n = 10$)	8.90	0.76	8.64	3.10	2.17	2.53	2.51	0.23	0.30	103	107	283	128	168	193	411	110	119	215
(d) Mayanmar margin ($n = 5$)	9.70	0.52	7.06	3.27	5.50	2.96	2.67	0.90	0.35	43	57	868	278	310	200	255	107	211	236
Andaman Sea and eastern flank of Nicobar Fan																			
RV *Samudra Manthan* samples																			
SM28 ($n = 28$)	13.84	0.56	6.04	2.25	4.77	3.39	2.18	1.59	0.18	31	91	20	129	131	74	661	12	239	110
SM30 ($n = 7$)	9.46	0.37	3.60	1.64	22.38	2.10	1.27	0.39	0.11	24	34	10	69	85	56	404	8	1433	64

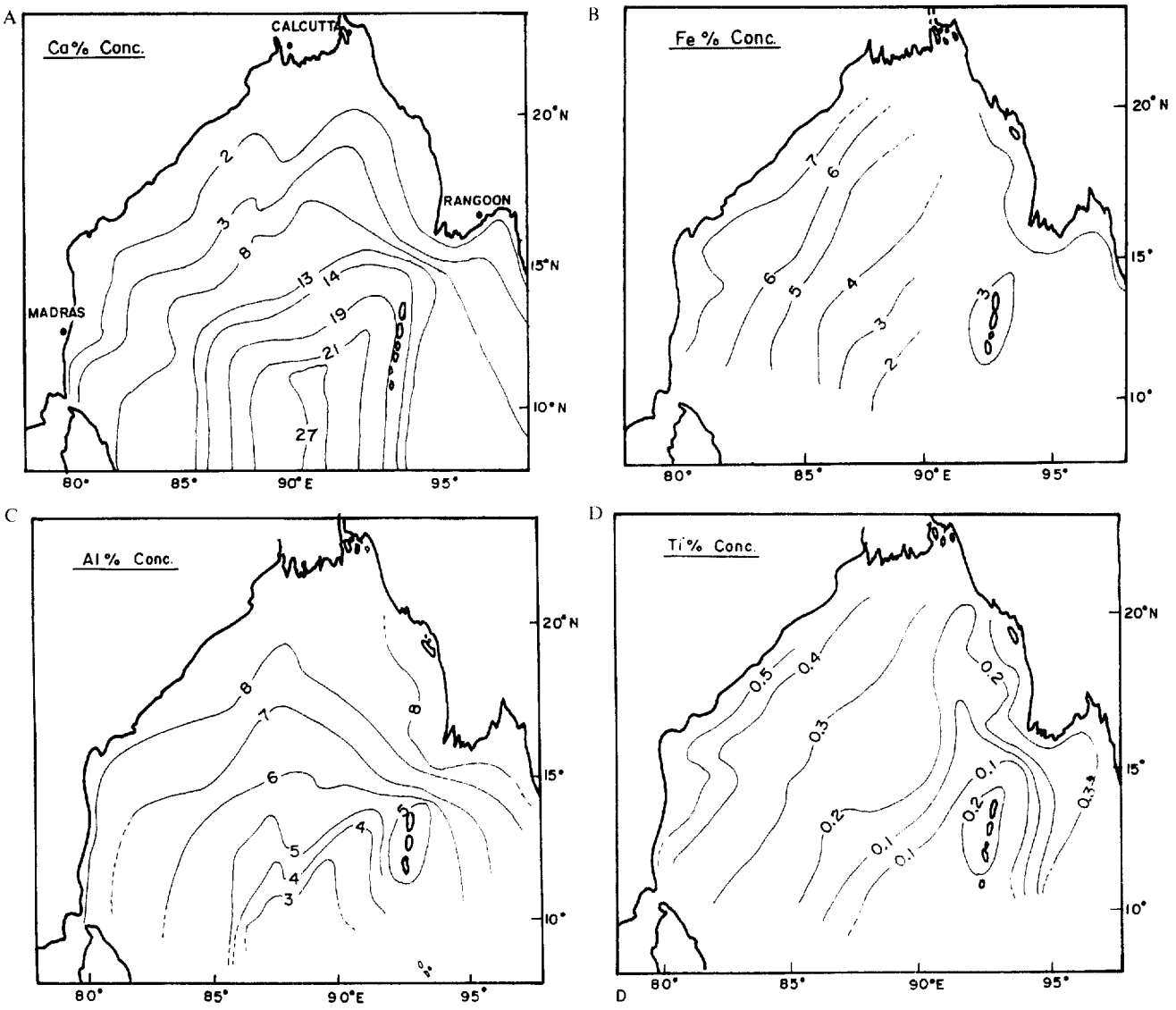

Fig. 5. Schematic maps showing the distribution of (a) calcium, (b) iron, (c) aluminium and (d) titanium concentrations in surface sediments of the Bengal Fan.

The areal distribution of selected elements in the Bengal Fan sediments are shown in Fig. 5. There is a distinct gradation in the element distributions, which is controlled by three major factors:

- input of Ganges–Brahmaputra-transported detritus, which is derived mainly from granite, gneiss, schist, slate, quartzite and sandstone;
- input of river-borne detritus from the Indian Peninsula derived mainly from basalt, crystalline rocks and laterites; and
- deposition of calcareous sediments on the eastern flank of the Nicobar Fan (adjacent to Ninetyeast Ridge).

Considering the distribution of the various elements, calcium varies between 0.74% in the terrigenous sediments and 22.8% in the sediments from station 29 (Fig. 5(a)). The high calcium content at station M29 is in agreement with the findings of Kolla and Kidd (1982), who reported more than 50% $CaCO_3$ in the sediments in the vicinity of this station.

Iron shows an opposite trend than that of calcium (Fig. 5(b)) and varies between 8.2 and 1.6%. The highest iron contents are encountered in the continental margin and result from the input of coarse terrigenous detritus (Wijayananda and Cronan, 1994). A terrigenous input of iron is also observed adjacent to the Andaman and Nicobar Islands and to Myanmar (Burma). The lowest iron contents are encountered near the Ninetyeast Ridge where calcareous sediments predominate. The principal source of iron appears to be Peninsular basalts and mafic rocks, the influence of which decreases with distance from source. Iron also shows a tendency to be preferentially concentrated in the fine sediments fraction adjacent to the continent, in accordance with the widely observed inverse correlation between iron content and grain size.

The aluminium content of the sediment is strongly determined by the terrigenous component (*cf.* Wijayananda and Cronan, 1994). It varies between 13.2 and 2.3% (Fig. 5(c)) and decreases away from the continent with the lowest value found at station 24 (2.3%), which also has the lowest Ti content (0.01%) (Fig. 5(d)).

The titanium content is the highest (>5%) in the shelf areas adjacent to the Indian Peninsula, Myanmar and the Andaman Islands (Fig. 5(d)). The titanium contents of sediments from the Ganges–Brahmaputra river

Table 3. Correlation matrix showing interelement correlations for sediments from the Bengal Fan (HMS *Investigator* samples)

	Al	Ti	Fe	Mg	Ca	Na	K	Mn	P	Ni	Co	Ca	V	Zn	Mo	Cr	Pb	Sr	Ba
Al	1																		
Ti	0.49	1																	
Fe	0.52	0.72	1																
Mg	0.40	0.43	0.44	1															
Ca	−0.88	0.49	−0.89	−0.83	1														
Na	−0.11	0.07	−0.08	−0.14	−0.22	1													
K	0.56	0.47	0.50	0.39	0.78	−0.14	1												
Ma	−0.20	−0.25	−0.16	−0.29	−0.15	−0.18	−0.01	1											
P	0.30	0.32	0.34	0.21	−0.72	0.02	0.29	−0.23	1										
Ni	0.44	0.22	0.29	0.53	−0.06	0.59	0.30	−0.09	0.62	1									
Co	0.10	0.29	0.31	0.13	−0.19	−0.04	0.12	−0.25	0.06	−0.01	1								
Cu	−0.13	0.02	0.09	−0.19	−0.13	−0.26	−0.03	0.29	−0.17	0.16	0.16	1							
V	0.44	0.33	0.34	0.41	−0.27	0.33	0.37	−0.20	0.45	0.53	0.03	0.02	1						
Zn	0.12	0.03	0.07	0.09	−0.24	−0.04	0.24	0.16	0.02	0.44	−0.03	0.18	0.48	1					
Mo	−0.26	0.09	0.13	−0.41	0.49	−0.65	−0.20	−0.18	−0.29	−0.26	0.12	−0.13	−0.11	−0.34	1				
Cr	−0.28	−0.22	−0.27	0.26	0.36	0.04	−0.22	−0.01	−0.27	0.001	−0.06	−0.03	−0.08	−0.16	−0.18	1			
Pb	−0.17	0.03	0.07	0.11	0.24	−0.08	−0.12	−0.14	0.13	0.05	−0.01	−0.20	0.61	0.08	0.05	0.05	1		
Sr	0.92	−0.84	−0.92	−0.90	0.83	0.27	−0.80	0.14	−0.76	−0.09	−0.19	−0.17	−0.26	−0.24	−0.55	0.24	−0.25	1	
Ba	−0.66	−0.64	−0.61	−0.73	0.49	−0.39	−0.50	−0.46	−0.55	−0.10	−0.12	−0.17	−0.26	−0.14	−0.32	−0.18	−0.21	0.45	1

system decrease away from source. The titanium content is much lower in sediments from the Andaman Sea compared to the Bengal Fan. This reflects the different sources of terrigenous sediments to these two areas (Roonwal *et al.*, in press).

The Nicobar Fan sediments show differences in composition from those of Bengal Fan, with higher contents of CaO and strontium and lower contents of iron, phosphorus, cobalt, copper, lead, nickel, vanadium, molybdenum and chromium. These differences reflect, in part, the higher biogenic carbonate content of the Nicobar Fan sediments. In fact these sediments were cut off from a supply of material from the Bengal Fan as a result of convergence of Ninetyeast Ridge with a Java Trench during the Pleistocene (Bowles *et al.*, 1978; Curray *et al.*, 1982). As a result, the entire surface sediments of the Nicobar Fan are receiving only pelagic deposition at present. However, the transition metal contents of these sediments appear to be very low compared to those of deep-sea clays (Chester, 1990).

Table 3 shows that calcium is strongly associated with strontium and, to a lesser extent, barium in the sediments from the Bengal Fan but is negatively correlated with phosphorus. The correlation of iron, magnesium, potassium, aluminium and titanium confirms a terrigenous source of these elements, which is in agreement with the findings of Nath *et al.* (1989) for sediments from the Central Indian Basin. However, in contrast to the findings of Nath *et al.* (1989), there are no marked interelement associations between the transition elements, manganese, nickel, copper and iron, which these authors attribute to distribution from a hydrogenetic–diagenetic source. Since the concentrations of nickel, copper and iron (but not manganese) in the lower fan sediments are well below those given by Chester and Aston (1976) for average Pacific deep-sea clays, and since the samples lie within the Ganges province as defined by Kolla and Kidd (1982), this may simply reflect the fact that the sediments have a strongly terrigenous rather than an authigenic origin.

In summary, the present mineralogical and geochemical data are consistent with there being two main sources of the surface sediments of the Bengal Fan, the Himalayas and the Deccan Traps from the Indian Peninsula.

Acknowledgements—This work was carried out under the grant DST/ES/003/87 (IX) from the Department of Science and Technology, New Delhi. Sediment samples were kindly supplied by the British Museum, London (Mr A. Buckley) and the Oil and Natural Gas Commission, Dehra Dun. Part of this work was carried out while one of the authors (GSR) was at BGR (Hannover) on an EC Bursary in 1991. The authors thank Dr S. Crowley (University of Liverpool), who kindly made a preprint of his paper available to us, and Dr P. K. S. Chauhan for much help during the preparation of this manuscript.

REFERENCES

Amano K. and Taira A. (1992) Two-phase uplift of higher Himalayas since 17 Ma. *Geology* **20**, 391–394.

Anon. (1992) *Recent Geoscientific Studies in the Bay of Bengal and the Andaman Sea*. Geol. Surv. India, Spec. Publ. No. 29, 278 pp.

Aoki S., Kohyama N. and Ishizuka T. (1991) Sedimentary history and chemical characteristics of clay minerals in cores from the distal part of the Bengal Fan (ODP 116). *Mar. Geol.* **99**, 175–185.

Biscaye P. E. (1965) Mineralogy and sedimentation of Recent deep-sea clay in the Atlantic Ocean and adjacent seas and oceans. *Geol. Soc. Am. Bull.* **76,** 803–832.

Borole D. V. (1993) Late Pleistocene sedimentation: a case study of the Central Indian Ocean Basin. *Deep-Sea Res.* **40,** 761–775.

Bouquillon A., Chamley H. and Frohlich F. (1989) Sédimentation argileuse au Cénozoique supérieur dans l'Ocean Indien nord-oriental. *Oceanol. Acta* **12,** 133–147.

Bouquillon A., France-Lanord C., Michard A. and Tircelin J.-J. (1990) Sedimentary and isotopic chemistry of Bengal Fan sediments: the denudation of the Himalaya. *Proc. Ocean Drilling Progr., Scient. Res.* **116,** 43–58.

Bowles F. A., Ruddiman W. F. and Jahn W. H. (1978) Acoustic stratigraphy, structure, and depositional history of the Nicobar Fan, eastern Indian Ocean. *Mar. Geol.* **26,** 269–288.

Brass G. W. and Raman C. V. (1990) Clay mineralogy of sediments from the Bengal Fan. *Proc. Ocean Drilling Progr., Scient. Res.* **116,** 35–41.

Chauhan O. S., Gujar A. R. and Rao Ch. M. (1994) On the occurrence ferromanganse micro nodules from the sediments of the Bengal Fan: a high terrigenous sediment input region. *Earth Planet. Sci. Lett.* **128,** 563–573.

Chauhan O. S., Mascarenhas A., Paropkari A. K. and Rao Ch. M. (1992) Late Quaternary sedimentation in the eastern Bay of Bengal. In *Oceanography of the Indian Ocean* (edited by Desai B. N.), pp. 479–486. Oxford & IBH Publishing, New Delhi.

Chester R. (1990) *Marine Geochemistry*, 698 pp. Unwin Hyman, London.

Chester R. and Aston S. R. (1976) The geochemistry of deep-sea sediments. In *Chemical Oceanography*, 2nd Edn. Vol. 6 (edited by Riley J. P. and Chester R.), pp. 281–390. Academic Press, London.

Class C., Goldstein S. L., Galer S. J. G. and Weiss D. (1993) Young formation age of a mantle plume source. *Nature* **362,** 715–721.

Copeland P. and Harrison T. M. (1990) Episodic rapid uplift in the Himalaya revealed by $^{40}Ar/^{39}Ar$ analysis of detrital K-feldspar and muscovite, Bengal Fan. *Geology* **18,** 354–357.

Cronan D. S. and Wijayananda N. P. (1991) Sediments and marine mineral resources of the eastern Indian Ocean. *Mar. Mining* **10,** 103–116.

Crowley S. (in press) Mineralogy and geochemistry of Bay of Bengal deep sea fan sediments. ODP Leg 116: evidence for an Indian subcontinent contribution to distal fan sedimentation. In *Geological Evolution of Ocean Basins: Results from the Ocean Drilling Program*. Geological Society Special Publication.

Curray J. R. (1991) Possible greenschist metamorphism at the base of a 22-km sedimentary section, Bay of Bengal. *Geology* **19,** 1097–1100.

Curray J. R. (1994) Sediment volume and mass beneath the Bay of Bengal. *Earth Planet. Sci. Lett.* **125,** 371–383.

Curray J. R. and Moore D. G. (1971) Growth of the Bengal deep-sea fan and denudation of the Himalayas. *Geol. Soc. Am. Bull.* **82,** 563–572.

Curray J. R. and Moore D. G. (1974) Sedimentary and tectonic processes in the Bengal deep sea fan and geosyncline. In *The Geology of Continental Margins* (edited by Burk C. A. and Drake C. L.), pp. 617–627. Springer-Verlag, Heidelberg.

Curray J. R., Emmel F. J., Moore D. G. and Raitt R. W. (1982) Structure, tectonics, and geological history of the northeast Indian Ocean. In *The Ocean Basins and Margins*, Vol. 6 *The Indian Ocean* (edited by Nairn A. E. M. and Stehli F. G.), pp. 399–450. Plenum Press, New York.

Debrabant P., Fagel N., Chamley H., Bout V. and Caulet J. P. (1993) Neogene to Quarternary clay mineral fluxes in the Central Indian basin. *Palaeogeogr., Palaeoclimatol., Palaeoecol.* **103,** 117–131.

Derry L. A. and France-Lanord C. (1996) Neogene Himalayan weathering history and river $^{87}Sr/^{86}Sr$: impact on the marine sedimentary record. *Earth Planet. Sci. Lett.* **142,** 59–74.

Dia D., Dupre B. and Allegre C. J. (1992) Nd isotopes in Indian Ocean sediments used as a tracer of supply to the ocean and circulation paths. *Mar. Geol.* **103,** 349–359.

Duncan R. A. (1990) The volcanic record of the Reunion hotspot. *Proc. Ocean Drilling Program, Scient. Res.* **115,** 3–10.

Einsele G., Ratschbacher L. and Wetzel A. (1996) The Himalaya–Bengal Fan denudation–accumulation system during the past 20 Ma. *J. Geol.* **104,** 163–184.

Emmel F. J. and Curray J. R. (1984) The Bengal Submarine Fan, northeastern Indian Ocean. *Geo-Mar. Lett.* **3,** 119–124.

France-Lanord C. and Derry L. A. (1994) $\delta^{13}C$ of organic Carbon in the Bengal Fan: source evolution and transport of C 3 and C 4 plant carbon to marine sediments. *Geochim. Cosmochim. Acta* **58,** 4809–4814.

France-Lanord C., Derry L. and Michard A. (1993) Evolution of the Himalaya since Miocene time: isotopic and sedimentological evidences from Bengal Fan. In *Himalayan Tectonics* Geological Society Special Publication No. 74, (edited by Trelor P. J. and Searle M. P.), pp. 603–621.

Hovan S. A. and Rea D. K. (1992) The Cenzoic record of continental mineral deposition on Broken and Ninetyeast Ridges, Indian Ocean: South African aridity and sediment delivery from the Himalayas. *Paleoceanography* **7,** 833–860.

Ingersoll R. V. and Suczek C. A. (1979) Petrology and provenance of Neogene sand from Nicobar and Bengal Fans, DSDP Sites 211 and 218. *J. Sedim. Petrol.* **49,** 1217–1228.

Ittekkot V., Safiulla S., Mycke B. and Seifert R. (1985) Seasonal variability and geochemical significance of organic matter in River Ganges, Bangladesh. *Nature* **317,** 800–802.

Ittekkot V., Nair R. R., Honjo S., Ramaswamy V., Bartsch M., Manganini S. and Desai B. N. (1991) Enhanced particle fluxes to the deep ocean induced by freshwater inputs. *Nature* **351,** 385–387.

Ittekkot V., Haake B., Bartsch M., Nair R. R. and Ramaswamy V. (1992) Organic carbon removal from the Sea: the continental connection. In *Upwelling Systems: Evolution since the Early Miocene*. Geol. Soc. Spec. Publ. No. 64, (edited by Summerhayes C. P., Prell W. L. and Emeis K. C.), pp. 167–176.

Johnson M. R. W. (1994) Volume balance of erosional loss of sediments deposition related to Himalayan uplift. *J. Geol. Soc. London* **151,** 217–220.

Klootwijk C. T., Gee J. S., Peirce J. W. and Smith G. M. (1991) Constraints on the India-Asia convergence: paleomagnetic results from Ninetyeast Ridge. *Proc. Ocean Drilling Progr., Scient. Res.* **121,** 777–882.

Kolla V. and Kidd R. B. (1982) Sedimentation and sedimentary processes in the Indian Ocean. In *The Ocean Basins and Margins*, Vol. 6 *The Indian Ocean* (edited by Nairn A. E. M. and Stehli F. G.), pp. 1–50. Plenum Press, New York.

Kolla V., Moore D. G. and Curray J. R. (1976) Recent bottom-current activity in the deep western Bay of Bengal. *Mar. Geol.* **31,** 255–270.

Krishnaswami S., Trevedi J. R., Sarin M. M., Ramesh R. and Sharma K. K. (1992) Strontium isotopes and rubidium in the Ganga–Brahmaputra river system: weathering in the Himalaya, fluxes to the Bay of Bengal and contributions to the evolution of oceanic $^{87}Sr/^{86}Sr$. *Earth Planet. Sci. Lett.* **109,** 243–253.

Kuehl S. A., Hariu T. N. and Moore W. S. (1989) Shelf sedimentation off the Ganges-Brahmaputra river system: evidence of sediment bypassing to the Bay of Bengal. *Geology* **17,** 1132–1135.

Kumar M. D., George M. D. and Sen Gupta R. (1992) Inputs from Indian rivers to the Ocean: a synthesis. In *Oceanography of the Indian Ocean* (edited by Desai B. N.), pp. 347–358. Oxford & IBA Publishing, New Delhi.

Levchenko O. V., Milanovskiy V. Ye. and Popov A. A. (1993) A sediment thickness map and the tectonics of the distal Bengal Fan. *Oceanology* **33,** 232–238.

Lisitizin A. P. (1972) Sedimentation in the world Oceans. *Soc. Econ. Paleontol. Mineral. Spec. Publ.* **17,** 135–148.

Mallik T. K. (1976) Shelf sediments of the Ganges with special emphasis on the mineralogy of the western part, Bay of Bengal, Indian Ocean. *Mar. Geol.* **27,** 1–32.

Milliman J. D. and Meade R. H. (1983) World-wide delivery of river sediment of the Oceans. *Geology* **91,** 1–21.

Mukhopadhyay M. and Krishna M. B. R. (1995) Gravity anomalies and deep structure of the Ninetyeast Ridge north of the equator, eastern Indian Ocean—a hot spot trace model. *Mar. Geophys. Res.* **17,** 201–216.

Naidu A. S., Mowatt T. C., Somayajulu B. L. K. and Sreeramachandra Rao K. (1985) Characteristics of clay minerals in the bed loads of major rivers of India. *Mitt. Geol.-Paläont. Inst. Univ. Hamburg* **58,** 559–568.

Naini B. R. and Leyden R. (1973) Ganges cone: a wide angle seismic reflection and refraction study. *J. Geophys. Res.* **78,** 8711–8720.

Nath B. N., Rao V. P. and Becker K. P. (1989) Geochemical evidence of terrigenous influence in deep-sea sediments up to 8 S in the Central Indian Basin. *Mar. Geol.* **87,** 301–313.

Ormond A., Boulégue J. and Genthon P. (1995) A thermoconvective interpretation of heat flow data in the area of the Ocean Drilling Program Leg 116 in a distal part of the Bengal Fan. *J. Geophys. Res.* **100,** 8083–8095.

Ramana M. V., Nair R. R., Sarma K. V. L. N. S., Ramprasad T., Krishna K. S., Subrahmanyan V., D'Cruz M., Subramanyan C., Paul J., Subrahmanyan A. S. and Chandra Shekar D. V. (1994) Mesozoic anomalies in the Bay of Bengal. *Earth Planet Sci. Lett.* **121,** 469–475.

Rao D. G. *et al.* (1993) Analysis of multi-channel seismic reflection and magnetic data along 13 N latitude across the Bay of Bengal. *Mar. Geophys. Res.* **16,** 225–236.

Rea D. K. (1992) Delivery of Himalayan sediments to the northern Indian Ocean and its relation to global climate, sea level, uplift, and seawater strontium. In *Synthesis of Results from Scientific Drilling in the Indian Ocean*, Am. Geogeophys. Un. Geophys. Monogr. 70, (edited by Duncan R. A., Rea D. K., Kidd R. B., Von Rad U. and Weissel J. K.), pp. 387–402.

Reetsma T., Ittekkot V., Bertsch M. and Nair R. R. (1993) River inputs and organic matter fluxes in the northern Bay of Bengal: fatty acids. *Chem. Geol.* **103,** 55–71.

Rodolfo K. S. (1969) Bathymetry and marine geology of the Andaman Basin, and tectonic implications for Southeast Asia. *Geol. Soc. Am. Bull.* **80,** 1203–1230.

Roonwal G. S. (1986) *The Indian Ocean: Exploitable Mineral and Petroleum Resources*, 198 pp. Springer-Verlag, Heidelberg.

Roonwal G. S. and Srivastava S. K. (1991) Clay mineralogy of the pelagic sediments: along a west-east transect in the Indian Ocean. *J. Geol. Soc. India* **38,** 37–54.

Roonwal G. S., Glasby G. P. and Roelandts I. (in press). Mineralogy and geochemistry of surface sediments from the Andaman Sea and upper Nicobar Fan, northeast Indian Ocean. J. Indian Asso. Sedimentol.

Royer J. Y., Peirce J. W. and Weissel J. K. (1991) Tectonic constraints on the hot-spot formation of Ninetyeast Ridge. *Proc. Ocean Drilling Program, Scient. Res.* **121,** 763–776.

Sarin M. M., Krishnaswami S., Dill K., Somayajulu B. L. K. and Moore W. S. (1989) Major ion chemistry of the Ganga-Brahmaputra river system: weathering processes and fluxes to the Bay of Bengal. *Geochim. Cosmochim. Acta*, **53,** 997–1009.

Sarin M. M., Krishnaswami S., Somayajulu B. L. K. and Moore W. S. (1990) Chemistry of uranium, thorium, and radium isotopes in the Ganga-Brahmaputra rivers system: weathering processes and fluxes to the Bay of Bengal. *Geochim. Cosmochim. Acta* **54,** 1387–1396.

Sarin M. M., Krishnaswami S., Sharma K. K. and Trevedi J. R. (1992a) Uranium isotopes and radium in the Bhagirathi Alaknanda river system: evidence for high uranium mobilization in the Himalaya. *Curr. Sci.* **62,** 801–804.

Sarin M. M., Krishnaswami S., Trivedi J. R. and Sharma K. K. (1992b) Major ion chemistry of the Ganga source waters: weathering in the high altitude Himalaya. *Proc. Indian Acad. Sci. (Earth Planet. Sci.)* **101,** 89–98.

Schmitz B. (1987a) Barium equatorial high productivity and the northward wandering of the Indian continent. *Paleoceanography* **2,** 63–77.

Schmitz B. (1987b) The TiO_2/Al_2O_3 ratio in the Cenozoic Bengal abyssal fan sediments and its use as a paleostream energy indicator. *Mar. Geol.* **76,** 195–206.

Sharma K. K. (1984) The sequence of phased uplift of the Himalaya. In *The Evolution of the East Asian Environment* (edited by Whyte R. O., Chiu T. N., Leung C. K. and So C. L.), Vol. I, pp. 56–70. Centre for Asian Studies, University of Hong Kong.

Stow D. A. V., Cochran J. R. and ODP Leg 116 Shipboard Scientific Party (1989) The Bengal Fan: some preliminary results from ODP drilling. *Geo-Mar. Lett.* **9,** 1–10.

Stow D. A. V., Amano K., Balson P. S., Brass G. W., Corrigan J., Raman C. V., Tiercelin J-J., Townsend M. and Wijayananda N. P. (1990) Sediment facies and processes on the distal Bengal Fan, Leg 116. *Proc. Ocean Drilling Program, Scient. Res.* **116,** 377–396.

Subramaniam V. (1980) Mineralogical input of suspended matter by Indian rivers into the adjacent area of the Indian Ocean. *Mar. Geol.* **36,** M29–M34.

Subramaniam V. (1985) Geochemistry of river basins in the Indian subcontinent. Part I: water chemistry, chemical erosion and water-mineral equillibira. *Mitt. Geol.-Paläont. Inst. Univ. Hamburg* **58,** 495–512.

Subramaniam V., Van't Dack L. and Van Grieken R. (1985) Chemical composition of river sediments from the Indian sub-continent. *Chem. Geol.* **48,** 271–279.

Subramaniam V., Jha P. K. and Van Grieken R. (1988) Heavy metals in the Ganges Estuary. *Mar. Pollut. Bull.* **19,** 290–293.

Subramaniam V., Ramanathan A. C., Vaithanathan P. (1989) Distribution and fractionation of heavy metals in the Cauvery estuary, India. *Mar. Pollut. Bull.* **20,** 286–290.

Suresh N. (1993) Sediment dispersal in the Bay of Bengal with special emphasis on mineralogy and geochemistry. Ph.D. thesis, Garhwal University, Srinagar, U.P.

Suryanarayana A., Murty V. S. N. and Rao D. P. (1993) Hydrography and circulation of the Bay of Bengal during the winter, 1983. *Deep-Sea Res.* **40,** 205–217.

Venkatarathnam K. and Biscaye P. E. (1973) Clay mineralogy and sedimentation in the eastern Indian Ocean. *Deep-Sea Res.* **20,** 727–738.

Verma R. K. (1991) *Geodynamics of the Indian Peninsula and the Indian Plate Margin*, 357 pp. A. A. Balkema, Rotterdam.

Wetzel A. and Balson P. (1992) Sedimentology of fine-grained turbidities inferred from continously recorded physical properties data. *Mar. Geol.* **104,** 165–178.

Wijayananada N. P. and Cronan D. S. (1994) The geochemistry and mineralogy of marine sediments from the eastern Indian Ocean. *Mar. Geol.* **117,** 275–285.

Windom H. L. (1976) Lithogenous material in marine sediments. In *Chemical Oceanography*, Vol. 5, 2nd Edn. (edited by Riley J. P. and Chester R.), pp. 103–135. Academic Press, London.

Yokoyama K., Amano K., Taira A. and Saito T. (1990) Mineralogy of silts from the Bengal Fan. *Proc. Ocean Drilling Program., Scient. Res.* **116,** 59–73.

Annex B60

Mead A. Allison, "Geologic Framework and Environmental Status of the Ganges-Brahmaputra Delta", *Journal of Coastal Research*, Vol. 14, No. 3 (1998)

Journal of Coastal Research	14	3	826–836	Royal Palm Beach, Florida	Summer 1998

Geologic Framework and Environmental Status of the Ganges-Brahmaputra Delta

Mead A. Allison

Department of Oceanography
Texas A&M University
5007 Avenue U.
Galveston, TX 77551, U.S.A.

ABSTRACT

ALLISON, M.A., 1998. Geologic Framework and Environmantal Status of the Ganges-Brahmaputra Delta. *Journal of Coastal Research,* 14(3), 826–836. Royal Palm Beach (Florida), ISSN 0749-0208.

The enormous delta of the Ganges-Brahmaputra River in Bangladesh, and surrounding areas of India, is the lifeblood for one of the largest populations on Earth. Decending from the Himalayan plateau to a lowland upper delta plain, the rivers experience rapid lateral migration, producing a patchwork of flood plains of various ages. In the eastern lower (tidal) delta plain, the rivers enter the sea through the Meghna estuary, a 100-km-wide zone of multiple distributary channels and migrating islands. Coalescing subaqueous sand shoals in the river mouths form a delta front clinoform that is prograding seaward over the topset beds of a muddy subaqueous delta on the continental shelf. West of the river mouths, the lower delta plain is covered by a mangrove forest (Sunderbans), drained by a network of river distributary and secondary tidal channels and formed in an earlier phase of Holocene delta progradation. The Ganges-Brahmaputra delta is under increasing environmental pressure today in response to the needs of a rapidly growing and modernizing population.

ADDITIONAL INDEX WORDS: *Bangladesh, India, delta plain, Meghana estuary, Holocene.*

INTRODUCTION

The Ganges-Brahmaputra delta was formed by the confluence of two of the world's great rivers. With headwaters at elevations above 5000 m, the Ganges and Brahmaputra Rivers are the 2 largest of the 8 south Asian rivers (others are the Irrawaddy, Hungho, Mekong, Narmada, Indus, and Godavari) draining the Himalayas that number among the top 15 on earth in sediment discharge to the oceans (MILLIMAN and MEADE, 1983; MILLIMAN and SYVITSKI, 1992). Gathering runoff from a combined drainage basin of over 1.7 million km^2, the high-gradient, braided Brahmaputra and meandering Ganges each deliver sediment-laden water with distinct grain size and mineralogical character to a deltaic plain in the Bengal Basin (Figure 1). A sequence of up to 16 km of fluvio-deltaic sediments have filled this basin since the Paleogene (PAUL and LIAN, 1975). Regional tectonic uplift and subsidence are ongoing in the basin, making the Ganges-Brahmaputra subject to relatively rapid (10^2 yr) channel avulsions that have created a complex subaerial delta morphology. Virtually all of the nation of Bangladesh and surrounding areas of India are part of this fertile deltaic plain, which supports a population of approximately 200 million people in the 1990s. Although the delta has been extensively impacted by human activity for hundreds of years—British surveyor James Rennell observed earthen levees along the Ganges in 1764 (RENNELL, 1781)—the combination of river channel mobility and the persistence of traditional agricultural and rural settlement practices have retarded implementation of modern river control practices. Only since the 1960s has there been a significant impact on the delta from the construction of artificial levees, road embankments, and tributary dams.

The Ganges-Brahmaputra discharges into the Bay of Bengal along a delta front of 380 km. High-velocity tidal currents and frequent tropical cyclones in the Bay are major factors in shaping the subaerial delta front and in sediment delivery offshore. Sediment partitioning across the river-ocean interface has led to the formation of a subaqueous mud clinoform on the continental shelf adjacent to the river mouths. On the western edge of the delta, Swatch of No Ground submarine canyon incises the shelf to within 40 km of the shoreline. The submarine canyon is one of the few associated with major rivers that is an active conduit for sediment delivery to the deep sea, trapping sediment migrating westward along the subaqueous delta front. At the base of the submarine canyon is the world's largest submarine fan (Bengal Fan) which covers 3 million km^2 of seafloor (CURRAY *et al.*, 1982).

The objective of this paper is to provide a summary of the state of knowledge regarding the natural environment (e.g., geologic framework, ecology, physical processes) of the Ganges-Brahmaputra delta. A secondary objective is to identify some of the emerging issues that impact the natural environment of the region in response to a burgeoning population and the attendant socioeconomic growth.

PHYSICAL SETTING

The climate of the Ganges-Brahmaputra delta in Bangladesh is dominated by the monsoon cycle. Monsoon season,

98146 received and accpeted in revision 25 May 1998.

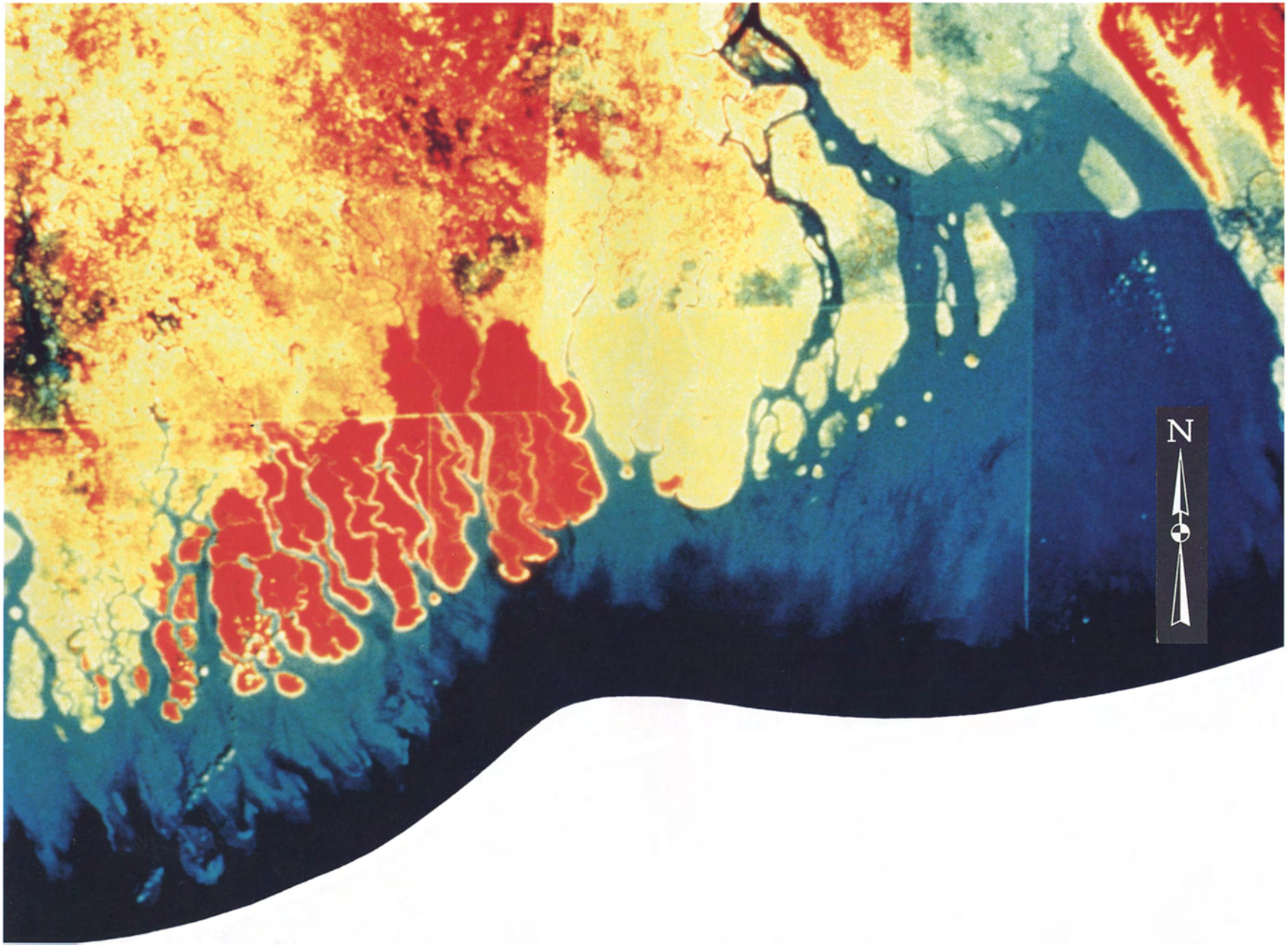

Plate 1. The Ganges-Brahmaputra delta was formed by the confluence of two great rivers, the Ganges and the Brahmaputra. Descending from the Himalaya plateau to a lowland upper delta plain, the rivers experience rapid lateral migration, which produces a patchwork of flood plains of various ages. Gathering runoff from a combined basin of over 1.7 million km^2, the high-gradient, braided Brahmaputra (right) and the meandering Ganges (left) each deliver sediment-laden water to a deltaic plain in the Bengal Basin.

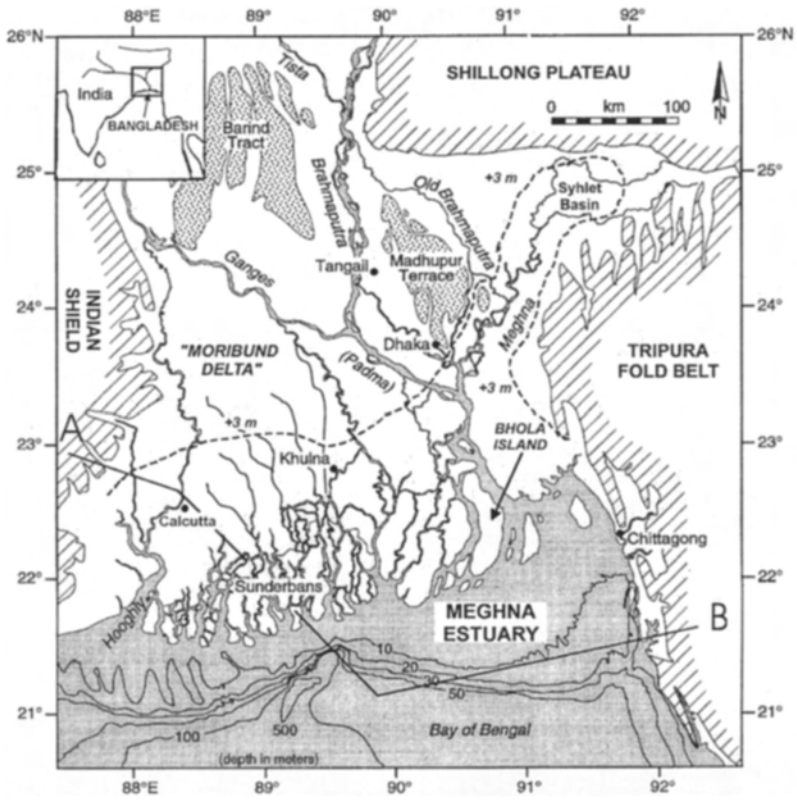

Figure 1. Map of the Ganges-Brahmaputra delta and adjacent areas of the Bengal shelf (modified from Kuehl *et al.*, 1997). Line A-B is the geologic cross-section in Figure 2.

which extends from late May to September, is the period when 80% of the rainfall occurs and winds blow from the Indian Ocean (*e.g.* southeast to southwest). Annual rainfall in the delta ranges from 125 cm in western Bangladesh to more than 300 cm in the river mouth region, and more than 500 cm in the extreme northeast bordering the Himalayan plateau (BRAMMER, 1996). Everywhere in the delta annual rainfall exceeds potential evapotranspiration rates. Mean daily temperature ranges from about 18°C in the dry season of continental winds (December–February) to 30°C prior to the onset of monsoon in April–May. Temperature extremes of 4°C and 43°C have been recorded in the region, with a narrower range along the coast (BRAMMER, 1996).

Tidal currents are perhaps the strongest hydrodynamic influence on the subaerial delta front and subaqueous part of the Ganges-Brahmaputra delta. The tide is semidiurnal and approximately synchronous along the delta front. Interaction of the M_2 and S_2 major components produces a distinct daily inequality of successive tides (EYSINK, 1983). Mean tidal amplitude is approximately 2.8 m on the east side of the delta, decreasing to approximately 1.9 m on the west (BITWA, 1987). Deformation of the tide front entering the islands and channels of the Meghna estuary produces tidal amplitudes exceeding 4 m and tidal currents up to 300 cm/sec in the river mouth (BARUA, 1990). Differences in the channel aspect ratio (water depth : width) and tidal assymetry in the river mouth estuary leads to flood dominance in the eastern tidal channels and ebb dominance in the western (BARUA, 1990). Saline water penetrates as far upstream as the Padma confluence 100 km inland during the dry season, and tides are measurable up to the Ganges-Brahmaputra confluence. The inland limit of saline influence follows an irregular line west of the Meghna estuary seaward of the 3 m elevation contour (Figure 1) and depends on the size and separation of the 20+ distributary channels that dissect the Ganges-Brahmaputra delta front. An estimate of the vector sum tidal and non-tidal residual transport by BARUA *et al.* (1994) reveals generally southwestward water and sediment delivery on the subaqueous delta during the dry season. Their measurements show a strong influence of the Ganges-Brahmaputra outflow on the coastal circulation in August. Models of the freshwater plume during high discharge in June–September also show net advection toward the west of the Bay of Bengal circulation gyre (SHETYE *et al.*, 1996).

The northern Bay of Bengal has a moderate wave climate with average wave heights of less than 0.5 m and 3–4 second wave periods. During the monsoon season wave heights average 0.5–1.0 m, with occasional waves up to 2 m with corresponding periods of 6 seconds. Larger waves of up to 5 m have been observed during cyclones (NEI, 1978). Tropical cyclones can affect coastal areas of the delta in both the premonsoon (March–June) and post-monsoon (September–De-

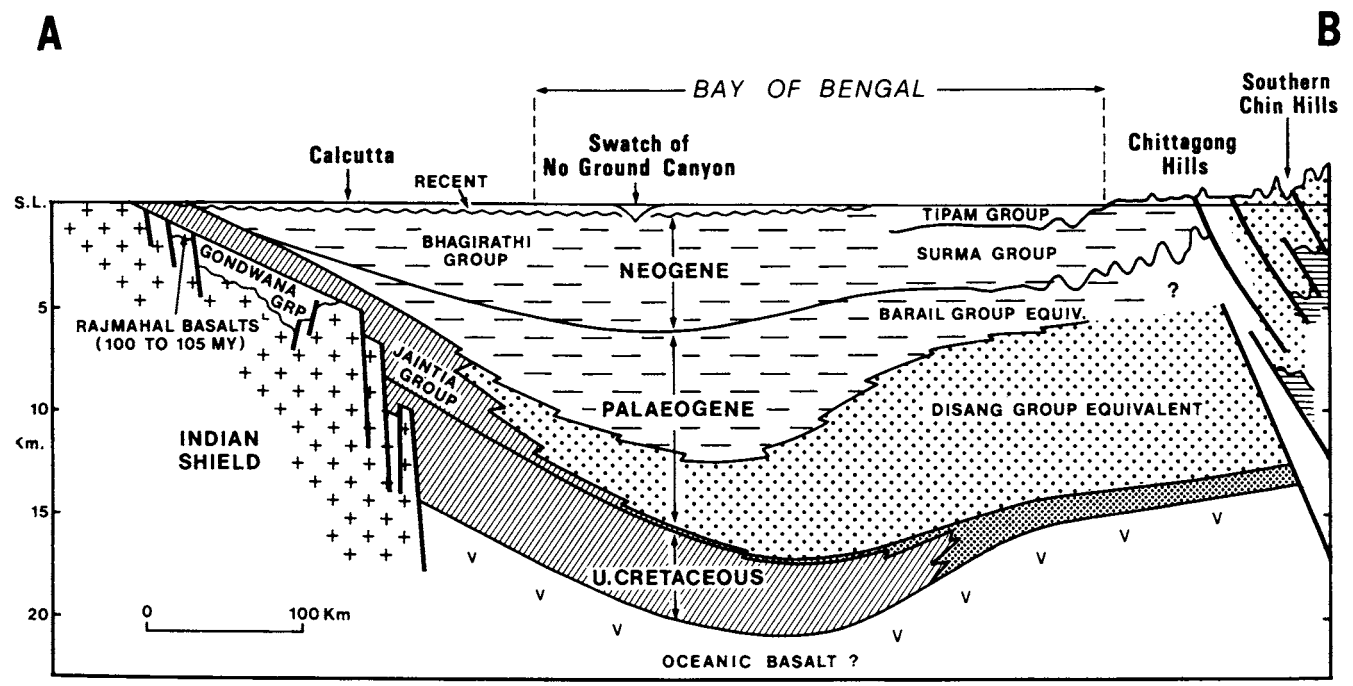

Figure 2. Regional cross-section of the Bengal Basin from line A-B in Figure 1 (from Imam and Shaw (1985).

cember) period (MURTY *et al.*, 1986). A total of 77 of these storms made landfall somewhere along the northern Bay of Bengal coast in the present century up to 1985. Owing to the low elevation of the Ganges-Brahmaputra deltaic plain, the resulting storm surges can penetrate as far as 100 km inland and have resulted in the death of an estimated 4.5 million persons in the period 1737–1985 (EMERY and AUBREY, 1989).

BENGAL BASIN

Collision between the continental masses of India and Asia began in the mid-Oligocene; the onset of major uplift of the Himalayas and the Indo-Burman range to the east was underway by the mid-Miocene (CURRAY *et al.*, 1982). A subsiding region along the front of the mountain belts, the Himalayan foredeep, became the repository for large volumes of clastic sediments shed off the rising mountains. The Bengal Basin evolved out of this area bordered by the Precambrian Shillong Massif and Indian Shield to the north and west, and the Neogene Tripura Fold Belt to the east (Figure 1). A stable shelf on the west and northwest side of the Basin bordering the Indian Shield contains a sequence of 1–8 km of Permian-Recent clastics (IMAM and SHAW, 1985). To the south and east, tectonic activity continues in the Bengal foredeep centered below the present Ganges-Brahmaputra river mouths. Up to 16 km of Tertiary and Quaternary fluvio-deltaic sediments have accumulated in the foredeep (Figure 2). The two parts of the Basin are separated by a hinge zone marked by high gravity and magnetic anomalies (SENGUPTA, 1966).

The Bengal foredeep contains a number of sub-basins, structural troughs, and highs bounded by basement-controlled lineaments that exhibit regional uplift and subsidence (FAO, 1987). In the northeast, the Sylhet subbasin is subsiding at rates up to 2.1 cm/year because of down-thrusting under the Shillong Massif (JOHNSON and ALAM, 1991). During the monsoon season this area is subject to extensive rainwater (*i.e.* non-turbid) flooding. Although the overall effect of regional tectonic subsidence, intrabasin fault activity, and local compaction is not known, a sense of its magnitude and continuing nature is evident from observations of sinking buildings, buried forests, and active fault scarps in the delta plain (MORGAN and MCINTIRE, 1959; COATES *et al.*, 1988; COATES, 1990).

A vast flat alluvial plain, encompassing Bangladesh and parts of the adjacent Indian states of West Bengal, Assam, and Tripura, forms the surface of the Bengal Basin. The plain is covered almost entirely by Quaternary and Recent alluvium of the Ganges, Brahmaputra, and Meghna rivers with Tertiary sediments exposed on the northern edge and in the Tripura Fold Belt to the east (FAO, 1987). Overall relief is slight with a gradual seaward elevation drop from 90 m in the extreme northwest of Bangladesh to a coastal plain of less than 3 m south of 24° N latitude. In the northeast along the axis of the Sylhet subbasin, the 3 m elevation contour extends more than 150 km inland (Figure 1). Two fault-bounded terraces, the Barind and Madhupur (Figure 1), outcrop in the deltaic plain and are elevated 3–15 m above the Holocene alluvium. Both are composed of the Pleistocene Madhupur Clay, an older alluvial unit that has been uplifted and deeply dissected by streams (MORGAN and MCINTIRE, 1959). The presence of these raised terraces on the deltaic plain is a first-order control on the Ganges and Brahmaputra channel paths.

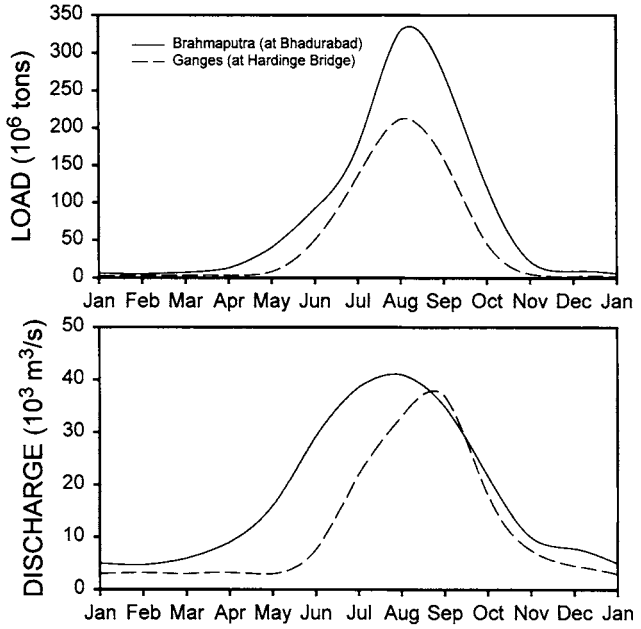

Figure 3. Water and suspended sediment discharge figures for the Brahmaputra and Ganges Rivers above the Padma confluence. Water discharge figures are 1969 to 1975 montly averages compiled by Emery and Aubrey (1989). Suspended sediment discharge rates for the Brahmaputra are 1958 to 1962 monthly averages; the Ganges are 1969 to 1970 monthly averages compiled by Barua, *et al.* (1994).

THE RIVERS

Approximately 85% of the surface runoff entering the fluvio-deltaic plain in Bangladesh is carried by three rivers: the Brahmaputra, Ganges, and Meghna. The Brahmaputra originates in Tibet and flows eastward along the northern slope of the Himalayas before turning south through Assam and merging with the Ganges 250 km inland of the Bay of Bengal. The Ganges rises west of the Brahmaputra along the Tibet-India border and flows 2200 km southeastward across India and Bangladesh. While the Brahmaputra catchment area is only half that of the Ganges (0.57 to 1.09 million km^2), its mean annual water discharge exceeds the Ganges (19,600 to 11,000 m^3/sec; FAO, 1987b) because of the tremendous monsoonal rainfall and snowmelt in the catchment. Both rivers have an enormous seasonal discharge range; in the Brahmaputra discharges have been measured from 2820 m^3/sec in mid-dry season (February–March) to an estimated 100,000 m^3/sec during the extreme flood of 1988 (EGIS, 1997). The Brahmaputra begins to rise a month before the Ganges in March–April in response to snowmelt in the Himalayas, reaching a peak discharge usually in late July–early August; the Ganges reaches its peak in late August–early September (Figure 3). Annual Ganges discharge figures have decreased since 1975 with the construction of the Farakka Barrage, which is designed to divert water into distributaries in eastern India to augment low dry season flows. The combined Ganges-Brahmaputra flow eastward for 120 km along the Padma reach where they meet the Meghna River. The Meghna drains the Shillong and Tripura hills in northeastern Bangladesh and contributes an additional mean annual water discharge of 2040 m^3/sec (COLEMAN, 1969).

SARIN *et al.* (1989, 1990) examined major ion chemistry of the Ganges and Brahmaputra rivers and calculated dissolved fluxes to the oceans. Their data show an average concentration of dissolved components of 178 mg/l in the Ganges and 100 mg/l in the Brahmaputra. The figures are relatively high compared to other major rivers—the Amazon is about 5 to 50 mg/l (GIBBS, 1972)—and are a result of chemical denudation rates 2 to 3 times higher than the world average (36 tons km^{-2} yr; HU *et al.*, 1982). SARIN *et al.* (1989) attribute this to high relief and heavy rainfall in the catchment area. Ganges water carries more Na^+, HCO_3^- and Cl^- than Brahmaputra water as a result of high concentrations of soil salts in the lowland reach. Together, the dissolved flux of the Ganges-Brahmaputra (~130 million tons) accounts for about 3% of the annual global riverine source of dissolved ions to the oceans.

Estimates of the discharge rate for particulates in the rivers vary by a factor of two as a result of measurement differences and interannual river variability. At approximately 50 km above the confluence, the Brahmaputra has a mean annual sediment discharge of 387 to 650 million tons (FAO, 1987b; HOSSAIN, 1992) and the Ganges ranges from 196 to 480 million tons (CBJET, 1991; HOSSAIN, 1992). Data for the Meghna is more scattered but COLEMAN (1969) reports a maximum annual mean of 20 million tons. Combined sediment discharge of most estimates is about 1 billion tons annually, placing the Ganges-Brahmaputra in the top three in the world (*e.g.* Amazon, Huangho; MILLIMAN and SYVITSKI, 1992). Sediment discharge figures are made far upstream of the river mouth to avoid tidal influence. Recent examination of downstream sediment discharge trends by BARUA *et al.* (in press) suggest that at least 17% of this sediment never reaches the ocean and is likely deposited on the lowland flood plain by overbank flooding.

Most of the sediment transported by the Ganges-Brahmaputra (80%) is silt and fine sand with little clay supplied by the young catchment area (COLEMAN, 1969). Suspended sediment concentrations are about 190–1,400 mg/l in the Ganges and 220–1,600 mg/l in the Brahmaputra (BARUA, 1990). Bed material is coarser in the braided Brahmaputra channel with a median grain size of 0.22 mm, compared to 0.12 mm in the Ganges (BARUA *et al.*, in press). The sand fraction of the Ganges and Brahmaputra river load is 31 to 78% quartz, 15 to 30% alkali and plagioclase feldspars, 5 to 30% micas, and 2 to 9% heavy minerals (BRAMMER, 1996). Mica percentage is higher in Ganges material and makes up as much as 80% of the silt fraction. SARIN *et al.* (1989) examined the clay mineral composition and found major differences between the lowland Ganges and Brahmaputra and their upland tributaries, which they attributed to differences in the regional geology of the lowland reach. Lowland Ganges averages are 42% smectite, 43% illite, 7% kaolinite, and 8% chlorite; the Brahmaputra averages 5, 61, 18, and 16%, respectively. The enrichment of smectite in the Ganges has been attributed to the weathering of basaltic traps in India by lowland tribu-

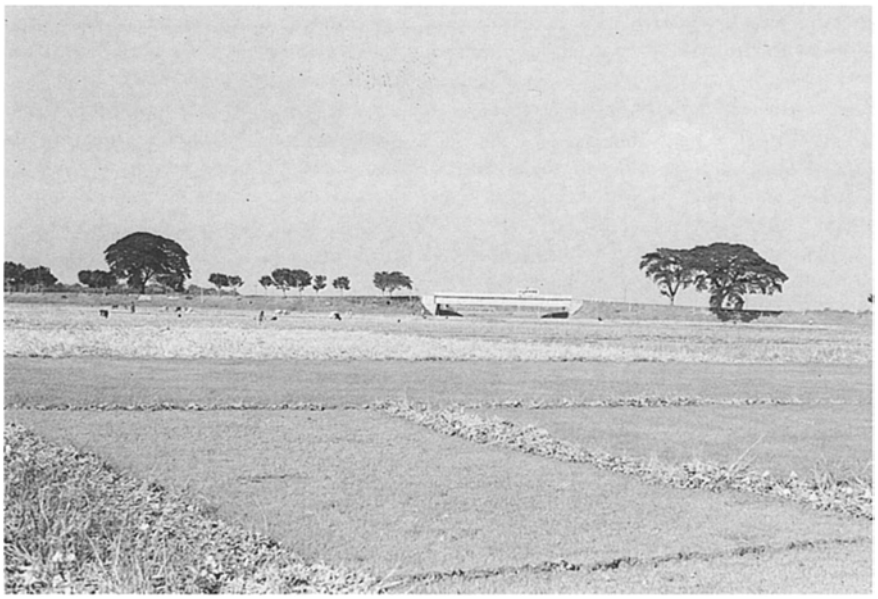

Figure 4. Characteristic lowland flood plain under cultivation near Tangail, Bangladesh. Farm plots are usually small (<200 m²) and worked by human labor and draft animals. The viaduct on the road embankment in the background (bus on viaduct for scale) was the only feature in the area above water level in the 1988 flood.

taries such as the Chambak, Betwa, and Ken (SUBBA RAO, 1964; SARIN *et al.*, 1989).

GANGES-BRAHMAPUTRA DELTA

Lowland Flood Plain

Two main subaerial facies are formed by delta progradation: the saline-influenced lower delta plain, and the generally higher-elevation and freshwater upper delta plain. In the "Mississippi model" of delta evolution, the upper delta plain is a complex network of well and poorly drained swamps, freshwater marshes, and lakes. The heavily cultivated lowland flood plains of Bangladesh (Figure 4) are the equivalent in the Ganges-Brahmaputra delta. Entering this 3 to 20 m elevation plain, the Ganges, Brahmaputra, and Meghna rivers and their distributaries have left a Holocene alluvial stratigraphy that averages 40 m in thickness (UMITSU, 1987, 1993). Strata are composed of overbank and crevasse splay facies cut by coarse channel sequences.

Channel morphology of the Ganges-Brahmaputra was examined in detail by COLEMAN (1969). The Brahmaputra in Bangladesh, known as the Jamuna reach below the Old Brahmaputra offtake (Figure 1), is a braided channel characterized by multiple thalwegs, numerous mid channel bars exposed at low flow (*e.g.* chars), and vegetated islands. Channel aggradation and char formation result from sediment loads that exceed the carrying capacity of the wide and shallow channel. The channel belt is subject to rapid lateral migration (up to 800 m/yr) and frequent, overlapping crevasses that build up a broad (100 to 1000 m wide) natural levee of silty sand on the channel margins. Other stretches of the channel belt are relatively stable "node points," one such area 40 km above the Ganges confluence is the site of the Jamuna Bridge, slated for completion in 1998–1999. The Jamuna Bridge will provide the first road link to the isolated northwest of Bangladesh. The Ganges in Bangladesh exhibits characteristics of a meandering river with a few braided reaches. Since 1780, the river has occupied and abandoned several large meander loops 70 km above the confluence at Hardinge Bridge (COLEMAN, 1969). Constructed early in the century, Hardinge Bridge remains the only road connection across the Ganges in Bangladesh.

Historical records indicate the Ganges-Brahmaputra is subject to periodic major avulsions in the lowland flood plain. Major Rennell's survey maps from the 1760's show the Brahmaputra flowing down a channel now known as the Old Brahmaputra (Figure 1) east of the Madhupur Tract, and joining the Meghna southeast of Dhaka. Avulsion into the present Jamuna channel west of the Madhupur Tract seems to have occurred gradually over a 30 yr period following a severe earthquake in 1782 and a major flood in 1787 (BRAMMER, 1996). Geomorphic evidence from aerial photos suggests the Brahmaputra successively occupied and abandoned at least three other channel belts to the northeast of the Old Brahmaputra course prior to that time (COLEMAN, 1969). The Ganges has been migrating toward the northwest in the last 250 years, perhaps in response to tectonic uplift in the west which has raised areas as much as 6 m above present flood levels (BRAMMER, 1996). Known as the moribund delta, this area south of the Ganges is crossed by a number of old, silted up distributaries (*e.g.* Hoogley, Gorai, Arial Khan) that remain connected to the Bay of Bengal. The Padma reach is also actively migrating; in the 1966 flood near Faridpur, the channel moved northward by 1.5 km, excavating a 30 m deep

channel (ISPAN, 1989). In Rennell's time, the Ganges and Brahmaputra had separate discharge points, with the Ganges flowing south of the present Padma course and entering the Bay of Bengal west of Bhola Island (Figure 2).

The upper delta plain of the Ganges-Brahmaputra has been divided into 17–20 distinct flood plains (ALAM et al. 1990). The quantity and characteristics of sediment received in these flood plains varies considerably with flooding characteristics of individual rivers, flood plain elevation, the presence of offtakes, local subsidence induced by groundwater withdrawal and sediment compaction, tectonic uplift and subsidence, and the presence of artificial embankments (ALLISON *et al.*, 1998). Flooding occurs during the monsoon season with average floods inundating about 20% of Bangladesh, while the extreme flood of 1988 inundated 46% (ISPAN, 1989). Much of the inundation, which in normal years can exceed 3 m in low-lying areas, is rainwater (*e.g.* non-turbid) flooding. Heavy rainfall in the delta in May-September coincides with high river levels caused by delivery of large volumes of water from upper catchment areas. High river levels elevate the water table and block drainage of rainwater. Turbid flooding is limited to areas proximal to river channels and is delivered to the flood plain by overbank flow and through secondary channel offtakes from the main channel.

ALLISON *et al.* (1998) presented the first quantitative sediment accumulation rates in the lowland flood plain utilizing ^{137}Cs geochronology. Their study of the east bank of the Jamuna flood plain (about 7% of the total lowland flood plain) showed strong correlation with distance from the main river channel and from secondary distributaries. Rates decreased from about 4 cm/yr adjacent to the natural levees to mm/yr in the distal flood plain. Satellite images suggest distal areas only experience turbid water inundation during extreme (1988-type) floods. GIS extrapolation of site data indicates an average of 23 million tons of Jamuna sediment is deposited annually in the region; supporting the BARUA *et al.* (in press) discharge study of downstream sediment discharge patterns that showed the lowland flood plains are a significant storage area for modern riverine sediment. A report on flood plain sedimentation by ISPAN (1993) demonstrated that soil type is closely allied to relative sediment accumulation rate. Older flood plains receiving limited riverine sediment today, such as along the Old Brahmaputra, for instance, have thick (>75 cm), organic-rich soils with original alluvial stratification destroyed by biological mixing. Soils are less well-developed and lower in organic content in "younger" flood plain areas proximal to the river. Duration and depth of annual flooding also has an effect on flood plain soil development (ISPAN, 1993).

Grain size in the flood plain is dominantly in the silt range, with an overall decrease in mean grain size away from the channel (COLEMAN, 1969; ALLISON *et al.*, 1998). Surface soils in inactive areas such as the Old Brahmaputra flood plain can be enriched in clay-sized material due to elevation-controlled sediment redistribution (BRAMMER, 1996). Permanently flooded water bodies (*e.g.* bils) can be observed in low-lying distal flood plains, and probably form by tectonic and compaction-induced subsidence.

The lowland flood plain of Bangladesh is one of the most densely populated regions on Earth, with the majority of the population living by subsistence farming. Per capita income averages about $150 per year. Bangladesh has 11.6 people per hectare of arable land compared to 1.3 in the United States (ISPAN, 1989). At present estimates of population growth indicate that figure will increase to 38.5 by the time the population reaches a stationary level in about 100 years (ISPAN, 1989). Introduction of modern high-yield rice hybrids, groundwater irrigation in the dry season, crop rotation, and food banking in recent years have averted widespread famine—the catastrophic famine of 1971 was the result of disruption of agriculture by the Independence War in Bangladesh—but these advances have had environmental costs. Large-scale groundwater withdrawal for land irrigation and drinking water, for instance, is likely to accelerate land subsidence, and recently has been identified as a source of widespread arsenic poisoning in Bangladesh, likely from Ar leached from aquifer sediments (K. ALAM, pers. comm.).

Increasing use of earthen and hardened artificial levees along river and distributary channels may have far-reaching consequences. Since the 1960's, a significant percentange of arable land in the flood plains has been walled off from river flooding by these embankments, and indirectly by the construction of raised roads. Virtually the entire west bank of the Jamuna, for example, is protected by a 5–6 meter high levee today. Bangladeshi culture has evolved many ingenious methods over hundreds of years, including raised villages, to cope with the effects of monsoonal floods. In other river deltas, the denial of river water and sediment has resulted in decreased soil fertility and the deleterious effects of reliance on chemical fertilizers, as well as land subsidence that increases saline intrusion and the damage caused by storm surges. Continued aggradation of high-load rivers, such as the Ganges-Brahmaputra, raises bed level, creating an expensive and potentially dangerous situation. Embankments will also influence many of the beneficial effects of the monsoon, including the wet season fishery, which contributes over 70% of the Bangladeshi animal protein intake, and which is the second largest export after jute, itself a flood-dependent crop (ISPAN, 1989). Fish stocks have declined in the main Ganges channel in recent years as a result of flood control and land use practices (NATARJAN, 1989). Political tension has also arisen because all of the river's upland tributaries lie outside Bangladesh and water supply to the delta plain is impacted by the tributary dams and water diversion projects intended for the benefit of other nations.

Lower Delta Plain

It is convenient to consider the lower (tidal) delta plain as two distinct regions, the Meghna estuary in eastern Bangladesh, which is the focus of modern Ganges-Brahmaputra discharge, and the Sunderbans mangrove forest in western Bangladesh and adjacent India (Figure 1). While the Holocene evolution of this region remains poorly understood, all available evidence indicates that maximum sea level transgression occurred at about 6,500 BP when the shoreline was 100 to 300 km inland of the present shoreline (VISHNU-MITTRE and GUPTA, 1970; BRAMMER and BRINKMAN, 1977; UMITSU, 1987; BANARJEE and SEN, 1988; UMITSU, 1993). The

Figure 5. Characteristic mangrove forest in the Sunderbans. Note the mangrove pneumatophores protruding above the sediment surface.

paleo-shoreline follows approximately the present 3 m elevation contour (Figure 1). Shoreline progradation and basin infilling by the Ganges, Brahmaputra, and Meghna rivers subsequent to this time accounts for ~30,000 km² of growth, comprising 30% of the modern delta plain.

As the focus of freshwater discharge and tidal energy, the Meghna estuary region is extremely dynamic, composed of migrating channels and islands of <2 m above sea level. West of about 90.5° E longitude, away from the active river discharge, islands have coalesced to form peninsulas separated by tidal channels. The islands and peninsulas are densely settled and cultivated. Sediments are sandy silts that below the cultivated horizon exhibit mm-scale tidal interlaminations of silt and micaceous fine sand (BRAMMER, 1996). In a comparative study of historical charts from the 18th to early 20th centuries with satellite imagery, ALLISON (1998) demonstrated that the Meghna estuary region is undergoing net land accretion at an average rate of 7.0 km²/yr since 1792 south of 22.9° N latitude (4.4 km²/yr since 1840). A comprehensive analysis of LANDSAT imagery by MARTIN and HART (1997) gave a figure of 16.4 km²/yr south of 23.1°N for 1973–1996, with significant interannual variation: the 1973–4 to 1979 period was marked by net erosion of 70 km²/yr. Over the last 200 yrs the Meghna estuary has evolved by seaward acoretion of the islands and their subaqueous shoal extensions by up to 50 km, and gradual welding of the landward end to the mainland to form peninsulas (ALLISON, 1998). The river mouth has also stepped eastward during this time by silting up and abandoning channels. A digitate peninsula morphology is present across the entire 380 km delta front shoreline, suggesting areas to the west of the Meghna estuary were formed in an older phase(s) of this process.

The eastern lower delta plain and adjacent coastal areas along the Chittagong coast have a population of over 20 million persons who make their living primarily by agriculture, fishing, and, increasingly, by shellfish aquiculture. Living near sea level, this population is extremely vulnerable to rising sea levels and to storm surges associated with tropical cyclones: the cyclones of 1970 and 1991 each killed 300,000–400,000 persons. The government of Bangladesh is addressing this issue by constructing a network of raised emergency shelters and by building earthen coastal embankments (*e.g.* polders). While scattered polders built by local landlords (Zamindars) have existed since at least the 17th century, beginning in 1965–1966 with the Coastal Embankment Project (CEP), the government has extended and improved the polder system in the eastern half of the lower delta plain and inland of the Sunderbans. The project and its successors had the twin goals of protection from cyclonic surges and reclamation of tidal wetlands for cultivation. Experimental cross-dams spanning small channels in the Meghna estuary and designed to stimulate land accretion were also tested in 1957 and 1964 by the Land Reclamation Poject (EYSINK, 1983). Within ten years of the inception of the CEP, problems with land flooding began as sluice gates in the polders were silted up by bed aggradation of adjoining channels. Over one million persons had been affected by 1997 with an estimated 114,000 hectares of year-round flooding (S. AMIN, pers. comm.). This problem is likely exacerbated by land subsidence induced by polder cutoff of tidal sediment supply to these areas.

Sundarbans National Park and adjacent areas in India are the largest mangrove forest on Earth (Figure 5). Total area of the forest today is approximately 5,993 km², of which 29% is tidal channels. At the advent of British rule in the 18th century, the forest was double its present extent, but Zamindars were allowed to reclaim much of the northern area (AHMED, 1968). The Sunderbans was first declared a reserved forest in 1875 as a refuge for the Bengal Tiger (*Pan-*

thera tigris) and other endangered species. Over 60% of the forest is composed of two mangrove species, Sundri (*Heritiera fomes*) and Gewa (*Excoecaria agallocha*), with a decrease in species diversity in the more saline southern region (ISLAM and KHAN, 1988). Sediments in the forest are relatively organic-poor (*e.g.* non peaty) clayey to sandy silts exhibiting mm-scale tidal lamination below the biologically mixed horizon. The forest floor exhibits a microtopography of elevations from 0.9 to 2.1 m above mean sea level (KATEBI and HABIB, 1989). Although the entire region is affected by tides, saline penetration varies seasonally, reaching a maximum of 100 km inland during the dry season. It is unknown to what extent sediment is supplied to the Sunderbans either from Ganges distributaries or from the marine side, although SEGALL and KUEHL (1992) report high smectite clay concentrations at the mouth of these distributaries that they attribute to a Ganges origin.

The Sunderbans is a managed forest where an estimated 350,000 people earn a livelihood as wood cutters, fisherman, and honey gatherers through a system of auctions and licences (JALAL, 1989). The most serious environmental threat to the forest today is increased saline intrusion. In the 1930's, sporadic mortality of Sundri trees was noted by a process known as "top-dying" (KHAN *et al.*, 1990). By 1970, timber loss was estimated at 1.44 million m^3 and harvesting of Sundri was halted for a time (SHAFI, 1982). Although the ultimate cause of top-dying of Sundri is a fungal cankar (*Botryoshaeria ribis*), it is associated with increased soil salinity (CHAFFEY *et al.*, 1985) related to siltation of the Ganges distributaries that provide freshwater runoff to the Sunderbans. To what extent this process is natural, caused by shifting of the Ganges discharge eastward, or has been accelerated by dry season water withdrawal upstream at the Farrakka Barrage, remains a subject of debate. ALLISON (1998) documents net erosion of the Sunderbans shoreline, increasing to the west, where 3 to 4 km of retreat have occurred since 1840. The alongshore difference in erosion rates suggest the western Sunderbans is sediment-starved, either by eastward migration of the river mouths or by decreased Ganges sediment delivery via the local distributaries. Whatever the case, shoreline erosion and saline intrusion may also be compounded by regional subsidence (tectonic and compaction) process.

Continental Shelf

The Bengal continental shelf seaward of the Ganges-Brahmaputra delta plain is an important fishery for Bangladesh, with the bulk of this fish and shrimp resource (75%) exploited by small-scale, non-mechanized operations that involve some 200,000 persons (JALAL, 1989). Petroleum exploration is in an embryonic stage on the Bengal shelf at present compared with other deltas of the world, but is a potential economic boon of the future to Bangladesh and India.

The subaqueous component of the Ganges-Brahmaputra delta resembles other large river systems entering an energetic continental shelf environment. KUEHL *et al.* (1989) first identified a mud clinoform on the Bengal shelf, similar to those previously discovered on the continental shelf adjacent to the Amazon (NITTROUER *et al.*, 1986), Huangho (ALEXANDER *et al.*, 1991) and Fly (HARRIS *et al.*, 1993). Topset beds in less than 30 m water depth dip gently (0.036°) and diverge offshore (KUEHL *et al.*, 1997). Surface sediments are sandy silts (2–6 phi mean diameter) that landward of the 15 m isobath are tidally laminated (KUEHL *et al.*, 1989; SEGALL and KUEHL, 1994). Discontinuous ephemeral mud layers 2 to 3 m thick overlie the coarser-grained surface; SEGALL and KUEHL (1992) suggest these muds may buildup during successive high discharge periods for the 3 to 5 years on average between cyclones. Historical charts show that a lobate apron has formed from the coalescence of island shoal extensions off the Meghna estuary mouth in 8 to 15 m water depths (ALLISON, 1998). Progradation of a coarse-grained subaerial delta front clinoform over the subaqueous mud clinoform is a characteristic that is absent in the clay-rich Amazon and Fly systems.

On the middle shelf (30–60 m), more steeply dipping (0.19°) foreset beds form the thickest (40–60 m) part of the subaqueous delta (KUEHL *et al.*, 1997). Rapid sediment accumulation (up to 9 cm/yr; KUEHL et al., 1989) of fine to medium silts (mean grain size 7–8.5 phi) is characteristic of the foreset region. Further offshore (>60 m), the modern sediment wedge thins seaward into gently dipping (0.022°) bottomset muds over an erosional surface that is likely the Pleistocene lowstand surface (KUEHL *et al.*, 1997). Evidence of growth faults, slumps, and mass wasting near the head of Swatch of No Ground submarine canyon, which incises the shelf to about the 20 m isobath, suggest that the canyon is intercepting deltaic sediment transported alongshore to the west, funnelling a fraction of this material to the deep sea (KUEHL *et al.*, 1997). Studies of clay mineralogy on the Bangladesh and Indian shelves indicate that the canyon acts as a barrier to the transport of Ganges-Brahmaputra sediment to the Indian shelf (SEGALL and KUEHL, 1992).

CONCLUSION

In the new millenium, the Ganges-Brahmaptra delta faces a number of environmental issues stemming from habitat modification and rapid population growth. Among these are rising sea level and saline intrusion, water rights, inland and offshore fish stocks, flood control, soil fertility, water-borne pollutants, and river channel migration. A number of poorly understood geological processes need to be better studied to allow informed decision-making on these environmental issues. Among these are:

(1) The quantities and processes of river sediment supply to the lowland flood plain, lower delta plain, and marine end-member.

(2) The character of river sediment supply to the lowland flood plains and its contribution to soil fertility.

(3) The regional pattern and rates of tectonic and sediment compaction-induced subsidence and uplift in the delta plain.

(4) The Holocene evolution of the delta plain-subaqueous delta since maximum sea level transgression at 6,500 yBP.

LITERATURE CITED

ALAM, M.K.; HASAN, A.K.M.S.; KHAN, M.R., and WHITNEY, J.W., 1990. *Geological Map of Bangladesh*. Geological Survey of Bangladesh.

ALEXANDER, C.R.; DEMASTER, D.J., and NITTROUER, C.A., 1991. Sediment accumulation in a modern epicontinental-shelf setting: The Yellow Sea. *Marine Geology,* 98, 51–72.

ALLISON, M.A., 1998. Historical changes in the Ganges-Brahmaputra delta front. *Journal of Coastal Research,* 14(4).

ALLISON, M.A.; KUEHL, S.A.; MARTIN, T.C., and HASSAN, A., 1998. Importance of flood-plain sedimentation for river sediment budgets and terrigenous input to the oceans: insights from the Brahmaputra-Jamuna River. *Geology,* 26, 175–178.

AMHED, N., 1968. *An Economic Geography of East Pakistan.* Oxford University Press, London, 210p.

BANERJEE, M. and SEN, P.K., 1988. Paleobiology and environment of deposition of Holocene sediments of the Bengal Basin, India. *In: Palaeoenvironment of East Asia from the mid-Tertiary: Proceedings of the Second Conference.* Hong Kong, Centre of Asian Studies, University of Hong Kong, pp. 703–731.

BARUA, D.K., 1990. Suspended sediment movement in the estuary of the Ganges- Brahmaputra-Meghna River system. *Marine Geology,* 91, 243–253.

BARUA, D.K.; KUEHL, S.A.; MILLER, R.L., and MOORE, W.S., 1994. Suspended sediment distribution and residual transport in the coastal ocean off the Ganges-Brahmaputra river mouth. *Marine Geology,* 120, 41–61.

BARUA, D.K.; MARTIN, T.C.; HASSAN, A.; MAHMOOD, S., and KUEHL, S.A., in press. Suspended sediment transport through the Ganges-Brahmaputra fluvial system: implications for floodplain sedimentation and sediment delivery to the ocean. *Sedimentology.*

BITWA (Bangladesh Inland Water Transport Authority), 1987. Bangladesh Tide Tables. BITWA, Dhaka, 151p.

BRAMMER, H.B., 1996. *The Geography of the Soils of Bangladesh.* University Press Limited, Dhaka, Bangladesh, 287p.

BRAMMER, H.B. and BRINKMAN, R., 1977. Surface-water gley soils in Bangladesh: environment, landforms, and soil morphology. *Geoderma,* 17, 91–109.

CBJET (China-Bangladesh Joint Expert Team), 1991. *Study Report on Flood Control and River Training Project on the Brahmaputra River in Bangladesh. Vol. 1: Analysis of Hydrology and River Morphology of the Brahmaputra River,* Dhaka, Bangladesh.

CHAFFEY, D.R.; MILLER, F.R., and SANDOM, J.H., 1985. *A Forest Inventory of the Sunderbans, Bangladesh.* Overseas Development Administration Main Report. Overseas Development Administration, Dhaka, 196p.

COATES, D.A., 1990. The Mymensingh Terrace: evidence of Holocene deformation in the delta of the Brahmaputra River, central Bangladesh. *Geological Society of America Bulletin Abstracts with Programs,* 22, 310.

COATES, D.A.; WHITNEY, J.W., and ALAM, A.K.M., 1988. Evidence of neotectonic activity on the Bengal delta, Bangladesh. *Geological Society. of America Bulletin Abstracts with Programs,* 20, 54.

COLEMAN, J.M., 1969. Brahmaputra River: channel processes and sedimentation. *Sedimentary Geology,* 3, 129–239.

CURRAY, J.R.; EMMEL, F.J.; MOORE, D.G., and RAITT, R.W., 1982. Structure, tectonics and geological history of the northern Indian Ocean. *In:* A.E. Nairn and F.G., Stehli (Editors)*: The Ocean Basins and Margins.* New York: Plenum, 6, pp. 107–112.

EGIS (Environment and GIS Support Project for Water Sector Planning), 1997. *Morphological dynamics of the Brahmaputra-Jamuna River.* Environment and GIS Support Project for Water Sector Planning, Dhaka, Bangladesh, 76p.

EMERY, K.O. and AUBREY, D.G., 1989. Tide gauges of India. *Journal of Coastal Research,* 5, 489–501.

EYSINK, W.D., 1983. *Basic Considerations on the Morphology and Land Accretion Potentials in the Etuary of the Lower Meghna River.* Bangladesh Water Development Board Land Reclamation Project, Technical Report No. 15. Chittagong, Bangladesh, 85p.

FAO (United Nations Food and Agricultural Organization). 1987. *Geology of Bangladesh.* Master Plan Organization, Ministry of Irrigation, Water Development and Flood Control, Bangladesh. MPO-UNDP-IBRD Technical Report No. 4, 169pp.

FAO (United Nations Food and Agricultural Organization). 1987b. *Floods and Storms.* Master Plan Organization, Ministry of Irrigation, Water Development and Flood Control, Bangladesh. MPO-UNDP-IBRD Technical Report No. 11, 305pp.

GIBBS, R.J., 1972. Water chemistry of the Amazon River. *Geochemica Cosmochemica Acta,* 36, 1061–1066.

HARRIS, P.T.; BAKER, E.K.; COLE, A.R., and SHORT, S.A., 1993. A preliminary study of sedimentation in the tidally dominated Fly River Delta, Gulf of Papua. *Continental Shelf Research,* 13, 441–472.

HOSSAIN, M.M., 1992. *Total Sediment Load in the Lower Ganges and Jamuna.* Bangladesh University of Engineering and Technology Internal Report, Dhaka, 15p.

HU, M.; STALLARD, R.F., and EDMOND, J.M., 1982. Major ion chemistries of some large Chinese rivers. *Nature,* 298, 550–553.

IMAM, M.B. and SHAW, H.F., 1985. The diagenesis of Neogene clastic sediments from the Bengal Basin, Bangladesh. *Journal of Sedimentary Petrology,* 55, 665–671.

ISLAM, M.J. and KHAN, F.A., 1988. Timber volume inventory. *UNDP/UNESCO Mangrove Ecosystems Occasional Papers,* No. 2., United Nations Development Program, New Delhi, 31p.

ISPAN (Irrigation Support Project for Asia and the Near East), 1989. *Eastern Waters Study.* U.S. Agency for International Development, 83p.

ISPAN (Irrigation Support Project for Asia and the Near East), 1993. *A Study of Sedimentation in the Brahmaputra-Jamuna Floodplain.* Bangladesh Ministry of Water Resources, Dhaka, 133p.

JALAL, K.F., 1989. Towards a national strategy on coastal resource management in Bangladesh. *In: Coastal Area Resource Development and Management, Part II.* Coastal Area Resource Development and Management Association, Dhaka, pp. 67–78.

JOHNSON, S.Y. and ALAM, A.M.N., 1991. Sedimentation and tectonics of the Sylhet trough, Bangladesh. *Geological. Society of America Bulletin,* 103, 1513–1527.

KATEBI, M.N.A. and HABIB, G., 1989. Sunderbans and forestry. In: *Coastal Area Resource Development and Management, Part II.* Coastal Area Resource Development and Management Association, Dhaka, pp. 79–100.

KHAN, F.A.; CHOUDHURY, A.M., and ISLAM, M.J., 1990. Timber volume inventory in the Sunderbans using aerial photography and other remote sensing techniques. *UNDP/UNESCO Mangrove Ecosystems Occasional Papers,* No. 9, United Nations Development Program, New Delhi, 21p.

KUEHL, S.A.; HARIU, T.M., and MOORE, W.S., 1989. Shelf sedimentation off the Ganges- Brahmaputra river system: evidence for sediment bypassing to the Bengal Fan. *Geology,* 17, 1132–1135.

KUEHL, S.A.; LEVY, B.M.; MOORE, W.S., and ALLISON, M.A., 1997. Subaqueous delta of the Ganges-Brahmaputra river system. *Marine Geology,* 144, 81–96.

MARTIN, T.C. and HART, T.C. 1997. *Time Series Analysis of Erosion and Accretion in the Meghna Estuary.* Meghna Estuary Study Internal Report, Bangladesh Ministry of Water Resources, Dhaka, 20p.

MILLIMAN, J.D. and MEADE, R.H., 1983. World-wide delivery of river sediments to the oceans. *Journal of Geology,* 91, 1–22.

MILLIMAN, J.D. and SYVITSKI, J.P.M., 1992. Geomorphic/Tectonic control of sediment discharge to the ocean: the importance of small mountainous rivers. *Journal of Geology,* 100, 525–544.

MORGAN, J.P. and MCINTIRE, W.G., 1959. Quaternary geology of the Bengal Basin, East Pakistan and India. *Geological Society of America Bulletin,* 70, 319–342.

MURTY, T.S.; FLATHERS, R.A., and HENRY, R.F., 1986. The storm surge in the bay of Bengal. *Progress in Oceanography,* 16, 195–233.

NATARAJAN, A.V., 1989. Environmental impact of Ganga Basin development on gene-pool and fisheries of the Ganga River system. *In:* D.P. Dodge (editor): *Proceedings of the International Large River Symposium.* Can. Spec. Publ. Fish. Aquat. Sci., 106, 545–559.

NEI (Netherlands Economic Institute), 1978. *Chittagong Port Entrance Study: Hydrologic and Hydrographic Survey,* Netherlands Economic Institute, 362p.

NITTROUER, C.A.; KUEHL, S.A.; DEMASTER, D.J., and KOWSMANN, R.O., 1986. The deltaic nature of Amazon shelf sedimentation. *Geological Society of America Bulletin,* 97, 444–458.

PAUL, D.D. and LIAN, H.M., 1975. Offshore Tertiary basins of southeast Asia: Bay of Bengal to South China Sea. *9th World Petroleum Congress,* 3, 107–121.

RENNELL, J., 1781. An account of the Ganges and Burrampooter Rivers. *Philosophical. Transactions of the Royal Society of London,* 71, 87–114.

SARIN, M.M.; KRISHNASWAMI, S.; DILLI, K.; SOMAYAJULU, B.L.K., and MOORE, W.S., 1989. Major ion chemistry of the Ganges-Brahmaputra river system: weathering processes and fluxes to the Bay of Bengal. *Geochemica Cosmochemica Acta,* 53, 997–1009.

SARIN, M.M.; KRISHNASWAMI, S.; SOMAYAJULU, B.L.K., and MOORE, W.S., 1990. Chemistry of uranium, thorium, and radium isotopes in the Ganges-Brahmaputra river system: weathering processes and fluxes to the Bay of Bengal. *Geochemica Cosmochemica Acta,* 54, 1387–1396.

SEGALL, M.P. and KUEHL, S.A., 1992. Sedimentary processes on the Bengal continental shelf as revealed by clay mineralogy. *Continental. Shelf Research,* 12, 517–541.

SEGALL, M.P. and KUEHL, S.A., 1994. Sedimentary structures on the Bengal shelf: a multi-scale approach to sedimentary fabric interpretation. *Sedimentary Geology,* 93, 165–180.

SENGUPTA, S. 1966. Geological and geophysical studies in the western part of the Bengal Basin, India. *American Association of Petroleum Geologists Bulletin,* 50, 1001–1017.

SHAFI, M., 1982. Adverse effect of Farrakka on the forest of south west region of Bangladesh- (Sunderbans). *In: Proceeding of the Second Bangladesh National Conference on Forestry,* Dhaka, p. 30–45.

SHETYI, S.R.; GOUVEIA, A.D.; SHANKAR, D.; SHENOI, S.S.C.; VINAYACHANDRAN, P.N.; SUNDAR, D.; MICHAEL, G.S., and NAMPOOTHIRI, G., 1996. Hydrography and circulation in the western Bay of Bengal during the northeast monsoon. *Journal of Geophysical Research,* 101(C6), 14011–14025.

SUBBA RAO, M., 1964. Some aspects of continental shelf sediments off the east coast of India. *Marine Geology,* 1, 59–87.

UMITSU, M., 1987. Late Quaternary sedimentary environment and landform evolution in the Bengal Lowland. *Geographical Review of Japan, Series B.,* 60, 164–178.

UMITSU, M., 1993. Late Quaternary sedimentary environments and landforms in the Ganges Delta. *Sedimentary Geology,* 83, 177–186.

VISHNU-MITTRE, S. and GUPTA, H.P., 1970. Pollen analytical study of Quaternary deposits in the Bengal Basin. *Paleobotanist,* 19, 297–306.

Annex B61

Mead A. Allison, "Historical Changes in the Ganges-Brahmaputra Delta Front", *Journal of Coastal Research*, Vol. 14, No. 4 (1998)

Journal of Coastal Research	14	4	1269–1275	Royal Palm Beach, Florida	Fall 1998

Historical Changes in the Ganges-Brahmaputra Delta Front

M. A. Allison

Department of Oceanography
Texas A&M University
5007 Avenue U.
Galveston, TX 77551, U.S.A.

ABSTRACT

ALLISON, M.A., 1997. Historical Changes in the Ganges-Brahmaputra Delta Front. *Journal of Coastal Research*, 14(4), 1269–1275. Royal Palm Beach (Florida), ISSN 0749-0208.

Detailed early chartmaking by the British East India Company and the Royal Navy in India and present-day Bangladesh provide one of the most accurate databases available to track the evolution of a major delta front over the last 200 years. Digital databases of shoreline position and shallow bathymetry of the Ganges-Brahmaputra delta front were constructed using geo-referenced and projection-corrected early and modern charts, and using LANDSAT imagery. In contrast with earlier published studies, these databases indicate the Ganges-Brahmaputra has an actively prograding subaerial delta: an average of approximately 7.0 km²/yr of new land have accreted in the river mouth region since 1792. Digitate shoals, forming in association with accretion of elongate islands in the river mouth region, are coalescing in 8–15 m water depth to form a relatively coarse-grained lobate feature that is prograding over the muddy, subaqueous delta on the inner shelf. The morphology of shoal growth suggests the Ganges-Brahmaputra mouth has evolved eastward over the late Holocene as a series of digitate shoal-channel complexes. West of the active river mouth in historical times, the delta front is sediment starved and is undergoing retreat at rates of about 1.9 km²/yr.

ADDITIONAL INDEX WORDS: Ganges-Brahmaputra Delta, shoreline change, deltaic sedimentation, coastal subsidence, Bangladesh, India.

INTRODUCTION

The Ganges-Brahmaputra River is one of the three largest riverine sources of water and sediment to the world ocean; 1.06 billion tons/yr according to Milliman and Syvitski (1992). The Ganges and Brahmaputra rivers are young, sediment-rich rivers that drain the Himalayan highlands, and, joining with the Meghna River in Bangladesh, enter the Bay of Bengal through several distributary channels (Figure 1). Sediment and water discharge peaks during the May-November monsoon season. The delta front of the Ganges-Brahmaputra is strongly dominated by tidal processes: tides are semi-diurnal with a range of up to 4 m, and generate shore-normal tidal currents up to 300 cm/sec (BARUA *et al.*, 1994). BARUA (1990) notes that during periods of low river discharge, the eastern distributary channels (Hatia and Sandwip) serve as flood channels, while net seaward water transport occurs in the Tetulia and Shahbazpur channels to the west (see Figure 2).

Approximately 85% of Bangladesh is underlain by the deltaic and alluvial deposits of these rivers (ALAM *et al.*, 1990; UMITSU, 1990), which have formed the 5–15-km-thick Bengal Basin (CURRAY *et al.*, 1982) since the early Tertiary. A majority of the tidally influenced zone (Figure 1) of the delta is less than 3 m above mean sea level (MSL), with other areas of Holocene alluvium generally less than +15 MSL. The Madhupur tract in central Bangladesh (Figure 1) is a highly-weathered Pleistocene clay uplifted to +10–30 MSL that separates the 18th century Old Brahmaputra channel from the modern (Jamuna) channel of the Brahmaputra.

Research has shown that other large, energetic river mouths, such as the Amazon (NITTROUER *et al.*, 1986; KUEHL *et al.*, 1986), Huangho (ALEXANDER *et al.*, 1991), and Fly (HARRIS *et al.*, 1993) exhibit delta growth in the form of a subaqueous mud clinoform on the continental shelf. It is believed that tidal focusing and wave-induced seabed reworking inhibit sediment accumulation in the river mouth region, preventing formation of a "Mississippi-model" subaerial delta (NITTROUER *et al.*, 1986). This produces a throat-shaped river mouth containing sandy shoals and islands. Recent studies by KUEHL *et al.* (1989, in press) have identified a subaqueous mud delta on the inner shelf off the Ganges-Brahmaputra River mouths. Sedimentation rates on the foreset beds of this feature reach 9 cm/yr in some areas (KUEHL *et al.*, 1989). EYSINK (1983) published evidence, based on a comparison of early (1770's-1780's) maps of the British geographer James Rennell, that while the location of channels and shoal islands in the river mouth area is extremely dynamic, little or no net shoreline progradation has occurred in the last 200 years. Rennell's data led COLEMAN (1969) and EYSINK (1983) to suggest that loss offshore from the strong tidal currents, combined with regional subsidence in the Bengal Basin, offset the large sediment input at the river mouth. Modern texts (FRIEDMAN *et al.*, 1992; p. 478) now suggest the Ganges-Brahmaputra mouth region is an estuary, without a subaerial deltaic component.

96157 received 29 December 1996; accepted in revision 22 April 1997.

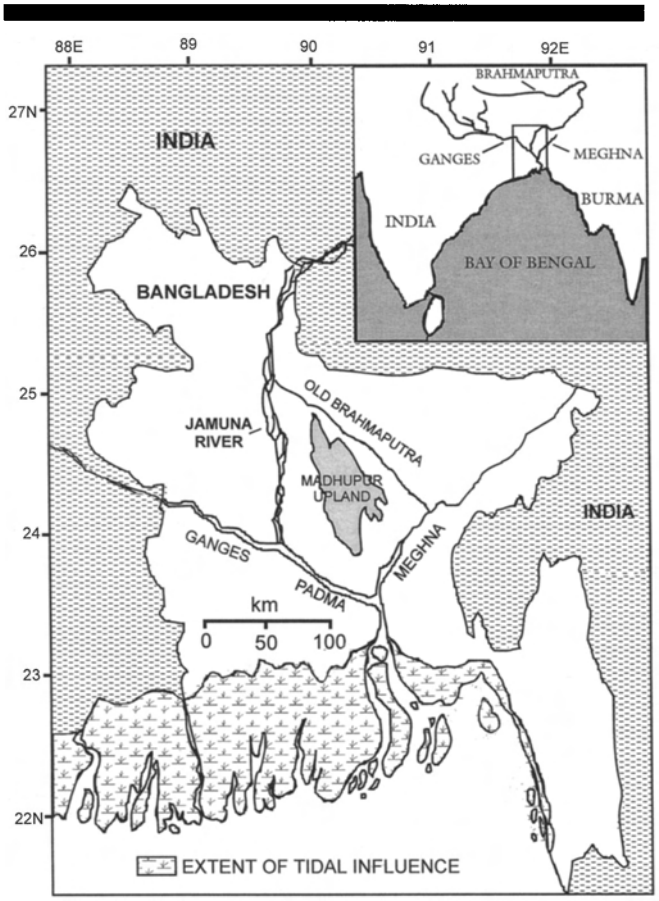

Figure 1. Map of the study area.

While saline penetration occurs in the distributary mouths of the river during low discharge periods (BARUA, 1990), several lines of evidence suggest the description of the Ganges-Brahmaputra mouth as an estuary should be reevaluated. Unlike tropical rivers like the Amazon and Fly, which carry about 70% clay, the Ganges-Brahmaputra is a relatively coarse-grained system, with a sediment load composed of 80% silt and sand (COLEMAN, 1969). In addition, the Ganges-Brahmaputra is the only major river mouth classified as an "estuary" that has a high mean suspended sediment load (1,799 mg/l; LISITZEN, 1972). Detailed chartmaking of the Bay of Bengal conducted by the British East India Company and the Royal Navy in the 18th and 19th centuries was not utilized by EYSINK (1983) in concluding that there has been no shoreline progradation in historical times. The present study was undertaken to evaluate these additional historical sources, and to apply modern image processing and GIS technology to the study of processes in the Ganges-Brahmaputra river mouth. The objective of this paper is to reexamine the question of whether the Ganges-Brahmaputra River has a subaerial deltaic component in order to gain insight into the process of delta formation in energetic river mouths.

MAP GENERATION

Early maps and charts utilized in the present study were obtained as full-size microphotographic transfers from the Map Room and India Office of the British Library. Shoreline geometries for 1792, 1840, and 1904/8 were created using LACAM (1794), LLOYD (1840), and ADMIRALTY (1904;1908), respectively. A LANDSAT mosaic of images from 1984 was used to obtain modern shoreline boundaries. In addition to shoreline position, the 1837–1840 survey of the delta front by Commander Lloyd of the Royal Navy (LLOYD, 1840) includes over 10,000 soundings taken at quarter-fathom intervals in water depths of less than 50 m. This information was compared with modern charts (DMA, 1990) to examine bathymetric changes along the Ganges-Brahmaputra delta front.

Chart information was digitized and georeferenced on MAPINFO© software using a series of fixed points (*i.e.*, city locations, surveyed benchmarks). Charts from 1792 and 1840 required a longitude correction to compensate for systematic errors in early benchmark surveys. All maps/charts were geocorrected to a standard Mercator projection. LANDSAT images were georeferenced using PCI© image analysis software. The VERTICAL MAPPER© module in MAPINFO was used to calculate area changes between map sets.

RESULTS

Shoreline Change

Table 1 demonstrates that the river mouth region of the Ganges-Brahmaputra delta front east of the Haringhata River (Figure 2, 4) has experienced net land accretion between 1792 and 1984 that averages 7.0 km²/yr. Comparison of the 1792 and 1840 surveys suggest an even more rapid land accretion rate (14.8 km²yr). However, the large longitude correction and small scale (1:850,000) indicate a relatively large error associated with the 1792 survey. Using Commander Lloyd's more reliable data from 1840 (plotted in Figure 3), gives an average accretion rate of 4.4 km²/yr. The 1904 survey of the eastern part of the delta is an exception to the overall trend of net land accretion. Although not listed on the 1904 chart, it is evident from the digital overlays that some of the 1904 shorelines are identical with 1840, and hence, are older data plotted for areas not remapped in the 1904 survey. This problem was not observed in the 1908 survey of the western delta (west of the Haringhata River).

West of the Haringhata River and away from the active river mouths, the delta front is undergoing net land loss. Erosion rates of the islands and peninsulas that form the western delta front are progressive over the period (1792–1984); land loss over this area averages 1.9 km²/yr. Land loss increases to the west (Figure 3); seaward-facing shorelines adjacent to the east bank of the Hoogly River in India have retreated as much as 3–4 km since 1840. Large tidal channels that extend inland have experienced considerable migration (Figure 3), but show no evidence of net infilling or widening. However, minor tidal channels are only plotted in the early data to about 30 km inland from the sea face of the delta, and, hence, any net effect of their growth or silting up is unknown.

Bathymetric Change

Table 2 displays the volume gain or loss in seabed elevation in the river mouth region (Figure 3,4) and in the extreme

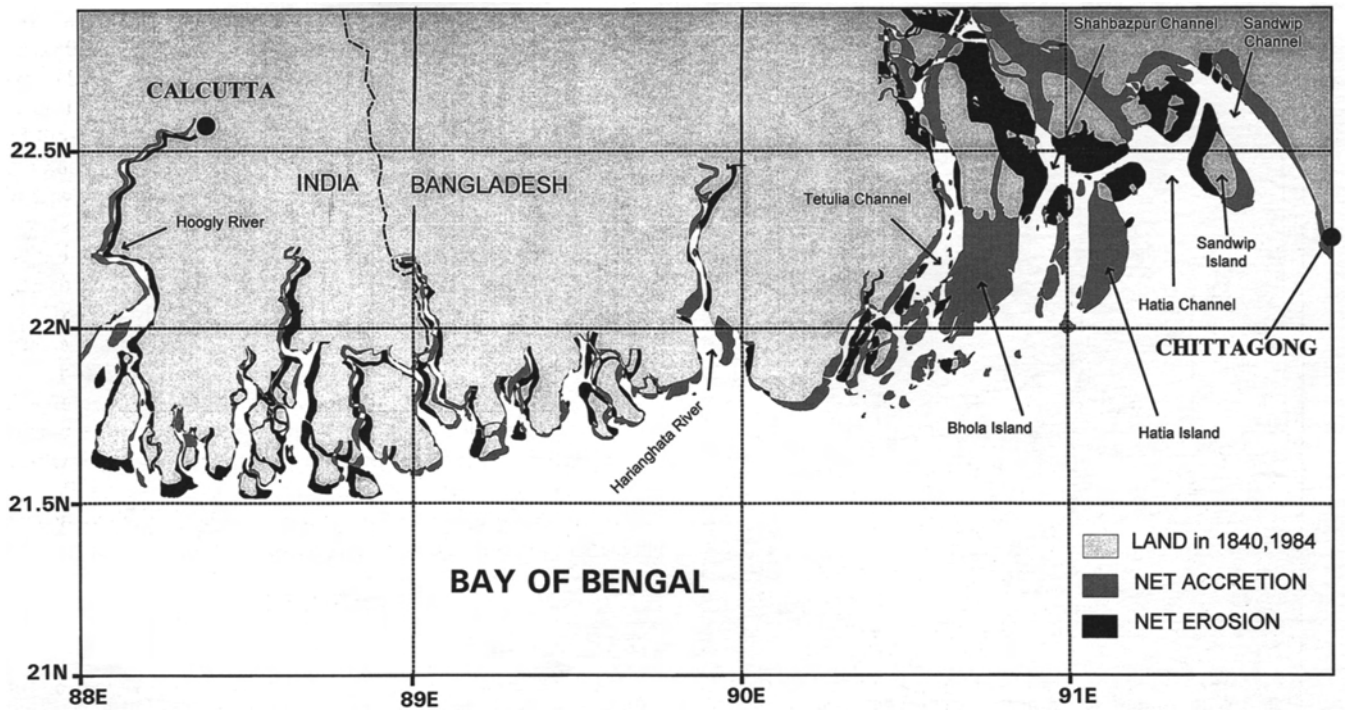

Figure 2. Map overlay of shoreline positions from the Lloyd survey in 1840 and a 1984 LANDSAT mosaic showing land accretion and erosion occurring in the intervening 144 years. Note the concentration of accretion in the area of the present mouths of the Ganges-Brahmaputra (90–92°E), and the net erosion in the older, sediment starved deltaic deposits to the west. Comparison extends inland along distributary channels to the limit of the 1840 survey. Modern surveys show that the tidal channel network continues further inland and several old distributaries (*e.g.*, the Hoogly) remain connected to the Ganges or Padma River channels.

western delta (Figure 4) between 1840 and 1990. The central delta front region is not included in these calculations because these areas were not remapped in the 1990 survey. Each depth interval between isobaths in Table 2 reflects a 1990 region where changes (either higher or lower elevation) from the 1840 bathymetry are recorded as volumes and averaged for the entire region. These regions are then averaged overall to provide a net value of volume change in areas of less than 50 m water depth (40 m in the western delta). Land areas are assumed to be 2 m above mean sea level for the calculations. This methodology does not differentiate between bathymetric changes caused by seabed accretion/erosion from changes induced by regional subsidence/uplift.

Table 1. *Shoreline land area change of the delta front between 1792 and 1984.*

Date	River Mouth Area (km²)	Western Delta Area (km²)
1792	5,122.4	5,500.0
1840	5,830.7	5,359.1
1904/8	5,447.3**	5,255.4
1984	6,468.3	5,131.9
Total (1792–1984)	**+1,345.9**	**−368.1**

**May reflect reuse of 1840 data in some areas

DISCUSSION

Pathways of River Sediment Dispersal

Comparison of historical and modern data for shorelines and shallow bathymetry demonstrate the progressive growth of a deltaic feature at the mouths of the Ganges-Brahmaputra River in Bangladesh. These results contradict the EYSINK (1983) study. This is attributed to the inaccuracy of the earliest surveys used by Eysink, as well as difficulties in georeferencing maps possessing different projections without modern computer tools. EYSINK (1983) does note that Survey of Pakistan maps of the river mouth region in 1940 and 1963 show net shoreline progradation that averages 12.1 km²/yr; in relative agreement with the 7.0 km²/yr since 1792 observed in the present study considering the nature of the data and the probable interannual variations in river sediment supply and marine reworking (*i.e.*, as by cyclones). The Eysink total also includes areas further upriver, beyond the boundaries of the historical datasets utilized in the present study. Significantly, UMITSU (1990) places the maximum sea level transgression on the delta front at 6.5–7 ka. Comparing this paleoshoreline with the modern indicates about 30,000–35,000 km² of shoreline progradation, an average of 4–5 km²/yr; in close agreement with the most reliable data from the Lloyd survey (4.4 km²/yr).

Considering only the more reliable data from LLOYD (1840)

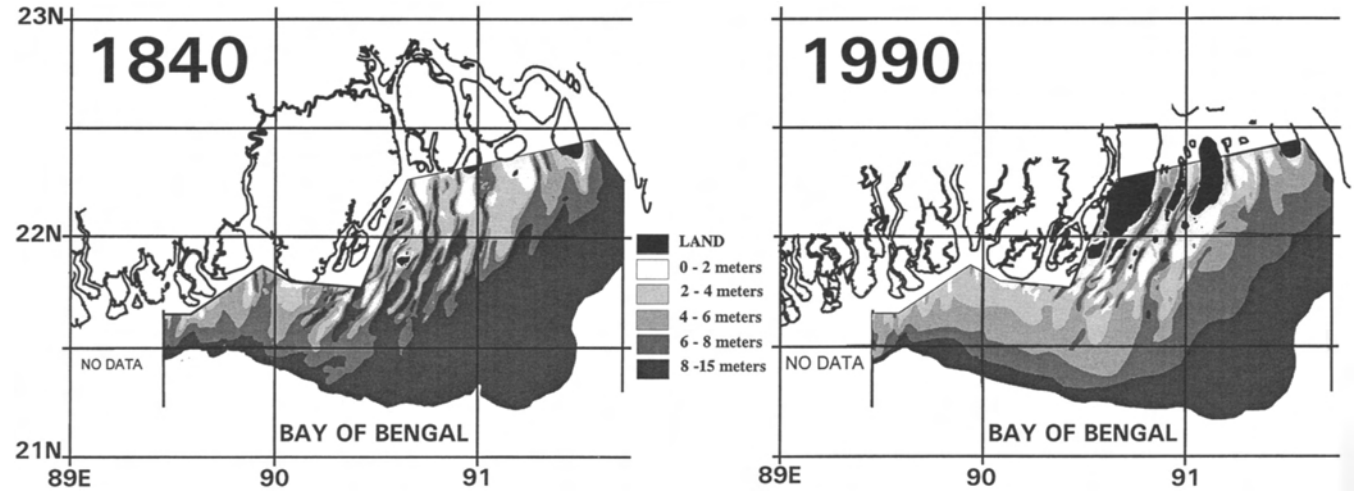

Figure 3. Bathymetry of the delta front in the area of the Ganges-Brahmaputra River mouths from the Lloyd survey in 1840 and from Defense Mapping Agency charts (1990). Within the study box (12,530 km^2), islands and their associated subaqueous shoals have accreted seaward as much as 50 km during the period. The 6–8 m isobaths also demonstrate that individual digitate shoals are coalescing offshore to form a lobate feature of coarse grained material on the inner shelf.

in Table 1 and 2, and assuming an average land elevation change from MSL to +2 m, an estimated 9.7×10^6 tons of annual land accretion (at a sediment density of 1100 kg/m^3) occurs in the river mouth region (*i.e.*, east of the Haringhata River). This first-order estimate serves to illustrate that only 1–2% of the annual sediment Ganges-Brahmaputra sediment discharge is necessary to account for observed land accretion rates. West of the Haringhata to the mouth of the Hoogly River in India, there has been net shoreline erosion since 1840, equivalent to an annual release of 3.5×10^6 tons of sediment. These areas, distal to the present river sediment point source, are probably eroding in response to eustatic and

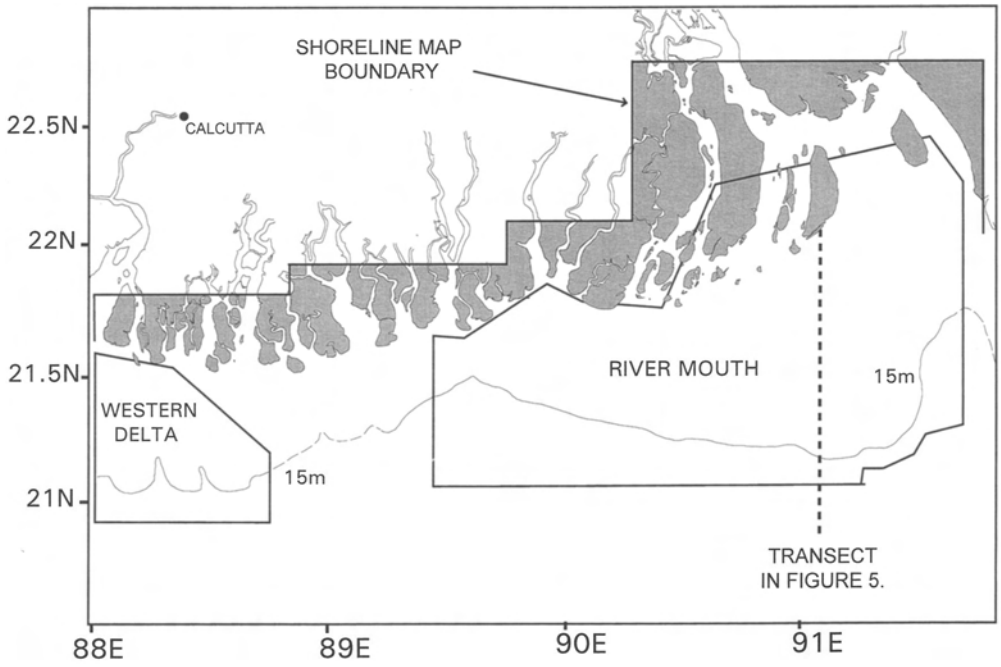

Figure 4. Map of the shoreline and bathymetric boundaries used for calculating land accretion/erosion and changes in sediment volume offshore. Offshore areas in the area of 89°E are not included because they have not been remapped since the Lloyd survey. Location of the transect in Figure 5 is noted.

Table 2. *Delta front bathymetric change between 1840 and 1990.*

Water Depth (m)	Volume of Gain(+)/Loss(−) in Seabed Elevation ($\times 10^7$ m^3)	
	River Mouth	Western Delta
Land (+2 m elevation)	(+) 203.8	(−) 3.7
0–5	(−) 738.1	(+) 107.9
5–10	(+) 2,960.1	(−) 300.2
10–15	(+) 188.9	(−) 20.6
15–20	(+) 398.9	(−) 482.7
20–30	(+) 749.3	(−) 148.0
30–40	(+) 684.4	(−) 19.3
40–50	(+) 379.1	No data
Net value	**(+) 4,826.6**	**(−) 866.4**

subsidence-induced rises in relative sea level (RSL). Westward sediment fining and increased sediment accumulation rates on the Bay of Bengal inner shelf (KUEHL *et al.*, 1989) suggest that shelf sediment dispersal is toward the west, and hence, sediment erosion in the western delta is not contributing to the land accretion in the river mouth area.

Figure 3 demonstrates that the bulk of accretion in the Ganges-Brahmaputra river mouth area occurs subaqueously on the inner shelf between 90° and 92°E longitude. These are the topset (<20 m water depth) and upper foreset (20–50 m) areas of the subaqueous delta identified by KUEHL *et al.* (1989; in press). Within the 12,530 km^2 study area outlined in Figure 4, bathymetric changes between 1840 and 1990 indicate an increase in sediment volume of 3.0×10^{10} m^3 (22.1×10^7 tons/yr) in the topset area and 1.8×10^{10} m^3 (13.3×10^7 tons/yr) in the upper foreset area (assuming $\rho_{dry} = 1100$ g/cm^3). This corresponds to an estimated 21% and 12.5% of the annual Ganges-Brahmaputra sediment budget, respectively, or an average of 2.8×10^4 tons/km^2/yr. Together, these estimates for the last 150 years exceed a Holocene average for the entire delta front of 27% (including the entire subaqueous delta) calculated by KUEHL *et al.* (in press) using UMITSU's (1990) Holocene stratigraphic thicknesses since the onset of estuarine infilling. In the 1410 km^2 of the western delta (Figure 4) mapped in 1840 and 1990, a decrease in sediment volume of 8.5×10^9 m^3 (6.3×10^7 tons/yr) occurs in water depths to 40 m, indicating net erosion and/or increasing RSL of 4.5×10^4 tons/km^2/yr.

Before these figures for subaerial and subaqueous sediment accumulation and erosion of Ganges-Brahmaputra delta can be considered quantitative, a better understanding of subsidence-induced RSL change along this section of coastline is required. Long-term tide gauge records from the Indian subcontinent (EMERY and AUBREY, 1989) range from −1.3 to +2.1 mm/yr of RSL rise, with an average of +0.5 mm/yr. However, the closest stations to the delta are in the Calcutta area at the extreme western edge of the Bengal Basin. Anecdotal information of buried historical structures and buried coastal forests collected by MORGAN and MCINTIRE (1959) and COLEMAN (1969) led these authors to suggest that subsidence-induced RSL rise may approach 1–2 cm/yr in some areas of the delta plain. Several NE-SW trending structural troughs and gravimetric highs extend across the Bengal Basin, possibly indicating that regional subsidence-uplift patterns may overlay the overall sediment accretion trend in the river mouth region. These patterns are likely to be at least partially responsible for the rapid switching of river channels in the alluvial plain of the Ganges-Brahmaputra observed in historical times. West of the active delta front, these trends may exacerbate shoreline retreat and bathymetric deepening induced by eustatic sea level rise and erosion by waves, tidal currents, and cyclonic storms. A comparison of average infilling/erosion rates in the river mouth and western delta (+2.8 vs. -4.5×10^4 tons/km^2/yr) suggests that RSL rise is quite dramatic in areas not receiving significant Ganges-Brahmaputra sediment in historical times. River mouth infilling rates may be considerably higher than the figures presented in this paper, in order to compensate for the delta-wide rise in RSL.

Morphology of the Ganges-Brahmaputra Delta

Delta front morphologic changes in historical times give evidence of the overall effect of sediment accumulation on delta growth. The transect of seafloor elevation change in the river mouth region (Figure 5) indicates that there is aggradation and progradation of the outer topset and foreset region. This supports the observations of subaqueous delta growth made by KUEHL *et al.* (1989) using sediment geochronology data. Figure 3 demonstrates that there is also a second depocenter of delta growth centered in the upper topset region (<15 m water depth) immediately seaward of the river mouths. Modern deposits of fine sands and silts (mean diameter 2–6 ϕ) mantle much of this region, with generally finer mud deposits further seaward on the outer topset and foreset region (KUEHL *et al.*, 1989). During the period from 1792-present, two processes are observed in this inner topset region. Bhola and Hatia Islands (Figure 2), and the shoals extending seaward from their downstream ends, have accreted on the seaward end by up to 50 km. In addition, across the entire river mouth region, but particularly on the eastern side, these coarse-grained deposits are coalescing to form a lobate feature at about 8–15 m water depth. Upriver, there has been a complex rerouting of channels flowing between the island-shoal complexes.

Delta front morphology changes occurring in historical times suggests an overall mechanism for Ganges-Brahmaputra delta growth during the Holocene. Because of the strong tidal influence in the mouth region, the river discharges through several distributary channels. Newly formed islands and associated subaqueous sand shoals accrete south-southeastward (seaward) forming a digitate river mouth region. This digitate morphology is present across the entire delta front to the mouth of the Hoogly River in India, suggesting that the Ganges tributary has progressively moved eastward during the Holocene, occupying and abandoning a series of distributary channels that are left behind as moribund tidal channels no longer receiving significant water and sediment from the main river. Progressive downstream abandonment of distributaries of the lower Ganges has been observed in historic times (ISPAN, 1995). Silting up and reduced competence with continued channel extension by growth of the interdistributary island-shoal complex may ex-

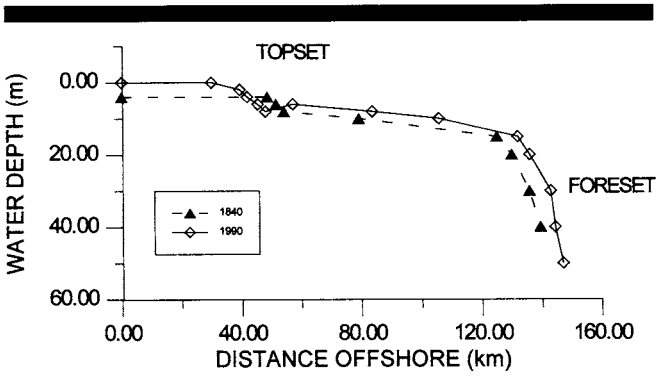

Figure 5. A comparison cross-shore transect of bathymetry across the inner shelf from the Lloyd survey in 1840 with modern charts (1990). Note the overall accretion along the outer topset and foreset areas of the subaqueous mud delta first identified by KUEHL *et al.* (1989). Net accretion is also present in the inner topset area, corresponding to the growth and coalescence of the digitate shoals at the river mouths.

plain the eventual abandonment of channels. The Hoogly is an exception to this process; its connection to the Ganges is kept open by human modification (Hossain, 1993). The shoal growth and channel abandonment process is best observed in historical times in the Tetulia channel-Bhola Island area (Figure 2). Control(s) on eastward migration of the river are unresolved, but may be related to basin tectonics. Further seaward, these digitate shoal complexes merge into a relatively coarse sediment sheet draped over older and finer-grained topset sediments of the mud clinoform accreting offshore.

The development of a subaerial delta over a subaqueous mud delta in the Ganges-Brahmaputra system differs from Amazon and Fly River morphologies, which lack the subaerial component (NITTROUER *et al.*, 1986; HARRIS *et al.*, 1993). All are energetic, macrotidal river mouths, but the Ganges-Brahmaputra possesses a significantly larger fraction of "coarse" material that remains inshore to occlude the river mouth. Grain size of river sediment load has recently been recognized by ORTON and READING (1993) to have as significant an effect on delta morphology as the triad of sediment volume, wave, and tidal energies (WRIGHT and COLEMAN, 1973). Each of the digitate island-shoal complexes in the Ganges-Brahmaputra system can be considered the equivalent of distributary lobes in the Mississippi model of delta growth. Sunderbans National Park in western Bangladesh is the only section of the delta front that remains in a relatively natural state. This area suggests that, unlike lobes in the Mississippi, which are colonized by saline and freshwater marshes, before human disturbance, the entire Ganges-Brahmaputra delta front was probably a vast network of mangrove-colonized islands separated by old distributary channels interconnected through minor channels. This has been confirmed by the limited coring to date of the delta front conducted by UMITSU (1990).

CONCLUSIONS

Historical data indicates the following about the Ganges-Brahmaputra delta front:

(1) The mouth of the Ganges-Brahmaputra does exhibit the characteristics of an actively prograding subaerial delta. An average of 7.0 km²/yr of new land has accreted in this area since 1792 (4.4 km²/yr since 1840). This accounts for about 1–2% of the overall river sediment budget.
(2) The deltaic region at the river mouth has two depocenters of progradation/aggradation, with a subaqueous mud delta forming offshore (cf. KUEHL *et al.*, 1989) and a subaerial delta forming above the inner topset beds of the subaqueous delta.
(3) Bathymetric changes observed on the delta front east of the Haringhata River between 1840 and 1990 indicate that about 21% of the annual river sediment budget is supplying aggradation and progradation of the topset depocenter, and an additional 12.5% is sequestered in the upper foreset area (20–50 m water depth).
(4) The morphology of shoal evolution in the river mouth region suggests that the Ganges-Brahmaputra has evolved by a series of eastward steps of the river mouth that are controlled by channel margin accretion and infilling, followed by channel abandonment.
(5) The shoreline and shallow offshore areas of the western delta front are in a net erosional state. Seaward-facing shoreline areas have retreated as much as 3–4 km since 1792. This is attributed to the area being composed of inactive deltaic digitate shoal complexes that receive minimal modern Ganges-Brahmaputra sediment.
(6) Shoreline erosion and increasing depths offshore are a function of eustatic sea level rise and erosion by oceanographic processes, possibly exacerbated by regional subsidence

ACKNOWLEDGMENTS

Funding for this study was provided the National Science Foundation (INT-9322601) and a grant from the Coastal Research Center of Woods Hole Oceanographic Institution. Thanks are due to S. Kuehl, S. Goodbred, T. Martin, J. Kelley, and H. Walker for their reviews and constructive comments.

LITERATURE CITED

ADMIRALTY, 1904. Chart of the Matla River to Elephant Point, London.

ADMIRALTY, 1908. Chart of The Sandheads: False Point to the Mutlah River, London.

ALAM, M.K.; HASAN, A.K.M.S.; KHAN, M.R., and WHITNEY, J.W., 1990. *Geological Map of Bangladesh.* Geological Survey of Bangladesh.

ALEXANDER, C.R., DEMASTER, D.J., and NITTROUER, C.A., 1991. Sediment accumulation in a modern epicontinental-shelf setting: the Yellow Sea. *Marine Geology,* 98, 51–72.

BARUA, D.K., 1990. Suspended sediment movement in the estuary of the Ganges-Brahmaputra-Meghna river system. *Marine Geology,* 9, 243–253.

BARUA, D.K; KUEHL, S.A.; MILLER, R.L., and MOORE, W.S., 1994. Suspended sediment distribution and residual transport in the coastal ocean off of the Ganges-Brahmaputra river mouth. *Marine Geology,* 120, 41–61.

COLEMAN, J.M., 1969. Brahmaputra River: channel processes and sedimentation. *Sedimentary Geology,* 3, 129–239.

CURRAY, J.R.; EMMEL, F.J.; MOORE, D.G., and RAIT, R.W., 1982. Structure, Tectonics and Geological History of the Northeastern Indian Ocean. *In:* A.E. Nairn and F.G. Stehli, (eds.). 6, New York: Plenum, The Ocean Basins and Margins pp. 399–450.

DEFENSE MAPPING AGENCY, 1990. Bay of Bengal: Raimangail River to Elephant Point and Devi River to Pusur River, Washington, D.C.

EMERY, K. O. and AUBREY, D.G., 1989. Tide gauges of India. *Journal of Coastal Research,* 5, 489–501.

EYSINK, W.D., 1983. Basic considerations on the morphology and land accretion potentials in the estuary of the lower Meghna River. *Bangladesh Water Development Board Land Reclamation Project,* Technical Report 15, Chittagong, 85p.

FRIEDMAN, G.M.; SANDERS, J.E., and KOPASKA-MERKEL, D.C., 1992. *Principles of Sedimentary Deposits: Stratigraphy and Sedimentology,* New York, Macmillan 717p.

HARRIS, P.T.; BAKER, E.K.; COLE, A.R., and SHORT, S.A., 1993. A preliminary study of sedimentation in the tidally dominated Fly River delta, Gulf of Papua. *Continental Shelf Research,* 13, 441–472.

HOSSAIN, M.M., 1993. Morphology and sediment transport aspects of the lower Ganges. *In: International Workshop on Morphological Behaviour of the Major Rivers of Bangladesh.* Dhaka, Bangladesh.

KUEHL, S.A.; NITTROUER, C.A., and DEMASTER, D.J., 1986. The nature of sediment accumulation on the Amazon continental shelf. *Continental Shelf Research,* 6, 209–225.

KUEHL, S.A.; HARIU, T.M., and MOORE, W.S., 1989. Shelf sedimentation off the Ganges-Brahmaputra river system: evidence for sediment bypassing to the Bengal Fan. *Geology,* 17, 1132–1135.

KUEHL, S.A.; LEVY, B.M.; MOORE, W.S., and ALLISON, M.A., in press. Subaqueous delta of the Ganges-Brahmaputra River system. *Marine Geology.*

ISPAN (Irrigation Support Project for Asia and the Near East), 1993. *A Study of Sedimentation in the Brahmaputra-Jamuna Floodplain.* Bangladesh Ministry of Water Resources, Dhaka, 133p.

LACAM, B., 1794. A chart of the northern part of the Bay of Bengal from Point Palmiras and the Aracan shore. Londong: Laurie and Whittle.

LISITZEN, A.P. 1972. *Sedimentation in the World Ocean.* SEPM Special Publication 17, 218p.

LLOYD, R., 1840. A survey of the sea face of the Soondurbuns. London; W.H. Allen.

MILLIMAN, J.D. and SYVITSKI, P.M., 1992. Geomorphic/tectonic control of sediment discharge to the ocean: the importance of small mountainous rivers: *Journal of Geology,* 100, 525–544.

MORGAN, J.P. and MCINTYRE, W.G., 1959. Quaternary geology of the Bengal Basin, East Pakistan and India. *Geological Society of America Bulletin,* 70, 319–342.

NITTROUER, C.A.; KUEHL, S.A.; DEMASTER, D.J.; and KOWSMANN, R.O., 1986. The deltaic nature of Amazon shelf sedimentation. *Geological Society of America Bulletin,* 97, 444–458.

ORTON, G.J. and READING, H.G., 1993. Variability of deltaic processes in terms of sediment supply, with particular emphasis on grain size. *Sedimentology,* 40, 475–512.

UMITSU, M., 1990. Late Quaternary environments and landforms in the Ganges delta. *Sedimentary Geology,* 83, 177–186.

WRIGHT, L.D. and COLEMAN, J.M., 1973. Variations in morphology of major deltas as functions of ocean wave and river discharge regimes, *American Association of Petroleum Geologists Bulletin,* 57(2), 370–398.

Annex B62

S. Kuehl and S.L. Goodbred, "Holocene and modern sediment budgets for the Ganges-Brahmaputra River: Evidence for highstand dispersal to flood-plain, shelf, and deep-sea depocenters", *Geology,* Vol. 27, No. 6 (1999)

Holocene and modern sediment budgets for the Ganges-Brahmaputra river system: Evidence for highstand dispersal to flood-plain, shelf, and deep-sea depocenters

Steven L. Goodbred, Jr.
Steven A. Kuehl
Virginia Institute of Marine Science, College of William and Mary, Gloucester Point, Virginia 23062, USA

ABSTRACT

The partitioning of fluvial sediment load across continental margins is an important control on strata formation and sequence development; however, few quantitative sediment budgets that encompass entire dispersal systems exist. For the Ganges-Brahmaputra river system, sediment discharge is estimated to be 10^9 t/yr at gauging stations ~300 km inland of the coast, but little has been known of the downstream fate of this material. Geochronological, geophysical, and stratigraphic investigations of the lowland flood plain, delta plain, and shelf help to delineate the extent of Holocene fill and allow calculation of a first-order sediment budget. Results reveal that 1500×10^9 m^3 of sediment fill has been sequestered within the flood plain and delta plain since ca. 7000 yr B.P., or about one-third of the annual discharge. The remaining load appears to be apportioned between the prograding subaqueous delta (1970×10^9 m^3) and transport to the deep-sea Bengal fan via a nearshore canyon. Modern (<100 yr) budget estimates based on short-term accretion rates indicate a similar dispersal pattern and show that contemporaneous deposition continues within these disparate depocenters. The roughly equal partitioning of sediment among flood-plain, shelf, and deep-sea settings reflects the respective influence of an inland tectonic basin, a wide shelf, and a deeply incised canyon system. The findings also support new sequence stratigraphic models for these settings and indicate the important insight that modern river deltas can provide for ancient margin systems. Furthermore, results affirm that values of riverine sediment flux to the oceans may be considerably overestimated by not accounting for loss to the flood plains downstream of the gauging stations.

INTRODUCTION

Rivers are the main source of terrigenous sediment to the world oceans; however, much of this point-source material is trapped at the continental margin, commonly in a deltaic setting as lower flood-plain, delta-plain, shelf, and slope deposits. At present, although fairly accurate load estimates exist for many rivers, little is known about the fate of fluvial sediment downstream of the final gauging stations of rivers (Milliman and Syvitski, 1992). Many gauging sites are located hundreds of kilometers from the coast, and a considerable portion of a river's load may be sequestered to extensive downstream flood-plain and delta-plain environments. Partitioning of this load among fluvial, coastal, shelf, and deep-sea settings is important for understanding flood-plain and delta formation, coastal response to sea-level change and subsidence, and long-term sequence development.

Current ideas of sediment partitioning are based on somewhat circular reconstructions of preserved deltaic sequences and limited data from modern systems. For example, early sequence stratigraphic models suggested that alluvial, shelf, and slope facies develop in general concordance with transgressive, highstand, and lowstand sea-level stages, respectively. These ideas have now been refined for fluvial systems by addressing the locally high sediment input and complex response to base-level change that may shift the timing and location of sequence development (e.g., Schlager, 1993; Wescott, 1993). Other studies have also extended the original passive-margin sequence model to include different tectonic and physiographic settings (e.g., Posamentier and Allen, 1993a, 1993b). However, there remain few quantitative data from modern and late Quaternary examples to test these current views.

In the modern system, sediment budgets for the lower flood plains and delta plains of the Amazon, Ganges-Brahmaputra, and Mississippi Rivers indicate that 24%–39% of riverine sediment load is being sequestered to these regions (Dunne et al., 1998; Goodbred and Kuehl, 1998; Kesel et al., 1992). Offshore of some large rivers, the presence of a subaqueous delta demonstrates that the shelf is also a major highstand depocenter for fluvial sediment (Kuehl et al., 1986, 1997), although constraining offshore budgets can be complicated where sediment plumes are widely dispersed. A comprehensive fluvial sediment budget is difficult to establish because discharge may be distributed across terrestrial, coastal, and pelagic realms and controlled by varying sea level, fluvial and littoral processes, and tectonics. For the delta of the Ganges-Brahmaputra river system, an opportunity exists for calculating sediment volumes because of physical boundaries that laterally confine the basin. Furthermore, tectonic activity, basin physiography, and the large sediment load favor accommodation and widespread sediment dispersal. In this study we use stratigraphic and geochronologic data to determine first-order Holocene (since ca. 7000 yr B.P.) and modern (~100 yr) sediment budgets for the lower Ganges-Brahmaputra river system that distinguish between flood-plain, shelf, and deep-sea depocenters.

BENGAL BASIN AND GANGES-BRAHMAPUTRA RIVER SYSTEM

The Ganges and Brahmaputra Rivers debouch into the Bengal basin, where they currently coalesce ~150 km upstream of the coastline. The rivers are gauged separately; the main stations are situated ~300 km above the mouth (see Fig. 1). Load estimates indicate a combined sediment discharge of $\sim 1 \times 10^9$ t/yr for the rivers (Milliman and Syvitski, 1992). The receiving Bengal basin comprises ~100 000 km^2 of lowland flood plain and delta plain and is bounded by Tertiary highlands. These same uplands confine the continental shelf (~40 000 km^2) and upper Bay of Bengal, restricting longshore advection of the sediment plume (Barua et al., 1994). The shelf is also incised by a major canyon system, the Swatch of No Ground, that is within

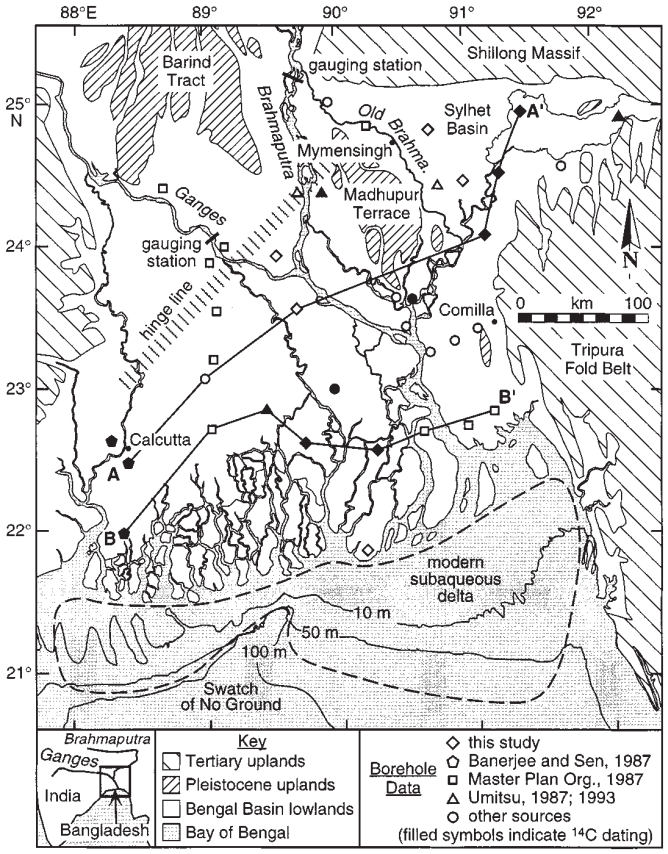

Figure 1. Physiographic map of Bengal basin and locations of borehole data and cross-sectional profiles (A-A′ and B-B′) for Figure 2.

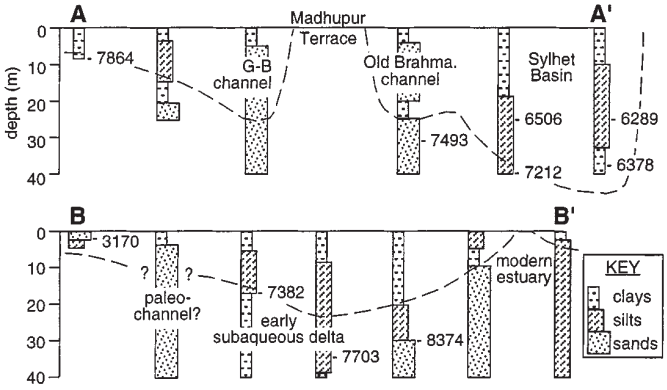

Figure 2. Cross-sectional profiles showing generalized stratigraphy of flood-plain and delta-plain deposits (above dashed line) with calibrated radiocarbon ages. Sediments below dashed line are either marine or were deposited before ca. 7000 yr B.P. Locations are shown in Figure 1. Note thick sequences in subsiding Sylhet basin (near B′). G-B = Ganges-Brahmaputra (Brahma.).

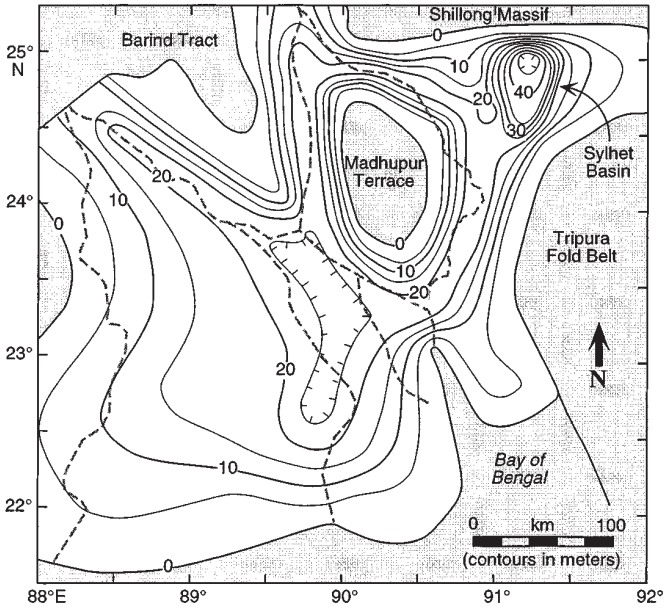

Figure 3. Isopach map of flood-plain and delta-plain sediments deposited since middle Holocene slowdown in sea-level rise, ca. 7000 yr B.P. Volume calculations indicate 1500 × 10^9 m^3 of sediment fill in this region, corresponding to ~30% of annual discharge. Dashed lines represent modern river channels, as shown in Figure 1.

30 km of the modern shoreline and serves as a conduit to the deep-sea Bengal fan (Kuehl et al., 1989, 1997; Weber et al., 1997).

The Bengal region is tectonically active, vertical displacement dominating Quaternary movements. The Madhupur terrace and Barind tract are Pleistocene uplifted alluvial deposits (Morgan and McIntire, 1959), and neotectonic uplift is occurring around the Mymensingh, Calcutta, and Comilla areas (Coates, 1990; Khandoker, 1987). The expansive Sylhet basin is a foreland-trough system that is subsiding at 1–3 mm/yr because of overthrusting of the adjacent Shillong massif (Goodbred, 1999; Johnson and Alam, 1991). Across much of the Bengal region, compaction and/or isostatically induced subsidence are clearly active, but rates are poorly constrained by existing data.

METHODS

Stratigraphic and geochronologic data from the flood-plain and delta plain were compiled from various sources, including published studies (Banerjee and Sen, 1987; Master Plan Organization, 1987; Umitsu, 1993) and results from our ongoing research (Figs. 1 and 2; Goodbred, 1999; Goodbred and Kuehl, 1998). Calibrated radiocarbon ages (CALIB 3.0; Stuiver and Reimer, 1993) were used to establish the 7000 yr B.P. surface across the region. The eastern, western, and northern boundaries of basin fill are delineated by the abrupt exposure of Tertiary highlands, and the southern limit is taken as the modern shoreline at 0 m thickness. Geographic positions were converted to UTM (universal transverse mercator) units to correct for projection. An isopach map was contoured by hand from available data, and fill volume was calculated by using Surfer graphing software. Kuehl et al. (1997) used similar methods to determine the volume of the subaqueous delta from seismic-reflection data. Volume to mass conversions were made by using a 1.5 g/cm^3 dry bulk density based on in situ measurements reported by the Food and Agriculture Organization (1971) and Michels et al. (1998). Data for the modern budget were compiled from various studies, including values for the flood plain and delta plain (Goodbred and Kuehl, 1998), nearshore (Allison, 1998), and delta front (Michels et al., 1998).

FLUVIAL SEDIMENT BUDGET

The isopach map (Fig. 3) indicates 1500 × 10^9 m^3 of sediment fill in the Bengal basin since the middle Holocene slowdown in sea-level rise ca. 7000 yr B.P. (Table 1). This value equates to 0.32 × 10^9 t/yr, or about one-third of the estimated annual load (Table 2). Maximum fill thickness in the Bengal basin is found within the subsiding Sylhet basin (>40 m), and

TABLE 1. SEDIMENT-FILL VALUES FOR THE BENGAL BASIN SINCE ca. 7 ka

	Fill volume (10^9 m^3)	Load stored (10^9 t/yr)*
Flood plain and delta plain	1500	0.32
Subaqueous delta	1970†	0.42

*Value using 1.5 t/m^3 dry bulk density.
†Kuehl et al. (1997).

TABLE 2. SEDIMENT BUDGETS FOR THE GANGES-BRAHMAPUTRA RIVER DELTA

	Flood plain/ delta plain	Subaqueous delta	Canyon/fan
Holocene*	32 (this study)	42 (Kuehl et al., 1997)	26?
Modern	30 (Goodbred and Kuehl, 1998)	21, topset (Allison, 1998)	29?
		20, foreset (Michels et al., 1998)	

Note: Values are percentage of load based on 1×10^9 t/yr sediment discharge.
*Calculated since 7 ka.

other thick sequences fill modern river and paleoriver channels. We suspect there may be a paleochannel course in the southwestern area, but this could not be confirmed with our data. To address this potential error, sediment volume was recalculated by assuming maximum fill depth in these areas, resulting in a <10% deviation from the stated value. On the shelf, the subaqueous delta began to form ca. 7000 yr B.P., and Kuehl et al. (1997) calculated 1970×10^9 m^3 of fill since that time, representing 0.42×10^9 t/yr of sediment storage. Together the flood-plain and subaqueous delta deposits account for ~75% of the estimated fluvial sediment discharge. About 25% of the load remains unaccounted for and apparently escapes the shelf through the Swatch of No Ground canyon. Although no comprehensive volume measures could be made for the canyon or the Bengal fan, direct local accumulation measurements show that a considerable volume of sediment is reaching these depocenters (Michels et al., 1998; Weber et al., 1997).

For comparison, a modern sediment budget (Table 2) was determined by using published ^{137}Cs and ^{210}Pb geochronologies from the flood plain (Goodbred and Kuehl, 1998) and delta foresets (Michels et al., 1998). Allison (1998) quantified sediment aggradation between the shoreline and 50 m isobath (topset region) by using a geographic information system–based comparison of current and eighteenth century British bathymetric charts. Together these studies reveal that the recent load distribution is similar to the overall Holocene system; ~30% of the load is sequestered to the flood plains and ~40% is sequestered to the subaqueous delta. The remaining ~30% is presumed to reach the Swatch of No Ground (Kuehl et al., 1997), a conclusion that is supported by rapid modern sediment accretion in the canyon head (>50 cm/yr; Kudrass et al., 1998).

These results are consistent among the various studies, methods, and time scales used, but potential sources of error should be acknowledged. Perhaps foremost is variation in fluvial sediment load, which is largely controlled by climate, tectonics, and land use. Paleoclimatic records constructed from the Tibetan Plateau indicate onset of the Southwest Monsoon (the main source of regional precipitation) ca. 12 000 yr B.P., relatively stable conditions after ca. 5700 yr B.P., and near-present conditions since ca. 3600 yr B.P. (Gasse et al., 1991; Thompson et al., 1989). Although this climate record does not discount variation in the sediment load, no major climatic shifts have occurred during the past 7000 yr. In the modern Ganges-Brahmaputra system, the effects of short-term climate change, basin tectonics, and shifting land uses should be tempered by the immense size of the drainage basin (1.8×10^6 km^2). This mitigation reflects a basin's capacity to store eroded sediments for hundreds to thousands of years before downstream release (Meade, 1996). An example from the Changjiang River drainage basin (1.3×10^6 km^2) reveals no evidence for a modern or late Holocene increase in sediment load, despite two millennia of extensive anthropogenic activity and a >50% loss of remaining forest cover in recent decades (Chen Xiqing, 1996). Increased erosion in the catchment was shown to be accommodated by channel and flood-plain adjustments along the middle and upper reaches of the river.

DISCUSSION

Recent studies of the Ganges-Brahmaputra delta indicate active sedimentation within flood-plain, shelf, and canyon depocenters during the late Holocene and continuing to the present. Our data also suggest that sediment distribution has been roughly equally apportioned among these areas. Many factors affect sediment dispersal and sequence development along continental margins, but eustasy, tectonics, and sediment supply are generally considered the most important (Jervey, 1988). For the Ganges-Brahmaputra river system, slow eustatic sea-level rise during the past 7000 yr would presumably focus deposition on the shelf (nearest accommodation) and cannot account for the observed widespread distribution of sediment. The immense sediment and water discharge favor dispersal seaward of the coast, but they do not explain the large volume sequestered to the Bengal flood plains. The remaining influence that we believe to be one of the main controls on sediment dispersal in this system is tectonics.

Accommodation on the Ganges-Brahmaputra flood plains is continually generated via overthrust faulting, isostatic loading, compaction, and neotectonic (fault) movements. The impact of these processes on sediment dispersal is supported by our calculation that one-third of the sediment load is sequestered to the low-lying flood plains. Subsidence sustains this flood-plain storage capacity, and exceeds 3 mm/yr in some areas (Goodbred, 1999). The relative contribution of compaction to this signal is not known, but it is presumably less significant than in finer grained delta sequences (e.g., Mississippi River delta). Extrapolating known rates from the Bengal basin through the middle Holocene, subsidence can account for 5–25 m of accommodation compared to ~10 m by sea-level rise. Offshore, compaction is believed to be significant in the muddy subaqueous delta and, along with isostatic loading, can account for continued production of accommodation on the shelf. Around the Swatch of No Ground, growth faults reflect rapid deposition and oversteepening and serve to feed massive sediment blocks into the canyon (Kuehl et al., 1997; Kudrass et al., 1998). Furthermore, that the canyon today remains unfilled suggests the successive removal of accumulated sediment to the Bengal fan via mass wasting (Weber et al., 1997).

Large modern deltas may serve as important analogs for ancient margin systems, because abundant accommodation and sediment supply favor the formation of comparable stratigraphic sequences (e.g., Mississippi River delta; Boyd et al., 1989). The Ganges-Brahmaputra delta provides a modern example of sequence development along a high-yield, tectonically active margin. For passive-margin settings, it is generally believed that most sediment bypasses the flood plain and is trapped on the shelf during highstands of sea level. This pattern is controlled by the seaward increase in accommodation resulting from subsidence and the sloping shelf. In contrast to this, Posamentier and Allen (1993a) presented a revised sequence stratigraphic model for foreland basin systems and noted that subsidence increases landward as a result of overthrust-driven subsidence. Resulting sequence development during highstand conditions largely occurs in the updip (landward) region.

The pattern of highstand sediment dispersal for the Ganges-Brahmaputra delta appears to reflect both of the these sequence models, with considerable storage in landward and seaward basins. This situation can be explained by

the tectonic complexity of the Bengal basin, which comprises both foreland and passive margin elements. In the northeast, the Sylhet basin is a local tectonic foreland subsiding at a rate that increases toward the overthrusting Shillong massif (Goodbred, 1999; Johnson and Alam, 1991). However, the lower Ganges-Brahmaputra delta plain and subaqueous delta are situated along a classic passive margin, where isostatic subsidence increases seaward of a hinge line (Fig. 1; Lindsay et al., 1991). Furthermore, the Swatch of No Ground canyon is an important control on highstand sediment dispersal on the shelf that serves as a conduit to the Bengal fan (Kuehl et al., 1989). The canyon head incises within 30 km of the modern coast (unlike most passive margin canyons) and presents a situation comparable to the narrow, deeply incised shelves of collision margins (May et al., 1983), thus adding a third dimension to the tectonic-physiographic setting of the Bengal basin. It is clear that the Ganges-Brahmaputra system does not fall into a typical margin setting or established model of sediment dispersal. However, the roughly equal and contemporaneous partitioning of sediment among these different depocenters affirms recent refinement of sequence stratigraphic models (e.g., Posamentier and Allen, 1993a, 1993b) and supports the application of modern delta studies to these efforts.

Regarding modern geologic systems, the magnitude of sediment trapping in the Bengal basin has major implications for estimates of sediment flux to the world ocean. Milliman and Syvitski (1992) suggested that terrigenous sediment flux from rivers may be overestimated because of failure to account for flood-plain deposition downstream of the gauging stations (see Fig. 1). Results of this study substantiate their ideas; the 30% storage of Ganges-Brahmaputra sediment load in the flood plain equates to a 1%–3% reduction in *global* estimates of riverine sediment flux to the oceans from this system alone. Tectonic subsidence, broad flood plains, and widespread overbank flooding are important factors contributing to flood-plain sequestration in this system (Goodbred and Kuehl, 1998).

ACKNOWLEDGMENTS

This project was completed with support from National Science Foundation (NSF) grant (EAR-9706274), Flood Action Plan 24: River Survey Project (European Union–sponsored), and the NSF Summer Institute in Japan. We thank Masatomo Umitsu of Nagoya University for sharing his collection of unpublished borehole data, and John Milliman, Peter Southgate, and Michael Williams for constructive reviews. Virginia Institute of Marine Science contribution 2200.

REFERENCES CITED

Allison, M. A., 1998, Historical changes in the Ganges-Brahmaputra delta front: Journal of Coastal Research, v. 14, p. 480–490.

Banerjee, M., and Sen, P. K., 1987, Paleobiology in understanding the change of sea level and coast line in Bengal Basin during the Holocene period: Indian Journal of Earth Sciences, v. 14, p. 307–320.

Barua, D. K., Kuehl, S. A., Miller, R. L., and Moore, W. S., 1994, Suspended sediment distribution and residual transport in the coastal ocean off the Ganges-Brahmaputra River mouth: Marine Geology, v. 120, p. 41–61.

Boyd, R., Suter, J., and Penland, S., 1989, Relation of sequence stratigraphy to modern sedimentary environments: Geology, v. 17, p. 926–929.

Chen Xiqing, 1996, An integrated study of sediment discharge from the Changjiang River, China, and delta development since the mid-Holocene: Journal of Coastal Research, v. 12, p. 26–37.

Coates, D. A., 1990, The Mymensingh terrace: Evidence of Holocene deformation in the delta of the Brahmaputra River, central Bangladesh: Geological Society of America Abstracts with Programs, v. 22, no. 7, p. 310.

Dunne, T., Mertes, L. A. K., Meade, R. H., Richey, J. E., and Forsberg, B. R., 1998, Exchanges of sediment between the flood plain and channel of the Amazon River in Brazil: Geological Society of America Bulletin, v. 110, p. 450–467.

Food and Agriculture Organization, 1971, Soil survey project, Bangladesh: Soil resources: Rome, United Nations Development Program—Food and Agriculture Organization, 211 p.

Gasse, F., Arnold, M., Fontes, J. C., Fort, M., Gilbert, E., Huc, A., Li Bingyan, Li Yuanfang, Liu Qing, Mélières, F., Van Campo, E., Wang Fubao, and Zhang Quingsong, 1991, A 13,000-year climate record from western Tibet: Nature, v. 353, p. 742–745.

Goodbred, S. L., Jr., 1999, Sediment dispersal and sequence development along a tectonically active margin: Late Quaternary evolution of the Ganges-Brahmaputra River delta [Ph.D. thesis]: Gloucester Point, Virginia, College of William and Mary, 132 p.

Goodbred, S. L., Jr., and Kuehl, S. A., 1998, Floodplain processes in the Bengal Basin and the storage of Ganges-Brahmaputra River sediment: An accretion study using ^{137}Cs and ^{210}Pb geochronology: Sedimentary Geology, v. 121, p. 239–258.

Jervey, M. T., 1988, Quantitative geological modeling of siliciclastic rock sequences and their seismic expression, *in* Wilgus, C. K., Hastings, B. S., Kendall, C. G. S. C., Posamentier, H. W., Ross, C. A., and Van Wagoner, J. C., eds., Sea-level change: An integrated approach: Society of Economic Paleontologists and Mineralogists Special Publication 42, p. 47–70.

Johnson, S. Y., and Alam, A. M. N., 1991, Sedimentation and tectonics of the Sylhet trough, Bangladesh: Geological Society of America Bulletin, v. 103, p. 1513–1527.

Kesel, R. H., Yodis, E. G., and McCraw, D. J., 1992, An approximation of the sediment budget of the lower Mississippi River prior to major human modification: Earth Surface Processes and Landforms, v. 17, p. 711–722.

Khandoker, R. A., 1987, Origin of elevated Barind-Madhupur areas, Bengal Basin: Results of neotectonic activities: Bangladesh Journal of Geology, v. 6, p. 1–9.

Kudrass, H. R., Michels, K. H., Wiedicke, M., and Suckow, A., 1998, Cyclones and tides as feeders of a submarine canyon off Bangladesh: Geology, v. 26, p. 715–718.

Kuehl, S. A., DeMaster, D. J., and Nittrouer, C. A., 1986, Nature of sediment accumulation on the Amazon continental shelf: Continental Shelf Research, v. 6, p. 209–225.

Kuehl, S. A., Hariu, T. M., and Moore, W. S., 1989, Shelf sedimentation off the Ganges-Brahmaputra river system: Evidence for sediment bypassing to the Bengal fan: Geology, v. 17, p. 1132–1135.

Kuehl, S. A., Levy, B. M., Moore, W. S., and Allison, M. A., 1997, Subaqueous delta of the Ganges-Brahmaputra river system: Marine Geology, v. 144, p. 81–96.

Lindsay, J. F., Holliday, D. W., and Hulbert, A. B., 1991, Sequence stratigraphy and the evolution of the Ganges-Brahmaputra delta complex: American Association of Petroleum Geologists Bulletin, v. 75, p. 1233–1254.

Master Plan Organization, 1987, Geology of Bangladesh: Harza Engineering Company International, Technical Report 4, 178 p.

May, J. A., Warme, J. E., and Slater, R. A., 1983, Role of submarine canyons on shelf-break erosion and sedimentation: Modern and ancient examples, *in* Stanley, D. J., and Moore, G. T., eds., The shelfbreak: Critical interface on continental margins: Society of Economic Paleontologists and Mineralogists Special Publication 33, p. 315–332.

Meade, R. H., 1996, River-sediment input to major deltas, *in* Milliman, J. D., and Haq, B. U., eds., Sea level and coastal subsidence: Causes, consequences, and strategies: Dordrecht, Netherlands, Kluwer Academic Publishers, p. 63–85.

Michels, K. H., Kudrass, H. R., Hübscher, C., Suckow, A., and Wiedicke, M., 1998, The submarine delta of the Ganges-Brahmaputra: Cyclone-dominated sedimentation patterns: Marine Geology, v. 149, p. 133–154.

Milliman, J. D., and Syvitski, J. P. M., 1992, Geomorphic/tectonic control of sediment discharge to the ocean: The importance of small mountainous rivers: Journal of Geology, v. 100, p. 525–544.

Morgan, J. P., and McIntire, W. G., 1959, Quaternary geology of the Bengal basin, East Pakistan and India: Geological Society of America Bulletin, v. 70, p. 319–342.

Posamentier, H. W., and Allen, G. P., 1993a, Siliciclastic sequence stratigraphic patterns in foreland ramp-type basins: Geology, v. 21, p. 455–458.

Posamentier, H. W., and Allen, G. P., 1993b, Variability of the sequence stratigraphic model: Effects of local basin factors: Sedimentary Geology, v. 86, p. 91–109.

Schlager, W., 1993, Accommodation and supply—A dual control on stratigraphic sequences: Sedimentary Geology, v. 86, p. 111–136.

Stuiver, M., and Reimer, P. J., 1993, Extended ^{14}C data and revised CALIB 3.0 ^{14}C age calibration program: Radiocarbon, v. 35, p. 215–230.

Thompson, L. G., Mosley-Thompson, E., Davis, M. E., Bolzan, J. F., Dai, J., Yao, T., Gundestrup, N., Wu, X., Klein, L., and Xie, Z., 1989, Holocene–late Pleistocene climatic ice core records from Qinghai-Tibetan Plateau: Science, v. 246, p. 474–477.

Umitsu, M., 1987, Late Quaternary sedimentary environment and landform evolution in the Bengal lowland: Geographical Review of Japan, v. 60, p. 164–178.

Umitsu, M., 1993, Late Quaternary sedimentary environments and landforms in the Ganges delta: Sedimentary Geology, v. 83, p. 177–186.

Weber, M. E., Wiedicke, M. H., Kudrass, H. R., Hübscher, C., and Erlenkeuser, H., 1997, Active growth of the Bengal fan during sea-level rise and highstand: Geology, v. 25, p. 315–318.

Wescott, W. A., 1993, Geomorphic thresholds and complex response of fluvial systems—Some implications for sequence stratigraphy: American Association of Petroleum Geologists Bulletin, v. 77, p. 1208–1218.

Manuscript received October 29, 1998
Revised manuscript received February 9, 1999
Manuscript accepted February 19, 1999

Annex B63

M. A. Allison & E.B. Kepple, "Modern Sediment Supply to the Lower Delta Plain of the Ganges-Brahmaputra River in Bangladesh", *Geo-Marine Letters*, Vol. 21 (2001)

Geo-Marine Letters (2001) 21: 66–74
DOI 10.1007/s003670100069

M.A. Allison · E.B. Kepple

Modern sediment supply to the lower delta plain of the Ganges-Brahmaputra River in Bangladesh

Received: 26 May 2000 / Revision accepted: 17 May 2001 / Published online: 30 June 2001

Abstract Vibracores and auger samples collected from the lower (tidal) delta plain of the Ganges-Brahmaputra River in Bangladesh were examined to determine whether the area is a significant sink for riverine sediments. Measurements of ^{137}Cs activity and radiocarbon in the sediments indicate sediment accumulation is taking place on decadal and millennial time scales at rates reaching 1.1 cm/year. The sediment of the lower delta plain is primarily derived from an offshore source after having originally been supplied by the Ganges-Brahmaputra river system, carried westward by prevailing currents and advected inland by monsoonal coastal setup and cyclonic events.

Introduction

The lower delta plain has been defined as the low-elevation subaerial portion of a river delta adjacent to the ocean which is subject to tidally driven, periodic saline flooding. Such areas are primarily colonized by mangroves in tropical regions and salt marshes at higher latitudes, grading inland into a variety of freshwater wetlands. In major rivers this region may reach 100 km or more inland, and it is a highly productive ecosystem which serves as an important fishery for local populations. In most deltas, the lower delta plain was deposited over Pleistocene fluvial (lowstand) strata after post-glacial eustatic sea-level rise, and the associated landward migration of coastal environments slowed at 6,000–8,000 years B.P. (Stanley and Warne 1994). The lower delta plain develops in stages, associated with river distributary depocenters which remain active for 10^2–10^3 years, with depositional morphology dependent on the balance between sediment supply and wave/tidal reworking in each delta (Wright and Coleman 1973). The rapid sedimentation of thick sequences of fine-grained strata over older deltaic units in the deltaic plain creates conditions of compaction-induced subsidence independent of the subsidence or uplift associated with tectonically active sedimentary basins. In the Mississippi delta, for instance, long-term tide-gauge records indicate ongoing subsidence at rates of 1 cm/year or more (Penland and Ramsey 1990; Roberts et al. 1994). Lower delta plain areas can be thought of as undergoing a natural cycle of growth, followed by abandonment and subsidence-induced marine flooding and shoreline erosion, and finally by eventual reoccupation and sediment supply from new river distributaries. The loss of lower delta plain wetlands in rivers like the Mississippi (Britsch and Dunbar 1993) and Nile (Stanley and Warne 1998) has been accelerated by a variety of anthropogenic processes, such as distributary network alteration for transportation, artificial levees for flood control, tributary dams in the catchment, and water withdrawal for irrigation. These processes affect sediment supply through the distributaries. In addition, the lower delta plain may receive sediment from offshore during tidal and storm high-water events, ameliorating wetland loss through subsidence. Studies of Mississippi River salt marshes using sediment traps and marker horizons (Baumann et al. 1984; Rejmanek et al. 1988; Reed 1989; Cahoon et al. 1995) have shown that tidal sediment input is small due to the limited tidal range (30–40 cm). However, coastal setup associated with winter cold fronts and cyclonal storms can add substantial amounts of sediment to the marsh surface. The importance of this process for sediment supply to the lower delta plain remains largely undefined for deltas in other tidal and climatic regimes. The present study reports the first widespread measurements of sediment supply to the

M.A. Allison (✉)
Department of Geology, Dinwiddie Hall,
Tulane University, New Orleans LA 70118, USA
E-mail: malliso@tulane.edu
Tel.: +1-504-8623197
Fax: +1-504-8655199

E.B. Kepple
Department of Geology and Marine Sciences,
University of South Carolina, Columbia SC 29208, USA

lower delta plain of a large river system which discharges onto a macrotidal margin within the tectonically active Bengal Basin.

Sediment accumulation rates were derived in the present study by using ^{137}Cs geochronology. ^{137}Cs ($T_{1/2} = 30.2$ years) is a particle-reactive, bomb-fallout radiotracer which was first introduced into terrestrial, wetland, and aquatic systems in 1954 with the advent of atmospheric hydrogen bomb testing (DeLaune et al. 1978). A number of studies in these settings (DeLaune et al. 1978; Ritchie and McHenry 1990; Walling et al. 1992; He and Walling 1996; Walling and He 1997) have utilized the first appearance of ^{137}Cs (or the 1963 peak fallout) as a marker horizon for sediment accumulation, sometimes in conjunction with naturally occurring radiotracers like ^{210}Pb ($T_{1/2} = 22.3$ years). In the Ganges-Brahmaputra (G-B) delta, Allison et al. (1998) utilized ^{137}Cs penetration depths to examine Brahmaputra floodplain sedimentation, whereas Goodbred and Kuehl (1998) examined sedimentation rates in a number of fluvio-deltaic G-B subenvironments, using a combination of penetration depths and sediment inventories of ^{137}Cs and ^{210}Pb. The present study builds upon this work by presenting ^{137}Cs, ^{210}Pb, and radiocarbon results for the relatively unstudied lower delta plain of the Ganges-Brahmaputra River.

Study area

The combined Ganges-Brahmputra river system is one of three (cf. Amazon, Huanghe) on Earth which deliver in excess of a billion metric tons of sediment to the ocean annually (Milliman and Syvitski 1992). Both rivers rise in the Himalayas, and converge 150 km inland of the Bay of Bengal on the vast lowland floodplain and delta plain centered over the Bengal Basin in Bangladesh and adjacent India (Fig. 1). West of the active river mouths for a distance of 300 km, a lower (tidal) delta plain extends inland as far as 100 km, dissected by a network of N-S-oriented tidal channels which, in some cases, are G-B distributaries which branch off the main rivers upstream of the estuarine throat. Historical charts and remote sensing data (Allison 1998) as well as stratigraphic information (Allison et al. 2001) indicate that the digitate lower delta plain morphology has evolved since maximum sea-level transgression at about 6,500 years B.P. (Umitsu 1993), by a process of seaward accretion of islands and their subaqueous shoal extensions. These islands are gradually welded to the lower delta plain to form N-S-oriented peninsulas, followed by an eastward shift of the G-B which results in later alteration of the channels by estuarine processes.

The lower delta plain of the Ganges-Brahmaputra can be divided into three zones. The Meghna Estuary region east of 90°10′ longitude (Fig. 1) is where G-B riverine discharge is focused and island/shoal complex accretion is active (Allison 1998). The western lower delta plain (west of the Haringhata river mouth

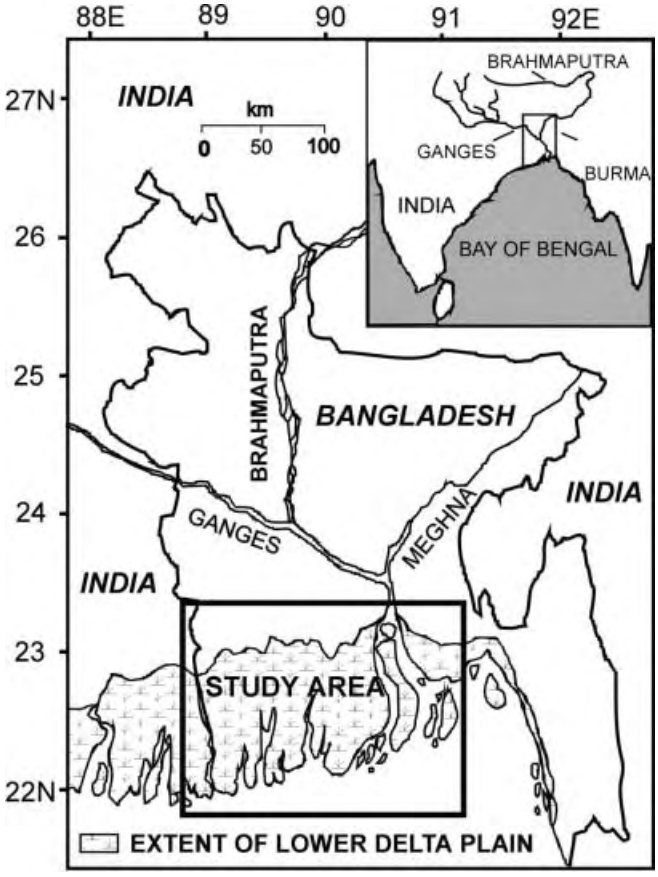

Fig. 1 Location map of the Ganges-Brahmaputra delta and the extent of the lower (saline) delta plain west of the present river mouths

estuary; Fig. 2) is a complex network of mangrove-vegetated islands and peninsulas (Sunderbans National Park) which forms the world's largest contiguous mangrove swamp. The forest floor exhibits a microtopography of 0.9–2.1 m above mean sea level (Katebi and Habib 1989). Although saline water may extend inland along tidal channels as far as 100 km during the dry season (September–May), significant tidal inundation of the Sunderbans occurs only during the monsoonal season (June–September) when southwest to southeast winds induce coastal setup and rivers are at peak water discharge. The central peninsula between the Haringhata River and the Meghna Estuary (Fig. 2) has elevations and an underlying geology similar to the Sunderbans. This region has been cleared for cultivation and is protected in some areas from saline water penetration by tides and tropical cyclones with earth embankments (polders). Historical maps from the 18th century show that there was a continuous belt of coastal mangroves from the Meghna Estuary to the Hoogly River in India prior to the onset of intense human cultivation. The entire G-B lower delta plain surface is composed of silt-rich alluvium which is undergoing rapid soil formation in response to the wet, tropical location of the delta, with an annual rainfall of

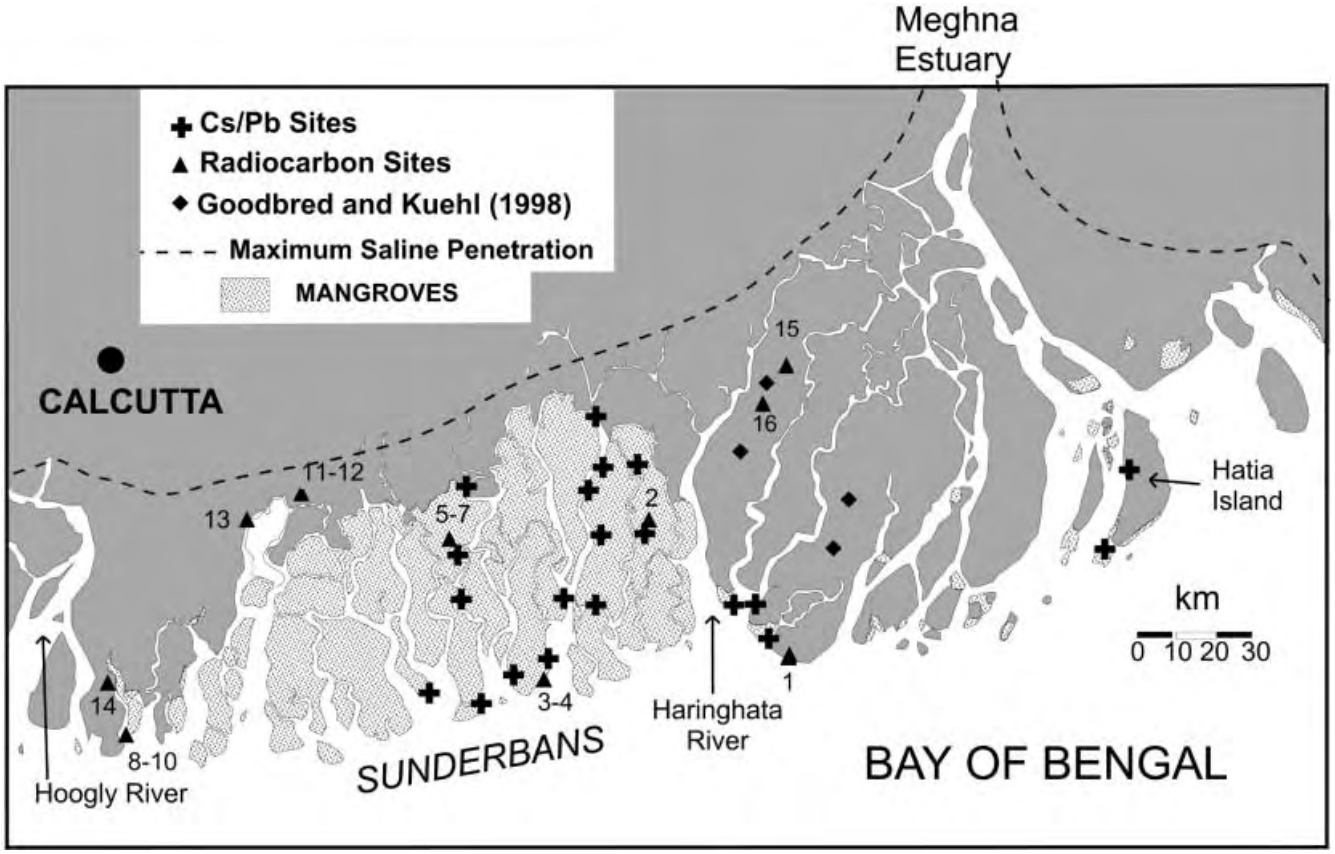

Fig. 2 Map of the core sites in the Ganges-Brahmaputra for Cs/Pb geochronology used in the present study as well as four sites measured by Goodbred and Kuehl (1998). Numbered sites *1–7* for radiocarbon were collected in the present study, sites *8–16* are data from previous studies (see Table 2)

150–300 cm, 85–90% of which falls during the monsoon period (Brammer 1996).

Methods

Sediment core samples were collected from 31 lower delta plain sites in Bangladesh in March 1998 and January 1999, 20 of which are utilized in the present study (Table 1). Areas not accessible by vehicle, including the Sunderbans National Park, were reached onboard M/V *Morzat* (Bangladesh Department of Forest) as well as various local ferries and fishing boats. Because of the presence of tigers, all samples from the Sunderbans area were taken within 100 m of tidal channel banks navigable by boat. Cores up to 5 m long were collected with a portable vibracorer using 7.5-cm diameter aluminum tubes. The cores were cut into 1-m sections and sealed on site. Upon return to the laboratory in Dhaka, the cores were sectioned lengthwise, photographed, X rayed, examined visually, and cut into 5-cm depth sections for transport to the USA. Sample sites not accessible with the vibracorer were sampled with an auger. A spoon (peat) sampler was used to obtain 7-cm-diameter cores from the upper meter which were described and subsampled at 5-cm intervals in the field. Below one meter, a Dutch auger head was used to collect samples at every 25-cm interval to a depth of 6–7 m in the sediment.

Analyses for ^{137}Cs, ^{210}Pb, and ^{226}Ra activities were conducted on sediment samples from 20 cores. Samples were dried at 60 °C, ground, and packed in 50-mm-diameter polycarbonate petri dishes (~10–15 g). Dishes were sealed for at least 21 days prior to counting to allow for ingrowth to secular equilibrium of ^{226}Ra daughter isotopes. Samples were counted for 1–3 days by gamma spectrometry, using a low-energy, planar germanium detector coupled to a multichannel analyzer. Activities were calculated using net peak areas of the 661.6- (^{137}Cs), 46.5- (^{210}Pb), and 352-keV (^{226}Ra) photopeaks. Activities were corrected for self-absorption using the methods of Cutshall et al. (1983). Excess ^{210}Pb activities were calculated by subtracting the supported levels obtained from ^{226}Ra activities. Five cores were also counted for ^{210}Pb, using alpha spectrometry of the ^{210}Po daughter following the methods of Nittrouer et al. (1979). Approximately 2 g of dried sample was spiked with a ^{209}Po yield determinant, leached with hot HNO_3 and HCl, and plated onto silver planchets. All counting statistics are based on 2σ standard errors.

Samples for grain-size analysis were wet sieved into sand and mud components using a 63-μm sieve. Mud fractions were analyzed wet, using a Sedigraph model 5100 X-ray particle analyzer on water-diluted slurries treated with sodium hexametaphosphate to inhibit

Table 1 Non-normalized ^{137}Cs inventories and accretion rates calculated by the penetration and inventory methods for all Cs sites in the G-B lower delta plain

Core	Latitude (N)	Longitude (E)	Depth of penetration (cm)	Penetration accretion (cm/year)	Cs inventory (dpm/cm^2)	Inventory accretion (cm/year)
7BP98	21°51′45″	90°04′18″	> 62	> 1.18	> 7.3	> 0.52
8BP98	21°56′59″	90°02′07″	55–100	1.53	5.3	0.35
12BP98	21°56′52″	89°58′34″	55–100	1.53	3.0	0.15
13BS98	22°25′44″	89°35′43″	20–25	0.28	1.2	0
14BS98	22°17′58″	89°36′54″	25–30	0.40	1.5	0.03
15BS98	22°14′25″	89°34′29″	30–35	0.51	2.6	0.12
16BS98	22°07′35″	89°36′33″	50–55	0.97	2.3	0.09
17BS98	21°57′54″	89°30′25″	35–40	0.63	4.3	0.26
18BS98	21°56′53″	89°35′43″	55–75	1.25	6.1	0.42
19BS98	22°07′46″	89°42′56″	100–105	2.10	14.4	1.13
20BS98	22°18′23″	89°42′37″	15–20	0.17	1.7	0.04
3BH99	22°25′44″	91°04′00″	> 155	> 3.22	> 13.4	> 1.0
6BH99	22°05′26″	90°59′56″	> 95	> 1.93	> 10.8	> 0.82
7BS99	21°49′06″	89°27′37″	45–50	0.83	4.1	0.25
8BS99	21°46′38″	89°22′50″	35–40	0.61	3.2	0.17
9BS99	21°41′47″	89°16′47″	50–55	0.94	6.9	0.49
10BS99	21°43′24″	89°08′10″	30–35	0.50	9.0	0.67
11BS99	21°57′44″	89°13′28″	60–65	1.17	7.2	0.51
12BS99	22°04′55″	89°13′30″	45–50	0.83	4.6	0.29
13BS99	22°15′08″	89°14′19″	10–15	0.06	1.7	0.04

flocculation. Sand fractions were dried at 60 °C for 24 hours and analyzed on an automated 180-cm settling column. Sand and mud analyses were reintegrated using total dry weight of sand prior to the column analysis, and dry weight of mud (silt + clay) obtained from an aliquot of the wet-sieved mud collected prior to Sedigraph analysis which was dried at 60 °C for 24 hours. Radiocarbon analyses were performed by AMS methods by the NAMS facility at Woods Hole, MA and Beta Analytic in Miami, FL. All dates are reported in calibrated sidereal (calendar) years using the CALIB 4.2 program of Stuiver et al. (1998).

Results

^{137}Cs was present in all 15 cores from the mangrove-vegetated Sunderbans region west of the Haringhata River to depths between 10 and 105 cm, with depth-integrated inventories varying between 1.2 and 14.4 dpm/cm^2, assuming an average grain density of 2.65 g/cm^3 (Table 1). Activities were generally low and ranged from the detectability limit of about 10 dpm/kg to a maximum of 200 dpm/kg. A subsurface peak which may correspond to the 1963 peak in bomb testing was observed in a few cores (e.g., at about 40 cm in core 11BS99; Fig. 3), but most showed variable activities downcore, including intervals where activity was below the detectability limit. ^{137}Cs inventories in the sediment cores decreased with increasing distance from the bay (Fig. 4).

Total ^{210}Pb activity in the surface sediments, for both gamma and alpha methods, was about 1,200–1,800 dpm/kg and varied downcore with no clear decay-induced slope (Fig. 3). ^{226}Ra activities in the cores, counted by gamma spectrometry, also fall in this range, close to the total ^{210}Pb activity. Measurement error (± 5%) makes it impossible to say whether all ^{210}Pb activity in the cores is supported or whether 100–300 dpm/kg of excess ^{210}Pb is present. Radiocarbon accumulation rates were also calculated for seven sites in the lower delta plain from the same cores as the Cs and Pb data, using calendar radiocarbon ages (Table 2). The resulting rates (0.13–0.70 cm/year) are averages for sediment accumulation over the last 2,500 years.

Discussion

Depth of ^{137}Cs penetration has been utilized in the Ganges-Brahmaputra floodplain (Allison et al. 1998; Goodbred and Kuehl 1998) and elsewhere (Ritchie et al. 1975; Walling and Bradley 1989) as an indicator of total sediment accumulation since the date of significant global fallout (1954) to the land surface (Cambray et al. 1982). In the G-B floodplain studies (Allison et al. 1998; Goodbred and Kuehl 1998), penetration accumulation rates were calculated after subtracting a general mixing depth of 10 cm which was interpreted to represent the integrated effect of processes which downmix ^{137}Cs (e.g., non-mechanized cultivation, diffusion, bioturbation, clay infiltration). Applying this method to the lower delta plain sediments yields accretion rates of 0.06–2.1 cm/year with a general trend of decreasing rates with increasing distance from the Bay of Bengal (Table 1).

^{210}Pb activity profiles have been used in many studies of floodplains and other coastal environments in concert with ^{137}Cs as an indicator of sediment accumulation which, because of the different fallout history of a naturally occurring radiotracer, provides a

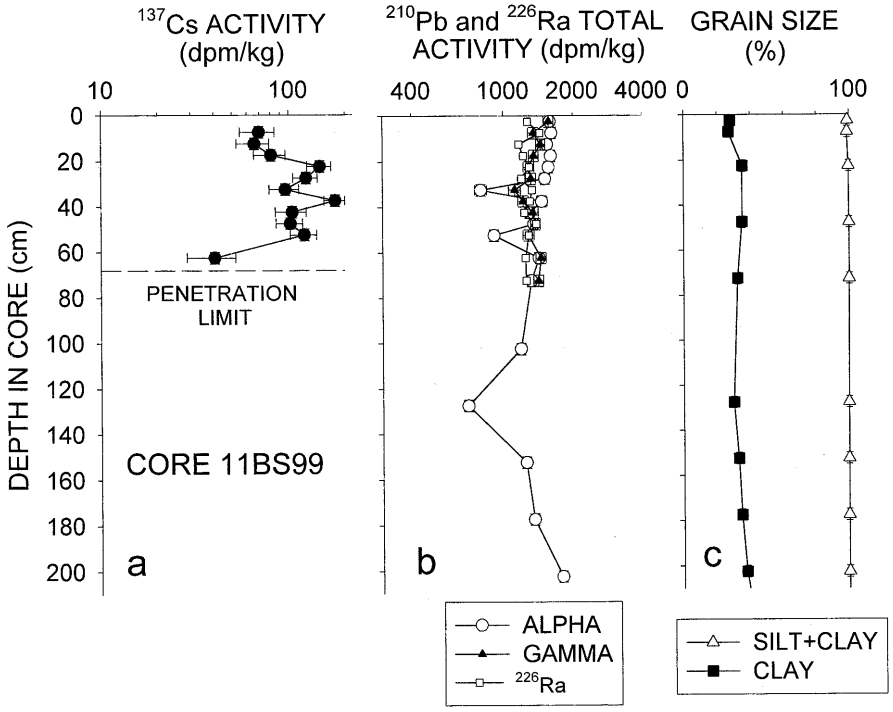

Fig. 3a–c Representative core from the Sunderbans lower delta plain region showing **a** downcore ^{137}Cs activities (activities are relatively low and ^{137}Cs penetrates to a depth of about 65 cm), **b** downcore total ^{210}Pb activities obtained by both alpha and gamma spectrometry, plotted against supported levels obtained from ^{226}Ra activities in the same gamma sample (data in this and other cores are inconclusive about whether ^{210}Pb above ^{226}Ra supported levels is present), and **c** clay and mud contents (< 4- and < 63-μm fractions, respectively; note that grain size is a relatively invariant clayey silt throughout the core)

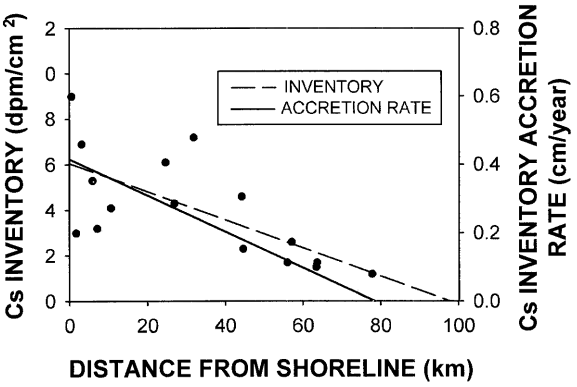

Fig. 4 Plot showing the decreasing non-normalized sediment inventories of ^{137}Cs for sites from the lower delta plain (• and *solid line*) in the Sunderbans and central lower delta plain with increasing distance from the Bay of Bengal. *Dashed line* shows the normalized ^{137}Cs accretion rates corresponding to this data set

powerful comparative tool. ^{210}Pb accumulation rates are determined by calculating the slope of the downcore decay of the excess ^{210}Pb carried by particles to the sediment surface in addition to the ^{210}Pb supplied by ^{226}Ra decay in the sediments (Nittrouer et al. 1979). In gamma-counted sediment samples where ^{226}Ra activities are measured directly, sediment accumulation has also been calculated from the excess inventory of ^{210}Pb by subtracting an atmospheric input term to yield a value for excess activity resulting from sediment deposition (He and Walling 1996). In the present study, the use of ^{210}Pb geochronology as a check on ^{137}Cs penetration-derived accretion rates has been unsuccessful because of the low excess ^{210}Pb activities of the lower delta plain sediments.

In the present study, the possibility that ^{210}Pb-supported levels were located at the sediment surface suggests that the occurrence of ^{137}Cs below the 10-cm mixing depth might be a function of post-depositional desorption and migration rather than sediment accumulation. ^{137}Cs has been shown to have a strong particle affinity except where the sediments are subject to fluctuations in pore-water salinity (Santschi et al. 1983; Sholkovitz and Mann 1984; Alexander et al. 1991). The lower delta plain would be expected to undergo such fluctuations because of diurnal and seasonal variations in tidal inundation and rainfall. Cs migration is supported by the fact that, in most of the cores, no Cs was detected in the uppermost (0–5 cm) intervals. In addition, ^{137}Cs inventories in the cores were low (< 14.4 dpm/cm^2). Because the atmospheric input of Cs to land surfaces has been nonsteady since 1954, Goodbred and Kuehl (1998) used sediment cores from exposed Pleistocene soil horizons in the G-B delta in Bangladesh as a proxy for determining the atmospheric input for the region. The mean inventory from three soil cores gave a ^{137}Cs value of 9.5 ± 3.7 dpm/cm^2. Values above this level were interpreted as the product of ^{137}Cs brought in on riverine particles during sediment accumulation. The Sunderbans lower delta plain sites from the present study have inventories of only 12–95% of atmospherically supported levels for all but one core (19BS98). One possible explanation is the effect of grain size. Goodbred and Kuehl (1998) demonstrated that Cs was sorbed almost entirely onto the < 10-μm fraction in Ganges-Brahmputra floodplain sediments. They corrected for grain-size variation within the cores by normalizing Cs inventories to a typical clay (< 4 μm) content of 50%. The lower delta plain cores, which

Table 2 Radiocarbon ages and accumulation rates for the GB lower delta plain

Key	Latitude (N)	Longitude (E)	Site	Depth (m)	Material	Radiocarbon age (year B.P.)	Calender age (year B.P. $\pm 2\sigma$)	Accumulation rate (cm/year)	Reference
1	21°49′25″	90°08′12″	6BP98	1.5	Buried tree	495 ± 45	614 ± 14	0.24	This study
2	22°07′46″	89°42′56″	19BS98	1.4	Marine shell	1,200 ± 30	730 ± 59	0.19	This study
3	21°49′06″	89°27′37″	7BS99	0.7	Wood	90 ± 40	227 ± 48	0.31	This study
4	21°49′06″	89°27′37″	7BS99	2.2	Crab claw	127 ± 7	309 ± 8	0.70	This study
5	22°04′55″	89°13′30″	12BS99	1.5	Peat	570 ± 50	584 ± 64	0.26	This study
6	22°04′55″	89°13′30″	12BS99	3.2	Peat	2,300 ± 40	2,378 ± 29	0.13	This study
7	22°04′55″	89°13′30″	12BS99	5.8	FW shell	2,690 ± 40	3,192 ± 17	0.18	This study
8	21°37′	88°18′	BS1159	8.4	Wood	4,710 ± 120	5,430 ± 230	0.15	Hait et al. (1996)
9	21°37′	88°18′	OS19420	12.2	Wood	4,790 ± 30	5,582 ± 63	0.22	Stanley and Hait (2000)
10	21°37′	88°18′	OS16697	23.4	Shell	6,040 ± 35	6,921 ± 85	0.34	Stanley and Hait (2000)
11	22°14′	88°47′	BS1156	22.3	Wood	7,530 ± 180	8,748 ± 13	0.25	Hait et al. (1996)
12	22°14′	88°47′	SH9	4.9	Wood	4,250 ± 40	4,889 ± 61	0.10	Stanley and Hait (2000)
13	22°10′	88°38′	BS1160	31.7	Wood	6,250 ± 140	7,137 ± 288	0.44	Hait et al. (1996)
14	21°45′	88°15′	Grn7137	1.8	Kankar	3,170 ± 70	3,382 ± 144	0.05	Gupta (1981)
15	22°33′	90°03′	BVC16	1.1	Peat	910 ± 60	820 ± 111	0.13	Brammer (1996)
16	22°32′56″	90°05′56″	GVC16	3.2	Peat	2,120 ± 70	2,267 ± 47	0.14	Goodbred and Kuehl (2000)

have relatively invariant downcore grain size and which were corrected to 50% clay content, exhibit normalized ^{137}Cs inventories of 2.0–12.1 dpm/cm^2 (Fig. 5a), still well below atmospherically supported levels in most cases.

Although desorption and migration of ^{137}Cs is indicated and might be an explanation for intercore differences in Cs penetration depth, it cannot explain the observed trend of increased normalized Cs inventories in cores close to the Bay of Bengal shoreline (Fig. 4). A linear regression analysis shows that there is a significant positive relationship between ^{137}Cs penetration depths and normalized ^{137}Cs inventories for the lower delta plain cores (t-test, $p < 0.05$, $n = 17$; Fig. 5a), which was also observed by Goodbred and Kuehl (1998) in the G-B floodplain and was interpreted as indicating a slow, steady-state release of ^{137}Cs-carrying particles from the G-B drainage basin to the sediment deposit. Their results show close relationships between accretion rates calculated by ^{137}Cs or ^{210}Pb inventories and penetration accretion rates. Dividing the lower delta plain core values by a correction term gives a penetration:inventory linear regression line which closely matches the adjacent floodplain values obtained by Goodbred and Kuehl (1998). A value of 0.26 for the correction term provides the highest correlation with the floodplain regression line (Fig. 5b). The low ^{137}Cs inventories relative to penetration depth in the lower delta plain, necessitating this correction factor, are interpreted to be partly a function of Cs desorption and migration. Low activities of ^{137}Cs and unsupported ^{210}Pb observed in the lower delta plain may also be generated by lower sorption efficiency, possibly due to organic content or composition, post-depositional ion exchange of surface sediments during tidal immersion, or dilution with low-activity sediment particles.

If normalized ^{137}Cs inventories above the lowest calculated value (2.0 dpm/cm^2) in lower delta plain cores are interpreted as sediment accumulation, inventories can be utilized to calculate sediment accretion rates in the presence of Cs migration in the sediments. Normalized inventory accretion rate (R_{Cs} cm/year) is

$$R_{Cs} = \frac{\lambda_{Cs}}{\left(1 - e_{Cs}^{-\lambda T}\right)} \frac{I_{total} - cI_{atm}}{f_{clay} \rho A_{clay}} \quad (1)$$

where λ_{Cs} is the decay constant for Cs, I_{total} is the non-normalized inventory of the core (dpm/cm^2), I_{atm} is the atmospheric component of 9.5 ± 3.7 dpm/cm^2, corrected with the term ($c = 0.26$) for the low activities observed in the lower delta plain, f_{clay} is the percentage of sediments finer than 4 μm, T is the time (years) of Cs input between 1954 and the year the core was collected, ρ is an estimated mean bulk density (1.3 g/cm^3) for the upper meter of lower delta plain sediments (Allison et al. 2001), and A_{clay} is the mean clay-normalized activity (dpm/g). The results (Table 1) give sediment accumulation rates of 0–1.13 cm/year for the cores, considerably lower than the rates calculated by the penetration depth method. Excluding the anomalously high value at site 19BS98, the accretion rates preserve the trends of decreasing values with increasing distance of the core site from the Bay of Bengal observed for the inventories and penetration depths (Fig. 4).

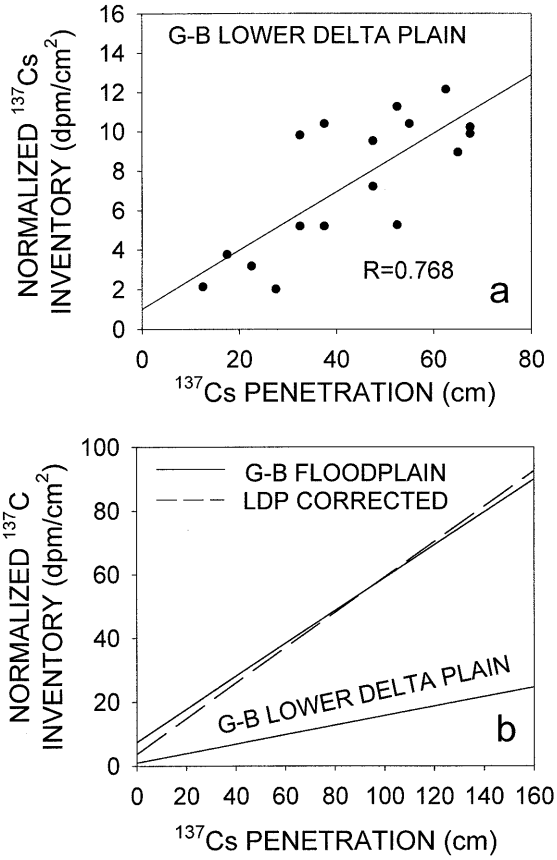

Fig. 5 **a** Plot of ^{137}Cs inventories normalized to 50% clay content vs. penetration depths of Cs for core sites from the Sunderbans region of the lower delta plain. **b** The same linear regression line for the lower delta plain (see **a**), compared with the values obtained for the Ganges-Brahmaputra floodplain by Goodbred and Kuehl (1998), as well as the lower delta plain values corrected by term (*c*) described in the text (*dashed line* LDP corrected). The LDP ^{137}Cs inventories increase with penetration in a similar manner to the floodplain, and therefore can be interpreted as a result of differing rates of sediment accumulation in the lower delta plain

In their study of floodplain accretion, Goodbred and Kuehl (1998) measured Cs at four sites under cultivation on the lower delta plain east of the Sunderbans region (Fig. 2). Their results showed penetration depths of 10 cm or less and no sediment accretion by the normalized inventory method used above. The contrast between these findings and the present study can be explained by (1) differences in the detection limits of ^{137}Cs in the gamma spectrometers (although both studies used the same Canberra model) in the two studies, (2) differences in the sorption efficiency and/or cation exchange capacity of surface sediments in the two areas, perhaps due to the cultivated versus undisturbed mangrove settings, or (3) spatial variations in sedimentation rates. The ^{137}Cs measurement at five cultivated/mangrove sites on the lower peninsula east of the Sunderbans and on Hatia Island in the river mouth (Fig. 2) served to investigate this aspect. In the latter area, remote sensing has provided evidence of accretion since the onset of bomb testing (Martin and Hart 1997; Allison 1998). The three cores from the south central lower delta plain (7BP98, 8BP98, 12BP98) show ^{137}Cs penetration depths and inventories equivalent to the Sunderbans cores (Table 1). The modern river-mouth cores (3BH99, 6BH99) also exhibit equivalent activities to the level of the deepest sample measured (155 and 95 cm, respectively). These data suggest that the ^{137}Cs results of Goodbred and Kuehl (1998) can be explained by either higher detection limits in their gamma detector, the inland location of the sites (34–69 km from the Bay of Bengal), or relatively high local elevations. In addition, the apparent accretion measured in the Sunderbans cores is evidently real, and is probably also taking place in the south central lower delta plain. These findings support the notion that, even in the modern river mouth, lower delta plain sediments show lower ^{137}Cs activities relative to G-B floodplain deposits of the same grain size, regardless of whether the sites are vegetated by mangroves or are under cultivation.

^{137}Cs inventory accretion rates can be compared with longer-term accretion rates obtained from radiocarbon dates converted to calendar years for wood, peat and shell samples from late-Holocene strata (<25 m below present surface) of the lower delta plain. A compilation of these data from the present study and other sources generally shows ^{14}C rates of 0.05–0.44 cm/year for the lower delta plain west of the active river mouth region (Table 2). The anomalous value (0.7 cm/year) obtained in core 7BS99 is from a crab claw which, as a result of burrowing, may have been located up to 50 cm or more below the sediment surface at the time of emplacement. For the five sites of the present study for which there are both Cs and radiocarbon data, ^{14}C accretion rates are 55–110% of ^{137}Cs rates (omitting the anomalous ^{137}Cs value at 19BS98). The finding suggests that ^{137}Cs-normalized inventory rates are valid, and that sedimentation has been relatively constant in the area for the last several thousand years. The ^{14}C accumulation rate interval is sufficiently long to reflect the seaward progradation of the subaerial strata unit as well as later aggradation of the mangrove surface. This complicates its application for estimating the rate of accommodation space created by relative sea-level rise (either by eustatic sea-level change and/or regional subsidence). The relatively constant rates of 0.1–0.4 cm/year observed at multiple depths at one site (core 12BS99) and at sites on the entire lower delta plain, as well as the elevation of the Sunderbans surface above all but the highest tides suggest, however, that rates of relative sea-level rise are unlikely to exceed these values. This contradicts older, anecdotal evidence of buried forests and buildings in the region being attributed to rapid tectonic and/or compaction-induced subsidence (Morgan and McIntire 1959).

Two possible vectors exist for sediment supply to the lower delta plain west of the active river mouths, i.e., delivery from upstream Ganges distributaries which discharge into the Sunderbans region (e.g., the Hoogly, Gorai) and from Ganges-Brahmaputra sediment

discharged onto the shelf and carried westwards by the prevailing coastal currents. The Ganges distributaries have undergone siltation in historical times which, in the Hoogly River in India, has necessitated the construction of barrages and dredging to maintain water flow during the dry season. This reduction in water and sediment discharge through older distributaries which dissect the Sunderbans lower delta plain suggests that much of the sediment reaching the lower delta plain is suspended sediment discharged through the G-B river mouth and carried westwards by residual (non-tidal and tidal) coastal currents for most of the year (Barua et al. 1994). Common surface suspended sediment concentrations are 150–200 mg/l in the nearshore area (< 5-m water depth) and in the tidal portions of the Ganges distributary channels (Barua 1990; Barua et al. 1994). The mangrove surface of the lower delta plain remains subaerially exposed during low G-B river discharge periods, but is flooded periodically by saline water from the 1–2 m coastal setup produced by onshore-oriented monsoonal winds in June–September (Katebi and Habib 1989). In addition, tropical cyclones make landfall along the northern Bay of Bengal coast every 3.1 years on average (Murty et al. 1986), producing storm surges of up to 6–7 m elevation. The observed pattern of decreasing ^{137}Cs sediment accretion rates with distance from the Bay of Bengal is attributed to an offshore source introduced during monsoonal high tides and cyclonic events. This sediment is likely a combination of recent suspended sediments from the river mouth and reworked inner shelf ephemeral mud deposits, the latter observed previously by Segall and Kuehl (1994), and Kuehl et al. (1997).

A first-order estimate of the sediment supply to the lower delta plain can be obtained from the ^{137}Cs accretion rate relationship with distance from the Bay of Bengal. Assuming a mean sediment density of 1.3 g/cm^3, a total of 3.7×10^7 tonnes/year is accumulating on the lower delta plain in the Sunderbans region (Haringhata river mouth to the Hoogly river mouth) from the shoreline to 75 km inland where the site data indicate that accumulation drops to negligible values. The central lower delta plain east of the Haringhata mouth and the river-mouth region to 91°15′ stores an additional 3.8×10^7 tonnes/year, assuming the same rates with distance measured for the Sunderbans region. Allison (1998) calculated that the average annual land accretion in the river-mouth region of the G-B delta was 5.5 km^2/year, which accounted for 0.97×10^7 tonnes/year of riverine sediment. This total is about 1–2% of the 59.9–108.7×10^7 tonnes of annual sediment load reported for the combined Ganges-Brahmaputra discharge (Coleman 1969; Master Plan Organization 1987). By contrast, lower delta plain sediment storage contributes 7–13% (7.5×10^7 tonnes/year) to the overall sediment budget. This modern riverine sediment contribution is clearly important for maintaining coastal land elevations in response to rising relative sea level in the area. Comparisons of historical and remote sensing evidence from the 1970s–1990s (Allison 1998) show that shoreline erosion is taking place, particularly in the western Sunderbans of Bangladesh and adjacent India where retreat rates reach 20 m/year, in spite of the large influx of sediment. It may be that the polders which are being constructed along the lower delta plain shoreline in Bangladesh will ultimately have a detrimental effect on land elevation by reducing the influx of G-B sediment during tidal and cyclonic floods.

Conclusions

^{137}Cs geochronologies from sediment cores in the Sunderbans lower delta plain west of the modern Ganges-Brahmaputra river mouths in Bangladesh show that the area is still a significant depocenter for riverine sediment. Sediment accumulation rates calculated from grain size-normalized ^{137}Cs inventories exceed the regional atmospheric contribution (range 0–1.1 cm/year), and show a trend of decreasing accretion with increasing distance inland from the Bay of Bengal. This accumulation accounts for 7–13% of the overall Ganges-Brahmaputra sediment load, and is likely delivered via onshore advection during monsoonal and cyclonic coastal setup events. ^{137}Cs inventories in the Sunderbans and river-mouth areas are less than one third those measured by other investigators in adjacent Ganges-Brahmaputra floodplain cores of comparable grain size, suggesting that surface-particle ^{137}Cs absorption efficiency is reduced in the lower delta plain and that desorption and downcore migration has taken place. Evidence of recent lower delta plain accretion is supported by general agreement with longer term, radiocarbon accumulation rates obtained from the same cores and from previous studies. This constancy of sedimentation in an environment which has undergone a progradation of facies in the late Holocene suggests that regional relative sea-level rise ranges from 0.1 to 0.4 cm/year.

Acknowledgements Funding for this study was provided by grant EAR-9707067 from the National Science Foundation. Logistical support for the fieldwork was given by the Bangladesh Geological Survey, Bangladesh Department of Forest, and EGIS II (Environment and Geographic Information Support) in Dhaka. The Department of Forest also granted permission to work in the Sunderbans National Park, and provided guards. Thanks are offered to all those who helped with sample collection, and for discussions on the interpretation of these data, including S.R. Khan, M. Lee, M. Kershaw, D. Lanier, S. Goodbred, and S. Kuehl. Two anonymous reviewers suggested many improvements in the final manuscript.

References

Alexander CR, Nittrouer CA, DeMaster DJ (1991) Macrotidal mudflats of the southwestern Korean coast: a model for interpretation of intertidal deposits. J Sediment Res 61:805–824

Allison MA (1998) Historical changes in the Ganges-Brahmputra delta front. J Coast Res 14:480–490

Allison MA, Kuehl SA, Martin TC, Hassan A (1998) The importance of floodplain sedimentation for river sediment budgets and terrigenous input to the oceans: insights from the Brahmaputra-Jamuna River. Geology 26:175–178

Allison MA, Khan SR, Goodbred SL, Kuehl SA (2001) Holocene stratigraphy and evolution of the Ganges-Brahmaputra lower delta plain in Bangladesh. Sediment Geol Spec Issue (in press)

Barua DK (1990) Suspended sediment movement in the estuary of the Ganges–Brahmaputra–Meghna River system. Mar Geol 91:243–253

Barua DK, Kuehl SA, Miller RL, Moore RS (1994) Suspended sediment distribution and residual transport in the coastal ocean off the Ganges-Brahmaputra River mouth. Mar Geol 120:41–61

Baumann RH, Day JW, Miller CA (1984) Mississippi deltaic wetland survival: sedimentation versus coastal submergence. Science 224:1093–1095

Brammer H (1996) The Geography of the soils of Bangladesh. University Press, Dhaka

Britsch LD, Dunbar JB (1993) Land loss rates: Louisiana coastal plain. J Sediment Res 9:324–338

Cahoon DR, Reed DJ, Day JW, Steyer GD, Boumans RM, Lynch JC, McNally D, Latif N (1995) The influence of Hurricane Andrew on sediment distribution in Louisiana coastal marshes. J Coast Res Spec Issue 21:280–294

Cambray RS, Playford K, Lewis GNJ (1982) Radioactive fallout in air and rain: results to end of 1981. UK Atomic Energy Authority Rep AERE-R 10485

Coleman JM (1969) Brahmaputra River: channel processes and sedimentation. Sediment Geol 3:129–239

Cutshall NH, Larsen IL, Olsen CR (1983) Direct analysis of ^{210}Pb in sediment samples: self-absorption corrections. Nucl Instr Methods 206:309–312

DeLaune RD, Patrick Jr WH, Buresh RJ (1978) Sedimentation rates determined by ^{137}Cs in a rapidly accreting salt marsh. Nature 275:532–533

Goodbred SL, Kuehl SA (1998) Floodplain processes in the Bengal Basin and the storage of Ganges-Brahmaputra river sediment: an accretion study using ^{137}Cs and ^{210}Pb geochronology. Sediment Geol 121:239–258

Goodbred SL, Kuehl SA (2000) Late Quaternary evolution of the Ganges-Brahmaputra River delta: significance of high sediment discharge and tectonic processes on margin sequence development. Sediment Geol 133:227–248

Gupta HP (1981) Palaeoenvironments during Holocene time in Bengal Basin, India as reflected by palynostratigraphy. Paleobotanist 27:138–160

Hait AK, Das HK, Ghosh S, Ray AK, Saha AK, Chanda S (1996) New dates of Pleisto-Holocene subcrop samples from South Bengal, India. Indian J Earth Sci 23:79–82

He Q, Walling DE (1996) Use of fallout ^{210}Pb measurements to investigate longer-term rates and patterns of overbank sediment deposition on floodplains of lowland rivers. Earth Surface Proc Landforms 21:141–154

Katebi MNA, Habib G (1989) Sunderbans and forestry. In: Coastal area resource development and management, part II. Coastal Area Resource Development and Management Association, Dhaka, pp 79–100

Kuehl SA, Levy BM, Moore WS, Allison MA (1997) Subaqueous delta of the Ganges-Brahmaputra river system. Mar Geol 144:81–96

Martin TC, Hart TC (1997) Time series analysis of erosion and accretion in the Meghna Estuary. Meghna Estuary Study Internal Rep, Bangladesh Ministry of Water Resources, Dhaka

Master Plan Organization (1987) Floods and storms. Tech Rep No 11 Master Plan Organization, Bangladesh Ministry of Irrigation, Water Development and Flood Control, Dhaka

Milliman JD, Syvitski JPM (1992) Geomorphic/tectonic control of sediment discharge to the ocean: the importance of small mountainous rivers. J Geol 100:525–544

Morgan JP, McIntire WG (1959) Quaternary geology of the Bengal basin, East Pakistan and India. Geol Soc Am Bull 70:319–342

Murty TS, Flathers RA, Henry RF (1986) The storm surge in the Bay of Bengal. Prog Oceanogr 16:195–233

Nittrouer CA, Sternberg RW, Carpenter R, Bennett JT (1979) The use of Pb-210 geochronology as a sedimentological tool: application to the Washington continental shelf. Mar Geol 31:297–316

Penland S, Ramsey K (1990) Relative sea level rise in Louisiana and the Gulf of Mexico: 1908–1988. J Coast Res 6:323–342

Reed DJ (1989) Patterns of sediment deposition in subsiding coastal marshes, Terrebonne Bay, Louisiana: the role of winter storms. Estuaries 12:222–227

Rejmanek M, Sasser CE, Peterson GW (1988) Hurricane-induced sediment deposition in a Gulf coast marsh. Estuarine Coastal Shelf Sci 27:217–222

Ritchie JC, McHenry HR (1990) Application of radioactive fallout Cesium-137 for measuring soil erosion and sediment accumulation rates and patterns: a review. J Environ Qual 19:215–233

Ritchie JC, Hawks PH, McHenry HR (1975) Deposition rates in valleys determined using fallout Cesium-137. Geol Soc Am Bull 86:1128–1130

Roberts HH, Bailey A, Kuecher GJ (1994) Subsidence in the Mississippi River delta: important influences of valley filling by cyclic deposition, primary consolidation phenomena, and early diagenesis. Trans Gulf Coast Assoc Geol Soc 44:619–629

Santschi PH, Ki YH, Adler DM, Amdurer M, Bell J, Nyffeler UP (1983) The relative mobility of natural (Th, Pb, and Po) and fallout (Pu, Am, Cs) radionuclides in the coastal marine environment: results from model ecosystems (MERL) and Narragansett Bay. Geochim Cosmochim Acta 47:201–210

Segall MP, Kuehl SA (1994) Sedimentary structures on the Bengal shelf: a multi-scale approach to sedimentary fabric interpretation. Sediment Geol 93:165–180

Sholkovitz ER, Mann DR (1984) The pore water chemistry of Pu-239/240 and Cs-137 in sediments of Buzzards Bay, Massachusetts. Geochim Cosmochim Acta 48:1107–1114

Stanley DJ, Hait AK (2000) Holocene depositional patterns, neotectonics and Sunderbans mangroves in the western Ganges-Brahmaputra delta. J Coast Res 16:26–39

Stanley DJ, Warne AG (1994) Worldwide initiation of Holocene marine deltas by deceleration of sea-level rise. Science 265:228–231

Stanley DJ, Warne AG (1998) Nile delta in its destruction phase. J Coast Res 14:794–825

Stuiver M, Reimer PJ, Braziunas TF (1998) High-precision radiocarbon age calibration for terrestrial and marine samples. Radiocarbon 40:1127–1151

Umitsu M (1993) Late Quaternary sedimentary environments and landforms in the Ganges Delta. Sediment Geol 83:177–186

Walling DE, Bradley SB (1989) Rates and patterns of contemporary floodplain sedimentation: a case study of the River Culm, Devon, UK. Geojournal 19:53–62

Walling DE, He Q (1997) Use of fallout ^{137}Cs in investigations of overbank sediment deposition on river floodplains. Catena 29:263–282

Walling DE, Quine TA, He Q (1992) Investigating contemporary rates of floodplain sedimentation. In: Carling A, Petts GE (eds) Lowland floodplain rivers: geomorphological perspectives. Wiley, London, pp 165–184

Wright LD, Coleman JM (1973) Variations in morphology of major river deltas as functions of ocean wave and river discharge regimes. AAPG Bull 57:370–398

Annex B64

Md. Ferdous Alam and Kenneth J. Thompson, "Current Constraints and Future Possibilities for Bangladesh Fisheries", *Food Policy,* Vol. 26, No. 3 (2001)

Pergamon

Food Policy 26 (2001) 297–313

FOOD POLICY

www.elsevier.com/locate/foodpol

Current constraints and future possibilities for Bangladesh fisheries

Md. Ferdous Alam [a], Kenneth J. Thomson [b,*]

[a] *Department of Agricultural Finance, Bangladesh Agricultural University, Mymensingh, Bangladesh*
[b] *Department of Agriculture, University of Aberdeen, 581 King Street, Aberdeen AB24 5YA, UK*

Received 1 May 1999; received in revised form 1 March 2001; accepted 19 March 2001

Abstract

Fisheries are an important source of animal protein, foreign exchange earnings and employment generation in Bangladesh. This paper examines the current status of fisheries in Bangladesh, for each of the major sub-sectors — inland open waters, inland closed waters (aquaculture), and marine fisheries. Production has been on the increase for all types of fisheries, but the productivity of rivers and estuaries is variable, there are many constraints on expansion, and it is difficult to identify significant achievements from government policy efforts. A host of factors are responsible for the under-utilisation of fishing areas, including resource limitations, poor implementation of fisheries laws, the limited spread of fish farming technology, low financial capacities and ineffective extension practices. These constraints are discussed for the three sub-sectors, and some possibilities for future improvements are suggested.

Keywords: Bangladesh; Fisheries; Open water; Closed water; Aquaculture; Marine; Policy

Introduction

With a total land area of 147,570 km^2, Bangladesh is characterised by a high population (127.6 million; 1998 estimate), rapid population growth (1.76% per annum since 1990), high population density (about 800 persons per km^2, or only 0.57 ha per head) and low per capita income (US$276 per year: World Bank, 1997). Agriculture (including fishing) is the major contributor to the economy, accounting

* Corresponding author. Tel.: +44-1224-274122 fax: +44-1224-273731.
E-mail address: k.j.thomson@abdn.ac.uk (K.J. Thomson).

for 32% of GDP. About 80% of the population live in rural areas where poverty is prevalent although its magnitude has reduced considerably over the last decade or so: 21.3% of aggregate income accrues to the bottom 40% of households, while the top 5% share 18.1%, the Gini ratio being 0.45 (World Bank, 1997, p. 37). About 46% of the rural population are inadequately fed, with a daily intake below 2122 kcal.

Fish and fisheries have been an integral part of the life of the people of Bangladesh from time immemorial, and play a major role in employment, nutrition, foreign exchange earnings and other aspects of the economy. Fish is a natural complement to rice in the national diet, giving rise to the adage *Maache-Bhate Bangali* ("a Bengali is made of fish and rice"): fish alone supplies about 60% of animal protein intake.[1] The fisheries sector provides full-time employment to an estimated 2 million fishermen, small fish traders, fish transporters and packers, etc. (World Bank, 1989), and another 10 million people are partly dependent on fishing, e.g. part-time fishing for family subsistence (BFRSS, 1986). The sector contributes about 5% of GDP (Ali, 1998), 14% of Gross Agricultural Product (Amin, 1998) and about Tk.18 billion[2] (9%) of export earnings, of which frozen shrimp constitutes about 82% while the rest are fish and other aquatic products such as frogs' legs, shark and shark fins (Banik and Humayun, 1998). Fisheries exports comprise frozen shrimp, frozen frogs' legs, frozen fish, dry fish, salted and dehydrated fish, turtles, tortoises and crabs, and shark fin and fish maws.

The objectives of this paper are to examine recent developments in the Bangladesh fisheries sector, and to assess the problems constraining fuller utilisation of its potential. This is done both by looking at physical and economic performance as far as this can be ascertained, and at constraints to successful policy implementation. This leads us to conclude with an assessment of some opportunities for future improvements.

Fisheries resources

Bangladesh is ideally suited for fish production, having one of the highest man–water ratios in the world, at 20 persons per ha of water area (Task Force, 1991). The country is very rich in inland water for fish production, being the delta of the three major river systems, i.e. the *Ganges*, *Brahmaputra* and *Meghna*. Altogether, a total of 230 large and small rivers (BBS, 1997) with their tributaries and branches criss-cross the country, with extensive floodplains along their banks. The estimated total floodplain area is 6.3 million ha (Mha), of which 0.8 Mha have been permanently dried up by flood protection measures. The balance of 5.5 Mha (MPO, 1989) is inundated at various depths ranging from very shallow (0–30 cm) to deeply flooded (more than 1.8 m) during the monsoon season. The fisheries are multi-species in

[1] FAO statistics show fish providing 47% of animal protein and 6% of total protein intake in 1993. Also, amongst UN-defined Low-Income Food Deficit Countries, Bangladesh has an unusually low consumption of animal proteins.

[2] Tk.1000 equals US$20 approximately.

nature: there are about 300 species of fish and 20 species of prawns in Bangladesh (Rahman, 1989). The most common species is *hilsha*,[3] which accounts for nearly half of the total marine catch, and about 18% of total fish production.

The fisheries resources[4] of the country are generally classified as: (i) inland open waters; (ii) inland closed waters; and (iii) marine waters (see Table 1).

- Inland open water bodies, where capture fishing is mainly carried out, comprise rivers and estuaries, *beels* (small lakes, low-lying depressions, permanent bodies of floodplain water, or bodies of water created by rains or floods that may or may not dry up in the dry season; in the wet season, *baors* or shallow lakes may be formed as smaller water bodies are joined up), Kaptai Lake (a man-made lake created for hydroelectricity) and floodlands (annually flooded, low-lying areas associated with rivers). The total area of inland open water bodies is 4.05 Mha, comprising 1 Mha of rivers and estuaries, 2.8 Mha of floodlands, and small areas of *beels* and Kaptai Lake.
- Inland closed water bodies, where aquaculture (fish farming) at various intensities is carried out, include ponds, *dighis* (big ponds) and *baors* (oxbow lakes), and also some coastal waters. The 0.3 Mha of inland closed water areas include 0.15 Mha of ponds and *dighis*, 0.14 Mha of traditional shrimp farms in coastal

Table 1
Water areas for Bangladesh fisheries, 1998. Source: Department of Fisheries (DOF, 1998)

Type of water body	Water areas (ha)	Percent of total inland waters
A. *Inland open waters:*		
Rivers and estuaries	1,031,563	23.77
Beels	114,161	2.63
Kaptai Lake	68,800	1.58
Floodlands	2,832,792	65.28
Total inland open waters	4,047,316	93.26
B. *Inland closed waters:*		
Ponds and *dighis*	146,890	3.38
Baors	5488	0.13
Coastal shrimp farms	140,000	3.22
Total inland closed waters	292,378	6.74
Total inland waters (A+B)	4,339,694	100.00
C. *Marine waters (Bay of Bengal):*	16,607,000	
Total waters (A+B+C)	20,946,694	

[3] *Hilsha*, also called *toli shad* (*Tenualosa toli*), is a basically marine diadromous species. For spawning, it migrates to rivers where a large number get caught. It is also caught in marine waters.

[4] See remarks later in the paper about Bangladeshi fisheries statistics.

areas, and small areas of *baors*, drains and ditches, and semi-intensive shrimp farms.

- Marine waters extend over 166,000 km^2 (16.6 Mha) of sea area, following the 1974 declaration of a 200-nautical mile Exclusive Economic Zone (EEZ), within which Bangladesh also has the right to exploit and manage living and non-living resources.

Fish production and yields

Total fish production in Bangladesh in 1997–1998 (provisional figures) was reported to be 1.491 million tonnes (Mmt), of which 0.62 Mmt (42%) was from inland open waters, 0.57 Mmt (38%) from inland closed waters and 0.30 Mmt (20%) from marine fisheries (Table 2). The largest three contributors to total inland production (including culture and capture) are ponds (35%), floodplains (32%), and rivers and estuaries (14%). The overall annual growth rate of fish production of

Table 2
Reported total fish production, Bangladesh, 1984–1985 to 1997–1998 (units: thousand metric tonnes). Source: Department of Fisheries (*Fish Catch Statistics*, various issues)

Year	Inland capture		Inland culture		Marine		Total	
	Quantity	%	Quantity	%	Quantity	%	Quantity	%
1984–1985	463.0	60	123.0	16	188.0	24	774.0	100
1985–1986	441.8	56	144.7	18	207.4	26	793.0	100
1986–1987	431.0	53	166.1	20	217.6	27	814.7	100
1987–1988	423.6	51	175.9	21	227.6	28	827.1	100
1988–1989	424.1	50	183.5	22	233.3	28	841.0	100
1989–1990	423.9	50	192.6	23	239.1	28	855.5	100
1990–1991	443.4	49	211.0	24	241.5	27	895.9	100
1991–1992	479.4	50	226.8	24	245.5	26	952.1	100
1992–1993	532.4	52	237.7	23	250.5	25	1020.6	100
1993–1994	573.0	53	264.0	24	253.0	23	1091.0	100
1994–1995	570.0	49	330.0	28	270.0	23	1170.0	100
1995–1996	595.0	47	390.0	31	279.0	22	1264.0	100
1996–1997	659.0	48	420.0	31	294.0	21	1373.0	100
1997–1998[a]	620.0	42	570.0	38	301.0	20	1491.0	100
Rates of growth to 1997–1998[b] from:								
1984–1985	3.39		10.47		3.07		5.02	
	(3.41)		(9.32)		(3.03)		(4.69)	
1989–1990	5.35		13.03		3.07		7.10	
	(6.13)		(11.61)		(2.93)		(6.80)	

[a] Provisional figures.
[b] Figures within parentheses are production growth rates excluding 1997–1998 data.

Bangladesh for the period 1984–1985 to 1997–1998 was 5.02% (4.69% excluding 1997–1998 provisional figures).

Data presented in Table 2 display several important features. First, although inland open water fisheries are still the largest contributors to total production, their share has declined, from 60% in 1984–1985 to only 42% in 1997–1998, while inland closed water (culture) fisheries have been contributing increasingly, from 16% in 1984–1985 to 38% in 1997–1998. Meantime, the share of marine fisheries fell from 24 to 20%. For each of these types, the overall production growth rate has been positive, but capture production from inland open waters fell at 1.66% per year in the 1980s. Almost all the growth has occurred since 1989–1990: since then, total production nearly doubled by 1997–1998, led by aquaculture in inland closed waters, which increased output at a remarkable 13% per year. Even excluding the provisional 1997–1998 figure, aquaculture is estimated to have grown by 11.6% per year. In the Bay of Bengal, production from the marine fisheries has grown steadily but relatively slowly since 1983–1984 (Table 2).

Turning to yield (annual production per hectare) statistics (Table 3), the average yield in open inland waters declined throughout the 1980s but recovered strongly thereafter, both overall and in each open-water category, with the possible exception of rivers and estuaries.

Current policy goals and constraints

The government of Bangladesh has looked to the fisheries sector to increase production, in order to improve nutrition, create employment and increase export earnings. The current Fifth Five-Year Plan (Planning Commission, 1998) targets per capita daily consumption to be raised from the current level of 25.6–34.4 g by the terminal year 2002. Based on an estimated population of 132.5 million, the required production of fish is thus 1.965 Mmt. In addition, the Planners assume that 95,000 tonnes of shrimp, fish and fish products will be exported in 2001–2002[5] and that another 15,000 tonnes of fish will be required for industrial and other uses. The fish production target for the terminal year has thus been set at 2.075 Mmt. The major thrusts of the current development budget are: (i) the promotion of rice–fish farming systems; and (ii) improved conservation and management along with institutional and manpower development for equitable distribution of benefits from common property water resources through social research with non-governmental organisations (NGOs).

These policy targets are thus clearly linked, but the interdependencies are complex and not always self-reinforcing. For example, under prevailing socio-economic conditions, it is unlikely that higher production alone will guarantee better nutrition for the majority of the people. There are considerable disparities — believed to be

[5] Export earnings from shrimp, fish and fish products and other aquatic organisms in 1999–2000 were Tk.18,100 million, and are expected to be Tk.23,028 million by 2001–2002.

Table 3
Reported yield of inland water bodies, Bangladesh, 1983–1984 to 1997–1998 (units: kg/ha/year). Source: calculated by the Department of Fisheries (*Fish Catch Statistics*, various issues)

Year	Inland capture (open water)					Inland culture (closed water)				All inland waters
	Rivers and estuaries	Flood-lands	*Beels*	Kaptai Lake	All inland capture	Ponds	*Baors*	Shrimp farms	Inland culture	
1983–1984	209	71	450	59	117	735	157	159	573	138
1984–1985	213	69	402	39	114	760	175	176	572	138
1985–1986	200	66	396	35	109	843	176	229	604	137
1986–1987	195	65	369	58	106	973	214	253	693	139
1987–1988	186	64	399	59	105	1017	228	269	714	140
1988–1989	176	66	412	50	105	1055	241	251	704	141
1989–1990	168	68	408	54	105	1115	247	254	739	143
1990–1991	131	88	420	64	109	1232	281	263	810	152
1991–1992	121	104	431	61	118	1328	306	278	870	164
1992–1993	135	116	464	60	132	1376	329	312	912	179
1993–1994	139	127	487	96	142	1515	401	286	910	193
1994–1995	155	130	511	81	130	1820	448	338	1084	209
1995–1996	168	130	534	87	150	2097	546	486	1296	228
1996–1997	152	132	587	116	149	2424	546	821	1621	249
1997–1998	156	134	622	131	153	2832	729	1071	1950	274

widening — in fish consumption between rich and poor households, and between urban and rural areas (Gupta and Shah, 1992). Annual per capita fish consumption in rural areas, as reported by them, is 4.4 kg for low-income people and 22.1 kg among higher-income groups. Given the present pattern of income distribution and rural–urban population distribution, the lion's share of higher production will probably be consumed by the urban population and by higher-income groups. However, an increase in fisheries exports often involves redirecting products from local consumption to buyers abroad (Kent, 1997). Access by the rural poor — and even by

fishermen households themselves — to fish as a source of protein to supplement others (e.g. pulses) is subject to the problems of direct and trade "entitlement failure" (Sen, 1981, p. 51).

In addition to these difficulties in setting policy objectives, many factors constrain the utilisation of the full potential of the fisheries in Bangladesh. Many of these constraints are known to the policy planners but cannot be overcome by individual government departments. Inter-government departmental co-ordination, co-ordination between departments and NGOs, and the stimulation of public response are important to deal with such a multitude of problems. Several of these constraints are discussed for the three sub-sectors — inland open waters, closed inland waters, and marine fisheries — in more general terms.

Inland open waters

The past trend of declining production of inland open water fisheries was of great concern to the government. Some of the important factors identified as responsible for the decline were (World Bank, 1991; Lewis, 1997; Planning Commission, 1998):

1. over-fishing caused by population pressure;
2. indiscriminate killing of juveniles and destruction of spawning grounds;
3. obstruction of migration routes due to unplanned construction of dams and embankments under flood control, drainage and irrigation (FCDI) projects;
4. shrinkage of floodplains due to growth of irrigation-based food grain production by paddy cultivation;
5. siltation, flood prevention controls, and changing water management practices; and
6. reduced availability of wild fish through increased use of agri-chemicals.

The use of agri-chemicals (fertilisers, pesticides and herbicides) in Bangladesh agriculture can probably not be reduced significantly in the foreseeable future because of the country's tremendous dependence on rice. The country is theoretically self-sufficient in food production but natural disasters such as floods continually threaten this balance. Foodgrain imports to meet emergencies have averaged 0.5–1.5 Mmt during the 1990s (World Bank, 1997). Public investment in agriculture for the last 20 or 30 years has been geared around rice, and the lion's share of the agricultural development budget has been used in this sector. In order to feed the growing population and because additions to land for crop cultivation is hardly possible, further intensification of foodgrain production may demand even more use of agri-chemicals.

The development of irrigation and drainage projects is also necessary because of dry-season water requirements for rice, wheat and some *rabi* crops like potatoes. Constructing embankments and other flood control devices is also unavoidable, but these have resulted in considerable obstructions to the migration of fish and damage to fish habitats. Hydraulic structures and sluice gates can reduce the problems, but these efforts are constrained by limited ability of the government to erect such structures in needed points, and to manage them after construction. The siltation of river

basins is another big problem, not permanently soluble by dredging rivers and estuaries.[6]

The improvement in the productivity of inland openwaters may be due to several government initiatives. These include as the New Fisheries Management Policy (NFMP), integrated pest management (IPM) and stocking programmes, the involvement of NGOs in fisheries management, the application of community-based fisheries management (CBFM), and the efforts of the fisheries and other departments such as tightening of fisheries law enforcement and openwater management measures.

The NFMP was initiated for inland open water fisheries (known as *jalmahals*) in 1987, and is aimed at protecting fishers from exploitation by influential middlemen, and at conserving fishery resources by limiting the number of fishers to ensure maximum sustainable catches[7] (Ahmed et al., 1997). The main elements of the NFMP are to: (a) identify genuine fishermen and organise them into groups; (b) provide them with fishing rights via licenses to fish in well-defined water areas via the gradual replacement of the revenue-oriented yearly leasing system; and (c) provide needed technical, marketing, and credit facilities. The NFMP has had beneficial effects on income distribution from open water fisheries, and was early reported as largely or potentially successful (BCAS, 1989). However, further state initiatives have been needed, such as the current World Bank-financed Fourth Fish Project costing Tk.3000 million.

Integrated pest management (IPM) techniques have been encouraged to reduce the use of chemical fertilisers and pesticides. Introduction of fish bypasses (rubber dams) to facilitate fish movement, establishing fish sanctuaries in strategic river locations, expansion of fish culture in paddy fields are some of the important initiatives. Stocking programmes of openwaters and floodplains is ideally a very promising initiative but so far have not proved satisfactory (Planning Commission, 1998). Nevertheless, the initiative has remained an important strategy to augment stock of openwater fisheries. Increasing emphasis has been placed on conserving fish resources through rigorous implementation of fishing legislation, and the education of and information to fishermen. All these initiatives have certainly contributed towards improving the situation of the openwater fisheries.

Inland closed waters

Given the vast areas of ponds, *baors*, and coastal shrimp farms, fish farming in the more manageable inland closed waters provides greater promise (see Table 3). Of the total 1.47 Mha of pond area, 52.2% is accounted for by cultured ponds, which are stocked with fingerlings, provided with inputs and feeding, and managed on some

[6] A permanent solution requires reforestation amongst the headwaters in India.

[7] Prior to the introduction of NFMP, the water bodies of Bangladesh used to be leased through auction, since a major concern of the government was to collect revenue. As a result of auctioning, influential persons who were usually non-fisherman would get the usage rights, and genuine fisherman had very limited access. Moreover, successful bidders tended to extract fish to the fullest extent without regard to conservation.

sort of scientific basis. The rest of the total, i.e. about 31% are culturable ponds having potential for culture without improvement but where fish fry are not released, and 17% are derelict ponds not suitable for fish culture without improvements. The average annual yield of the cultured ponds is around 2.0 t/ha, which is lower as compared to many private farms and projects run by NGOs. Some fish farmers are successfully achieving 4–5 t/ha or even more. The average yield of culturable and derelict ponds is even lower: 928 and 508 kg/ha/year, respectively. Fish feed being costly, is perhaps the most important constraint towards the expansion of semi-intensive or intensive aquaculture.

The yield of ponds, *baors* and shrimp farms increased consistently and more than doubled during the period 1983–1984 to 1997–1998. In particular, pond yields appeared nearly to quadruple over that period. For all inland waters, yield per hectare doubled almost exactly. The Bangladesh Fisheries Research Institute (BFRI) and the International Centre for Living Aquatic Resources Management (ICLARM) have generated new and profitable technologies (farming systems involving species suitable for polyculture, monoculture, and integrated culture, e.g. fish–rice, fish–poultry–duck). Moreover, demonstration projects have contributed significantly to the adoption of these and other technologies. Such projects include the Mymensingh Aquaculture Extension Project (MAEP) funded by the Government of Bangladesh and the Danish agency DANIDA, the North-western Fisheries Project funded by the UK agency DFID, and the efforts of NGOs such as the Grameen Bank, BRAC, CARE, Proshika and CARITAS. A large number of other NGOs have fish and shrimp culture projects with landless, small and marginal farmers, and the productivity these ponds is usually higher than many privately managed ponds. These continued initiatives have certainly led to increases in overall production as well as productivity of the culture fisheries. However, many of these efforts are localised, and their widespread adoption is hampered by the poverty of the fishermen, and the lack of credit access.

Marine waters

The factors constraining production of the marine fisheries are: (i) the high levels of capital required to exploit resources of the deep sea; (ii) congestion by artisanal fishermen in inshore waters; (iii) inadequate knowledge and information on fish stocks, particularly the pelagic stock; (iv) lack of modern fishing know-how and equipment; (v) inadequate harbour and landing facilities; and (vi) risks regarding fishing equipment and lives. Low preferences (domestic demand) for the marine species are an additional factor, which has perhaps failed to attract adequate attention.

Many of these constraints are hard to measure. Most of the marine resource surveys[8] carried out in the 1960s and 1970s are outdated, and uncertainty exists as to whether the marine fisheries are under- or over-exploited (see for example Alam,

[8] Marine fishing surveys were carried out by the Japanese in 1960–1961, by FAO in 1968–1971 and 1979–1980, by the Bangladesh Ministry of Fisheries and Livestock and Japan jointly in 1976–1977, and by Bangladesh and Thailand jointly in 1979.

1993). The Department of Fisheries believes that marine fisheries are over-exploited, and the World Bank (1991) has commented that marine fishing has reached a maximum sustainable level and thus offers limited scope for expansion. However, the rather slowly increasing production trend of marine fish suggests the contrary, and it is often said that the potential for deep-sea fishing is yet unexplored. However, detailed surveys in the vast EEZ are very expensive, and benefit–cost analysis is likely to provide little support for such survey investment. Moreover, the operation of only 47 shrimp trawlers and 13 fish trawlers in the vast area of the EEZ (Ali, 1998; DOF, 1998) reflects the capital constraint which has limited the number of large deep-sea trawlers.

Also, the capital and operating costs of large boats such as deep-sea trawlers are formidable, and investment in processing industries can hardly be justified since many existing plants are under-utilised: only about 15–20% of total installed capacity is fully used (World Bank, 1991).

Finally, given the limited size of the domestic market (both fresh and processed),[9] higher production of marine species will create considerable disposal problems unless an export market can be created. However, market preferences cannot be developed overnight. While it is true that poor people would consume marine fish instead of starving, it has to be made available. Alternatively, the low-value and trash fish could be used to make fish meal and/or animal feed. The fishermen would rather utilise their storage space for more valuable species, most of which are meant for the export market, and the bulk of the low-value species are dumped into the sea. Therefore, unless some way of retaining low-value and trash species is found, domestic consumption cannot be increased. It is therefore unlikely that marine fishing can be significantly increased to supplement the fish consumption of the country. At best, exports may be enhanced (as is happening), but this is likely to benefit only the richer segments of the population.

Statistics, credit and public administration

A basic problem for fisheries analysis, planning and evaluation in Bangladesh is that the national statistics are very poor and often conflict with the actual situation and with each other. For example, statistics on pond areas show no change for the last 10–12 years or so, whereas aquaculture (both fish and shrimp culture) has opened a new era for fish farming during this period. Many new entrepreneurs have entered this sub-sector and have excavated new ponds, not reflected in official statistics. In the marine sector, official statistics on the numbers of fishing boats, vessels and fishermen conflict with many field observations, and there is continuing uncertainty over deep-sea exploitation in terms of stocks and harvesting rates by both domestic and foreign boats. The production statistics may be less free of such doubts, but are still unreliable. Because of these and other problems, future projections and targets for fisheries policies can only be weakly based.

[9] *Hilsha* caught in rivers fetch higher prices than those from marine waters.

The greater provision of credit has long been advocated for the development of all types of fisheries. Millions of Taka have been disbursed over the years for the crop sector, but fisheries credit accounts for only 1.5–4.5% of the agricultural sector total and 0.09–0.35% of that for all sectors (World Bank, 1991, p. 25). Moreover, the allocated credit budget is not made available timeously. Rahman (1990) showed that processing plant owners found it difficult to obtain institutional credit for working capital, and hatchery and nursery operators found the credit process too complex and bureaucratic. Fish and shrimp farmers and fishermen without collateral often fail to qualify for institutional credit. Rich farmers and other affluent people have enjoyed most of the benefits of easy credit. With the existing rural power structure, it is very hard to devise credit programmes to target exclusively the small- and medium-sized fish farmers. Most pond owners are small and marginal farmers and have very small ponds used for non-commercial home fish supply. Although this is what is being encouraged, capital constraints often limit pond fish farming due to the very poor accessibility of the fish farmers to banks and credit institutions. Several years of experimentation have elapsed, but as yet no effective model of credit has been evolved to give exclusive benefit to the landless, small- or medium-sized farmers and fishermen.

Budget allocations to the fisheries sector have declined over time in spite of its increasing role to the economy. During the Third Five-Year Plan, the allocation was 1.58% of the total budget, increasing to 1.78% during the Fourth Five-Year Plan, but reduced (from Tk.7500 to Tk.5862 million, i.e. by 22%) to only 0.29% during the Fifth Five-Year (1997–2002) Plan (Ali, 1998).

While various costly public programmes such as stocking floodplains, establishing fish sanctuaries, and constructing fish bypasses are being actively implemented or at least considered, inactive law enforcement jeopardises the positive effect of such programmes for open water fisheries. Activities such as catching under-sized, juvenile and brood fish, and the use of prohibited gear such as "current *jal*" (nets having very small mesh size), are clear violations of fisheries law. During the Fish Fortnight,[10] recommendations for strengthening the implementation of laws are repeatedly made, but policy makers and implementers appear to forget these subsequently. This attitude reflects a lack of commitment to fisheries development and is an example of a major policy deficiency. In the marine sector, there is inadequate monitoring and control over exploitation, e.g. over-catching by trawlers in coastal waters, and by foreign boats in deep-sea areas.

Adoption and spread of fishing technologies depend mainly on extension services. The responsibility for fisheries extension lies with the Department of Fisheries (DOF) but like many other government agencies the DOF is hampered by a severe lack of resources and a rigid hierarchical institutional culture, which inhibits proactive work. The Thana Fisheries Officers (TFOs) lack proper training and field experience, and

[10] Each year, during a fortnight in August or September, the Department of Fisheries and the Ministry of Fisheries and Livestock conduct a programme to display and demonstrate new technologies, and to educate or inform fish farmers, fishermen and related parties by means of seminars, symposiums, pamphlets and posters.

are often constrained by lack of transport and the non-reimbursement of fuel costs. These problems make the extension services ineffective, hamper the transfer of technologies, and are partly responsible for the low adoption of semi-intensive fish culture.

Future possibilities for improved fisheries

Poor developing countries face a number of problems in designing and implementing governmental policies, and many of these difficulties are fully reflected in the Bangladesh fisheries sector. Not much can be done at a sectoral level about some problems but there are others for which solutions may exist, or at least which require the best or least-worst solution to be attempted. Some problems have the nature of conflicts or trade-offs, where difficult choices, often involving a mixture of efficiency and equity goals, or a balancing of short- and long-term costs and benefits, must be made. Others involve trying to improve the management and administration of private- and public-sector activities, through additional resources or appropriate information. Some of these possibilities are discussed below.

Food requirements

The best way to enable the poor to improve nutritional intake from fish appears to be through subsistence fishing in the floodplains. Quick-growing species, and species that have been already fished out, should be re-stocked so that species diversity is restored. The poor can also benefit from the consumption of small fish. A stocking programme combined with increasing public awareness in favour of ‘no immediate catching of released fry/fingerlings’ would probably allow the subsistence fishers to improve nutritional intake from fishing.

Inland open waters

It is often argued that the use of fertilisers, pesticides and herbicides should be reduced to improve the fish habitats and increase fish production of the floodplains. However, given the national food import requirement, it is unlikely that use of fertiliser and other chemical inputs can be reduced in the foreseeable future. In fact, statistics show that the consumption of chemical fertilisers, insecticides, herbicides, etc. has been on the increase (MOA, 1995; World Bank, 1997). Therefore, in the context of a country like Bangladesh, one probably has to accept the increasing use of agri-chemicals in crop production, and plan for the development of floodplain fisheries accordingly.

Other environmental problems such as reduced fish habitat due to construction of flood control and drainage projects and to industrial pollution of inland waters can be controlled to some extent. Mechanisms for establishing links between waters affected by flood control projects with the open waters of other floodplain fisheries are very important in improving the productivity of floodplain fisheries. In its Fifth

Five-Year Plan, the government has included such a strategy. Strict enforcement of pollution regulations, and regulation concerning catching of fish and fries and brood fish, are urgently needed. The establishment of fish bypasses and sanctuaries are under active consideration, and a stocking programme has been continued for more than a decade. Therefore, it appears that it is not the lack of policy strategy but the commitment of the government machinery to implement these measures which is missing.

Fisheries management is also partly responsible for the poor performance of the much-talked-about strategies. Adoption of the NFMP, CBFM, and increasing public disapproval of environmental degradation, of the use of destructive gears, and of the indiscriminate immediate (without allowing time for fish to grow) catching of stocked fry/fingerlings are very important to improve the floodplain fishery. Some of these measures have already started producing positive results. CBFM has been benefiting the fishermen and fish stock (see Hossain and Nazmul Alam, 1998; Thompson et al., 1999). Given the increasing fishing pressure, a stocking programme is necessary to the successful management of floodplain fisheries. The DOF believes that artificial stocking of the rivers and floodplains has reversed the downward production trend, but its impact may or may not be sustained depending upon how the fisheries is managed. Moreover, research is needed into the construction of fish bypasses for better movement of fish and restoration of fish habitat, the establishment of fish sanctuaries to protect brood fish, and CBFM systems in order to arrive at appropriate decision.

Inland closed waters

In the field of culture fisheries, important investigation needs are genetic research on quick-growing species, and research on fish farming systems and into the status and activities of hatcheries. An overwhelming majority of the fish farmers do not use artificial feed as it is very costly. The common material input (feed) applied is rice bran. Therefore, research is urgently needed to develop cheap fish feed. In addition, some researchable topics are the actual adoption of recommended input levels and technologies, and benefit–cost analysis of different fish farming systems and fishing technologies. The fisheries extension service should intensify its efforts to familiarise farmers with the combinations and dosage levels of input use. The culturable and derelict ponds must be brought to culture, and all impediments in connection with this should positively be removed in order to take advantage of the additional production which is currently foregone.

The potential of aquaculture may be seen from three angles. First, the yields of cultured ponds can be at least doubled by adopting semi-intensive management, or even more by adopting more capital-intensive systems. The use of artificial feed under semi-intensive management of some ponds in Kishoreganj has given more than 8 t/ha. The possibility of disease exists, but under such management can be taken care of. Extensive management of ponds will not suffice to raise consumption levels and meet export requirements as the number of ponds and total pond area is limited. Therefore, pond management must be made at least semi-intensive if not

fully capital-intensive in the long run. Second, culturable and derelict ponds, which constitute a big proportion of the total pond area, could be brought under semi-intensive or intensive fish culture with some excavation and re-excavation.[11] Third, in addition to 1.3 million perennial ponds, there are hundreds of thousands of shallow seasonal ponds and ditches, road-side canals, and borrow-pits (artificial canals created for flood control embankments and irrigation projects for rice production) which retain water for only a part of the year (mostly 4–7 months). These have tremendous potential for culturing species like Nile Tilapia (*Oreochromis niloticus*) and silver barb (*Puntius gonionotus*) (Gupta and Rab, 1994). At the current state, many of these resources are unutilised, expansion of aquaculture in such utilised resources would provide additional fish and employment of the subsistence fishers.

In addition, Bangladesh conditions are very suitable for pen and cage culture, which could greatly supplement the fish production of the country. Cage culture was attempted in Lake Kaptai (Karim, 1988; ADB, 1989) but has not yet spread over the country. Another type of potential fish farming is integrated rice–fish culture. Fish has traditionally been a natural component of the rice field ecosystem in Bangladesh and provides farmers with a convenient source of protein and income. Some NGOs have already started practising rice–fish integrated culture. Dewan (1985) and Gupta et al. (1998) emphasise that good prospects exist for paddy–fish farming in Bangladesh.

Marine fisheries

As discussed above, it is also necessary to determine whether marine fisheries are really over-exploited. Important concerns are resource surveys for the identification of fishing grounds for both demersal and pelagic fish, the determination of over-fishing, and the number of operating fishing boats, vessels and fishermen. Also needed are market surveys into preferences for marine species, and investigations into crew income-sharing systems. The Fisheries Development Corporation (FDC) has been set up to create infrastructure for the marine fisheries sector, but has been subject to inefficiencies and political disturbance.

Fisheries infrastructure

The provision of improved landing centres (stages) is sometimes advocated as a means of assisting coastal and marine fishermen to land and market their catch more efficiently. However, given the scarcity of capital, there is a great need to avoid investments that bring low returns compared to other sectors. Fishing in Bangladesh is carried out in innumerable rivers, estuaries and floodplains all over the country. Of the thousands of fishermen operating in open waters at different locations, a significant proportion are subsistence or artisanal fishermen. Public investment in the

[11] Rough calculations suggest that an additional 100,000 t might be produced if these ponds were bought into semi-intensive culture.

construction of large-scale landing centres can hardly be justified for this kind of subsistence fishing. Throughout the country, NGOs have better networks close to the grassroots, and could be used as channels for more effective credit delivery and utilisation.

What is needed more is improvements in marketing infrastructure. It is believed that 10–12% of all fish caught becomes spoiled and unsuitable for human consumption (Karim and Ahsan, 1989). Shahidullah (1986) has remarked that "…harvested shrimp arrives at the landing centers without ice, and is usually held there with insufficient ice".[12] During the monsoon season, *Hilsha* is caught in abundance but every year is wasted due to shortage of ice. An insulated and refrigerated transport system is almost completely absent, except in the metropolitan cities of Dhaka, Chittagong and Khulna. In addition, more ice factories, auctioning improvements, and better wholesaling and retailing market places are all required.

Marketing improvements are needed even more urgently in terms of the export market, which as mentioned above is an important component of both the current trade balance and of the Five-Year Plan. However, the 1997 ban by the European Union (EU) on seafood imports from Bangladesh, based on serious deficiencies found in EU inspections of infrastructure and hygiene in the Bangladesh processing sector (Cato and dos Santos, 1998), cost the country some US$15 million for shrimp exports alone. The need to secure high-value markets in developed countries against sudden and unexpected crises of this type has led to significant improvements, but there is much yet to be done.

Extension and management

To expand aquaculture, the fisheries extension services need to be strengthened in order to popularise semi-intensive fish culture and bring culturable and derelict ponds and other water bodies into fish culture. Low-cost fish feed must be developed and made available to enable farmers to use in their ponds. Government programmes for water management should be designed so as not to affect fishing habitats in particular and fisheries in general. Community participation in the utilisation of *khas* ponds and other water bodies should be ensured to handle social problems such as poaching (and to some extent economic problems such as finance), side by side with present efforts in stocking water bodies, establishing sanctuaries, and facilitating fish movement. The New Fisheries Management Policy should be fully implemented for management of open water bodies. Public disapproval of the breaking of fisheries laws must be fostered, and strict enforcement of laws is necessary for making public efforts meaningful. The active participation of community and the involvement of NGOs (at least initially) is particularly necessary for fisheries resources lacking property rights. The close co-operation of the DOF and NGOs (ultimately community) is essential for better fisheries management. Finally, up-to-date fisheries statistics are needed for making and monitoring sound plans.

[12] See also the *Bangladesh Independent* Internet edition, 17.02.01

Acknowledgements

The first author expresses his gratitude to the Association of Commonwealth Universities for a fellowship to pursue post-doctoral research at the University of Aberdeen.

Both authors are grateful to Dr Peter Howgate for most useful comments and suggestions on an initial draft, and to two anonymous reviewers for further comments and suggestions. However, responsibility for the content of the paper is entirely theirs.

References

Ahmed, M., Capistrano, A.D., Hossain, M., 1997. Co-management of Bangladesh fisheries. Fisheries Management and Ecology 4 (3), 233–248.

Alam, M.F., 1993. An economic study on the utilization and potential of marine fisheries in Bangladesh. Research Report submitted to Winrock International. Department of Agricultural Finance, Bangladesh Agricultural University, Mymensingh, Bangladesh.

Ali, M.L., 1998. Matshyasampad Unnayon O Babosthapona Koushal (Fisheries Development and Management Strategy). Sankalan: Matsya Sampad Unnayan, Fish Week 98. Directorate of Fisheries and Ministry of Fisheries and Livestock, Government of the People's Republic of Bangladesh, Dhaka (in Bengali).

Amin, N.M., 1998. Matshyasampad Babosthaponai Prathisthanik Samonnoyer Guruttya (Importance of Institutional Co-ordination in Managing Fisheries Resources. Sankalan: Matsya Sampad Unnayan, Fish Week 98. Directorate of Fisheries and Ministry of Fisheries and Livestock, Government of the People's Republic of Bangladesh, Dhaka (in Bengali).

Asian Development Bank (ADB), 1989. Project Completion Report of the Aquaculture Development Project in Bangladesh, Manila.

Banik, R.C.K., Humayun, N.M., 1998. Matsya Sakranto Parishankhan (Fish-Related Statistics). Sankalan: Matsya Sampad Unnayan, Fish Week 98. Directorate of Fisheries and Ministry of Fisheries and Livestock, Government of the People's Republic of Bangladesh, Dhaka (in Bengali).

Bangladesh Bureau of Statistics (BBS), 1997. Statistical Pocket Book of Bangladesh, 1997. Statistical Division, Ministry of Planning, Government of the People's Republic of Bangladesh, Dhaka, Bangladesh.

Bangladesh Center for Advanced Studies (BCAS), 1989. Final report on the Project for Experiment on Approaches to New and Improved Management of Openwater Fisheries in Bangladesh (ENIMOF), Department of Fisheries and Ministry of Fisheries and Livestock, Dhaka, August 1989.

Bangladesh Fisheries Resources Survey System (BFRSS), 1986. Water Area Statistics of Bangladesh. Fisheries Information Bulletin, vol. 1, Dhaka, Bangladesh.

Cato, J.C., Dos Santos, C.A.M.L., 1998. Bangladesh seafood exports: safety, hygiene and the EU ban. INFOFISH International 6, 52–58.

Department of Fisheries (DOF), 1994–1998. Fish Catch Statistics, various issues. Department of Fisheries, Government of the People's Republic of Bangladesh.

Dewan, S., 1985. Prospect of paddy-cum-fish culture in Bangladesh. Proceedings of the Workshop on Farming System Development, 5–6 June. NRDP/DANIDA Project, Noakhali, pp. 59–67.

Gupta, M.V., Rab, M.A., 1994. Adoption and Economics of Silver Barb (*Puntius gonionotus*) Culture in Seasonal Waters in Bangladesh. ICLARM Technical Report no. 41, International Centre for Living Aquatic Resources Management, Manila, Philippines.

Gupta, M.V., Shah, M.S., 1992. NGO Linkages in Developing Aquaculture as a Sustainable Farming Activity: a Case Study from Bangladesh. Paper presented at the Asian Farming Systems Symposium, Colombo, Sri Lanka.

Gupta, M.V., Sollows, J.D., Mazid, M.A., Rahman, A., Hussain, M.G., Dey, M.M., 1998. Integrating Aquaculture with Rice Farming in Bangladesh: Feasibility and Economic Viability, Its Adoption and Impact. International Centre for Living Aquatic Resources Management (ICLARM) Technical Report no. 55, Manila, Philippines, 90pp.

Hossain, M.M., NazmulAlam, S.M., 1998. Samajbhittik Matsya Abhoyasram: Matsya Utpadon Briddhir Koushol (Community-based Fish Sanctuaries: Strategy for Increasing Fish Production). Fish Week 98. Directorate of Fisheries and Ministry of Fisheries and Livestock, Government of the People's Republic of Bangladesh, Dhaka (in Bengali).

Karim, M., 1988. Status and Prospects for Pen and Cage Culture in Bangladesh. Report No. 12, FAO/UNDP Technical Assistance Project, IDA Agricultural Research II, Mymensingh, Bangladesh.

Karim, M., Ahsan, A.K.M., 1989. Policy Recommendation for Fisheries Development in Bangladesh. Paper presented for the Ministry of Fisheries and Livestock, Dhaka.

Kent, G., 1997. Fisheries, food, security and the poor. Food Policy 22 (5), 393–404.

Lewis, D., 1997. Rethinking aquaculture for resource poor farmers: perspective from Bangladesh. Food Policy 22 (6), 533–546.

Ministry of Agriculture (MOA), 1995. Handbook of Agricultural Statistics. Sector Monitoring Unit, Ministry of Agriculture, Government of the People's Republic of Bangladesh.

Master Plan Organisation (MPO), 1989. Fisheries and Flood Control, Drainage and Irrigation Development, Technical Report No. 17, March.

Planning Commission, 1998. Fifth Five-Year Plan, 1997–2002. Planning Commission, Government of the People's Republic of Bangladesh, Dhaka.

Rahman, A.K.A., 1989. Freshwater fishes in Bangladesh. Zoological Society of Bangladesh.

Rahman, A., 1990. Socio-economic aspects of shrimp culture project: analysis of field level data. Bangladesh Institute of Development Studies, Dhaka.

Sen, A., 1981. Poverty and Famines: An Essay on Entitlement and Deprivation. Clarendon Press, Oxford.

Shahidullah, M., 1986. Current status of shrimp fishery of Bangladesh. Marine Fisheries Bulletin, no. 4 (June), Chittagong.

Task Force, 1991. Managing the Development Process: Bangladesh Development Strategies, vol. 2. University Press Limited, Dhaka.

Thompson, P.M., Parvin, S., Md. Nurul, I., Md. Manjur, K., 1999. An assessment of co-management arrangements developed by the Community-Based Fisheries Management Project in Bangladesh. Paper presented at the International Workshop on Fisheries Co-management, 23–28 August 1999. Derived from http://www.co-management.org/.

World Bank, 1989. Bangladesh Action Plan for Flood Control. 11 December.

World Bank, 1991. Bangladesh Fisheries Sector Review, Report #8830-BD. Agriculture Operations Division, Asia Country Department 1.

World Bank, 1997. Bangladesh: Annual Economic Update 1997: Economic Performance, Policy Issues and Priority Reforms. South Asia Regions.

Annex B65

Joseph R. Curray et al., "The Bengal Fan: Morphology, Geometry, Stratigraphy, History and Processes", *Marine and Petroleum Geology*, Vol. 19, No. 10 (2002)

ELSEVIER

Marine and Petroleum Geology 19 (2003) 1191–1223

Marine and Petroleum Geology

www.elsevier.com/locate/marpetgeo

The Bengal Fan: morphology, geometry, stratigraphy, history and processes

Joseph R. Curray[a,*], Frans J. Emmel[b], David G. Moore[c]

[a]*Scripps Institution of Oceanography, La Jolla, CA 92093-0220, USA*
[b]*10162 Ramona Dr., Spring Valley, CA 91977, USA*
[c]*P.O. Box 1188, Willow Creek, CA 95573, USA*

Received 20 October 2002; received in revised form 16 February 2003; accepted 12 March 2003

Abstract

The Bengal Fan is the largest submarine fan in the world, with a length of about 3000 km, a width of about 1000 km and a maximum thickness of 16.5 km. It has been formed as a direct result of the India–Asia collision and uplift of the Himalayas and the Tibetan Plateau. It is currently supplied mainly by the confluent Ganges and Brahmaputra Rivers, with smaller contributions of sediment from several other large rivers in Bangladesh and India.

The sedimentary section of the fan is subdivided by seismic stratigraphy by two unconformities which have been tentatively dated as upper Miocene and lower Eocene by long correlations from DSDP Leg 22 and ODP Legs 116 and 121. The upper Miocene unconformity is the time of onset of the diffuse plate edge or intraplate deformation in the southern or lower fan. The lower Eocene unconformity, a hiatus which increases in duration down the fan, is postulated to be the time of first deposition of the fan, starting at the base of the Bangladesh slope shortly after the initial India–Asia collision.

The Quaternary of the upper fan comprises a section of enormous channel-levee complexes which were built on top of the preexisting fan surface during lowered sea level by very large turbidity currents. The Quaternary section of the upper fan can be subdivided by seismic stratigraphy into four subfans, which show lateral shifting as a function of the location of the submarine canyon supplying the turbidity currents and sediments. There was probably more than one active canyon at times during the Quaternary, but each one had only one active fan valley system and subfan at any given time. The fan currently has one submarine canyon source and one active fan valley system which extends the length of the active subfan. Since the Holocene rise in sea level, however, the head of the submarine canyon lies in a mid-shelf location, and the supply of sediment to the canyon and fan valley is greatly reduced from the huge supply which had existed during Pleistocene lowered sea level. Holocene turbidity currents are small and infrequent, and the active channel is partially filled in about the middle of the fan by deposition from these small turbidity currents.

Channel migration within the fan valley system occurs by avulsion only in the upper fan and in the upper middle fan in the area of highest rates of deposition. Abandoned fan valleys are filled rapidly in the upper fan, but many open abandoned fan valleys are found on the lower fan. A sequence of time of activity of the important open channels is proposed, culminating with formation of the one currently active channel at about 12,000 years BP.

Keywords: Indian ocean; Bengal Fan; Submarine fans; Turbidity currents

1. Introduction

The Bengal Fan was apparently first recognized as a submarine fan by Dietz (1953). He had seen echograms collected in 1948 by the Swedish deep sea expedition from the research vessel ALBATROSS, which showed small depressions or notches in the otherwise flat topography in a transect running southeast from Sri Lanka. Scientists on the expedition had speculated that these depressions might be tectonic features or grabens in a smooth lava flow on the sea floor. Dietz drew on observations by Buffington (1952) and Menard and Ludwick (1951) of natural levees bordering turbidity current channels across sediment-covered sea floor off southern California, and he speculated that these depressions were also turbidity current channels. He pointed

* Corresponding author. Fax: +1-858-534-0784.
E-mail address: jcurray@ucsd.edu (J.R. Curray).

0264-8172/03/$ - see front matter © 2003 Elsevier Science Ltd. All rights reserved.
doi:10.1016/S0264-8172(03)00035-7

out that the bathymetry in the Bay of Bengal (op. cit., 1953, Fig. 1) is a smooth plain gently sloping away from a submarine canyon located off the Mouths of the Ganges River. "The uniform gradient suggests that this gradient is determined by the profile of equilibrium of some sea-floor process. Could not this process be turbidity currents?" (Op. cit., 1953, p. 377).

This region was subsequently illustrated in the early physiographic maps of Heezen and Tharp (1964), and the fan was named the Ganges Cone. The first real survey and delineation of the fan was by Curray and Moore (1971), who proposed the name Bengal Fan. This name has subsequently totally replaced the earlier name of Ganges Cone. These early physiographic maps diagrammatically showed fans as

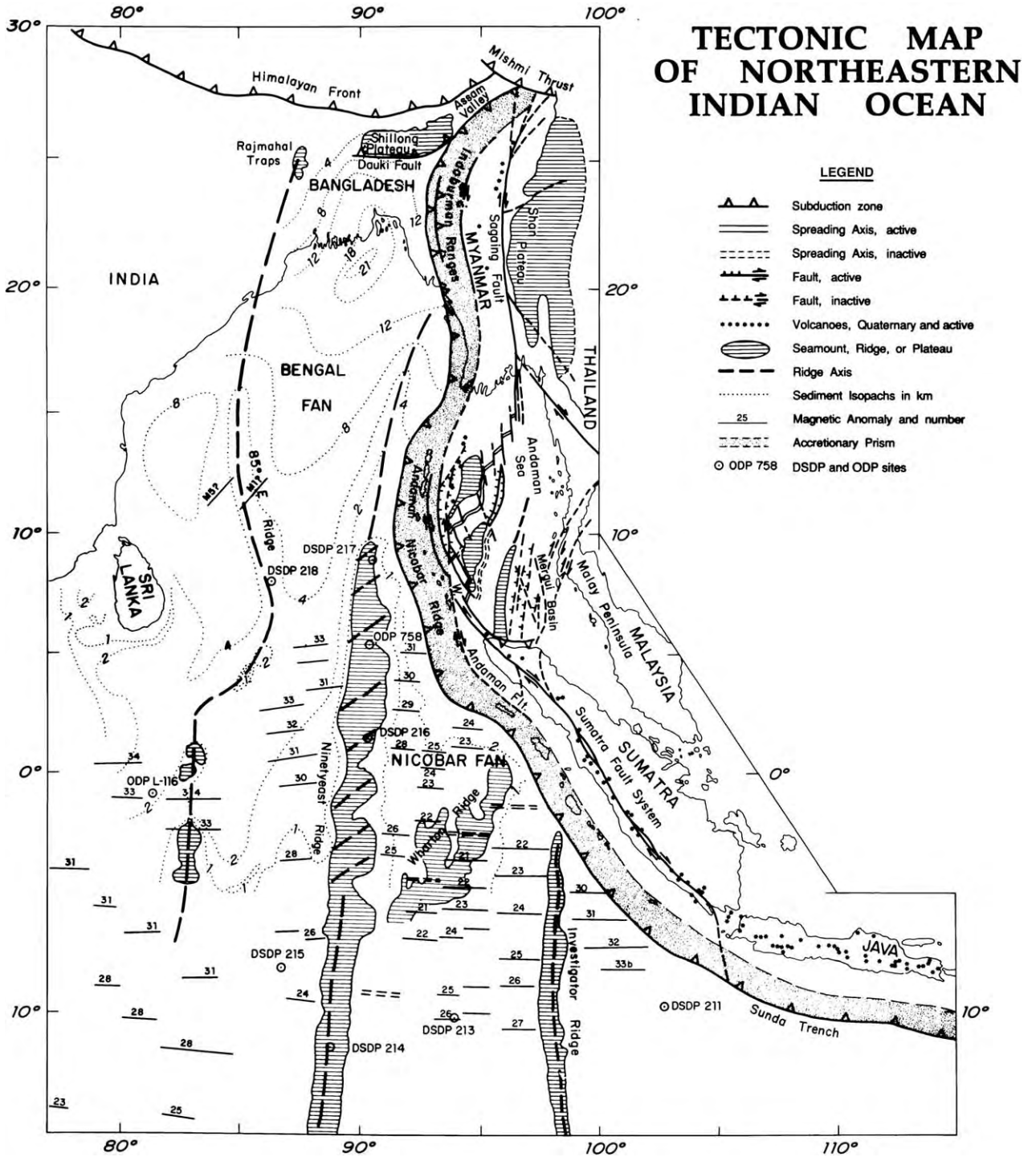

Fig. 1. Tectonic map of the northeastern Indian Ocean. From Curray (1991).

having a distributary pattern of turbidity current channels. Subsequent surveys have shown that this was a misinterpretation, and that most of the channels shown in this pattern are abandoned channels.

The western margin of the Bengal Fan is the continental slope of eastern India (Figs. 1 and 2); the northern proximal or upper fan lies off the Bangladesh continental slope; and the eastern margin is the northern end of the Sunda trench and the accretionary prism of the Sunda Subduction Zone, extending from Myanmar (Burma), through the Andaman–Nicobar Ridge, into the Mentawai Islands off Sumatra. Much Bengal Fan sediment has been subducted and/or uplifted into this accretionary prism.

The Bay of Bengal was created by the initial Paleocene–Eocene collision of India with the subduction zone of the north side of the Tethys Ocean (Alam, Alam, Curray,

Fig. 2. Physiographic diagram of the northeastern Indian Ocean and adjacent land areas.

Fig. 3. Bathymetry and topography of northeastern Indian Ocean and adjacent land areas, in corrected meters. R–S Gap is the Rajmahal–Shillong Gap; MR is Mahanadi River; GR is Godavari River; KR is Krishna River.

Chowdhury, & Gani, 2003; Curray, Emmel, Moore, & Raitt., 1982; Curray & Moore, 1974; Lee & Lawver, 1995). Prior to collision, a thick continental rise prism of sediment had formed off the eastern margin of India. Rapid clastic sedimentation in the Bengal Basin and fan formation on top of this continental rise commenced during continuing collision in the Eocene, and prograded southward during the Tertiary.

The Ganges River flows through the Rajmahal–Shillong gap (Figs. 1 and 3), and the Brahmaputra River flows through a deep gap in the eastern Himalayas, down the Assam Valley, and between the Shillong Hills and the accretionary prism of the Indoburman Ranges. These rivers, confluent in the Bengal Delta, drain the south and north slopes of the Himalayas, respectively, and deliver their huge sediment load to the Bengal Basin and the Bay of Bengal. The Bengal Delta has filled the Bengal Basin, and the sediment which has passed on through has been distributed across the entire Bay of Bengal to form the largest submarine fan in the world. Two distinct fans, separated by the Ninetyeast Ridge, are recognized; the eastern subfan is called the Nicobar Fan, and the western fan is the Bengal Fan proper (Fig. 1) (Curray & Moore, 1971, 1974). The Nicobar Fan has been inactive since

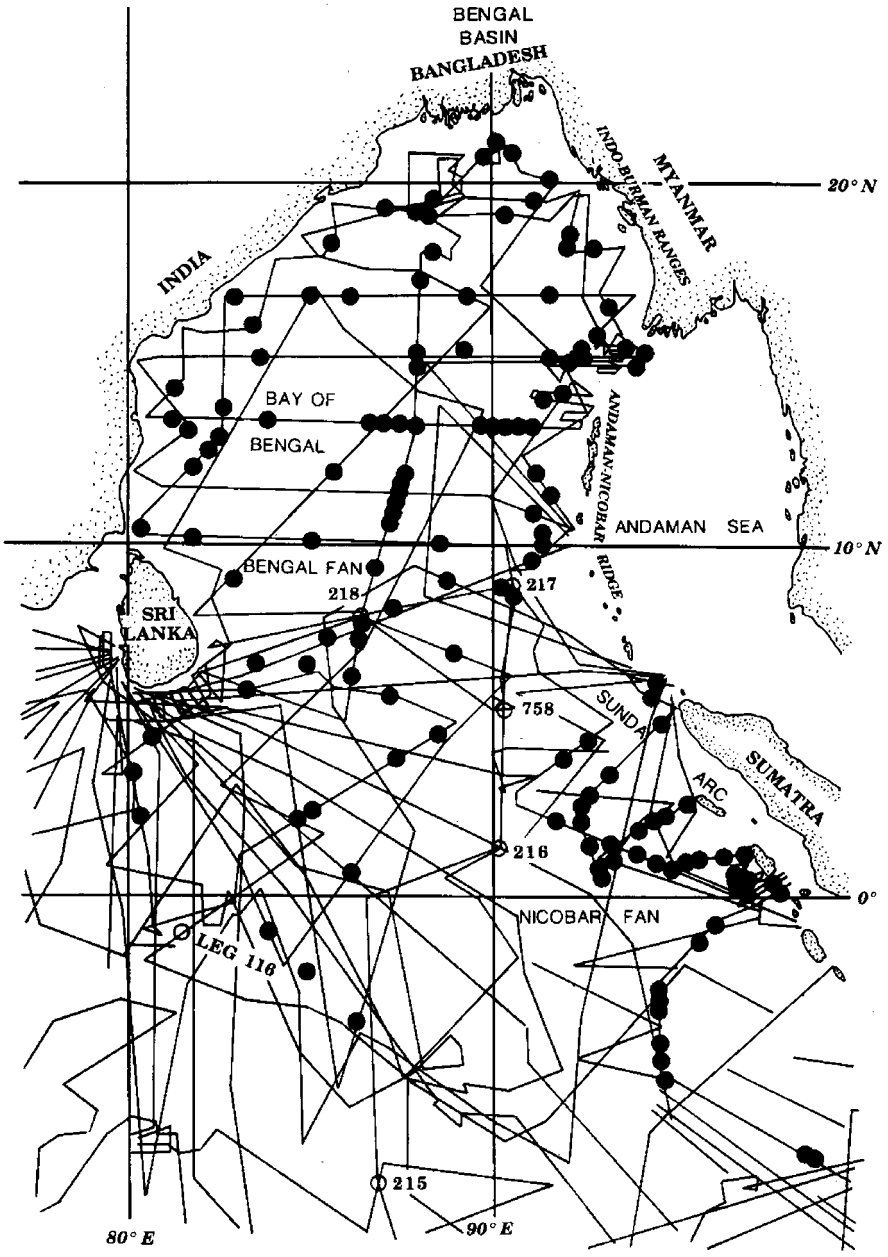

Fig. 4. Geophysical track lines and DSDP (215, 216, etc.) and ODP Leg 116 drill sites. Geophysical tracks include 3.5 kHz bathymetry, seismic reflection, gravity and magnetics. Dots are seismic refraction and/or wide angle reflection stations.

Table 1
Dimensions of some well-studied fans

Fan	Length (km)	Width (km)	Area (10^3 km^2)	Maximum thickness (m)	Volume (km^3)	Water depth apex (m)	Water depth distal end	Depth range (m)
Bengal and Nicobar (1)	3800?	~2000	?	16,500	?	1400	5500	4100
Bengal (1)	3000	830–1430	2800–3000	16,500	12.5×10^6	1400	5000	3600
Indus (2,3)	1500	<960	1100	>9000	1×10^6	~1500?	~4600?	~3100?
Amazon (4)	>700	250–700	330	4200	$>7 \times 10^5$	1500	4800	3300
Mississippi (4)	540	570	>300	4000	2.9×10^5	1200	3300	2100
Monterey (4)	400	250	75	2000	5×10^4	1280	4570	3290
Astoria (4)	>250	130	32	2200	2.7×10^4	1140	2840	1700
La Jolla (4)	40	50	1.2	1600	1175?	550	1100	550

Sources of data: (1) this study; (2) Kolla and Coumes (1987); (3) Clift et al. (2001); (4) Barnes and Normark (1985).

mid-Pleistocene time because the channel system which fed it was cut off by convergence of the Ninetyeast Ridge with the Sunda Trench (Curray & Moore, 1974). Most of our discussion will, therefore, be of the Bengal Fan. The most distal sediments which can be attributed to the Bengal and/or Nicobar Fan are Pliocene silt and sand turbidites in DSDP Site 211, south of eastern Sumatra, 3800 km from the present fan apex (Fig. 1).

The Bengal Fan has been largely unaffected by tectonic disturbances; contour currents are probably a minor influence (Kolla, Moore, & Curray, 1976); and while several very large rivers enter the western side of the Bay of Bengal from eastern India, the overall morphology is dominated by the massive sediment supply from the present and past canyons fronting the Bengal Delta of the Ganges and Brahmaputra Rivers. Because it is a very large fan, it is probably quite representative for studies of processes acting in the deposition of extensive turbidite sections. An ancient sediment body like the Bengal Fan preserved in the geological record would probably not be recognized as a submarine fan. It would instead probably be called a sedimentary basin, or in earlier terminology, be labeled a 'geosyncline'. Total volume of the Bengal Fan is comparable to the volume of the 'Appalachian Geosyncline' (Curray, 1991; Drake, Ewing, & Sutton, 1959).

Many descriptions of modern submarine fans have been published during the last few decades, and many models for formation and growth have been proposed (see, for example: Bouma, Steltin, & Coleman, 1985; Damuth & Flood, 1985; Mutti, 1974; Nelson & Nilsen, 1984; Normark, 1970, 1978; Normark, Posamentier, & Mutti, 1993; Piper & Normark, 2001; Shanmugam & Moiola, 1988; Stow, Howell, & Nelson, 1984; Walker, 1978; and many others). We have previously published several discussions of the Bengal Fan (see, for example: Curray et al., 1982; Curray & Moore, 1971; Curray & Moore, 1974; Emmel & Curray, 1985; Moore, Curray, Raitt, & Emmel, 1974; and others). This paper is an update to those papers, with inclusion of

Table 2
Bay of Bengal morphological divisions and valley gradients

Morphological divisions	Fan gradient (m/km)	Depth (m)	Channel thalweg divisions	Thalweg gradient (m/km)
Bengal Delta				
Inner shelf	~0.4–1.3	0		
Outer shelf	~0.7–2.7	38	Swatch of No Ground Canyon	8.2
Continental slope	~20–50	150		
Upper fan	5.7	1400	Upper fan valley	2.39
Middle fan	1.68	2250	Middle fan valley	1.68
Lower fan	0.88	2900	Lower fan valley	0.85
		3330	Lower fan valley	1.05
		3800	Lower fan valley	0.74
Central Indian Ocean Basin		5000		

new observations and interpretations. Our objective here is to review the geometry, stratigraphy, history and processes of the Bengal Fan. We will not attempt to fit this fan into previously published classifications of submarine fans, we will not apply previously published models of formation, nor will we cite many comparisons of our observations on the Bengal fan to observations on other large passive margin fans. We will, however, propose our model for processes of formation of this fan.

This study is based mainly on data collected during cruises of the Scripps Institution of Oceanography, between 1968 and 1986, utilizing 3.5 kHz bottom-penetrating (~100 m

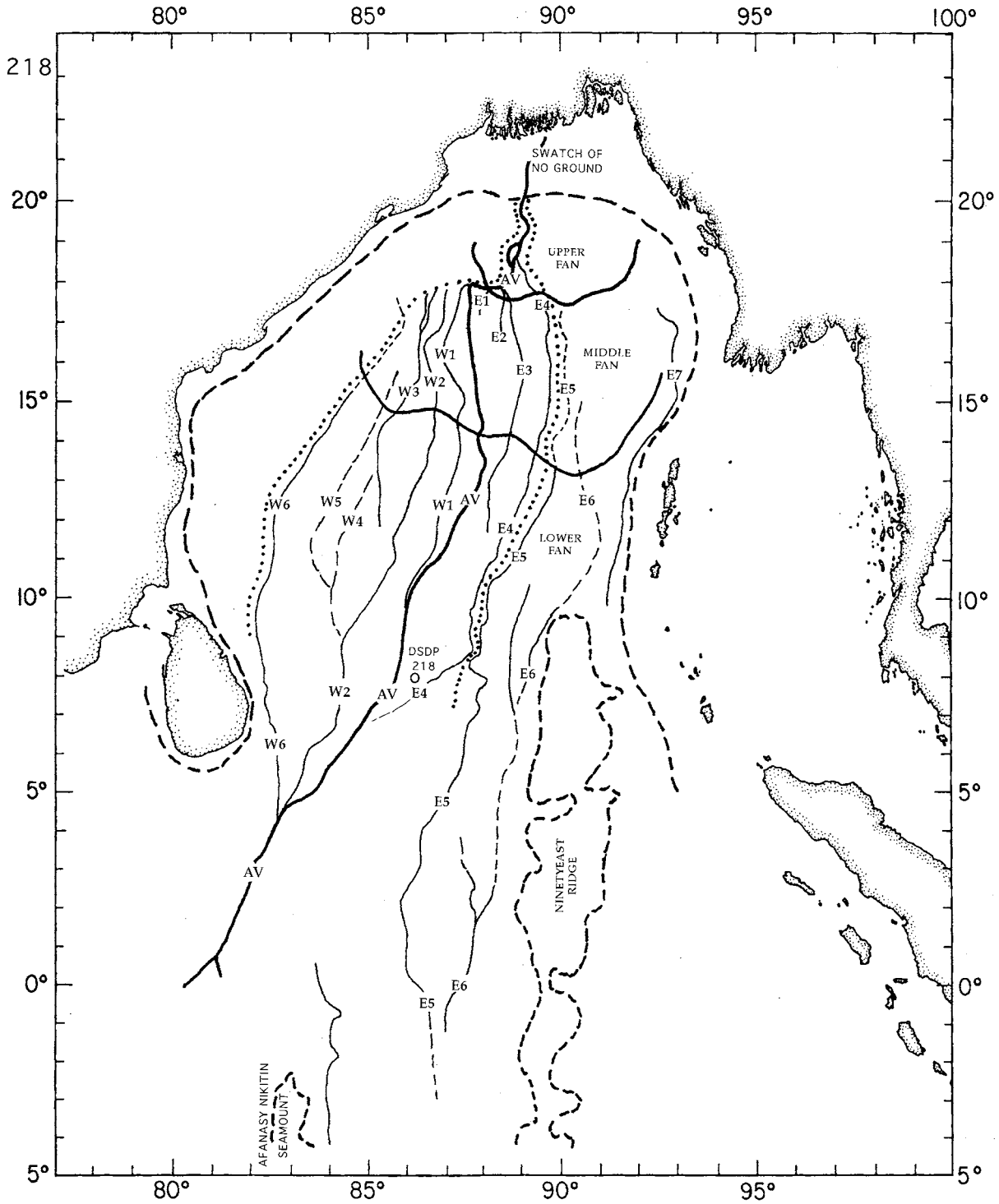

Fig. 5. The Bengal Fan, showing the subdivisions, outline of the active subfan and the reference names of the principle channels. AV is the 'active' channel. Heavy dashed line is shelf edge and bathymetric highs. Light dashed lines are less certain channels. Dotted line is outline of most recently active subfan, 'D' of Fig. 15D.

maximum) echo sounder and airgun seismic reflection profiling, mainly analog, but with some multichannel digital seismic reflection data. For most of our seismic reflection surveys, data were collected with two different sweep times and filter settings: a slower sweep, generally 5 s, filtered to 20–60 Hz; and a faster sweep, generally 2 s, filtered to 50–150 Hz for higher resolution. We did not have swath-mapping capability until the 1986 cruise, so although we knew from some detailed surveys that all of the fan valleys meandered, we could not document that fact. Tracks of these expeditions are shown in Fig. 4. Our contour chart (Fig. 3) is based on many additional ship tracks. Because of the very large area of the fan and limitations of time, the survey over some of the flat area of the fan was conducted at speeds of 8–10 knots or more. Thus, our bathymetric and reflection profiles commonly exhibit a large vertical exaggeration averaging about 25 X.

2. Morphology

The Bengal Fan has an area of approximately 2.8–3.0 × 10^6 km^2, not including the Nicobar Fan. The length of the Bengal Fan is between 2800 and 3000 km, extending from 20°10′N to 7°S latitude. Its greatest width is 1430 km at 15°N, and its narrowest part is at 6°N, 830 km between Sri Lanka and the Ninetyeast Ridge. Depths at its apex and distal end are 1400 and almost 5000 m, respectively. The fan volume is about 12.5 × 10^6 km^3, and the mass of the sediments and metasediments in the fan is about 2.88 × 10^{16} t (Curray, 1994). These dimensions make it the largest fan in the world. Including the Nicobar Fan, its now-detached eastern subfan, it is even larger. A comparison of overall dimensions of a few well-studied fans is shown in Table 1.

The shelf off the Bengal Delta of the confluent Ganges and Brahmaputra Rivers has an average width of about 150 km, and is wider east of the canyon than west of it (Figs. 2 and 3). The juncture between the base of the continental slope and the head of the fan is at about the 1400-m contour. The overall surface of the fan is remarkably smooth and has gradients varying from about 5.7 m/km on the uppermost fan to less than 1 m/km on its lower reaches (Table 2).

Although relatively smooth when viewed as a whole, the Bengal Fan is marked by a series of channels or fan valleys that are open for various distances along the length of the fan (the terms channel and fan valley will be used interchangeably and synonymously in this paper). Only the more distinct valleys which we can correlate between our widely spaced survey lines will be discussed; these are given names for convenience of reference, and will be discussed later (Fig. 5). The main central channel (AV) shown prominently in Figs. 2 and 5 is the most important, because it appears to be the only valley directly connected to the submarine canyon at the present time. This most recently active valley (AV), has been cut off from the direct supply of sediment from the rivers since about the time sea level rose above the head of the Swatch of No Ground Canyon, at a depth of about 38 m of water in mid-shelf (Figs. 2 and 3).

A three-fold division of the fan is based on the gradients of the central ‘active’ valley and of the fan surface (Table 2 and Fig. 5).

1. Upper fan, with average valley gradients of about 2.39 m/km, and a fan gradient of about 5.7 m/km. The thalweg of the active fan valley lies above the level of the adjacent fan, and the lower boundary of the upper fan is placed where the thalweg of the channel is cut into the fan surface, rather than being built above it.
2. Middle fan, where both the fan and fan valley gradients average about 1.68 m/km, and the valleys are smaller in cross-sectional area.
3. Lower fan, where the gradients drop to less than about 1 m/km, except locally where the gradient may increase because of valley fill.

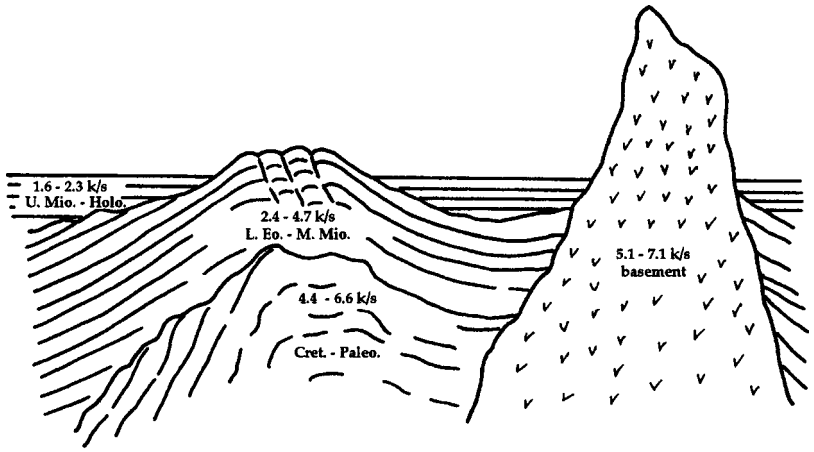

Fig. 6. Diagrammatic, composite seismic stratigraphic subdivision of sedimentary section of the Bengal Fan, based on tracing two regional onlap unconformities. Velocities are from seismic refraction and wide-angle reflection stations. Age assignments are from DSDP Leg 22 drilling results (Moore et al., 1974).

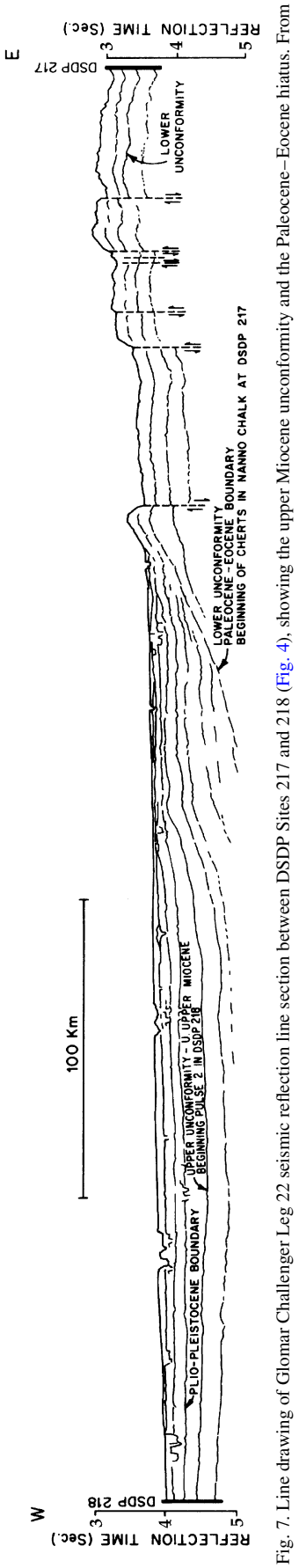

Fig. 7. Line drawing of Glomar Challenger Leg 22 seismic reflection line section between DSDP Sites 217 and 218 (Fig. 4), showing the upper Miocene unconformity and the Paleocene–Eocene hiatus. From Moore et al. (1974).

The boundaries between the upper, middle, and lower fan can be approximated by the 2250 and 2900 m contours, respectively.

The size, morphology, and structure of the fan valleys on the upper fan contrast significantly with those of the middle and lower fan regions. We will describe these contrasting valleys later and discuss their significance in overall fan growth.

3. Stratigraphy

3.1. Tertiary stratigraphy

Very early in our studies of the seismic stratigraphy of the Bengal Fan, we recognized two major unconformities in the localities of deformation in the southern or lower fan (Fig. 6) (Curray & Moore, 1971). We could trace these onlap unconformities from one deformed locality through the conformable section to the next. On the basis of these unconformities, we subdivided the section into the basement, an older sequence shown with velocities from about 4.4 to 6.6 km/s, and two younger sequences with velocities of 1.6–2.3 and 2.4–4.7 km/s.

We could not assign ages until the first drilling was done at DSDP Sites 217 and 218 in 1972 (Figs. 4 and 7) (von der Borch & Sclater et al., 1974; Moore et al., 1974). The age of the upper unconformity between the two younger units was found to be upper Miocene. This age was confirmed many years later with drilling of Leg 116 over a thousand km away near the equator (Figs. 1 and 4) (Cochran & Stow et al., 1990). This was estimated to be the time of onset of the intraplate or diffuse plate edge deformation (Curray & Munasinghe, 1989).

Site 217 drilled the lower unconformity on the Ninetyeast Ridge, and encountered a hiatus in the lower Eocene. The same hiatus was present in ODP Site 758 (Peirce et al., 1989) and DSDP Site 216 drilled farther south on the ridge (Figs. 1 and 4). Inasmuch as sedimentation on the Ninetyeast Ridge is pelagic rather than turbidites of the fan, one can question the validity of the correlation into the fan, but it appears to be a reasonable correlation from the 217 site into the adjacent fan, as it is present in many of our other seismic sections passing on and off the Ninetyeast Ridge. Furthermore, a similar but longer hiatus was found at DSDP sites 212 and 215 located much farther to the south and east in the very distal fan.

Our seismic reflection and refraction data (Fig. 4) permitted us to isopach the total sedimentary section in the Bay of Bengal (Curray et al., 1982; Curray & Moore, 1971, 1974; Moore et al., 1974). Later, Brune, Curray, Dorman, and Raitt (1991, 1992) and Curray (1991) reinterpreted the total sedimentary section in the light of probable load pressure and temperature metamorphism of the deeper part of the section to greenschist facies metasediments (Fig. 8A). Thus, as discussed by Curray

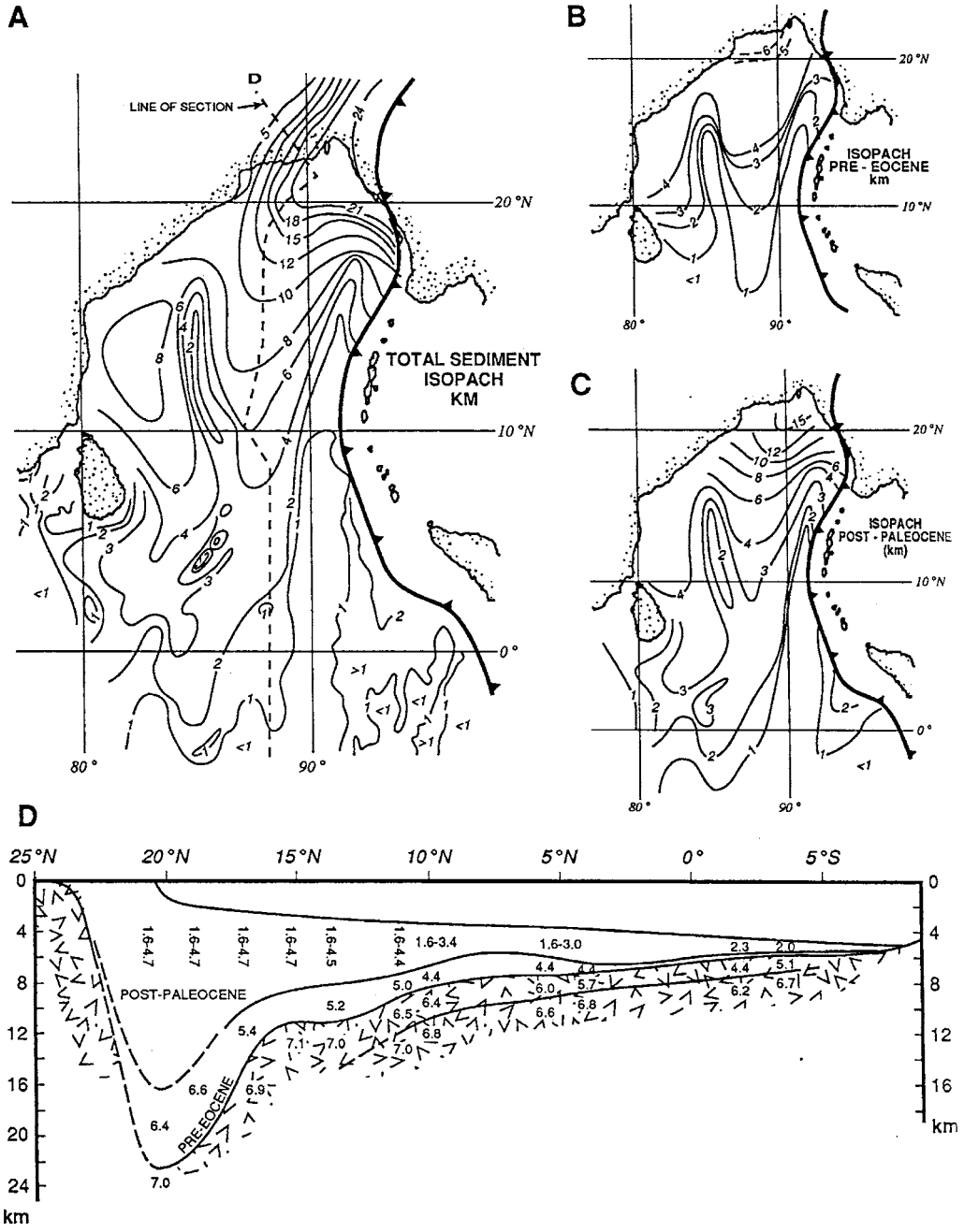

Fig. 8. Isopach maps and longitudinal section in Bay of Bengal and Bengal Basin, from seismic refraction and reflection data of Scripps Institution of Oceanography, some reflection data from Lamont-Doherty Geological Observatory and published drilling information in the Bengal Basin. Numbers in figure D are velocities in kilometers per second. The post-Paleocene part of the section is interpreted as the Bengal Fan, as explained in the text. From Curray (1991).

(1994), the rocks with a velocity of 7.0 km/s beneath the Bangladesh shelf (Fig. 8D) at 20°N are interpreted to be oceanic crust metamorphosed to amphibolite facies and the overlying rocks with velocities of 6.4–6.6 km/s are greenschist facies metasediment.

If we accept the correlations from the drilling sites (Figs. 1 and 7), it now allows us to assign ages to the units we defined earlier. We interpret the upper unit (Fig. 8C and D) as post-Paleocene, the Bengal Fan. We interpret the older sedimentary unit (Fig. 8B) as pre-Eocene pre-Bengal Fan deposition, perhaps a continental rise off the east coast of India, with pelagic or hemipelagic sediments farther offshore. The greater thickness off present northeastern India and west of the Bengal Basin might reflect coalesced fans of ancestral Mahanadi and other rivers, but the correlations and isopachs in that region are very tenuous.

The eastern edge of the Bengal Fan lies along the Sunda subduction zone, which extends from off Java and Sumatra, northward to the west side of the Andaman and Nicobar Ridge and into the Indoburman Ranges of Myanmar. The fan is passing obliquely into this subduction zone and some of the older sediments have been scraped off into

the accretionary wedge. If rocks are too deep to be sampled by drilling, one should try to sample them either where they are not as deep or where they crop out.

A very simplified geological section in part of the Indoburman Ranges is shown in Fig. 9A (interpreted from descriptions from Acharyya, 1998; Brunnschweiler, 1966; Mitchell, 1989; and others). We suggest that these Eocene Indoburman rocks are early Bengal Fan sediments. Where they are exposed along the coast of Myanmar, they are turbidites such as we might expect from this part of the fan. Similarly, the section in the Andaman–Nicobar Ridge consists of upper Eocene and Oligocene turbidites overlying pelagic sediments and ophiolite (Fig. 9B) (Chatterjee, 1967; Gee, 1927; Karunakaran, Ray, & Saha, 1968; Roy, 1983; and others).

Drilling (von der Borch et al., 1974) done in the very distal parts of the fan at site 215 (Figs. 1 and 4) shows a hiatus from middle Eocene to upper Miocene silty clays and clayey silts (Fig. 9C). Site 211 (Fig. 1) even farther

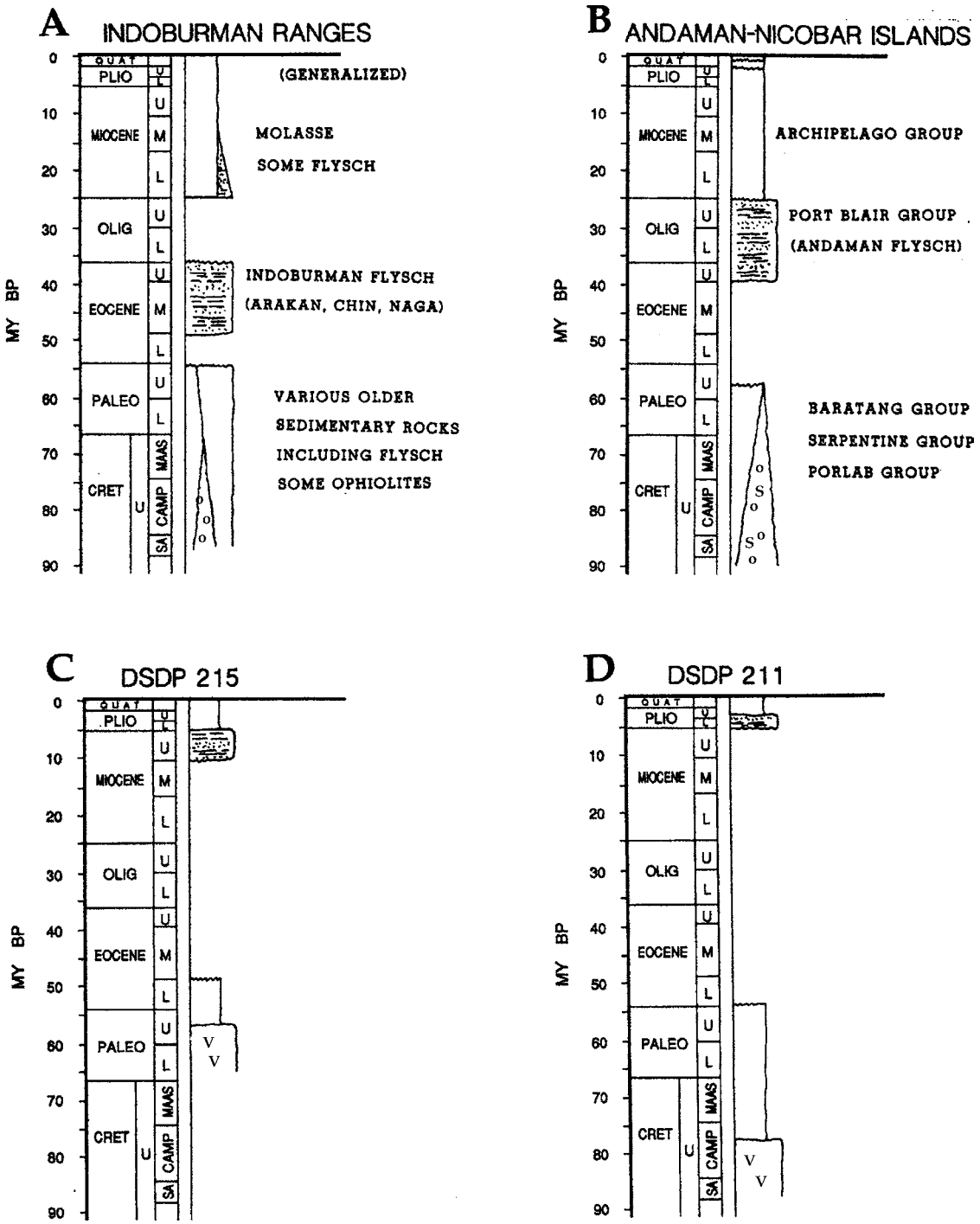

Fig. 9. Simplified geological sections from the Indoburman Ranges and the Andaman and Nicobar Islands, interpreted as Bengal Fan sediments offscraped at the Sunda subduction zone, and DSDP Sites 215 and 211. Locations in Fig. 1, and references are discussed in text.

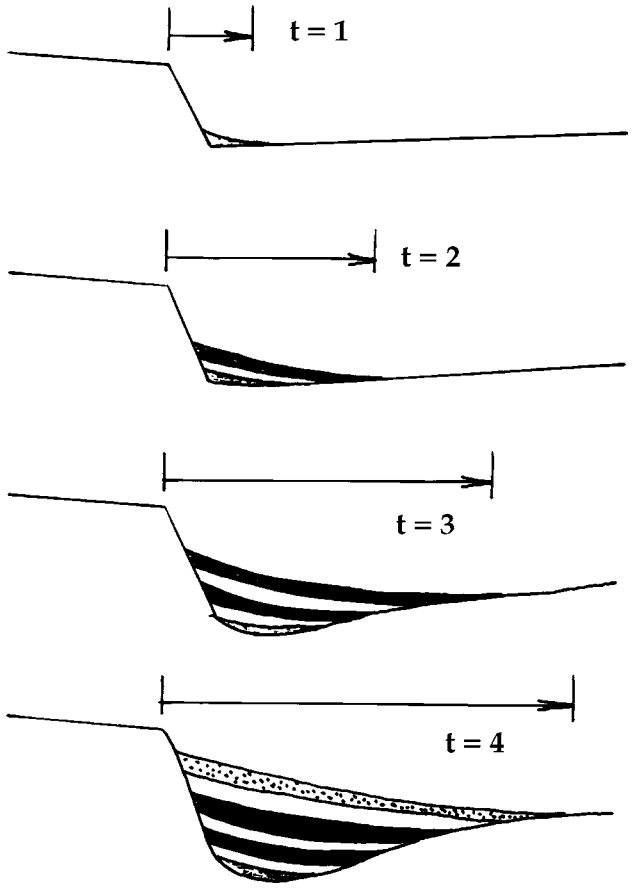

Fig. 10. Progradation of a submarine fan, showing that the hiatus at the base of the fan increases in length down the fan.

away in the distal Nicobar Fan shows a hiatus from the end of Paleocene to lower Pliocene silty sands and clayey silts (Fig. 9D). The lower unconformity (Fig. 6) is a hiatus, a period of non-deposition or greatly reduced rate of deposition. The farther from the head of the fan, the longer the hiatus, because fans prograde (Fig. 10).

Fig. 11 shows the apparent length of the hiatus, or condensed section, as a function of distance from the present head of the fan. DSDP 218 was far from reaching the base of the fan. The Leg 116 sites, ODP 717–719, also did not reach the base, but extrapolation of rates of deposition suggests an Oligocene age for the base at this latitude. Sites 215 and 211 each show a very long hiatus or condensed section. The turbidites in the Indoburman Ranges (IB) and the Andaman–Nicobar Ridge (A–N) date from very near the time of presumed initiation of Bengal Fan deposition.

3.2. Quaternary stratigraphy

Four units can be distinguished within the Pleistocene upper fan sediments by seismic structure and stratigraphy (Figs. 12 and 13). These units are most evident in our seismic reflection network on the upper fan, where large valleys and levees are best developed. Because of the limited density of coverage of our seismic reflection data, we cannot correlate these entire units to the middle and lower fan, but we can correlate the base of the oldest unit to DSDP 218 (Figs. 4 and 5). Each unit shows periods of active channel and levee formation, interpreted as coeval with one or more periods of low stands of sea level when most fan building occurs, and the boundaries between the units which probably represent high sea level times of valley filling, when turbidity current activity was diminished. For discussion, we refer to these units as A, B, C, and D from oldest to youngest.

To determine the stratigraphic ages of these units, we have carefully correlated the base of Units A and B from the upper fan through our network of seismic reflection records to DSDP Site 218, located on the lower fan (Figs. 4 and 5). Our seismic coverage and linkage are not good enough to be able to correlate with the ODP Leg 116 sites, which are located at the distal end of the lower fan (Figs. 1 and 4). The base of Unit A appears to correlate with the Pliocene–Pleistocene boundary at 205 m in DSDP Site 218 (von der

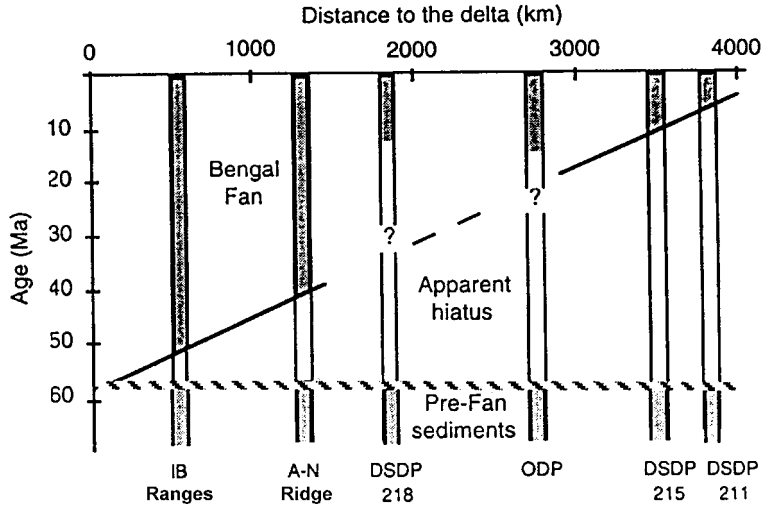

Fig. 11. Length of the Paleocene–Eocene hiatus plotted by distance from the apex of the present Bengal Fan. IB is Indoburman Ranges; A–N is Andaman–Nicobar Ridge. Locations in Fig. 1.

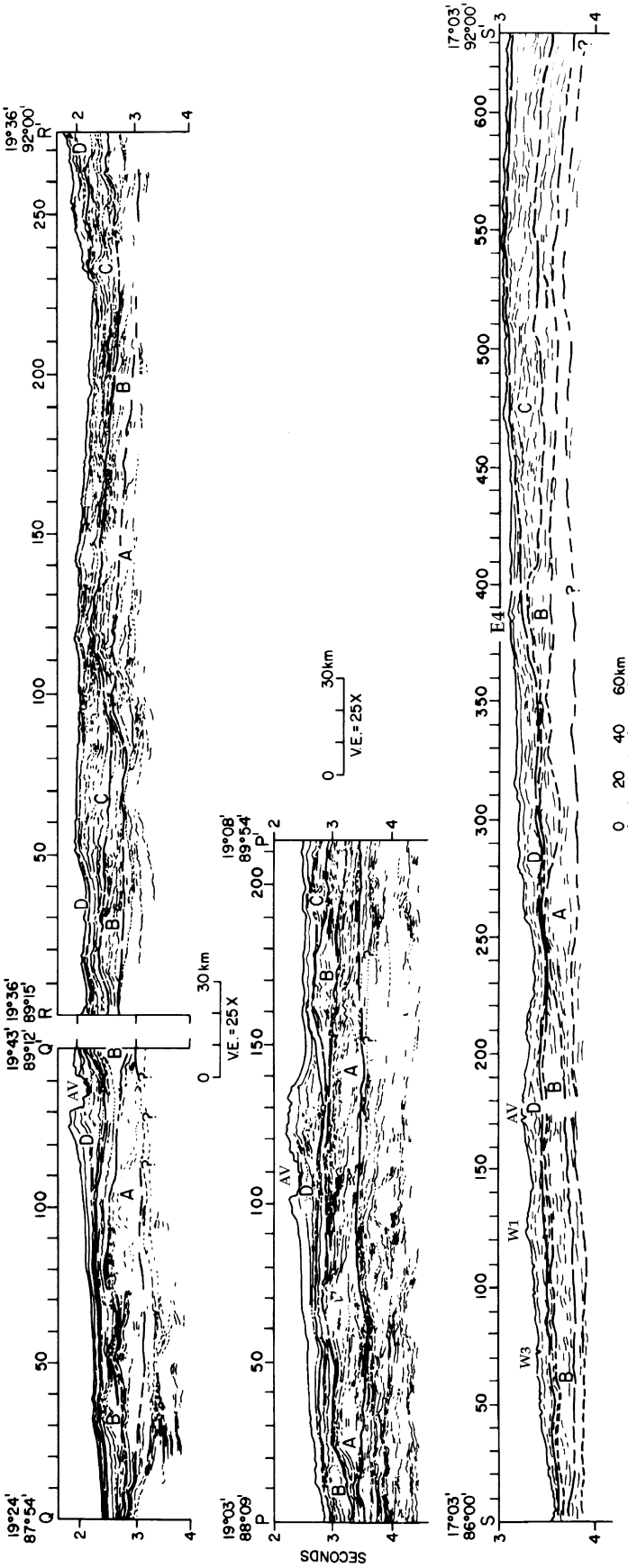

Fig. 12. Interpreted line drawings of seismic reflection records of the upper fan, showing delineation into Quaternary sequences A, B, C and D. For channel locations, see Fig. 5.

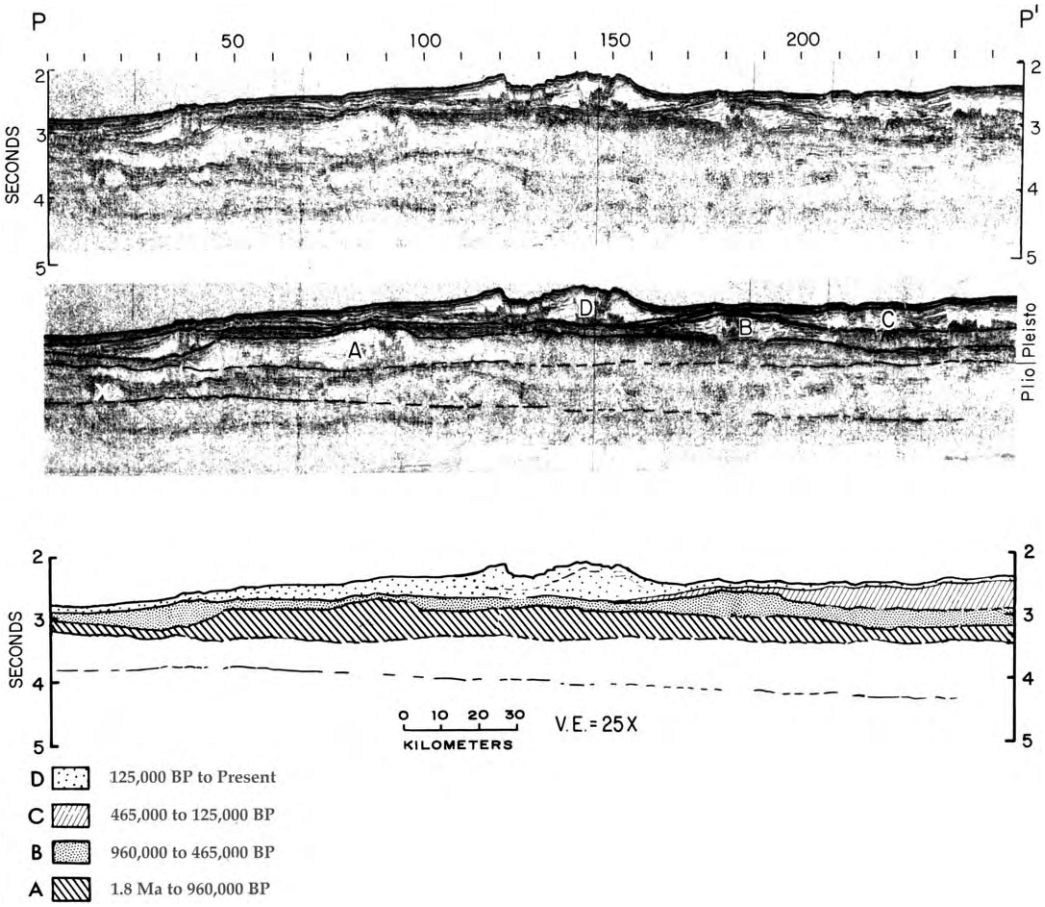

Fig. 13. Reflection profile of section P–P′ in Fig. 12. Upper section uninterpreted; middle section interpreted showing the channel-levee complexes of subfans A, B, C and D; lower section is an interpreted line drawing of the section. Xs on middle section are older unidentified channel-levee complexes.

Borch et al., 1974), with an age of 1.8 my; and the B/A boundary correlates with a reflector at a depth of 120 m at the DSDP site (Fig. 14).

The lithology and the implied genesis of the Quaternary sediments drilled in the upper section of DSDP 218 can be divided into three units of Pleistocene and Holocene age (Fig. 14):

1. 205–70 m: A mixed clayey silt turbidite and nanno ooze implies that fan valleys were not too distant, and that overbank sheet flows were intermittent.
2. 70–9 m: Sand and silty sand. This turbidite pulse indicates that fan valleys were nearby and active.
3. 9–0 m: Nanno ooze. During this period, fan valleys were too far away to be of influence, or were relatively inactive.

An important fossil for our correlations in the Bengal Fan is Pseudoemiliania lacunosa (Gartner, 1974), the last occurrence of which is dated at 465,000 years (Gartner, 1990), at 70 m in DSDP 218. If the base of Unit A at 205 m is 1.8 my, and assuming a constant rate of sediment accumulation between 205 and 70 m, the B/A at 120 m contact interpolates to about 960,000 BP. Because Unit C appears to be present only in the eastern part of the fan, we assume that it

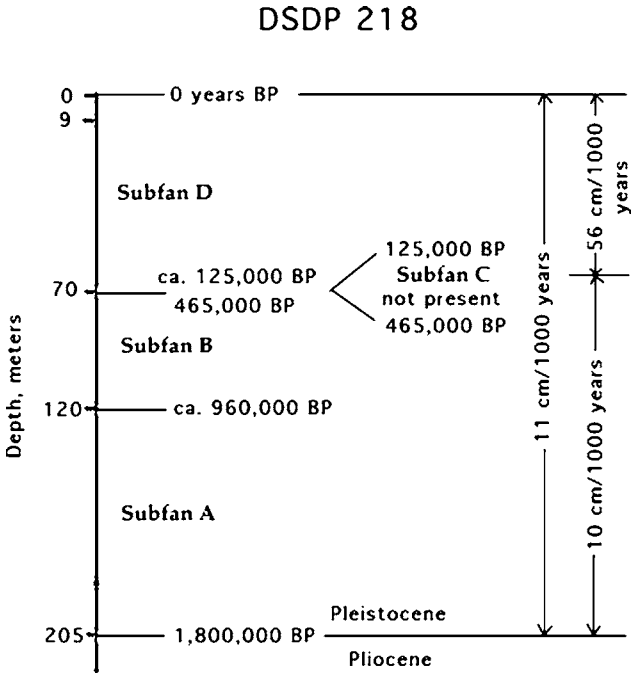

Fig. 14. The sedimentary section drilled in DSDP 218, interpreted into the drilling units or subfans shown in Fig. 12, with the ages discussed in the text. Average rates of accumulation are shown. We suggest that unit or subfan C is not present in this location, as discussed in the text.

is not present in DSDP 218, and that the end of deposition of unit B coincides with the 465,000 age at 70 m. Since unit D is the presently active subfan, we assign it an age of Wisconsin to present, 125,000 years to present and a depth range in DSDP 218 of 70–0 m. Thus we arrive at the estimated time periods for deposition of the four units in Figs. 12 and 13.

The distribution of our oldest sequence, unit A, from 1.8 Ma to 960,000 BP (Fig. 15A) suggests that there may have been two active submarine canyons supplying the fan. We cannot determine if these canyons were active simultaneously or consecutively. The second sequence, 'B', from 960,000 to 465,000 BP (Fig. 15B) had as many as four canyons supplying the fan, but again we do not know if they were simultaneous or sequential.

The third sequence, 'C', from 465,000 to 125,000 BP (Fig. 15C) lies on the eastern side of the fan, but once again

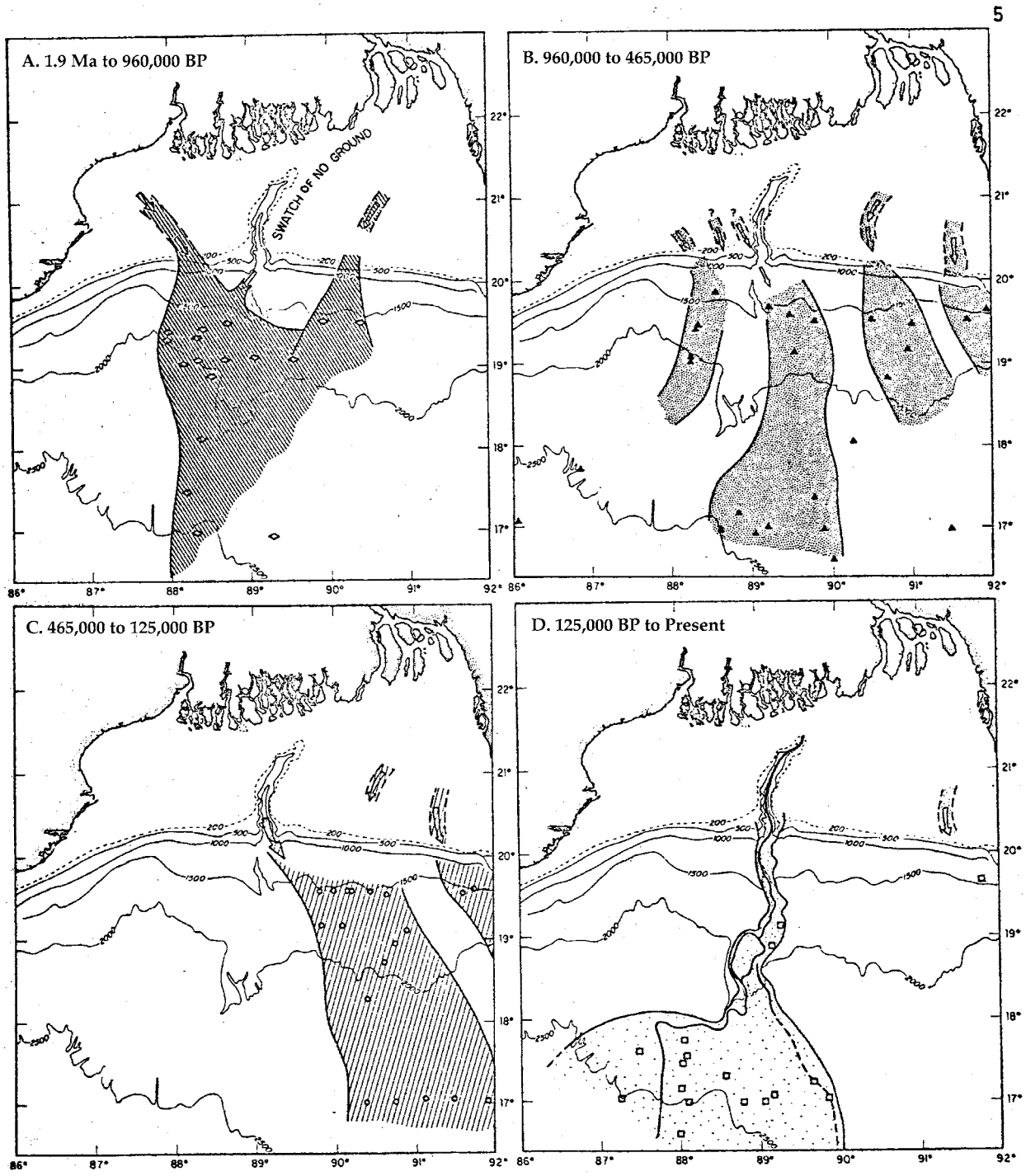

Fig. 15. Quaternary subfans, showing major shifting of submarine canyons and fan valley systems of the sequences in Figs. 12–14. Squares, triangles, etc. are channel crossings in our seismic records.

with a hint of more than one source. Notice that one of the principal canyon sources appears to be the present Swatch of No Ground submarine canyon. We assume that the present system 'D' issuing from the Swatch of No Ground (Fig. 15D) started about 125,000 years ago. Within this unit there was a shift in activity from a channel on the east side of this subfan (E 4) shown with a dashed line to the presently active channel (AV). This occurred not by shift to a new submarine canyon source, but by a major channel shift at about 19°N. Many subsequent channel shifts, probably by the river-like processes of avulsion, have occurred at the sharp bend in the channel at about 18°N, the area of most rapid deposition of sediment. These channel processes will be discussed later in this paper.

It appears from the distribution of submarine canyons and fan valleys supplying these different subfans (A, B, C and D) that the last supply to go east of the Ninetyeast Ridge to the Nicobar Fan was cut off by about 125,000 BP.

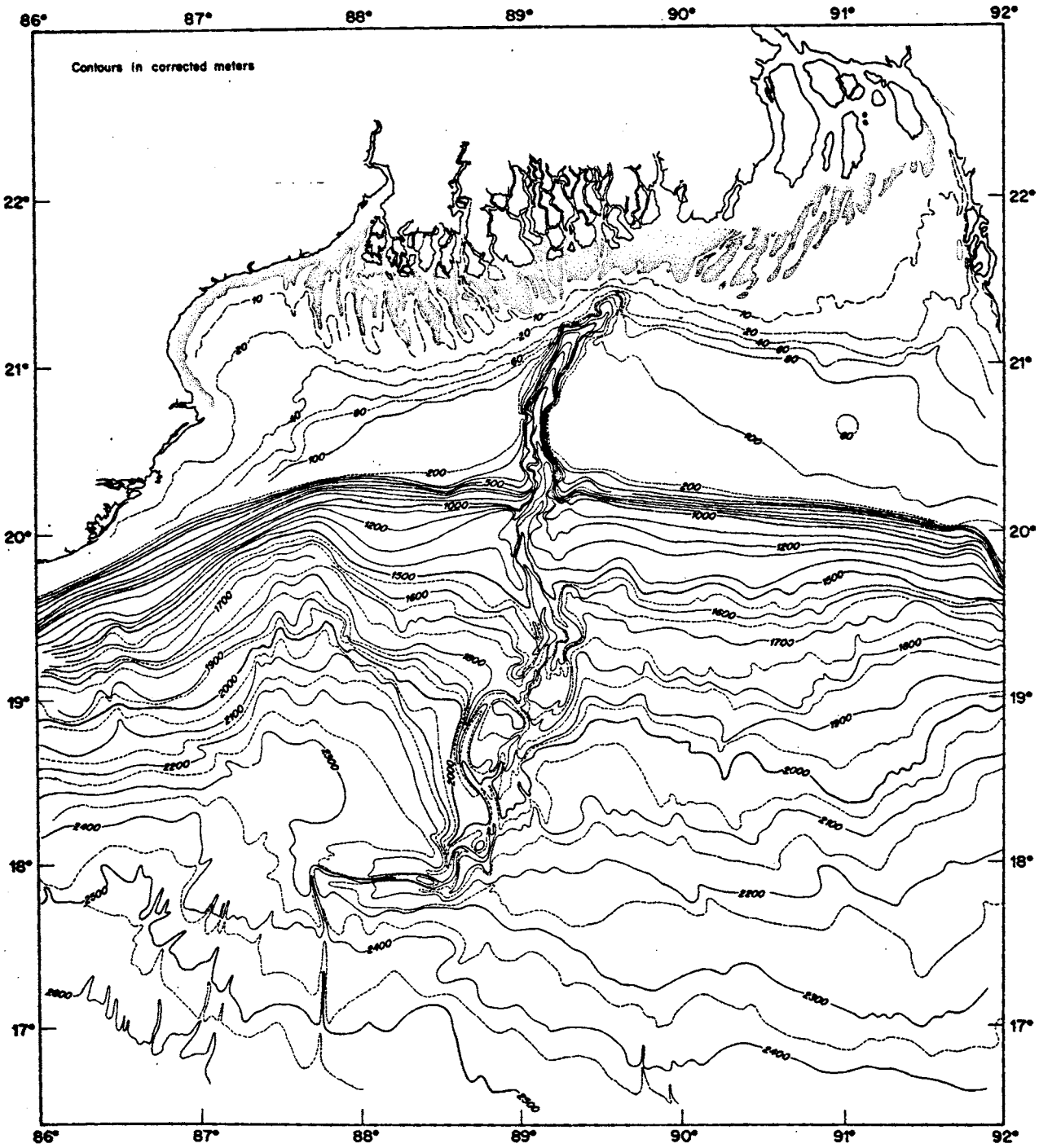

Fig. 16. Bathymetry of the continental shelf, the Swatch of No Ground, and the upper fan.

4. The submarine drainage system of the Bay of Bengal

The present submarine drainage system of the Bay of Bengal and Bengal Fan consists of one active submarine canyon, the Swatch of No Ground, lying on the Bangladesh continental shelf off the Bengal Delta. It serves as a point source for one active fan valley or channel, AV (Fig. 5). At times in the past other submarine canyons cut into this shelf, which is a broad delta front. In this regard the Bengal Fan is different from some other large fans, which have had only one submarine canyon supplying them throughout their histories. And, as we will discuss, fan valleys or channels may be active for relatively short periods of time compared with the life of a submarine canyon.

Recorded graphic sections are effective for displaying local details or regional profiles, but they generally have the notable characteristic of exaggeration of vertical scales. Vertical exaggeration is helpful and, in many cases, even necessary to display the features of interest within reasonable size limitations; but unfortunately even the most experienced observers tend to describe the illustrated features in terms of the vertically exaggerated sections, such as 'vertical', 'steep', 'pinnacle', etc. Very broad shallow channels become 'U-shaped or V-shaped troughs'; gentle slopes of a few degrees inclination become 'escarpments'; and dips of a few degrees become steep dips. In the descriptions and interpretations of the following sections, we have attempted to maintain a proper perspective of true scale of structural and topographic features, and we ask that our readers give serious attention to the notations of vertical scale exaggeration that accompany the illustrated sections. When we use the terms V-shaped or U-shaped, we mean very broad Vs and Us.

Most of the slopes in this study are very low (Table 2), and are expressed in meters per kilometer. For reference, 0.1° = 1.75 m/km; 1° = 17.5 m/km; 2° = 35 m/km; 5° = 87 m/km. At 200 times vertical exaggeration, 0.1° or 1.75 m/km looks like a 19° slope, and at 400 times, it looks like a 35° slope.

4.1. The Swatch of No Ground submarine canyon

The head of the Swatch of No Ground lies in about 38 m water depth at 21°27′N, 89°41′E (Fig. 16), and the canyon continues south for 160 km as a long, straight trough to about 20°12′N and 89°12′E at a depth of 1406 m, with an average gradient of 8.2 m/km. Detailed bathymetry suggests that some smaller filled tributaries may exist on the northwestern side, but we have no evidence that the main canyon extended closer to shore than it now does.

The canyon is the presumed location of the river mouth at the last glacial sea level low. The curve of the canyon across the inner shelf may represent a westward migration of the river mouth during some stage of falling sea level in middle Pleistocene (Fig. 15). The confluent Ganges and Brahmaputra Rivers presently flow into the sea about 90 km farther east at 22°10′N and 90°30′E, and very little sediment now enters the canyon directly from these rivers.

High rates of deposition have been demonstrated in the subaqueous parts of the Bengal Delta and on the inner continental shelf (Hübscher, Spiess, Breitze, & Weber, 1997; Kuehl, Hariu, & Moore, 1989; Kuehl, Levy, Moore, & Allison, 1997; Michels, Kudrass, Hübscher, Suckow, & Wiedecke, 1998). Similarly, high rates of deposition have been shown for the inner end of the floor of the Swatch of No Ground, interpreted as trapping of sediment mobilized on the delta topset by storms and tidal currents (Kudrass, Michels, Wiedecke, & Suckow, 1998). However, on the basis of lack of evidence of cable breaks and of large modern turbidity current activity in the channel system on the fan, we believe (Curray et al., 1982; Curray & Moore, 1974; Emmel & Curray, 1985) that late Holocene and modern slides and turbidity currents are small and infrequent compared to those of lowered sea level. This will be discussed in more detail later in this paper.

Two single-channel seismic reflection lines are shown in Fig. 17, across the canyon, one at mid-shelf and one just beyond the shelf break. The broad U-shaped trough at mid-shelf has a width of 20 km from rim to rim. The bottom is 8 km wide, and the depth 862 m below the rims; these dimensions add up to a cross-sectional area of approximately 11,200,000 m^2. Visible fill in the canyon is about

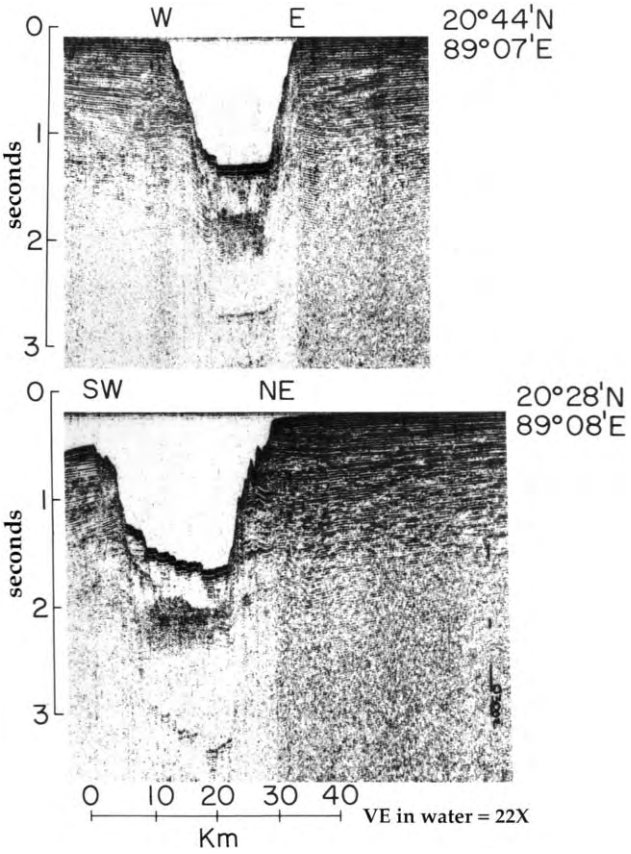

Fig. 17. Seismic reflection profiles across the Swatch of No Ground submarine canyon.

0.8 s (approximately 800 m). The upper half of this fill is faintly bedded, but the lower part is chaotic in appearance beneath a very strong reflector, suggesting that it is made up of irregular sandy beds or lenses. Both crossings display step-like terraces, especially on the west side of the canyon. These and similar terraces have been attributed to faulting and slumping (Shepard, 1973). Another possible explanation is that they are the result of either lateral cutting of valley fill, or of natural levee deposition of smaller flows confined within the broad Swatch of No Ground trough. We have no basis for selecting a preferred mechanism.

The location of an active submarine canyon is related to river mouth migrations, sedimentation, and Quaternary sea level fluctuations. At high stands of sea level, as today, rivers are free to migrate back and forth across the delta landward of the shoreline, without regard to locations of abandoned submarine canyons they formerly occupied. During a falling sea level a river channel may be incised both landward and seaward of the former high stand shoreline while the river seeks grade above its new base level; but as the shoreline continues to regress, the river is free to select a new course across the shelf in response to shelf topography, wave approach, and longshore current influence. At any time the river could fall into an old submarine canyon head, and the canyon would be rejuvenated.

The locus of a new submarine canyon is probably selected by position of the river mouth at a low stand of sea level, unless it already lies in a submarine canyon. The full sediment load of the river is deposited off the river mouth. If large amounts of sediment fall over the shelf break onto the upper continental slope, deposition, and hence slope failure leading to erosion, are concentrated there. Headward erosion can start and form a new submarine canyon.

During the subsequent rise of sea level with waning of continental glaciers, a river will tend to retreat up its own channel or canyon. With a rapid sea level rise and/or inadequate sediment supply, an estuary can be formed, confining the river and preventing its migration. With a slowing of the rate of rise, however, as occurred in the late Quaternary at about 6000–7000 BP (Curray, 1964; Fairbanks, 1989), and/or with a local increase in sediment supply, a river mouth could fill its channel or estuary and escape. This is, we believe, what has occurred here with the present Bengal Delta river mouths and with the Swatch of No Ground Canyon heading at about 38 m of water depth. Without allowing for subsidence, sea level would have been at that level at approximately 9000 BP (Curray, 1964; Fairbanks, 1989). With the estimated high rates of subsidence in Bangladesh of from 1 cm/yr (Milliman, Broadus, & Gable, 1989; Morgan & McIntire, 1959) to as high as 2.5 cm/yr (Alam, 1989), however, the shoreline could have been at the present canyon head as recently as 1500–3800 years ago. The fact that the edge of the continental shelf lies at about 150 m, not much lower than the world-wide average of about 120–130 m, suggests that the estimated rates of subsidence cited above might not apply far out onto the shelf. If we assume that the river or rivers abandoned the canyon lip at 38 m at the slowing of the rate of rise of sea level at about 6500 BP, the subsidence rate at that location would have averaged a modest and reasonable 3 mm/yr.

In conclusion, we suggest that the locations of new canyons are determined at low stands of sea level by locations of river mouths. Initial canyon erosion occurs during low sea level and early rapidly rising sea level. Canyon abandonment occurs during late slowly rising sea level and high sea level. And finally, canyon filling and selection of a new river course occurs during high sea level and falling sea level. A similar scenario has been proposed for the Amazon Fan (Flood & Piper, 1997).

4.2. Fan valleys or turbidity current channels

Mapping of the pattern of valleys or turbidity current channels on a fan is essential to understanding the processes in fan development. The degree of difficulty in mapping without swath-mapping bathymetric or wide swath side scan sonar data is related to the number of valley crossings available and the accuracy of navigation of the survey vessels recording these crossings. The task of correlating valleys would, of course, have been greatly facilitated with many more survey lines on this huge fan or with swath-mapping bathymetric data or wide swath side scan sonar. Unfortunately, these were not options at the time most of our surveys were run, and we have only two swath-mapping tracks across the lower fan, which do show the extensive meandering known to be present on the entire fan.

An important conclusion of our early surveys and study of the Bengal Fan is that there is only one active fan valley system connected to the submarine canyon and active at the present time. We attempted to identify that present channel (Curray & Moore, 1974). Other later investigators have accepted our interpretation of the active channel, and have limited most of their surveying to that channel (Hübscher et al., 1997; Moe, Tokuyama, & Murayama, et al., 2001; Weber, Wiedicke, Kudrass, Hübscher, & Erlenkeuser, 1997). Close examination of the surveys by Moe et al. (2001), however, had cast some doubt about present continuity of this channel in the upper lower fan, at about 11°N. This prompted us to reexamine our fan valley correlations between about 18 and 11°N. Our conclusion from this reexamination is that our original selection of the active valley is valid. Turbidity current activity, however, is greatly reduced from Pleistocene lowered sea level conditions, and 'AV' has been modified during the rising sea level by back-filling at about 10–11°N.

The most important and obvious surface channels are shown in Fig. 5, and the presently active subfan (Fig. 14D) is outlined and extrapolated farther south. The channels are identified as AV, the active channel, and W 1, W 2, W 3, etc. lying to the west of AV, and E 1, E 2, E 3, etc. to the east.

The gradients of the canyon, the active fan valley and the adjacent fan are shown in Fig. 18A, expressed in m/km. The boundary between the canyon and the active fan valley is at 20°12′N, at about 1400 m water depth, at the base of the continental slope (Table 2). At this juncture the gradient changes from an average of 8.2 m/km for the canyon to 2.39 m/km for the upper fan valley. The depth of the canyon thalweg below the adjacent outer shelf is about 700 m (Fig. 17); the thalweg depth below the crests of the natural levees in the uppermost fan valley at 20°N is about 325 m (Fig. 18B). It is here that the immense leveed valleys are first developed, and the thalweg of the active channel lies above the level of the adjacent upper fan. In a sense they are 'elevated expressways' because the thalweg of the channel is built above the level of the underlying fan surface, which is now depressed by the weight of the channel-levee system. Examples are shown as line drawings in Fig. 19 and in Fig. 20 as a seismic reflection record of a crossing at 19°05′N, where the channel is about 220 m deep. Some of these large channel-levee complexes are as wide as 50–60 km and 800–1000 m thick. The complex ones with a younger channel built on the flanks of older levees are much wider than that. The boundary on the fan below which the thalweg is eroded into the fan surface defines the southern edge of the upper fan (Figs. 5 and 18A).

An important difference between the canyon and upper fan valley is the cross-sectional area. The cross-sectional area of the outer crossing of the canyon in Fig. 17 at 20°28′N is about 11,200,000 m^2, while the cross-sectional area of the fan valley at 20°N is about 3,150,000 m^2, of which 166,000 m^2 is in an incised inner valley. Fifty kilometers farther down (Fig. 18B) the depth of the fan valley is 220 m, although its width is still 16.5 km, and the cross-sectional area of about 1,500,000 m^2. Our last crossing of the valley on the upper fan is at 18°03′N, where the cross-sectional area is about 1,000,000 m^2 and the channel depth is about 165 m. A drastic reduction of over 90% to about 80,000 m^2 occurs near the boundary between the upper and middle fan. The mid-fan valleys are almost as deep, but are much narrower.

All of the upper fan channel crossings show inner incised channels (Fig. 19). The reduction in cross-sectional area from these inner incised valleys of the upper fan channels to the 80,000 m^2 size of the upper middle fan channels is about

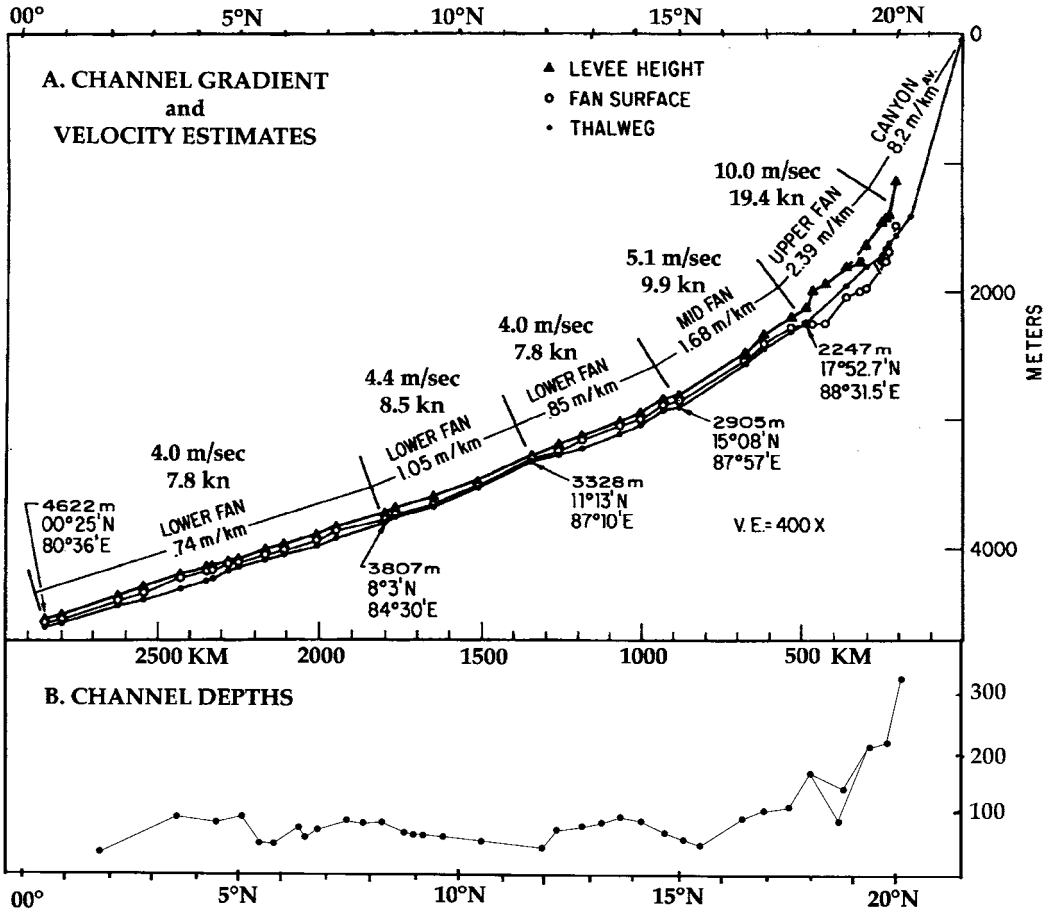

Fig. 18. A. Gradient of the active valley and the adjacent fan surface. Velocity estimates will be discussed later. B. Channel depths of the active valley. Notice that at about 400 km below the canyon mouth, two channel depths are shown, for the 'West Fork' (WF) and for the 'East Fork' (EF). The events of the channel shifting are detailed in Fig. 19.

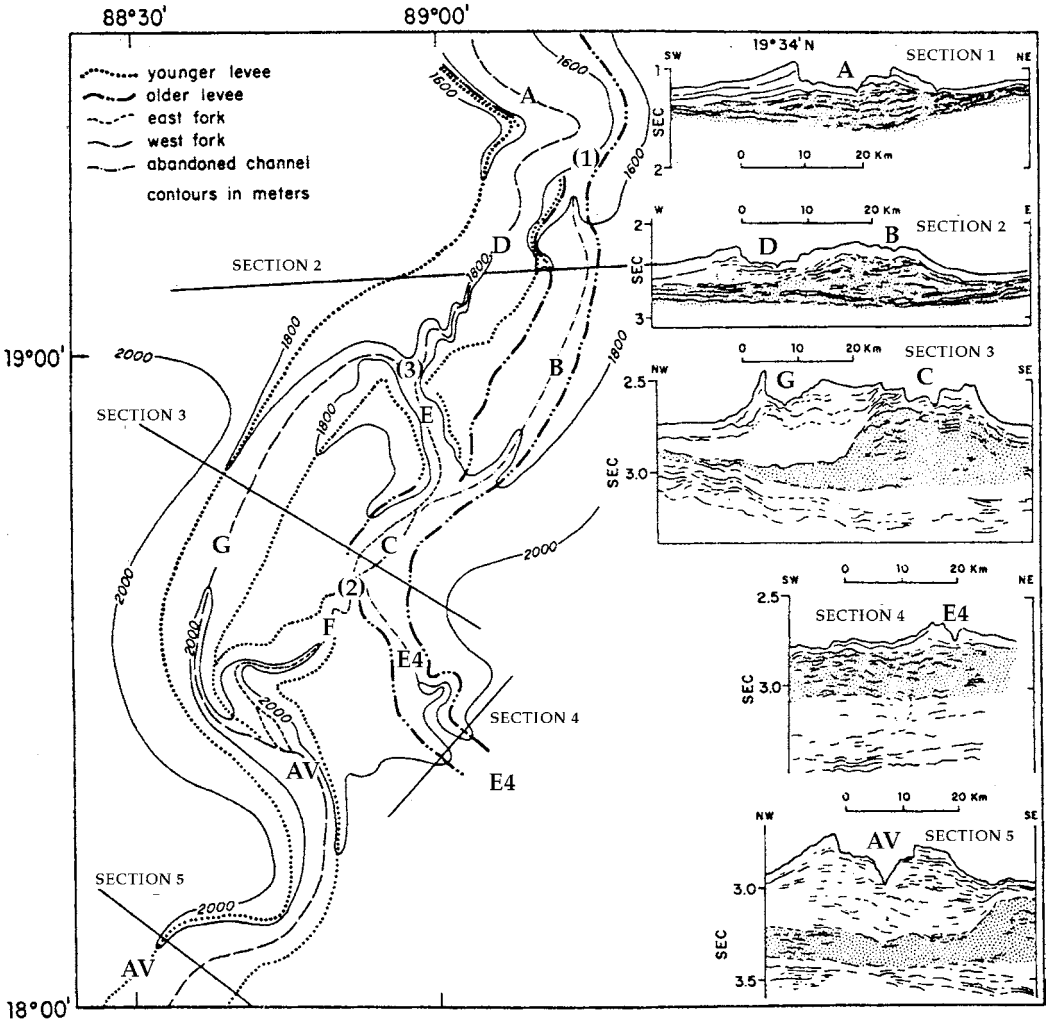

Fig. 19. Detailed bathymetry in the region of the bifurcation of the active valley in the upper fan. Numbers (1), (2) and (3) indicate areas of bifurcations by avulsion discussed in text. Section 1 is at 19°34′N, north of the map.

50%. This suggests a change in flow regime from huge channel-filling Pleistocene turbidity currents to the reduced size of Holocene turbidity currents, as previously suggested by Curray and Moore (1974) and Hübscher et al. (1997). During conditions of high sea level, as today, the turbidity currents are relatively small and infrequent and only the inner incised valley in the upper fan is adjusted to that smaller size. Any down-slope decrease in cross-sectional

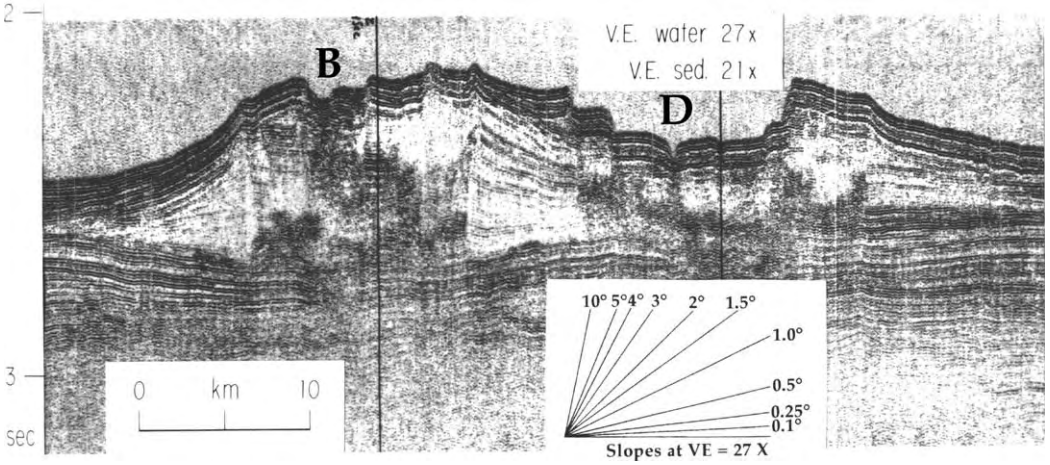

Fig. 20. Seismic reflection profile of Section 2, Fig. 19 at 19°05′N, showing the active channel D, on the right, and the inactive channel B on the left. This section is reversed from the line drawing in Fig. 19; east is on the left.

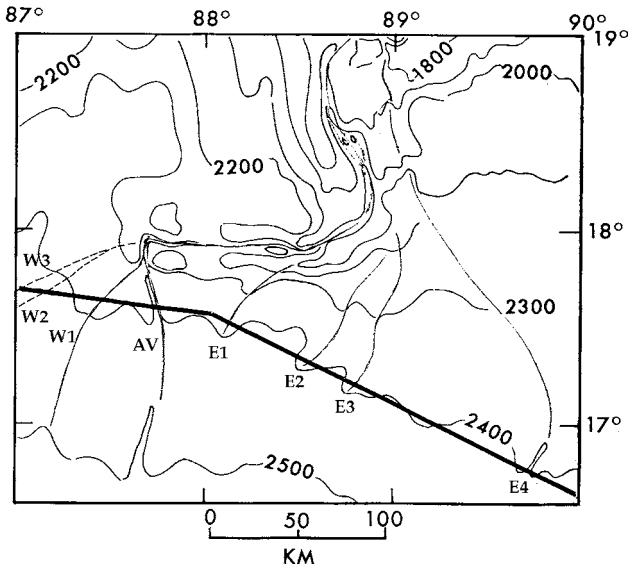

Fig. 21. Track of seismic line shown in Fig. 22, with interpreted channel migrations westward from E 4, to E 3, E 2, E 1, to W 3, and back eastward to W 2, W 1 and to AV.

area of the large levee-flanked valleys implies significant overbank flow outward and downward across the fan.

At about 400 km (Fig. 18B) two channel depths are shown. At 175 km below the canyon the valley bifurcates into an east and a west fork, which rejoin again 100 km farther to the south (Fig. 19). The sections shown in Fig. 19 are line drawings of seismic sections. Section 2 is the same as the seismic line in Fig. 20, but is reversed to show west on the left. Each individual channel thalweg segment is given a designation (A, B, etc.), and the locations of the three channel avulsion events are numbered (1), (2), and (3).

The presently active channel is shown as 'west fork'. The initial active channel included thalweg segments A, B, C and E 4, showing that E 4 was probably the single active fan valley during the early part of period D, ~125,000–0 BP (Fig. 15D). South of section 1, at about 19°20′N, a first channel break occurred, avulsion #1 in Fig. 19. The active channel then followed thalweg segments A, D, E, C and E 4. Next channel avulsion avulsion #2 changed the active segments to A, D, E, C, F and AV. Finally avulsion event #3 changed the active segments to A, D, G and AV, the present course of AV, and the east fork is being abandoned and filled.

Fig. 21 shows the area immediately south of the area of Fig. 20, where the next series of channel shifts lower on the upper fan appears to have occurred, and Fig. 22 shows a line drawing of part of the seismic line plotted in Fig. 21. The pattern appears to be first a westward shifting of the active channel, followed by an eastward shifting. The sequence appears to have been E 4 first, followed by E 3, E 2, E 1, W 3, W 2,W 1 and finally the move to AV, the presently active channel. Our best estimates of timing of these events are that the shift from E 4 to E 3 may have been early in Quaternary period D, 125,000–0 years BP, and as will be discussed later, that the shift from W 1 to AV was between 9700 and 12,800 BP.

The maximum number of valleys recorded on east–west survey lines across the Bay of Bengal occur between 11 and 17°N latitude. The average is about 10. This is fewer channels than we had previously believed because we had earlier interpreted all as separate channels instead of some being meanders of the same valley. South of 10°, the total number of valleys decreases until at 5°N only six valleys are found, three of which are deeper than 40 m. At the equator, five valleys are possibly present, including two possible branches of AV, although our southernmost crossings are slightly north of the equator (Fig. 4). The implication of this decrease is that migration processes active on the upper fan tend to create new valleys, and that these, in turn, tend to reoccupy and rejuvenate a few longer lived valleys down-fan. This is the reverse of the branching or distributary pattern of fan drainage systems commonly shown in artists' concepts of submarine fans.

The Bengal Fan is different from other large passive margin fans. Whereas the Indus, Amazon, Mississippi and Congo Fans have always had one single point source of sediments issuing from a single canyon, the Bengal Fan has clearly had many canyon sources throughout the Quaternary, and probably throughout its Tertiary history. Furthermore, the Bengal Fan is more than twice the length of these other fans.

It was apparent during our surveys that some valleys, although reasonably deep, are open only a relatively short distance down-fan, while others display much more continuity and occur over long distances before becoming inactive. Valleys W 2 and W 3, situated just west of AV, for example, are completely filled north of 17°N.

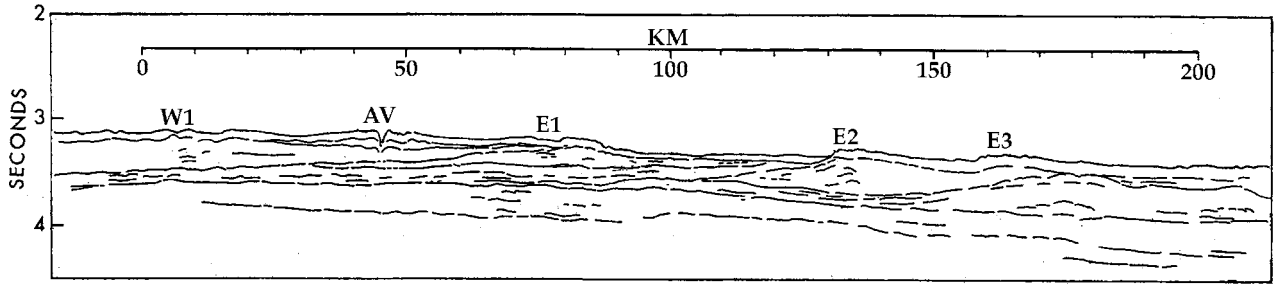

Fig. 22. Line drawing of part of seismic reflection line showing the locations of the channel crossings in Fig. 21.

4.2.1. Active valley, middle and lower fan

Fig. 23 is a compilation of line drawings of crossings of AV, in the middle and lower fan. All of the sections are at approximately the same scale and vertical exaggeration. They are, however, not strictly comparable, and we cannot easily calculate and demonstrate quantitatively the changes in cross-section area of the channels because of the extreme meandering nature of the channels in the middle and lower fan (Moe et al., 2001), and because our crossings are not necessarily orthogonal to the channel trends. Many of the channel crossings are multiple because of meanders and oxbows. In some cases the oxbow channels are filled; in other examples they are open. What can be observed and compared is maximum depth (Fig. 18B), whether the channels have flat bottoms and are being filled, or whether they are open. Open channels may be currently active, or they may simply be abandoned in regions of the fan far from current sources of sedimentation.

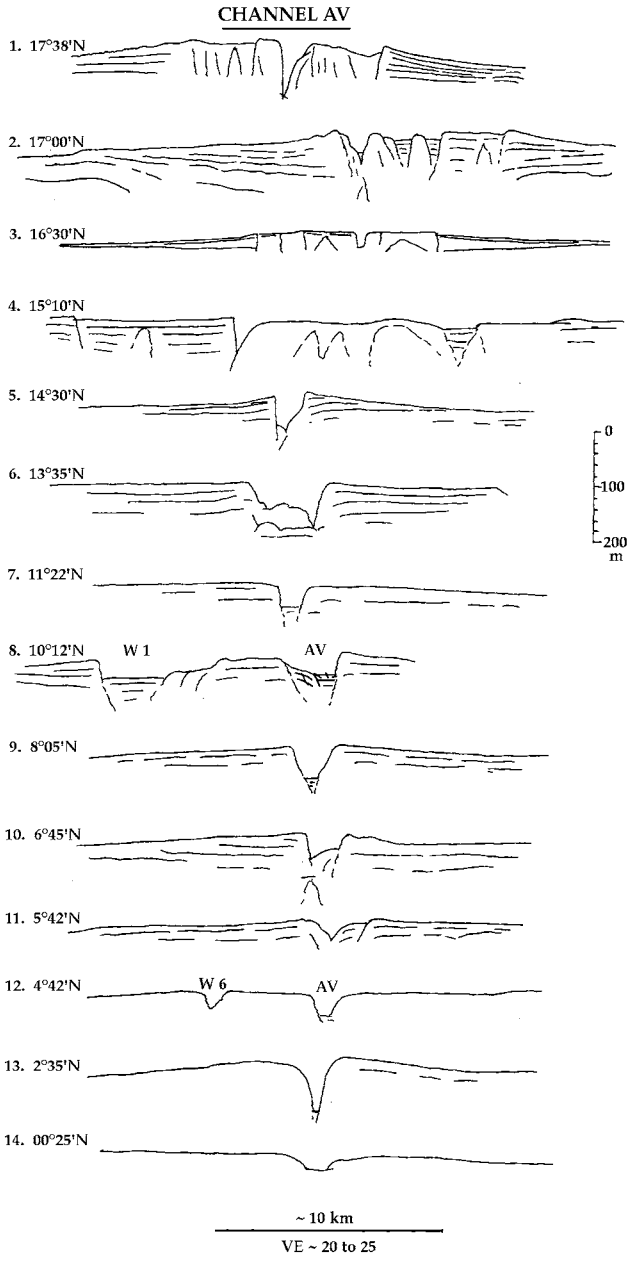

Fig. 23. Line drawings of 3.5 kHz records of selected crossings of the active valley AV. Section #8 shows crossings of both AV and the W 1 channels. Section #12 shows crossings of both AV and the W 6 channels. Refer to Fig. 5. Section #3 is adapted from Hübscher et al. (1997) and Weber et al. (1997).

The large elevated fan valley of AV ends abruptly at about 18°N, about 400 km from the canyon mouth, and at southern boundary of the upper fan. A completely different type of valley of much smaller dimension is encountered there. Whereas the thalwegs of the large upper fan valleys are built above the underlying fan surface, the middle and lower fan valley thalwegs are incised into the fan surface. The average fan surface gradient is 5.7 m/km in the upper fan, and 1.68 m/km in the middle fan, and the thalweg gradients are 2.39 and 1.68 m/km, respectively (Table 2 and Fig. 18A). The valleys on the middle and lower fan have small levees, and overbank deposition occurs along the whole length of the valley. AV can be traced down-fan to south of Sri Lanka, where our last crossing is at 0°25′N, 80°36′E, a distance of about 2220 km (Fig. 5).

Sections #1–6 (Fig. 23, have a V-shaped channel, with indications of filled meanders nearby, for example in sections 1, 2 and 4. Section #3 is a special study, and will be discussed below. Sections #5 and 6 channels may have slumped material on the channel floor. Section #7 is notably smaller and has a flat bottom. Section #8 also has some flat bottom fill and lies very close to the confluence with channel W 1, also labeled. Section #9 also has a flat bottom, whereas sections #10, 11, 12 and 13 have V-shapes with only suggestions of some deposition on the bottom. The last section we have of AV is #14, which is small with a generally flat bottom. The right hand levees of these channels appear to be higher than the left hand levees, a phenomenon observed and attributed to Coriolis force by Menard (1960), but we cannot evaluate this statistically because our crossings are not necessarily orthogonal to the alignments of the channels.

We interpret a flat bottom fill in a channel as indicating some degree of inactivity or abandonment, including declining turbidity current activity or size; and we interpret open, V-shaped channels as indicating turbidity current activity or else abandonment out of the reach of overflow deposition from nearby channels. Thus, in summary, AV looks like it could be active on a small scale through section #6 at about 13°N; less active and undergoing deposition in sections #7 and #8 to south of 10°N, and open but less active from section #9 to the southern end.

Valleys W 6 and W 2 join with AV at about 5°N as hanging valleys, an example of channel piracy by AV (Emmel & Curray, 1981b). The hanging valley of W 6 is shown in section #12, shortly before its confluence with AV. Two shallow filled channels are found on the south side of AV in line with W 6 and W 2, which may have been their

continuations beyond the region of piracy, but we have not shown them in Fig. 5.

Moe et al. (2001) conducted a swath mapping survey following AV northward from about 9°45′N to where they appear to lose AV at about 11°N, and followed W 1 (Fig. 5) from that point to about 11°45′N. They interpreted the sections of W 1 to be inactive, whereas they interpreted sections of AV from between 14° and 15°N to be active. These interpretations agree with ours, that AV is active southward to between sections #6 and 7, between 13°35′N and 11°22′N (Fig. 23). South of about 8°N, it is open, but we suggest that it is not very active, and is instead isolated from a source of sediment. We believe that this is the high sea level effect of the Holocene. Small turbidity currents late in the rise and during the high stand of sea level do not fill the upper fan channels bank to bank, so instead of spilling over the banks to send sediment by sheet flow to the adjacent upper fan, most of the sediment in the turbidity current is confined to the channel and some is deposited there. Hence the channel in the region of about 12–10°N has flat bottom fill, and the large channels south of about 8–10°N are receiving small amounts of sediment but are residually open and large.

Section #3, Fig. 23 is adapted from Hübscher et al. (1997) and Weber et al. (1997), who have published high resolution surveys of seismic, swath mapping, coring and dating from channels in AV. Their dating of AV channel at 16°30′N (Fig. 24) shows that this channel-levee complex was formed between 12,800 and 9700 BP over a pre-existing fan surface 12,800 years old. The levees were built to a height of over 40 m by 9700 BP, and the large channel was filled to a depth of over 70 m before 6000 BP, leaving only the small cross-section inner channel, similar in size to those above and below this level in AV system. As discussed previously, we interpret the time of cutoff of the direct discharge of sediment from the confluent Ganges and Brahmaputra Rivers into the Swatch of No Ground as about 6500 BP. We conclude that AV was formed and became the active channel approximately 12,000 years BP, and turbidity current activity diminished in AV at about 6000–6500 BP.

Both Hübscher et al. (1997) and Weber et al. (1997) concluded that the Bengal Fan is unique, in that sediment supply was continued through the Holocene, and that significant growth occurred during the sea level rise and highstand. They cite references to work in the Amazon, Rhone and Mississippi Fans that they were inactive during the late sea level rise and highstand. In addition, they slightly misinterpreted one of our statements (Emmel & Curray, 1985) to imply that the channel has been ‘abandoned’ since the last sea level rise, when in fact we have described and illustrated in another paper (Curray et al., 1982, Fig. 22b) our model for the reduced turbidity current activity during high stands of sea level.

The real significance of section #3 and the excellent seismic work correlated with radiocarbon dates is: 1. The AV, was first formed about 12,000 years ago on a fan surface about 12,800 years old; 2. Turbidity current activity deposited levees about 40 m high before 9700 years ago, enclosing a large cross-section channel; 3. By about 6000 years ago, the time we suggest the canyon was cut off from its direct supply of sediment from the confluent Ganges and Brahmaputra Rivers, this large channel had been filled, except for a relatively small cross-section area inner channel, by deposition from turbidity currents contained within the larger channel; and 4. In the past 6000 years, about seven meters of additional sediment have been deposited on the top of this channel fill, showing a continuing occurrence of turbidity current activity with some lesser amount of channel overflow even since the submarine canyon has been cut off from its direct supply of sediment from rivers.

Channel depths and the gradient of AV along its course vary down-fan (Fig. 18). Near the boundary of upper and middle fan (section #1, Fig. 23), the channel depth is 159 m, and decreases down-fan to about 37 m at 15°10′N, section

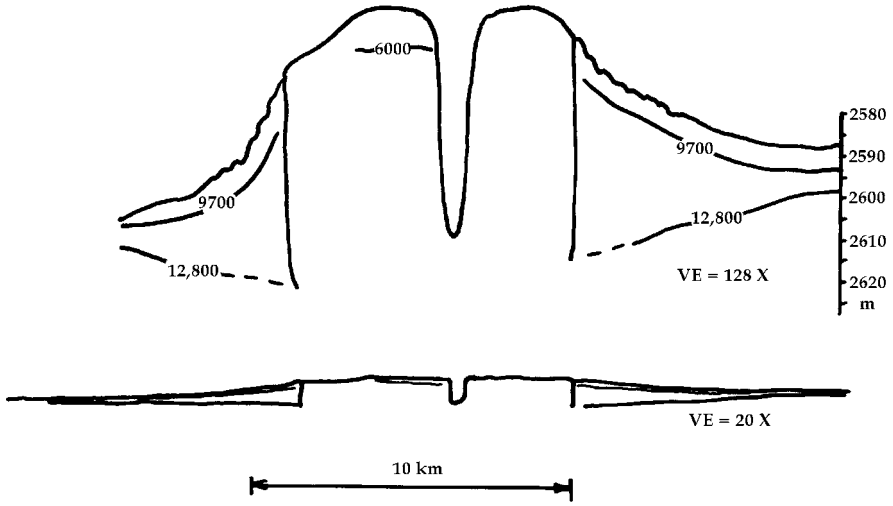

Fig. 24. Section 3 from Fig. 23, adapted from Hübscher et al. (1997) and Weber et al. (1997). See text for discussion of radiocarbon dates shown.

#4. South of this point, it increases to about 90 m at 13°35′N, section #6, and then shoals again at 11°22′ to 10°12′N to 41 and 37 m. Beyond this point, depths again are variable, with minimum values in the region where two hanging valleys, W 2 and W 6, join it at about 5°N. It is very deep and open at section 13, at 2°35′N, almost 100 m. It is shallow again at our most southerly two crossings below the only known bifurcation on the lower fan, with depths of 30 and 14 m, and the valleys probably disappear farther beyond that point. The ODP Leg 116 drilling sites are located in this region, in the extreme distal end of this subfan which was active during the Wisconsin and Holocene, subfan D (Figs. 14 and 15D).

Menard (1960) observed that many submarine channels attain a maximum depth part way along their paths, and decrease in depth below this maximum. Komar (1973) explained this phenomenon as increase in thickness of the turbidity current as the velocity decreases down the channel. AV does not follow this pattern. Channel depths are greater in the upper fan (Fig. 18B), decrease in the lower middle fan, increase in the upper lower fan, but then reach a minimum at 10° to 11°N. We will further discuss possible reasons for these channel size variations again later.

4.2.2. The eastern fan valleys

In addition to AV, other open fan valleys are found in the upper part of the middle fan (Fig. 5). A clear correlation between these middle fan valleys and those of the upper fan is generally not possible. An exception is E 4 (Figs. 5, 19 and 21), which we believe is of early Wisconsin age (Figs. 14D and 5). Fig. 25 is a compilation of sections of channel E 4, from 17°N, section#1, to the last crossing in which we can observe it at 7°24′N, section #9, a distance of about 1550 km from the canyon mouth. It appears in that region that it may join the channel now occupied by AV. If this is correct, it implies that the lower part of AV is older than 12,000 years, and that when AV was formed by channel shifting, it reoccupied this older segment of channel.

In our northernmost crossing, section #1, Fig. 25, the channel is filled, undoubtedly by the rapid deposition of shifting large channel-levee complexes in this region. Sections 2–4 show an open channel down to 13°27′N. In the next crossing at 13°10′N, the channel is partly filled. The channel is open in sections 6, 7 and 8 and is very deep, about 100 m. It has flat-bottom fill in our last crossing, # 9 at 7°24′N. This pattern of filling is somewhat similar to the AV: channel deposition and back-filling occurred in the middle fan at about 13°N (section 5, Fig. 25), perhaps during decreased turbidity current activity before this channel was abandoned at some time early in period D, after 125,000 years BP. Filling at 7°24′N is due to the continuing deposition from the later valleys, probably some of the west valleys and then by AV. The turbidity currents which eroded E 4 must have been large, as judged by the valley's size over the last 160 km of its course, where it often exceeds 100 m in depth.

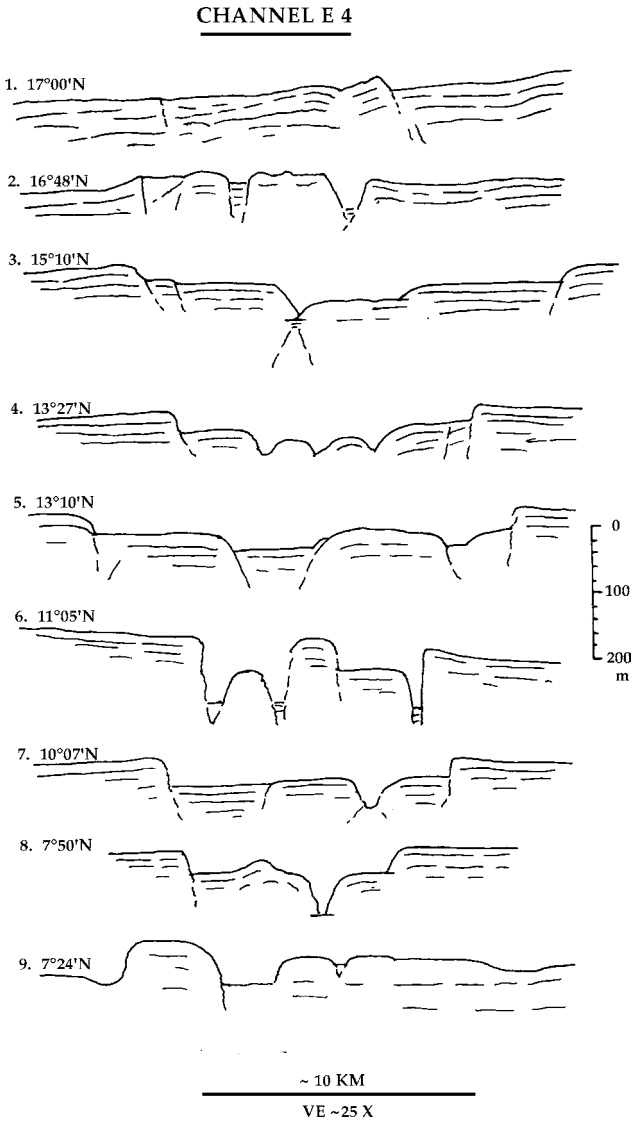

Fig. 25. Line drawings of 3.5 kHz records of selected crossings of channel E 4.

One of the most prominent of the older eastern channels is E 5 (Fig. 26). Our most northerly crossing is section 1, Fig. 26, at 13°16′N and 90°04′E; lines north of this latitude show only filled remnants, as observed in our seismic and 3.5 kHz lines. Our section #2 at 12°36′N has some open channel, increasing down-fan in sections 3, 4, 5 and 6 at 7°20′N. Section 7 shows our deepest channel crossing, with the rather remarkable depth of 143 m, where the channel has eroded to below the Pleistocene–Pliocene boundary which we extrapolate from DSDP Site 218 (Figs. 1 and 4). Between this latitude and the equator, it is more than 100 m deep in most crossings. For comparison, at about the same latitude AV is much smaller (Fig. 23). We cannot determine which of the channels in sections 5 and 6 is E 5 nor what the other channel is.

We assume that this valley is pre-Wisconsin in age, and presume that it formed late in period C (Fig. 14C). This valley can be traced down-fan to 2°S, but unfortunately, the

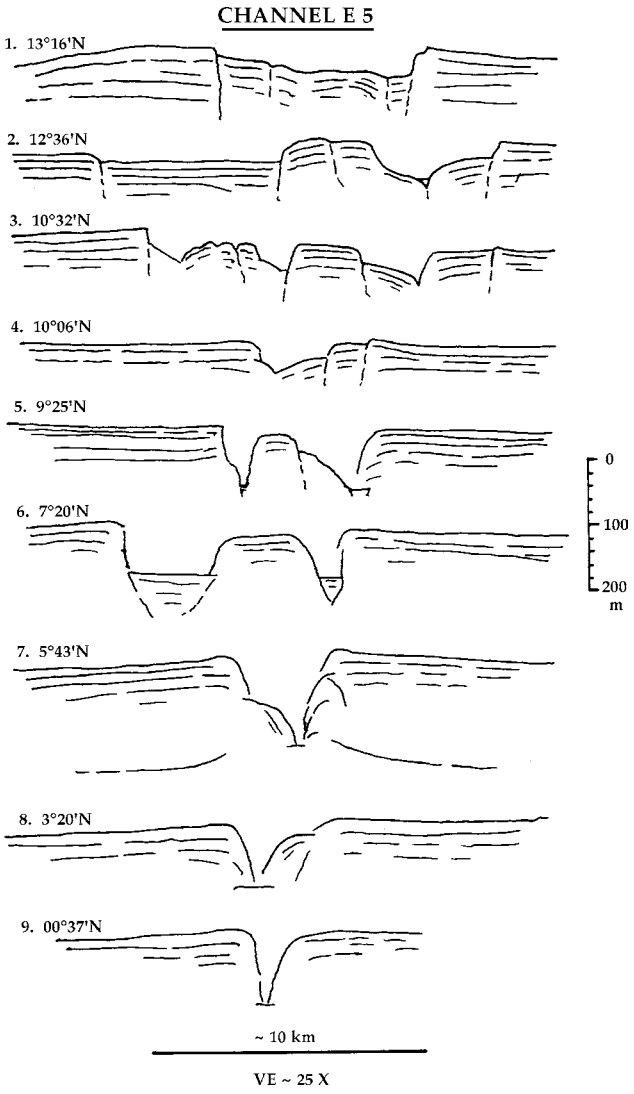

Fig. 26. Line drawings of 3.5 kHz records of selected crossings of channel E 5.

course south of the equator is based only on soundings of unknown accuracy, and the exact depth is not known. Its total length, measured from the present canyon mouth, is almost 2500 km.

The deep remnants of E 4 and E 5 on the lower fan were excavated by extremely large currents during lowered sea levels. Furthermore, as in the case of E 5, they may have been reoccupied and eroded during several sea level lows. On the upper fan, at about 19°35′N, and between 89°44.5′E and 90°17′E, there are large buried valleys which support these conclusions. The largest valleys of subfans B and C are found here (Fig. 15B and C).

Between 0°45′N, 83°52.5′E and approximately 4°00′S, 84°00′E, another relict valley was crossed several times (Fig. 5). Its depth exceeds 100 m in several locations, and its course is remarkably parallel to that of the E 5. We believe that this valley also belongs to the drainage system of the pre-Wisconsin fan and that its upper course was filled in by overflow sediments transported down-fan by later valleys.

In the northeastern part of the bay, we mapped a valley which we had previously named the 'Box Valley' (Moore, Curray, & Emmel, 1976) (Fig. 5, E 7), because of its curious U shape in recorded cross-section. It can be followed between 17°N and about 10°N off Myanmar and the Andaman Islands, and its course roughly parallels the base of the continental slope (Fig. 3). Between the latitudes of 15°30′ and 14°18′, this valley is completely filled by a mudflow resulting from the very large Bassein submarine slide. We suggest that the channel has this characteristic shape both north and south of the immediate vicinity of the Bassein slide (Moore et al., 1976) because of deposition from either large slides such as the Bassein slide or from the many mud volcanoes on this western slope of the accretionary prism (Fig. 1).

4.2.3. The western fan valleys

Of the valleys reviewed this far, we have suggested that E 5 was active in pre-Wisconsin time and that E 4 was active some time during the Wisconsin latest glacial, probably early in period D (Fig. 15). Since E 4 was abandoned, activity has been west of E 4, first perhaps at E 3, then E 2 and E 1, and then to the west channels. We cannot be certain, but we suggest that a reasonable sequence would be E 5, E 4, E 3, E 2, E 1, W 3, W 2, W 1, and finally AV.

We do not know when W 6 was active, but it is a special case. In fact, it may be a channel primarily related to the Mahanadi, Godavari and Krishna Rivers of India (Fig. 3), and this western part of the Bay of Bengal could be considered a subfan, the Orissa Fan (Emmel & Curray, 1981a). It may still be receiving some input from those rivers, because they have deltas on a narrow continental

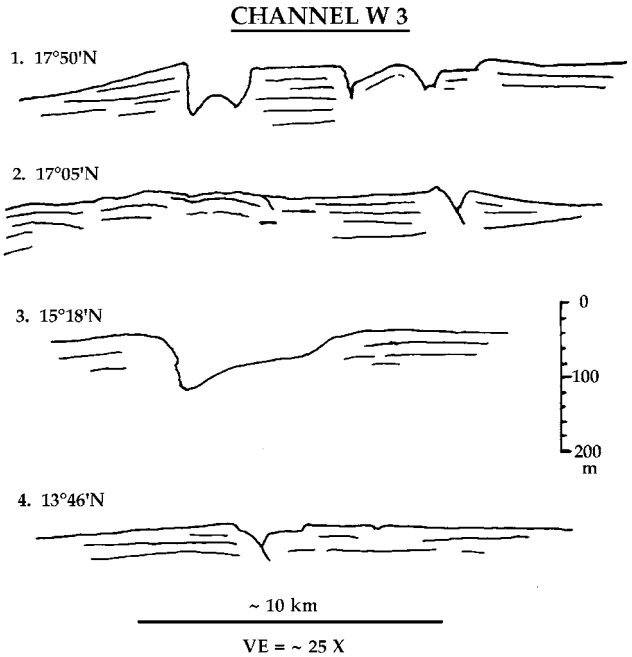

Fig. 27. Line drawings of 3.5 kHz records of selected crossings of channel W 3.

shelf. The northern end of W 6 could be related to small canyons shown in the depth contours on the continental slope south of the Mahanadi delta (Fig. 3) and sediment could come down the continental slope off the Godavari and Krishna Rivers. The bottom sediments of this subfan show mineralogy of Indian subcontinental origin (Kolla & Biscaye, 1973; Kolla et al., 1976). The OPD Leg 116 sites (Figs. 1 and 4) show that some sediment has a provenance suggestive of India and Sri Lanka (Brass & Rahman, 1990; Yokuyama, Amano, Tairo, & Saito, 1990).

Figs. 27–29 show compilations of sections of channels W 3, W 2 and W 1, respectively. Each shows multiple channels in the northernmost section. We cannot determine which is the channel which connects with the next section to the south.

Channel W 3 can be traced only to about 12°N (Figs. 5 and 27). It is generally open in the upper middle fan, sections 1, 2 and 3, Fig. 27, but by 13°N, it is small and probably filled. It disappears shortly south of there, probably filled by channel overflow from the subsequently active channel, W 2.

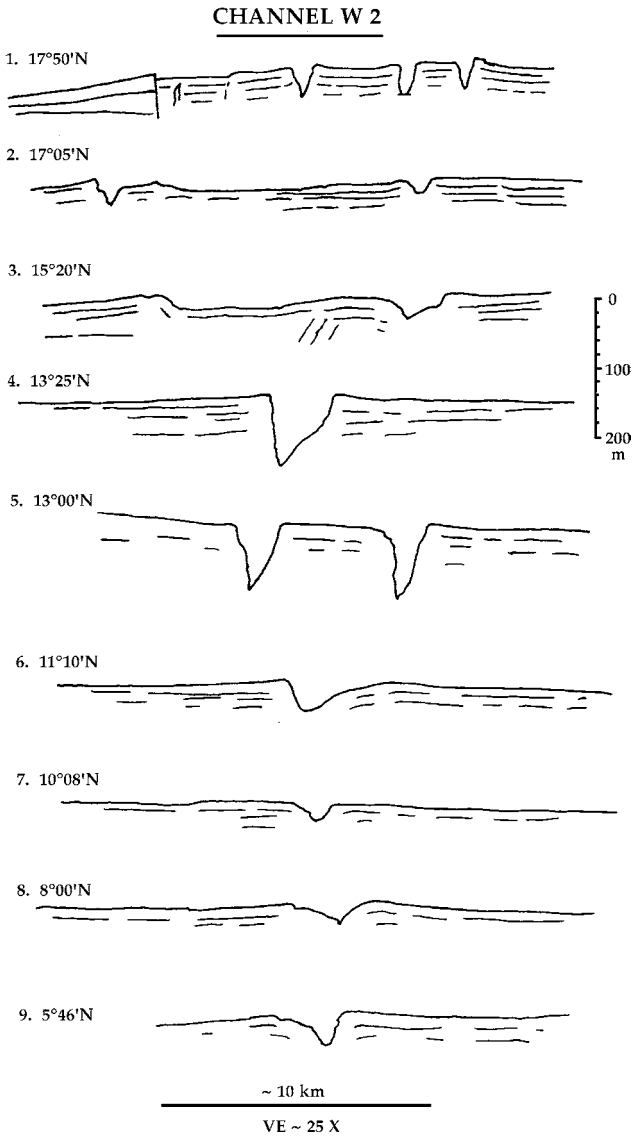

Fig. 28. Line drawings of 3.5 kHz records of selected crossings of channel W 2.

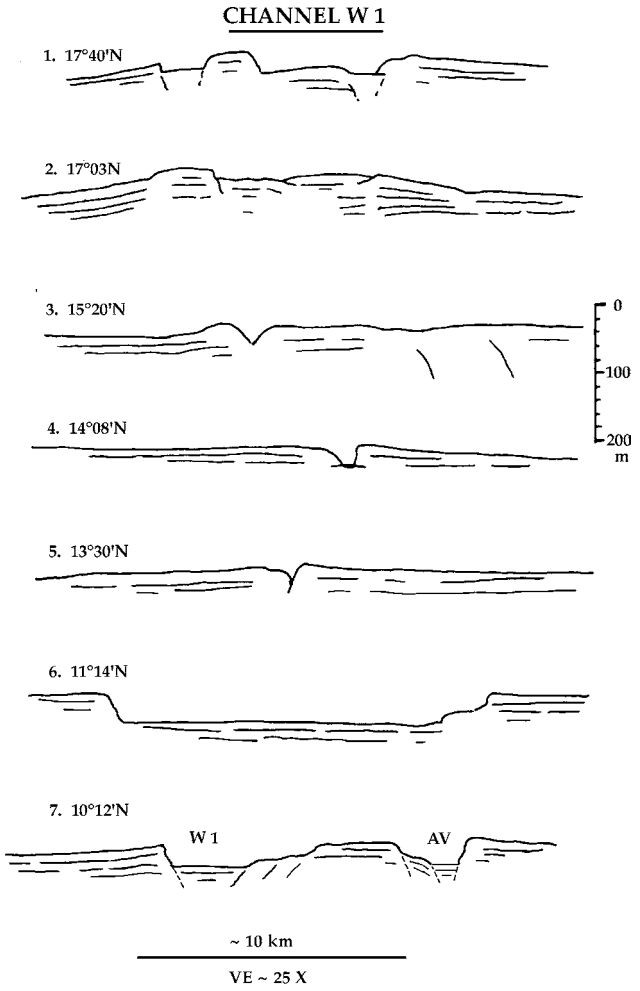

Fig. 29. Line drawings of 3.5 kHz records of selected crossings of channel W 1. Section 7 also shows channel AV.

Channel W 2 (Fig. 28) is small and shows filling in the upper middle fan, sections #1, 2 and 3. By 13°N, it is very large, exceeding 100 m. It then continues open but smaller to where it joins AV as a hanging valley at about 5°N (Fig. 5).

We believe that W 1 was the active channel prior to formation of AV about 12,000 years ago. It is generally small and filled down to about 11°N, sections 1–5, (Fig. 29). Section 6 shows a very large flat bottom channel, but we suspect that this section runs through an east–west meander, making it appear too wide. Section 7, the same as section 8 in Fig. 23, shows W 1 just before it merges with AV. Thus the channel below this merge was occupied earlier by W 1. Farther south, it may have been occupied even earlier by E 4.

We believe that W 3 is older than W 2, because its lower end appears to have been buried by sheet flow from W 2. We believe that W 1 is younger than W 2 because W 1 and AV merge at grade, and W 2 is a hanging valley when it enters

AV. When W 1 was abandoned and AV was formed, it reoccupied the W 1 channel south of 10°N. W 1 had already probably reoccupied the E 4 channel south of 7°N., and E 4 had perhaps already eroded deeply enough to cut off the W 6 and W 2 channels at 5°N. These are only assumptions, and we cannot be absolutely confident about this interpreted sequence. The most important event in timing has been made possibly by the studies of Hübscher et al. (1997) and Weber et al. (1997), that AV is only about 12,000 years old.

AV has obviously reoccupied earlier channels. The oldest valley we know of in this subfan (Fig. 14D) is E 4, and it extends to the end of the valley we label AV at about the equator. E 3, E 2 and E 1 presumably occupied parts of the lower end of E 4's channel, as did W 3, W 2 and W 1. W 5 and W 4 are presumably older than W 3, but we have little information on them. We know nothing about the relative age of W 6. Reoccupation of older channels on the lower fan is one of the dominant processes of channel migration on the Bengal Fan.

4.3. Velocity estimates for turbidity currents

Turbidity current velocities have been estimated by direct observations in other parts of the world, by laboratory simulation and by mathematical calculations. These various methods have yielded estimates that range from 25 m/s (about 50 knots) (Heezen & Ewing, 1952) off the Grand Banks, northern Atlantic Ocean, to very slow drift, 25 cm/s (0.5 knot) in Lake Meade (Gould, 1951).

We have attempted some estimates of velocity with a Chezy-type equation used by Komar (1970) (M. Baltuck, personal communication). The equation is:

$$\mu = \left[\frac{\rho_t - \rho}{\rho_t} gh \frac{\sin \beta}{(1-\alpha)c_f} \right]^{1/2}$$

where

h	channel depth
β	channel slope
ρ_t	density of turbidity current. We have used 1.15 g/cm^3 (Komar, 1972)
ρ	density of sea water, ~1.027 g/cm^3
c_f	drag coefficient. We used 0.0035 (Johnson, 1964; Komar, 1973)
g	acceleration due to gravity, 9.807 m/s^2
α	ratio of the drag on the flow at the upper interface of the turbidity current to drag at the current slope interface, the bottom of the flow, and is dependant upon the Froude number.

These estimates are shown in Fig. 18A, plotted above the gradients for AV and the adjacent fan surface. Although AV is only about 12,000 years old, the overall gradient of the fan and the thalweg is a profile of equilibrium for maximum turbidity activity during low stands of sea level. These estimates would, therefore, be maximum velocities during lowered sea level. The estimates range from about 10 m/s (20 knots) in the upper fan to about 4 m/s (8 knots) in the lower fan. Thus turbidity currents slow going down the fan, as one would expect, although the reasoning is circular because gradient of the channel is one of the variables in the equation. Nevertheless, we suggest that these estimates may be reasonable for maximum size turbidity currents during lowered sea level conditions. We presume that present day velocities of the smaller flows would be slower.

At the same time as the velocity decreases, the cross-sectional area of the channel also decreases. Obviously, if a turbidity current slows in velocity and if the channel decreases in size, most of the volume of the turbidity current must overflow the banks of the natural levees and pour out over the fan. This lateral flow, probably diagonally down the gradient of the fan surface, is the source of the sediment comprising the great bulk of the fan, and by analogy, the most common sediment of some ancient sedimentary basins. The residual turbidity current that remains in the flow in the channel may end up as primarily sand or silt, and is deposited where the turbidity current loses its momentum and dies out. With large turbidity currents such as occurred during Pleistocene lowered sea level, some of this coarser sediment may have been deposited at the distal end of the fan. During high stands of sea level as today, with smaller and less frequent turbidity currents, much the sand and silt may be deposited in the channel itself.

An interesting result of these estimates is that a large turbidity current would require about 72 h to reach the equator, following AV. An interesting question is how long would this river of sediment-suspension flow past any point along the channel? The answer must lie in how the slumping occurs in the fill in the submarine canyon. Again, we do not know, but the slumping event must not be simultaneous along the 160 km of canyon axis, but may in fact be a sequence of small slumps starting at the outer or lower end. Each successive slump would oversteepen the fill up-canyon from it, so a shoreward progression of slumping would occur. This would imply a discrete period of time, so we might speculate that an observer sitting on one of the natural levees along this channel, if he or she were not swept away by the overflow from the turbidity current, might have been able to watch the current passing by for at least several hours.

5. Discussion and conclusions

5.1. One active canyon, one active fan valley

One of the important conclusions from this study and our previous publications is that there is only one active fan valley at the present time, issuing from the one active submarine canyon. As the fan valleys migrated, two active channels could have coexisted during the short time

required to fill an old channel and stabilize a new one. In contrast, our investigations of the Quaternary stratigraphy (Fig. 15) suggests that during some periods of time, there may have been more that one active canyon. As we have stated, we do not know whether these canyons were active simultaneously or sequentially. Today the major rivers, the Ganges and Brahmaputra are confluent in the delta, but this has probably not always been the case. During much of Holocene and Pleistocene time they may have entered the Bay of Bengal separately, as some of the other large rivers may also have done. Thus, during much of the Pleistocene, and presumably during the late Tertiary, several rivers may have flowed separately into the Bay, each with its own submarine canyon system and active fan valley.

5.2. Channel size and gradient variations

Dramatic changes occur in channel sizes down the length of the fan, from the immense channel-levee complexes of the upper fan, to the much smaller incised channels of the middle fan, to the partially filled channels of the upper lower fan, and finally to the open but probably inactive channels of the lower fan. While we would like to be able to plot the change in cross-sectional area down the length of the fan, we are unable to do so because of the meandering and the fact that our sections are not necessarily at right angles to the trends of the channels. The best we can do is to discuss channel depth changes.

Menard (1960) observed that many such channels show a maximum depth part way down their respective fans or continental rises, with a decrease in depth below that point. Komar (1973) explained this as increase in thickness of the turbidity currents with a decrease in gradient. Channels in the Bengal Fan, and especially the active channel, in contrast, show a general down-fan decrease in depth, with minimum channel depths in the lower middle fan at about 16°N and again at about 10–11°N in the lower fan (Figs. 18 and 23). Both of these minima coincide with local decreases in fan gradient, probably caused by deposition within the channel. Sections 7 and 8 at 11 and 10°N show some flat ponded sediment. We suggest that back filling started at 10 and 11°N early in the rise of sea level at the end of the Wisconsin, and that it may have progressed northward later in the rise.

Komar (1972) estimated the relative thickness of the head of a turbidity current compared with the thickness of the body of the current. He concluded that with Froude number about 0.75, which corresponds to a gradient of 0.0022 (2.2 m/km), head and body thicknesses are equal. Above that point, where the gradient exceeds 2.2 m/km, head thickness is greater, so more of the overflow of the channels would come from the head. Below that point at lower gradients, more of the overflow would come from the body. Significantly, this change in average gradient occurs precisely at the boundary between our upper and middle fan. This is where the thalwegs of the channels change from lying above the underlying fan surface to where they are incised into the fan surface. And this is where the cross-sectional area of the channel decreases by about 90%. The upper fan is the region of maximum rate of deposition of the levees. The huge levees end at the boundary between upper and middle fan, and deposition below that point is probably spread farther across the fan rather than being concentrated in the levees.

If the sediment suspended in the head of a turbidity current is coarser than the sediment suspended in the body of a turbidity current, this would suggest that some of the sand would overflow the channels in the upper fan, and that predominantly finer sediment would overflow the channels in the middle and lower fan. Observations do not support this assumption, and we will discuss this problem later when we address the problem of where the sand is deposited.

5.3. Channel shifting and formation of new channels

Channel avulsion occurs only on the upper fan and the upper part of the middle fan. It is a rapid process, and the rate of deposition is highest in this region. Slow channel migration by lateral erosion probably occurs farther down on the middle and lower fan, but this process is much less important.

We have shown (Fig. 19) a scenario to explain the sequence of events in the change from flow down channel E 4 to AV on the upper fan. This process of cut and fill could have been very rapid. The distance over which we can recognize this filled valley is about 25–30 km. If we take a conservative figure of 1,500,000 m^2 for the cross-sectional area of an upper fan valley, then the sediment fill involved is in the order of 35–45 km^3. Compare this with a migration and fill episode in historic time in Bangladesh (Coleman, 1969). The Brahmaputra River carved a valley 200 km long, with an average width of 12 km. Subsequently an average thickness of 18 m of sand was deposited in the valley. This migration and subsequent fill of about 45 km^3 took about 200 years.

Channel avulsion on the upper fan probably occurs much less frequently than channel avulsion at the southern boundary of the upper fan, where the channel changes from huge channel-levee complexes to smaller channels incised into the underlying fan. This is where the gradient of the thalweg decreases to less than 2.2 m/km, where the channel cross-sectional area decreases by as much as 90%, and where the thickness of the body of large turbidity currents would exceed the thickness of the heads of the turbidity currents. Thus a great amount of overflow of the banks of the channels would occur. We have shown that as many as eight valleys are thought to have connected at different times to the channel in the upper fan (Figs. 5, 21 and 22). During short periods, two could have existed at the same time, while the abandoned channel was being filled. Middle fan filling between 16 and 18°N is by a combination of deposition within the valley during the time that it is still connected to the large fan valley as more of the flow is being

diverted to the new middle fan valley, and by overbank sheet flows from later adjacent valleys.

The dominant process of sedimentation on the distal fan and the flanks of the active subfan far from the active channel is probably hemiturbidite deposition, by diffuse clouds of suspended fine sediment deposited slowly from suspension over a long period of time, perhaps weeks to months, at the dying end of large turbidity currents (Stow & Wetzel, 1990).

5.4. Where is the sand deposited?

The Ganges and Brahmaputra Rivers, the major sources of sediment for the Bengal Fan, are relatively sandy rivers as compared with other major rivers of the world (Coleman, 1969; Thorne, Russel, & Alam, 1993), i.e., they carry an unusually high proportion of bed load. Huge amounts of sand and other coarse sediment must have been carried to the Bengal Fan during Pleistocene lowered sea levels. Where was this coarse sediment deposited? Is it concentrated in certain parts of the fan that could constitute potential hydrocarbon reservoirs, or is it distributed more uniformly? We do not know, because insufficient coring and drilling have been done to form any firm conclusions. We can only speculate or surmise from the little sampling done on this fan and from what is known about other better-sampled fans.

Possible loci of preferential accumulation of the sands in the Bengal Fan are overbank deposits in the upper fan levees, in inter channel-levee lows, in the channels, in overbank deposits in the mid and lower fan, and/or in terminal lobes.

Sand turbidites have been sampled in DSDP 218 (Figs. 1 and 4) in the lower fan in five pulses, ranging from late Quaternary to middle Miocene (Thompson, 1974). The site is near channel E 4 (Fig. 5), and the late Quaternary pulse could be related to the time of activity of that channel. Although we see many buried older channels in our seismic reflection lines, we do not have sufficient coverage to correlate these channels from line to line, as we can do with surface channels. We, therefore, have no way of knowing proximity to channels for the older three pulses in this lower fan environment. The ODP Leg 116 sites (Figs. 1 and 4) sampled silt turbidites, but it is located in the far distal part of the fan, rather remote from the mapped termination of our AV.

Sand has been cored in and near various channels on the fan, including in a few of our own cores and in Lamont-Doherty Geological Observatory cores. Otherwise our Scripps coring efforts on the fan have yielded fine grain sediments with occasional thin sand and silt layers and burrow fillings. In particular, although we have very few cores on the levees of the upper fan, none have shown sand deposits. Our cores are, however, short and may not be sampling the lowered sea level strata of those levee deposits.

An argument can be made that extensive sand deposits may lie in the natural levees or between the channel-levee complexes in the upper fan. Komar (1973) has postulated that in the upper part of a turbidity current channel out to a gradient of 2.2 m/km, the thickness of the head of the flow exceeds the thickness of the body of the flow, and is more likely to overflow the banks. If the head contains more of the sand, then the levee surfaces could be partly sand. A more plausible explanation was offered by Pirmez, Hiscott, and Kronen, (1997) based on drilling in the Amazon Fan. They discovered that the 'high-amplitude reflection packets' (HARPs) include significant sand beds and lie preferentially in the inter-channel areas adjacent to areas of channel shifting by avulsion. When levee breaching occurs during avulsion, the turbidity currents spill out into the lows between the channel-levee complexes and the sands in suspension in the turbidity current heads and in the lower parts of the body are deposited as the currents flow through the breach.

An example may be the Eocene turbidite sands in the Indoburman Ranges, which we have interpreted as 'proximal' Bengal Fan sediments offscraped in the subduction zone and uplifted into the accretionary prism (Fig. 9A). We have no direct evidence for the existence of such upper or middle fan turbidite sands in the Bengal Fan, but HARPs can perhaps be identified in some of our reflection profiles and line drawings, for example in Figs. 13, 19 and 20.

The only other large fan which has been drilled is the Mississippi Fan (Bouma, Coleman, & Meyer et al., 1986). No drilling was done in the upper fan, but sand was found in mid-fan channels and in the lower overbank deposits of the fan. Sand was also found in channel fill and in overbank deposits in mid and lower fan on the Amazon Fan. Insignificant amounts of sand were found in upper fan overbank deposits.

Studies of ancient fans and of other modern fans also show that sands are frequently found in channel deposits and in terminal lobes (see, for example, Mutti & Normark, 1991; Normark, 1978; Piper & Normark, 2001; Shanmugam & Moiola, 1988; Walker, 1978). Terminal sandy lobes have been described both in midfan and distal fan locations. We suggest that the midfan lobes, previously called suprafans (Normark, 1970, 1978), are Holocene high sea level deposits from small Holocene turbidity currents, and are analogous to the channel backfill we observe on the Bengal Fan between about 13 and 10°N. Terminal sandy lobes may possibly exist at the distal end of Bengal Fan channels, and were presumably deposited by sheet flow at the lower ends of channels carrying large turbidity currents, which deposited the last sands carried by those currents. We have no direct evidence by sampling regarding the existence of terminal lobe in the Bengal Fan.

5.5. Fan depositional models

Our depositional model for the Bengal Fan, for which we do not claim total originality (see, for example, Kolla & Coumes, 1987; Stow et al., 1984; and many others) is shown in Fig. 30. This is an elaboration of the model in our earlier paper (Curray et al., 1982, Fig. 22).

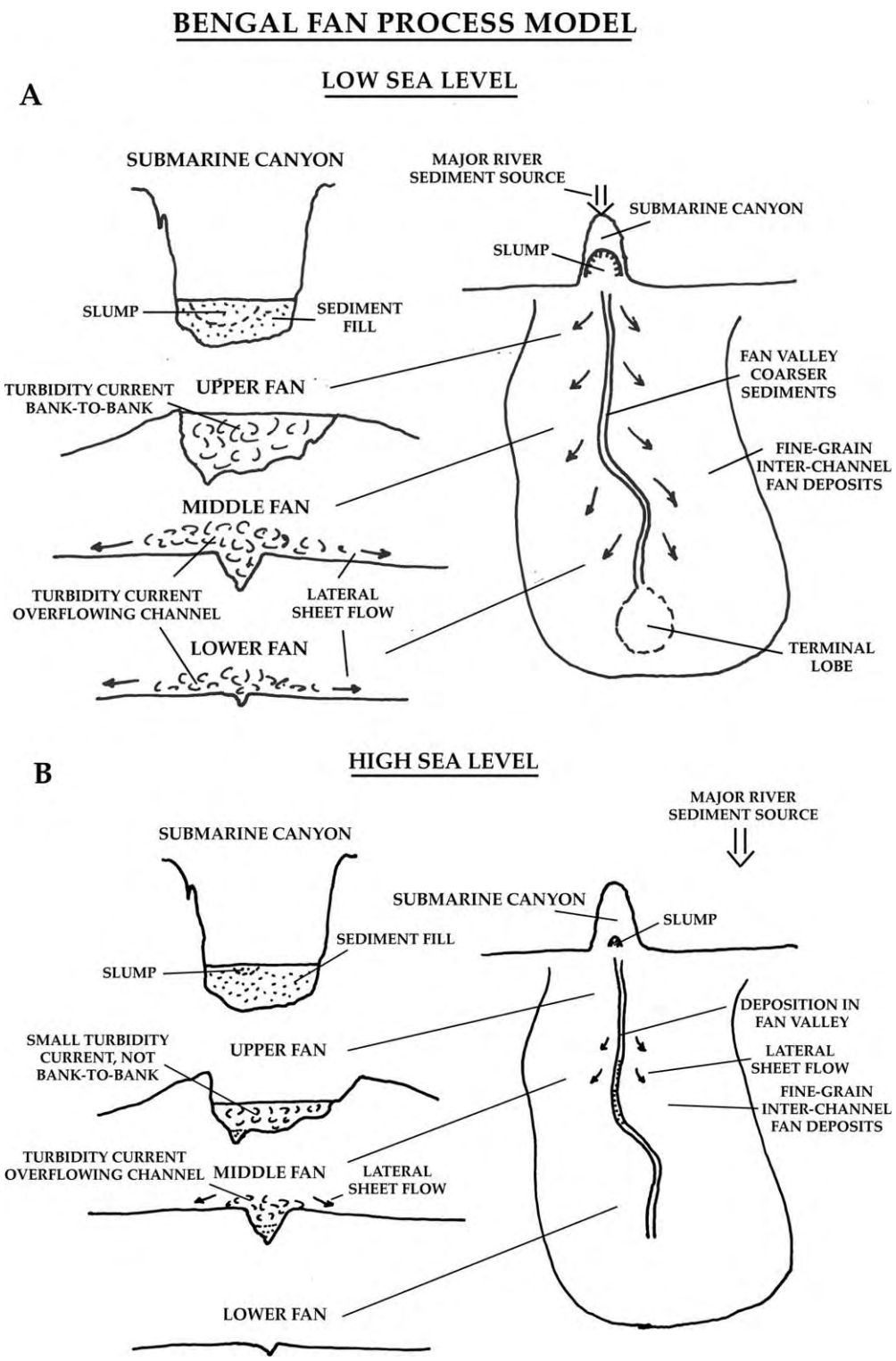

Fig. 30. Model of turbidity current deposition for the Bengal Fan. A. Conditions during lowered sea levels when turbidity current activity is at a maximum. B. Conditions during a high stand of sea level as today with minimum turbidity current activity.

Processes during lowered sea level conditions are illustrated in Fig. 30A. Rapid deposition occurred in the submarine canyon because the full discharge of the confluent Ganges and Brahmaputra Rivers entered the canyon head. At times, other rivers may have had their own submarine canyons and channel systems. Where the rivers did not occupy preexisting canyons, slumping on the upper continental slope started the formation of new canyons. Slumping occurred in unstable fill in the canyon heads or on the slope, generating huge turbidity currents, which filled the upper fan channels to levee level. Smaller turbidity currents were totally contained within the levees, but larger than

average flows would have spilled over the levee crests, further increasing their height. The heights of the levees were therefore determined by the size of the largest turbidity currents (also see Komar, 1973). As the currents moved down the channel, they slowed as the gradient decreased and as the channel cross-sections decreased. The turbidity currents spilled over the levee crests as sheet flows down-slope diagonally away from the channels, and deposited the finer grain parts of the load as fan surface deposits. Some of the coarser sediments were deposited within the channels, and during maximum turbidity current activity, some of it might have passed through the canyon to form terminal lobes of relatively course sediment.

Processes during high stands of sea level, like the present time, are shown in Fig. 30B. The canyon does not receive the direct load of the large rivers, but does intercept sediment moving on the continental shelf (Hübscher et al., 1997; Kudrass et al., 1998; Kuehl et al., 1997; Weber et al., 1997). The resulting slumps and turbidity currents are smaller, probably less frequent, and probably contain less coarse sediment than during lowered sea level. The currents are, therefore, contained within the large channels, and less overflow occurs. Because the flows are smaller, they are probably slower and do not carry as far down the channel. Deposition occurs within the channel in the middle fan at the termination of flow, and little or no turbidity current deposition reaches the lower fan.

Acknowledgements

The work at sea and initial analysis and publication of data for this project, many years ago, was funded by various grants from the Office of Naval Research and the National Science Foundation. Funding for the expenses of this long overdue summary publication have come from our own personal resources. During the cruises and the reduction of data, we had the assistance of many colleagues, some of whom have coauthored publications with us, as listed in the references below. We cannot list them all by name, but thank them all. However, we are especially grateful for the help we received from Russell Raitt, Ed Hamilton, Bill Huckabay, Perry Crampton, Tissa Munasinghe, George Hohnhaus and Jim Yount. We have also benefited greatly from thoughtful and careful reviews and suggestions of an earlier version of this manuscript by Ven Kolla and Dave Piper, and we thank them.

References

Acharyya, S. K. (1998). Break-up of the greater Indo-Australian continent and accretion of blocks framing south and east Asia. *Journal of Geodynamics*, *26*, 149–170.

Alam, M. (1989). Geotectonics and subsidence of the Ganges–Brahmaputra Delta of Bangladesh and accompanied drainage, sedimentation and salinity problems. In J. D. Milliman, & S. Sabhasri (Eds.), *Sea level rise and coastal subsidence: Problems and strategies*. New York: Wiley.

Alam, M., Alam, M. M., Curray, J. R., Chowdhury, M. L. R., & Gani, M. R. (2003). An overview of the sedimentary geology of the Bengal Basin in relation to the regional tectonic framework and basin-fill history. *Sedimentary Geology*, *155*, 179–208.

Barnes, N. E., & Normark, W. R. (1985). Diagnostic parameters for comparing modern and ancient fans. In A. H. Bouma, W. R. Normark, & N. E. Barnes (Eds.), *Submarine fans and related turbidite systems, wall chart*. Berlin: Springer.

von der Borch, C. C., Sclater, J. C., et al. (1974). *Initial reports of the Deep Sea Drilling Project, Leg 22*. Washington, DC: US Government Printing Office, 890 pp.

Buffington, E. C. (1952). Submarine 'natural levees'. *Journal of Geology*, *60*, 473–479.

Bouma, A. H., Coleman, J. M., Meyer, A. W., et al. (1986). *Initial reports, Deep Sea Drilling Project, Leg 96*. Washington, DC: US Government Printing Office, 824 pp.

Bouma, A. H., Stelting, C. E., & Coleman, J. M. (1985). Mississippi Fan: Internal structure and depositional processes. *Geo-Marine Letters*, *3*, 147–153.

Brass, G. W., & Rahman, C. V. (1990). 4. Clay mineralogy of sediments from the Bengal Fan. In J. R. Cochran, D. A. V. Stow, et al. (Eds.), (*vol. 116*) (pp. 35–41). *Proceedings of the Ocean Drilling Project, Scientific Results*, College Station, TX (Ocean Drilling Program).

Brune, J. N., Curray, J. R., Dorman, L. M., & Raitt, R. W. (1991). Super-thick sedimentary Basin, Bay of Bengal. *Journal of the Association of Exploration Geophysicists*, *XII*.

Brune, J. N., Curray, J. R., Dorman, L. M., & Raitt, R. W. (1992). A proposed super-thick sedimentary Basin, Bay of Bengal. *Geophysical Research Letters*, *19*, 565–568.

Brunnschweiler, R. O. (1966). On the geology of the Indoburman Ranges. *Geological Society Australia Journal*, *13*, 127–194.

Chatterjee, P. K. (1967). Geology of the Main Islands of the Andaman Area. *Proceedings Symposium on Upper Mantle Project*, 348–360. Geophysical Research Board, National Geophysical Research Institute, Hyderabad, India.

Clift, P. D., Shimizu, N., Layne, G. D., Blusztajn, J. S., Gaedicke, C., Schlüter, H.-U., Clark, M. K., & Amjad, S. (2001). Development of the Indus Fan and its significance for the erosional history of the Western Himalaya and Karakoram. *Geological Society of America Bulletin*, *113*, 1039–1051.

Cochran, J. R., & Stow, D. A. V., et al (1990). *Proceedings of the Ocean Drilling Project, Leg. 116, Scientific Results*. College Station, TX, Ocean Drilling Program, 1445 p

Coleman, J. M. (1969). Brahmaputra river: Channel processes and sedimentation. *Sedimentary Geology*, *3*, 129–239.

Curray, J. R. (1964). Transgressions and regressions. In R. Miller (Ed.), *Papers in marine geology, shepard commemorative volume* (pp. 175–203). New York: Macmillan.

Curray, J. R. (1991). Possible greenschist metamorphism at the base of a 22 km sediment section, Bay of Bengal. *Geology*, *19*, 1097–1100.

Curray, J. R. (1994). Sediment volume and mass beneath the Bay of Bengal. *Earth and Planetary Science Letters*, *125*, 371–383.

Curray, J. R., Emmel, F. J., Moore, D. G., & Raitt, R. W. (1982). Structure, tectonics, and geological history of the northeastern Indian Ocean. In A. E. M. Nairn, & F. G. Stehli (Eds.), (*vol. 6*) (pp. 399–450). *Ocean basins and margins*, New York: Plenum Press.

Curray, J. R., & Moore, D. G. (1971). Growth of the Bengal deep-sea fan and denudation in the Himalayas. *Geological Society of America Bulletin*, *82*, 563–572.

Curray, J. R., & Moore, D. G. (1974). Sedimentary and tectonic processes in the Bengal Deep-sea Fan and Geosyncline. In C. A. Burk, & C. L. Drake (Eds.), *Continental margins* (pp. 617–627). New York: Springer.

Curray, J. R., & Munasinghe, T. (1989). Timing of intraplate deformation, northeastern Indian Ocean. *Earth and Planetary Science Letters*, *94*, 71–77.

Damuth, J. E., & Flood, R. D. (1985). Amazon Fan, Atlantic Ocean. In A. H. Bouma, W. R. Normark, & N. E. Barnes (Eds.), *Submarine fans and related turbidite systems* (pp. 97–106). New York: Springer.

Dietz, R. S. (1953). Possible deep-sea turbidity-current channels in the Indian Ocean. *Geological Society of America Bulletin*, *64*, 375–378.

Drake, C. L., Ewing, M., & Sutton, G. H. (1959). Continental margins and geosynclines; the east coast of North America north of cape Hatteras (*vol. 3*) (pp. 110–198). *Physics and chemistry of the earth*, New York: Pergamon Press.

Emmel, F. J., & Curray, J. R. (1981a). Dynamic events near the upper and mid-fan boundary of the Bengal Fan. *Geo-Marine Letters*, *1*, 201–205.

Emmel, F. J., & Curray, J. R. (1981b). Channel piracy on the lower Bengal Fan. *Geo-Marine Letters*, *1*, 123–127.

Emmel, F. J., & Curray, J. R. (1985). Bengal Fan, Indian Ocean. In A. H. Bouma, N. E. Barnes, & W. R. Normark (Eds.), *Submarine fans and related turbidite sequences* (pp. 107–112). New York: Springer.

Fairbanks, R. G. (1989). A 17.000-year glacio-eustatic sea level record: influence of glacial melting rates on the Younger Dryas event and deep-ocean circulation. *Nature*, *342*, 637–642.

Flood, R. D., & Piper, D. J. W. (1997). Amazon Fan sedimentation: The relationship to equatorial climate change, continental denudation, and seal-level fluctuations. In R. D. Flood, D. J. W. Piper, A. Klaus, & L. C. Peterson (Eds.), (*vol. 155*) (pp. 653–675). *Proceedings of the Ocean Drilling Project, Scientific Results*, College Station, TX.

Gartner, S. (1974). 26. Nannofossil biostratigraphy, Leg 22, Deep Sea Drilling Project. In C. C. von der Borch, J. C. Sclater, et al. (Eds.), *Initial reports of the Deep Sea Drilling Project, Leg 22* (pp. 577–599). Washington, DC: US Government Printing Office.

Gartner, S. (1990). 15. Neogene calcareous nannofossil biostratigraphy, Leg 116 (Central Indian Ocean). In J. R. Cochran, D. A. V. Stow, et al. (Eds.), *Proceedings of the Ocean Drilling Project, Leg 116, Scientific Results* (pp. 165–187), College Station, TX, Ocean Drilling Program.

Gee, F. R. (1927). The geology of the Andaman and Nicobar Islands, with special reference to Middle Andaman Island. *Records of the Geological Survey of India*, *LIX*, 208–232.

Gould, H. R. (1951). Some quantitative aspects of Lake Mead turbidity currents. *Turbidity currents and the transportation of coarse sediments to deep water* (pp. 34–52). *Society of Economic Paleontologists and Mineralogists, Special Publication No. 2*.

Heezen, B. C., & Ewing, M. (1952). Turbidity currents and submarine slumps, and the Grand Banks earthquake. *American Journal of Science*, *250*, 849–873.

Heezen, B. C., & Tharp, M. (1964). Physiographic diagram of the Indian Ocean, the Red Sea, the South China Sea, the Sulu Sea and the Celebes Sea. *Geological Society of America, scale 1:11,000,000*.

Hübscher, C., Spiess, V., Breitzke, M., & Weber, M. E. (1997). The youngest channel-levee system of the Bengal Fan: Results from digital sediment echosounder data. *Marine Geology*, *141*, 125–145.

Johnson, M. A. (1964). Turbidity currents. *Oceanography and Marine Biology, Annual Reviews*, *2*, 31–43.

Karunakaran, C., Ray, K. K., & Saha, S. S. (1968). Tertiary sedimentation in the Andaman–Nicobar geosyncline. *Journal Geological Society of India*, *9*, 32–39.

Kolla, V., & Biscaye, P. (1973). Clay mineralogy and sedimentation in the eastern Indian Ocean. *Deep Sea Research*, *20*, 727–738.

Kolla, V., & Coumes, F. (1987). Morphology, internal structure, seismic stratigraphy and sedimentation of Indus Fan. *American Association of Petroleum Geologists Bulletin*, *71*, 650–677.

Kolla, V., Moore, D. G., & Curray, J. R. (1976). Recent bottom-current activity in the deep western Bay of Bengal. *Marine Geology*, *21*, 255–270.

Komar, P. D. (1970). The competence of turbidity current flow. *Geological Society of America Bulletin*, *81*, 1555–1562.

Komar, P. D. (1972). Relative significance of head and body spill from a channelized turbidity current. *Geological Society of America Bulletin*, *83*, 1151–1166.

Komar, P. D. (1973). Continuity of turbidity current flow and systematic variations in deep-sea channel morphology. *Geological Society of America Bulletin*, *84*, 3324–3338.

Kudrass, H. R., Michels, K. H., Wiedecke, M., & Suckow, A. (1998). Cyclones and tides as feeders of a submarine canyon off Bangladesh. *Geology*, *26*, 715–718.

Kuehl, S. A., Hariu, T. M., & Moore, W. S. (1989). Shelf sedimentation off the Ganges–Brahmaputra river system: Evidence for sediment bypassing to the Bengal Fan. *Geology*, *17*, 1132–1135.

Kuehl, S. A., Levy, B. M., Moore, W. S., & Allison, M. A. (1997). Subaqueous delta of the Ganges–Brahmaputra river system. *Marine Geology*, *144*, 81–96.

Lee, T. T., & Lawver, L. A. (1995). Cenozoic plate reconstruction of Southeast Asia. *Tectonophysics*, *251*, 85–138.

Menard, H. W. (1960). Possible pre-Pleistocene deep-sea fans off central California. *Geological Society of America Bulletin*, *71*, 1271–1278.

Menard, H. W., & Ludwick, J. C. (1951). Applications of hydraulics to the study of marine turbidity currents. *Society of Economic Paleontologists and Mineralogists, Special Publication No. 2, Tulsa, Oklahoma*, 2–13.

Michels, K. H., Kudrass, H. R., Hübscher, C., Suckow, A., & Wiedecke, M. (1998). The submarine delta of the Ganges–Brahmaputra: Cyclone dominated sedimentation patterns. *Marine Geology*, *149*, 133–154.

Milliman, J. D., Broadus, J. M., & Gable, F. (1989). Environmental and economic implications of rising sea level and subsiding deltas: the Nile and Bengal examples. *AMBIO, Royal Swedish Academy of Sciences*, *18*, 340–345.

Mitchell, A. H. G. (1989). The Shan Plateau and western Burma: Mesozoic–Cenozoic plate boundaries and correlations with Tibet. In A. M. C. Sengor (Ed.), *Tectonic evolution of the Tethyan Region* (pp. 567–583). Dordrecht: Kluwer.

The KH 00-5 Scientific Party, Moe, K. T., Tokuyama, H., & Murayama, M. (2001). HINDOO cruise deep-sea channel survey in the Bay of Bengal. *Bulletin of the Geological Society of Japan*, *107*, XIX–XX.

Moore, D. G., Curray, J. R., & Emmel, F. J. (1976). Large submarine slide (olistostrome) associated with Sunda Arc subduction zone, northeast Indian Ocean. *Marine Geology*, *21*, 211–226.

Moore, D. G., Curray, J. R., Raitt, R. W., & Emmel, F. J. (1974). Stratigraphic-seismic section correlations and implications to Bengal Fan history. In C. C. von der Borch, J. C. Sclater, et al. (Eds.), *Initial reports of the Deep Sea Drilling Project, Leg 22* (pp. 403–412). Washington, DC: US Government Printing Office.

Morgan, J. P., & McIntire, W. G. (1959). Quaternary geology of the Bengal Basin, East Pakistan and India. *Geological Society of America Bulletin*, *70*, 319–342.

Mutti, E. (1974). Examples of ancient deep-sea fan deposits from circum-Mediterranean geosynclines. R. H.Dott, R. H.Shaver, *Society of Economic Paleontologists and Mineralogists, Special Publication No. 19, Tulsa, Oklahoma*, 92–105.

Mutti, E., & Normark, W. R. (1991). An integrated approach to the study of turbidite systems. In P. Weimer, & M. H. Link (Eds.), *Seismic facies and sedimentary processes of submarine fans and turbidite systems* (pp. 75–106). New York: Springer.

Nelson, C. H., & Nilsen, T. H. (1984). Modern and ancient deep-sea sedimentation. *Society of Economic Paleontologists and Mineralogists, Short Course*, *14*, 404.

Normark, W. R. (1970). Growth patterns of deep-sea fans. *American Association of Petroleum Geologists Bulletin*, *54*, 2170–2195.

Normark, W. R. (1978). Fan valleys, channels, and depositional lobes on modern submarine fans: Characters for recognition of sandy turbidite environments. *American Association of Petroleum Geologists Bulletin*, *62*, 912–931.

Normark, W. R., Posamentier, H., & Mutti, E. (1993). Turbidite systems: State of the art and future directions. *Reviews of Geophysics*, *31*, 91–116.

Peirce, J. W., Weissel, J. K., et al. (1989). *Proceedings of the Ocean Drilling Program, Leg 121, Scientific Results*. College Station, TX, Ocean Drilling Program, 990 p.

Piper, D. J. W., & Normark, W. R. (2001). Sandy fans-from Amazon to Hueneme and beyond. *American Association of Petroleum Geologists Bulletin*, *85*, 1407–1438.

Pirmez, C., Hiscott, R. N., & Kronen, J. D. J. (1997). Sandy turbidite successions at the base of channel-levee systems of the Amazon Fan revealed by FMS logs and cores: Unravelling the facies architecture of large submarine fans. In R. D. Flood, D. J. W. Piper, A. Klaus, & L. C. Peterson (Eds.), (*vol. 155*) (pp. 7–33). *Proceedings of the Ocean Drilling Project, Scientific Results*.

Roy, T. K. (1983). Geology and hydrocarbon prospects of the Andaman–Nicobar basin. *Petroleum Asia Journal*, 37–50.

Shanmugam, G., & Moiola, R. J. (1988). Submarine fans: Characteristics, models, classification, and reservoir potential. *Earth-Science Reviews*, *24*, 383–428.

Shepard, F. P. (1973). *Submarine geology* (3rd ed). New York: Harper & Row, 517 pp.

Stow, D. A. V., Howell, D. G., & Nelson, C. H. (1984). Sedimentary, tectonic and sea-level controls on submarine fan and slope-apron turbidite systems. *Geo-Marine Letters*, *3*, 57–64.

Stow, D. A. V., & Wetzel, A. (1990). 3. Hemiturbidite: A new type of deep-water sediment. In J. R. Cochran, D. A. V. Stow, et al. (Eds.), *Proceedings of the Ocean Drilling Project, Leg 116, Scientific Results* (pp. 25–34), College Station, Texas, Ocean Drilling Program.

Thompson, R. W. (1974). 38. Mineralogy of sands from the Bengal and Nicobar Fans, Site 218 211, Eastern Indian Ocean. In C. C. von der Borch, J. C. Sclater, et al. (Eds.), *Initial reports of the Deep Sea Drilling Project, Leg 22* (pp. 711–713). Washington, DC: US Government Printing Office.

Thorne, C. R., Russell, A. P. G., & Alam, M. K. (1993). Planform pattern and channel evolution of the Brahmaputra River, Bangladesh. J. L.Best, C. S.Bristow, *Geological Society of London Special Publication*, *75*, 157–276.

Walker, R. R. (1978). Deep-water sandstone facies and ancient submarine fans: Models for exploration for stratigraphic traps. *American Association of Petroleum Geologists Bulletin*, *62*, 932–966.

Weber, M. E., Wiedicke, M. H., Kudrass, H. R., Hübscher, C., & Erlenkeuser, H. (1997). Active growth of the Bengal Fan during sea-level rise and highstand. *Geology*, *25*, 315–318.

Yokuyama, K., Amano, K., Tairo, A., Saito, Y., et al. (1990). 6. Mineralogy of silts from the Bengal Fan. In J. R. Cochran, D. A. V. Stow, et al. (Eds.), (*vol. 116*) (pp. 59–73). *Proceedings of the Ocean Drilling Project, Scientific Results*, College Station, TX, Ocean Drilling Program.

Annex B66

M. Alam et al., "An Overview of the Sedimentary Geology of the Bengal Basin in Relation to the Regional Tectonic Framework and Basin-fill History", *Sedimentary Geology*, Vol. 155, No. 3-4 (2003)

Available online at www.sciencedirect.com
SCIENCE DIRECT®
Sedimentary Geology 155 (2003) 179–208
Sedimentary Geology
www.elsevier.com/locate/sedgeo

An overview of the sedimentary geology of the Bengal Basin in relation to the regional tectonic framework and basin-fill history

Mahmood Alam [a], M. Mustafa Alam [a,*], Joseph R. Curray [b], M. Lutfar Rahman Chowdhury [c], M. Royhan Gani [a,1]

[a] *Department of Geology, University of Dhaka, Dhaka 1000, Bangladesh*
[b] *Scripps Institution of Oceanography, La Jolla, CA 92093-0220, USA*
[c] *Bangladesh Petroleum Exploration and Production Company Ltd. (BAPEX), House No. 39, Road No. 116, Gulshan, Dhaka 1212, Bangladesh*

Received 18 July 2001; received in revised form 26 September 2001; accepted 13 March 2002

Abstract

The Bengal Basin in the northeastern part of Indian subcontinent, between the Indian Shield and Indo-Burman Ranges, comprises three geo-tectonic provinces: (1) The Stable Shelf; (2) The Central Deep Basin (extending from the Sylhet Trough in the northeast towards the Hatia Trough in the south); and (3) The Chittagong–Tripura Fold Belt. Due to location of the basin at the juncture of three interacting plates, viz., the Indian, Burma and Tibetan (Eurasian) Plates, the basin-fill history of these geo-tectonic provinces varied considerably. Precambrian metasediments and Permian–Carboniferous rocks have been encountered only in drill holes in the stable shelf province. After Precambrian peneplanation of the Indian Shield, sedimentation in the Bengal Basin started in isolated graben-controlled basins on the basement. With the breakup of Gondwanaland in the Jurassic and Cretaceous, and northward movement of the Indian Plate, the basin started downwarping in the Early Cretaceous and sedimentation started on the stable shelf and deep basin; and since then sedimentation has been continuous for most of the basin. Subsidence of the basin can be attributed to differential adjustments of the crust, collision with the various elements of south Asia, and uplift of the eastern Himalayas and the Indo-Burman Ranges. Movements along several well-established faults were initiated following the breakup of Gondwanaland and during downwarping in the Cretaceous. By Eocene, because of a major marine transgression, the stable shelf came under a carbonate regime, whereas the deep basinal area was dominated by deep-water sedimentation. A major switch in sedimentation pattern over the Bengal Basin occurred during the Middle Eocene to Early Miocene as a result of collision of India with the Burma and Tibetan Blocks. The influx of clastic sediment into the basin from the Himalayas to the north and the Indo-Burman Ranges to the east rapidly increased at this time; and this was followed by an increase in the rate of subsidence of the basin. At this stage, deep marine sedimentation dominated in the deep basinal part, while deep to shallow marine conditions prevailed in the eastern part of the basin. By Middle Miocene, with continuing collision events between the plates and uplift in the Himalayas and Indo-Burman Ranges, a huge influx of clastic sediments came into the basin from the northeast and east. Throughout the Miocene, the depositional settings continued to vary from deep marine in the basin to shallow and coastal marine in the marginal parts of the basin. From Pliocene onwards, large amounts of sediment were filling the Bengal Basin from the west and northwest; and major delta building processes continued to develop the present-day delta morphology. Since the Cretaceous, architecture of the Bengal Basin has been changing due to the collision pattern and movements of the major plates in the region. However, three notable changes in basin configuration can be

* Corresponding author.
E-mail address: mmalam@bdcom.com (M.M. Alam).
[1] Present address: Geoscience Department, University of Texas at Dallas, 2601 North Floyd Road, Richardson, TX 75038-0688, USA.

PII: S0037-0738(02)00180-X

recognized that occurred during Early Eocene, Middle Miocene and Plio-Pleistocene times, when both the paleogeographic settings and source areas changed. The present basin configuration with the Ganges–Brahmaputra delta system on the north and the Bengal Deep Sea Fan on the south was established during the later part of Pliocene and Pleistocene; and delta progradation since then has been strongly affected by orogeny in the eastern Himalayas. Pleistocene glacial activities in the north accompanied sea level changes in the Bay of Bengal.

Keywords: Bengal basin; India–Asia collision; Tectonic framework; Geo-tectonic province; Paleogeographic setting; Basin-fill

1. Introduction

The Bengal Basin in the northeastern part of Indian subcontinent, between the Indian Shield to the west and north, and the Indo-Burman Ranges to the east, covers Bangladesh, parts of West Bengal and Tripura states of India and the Bay of Bengal (Fig. 1). The basin draws broad international interest because of its relation to three spectacular geologic systems—the world's largest orogenic system, the Himalayan Range; which is drained by the Ganges–Brahmaputra Rivers to develop the world's largest fluvio-deltaic system, the Bengal Delta (the present Bengal Basin), covering an area of about 200,000 km^2; and the world's largest submarine fan system, the Bengal Deep Sea Fan, extending as far south as 7°S latitude.

The Bengal Basin is well known for the development of a thick ($\pm$ 22 km) Early Cretaceous–Holocene sedimentary succession (Curray, 1991a; Curray and Munasinghe, 1991) that has long been of interest from the hydrocarbon exploration point of view. The Bangladesh Oil, Gas and Mineral Corporation (BOGMC, 1997) summarized the exploration history of the Bangladesh part of the basin. Earlier comprehensive accounts pertaining to the regional stratigraphic scenario (e.g. Evans, 1932) and tectonic scenario (e.g. Evans, 1964; Sengupta, 1966; Raju, 1968) have set up the initial platform for our understanding of the basin generation and sediment-fill history of the basin. Bakhtine (1966) outlined the tectonic elements within the Bangladesh part of the basin for the first time. Subsequently, Alam (1972) described the geological evolution of the basin in terms of the then popular geosynclinal model; Desikacher (1974) reviewed the geological history of eastern India in the light of plate tectonic theory; and Curray and Moore (1974), Graham et al. (1975), Paul and Lian (1975) and Curray et al. (1982) established the plate tectonic scenario for evolution of the basin within the broader context of the Southeast Asia region.

During the past few decades, as a result of geological activities by both local and international hydrocarbon exploration agencies in different parts of Bangladesh, considerable subsurface data have been accumulated. Although most of the data recently acquired by the foreign oil companies are not accessible yet, earlier data outline the overall tectonic and stratigraphic framework of the basin (e.g. Salt et al., 1986; Murphy and Staff BOGMC, 1988; Lindsay et al., 1991; Reimann, 1993; Lohmann, 1995; Shamsuddin and Abdullah, 1997; Uddin and Lundberg, 1999), and refined our current understanding of the Bengal Basin configuration. In addition, Alam (1989, 1997) discussed the overall stratigraphic and tectonic history of the basin, and Johnson and Alam (1991) described the sedimentation and tectonics of the Sylhet Trough in the northeastern part of the basin. From the standpoint of facies analysis, Alam (1995a) has demonstrated the tide-dominated shallow marine sedimentation in the Miocene rocks in the southeastern Bengal Basin. Describing the deep-water clastics from the southeastern part of the basin, recently Gani and Alam (1999) have partly refined the conventional thinking regarding the sedimentation and tectonics of the basin, particularly the Chittagong–Tripura Fold Belt (CTFB) region. It is important to point out here that the geology of Bangladesh and its basin-fill history has to rely to a large extent on seismic evidence from the subsurface, because only in a minor part of the country (i.e. the CTFB) the basin-fill is exposed.

In spite of the above-mentioned studies, it appears that the state-of-the-art of sedimentary geology of the Bengal Basin suffers from oversimplification. There is a common tendency to relate the tectonic evolution of the basin only to the orogenic phases of the mighty Himalayas, although the Cenozoic evolutionary his-

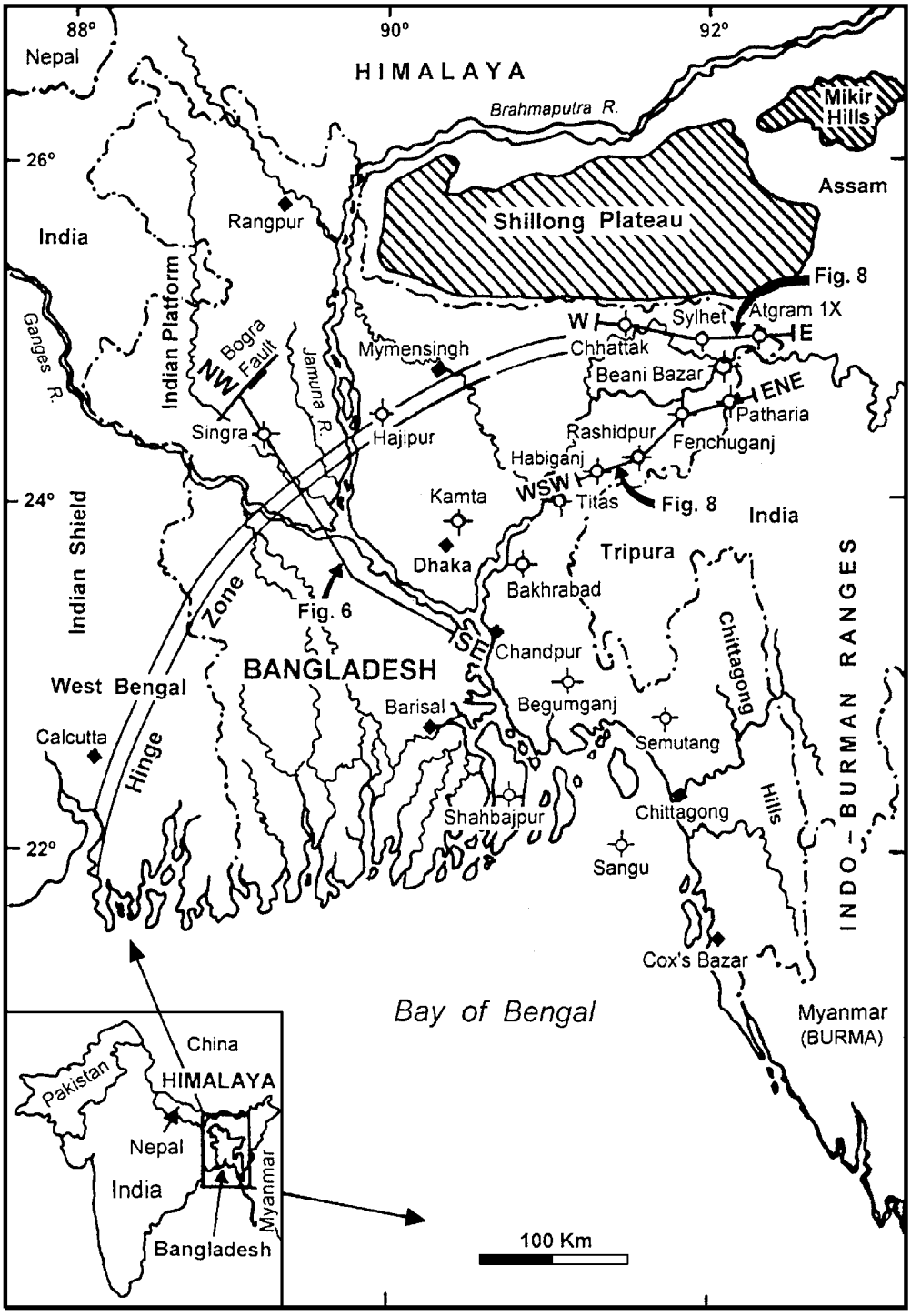

Fig. 1. Index map of Bangladesh and adjoining areas in the eastern part of the Indian subcontinent. This map shows location of the exploratory wells, lines of geological cross-sections shown in Figs. 6 and 8, and also the major tectonic features surrounding the Bengal Basin.

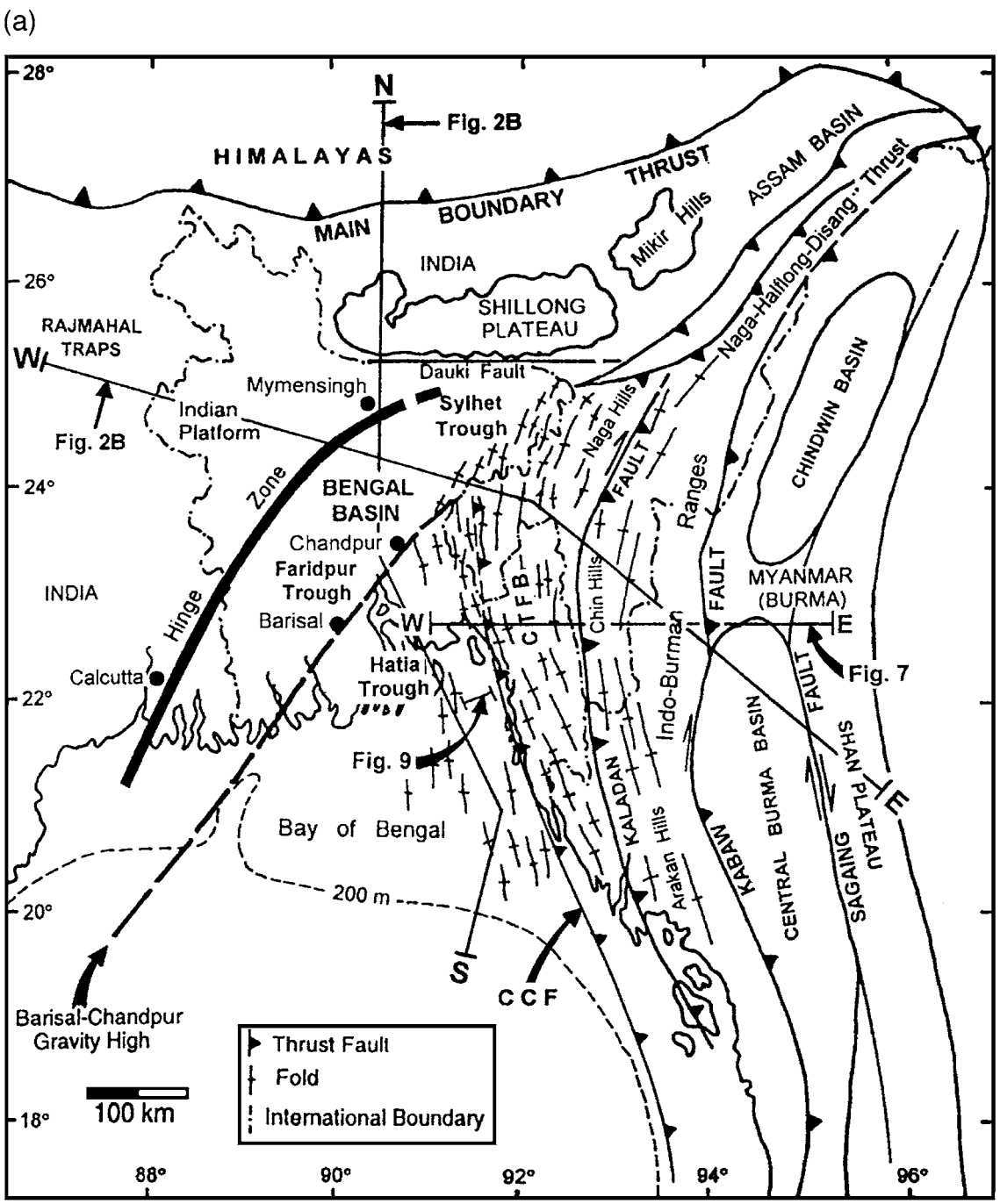

Fig. 2. (a) Regional map showing the tectonic elements of the Bengal Basin and surrounding areas (modified from Johnson and Alam, 1991; BOGMC, 1997; Uddin and Lundberg, 1999). The Hinge zone, lying above the Calcutta–Mymensingh gravity high, separates the *Stable Shelf Province* from the *Central Deep Basin Province* (see text for details). CTFB = Chittagong–Tripura Fold Belt and CCF = Chittagong–Cox's Bazar fault. Lines of cross-sections in Figs. 2b and 7, and the seismic section in Fig. 9 are also shown. (b) North–south and east–west crustal cross-sections through the Bengal Basin (modified from Murphy and Staff of BOGMC, 1988; BOGMC, 1997). See (a) for location of the section lines.

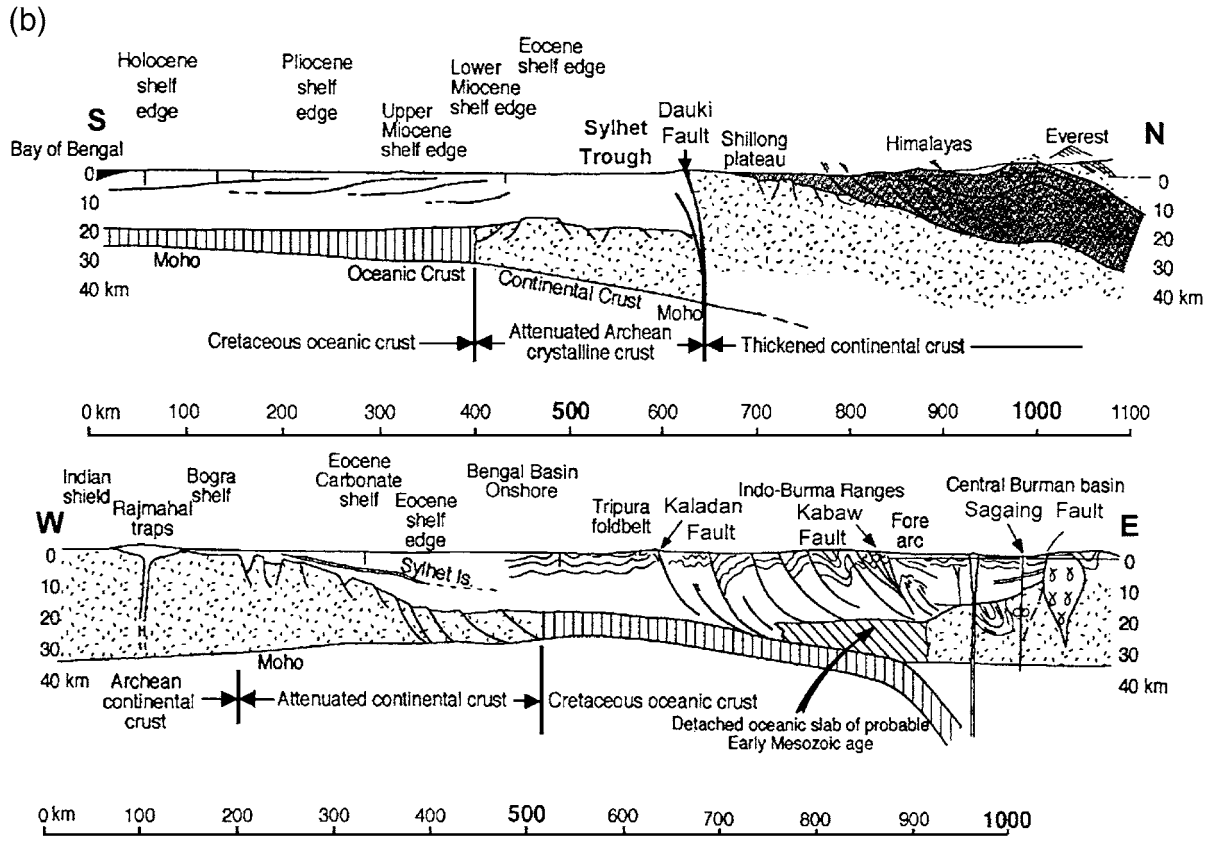

Fig. 2 (*continued*).

tory of the eastern Bengal Basin is mainly related to the oblique subduction phases of the Indian plate beneath the Burma plate. This oblique subduction has formed the westward migrating accretionary prism complexes (Dasgupta and Nandy, 1995; Gani and Alam, 1999). A major confusion arises from attempting to simplify the basin evolution within the broader regional scale and in comparing it with the 'foreland basin' model related to the Eastern Himalayan collision orogeny (e.g. Johnson and Alam, 1991; Uddin and Lundberg, 1999). There is indeed some rationale to explain the tectonic evolution of the basin in terms of the 'remnant ocean basin' model of Graham et al. (1975) and Ingersoll et al. (1995). From the stratigraphic point of view, another confusion pertains to the application of the stratigraphic scheme of Evans (1932), established for the Tertiary succession in the Lower Assam basin, northeastern India (Fig. 1), for the entire Bengal Basin, mainly on the basis of loosely defined lithologic similarity of the rock types.

It is time to look at the Bengal Basin in greater detail for a rational understanding of its evolution without being prejudiced by conventional thinking. Previous and newly acquired data can be reinterpreted in order to have a better understanding about the origin of the Bay of Bengal and the Bengal Basin. Gani (1999) and Gani and Alam (1999) consider the Bengal Basin to be a remnant ocean basin. They think that even if their interpretation is speculative, it is compatible with current knowledge and understanding of the eastern Bay of Bengal region. It has implications concerning the tectonic framework of the basin during the greater part of the Tertiary. The concept that the closing history of the basin represents a remnant ocean basin offers a general explanation for the existence of three distinct geo-tectonic provinces and the generation and devel-

opment of three stratigraphic successions representing each of these provinces. However, in a broader sense, most large sedimentary basins may be considered as remnant ocean basins, and this does not explain the special features of the Bengal Basin and surrounding areas.

Therefore, the primary objective of this overview is to provide the reader with a better understanding about the Bengal Basin, extending into the Bay of Bengal, its origin, stratigraphy and geological history. The paper discusses the regional tectonic setting and describes the structural framework of the basin in terms of its three geo-tectonic provinces. The paper then establishes separate stratigraphic schemes for each of the provinces based on the available data and comments on the general implications of our interpretation. And finally in the discussion and conclusions, emphasis is given to future lines of research in relation to the tectono-sedimentary evolution of the basin.

2. Regional tectonic setting

In order to comprehend the paleo-tectonics of the basin, it is essential to view the greater Bengal Basin in its regional perspective. The dynamic nature of the basin can be attributed to the interaction of three plates, namely, the Indian, Tibetan (Eurasian) and Burma (West Burma Block) Plates. The intensity and pattern of plate-to-plate interaction varied with time, affecting the basin architecture and sedimentation style throughout the basin. In the past, evaluation of the geological history of the Assam–Bengal Basin in relation to the plate movements on the eastern side of the Indian Subcontinent had been difficult because of the lack of reliable subsurface data from the region.

Since the late 1950s, a number of studies have dealt with plate reconstruction of the Southeast Asia region. Most workers agree that the region records the accretion of several plates and platelets of Gondwana affinity (Falvey, 1974; for an updated review, see Varga, 1997). It is believed that India rifted from the combined Antarctica–Australia part of Gondwanaland and began its spectacular journey, initially northwestward and then northward, sometime in the Early Cretaceous (Curray and Moore, 1974; Curray et al., 1982; Hutchison, 1989; Lee and Lawver, 1995; Acharyya, 1998; and others).

Thick sediment cover in the Bengal Basin conceals the basement configuration and makes the reconstruction or exact location of plate boundaries and sutures more difficult. Plate movement patterns and evolution of the Bengal Basin and the Bay of Bengal are carried out mostly with data and interpretation from the Indian Ocean, following early work by McKenzie and Sclater (1971), Sclater and Fisher (1974) and others.

One of the problems of plate reconstruction for the Indian Subcontinent is determining the eastern limit of Indian continental crust. Most of the earlier plate reconstruction scenarios (Curray and Moore, 1974; Graham et al., 1975; Curray et al., 1982) considered the eastern limit of the Indian continental crust to be approximately along the Hinge Zone, which lies above the Calcutta–Mymensingh Gravity High, with the oceanic part of the Indian Plate subducting beneath the Indo-Burman Ranges west of the Burma Block (the ‘Mt. Victoria Land Block’ of Mitchell, 1989; the Indo-Burma-Andaman or IBA Block of Acharyya, 1994, 1998; or the West Burma Block of Hutchison, 1989). They all considered the Burma Block to be of continental origin from Gondwana. Murphy and Staff BOGMC (1988) and BOGMC (1997) show the area between the Hinge Zone and Barisal–Chandpur Gravity High to be attenuated or thinned continental crust, so that the continent–ocean crust boundary lies along the Barisal–Chandpur Gravity High (Fig. 2a and b).

Acharyya (1998) places the present subduction zone on the western side of the Chittagong Hill Tracts (i.e. the CTFB), in the middle of the Bengal Foredeep or the deep basin. This is certainly the deformation front of the subduction zone, although the underlying crust and lithosphere do not descend rapidly until much farther east (Mukhopadhyay and Dasgupta, 1988). Ophiolite on the eastern side of Mt. Victoria is explained by Hutchison (1989) and Mitchell (1989) as a suture formed during eastward subduction; by Mitchell (1993) as a suture formed by westward subduction; and by Acharyya (1998), not as a suture, but instead as a flat-lying klippen rooted in the IBA (Indo-Burma-Andaman)-SIBUMASU (Siam, Burma, Malaysia and Sumatra) suture lying farther to the east beneath the central Burma Basin. Acharyya (1998) further suggests that the continental metamorphic

rocks of the Mt. Victoria region are a basement nappe over the ophiolites, rooted in the SIBUMASU Block. Brunnschweiler (1966, 1974) also interpreted the Mt. Victoria dome as a west-vergent nappe over Eocene flysch.

For our purpose here, we conclude that the continent ocean boundary (COB) beneath the Bengal Basin is located between the Hinge Zone and Barisal–Chandpur Gravity High, so that it lies along the northwest side of the gravity high and passes offshore approximately down the axis of the upper part of the Swatch-of-no-Ground submarine canyon. We also conclude that the continental Burma Block from Gondwana docked against the continental SIBUMASU Block, also from Gondwana, during Late Cretaceous to Paleogene: Mitchell (1989) says Early Cretaceous; Hutchison (1989) says Late Cretaceous; Mitchell (1993) says Mid-Eocene; and Acharyya (1998) says Late Oligocene. Most of these authors correlate the Lhasa or South Tibet Block with the Burma Block, but place the South Tibet collision with Asia at Late Jurassic or Early Cretaceous. These same authors agree that the India–Asia collision occurred during the Paleogene, probably with a 'soft collision' as early as Mid-Paleocene and a 'hard collision' later in Middle Eocene (Fig. 3).

For our collision scenarios, we will use the rate and angle of convergence compilation of Lee and Lawver (1995), calculated from rotations based on oceanic magnetic anomalies (Fig. 3). The times of major changes in convergence rates are about 70, 59, 44, 22 and 11 Ma. The 70, 44, 22 and 11 Ma events appear to correspond also with significant changes in the angle or direction of convergence. As stated previously, initial separation in Early Cretaceous of India from Australia and Antarctica was northwestward, but plate reorganization occurred in Late Cretaceous, perhaps about 90–96 Ma, changing the direction to more northward (Curray et al., 1982; Veevers, 1982; and others).

Before the departure of India from Australia and Antarctica in the Early Cretaceous, South Tibet, the Burma and SIBUMASU Blocks had already spun off northward and had docked against Asia. The three large continental masses were closely joined (Fig. 4a), with 'Greater India' extending an unknown distance into the Tethys Sea. With the break-up, a continuous zone of subduction was established along the southern margin of the Asian and Tibetan Plates. The initial alignment of these subduction zones is speculative, but was probably about east–west or southeast–northwest. A continuous zone of subduc-

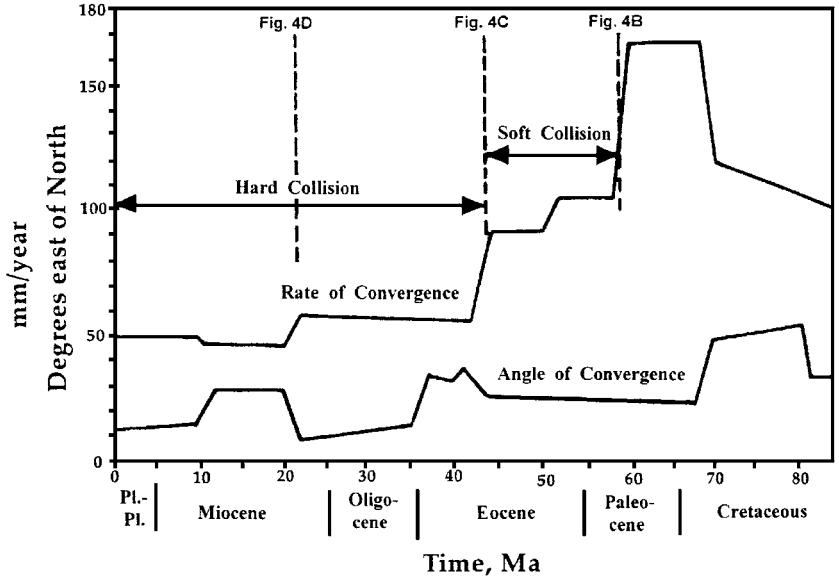

Fig. 3. Rate and angle of convergence between India and Eurasia. Modified from Lee and Lawver (1995).

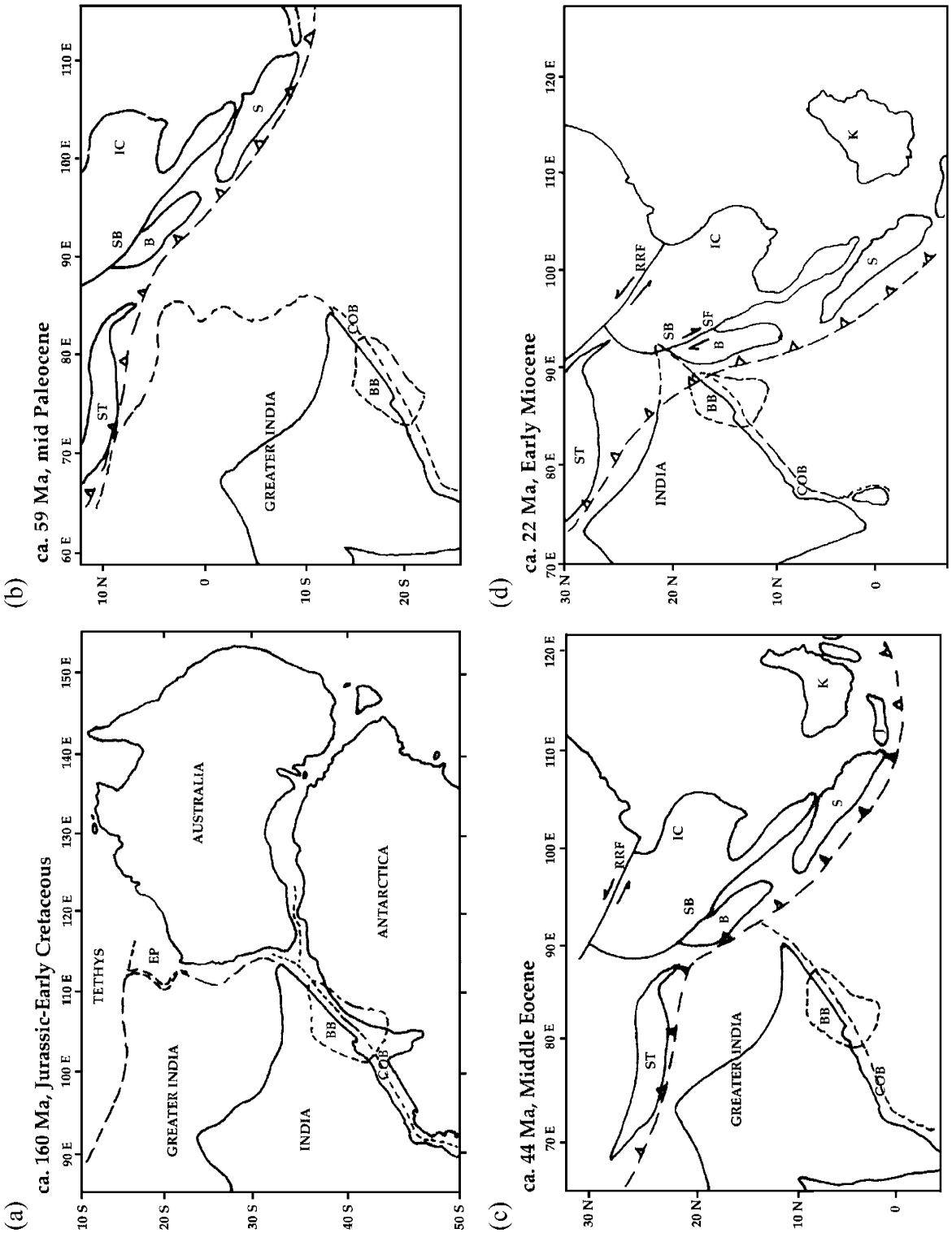
(a)
ca. 160 Ma, Jurassic-Early Cretaceous
TETHYS
EP
GREATER INDIA
AUSTRALIA
INDIA
ANTARCTICA
BB
COB
(b)
ca. 59 Ma, mid Paleocene
ST
IC
SB
B
S
GREATER INDIA
BB
COB
(c)
ca. 44 Ma, Middle Eocene
RRF
IC
SB
B
S
K
ST
GREATER INDIA
BB
COB
(d)
ca. 22 Ma, Early Miocene
RRF
IC
SB
SF
B
S
K
ST
INDIA
BB
COB

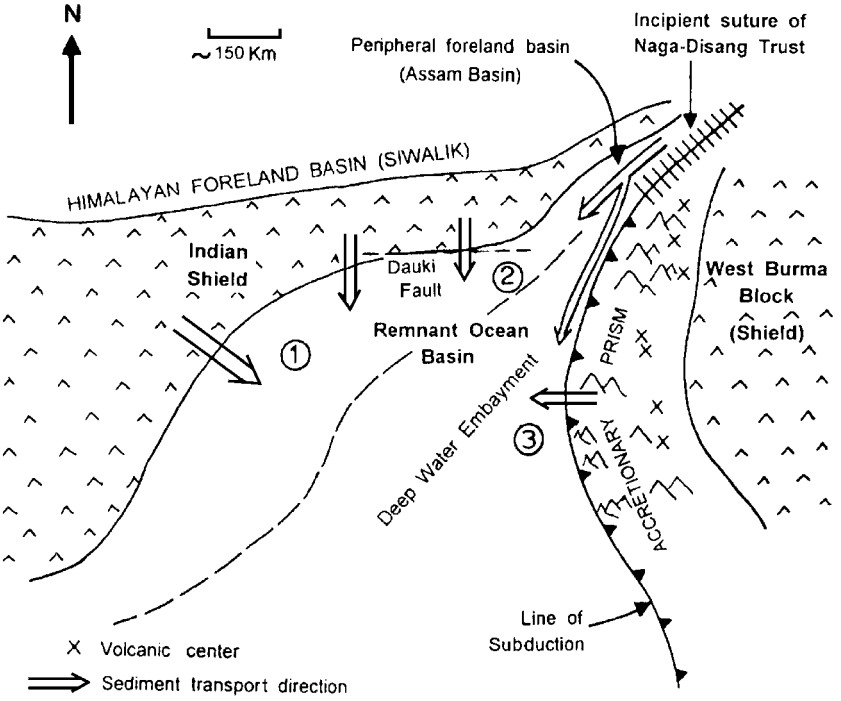

Fig. 5. Schematic Early Miocene paleogeographic representation of the Bengal Basin and surrounding region in terms of the plate tectonic model. Positions of the three geo-tectonic provinces of the basin are shown by encircled numbers: (1) *The Stable Shelf*; (2) *The Central Deep Basin*; and (3) *The Chittagong–Tripura Fold Belt* (after Gani and Alam, this volume).

tion also lay off the southwest side of the Burma Block (IBA), again at an unknown alignment. There is disagreement about rotation of both the Burma and SIBUMASU Blocks. Richter and Fuller (1996) uses paleomagnetic evidence to demonstrate that much of Malaysia, a part of SIMUBASU, rotated 30–40° CCW between Late Eocene and Late Miocene. This presents an enigma in our and other plate tectonic scenarios, which we cannot resolve. No such definitive paleomagnetic data have been collected in the Burma Block (Bender, 1983; Everett et al., 1989), but most authors assume CW rotation (e.g. Curray and Moore, 1974; Ninkovich, 1976; Tapponnier et al., 1982; Mitchell, 1989; Lee and Lawver, 1995; Varga, 1997; and many others). Our reconstructions (Fig. 4), adapted mainly from Lee and Lawver (1995), show somewhat more rotation than they showed, on the assumption of deep indentation by India into the Asian margin by the collision and extrusion as postulated by Tapponnier et al. (1982).

We have assumed (Fig. 4b) that the margin of Asia before the India–Asia collision was farther south and was a continuous subduction zone. During the collision process, India indented Asia, and Indochina and Southeast Asia were extruded eastward and southeastward. Klootwijk et al. (1992) show the initial collision between the northwest corner of Greater India and the subduction zone off Tibet at about the equator; Chen et al. (1993) and Patzelt et al.

Fig. 4. Plate reconstructions modified mainly from Lee and Lawver (1995). EP = Exmouth Plateau; COB = continent ocean boundary; ST = South Tibet; B = Burma Block or IBA (Indo, Burma, Andaman); SB = SIBUMASU (Siam, Burma, Malaysia, Sumatra); IC = Indochina; S = Sumatra; BB = Bengal Basin; K = Kalimantan; J = Java; RRF = Red River Fault; SF = Sagaing Fault. (a) Eastern Gondwana fit of the margins of "Greater India", Australia and Antarctica. (b) Plate reconstruction at about 59 Ma, Mid-Paleocene, the start of "soft collision" between India and Southeast Asia. (c) About 44 Ma, Middle Eocene, the start of "hard collision" between India and South Asia. (d) About 22 Ma, Early Miocene, a time of major collision between India and South Tibet in the north and India and Burma in the east.

(1996) show it at about 10°N; while Lee and Lawver (1995) shows it at about 20°N. Our reconstruction shows it at about 10°N, although for purposes of our story of the tectonic setting of the Bengal Basin, it is irrelevant.

In Mid-Paleocene, about 59 Ma, soft collision occurred between the northwest corner of the Indian Shield and South Tibet (Figs. 3 and 4b). India underwent some CCW rotation from about 60–55 Ma (Klootwijk et al., 1992), at which time the suture was completely closed. Since then India passed obliquely into and/or under Asia. Tibet had previously docked against south Asia, which at that time lay farther south. Subsequent crustal shortening and tectonic escape, i.e. extrusion of Indochina, Southeast Asia and South China, created the indentation where India is now situated.

During the 'soft collision', ca. 59–44 Ma, the northward or NNE motion of India continued, and was slowed perhaps by closing up formerly relatively undercompressed sutures between the other accreted terraines of South Asia: Junggar, Tarim, Kunlun, Qaidam, Qiangtang, etc. (Chen et al., 1993).

By Early Eocene, about 44 Ma, hard continent–continent collision related to the Himalayan orogeny commenced (Fig. 4c). By this time the older sutures were more fully compressed. This was also a time of major plate reorganization in the eastern Indian Ocean, when the Indian and Australian plates joined to form a single plate and the Australia–Antarctica separation started to accelerate. Some change in spreading direction also occurred (Fig. 3) and this was approximately the time when tectonic extrusion of the Burma and SIBUMASU Block and Indochina started (Tapponnier et al., 1982, 1986).

The Bengal Basin became a remnant ocean basin (Ingersoll et al., 1995) (Fig. 4d) at the beginning of Miocene because of the continuing oblique subduction of India beneath and southeast extrusion of Burma (West Burma Block). The Bengal Basin, as a remnant ocean basin, has three distinct geo-tectonic provinces (Fig. 5): (1) Passive to extensional cratonic margin in the west, the *Stable Shelf Province*; (2) the *Central Deep Basin Province* or remnant ocean; and (3) the subduction-related orogen in the east, the *Chittagong–Tripura Fold Belt (CTFB) Province*. These geo-tectonic provinces have been related to a regional plate tectonic scenario. Each of these provinces has its own distinctive tectonic and stratigraphic framework and history of sediment-fill.

3. Structural and tectonic framework of the Bengal Basin

The evolution of *Provinces 1 and 2* commenced with the Early Cretaceous rifting and concomitant volcanic eruptions along the northeastern margin of the Indian Shield. Pre-rift sediments of the Permo-Carboniferous age have only been penetrated in drill holes in *Province 1* within the subsurface graben basins on top of the Precambrian basement complex. These sediments may also exist on the continental crust part of *Province 2* (Sylhet Trough) hidden beneath the thick Late Cenozoic cover. There are, in fact, southwest–northeast trending lineations in both the aeromagnetic anomaly map of Rahman et al. (1990a) and in the Bouguer gravity anomaly map of Rahman et al. (1990b), which could reflect grabens on the continental crust.

It is important to delineate the exact position of the initial break-up line, along which the first oceanic crust of Indian Ocean formed. It has been suggested that the Barisal–Chandpur Gravity High could indicate the presence of a rift valley formed during the break-up of Gondwanaland and formation of the Indian Plate. This seems unlikely. We have interpreted the basement configuration from the PK-1 seismic line (Fig. 6). The line shows that landward from SP 1200 there is clear indication of the continental basement; and between SP 1200 and SP 1550 there are several phases of basalt flow (Lohmann, 1995) associated with the rifting of the Indian plate. This part of the basement can be considered as the transitional crust. Basinward from SP 1550 the seismic signature on top of the basement is characterized by numerous cross-cutting and down-going reflectors associated with basalt flows, which indicate the existence of oceanic crust below (Fig. 6). This change occurs below the Hinge Zone shown in Fig. 2. Furthermore, the alternating high and low magnetic values along the Hinge Zone (Rahman et al., 1990a) and immediately west of it, respectively, also indicate that this zone could represent a probable transition from continental to oceanic crust. We also speculate that the C–O boundary bends eastward beneath the Sylhet

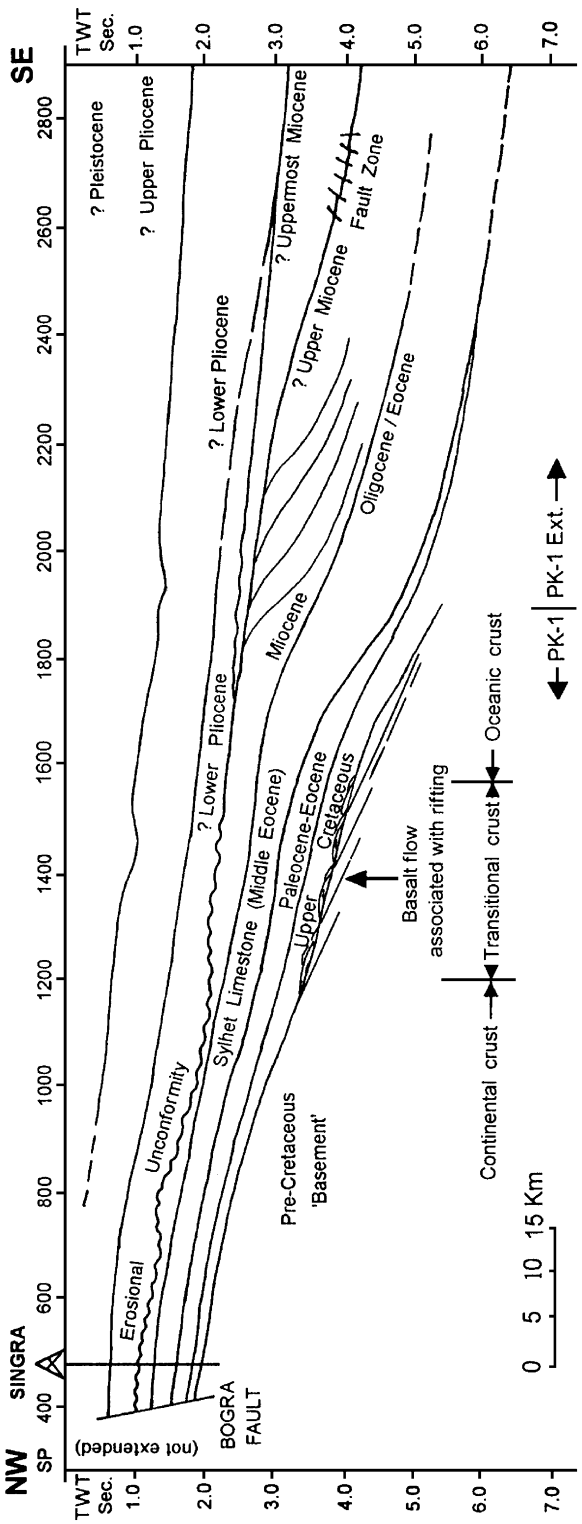

Fig. 6. Geological cross-section through the *Stable Shelf Province* and southern part of the *Central Deep Basin Province* of the Bengal Basin (see Fig. 1 for location of the section line). Note significant thickening of the Tertiary sedimentary succession from northwest towards southeast. The nature of the crust beneath the sedimentary succession is also indicated (detailed explanation is given in the text).

Trough area and probably continues towards the Halflong Thrust, so that at least the northern part of the trough is floored by the continental crust. Curray (1991b) reported that beneath the continental shelf southeast of this boundary in excess of 22 km of sedimentary and metasedimentary rocks overlie velocities suggestive of oceanic crust. BOGMC (1997) also postulates similar thickness southeast of this line in the Bengal Basin. Isostatic considerations also favor the interpretation that the basement rocks are oceanic rather than of continental origin.

Another element, the so-called 'Hinge Zone', a zone of presumed deep-seated normal faults in the basement complex, is conventionally thought of as representing the dividing line between the Indian Platform with full thickness of continental crust and the Bengal Foredeep (Fig. 2). Although the position of the Hinge Zone within *Province 1* is well established, it is usually shown to truncate against the Dauki Fault in the northeast. Another interpretation is that within *Province 2*, the Hinge Zone passes somewhere through the Sylhet Trough and probably continues towards the Halflong Thrust at the northeastern corner of the Bengal Basin. Counter to the suggestion that the Hinge Zone turns toward the Halflong Thrust, however, is that the very strong linear aeromagnetic map (Rahman et al., 1990a) closely coincides with the Hinge Zone and does truncate against the Dauki Fault. The Calcutta–Mymensingh gravity high (Rahman et al., 1990b) is not as strong and linear, and also appears to truncate against the Dauki Fault.

It can be argued that at least up to the Oligocene, *Provinces 1 and 2* underwent similar tectonic and sedimentary evolution. From the Late Oligocene, when the remnant ocean basin took shape due to the collisional orogeny of the Barail–Cachar Hills at the northeastern corner of India (Nandy, 1986), *Province 2* has been experiencing its own evolutionary history. Major upthrust movements of the Shillong Plateau (Fig. 2a and b) along the Dauki Fault (Seeber and Armbruster, 1981), probably in the Early Miocene, greatly influenced the sedimentation pattern in *Province 2*. Hiller and Elahi (1988) considered the Dauki Fault as a south-directed normal fault, whereas Johnson and Alam (1991) considered it as a north-directed low-angle (5–10°) thrust fault. We disagree with both of these interpretations, and suggest that the Dauki Fault should be considered as an upthrust fault (e.g. Murthy et al., 1969; Molnar, 1987; Murphy and Staff BOGMC, 1988; Chen and Molnar, 1990). It can also be logically concluded that, as suggested by Lohmann (1995), the Dauki Fault is at greater depth a high-angle reverse fault, but near the surface an apparent right-lateral strike–slip fault. However, recent studies (Bilham and England, 2001) suggest that the Shillong Plateau is a pop-up structure bounded by two reverse faults, the Oldham fault on the north and the Dauki fault on the south. Plateau uplift in the past 2–5 million years has caused the Indian plate to contract locally by 4–2 mm/year, reducing seismic risk in Bhutan and increasing the risk in the northern part of Bangladesh. The surface of the Shillong plateau is about 2 km high, consisting of Archaean rocks; and equivalent rocks lie 4–5 km and nearly 20 km below sea level to the north and south of the plateau, respectively. During the great 1897 Assam earthquake, the Shillong plateau rose violently by at least 11 m, and this was due to rupture of a buried reverse fault (Oldhan fault) approximately 110 km in length and dipping steeply away from the Himalayas (Bilham and England, 2001).

Paleogeographic analysis of the Bengal Basin suggests that in the Late Pliocene, when *Province 3* (CTFB) developed at the eastern margin, *Province 2* started to evolve as a foreland basin (sensu stricto); whereas *Province 1* may be considered as a future locus of the foreland basin when foredeep sediments will be thrust northwestward.

The structural evolution of *Province 3* (Fig. 7) is believed to have been largely controlled by the accretionary prism development and major east-dipping thrust faults produced by off-scraping of the oceanic sediments as a result of oblique subduction of the Indian plate beneath the Burma plate in an arc-trench setting (Gani and Alam, 1999). Within major individual thrust sheets, the sediments in the upper part have been deformed by the process of thin-skinned tectonics giving rise to a series of elongate, north–south trending curvilinear anticlines and synclines in this province (Fig. 6; Sikder and Alam, 2003). Lohmann (1995) and Sikder (1998) have pointed out some duplex structures in the western part of *Province 3*. They have also suggested thin-skinned detachment and shear-off tectonics to explain the structural style of the region, but did not relate these processes directly to the subduction complex. We believe that the tectonic and structural development of *Province 3*

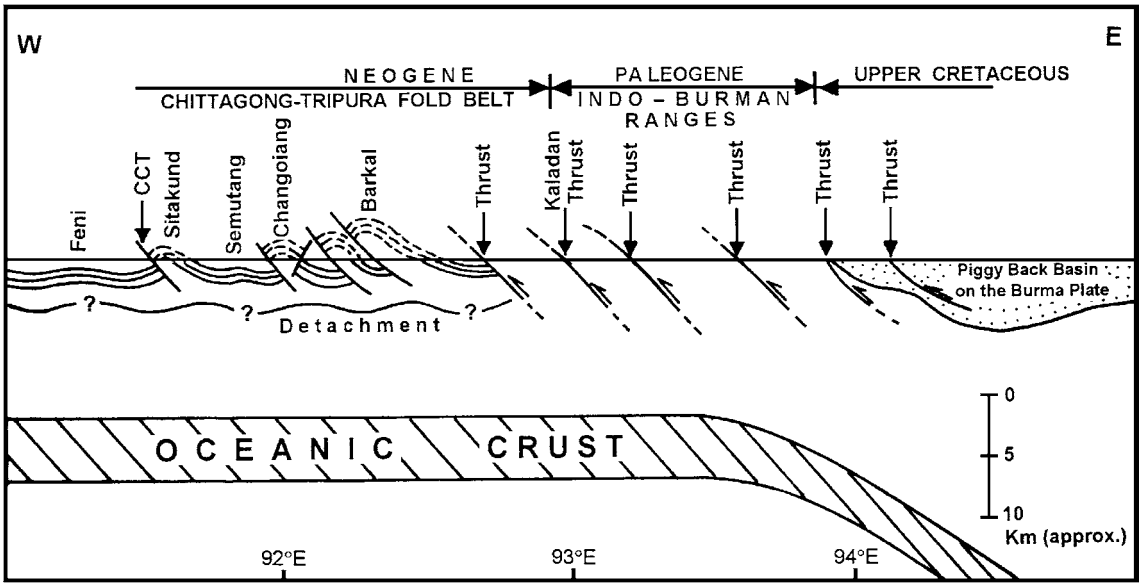

Fig. 7. Schematic cross-sectional profile through the *Chittagong–Tripura Fold Belt Province* (see Fig. 2a for location of the section line) showing the structural elements and development of Neogene accretionary prism complex resulting from the process of thin-skinned tectonics (after Sikder and Alam, 2003).

may more readily be explained by the accretionary prism formation. Compressive (north–south) wrench tectonics, as a result of convergent-oblique movement of the Indian plate relative to the Burma plate, and the opening of the Andaman Sea during Miocene time has significantly influenced the overall structural architecture of the region (Murphy and Staff BOGMC, 1988; Sikder, 1998). It is anticipated that future identification of the major individual thrust sheets (accretionary wedges) will provide vital information in determining the chronological order of the Tertiary rock succession in the region, since it is well known that the accretionary complex as a whole youngs towards the west (Dasgupta and Nandy, 1995; Gani and Alam, 1999). Intuitively, one such major thrust, the Kaladan thrust in the east of CTFB (Fig. 2a), has recently been described by Sikder (1998), but its significance is yet to be known.

4. Stratigraphic successions

The existing stratigraphic scheme of the Bengal Basin was originally established on the basis of the exposures along the fold belt in the eastern part of the basin and their purely lithostratigraphic correlation with the type sections in Assam, northeastern India, described by Evans (1932). The stratigraphic age assignments given by Evans for the Assam sequences are by no means reliable because they were based on long distance correlations of brackish marine macrofauna and vertebrate finds. While some parts of Evans' scheme may be usable in the regional lithostratigraphic or seismic correlation (e.g. the boundary between the Surma and Tipam Groups), other parts of his classification (e.g. the contact between the Bhuban and Bokabil Formations or the internal units of these formations) are difficult to apply to the lithostratigraphic succession throughout the basin. Therefore, over the years several workers have attempted to refine this scheme on the basis of palynological studies (e.g. Chowdhury, 1982; Uddin and Ahmed, 1989; Reimann, 1993); micropaleontological studies (Ahmed, 1968; Ismail, 1978; and unpublished reports of Petrobangla); and seismo-stratigraphic studies (Lietz and Kabir, 1982; Salt et al., 1986; Lindsay et al., 1991; and unpublished reports of Bangladesh Petroleum Exploration and Production Company). Some of these works, especially on micropaleontology (Ahmed, 1968; Ismail, 1978) and seismic strati-

graphic works by Salt et al. (1986) and Lindsay et al. (1991), assisted in solving some of the stratigraphic problems of the basin.

The first point to be noted while considering the stratigraphic successions in the three provinces of the Bengal Basin is that the shelfal facies should differ markedly from the time-equivalent basinal facies. Thus it is unwise to designate, for example, the Miocene strata of both the shelfal and basinal parts with the same rock-unit term, like the 'Surma Group'. Second, although the lithostratigraphic units are extremely diachronous in nature, the concept of diachronism (e.g. as depicted by Imam and Shaw, 1985) is difficult to apply in solving the problem of traditional stratigraphic nomenclature because of the complex nature of sedimentation pattern within the basin. As Brunnschweiler (1980) pointed out, there had never been a broad front of steady coastal advancement across the basin, giving rise to the regularly diachronic units leading to ''lithostratigraphic monsters''. However, due to lack of agreement among the geologists working on the Bengal Basin, stratigraphic formation names used for the Sylhet Trough are generally extended to the stable shelf and to the CTFB. The present paper suggests some new stratigraphic formation names to highlight the differences in stratigraphic successions in different parts of the basin. This approach should be seen as an encouragement for further research work and the necessity for a basinwide seismo-stratigraphic breakdown with integration of the exposed succession in the CTFB, as well as integration of reliable age dating information.

From the discussion above and in the previous sections it is suggested that a rational approach to the stratigraphy of Bangladesh will be to divide the Bengal Basin into three stratigraphic provinces corresponding to the geo-tectonic provinces mentioned earlier (Fig. 5). These are: (1) Stable Shelf or *Geo-tectonic Province 1*; (2) Central Deep Basin (including the Sylhet and Hatia Troughs) or *Geo-tectonic Province 2*; and (3) Chittagong–Tripura Fold Belt or *Geo-tectonic Province 3*. The Hatia Trough in *Province 2* (Fig. 2a) is considered to be the present active sediment depositional center or depocenter. However, the Bengal Deep Sea Fan may also be considered as an extension of the present sediment depocenter.

Sedimentation within the Bengal Basin is thought to have taken place in five distinct phases: (I) Permo-Carboniferous to early Cretaceous; (II) Cretaceous–Mid-Eocene; (III) Mid-Eocene–Early Miocene; (IV) Early Miocene–Mid-Pliocene; and (V) Mid-Pliocene–Quaternary. Each of these sedimentation phases has been controlled by the tectonic cycles, which involved the interaction and collision pattern of the major plates. In terms of the tectonic evolution of the basin, these phases could be called: (I) Syn-rift stage; (II) Drifting stage; (III) Early collision stage; and (IV) and (V) Late collision stage.

The initial sedimentation phase I (Permo-Carboniferous to early Cretaceous) started within the graben basins on the stable shelf (*Province 1*) well before the break-up of Gondwanaland. The break-up of Gondwanaland, which initiated sedimentation phase II, occurred in Early Cretaceous, possibly as early as M-11 time, 123–132 Ma, depending upon the time scale used (Ramana et al., 1994). This was the time of subsidence and marine transgression into the area of *Provinces 1 and 2* of the Bengal Basin (Banerji, 1981).

The rate of sedimentation increased in the Santonian (about 84–88 Ma) with sediment accumulation on the continental margin of India. This event could possibly be correlated with the postulated 90–96 Ma plate reorganization of Curray et al. (1982) and Veevers (1982) mentioned earlier. Most of these sediments were deposited on the northern continental margin of India, what is now the Himalayas. At this time sedimentation in the deeper part of the basin was rather slow, and perhaps dominated by hemipelagic deposition.

In the Paleocene, soft collision occurred between the northern Greater Indian continental crust and the subduction zone lying south of Asia (Fig. 4b). This should have had little or no effect on sedimentation in the future Bengal Basin. At the beginning of sedimentation phase III, in the Mid-Eocene (Fig. 4c), another important event of marine transgression occurred in *Province 1* that was dominated by carbonate deposition, which can also be traced all along the Himalayas. During the latter half of this sedimentation phase, gradual marine regression accumulated shelfal to deltaic deposits on *Provinces 1* and *2,* whereas submarine fan turbidite sedimentation dominated in the southwestern portion of *Province 2* and in *Province 3*.

By Early Miocene, i.e. the beginning of sedimentation phase IV, or the late collision stage, the Bengal Basin took the shape of a remnant ocean basin (Fig. 5), so that *Provinces 2 and 3* started to act as active sediment depocenters. A major collision of the Indian plate with South Tibet and Burma plates (Fig. 4d) took place in the Early Miocene, and rapid uplift occurred in the Himalayas and Tibet. Also, at about the same time a major upthrust movement occurred along the Dauki Fault resulting in separation of the Sylhet Trough from the stable shelf, and the trough formed an important sediment depocenter. Repetitive marine transgressions and regressions dominated the depositional processes over the entire Bengal Basin during phase IV.

At the beginning of sedimentation phase V (Mid-Pliocene), the final marine regression from most of the Bengal Basin concomitant with the tectonic upheaval of the eastern Bengal Basin, established a fluvio-deltaic environment of deposition. With continued Plio-Pleistocene collision of India with Tibet and Burma, and rapid rise of the Himalayas and the CTFB, the sediment depositional center was shifted further south and the present Faridpur and Hatia Troughs became the major sediment depositional centers.

4.1. Stratigraphic succession of Province 1

The stratigraphic succession of *Province 1* is presented in Table 1. A generalized correlation of the lithostratigraphic formations with the seismic sequences and major tectonic events (BOGMC, 1986) are also shown in Table 1. The sedimentary succession unconformably overlies the Precambrian basement rocks. It should be mentioned here that the rock successions described below are nearly all known only by drill holes.

The Precambrian rocks of the Indian Shield represent the oldest rocks encountered in drill holes of *Province 1*. These basement rocks are similar in nature to those in West Bengal and Shillong Plateau; and commonly consist of gneiss, schist, diorite, granodiorite and granite (Zaher and Rahman, 1980). Recent studies reveal that these rocks are predominantly composed of tonalite, diorite and granodiorite, with subordinate granite, gneiss and schist (Khan et al., 1997; Ameen et al., 1998, 2001). Precambrian stratigraphy of *Province 1* is poorly known, but data from the Indian part of the stable shelf suggest that the rocks are most probably of Archean age, and equivalent to the Bundelkhand Complex (Saxena et al., 1997). During this time, the Bengal Basin had not formed, and the area was part of the Gondwana Supercontinent around the south pole. The first phase of sedimentation in the Bengal Basin on top of the Precambrian rocks started during the Permian–Carboniferous (Table 1).

Thickness of the sedimentary succession in *Province 1* varies from about 200 m in the northwest near Rangpur (Fig. 1) to more than 6000 m in the southeast near the Calcutta–Mymensingh Gravity High. The oldest sedimentary rocks known from the subsurface of *Province 1* belong to the Gondwana Group (Table 1) that occurs in isolated grabens in the basement. The group is divided into two formations: the Kuchma and the Paharpur Formations (Zaher and Rahman, 1980). The Kuchma Formation is about 490 m thick and consists of sandstone, siltstone, mudstone and coal seams. Sandstone of the formation is unweathered, less feldspathic and moderately hard and compact. The tillites at the base of the Gondwana Group indicate that sedimentation followed a major glaciation in the region; and the Gondwana coal measures also suggest that deposition occurred under cold to cool climatic conditions (Wardell, 1999). The tillites consist of boulder beds with clasts of unsorted sedimentary, igneous and metamorphic rocks interbedded with occasional units of mudstone, siltstone and coal, indicating interglacial sedimentation. The Paharpur Formation is about 465 m thick and consists of fine to coarse arkosic sandstones with thick coal beds and occasional conglomerates. The sandstones are relatively weathered, moderately soft and strongly kaolinized resulting in a white clay matrix throughout the formation (Wardell, 1999). The Gondwana sediments are interpreted to have been deposited in low-sinuosity braided fluvial systems flanked by vegetated overbank and swampy floodplain areas (Uddin and Islam, 1992; Uddin, 1994).

The Rajmahal Group (Jurassic to Early Cretaceous) unconformably overlies the Gondwana Group and the Precambrian rocks; and comprises two formations: the Rajmahal Traps and the Sibganj Trapwash (Table 1).

Table 1
Stratigraphic succession of the Stable Shelf Province of the Bengal Basin, Bangladesh (modified from Zaher and Rahman, 1980; Khan, F.H, 1991; Lindsay et al., 1991; Reimann, 1993; Alam, 1997; BOGMC, 1997). * Denote equivalent formation of West Bengal, India.

Series	Group	Formation	Lithology	Depositional environment	Seism. seq.	Refl. no.	Age MY	Tectonic events	Sed'n phase
Holocene		Alluvium	Silt, clay, sand and gravel						
Pleistocene - Late Pliocene	Barind (200 m)	Barind Clay (50 m)	Yellowish brown to reddish brown clay, silty-clay and silty-sand with minor sand	Fluvial-alluvial and rapidly prograding delta	G				V
		Dihing (150 m)	Oxidized sand with clay and silicified wood fragments			R-17	? 1.6	Folding in Eastern Bangladesh	
						R-16	3.0		
Early Pliocene - Late Miocene	Dupi Tila (280 m)	Dupi Tila (280 m) *(Debagram and Ranaghat)**	Claystone, siltstone, sandstone and gravel	Fluvial and prograding delta-shelf	F	R-15	3.8		IV
						R-14	5.5		
						R-13	6.3		
						R-12	8.2		
Early to Middle Miocene	Jamalganj (415 m)	Jamalganj (415 m) *(Pandua)**	Alternating sandstone, siltstone and shale	Delta front to shelf and slope		R-11	10.5		
Oligocene	Bogra (165 m)	Bogra (165 m) *(Memari and Burdwan)**	Siltstone, carbonaceous shale and fine-grained sandstone	Increasing sedimentation rates	E	R-10	21	Folding in Indo-Burman Ranges (Fig. 4D)	III
Late Eocene	Jaintia (735 m)	Kopili Shale (240 m)	Sandstone, locally glauconitic and highly fossiliferous; shale with thin calcareous bands	Deltaic to slope	D	R-9	30		
Middle Eocene		Sylhet Limestone (250 m)	Nummulitic limestone with sandstone interbeds	Carbonate platform	C	R-8	39.5	Hard Collision (Fig. 4C)	II
Early Eocene		Tura sandstone (245 m) *(Jalangi)**	Sandstone, coal and shale	In western Bangladesh only: Deltaic to outer shelf		R-7	54		
Paleocene						R-6	58.5	Soft Collision Close Sutures (Fig. 4B)	
Middle to Late Cretaceous		Sibganj Trapwash (230 m) *(Ghatal and Bolpur)**	Coarse yellowish brown sandstone; volcanic materials with clay	Coastal to fluvial-alluvial	B	R-5	68		
Early Cretaceous - Jurassic	Rajmahal (840 m)	Rajmahal Traps (610 m)	Amygdaloidal basalt, andesite, serpentinized shale and agglomerate	Subaerial lava flows		R-4	126	Main Break-up Unconformity	I
				Fluvio-deltaic to shallow marine		R-3	Age poorly defined		
Late Permian	Gondwana (955 m)	Paharpur (465 m)	Feldspathic sandstone with thick coal seams	Fluvial to delta plain, coal swamps	A	R-2		Rapid Extension	
Permian - Carboniferous		Kuchma (490 m)	Coarse-grained sandstone and conglomerate with thick/thin coal seams					Graben Formation	
Precambrian		Basement complex		Stable Gondwana Continent		R-1	Stable Gondwana Continent (Fig. 4A)		

The Rajmahal Traps are about 610 m thick and consists of hornblende basalt, olivine basalt and andesite with minor agglomerate, tuff and ash beds (Khan, F.H., 1991). The Rajmahal Traps and its equivalent Sylhet Traps on the eastern side of *Province 1* are thought to be more extensive than revealed by limited outcrops (Kent, 1991; Curray and Munasinghe, 1991) and drill hole data. The Sibganj Trapwash unconformably overlies the volcanic rocks of the Rajmahal Traps (Table 1); and consists of poorly sorted coarse sandstones (trapwash), shale/claystone with locally kaolinitic sandstone. The rocks of the formation are thought to have been deposited in fluvial and coastal settings, particularly tidal flats, deltaic and lagoonal environments. In West Bengal, India, the Ghatal (120 m) and Bolpur (160 m) Formations (Table 1) represent the Sibganj Trapwash equivalent rocks.

The Rajmahal Group is unconformably overlain by the Jaintia Group, which consists of the Tura Sandstone, Sylhet Limestone and Kopili Shale Formations. The Tura Sandstone, equivalent of the Jalangi Formation of West Bengal (Lindsay et al., 1991), is about 245 m thick and consists of sandstones, siltstone, carboniferous mudstone and thin coal seams. The sandstones often contain foraminifera, shell debris and glauconite. The Sylhet Limestone (Middle Eocene), representing the most prominent seismic marker in *Province 1*, characterizes both the maximum marine transgression on the stable shelf of the Bengal Basin as well as defines the southern limit of the shelf. The limestone is massive and compact containing abundant foraminifera with minor algal debris; and may be classified as foraminiferal biomicrites. Banerji (1981) described diverse marine fauna including crinoids, corals and bryozoans from the Sylhet Limestone in the Lower Assam Basin. Seismic data (BOGMC, 1986) suggest that the lower part of Sylhet Limestone forms a broad time-transgressive facies extending from the shelf edge to the upper shelf area. Thickness of the formation decreases from over 800 m on the shelf edge in the southeast to about 250 m in wells located in the northwestern part of *Province 1*.

The Kopili Shale (Late Eocene) conformably overlies the Sylhet Limestone and comprises thin-bedded sandstone and shale in varying proportions, and occasional fossiliferous limestone. These rocks are interpreted as deposits of distal deltaic to shelf and/or slope environments. Maximum thickness of the formation is 240 m in Bangladesh. In outcrop section of the Kopili Hill (Assam) the formation is about 500 m thick, while in West Bengal it is much thinner, probably about 30 m (Banerji, 1984).

The Bogra Formation (Oligocene) unconformably overlies the Jaintia Group. The formation is about 165 m thick; and consists of interbedded sandstone and mudstone with a high sand/mud ratio. These rocks represent deposits of distal deltaic to marine environments (inner to outer shelf). In West Bengal, the Bogra Formation equivalent rocks comprise the Memari and Burdwan Formations (Table 1). The Burdwan Formation (about 200 m thick) represents the sandier proximal facies, while the Memari Formation (about 150 m) is the more distal and muddy deltaic facies (BOGMC, 1986; Lindsay et al., 1991). The Bogra Formation equivalent unit, known as the Barail Formation, is well developed in Assam, India (Fig. 1) and also occurs in the northern part of *Province 2*.

The Bogra Formation is unconformably overlain by the Early–Middle Miocene Jamalganj Formation, which comprises alternating sandstone, siltstone and shale. The formation is about 415 m thick in *Province 1*, whereas its equivalent Pandua Formation in West Bengal is more than 1500 m thick (Banerji, 1984). The rocks of the Jamalganj Formation are thought to have been deposited in a large delta complex. The Jamalganj Group is considered to be equivalent of Surma Group of *Province 2*. The Dupi Tila Formation (Table 1) unconformably overlies the Jamalganj Formation, and consists of light grey to yellowish grey clayey sandstone, siltstone and claystone with minor gravel. The formation is about 280 m thick in *Province 1*, while the equivalent Debagram and Rangahat Formations in West Bengal is 750 m thick.

The Barind Group, consisting of the Barind Clay and Dihing Formations, unconformably overlies the Dupi Tila Group. The Dihing Formation consists of coarse sand and sandstone, siltstone and claystone with some poorly consolidated pebble beds. The Barind Clay predominantly consists of yellowish to reddish brown clay, silty-clay and silty-sand with minor pebble. Thickness of the Barind Group in *Province 1* is about 200 m.

4.2. Stratigraphic succession of Province 2

The stratigraphic succession of *Province 2* was initially established by lithostratigraphic correlation to type sections in the Assam Basin, northeastern India (Fig. 2a; Evans, 1964; Holtrop and Keizer, 1970; Khan and Muminullah, 1980). On the basis of basin-wide seismostratigraphic correlation, Lietz and Kabir (1982) have partly refined the conventional stratigraphic framework for most parts of the Bengal Basin, including the Sylhet Trough. Seismic data indicate that the Sylhet Trough of *Province 2* contains about 17,950 m of Eocene to Holocene clastic sediments (Table 2; Hiller and Elahi, 1988) that appear to correspond fairly well with the maximum of 17,000 m Eocene–Holocene succession in the adjacent Assam Basin (Das Gupta, 1977). This section is thicker in the southern part of the province in the Faridpur and Hatia Troughs, but the stratigraphy is little known there.

4.2.1. The Sylhet Trough

The pre-Oligocene rocks, the Jaintia Group, (Table 2) have not been penetrated in the subsurface of *Province 2* (Fig. 8), but they crop out in the northern margin of the Sylhet Trough. In the southern Shillong Plateau these rocks reflect transgressive sedimentation on a passive margin (Banerji, 1981; Salt et al., 1986). Rao (1983) divided the equivalent pre-Oligocene Disang Group in the Naga Hills of India (east of the Sylhet Trough) into lower and upper units, representing basinal and shallow-marine facies, respectively. In the Sylhet Trough, the pre-Oligocene rocks consist of: (i) the Paleocene Tura Sandstone Formation, 170–360 m thick, consisting of poorly sorted sandstone, mudstone and fossiliferous marl, with minor carboniferous material and impure limestone; and interpreted as shallow-marine to marine deposits; (ii) the Middle Eocene Sylhet Limestone, a 250-m thick nummulitic unit interbedded with minor sandstone, interpreted as shallow-marine carbonate deposits; and (iii) the overlying 40–90 m thick, Upper Eocene Kopili Shale Formation, the lithology and fossil content of which indicate deltaic to slope depositional environments for the stable shelf of the Bengal Basin and Assam Basin. There are also possibilities that some of the Kopili Shale could have been deposited in deep sea fan environment and are stratigraphically equivalent to the Sylhet Limestone in the deeper part of the Bengal Basin.

Table 2
Stratigraphic succession of the Sylhet Trough in the northeastern part of Province 2 (revised from Hiller and Elahi, 1988)

Age (approx.)	Group	Formation	Seismic marker	Thickness (max.) (m)
Holocene	Dihing	Alluvium	→ Yellow	3350
Pleistocene		Dihing		
Late Pliocene	Dupi Tila	Upper Dupi Tila		
		Lower Dupi Tila		
Mid-Pliocene	Tipam	Girujan Clay Tipam Sandstone	→ Brown	3500
Early Pliocene Miocene	Surma	Upper Marine Shale Upper Lower	→ Red → Violet	3900
Oligocene	Barail	Undifferentiated		7200
Paleocene-Eocene	Jaintia	Kopili Shale Sylhet Limestone Tura Sandstone	→ Blue	
Pre-Paleocene	Undifferentiated sedimentary rocks (with some volcanics ?) on the continental basement complex			

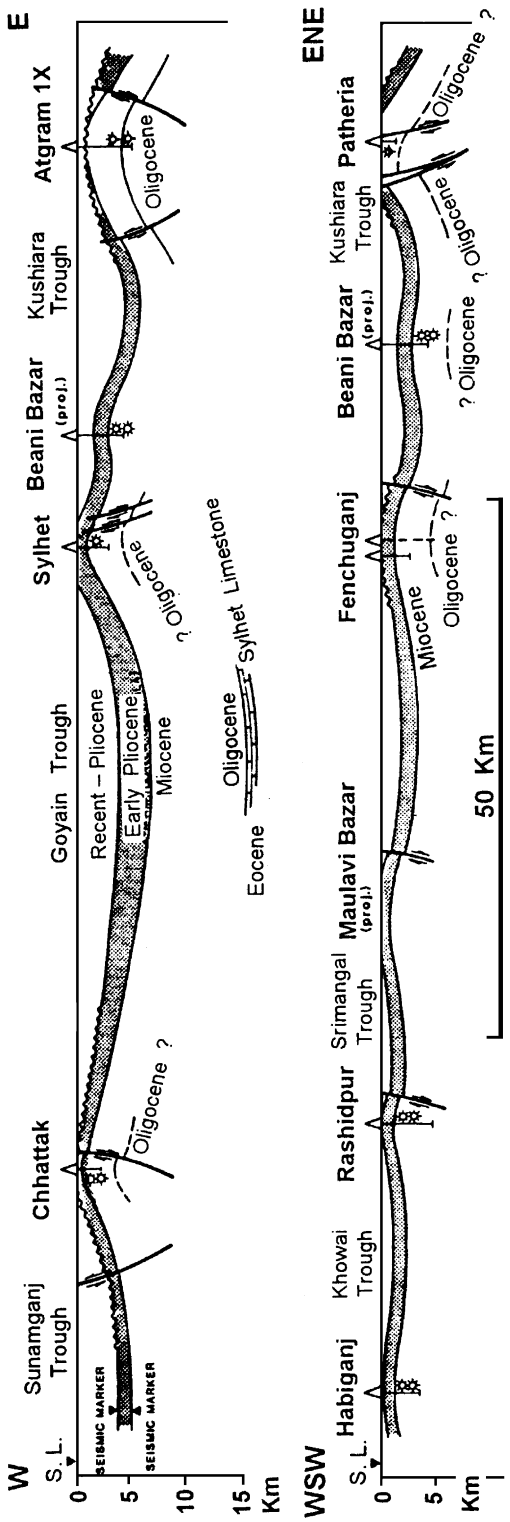

Fig. 8. Geological cross-sections through the northern (E–W line) and the southern (ENE–WSW line) portions of the Sylhet Trough in the northeastern part of *Province 2*. See Fig. 1 for location of the section lines.

The Oligocene rocks, informally termed as the Barail Group, are exposed along the northern fringe of the Sylhet Trough near the Dauki Fault area, and range in thickness from 800 (Johnson and Alam, 1991) to 1600 m (Ahmed, 1983). It is believed that these rocks have been encountered in the subsurface in the Atgram 1X and Rashidpur 2 wells (Fig. 1). The Barail equivalent rocks of the Bogra Formation (Khan and Muminullah, 1980) have been penetrated in *Province 1*, where they are less than 200 m thick (Table 1). The Barail rocks in the Sylhet Trough, which are not formally subdivided, have been interpreted as deposits of predominantly tide-dominated shelf environments (Alam, 1991). On the basis of facies analysis, Dasgupta et al. (1991) have interpreted the Barail Group (3500 m thick) from the basinal facies of the Lower Assam Basin, India, as deposits of a basinward migrating progradational submarine fan complex, and suggested that sedimentation continued into the overlying Surma Group. The contact of the Surma Group with the underlying Barail Group appears to be a transgressive onlap, approximately at the Oligocene–Miocene boundary (Banerji, 1984; Salt et al., 1986). This marine transgression on the shelf part of *Province 2* may be the result of a major upthrust movement along the Dauki Fault at the Early Miocene or by subsidence because of approach to the subduction zone (Fig. 4d). Following Evans' (1932) stratigraphic scheme, the Surma Group has traditionally been divided by workers in Bangladesh into two units—a lower Bhuban and an upper Boka Bil Formations (e.g. Holtrop and Keizer, 1970; Hiller and Elahi, 1988; Khan et al., 1988; and others) throughout the Bengal Basin. However, Johnson and Alam (1991) consider the group as a single stratigraphic unit because they observed no significant lithologic and petrologic differences between these formations. Khan, F.H. (1991) also considers the group as a single unit based on the lithological similarity and lateral facies variations within the group. We suggest that on the basis of the presence of a prominent seismic marker within the Surma Group (Hiller and Elahi, 1988), the group may informally be divided into a lower and an upper unit (Table 2). Similarly, Lee et al. (2001) divided the Surma Group into two formations on the basis of a seismic marker defined as maximum flooding surface. Perhaps this time of maximum flooding correlates with the changes in convergence rate and direction of India into Asia (Figs. 3 and 4d). It is important to realize that the divisions of the Surma Group in the Sylhet Trough are independent of the Bhuban and Bokabil divisions of the group in the Assam Basin (Fig. 2a). However, to formalize these units into the stratigraphic scheme for the Sylhet Trough part of *Province 2*, further detailed work on both the subsurface and exposed sections will be needed.

It should be mentioned here that the problem of facies variations within the Surma Group has been noted by Banerji (1984), who observed that rocks of the group from different outcrops and subsurface sections show variable conditions of deposition ranging from open marine to interdeltaic types. It appears from earlier works (Banerji, 1984; Khan et al., 1988; Reimann, 1993) that facies variations associated with alternating cycles of marine transgressions were of variable extent and affected by localized regressive phases; and therefore subdivision of the group over a wider area based on sand/shale ratio alone is probably prone to miscorrelation (Alderson, 1991). The top of the group constitutes a predominantly shaly unit, designated as the 'Upper Marine Shale' (Table 2; Holtrop and Keizer, 1970), which represents a 230-m thick pelitic sequence marking the last marine incursion, and is probably the sole seismic marker horizon throughout the Sylhet Trough. In Atgram 1X well, this shaly unit is eroded, as evidenced by seismic and well logs (Fig. 8; Hiller and Elahi, 1988).

Thickness of the Surma Group varies from 2700 m (in Atgram 1X well) to over 3900 m (in Fenchuganj 2 well) (Fig. 1), which is in good concurrence with the thickness of 2800–3250 m in the Naga Hills to the east (Rao, 1983). Johnson and Alam (1991) have interpreted the lower Surma Group (i.e. Bhuban Formation) as prodelta and delta-front deposits of a mud-rich delta system similar to the modern Bengal delta. The sediments of the upper Surma Group (i.e. Boka Bil Formation) represent deposits of subaerial to brackish environments, based on mudrocks and pollen types (*Hystrichosphroedis*; Holtrop and Keizer, 1970). Alderson (1991) noted marine influence within the Boka Bil Formation in eastern Sylhet Trough. On the basis of detailed facies analysis of core samples and wireline log interpretation, Alam (1995b) envisaged a micro-tidal coastal setting with

extensive development of intertidal and subtidal environments within a proto-Surma delta embayment, for the Surma Group sediments in the Sylhet Trough. Similarly, on the basis of comprehensive logging of the core samples from the Sylhet Trough, Sultana and Alam (2001) have interpreted the sediment of the group as deposits of environments ranging from shallow marine to tide-dominated coastal settings within a cyclic transgressive–regressive regime.

The Surma Group is overlain unconformably by the Middle Pliocene Tipam Group, consisting of the Tipam Sandstone and Girujan Clay Formations. The Tipam Sandstone comprises coarse-grained, cross-bedded sand and pebbly sand, with common carbonized wood fragments and coal interbeds; and interpreted as deposits of bed-load dominated braided-fluvial systems (Johnson and Alam, 1991). The Girujan Clay, composed mainly of mottled clay, accumulated in subaerial conditions as lacustrine and fluvial overbank deposits (Reimann, 1993).

The Dupi Tila Group, unconformably overlying the Tipam Group, comprises a sandy lower unit and an upper argillaceous unit (Hiller and Elahi, 1988). Khan et al. (1988) noted that sediments of the Lower Dupi Tila Formation are similar to the Tipam Sandstone, except that they tend to be poorly consolidated. Sediments of the Upper Dupi Tila Formation are characteristically fine to medium-grained sandstones, commonly silty and containing lignite fragments and fossil woods, with intercalation of mottled clay horizons. The fining-upward sequences of the Lower Dupi Tila Formation, with alternating channel and floodplain deposits, have been interpreted as meandering river deposits (Johnson and Alam, 1991). The younger Pleistocene sediments of the Dihing Formation have been identified only locally as relatively thin subaerial deposits unconformably overlying the Dupi Tila Group.

It is apparent from Table 2 that a huge thickness of sediment (nearly 7 km) has been deposited in the Sylhet Trough from Mid-Pliocene onward that could be due to the Mio-Pliocene uplift of the Chittagong–Tripura Fold Belt and the Himalayas.

4.2.2. The Hatia and Faridpur Troughs

We think that the stratigraphy and sedimentation pattern in the southern part of the Central Deep Basin (i.e. the Hatia and Faridpur Troughs of *Province 2*) (Fig. 2) should be considered separately. This is because these troughs are centrally located with respect to the geo-tectonic provinces described earlier; and more importantly they have been receiving sediment from the directions of all the provinces, although at different times and rates from different provinces.

During sedimentation phase II (Cretaceous–Mid-Eocene) the southern part of the Central Deep Basin had received little sediment (mainly hemipelagic) from *Province 1*. During phase III (Mid-Eocene–Early Miocene) and most of phase IV (Early Miocene–Mid-Pliocene) deep-water submarine fan sedimentation occurred in this deep basin area with sediment coming from the directions of *Provinces 1* and the Sylhet Trough of *Province 2*, and probably at a later time from *Province 3*. At the beginning of the Pliocene shallow marine sedimentation with a rapidly increased rate of sedimentation from the directions of all three provinces started to take place in this part of the Bengal Basin. The present basin configuration with the development of the Ganges–Brahmaputra Delta system in the onshore part of Bangladesh and the Bengal Deep Sea Fan in the offshore was established during the later part of Pliocene; and the delta progradation since then has been affected by orogeny in the eastern Himalayas. The oldest sediments yet sampled by drilling in the Bengal Fan are early Miocene, but it is believed that deposition of the fan may have started as early as Middle Eocene.

Because of the lack of deep seismic sections and deep well data from the southern part of *Province 2*, the pre-Pliocene stratigraphy of the region is poorly known. Borehole data from the Shahbazpur 1 well in the Hatia Trough (Figs. 1 and 2a) indicate the presence of more than 2000 m of Plio-Pleistocene sediments underlying 480 m of Holocene deposits. The Plio-Pleistocene sediments consist predominantly of shale with occasional interbedded sandstone and calcareous siltstone, and traces of lignite and bituminous coal (BAPEX, 1994). A well-documented seismic stratigraphy (Fig. 9), established recently for the Sangu gas field in the Hatia Trough (Figs. 1 and 2a), could be useful in depicting the general scenario of the sedimentation phase V in the region. On the basis of nannofossil analysis (NN 15-*Sphenolithus abies*) from the lower part of Megasequence 1 of the Sangu field stratigraphic succession (Fig. 9),

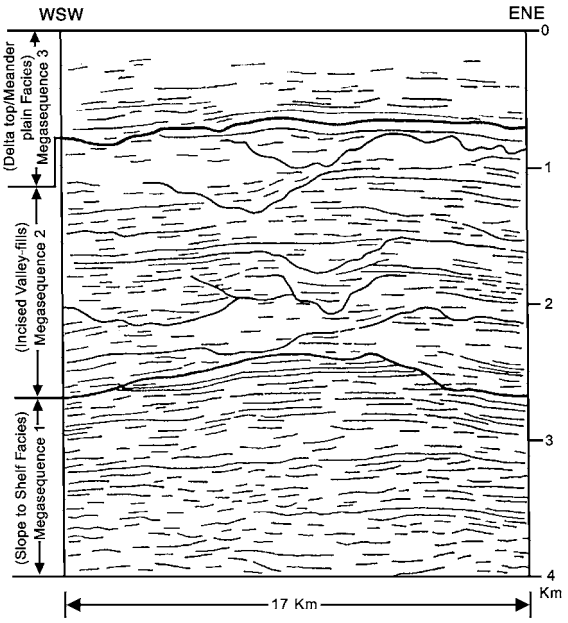

Fig. 9. Subsurface seismic profile (see Fig. 2a for location) through the offshore Sangu structure in the Hatia Trough, southern part of the *Central Deep Basin Province* (after BOGMC, 1997) showing the subsurface stratigraphy based on major sequence boundaries.

Partington (2001) has established the oldest age of Early Pliocene for sediments of this unit.

4.3. Stratigraphic succession of Province 3

On the basis of regionally correlatable bounding discontinuities the exposed Neogene succession of *Province 3* (CTFB) has been divided into three discrete composite sequences C, B and A, from oldest to youngest (Table 3; Gani and Alam, this volume). These workers acknowledge that without any regional marker bed or precise biostratigraphic zonation it is difficult to establish a stratigraphic scheme; and hence an allostratigraphic framework has been adopted, giving emphasis on bounding discontinuities, to analyze the sedimentation and basin-fill history of the Neogene clastic succession. It has been recognized that allostratigraphic units are more natural subdivisions of the rock record than conventional lithostratigraphic units (Walker, 1990; Miall, 1997). Therefore the allostratigraphic scheme formally adopted by the North American Commission of Stratigraphic Nomenclature North American Commission on stratigraphic Nomenclature (NACSN), 1983) has been incorporated in establishing a separate stratigraphy for the CTFB. Table 3 shows such a tentative stratigraphic classification for the CTFB that recognizes four Groups (more precisely allogroups) equivalent to the composite sequences. A brief description of each Group (from Gani and Alam, this volume), from oldest to youngest, is given below.

Chittagong group: The group is speculated to exist in the subsurface and has not yet been reported from the outcrop. The Group is thought to represent large-scale submarine fan complex as envisioned by Gani and Alam (1999) and to exist beneath the slope apron deposits of the composite sequence C. The Group probably ranges in age from the Eocene (?) or Oligocene to the Early Miocene and is equivalent to the traditional Barail Group and the lower part of the Surma Group.

Sitapahar Group (composite sequence C, equivalent to the traditional middle Surma Group): It is probably Middle Miocene in age and ranges in thickness from 1000 m to 1500 m. However, recent study based on *Dinoflagellates* (Uddin and Uddin, 2001) indicates that the exposed sediments of the CTFB are probably not older than Late Miocene/Early Pliocene. The Rangamati–Chittagong road section of the Sitapahar anticline could be the type section for this Group. In the type section it is represented by the oldest 1128+ m of the rock succession (composite sequence C) exposed in the eastern flank of the anticline (Gani and Alam, this volume). This Group represents a progressive basin filling from deep marine slope apron to shallow marine nearshore deposits, and would represent the period of closing of the suture between the Bengal Basin and the subduction zone lying off the Burma Block (Fig. 4b). No major erosion surface of sea level lowstand condition has been encountered within this Group, in which a low sand/shale ratio indicates that the basin was accommodation-dominated during this time. The Sitapahar Group may be further divided into several alloformations depending on the bounding discontinuities (mainly the marine flooding surfaces).

Mirinja Group (composite sequence B, equivalent to the traditional upper Surma Group): It is probably Late Miocene in age and ranges in thickness from

Table 3
Proposed allostratigraphic nomenclature for province 3 (CTFB) (after Gani and Alam, this volume)

Age (approx.)			Traditional nomenclature*		Proposed nomenclature	Thickness (m)	Brief description
Quaternary	Recent		Alluvium		Alluvium		
Neogene	Plio-Pleistocene		Dupitila Fm.		Kaptai Group (A)	1100 to 1600	Large-scale, low-sinuosity braided river deposits grading upward into high-sinuosity meandering river deposits. Very high sand-shale ratio. Characteristically yellowish-brown very coarse to fine sand.
			Tipam Group	Girujan Clay Fm.			
				Tipam Sst. Fm.			
	Miocene	Late	Surma Group	Boka Bil Fm.	Mirinja Group (B)	1200 to 1600	Alternating nearshore sand and shelfal mud with regional erosion surfaces related to relative sea level cycles. High sand-shale ratio. Predominance of tidal structures is obvious.
		Middle		Bhuban Fm.	Sitapahar Group (C)	1000 to 1500	Slope mud predominant; sandy deposits ranging from base-of-slope turbidites to nearshore tidal sands. No major erosion surfaces.
Paleogene	Oligocene	Early			boundary not established	2000 +	Speculated submarine fan complex in trench setting; mud dominated.
			base not exposed		Chittagong Group (mostly in subsurface)		
			Barail Group (in subsurface)				

Composite sequences C, B and A are shown in parenthesis. For convenience, the traditional lithostratigraphic classification (* based on Evans, 1932) is compared at the left.

1200 to 1600 m. The Lama–Fashiakhali road section of the Mirinja anticline could be the type section for this Group. In the type section the Group is represented by the 1293 m thick shelfal to coastal succession (composite sequence B) exposed in the western flank of the anticline (Gani and Alam, this volume). The Group may conveniently be divided into several alloformations corresponding to the individual sequences, which in turn can be divided further into allomembers depending on the transgressive erosion surface and transgressive surface/marine-flooding surface. The high sand/shale ratio of this Group indicates that the basin was supply-dominated during this period.

Kaptai Group (composite sequence A, equivalent to the traditional Tipam Group and Dupi Tila Formation): It is probably Plio-Pleistocene in age and ranges in thickness form 1100 to 1600 m. The stratigraphic succession in the western flank of the Sitapahar anticline along the Kaptai–Chandraghona road section could tentatively serve as a type section for this Group. The lower part of the Group represents braided stream coastal to fluvial deposits, whereas the uppermost part represents deposits of meandering river system. A 100–200 m thick and rather patchy clay deposits (traditional Girujan Clay) sometimes divides the Group into the above-mentioned traditional units.

5. Discussion

The tectonic evolution of the greater Bengal Basin is fundamentally related to the collision pattern of the Indian Plate with the Burma and Tibetan (Eurasian) Plates. From a simplistic point of view, the collision of

these plates can be visualized in two different forms: (i) the north to northeasterly continent–continent collision of the Indian Plate into the Tibetan Plate, which is mainly expressed by thrusting, lateral displacements, and uplift associated with the development of eastern Himalayas; and (ii) the oblique subduction of the oceanic crust beneath the Burma Plate resulting in the development of accretionary wedges, which together with thrusting and folding has subsequently uplifted the Indo-Burman Ranges and associated fold belt of the CTFB region (Gani and Alam, 1999; Sikder and Alam, 2003).

The sedimentation phases, described in Section 4, are crucial to our understanding of the stratigraphic scenario within each of the geo-tectonic provinces of the Bengal Basin. These phases are related to major tectonic events of regional implication; and also associated with periods of uplift and/or subsidence accompanied by relative sea level fluctuation. We believe that the stratigraphic successions of the Bengal Basin presented in this study are the consequence of relative positions of the provinces with respect to the collision pattern of the Indian, Tibetan and Burma Plates during the basin evolution (Fig. 4). Therefore, we also emphasize the necessity of a new seismo-stratigraphic framework for the Bengal Basin integrating all the different geo-tectonic provinces; and this should be an important future research target.

Sedimentation in *Province 1* has been remarkably variable and controlled by both the rise and fall of sea level and tectonic activities around the Bengal Basin; and deposition occurred predominantly on a passive continental margin setting. The stratigraphic record of *Province 1* (Table 1) reveals that the time between Precambrian and Carboniferous had been a period of erosion and peneplanation represented by a major unconformity on top of the basement complex. The initial phase of Permo-Carboniferous sedimentation occurred mainly in isolated graben-controlled basins; and the Gondwana Group is interpreted as the pre-continent break-up succession that was refaulted along some well-defined northwest–southeast trends during the period of extensional faulting, which led to rifting in the Early Cretaceous (Table 1; BOGMC, 1986).

Several workers (e.g. Morgan, 1972; Royer and Sandwell, 1989; Kent, 1991) have suggested that the volcanics of the Rajmahal Traps (Table 1) are associated with the Kerguelen hotspot that later formed the Ninetyeast Ridge. However, Curray and Munasinghe (1991) proposed that the Rajmahal Traps, the 85°E Ridge, and Afanasy Niktin Seamount were formed as traces of the hotspot on the Indian Plate that subsequently formed Crozet Island on the Antarctic Plate. Baksi et al. (1987) presented data suggesting an age of the Rajmahal Traps at around 115–117 Ma. The basalt flows of the Rajmahal Traps probably indicate crustal fracturing associated with the break-up of Gondwanaland (Alam, 1997; BAPEX, 1996). It has also been suggested that continued crustal extension and rifting during Mid–Late Cretaceous resulted in the development of restricted coastal-marine settings in which the sediments of the Sibganj Formation were deposited (BOGMC, 1986). Evidence of Cretaceous sea level oscillation in the Bengal Basin (Lindsay et al., 1991) shows some correlation with global sea-level curves of Haq et al. (1988). The sea level changes have caused local and regional facies variations documented by lithological variations between the Ghatal and Boalpur Formations of West Bengal and the Sibganj Trapwash of *Province 1* (Lindsay et al., 1991).

The sedimentation pattern within *Province 1* changed considerably at about the Cretaceous–Tertiary boundary. At this time marine transgression occurred throughout the province; and stratigraphic and seismic records suggest that the sediment depocenter was towards the south as evidenced by thick Cretaceous–Paleocene succession of the Jalangi, Ghatal and Bolpur Formations in the West Bengal part of *Province 1*. During the Middle Eocene, extensive marine transgression resulted in large-scale carbonate deposition (the Sylhet Limestone) in *Province 1* and also in the shelf part of *Province 2*. In terms of depositional lithofacies, the thick succession of carbonate, reflection-free internal character, and shelf-margin setting, are all favorable indicators of shelf-edge build-ups, such as reefs. With continued marine transgression fine clastics of the Kopili Shale occurred throughout the shelf of both *Provinces 1 and 2*.

By the Oligocene, basin-wide emergence and marine regression resulted in clastic sedimentation (Bogra Formation) in *Province 1*. At this time the northern part of *Province 2* was receiving clastic input (Barail Group) from the northeast. With major

uplift of the eastern Himalayas, the Bengal Basin was subjected to active tectonism during the Early Miocene (Fig. 4d) when sediment influx increased significantly. Major basin filling started with large-scale delta systems prograding from the northeast into *Provinces 2 and 3* (Johnson and Alam, 1991). In Late Miocene, with continued Himalayan movements regression occurred that produced an important unconformity, which correlate with the unconformity in seismic reflection records from offshore of the Bay of Bengal (Curray and Munasinghe, 1989). From Late Pliocene onward sedimentation in *Provinces 1 and 2* has been affected by the glacio-eustatic oscillations superimposed on a general regression that has left widespread traces in the Bengal Basin (Bakr, 1977).

For the Sylhet Trough in *Province 2*, the plate collisions resulted in various stress regimes affecting the region at different times. As mentioned earlier, the trough had undergone a complex history of evolution recording the transition from a passive and rifted continental margin to a foreland basin (sensu stricto) on the edges of two mobile belts—the Indo-Burman Ranges to the east and the Himalayas to the north. The dominant feature, considered to be the result of the north–south collision, is the major upthrust movement along the Dauki Fault during the Early Miocene. The north–south to northeast–southwest trending folds in the Sylhet Trough are thought to have been developed dominantly by the component of east–west directed compressional force associated with plate collision and crustal shortening (Hiller and Elahi, 1988). The northern extension of the north–south trending folds of the CTFB commonly 'swing round' eastward in the subsurface of the Sylhet Trough. This feature can be explained by the buttressing effect of the Shillong Plateau in westward propagation of the fold-thrust system of the CTFB. Another rapid sedimentation phase of fluvial deposition started in the Sylhet Trough in Mid-Pliocene when the CTFB developed at the eastern margin of *Province 2*.

The oblique subduction between the Indian and Burma plates indicates that *Province 3* is a zone of transpression. The manifestation of both the tectonic styles (i.e. subduction and strike–slip components) in a regional context is observed in outboard subduction systems coupled to inboard strike–slip faults, which is the common case worldwide (Dickinson and Seely, 1979; Mann et al., 1999). Three compartments can be delineated within the regional oblique subduction zone between the Indian and Burma plates. These are from east to west—(i) the Central Burma Basin situated between the Sagaing fault in the east and the Kabaw fault in the west; (ii) the Indo-Burman Range situated between the Kabaw fault and Kaladan fault; and (iii) CTFB situated between the Kaladan fault and the Chittagong–Cox's Bazar fault (Fig. 2) (Eastern thrust of Khan, A.A., 1991). These four fault systems show a combination of right-lateral transform fault and east-dipping thrust fault, in which the thrust component increases westward. For example, the Sagaing fault is a transcurrent fault with little or no thrust component, whereas the Chittagong–Cox's Bazar fault is a thrust fault with probably little transform component. The shallow contractile structures within the transpressive zone of *Province 3* may be the product of wrench deformation related to distributed shear (applying the model of Wilcox et al., 1973, to the right-lateral Kaladan fault?); or the contractile component of partitioned strain related to the development of a decollement beneath the CTFB (Fig. 6; Sikder and Alam, 2003). Considering the regional tectonic history the latter process is thought to have been dominant. Since the beginning of counter-clockwise rotation, India has been moving both northward and eastward, with the northward movement aided by the Mid-Miocene opening of the Andaman Sea. However, a few workers believe that at present the subduction slab is being dragged northward, and that subduction is overshadowed by the north-directed strike–slip movement (e.g. Pivnik et al., 1998).

Province 3 deserves especial consideration following the works of Gani and Alam (1999; and this volume). It is apparent from earlier studies and several published cross-sections through the CTFB and Indo-Burman Ranges (e.g. Mitchell, 1981; Curray et al., 1982; Hutchison, 1989; Dasgupta and Nandy, 1995; Pivnik et al., 1998) that the area represents a Cretaceous–Holocene accretionary prism complex developed due to the subduction of the Indian plate beneath the Burma plate. Gani and Alam (1999) depicted the CTFB as the westward continuation of this Indo-Burman accretionary prism, which is younging towards the west. Active development of *Province 3* began from the end of Late Oligocene when the Indo-

Burman Range had already emerged above sea level; and sedimentation started in a trench-slope setting (migrated from the east).

In the past, limitations in age determination of the Tertiary clastics has been a major problem in depicting the stratigraphic and tectonic scenario of the Bengal Basin. Recently, Partington (2001) has applied the nannofossil technique successfully in age determination of the sediments from the subsurface stratigraphic succession of the Sangu field in the Hatia Trough (Fig. 2a). This convenient and reliable technique has opened a new direction in age determination of the thick clastic succession in the Bengal Basin.

6. Conclusions

The Bengal Basin in the northeastern Indian subcontinent evolved from a passive continental margin (pre-Oligocene) to a remnant ocean basin (beginning of Miocene) comprising three geo-tectonic provinces: (1) Passive to extensional cratonic margin in the west, the *Stable Shelf*; (2) the *Central Deep Basin* or remnant ocean basin; and (3) the collision and subduction-related orogen in the east, the *Chittagong–Tripura Fold Belt* (Fig. 5). These geo-provinces have been related to a regional plate tectonic scenario, especially the collision pattern of the Indian Plate with the Burma and Tibetan (Eurasian) Plates.

The sedimentary evolution of the Bengal Basin is thought to have taken place in five main phases, proper understanding of which are crucial to the establishment of separate stratigraphic framework for each of the provinces. The existing stratigraphic schemes for the different provinces have only been partly revised in this study in the light of the tectonic events of regional implications. However, we emphasize that more systematic research, especially on seismic stratigraphy and the paleontological aspects of the sedimentary successions within the provinces with proper age dating will be necessary to formalize these schemes and to improve the correlation between tectonic events and stratigraphy.

Available data suggest that the sediment depocenter of the Bengal Basin changed as the basin configuration changed through time. The Cretaceous sediment depocenter was on the stable shelf in the West Bengal part of the basin. In Eocene, the sediment depocenter shifted to Assam and is represented by well-developed Jaintia Group of sediments of Assam. This also represents the soft collision on the northeastern part of the Indian Plate. By Miocene, the depocenter moved to northeastern part of the Bengal Basin in the Sylhet Trough. During the Pleistocene oscillation of sea level, the sediment depocenter moved throughout the basin. The present sediment depocenter is located in the Hatia Trough and extends to the Bengal Deep Sea Fan.

In recent years, hydrocarbon exploration activities in different parts of the Bengal Basin have gained momentum with the participation of international oil companies. Through their activities new subsurface well-log and seismic data are becoming available, which will be the key to our understanding of the basin-fill history, and also be very useful for the establishment a basinwide stratigraphic framework. We believe that proper understanding of the basinwide stratigraphic framework is essential from the viewpoint of hydrocarbon exploration within the Bengal Basin.

Acknowledgements

We would like to thank the Chairman of BOGMC for giving us permission to use the seismic profiles and well log data from BOGMC and BAPEX. We are grateful to the staff of BAPEX for providing valuable logistic support. Special thanks are due to Dick Murphy and Juergen Lietz for their constructive comments and useful suggestions that benefited the manuscript.

References

Acharyya, S.K., 1994. Accretion of Indo-Australian Gondwanic blocks along Peri-Indian collision margins. 9th International Gondwana Symposium, Hyderabad, India, 1029–1049.

Acharyya, S.K., 1998. Break-up of the greater Indo-Australian continent and accretion of blocks framing south and east Asia. J. Geodyn. 26, 149–170.

Ahmed, S.T., 1968. Cenozoic Fauna of the Cox's Bazar Coastal Cliff. Unpubl. MSc Thesis, Univ. of Dhaka, Dhaka, 68 pp.

Ahmed, A., 1983. Oligocene Stratigraphy and Sedimentation in the

Surma Basin, Bangladesh. Unpubl. MSc Thesis, University of Dhaka, 96 pp.
Alam, M., 1972. Tectonic classification of the Bengal Basin. Geol. Soc. Am. Bull. 83, 519–522.
Alam, M., 1989. Geology and depositional history of Cenozoic sediments of the Bengal Basin of Bangladesh. Palaeogeogr., Palaeoclimetol., Palaeoecol. 69, 125–139.
Alam, M., 1997. Bangladesh. In: Moores, E.M., Fairbridge, R.W. (Eds.), Encyclopedia of European and Asian Regional Geology. Chapman & Hall, London, pp. 64–72.
Alam, M.M., 1991. Paleoenvironmental study of the Barail succession exposed in northeastern Sylhet, Bangladesh. Bangladesh J. Sci. Res. 9, 25–32.
Alam, M.M., 1995a. Tide-dominated sedimentation in the upper tertiary succession of the sitapahar anticline, Bangladesh. In: Flemming, B.W., Bortholma, A. (Eds.), Tidal Signatures in Modern and Ancient Sediments. Int. Assoc. Sedimentol., Spec. Publ. 24, pp. 329–341.
Alam, M.M., 1995b. Sedimentology and depositional environments of the Bengal Basin subsurface Neogene succession based on detailed facies and electrofacies analysis: A case study of the Kailashtila, Rashidpur and Bakhrabad structures in northeastern Bangladesh. NORAD Project BGD-023, Bangladesh Petroleum Institute, Dhaka, 74 pp.
Alderson, A., 1991. The Surma Basin, Bangladesh: A palynostratigraphical manual, geological synthesis and comparison with the adjacent hydrocarbon provinces of N.E. India and Myanmar. Geochem Group, Project No. 4707/003, 194 pp.
Ameen, S.M.M., Khan, M.S.H., Akon, E., Kazi, A.I., 1998. Petrography and major oxide chemistry of some Precambrian crystalline rocks from Maddhapara, Dinajpur. Bangladesh Geosci. J. 4, 1–19.
Ameen, S.M.M., Chowdhury, K.R., Khan, M.S.H., Akon, E., Kabir, M.Z., 2001. Chemical petrology of the Precambrian crystalline basement rocks from Maddhapara, Dinajpur District, Bangladesh. 10th Geological Conf. Bangladesh Geol. Soc., Dhaka, Abstr., p. 63.
Bakhtine, M.I., 1966. Major tectonic features of Pakistan: Part II. The Eastern Province. Sci. Ind. 4, 89–100.
Bakr, M.A., 1977. Quaternary geomorphic evolution of the Brahmanbaria–Noakhali area, Comilla and Noakhali Districts, Bangladesh. Rec. Geol. Surv. Bangladesh 1 (2), 44 pp.
Baksi, A.K., Barman, T.R., Paul, D.K., Farrar, E., 1987. Widespread early Cretaceous flood basalt volcanism in eastern India: geochemical data from the Rajmahal–Bengal–Sylhet Traps. Chem. Geol. 63, 133–141.
Banerji, R.K., 1981. Cretaceous–Eocene sedimentation, tectonism and biofacies in the Bengal basin, India. Palaeogeogr., Palaeoclimetol., Palaeoecol. 34, 57–85.
Banerji, R.K., 1984. Post-Eocene biofacies, palaeoenvironments and palaeogeography of the Bengal basin, India. Palaeogeogr., Palaeoclimetol., Palaeoecol. 45, 49–73.
BAPEX, 1994. Core analysis report of Shahbazpur well no. 1. Unpubls. Report, BAPEX, Dhaka.
BAPEX, 1996. The petroleum geology and hydrocarbon potential of Bangladesh. BAPEX-CORE LAB Report, Petrobangla, Dhaka.
Bender, F., 1983. Geology of Burma. Borntraeger, Berlin, 260 pp.
Bilham, R., England, P., 2001. Plateau "pop-up" in the great 1897 Assam earthquake. Nature 410, 806–809.
BOGMC, 1986. The oil and gas seismic exploration project. The 'Hinge Zone' survey, Western Bangladesh. Interpretation Report, vol. 1, 114 pp.
BOGMC, 1997. Petroleum exploration opportunities in Bangladesh. Bangladesh Oil, Gas and Mineral Corporation (Petrobangla), Dhaka, March, 1997.
Brunnschweiler, R.O., 1966. On the geology of the Indoburman Ranges. Geol. Soc. Aust. J. 13, 127–194.
Brunnschweiler, R.O., 1974. Indoburman ranges. In: Spencer, A.M. (Ed.), Mesozoic–Cenozoic Orogenic Belts. Geol. Soc. London, Spec. Publ., vol. 4, pp. 279–299.
Brunnschweiler, R.O., 1980. Lithostratigraphic monster in modern oil exploration. Proc. 3rd Offshore Southeast Asia Conference, Singapore, 1–7.
Chen, W.P., Molnar, P., 1990. Source parameters of earthquakes beneath the Shillong Plateau and the northern Indo-Burman Ranges. J. Geophys. Res. 95, 12.527–12.552.
Chen, Y., Courtillot, V., Cogné, J.P., Besse, J., Yang, Z., Enkin, R., 1993. The configuration of Asia prior to the collision of India: Cretaceous paleomagnetic constraints. J. Geophys. Res. 98, 21.927–21.941.
Chowdhury, S.Q., 1982. Palynostratigraphy of the Neogene sediments of the Sitapahar anticline (western flank), Chittagong Hill Tracts, Bangladesh. Bangladesh J. Geol. 1, 35–49.
Curray, J.R., 1991a. Geological history of the Bengal geosyncline. J. Assoc. Explor. Geophys. XII, 209–219.
Curray, J.R., 1991b. Possible green schist metamorphism at the base of a 22 km sedimentary section, Bay of Bengal. Geology 19, 1097–1100.
Curray, J.R., Moore, D.G., 1974. Sedimentary and tectonic processes in Bengal deep-sea fan and geosyncline. In: Burk, C.A., Drake, C.L. (Eds.), The Geology of Continental Margins. Springer-Verlag, New York, pp. 617–628.
Curray, J.R., Munasinghe, T., 1989. Timing of intraplate deformation, northeastern Indian Ocean. Earth Planet. Sci. Lett. 94, 71–77.
Curray, J.R., Munasinghe, T., 1991. Origin of the Rajmahal Traps and the 85°E Ridge: preliminary reconstructions of the trace of the Crozet hotspot. Geology 19, 1237–1240.
Curray, J.R., Emmel, F.J., Moore, D.G., Raitt, R.W., 1982. Structure, tectonics and geological history of the northeastern Indian Ocean. In: Nairn, A.E.M., Stehli, F.G. (Eds.), The Ocean Basins and Margins. The Indian Ocean, vol. 6. Plenum, New York, pp. 399–450.
Das Gupta, A.B., 1977. Geology of Assam–Arakan region. Oil Commentary, India 15, 4–34.
Dasgupta, S., Nandy, D.R., 1995. Geological framework of the Indo-Burmese convergent margin with special reference to ophiolitic emplacement. Indian J. Geol. 67 (2), 110–125.
Dasgupta, P.K., Chakrabarti, P.K., Datta, D., 1991. Basinward migrating submarine fan environments from the Barail group in the north Cachar Hills, Assam–Arakan Orogen, India. In: Bouma, A.H., Carter, R.M. (Eds.), Facies Models, pp. 195–217, VSP.

Desikacher, S.V., 1974. A review of the tectonic and geological history of eastern India in terms of plate tectonic theory. J. Geol. Soc. India 15, 134–149.

Dickinson, W.R., Seely, D.R., 1979. Structure and stratigraphy of forearc regions. Am. Assoc. Pet. Geol. Bull. 63, 2164–2182.

Evans, P., 1932. Tertiary succession in Assam. Trans. Min. Geol. Inst. India 27, 155–260.

Evans, P., 1964. Tectonic framework of Assam. J. Geophys. Soc. India 5, 80–96.

Everett, J.R., Orville, R.R., Staskowski, R.J., 1989. Regional tectonics of Myanmar (Burma) and adjacent areas. 7th Thematic Conference on Remote Sensing for Exploration Geology, Calgary, Canada, 1141–1154.

Falvey, D.A., 1974. The development of continental margins in plate tectonic theory. J. Aust. Pet. Explor. Assoc. 14, 95–106.

Gani, M.R., 1999. Depositional history of the Neogene succession exposed in the southeastern fold belt of the Bengal Basin, Bangladesh. MSc Thesis, Univ. of Dhaka, Dhaka, Bangladesh, 61 pp.

Gani, M.R., Alam, M.M., 1999. Trench-slope controlled deep-sea clastics in the exposed lower Surma group in the southeastern fold belt of the Bengal Basin, Bangladesh. Sediment. Geol. 127, 221–236.

Gani, M.R., Alam, M.M., 2002. Trench-slope controlled deep-sea clastics in the exposed lower Surma Group in south-eastern Fold Belt of the Bengal Basin, Bangladesh. Sediment. Geol. (this volume).

Graham, S.A., Dickinson, W.R., Ingersoll, R.V., 1975. Himalayan–Bengal model for flysch dispersal in the Appalachian–Ouachita system. Geol. Soc. Am. Bull. 94, 273–286.

Haq, B.U., Hardenbol, J., Vail, P.R., 1988. Mesozoic and Cenozoic chronostratigraphy and cycles of sea level change. In: Wilgus, C.K., et al. (Eds.), Sea Level Changes: and Integrated Approach, vol. 42, SEPM Special Publications, pp. 71–108.

Hiller, K., Elahi, M., 1988. Structural growth and hydrocarbon entrapment in the Surma basin, Bangladesh. In: Wagner, H.C., Wagner, L.C., Wang, F.F.H., Wong, F.L. (Eds.), Petroleum Resources of China and Related Subjects, Houston, Texas. Circum-Pacific Council for Energy and Mineral Resources Earth Sci. Series, vol. 10, 657–669.

Holtrop, J.F., Keizer, J., 1970. Some aspects of the stratigraphy and correlation of the Surma basin wells, East Pakistan. ESCAFE Miner. Resour. Dev. Ser. 36, 143–154.

Hutchison, C.S., 1989. Geological evolution of South-East Asia. Clarendon Press, London, 368 pp.

Imam, M.B., Shaw, H.F., 1985. The diagenesis of Neogene clastic sediments from the Bengal Basin, Bangladesh. J. Sediment. Pet. 55, 665–671.

Ingersoll, R.N., Graham, S.A., Dickinson, W.R., 1995. Remnant ocean basins. In: Busby, C.J., Ingersoll, R.V. (Eds.), Tectonics of Sedimentary Basins. Blackwell, Oxford, pp. 363–391.

Ismail, M., 1978. Stratigraphical position of Bogra limestone of the platform area of Bangladesh. Proc. 4th Annu. Conf. Bangladesh Geol. Soc., 19–26.

Johnson, S.Y., Alam, A.M.N., 1991. Sedimentation and tectonics of the Sylhet Trough, Bangladesh. Geol. Soc. Am. Bull. 103, 1513–1527.

Kent, R., 1991. Lithospheric uplift in eastern Gondwana: evidence for a long-lived mantle plume system? Geology 19, 19–23.

Khan, A.A., 1991. Tectonics of the Bengal Basin. J. Himalayan Geol. 2 (1), 91–101.

Khan, F.H., 1991. Geology of Bangladesh. The Univ. Press, 207 pp.

Khan, M.R., Muminullah, M., 1980. Stratigraphy of Bangladesh. Petroleum and Mineral Resources of Bangladesh. Seminar and Exhibition, Dhaka, pp. 35–40.

Khan, M.S.H., Ameen, S.M.M., Akon, E., 1997. Petrographic study of some core samples from Precambrian basement, Maddhapara, Dinajpur District, Bangladesh. Bangladesh J. Geol. 16, 55–64.

Khan, M.A.M., Ismail, M., Ahmed, M., 1988. Geology and hydrocarbon prospects of the Surma Basin, Bangladesh. Proc. 7th Offshore Southeast Asia Conference, Singapore, 354–387.

Klootwijk, C.T., Gec, J.S., Peirce, J.W., Smith, G.M., McFadden, P.L., 1992. An early India–Asia contact: paleomagnetic constraints from Ninetyeast Ridge, ODP Leg 121. Geology 20, 395–398.

Lee, T.T., Lawver, L.A., 1995. Cenozoic plate reconstruction of Southeast Asia. Tectonophysics 251, 85–138.

Lee, Y.F.S., Brown, T.A., Shamsuddin, A.H.M., Ahmed, N.U., 2001. Stratigraphic complexity of the Bhuban and Bokabil Formations, Surma Basin, Bangladesh: implications for reservoir management and stratigraphic traps. 10th Geological Conf., Bangladesh Geol. Soc., Dhaka, Abstr., p. 25.

Lietz, J.K., Kabir, J., 1982. Prospects and constraints of oil exploration in Bangladesh. Proc. 4th Offshore Southeast Asia Conference, Singapore, 1–6.

Lindsay, J.F., Holliday, D.W., Hulbert, A.G., 1991. Sequence stratigraphy and the evolution of the Ganges–Brahmaputra Delta complex. Am. Assoc. Pet. Geol. Bull. 75, 1233–1254.

Lohmann, H.H., 1995. On the tectonics of Bangladesh. Swiss Assoc. Pet. Geol. Eng. Bull. 62 (140), 29–48.

Mann, P., Grindlay, N.R., Dolan, J.F., 1999. Subduction to strike–slip transitions on plate boundaries. Geol. Soc. Am. Today 9 (7), 14–16.

Mckenzie, D., Sclater, J.G., 1971. The evolution of the Indian Ocean since the Late Cretaceous. R. Astron. Soc., Geophys. J. 24, 437–528.

Miall, A.D., 1997. The Geology of Stratigraphic Sequences Springer-Verlag, Berlin, 433 pp.

Mitchell, A.H.G., 1981. Phanerozoic plate boundaries in mainland SE Asia, the Himalayas and Tibet. J. Geol. Soc. London 138, 109–122.

Mitchell, A.H.G., 1989. The Shan Plateau and western Burma: Mesozoic–Cenozoic plate boundaries and correlations with Tibet. In: Sengor, A.M.C. (Ed.), Tectonic Evolution of the Tethyan Region. Kluwer Academic Publishing, pp. 567–583.

Mitchell, A.H.G., 1993. Cretaceous–Cenozoic tectonic events in the Western Myanmar (Burma)-Asia region. J. Geol. Soc. London 150, 1089–1102.

Molnar, P., 1987. The distribution of intensity associated with the great 1897 Assam earthquake and bounds on the extent of the rupture zone. Geol. Soc. India J. 30, 13–27.

Morgan, W.J., 1972. Deep mantle plumes and plate motions. Am. Assoc. Pet. Geol. Bull. 56, 8563–8569.

Mukhopadhyay, M., Dasgupta, S., 1988. Deep structure and tectonics of the Burmese arc: constraints from earthquake and gravity data. Tectonophysics 149, 299–322.

Murphy, R.W., Staff of BOGMC, 1988. Bangladesh enters the oil era. Oil Gas J., 76–82, Feb. 29, 1988.

Murthy, M.V.N., Talukdar, S.C., Bhattacharya, A.C., Chakrabarti, C., 1969. The Dauki fault of Assam. Bull. Oil Nat. Gas Comm. (India) 6, 57–64.

Nandy, D.R., 1986. Tectonics, seismicity and gravity of northeastern India and adjoining areas. Geology of Nagaland Ophiolites. Geol. Surv. India, Mem., vol. 119, pp. 13–17.

Ninkovich, D., 1976. Late Cenozoic clockwise rotation of Sumatra. Earth Planet. Sci. Lett. 29, 269–275.

North American Commission on stratigraphic Nomenclature (NACSN), 1983. North American stratigraphic code. Am. Assoc. Pet. Geol. Bull. 67, 841–875.

Partington, M., 2001. The role of nannofossils and palynomorphs in unveiling the Cenozoic stratigraphy of Bangladesh. 10th Geological Conf., Bangladesh Geol. Soc., Dhaka, Abstr., p. 57.

Patzelt, A., Li, H., Wang, J., Appel, E., 1996. Paleomagnetism of Cretaceous to tertiary sediments from southern Tibet: evidence for the extent of the northern margin of India prior to the collision with Eurasia. Tectonophysics 259, 259–284.

Paul, D.D., Lian, H.M., 1975. Offshore basins of southwest Asia—Bay of Bengal to South Sea. Proc. 9th World Petrol Congress, Tokyo, vol. 3, pp. 1107–1121.

Pivnik, D.A., Nahm, J., Tucker, R.S., Smith, G.O., Nyein, K., Nyunt, M., Maung, P.H., 1998. Polyphase deformation in a fore-arc/back-arc basin, Salin Subbasin, Myanmar (Burma). Am. Assoc. Pet. Geol. Bull. 82, 1837–1856.

Rahman, M.A., Blank, H.R., Kleinkopf, M.D., Kucks, R.P., 1990a. Aeromagmetic anomaly map of Bangladesh, scale 1:1 000 000. Geol. Surv. Bangladesh, Dhaka.

Rahman, M.A., Mannan, M.A., Blank, H.R., Kleinkopf, M.D., Kucks, R.P., 1990b. Bouguer gravity anomaly map of Bangladesh, scale 1:1 000 000. Geol. Surv. Bangladesh, Dhaka.

Raju, A.T.R., 1968. Geological evolution of Assam and Cambay Basins of India. Am. Assoc. Pet. Geol. Bull. 52, 2422–2437.

Ramana, M.V., Nair, R.R., Sarma, K.V.L.N.S., Ramprassad, T., Krishna, K.S., Subramanyam, V., D'Cruz, M., Subramanyam, C., Paul, J., Subramanyam, A.S., Chandra Sekhar, D.V., 1994. Mesozoic anomalies in the Bay of Bengal. Earth Planet. Sci. Lett. 121, 469–475.

Rao, A.R., 1983. Geology and hydrocarbon potential of a part of Assam–Arakan basin and its adjoining region. Pet. Asia J. 6, 127–158.

Reimann, K.-U., 1993. Geology of Bangladesh. Borntraeger, Berlin, 160 pp.

Richter, B., Fuller, M., 1996. Paleomagnetism of the Sibumasu and Indochina blocks: implications for the extrusion tectonic model. In: Hall, R., Blundell, D. (Eds.), Tectonic Evolution of Southeast Asia. Geol. Soc. Spec. Publ., vol. 106, pp. 203–224.

Royer, J.Y., Sandwell, D.T., 1989. Evolution of the eastern Indian Ocean since late Cretaceous: constrains from Geosat altimetry. J. Geophys. Res. 94, 13755–13782.

Salt, C.A., Alam, M.M., Hossain, M.M., 1986. Bengal Basin: current exploration of the hinge zone area of southwestern Bangladesh. Proc. 6th Offshore Southeast Asia Conference, Singapore, pp. 55–57.

Saxena, M.N., Naini, B.R., Krishnan, M.S., 1997. India. In: Moore, E.M., Fairbridge, R.W. (Eds.), Encyclopedia of European and Asian Regional Geology. Chapman & Hill, pp. 352–372.

Sclater, J.G., Fisher, R.L., 1974. Evolution of the east central Indian Ocean, with emphasis on the tectonic setting of the Ninetyeast Ridge. Geol. Soc. Am. Bull. 85, 683–702.

Seeber, L., Armbruster, J., 1981. Great detachment earthquakes along the Himalayan arc and long-term forecasts. In: Simpson, D.W., Richards, P.G. (Eds.), Earthquake prediction—an international review. Washington, D.C. Am. Geophy. Union, Maurice Ewing Ser., vol. 4, pp. 259–277.

Sengupta, S., 1966. Geological and geophysical studies in the western part of Bengal Basin, India. Am. Assoc. Pet. Geol. Bull. 50, 1001–1017.

Shamsuddin, A.H.M., Abdullah, S.K.M., 1997. Geological evolution of the Bengal Basin and its implication in hydrocarbon exploration in Bangladesh. Indian J. Geol. 69, 93–121.

Sikder, A.M., 1998. Tectonic Evolution of Eastern Folded Belt of Bengal Basin. Unpubl. PhD Thesis, Dhaka Univ., Dhaka, 175 pp.

Sikder, A.M., Alam, M.M., 2003. 2-D modelling of the anticlinical structures and structural development of the eastern fold belt of the Bengal basin, Bangladesh. Sediment. Geol. (this volume).

Sultana, D.N., Alam, M.M., 2001. Facies analysis of the Neogene Surma group succession in the subsurface of the Sylhet Trough, Bengal Basin, Bangladesh. 10th Geological Conf., Bangladesh Geol. Soc., Dhaka, Abstr., p. 70.

Tapponnier, P., Peltzer, G., Le Dain, A.Y., Armijo, R., Cobbold, P., 1982. Propagating extrusion tectonics in Asia: new insights from simple experiments with plasticine. Geology 10, 611–616.

Tapponnier, P., Peltzer, G., Armijo, R., 1986. On the mechanics of the collision between India and Asia. In: Coward, M.P., Ries, A.C. (Eds.), Collision Tectonics. Blackwell, Oxford, pp. 115–157.

Uddin, M.N., 1994. Structure and sedimentation in the Gondwana basins of Bangladesh. Gondwana Nine, 9th Int. Gondwana Symposium, Hydrabad, India, vol. 2, pp. 805–819.

Uddin, M.N., Ahmed, Z., 1989. Palynology of the Kopili formation at GDH-31, Gaibandha District, Bangladesh. Bangladesh J. Geol. 8, 31–42.

Uddin, M.N., Islam, M.S.U., 1992. Depositional environments of the Gondwana rocks in the Khalashpir basin, Rangpur District, Bangladesh. Bangladesh J. Geol. 11, 31–40.

Uddin, A., Lundberg, N., 1999. A paleo-Brahmaputra? Subsurface lithofacies analysis of Miocene deltaic sediments in the Himalayan–Bengal system, Bangladesh. Sediment. Geol. 123, 239–254.

Uddin, M.F., Uddin, M.J., 2001. Stratigraphy of Chittagong Hill Tracts: some new concepts. 10th Geological Conf., Bangladesh Geol. Soc., Dhaka, Abstr., p. 59.

Varga, R.J., 1997. Burma. In: Moores, E.M., Fairbridge, R.W. (Eds.), Encyclopedia of European and Asian Regional Geology. Chapman & Hall, London, pp. 109–121.

Veevers, J.J., 1982. Western and northwestern margin of Australia. In: Nairn, A.E.M., Stehli, F.G., (Eds.), The Ocean Basins and

Margins: The Indian Ocean, vol. 6, Plenum Press, New York, pp. 513–544.
Wardell, A., 1999. Barapukuria Coal Deposits, Stage 2, Feasibility Study, Geol. Survey Bangladesh–UK Coal Project, No. 4298/7B, Petrobangla, Dhaka.
Walker, R.G., 1990. Facies modeling and sequence stratigraphy. J. Sediment. Pet. 60, 777–786.
Wilcox, R.E., Harding, T.P., Seely, D.R., 1973. Basic wrench tectonics. Am. Assoc. Pet. Geol. Bull. 57, 74–96.
Zaher, M.A., Rahman, A., 1980. Prospects and investigations for minerals in the northwestern part of Bangladesh. Petroleum and Mineral Resources of Bangladesh. Seminar and Exhibition, Dhaka, pp. 9–18.

Annex B67

Nanna Roos et al., "Small Indigenous Fish Species in Bangladesh: Contribution to Vitamin A, Calcium and Iron Intakes, Animal Source Foods to Improve Micronutrient Nutrition and Human Function in Developing Countries", *Journal of Nutrition*, Vol. 133, No. 11 (2003)

JN THE JOURNAL OF NUTRITION

Animal Source Foods to Improve Micronutrient Nutrition and Human Function in Developing Countries

Small Indigenous Fish Species in Bangladesh: Contribution to Vitamin A, Calcium and Iron Intakes[1,2]

Nanna Roos,*[3] Mohammed M. Islam† and Shakuntala H. Thilsted*

*Research Department of Human Nutrition, The Royal Veterinary and Agricultural University, Frederiksberg, Denmark and †Mymensingh Aquaculture Extension Project, Mymensingh, Bangladesh

ABSTRACT Fish play an important role in the Bangladeshi diet, constituting the main and often irreplaceable animal source food in poor rural households. Fish consumption is dominated by wild small (length <25 cm) indigenous fish species (SIS). The vitamin A content in SIS varies, from <100 μg of retinol equivalents (RE)/100 g raw edible parts, to >2,500 μg RE/100 g raw edible parts in mola (*Amblypharyngodon mola*). The study addressed the dietary contribution of fish to vitamin A, calcium and iron intakes and the potential of integrating SIS, including mola, into existing carp polyculture ponds. Fish consumption (wild and cultured fish) was surveyed by 5-d recall interviews in 84 poor rural households in Kishoreganj district in 1997–1998. Fifty-nine of the households cultured carp and SIS in small (mean size 400 m^2) domestic ponds. Total household fish consumption was unaffected by the domestic aquaculture production. SIS from wild sources contributed 84% of the total fish consumption. In the peak season (October), SIS contributed 40% (median 23%) of the recommended vitamin A intake at the household level ($n = 84$). Thirty-four households cultured mola along with carp. Cultured mola used for household consumption contributed 20% (median 18%) of the recommended intake of vitamin A at the household level. Wild SIS is an important source of vitamin A and calcium in Bangladesh. Mola can be integrated in existing carp culture without negative effects and can contribute to increased vitamin A intake in rural households. J. Nutr. 133: 4021S–4026S, 2003.

KEY WORDS: • *Bangladesh* • *vitamin A* • *calcium* • *iron* • *aquaculture*

Rice and fish dominate the diet of Bangladeshis to such an extent that the old proverb, "machee bhatee bangali," which can be translated as "fish and rice make a Bengali," continues to hold true. Fish is an essential and irreplaceable food in the rural Bangladeshi diet. Together with boiled rice, which is eaten at least twice per d, small amounts of vegetables and fish make up the typical meal. Meat, pulses and fruits are eaten less frequently and in smaller amounts. In the national nutrition survey conducted in rural Bangladesh in 1981–1982, average fish intake was 23 g raw fish/person/d, whereas average meat consumption was 5 g/person/d (1). Rice contributed >80% of the dietary energy and protein. In terms of weight of food consumed, fish ranks third after rice and vegetables. More recent regional studies have confirmed the importance of fish in the Bangladeshi diet (2,3). Fish intake is affected by several factors, such as year, season, location, water level and household income. **Table 1** shows regional and seasonal fish intakes from selected studies in Bangladesh.

Small indigenous fish species (SIS)[4], which are defined as species attaining a maximum length of 25 cm (4,5) contribute considerably to total fish intake. A study conducted in Mymensingh, Northern Bangladesh showed that fish intake increased with income (6).

Fish provide the main source of income to ~2 million households that either fish for a profession or are involved in related trades (7). Many more households catch fish for a part-time income and for food. In communities with access to fisheries, studied by the International Center for Living Aquatic Resources Management, an estimated 87% of all households caught fish for some part of the year (8).

The role of fisheries and aquaculture

Bangladesh is dominated by floodplains and rivers, which are rich ecosystems for freshwater fish. The floodplains, which comprise over half of the country, are inundated annually

[1] Presented at the conference "Animal Source Foods and Nutrition in Developing Countries" held in Washington, D.C. June 24–26, 2002. The conference was organized by the International Nutrition Program, UC Davis and was sponsored by Global Livestock-CRSP, UC Davis through USAID grant number PCE-G-00-98-00036-00. The supplement publication was supported by Food and Agriculture Organization, Land O'Lakes Inc., Heifer International, Pond Dynamics and Aquaculture-CRSP. The proceedings of this conference are published as a supplement to *The Journal of Nutrition*. Guest editors for this supplement publication were Montague Demment and Lindsay Allen.

[2] The study was funded by The Council for Development Research, Danish International Development Assistance (DANIDA), Ministry of Foreign Affairs, Denmark (project no. 104.Dan.8/684).

[3] To whom correspondence should be addressed. E-mail: nanna.roos@get2net.dk.

[4] Abbreviations used: MAEP, Mymensingh Aquaculture Extension Project; NCR, Nutrient Contribution Ratio; SIS, small indigenous fish species.

TABLE 1

Fish intake in Bangladesh from selected studies[1]

Location	Year/season		SIS[2] g/person/d	Large fish[3] g/person/d	Total fish g/person/d	Method	Reference
Rural Bangladesh	1981–1982	Annual	NA	NA	23	600 hh, 12 locations, 24-h food weighing	(1)
Manikganj	1995	Oct–Nov	28 ± 45(8)	29 ± 51(0)	57 ± 62(42)	152 hh, 769 individuals, 24-h food weighing	Inge Tetens (unpublished); (3)
	1996	Jan–Mar	25 ± 47(0)	12 ± 36(0)	37 ± 56(19)	145 hh, 717 individuals, 24-h food weighing	
Mymensingh	1995	Oct–Nov	14 ± 33(0)	24 ± 38(6)	38 ± 47(25)	152 hh, 765 individuals, 24-h food weighing	
	1996	Jan–Mar	12 ± 22(0)	20 ± 34(0)	32 ± 37(24)	146 hh, 729 individuals, 24-h food weighing	
Kapasia							
Small farm	1998–1999	Aug–Jul	NA	NA	83	20 hh, 84 d, 24-h food weighing	(19)
Medium farm	1998–1999	Aug–Jul	NA	NA	85	36 hh, 84 d, 24-h food weighing	
Large farm	1998–1999	Aug–Jul	NA	NA	96	12 hh, 84 d, 24-h food weighing	
Mymensingh							
Low income	1997	Feb–May	12 ± 17(4)	8 ± 13(2)	20 ± 21(14)	104 hh, 24-h recall	(6)
Medium income			13 ± 19(4)	12 ± 18(3)	26 ± 26(19)	104 hh, 24-h recall	
High income			14 ± 19(6)	16 ± 21(3)	29 ± 26(24)	105 hh, 24-h recall	
Low income	1997	Jun–Sep	21 ± 24(136)	9 ± 16(0)	30 ± 27(23)	104 hh, 24-h recall	
Medium income			30 ± 38(18)	11 ± 17(3)	41 ± 38(30)	104 hh, 24-h recall	
High income			28 ± 31(21)	13 ± 26(0)	41 ± 37(32)	105 hh, 24-h recall	
Dinajpur (Ashurar Beel)	1999	Feb–May	8 ± 7(6)	5 ± 8(3)[4]	13 ± 11(11)	90 hh, 24-h food weighing, 7 d/mo	Paul Thompson (unpublished)
		Jun–Sep	24 ± 19(20)	2 ± 4(0)[4]	26 ± 19(23)		
		Oct–Dec	29 ± 17(25)	5 ± 7(3)[4]	34 ± 19(31)		
Kishorganj (Kali Nadi)	1999	Jan–May	18 ± 9(16)	8 ± 7(6)[4]	26 ± 14(23)	90 hh, 24-h food weighing, 7 d/mo	
		Jun–Sep	20 ± 10(19)	9 ± 8(7)[4]	28 ± 13(26)		
		Oct–Dec	28 ± 15(25)	12 ± 12(8)[4]	40 ± 21(36)		

[1] Values are means ±SD (median). All values are raw whole fish, except values from Manikganj and Mymensingh 1995–1996, which are raw edible parts.
[2] Small indigenous fish species defined as species attaining a maximum length of 25 cm.
[3] Large fish include fish species attaining a maximum length of >25 cm.
[4] The species magur, rita, baila, bara baim, bhangon and kakila are included as large fish in this study.
hh, households; NA, data not available.

during the monsoon season, and agriculture and natural fisheries complement one another. In the monsoon to postmonsoon season (June–November), the floodplains provide an ideal habitat for the wide diversity of wild fish species, whereas in the dry season, the land is cultivated with rice.

Since the green revolution, Bangladesh has made tremendous strides in increasing rice production. This success has taken place through many changes in the overall agricultural production and the management of land and water. More areas have been brought under rice production, irrigation has expanded greatly and large areas have been drained and protected by flood control embankments. These changes have been at the expense of fish: the area of inland water and the duration of inundation have decreased, so there has been a reduction in the habitat for fish.

Fish catches relative to area are reported to have decreased by 81% in waters affected by flood protection (9). Although official figures show that the number of floodplain fisheries increased in the 1990s, after decreasing in the 1980s, it is widely held that floodplain catches have been falling. This apparent discrepancy may be due to more intensive monitoring of floodplain stocking in the early to mid-1990s as well as differences in the areas monitored (7,10).

Although capture fisheries dominate total production, freshwater aquaculture production has grown rapidly, and contributes an increasing share of fish available for consumption. Fish from aquaculture trebled in the period from 1989 to 1999 (11). The proportion of cultured ponds increased from 27% to 52% between 1984 and 1996 (12). Cultured ponds typically yield 1.0–3.7 tons fish/hectare/y (t/ha/y) (7), whereas noncultured ponds yield ~0.5 t/ha/y. About 85% of fish produced in ponds are carp (11), either exotic carp species such as silver carp (*Hypothalmichthys molitrix*) or common carp (*Cyprinus carpio*), or indigenous carp species such as rui (*Laboe rohita*) and mrigal (*Cirrhinus cirrhosus*; alternative scientific name is *Cirrhinus mrigala*). This has important implications for the availability of fish for poor people and the nutritional contribution of the fish that is consumed.

Nutritional contribution of fish

The importance of fish as a rich source of animal protein is well established and this is frequently used to justify fish as a valuable food, whereas very little attention has been given to the role of fish in supplying vitamin A and minerals in the diet. The protein content of fish ranges from 14 to 18 g/100 g raw

edible parts (13). From the last national survey in rural Bangladesh, the mean total protein intake was 48 g/person/d, of which fish contributed 3 g (1). The value of fish in the Bangladeshi diet should not focus on the contribution made to protein, because protein recommendations in the typical diet are met provided that the energy recommendations are met (5). Rather, focus should be placed on the composition of the fish and the contribution of micronutrients, especially vitamin A and minerals, from the different types of fish species.

The variation in vitamin A content in fish species is extreme (14). The content per 100 g raw edible parts in 27 species ranged from <100 μg RE in most species to 2680 μg RE (SD = 220, $n = 7$ samples) in mola (*Amblypharyngodon mola*). Based on their vitamin A content, species can be categorized as shown in **Table 2**. Species with very high, high and medium vitamin A content are all SIS, whereas other SIS and cultured carp species have a low vitamin A content.

Most of the vitamin A in fish is concentrated in the eyes and viscera (14). This distribution makes the cleaning practice extremely important for the retention of vitamin A. Cleaning practices depend on the fish species, size of fish and the person cleaning the fish. The waste can include the gill cover, jaw, head, tail and/or viscera (partial or full). For mola, the head and eyes are normally included as edible parts (5,14). Vitamin A in fish is found as retinol and dehydroretinol isomers. In mola, 80–90% of the total vitamin A is present as dehydroretinol (14). In estimating the total vitamin A content, it is estimated that the dehydroretinol isomers have 40% of the biological activity of all-*trans* retinol (15).

The mineral content of fish, unlike its vitamin A content, is apparently not species specific. The content of total iron and calcium in some commonly consumed Bangladeshi fish is shown in **Table 3**. Small fish are generally eaten with bones, although some bones may be discarded as plate waste, whereas in large fish most or all bones are discarded as plate waste. Therefore, small fish are an excellent source of calcium. In studies with both humans and rats it is shown that the bioavailability of calcium from whole small fish (mola) is as high as that from milk. In humans, the fractional calcium absorption is found to be 24 ± 6% from small fish and 22 ± 6% from milk (16).

SIS in aquaculture

Floodplain fisheries are still the main source of fish eaten by rural people, with SIS contributing the most. However, with the present trends of decreasing floodplain fisheries and increasing aquaculture, the total fish intake may fall and a larger proportion of SIS in the Bangladeshi diet will be substituted by carp. This will have a negative impact on the nutritional contribution from fish, especially because the content of vitamin A and calcium is very much less in carp species than in SIS. To maintain and enhance SIS intake, sustainable management and restoration of floodplain fisheries must be given high priority. However, the drainage of floodplains and the increasing population limit the scope. Rather, incorporating nutrient-dense fish species in the production systems used in the continued expansion of aquaculture is a means of abating the above trends.

TABLE 2

Categories of Bangladeshi fish species based on vitamin A content in edible parts[1]

Category of fish species	Vitamin A content RE/100 g raw edible parts	Common name[2]	Scientific name
Very high content	>1500	Mola (SIS)	*Amblypharyngodon mola*
		Chanda (SIS)	*Parambassis baculis*
High content	500–1500	Dhela (SIS)	*Osteobrama cotio cotio*
		Darkina (SIS)	*Esomus danricus*
Medium content	100–500	Chanda (SIS)	*Parambassis ranga*
		Koi (SIS)	*Anabas testudineus*
		Golsha tengra (SIS)	*Mystus bleekeri*
		Chanda (SIS)	*Chanda nama*
		Taki (SIS)	*Channa punctata*
		Chela (SIS)	*Chela cachius*
Low content	<100	Baim (SIS)	*Macrognathus aculeatus*
		Baim (SIS)	*Macrognathus pancalus*
		Kachki (SIS)	*Corica soborna*
		Gutum (SIS)	*Lepidocephalus guntea*
		Chapila (SIS)	*Gudusia chapra*
		Puti (SIS)	*Puntius chola*
		Puti (SIS)	*Puntius sophore*
		Khalisha (SIS)	*Colisha fasciatus*
		Shing (SIS)	*Heteropneustes fossilis*
		Magur (SIS)	*Clarias batrachus*
		Baim (SIS)	*Mastacembelus armatus*
		Puti (SIS)	*Puntius ticto*
		Chata (SIS)	*Colisa lalia*
		Tilapia (small exotic species)	*Oreochromis niloticus*
		Mrigel (large indigenous species)	*Cirrhinus cirrhosus*
		Rui (large indigenous species)	*Labeo rohita*
		Silver carp (large exotic species)	*Hypophthalmichthys molitrix*
		Hilsha (large indigenous species)	*Tenualosa ilisha*
		Common carp[2] (large exotic species)	*Cyprinus carpio*
		Grass carp[2] (large exotic species)	*Ctenopharyngodon idella*

[1] Fish species listed in descending order of vitamin A content in each category.
[2] From (20).

JN THE JOURNAL OF NUTRITION

TABLE 3

Mineral content in some commonly consumed Bangladeshi fish species[1]

Common name	Scientific name	n[2]	Fe (mg/100 g raw edible parts)	Ca (mg/100 g raw edible parts)	Ca[3] (mg/100 g raw edible parts corrected for plate waste)	Dry matter (%)
SIS:						
Baim/Chikra	Macrognathus aculeatus, Macrognathus pancalus, Mastocembelus armatus	5	2.4 ± 0.4	462 ± 56	203 ± 25	25 ± 1
Chanda	*Parambassis ranga, Parambassis baculis*, Chanda nama	5	1.8 ± 0.7	955 ± 342	878 ± 314	24 ± 2
Chapila	Gudusia chapra	3	7.6 ± 5.3	1063 ± 51	786 ± 38	27 ± 3
Darkina	Esomus danricus	3	12.0 ± 9.1	891 ± 357	775 ± 321	23 ± 3
Kachki	Corica soborna	2	2.8 ± 1.2	476 ± 37	347 ± 34	16 ± 1
Mola	Amblypharyngodon mola	3	5.7 ± 3.7	853 ± 86	776 ± 78	20 ± 1
Puti	*Puntius sophore, Puntius chola*, Puntius ticto	4	3.0 ± 0.9	1171 ± 216	784 ± 145	25 ± 1
Taki	Channa punctuatus	3	1.8 ± 0.4	766 ± 183	337 ± 81	22 ± 1
Tengra	Mystus vittatus	2	4.0 ± 0.4	1093 ± 334	480 ± 147	26 ± 4
Shrimp (Chingri)	Macrobracium sp.	3	3.1 ± 2.2	687 ± 23	687 ± 23	21 ± 2
Large fish						
Mrigel	Cirrhinus cirrhosus	3	2.5 ± 1.3	960 ± 104	0 ± 0	24 ± 3
Silver carp	Hypophthamichthys molitrix	3	4.4 ± 1.8	903 ± 361	37 ± 14	23 ± 2

[1] Values are means ± SD of n samples.
[2] n = number of samples. A sample contained 10–300 fish for SIS and 1–2 fish for larger fish.
[3] Calcium content of raw edible parts is corrected for plate waste using a correction factor based on the proportion of a species reported to be eaten without bones (5).

A field study was therefore conducted with the aim of investigating the production potential and nutritional benefits of integrating mola and other SIS in carp polyculture in small seasonal ponds. The readily available carp polyculture production systems practiced in ponds can be altered to include the production of SIS by using simple technologies and local resources. The production and profitability of carp and SIS cultures were measured, as well as the nutritional contribution of the fish produced in relation to the total fish consumption in the household. The study was conducted in collaboration with the Mymensingh Aquaculture Extension Project (MAEP) in Kishoreganj district, northern Bangladesh. Through local extension officers, MAEP trains poor farmers in carp culture in small homestead ponds. A semiintensive carp production system is practiced, based on the use of local low grade feeds and fertilizers (rice bran, banana leaves, manure) supplemented by chemical fertilizers (urea and phosphate). A production of 2–4 t/ha/y is obtained compared to 0.5 t/ha/y in ponds having wild fish. From 1989 to 1999, >40,000 farmers were trained. MAEP is implemented jointly by the government of Bangladesh, Danish International Development Assistance and a number of local nongovernmental organizations.

METHODS AND SUBJECTS

Fifty-nine poor rural households with small seasonal ponds were selected in Kishoreganj District. The households owned <0.8 ha land and had an annual income of <35,000 taka ($780 in U.S. dollars). From June 1997 to January 1998, the field trial was conducted. The ponds (mean size 396 m^2, range 212–850 m^2) were stocked with fingerlings of silver carp, grass carp (*Ctenopharyngodon idella*), mrigal, common carp and rui, with a mean fish size of 35 g, a ratio of 8:4:4:1 and at a density of 8,500/ha. In 34 of the ponds, mature mola, with a mean size of 1.6 g/fish, was stocked with the carps at a density of 25,000 mola/ha. Mola was collected from local ponds that had natural stocks. In 25 ponds, carp species were cultured with the other SIS. The culture period ranged from 6 to 8 mo. Small amounts of cheap local feed (rice bran, duckweed and banana leaves) were used and the ponds were fertilized with cow dung, urea and phosphate. Details of the pond management have been reported (5,17).

The total fish consumption, including fish bought in the local markets, captured from wild stocks and harvested from the ponds, was surveyed in the 59 households participating in the trial, as well as in a control group of 25 neighboring nonfish-producing households with similar socioeconomic status. This was done three times: preharvest season (July, 1997), harvest season (October, 1997) and postharvest season (February, 1998), using a recall method. The head of the household and the housewife were jointly interviewed about the fish consumption of the household in the past 5 d. Fish species, origin, price, amount of raw fish cooked and the parts of the fish consumed were recorded. The amount of fish was estimated from fish models, and the amount of raw edible parts was calculated by subtracting the cleaning waste (5). The average cleaning waste of SIS was 13% of the whole fish, whereas for large fish it was 22% of the whole fish, including 8% plate waste consisting mainly of bones. The nutritional contribution from fish is presented as a Nutrient Contribution Ratio

TABLE 4

The economics of carp and mola production in ponds[1]

	Taka × 1,000/ha/season[2]
Carps, value	73.6 ± 26.6
Mola, value	5.0 ± 4.6
Expenditures	48.7 ± 11.1
Net profit	28.1 ± 23.9

[1] Values are means ± SD for 34 ponds.
[2] U.S. $1 = 48 taka (1997). The production season ranged from 6 to 8 mo.

TABLE 5

Seasonal household fish consumption and Nutrient Contribution Ratio (NCR) in rural households[1,2]

		Consumption			NCR		
	N	SIS[3] (g/person/d)	Large fish (*g/person/d*)	Total (*g/person/d*)	Vitamin A (%)	Calcium (%)	Iron[4] (%)
July, 1997	84	28 ± 26(21)	10 ± 17(5)	37 ± 33(27)	16 ± 20(8)	16 ± 10(14)	4 ± 3(3)
October, 1997	84	65 ± 55(45)	18 ± 25(7)	82 ± 65(64)	40 ± 49(23)	31 ± 21(26)	9 ± 7(6)
February, 1998	84	38 ± 40(25)	16 ± 18(12)	55 ± 48(42)	20 ± 29(6)	20 ± 19(14)	7 ± 5(5)

[1] Values are means ±SD (median).
[2] Expresses a nutrient intake relative (%) to the sex- and age-specific recommended intakes (20) on household level. Values are means ± SD (median).
[3] SIS, small indigenous fish species.
[4] Based on recommended iron intakes for diets with low iron bioavailability.

(NCR), which expresses the intake of a nutrient from fish as a percentage of the FAO/WHO recommended intake (18). Fish consumption was recorded at the household level, and the recommended intake was totaled for all household members, based on sex- and age-specific recommendations.

RESULTS

Fish production and profit

The average total fish production was 2.87 t/ha (SD = 0.9, n = 59) for a 7-mo production season. The mean fish production was similar in the 34 ponds in which carp species were cultured with mola and the 25 ponds with carp and other SIS. The mean production of mola was 0.34 t/ha/season (SD = 0.21, n = 34). Mola contributed 10.3% of the total fish production in the 34 carp-mola ponds. A summary of the economics of the carp-mola ponds is shown in **Table 4**. The mean net income from pond production, including the value of the consumed fish, was 1230 taka/household/season ($30/household/season in U.S. dollars).

Within the range of a total fish production of 0.71–4.42 t/ha/season recorded in the 59 trial ponds, there was no indication of a negative correlation between the production of SIS and total carp production when either parametric (analysis of covariance) or nonparametric (similarity ranking) statistical methods were used (5).

Fish consumption and contribution to vitamin A and calcium intakes

Fish was consumed daily in 48% of the households in October 1997 and in 25% of the households in July 1997 and February 1998. Ninety-eight percent of the households consumed fish at least 1 d out of the 5 d surveyed in all seasons. The diversity of fish species in the diet was high. A total of 44 fish species by common names was recorded, comprising up to 60 scientifically distinct species. SIS dominated the total fish intake in terms of amount as well as frequency of consumption, contributing 84% of the total fish intake. There was no difference in fish intake in the fish-producing households (n = 59) and the nonfish-producing control households (n = 25). Fish bought in the local markets and wild-captured fish contributed >90% of the total fish consumption in both the fish-producing as well as the nonfish-producing households. The seasonal fish consumption and the NCR for vitamin A, calcium and iron are shown in **Table 5**. The contribution to the recommended iron intake was modest and depended on the assumption made for bioavailability. Fish contributed <10% of the recommended protein intake.

Forty-seven percent of the mola harvested from the 34 carp-mola ponds was consumed in the households, contributing an average of 4 g raw edible parts/person/d. This amount of mola was sufficient to cover 21% (median = 18%) of the recommended intake of vitamin A of the household in the 7-mo production season. NCR for iron, calcium and protein from SIS harvested from the ponds were all low, <5%.

The consumption survey confirmed that fish is an important part of the diet of most people in rural Bangladesh. Fish was eaten in small amounts, but with a high frequency in nearly all households. Changes in fish supply and species available for consumption therefore affect the diets of most people in rural Bangladesh. Floodplain fisheries are the main source of fish for consumption, and aquaculture in small homestead ponds has little impact on the household fish consumption. In Bangladesh, aquaculture is typically a secondary activity, supplementing more traditional farming activities. Nevertheless, aquaculture can make an important nutritional contribution through the production of vitamin A–dense SIS. By integrating vitamin A–dense SIS, such as mola, with existing carp production in semiintensive cultured ponds, the nutritional quality of the production can be improved without any negative impact on the total fish production. This production system offers great potential for providing a valuable source of dietary vitamin A in rural Bangladesh. If only 10 kg/y of mola were produced in each of the estimated 1.3 million ponds in Bangladesh, the annual recommended vitamin A intake of >2 million children would be met.

LITERATURE CITED

1. Ahmad, K. & Hassan, N. (1983) Nutritional Survey of Rural Bangladesh 1981–82. Institute of Nutrition and Food Sciences, Dhaka University, Dhaka, Bangladesh.
2. Minkin, S. F., Rahman, M. M. & Halder, S. (1997) Fish biodiversity, human nutrition and environmental restoration in Bangladesh. In: Openwater Fisheries of Bangladesh (Tsai, C. & Ali, M. Y., eds.), pp. 75–88. The University Press Limited, Dhaka, Bangladesh.
3. Hels, O., Hassan, N., Tetens, H. & Thilsted, S. H. (2002) Food consumption, energy and nutrient intake and nutritional status in rural Bangladesh: changes from 1981–82 to 1995–96. Eur. J. Clin. Nutr. 57: 586–594.
4. Felt, R. A., Rajts, F. & Akhteruzzaman, D. (1998) Small Indigenous Fish Species Culture in Bangladesh. Project ALA/92/05/02. Integrated Food Assisted Development Project (IFADEP), Dhaka, Bangladesh.
5. Roos, N. (2001) Fish consumption and aquaculture in rural Bangladesh: nutritional contribution and production potential of culturing small indigenous fish species (SIS) in pond polyculture with commonly cultured carps. Doctoral

thesis. Research Department of Human Nutrition, The Royal Veterinary and Agricultural University, Frederiksberg, Denmark.

6. Bouis, H., de la Briére, B., Hallman, K., Hassan, N., Hels, O., Quabili, W., Quisumbing, A., Thilsted, S. H., Zihad, Z. H. & Zohir, S. (1998) Commercial vegetable and polyculture fish production in Bangladesh: their impacts on income, household resource allocation and nutrition. Final project report to DANIDA and USAID. International Food Policy Research Institute (IFPRI), Washington D.C.

7. Thompson, P. M., Sultana, P., Roos, N., & Thilsted, S. H. (2002) Changing significance of inland fisheries for livelihoods and nutrition in Bangladesh. J. Crop. Prod. 6: 249–318.

8. Thompson, P. M. & Hossain, M. M. (1998) Social and distributional issues in open water fisheries management in Bangladesh. In: Inland Fishery Enhancements. FAO expert consultation on inland fishery enhancements, April 7–11 1997. FAO Technical Paper No. 374, pp. 351–370. Food and Agriculture Organization of the United Nations (FAO), Rome, Italy.

9. Overseas Development Administration of United Kingdom. (1997) Impacts of flood control and drainage with or without irrigation (FCD/I). Project on fish resources and fishing community in Bangladesh: executive summary of Flood Action Plan (FAP)—17. In: Openwater Fisheries of Bangladesh (Tsai, C. & Ali, M. Y., eds.), pp. 199–212. The University Press Limited, Dhaka, Bangladesh.

10. Ali, M. Y. (1999) Openwater fisheries management issues and future strategies. Paper presented at the National Workshop on Community-Based Fisheries Management and Future Strategies for Inland Fisheries in Bangladesh, October 24–25, 1999. Dhaka, Bangladesh.

11. DOF. (2000) Fish catch statistics of Bangladesh 1998–1999. Department of Fisheries (DOF), Dhaka, Bangladesh.

12. DOF. (1996) Fish catch statistics of Bangladesh 1995–1996. Department of Fisheries (DOF), Dhaka, Bangladesh.

13. Darnton-Hill, I., Hassan, N., Karim, R. & Duthie, M. R. (1988) Tables of nutrient composition of Bangladeshi foods. English version with particular emphasis on vitamin A content. Helen Keller International, Dhaka, Bangladesh.

14. Roos, N., Leth, T., Jakobsen, J. & Thilsted, S. H. (2002) High vitamin A content in some small indigenous fish species in Bangladesh: perspectives for food-based strategies to reduce vitamin A deficiency. Int. J. Food Sci. Nutr. 53: 425–437.

15. Shantz, E. M. & Brinkman, J. H. (1950) Biological activity of pure vitamin A2. J. Biol. Chem. 183: 467–471.

16. Larsen, T., Thilsted, S. H., Kongsbak, K. & Hansen, M. (2000) Whole small fish as a rich calcium source. Br. J. Nutr. 83: 191–196.

17. Roos, N., Islam, Md. M., Thilsted, S. H., Ashrafuddin, Md., Mursheduzzaman, Md., Mohsin, D. M. & Shamsuddin, A. B. M. (1999) Culture of mola (*Amblypharyngodon mola*) in polyculture with carps—experience from a field trial in Bangladesh. NAGA-ICLARM Quarterly. 22: 16–19.

18. FAO/WHO. (2002) Human vitamin and mineral requirements. Report of a joint FAO/WHO consultation, Bangkok, Thailand. Food and Agriculture Organization of the United Nations (FAO), Rome, Italy.

19. Thompson, P. M., Sultana, P., Nuruzzaman, M., Khan, A. K. M. F. & Islam, S. M. N. (2000) Fisheries extension evaluation project. Final Report. International Center for Living Aquatic Resource Management (ICLARM) and Department of Fisheries (DOF), Dhaka, Bangladesh.

20. Puwastien, P., Burlingame, B., Raroengwichit, M. & Sungpuag, P. (2000) ASEAN food composition tables. Institute of Nutrition, Mahidol University (INMU), ASEANFOODS Coordinator and INFOODS Regional Database Centre, Bangkok, Thailand.

JN THE JOURNAL OF NUTRITION

Annex B68

T. Pal et al, "Geodynamic evolution of the outer-arc-forearc belt in the Andaman Islands, the central part of the Burma-Java subduction complex", *Geological Magazine,* Vol. 140, No. 3 (2003)

Geol. Mag. **140** (*3*), *2003, pp. 289–307.* © *2003 Cambridge University Press*
DOI: 10.1017/S0016756803007805 *Printed in the United Kingdom*

Geodynamic evolution of the outer-arc–forearc belt in the Andaman Islands, the central part of the Burma–Java subduction complex

TAPAN PAL*, PARTHA PRATIM CHAKRABORTY†,
TANAY DUTTA GUPTA* & CHANAM DEBOJIT SINGH*

*Op: WSA, ER, Geological Survey of India, DK-Block, GSI Complex, Karunamoyee, Salt Lake, Kolkata-700 091, India
†Department of Applied Geology, Indian School of Mines, Dhanbad-926 004, India

(*Received* 14 May 2002; *accepted* 30 January 2003)

Abstract – The Andaman Islands, the central part of Burma–Java subduction complex, expose tectonostratigraphic units of an accretionary prism in an outer-arc setting and turbidites of a forearc setting. A number of N–S-trending dismembered ophiolite slices of Cretaceous age, occurring at different structural levels with Eocene trench-slope sediments, were uplifted and emplaced by a series of E-dipping thrusts. Subsequently, N–S normal and E–W strike-slip faults resulted in the development of a forearc basin with deposition of Oligocene and Mio-Pliocene sediments. Metapelites and metabasics of greenschist to amphibolite grade occur in a melange zone of ophiolites. The Eocene Mithakhari Group represents pelagic trench sediments and coarser clastics derived from ophiolites. Evidence of frequent facies changes, predominance of mass flow deposits, syn-sedimentary basinal disturbance and wide palaeogeographic variation indicate deposition of Eocene sediments in isolated basins of an immature trench-slope setting. Deposition of the Oligocene Andaman Flysch Group in a forearc setting is indicated by the large-scale persistence of beds, lack of small-scale lithological variation, bimodal provenance, less deformation, a well-defined submarine fan sequence and development predominantly on the eastern part of the outer arc. The Mio-Pliocene Archipelago Group includes alternations of siliciclastic turbidites and subaqueous pyroclastic flow deposits in the lower part and carbonate turbidites in the upper part, suggesting its deposition in the shallower forearc compared to the siliciclastic Oligocene sediments.

Keywords: accretionary prisms, ophiolite, Andaman Islands, Java Trench, fore-arc basins, trenches.

1. Introduction

In modern subduction settings the relationships of different geological processes and their products are poorly understood due to the limited scope for on-land studies and variable tectonic controls in different convergent margins (Dickinson & Seely, 1979; Underwood & Bachanan, 1982; Moore, Curray & Emmel, 1982). The understanding of accretionary processes in trench-slope basin margins depends heavily on geological and geophysical data obtained from the DSDP and ODP projects (Karig, 1974; Seely, Vail & Walton, 1974; Karig & Sharman, 1975). Geological mapping of the subaerially exposed parts of active subduction zone, coupled with marine geophysical transects across trenches, helps in understanding the processes and their products of modern subduction (Moore *et al*. 1980).

The Andaman Islands, representing the central part of the 5000 km long Burma–Sunda–Java subduction complex, display major tectono-stratigraphic elements striking approximately parallel to the trend of the Java Trench (Fig. 1a). West of the Andaman Islands the oceanic part of the Indian plate is subducting towards the east below the oceanic part of the Southeast Asian plate (Seely, Vail & Walton, 1974). The Andaman Sea, lying east of these Islands, is a pull-apart basin rather than a typical backarc basin (Curray, 1988; Maung, 1987). Young volcanoes of the Barren and Narcondam Islands, lying 150 km east of the main islands within the Andaman Sea, are interpreted as the inner arc. West of the Andaman Islands the Java trench has little expression in the gravity field (20 mgal) towards Burma but stronger signatures (100 mgal) towards the south (near Nicobar) (Mukhopadhyay, 1988). The subducted slab dips towards the east below Burma but whether or not it is active at present is uncertain (Satyabala, 1998; Guzman-Speziale & Ni, 2000). Seismic data from the Andaman Islands and Andaman Sea also indicate a Benioff zone dipping 40–55° towards the east and record epicentres at 200 km focal depth (cf. Mukhopadhyay, 1988). This terrain offers scope for in-depth study of different tectono-sedimentary processes in the evolution of the outer-arc and associated forearc belt.

The southern margin of Tibet and the Sunda Arc possibly formed a continuous arc system before the

† Author for correspondence: partha_geology@yahoo.co.in

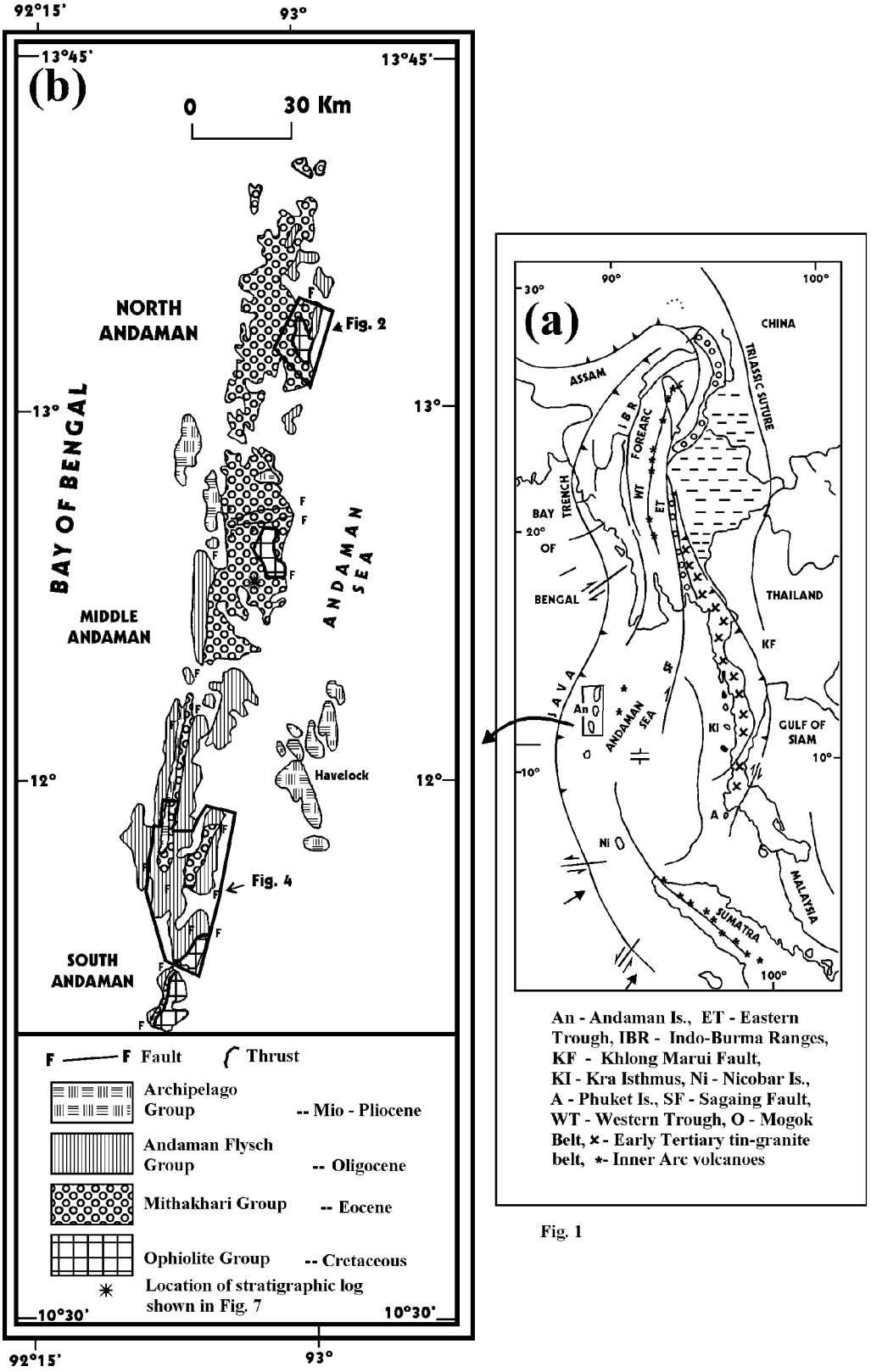

Fig. 1

Figure 1. (a) Regional tectonic framework of southeast Asia after Mitchell (1985) An – Andaman Islands; ET – Eastern Trough; IBR – Indo-Burma Ranges; KF – Khlong Marui Fault; KI – Kra Isthmus; Ni – Nicobar Island; A – Phuket Island; SF – Sagaing Fault; WT – Western Trough. (b) Generalized geological map of Andaman Islands showing distribution of Ophiolite and sedimentary units. Areas outlined by polygons are shown in Figures 2 and 4.

clockwise rotation of Southeast Asia to its present position (Tapponnier *et al*. 1982; Mitchell, 1985). Palaeomagnetic data, however, indicate that clockwise rotation was not present in the entire arc length and was limited only to the south of North Malay. Further south and east the plate underwent anticlockwise rotation (Hall, 2002). The complete arc system has been recorded from Burma, the northern segment of this arc (cf. Curray *et al*. 1978; Mitchell, 1984). The earliest tectono-sedimentary events of this mobile belt, represented by accretion of Triassic flysch sediments in Late Jurassic time, are recorded from the Indo-Burma ranges (Gramman, 1974; Mitchell, 1985). The accretion–collision complex in central Indonesia also records well-developed litho-tectonic packages of an arc system from the Cretaceous period onwards (Parkinson *et al*. 1998; Wakita, 1997; Wakita *et al*. 1998; Wakita, 2000). In the southern part of this subduction complex, an accretionary prism has been studied in detail from Nias Island, west of central Sumatra (Moore *et al*. 1980; Samuel & Harbury, 1996). In the whole of southeast Asia widespread changes in tectonic events have been recorded in three major periods, that is, at about 45, 25 and 5 Ma (Hall, 2002).

The tectonic evolution of the Andaman and Nicobar Islands, the central part of the Sunda Arc, has so far been modelled based on (1) tectonic elements recorded from the sea (Moore, Curray & Emmel, 1982), (2) seismic records (Das Gupta & Mukhopadhyay, 1993) and (3) regional correlation of tectonic elements of the eastern part of the Himalaya (Sengupta, Ray & Acharyya, 1990). Two schools of thought exist on the temporal history of subduction in this part of arc. According to one school (Acharyya, Ray & Roy, 1989; Sengupta, Ray & Acharyya, 1990) the present subduction, all around the western Sunda arc, began during Miocene times and on-land emplacement of ophiolites took place during terminal collision in Oligocene times. In their model, a second trench further east of the present trench with a proto-continent was postulated. In that model, Cretaceous ophiolites and Eocene sediments were considered as a part of an accretionary prism related to that second subduction margin and were subsequently emplaced as east to west propagating allochthonous nappe sheets onto the present subduction margin. The presence of melange and the highly deformed character of sediments provoked other workers to suggest onset of subduction during Late Cretaceous times, after the Early Cretaceous break-up of Gondwanaland (Curray & Moore, 1974; Karig *et al*. 1979) or from Late Palaeozoic times (Hamilton, 1979; McCourt *et al*. 1996). In Sumatra, accretion of Permo-Carboniferous continental crust during Mesozoic times has also been reported (Pulunggono & Cameron, 1984).

Despite the presence of all morphotectonic elements of a subduction complex, namely, the trench-slope, outer arc, forearc, etc., no comprehensive study from land-based field data has been undertaken so far. To establish the interrelationship of different stratigraphic units and to decipher the tectonic evolution of the islands, mapping on a 1:12 500 scale was carried out in key sectors of the North, Middle and South Andaman Islands and Havelock Island (Fig. 1b). In the present study, structural grain, emplacement and origin of Cretaceous ophiolites, and basin evolution of Tertiary sediments have been evaluated collectively to assess the evolution of these islands in a regional tectonic context.

2. Lithology

The Andaman Islands expose dismembered bodies of Cretaceous ophiolite slices and Tertiary sediments representing a trench-slope–forearc setting. The following stratigraphic sequence was established on the basis of the data collected by the present and earlier workers (Table 1). The lithological details of different geomorphotectonic domains recorded from the present study are detailed below. Although parts of the North Andaman, Middle Andaman and South Andaman Islands were mapped, representative detailed maps of the North Andaman (Fig. 2) and South Andaman Islands (Fig. 4) are presented here. Representative geological sections of parts of the North and South Andaman Islands are shown in Figures 3 and 5, respectively.

3. Accretionary slices (Ophiolite Group)

Metamorphic rocks, melange and ophiolitic rocks with pelagic cover sediments constitute the Ophiolite Group rocks and these occur as dismembered bodies. A tectonic stack of ophiolitic rocks is interleaved with ophiolite-derived clastic sediments. The ophiolite slices invariably show thrust contacts with underlying sediments and occasionally with overlying sediments. Towards the west, ophiolites are exposed in small isolated patches, whereas in the east, individual ophiolite slices are narrow and their along-strike extensions are traced for kilometres (Fig. 4). In the eastern part, most ophiolitic rocks occur in sequences with normal ophiolite stratigraphy (Figs 2, 4). Dominantly N–S- to NE–SW-trending discontinuous slices of ophiolites occurring at different structural levels and having tectonic contacts with underlying sediments indicate thrust-controlled emplacement in an accretionary environment.

3.a. Metamorphic rocks

This packet comprises metasediments and metabasics, which have undergone greenschist to amphibolite facies metamorphism. These rock units occur either as blocks in a melange zone in the Middle Andaman Islands or as discontinuous patches along the thrust

Table 1. Generalized stratigraphy (revised after Karunakaran, Ray & Saha, 1967; Ray, 1982)

Tectonic setting	Age	Stratigraphic unit	Lithocharacters	Fossil record	Palaeocurrent direction
Forearc	Pliocene (cf. Ray, 1982) Miocene (Chatterjee, 1964)	Archipelago Group (400 m thick)	Interbedded sequence of tuff, limestone, sandstone and clay (Limestone is biohermal and biostromal)	Nanofossils Pelagic foraminifers, *Lepidocyclina, Miogypsina,* bryozoan and algae	East, west and majority in southwest
			—Unconformity—		
	Upper Eocene-Oligocene (Pawde & Ray, 1963) Oligocene–Lower Miocene (Present work)	Andaman Flysch Group (300 m thick)	interbedded sequence of sandstone, siltstone and shale	*Rotalia, Nodosaria, Amphistegina, Globorotalia, Opimanana, Globigerinoids*	Northeast, southwest and majority in southeast
			—Unconformity/transitional—		
Trench-slope	Middle to Late Eocene (Karunakaran Ray & Saha, 1967)	Mithakhari Group (1400 m thick)	Conglomerate, sandstone and shale	*Cumulates atacicus, Assilina papillata, Pelatispira, Biplanispira*	Northwest; a few show northeast–southeast trend
			—Tectonic/unconformity—		
Accretionary slices	Cretaceous to Paleocene (Roy *et al*. 1988)	Ophiolite Group	Metamorphics, tectonites, cumulates, plagiogranite-diorite-andesite suite, basalt and pelagic sediments	Radiolaria: *Nasselaria spumellarion* Planktonic foraminifera: *Globigerina eugubina, G. trilloculinsides, G. fringa, G. velascoensis.Globorotalia compressa, Globigerinelloides sp., Pseudotextularia sp., Globotruncana arca, Reugoglobigerina sp*.	
	Early Cretaceous (Jafri, 1986)			Hagiastrids	

N.B. Age connotation is based purely on palaeontology; no isotopic ages are available.

contact between ophiolite and underlying trench-slope sediments (Mithakhari Group) in the North Andaman Islands. Quartzites, quartz-mica schists and phyllites represent the metasediments, whereas metabasics are principally amphibole-bearing chlorite–epidote–carbonate schists. In the metabasics, epidote and carbonate occur as syntectonic porphyroblasts, and hornblende grains are present as pre-tectonic retrograde grains. Close to the thrusts, rocks are intensely schistose.

3.b. Melange

Melange, a chaotic mixture of diverse rocks, occurs at the base of the ophiolite and is exposed mainly in the eastern part of the Middle Andaman Islands. The fragments of basalt, ultramafic rocks, metamorphic rocks, brecciated sandstone and chert are embedded in a sheared basaltic and serpentinized matrix (Fig. 6).

3.c. Ophiolite suite

Except for the sheeted dyke complex, all other members of a classic ophiolite stratigraphy are exhibited with the sequence of a plutonic complex, intrusives, extrusive lava series and pelagic sediments. The presence of a pre-subduction tectonic fabric in the harzburgite of the ophiolite package leads to a two-fold subdivision: a mantle sequence and a crustal sequence. The distinctive level that separates layered cumulates of crustal section from the underlying mantle sequence is believed to be the onland expression of the Moho (Corfield, Searle & Pederson, 2001). A complete sequence from the Moho is exposed in the South Andaman Islands.

Serpentinized harzburgite and pods of altered dunite represent the mantle sequence. Harzburgite showing tectonic fabric contains 20 to 30 % orthopyroxene. The remainder of the harzburgite is serpentine and chlorite. In dunite pods, relics of olivine are set in serpentine with some cumulus and intercumulus chromite.

Overlying the mantle sequence, an assemblage of plutonic rocks and extrusives represents the crustal sequence. The plutonic unit of crustal sections is represented by layered cumulates of peridotite–gabbro, overlain by non-cumulate gabbro and high-level intrusives of a plagiogranite–diorite–andesite suite of rocks with thin dykes of basalt and diabase.

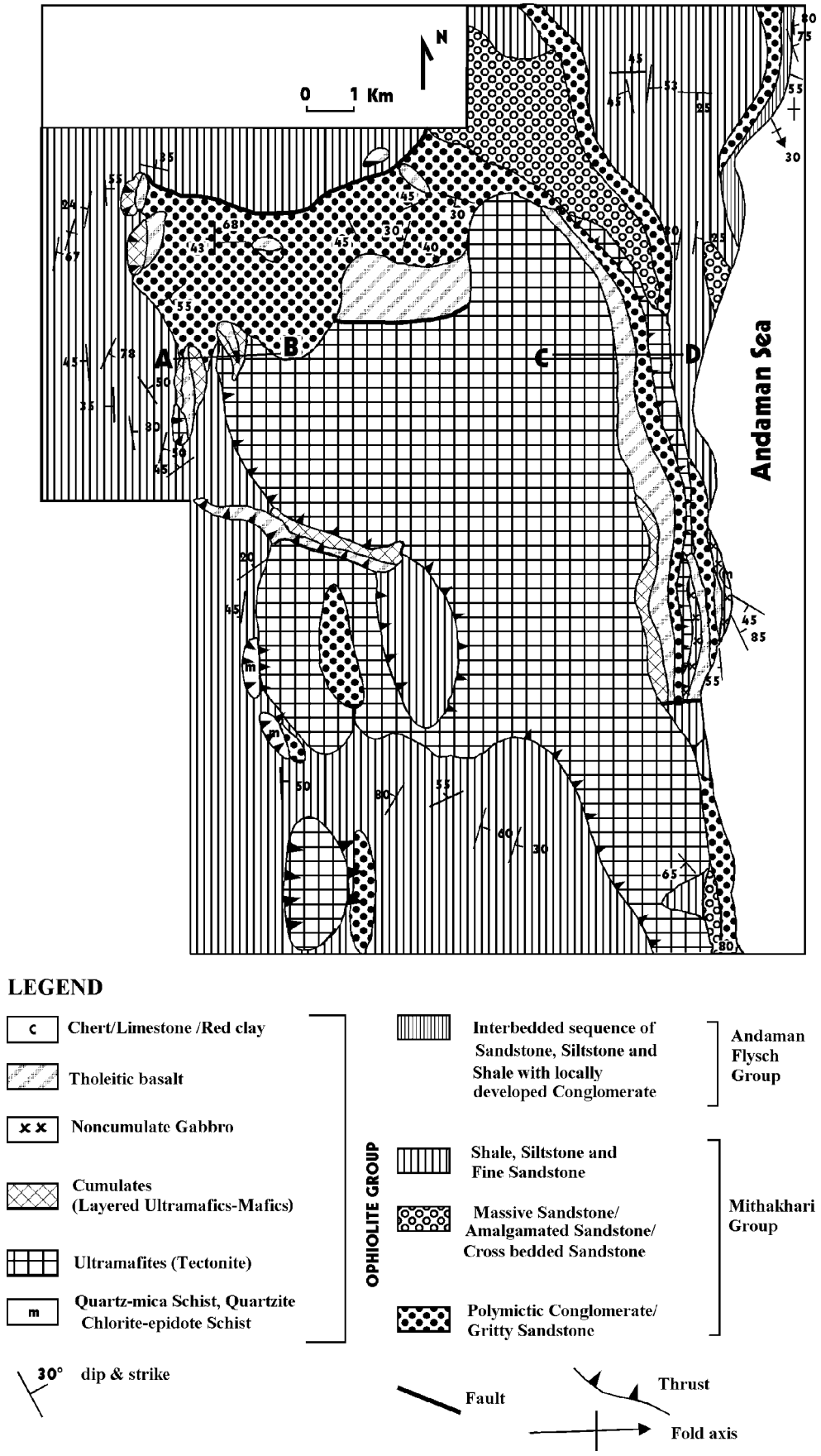

Figure 2. Detailed geological map of parts of North Andaman Islands showing lithostratigraphic units and tectonic elements. Sections A–B and C–D illustrated in Figure 3.

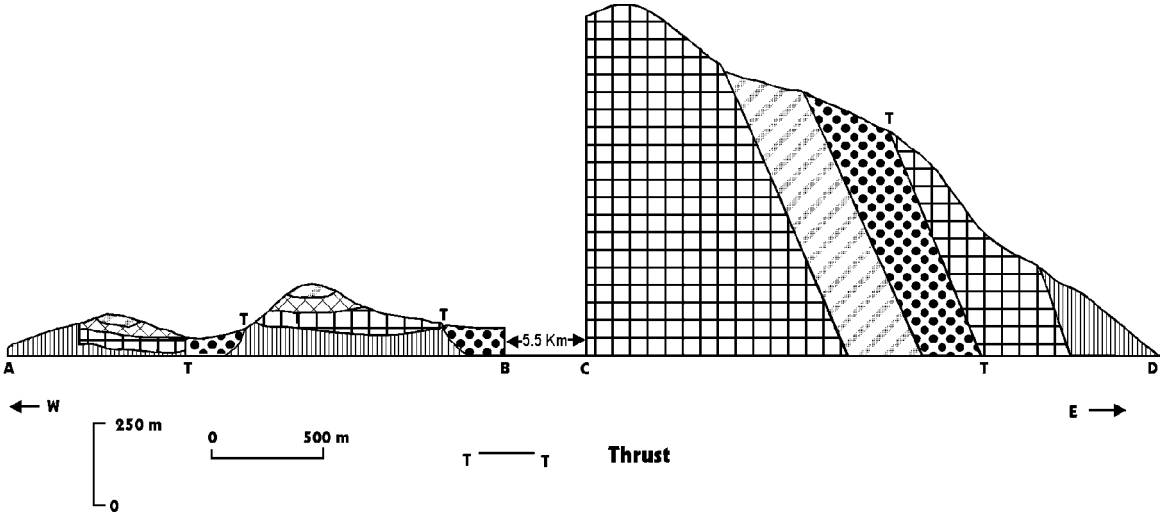

Figure 3. Representative geological sections of part of the North Andaman Island showing thrust contacts of ophiolites. Legend for lithological units are same as in Figure 2.

The layered cumulate unit is composed of serpentinized dunite–harzburgite–lherzolite–wehrlite, pyroxenite and gabbro with pods and stringers of chromitite. Individual layers can be traced at an outcrop scale. The eastward dip of these magmatic layers is consistent with an overall thrust-related emplacement history for these slices. In most of the rocks olivine is mostly serpentinized, producing mesh to hourglass textures. In the lherzolite, clinopyroxenes are relatively fresh, whereas olivine and orthopyroxene occur as cumulus and intercumulus phases, showing subsolidus re-equilibration textures. The harzburgites of this section have chemical compositions similar to the mantle section (Vohra, Haldar & Ghosh Roy, 1989).

Non-cumulate gabbro occurs as intrusives in the cumulate sequence. These units are mappable in both the North and South Andaman Islands and typically contain primary amphibole along with gabbroic minerals.

The non-layered plutonic rocks (high-level intrusives), represented by a plagiogranite–diorite–andesite suite of rocks, are closely intermingled with each other and show marginal intrusive relations with cumulates. Micrographic intergrowth of quartz and feldspar, with clots and veins of pyrite and chalcopyrite are common in plagiogranite. Major oxide analyses of these lithotypes show similarity with other ophiolitic plagiogranites (Jafri, Charan & Govil, 1995). Ray (1985) explained these plagiogranite–diorite suites of rocks as separate plutons. However, on the eastern coast of the Beadonabad–Rangachang sector of the South Andaman Islands, the plagiogranite suite of rocks occurs only as a member of the ophiolite, underlain and overlain by non-cumulate gabbro and basalt, respectively.

The sheeted dyke complex typical of other ophiolites is not exposed in the area, but near-vertical thin dykes of altered dolerite to basalt occur as intrusives in the plagiogranite–diorite suite of rocks in the coastal sector of the South Andaman Islands. The dykes are often offset by microfaults. The aphyric to sparsely phyric basalts of this unit show subophitic to intergranular textures.

The uppermost part of the ophiolite overlying the dyke complex consists of both pillowed and non-pillowed lavas. Physiochemically two types of lava are present as: (1) dacitic to andesitic basalt and (2) tholeitic basalt (Ray, Sengupta & Van Den Hui, 1988; Vohra, Haldar & Ghosh Roy, 1989). Dacitic to andesitic basalts contain phenocrysts of pyroxene, altered feldspar and minor quartz often set in a groundmass of epidote–chlorite–glass. Tholeitic basalt occurs as pillowed, brecciated and massive varieties and volumetrically constitutes the major part of the ophiolite in the South Andaman Islands.

Thin layers of red clay, red chert and limestone, either alternated with basalt or in short successions (*c*. 2.5 m thick) immediately overlying the extrusives, represent pelagic sediments and are volumetrically only a minor constituent of the ophiolites. Thin micritic limestone is interbedded with red shale showing gradational upper and lower contacts. Cherts, both massive and bedded varieties, are recrystallized. Jafri (1986), from the occurrence of *Hagiastrids* in radiolarian chert, assigned an Early Cretaceous age to these pelagic sediments. Roy *et al*. (1988) have reported *Nassellarian* and *spumellan* taxa or radiolaria from red chert and planktonic foraminifera from limestones, suggesting an Early Eocene to Paleocene age for these sediments. The present study, however, identified *Globoratalia* sp. and *Discocyclina* sp. in these sediments, suggesting a Late Cretaceous to Paleocene age.

4. Trench-slope deposit (Mithakhari Group)

Polymictic conglomerate, sandstone, and shale compose the Mithakhari Group. This ~1.4 km thick

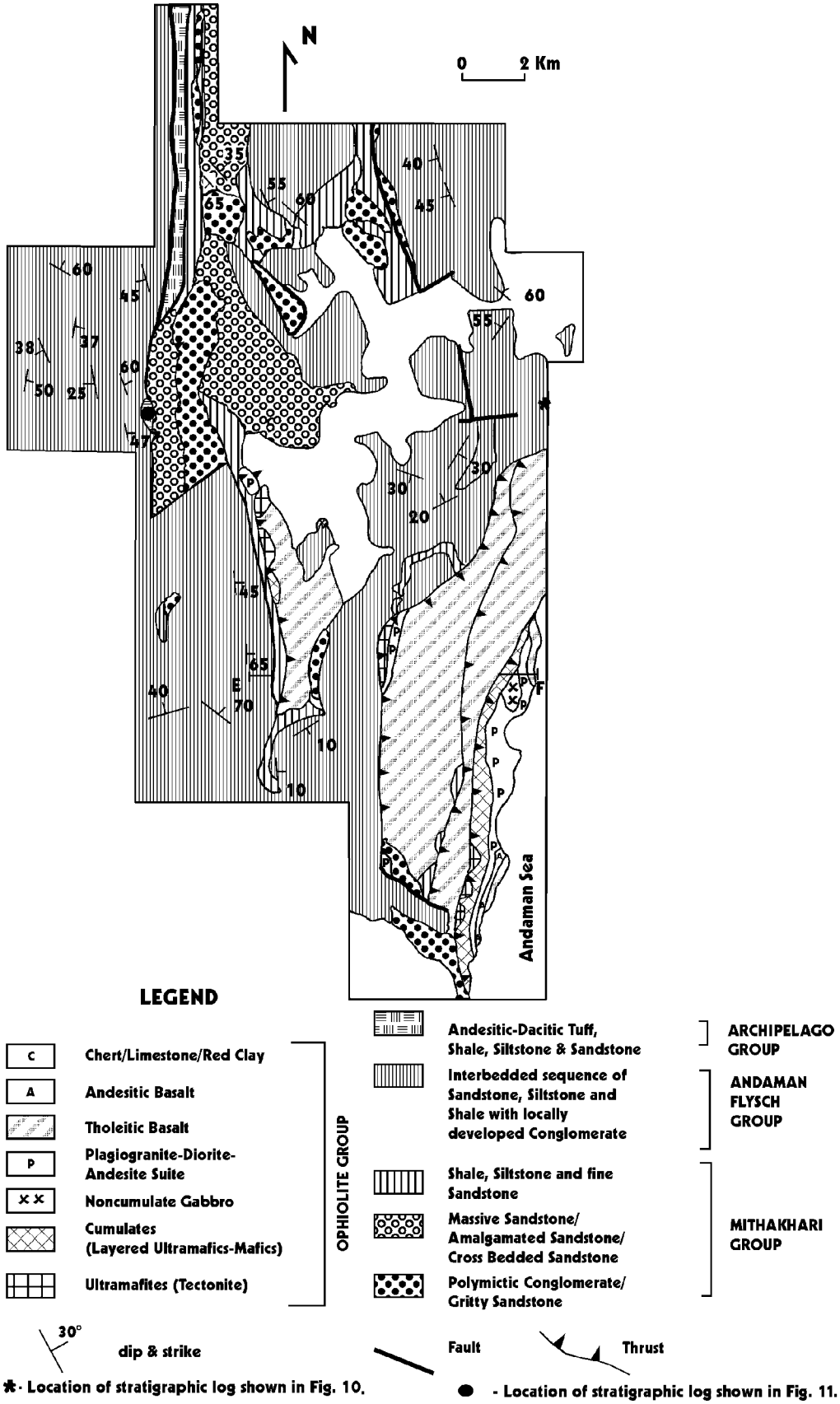

Figure 4. Detailed geological map of parts of the South Andaman Islands showing lithostratigraphic units and tectonic elements.

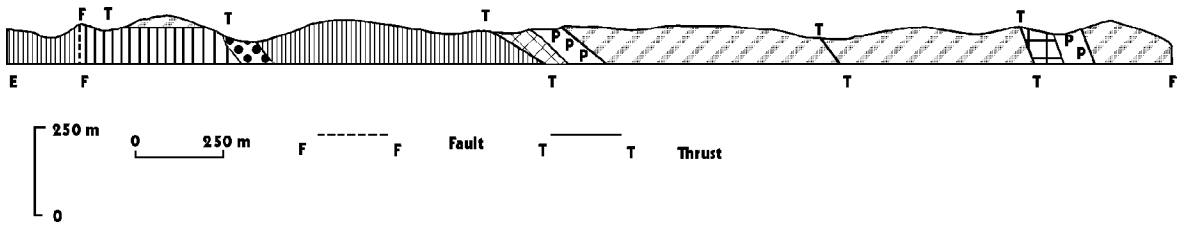

Figure 5. Representative geological sections of part of the South Andaman Islands showing thrust contact of ophiolites. Legend for lithological units as in Figure 4.

Figure 6. Tectonic melange showing clasts in sheared matrix developed at the base of ophiolite slices. Length of ruler = 0.12 m.

sedimentary unit (Ray, 1982) contains larger foraminifera and calcareous algae of Middle to Late Eocene age (Karunakaran, Ray & Saha, 1967; Roy *et al*. 1988) and can be mapped as three major formations: (1) conglomerate, (2) sandstone and (3) shale (Figs 2, 4). These formations are further subdivided into eight different lithofacies based on bed geometry and sedimentary structures present (Fig. 7): (1) disorganized matrix supported conglomerate, (2) graded matrix supported conglomerate, (3) graded pebbly sandstone, (4) massive and thick bedded sandstone, (5) plane-laminated and cross-stratified sandstones, (6) interbedded sandstone and mudstone, (7) massive to faintly laminated shale and (8) interbedded shale and coal.

In both disorganized and graded conglomerates, clasts of vein quartz and lithic fragments of shale, limestone, sandstone, chert, ultramafic rocks, porcellinite and basalt are set in a poorly sorted sandy matrix. Parallel-sided massive and thickly bedded sandstones (lithic wacke in character) are present as amalgamated beds and generally lack any grading. Plane-laminated and cross-stratified sandstone facies constitute an interbedded succession and often coarsen upward. Massive to faintly laminated pyritiferous shale interbedded with thin stringers of silt/fine sandstone form parallel-sided units laterally continuous at outcrop scale. Interbedded shale and coal facies contain occasional desiccation cracks and locally gypsum crystals. In the shale-dominated facies of the Mithakhari Group, a number of mud volcanoes are reported in the Middle Andaman and North Andaman Islands.

In plane-laminated and cross-stratified sandstone facies the palaeocurrent direction derived from chevron cross-stratification trends NW–SE (Fig. 8a) and that from tabular cross-strata is towards the SSW (Fig. 8b). Clast imbrication, sole marks, wave ripple trends (Fig. 8c) and large-scale channel bedform migration show dominant sediment influx was from the NE.

5. Forearc deposits

The rocks of this domain can be classified into two groups as discussed below.

5.a. Siliciclastic turbidites (Andaman Flysch Group)

This sequence (~3 km thick) overlies and onlaps the Mithakhari Group. Laterally persistent (over hundreds of metres) turbidite units with both top-truncated (T_{a-c}) and bottom-truncated (T_{de}) Bouma cycles and common

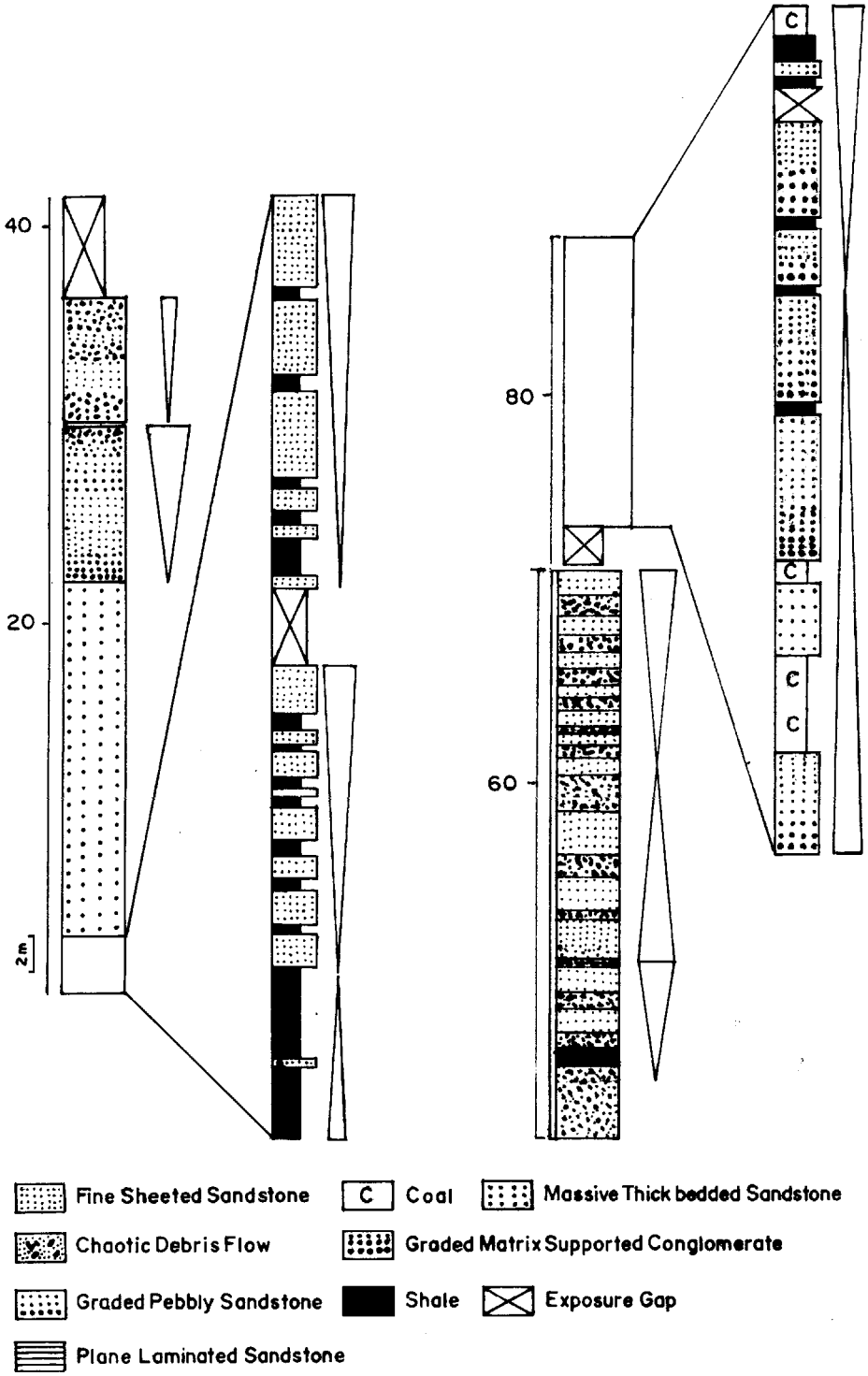

Figure 7. Representative stratigraphic log of Mithakhari sediments measured at Kaushalyanagar, Middle Andaman.

fluidization structures are characteristic of this unit. High-resolution facies analysis shows three different facies associations representing the inner or upper fan, middle fan and basin plain (Chakraborty & Pal, 2001).

5.a.1. The inner or upper fan facies

This facies is exposed in the eastern part of the North Andaman Islands and is characterized by: (1) considerable grain size variation, (2) abrupt vertical facies transitions, (3) close association of high-density turbidity current or channelized debris flows with fine-grained overbank deposits, (4) decrease in depth and increase in width:depth ratio of the channels up the section, (5) occurrence of poorly sorted and rounded large clasts of ophiolite in the conglomerate suggesting nearby provenance and (6) dominantly NE-directed palaeocurrents (Fig. 9a).

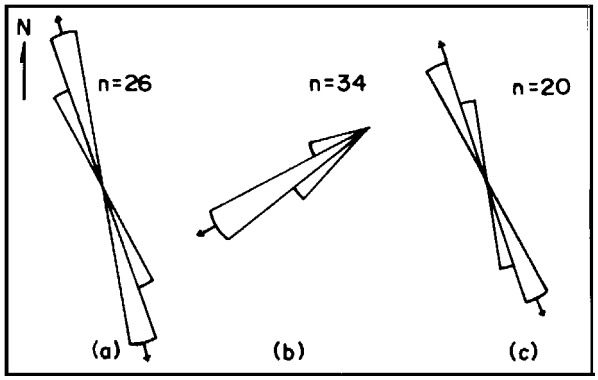

Figure 8. Palaeocurrent patterns of Eocene sediments measured from Kaushalyanagar section and other parts of the exposure belt. (a) Chevron cross-stratification; (b) tabular cross-stratification; (c) wave-ripple crestal trend.

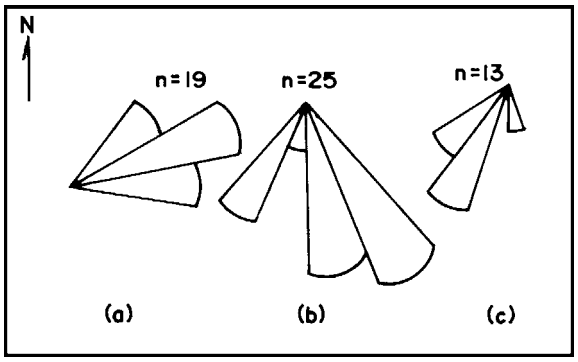

Figure 9. Palaeocurrent patterns of Oligocene sediments over entire exposure belt for (a) facies association 1, (b) facies association 2, and (c) facies association 3.

5.a.2. Mid-fan facies

Characteristics of this facies are: (1) parallel-sided sandstone beds which are laterally continuous over hundreds of metres, (2) well-defined Bouma cycles of T_{a-e}, T_{b-e}, T_{c-e}, T_{de}, T_{be}, (3) absence of basal channelling and frequent amalgamation of beds, (4) stacked sheets of coarse to fine sand with no distinct vertical variation in bed thickness (Fig. 10), (5) occurrence of laterally persistent slumped layers, (6) presence of tabular scour marks and flute marks and (7) broadly S-directed palaeocurrents from sole features (Fig. 9b). In general, these sandstones are poorly sorted matrix-supported quartz wackes with framework grains of detrital quartz, lithic fragments, feldspar and pyroxene. The siliciclastic matrix is dominantly clay minerals, chlorite, fine quartz and feldspar, and lithic fragments occasionally produce pseudomatrix.

5.a.3. Basin plain facies

This facies is characterized by hemipelagic mudstone interbedded with thin sandstone/siltstone beds,

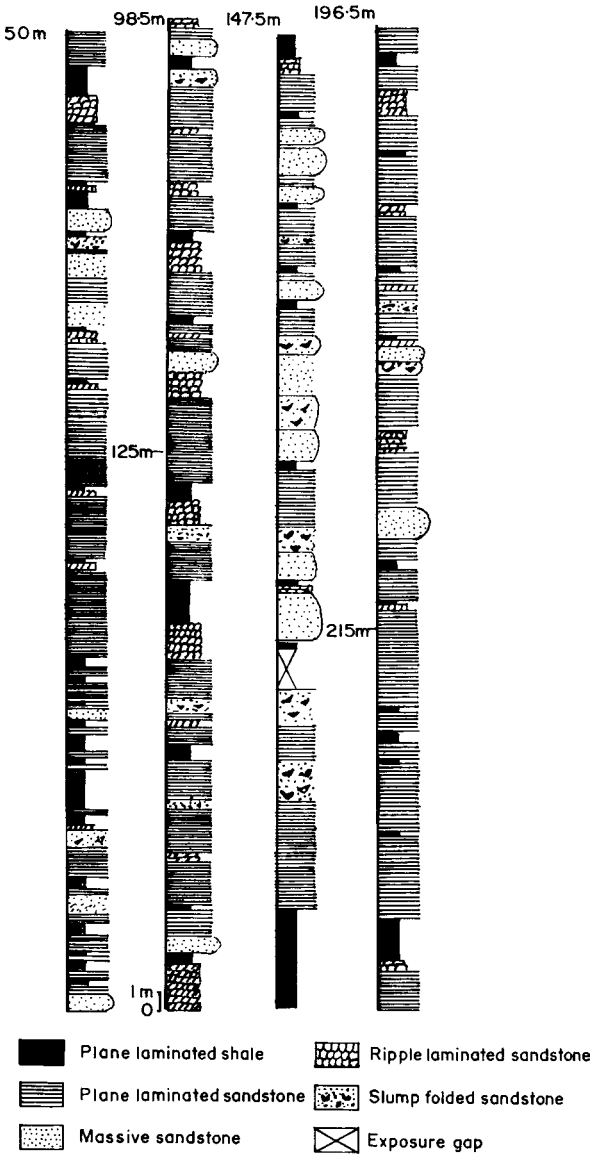

Figure 10. Stratigraphic log representing middle fan lobe of Andaman Flysch sediments measured at Corbyn's cove, South Andaman.

similar to classical distal turbidites. These fine-grained turbidite beds contain irregular and lenticular silt laminae (2–10 mm) and thin sand beds (> 10 mm) alternating with mud veneers. This unit is characterized by: (1) lack of channels and large scale scours at the base of sandy/silty interbeds, (2) absence of sole features, (3) presence of load casts and mud injection structures. Compared to the inner fan facies association, these sediments show continuity of bedding, lack of slump features, thinning and fining-upward depositional cycles. These sediments, in general, show S-directed palaeocurrents (Fig. 9c). Although exposed dominantly on the eastern side of the Andaman Islands, these turbidites are also exposed on the western side of the South Andaman and part of the Middle Andaman Islands with fault contacts against

the Eocene Mithakhari Group. A post-depositional N–S fault probably brought those sediments from further southeast (J. R. Curray, pers. comm.).

5.b. Pyroclastic flow–siliciclastic–carbonate turbidites (Archipelago Group)

Two major lithoassemblages, namely (A) alternation of subaqueous pyroclastics and siliciclastic turbidites in the lower part and (B) typical ash turbidite overlain by carbonate turbidites in the upper part constitute this group. Within the study area, unit A is well developed in the South and Middle Andaman Islands, whereas unit B is exposed in the Havelock Islands in the east. Unit A shows a repeated succession of tuffs and non-volcanogenic sediments including greywacke, siltstone and mud. Greywackes are normally graded turbidite sequences with coarse-graded beds, cross-laminated beds and parallel laminated beds (T_{ace}). Tuffs of unit A show amalgamated massive beds with ill-defined bedding contacts. Towards the upper part, tuff beds show a change from normal graded bedding with scoured bases to thin parallel lamination to ripple drift lamination (Fig. 11). In the massive tuffs, vitric to crysto-vitric varieties show delicately shaped glass shards and broken phenocrysts of euhedral quartz, plagioclase, muscovite, orthoclase, zircon and ilmenite. Glass shards are altered to zeolites. The tuffs have dacitic compositions (Pal, Dutta Gupta & Das Gupta, 2002).

In unit B typical ash turbidites show normal grading with T_{abcd} Bouma cycles. Sedimentary structures indicate transport of material dominantly from the north with occasional supply from the east and west (Karunakaran, Ray & Saha, 1968). Common micrograbens and slumps indicate synsedimentary basinal disturbance.

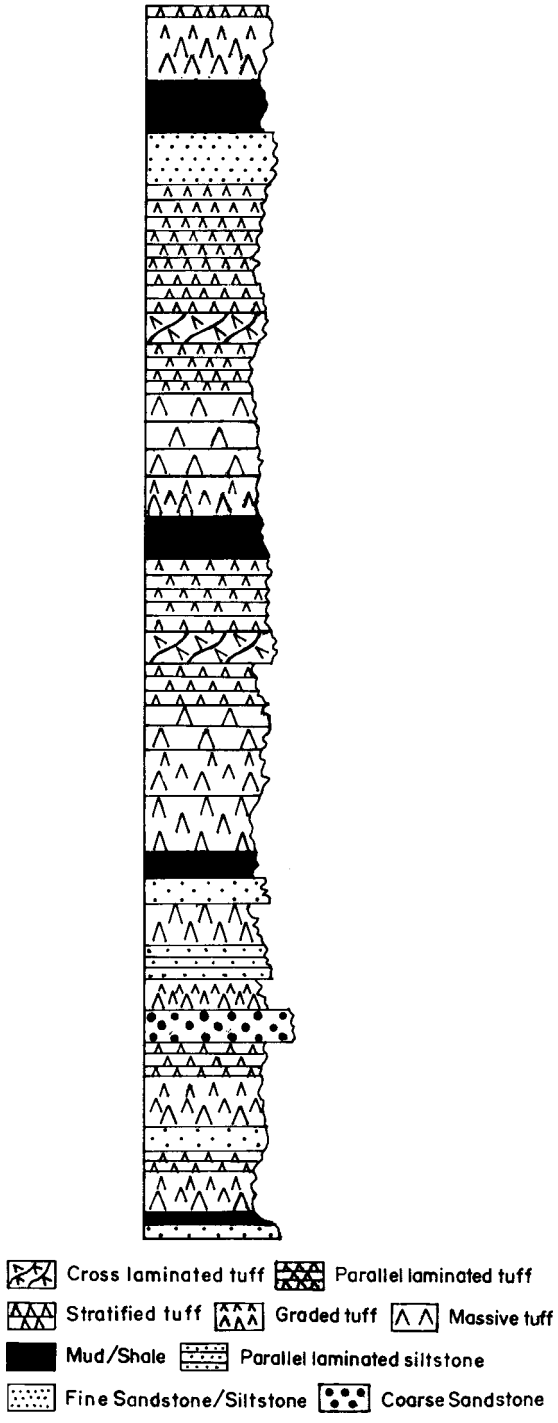

Figure 11. Stratigraphic log of tuff beds at Hubdeypur, South Andaman Islands showing turbidite features.

6. Structure

In comparison to the Andaman Flysch and Archipelago Group, rocks of the Mithakhari Group show a complex deformation pattern. The Eocene Mithakhari Group has highly variable bedding orientation (Fig. 12a). Axes of the minor folds show wide variation in direction from 050° to 240° with no apparent concentration and their plunge amount varying between 30° and 70°. The axial planes vary from inclined to vertical. In contrast, the Oligocene Andaman Flysch Group exhibits folds with comparatively regular geometry. These folds are open asymmetrical, with plunges from 18° to 25° either towards 030° or 225°. The β-pole data (Fig. 12b) define a girdle distribution with a low-plunging axis toward the southwest. The Mio-Pliocene Archipelago Group of rocks shows very regular fold geometry. In the Havelock area mesoscopic folds plunge at low angles (015°) to the south.

Several N–S-trending and E-dipping thrust sheets are present in the area. Due to lack of good exposures, direct measurement of the thrusts is difficult. Thrusts are principally delineated through mapping of ophiolite slices and tracing of lenticular bodies of mylonitic rocks. At some places in the North Andaman and Middle Andaman Islands, mylonitic rocks exhibit fluxion banding (Fig. 14a) and asymmetrical pressure tails (Fig. 14b). Intense recrystallization and subgrain formation are distinct in quartzose layers. In general,

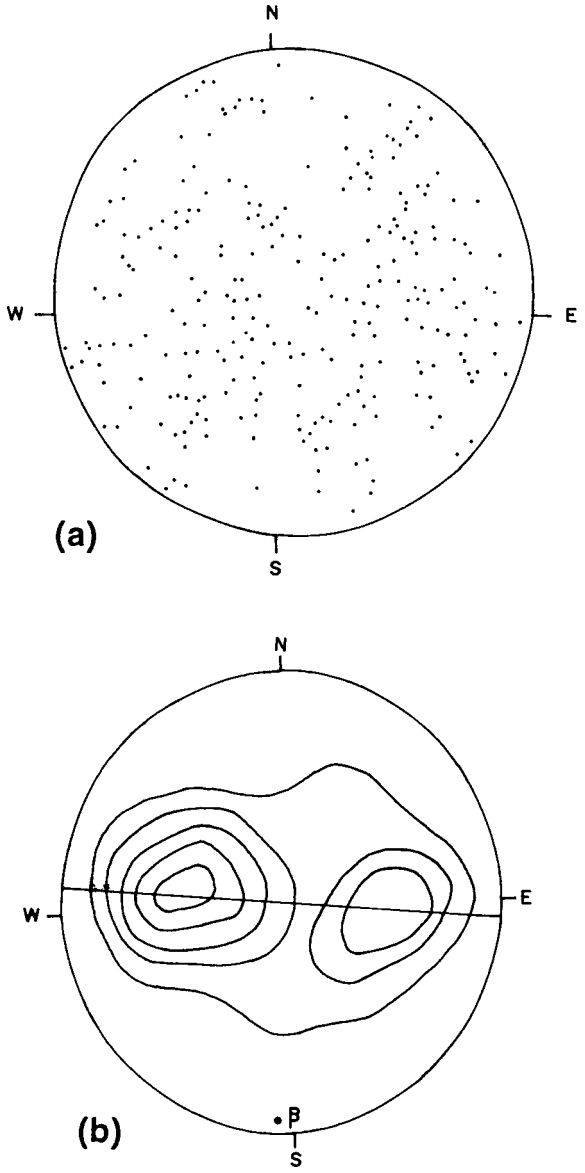

Figure 12. Stereo diagrams of bedding attitudes. (a) π diagram of Mithakhari sediments; (b) β diagram of Andaman Flysch sediments.

the dip of thrusts gradually increases from west to east. In the west, thrusts show low eastward dips (8–10°) whereas in the east, thrusts have steep (65–70°) easterly dips (Figs 3, 5, 13, 15).

The western thrusts, in general, have a ductile character while brittle behaviour is observed in a few thrusts of the eastern tract. Anastomosing shear planes producing shear lenses, wavy shear surfaces and foliations in basalt are commonly seen in the vicinity of the western thrusts. Brittle behaviour is exemplified by fault gouges, brecciation in basalt and gabbro as observed in the eastern part of the North Andaman Islands. In the North Andaman Islands, repetition of ophiolite members in a narrow belt is considered to be tectonic imbrication.

Besides the E-dipping N–S-trending thrusts some W-dipping N–S-trending backthrusts are present in the

Figure 13. Moderately steep dip of thrust in between ophiolite (OP) and Mithakhari sediment (M) in South Andaman. Width of the field of view is 3.85 m.

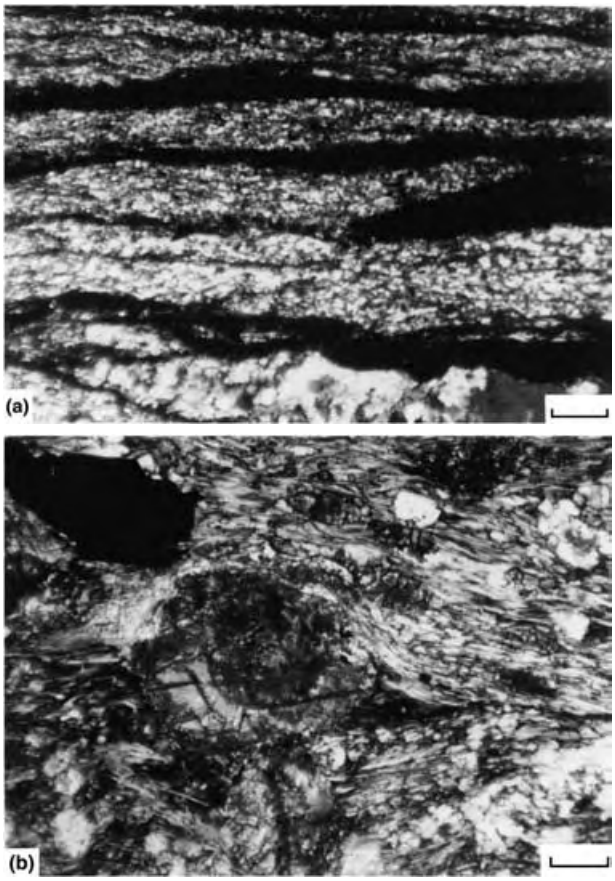

Figure 14. Photomicrographs showing (a) fluxion bands, (b) S–C foliation and shear fabric in sheared metamorphic rocks. (a, b) Scale bar = 0.14 mm.

area. In addition, a few out-of-sequence thrusts trending E–W (Fig. 2) are present.

A number of N–S-trending normal and E–W-trending strike-slip faults have affected the rocks of this area. The latter type faults are common within the Mithakhari, Andaman Flysch and Archipelago Group of rocks.

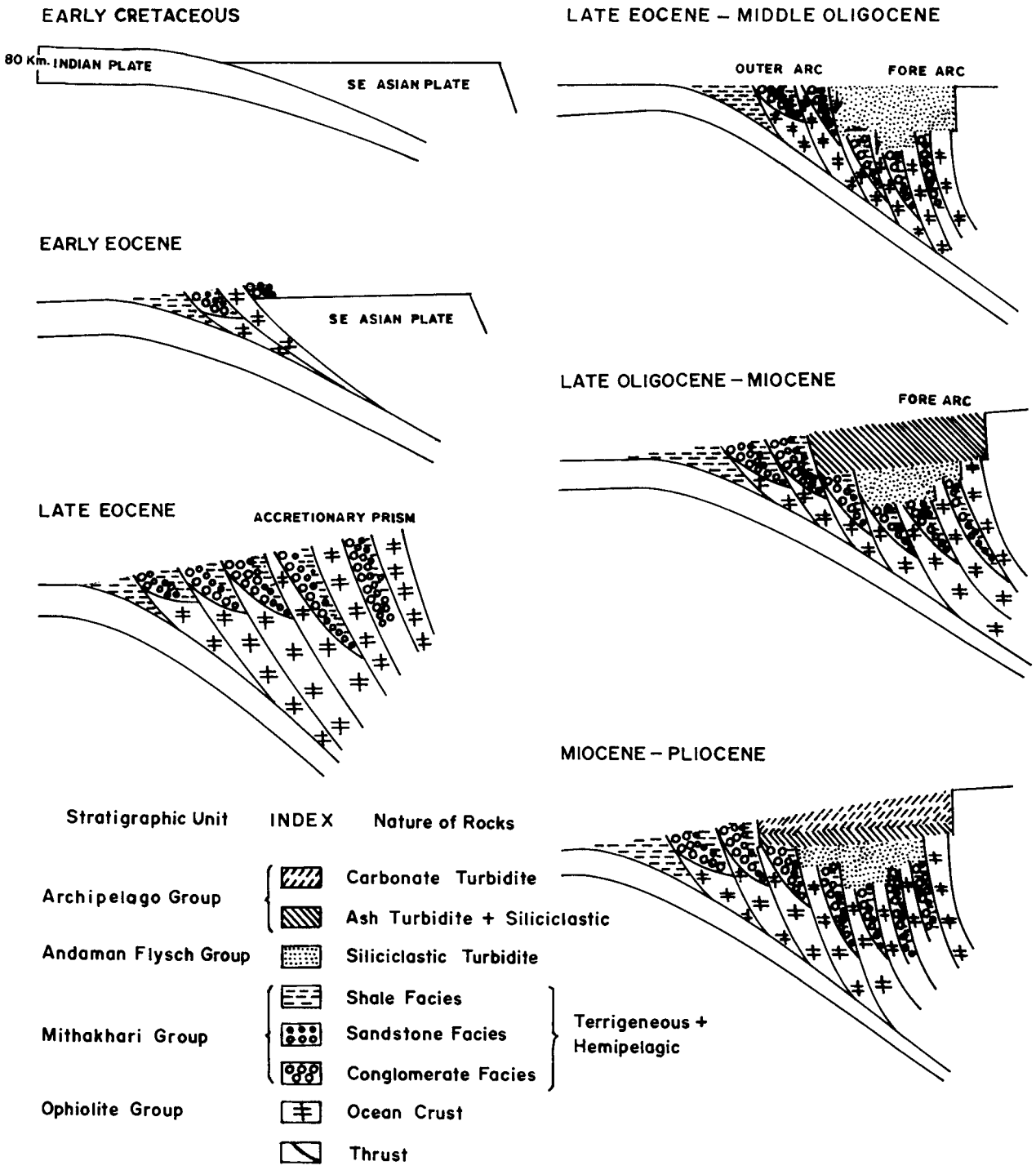

Figure 15. Sketch diagrams showing tectono-sedimentary events in different time periods. Note accretionary thrust emplacement of ophiolites, isolated thrust bounded trench-slope basins and fault bounded forearc basin.

7. Evolution of outer arc

7.a. Accretionary ophiolite slices

Discontinuous slices of ophiolite, present at different structural levels and in thrust contact with associated sediments, indicate thrust-controlled emplacement in an accretionary prism setting through offscraping from the subducting plate or from the lower part of the wedge (cf. Condie, 1989; Platt, 1986; Moores *et al.* 1984). Subduction-related deformation recorded in Cretaceous sediments of the Bengal fan in the west of Andaman Islands indicates that subduction began in the Cretaceous period (Moore, Curray & Emmel, 1982). As a result of subduction, ocean crust (ophiolite) of the subducting slab was scraped off and emplaced as a thrust slice. With continuous subduction from the Cretaceous onwards, a series of thrust slices of ophiolites were thus emplaced (Fig. 15, Table 2).

Table 2. Tectonic evolution of Andaman Islands

Age	Events
Late Cretaceous	(1) Formation of ophiolite involving crustal mantle processes (2) Initiation of oblique subduction of Indian plate below Southeast Asian plate
Late Cretaceous – Early Eocene	(1) Thrust controlled emplacement of ophiolite
Lower to late Eocene	(1) Continuation of emplacement of ophiolite by N–S-trending E-dipping thrusts (2) Deposition of ophiolite-derived clastics and trench sediments representing Mithakhari Group in small isolated basin of outer arc region (3) Formation of accretionary prism in compressional regime by tectonic slices of ophiolite and Mithakhari sediments through frontal accretion process (4) Formation of back thrust and out of sequence thrust to maintain the slope stability of prism
Oligocene	(1) Change of compressional regime to extensional regime at the rear of wedge (2) Formation of forearc basins through E–W- and N–S-trending strike-slip and dip-slip faults respectively (3) Deposition of siliciclastic turbidites of Andaman Flysch Group in forearc region (4) Post-depositional normal and strike-slip faults
Mio-Pliocene	(1) Subaqueous pyroclastic flow deposit in the form of ash turbidites alternated with siliciclastic turbidite in lower part of Archipelago Group in forearc region (2) Transition of siliciclastic to carbonate turbidites along with pyroclastic flow deposit in forearc region (3) Dominance of deposition of carbonate turbidite in upper part of Archipelago Group (4) Deformation to form plunging folds
Pleistocene to Recent	(1) Formation of recent conglomerate, shell limestone, volcanism of Barren and Narcondam Islands in inner arc region

The typical association of low-grade metamorphism with ophiolites worldwide suggests that metamorphism observed here is also related to emplacement of ophiolite. The continental origin of these metamorphic rocks as proposed earlier by Sengupta, Ray & Acharyya (1990) is rejected because of the absence of any gneissic rocks and presence of metapelites and metabasics only. The character of the metamorphic rocks is consistent with an origin as metamorphic soles by successive underplating and welding onto the base of an ophiolite as it moves from the mantle to the surface (cf. Condie, 1989). The heat source was probably a combination of residual heat from the mantle and shear heating during ophiolite emplacement (Platt, 1986).

A tectonic origin of melange is interpreted because these are diverse rocks embedded in sheared basalt and serpentinized rocks. Melange at thrust contacts of the ophiolites also suggests an origin linked with emplacement of ophiolite.

The ophiolite bodies show interplay of mantle–crustal processes. High Cr-chromite, high Mg olivine, enstatitic orthopyroxene and highly fractionated PGE patterns suggest that ophiolites were derived from a boninitic parental melt (Pal, Chakraborty & Ghosh, in press). In the upper mantle during adiabatic uprise, the rock–melt system was deformed in a plastic shear regime by convective forces dominantly in a horizontal direction, and that produced shear foliation in tectonized harzburgite (cf. Gass, 1990). Major oxides and trace element patterns of the plagiogranite suite of rocks suggest low-pressure crystal fractionation of a low-K tholeitic magma derived from the parental melt (Jafri, Charan & Govil, 1995). The plagiogranites may have been produced from the melt chilling against the magma chamber roof and crystallized under hydrous conditions (cf. Stakes, Taylor & Fisher, 1984) or formed from residual melts by fractionational crystallization (cf. Aldiss, 1981). The different compositions of lower lava and upper lava series from picritic to andesitic to tholeitic basalt, and gabbro dykes in the cumulate section, suggest that the Andaman ophiolites were derived from multiple parental magmas.

7.b. Trench-slope basins

Fossil assemblages indicate an Eocene age for the trench-slope deposits represented by the Mithakhari Group rocks. The sedimentary characters of the Mithakhari Group, namely (1) rapid facies changes both along and across depositional strike, (2) coarse-grained deposits with synsedimentary basinal disturbance, (3) isolated sedimentary successions with unrelated depositional patterns and widely variable palaeocurrent, (4) wide palaeogeographic variation ranging from non-marine deltaic to submarine, (5) short truncated sedimentary successions and (6) mass flow units containing blocks of underlying accretionary slices, indicate sedimentation in isolated small basins separated by structural ridges of ocean basement. Bounded between active thrust faults the isolated basinal character with unrelated palaeocurrent and sedimentation pattern prompted visualization of a trench-slope situation (Fig. 15; Chakraborty *et al*. 1999). The discontinuous nature of these basins in the entire Sunda Arc area has also been reported from seismic reflection studies (Karig *et al*. 1980; Moore, Curray & Emmel, 1982). In trench-slope basins along with fine sediments of trench there may be coarse detritus derived from accreted ophiolite slices. Sedimentation in these basins was dominated either by channellized laminar debris flows (Ricci Lucci, 1985) or high concentration flow dispersion (Dickie & Hein, 1995). The shale-dominated association in this setting indicates both distal and proximal palaeogeography. The distal units are hemipelagic in origin with siltstone stringers representing low-density turbidites.

Evidence of shearing in trench-slope sediments in contact with ophiolites and the profusion of progradational cycles in these sediments suggests structural uplift during and after sedimentation. Well-developed slope and distal facies associations without any wave signature suggest deposition in a slope delta model below storm wave base. Frequent delta abandonment further corroborates a deep-water immature environment (Postma & Cruikshank, 1988). Tectonic disturbance on a steeply sloping and structurally controlled substrate in an otherwise starved setting resulted in frequent mass failure. The association of coal, gypsum, cross-bedded sandstone lenses and pyrite-bearing shale suggests development of a low gradient alluvial plain in the top part of the section that suffered occasional marine inundation and extreme desiccation. With gradual uplift and concomitant progradation the depositional surface may have been raised from below storm wave base to a shallow coal-depositing paralic setting. Certain coarse-grained facies towards the top of these sedimentary successions suggest the presence of a submarine canyon that with time became sediment-starved due to structural blockage in its proximal part which was then overlain by basinal sediments (cf. Underwood & Bachanan, 1982). Integration of these features supports a model of an immature stepped trench-slope basinal environment with dominant NW–SE depositional strike in an accretionary prism. Individual small basins separated by structural highs with local sources of coarse detritus were uplifted and became part of the accretionary complex (Fig. 15). Such tectonic shoaling and sediment recycling are reflected in the coarsening and thickening upward progression of lithofacies and well-developed grain roundness in these trench-slope basin fills. McCrory (1995) recorded similar shoaling depositional history and development of fluvial to paralic environment from a trench-slope basin within the Cascadia subduction margin. With continuing subduction the pelagic sediments might have been dragged beneath the accretionary prism leading to compaction and expulsion of large amounts of pore fluids. Active mud volcanoes and diapirs in the area may be the direct evidence of such pore fluid expulsion through fault/fracture systems.

With continued subduction the scraped-off sediments and parts of the oceanic crust were accreted at the back of earlier thrusts, which resulted in the earlier thrust of the accretionary prism steepening further (Fig. 15). Progressive accretion at the tip of the wedge, which thereby lengthened the wedge, led to extensional tectonics. To adjust the internal shortening, backthrusts and out-of-sequence thrusts developed, cutting across the earlier accretionary prism (cf. Platt, 1986) formed by the Ophiolite–Mithakhari Group complex. Backthrusts allowed it to be thick and to maintain its surface slope (Davis, Suppe & Dahden, 1983).

Irregular patterns of mesoscopic folds and wide scatter of bed poles in trench-slope (Mithakhari) sediments (Fig. 12a) were possibly linked with thrust emplacement. Poorly developed mesoscopic folds and the presence of frequent nonconformities suggest that the irregular pattern of the folds was linked with episodic changes in basin floor topography.

8. Evolution of forearc

Forearc basins, in general, are younger and less deformed than those of accretionary origin (Macdonald, 1993). Less deformation overall, regular fold patterns, wide lateral extent of beds and development of a large-scale submarine fan are suggestive of a simpler basinal configuration for the Andaman Flysch and Archipelago group of rocks in a forearc environment. With gradual shoaling of the outer arc and the inception of carbonate buildups on its fringe areas, the forearc basin was marked by a change in deposition from siliciclastic to carbonate turbidites with recurrent influx of pyroclastics.

The forearc developed either because of (1) oblique subduction of the Indian plate (cf. Uyeda & Kanamori, 1979), resulting in margin-normal and margin-parallel strike-slip faults or (2) failure of the wedge stability through normal/strike-slip faults, transverse and parallel to the strike of the accretionary prism (east–west) (Fig. 15) (cf. Platt, 1986). Ophiolite-derived clasts within the inner fan part of the forearc siliciclastic submarine fan suggest the outer arc as an important sediment source. Apart from local ophiolite provenance, quartz-rich sediments derived dominantly from the north indicate the Irrawardy delta of Burma as another possible source of sediment. Sediment transport from Burma to the south of Sumatra along the trench axis has also been suggested earlier by Moore, Curray & Emmel (1982). During Mio-Pliocene times, the inner arc also probably supplied huge amounts of pyroclastic sediments in the form of either ash fall or subaqueous pyroclastic flows (Table 2; Srinivasan, 1988). The dominance of shallow-water carbonate clastics in the top part of the Mio-Pliocene section suggests the proximal part of the basin might have been uplifted at least above the storm wave base and resulted in shedding of carbonate clastics in the deeper part. Sediment supply from the Bengal fan to the forearc through debris flows and distal turbidites is, however, barred by an uplifted outer-arc ridge.

A decline in the intensity and recurrence of volcanic activity through the Mio-Pliocene pyroclastic section is expressed in the dominance of subaqueous debris flows (cf. Nemec & Steel, 1984) in the lower part, low concentration currents with limited turbulence (Middleton & Hampton, 1973; Wright & Mutti, 1981) in the middle, and thin ash turbidites of distal character in the topmost part. A retrogradational basin filling history is inferred, as the distal facies association

overlies the proximal one. A change in facies stacking motif from a retrogradational to progradational pattern is recorded only towards the end of Mio-Pliocene time where a thickening-upward amalgamated carbonate turbidite unit overlies the pyroclastic section (Fig. 15, Table 2).

9. Discussion and conclusions

The subduction–accretion complex around the Andaman and Nicobar Islands can be considered as a tectonic prism resting on the subducting Indian plate with the Burma platelet as a rigid buttress behind the prism. The deformations recorded in Cretaceous sediments of the Bengal fan to the west of the Java Trench (Moore, Curray & Emmel, 1982) do not favour onset of subduction during Miocene times as suggested by Sengupta, Ray & Acharyya (1990). Seismic profiles in the Andaman Sea, particularly to the east of the Middle Andaman Islands, also show a series of folded thrust packets of Cretaceous age which supports the onset of subduction in Cretaceous times (Roy, 1992). Furthermore, an accretionary wedge formed by the accretion of ocean plate along with sediments during Cretaceous times has also been recorded from Java, the southern extension of this subduction complex (cf. Wakita, 2000). The beginning of subduction in Late Jurassic to Early Cretaceous times is suggested by (1) the tectonic accretion of Triassic foreland flysch sediments (cf. Mitchell, 1985) and (2) granodiorite plutons yielding Cretaceous K–Ar ages (Gansser, 1964).

The sequential change in the dip of thrusts from west to east in the mapped area suggests accretion of ophiolite slices in their present position rather than their emplacement as allochthonous nappe sheets. In the South Andaman Islands, Oligocene sediments show onlapping relations with Eocene sediments. Drilling records from west to east of the Andaman Islands and surrounding sea even up to 4 km depth do not record Oligocene sediments below Cretaceous ophiolites (Roy & Das Sharma, 1993). With continuous subduction from the Cretaceous onwards, a number of ophiolite slices along with pelagic sediments were scraped off to form an accretionary prism. During Eocene times, basins were isolated and separated by thrust-bounded structural ridges of ophiolite basement. Western basins in this accretionary prism are probably younger than the eastern ones. Individual basins with ophiolitic provenance and overlying coarse detritus were uplifted and became part of the accretionary complex. The irregular fold pattern of these sediments may be the effect of tectonically induced episodic changes in basin floor geometry on a trench slope. The depositional pattern of these Eocene sediments indicates that the basins were originally isolated from a terrigenous supply source and this allowed accumulation of hemipelagites with occasional intrabasinal mass flows. With progressive shoaling and lowering of relative sea level, accretionary processes became dominant and detritus was supplied through submarine canyons cutting through tectonically generated slopes. Progadational depositional cycles and evidence of emergence indicate frontal accretion and tectonic shoaling in these basins (Chakraborty *et al*. 1999). Uplift of ophiolites along with sediments during Late Cretaceous to Eocene times has also been reported from the Sumatra and Java areas (cf. Hall, 1996, 2002).

Frontal accretion eventually led to a gradual increase in the slope of the wedge and ultimately to extension during late Eocene–Oligocene times. A fault-controlled forearc basin was initiated at the back of the prism. Uplift of the accretionary complex and its erosion influenced fan development in the adjacent forearc. During Late Oligocene times, this turbidite package became juxtaposed with units of accretionary prism. In addition to siliciclastic turbidites the forearc was also fed by recurrent pyroclastic influx in Miocene time. Towards the end of forearc deposition the shallowing of the basin favoured carbonate deposition. Further south of the subduction zone, for example, between Sumatra and Java, the absence of volcanic activity from Early Eocene to Early Miocene times has been correlated to northwards advancement of the subduction zone during anticlockwise rotation of Sundaland (Hall, 2002) which may be valid for the Andaman region also.

Inner-arc volcanic activity from the Andaman and Nicobar Islands has so far been reported from Quaternary age (Narcondam and active Barren) volcanoes. Cretaceous and Cenozoic arc volcanic activity has been reported from Burma (cf. Mitchell, 1985) and in many on-land places in Sumatra and Java (Heryanto *et al*. 1994, cited in Wakita, 2000; Wakita *et al*. 1998; Hall, 2002). Recent reports of pyroclastic flow deposits interbedded with Mio-Pliocene turbidites indicate arc volcanism from the Mio-Pliocene in this part of the plate margin (Pal, Dutta Gupta & Das Gupta, 2002). Dating of seamounts in the Andaman Sea (such as Sewell and Alcock seamounts) along with the search for pyroclastics in Eocene and Oligocene sediments will help in understanding the evolution of the inner arc in the Andaman and Nicobar areas. In the easternmost part of the Andaman Sea (Kra Isthmus and Phuket Islands of Thailand), Carboniferous to Permian rocks (Garson, Amos & Mitchell, 1976) are intruded by tin-tungsten bearing granite plutons of Paleocene age (cf. Mitchell, 1985). The tectonic belt containing similar rocks extends up to the western part of the Mogok belt of Burma (Maung Thein & SoeWin, 1970). Paleocene granites with a high Sr^{87}/Sr^{86} ratio (0.717) and abundant muscovite suggest melting of metasedimentary rocks (cf. Mitchell, 1985). The outer-arc ridge of this arc system is continuous from north of the Andaman Islands to southwest of Java (Hamilton, 1973, 1977). The onland outer arc

with associated forearc represented in the Andaman and Nicobar Islands have parallels in the Indo-Burma Ranges, the Western Trough of Burma and in central Java. The sediments and tin-granite belt extend from the eastern part of the Andaman Sea northwards to Burma. A zone of imbricate en-echelon E-verging thrusts in the western part of the Shan Plateau passes through Thailand and Burma into the western margin of the Gulf of the Siam and possibly along the Khlong Marua strike-slip fault up to eastern part of Sumatra (cf. Mitchell, 1985). All these features suggest that the Burma–Andaman Nicobar–Indonesia arc formed in a continuous belt on the western margin of Southeast Asia before opening of the Andaman Sea by Late Cenozoic dextral movement along the Sagaing fault (cf. Maung, 1987; Mitchell, 1985).

Deformation of Eocene–Oligocene–Mio-Pliocene sediments in the Andaman Islands, accretion of Cretaceous–Eocene sediments, arc volcanic activity in Mio-Pliocene time and young volcanoes in the Andaman and Nicobar Islands suggest that subduction-related processes in the Java trench were operative either continuously or intermittently from Cretaceous times onwards. These tectonic events concluded at the end of Eocene times in the northern part of complex, that is, in Burma and in the southern part of complex, in Indonesia. Since Burma and India were juxtaposed from the end of Eocene times (Mitchell, 1985), the arc and forearc development of the Andaman and Nicobar Islands can have parallels with the southern part of subduction complex, that is, Sumatra and Java. The dextral displacement along the Sagaing fault and spreading of the Andaman Sea accelerated the separation of the Burma plate from North Sumatra during Middle Miocene times (Hall, 2002). The Andaman Sea is recognized as a pull-apart basin (Curray, 1988) rather than a typical backarc basin. Right lateral movement along the Sagaing fault in the central part initiated the opening of basin (Curray *et al*. 1978). This is indicated by the presence of a series of E–W/NE–SW seismogenic faults at the leading edge of the Indian plate all along the subduction complex (cf. Das Gupta & Nandy, 1995). The subduction direction was oblique in the Andaman region and orthogonal between Sumatra and Java (cf. Hall, 2002). The oblique plate motion was resolved into trench normal subduction and dextral movements, which generated strike-slip faults and developed the forearc basin in this part of the subduction complex.

Acknowledgements. This work is an output of five years of field season programmes of the Geological Survey of India (GSI) from 1996–97 to 2000–2001.The authors are thankful to Dr S. K. Ray, Sri M. K. Dhara, former Directors, Proj. Andaman and Dr S. C. Das Gupta, Director, Proj. Andamans, Eastern Region, Geological Survey of India for their guidance. The authors are grateful to Sri R. N. Ghosh and Sri D. Chatterjee, former Dy Director Generals, Geological Survey of India, for their inspiration and permission to publish the geological maps of the area. The authors acknowledge the help of Dr A. Roychowdhury for fossil study and Dr Sabyasachi Das Gupta for his valuable suggestions to improve the manuscript. The authors are very much thankful to Prof. Robert Hall for his critical review and valuable suggestions, which have improved the manuscript significantly.

References

ACHARYYA, S. K., RAY, K. K. & ROY, D. K. 1989. Tectonostratigraphy and emplacement history of the ophiolite assemblage from Naga Hills and Andaman Island arc, India. *Journal of the Geological Society of India* **33**, 4–18.

ALDISS, D. R. 1981. Plagiogranites from the ocean crust and ophiolites. *Nature* **289**, 577–8.

CHAKRABORTY, P. P. & PAL, T. 2001. Anatomy of a Forearc Submarine Fan: Upper Eocene–Oligocene Andaman Flysch Group, Andaman Islands, India. *Gondwana Research* **4**(3), 477–86.

CHAKRABORTY, P. P., PAL, T., DUTTA GUPTA, T. & GUPTA, K. S. 1999. Facies pattern and depositional motif in an immature trench-slope basin, Eocene Mithakhari Group, Middle Andaman, India. *Journal of the Geological Society of India* **53**, 271–84.

CHATTERJEE, P. K. 1964. Geology of the main islands of the Andaman area. In *Proceedings of the Symposium on the Upper Mantle Project*, pp. 348–60. National Geophysical. Research Institute of India.

CONDIE, K. C. 1989. *Plate Tectonics and Crustal Evolution* (3rd edition). Pergamon Press, 469 pp.

CORFIELD, R. I., SEARLE, M. P. & PEDERSON, R. B. 2001. Tectonic setting, origin and obduction history of the Spontang ophiolite, Ladakh Himalaya, NW India. *Journal of Geology* **109**, 715–36.

CURRAY, J. R. 1988. The Sunda Arc: a model for oblique plate convergence. In *Proceedings of the Snellius II Symposium, Jakarta, Nov. 23–28, 1987* V. I. Geology and geophysics of the Sunda arc and adjacent areas (eds J. E. van Hinte, Tj. C. E. Weering and A. R. Fortuin), pp. 89–108. *Netherlands Journal of Sea Research* 1.

CURRAY, J. R. & MOORE, D. G. 1974. Sedimentary and tectonic processes in the Bengal deep sea fan and geosyncline. In *The geology of continental margins* (eds C. A. Burke and C. L. Drake), pp. 617–27. New York: Springer Verlag.

CURRAY, J. R., MOORE, D. G., LAWVER, L. A., EMMEL, F. J., RAITT, R. W., HENRY, M. & KIECKHEFER, R. 1978. Tectonics of the Andaman Sea and Burma. In *Geological and Geophysical Investigations of Continental Margins*, pp. 189–98. American Association of Petroleum Geology, Memoir no. 29.

DAS GUPTA, S. & MUKHOPADHYAY, M. 1993. Seismicity and plate deformation below the Andaman Arc, northeastern Indian Ocean. *Tectonophysics* **225**, 529–42.

DAS GUPTA, S. & NANDY, D. R. 1995. Geological framework of the Indo-Burmese convergent margin with special reference to ophiolite emplacement. *Indian Journal of Geology* **67**(2), 110–25.

DAVIS, D., SUPPE, J. & DAHDEN, F. A. 1983. Mechanics of fold and thrust belts and accretionary wedges. *Geophysical Research* **88**, 1153–72.

DICKIE, J. R. & HEIN, F. J. 1995. Conglomeratic fan deltas and submarine fans of the Jurrasic Labarge Group. Whitehorse Trough. Yukon Territory, Canada: fore-arc

sedimentation and unroofing of a volcanic island-arc complex. *Sedimentary Geology* **98**, 263–92.

DICKINSON, W. R. & SEELY, D. R. 1979. Structure and stratigraphy of forearc regions. *American Association of Petroleum Geologists Bulletin* **63**, 2–31.

GANSSER, A. 1964. *Geology of the Himalayas.*New York: Wiley-Interscience, 289 pp.

GARSON, M. S., AMOS, B. J. & MITCHELL, A. H. G. 1976. *The geology of the area around Neyaungga and Yengan, Southern Shan State, Burma.* Institute of Geological Science, London. Overseas Memoir 2, 70 pp.

GASS, I. G. 1990. Ophiolites and Oceanic lithospheres. In *Proceedings of the Symposium "Troodos 1987": Ophiolites and Oceanic Crutal Analogues* (eds J. Malpas, E. M. Moores, A. Panayiotou and C. Xenophontos), pp. 1–10. Geological Survey of Cyprus.

GRAMMAN, F. 1974. Some palaeontological data on the Triassic and Cretaceous of the western part of Burma. *Newsletter Stratigraphy* **3**, 277–90.

GUZMAN-SPEZIALE, M. & NI, J. F. 2000. Comment on Subduction in the Indo-Burma region: Is it still active? by S. P. Satyabala. *Geophysical Research Letters* **27**, 1065–6.

HALL, R. 1996. Reconstructing Cenozoic SE Asia. In *Tectonic evolution of SE Asia* (eds R. Hall and D. J. Blundell), pp. 153–84. Geological Society of London, Special Publication no. 106.

HALL, R. 2002. Cenozoic geological and plate tectonic evolution of SE Asia and the SW Pacific: computer-based reconstructions and animations. *Journal of Asian Earth Sciences* **20**(4), 353–434.

HAMILTON, W. 1973. Tectonics of the Indonesian Region. *Geological Society of Malaysia Bulletin* **6**, 3–10.

HAMILTON, W. 1977. Subduction in the Indonesian region. In *Island arcs, deep sea trenches and back arc basins* (eds M. Talwani and W. C. Pitman III), pp. 15–31. American Geophysical Union. M. Ewing Series, 1.

HAMILTON, W. 1979. *Tectonics of the Indonesian Region.* U. S. Geological Survey Professional Paper 1078, 345 pp.

JAFRI, S. H. 1986. Occurrence of Hagistrids in chert associated with Port Blair Seies, South Andaman, India. *Journal of the Geological Society of India* **28**, 41–3.

JAFRI, S. H., CHARAN, S. N. & GOVIL, P. K. 1995. Palagiogranite from the Andaman ophiolite belt, Bay of Bengal, India. *Journal of the Geological Society, London* **152**, 681–7.

KARIG, D. E. 1974. Tectonic erosion at trenches. *Earth and Planetary Science Letters* **21**, 209–12.

KARIG, D. E. & SHARMAN, G. F. 1975. Subduction and accretion in members. *Geological Society of America Bulletin* **86**, 377–89.

KARIG, D. E., LAWRENCE, M. B., MOORE, G. F. & CURRAY, J. R. 1980. Structural framework of the forearc basin, NW Sumatra. *Journal of the Geological Society, London* **137**, 77–91.

KARIG, D. E., SUPARKA, S., MOORE, G. F. & HEHANUSSA, P. E. 1979. Structure and Cenozoic evolution of the Sunda arc in the Central Sumatra Region. In *Geological and geophysical investigations of continental margins* (eds J. S. Watkins, L. Montadert and P. W. Dickerson), pp. 223–37. American Association of Petroleum Geologists, Memoir no. 29.

KARUNAKARAN, C., RAY, K. K. & SAHA, S. S. 1967. A revision of the stratigraphy of Andaman and Nicobar Islands. India. *Bulletin of the National Institute of Science, India* **38**, 436–41.

KARUNAKARAN, C., RAY, K. K. & SAHA, S. S. 1968. Tertiary sedimentation in the Andaman-Nicobar geosyncline. *Journal of the Geological Society of India* **9**, 32–9.

MACDONALD, D. I. M. 1993. Controls on sedimentation at convergent plate margins. *Special Publication of International Association of Sedimentologists* **20**, 225–57.

MAUNG, H. 1987. Transcurrent movements in the Burma–Andaman sea region. *Geology* **15**, 911–12.

MAUNG THEIN & SOE WIN. 1970. The metamorphic petrology, structure and mineral resources of the Shantaung-u-Thandawmywet Range, Kayaukse District. *Union of Burma: Journal of Science and Technology* **3**, 487–514.

MCCRORY, P. A. 1995. Evolution of a trench-slope basin within the Cascadia subduction margin: the Neogene Humboldt Basin, California. *Sedimentology* **42**, 223–47.

MCCOURT, W. J., CROW, M. J., COBBING, E. J. & AMIN, T. C. 1996. Mesozoic and Cenozoic plutonic evolution of SE Asia: evidence from Sumatra, Indonesia. In *Tectonic evolution of SE Asia*(eds R. Hall and D. J. Blundell), pp. 321–35. Geological Society of London, Special Publication no. 106.

MIDDLETON, G. V. & HAMPTON, M. A. 1973. Sediment Gravity Flows: Mechanics of Flow and Deposition. In *Turbidites and Deep Water Sedimentation* (eds G. V. Middleton and A. H. Bouma), pp. 1–38. S.E.P.M. Pacific Section Short Course, Anaheim.

MITCHELL, A. H. G. 1984. Initiation of subduction by post-collision foreland thrusting and back thrustng. *Journal of Geodynamics* **1**, 103–20.

MITCHELL, A. H. G. 1985. Collision-related fore-arc and back-arc evolution of the Northern Sunda arc. *Tectonophysics* **116**, 323–34.

MOORE, G. F., BULLMAN, H. G., HEHANUSSA, P. E. & KARIG, D. E. 1980. Sedimentology and paleobathymetry of Neogene trench-slope deposits, Nias Island, Indonesia. *Journal of Geology* **88**, 161–80.

MOORE, G. F., CURRAY, J. R. & EMMEL, F. J. 1982. Sedimentation in the Sunda trench and forearc region. In *Trench-Forearc Geology: Sedimentation and Tectonics on Modern and Ancient Active Plate Margins*(ed. J. K. Legget), pp. 245–58. Geological Society of London, Special Publication no. 10.

MOORES, E. M., ROBINSON, P. T., MALPAS, J. & XENOPHONTOS, C. 1984. A model for the origin of the Troodos massif, Cyprus and other Mideast Ophiolites. *Geology* **12**, 500–3.

MUKHOPADHYAY, M. 1988. Gravity anomalies and deep structure of the Andaman-Arc. *Marine Geophysical Research* **9**, 197–211.

NEMEC, N. & STEEL, R. J. 1984. Alluvial and coastal conglomerates: Their significant features and some comments on gravity mass-flow deposits. In *Sedimentology of gravels and conglomerates* (eds E. H. Koster and R. J. Steel), pp. 1–31. Canadian Society of Petroleum Geologists, Memoir no. 10.

PAL, T., DUTTA GUPTA, T. & DAS GUPTA, S. C. 2002. Vitric tuff from Archipelago Group of rocks (Mio-Pliocene) of South Andaman. *Journal of the Geological Society of India* **59**, 111–14.

PAL, T., CHAKRABORTY, P. P. & GHOSH, R. N. in press. PGE distribution in Andaman ophiolites and its parental melt. *Journal of the Geological Society of India.*

PARKINSON, C. D., MIYAZAKI, K., WAKITA, K., BARBER, A. J. & CARSWELL, D. A. 1998. An overview and tectonic synthesis of the very high pressure and associated rocks of Sulawesi, Jaa and Kalimantan, Indonesia. *The Island Arc* **7**, 184–200.

PAWDE, M. B. & RAY, K. K. 1963. On the age of Graywackes in South Andaman. *Science and Culture* **30**, 279–80.

PLATT, J. P. 1986. Dynamics of orogenic wedges and the uplift of high-pressure metamorphic rocks. *Geological Society of America Bulletin* **97**, 1037–53.

POSTMA, G. & CRUICKSHANK, C. 1988. Sedimentology of a terraced Gilbert-type delta. In *Fan-Deltas: Sedimentology and Tectonic Setting* (eds W. Nemec and R. J. Steel), pp. 144–57. Glasgow: Blackie.

PULUNGGONO, A. & CAMERON, N. R. 1984. Sumatran microplates, their characteristics and their role in the evolution of the Central and South Sumatra basins. *Proceedings of Indonesian Petroleum Association*, 13th Annual Convention, 121–44.

RAY, K. K. 1982. A review of the geology of Andaman and Nicobar Islands. *Geological Survey of India Miscellaneous Publication* **42**(2), 110–25.

RAY, K. K. 1985. East Coast Volcanics – a new suite in the ophiolites of Andaman Islands. *Record Geological Survey of India* **116**(2), 83–7.

RAY, K. K., SENGUPTA, S. & VAN DEN HUI, H. J. 1988. Chemical characters of volcanic rocks of Andaman ophiolite, India. *Journal of the Geological Society, London* **145**, 393–400.

RICCI LUCCI, F. 1985. Influence of transport processes and basin geometry on sand composition. In *Provenance of Arenites* (ed. G. C. Zuffa), pp. 19–45. Dordrecht: Reidel.

ROY, D. K., ACHARYYA, S. K., RAY, K. K., LAHIRI, T. C. & SEN, M. K. 1988. Nature of occurrence and depositional environment of the oceanic pelagic sediments associated with the ophiolite assemblage, South Andaman Island. *Indian Mineralogy* **42**, 31–56.

ROY, S. K. 1992. Accretionary Prism in Andaman Forearc. *Geological Survey of India Special Publication* **29**, 273–8.

SAMUEL, A. & HARBURY, N. A. 1996. The Mentawai Fault zone and deformation of the Sumatran Forearc in the Nias Area. In *Tectonic evolution of SE Asia* (eds R. Hall and D. J. Blundell), pp. 337–51. Geological Society of London, Special Publication no. 106.

SATYABALA, S. P. 1998. Subduction in the Indo-Burma region: Is it still active? *Geophysical Research Letters* **25**, 3189–92.

SEELY, D. R., VAIL, D. R. & WALTON, G. G. 1974. Trench slope model. In *Geology of continental margins* (eds G. A. Burke and G. L. Drake), pp. 219–60. New York: Springer Verlag.

SENGUPTA, S., RAY, K. K. & ACHARYYA, S. K. 1990. Nature of ophiolite occurrences along the eastern margin of the Indian plate and their tectonic significance. *Geology* **18**, 439–42.

SRINIVASAN, M. S. 1988. Late Cenozoic sequences of Andaman Nicobar Islands; their regional significance and correlation. *Indian Journal of Geology* **60**, 11–34.

STAKES, D. S., TAYLOR, H. R. JR. & FISHER, R. I. 1984. Oxygen isotope and geochemical characterization of hydrothermal alteration in ophiolite complexes and modern oceanic crust. In *Ophiolites and oceanic lithosphere* (eds I. G. Gass, S. J. Lippard and A. W. Shelton), pp. 199–214. Geological Society of London, Special Publication no. 13.

TAPPONNIER, P., PELTZER, G., LE DANIN, A. Y., ARMIJO, R. & COBOLD, P. 1982. On the propagating extrusion tectonics in Asia: new insights from simple experiments with plasticine. *Geology* **10**, 611–16.

UNDERWOOD, M. B. & BACHANAN, S. B. 1982. Sedimentary facies associations within subduction complexes. In *Trench Forearc Geology: Sedimentation and Tectonics on Modern and Ancient Active Plate Margins* (ed. J. K. Legget), pp. 537–50. Geological Society of London, Special Publication no. 10. Oxford: Blackwell Scientific Publications.

UYEDA, S. & KANAMORI, H. 1979. Back-arc opening and the mode of subduction. *Journal of Geophysical Research* **82**, 1049–61.

VOHRA, C. P., HALDAR, D. & GHOSH ROY, A. K. 1989. The Andaman–Nicobar ophiolite complex and associated mineral resources – current appraisal: Phanerozoic ophiolites of India (ed. N. C. Ghosh), pp. 281–315. Summary Publication, Patna.

WAKITA, K. 1997. Oceanic plate stratigraphy and tectonics in East and Southeast Asia. *Proceedings of the International Conference on Stratigraphy and Tectonic Evolution of Southeast Asia and the South Pacific* (eds Phisit Dheeradilok, Chaiyan Hinthong *et al.*), pp. 12–16. Bangkok, Thailand.

WAKITA, K. 2000. Cretaceous accretionary–collision complexes in central Indonesia. *Journal of Asian Earth Sciences* **18**, 729–49.

WAKITA, K., MIYAZAKI, K., ZULKARNAIN, I., SOPAHELUWAKAN, J. & SANYOTO, P. 1998. Tectonic implication of new age data for the Meratus Complex of South Kalimantan, Indonesia. *Island Arc* **7**, 202–22.

WRIGHT, J. V. & MUTTI, E. 1981. The Dali ash, islands of Rhodes, Greece: A problem in interpreting submarine volcanogenic sediments. *Bulletin of Volcanology* **44**, 153–67.

Annex B69

A. Uddin & N. Lundberg, "Miocene Sedimentation and Subsidence During Continent–Continent Collision, Bengal Basin, Bangladesh", *Sedimentary Geology*, Vol. 164, No. 1-2 (2004)

Available online at www.sciencedirect.com
SCIENCE DIRECT®
Sedimentary Geology 164 (2004) 131–146
Sedimentary Geology
www.elsevier.com/locate/sedgeo

Miocene sedimentation and subsidence during continent–continent collision, Bengal basin, Bangladesh

Ashraf Uddin[a,*], Neil Lundberg[b]

[a] Department of Geology and Geography, 210 Petrie Hall, Auburn University, Auburn, AL 36849-5305, USA
[b] Department of Geological Sciences, Florida State University, Tallahassee, FL 32306, USA

Received 9 April 2003; received in revised form 1 September 2003; accepted 23 September 2003

Abstract

The Bengal basin, a complex foreland basin south of the eastern Himalayas, exhibits dramatic variability in Neogene sediment thickness that reflects a complicated depositional and tectonic history. This basin originally formed as a trailing margin SE of the Indian continental crust, complicated by convergence with Asia to the north and oblique convergence with Burma to the east. Newly compiled isopach data and previously reported seismic data show evidence of thickening of basin fill toward the south, opposite of the pattern typically seen in foreland basins. This is presumably due to sedimentary loading of voluminous deltaic sediments near the continent–ocean boundary and basinward downfaulting analogous to that in the Gulf of Mexico. Isopach data show that there is considerable vertical relief along the base of the Miocene stratigraphic sequence, probably due to down-to-the-basin faulting caused by focused deltaic sedimentation and associated crustal flexure. In contrast, when viewed in east–west profile, basin shape is more typical of a foreland basin, with strata thickening eastward toward the Indo–Burman ranges, which reflects east–west convergence with Southeast Asia.

Comparison of the lateral and vertical extent of the Bhuban and Boka Bil Formations with the Bouguer anomaly map of Bangladesh suggests that considerable subsidence of the Sylhet trough (in the northeastern part of the Bengal basin), which has the lowest gravity value of the region, had not taken place by the end of the Miocene. This post-Miocene subsidence is attributed to tectonic loading from southward thrusting of the Shillong Plateau along the Dauki fault. Relatively uniform Miocene isopachs across the Sylhet trough confirm that this began in the Pliocene, consistent with results of recent research on sediment provenance. In the northwest, in the region south of the Siwalik foreland basin, continental crust has not as yet been loaded, allowing relatively little accommodation space for sediment accumulation. The Miocene here is very thin. Deltaic progradation across most of Bangladesh during the Miocene followed earlier, more proximal progradation across Assam, immediately northeast of the Bengal basin, and has been followed by continued progradation into the southern Bangladesh coastal and offshore region.

Keywords: Bengal basin; Bangladesh; Himalayas; Isopach maps; Surma Group

1. Introduction

The Bengal basin is a composite basin with a varied tectonic history. Other than minor Carbonifer-

* Corresponding author. Tel.: +1-334-844-4885; fax: +1-334-844-4486.
E-mail address: uddinas@auburn.edu (A. Uddin).

0037-0738/$ - see front matter © 2003 Elsevier B.V. All rights reserved.
doi:10.1016/j.sedgeo.2003.09.004

ous coal measures preserved at least locally on Precambrian continental crust, the main phase of deposition in this basin began following the separation of India from Antarctica at about the beginning of Late Cretaceous time (Sclater and Fisher, 1974; Molnar and Tapponnier, 1975). The motion of the Indian continent slowed markedly from the Early Eocene to Early Oligocene and then resumed in a north–northwesterly direction (Sclater and Fisher, 1974). Thick Tertiary deposits accumulated in the Bengal basin beginning in the Late Eocene, with deposition accelerating with the arrival of clearly orogenic sediments in the earliest Miocene (Uddin and Lundberg, 1998a). The Bengal basin is a large basin occupied dominantly by the Ganges–Brahmaputra delta. From at least Miocene to the present, the Ganges–Brahmaputra and associated or ancestral rivers have been transporting clastic sediments to the Bengal basin.

Exploration for gas and oil by several national and international oil companies has been continuing in the Bengal basin since about 1910. The Bangladesh part of the Bengal basin is rich in natural gas deposits. Proven reserves of natural gas exceed 13 trillion ft^3 (Murphy, 1988), and production is currently being used for domestic and industrial purposes. Most of the gas fields are characterized as structural traps located in the Sylhet trough of northeastern Bangladesh. There is at least one well that is producing oil in the Sylhet trough (Murphy, 1988). The major hydrocarbon producing sediment horizon is the Boka Bil Formation, an Upper Miocene unit that comprises the upper portion of the Surma Group. Exploration efforts here have produced a number of data sets that are useful in helping to decipher the paleogeography of the Bengal basin, with most data focusing on strata of the Miocene.

Proximal deposition of a portion of the orogenic sediment from the eastern Himalaya and the Indo–Burman uplifts has built a thick sequence (~ 20 km) of deposits in the Bengal basin. These deposits hold considerable potential for recording the erosion of and thus the tectonic events in the Himalayan and Indo–Burman mountain belts. Although the Himalayan belt and the sediments along its northwestern foothills have been studied for a number of years, and drill cores from distal portions of the Bengal deep-sea fan have been recovered by several drilling cruises, the deltaic sediments of the Bengal basin, through which the orogenic detritus is transported to reach the deep-sea fan, have not been studied in detail.

Isopach maps have been drawn from electric logs obtained from oil and gas exploration in the region, and gravity data have been compiled, in an effort to study the Miocene sedimentation patterns in the Bangladesh part of the Bengal basin and fundamental issues of paleogeography during the critical time periods immediately prior to and following the Miocene. The purpose of this paper is to address questions about basin-scale patterns of subsidence and sedimentation. The fundamental question addressed here is the following: what are the overall patterns of subsidence across the Bengal basin, and what do they imply about the history of basin development and regional tectonic events? Also, when did the considerable subsidence of the Sylhet trough take place, and what does this mean for the evolution of the prograding delta?

2. Regional geology

Bangladesh constitutes the eastern continuation of the central broad Indo–Gangetic plains of India, which serve to physiographically divide the Peninsular (shield) area to the south from the extra-Peninsular region (Himalayan mountain ranges) to the north and northeast (Fig. 1). The Bengal basin is located primarily in Bangladesh, with a lesser part in the West Bengal State of India, and lies roughly between 20°34′ to 26°38′N and 88°01′ to 92°41′E. The basin is surrounded by India on three sides. The Shillong Plateau of Assam lies to the immediate north, and the Himalayas to the distant north. The Indo–Burmese Arakan-Chin uplifts lie to the east and the Indian shield to the west. The area is open toward the south and drains into the Bay of Bengal in the northern Indian Ocean (Fig. 1). Sediment carried by three major rivers, the Ganges, the Brahmaputra, and the Meghna, is distributed to the Bengal deep-sea fan by turbidity currents through the ‘Swatch of No Ground’ (Curray and Moore, 1971; Kuehl et al., 1989), a submarine canyon. The Bay of Bengal has been identified as a remnant ocean basin (Curray et al., 1982; Ingersoll et al., 1995) because the basin has been closing by easterly subduction beneath the Indo–Burman ranges and the Andaman and Sunda Arcs.

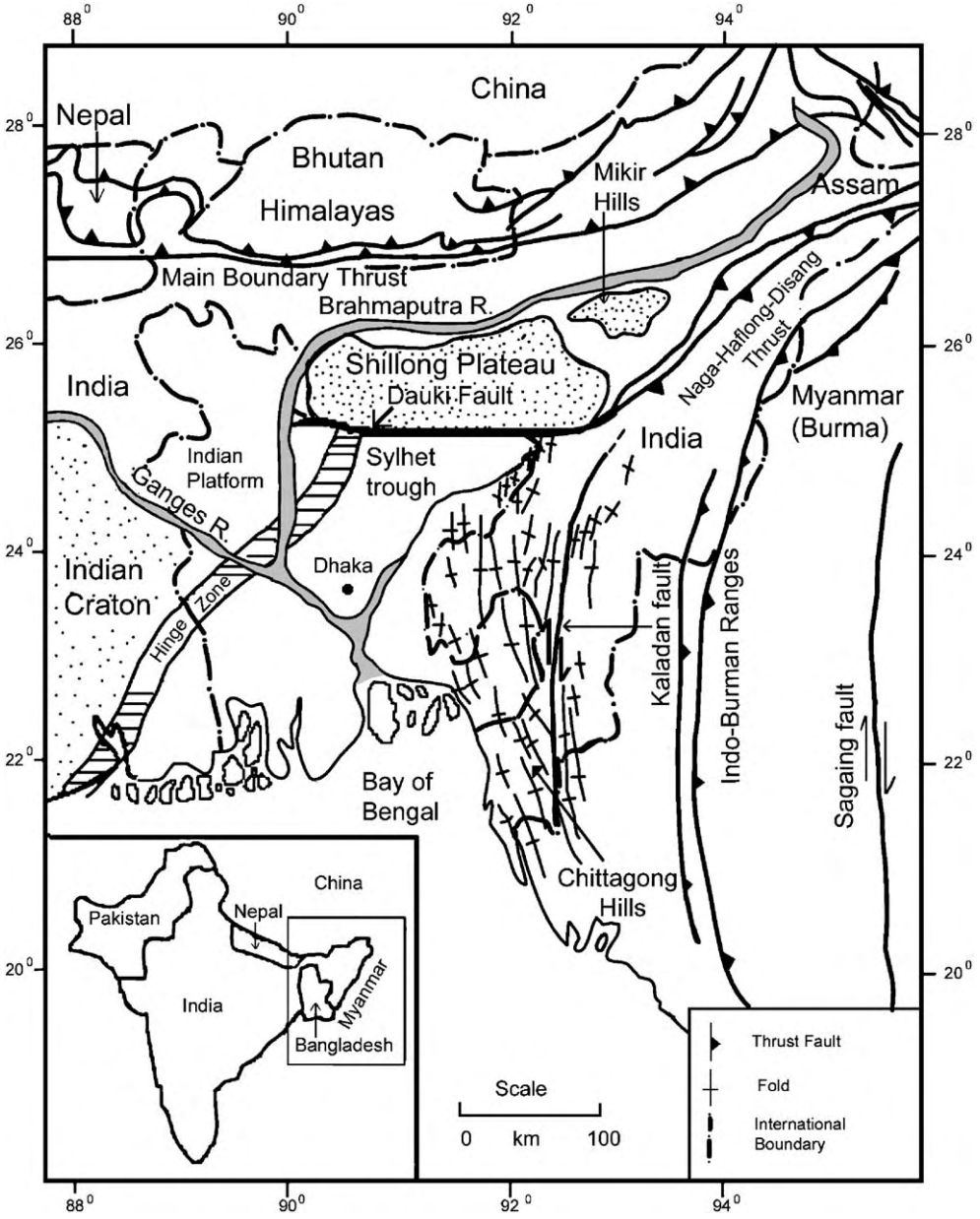

Fig. 1. Map showing major tectonic elements in and around the Bengal basin. Hinge zone demarcates the deeper basin from the Indian Platform area. Right-lateral N–S faults (e.g., Kaladan fault) are in the east. The Dauki fault separates the Sylhet trough from the uplifted Shillong Plateau at the north (after Uddin and Lundberg, 1998b).

The Shillong Plateau and the Mikir Hills to the north are underlain by Precambrian continental crust (Fig. 1). Previously, it was suggested that the Shillong Plateau was the result of right-lateral shear faulting having detached a block of Indian crust some 250 km eastward from the Rajmahal hills of India (Evans, 1964). More recently, vertical or dip-slip uplift has been suggested for the origin of the Shillong Plateau (Fig. 2a; Desikachar, 1974; Hiller and Elahi, 1984). The plateau appears presently as a horst block, bor-

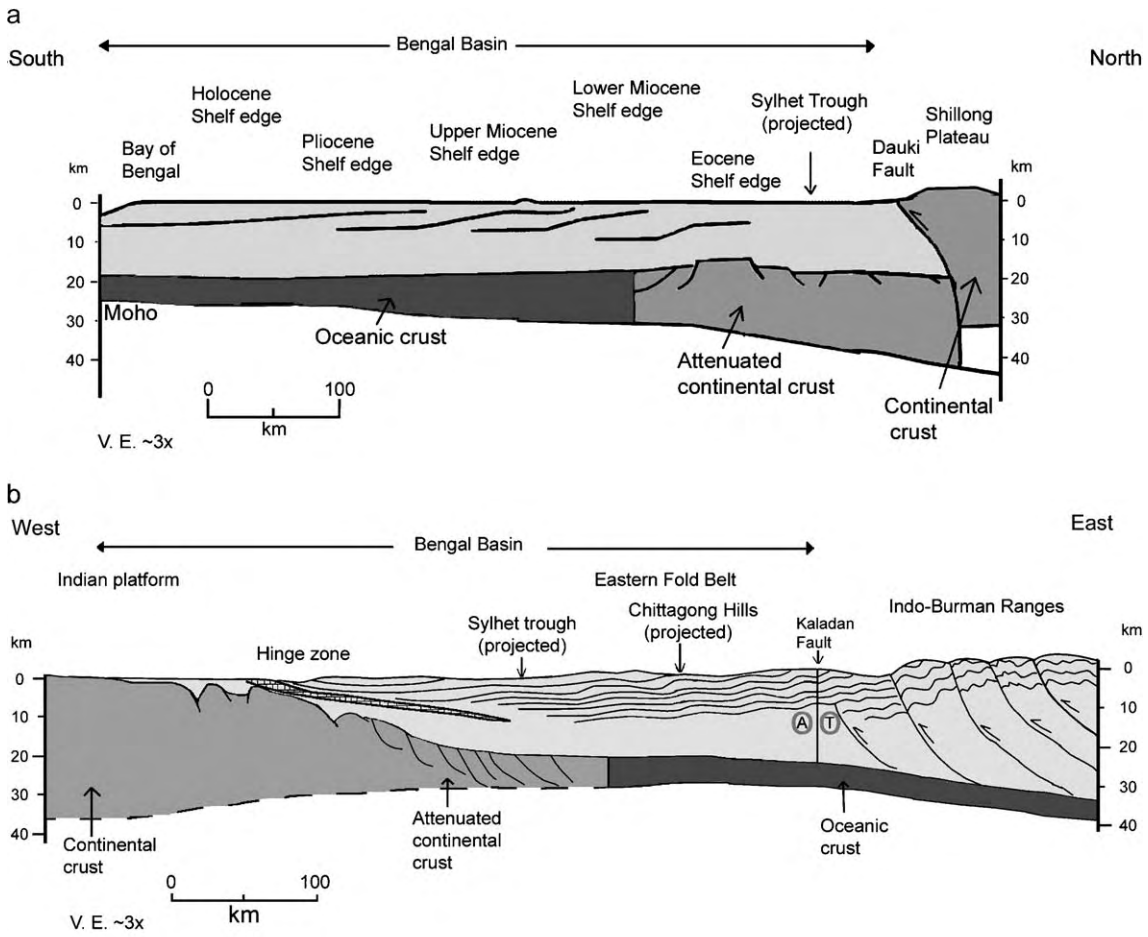

Fig. 2. Schematic cross-section of the Bengal basin; (a) N–S, through the Shillong Plateau; (b) E–W, through the northern Chittagong Hill region, after Murphy (1988). These show sediment thickening toward the south and east, respectively.

dered on all sides by faults (Khandoker, 1989) and drained by the Brahmaputra River on the north and west. The southern margin of the plateau is a south-dipping monocline, truncated by the prominent E–W trending Dauki fault, which marks the northern boundary of the Bengal basin (Fig. 1). Molnar (1987), based on interpretations of the seismotectonics of the region, interpreted the Dauki fault as an over-thrust. Johnson and Nur Alam (1991) also suggested that the Dauki fault is a thrust fault, with a dip similar to that of other frontal Himalayan thrusts (i.e., 5–10°; Molnar, 1987) and indicated that a few tens (28–80) of kilometers of horizontal tectonic transport would be required to carry the Shillong Plateau to its present elevation. Uplift of the Shillong Plateau also led to a 300 km westward shift of the Brahmaputra after the Miocene (Johnson and Nur Alam, 1991).

2.1. Tectonic setting

The Bengal basin is asymmetric; the thickness of the sediments increases toward the south and east to more than 16 km (Fig. 2a and b; Curray and Moore, 1971; Murphy, 1988). Interpretations of the tectonic setting of the basin are varied and rather convolute. Desikachar (1974) proposed a plate tectonic model of the region. He considered the Bengal basin as a peri-cratonic basin of the Indian plate. His proposition

suggests that the deeply subsided central portion of the Bengal basin forms part of the Indian plate, whereas the eastern basin margin is actually part of the Burmese plate. In his view, the Burmese plate has moved toward the Indian plate beginning in the Miocene, and just east of the Ninety-East ridge (or its northern extension), where he inferred maximum subsidence, the Burmese plate overrode the Indian plate to form a subduction zone between the two plates. Today most authors agree that convergence between India and Burma has resulted in subduction of oceanic crust beneath Burma, with the trailing margin of India currently passing obliquely into the foreland of the Indo–Burman ranges (Murphy, 1988; Mukhopadhyay and Dasgupta, 1988; Alam et al., 2003). This convergent margin has been complicated by right-lateral strike-slip motion (e.g., Kaladan fault, Sagaing fault; Fig. 1), possibly throughout the history of the collision (e.g., Ni et al., 1989).

Tectonically, the basin has two broad divisions: (1) the 'Indian platform' (also known as the 'Stable shelf' region) to the northwest and west, underlain by Precambrian continental crust, and (2) the deeper part of the basin in the south and east. The 'Hinge zone' (Sengupta, 1966) separates the two structural provinces. The basement of the 'Indian platform' slopes to the northwest and southeast from a central ridge, which has the shallowest occurrence (~ 140 m) of Precambrian rocks in Bangladesh. These basement rocks are generally considered to be an eastward subsurface continuation of rocks of the Indian Shield. From the Hinge zone, the southeastern slope of the Precambrian basement steepens rather abruptly (from 2–3° to 6–12°), and then dips more gently (1–2°) again in the deeper (SE) part of the basin. The narrow (25–100 km) 'Hinge zone' has also been known as the 'Calcutta–Mymensingh gravity high' (Sengupta, 1966; Khandoker, 1989), although more recent data (Khan and Agarwal, 1993) suggest that this term is somewhat misleading. The Hinge zone runs in a NE–SW direction (Fig. 1) between the Naga–Haflong–Disang thrust zone of Assam in the northeast to the Indian part of the Bay of Bengal, off the east coast of India to the south (Fig. 1).

The deeper part of the Bengal basin, a zone of very thick sedimentary strata lying over deeply subsided basement, is subdivided, based on gravity studies, into a northwestern platform flank, just east of the Hinge zone, and an eastern folded flank that includes the Chittagong Hills and the Sylhet trough in the northeastern part of the Bengal basin (Khandoker, 1989; Khan, 1991). The platform flank shows small-amplitude, isometric or geographically equant anomalies, whereas the folded flank exhibits large-amplitude, linear or elongate anomalies (Bakhtine, 1966). The Sylhet trough is a conspicuous trough of thick sedimentary fill along the northeastern part of the Bengal basin, and has been studied extensively as a result of successful petroleum exploration (Holtrop and Keizer, 1970; Woodside, 1983). The Sylhet trough is a depositional low located just south of the crystalline Shillong Plateau with a structural relief of about 20 km between the trough and the neighboring plateau (Murphy, 1988; Johnson and Nur Alam, 1991). The folded flank of the deeper basin is composed of elongated folds of north–northwest to south–southeast trend. Structural complexity of the folded flank increases from west to east and merges into the Indo–Burman ranges farther east (Khan, 1991). Strata exposed in the folded flank are broadly similar to those exposed along the length of the Sub-Himalayan belt of the Himalayas.

2.2. Stratigraphy

The stratigraphy of the basin (Fig. 3) is incompletely known because of thick sequences of alluvium cover and relative paucity of fossils. Comparative lithologic studies have been the only means to establish and to interpret the stratigraphy. The nomenclature and classification of the stratigraphy of the Bengal basin is established on the basis of type sections in the Assam basin (northeast India) (Khan and Muminullah, 1980). Stratigraphically, only the Tertiary rocks are exposed in the folded flank of the Bengal basin (Chittagong Hills and flanks of the Sylhet trough; Fig. 1) and the Permo–Carboniferous Gondwana coals are the oldest Phanerozoic sediments at the holes drilled into the Precambrian 'Indian platform' tectonic zone in northwest Bengal basin. These intracratonic, fault-bounded Gondwana coal deposits are exposed at the western fringe of the Bengal basin, in the Bihar State of India. There are also subsurface occurrences of volcanic rocks, equivalent to the Rajmahal traps of India, followed by trap-wash sediments

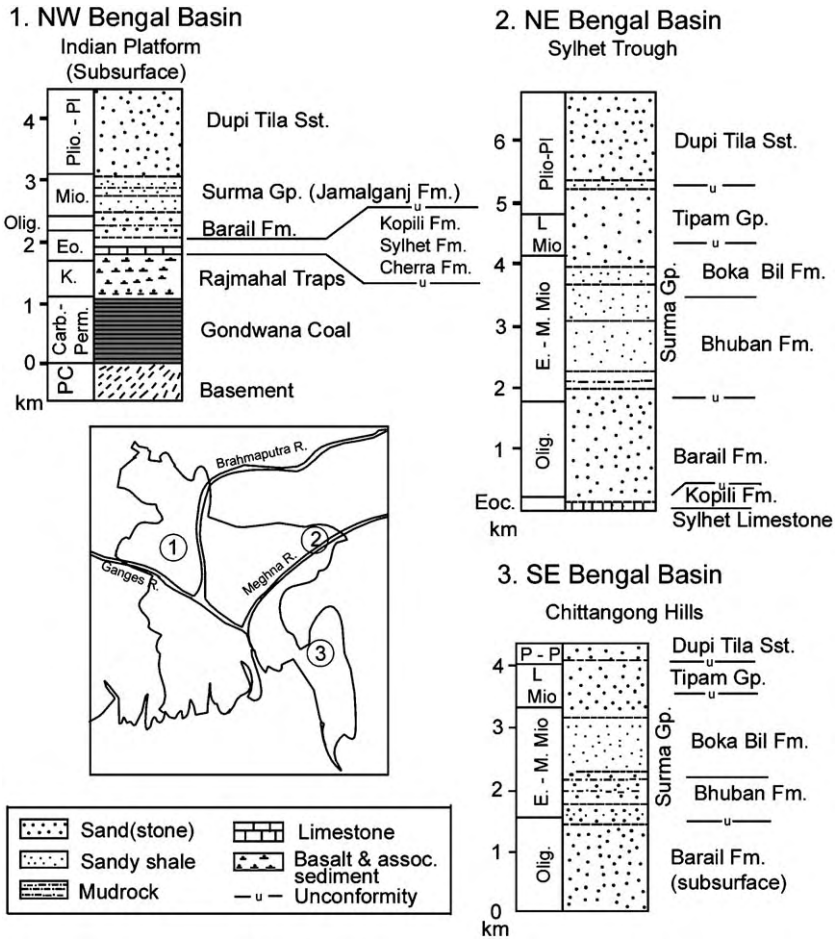

Fig. 3. Stratigraphic framework of the Bengal basin. Miocene sediment thickness is much lower near the Indian platform in the northwestern part of the basin. This shelf area of the basin is floored by continental crust (after Khan and Muminullah, 1980; Uddin and Lundberg, 1999; and many other sources).

present above the Gondwana coal formations at the NW of the Bengal basin.

Repeated submergence and emergence of the Bengal basin must have taken place in the shelf region during Late Cretaceous–Middle Eocene time, when the deeper parts of the Stable shelf of West Bengal, Bangladesh and Assam were invaded by the sea, whereas freshwater sedimentation of sandstone and carbonaceous mudrocks continued in most of the shallow shelf regions (Hoque, 1974; Banerji, 1981; Reimann, 1993). In the Bengal foreland and Indo–Burman ranges, sedimentation took place in a marine environment and turbidites probably played an important role in sedimentation (Graham et al., 1975). The Eocene interval is marked by an extensive marine transgression caused by conspicuous basin-wide subsidence. Clastic sediment input on the 'Stable shelf' was reduced and the shelf became the site of deposition of shallow, clear water, open marine, limestone. These limestones, commonly known as the Sylhet Limestone, are very rich in fossil nummulites. This limestone is exposed at the northern fringe of the Sylhet trough on the south slope of the Shillong plateau.

The Oligocene to Earliest Miocene time was characterized by a major marine regression exposing most of the 'Stable shelf.' The Bengal basin is bounded from the Burma basin to the east by the Indo–Burman

ranges. The Oligocene clastic rocks (Barail Group) are exposed in part of the Sylhet trough and drilled in some holes (Holtrop and Keizer, 1970; Reimann, 1993).

The Miocene Surma Group is a diachronous unit consisting of a succession of alternating mudrock, sandstone, siltstone and sandy shales with occasional thin conglomerates (Imam and Shaw, 1985). Overlying the Surma Group, the Upper Marine Shale represents a regional marine transgression in the region (Holtrop and Keizer, 1970). By Early Miocene time, a major phase of sedimentation started and huge amounts of clastic sediment were funneled into the basin from the northeast and the major Mio–Pliocene delta complex started to build from the northeast (Uddin, 1990). A considerable amount of sediment was also coming into the basin from the northwest and small deltas were building on the western side of the basin (Alam, 1989). Sedimentation was in deltaic and open-shelf environments along the basin margins, whereas turbidites were controlling the sedimentation in the central and southern areas (Alam, 1989). Deltaic sedimentation during the Miocene has been documented based on extensive studies of lithofacies (e.g., Alam, 1989; Uddin and Lundberg, 1999), and fossil assemblages (mostly palynology; as cited in Reimann, 1993), confirmed by studies of seismic reflection character (Salt et al., 1986; Lindsay et al., 1991). Many investigations of lithofacies have reported mainly coastal to shallow water deposits, with some reports of deep marine strata in SE Bangladesh (e.g., Reimann, 1993; Gani and Alam, 1999). Tests of foraminifers and hystrichospherids from the more shaly sequences in the Chittagong Hills also indicate brackish to marine environments. Remains of gastropods, lamellibranchiats, echinoids and burrows discovered in cross-bedded sandstone of the Bhuban Formation indicate nearshore depositional environments (Reimann, 1993). A paleogeographic reconstruction of the Bengal basin in the Miocene (Alam, 1989) shows several deltaic complexes prograding from the northeast, east, west and northwest into the basin. Strata of the overlying Tipam Formation were laid down under continental fluviatile conditions (Alam, 1989). During this time, strata along the eastern margin of the Bengal basin began to be actively deformed, producing a distinct mobile belt (folded flank of the deeper part of the basin) known as the Chittagong folded belt.

The Late Miocene–Pliocene time was a period of intense deformation and uplift in the mobile belts of the Bengal basin, contributing to widespread regression of the sea (Hoque, 1974). A regression during the Late Miocene (the Messinian) has also been seen in seismic reflections recorded far offshore in the Bay of Bengal (Curray and Moore, 1971). West-directed compression propagated westward, deforming strata in the area of the Chittagong Hill tracts. Deposition of fluviatile and deltaic sandstones and conglomerates (Dupi Tila Sandstone and Dihing Formation) took place in the eastern fold belt and in the Sylhet trough (Holtrop and Keizer, 1970).

The Quaternary in the Bengal basin was marked by a general regression presumably due to voluminous sediment influx from the highlands, although glacioeustatic oscillations have also been recorded (Morgan and McIntire, 1959). Much of the present geomorphic landscape of the Bengal basin and the regions surrounding it developed during this time (Hoque, 1974). Pleistocene and Holocene deposits are represented on land by three areas of red clay deposits, a coastal coral bed and several small sand bodies, but voluminous deltaic deposits of this age are restricted to the offshore regions of the Bay of Bengal.

3. Methods

The Miocene Surma Group is the stratigraphic interval that is of particular interest from the perspective of hydrocarbon occurrence in Bangladesh, because all natural gas pay zones are found in this group. Because these strata are well represented in the deeper parts of the basin, petroleum exploration has produced a wealth of subsurface data. Electric logs obtained during hydrocarbon exploration were analyzed to measure thicknesses of the Miocene units (the Bhuban and Boka Bil Formations) in 18 wells (Table 1). These Miocene units are bounded below by a basal-Miocene unconformity, and bounded above by a distinctive seismic reflector known as the "Upper Marine Shale" (Reimann, 1993). The contact between these two units is transitional, identified mainly on the basis of lithology and supported by palynomorphs and some foraminifers (Reimann, 1993). Related subsurface data were also studied to compare and decipher

Table 1
Thickness of two Miocene units (Bhuban and Boka Bil Formations) of the Surma Group in the Bengal basin in various wells of Bangladesh

Tectonic location		Wells	Thickness of Boka Bil Formation (in meters)			Thickness of Bhuban Formation (in meters)		
Major	Important subdivision		From	To	Total	From	To	Total
Shelf		Bogra-1	217	782	565	782	1593	811
		Kuchma-X1	340	1090	750	1090	1606	516
		Singra-IX	1290	1600	310	1600	1880	280
Hinge zone		Hazipur-1	1393	2247	854	2247	3130	883
Deeper basin	Surma basin (=Sylhet trough)	Chattak-1	626	1081	456	1082	2134	1052
		Sylhet-2	1240	1915	675	1915	2818	903
		Atgram-IX	1085	2256	1171	2256	4178	1920
		Kailastila-1	2150	2900	750	2290	4138	1238
		Beani Bazar-IX	2631	3640	1009	3640	4109	469
		Rashidpur-2	1036	2710	1674	2710	3851	1141
		Habiganj	1165	2326	1161	2326	3506	1180
		Kamta-1	1030	2740	1710	2740	3614	874
		Titas-1	832	2362	1531	2362	3758	1396
		Bakhrabad-1	560	1770	1210	1770	2838	1068
		Begumganj-1	1480	2580	1100	2580	3656	1076
		Muladi-1	750	2590	1840	2590	4395	1805
		Feni-1	1300	2440	1140	2440	3200	760
	Folded belt	Semutang-1	250	1530	1280	1530	3500	1970
		Jaldi-3	500	1380	880	1380	2930	1550
	Offshore	Kutubdia	1713	3606	1792	not drilled		

paleogeography. Gravity data (Brunnschweiler, 1980; Rahman et al., 1990; Khan and Agarwal, 1993) have been analyzed to interpret overall basin geometry in light of Miocene stratal variations. Most of the Miocene strata in the northwestern part of the Bengal basin are limited to very thin, mostly undifferentiated sequences and are not included in this study.

4. Depositional patterns

An isopach map of the lower to middle Miocene Bhuban Formation (Fig. 4) shows dramatic thickening of strata toward the south and toward the east. In the northwest part of the study area, Bhuban thicknesses generally range from about 500 to 900 m, with one area of reduced thickness (Singra well). This overall pattern is varied by a region of anomalously thin strata extending from the Bakhrabad well southeastward to the Jaldi well. Although we have no data in the Tripura area of India, there is an apparent offset of the isopachs of Bhuban strata between northeastern Bangladesh and the region to the south, called the Chittagong Hills.

An important observation about the Bhuban strata is that the maximum thicknesses in the south and along the eastern parts of the basin are the same (~ 1800 m), suggesting that crustal type and accommodation space were similar across these areas. The very regular pattern of thickening toward the south and toward the east, from 500 to 1800 m thick, suggests deltaic deposition prograding southward and eastward. This further suggests deeper marine sedimentation beyond the deltaic deposits to the south and east. This is certainly true in southeast Bangladesh where turbidites are reported in the Bhuban Formation in the Chittagong Hills (e.g., surface exposures near the Semutang well, see Akhter et al., 1998; Gani and Alam, 1999). Notably, there is no indication in the isopach data of barriers to sedimentation in the present-day region of the western foothills of the Indo–Burman ranges. This region in the Miocene was near the zone of plate convergence between India and Burma, with Bengal basin strata overlying the subducting oceanic crust of Indian plate. Thus, much of the Bhuban Formation in this region may have been deposited on an outer trench slope as Burma approached from the east, and so is likely to comprise

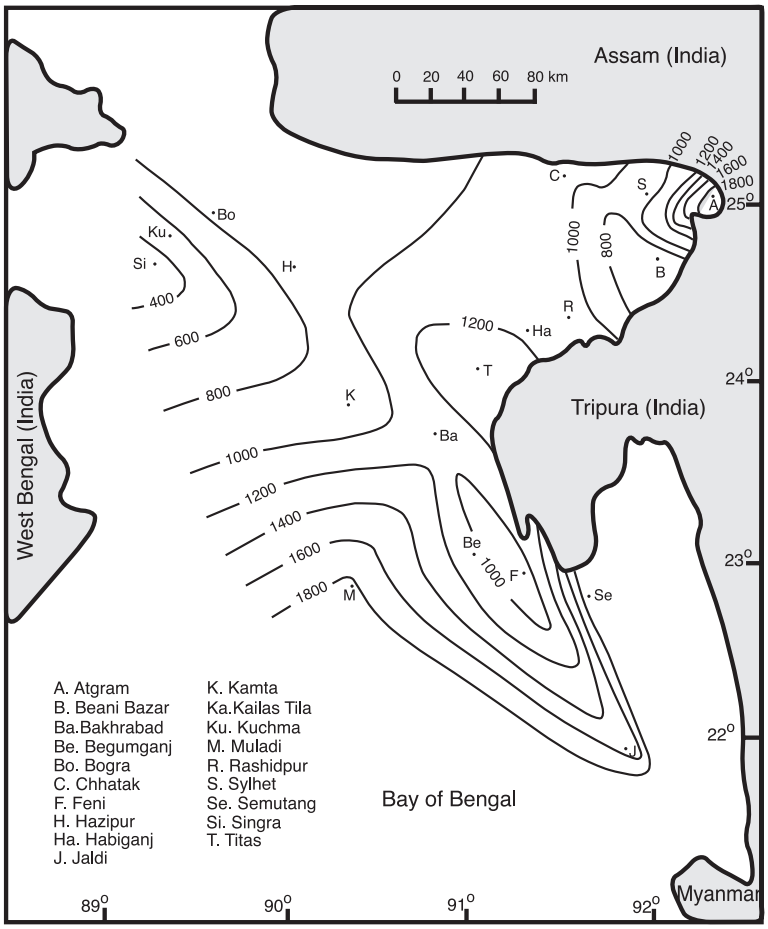

Fig. 4. Isopach map (in meters) of the lower to Middle Miocene Bhuban Formation. Well data from the southwest part of the basin not available. Index provides key to well names referred in text. The outline indicated by the shaded areas in Figs. 4, 5 and 6 correspond to the political boundary of Bangladesh.

deep-marine deposits. The one obvious anomaly to this regular pattern is the zone of thin strata extending from the Bakhrabad (Ba) well to the Jaldi (J) well. This area of anomalously thin Bhuban strata is enigmatic; perhaps it overlies a pre-existing bathymetric high, or for some reason relatively thin strata were deposited, or at least preserved here. The map pattern of isopachs in this region has been compressed by strong east–west shortening during the Late Neogene. The original depositional pattern would therefore have been considerably smoother, with thicknesses increasing more gradually to the east. Elsewhere, most Bhuban strata that have been analyzed are interpreted to be shallow-marine to subaerial deposits. We have no well data in the southwestern part of the basin; we presume that thickness variations here likely continue as shown, roughly parallel to the (SW-trending) continent–ocean boundary and Hinge zone.

An isopach map of the Boka Bil Formation (midd to upper Miocene; Fig. 5) shows one major depocenter in the central part of the basin, with stratal thickness ranges mimicking those of the Bhuban strata. The thickest deposition of Boka Bil strata is found at the Muladi (well M) area with strata gradually thinning toward the northwest, north and to a lesser degree to the east. Anomalously thick strata, however, are found in the area of Rashidpur (well R). Significantly, there is no extensive area of thick Boka Bil strata in southeast

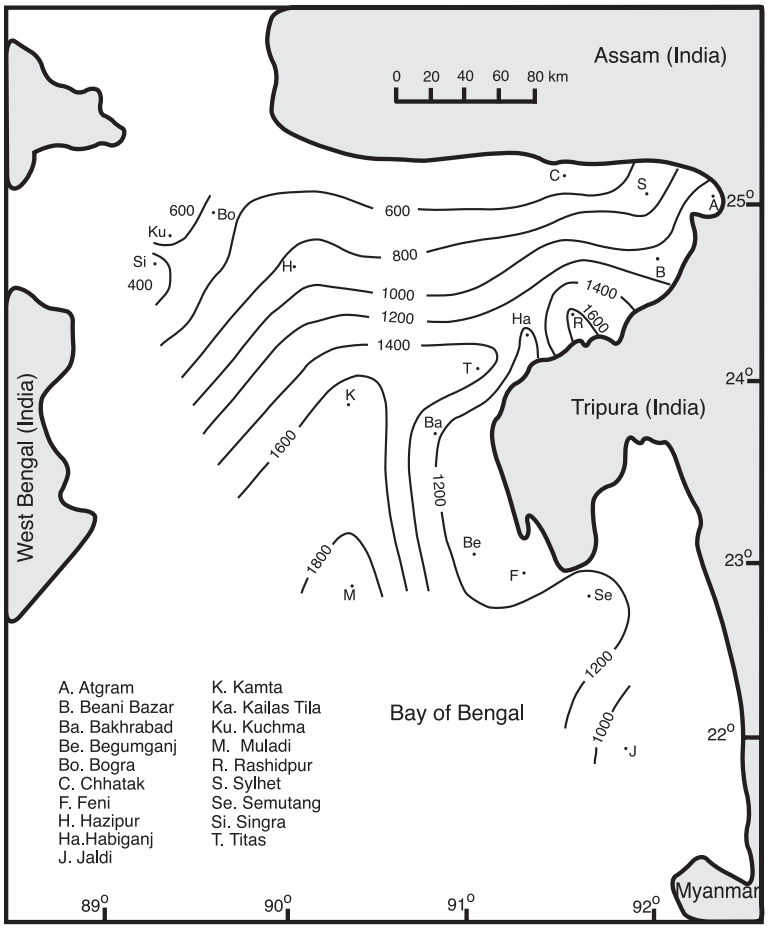

Fig. 5. Isopach map (in meters) of the Middle to Upper Miocene Boka Bil Formation of the Surma Group. Index provides key to well names referred to in the text.

Bangladesh, and no turbidites have been reported from these units. Continuing E–W plate convergence has closed the topographic embayment associated with the trench by this time, resulting in deposition of relatively uniform thickness of mostly shallow-marine Boka Bil strata in southeast Bangladesh. As was true for the Bhuban Formation, complex thickness variations along the eastern basin margin suggest that the Indo–Burman ranges were continuing to encroach on the Bengal basin throughout the Miocene, particularly in the area of the Chittagong Hills (far eastern portion of central and southern Bangladesh).

The thinnest section of both formations is located at the Singra well, which is closer to the exposed Indian craton to the west than are any other wells in this study. This area apparently experienced less subsidence than most of the rest of the basin through the Miocene.

4.1. Basin tectonics

The Bouguer anomaly map (Fig. 6) of Bangladesh helps recognize four key features that are important to discuss the tectonics of the Bengal basin:

(a) A linear gravity anomaly parallels the Hinge zone (slightly offset to northwest), marking rapid sediment thickening to the southeast, toward oceanic crust.

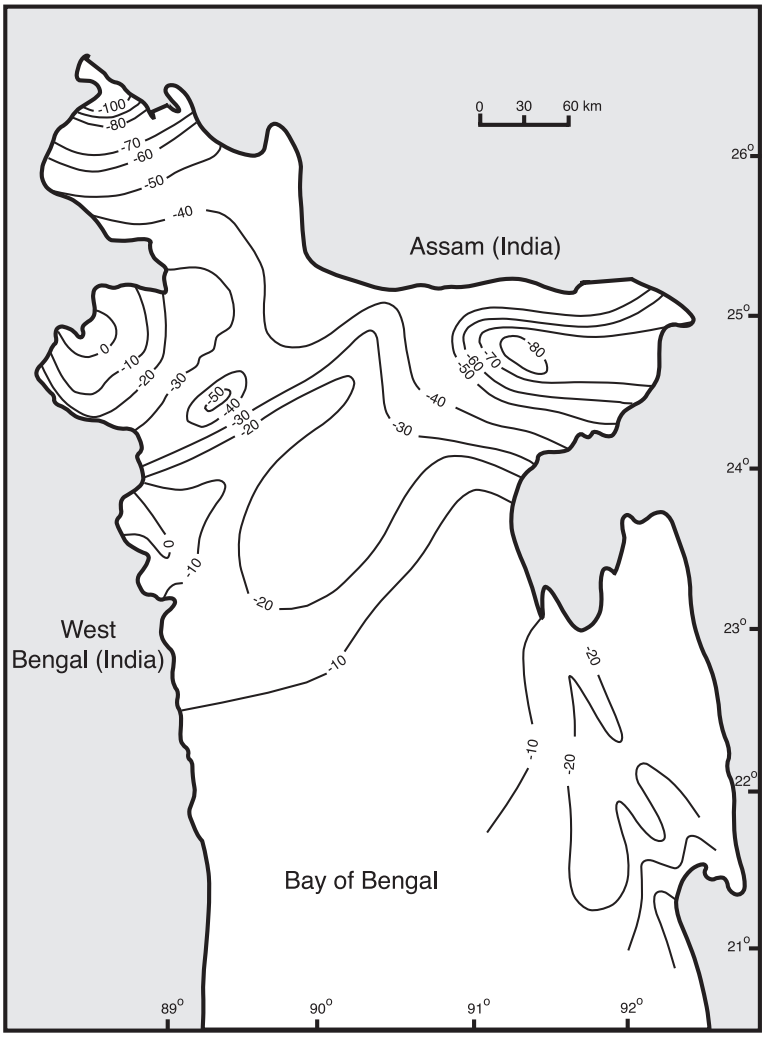

Fig. 6. Simplified Bouguer anomaly map of Bangladesh (from many different sources, including Brunnschweiler 1980; Rahman et al. 1990; Khan and Agarwal 1993). Bouguer data are in milligals.

(b) A high negative gravity anomaly in the extreme northwest of Bangladesh suggests marked thickening of basinal strata northward into the Siwalik foreland basin of the eastern Himalayas.
(c) A strong negative gravity anomaly over the Sylhet trough reflects thick basin strata, but the consistency of thickness of Miocene strata demonstrates that this is a Pliocene (and younger?) feature, indicating that the Shillong Plateau was uplifted after the Miocene.
(d) Linear north–south gravity anomalies in the Chittagong Hill region reflect the folded nature of the western basin margin, and the amplitudes of the gravity anomalies indicate that basement is involved in the folding. The eastward trend to greater negative gravity values reflects the deepening Moho, presumably due to lithospheric flexure caused by loading of the Indo–Burman ranges. This is much less pronounced than the dramatic gravity signature of the Himalayan foreland in northwestern Bangladesh.

The Bengal basin was essentially a southeast facing passive margin prior to involvement in the

Tertiary collision (Johnson and Nur Alam, 1991). Orogenic uplifts in the Indo–Burman ranges, the Naga Hills and the Himalayas in Assam began by the Late Eocene and Oligocene (Brunnschweiler, 1966; Rangarao, 1983; Uddin et al., 1999). There are several kilometers of thickness of Eo–Oligocene orogenic strata preserved in Assam (Rangarao, 1983), potentially far removed from the Bengal basin at the time (Uddin et al., 1999). Peripheral effects of crustal loading must have been observed in the Sylhet trough, which contains about 1.5 km of Oligocene Barail sediments. Barail sandstones in Bangladesh are shallow marine (Rangarao, 1983; Alam, 1991) and are extremely quartz-rich, suggesting a derivation probably from the Indian craton to the west and northwest (Uddin and Lundberg, 1998a).

Orogenic sedimentation had clearly been initiated by the deposition of the thick Surma Group of sediments. Encroachment of the Indo–Burman ranges from the east and the Himalayas from the north caused accelerated subsidence of the Sylhet trough and the Bengal basin where voluminous sediments were deposited in a prograding delta (Figs. 4 and 5). Sedimentation in the Bengal basin during Miocene time must have kept pace with subsidence of the basin (Hoque, 1974), except in southern and southeast Bangladesh, where turbidite deposits indicate excess accommodation space. These isopach maps do not obviously show a "closed contour" pattern of the Surma Group of sediments during Miocene time. The gravity map of Bangladesh suggests a Bouguer minimum (-80 mgl) for the Sylhet trough (Fig. 6). Comparison of this gravity anomaly does not match the Miocene stratigraphic thicknesses in the Sylhet trough. It can thus be inferred that maximum subsidence of the Sylhet trough did not take place during Miocene time (Uddin, 1990; Johnson and Nur Alam, 1991). Pliocene uplift of the Shillong Plateau (Johnson and Nur Alam, 1991) and the gradual encroachment of the Indo–Burman ranges toward the Bengal basin in the west suggest that the major subsidence of the Sylhet trough took place during Pliocene time.

An interesting question revolves around whether there was actual basin thickening due to tectonic loading in the Bengal basin during the Miocene. In the case of the Himalayan orogen, the mountain front was too far north of this region in the Miocene to have produced significant loading, or likely even a peripheral forebulge. On the other hand, the Indo–Burman ranges to the east were likely close enough to have driven basin flexure, resulting in additional accommodation space along the eastern margin of the basin. This eastern basin margin was a very complicated region during the Miocene, with deep-water turbidites reported by many workers who have studied the Bhuban unit. Thus, the Chittagong Hills area is the one part of the Bengal basin known to have been substantially deeper than shallow marine conditions during at least part of the Miocene. This area was the site of the northern extension of the Andaman–Nicobar trench, experiencing active east–west convergence. No turbidites have been reported in the younger Boka Bil Formation in this area (or elsewhere), and so apparently the combination of tectonic convergence and deposition of approximately 2 km of strata raised and/or filled this deep-water part of the basin by the Late Miocene. Across the remainder of the Bengal basin, deposition of the Bhuban Formation in the early to middle Miocene was dominated by deltaic processes (Alam, 1989). Very thick deposits at the Atgram well (Table 1, Figs. 4 and 5) are anomalous relative to nearby wells in Bangladesh. This likewise may be due to structural thickening related to east–west shortening of the Indo–Burman ranges, either by directly thickening this section by thrust faults or by tectonic loading relatively near the axis of Indo–Burman orogenic activity. The overall picture of deltaic sedimentation prograding southward in the Bhuban continued in the late Miocene, with similar thickness variations in the Boka Bil Formation, and without the complication of thick deep-water deposits in the region that is now southeastern Bangladesh.

4.2. Regional implications

The Eocene to Oligocene precollisional to syncollisional sediments in the Bangladesh portion of the Bengal basin are overwhelmingly quartzose and contain only small amounts of heavy minerals (mainly ultra-stable species of zircon, tourmaline, and rutile) of which about 60% are opaque varieties (Uddin and Lundberg, 1998a,b). The compositions and textures of Eocene and Oligocene sandstones in the Bengal basin

do not obviously suggest derivation from Himalayan or Indo–Burman orogenic sources, but rather point toward the low-relief, crystalline Indian craton adjacent to the west. Intense chemical weathering has also been suggested for Paleogene sediments in the Bengal basin because of their quartzose composition (Uddin and Lundberg, 1998a).

Increased thicknesses of Miocene strata and the composition of Miocene sandstones of the Surma Group in the eastern Bangladesh yield a clear record of orogenic unroofing (Uddin and Lundberg, 1998a). The source rocks from which these sands were derived were dominated by supracrustal rocks, producing detritus rich in monocrystalline quartz, sedimentary to low-grade metamorphic lithic fragments, and a host of various heavy minerals, including a substantial input of garnet, but also epidote, chlorites, tremolite, actinolite, staurolite, and kyanite (Uddin and Lundberg, 1998a,b). Preliminary isotopic studies of the Miocene sediments from the Bengal basin revealed relatively uniform $^{87}Sr/^{86}Sr$ isotope ratios (about 0.72–0.73), which suggests that the most likely source rocks in the Himalayas were relatively unchanged throughout the unroofing process during Miocene time (Uddin et al., 2000). Similar inferences have also been drawn from the sediments of the Bengal fan (France-Lanord et al., 1993). Sedimentation rates in the Bengal fan increased during this time, perhaps due to increased rate of erosion (Cochran, 1990). This represents a dramatic southward advance of the deformation front of the eastern Himalayas, whereas the deformation front of the Indo–Burman ranges has likely advanced more gradually westward, progressively encroaching on the Bengal basin.

Trends from the subsurface lithofacies maps of the Miocene sediments from Bangladesh suggest that deltaic deposits entered the Bengal basin from the northeast, and that the source terranes of this sediment included the eastern Himalayas and the north-trending Indo–Burman ranges immediately adjacent to the east. This is consistent with preservation of thick orogenic sequences immediately northeast in Assam (northeast India, Sinha and Sastri, 1973; Uddin et al., 2002). A consistent increase in sand percentages from the Bhuban to Boka Bil Formations in most of the eastern wells of Bangladesh suggests progradation of the delta, perhaps along with westward migration of the Indo–Burman ranges as a proximal source (Uddin and Lundberg, 1999).

Increases in sand percentages from the Bhuban to the Boka Bil Formations in northeastern Bangladesh may reflect westward advance of the Indo–Burman orogenic front toward the Sylhet trough and the Chittagong Hill tracts (Fig. 1; Uddin and Lundberg, 1998a). Consistent increase in the thickness of the Miocene sediments in the eastern Bengal basin suggests the presence of major river systems (i.e., paleo-Brahmaputra, paleo-Meghna, paleo-Karnafuli) delivering detritus from the Indo–Burman ranges and the eastern Himalayas straight to the Bengal fan through the Sylhet trough and the northern Chittagong Hill tracts forming a major delta complex at the northeastern part of Bangladesh. Some of these paleo-drainage systems may have been submarine, because marine sequences have been identified in the coeval rocks of the Chittagong Hill tracts (Akhter et al., 1998; Gani and Alam, 1999; Alam et al., 2003). These Miocene channels were likely distributaries of a major drainage system that transported orogenic sediment into the early Bengal fan. These Miocene deltas in Bangladesh migrated from east to west and from north to south, toward the Bay of Bengal, as underthrusting of India beneath southeast Asia along the present-day Java trench and its northern extension continued. Subsidence due to deltaic loading has been active since at least the Miocene, with subsidence near the mountain belts accelerated by loading of the advancing orogens. The lithofacies trends also indicate that the Shillong Plateau, an uplifted massif of Precambrian basement rocks standing adjacent on the north of the Bengal basin, was not a source of sediments during the Miocene time (Fig. 1; Johnson and Nur Alam, 1991; Uddin and Lundberg, 1999).

The isopach data also show evidence of thickening of basin fill toward the south, opposite of the normal foreland basin, presumably because of the transition to oceanic crust—like the Mississippi Delta, with downfaulting toward the basin (e.g., Worrall and Snelson, 1989). From west to east across the basin, in contrast, the overall shape is typical for a foreland basin, apparently because the continent-to-ocean transition has the ‘‘normal’’ polarity, with oceanic crust having subducted first, followed by transitional and then continental crust.

5. Conclusions

Miocene deposits of the Bengal basin of Bangladesh clearly record orogenic activity in the eastern Himalayas and the Indo–Burman ranges as a result of continent–continent collision. Isopach maps constructed from electric logs obtained from oil and gas exploration in the region, coupled with gravity data, document Miocene sedimentation and subsidence patterns in the Bangladesh part of the Bengal basin. These new data on sediment thickness and previously reported seismic data indicate that sedimentary lithofacies in the fill of this asymmetric basin were controlled mainly by subsidence due to deltaic progradation over the continent/ocean boundary, overprinted by tectonic loading and oblique convergence along its eastern boundary. Deltaic progradation through most of Bangladesh in the Miocene followed earlier deltaic accumulations closer to the Himalayas in the Eo–Oligocene (+6 km of largely pre-Miocene deltaic strata in Assam). Since the Miocene, the deltaic depocenter has continued to prograde southward toward the southern Bangladesh offshore and the Bengal deep-sea fan.

Isopach data of the Bhuban and Boka Bil formations across much of Bangladesh indicate that the considerable subsidence of the Sylhet trough in the northeast, which has the lowest gravity value of the region, did not take place in or by the Miocene. Because there are no depocenters represented in the Miocene isopachs of the Sylhet trough, subsidence must have taken place since Miocene time, consistent with results of recent research on sediment composition.

Isopach data show that there is considerable vertical relief along the base of the Miocene stratigraphic sequence. The southeast part of the basin overlies oceanic crust, and had considerable accommodation space, relative to the remainder of the basin, which is floored by (attenuated?) continental crust. Indeed, turbidites have been reported from the Bhuban Formation in the southeast Bengal basin. In part due to the transition from continental to oceanic crust, the Bengal basin as a whole thickens away from the Himalayas in a N–S profile. This is opposite to the pattern normally seen in foreland basins, due to the continent–ocean boundary, presumably exacerbated by sedimentary loading and basinward downfaulting analogous to that seen along the northern Gulf of Mexico. In an E–W profile, the basin shape is more typical of a foreland basin, with sediment thickening eastward toward the Indo–Burman ranges. This dramatic lowering of the base of the Miocene is apparently due to flexure associated with subduction beneath Southeast Asia and tectonic loading of the Indo–Burman ranges. Toward the north, regional lowering northward into the Sylhet trough is seen above the Miocene strata, and is attributed to flexure caused by southward thrusting of the Shillong Plateau along the Dauki fault.

Acknowledgements

We are thankful to BOGMC and BAPEX for providing data. M. Moinul Huq, Lutfar R. Chowdhury, M. Nazim Ahmed and M. Aminul Islam are thanked for their cooperation. Supported partly by a grant from NSF (INT-0117405). Pranav Kumar and Jeroen Sonke helped draft some figures. The manuscript was improved by thoughtful and constructive reviews by Eduardo Garzanti, Andrew Miall and Anthony Tankard.

References

Akhter, M.H., Bhuiyan, A.H., Hussain, M., Imam, M.B., 1998. Turbidite sequence located in Bangladesh. Oil and Gas Journal, (Dec. 21, 1998), 109–111.

Alam, M., 1989. Geology and depositional history of Cenozoic sediments of the Bengal Basin of Bangladesh. Palaeogeography, Palaeoclimatology, Palaeoecology 69, 125–139.

Alam, M.M., 1991. Paleoenvironmental study of the Barail succession exposed in north–eastern Sylhet, Bangladesh. Bangladesh Journal of Scientific Research 9, 25–32.

Alam, M., Alam, M.M., Curray, J.R., Chowdhury, M.L.R., Gani, M.R., 2003. An overview of sedimentary geology of the Bengal basin in relation to the regional framework and basin-fill history. Sedimentary Geology 155, 179–208.

Bakhtine, M.I., 1966. Major tectonic features of Pakistan: Part II. The Eastern Province. Science and Industry 4, 89–100.

Banerji, R.K., 1981. Cretaceous–Eocene sedimentation, tectonism, and biofacies in the Bengal Basin, India. Palaeogeography, Palaeoclimatology, Palaeoecology 34, 57–85.

Brunnschweiler, R.O., 1966. On the geology of the Indo–Burman ranges (Arakan coast and Yoma, Chin Hills, Naga Hills). Geological Society of Australia Bulletin 13, 137–194.

Brunnschweiler, R.O., 1980. Lithostratigraphic monsters in modern oil exploration. Offshore S.E. Asia Conference, SEAPEX Session. 7 pp.

Cochran, J.R., 1990. Himalayan uplift, sea level, and the record of Bengal Fan sedimentation at the ODP Leg 116 sites. In: Cochran, J.R., Stow, D.A.V., et al. (Eds.), Proceedings of the Ocean Drilling Program Scientific Results, vol. 116B. Ocean Drilling Program, College Station, TX, pp. 397–414.

Curray, J.R., Moore, D.G., 1971. The growth of the Bengal Deep-sea Fan and denudation in the Himalayas. Geological Society of America Bulletin 82, 563–572.

Curray, J.R., Emmel, F.J., Moore, D.G., Raitt, R.W., 1982. Structure, tectonics and geological history of the northeastern Indian Ocean. In: Nairn, A.E.M., Stehli, F.G. (Eds.), The Ocean Basin and Margins. The Indian Ocean, vol. 6. Plenum, New York, pp. 399–450.

Desikachar, O.S.V., 1974. A review of the tectonic and geological history of eastern India in terms of 'plate tectonics' theory. Journal of the Geological Society of India 33, 137–149.

Evans, P., 1964. The tectonic framework of Assam. Journal of the Geological Society of India 5, 80–96.

France-Lanord, C., Derry, L., Michard, A., 1993. Evolution of the Himalaya since Miocene time: isotopic and sedimentologic evidence from the Bengal Fan. In: Treloar, P.J., Searle, M. (Eds.), Himalayan Tectonics. Geological Society of London Special Paper, vol. 74, pp. 603–621.

Gani, M.R., Alam, M.M., 1999. Trench-slope controlled deep-sea clastics in the exposed lower Surma Group in south–eastern Fold Belt of the Bengal Basin, Bangladesh. Sedimentary Geology 127, 221–236.

Graham, S.A., Dickinson, W.R., Ingersoll, R.V., 1975. Himalayan–Bengal model for flysch dispersal in the Appalachian–Ouachita system. Geological Society of America Bulletin 86, 273–286.

Hiller, K., Elahi, M., 1984. Structural development and hydrocarbon entrapment in the Surma Basin, Bangladesh (northwest Indo–Burman Fold belt). Proceedings of 4th Offshore Southeast Asia Conference, Singapore, pp. 6-50–6-63.

Hoque, M., 1974. Geological framework of Bangladesh. In: Studies in Bangladesh Geography. Bangladesh National Geographic Association, pp. 1–18.

Holtrop, J.F., Keizer, J., 1970. Some aspects of the stratigraphy and correlation of the Surma Basin wells, East Pakistan. ECAFE Mineral Resources Development Series, vol. 36. United Nations, New York.

Imam, M.B., Shaw, H.F., 1985. The diagenesis of Neogene clastic sediments from the Bengal Basin, Bangladesh. Journal of Sedimentary Petrology 55, 665–671.

Ingersoll, R.V., Graham, S.A., Dickinson, W.R., 1995. Remnant ocean basins. In: Busby, C.J., Ingersoll, R.V. (Eds.), Tectonics of Sedimentary Basins. Blackwell Science, Cambridge, MA, pp. 362–391.

Johnson, S.Y., Nur Alam, A.M., 1991. Sedimentation and tectonics of the Sylhet trough, Bangladesh. Geological Society of America Bulletin 103, 1513–1527.

Khan, A.A., 1991. Tectonics of the Bengal basin. Journal of Himalayan Geology 2, 91–101.

Khan, A.A., Agarwal, B.N.P., 1993. The crustal structure of western Bangladesh from gravity data. Tectonophysics 219, 341–353.

Khan, M.R., Muminullah, M., 1980. Stratigraphy of Bangladesh. Proceedings of Petroleum and Mineral Resources of Bangladesh. Ministry of Petroleum and Mineral Resources, Government of Bangladesh, pp. 35–40.

Khandoker, R.A., 1989. Development of major tectonic elements of the Bengal Basin: a plate tectonic appraisal. Bangladesh Journal of Scientific Research 7, 221–232.

Kuehl, S.A., Hairu, T.M., Moore, W.S., 1989. Shelf sedimentation off the Ganges–Brahmaputra river system—evidence for sediment bypassing to the Bengal fan. Geology 17, 1132–1135.

Lindsay, J.F., Holliday, D.W., Hulbert, A.G., 1991. Sequence stratigraphy and the evolution of the Ganges–Brahmaputra Delta complex. American Association of Petroleum Geologists Bulletin 75, 1233–1254.

Molnar, P., 1987. The distribution of intensity associated with the great 1897 Assam earthquake and bounds on the extent of the rupture zone. Journal of the Geological Society of India 30, 13–27.

Molnar, P., Tapponnier, P., 1975. Cenozoic tectonics of Asia: effects of a continental collision. Science 189, 419–426.

Morgan, J.P., McIntire, W.G., 1959. Quaternary geology of the Bengal basin, East Pakistan and India. Geological Society of America Bulletin 70, 319–342.

Mukhopadhyay, M., Dasgupta, S., 1988. Deep structure and tectonics of the Burmese arc: constraints from earthquake and gravity data. Tectonophysics 149, 299–322.

Murphy, R.W., 1988. Bangladesh enters the oil era. Oil and Gas Journal, Feb. 29, 76–82.

Ni, J.F., Guzman-Speziale, M., Holt, W.E., Wallace, T.C., Saeger, W.R., 1989. Accretionary tectonics of Burma and the three dimensional geometry of the Burma subduction zone. Geology 17, 68–71.

Rahman, M.A., Mannan, M.A., Blank Jr., H.R., Kleinkopf, M.D., Mirchanikov, S.M., 1990, Bouguer gravity map of Bangladesh: Geological Survey of Bangladesh, scale 1:1,000,000.

Rangarao, A., 1983. Geology and hydrocarbon potential of a part of Assam–Arakan basin and its adjacent region. In: Bhandari, L.L., et al. (Ed.), Petroliferous Basins of India, Petroleum Asia Journal. The Himachal Times Group, Dehra Dun, India, pp. 127–158.

Reimann, K.-U., 1993. Geology of Bangladesh. Gebruder Borntraeger, Berlin. 160 p.

Salt, C.A., Alam, M.M., Hossain, M.M., 1986. Bengal basin: current exploration of the Hinge zone of southwestern Bangladesh. Proceedings of 6th Offshore Southeast Asia Conference, Singapore, pp. 55–67.

Sclater, J.G., Fisher, R.L., 1974. The evolution of the east central Indian Ocean, with emphasis on the tectonic setting of the Ninetyeast Ridge. Geological Society of America Bulletin 85, 683–702.

Sengupta, S., 1966. Geological and geophysical studies in western part of Bengal basin, India. American Association of Petroleum Geologists Bulletin 50, 1001–1017.

Sinha, R.N., Sastri, V.V., 1973. Correlation of the Tertiary geosynclinal sediments of the Surma Valley, Assam, and Tripura State (India). Sedimentary Geology 10, 107–134.

Uddin, A., 1990. Shift in depositional patterns during Miocene time

in the Bengal Basin, Bangladesh [abs.]. Geological Society of America Program with Abstracts 22, A366.

Uddin, A., Lundberg, N., 1998a. Cenozoic history of the Himalayan–Bengal system: sand composition in the Bengal basin, Bangladesh. Geological Society of America Bulletin 110, 497–511.

Uddin, A., Lundberg, N., 1998b. Unroofing history of the eastern Himalaya and the Indo–Burman ranges: heavy mineral study of the Cenozoic sediments from the Bengal basin, Bangladesh. Journal of Sedimentary Research 68, 465–472.

Uddin, A., Lundberg, N., 1999. A paleo-Brahmaputra? Subsurface lithofacies analysis of Miocene deltaic sediments in the Himalayan–Bengal system, Bangladesh. Sedimentary Geology 123, 227–242.

Uddin, A., Sarma, J.N., Kher, S., Lundberg, N., Odom, L.A., 1999. Pre-Miocene orogenic history of the eastern Himalayas: compositional studies of sandstones from Assam, India [Invited abs.]. Eos, Transactions of American Geophysical Union, Spring Meeting Supplement 80 (17), S313.

Uddin, A., Stracke, A., Odom, A.L., 2000. Isotopic constraints on provenance of Miocene sediments from the Bengal basin, Bangladesh [abs.]. Geological Society of America Programs with Abstracts 32, A-311.

Uddin, A., Kassos, G., Beasley, B., Logan, T., Sarma, J.N., 2002. Heavy minerals from Neogene deposits of Assam, India: unroofing history of the Eastern Himalayas [abs]. Geological Society of America Programs with Abstracts 34, 435.

Woodside, P.R., 1983. The petroleum geology of Bangladesh. Oil and Gas Journal 81 (32), 149–155.

Worrall, D.M., Snelson, S., 1989. Evolution of the northern Gulf of Mexico, with emphasis on Cenozoic growth faulting and the role of salt. In: Bally, A.W., Palmer, A.R. (Eds.), The Geology of North America—An Overview, DNAG, vol. A. Geological Society of America, Boulder, pp. 91–138.

Annex B70

C. Nielsen et al., "From Partial to Full Strain Partitioning Along the Indo-Burmese Hyper-oblique Subduction", *Marine Geology*, Vol. 209 (2004)

ELSEVIER

Marine Geology 209 (2004) 303–327

MARINE GEOLOGY
INTERNATIONAL JOURNAL OF MARINE GEOLOGY, GEOCHEMISTRY AND GEOPHYSICS

www.elsevier.com/locate/margeo

From partial to full strain partitioning along the Indo-Burmese hyper-oblique subduction

C. Nielsen[a,1], N. Chamot-Rooke[a,*], C. Rangin[b], the ANDAMAN Cruise Team[2]

[a] *Laboratoire de Géologie, CNRS, UMR 8538, Ecole normale supérieure, 24 rue Lhomond, 75231, Paris, France*
[b] *CNRS, UMR 6535, Collége de France, CEREGE, Aix-en-Provence, France*

Received 7 August 2003; received in revised form 5 April 2004; accepted 4 May 2004

Abstract

The Andaman–Nicobar Trench and its onshore prolongation—the Indo-Burmese wedge—is the least studied segment of the India–Australia subduction. New offshore geological and geophysical data have recently been collected along the Burma scarp during a marine survey conducted with the R/V *Marion Dufresne* (Andaman Cruise). Swath bathymetric mapping combined with shallow and deep seismic show that the dominant active tectonics is dextral strike-slip faulting accompanied by various amounts of shortening. The southern portion of the Burma scarp is transpressive (north Andaman Islands), the central portion is pure strike-slip on NNE-oriented segments (southern Myanmar), the northern portion shows sedimentary wedge growth along NW segments, both onshore and offshore (Arakan Yoma prism). Further north, the wedge bends to the west, while dextral shear faults more or less parallel to the Sagaing Fault develop within the internal part of the wedge and elongated NS folds form in its external part, abutting onto the Shillong Plateau. We propose a simple kinematic model involving evolution from partial to full partitioning from south to north along the West Burma Scarp (WBS), and we test it quantitatively using the most recent geodetic results. In the south, half of the 3.5 cm/year of India motion is taken at the trench itself, the other half being accommodated onto a single shear fault, the Sagaing Fault in Myanmar. In the north, where the Bangladesh fold system developed, dextral strike-slip faults are activated within the Arakan Yoma belt and at the accretionary prism–backstop contact, resulting in full partitioning there. Faults accommodating the oblique component of motion of India are progressively migrating in space from far field faults (Andaman–Sagaing) to near trench faults (Arakan Yoma belt and trench itself), the Burma sliver being "buttressed" by the Eastern Himalayas. This kinematic extends back to 4 Ma, which is the time of initiation of the last pulse of oceanic accretion in the Andaman Basin.

Keywords: Myanmar geology; Arakan Yoma belt; West Burma Scarp; accretionary wedge; oblique subduction; plate kinematics

1. Introduction

Northward motion of India with respect to SE Asia is accommodated along three main trenches: Java, Sumatra and Andaman–Nicobar. The curvature of these trenches implies a progressive increase of the

* Corresponding author. Fax: +33-1-44-32-20-00.
E-mail address: rooke@geologie.ens.fr (N. Chamot-Rooke).
[1] Now at Total, Paris la Défense.
[2] E. Bourdon, U. Min Han, U. Tin Tun Aung, U. Kyaw Htin, U. Min Swe, F. Farcy and D. Tsang Hin Sun.

0025-3227/$ - see front matter © 2004 Elsevier B.V. All rights reserved.
doi:10.1016/j.margeo.2004.05.001

obliquity of convergence, ranging from pure normal subduction at Java to oblique subduction at Sumatra and highly oblique motion towards the Andaman Islands and Myanmar (Fig. 1). The upper plate itself is shaped by this variation of obliquity. Off Sumatra, a large piece of crustal sliver is detached from the Sunda margin along the Great Sumatran, or Semangko, Fault. Northward, where obliquity becomes high, the Andaman Basin opened behind the Andaman–Nicobar Trench in a pull-apart setting between the northern tip of the Semangko Fault and the Sagaing Fault in Myanmar. The Andaman–Nicobar Trench is the least studied segment of the India–Australia subduction. The trench appears as a continuous trough from the northern tip of Sumatra to the southern extension of the Arakan Yoma accretionary prism, off Myanmar. It then vanishes towards the Bangladesh fold system.

Based on early versions of global plate kinematic models, Curray proposed the existence of an independent Burmese platelet absorbing the oblique motion of India with respect to SE Asia (Curray et al., 1979). The supposedly large NE motion of India (10 cm/year) was resolved, or partitioned (Fitch, 1972), into two large components: dextral strike-slip on the Sagaing Fault (>5 cm/year) and high rate normal subduction along the Indo-Burmese trench (>4 cm/year). Since these pioneering works, new constraints have been obtained from seismology, mantle tomography and GPS measurements. Seismicity and tomography delineate an eastward dipping Indian slab down to at least 250 km below the Andaman–Nicobar–Myanmar system (Verma et al., 1976a,b; Guzmàn-Speziale et al., 1987; Mukhopadhyay and Das Gupta, 1988; Guzmàn-Speziale and Ni, 1996). Seismicity distribution over the Burmese platelet and within the slab below indicate a more or less N–S trending P axis, suggesting that the entire area is subjected to north–south compression in relation to the nearby Himalayan Syntaxis (Le Dain et al., 1984; Guzmàn-Speziale and Ni, 1996). Virtually none of these studied focal mechanisms seemed to relate to the E–W subduction inferred by Curray. This absence of subduction earthquakes led Rao and Kumar (Rao and Kumar, 1999) to propose that although a deep lithospheric slab is indeed present at depth, subduction is now inactive. However, a recent re-examination of the seismicity suggests a still active oblique subduction (Satyabala, 2003). Satyabala further shows that the variation of slip vectors azimuths is compatible with a slip partitioning process similar to other oblique subductions, a conclusion that we share as will be shown later in this paper.

New kinematics constraints have recently been obtained through Global Positioning System (GPS) measurements. A major output of the GEODYSSEA Program was the discovery of a significant motion of a large Sundaland Block (Sumatra, Java, Vietnam, SE China, Borneo) with respect to Eurasia (Chamot-Rooke and Le Pichon, 1999; Simons et al., 1999; Michel et al., 2001). Global kinematics obtained by GPS (Holt et al., 2000; Kreemer et al., 2000a; Paul et al., 2001; Kreemer et al., 2003) as well as recent revision of India kinematics for the last 3 Myears (Gordon et al., 1999) also point to a slower than predicted motion of India. Finally, a local GPS network in Myanmar tied to other stations in SE Asia established a velocity of about 20 mm/year across the Sagaing Fault (Vigny et al., 2003), thus suggesting that only part of the motion of India is accommodated along the fault. A similar geological estimate was reached using the offset of a Quaternary volcano built on the fault (Bertrand et al., 1998; Bertrand, 1999).

Eastward motion of Sundaland, the new kinematics for India and slow shear on the Sagaing Fault put new kinematics constraints on the recent geodynamics of the Indo-Burma Trench. We report in this paper additional constraints based on a marine survey conducted along the Burma front (Andaman Cruise). The Burma scarp was surveyed in great detail between 14°N and 20°N, using swath mapping, shallow seismic and measurements of the gravity and magnetic fields. This new data set was combined with existing multichannel industrial lines from Compagnie Générale de Géophysique (CGG). We first describe the morphology of the Burma scarp and show that at present, the scarp is a major dextral strike-slip fault zone. Based on the pattern of active faults mapped both offshore and onshore (Myanmar), we further suggest that the degree of strain partitioning gradually increases from south Myanmar to north Myanmar, shearing being accommodated not only on the Sagaing Fault but also on additional strike-slip faults within the Arakan Yoma belt. We finally reconsider the general kinematic framework based

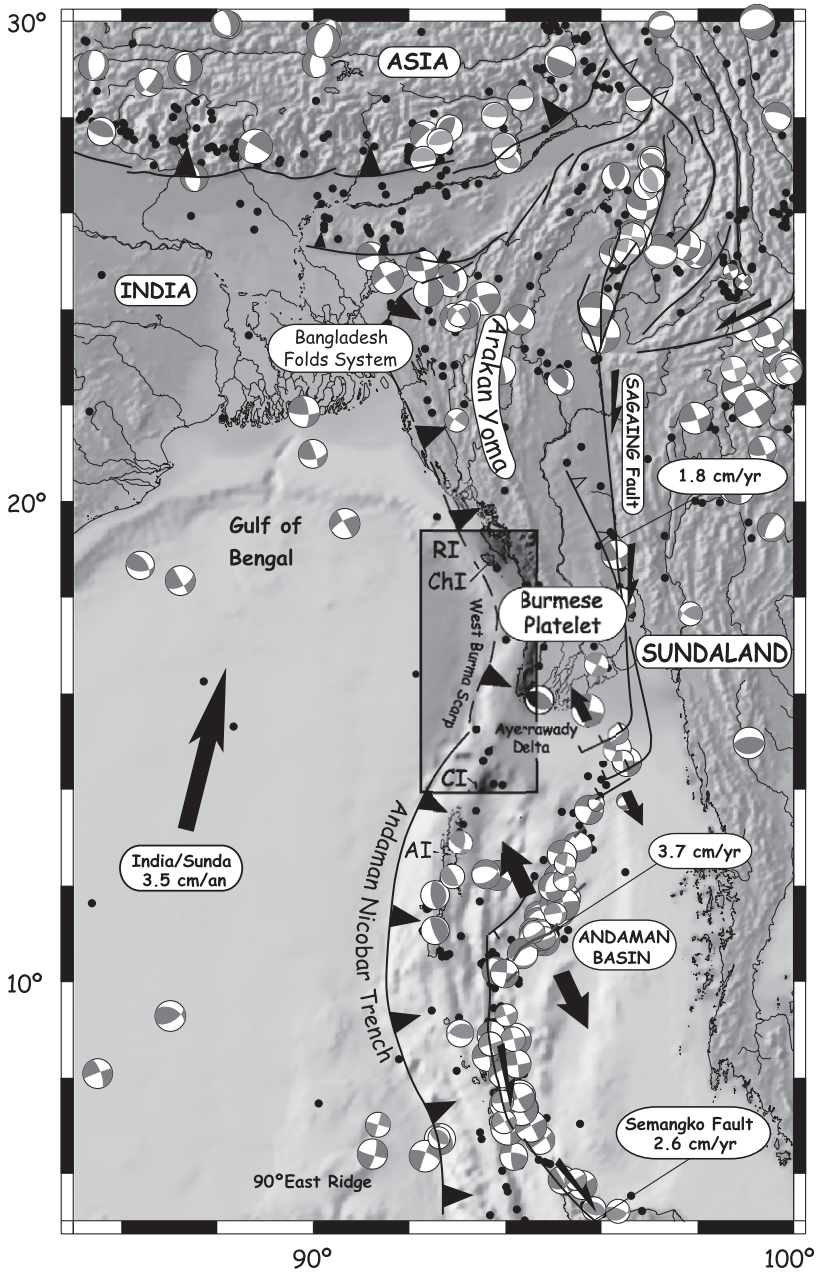

Fig. 1. Myanmar geodynamic setting. India–Sundaland convergence and shear motion on the Sagaing Fault are taken from the latest geodetic measurements (Vigny et al., 2003). The rectangle locates the Andaman Cruise survey along the Indo-Burma Margin. Focal mechanisms are from the HARVARD Catalogue and bibliographic references (Le Dain et al., 1984; Guzmàn-Speziale and Ni, 1996; Holt et al., 2000). AI: Andaman Islands. CI: Coco Islands. ChI: Cheduba Island. RI: Ramree Island.

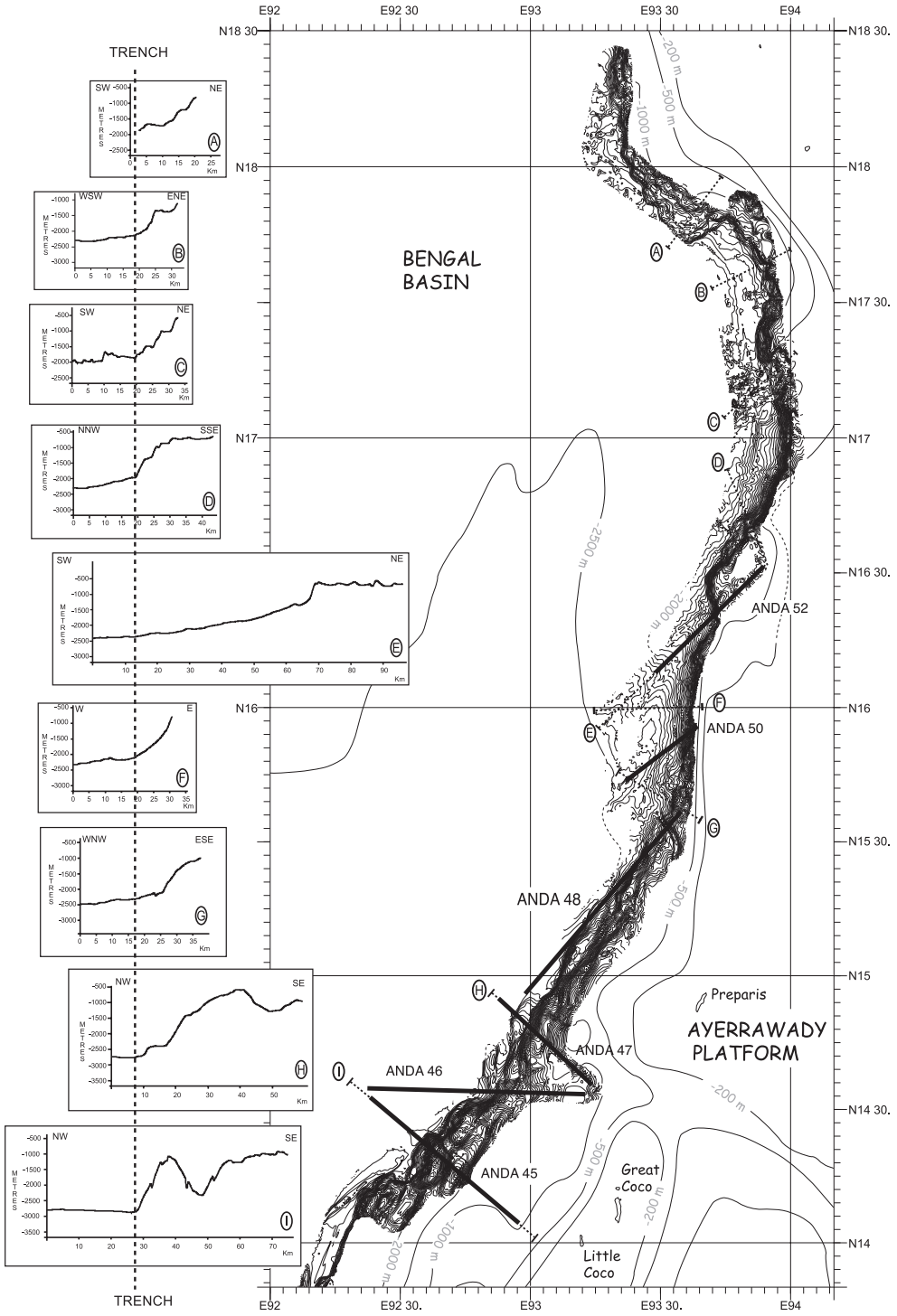
TRENCH
SW
NE
A
WSW
ENE
B
SW
NE
C
NNW
SSE
D
SW
NE
E
W
E
F
WNW
ESE
G
NW
SE
H
NW
SE
I
METERS
Km
TRENCH
E92
E92 30
E93
E93 30
E94
N18 30
N18
N17 30
N17
N16 30
N16
N15 30
N15
N14 30
N14
BENGAL
BASIN
-200 m
-500 m
-1000 m
-2000 m
-2500 m
ANDA 52
ANDA 50
ANDA 48
ANDA 47
ANDA 46
ANDA 45
Preparis
AYERRAWADY
PLATFORM
Great
Coco
Little
Coco

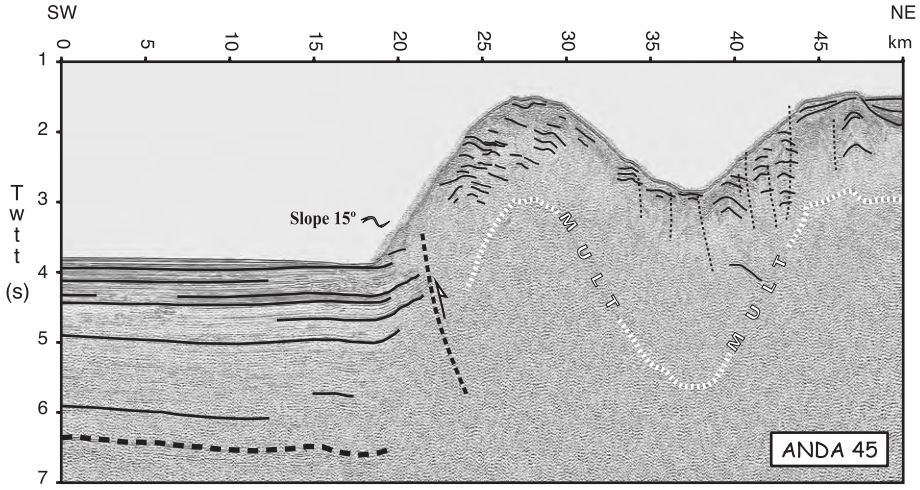

Fig. 3. Profile Andaman 45 and its interpretation. Track is located in Figs. 2 and 4. The Andaman seismic is a "light" seismic acquired at 10 knots (six channels, threefold). All Andaman profiles shown are migrated sections.

on the most recent plate tectonics models constrained by GPS measurements.

2. Morphology of the Indo-Burma trench along the West Burma Scarp (WBS)

The Andaman survey along the West Burma Scarp covers the Indo-Burma trench north of the Andaman Islands and south of the Arakan Yoma wedge in Myanmar (Fig. 1). The surveyed area is a 6–7-mile-wide strip extending from 14°N to 18°30′ N (Fig. 2). A single ship track was also run along the trench axis further South, so that the total length of trench surveyed is over 700 km. Morphologically, the WBS is a narrow and steep scarp between the flat 3000-m-deep Bengal Basin to the west and the bathymetric highs of the Coco Ridge to the east (Coco Islands and their extension, see Fig. 1). East of the Coco Ridge, the Ayerrawady platform and basins system is largely blanketed by fast infill of the prograding Ayerrawady delta.

A set of bathymetric sections across the West Burma Scarp (Fig. 2) clearly shows that the morphology is not typical of a trench. Most of these sections reveal the presence of a narrow and sharp slope break. Cross-sections B–H present wall morphology at short distance from the flat Bengal Basin. The slope of this narrow front is unusually high for a stable sedimentary wedge (12–15°), at contrast with the gentle slope observed at other accretionary prisms with a similar thick incoming section. Direct comparisons can be made with the Barbados and Eastern Mediterranean prisms, both being fed by large deltas (the Amazon and the Nile cones, respectively). The taper for those prisms does not exceed a few degrees (Lallemand et al., 1994; Chaumillon and Mascle, 1997). The steep gradient of the WBS actually shows more similarities with strike-slip dominated margins, such as the Puysegur Trench (Delteil et al., 1996; Lamarche and Lebrun, 2000; Lebrun et al., 2000) and the Hikurangi Trench (Collot et al., 1996, 2001) in New Zealand. The Burmese scarp swings south to north from a N40°E direction immediately north of the Andaman Islands to a N40°W trend at the location where the Arakan Yoma belt widens. This south to north swing coincides with three main tectonic styles, from trans-

Fig. 2. Andaman Cruise multibeam mapping along the Western Burma Scarp, contoured every 25 m. Contours lines outside the multibeam survey were merged with the GEBCO database. Seismic tracks are shown as thick black lines. A series of bathymetric profiles across the Western Burma Scarp are displayed to the left (sections A–I, dotted lines on the map). Notice that some, but not all, of these sections follow the seismic profiles.

pressive to pure dextral strike-slip in the south to accretion combined with dextral shear in the north.

2.1. The southern part of West Burma Scarp: a transpressive segment

South of 14°40′ N, the WBS morphology is characterized by a set of three N10°–N35°E *en échelon* highs. These blocks are bounded eastward by N30°E trending basins. One of these highs was imaged by seismic profile Andaman 45 (bathymetric section I in Fig. 2 and seismic line in Fig. 3). Thrusting onto the flat cover of the Bengal fan is suggested by the discrete flexure of the sediment pile deposited on the downgoing plate. The deepest reflector identified within the trench gently dips eastward and the section above shows clear fanning in relation to active thrusting (Fig. 3). The frontal thrust at the very base of the slope is buried beneath a sedimentary talus and thus does not break to the surface, the talus being probably fed by the unstable steep slope hanging above. The internal structure of the hanging wall shows rare eastward dipping reflectors. Although we cannot totally rule out that this tilting corresponds to the inherited structure of the upper margin (such as tilted blocks), a link with the recent activity of the bounding thrust is more likely. The simplest interpretation is that this set of *en échelon* highs are faulted wrenched anticlines. *En échelon* folds in a similar position (frontal wedge) and with similar orientation of their elongated axis have been observed south and north, although they all show less severe deformation. Estimate of the amount of shortening is difficult to obtain. On seismic line Andaman 45 (Fig. 3), the rare reflectors seen within the hanging wall may correspond to the well-stratified reflectors recognized in the trench, but the poor quality of the seismic does not allow a direct and reliable correlation. Furthermore, part of the hanging wall has clearly been eroded. The Neogene to Quaternary sedimentation rates in the area remain largely speculative. Based on multi-channel seismic data across the Bay of Bengal at 13°N latitude (150 km south of our survey), Gopala Rao et al. (1994) estimated a 250 m Ma^{-1} accumulation rate. Borehole data in the southern Bangladesh at 22°N latitude (about 400 km away from the northern tip of our survey) indicate a mean rate of 520 m Ma^{-1} for the post-Pliocene period (Alam et al., 2003). Using these rates as lower and upper bounds, and taking the sound velocity in the sediment in the range 1800–2000 m/s, the deepest reflector recognized on line Andaman 45 would be 5–10 Myears old (i.e., Early Pliocene or Late Miocene). The entire sequence above this reflector shows regular fanning towards the trench and upward folding at the slope break. This pattern is compatible with steady state thrusting since at least this age. The systematic *en échelon* disposition of those large anticlines (Figs. 2 and 4) strongly suggests that this portion of the WBS is an active transpressive dextral zone.

Between 14°N and 15°40′ N (Fig. 4), the WBS is a N40°E trending wall linking the flat Bengal Basin with the very shallow Burma shelf. North of 14°30′ N, the toe of the slope is affected by N10°E trending folds and thrusts with again an *en échelon* geometry (Fig. 5). The WBS is crosscut there by seismic profiles Andaman 46, 47 and 48 (Figs. 6, 8 and 9). We also show in Fig. 7 the line drawing of an unpublished CGG multichannel profile.

Along the east–west trending Andaman 46 profile (Fig. 6), a narrow elongated slice (slice A), thrust bounded west and east, occupies the base of the scarp. The internal structure of this slice shows again a series of small-scale *en échelon* folds trending N10°E. The CGG multichannel profile (Fig. 7) has a much better penetration than Andaman seismic lines, close to 3 twtt. The entire front of the wedge is affected by steep thrusts with double vergence. This reverse fault system is interpreted as the trace of a major N35°E trending dextral strike-slip fault. Part of this fault system is buried, as shown by dotted lines in Fig. 6, below 0.8–1 s twtt thick sediments. Profile Andaman 47 (Fig. 8) shows another pop-up structure (tectonic slice B). A small mound associated with a nascent strike-slip fault west of tectonic slice B is interpreted as a mud volcano. Although sediments are actively deformed at the toe of the slope, undeformed sediments blanket the scarp immediately east of the slope break, pointing again to localized deformation at the very base of the Burma scarp.

We interpret tectonic slices A and B (Fig. 5) as the surface expression of a dextral wrenched fault system at depth. The area thus appears as a positive flower structure, presently active only at the base of the scarp. The abyssal plain of the Bengal Basin is moderately affected by the *en échelon* structures. This could be the result of high sedimentation rate

versus low deformation rate. In any case, the shearing component seems to be higher than the frontal accretionary component.

Profile Andaman 48 (Fig. 9) is very oblique to the trend of the WBS. Its orientation parallels the trend of the scarp and helps to better confirm the fault dips. The westernmost fault (fault A) is subvertical, at least in the top of the section, and shows a minor thrust component towards the east close to the mudline. This fault is more or less in line with the westernmost fault identified on profile Andaman 47, but with opposite vergence. Another active fault can be observed immediately east of fault A in the middle part of profile Andaman 48 (Fig. 9) and is also probably a vertical strike-slip fault, marked by a discrete mud volcano.

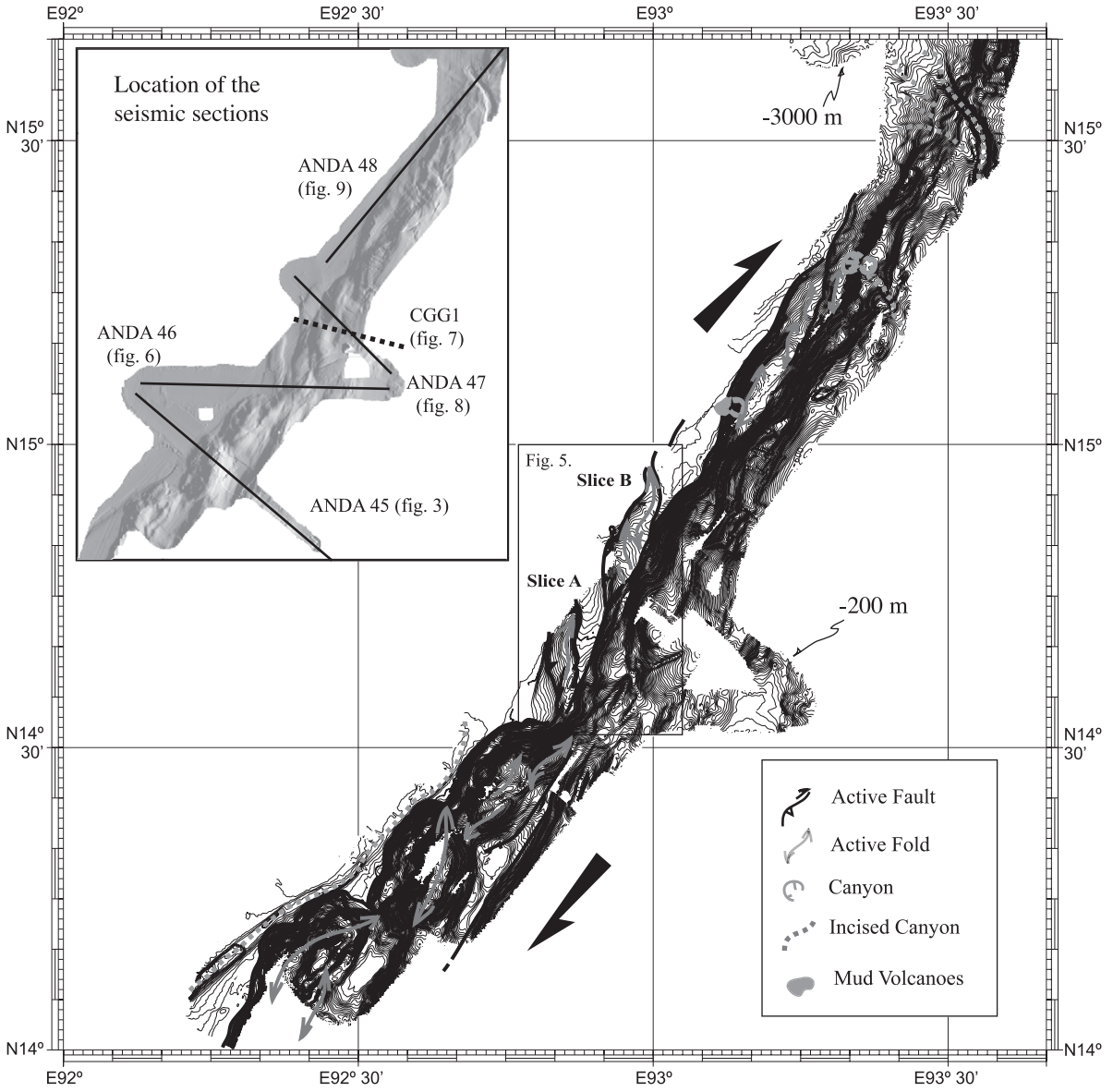

Fig. 4. Tectonic sketch for the southernmost portion of the surveyed Western Burma Scarp. Bathymetric data are contoured every 20 m.

Fault zone B below the lower terrace has a clear strike-slip component as indicated by its change of vergency approaching the surface. Eastward, the profile crosscuts fault zone C, which seems to be less active than fault zone B on profile Andaman 48. However, the bathymetric map confirms that fault zone C becomes the active one northward. Active deformation is thus concentrated along the two frontal *en échelon* duplex, less than 20 km wide, located at the base of the slope. Steepness and localization of the active structures support the fact that the deformation is concentrated in a narrow band at the base of the slope. The interpretation is that fault zones A, B and C are part of a larger *en échelon* dextral strike-slip system trending N35°E.

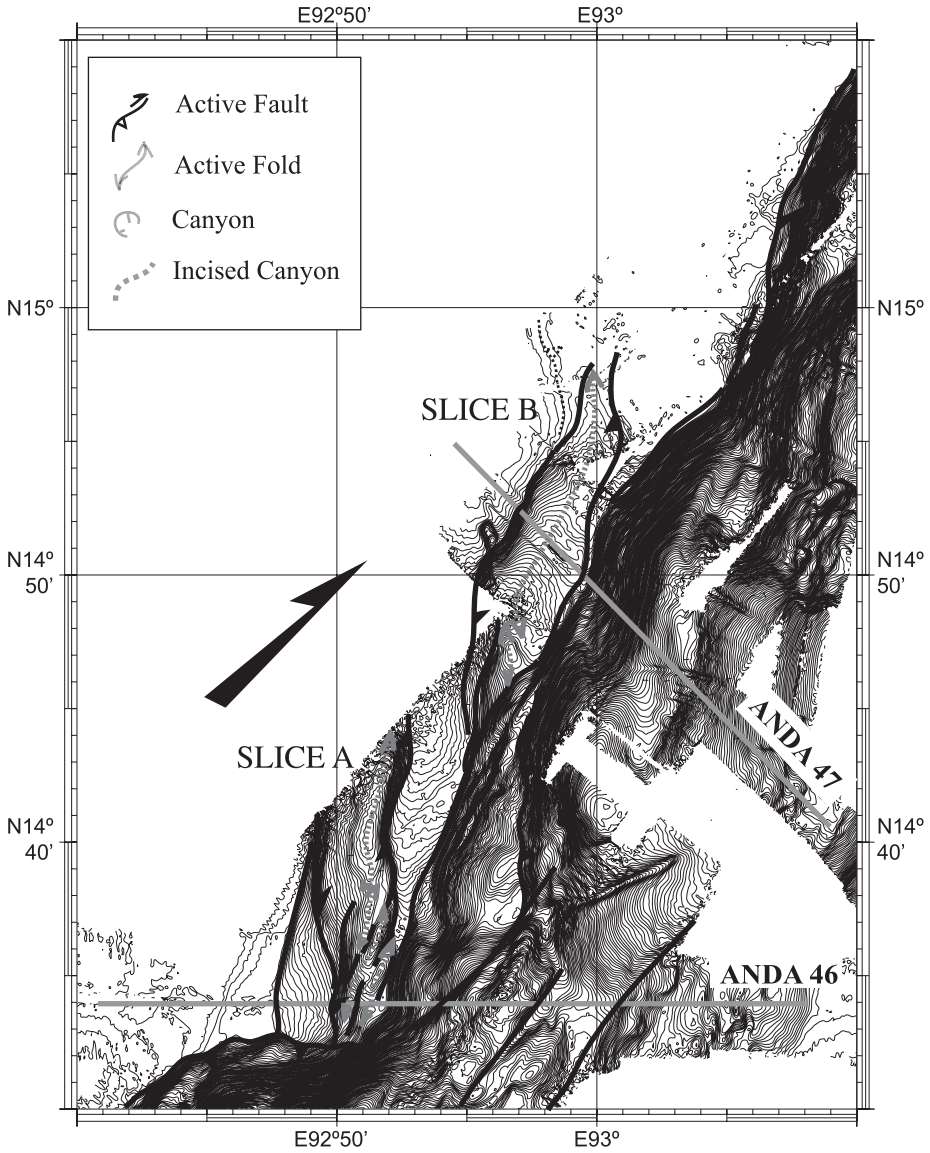

Fig. 5. Extract of the southern area showing *en échelon* tectonic slices at the base of the slope of the Western Burma Scarp. See location of the extract in Fig. 4.

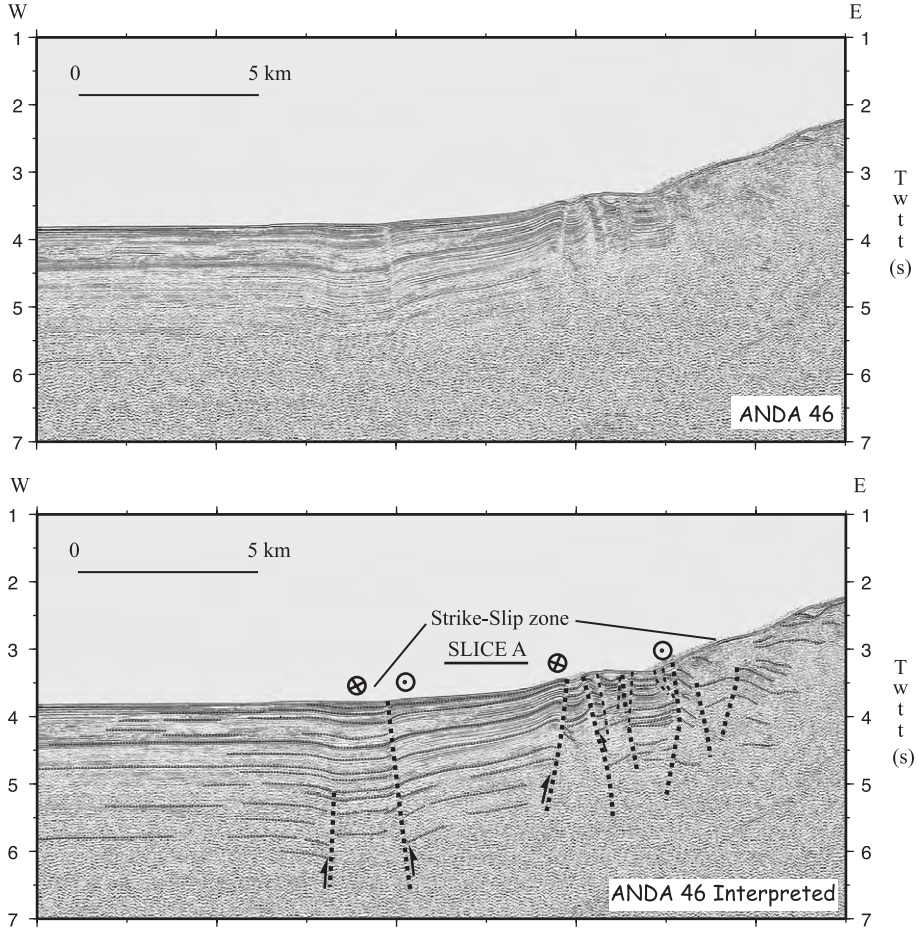

Fig. 6. Profile Andaman 46 and its interpretation. Track line position in Fig. 4.

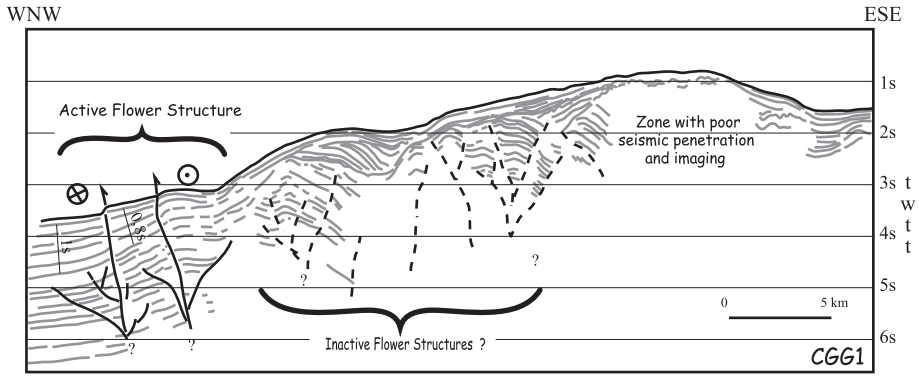

Fig. 7. CGG Profile interpretation. Track line position in Fig. 4.

2.2. The central part of the Western Burma Scarp: a transform segment

North of 15°30′ N, the WBS swings westward and bends to a N10°E orientation. In contrast to the southernmost segment, no tectonic slices are observed seaward of this portion of the scarp. The morphology is simple and corresponds to a relatively undeformed area. Between 15°40′ N and 15°50′ N (Fig. 10) prominent canyons, well seen on backscattering data, deeply incise the WBS. A large deep sea fan outlines the very unstable tectonic front, but no clear fault geometry can be observed there.

Absence of significant deformation at the toe of the scarp is illustrated along seismic line Andaman 50 (Fig. 11). The trench does not appear either in the morphology. The Bengal fan sediments actually lap gently the base of the WBS. This sequence is rather undeformed, with the exception of discrete strike-slip faulting affecting the Bengal fan sediments. The

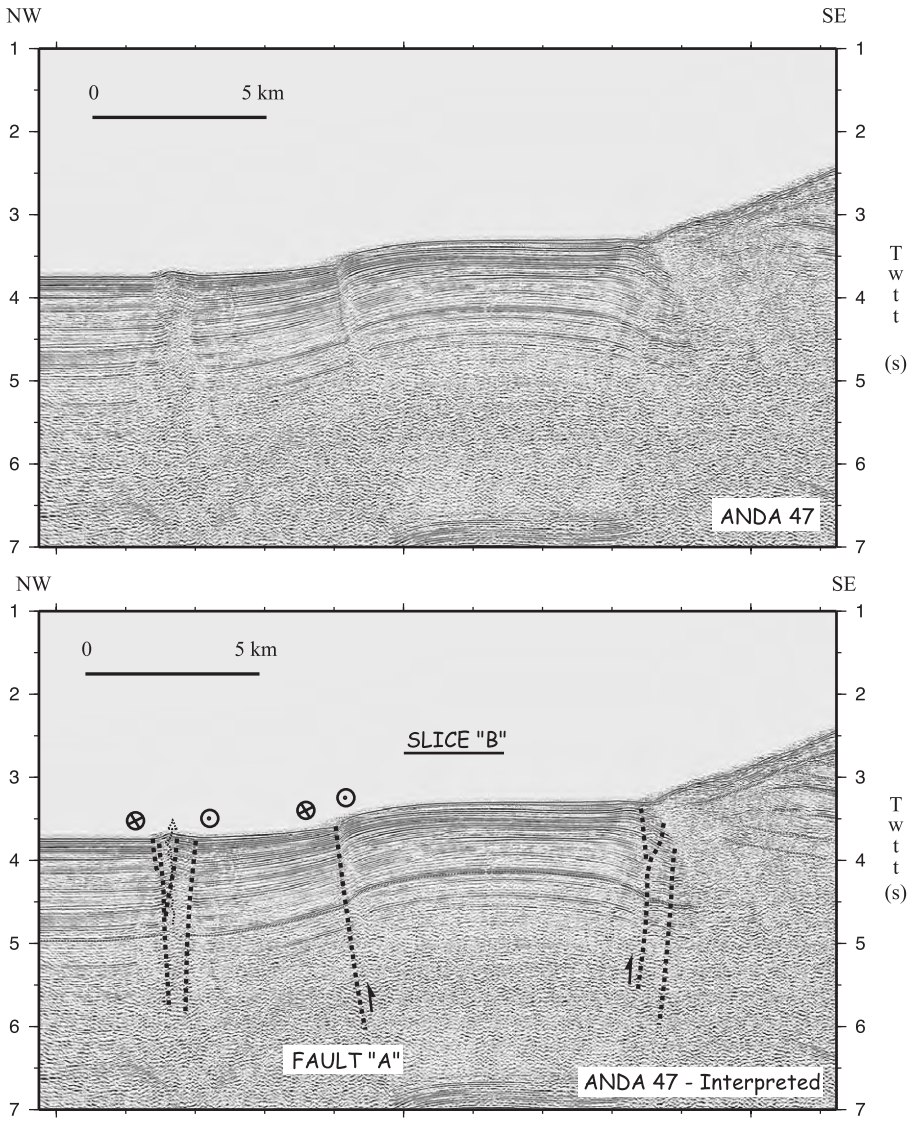

Fig. 8. Profile Andaman 47 and its interpretation. Fault A is followed on profile Andaman 48. Track line position in Fig. 4.

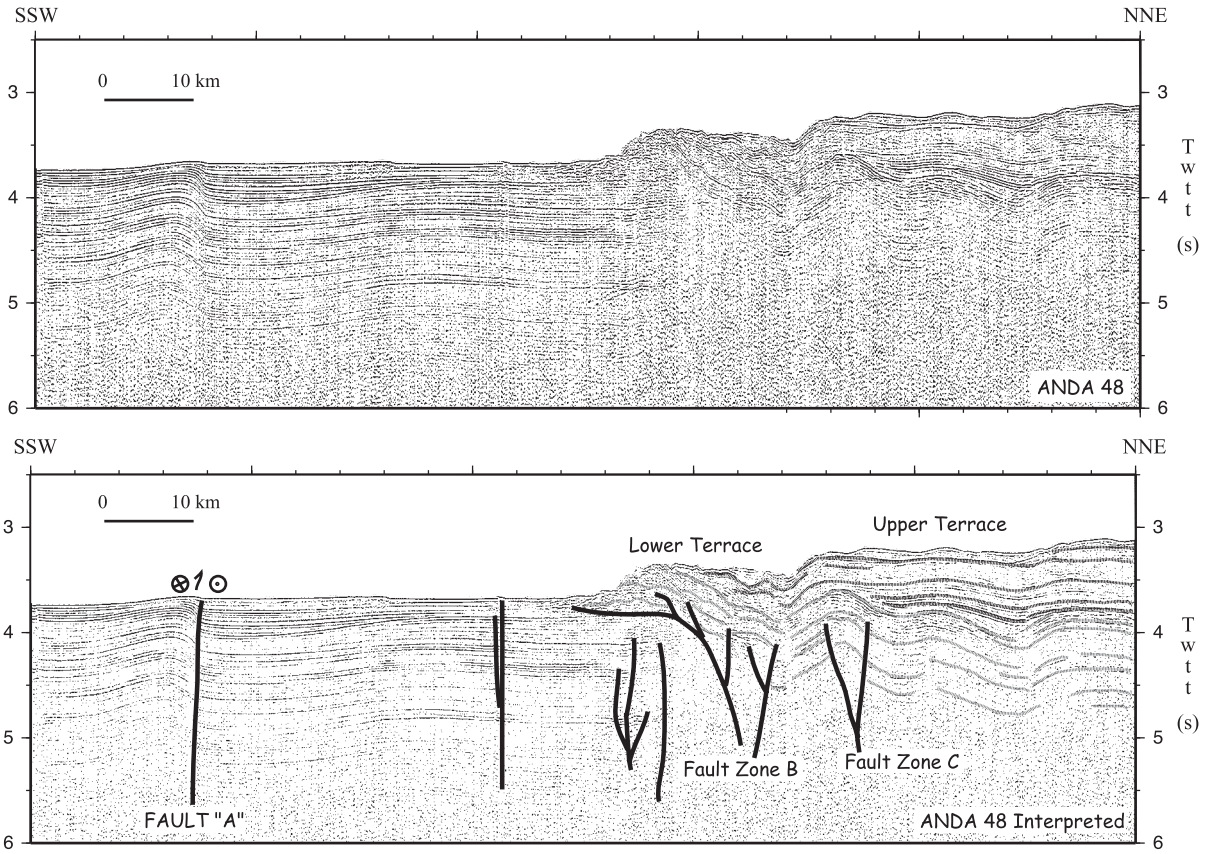

Fig. 9. Profile Andaman 48 and its interpretation. Track line position in Fig. 4.

sequence below is flexed upslope. This sequence was followed landward on a CGG multichannel line (Fig. 11) and forms the western flank of a high poorly imaged on seismic profiles.

A single active thrust was mapped east of the shelf break (CGG2, Fig. 11). The main orientation of this thrust is not well constrained due to poor spatial distribution of available seismic data. However, the regional tectonic orientations of the thrusts mapped northward, as well as correlation with onshore mapped structures along the Indo-Burma mountain ranges, indicate that this structure corresponds to a dogleg compressive arm (restraining bend) oriented in N140°E to 150°E, consistent with a N30°E to N40°E convergence.

Deformation is present north of 16°20′ N where the WBS is clearly framed by dominos with N160°E and N40°E segments. Andaman 52 seismic line (Fig. 11) indicates that sediments are thrusted westward onto the Bengal Basin along the largest N160°E segments. Several potential décollement levels are observed within the Bengal sediments, possibly merging along a single main décollement at depth. Clear and intense deformation is found further upslope, at the northeastern end of profile Andaman 52. Active folding associated with N160°E trending thrusts affects the recent sediments supplied by the Ayerawaddy delta. Despite discontinuous bathymetric mapping due to shallow waters, folds appear rather sigmoid in shape and connect with the N40°E trending structures interpreted as strike-slip faults. The northwestward part of this ‘‘domino’’ pattern is relayed northward (between 16°30′ N and 16°40′ N, Fig. 10) by a rather continuous and narrow strike-slip zone marked by *en échelon* folds and mud volcanoes. Here, the deformation takes place along

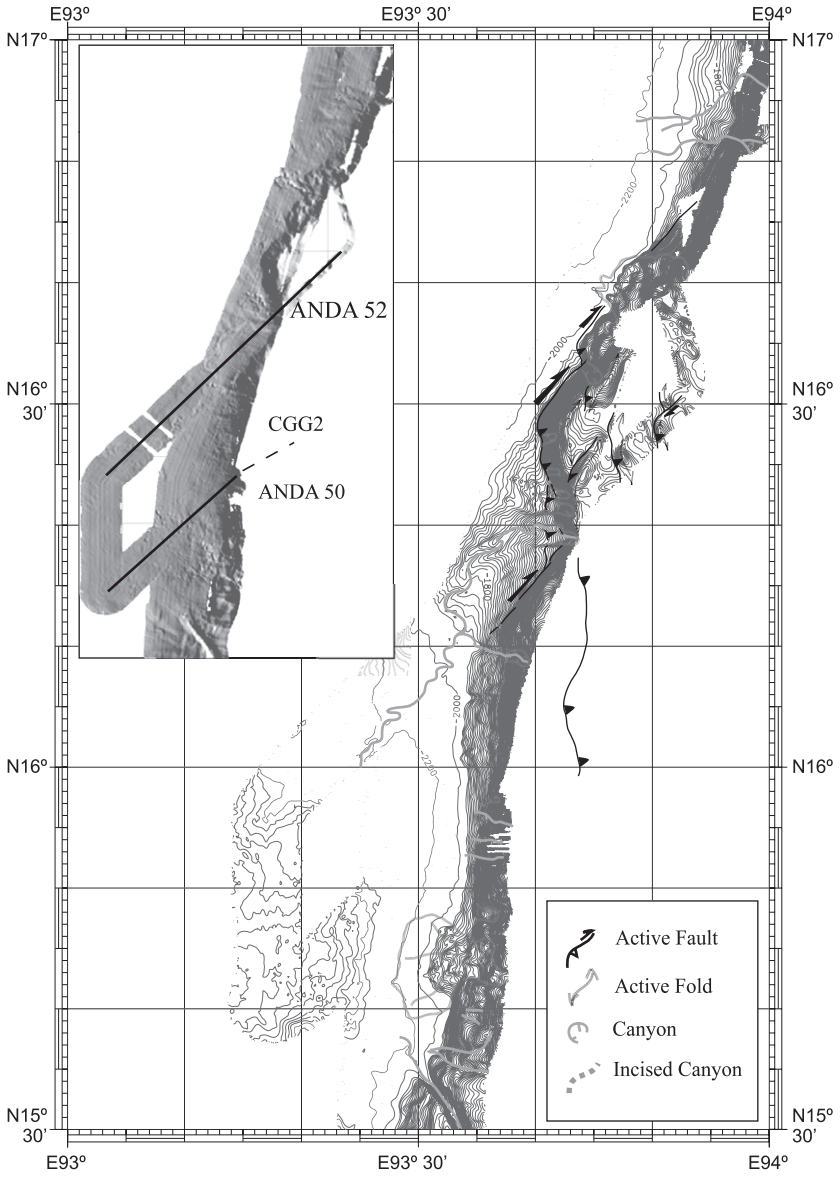

Fig. 10. Tectonic sketch of the central portion of the surveyed West Burma Scarp. Bathymetric data are contoured every 20 m.

short dogleg segments composed of N160°E trending thrusts and N40°E trending strike-slip faults. The same organization is followed northward where it guides the shape of the wall. Consequently, the entire central segment of the WBS corresponds to a multi-scale dogleg system consistent at larger scale with a rather straight N35°E dextral shear zone in a N35–40°E convergence.

2.3. The northern part of the West Burma Scarp: from transform to accretion

This northernmost part of our survey covers the very southern tip of the Arakan Yoma wedge (Fig. 12). Structurally, it coincides offshore with the first clear evidences of significant wedge type accretion. We name it the Ramree lobe, from the nearby

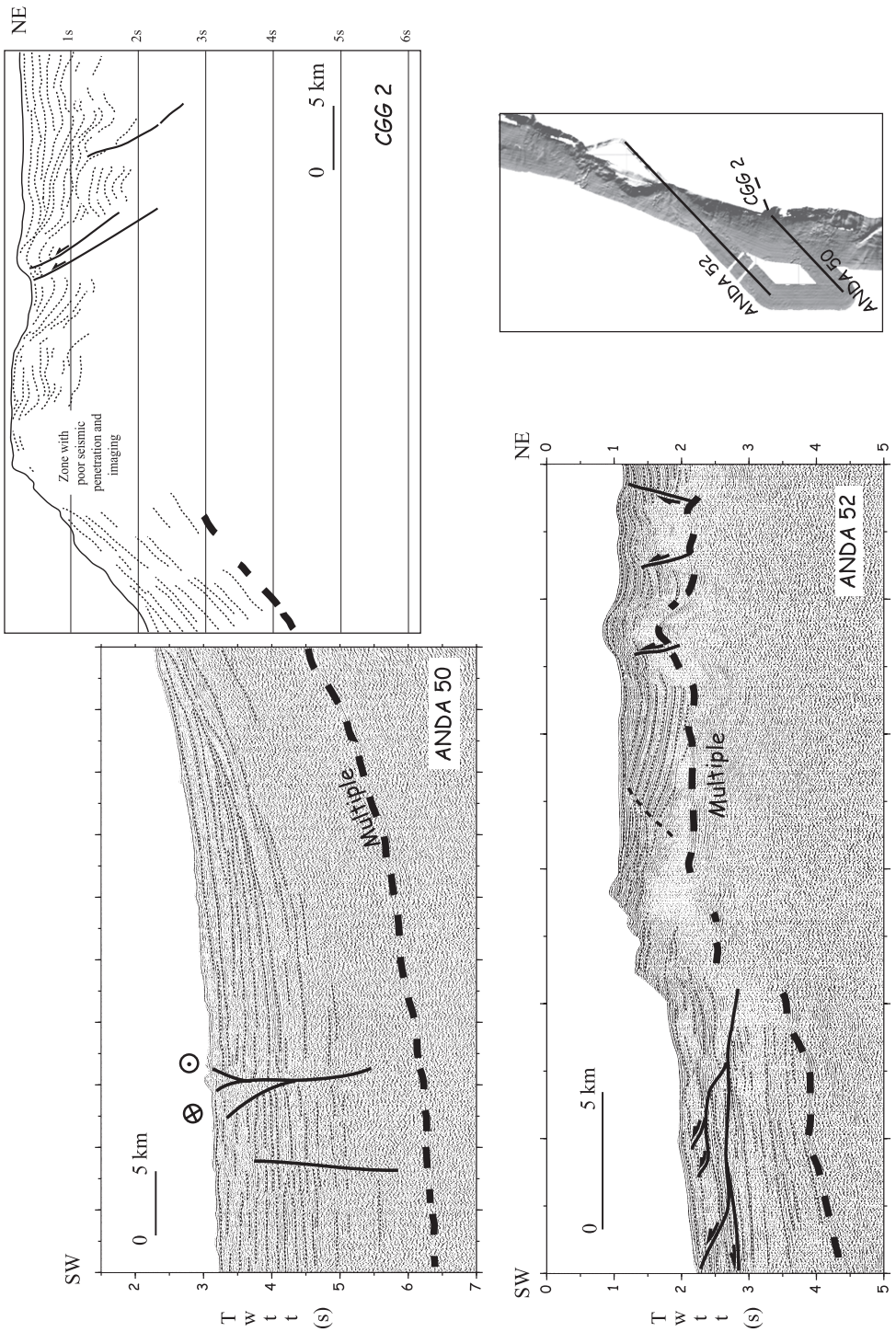

Fig. 11. Interpretations of seismic profiles Andaman 50, Andaman 52 and CGG2 multichannel line.

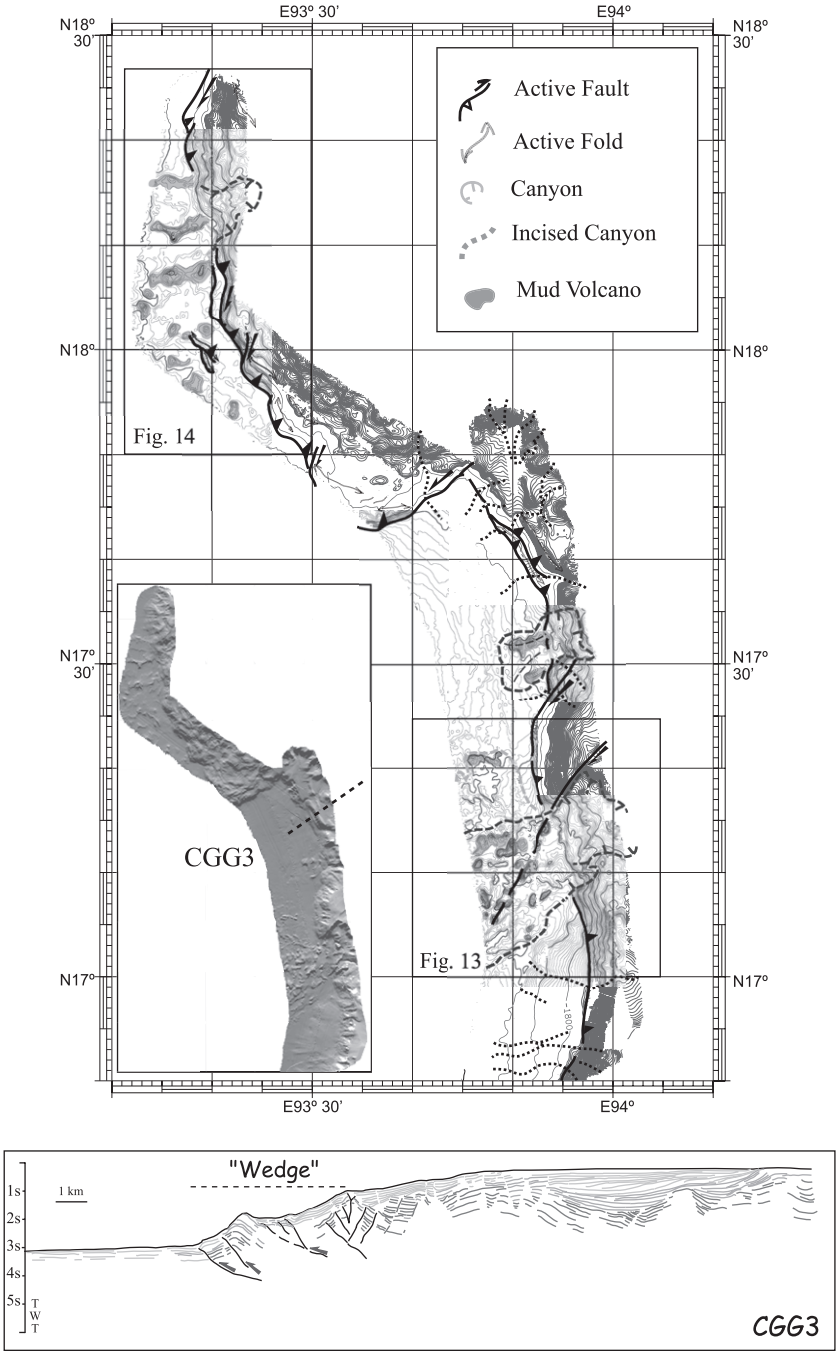

Fig. 12. (a) Tectonic sketch and bathymetric map of the northern portion of the Western Burma Scarp. Data are contoured every 20 m. (b) Interpretation of CGG3 multichannel line.

Ramree Island off Myanmar main coast. This is also the place of widespread mud diapirism and major gravity collapses, such as the Watthe Avalanche named from the closest city in Myanmar.

2.3.1. The Watthe Avalanche

Between 17°N and 17°35′ N, an important cinder cone abruptly cuts the linearity of the Western Burma Scarp. The area shows debris flows that poured out of large canyons. Bathymetric mapping reveals kilometer-size blocks lying on the flat seafloor of the Bengal Basin (Fig. 13). In addition to this blocky morphology, several mud volcanoes were identified on 3.5-kHz profiles. They appear as smoother bathymetric mounds within the Bengal plain. Our interpretation is that a large debris avalanche, the Watthe Avalanche, recently affected the steep and rather unstable slope of the Western Burma Scarp. Sudden loading of the non-

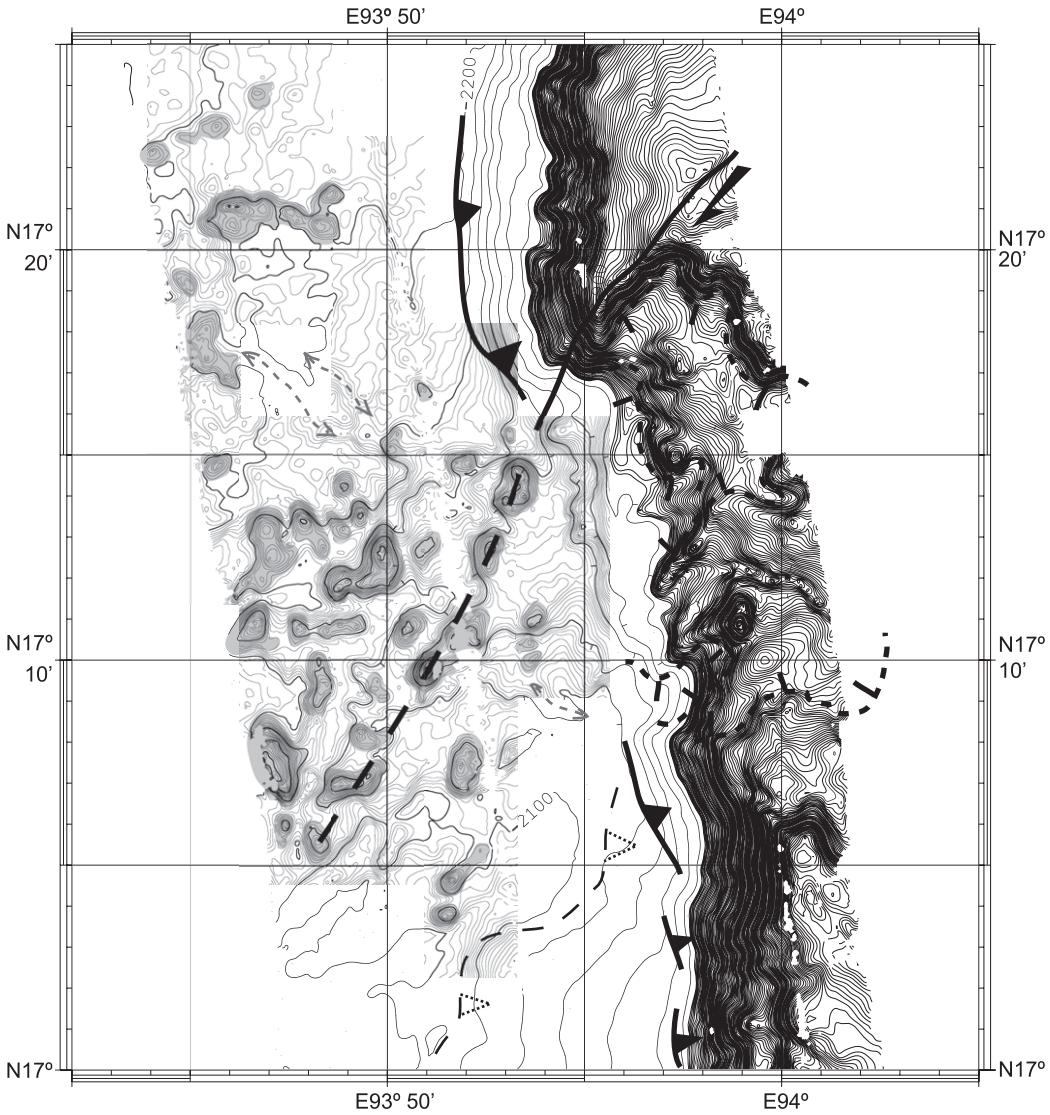

Fig. 13. Focus on the Watthe Avalanche and its debris cone. Mud volcanoes are in grey, black dotted lines are normal faults, black line is the strike-slip fault that generated the avalanche, and grey dotted lines are fold axis. Bathymetric data are contoured every 20 m.

compacted sediments of the Bengal fan probably resulted in the eruption of the mud volcanoes. Fast blanketing due to high sedimentation influx lead to rapid filling and progressive embedding of some of the debris, responsible for the peculiar "flat and blocks" morphology recognized by multibeam. Mud volcanoes are irregularly arranged into several N30°E trending ridges. Assuming that mud escaped through tension gashes, this orientation is compatible with stress orientation expected onto a more or less NS dextral strike-slip fault.

Similar avalanches have been observed along the Hikurangi Margin (Collot et al., 2001). The Ruatoria Debris Avalanche in New Zealand presents the same morphology, constituted by debris flows, with an almost circular indentation bounded by strike-slip scarp parallel to the Pacific Plate/Kermadec Arc convergence. The avalanche is interpreted there as resulting from the oblique subduction of a large seamount. The Watthe Avalanche seems to have occurred in a different tectonic setting, since the WBS shows no seamount-related indentation. The Avalanche would rather be the result of the high instability of the WBS along the main shearing segments. A similar instability, a large submarine olistostrome associated with the subduction motion, has been reported southward along the Sunda Arc subduction zone, facing the Andaman Islands (Moore et al., 1976).

2.3.2. The Ramree lobe

Offshore Ramree and Cheduba Islands, the Western Burma Scarp is a short accreting segment composed of imbricate folds and thrusts (Fig. 12). This portion of the WBS is the first clear evidence for wedge type accretion. The bathymetry shows a large semi-circular lobe sharply bounded to the southeast by a N55°E trending fault. Sigmoid folds there indicate sinistral motion compatible with the progressive outward growth of the wedge at the expense of the thick Bengal plain sediments. The main orientation of thrusting is N120°E, and a statistical study of the orientation of the imbricate slices and folds suggests a N35°E growth convergence.

North of 18°N (Fig. 14), although the overall course of the WBS generally trends northward, bathymetric details show dogleg segments with N140°E trending thrusts (accreting segments) and N10–20°E trending transfer faults (dextral strike-slip segments). However, the transfer faults do not show sharply in the bathymetry due to the soft and thick sediment cover.

Deformation also affects the flat sediments of the Bengal Basin, indicating outward propagation of the décollement level. The Bengal Plain facing this portion of the WBS is actually covered with mud volcanoes, either isolated or remarkably aligned along N70°E to EW trends. These mud ridges are particularly abundant in the northernmost part of the surveyed area. Notice that mud expulsion is also abundant upslope towards the continental margin, with Ramree and Cheduba Islands being the culminating points of larger mud volcano fields (Bender, 1983).

3. Tectonic interpretation of the Western Burma Scarp

The structures observed along a 700-km-long portion of the West Burma Scarp typically depict a dextral shear zone with wrenched accretionary wedge. The active tectonics evolves from transpression in the south to a multiscale restraining bend geometry in the north, connected by a localized strike-slip fault zone (Fig. 15). We do not see abrupt changes in the tectonic style, but subtle variations occur along the West Burma Scarp from south to north:

(1) In the south, the dominant tectonic process is dextral strike-slip faulting localized at the base of the slope, accompanied with significant shortening. Multiscale *en échelon* folds with axis trending N10°E to N35°E are compatible with NE convergence of the Indian plate with respect to the Burma margin.
(2) Further north, the WBS is shaped by a domino pattern framed by short N160°E and long N40°E segments. Motion along the N40°E trending segments is pure strike-slip.
(3) The WBS then swings N10°W, towards the Watthe Avalanche and N40°W towards the Ramree lobe. The WBS there shows a combination of N20°E dextral faults and NW–SE thrusts. The Ramree lobe itself shows discrete dogleg structures in its internal pattern.

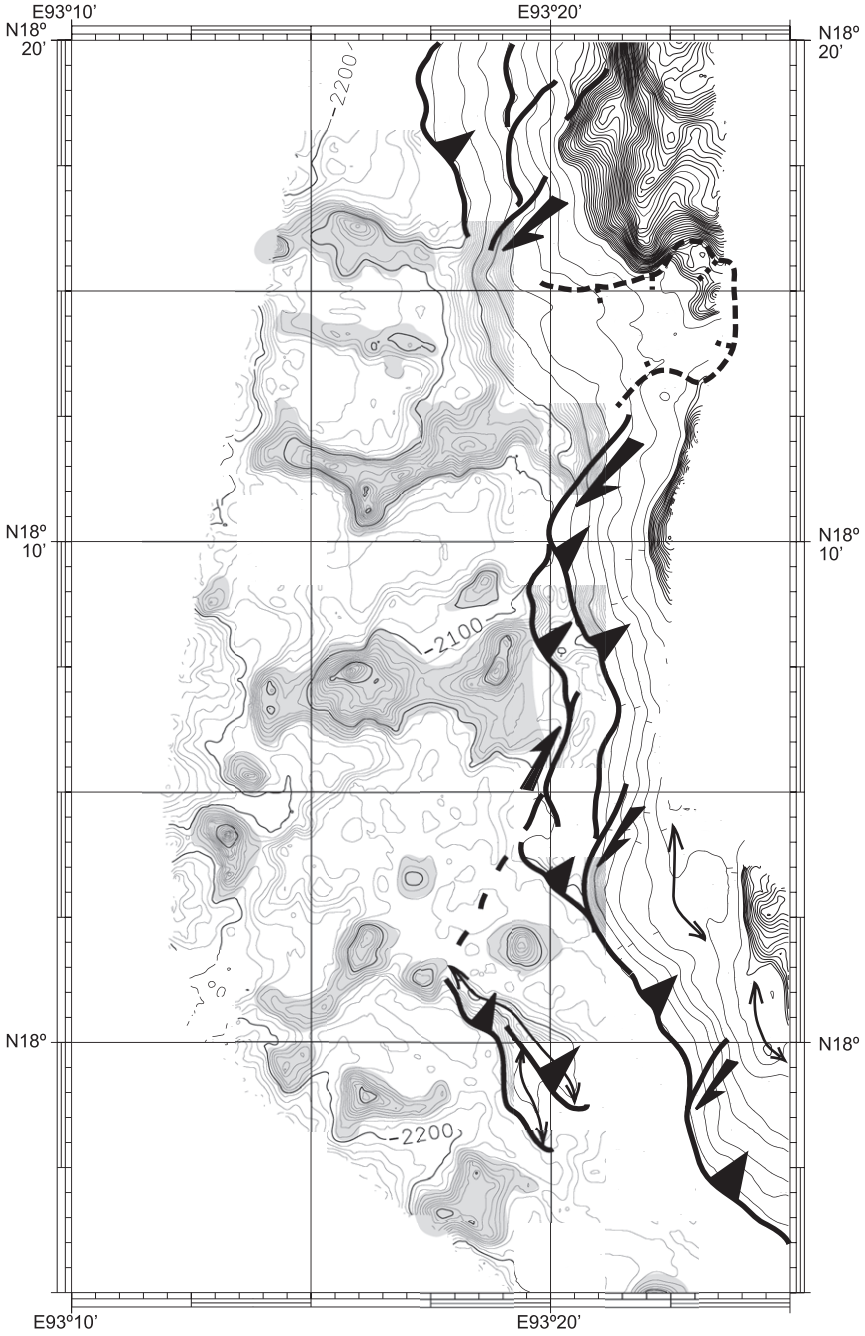

Fig. 14. Western flank of the Ramree Lobe, controlled by N10–20°E trending dextral strike-slip faults and N120–140°E trending thrusts. Bathymetric data are contoured every 20 m.

(4) Previous work on the offshore part of the Indo Burma wedge (Nielsen et al., 2001) also indicated, on the basis of industrial seismic data, that the same dogleg organization extends north outside the Andaman survey, up to 19°40′ N (Fig. 15). In this area, the Burma margin is controlled by

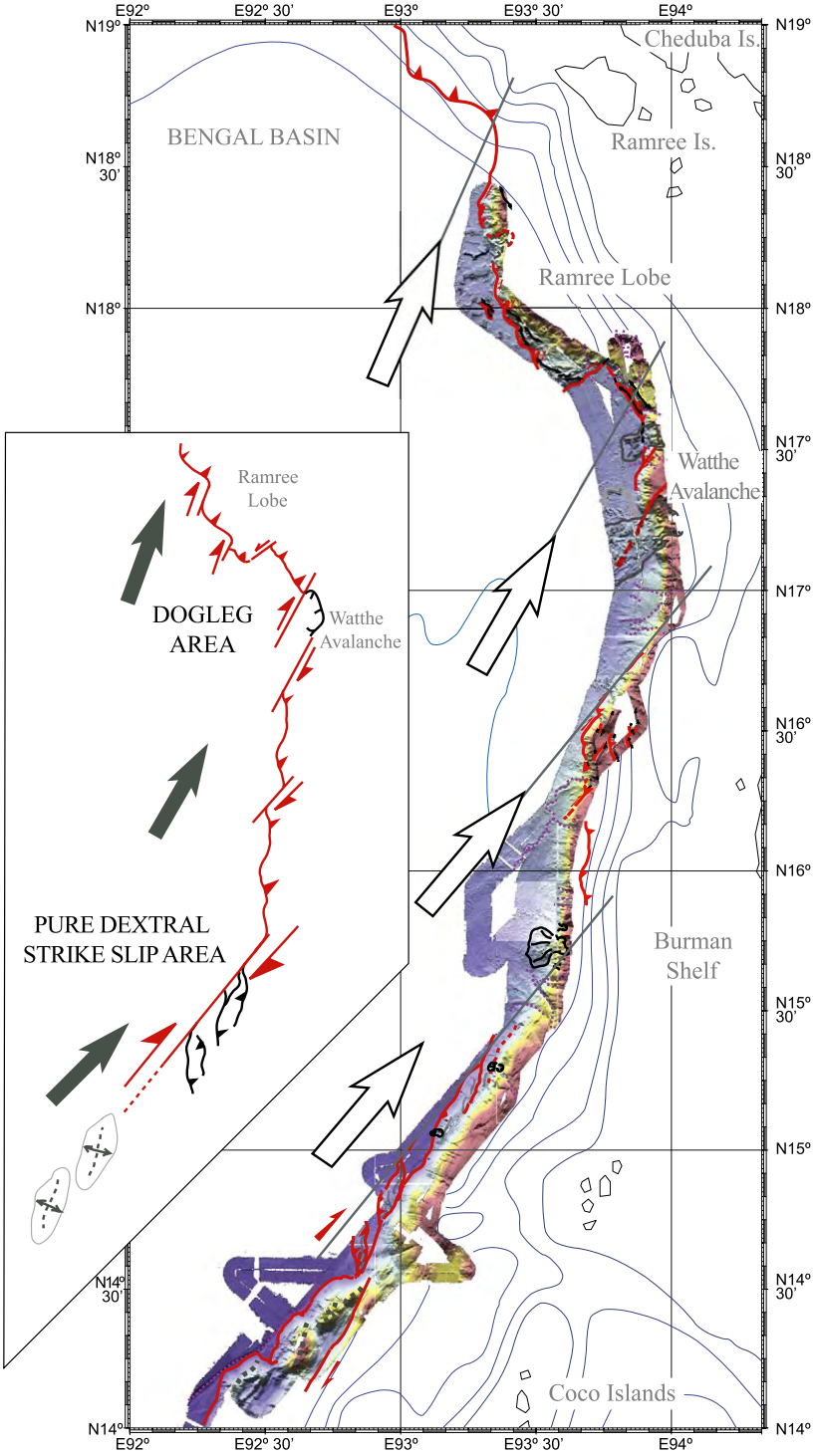

Fig. 15. Summary of the main tectonic features along the slope of the Western Burma Scarp. Arrows indicate inferred relative convergence between India and Burma margin.

N130°E thrust linked by NS to N20°E trending dextral transform segments, suggesting a N10–20°E relative convergence between India and Burma.

The mean N35°E trend of the pure shear segments, together with the N130–140°E trending thrusts, are compatible with a N30–40° convergence of India with respect to the Burma platelet. In details, the relative direction of convergence may evolve from N50° in the south to N20° in the north. We interpret those variations as resulting from latitudinal variations of the motion of the upper plate (or upper margin) with respect to India, either as an effect of rigid body rotation of the Burma platelet or as a result of internal deformation within it. The mean N30–40° convergence is to be compared to the predicted N10 ± 5° motion of India with respect to Sundaland. The main conclusion is that although the 20–30° clockwise rotation of the convergence vector does imply some amount of shear partitioning (if not relative convergence would be N10°), the degree of partitioning is rather small, at least along the portion of trench covered by the Andaman survey. We will show in a latter section that this observation is in agreement with reduced shearing motion on the Sagaing Fault.

4. Correlation of offshore data with seismicity and onshore structural fabric of the Indo-Burma range

Superficial as well as internal structures of the offshore Indo-Burmese wedge are poorly known. The active tectonic setting is mainly constrained by information provided by focal mechanisms of largest earthquakes (Harvard CMT and Engdahl catalogue) and some scarce morphological studies (Basu et al., 1992; Gopala Rao and Krishna, 1997). Off the Andaman Islands, seismicity indicates EW shortening, but strike-slip faulting is dominant. A few interplate earthquakes (i.e., slip on low-angle and east-dipping plane, see Fig. 1) suggest EW subduction (Kreemer et al., 2003). A recent model of the tsunami generated by the large 31/12/1881 submarine earthquake south of the Andaman Islands (Mw 7.9–10°N latitude) concludes to pure thrust slip onto an east-dipping plane (Ortiz and Bilham, 2003). Full partitioning would thus be reached there, in relation with the opening of the Andaman basin (Ortiz and Bilham, 2003). Immediately north of the Andaman Islands, major seismic events are absent, suggesting a seismic gap below the entire surveyed area. This gap was interpreted as further evidence for "locking" of the lower Indian and upper Burman plates (Le Dain et al., 1984; Guzmàn-Speziale and Ni, 1996). One large earthquake did occur recently quite close to the southern tip of our survey. This 13/09/2002 earthquake (Mw 6.5–13°N latitude), located west of the northern tip of the Andaman, is interpreted as oblique subduction of the Indian plate in a more or less northeast direction (Kayal et al., 2004). The subduction motion obtained solely from earthquakes would thus indicate gradual increase of the obliquity from southern to northern Andaman Islands.

North of 21°N in northern Myanmar, the core of the Arakan Yoma wedge is affected by strike-slip faults (Le Dain et al., 1984; Ni and Guzmàn-Speziale, 1989; Guzmàn-Speziale and Ni, 1996; Rao and Kumar, 1999). Faults seem to be distributed within the Arakan Yoma belt, but major ones may coincide with the main geological contacts (from west to east, Neogene prism-metamorphic Paleogene prism-Backstop formed by the Central Myanmar basin). At the same latitude, the toe of the Arakan Yoma wedge is exposed onshore and is characterized by NS trending folds and thrusts. Orientation of the maximum horizontal compressive stress from borehole breakouts suggests E–W compression in the external part of the Bangladesh fold system, although the data are somewhat scattered (Gowd et al., 1992). The E–W compression seems to be restricted to the sedimentary pile, since the mean P axis of earthquakes is only slightly east of north (Gowd et al., 1992, 1998). This would imply decoupling of the Tripura fold-and-thrust belt from the underlying basement.

Field studies at the latitude of the Andaman survey have shown that the dogleg structural organization recognized at sea is also observed on land along the southern part of the Indo-Burma range (Fig. 16). In its southernmost part, this range is mainly framed by N30°E trending dextral strike-slip faults and rare thrust faults, as far north as 18°N. North of this latitude, the N20°E dextral faults are combined with N120°E northeastward and southwestward vergent thrusts. The deformed area widens and changes orientation gradually, forming a major restraining bend.

Annex B70

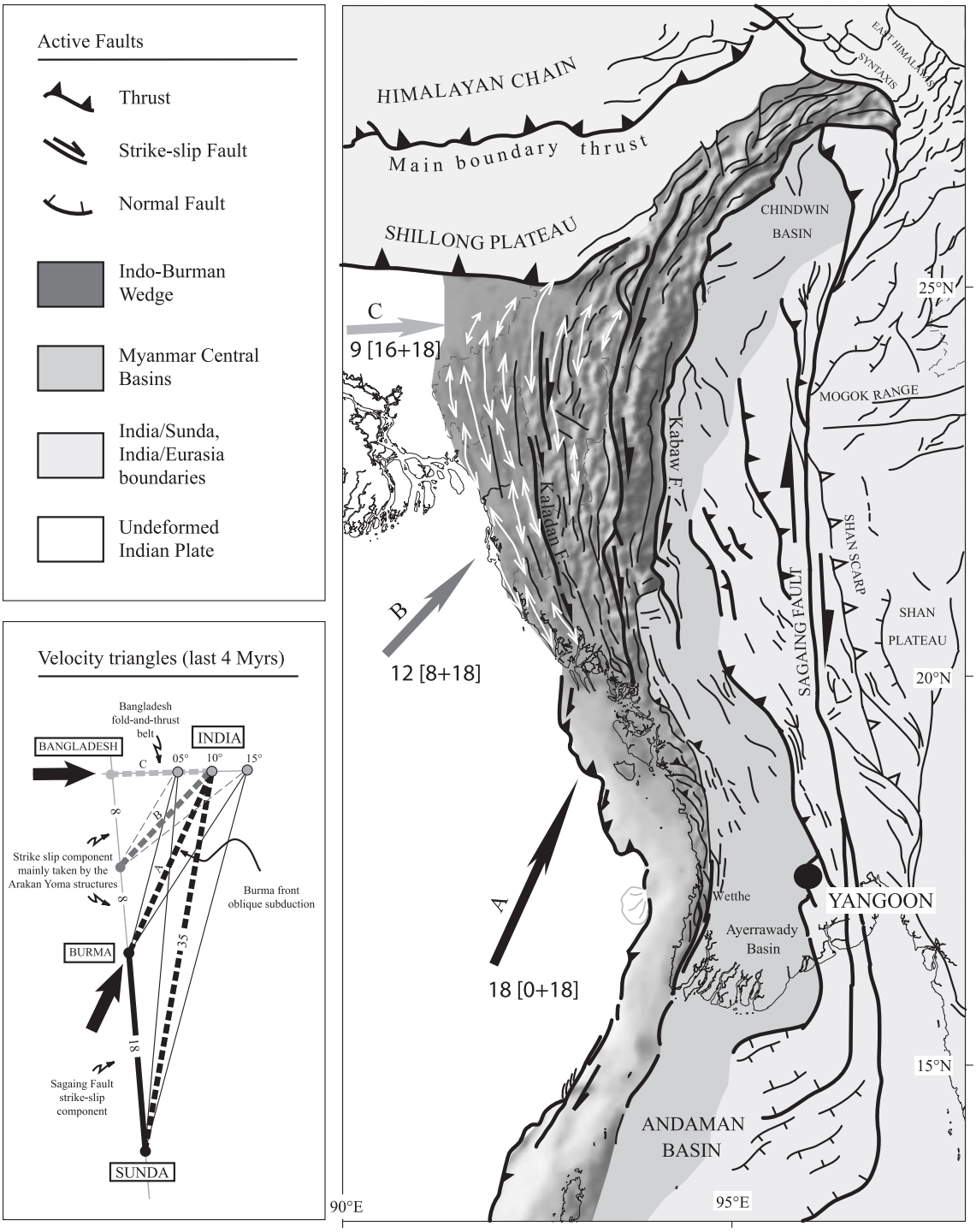
Active Faults
Thrust
Strike-slip Fault
Normal Fault
Indo-Burman Wedge
Myanmar Central Basins
India/Sunda, India/Eurasia boundaries
Undeformed Indian Plate
Velocity triangles (last 4 Myrs)
Bangladesh fold-and-thrust belt
BANGLADESH
INDIA
BURMA
SUNDA
Strike slip component mainly taken by the Arakan Yoma structures
Burma front oblique subduction
Sagaing Fault strike-slip component
HIMALAYAN CHAIN
Main boundary thrust
SHILLONG PLATEAU
EAST HIMALAYAN SYNTAXIS
CHINDWIN BASIN
MOGOK RANGE
Kaladan F.
Kabaw F.
SAGAING FAULT
SHAN SCARP
SHAN PLATEAU
C
9 [16+18]
B
12 [8+18]
A
18 [0+18]
Wetthe
YANGOON
Ayerrawady Basin
ANDAMAN BASIN
25°N
20°N
15°N
90°E
95°E

North of 20°N, the active structures are more linear and are represented by N–S to N170°E trending steep strike-slip faults that dissect the internal part of the range. The shallow seismicity outlines these strike-slip faults, which are sub-parallel to the Sagaing Fault.

The main conclusion from land studies is that dextral strike-slip faulting within the core of the Arakan Yoma wedge gradually increases northwards, while the relative convergence vector at the toe of the wedge becomes gradually purely frontal forming the Bangladesh folds. Our general interpretation is that partitioning along the Indo-Burma margin progressively evolves from poorly partitioned in the Andaman survey area to highly partitioned in the north. We next test this hypothesis through a simple kinematic model.

5. From partial to full partitioning along the Indo-Burma margin

Partitioning is a major mechanism of accommodation of oblique convergence (Mc Caffrey, 1994) at SE Asia trenches (including the Sunda trenches, and also the Philippine Trench and Nankai Trough). Sumatra, in particular, was long recognized as a case study, oblique motion of the Indo-Australian plate being resolved into trench-normal and arc-parallel components (Mc Caffrey, 1991; Bellier and Sébrier, 1995). Partitioning at Sumatra is active as far north as the northern tip of the Semangko Fault, where the fault enters into the Andaman Sea and connects to the active Andaman spreading centers. The Andaman Basin itself is generally considered as a pull-part basin between the Semangko and the Sagaing Fault, thus suggesting that partitioning observed at Sumatra is more or less transferred to Myanmar. This rather simple scheme is challenged by a number of complexities. First, the offshore tectonic pattern shows significant amount of shearing along a sizeable portion of the trench itself, indicating that full partitioning does not hold there. Second, the rate of motion on the Sagaing Fault is only two thirds of the rate on the northern Semangko Fault. A geological velocity of 10–25 mm/year was proposed using the offset of a Quaternary volcano built right on the fault (Bertrand et al., 1998; Bertrand, 1999). This is in good agreement with geodetic estimates. A local GPS geodetic network in Myanmar tied to other stations in SE Asia established an instantaneous velocity of about 18 mm/year around the ancient city of Mandalay (Vigny et al., 2003). Full transfer of the 26 mm/year Semangko motion to the Sagaing Fault thus does not seem to apply. Third, the series of NS elongated folds in Bangladesh suggest that convergence is back to trench-normal there. The degree of partitioning thus strongly varies with latitude. Fourth, vertical partitioning may also be important, stress indicators (borehole breakouts and P axis of earthquakes) show that at least the frontal portion of the Arakan prism is decoupled from the underlying basement.

Regardless of the mechanisms at work, we find that a simple kinematic model involving evolution from partial to full partitioning from south to north along the West Burma Scarp is compatible not only with the offshore tectonic style, but also with the reduced amount of shearing on the Sagaing Fault and the activation of additional dextral strike-slip faults within the core of the Arakan Yoma belt. We take as a basis to our model the most recent up-to-date for the motion of India with respect to Sundaland (Chamot-Rooke et al., 1998; Chamot-Rooke and Le Pichon, 1999; Simons et al., 1999; Becker et al., 2000; Holt et al., 2000; Kreemer et al., 2000b; Vigny et al., 2003). Geodetic measurements confirmed that Sundaland acts as an individual plate, so that the India/Eurasia kinematics inaccurately describes subduction motion at Sundaland trenches. Global kinematics obtained by

Fig. 16. Combined offshore and onshore structural map of Myanmar and surroundings. Schematically, the main units from west to east are: Indian plate, highly deforming and westward prograding Arakan Yoma Range and Bangladesh folds and thrust belt, deforming Myanmar Central Basins, undeforming Sunda Block. Arrows (and numbers next to them) indicate relative convergence of India with respect to the upper margin (all rates in mm/year), progressively rotating from 035°/18 mm/year (South Myanmar) to due East–West/9 mm/year (Bangladesh folds and thrusts belt). This is the result of progressive evolution from partial (south) to full partitioning (north), in relation with shear on Sagaing Fault only (south) to shear on Sagaing Fault plus NS dextral strike-slip faults in the Arakan Yoma (north). Numbers in brackets indicate the amount of dextral shear taken in the Arakan belt (first number, 0–8 and 16 mm/year) and onto the Sagaing Fault (second number, constant 18 mm/year rate assumed). These numbers were derived from the velocity triangles shown to the left.

GPS also point to a slower than expected motion of India. NUVEL-1A estimation at the latitude of Myanmar was about 50 mm/year (DeMets et al., 1990, 1994) where GPS measurements as slow as 35 mm/year have been reported (Holt et al., 2000; Kreemer et al., 2000a; Paul et al., 2001). A recent revision of the kinematics of India for the last 3 Myears, using up-to-date magnetic anomaly identification, also concludes to a slower motion of India (Gordon et al., 1999). Taking into account these revisions, the India–Sundaland convergence vector at the latitude of Myanmar is close to 35 mm/year, in a N10 ± 5° direction.

We test in Fig. 16 velocity triangles that may apply to the Indo-Burma region. Since geodetic (instantaneous) and geologic (finite motion for the last 3–4 Ma) estimates of India motion converge to similar values, we infer that the kinematic we describe here is valid for the last 4 Ma. The 4-Ma period also corresponds to the last pulse of oceanic accretion in the Andaman basin (Chamot-Rooke et al., 2001). India–Sunda motion is set to 35 mm/year, but we allow for the direction to vary in the range N5° to N15°. Shearing on the Sagaing Fault is constrained to 18 mm/year. The basic idea is that partitioning evolves from partial in the south (i.e., shearing on the Sagaing Fault only) to full partitioning in the north (i.e., shearing on the Sagaing Fault plus additional strike-slip faults active within the Arakan Yoma). Shearing on the Sagaing Fault alone leads to predicted convergence motion at the Burma Trench in the range N10° to N40°, in agreement with the structures described along the WBS. Dextral shearing on additional faults west of the Sagaing progressively re-orientates clockwise the direction of convergence to reach pure shortening in the very north (Bangladesh). The model requires an integrated rate of shear within the Arakan Yoma increasing northward (from small to 16 mm/year, see Fig. 16) which adds to the shear on the Sagaing Fault. We do not know at present whether this shear is located onto specific faults or distributed throughout the wedge. Major geologic discontinuities are likely to be activated. The Kabaw fault puts into contact the metamorphic rocks of the Paleogene accretionary complex with the Upper Cretaceous–Tertiary sediments of the Central basin. The fault is known to be reverse but with a strong right-lateral component (Pivnik et al., 1998). Other faults are active within the Indo-Burman Ranges, such as the Kaladan thrust, at the contact between the Paleogene accretionary complex and the Neogene accretionary prism, and additional east-dipping thrusts limiting successive slices of the accretionary prism (Sikder and Alam, 2003). We infer that these faults have a significant dextral strike-slip component.

Implicit in our kinematic model is that this additional shearing is taken in the Arakan Yoma belt rather than on the Sagaing Fault. If taken along the Sagaing Fault only, then the rate of strike-slip motion on it should increase northward. GPS measurements are restricted to Mandalay City, and at present, we do not know if the geodetic rate is constant along the entire Sagaing Fault. However, a northward rate increase would imply stretching of the Burma sliver, which is opposite to the observations. The Central basin in Myanmar is affected by transpression (see Fig. 16) active since Pliocene or Pleistocene time (Pivnik et al., 1998). This recent transpression followed a long period of extension, which led Pivnik et al. to suggest that northward motion of the Burma sliver is resisted by the Eastern Himalayas, following a "buttressing" model initially proposed by Beck (Beck et al., 1993). The entire variation that we see along the Burma front may actually be the result of this buttressing effect. Away from the Himalayas, obliquity of the subduction is fully accommodated by the opening of the Andaman basin. In Myanmar, motion of the sliver is resisted by the Himalayas, so that only half of the Andaman opening is transmitted to the Sagaing Fault. The remaining oblique component is then accommodated at the trench itself (this WBS study). In northern Myanmar, motion of the sliver may eventually drop, thus de-activating the Sagaing Fault. Dextral shearing would then migrate westward, re-activating major discontinuities found in the Arakan Yoma belt. In this extreme scenario, oblique motion of India is progressively transferred from a remote fault system (Andaman basin and eastern margin of the Central basin, i.e., the Sagaing Fault) to a close to trench fault system (Arakan belt and trench itself).

6. Conclusions

The West Burma Scarp is an active dextral strike-slip boundary accommodating part of the India–

Sunda motion. Detailed multibeam mapping and seismic imaging of the active structures found along the scarp suggests a relative convergence between India and Burma around N30°, implying pure strike-slip to pure shortening depending on the local orientation of the various segments of the margin. At a more regional scale, the Burma front progressively evolves to pure shortening northward towards the Bangladesh fold system. We infer that the evolution from shear (Burma scarp) to shortening (Bangladesh wedge) is the result of a gradual evolution from partial to full partitioning. Partial partitioning in the south is compatible with estimated motion of the Sagaing Fault, obtained from both instantaneous (GPS) and Quaternary (geological) fault slip rates (about 2 cm/year). The Sagaing Fault thus takes only half of the total India–Sundaland shear component of motion. Full partitioning in the north is the result of additional active strike-slip faults within the Arakan Yoma, localized at the prism–backstop contact but also within the Arakan Yoma belt. Faults accommodating the oblique component of motion of India are progressively migrating in space from far field faults (i.e., Andaman transforms/rift system and Sagaing Fault) to near trench faults (Arakan Yoma belt and the trench itself), as a result of the buttressing effect of the Eastern Himalayas that resist free escape of the Burma sliver.

Acknowledgements

We are particularly grateful to the people of the Institut Polaire Français Paul Emile Victor for their logistic support of the Andaman Cruise, in particular, G. Jugie and Y. Balut. Captain G. Foubert (Compagnie Maritime d'Affrètement) took us safely through the dangerous mounds of the Burma scarp, we warmly thank him and the entire crew of the *Marion Dufresne*. Swath bathymetry was successfully operated by B. Ollivier, chief of marine operators, and his team R. Cagna and X. Morin. We also thank G. Le Beuz and Y. Penaud, GENAVIR-Ifremer, for operating the seismic system. CGG and Total made available to us some of their industrial seismic lines, thanks to M. Le Vot. We also thank Serge Lallemand and Heidrun Kopp for their useful comments, and David Piper for his careful reading.

References

Alam, M., Alam, M.M., Curray, J.R., Chowdhury, A.L.R., Gani, M.R., 2003. An overview of the sedimentary geology of the Bengal Basin in relation to the regional tectonic framework and basin-fill history. Sediment. Geol. 155 (3–4), 179–208.

Basu, P.C., Bandyopadhaya, A., Bandyopadhaya, R.R., 1992. Bathymetry and echosignatures over parts of the accretionary wedge west of Andaman–Nicobar islands. Spec. Publ.-Geol. Surv. India 29, 219–228.

Beck, M.E., Rojas, C., Cembrano, J., 1993. On the nature of buttressing in margin-parallel strike-slip fault systems. Geology 21, 755–758.

Becker, M., Reinhart, E., Nordin, S.B., Angermann, D., Michel, G., Reigber, C., 2000. Improving the velocity field in South and South-East Asia: the third round of GEODYSSEA. Earth Planets Space 52 (10), 721–726.

Bellier, O., Sébrier, M., 1995. Is the slip rate variation on the great Sumatran fault accommodated by forearc stretching? Geophys. Res. Lett. 22 (15), 1969–1972.

Bender, F., 1983. Geology of Burma. Beiträge zur regionalen geologie der erde, vol. 16, Borntraeger, Stuttgart.

Bertrand, G., 1999. Tectonique Cénozoïque de l'Escarpement du Plateau Shan (Myanmar). Université Pierre et Marie Curie Paris VI, Paris.

Bertrand, G., Rangin, C., Maury, R., Htun, H.M., Bellon, H., Guillaud, J.P., 1998. Les basaltes de Singu (Myanmar): nouvelles contraintes sur le taux de décrochement récent de la faille de Sagaing. C. R. Acad. Sci., Paris 327, 479–484.

Chamot-Rooke, N., Le Pichon, X., 1999. GPS determined eastward Sundaland motion with respect to Eurasia confirmed by earthquakes slip vectors at Sunda and Philippine trench. Earth Planet. Sci. Lett. 173 (4), 439–455.

Chamot-Rooke, N., Le Pichon, X., Rangin, C., Huchon, P., Pubellier, M., Vigny, C., Walpersdorf, A., 1998. Sundaland motion in a global reference frame detected from GEODYSSEA GPS measurements: implications for relative motions at its boundaries with the Australia–Indian plates and the South China Block. In: Wilson, P., Michel, G. (Eds.), Scientific Technical Report STR98/14. GeofroschungsZentrum, Potsdam, pp. 39–75.

Chamot-Rooke, N., Rangin, C., Nielsen, C., 2001. Timing and Kinematics of Andaman Basin Opening. Eos. Trans. AGU 82 (20) (Spring Meet. Suppl., Abstract T42B-08, Boston).

Chaumillon, E., Mascle, J., 1997. From foreland to forearc domains: new multichannel seismic reflection survey of the Mediterranean ridge accretionary complex (Eastern Mediterranean). Mar. Geol. 138, 237–259.

Collot, J.Y., Delteil, J., Lewis, K., Davy, B., Lamarche, G., Audru, J.-C., Barnes, P., Chanier, F., Chaumillon, E., Lallemand, S., Mercier de Lepinay, B., Orpin, A., Pelletier, B., Sosson, M., Toussaint, B., Uruski, C., 1996. From oblique subduction to intra-continental transpression: structures of the southern Kermadec–Hikurangi margin from multibeam bathymetry, side-scan sonar and seismic reflection. Mar. Geophys. Res. 18, 357–381.

Collot, J.Y., Lewis, K., Lamarche, G., Lallemand, S., 2001. The giant Ruatoria debris avalanche on the northern Hikurangi mar-

gin, New Zealand: result of oblique seamount subduction. J. Geophys. Res. 19, 271–297.

Curray, J.R., Moore, D.G., Lawver, L.A., Emmel, F.J., Raitt, R.W., Henry, M., Kieckhefer, R., 1979. Tectonics of the Andaman Sea and Burma. In: Watkins, J.S., Montadert, L., Dickerson, P.W. (Eds.), Geology and Geophysics of Continental Margins. American Association of Petroleum Geologists Memoir 53, 189–198.

Delteil, J., Collot, J.-Y., Wood, R., Herzer, R., Calmant, S., Christoffel, D., Coffin, M., Ferrière, J., Lamarche, G., Lebrun, J.-F., Mauffret, A., Pontoise, B., Popoff, M., Ruellan, E., Sosson, M., Sutherland, R., 1996. From strike-slip faulting to oblique subduction: a survey of the Alpine Fault–Puysegur Trench transition, New Zealand, results of cruise Geodynz-sud Leg 2. Mar. Geophys. Res. 18, 383–399.

DeMets, C., Gordon, R.G., Argus, D.F., Stein, S., 1990. Current plate motions. Geophys. J. Int. 101, 425–478.

DeMets, C., Gordon, R.G., Argus, D.F., Stein, S., 1994. Effects of recent revisions to the geomagnetic reversal time scale on estimates of current plate motions. Geophys. Res. Lett. 21, 2191–2194.

Fitch, T.J., 1972. Plate convergence, transcurrent faults, and internal deformation adjacent to Southeast Asia and the western Pacific. J. Geophys. Res. 77, 4432–4460.

Gopala Rao, G.C., Krishna, K.S., 1997. Crustal evolution and sedimentation history of the Bay of Bengal since the Cretaceous. J. Geophys. Res. 102 (B8), 17747–17768.

Gopala Rao, G.C., Bhattacharya, M.V., Ramana, V., Subrahmanyam T., Ramprasad, T., Krishna, K.S., Chaubey, A.K., Murty, G.P.S., Srinivas, K., Desa, M., 1994. Analysis of multi-channel seismic reflection and magnetic data along 13°N latitude across the Bay of Bengal. Mar. Geophys. Res. 16, 225–236.

Gordon, R.G., Argus, D.F., Heflin, M.B., 1999. Revised estimate of the angular velocity of India relative to Eurasia. Eos. Trans. AGU 80 (46) Fall Meet. Suppl., F273, San Francisco.

Gowd, T.N., Srirama Rao, S.V., Gaur, V.K., 1992. Tectonic stress field in the Indian subcontinent. J. Geophys. Res. 97 (8), 11879–11888.

Gowd, T.N., Rao, S.V.S., Chary, K.B., 1998. Seismotectonics of northeastern India. Curr. Sci. 74 (1), 75–80.

Guzmàn-Speziale, M., Ni, J.F., 1996. Seismicity and active tectonics of the western Sunda Arc. In: Yin, A., Harrison, M. (Eds.), The Tectonic Evolution of Asia, Cambridge University Press, pp. 63–84.

Guzmàn-Speziale, M., Ni, J.F., Holt, W.E., Wallace, T., 1987. Seismotectonics of the Burma subduction zone. EOS, 1444.

Holt, W., Chamot-Rooke, N., Le Pichon, X., Haines, J., Shen-Tu, B., Ren, J., 2000. Velocity field in Asia inferred from Quaternary fault slip rates and Global Positioning System observations. J. Geophys. Res. 105 (B8), 19185–19209.

Kayal, J.R., Gaonkar, S.G., Chakraborty, G.K., Singh, O.P., 2004. Aftershocks and seismotectonic implications of the 13 September 2002 earthquake (M-w 6.5) in the Andaman Sea basin. Bull. Seismol. Soc. Am. 94 (1), 326–333.

Kreemer, C., Haines, A.J., Holt, W.E., Blewitt, G., Lavallée, D., 2000a. On the determination of a global strain rate model. Earth Planets Space 52, 765–770.

Kreemer, C., Holt, W.E., Goes, S., Govers, R., 2000b. Active deformation in eastern Indonesia and the Philippines from GPS and seismicity data. J. Geophys. Res. 105 (B1), 663–680.

Kreemer, C., Holt, W.E., Haines, A.J., 2003. An integrated global model of present-day plate motions and plate boundary deformation. Geophys. J. Int. 154, 8–34.

Lallemand, S.E., Schnurle, P., Malavieille, J., 1994. Coulomb theory applied to accretionary and nonaccretionary wedges—possible causes for tectonic erosion and or frontal accretion. J. Geophys. Res. Solid Earth 99 (B6), 12033–12055.

Lamarche, G., Lebrun, J.-F., 2000. Transition from strike-slip faulting to oblique subduction: active tectonics at the Puysegur Margin, South New Zealand. Tectonophysics 316, 67–89.

Lebrun, J.-F., Lamarche, G., Collot, J.-Y., Delteil, J., 2000. Abrupt strike-slip fault to subduction transition: the Alpine Fault–Puysegur Trench connection, New Zealand. Tectonics 19 (4), 688–706.

Le Dain, A.Y., Tapponnier, P., Molnar, P., 1984. Active faulting and tectonics of Burma and surrounding regions. J. Geophys. Res. 89, 453–472.

Mc Caffrey, R., 1991. Slip vectors and stretching of the Sumatran fore arc. Geology 19, 881–884.

Mc Caffrey, R., 1994. Global variability in subduction thrust zone–forearc systems. Pure Appl. Geophys. 142 (1), 173–224.

Michel, G.W., Yu, Y.Q., Zhu, S.Y., Reigber, C., Becker, M., Reinhart, E., Simons, W., Ambrosius, B.A.C., Vigny, C., Chamot-Rooke, N., Le Pichon, X., Morgan, P., Matheussen, S., 2001. Crustal motion and block behaviour in SE-Asia from GPS measurements. Earth Planet. Sci. Lett. 187 (3–4), 239–244.

Moore, D.G., Curray, J.R., Emmel, F.J., 1976. Large submarine slide (Olistostrome) associated with Sunda-Arc Subduction Zone, northeast Indian-Ocean. Mar. Geol. 21 (3), 211–226.

Mukhopadhyay, M., Das Gupta, S., 1988. Deep structure and tectonics of the Burmese arc: constraints from eathquake and gravity data. Tectonophysics 149, 299–322.

Ni, J.F., Guzmàn-Speziale, M., 1989. Accretionary tectonics of Burma and the three dimensional geometry of the Burma subduction zone. Geology 17, 68–71.

Ortiz, M., Bilham, R., 2003. Source area and rupture parameters of the 31 December 1881 M-w = 7.9 Car Nicobar earthquake estimated from tsunamis recorded in the Bay of Bengal. J. Geophys. Res. Solid Earth 108 (B4) DOI:10.1029/2002JB001941.

Paul, J., Buergmann, R., Gaur, V.K., Bilham, R., Larson, K.M., Ananda, M.B., Jade, S., Mukal, M., Anupama, T.S., Satyal, G., Kumar, D., 2001. The motion and active deformation of India. Geophys. Res. Lett. 28 (4), 647–650.

Pivnik, D.A., Nahm, J., Tucker, R.S., Smith, G.O., Nyein, K., Nyunt, M., Maung, P.H., 1998. Polyphase deformation in a fore-arc/back-arc basin, Salin subbasin, Myanmar (Burma). AAPG Bull.-Am. Assoc. Pet. Geol. 82 (10), 1837–1856.

Rao, P., Kumar, R., 1999. Evidences for cessation of Indian plate subduction in the Burmese arc region. Geophys. Res. Lett. 26 (20), 3149–3152.

Satyabala, S.P., 2003. Oblique plate convergence in the Indo-Burma (Myanmar) subduction region. Pure Appl. Geophys. 160 (9), 1611–1650.

Sikder, A.M., Alam, M.M., 2003. 2-D Modelling of the anticlinal

structures and structural development of the eastern fold belt of the Bengal Basin, Bangladesh. Sediment. Geol. 155 (3–4), 209–226.

Simons, W.J.F., Ambrosius, B.A.C., Noomen, R., Angermann, D., Wilson, P., Becker, M., Reinhart, E., Walpersdorf, A., Vigny, C., 1999. Observing plate motions in SE Asia: geodetic results of the GEODYSSEA project. Geophys. Res. Lett. 26 (14), 2081–2084.

Verma, R.K., Mukhopadhyay, M., Ahluwalia, M.S., 1976a. Earthquake mechanisms and tectonic features of northern Burma. Tectonophysics 32, 387–399.

Verma, R.K., Mukhopadhyay, M., Ahluwalia, M.S., 1976b. Seismicity, gravity and tectonics of northeast India and northern Burma. Bull. Seismol. Soc. Am. 66, 1683–1694.

Vigny, C., Socquet, A., Rangin, C., Chamot-Rooke, N., Pubellier, M., Bouin, M.N., Bertrand, G., Becker, M., 2003. Present-day crustal deformation around Sagaing fault, Myanmar. J. Geophys. Res. 108 (B11) DOI:10.1029/2002JB001999.

Annex B71

S. Kuehl et al., "The Ganges-Brahmaputra Delta", in *River Deltas--Concepts, Models, and Examples* (L. Giosan & J. Bhattachar eds., 2005)

RIVER DELTAS—CONCEPTS, MODELS, AND EXAMPLES

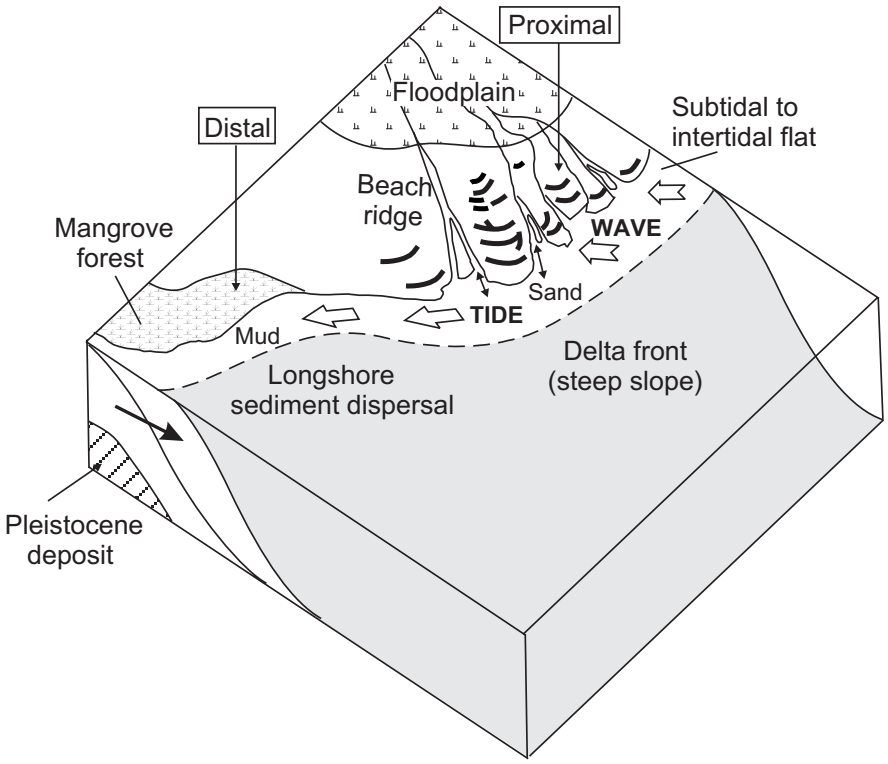

Edited by:

LIVIU GIOSAN
Department of Geology and Geophysics, Woods Hole Oceanographic Institution, MS # 22, Woods Hole, Massachusetts, 02543, U.S.A.

AND

JANOK P. BHATTACHARYA
Department of Geosciences, University of Texas at Dallas, P.O. Box 830688, Richardson, Texas 75083-0688, U.S.A.

Laura J. Crossey, Editor of Special Publications
SEPM Special Publication 83

Tulsa, Oklahoma, U.S.A. *August, 2005*

SEPM and the authors are grateful to the following
for their generous contribution to the cost of publishing

River Deltas—Concepts, Models, and Examples

University of Aberdeen

CASP

**Coastal Ocean Institute and Reinhart Coastal Research Center
at the Woods Hole Oceanographic Institution**

**The Mr. & Mrs. J.B. Coffman Endowment in Sedimentary Geology
at the University of Nebraska-Lincoln**

Natural Sciences and Engineering Research Council of Canada

Contributions were applied to the cost of production, which reduced the
purchase price, making the volume available to a wide audience

---

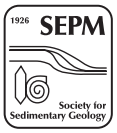

SEPM (Society for Sedimentary Geology) is an international not-for-profit Society based in Tulsa, Oklahoma. Through its network of international members, the Society is dedicated to the dissemination of scientific information on sedimentology, stratigraphy, paleontology, environmental sciences, marine geology, hydrogeology, and many additional related specialties.

The Society supports members in their professional objectives by publication of two major scientific journals, the Journal of Sedimentary Research (JSR) and PALAIOS, in addition to producing technical conferences, short courses, and Special Publications. Through SEPM's Continuing Education, Publications, Meetings, and other programs, members can both gain and exchange information pertinent to their geologic specialties.

For more information about SEPM, please visit **www.sepm.org.**

ISBN 1-56576-113-8

SEPM (Society for Sedimentary Geology)
6128 E. 38th Street, Suite 308
Tulsa, Oklahoma 74135-5814, U.S.A.

Printed in the United States of America

RIVER DELTAS—CONCEPTS, MODELS, AND EXAMPLES

Liviu Giosan and Janok P. Bhattacharya, Editors

CONTENTS

Introduction

Concepts and Reviews

Ancient Deltas (Pre-Holocene)

Modern Deltas (Holocene)

THE GANGES–BRAHMAPUTRA DELTA

STEVEN A. KUEHL
Department of Physical Sciences, Virginia Institute of Marine Science, College of William and Mary, Gloucester Point, Virginia, 23185, U.S.A.
e-mail: kuehl@vims.edu
MEAD A. ALLISON
Department of Earth & Environmental Sciences, Tulane University, New Orleans, Louisiana 70118, U.S.A.
e-mail: malliso@tulane.edu
STEVEN L. GOODBRED
Marine Sciences Research Center, Stony Brook University, Stony Brook, New York 11794, U.S.A.
e-mail: steven.goodbred@sunysb.edu
AND
HERMANN KUDRASS
Bundesanstalt für Geowissenschaften und Rohstoffe, 30631, Hannover, Germany
e-mail: kudrass@bgr.de

Abstract: Originating in the Himalayan Mountains within distinct drainage basins, the Ganges and Brahmaputra rivers coalesce in the Bengal Basin in Bangladesh, where they form one of the world's great deltas. The delta has extensive subaerial and subaqueous expression, and this paper summarizes the current knowledge of the Late Glacial to Holocene sedimentation from the upper delta plain to the continental shelf break. Sedimentation patterns in the subaerial delta are strongly influenced by tectonics, which has compartmentalized the landscape into a mosaic of subsiding basins and uplifted Holocene and Pleistocene terraces. The Holocene evolution of the delta also has been mediated by changing river discharge, basin filling, and delta-lobe migration. Offshore, a large subaqueous delta is prograding seaward across the shelf, and is intersected in the west by a major submarine canyon which acts both as a barrier for the further westward transport of the rivers' sediment and as a sink for about a third of the rivers' sediment discharge. Subaerial and subaqueous progradation during the Holocene has produced a compound clinoform, a feature which appears to be common for large rivers discharging onto an energetic continental shelf.

INTRODUCTION

The giant delta fed by the Ganges and Brahmaputra Rivers has only recently revealed its secrets to modern observational science. Early seminal studies by Morgan and McIntire (1959) and Coleman (1969) showcased much of the Quaternary geology of the Bengal basin and of the modern river system, respectively; however, it was not until late 1980s and 1990s that the submarine delta was described and numerous studies of coastal and delta-plain environments were published. As such, a comprehensive picture of the entire delta system could only recently be assembled. This paper summarizes the current knowledge of this major sedimentary system, based largely on published research of the last decade.

The Ganges and Brahmaputra Rivers currently contribute about a billion tons (10^{12} kg) of sediment annually to the Bengal Basin, and over the Holocene these sediments have built a deltaic feature with a subaerial surface area of 110,000 km^2. The modern delta continues offshore as a prograding clinoform, extending 125 km across the continental shelf from the river mouths, and about 250 km along shelf from the eastern coast of Bangladesh west to the "Swatch of No Ground" submarine canyon, roughly at the border of India and Bangladesh. Thus, the total area of the combined subaerial and submarine delta is about 140,000 km^2, an area roughly equivalent to the size of Britain.

One of the goals of this summary is to reflect on the lessons of the Ganges–Brahmaputra system with respect to sedimentary processes and deltaic facies compared with other major rivers. This exercise has both academic as well as societal importance as a result of the remarkable intersection of geology and human habitation within delta systems in general, and within the Ganges–Brahmaputra system in particular. Most of the Ganges–Brahmaputra delta is contained within, or seaward, of Bangladesh, a country of some 140 million inhabitants with a population density approaching 1,000 persons per km^2. The southwest sector of the delta extends into India, covering an area of approximately 25,000 km^2, or about 22% of the subaerial surface. People living on the delta have adapted to the harsh realities of frequent flooding and land loss and/or gain characteristic of lowland deltas, but they face an uncertain future as development of river control structures, global sea-level rise, and climate change threaten to alter the dynamic balance between sediment supply, subsidence, and sea level in various regions of the delta.

SETTING

Tectonics and Geologic Setting

While most of the world's major rivers enter the ocean along passive continental margins, the Ganges and Brahmaputra originate in the still rising Himalayan orogenic belt and reach the sea across the tectonically active Bengal Basin. Despite its proximity to the Himalayan foredeep, though, the Bengal Basin is situated seaward of the foreland hinge on a classic trailing-edge margin. Nevertheless, the margin is deformed within this complex, but poorly understood, tectonic setting. As evidence of this activity,

River Deltas—Concepts, Models, and Examples
SEPM Special Publication No. 83, Copyright © 2005
SEPM (Society for Sedimentary Geology), ISBN 1-56576-113-8, p. 413–434.

the Bengal Basin is bordered directly by the Precambrian Shillong Massif and Indian Shield to the north and west, and the Neogene Tripura Fold Belt to the east (Fig. 1). The tectonic activity of the basin has influenced riverine sediment distribution of all parts of the margin. Because of the ongoing collision of the Burmese plate overriding the eastern margin of the Indian continent and its adjacent oceanic crust, the Bengal Basin has been subsiding since the Eocene (Alam et al., 2003). The Eocene carbonate platform formed at the drifting Indian plate can easily be traced in seismic records and boreholes from a few hundred meters depth on the Indian side, dipping southeastwards under deltaic sediments to depths of about 6 km (Reimann and Hiller, 1993). The thickness of deltaic sediments overlying the oceanic crust in the central and eastern basin may reach up to 20 km (Johnson et al., 1976; Curray et al., 2002). Long-term tectonic subsidence in the eastern and southern basin of 1–2 mm y^{-1} has been balanced by the high sediment supply from Himalayan erosion (Alam, 1996). The approximate transition of the Indian continent to oceanic crust, which acts as a hinge line, is marked by high gravity and magnetic anomalies (Sengupta, 1966; Iman and Shaw, 1985).

Except for two possibly fault-bounded terraces that are elevated 3–15 m above the Holocene alluvium (Madhupur and Barind; Fig. 1), the basin surface over which the Ganges and Brahmaputra migrate is of low relief, dipping gently seaward from a mean elevation of 10–15 m in the upper delta plain. At the coast, the Holocene Ganges–Brahmaputra delta has prograded across a broad front (380 km) bordered by the Hoogly River in the west (India) and the Tripura fold belt of eastern Bangladesh.

Rivers

Both the Ganges and Brahmaputra rivers originate in mountains of the Himalaya, but they take distinctly different paths before joining together in the Bengal Basin and debouching to the Bay of Bengal (Fig. 2; Subramanian and Ramanathan, 1996). The Ganges source is the Gangotri glaciers on the southern slopes of the Himalaya. It crosses the Great and Lesser Himalayas southward before descending onto the Indo-Gangetic plain, where it flows eastward towards the Bengal Basin and is fed by numerous large tributaries. The Brahmaputra originates from glaciers along the northern slopes of the Himalayan range, travels eastward along the Tibetan plateau as the Tsangpo, and then traverses abruptly around the Himalayan syntaxis (Nanga Parbat) before descending southward to the Bengal Basin. The combined drainage basin area for the two rivers is about 2×10^6 km^2, with 1,114,000 km^2 for the Ganges and 935,000 km^2 for the Brahmaputra (Coleman, 1969).

The mainstream and various tributaries of the Ganges and Brahmaputra rivers drain a variety of geologic source rocks (Fig. 2). The highland streams of the Ganges largely drain Precambrian metamorphic rocks of the Himalaya southern slope, along with some Paleozoic–Mesozoic sedimentary sequences and Pleistocene alluvium. Lowland Ganges streams cross Mesozoic–Tertiary flood basalts, Precambrian metamorphics, and Archean granites and gneisses. In contrast, the Brahmaputra basin is dominated by Mesozoic sandstone, shale, and limestone, with Precambrian acid intrusives and Cambrian sedimentary rocks. The distinct geology of the two drainage basins leads to diagnostic differences in the mineralogy of modern sediments carried by the rivers (Heroy et al., 2003; Huizing, 1971). For the fine sand fraction (250–63 μm), the epidote-to-garnet ratio of Brahmaputra sediments is typically between 1.0 and 2.5, whereas ratios in Ganges sediments are < 1, with a typical value of about 0.5. For the clay-size mineralogy, Brahmaputra sediment is characterized by higher relative abundances of illite (63% vs. 41%), kaolinite (29% vs. 17%), and chlorite (2–3% vs. < 1%), whereas Ganges sediment contains significantly higher smectite (39% vs. 3%).

River waters of the Ganges and Brahmaputra contain a relatively high concentration of Sr (0.91 μmol l^{-1}) with a higher radiogenic $^{87}Sr/^{86}Sr$ ratio of 0.7295 than the global runoff. Therefore, the Sr input of the two rivers is considered to be a substantial source for the global Cenozoic increase of the seawater $^{87}Sr/^{86}Sr$ (Edmond, 1992; Galy et al., 1999). Total dissolved salt concentrations are also relatively high compared to other major rivers—178 mg l^{-1} in the Ganges and 100 mg l^{-1} in the Brahmaputra—and are a result of chemical denudation rates 2–3 times higher than the world average created by high relief and high rainfall in the catchment (Sarin et al., 1989). Combined total flux of dissolved ions to the oceans is 0.13×10^{12} kg y^{-1} (3% of world total).

Water and sediment discharge of the rivers is driven largely by the southwest monsoon, with maximum discharge for the Ganges and Brahmaputra occurring during June–November and May–November, respectively (Fig. 3) (Coleman, 1969). River discharge drops dramatically during the northeast monsoon and reaches a low during January–April that is about an order of magnitude below peak discharge. Overall, 80–90% of the water discharge for the Ganges occurs during the southwest monsoon; this figure rises to about 95% for the Brahmaputra (Subramanian and Ramanathan, 1996). Numerous estimates of sediment discharge for the combined system into the Bengal Basin converge at about 10^{12} kg y^{-1} (Abbas and Subramanian, 1984; Goswami, 1985; Subramanian, 1978). However, on the basis of a geochemical mass balance the amount of bedload into the basin could be almost twice as much (Galy and France-Lanord, 2001). Subramanian and Ramanathan (1996) conclude that the bulk of the sediment load for the rivers is delivered during moderate peaks in water discharge that occur during a normal wet season.

Oceanography

The coastal zone is strongly affected by the tidal wave, which has a range of 1.9 m on the western coast and is amplified to 2.8 m along the eastern coast by the funneling effect of the topography (Barua, 1990). Farther upstream in the estuary, the range increases to as much as 5 m. On the basis of 14 temporary stations where the current velocities and suspended-sediment concentrations on the inner shelf were examined, the suspended material is transported mainly southwestwards (Barua, 1990).

Surface circulation in the Bay of Bengal is dominated by reversing wind regimes and high variability of precipitation of the monsoonal seasons. During the summer monsoon, an anticlockwise gyre develops in the northwestern sector of the Bay, which reverses during winter (Tomczak and Godfrey, 1994). Precipitation during the summer monsoon (July–September) increases the joint outflow from the Ganges and Brahmaputra into the northern Bay of Bengal from about 10,000 $m^3 s^{-1}$ to about 100,000 $m^3 s^{-1}$. During the high-discharge period this fluvial runoff displaces marine waters seaward near the river mouths. Freshwater influence extends over much of the northern Bay, forming a surface layer of reduced salinity 50–100 m thick. Especially during the summer monsoon, the low-density, low-salinity surface layer damps the upwelling of deeper nutrient-rich water near the Indian coast and in general prevents the vertical exchange of water masses (Sheyte et al., 1991). This situation produces a permanent oxygen-minimum zone in the deeper Bay of Bengal, extending from the thermocline between 50–100 m to 600 m (Karstensen, 1999). In the shelf canyon, called the Swatch of No Ground, the slow vertical water exchange rate and the high flux of organic material results in nearly anoxic

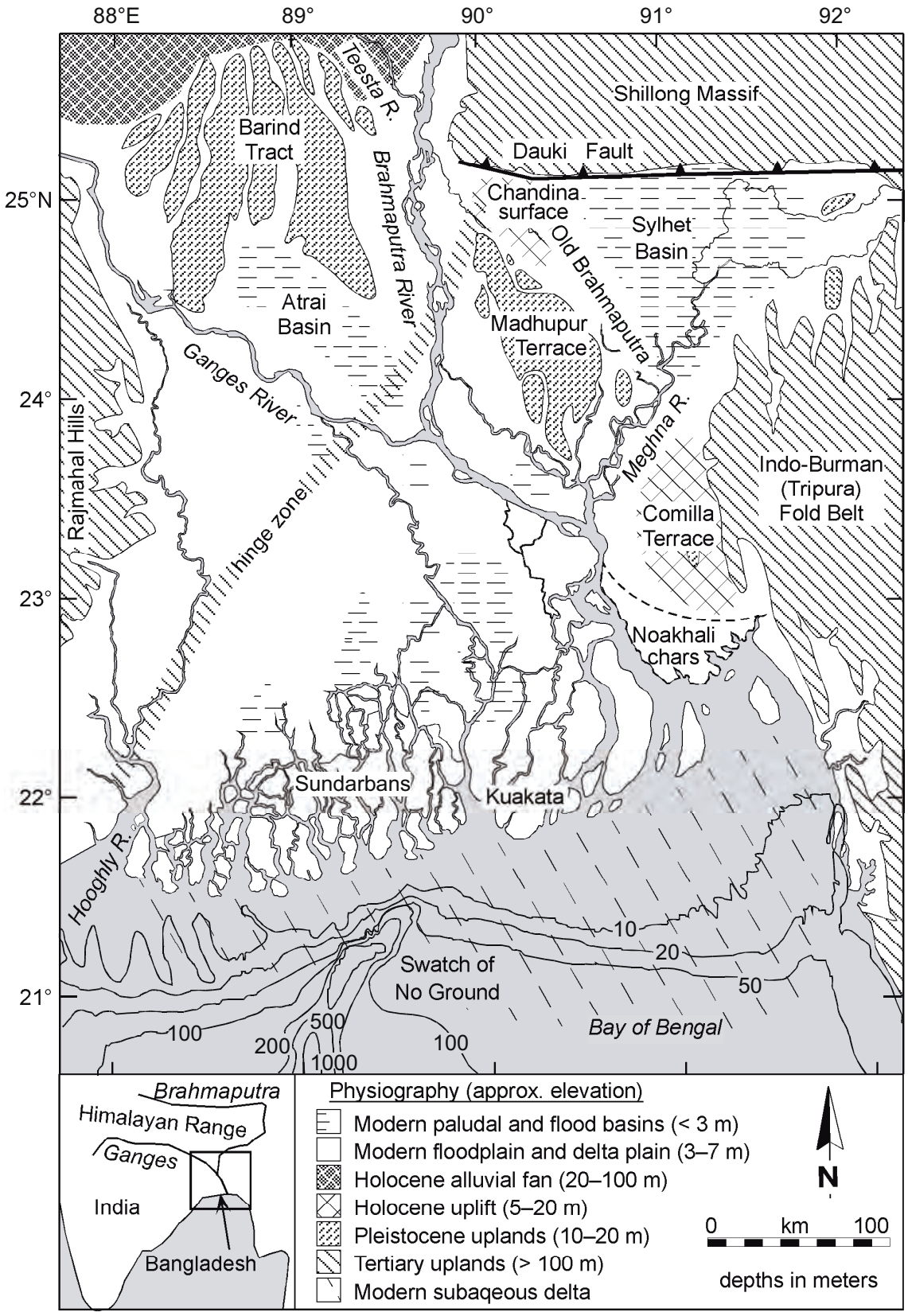

FIG. 1.—Physiographic and tectonic map of the subaerial Ganges–Brahmaputra Delta showing the distribution and ages of landforms in this tectonically complex Bengal Basin. The delta is surrounded by Tertiary uplands and contains uplifted Pleistocene and Holocene regions such as the Barind Tract, Madhupur, and Comilla Terraces.

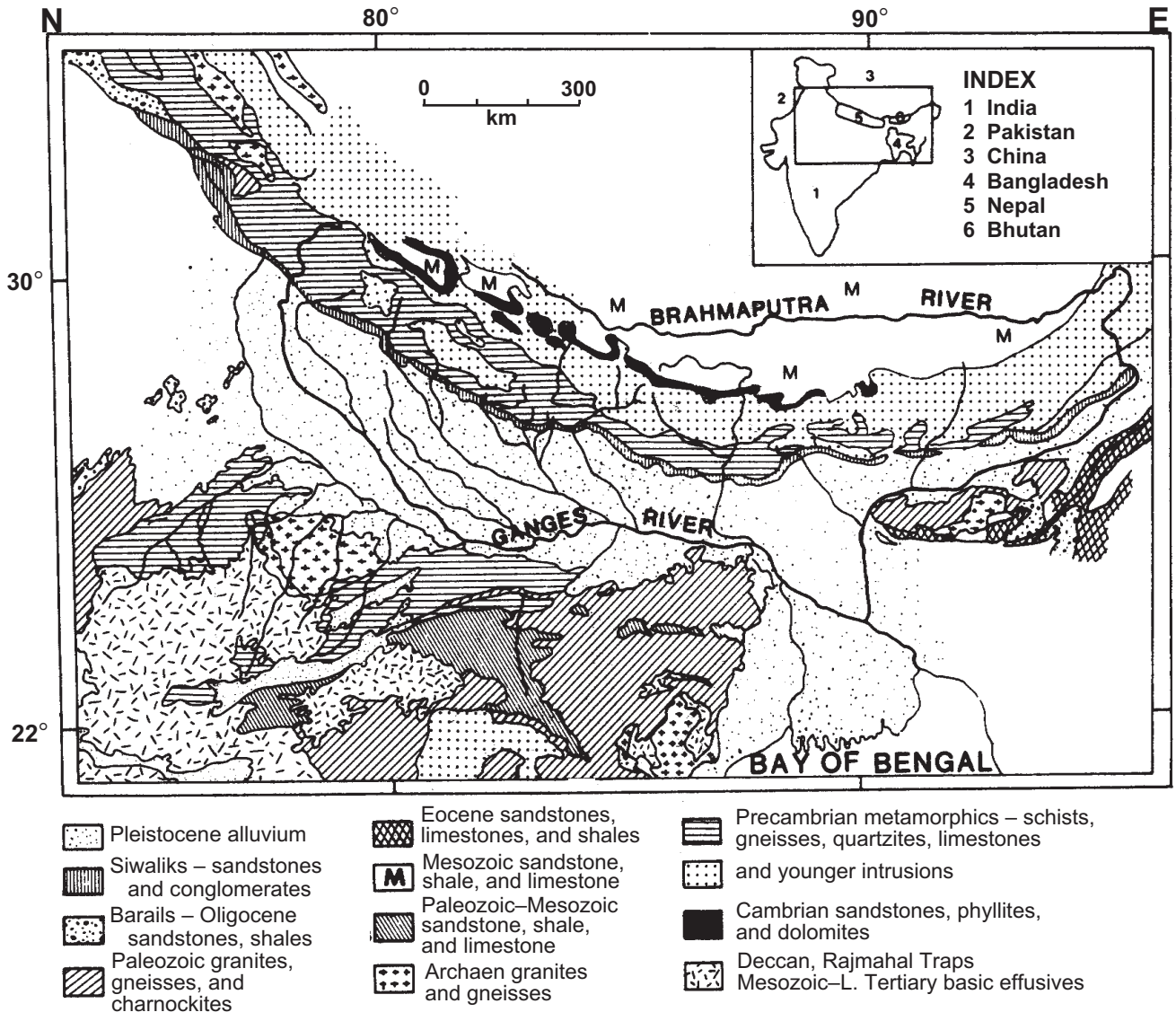

FIG. 2.—Map showing geology of drainage basins for the Ganges and Brahmaputra Rivers. The contrasting geology for the two rivers results in diagnostic mineralogical differences. The Ganges shows a lower epidote/garnet ratio (0.5) than the Brahmaputra (> 1) in the fine sand fraction. For the clay fraction, Brahmaputra sediment is characterized by higher relative abundances of illite (63% vs. 41%), kaolinite (29% vs. 17%), and chlorite (2–3% vs. < 1%); whereas Ganges sediment contains significantly higher smectite (39% vs. 3%).

bottom water (Berner et al., 2003).

The flux of sediment particles in the northern Bay is also governed by the monsoon periodicity. Sediment-trap deployments reveal that most of the lithogenic material is deposited during the summer monsoon, with monthly peak values of 300 $mg\,m^{-2}\,d^{-1}$, whereas most of the biogenic (carbonate and opal) flux is related to the increased convective mixing by wind forcing (Unger et al., 2003).

Cyclones

The northern Indian Ocean and, particularly, the Bay of Bengal are frequently affected by tropical cyclones. The large waves and storm surge produced by these storms mobilize huge amounts of sediment on the shelf and especially on the shallow delta topset and delta front. Consequent flooding of the southern delta islands by this highly turbid water contributes to their vertical growth by sedimentation (Allison and Kepple, 2001). Although the storms have formed in this region in every month of the year because of the relatively warm surface ocean waters in the Bay of Bengal (above 27° C much of the time), they are rare in January–March. Cyclones typically form in the area between 8° and 15° N latitude, with peaks in activity in both the premonsoon (April–May) and post-monsoon (October–November) period, often forming as disturbances in the Intertropical Convergence Zone (ITCZ). Activity decreases during the monsoon when the ITCZ is over south Asia, but it can occur north of 15° N during this period coincident with southward ITCZ

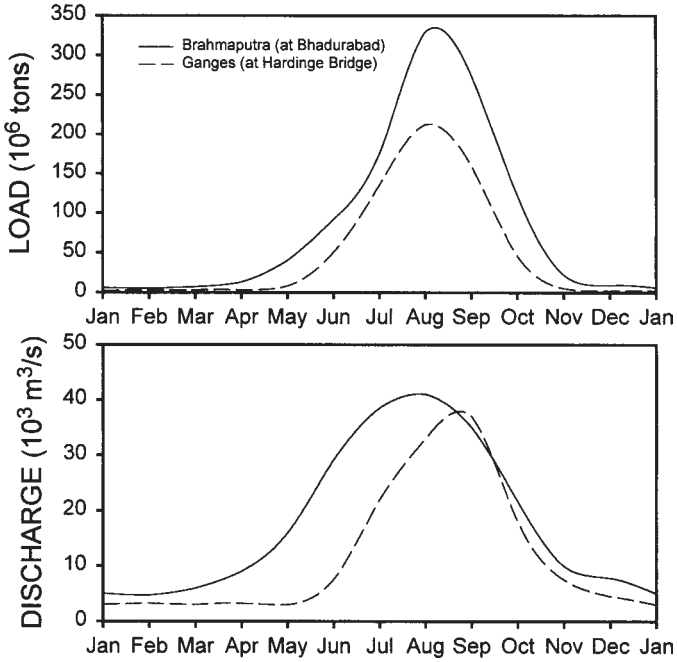

FIG. 3.—Water and suspended-sediment discharge for the Ganges and Brahmaputra Rivers. Water discharge represents monthly averages from 1969 to 1975. Suspended-sediment curves also represent monthly averages; from 1969 to 1970 for the Ganges, and from 1958 to 1962 for the Brahmaputra (from Barua et al., 1994).

migration. Analysis of cyclone frequency in the northern Indian Ocean from the 1870s to 1990s (Singh et al., 2000; Raghavan and Rajesh, 2003) suggests a slight decrease in activity over this period, with an average of almost 9 tropical cyclones per year. However, decadal variations in activity are observed (Kudrass et al., 1998).

Storm tracks of tropical cyclones in the Bay of Bengal between 1877 and 2001 were analyzed by Islam and Peterson (2003), who determined that 133 storms struck the coastline of Bangladesh over this period; 96 of these made landfall over the deltaic plain. Of these storms, 34 reached typhoon strength (> 119 km/hr). The most severe to make landfall on the deltaic plain was the November 1970 typhoon, which had measured peak winds of 222 km/hr and a storm surge of up to 6–10 m, resulting in an estimated 500,000 deaths in Bangladesh. Because the storm-surge-elevation was magnified by the timing of landfall with high tide, storm surge was recorded as far as 200 km inland over the low-elevation deltaic plain.

Coastal Morphology

The gently dipping basin surface continues offshore except along the Chittagong coast on the east side of the delta (Fig. 4), where the continental shelf is marked by a series of north–south trending structural ridges and troughs that mark the offshore extension of the Tripura Fold Belt. Kuehl et al. (1997) observed that these linear basins were floored with large sand waves, suggesting that local steering and intensification of tidal currents prevented the accumulation of fine-grained deltaic sediments. On the west side, opposite the India–Bangladesh border, the shelf surface is incised within 30 km of the shoreline by Swatch of No Ground Canyon, the lowstand course of the Ganges–Brahmaputra that is linked to the Bengal deep sea fan. Other than these features along the longitudinal boundaries of the delta, bathymetric relief on the inner-mid shelf is primarily the product of Ganges–Brahmaputra sedimentation since the Holocene deceleration of sea-level rise. A series of subaqueous shoals extend to about 8 m water depth seaward of the peninsulas and islands that separate the distributary channels (active and inactive) across the entire delta front. These shoals coalesce offshore into a topset platform that forms the inner section of a clinoform (topset–foreset–bottomset) deposit that is actively prograding seaward on the mid-shelf.

ENVIRONMENTS

Upper Delta Plain and Flood Basins

The upper delta plain (UDP) comprises about half of the Ganges–Brahmaputra delta system, extending 200 km landward of the salinity-influenced lower delta plain. This large area is dominated by fluvial processes that are overprinted by downstream coastal evolution and sea-level change. The landward boundary of the UDP is defined by the initiation of distributary development along the Ganges and by a point of frequent channel avulsion along the Brahmaputra (Fig. 5). The adjacent deltaic floodplains are clearly defined along their upland border by outcropping Tertiary uplands, and the downstream edge of the UDP is defined here by the inland dry-season extent of saline water, typically encompassing land > 3 m above sea level.

Physiography.—

In the UDP, several major environments reflect interactions between the fluvial systems and intrabasin tectonics. Among the prominent features of the area are the Barind Tract and the Madhupur Terrace, broad, fluvially dissected surfaces that are composed of much older alluvial deposits (Fig. 6). These elevated deposits are not flooded during the high-water season. Noted as early as the Nineteenth Century (Fergusson, 1863) and first described in detail by Morgan and McIntire (1959), these features have been found to exhibit a strong control on recent river courses, floodwater and sediment distribution, and Holocene delta development (Goodbred et al., 2003). The origin of these elevated sedimentary blocks has traditionally been ascribed to tectonic uplift (Morgan and McIntire, 1959) on the basis of apparent bounding faults, and this interpretation has remained prominent in the literature despite limited evidence. More recent field investigations have noted that previously interpreted fault boundaries may be more consistent with fluvial erosion (R. Caputo, personal communication), raising the possibility that these are geomorphic features (e.g., perhaps former highstand remnants), although a tectonic origin is not precluded. Furthermore, speculated ages for the Barind Tract and the Madhupur Terrace range widely from Holocene to Plio-Pleistocene. Single, unpublished surface exposure dates from each site, though, suggest an age range on the order of 70–130 ka (J. Whitney, personal communication).

The UDP is also influenced by "terraces" younger and less pronounced than the well-developed Barind Tract and Madhupur Terrace. These younger features include the Chandina and Comilla surfaces (Fig. 1), whose slightly incised drainage network, limited flooding, and unweathered sediments suggest moderate uplift of historical age (Coates et al., 1988; Coates, 1990). Both of these surfaces lie along the old Brahmaputra river course, which was abandoned after the late 1700s (Ascoli, 1912), and it is not unlikely

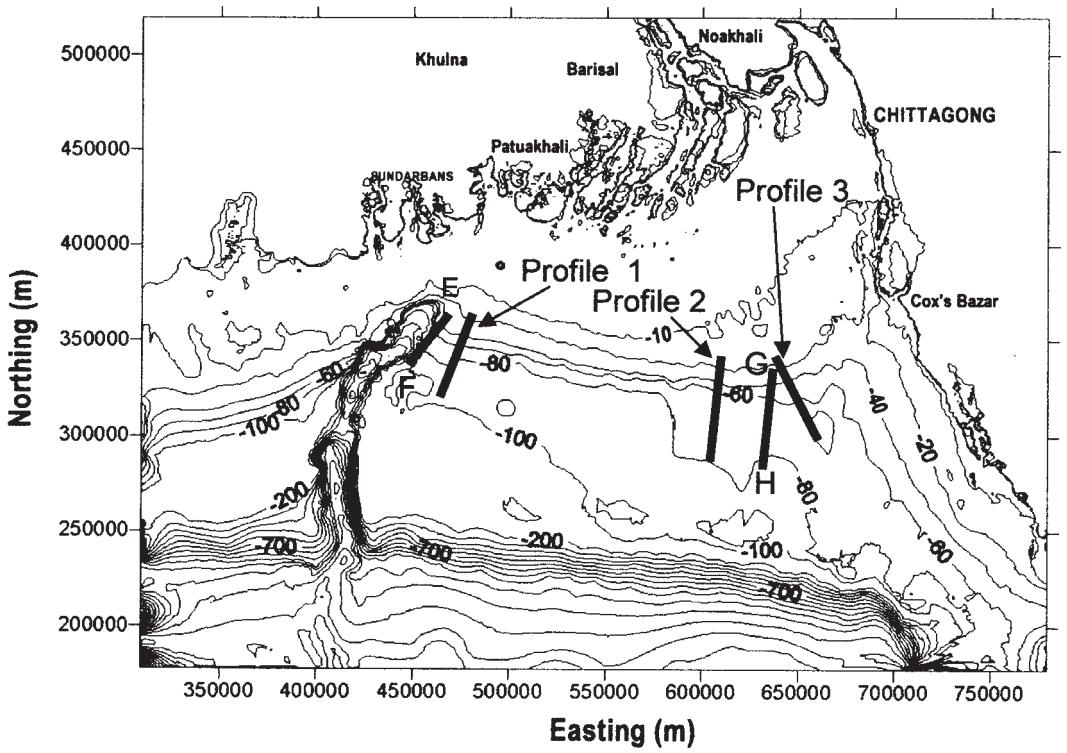

FIG. 4.—Bathymetric chart of the shelf and upper slope of the Ganges–Brahmaputra Delta (contours in meters). Transects are shown for boomer and 3.5 kHz reflection profiles (Figs. 11 and 13). The shelf clinoform morphology (subaqueous delta) can be clearly seen as inner shelf topsets grade into more steeply dipping foresets on the mid-shelf. A major feature of this shelf is the giant submarine canyon (Swatch of No Ground), which indents the shelf to the 20 m isobath on the western side of the Delta. This canyon currently acts as a conduit for the off-shelf transport of about 30% of the present river sediment discharge.

that these features and events are related, but formal studies are needed to test this assertion. Furthermore, the apparently young ages (< 10^3 yr) of the Chandina and Comilla surfaces and their elevation above major flooding imply a tectonic origin rather than being purely morphological features. Regardless of the absolute age and origin of elevated surfaces in the Bengal Basin, they clearly serve to partition the UDP into discrete sub-basins between which there is limited exchange of sediment and which, in many cases, contain distinct stratigraphy. These sub-basins can be divided into two major types, (1) relatively narrow alluvial corridors ("valley plains") and (2) broad, low-lying flood basins.

At present, and historically, the upper reaches of both the Ganges and Brahmaputra rivers flow 50–100 km through relatively narrow (40–80 km) corridors between adjacent uplands or terraces (Fig. 5). The corridors are situated mainly between the Tertiary uplands that bound the Bengal Basin and the intrabasinal highs discussed above. Within these restricted alluvial pathways, the occupying channel braidbelts are 5–15 km wide (i.e., up to 30% of the corridor width) and thus dominate sedimentation patterns (Goodbred et al., 2003). The river-channel braidbelts deposit almost solely sand-size sediments (Coleman, 1969), but overbank flooding also distributes fine-grained sediments across half of the alluvial corridors at any given time (Allison et al., 1998). At longer timescales (> 10^2 yr), however, most fine-grained floodplain deposits are removed by channel avulsion and braidbelt migration, leading to a predominance of clean channel sands in the subsurface stratigraphy (Fig. 7). This reworking process is presumably enhanced by the restricted space for channel migration within corridors. Despite this apparently limited accommodation space, the corridors are not merely throughputs for riverine sediment. In fact, channel aggradation and floodplain accretion sequester an appreciable portion of the fluvial load. Judging by ^{210}Pb- and ^{137}Cs-derived accretion rates, the Brahmaputra braidbelt traps > 50 x 10^9 kg y^{-1} of primarily coarse-grained sediment at rates > 10 mm y^{-1}, with the another 30 x 10^9 kg y^{-1} of fine material deposited on the adjacent floodplains at rates of 1–3 mm y^{-1} (Allison et al., 1998; Goodbred and Kuehl, 1998).

Major floodbasins also characterize large portions of the UDP, with the most prominent feature being the Sylhet basin. This broad depression covers about 10,000 km^2 in the northeast delta (Fig. 1). It is bordered by the Indo-Burman foldbelt, and the Madhupur Terrace to the east and west, respectively, and is bound by the Dauki Fault and Shillong Massif (cratonic fragment) to the north. Owing to north–south compression since at least the Pliocene, the Sylhet basin has supported long-term subsidence rates of 1–4 mm y^{-1} (Johnson and Alam, 1991; Goodbred and Kuehl, 2000a). This continuous generation of accommodation has favored the deposition and preservation of fine-grained sediments, which constitute 50% or more of the stratigraphic sequence (Goodbred et al., 2003). During the Holocene, the main trunk of the Brahmaputra River has periodically flowed through the Sylhet Basin, with major avulsions occurring at periods less than a few thousand years. Stratigraphy also suggests that its course at these times was restricted to the western part of the basin, near its pre–Twentieth Century channel (Fig. 1). Recent sedimentation rates in the Sylhet are 2–5 mm y^{-1}, thereby accounting for about 75 x 10^9 kg y^{-1} of the Brahmaputra load that is sequestered to this large basin (Goodbred and Kuehl, 1998).

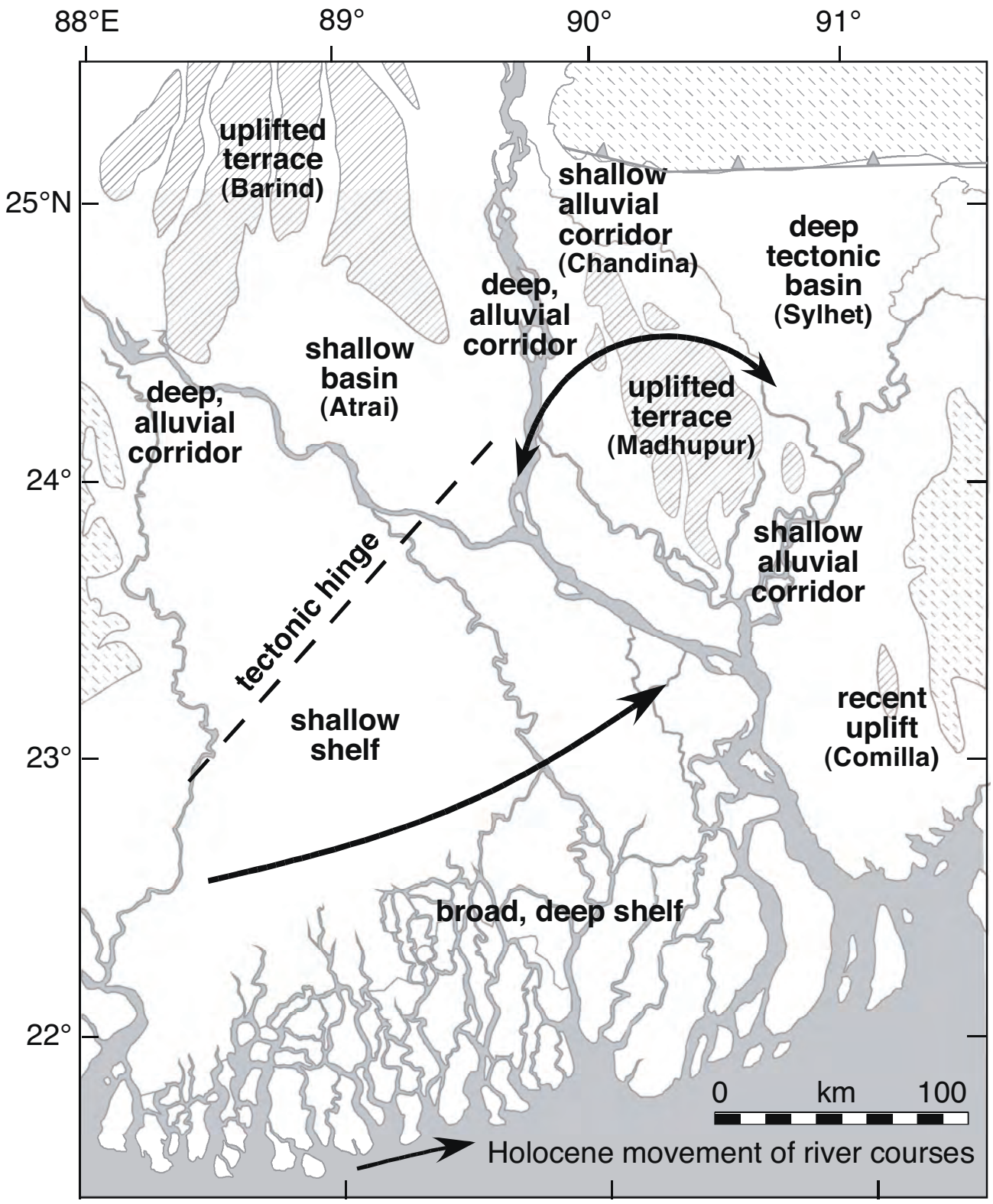

FIG. 5.—Map of tectonomorphic features and controls on the Ganges–Brahmaputra rivers and delta system. Note that areas of uplift serve to partition the delta into numerous sub-basins that each have characteristics salient to the nature of sedimentation and stratigraphic preservation (Goodbred et al., 2003). The large arrows show general Holocene pathways for the major river channels. The Ganges course is characterized by a stepwise eastward migration during the Holocene, whereas the Brahmaputra has largely occupied either its present or recent courses, switching on the order of every one thousand to two thousand years.

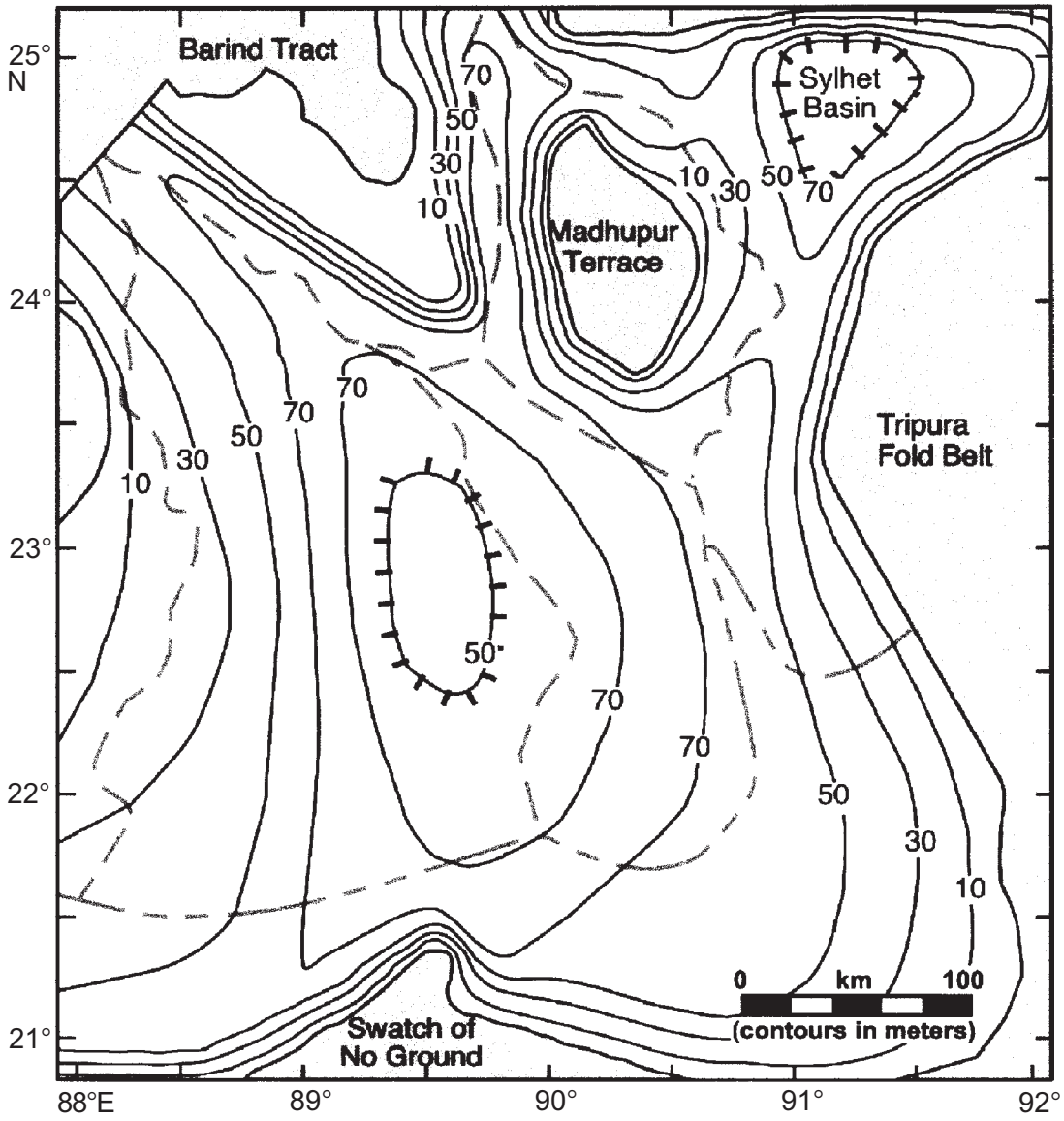

FIG. 6.—Isopach map of Ganges–Brahmaputra fluviodeltaic sediments, including subaerial and subaqueous deposits, deposited from ~ 12,000 yr BP to present. Representative cross sections of delta stratigraphy are shown in Figure 7. The dashed gray lines represent the modern river channels and shoreline. Total volume stored in the delta is about 8.5 x 10^{12} m^3, nearly 60% of which was deposited under the strengthened monsoon and increased river discharge of the early Holocene. Thickest sequences are in the alluvial lowstand valleys and in the subsiding Sylhet Basin. Representative cross sections of delta stratigraphy are shown in Figure 7. The dashed gray lines represent the modern river channels and shoreline.

The other major floodbasin in the delta is the Atrai basin (~ 1500 km^2), which is situated upstream of the Ganges and Brahmaputra confluence (Fig. 1). Unlike the Sylhet, the Atrai is not tectonically controlled but rather is a function of poor drainage caused by both natural and artificially raised levees along the major river channels. Holocene sediments in the basin are comparatively thin (< 10 m) and overlie Barind Tract sediments, which dip shallowly south of their surface exposure. What the Sylhet and Atrai basins have in common are extended periods (up to 6 months) of annual flooding that is 2–6 m deep. Such conditions favor the trapping of fine-grained sediments, which dominate the stratigraphy in both areas (Goodbred and Kuehl, 2000a).

Stratigraphy.—

At a general scale, shallow stratigraphic sequences within the UDP are relatively simple and comprise only a few sedimentary facies. As might be expected, the most common stratigraphy is a fining-up sequence where fine-grained floodplain sediments overlie sandy channel deposits. In these settings, the capping mud unit is typically 0.5–3 m thick and silt dominated, with predominantly oxidized conditions and rapid soil development (Brammer, 1996). Iron-carbonate (mainly Ganges floodplain) and iron-oxide concretions and root casts are not uncommon, and bioturbation by plants and burrowing is also rapid relative to accretion (Goodbred, 1999). These characteristics

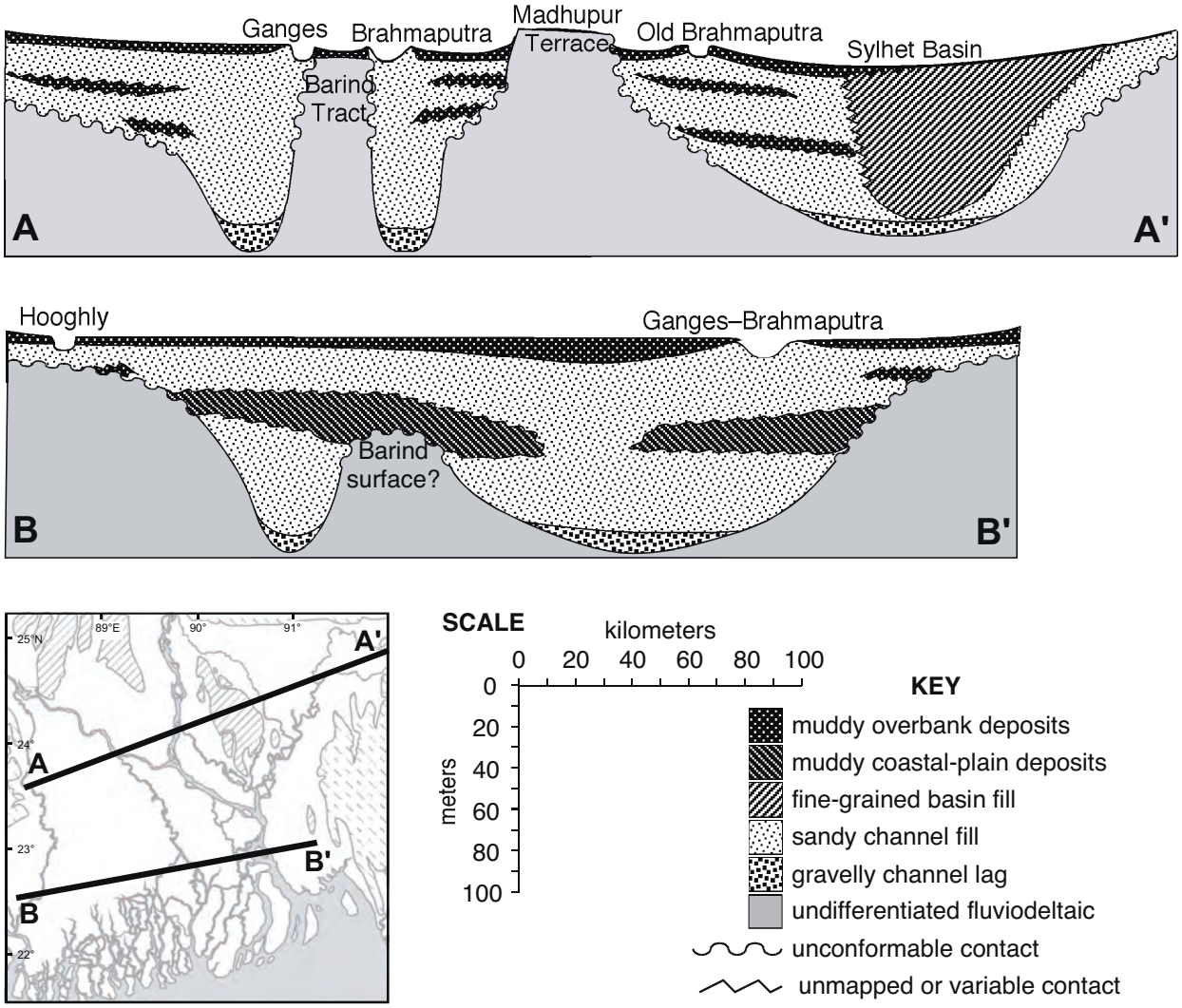

FIG. 7.—Generalized cross sections of the Bengal Basin showing typical distribution of coarse- and fine-grained postglacial fluviodeltaic deposits. Muddy floodplain deposits are not well preserved and tend to be highly localized within the stratigraphy, which is dominated by course silts and fine sands. Important exceptions to the coarse-grained stratigraphy are the tectonically subsiding Sylhet Basin and also the coastal plain, where a thick muddy mangrove facies reflects initial delta formation in the early Holocene.

typify the "floodplain soil" facies, which is the most common and widespread unit in the shallow stratigraphy of the UDP. Interestingly, this thin facies is rare in the subsurface, where preserved mud units are relatively local and almost always < 5 m thick. Presumably the surface soil facies is almost wholly removed by channel migration and avulsions on timescales > 1,000 yr (Goodbred et al., 2003). A related fine-grained facies can be found in local depressions called *bils*. The origin of bils is not well known, but they are apparently small interfluvial basins or channel-abandonment features. In the bils, mud deposits tend to be more clay rich than the adjacent floodplain soils and may reach 7 m thick. The sediments are more reducing under permanently flooded conditions, and concretions are generally absent. Bils are also the only sites in the UDP where organic-rich deposits are found. Even there they are relatively uncommon, forming discrete layers (5–20 cm thick) with combustible-carbon values < 30% dry wt. It is worth noting that organic content in all other settings of the UDP is < 2% dry wt. However, like the thin floodplain soils these bil deposits do not appear to be well preserved in the stratigraphy.

More significant in the overall stratigraphy are "floodbasin muds" of the Sylhet Basin. Here, continuous mud sequences are tens of meters thick and in places reach 80 m of fine-grained Holocene deposits (Figs. 6, 7). Unlike the thin floodplain soils, these deposits accumulate more rapidly because of tectonic subsidence and are thus better preserved (Goodbred et al., 2003), although their organic content remains low (< 2% dry wt). The sediments of the floodbasins are silt-dominated, similar to most of the Ganges–Brahmaputra surficial deposits. In the modern floodbasin deposits, sedimentary structure is limited and soil development is fairly rapid (Brammer, 1996; Goodbred, 1999). However, deposits of the early Holocene during rapid sea-level rise are likely to have more primary structure preserved. Overall, the Sylhet basin is a major repository for fine-grained sediments

transported by the Brahmaputra at multiple timescales from modern to the Pliocene.

In most of the UDP outside of Sylhet Basin, sandy deposits ubiquitously constitute the shallow stratigraphy from ~ 3 m to > 20 m deep. These coarse deposits are generally clean, relatively unweathered, fine to very fine sands with several percent heavy minerals (Heroy et al., 2003). Primary structure in the form of cross-stratification and planar beds are abundant and defined by micaceous and heavy-mineral layers at scales of millimeters to decimeters (Coleman, 1969; Bristow, 1993). Although detailed facies analyses have not been made outside of the modern river channel, limited trenches and pits in the floodplain suggest that underlying sand facies reflect channel deposits and bar complexes rather than splays or other fluvial subenvironments.

Lower Delta Plain and Delta Front

The lower delta plain (LDP) of the Ganges–Brahmaputra, defined here as the subaerial delta inland to the limit of saline penetration during periods of low river discharge, is a zone up to 100 km wide that increases only minimally in elevation inland (elevations are typically < 3 m above mean sea level at the northern limit of salt-water intrusion). Early colonial records from the Seventeenth and Eighteenth Centuries suggest that most of the LDP in Bangladesh and the adjacent Indian state of West Bengal was mangrove forest, but today reclamation for agriculture and logging have reduced the mangrove swamp to 5,993 km^2, primarily in Sunderbans National Park. In the Sunderbans, distributary channels associated with relict courses of the Ganges River subdivide the region into a series of north–south oriented, elongate peninsulas, which are dissected, in turn, by smaller anastomosing tidal channels. Farther east on the Kuakata peninsula, earthen coastal embankments (e.g., polders) created for cyclone protection and agricultural development have eliminated most of the smaller tidal channels that subdivide the peninsulas into islands. In the active distributaries of the Ganges–Brahmaputra that form the Meghna estuary, much of the island and peninsula land areas came under cultivation in the late Twentieth Century, or are used for tree (mangrove) farms.

The modern sediment character of the LDP is outlined in Allison et al. (2003). Surface sediments are generally silts to clayey silts (mode 6.5–7.5 ϕ) with < 5% sand. Clay content is slightly higher in the western LDP relative to the Meghna estuary. Total organic carbon content (TOC) is generally low, ranging from 0.05 to 1.1% except in the upper ~ 10 cm of sediments containing leaf litter in mangrove-vegetated areas. Clay mineralogy is mainly illite (40–65%), with lesser amounts of smectite, kaolinite, and chlorite. The upper 2 m of the LDP sediment column is predominantly two sedimentary facies: mottled mud in the Sunderbans and established agricultural areas in Kuakata, and interbedded mud in the Meghna estuary region. Interbedded mud also underlies the Mottled mud at 2–3 m depth in the Sunderbans. The only other observed facies in surficial sediments (peaty mud) is found in clay-rich peat basins immediately landward of the LDP. These basins are the product of internal drainage and standing-water conditions produced in areas between relict Ganges distributaries (Brammer, 1996; Goodbred, 1999).

Mottled mud is formed by partial homogenization of primary sedimentary structures by rooting, burrowing, or agricultural disturbance (Figs. 8A, 9). Mangrove areas often show overprinting by root structures and faint, laterally discontinuous centimeter-scale interbeds of silt-rich and silt-poor beds and laminae. Interbedded mud consists of millimeter- to centimeter-scale silt laminae separated by clayey silts (Figs. 8B, 9). Laminations often exhibit cyclicities in the thickness of clay–silt couplets that is characteristic of tidalites. Allison and Kepple (2001) have shown with ^{137}Cs geochronology that the LDP surface is accumulating sediment today at rates of up to 1.1 cm y^{-1}, with a trend of decreasing accumulation with increasing distance inland from the Bay of Bengal. They determined that this sediment is likely Ganges–Brahmaputra suspended sediment being advected alongshore by the westward-flowing coastal current (Barua et al., 1994) and transported inland during coastal setup events that inundate the LDP. Coastal setup is produced seasonally by the southwest monsoon, and episodically by cyclonic storms tracking north in the Bay of Bengal. The layers found in the interbedded mud facies are produced by this cyclic or episodic sediment flux, and preserved in surface LDP sediments in the Meghna estuary region by limited agricultural disturbance.

Historical and satellite-era remote-sensing studies (Martin and Hart, 1997; Allison, 1998a) have shown that the Meghna estuary region has been experiencing shoreline accretion at rates of 5.5–16 km^2/yr over the past several centuries. Accretion is mainly a process of seaward extension of interdistributary islands, coupled with a welding of individual islands farther up the estuary into peninsulas by silting up of tidal channels separating islands. The seaward faces of interdistributary islands have digitate subaqueous shoals that extend up to 80 km offshore and merge into a broad, lobate apron at 6–8 m water depth. These shoals have accreted seaward as much as 50 km since 1840 (Allison, 1998a). The term *delta front* is used here to refer to shallow-water deposits immediately off the river-mouth region where coarse-grained sediments are primarily deposited. The Ganges–Brahmaputra subaerial delta is advancing along a delta front 150 km wide that is punctuated alongshore by ebb- and flood-dominated channels and shoals extending from interdistributary islands (Fig. 1). The lobate apron merges offshore at about 10–15 m water depth with the lower-gradient topset beds of the subaqueous clinoform. The subaqueous delta-front deposits are not well sampled, but seismic transects from Kuehl et al. (1997) suggest that the highly reflective surface (limited seismic penetration) is characteristic of sands, covered by ephemeral silty layers (Kuehl et al., 1989). Meghna estuary islands show a fining-upward sequence with cross-bedded, muddy sands at depth (5–6 m), equivalent to shoal deposits, buried by the shoal-island complex consisting of interbedded mud and sand (Allison et al., 2003). West of the active river mouths opposite the Sunderbans, relict distributary shoals are found on the innermost shelf. Sea-facing shorelines have eroded as much as 3–4 km since 1792 (Allison, 1998b).

Sediment cores collected from the LDP on the Kuakata peninsula and in the Sunderbans show the same (~ 7 m thick) fining-upward stratigraphic transition from subtidal shoal to intertidal shoal to supratidal flat (seasonally flooded mangrove) as is observed in the modern prograding shoal-island complexes in the Meghna estuary (Allison et al., 2003). Borehole data from the LDP (Goodbred and Kuehl, 2000a) indicates that this progradational sequence lies directly on an early Holocene transgressive shelf sand. Several studies (Banerjee and Sen, 1988; Umitsu, 1993; Goodbred and Kuehl, 2000a) have shown that the entire modern LDP is seaward of the maximum sea-level transgression, and hence began prograding after about 5,000–6,000 yr BP. Limited radiocarbon data from the LDP sequence (summarized in Allison et al., 2003) suggest that the LDP accreted in a west-to-east pattern beginning about 5,000 yr BP in the Indian Sunderbans. The eastward shift of distributaries was related to the Ganges: the Brahmaputra was infilling shallow inland areas north and south of the Madhupur uplands. Radiocarbon and clay-mineral evidence (Heroy et al., 2003; Allison et al., 2003) suggests that the Sunderbans and Kuakata LDP deposits were created by the

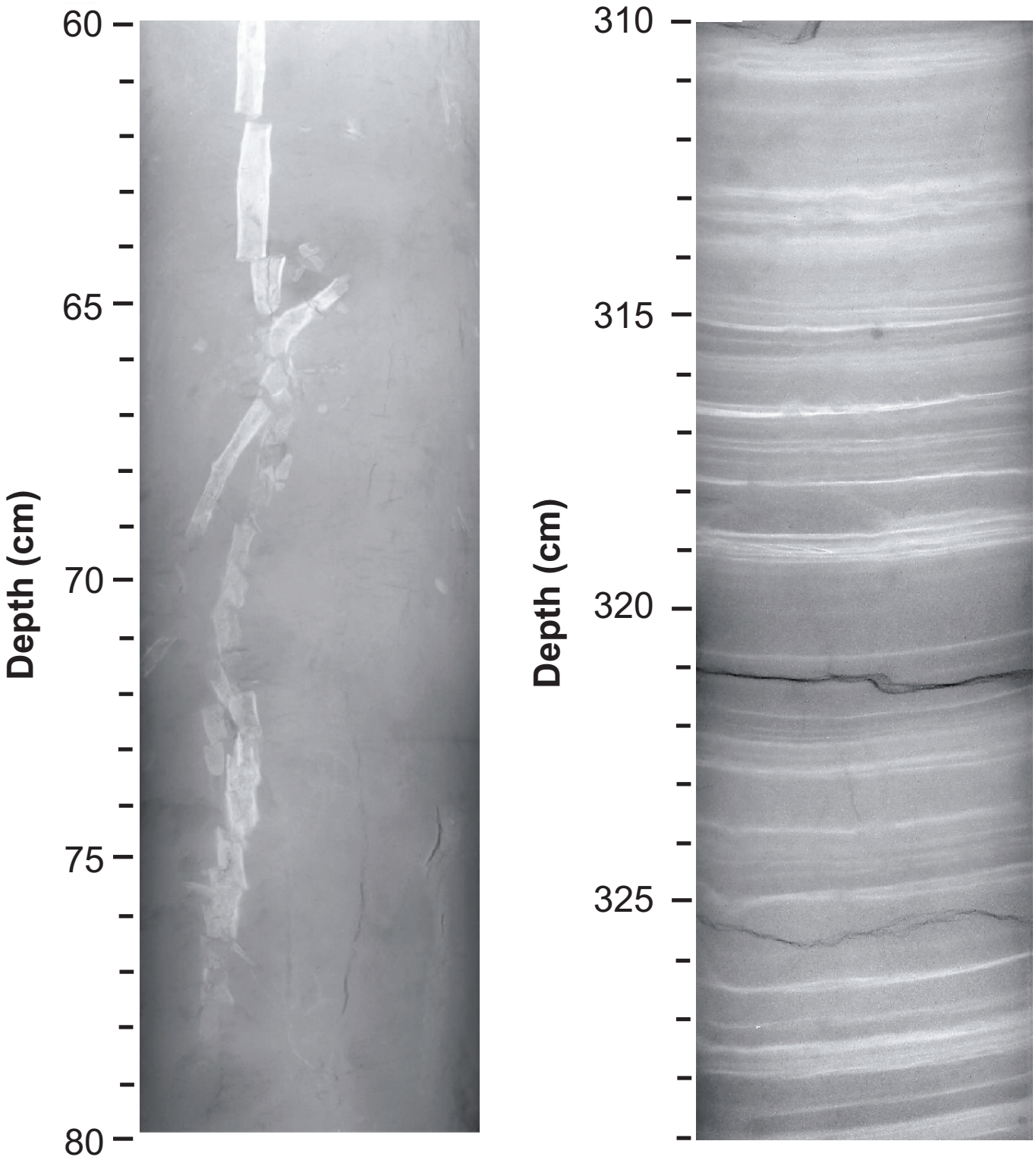

FIG. 8.—X-radiography positives from vibracores of typical facies in the delta plain. **A)** Except near active, major river channels, the delta plain is nearly everywhere capped by 1–3 m of muddy overbank deposits that are well mixed, showing little to no primary sediment structure. Weathering in these deposits has advanced to various states, forming soils with Fe-rich roots casts (shown) and concretions (not shown) that are most commonly siderite, rarely pyrite. **B)** Below the muddy surficial floodplain deposits are thick sequences (5–30 m) of muddy sand to sand deposits reflecting higher-energy fluvial or fluviotidal deposition. Shown is a typical tidalite sequence from the lower delta plain with alternating silt and sand layers tuned to fortnightly tidal cycles. In the upper delta plain, tidalites are replaced by clean, cross-bedded sands deposited in fluvially dominated settings.

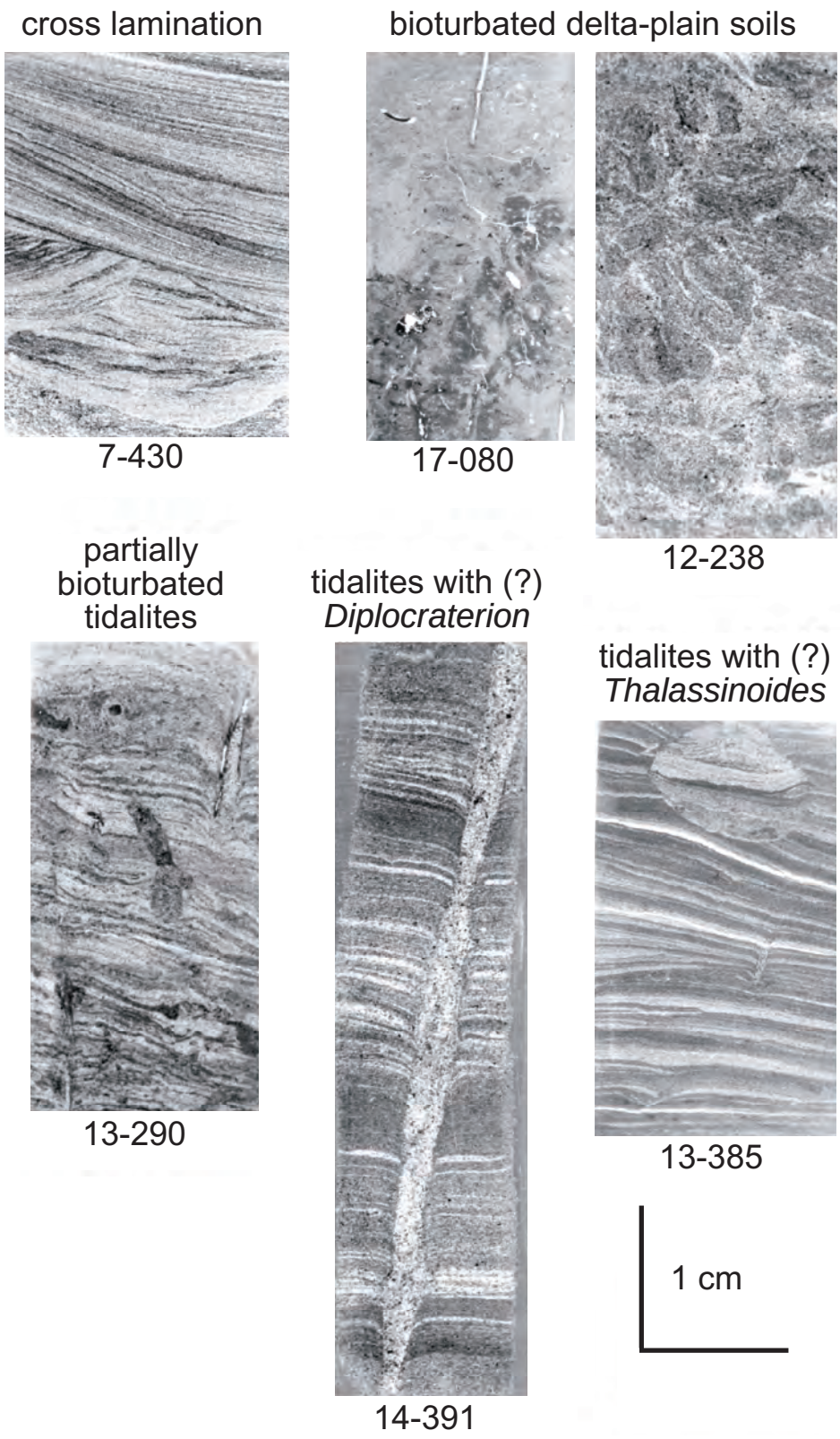

FIG. 9.—Petrographic thin sections showing fine-scale bedding and mixing in various settings of the delta plain (lower label, #-##, indicates core number followed by depth in centimeters). Note that sections < 3 m deep show the most mixing, reflecting soil development under upward-fining, reduced-sedimentation conditions. Section 7-430 shows the typical sandy, cross-bedded deposits that dominate upper-delta-plain facies below the capping floodplain muds. In the tidal deposits millimeter-scale beds appear to be deposited on each tidal cycle, with observable fortnightly spring–neap changes.

Ganges, and only in the last several hundred years has combined Ganges–Brahmaputra delta-front progradation been occurring in the Meghna estuary region.

Subaqueous Delta

The existence of an accretionary subaqueous delta on the Bengal shelf was first suggested by Kuehl et al. (1989) and later confirmed by Kuehl et al. (1997) and Michels et al. (1998) (Fig. 10). Topset beds extend seaward from the delta front to water depths of about 30 m, judging by the subtle change in seabed surface gradients observed in high-resolution seismic profiling (e.g., Fig. 11). Gradients increase from < 0.1° in the topset region to values ranging from 0.20° to 0.27° in the foreset region. The transition to bottomset beds occurs at depths ranging from 80 m for the western shelf, shoaling to 60 m for the eastern shelf, with bottomset gradients of < 0.1°. Consistent with other accretionary subaqueous deltas and with their sigmoidal geometry, maximum accumulations rates occur in the foreset region (5–9 cm y^{-1} based on ^{210}Pb, ^{14}C, and ^{32}Si geochronologies), with dramatically lower rates << 1 cm y^{-1} in topset and bottomset regions.

Volumetric and mass estimates of the subaqueous delta from boomer records indicate that the subaqueous delta contains about 30% of present river sediment discharge, extrapolated to about 10 ka (Kuehl et al., 1997). This estimate is also consistent with contemporary sedimentation rates and a budget determined by high-resolution seismic profiles and core samples dated by ^{210}Pb, ^{137}Cs, ^{14}C, and ^{32}Si, which reveal accumulation in the clinoform of 20% (Michels et al., 1998) to 30% (Suckow et al., 2001) of the estimated annual sediment load of the Ganges and Brahmaputra (10^{12} kg y^{-1}). The clinoform progrades seaward about 20 m y^{-1} across the Late Pleistocene deltaic floodplain surface presently exposed on the outer shelf.

Topset Beds.—

Although seabed surface texture of the topset region ranges from fine sand to clay, field data and acoustic observations suggest that this area is composed mainly of sand and silt. High-resolution acoustic studies using Parasound (3.5 kHz) show a strong bottom reflector with virtually no sub-bottom penetration (Michels et al., 1998). Multi-frequency (boomer) studies show limited sub-bottom penetration (15 m maximum) with strong reflectors just beneath the surface, consistent with the inferred coarse texture (Kuehl et al., 1997). This interpretation is also supported by seven vibracores (up to 3 m length) collected at the seaward edge of the topset region. Sediment texture in these cores is highly variable, but average sand:silt:clay is ~ 4:3:3. Cores reveal fining-upward beds (up to 70 cm thick) of fine to very fine, micaceous sand. Lacquer peels from these sands (Fig. 12) reveal thin lamination throughout. The bases of these units sometimes are marked by centimeter-size clay balls, and occasionally shells. The absence of bioturbation suggests rapid deposition and physical reworking, perhaps induced by frequent cyclone-generated waves and currents (Kuehl et al., 1991; Segall and Kuehl, 1994). A veneer of muddy sediment is observed from gravity cores from some locations, apparently indicating the presence of ephemeral mud deposits. Deep-water wave hindcasting using gale-force winds (average seven occurrences per year) yield near-bed orbital velocities that exceed the critical threshold of bottom sediments by an order of magnitude (Barua et al., 1994).

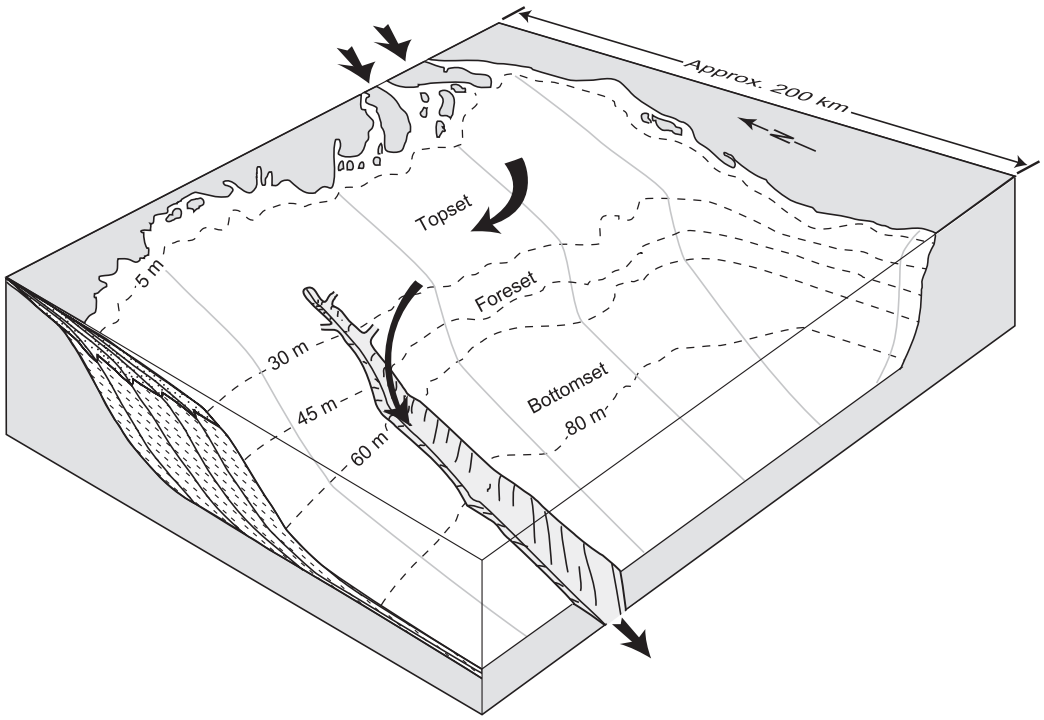

FIG. 10.—Cartoon showing the general morphology and inferred sediment transport pathways for the Ganges–Brahmaputra subaqueous delta. Currently, the major input to the shelf is from the eastern distributaries. The delta foresets are advancing seaward across the mid-shelf region at about 50 m/yr. A significant fraction (about 30%) of the rivers discharge is trapped within the canyon, which is episodically evacuated, presumably by turbidity currents which feed the Bengal Fan.

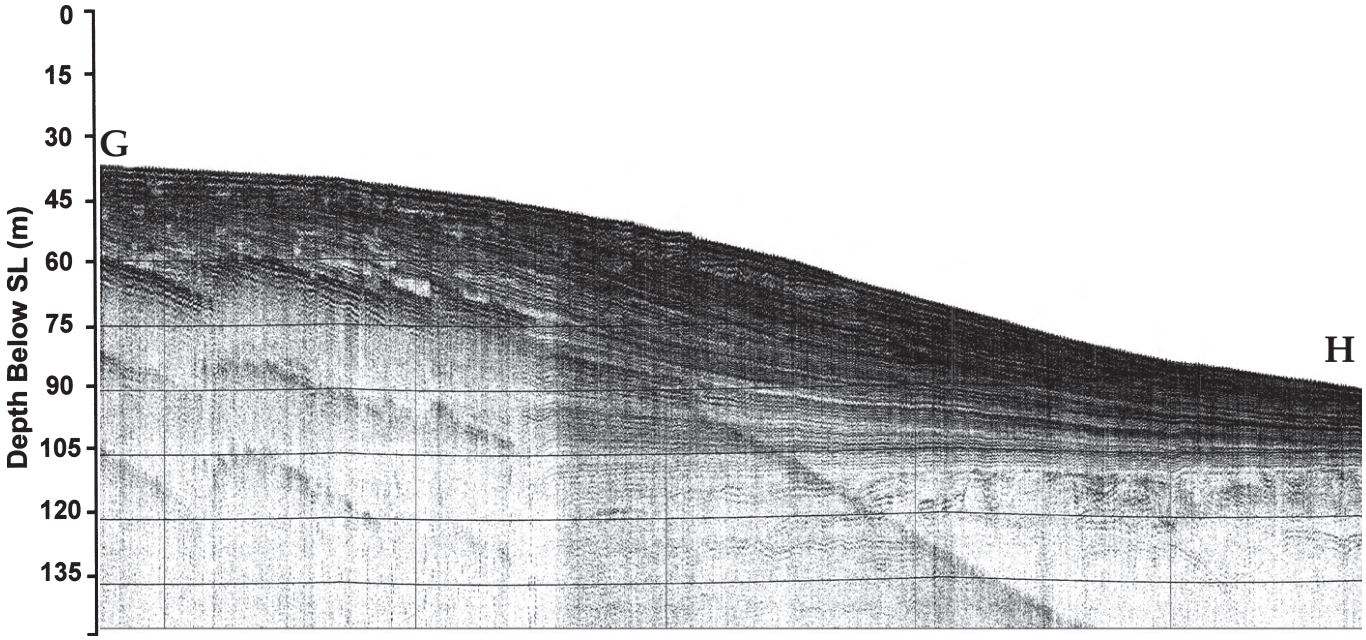

FIG. 11.—High-resolution (Boomer) profile from the Ganges–Brahmaputra subaqueous delta (see Fig. 3 for location). The sand and mud clinoform overlies the transgressive surface characterized by truncated bedding and channel-fill features.

Foreset Beds.—

Sea-bed texture fines seaward to a sandy mud in the foreset region (sand:silt:clay ~ 1:7:2), and the resulting increase in acoustic penetration reveals that the Pleistocene units underlying the clinoform are often erosionally truncated, with abundant cut-and-fill features characteristic of former channels active at the last glacial maximum (LGM). Within the foreset clinoform deposits, closely spaced, nearly parallel reflectors diverge from the topset to the mid-foreset region and converge farther seaward towards the bottomset region. Acoustically transparent beds are a common feature of the foreset region, covering an area of a few kilometers to tens of kilometers along and across the region, with a typical thickness of about 5 m. Parasound records demonstrate an increase in abundance of the transparent beds in the study area from west to east, with the vertical stacking of as many as five such layers for the eastern profiles (Fig. 13) (Michels et al,. 1998).

Compared to the topset beds, the proportion of sand and silt significantly decreases with increasing water depth. Most of the still numerous distinct sand and silt layers have sharp basal contacts, and fine upward. The upper mud sections are frequently bioturbated and may contain some thin-shelled mollusc shells and centimeter-size echinoid sand dollars. More than 50% of the foreset beds consist of these graded units, indicating that most accumulation in the foreset bed happens during discrete rapid-accumulation events and that the more continuous supply of sediment is relatively small. Storms and tropical cyclones, which dominate the sediment transport into the Swatch of No Ground (see below), have most probably also deposited the graded sequences of the foreset beds. However, the much smaller number of graded beds per time unit (< 0.5 graded beds y^{-1}) compared to the Swatch of No Ground tempestites (3 graded beds y^{-1}), is an indicator of nondeposition or even erosion along the foreset beds (Michels et al., 1998).

At the transition from foreset to bottomset beds, acoustically transparent beds form 1-km-wide lobes, occasionally displaying a terrace-like morphology. Vibracores collected from transparent and adjacent stratified beds reveal distinctly different characteristics. Stratigraphic and grain-size analyses (Fig. 14A) indicate that the acoustically transparent beds are unsorted and homogeneous. Thin-section photomicrographs reveal distinctive and contrasting structure from stratified and homogeneous beds (Fig. 14B), consistent with field observations. From the above evidence, we conclude that the acoustically transparent beds represent large-scale sediment gravity flows. Although the exact nature of these flows is unknown, the available data suggest that flow densities are moderately high, enough to prohibit the development of graded beds, but low enough that turbulent mixing can effectively homogenize the sea bed. The increasing frequency of transparent beds toward the river mouth is accompanied by a progressive decrease in foreset slope, from 0.27° to about 0.20°. Presumably, the increasing incidence of sediment gravity flows in the east causes a reequilibration of foreset slope, resulting in the lower observed gradient.

Because of the influence of strong cyclones in the Bay of Bengal, it is tempting to speculate that large wind-driven waves could trigger mass movement in the foreset region. However, major cyclones influence the area about once a year, whereas only about four distinct gravity flows have been observed in the past 250 years (Michels et al., 1998). Thus, although cyclones cannot be ruled out as a possible trigger, other factors should be considered. As another possibility, tectonic activity along the boundary between the Indian and Burmese plates creates strong earthquakes. For example, five quakes between magnitude 4.6 and 6.5 have occurred since 1955. Therefore, high rates of sedimentation, leading to pore pressurization, coupled with earthquake and/or cyclone activity, are the primary suspects in triggering sediment gravity flows in the foreset region of the Ganges–Brahmaputra subaqueous delta.

FIG. 12.—Lacquer peel from the sandy topset region showing thin lamination throughout.

Bottomset Beds and Outer Shelf.—

Extending from the toe of the foresets seaward to water depths of about 100 m, bottomset clinoform beds display regular horizontal bedding overlying the transgressive surface. The thickness of the bottomset beds as a unit, and as individual layers, decreases rapidly seaward. Most of the acoustically transparent slump deposits end near the gradual change in slope marking the transition to the foreset beds. The extent of bottomset beds onto the shelf differs considerably with respect to water depth, from 75 m in eastern delta to 120 m in the western part. Measured sedimentation rates in the western sector, close to the Swatch of No Ground, are close to 0.2 cm y^{-1} (Suckow et al., 2001). Correspondingly, bioturbation is more effective, and only some thick sand–silt layers are preserved in the predominantly muddy sequence.

The outer shelf, from the toe of the bottomsets to the shelf break at 150 m, exhibits outcropping relict deposits containing oolitic beach ridges (Wiedicke et al., 1999) and possible lowstand deltaic sequences (Hübscher et al., 1998). The modern submarine delta with its clinoforms is prograding southward over this Late Pleistocene–early Holocene transgressive surface. The surficial deposits on the outer shelf are discontinuous layers of muddy sand palimpsest, consisting of reworked fluvial sand mixed with Holocene biogenic debris (Michels et al., 1998). In the seismic records, numerous cut-and-fill structures and a stacked sequence of seaward-propagating clinoforms indicate that the outer shelf is built from sea-level-lowstand deltas (Hübscher et al., 1998). During the LGM, the former coastline on the central Bengal shelf was formed by a set of oolitic beach ridges in present water depth of 120–130 m. The occurrence of these ooids as far west as the margins of Swatch of No Ground Canyon (Sengupta et al. 1992) is an indication that this section of coastline had at least seasonally clear water, a situation which contrasts markedly with the present conditions. Apparently most of the fluvial mud was trapped within the valley that today forms the shelf canyon and was transferred directly to the Bengal deep-sea fan (Weber et al., 1997). In addition, the reduced fluvial runoff at LGM (Kudrass et al., 1998) also may have reduced the supply of mud to the former coastline. The shelf break lies at relatively great water depths of approximately 150 m.

SWATCH OF NO GROUND (SoNG)

The most prominent feature on the Bengal shelf is the deeply incised Swatch of No Ground canyon (SoNG). The SoNG bisects the shelf and ends in an amphitheater at the 20 m isobath, within 30 km of the modern shoreline. The canyon directly intersects the prograding foreset beds of the submarine delta and then deepens to > 500 m within 50 km of the coast and to 1200 m by the shelf break. The canyon itself is 20–30 km wide, with steep walls (> 10°) on its eastern side and shallower slopes (~ 5°) on the western wall. Both of the walls of the canyon are dissected by gullies, which apparently constitute a network for sediment transport into the canyon (Kuehl et al., 1989; Kuehl et al., 1997; Kottke et al., 2003).

Sedimentation fundamentally differs between eastern and western side of the SoNG. At the steep eastern wall, growth faults indicate a long-term instability (Kuehl et al. 1997; Kottke et al. 2003). The more gentle western wall is formed by a set of terraces and broad depressions, the latter of which serve as pathways for about 10 mud flows in a 100 m sedimentary column corresponding on the average to a slide event every fifth year. Most of the mudflows end or coalesce on the broad U-shaped canyon floor, where they interfinger with bedded sediments. Between the pathways for the mudflows and some deeply incised gullies, more steady sedimentation prevails, as

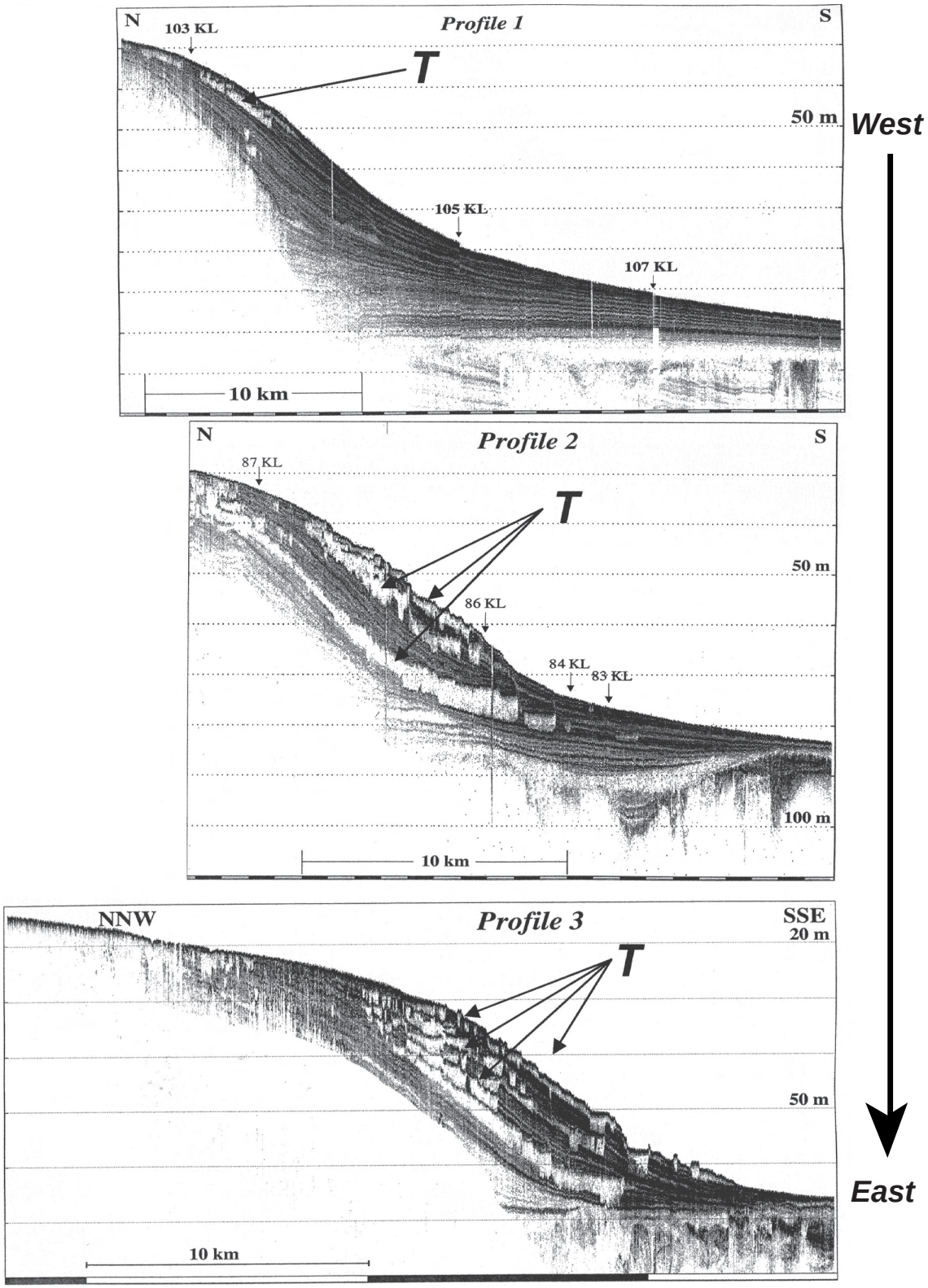

FIG. 13.—Three high-resolution (3.5 kHz) across-shelf profiles from west to east showing the increasing frequency of acoustically transparent layers (**T**) toward the active river mouths. These transparent layers are interpreted to represent sediment gravity flows, perhaps initiated by earthquakes common to the area. Profile 3 shows terraces formed by these flows deposited in the outer foreset and bottomset regions.

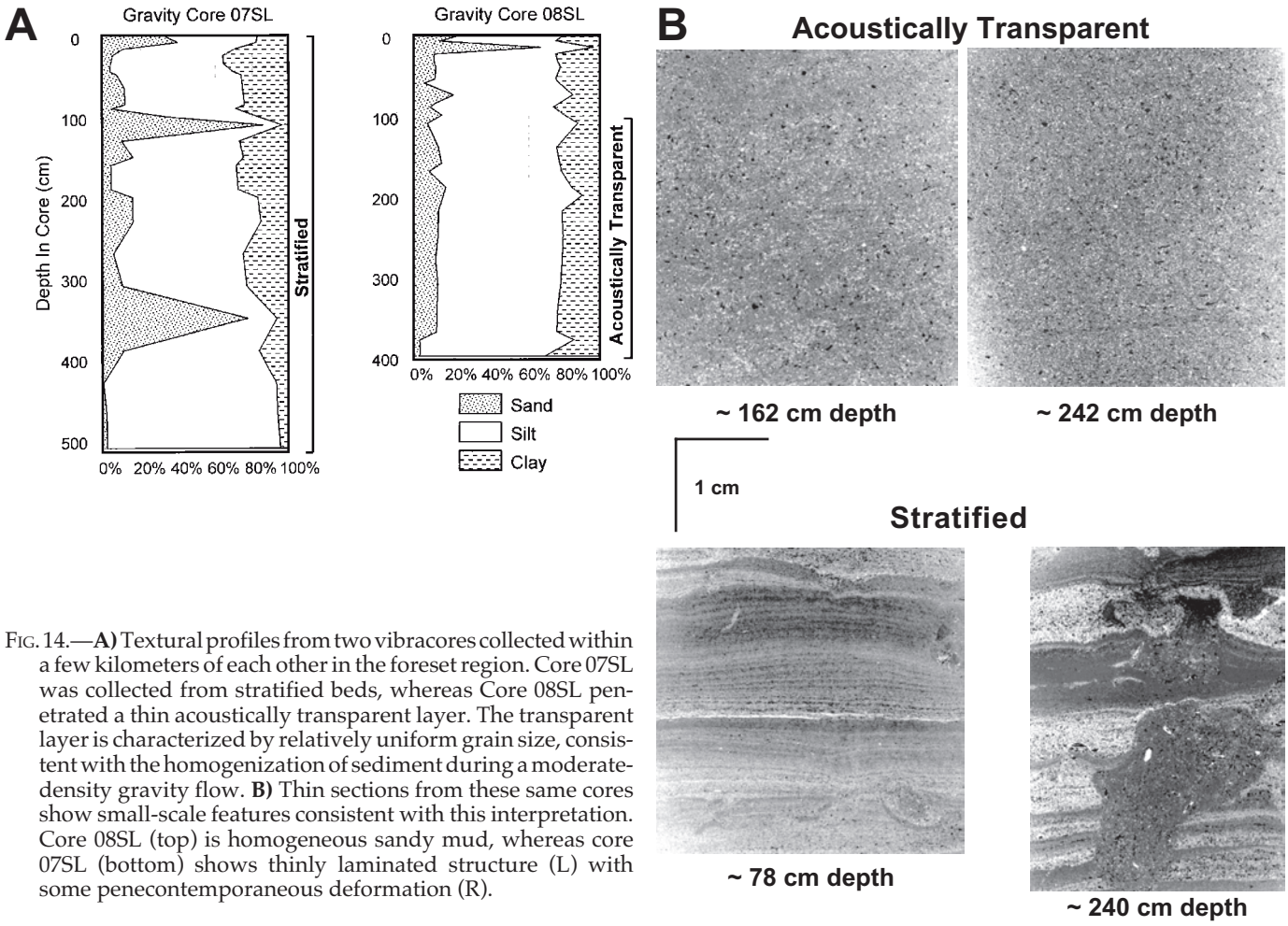

FIG. 14.—**A)** Textural profiles from two vibracores collected within a few kilometers of each other in the foreset region. Core 07SL was collected from stratified beds, whereas Core 08SL penetrated a thin acoustically transparent layer. The transparent layer is characterized by relatively uniform grain size, consistent with the homogenization of sediment during a moderate-density gravity flow. **B)** Thin sections from these same cores show small-scale features consistent with this interpretation. Core 08SL (top) is homogeneous sandy mud, whereas core 07SL (bottom) shows thinly laminated structure (L) with some penecontemporaneous deformation (R).

seen in the seismic records of draped, parallel-bedded sequences. Sedimentation rates in these areas are an order of magnitude higher than in the foreset beds, ranging from 50 cm y^{-1} at 230 m water depth to 20 cm y^{-1} at a site 15 km downcanyon at 570 m water depth (Michels et al., 2003). The draped sequence consists predominantly of graded sand–silt–clay sequences and numerous laminated mud sequences.

The graded units of the dated cores are assumed to have settled from suspension-rich surface water produced by the passage of storm- and cyclone-agitated water masses over the deep-water sediment trap of the shelf canyon. Indeed, the most prominent graded deposits appear to be correlated with the historical record of cyclones of the last 30 years (Kudrass et al., 1998).

The enormously high sedimentation rate in the upper reaches of the SoNG should have resulted in a rapid filling of the whole canyon. The present form of the canyon seems to be maintained by episodic mass wasting affecting the whole canyon, events that happened approximately 150 and 280 years BP (Michels et al., 2003). This episodic emptying is probably how sediments are transferred by turbidity currents to feed the huge Bengal fan, extending as far as to the Equator, more than 2000 km away.

LATE GLACIAL AND HOLOCENE DEVELOPMENT

At the lowstand LGM, approximately 18 ka, the Ganges–Brahmaputra river system had incised near to base level across most of the Bengal Basin, although the upstream extent of incision is not well known. The best constraint is along the Brahmaputra paleovalley, which is known to be ~ 110 m deep at the Jamuna Bridge site 200 km upstream of the modern coast (JICA, 1976). Outside of the alluvial valleys, most of the Bengal Basin was composed of broad, lateritic uplands situated at 45–55 m below present sea level (Goodbred and Kuehl, 2000a). Similar lateritic remains occasionally crop out on the outer shelf (Michels et al., 1998). The formation of ooids and oolitic beach ridges along the former coast, at 20–18 ka, indicate low terrigenous input (Wiedicke et al., 1999) as glacial rivers discharged into the fjord-like SoNG with generally reduced fluvial runoff (Kudrass et al., 2001). By ~ 15 ka, though, increasing rates of sedimentation are recorded contemporaneously with a strengthening summer monsoon and enhanced precipitation over the catchment (Goodbred, 2003). Intensification of the summer monsoon continued into the early Holocene, when higher-than-present precipitation (Prell and Kutzbach, 1987; Gasse et al., 1991; Kudrass et al., 1998; Goodbred and Kuehl, 2003) led to tremendous G–B sediment discharges of ~ 2.5 x 10^{12} kg y^{-1}, or more than 2.5 x the modern load, continuing for several thousand years (Goodbred and Kuehl, 2000b).

The initial period of high sediment discharge is recorded on the fan by the rapid growth of the still active channel–levee system of the Bengal fan between 13 and 9 ka (Weber et al., 1997). Supply to the fan dwindled once the lowstand surface of the Bengal Basin was transgressed, leading to deltaic sediment trap-

ping (Goodbred and Kuehl, 2000a). This initiation of delta formation at 10–11 ka is widely marked on the LDP by deposition of fine-grained mud (i.e., lower delta mud facies) over the lowstand laterite and alluvial sand units. These muds reflect an intertidal mangrove environment containing abundant wood fragments and estuarine shells (Umitsu, 1993). This relatively sensitive coastal setting persisted with little apparent change for the next 2000–4000 years, suggesting that shoreline position was relatively stable during a period in which eustatic sea level rose 30–35 m at a mean rate of ~ 1 cm y^{-1}. Such rapid glacio-eustasy was offset by the immense Ganges–Brahmaputra sediment discharge created by the strengthened monsoon (Goodbred and Kuehl, 2000b; Goodbred, 2003).

In addition to widespread coastal-plain deposition in the early Holocene, major fluvial and flood-basin sequences accreted across the UDP. Sandy channel sequences continued to be deposited in the central alluvial valleys, as well as sequestered to the backflooded Sylhet Basin from ~ 11 to 9 ka (Goodbred and Kuehl, 2000a). Fine-grained sediments were deposited in the Sylhet Basin after ~ 9 ka, indicating that the Brahmaputra flowed along its western (modern) course and delivered most of its coarse load to the coast. This bypassing of inland basins such as the Sylhet likely enhanced shoreline stability during the last phase of rapid sea-level rise. Although the Ganges–Brahmaputra delta sequence was largely aggradational from 11 to 7 ka, pollen abundances from coastal deposits indicate that peak marine influence occurred near the end of this period (Banerjee and Sen, 1988; Umitsu, 1993), corresponding to the maximum transgression. After 7 ka, much of the delta switched to a progradational mode, with alluvial sands prograding widely across the coastal plain as well as the initiation of subaqueous delta development (Goodbred and Kuehl, 2000a; Kuehl et al., 1997). This change characterizes the Ganges–Brahmaputra as a compound delta system with prograding subaerial and subaqueous clinoforms.

Mid-Holocene progradation was most prominent in the western delta, where the Ganges system discharged, and the coast there appears to have approached its present extent by 6 to ~ 5 ka (Allison et al., 2003). In the eastern delta, though, rapid infilling of the Sylhet Basin (> 2 cm y^{-1}) from ~ 7.5 to 6 ka indicates that the Brahmaputra River had switched to its eastern course, into the basin. Thus, much of the Brahmaputra load was sequestered inland, starving the eastern delta front and leading to a maximum transgression 1000–2000 years later than for the Ganges-fed western delta. By 5–6 ka, widespread deposition of muddy floodplain deposits in the Sylhet basin indicates that the Brahmaputra had switched again to its western course.

The main Ganges course migrated or avulsed eastward after ~ 5 ka, creating subaerial deposits extending to the modern coastline (Allison et al., 2003), while the Brahmaputra underwent at least one more cycle of course changes in the late Holocene, switching back to its modern western course only ~ 150 years ago (Fergusson, 1863). With slowed sea-level rise during this period (i.e., production of accommodation space), most of the Brahmaputra load likely bypassed the Sylhet basin and reached the coast. Progradation of the shoreline on the eastern side of the delta appears to have begun after about 3 ka, but constraints are limited because of a lack of radiocarbon dates, with infilling of the modern river-mouth estuary (Meghana estuary) accelerating after the last switch of the Brahamputra to its western course about 150 years ago. On the shelf, the muddy subaqueous delta continued to develop throughout the mid–late Holocene, with the modern foresets prograding up to 15–20 m/yr, the base of which presently reaches the ~ 80 m isobath on the outer shelf (Kuehl et al., 1997; Michels et al., 1998).

SPECIAL ATTRIBUTES OF THE GANGES–BRAHMAPUTRA DELTA

The enormous sediment load of the rivers has had a dramatic influence on the Holocene evolution of the Ganges–Brahmaputra delta, resulting in two phases of subaerial progradation in the Holocene. Goodbred and Kuehl (2000a) and Goodbred (2003) outline how strengthening of the southwest monsoon combined with rapid warming in the Himalayas during 11–7 ka to create sediment supply more than double that of the present. This led to deposition of a delta-plain unit ~ 50 m thick at a pace that exceeded the rate of sea-level rise. As this sediment pulse declined to present levels, sea-level transgression resumed and sediment infilling in inland areas of the Bengal Basin postponed resumption of the progradation of the present LDP until after 5 ka. In contrast, for most other deltas, Holocene delta progradation was restricted to a single phase after deceleration of the rate of sea-level rise (7.4–9.5 ka; Stanley and Warne, 1994).

The relative coarseness of the Ganges–Brahmaputra sediment load also has shaped the modern delta in combination with the large volume of sediment delivered. In the UDP, this can be observed in the rate at which channel avulsions occur (10^2 year intervals) and in the extreme rates of lateral migration within existing channel complexes (up to 800 m/yr) (Coleman, 1969; ISPAN, 1995; Goodbred and Kuehl, 2000b). This is particularly true in the high-gradient Brahmaputra, whose braided reach in Bangladesh has a median grain size in the channel bed of 0.22 mm (Barua et al., 1994) and a sediment load that is 80% silt and sand (Coleman, 1969). Clearly grain size is a contributing factor to rapid aggradation in the UDP and within river channels that leads to lateral migration and avulsion.

In the LDP, grain size may play a role in reducing sediment-compaction-induced subsidence relative to other deltas. In the Mississippi LDP, for instance, the dewatering of high-porosity, clay-rich Holocene sediments is a major part of the rapid subsidence (1–2 cm y^{-1}; Penland et al., 1989) that led to enormous loss of LDP wetlands to submergence in the Twentieth Century (Baumann et al., 1984; Walker et al., 1987; Boesch et al., 1994; Penland et al., 2000). Allison and Kepple (2001) have suggested that despite the thick Holocene section and overall deltaic sediment thicknesses up to 16 km (Paul and Lian, 1975) in the Ganges–Brahmaputra LDP, rates of relative regional sea-level rise are only 0.1–0.4 cm y^{-1}, at or below the rate new sediment is supplied by the coastal setup influx.

Whereas the magnitude of compaction-induced subsidence in the LDP may be relatively small, elsewhere in the Ganges–Brahmaputra delta subsidence rates are much higher, reflecting the complex tectonic setting of the delta. For example, as discussed above, high subsidence and resulting accommodation in the Sylhet and other inland basins apparently had a major influence on delta evolution as well as the timing and magnitude of sediment supply to the ocean. Moreover, it seems likely that subsidence rates in the Sylhet, while controlled primarily by tectonics, also reflect self-compaction of the finer-grained sediments that are deposited there. Unlike other "passive" margins, the tectonic control on the Ganges–Brahmaputra delta is quite striking. In addition to the inland basins mentioned above, relative motion (i.e., both uplift and subsidence) in the Bengal basin clearly has had a strong influence on the rivers' drainage patterns and more generally in dictating the basin boundaries.

Another special characteristic of the delta is the presence of a major submarine canyon, "Swatch of No Ground," which apparently has served as an important conduit for off-shelf escape of the sediment of the Ganges–Brahmaputra rivers throughout the

Late Quaternary. The location of the canyon may be constrained by a major NE–SW trending trough, and if so, is another example of the tectonic control on the dispersal of the rivers' sediment load. In any case, the canyon clearly is an important barrier for the westward transport of sediments to the Indian shelf (Segall and Kuehl, 1992), but it could also serve to limit the seaward progradation of the subaqueous delta. We have estimated that the amount of sediment accumulating in the subaqueous delta is equal to that escaping to the Bengal fan through the canyon (Goodbred and Kuehl, 1999). Hence, it is tempting to speculate that in the absence of such a major sediment sink the seaward progradation of the subaqueous delta, as well as its lateral extent, would be much greater. At present, the outer Bengal shelf does not receive a significant supply of modern river sediment, as evidenced by the exposed Pleistocene surface and oolitic beach ridges.

Although the subaqueous delta of the Ganges–Brahmaputra has many similarities to other major clinoforms forming off large rivers (e.g., Amazon, Huanghe, Fly), it also reveals significant differences. In particular, sand dominates the texture of topset beds for the Ganges–Brahmaputra subaqueous delta, whereas most other major subaqueous deltas are predominantly mud. The overall morphology of the modern delta front and subaqueous delta of the Ganges–Brahmaputra is that of a compound clinoform that generally coarsens up, with a capping of finer-grained supratidal muds (Fig. 15). Over the Holocene, as the delta progrades, much of this fine-grained cap is removed by river migration and is replaced in the stratigraphic record by channel fill. The high sand content of topset beds for the Ganges–Brahmaputra system is in part related to its relatively coarse sediment load, but also to the energetic shallow shelf setting punctuated by frequent cyclones and the resulting wave- and wind-induced bottom resuspension and winnowing. The coarse nature of this system makes the distinction between delta front and subaqueous delta more difficult than in other systems, where typically it is defined on the basis of the textural change from sand or mixed sand and mud, to mud (e.g., Fly; Dalrymple et al., 2003; Harris et al., 1993). At present, we lack sufficient

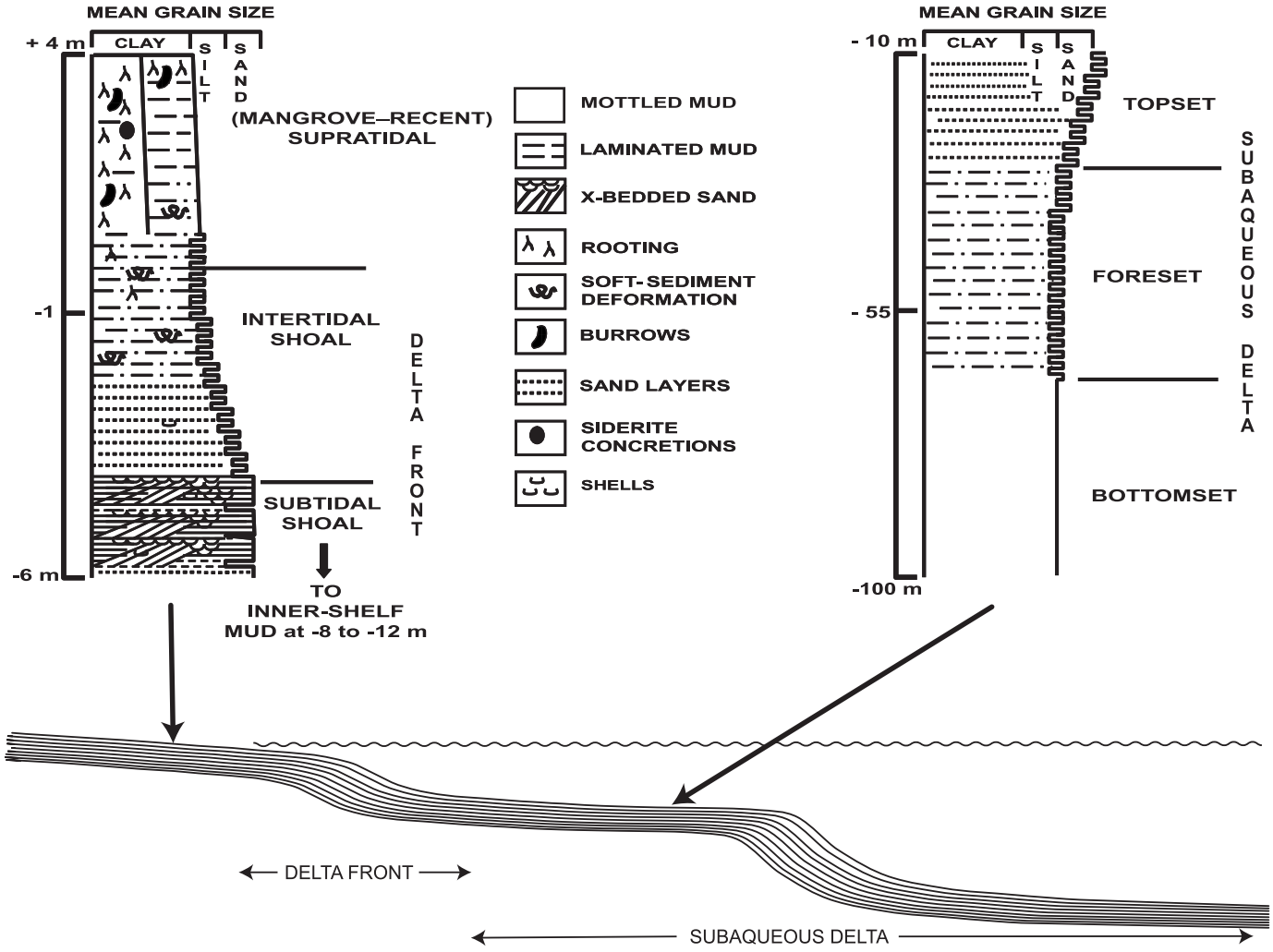

FIG. 15.—Cartoon showing facies succession of the modern Ganges–Brahmaputra Delta (top) with respect to the dual clinoform which comprises the subaerial and subaqueous regions (bottom). The formation of such features appears to be relatively common where large rivers discharge into an energetic marine shelf. The thin fine-grained cap of supratidal muds has a low likelihood of preservation during progradation, inasmuch as it is likely reworked by channel migration.

continuous stratigraphic control to determine whether our distinction between delta front and topset, based on surface morphology and shallow seismic reflection, could be resolved clearly at the outcrop scale.

REFERENCES

Abbas, N., and Subramanian, V., 1984, Erosion and sediment transport in the Ganges River basin (India): Journal of Hydrology, v. 69, p. 173–182.

Alam, M., 1996, Subsidence of the Ganges–Brahmaputra delta of Bangladesh and associated drainage, sedimentation and salinity problems, *in* Milliman, J.D., and Haq, B.U., Sea-Level Rise and Coastal Subsidence; Causes, Consequences, and Strategies: Dordrecht, The Netherlands, Kluwer Academic Publishers, p. 169–192.

Alam, M., Alam, M.M., Curray, J.R., Chowdhury, M.L.R., and Gani, M.R., 2003, An overview of the sedimentary geology of the Bengal Basin in relation to the regional tectonic framework and basin-fill history: Sedimentary Geology, v. 155, p. 179–208.

Allison, M.A., 1998a, Historical changes in the Ganges–Brahmaputra delta front: Journal of Coastal Research, v. 14, p. 1269–1275.

Allison, M.A., 1998b, Geologic framework and environmental status of the Ganges–Brahmaputra delta: Journal of Coastal Research, v. 14, p. 826–837.

Allison, M.A., and Kepple, E.B., 2001, Modern sediment supply to the lower delta plain of the Ganges–Brahmaputra River in Bangladesh: Geo-Marine Letters, v. 21, p. 66–74.

Allison, M.A., Kuehl, S.A., Martin, T.C., and Hassan, A., 1998, The importance of floodplain sedimentation for river sediment budgets and terrigenous input to the oceans: Insights from the Brahmaputra–Jamuna River: Geology, v. 26, p. 175-178.

Allison, M.A., Khan, S.R., Goodbred, S.L., and Kuehl, S.A., 2003, Stratigraphic evolution of the late Holocene Ganges–Brahmaputra lower delta plain: Sedimentary Geology, v. 155, p. 317–342.

Ascoli, F.D., 1912, Changes in the Ganges delta: The Geographical Journal (London), v. 39, p. 611–612.

Banerjee, M., and Sen, P.K., 1988, Paleobiology and environment of deposition of Holocene sediments of the Bengal basin, India, *in* The Palaeoenvironment of East Asia from the mid-Tertiary, Proceedings of the 2nd Conference: Centre of Asian Studies, University of Hong Kong, Hong Kong, p. 703–731.

Barua, D.K., 1990, Suspended sediment movement in the estuary of the Ganges–Brahmaputra–Meghna river system: Marine Geology v. 91, p. 243–253.

Barua, D.K., Kuehl, S.A., Miller, R.L., and Moore, W.S., 1994, Suspended sediment distribution and residual transport in the coastal ocean of the Ganges–Brahmaputra River mouth: Marine Geology, v. 120 p. 41–61.

Baumann, R.H., Day, J.W., and Miller, C.A., 1984, Mississippi deltaic wetland survival: sedimentation versus coastal submergence: Science, v. 224, p. 1093–1095.

Berner, U., Poggenburg, J., Faber, E., Quadfasel, D., and Frische, A, 2003, Methane in ocean waters of the Bay of Bengal: its sources and exchange with the atmosphere: Deep-Sea Research II, v. 50, p. 925–950.

Boesch, D.F., Josselyn, M.N., Mehta, A.J., Morris, J.T., Nuttle, W.K., Simenstad, C.A., and Swift, D.J.P., 1994, Scientific Assessment of Coastal Wetland Loss, Restoration and Management in Louisiana: Journal of Coastal Research, Special Issue no. 20, 103 p.

Brammer, H., 1996, The Geography of the Soils of Bangladesh: University Press, Dhaka, Bangladesh, 287 p.

Bristow, C.S., 1993. Sedimentary structures exposed in bar tops in the Brahmaputra River, Bangladesh, *in* Best, J.L. and Bristow, C.S., Braided Rivers: Geological Society of London, Special Publication 75, p. 277–289.

Coates, D.A., 1990, The Mymensingh terrace: Evidence of Holocene deformation in the delta of the Brahmaputra River, central Bangladesh (abstract): Geological Society of America, Abstracts with Programs, v. 22, p. 310.

Coates, D.A., Whitney, J.W., and Alam, A.K.M., 1988, Evidence of neotectonic activity on the Bengal delta, Bangladesh (abstract): Geological Society of America, Abstracts with Programs, v. 20, p. 54.

Coleman, J.M., 1969, Brahmaputra River: channel processes and sedimentation: Sedimentary Geology, v. 3, p. 129–239.

Curray, J.R., Emmel, F.J., and Moore, D.G., 2002, The Bengal Fan: morphology, geometry, stratigraphy, history and processes: Marine and Petroleum Geology, v. 19, p. 1191–1223.

Dalrymple, R.W., Baker, E.K., Harris, P.T., and Hughes, M.G., 2003, Sedimentology and stratigraphy of a tide-dominated, foreland-basin delta (Fly River, Papua New Guinea), *in* Sidi, F.J., Nummedal, D., Imbert, P., Darman, H., and Posamentier, H.W., Tropical Deltas of Southeast Asia: SEPM, Special Publication, 76, p. 147–173.

Edmond, J.M., 1992, Himalayan tectonics, weathering processes, and the strontium isotope record in marine limestones: Science, v. 258, p. 1594–1597.

Fergusson, J., 1863, On Recent changes in the delta of the Ganges: Geological Society of London, Quarterly Journal, v. 19, p. 321–354.

Galy, A., and France-Lanord, C., 2001, Higher erosion rates in the Himalaya: Geochemical constraints on riverine fluxes: Geology, v. 29, p. 23–26.

Galy, A., France-Lanord, C., and Derry, L.A., 1999, The strontium isotopic budget of Himalayan rivers in Nepal and Bangladesh: Geochimica et Cosmochimica Acta, v. 63, p. 1905–1925.

Gasse, F., Arnold, M., Fontes, J.C., Fort, M., Gilbert, E., Huc, A., Li, B., Li., Y., Liu, Q., Mélières, F., Van Campo, E., Wang, F., and Zhang, Q., 1991, A 13,000-year climate record from western Tibet: Nature, v. 353, p. 742–745.

Goodbred, S.L., 1999, Sediment dispersal and sequence development along a tectonically active margin: late Quaternary evolution of the Ganges–Brahmaputra River delta: Ph.D. Dissertation, College of William and Mary, 165 p.

Goodbred, S.L., Jr., 2003, Response of the Ganges dispersal system to climate change: a source-to-sink view since the last interstade: Sedimentary Geology, v. 162, p. 83–104.

Goodbred, S.L., and Kuehl, S.A., 1998, Floodplain processes in the Bengal Basin and the storage of Ganges–Brahmaputra river sediment: An accretion study using ^{137}Cs and ^{210}Pb geochronology: Sedimentary Geology, v. 121, p. 239–258.

Goodbred, S.L., and Kuehl, S.A., 1999, Holocene and modern sediment budgets for the Ganges–Brahmaputra River: Evidence for highstand dispersal to flood-plain, shelf, and deep-sea depocenters: Geology, v. 27, p. 559–562.

Goodbred, S.L., and Kuehl, S.A., 2000a, The significance of large sediment supply, active tectonism and eustasy on margin sequence development: Late Quaternary stratigraphy and evolution of the Ganges–Brahmaputra delta: Sedimentary Geology, v. 133 p. 227–248.

Goodbred, S.L., and Kuehl, S.A., 2000b, Enormous Ganges–Brahmaputra sediment discharge during strengthened early Holocene monsoon: Geology, v. 28, p. 1083–1086.

Goodbred, S.L., and Kuehl, S.A., 2003, The production, transport, and accumulation of sediment: a cross-section of recent developments with an emphasis on climate effects: Sedimentary Geology, v. 162, p. 1–3.

Goodbred, S.L., Kuehl, S.A., Steckler, M.S., and Sarker, M.H., 2003, Controls on facies distribution and stratigraphic preservation in the Ganges–Brahmaputra delta sequence: Sedimentary Geology, v. 155, p. 301–316.

Goswami, D.C., 1985, Brahmaputra River, Assam, India: Physiography, basin denudation, and channel aggradation: Water Resources Research, v. 21, p. 959–978.

Harris, P.T., Baker, E.K., Cole, A.R., and Short, S.A., 1993, A preliminary study of sedimentation in the tidally dominated Fly River delta, Gulf of Papua: Continental Shelf Research, v. 13, p. 441–472.

Heroy, D.C., Kuehl, S.A., and Goodbred, S.L., 2003, Mineralogy of the Ganges and Brahmaputra Rivers: implications for river switching and Late Quaternary climate change: Sedimentary Geology, v. 155, p. 343–359.

Hübscher, C., Breitzke, M., Michels, K., Kudrass, H.R., Spiess, V., and Wiedicke, M., 1998, Late Quaternary seismic stratigraphy of the eastern Bengal Shelf: Marine Geophysical Researches, v. 20, p. 57–71.

Huizing, H.G.J., 1971, A Reconnaissance study of the mineralogy of sand fractions from East Pakistan sediments and soils: Geoderma, v. 6, p. 109–133.

Iman, M.B., and Shaw, H.F., 1985, The diagenesis of Neogene clastic sediments from the Bengal Basin, Bangladesh: Journal of Sedimentary Petrology, v. 55, p. 665–671.

Islam, T., and Peterson, R.E., 2003, A climatological study on the landfalling tropical cyclones of Bangladesh (abstract): American Meterological Society, Annual Meeting Abstracts.

ISPAN, 1995, A Study of Sedimentation in the Brahmaputra–Jamuna Floodplain: Bangladesh Flood Action Plan 16, US Agency for International Development, 188 p.

JICA (Japan International Cooperation Agency), 1976, Geology and Stone Material, Jamuna Bridge Construction Project, p. 54.

Johnson, B.D., Powell, McA.C., and Veevers, J.J., 1976, Spreading history of the eastern Indian Ocean and Greater India´s northward flight from Antarctica and Australia: Geological Society of America, Bulletin, v. 87, p. 1560–1566.

Johnson, S.Y., and Alam, A.M.N., 1991, Sedimentation and tectonics of the Sylhet trough, Bangladesh: Geological Society of America, Bulletin, v. 103, p. 1513–1527.

Karstensen, J., 1999, Ueber die Ventilation der Thermokline des Indischen Ozeans: Dissertation, Fachbereich Geowissenschaften, Hamburg, 172 p.

Kottke, B., Schwenk, T., Breitzke, M., Wiedicke, M., Kudrass, H.R., and Spiess, V., 2003, Acoustic facies and depositional processes in the upper submarine canyon Swatch of No Ground (Bay of Bengal): Deep Sea Research Part II: Topical Studies in Oceanography, v. 50, p. 979–1001.

Kudrass, H.R., Michels, K.H., Wiedicke, M., and Suckow, A., 1998, Cyclones and tides as feeders of a submarine canyon off Bangladesh: Geology, v. 26, p. 715–718.

Kudrass, H.R., Hofmann, F., Doose, H., Emeis, K., and Erlenkeuser, H., 2001, Modulation and amplification of climatic changes in the Northern Hemisphere by the Indian summer monsoon during the past 80 k.y.: Geology, v. 29, p. 63–66.

Kuehl, S.A., Hariu, T.M., and Moore, W.S., 1989, Shelf sedimentation off the Ganges–Brahmaputra River system: Evidence for sediment bypassing to the Bengal fan: Geology, v. 17, p. 1132–1135.

Kuehl, S.A., Hariu, T.M., Sanford, M.W., Nittrouer, C.A., and DeMaster, D.J., 1991, Millimeter-scale sedimentary structure of fine-grained sediments: Examples from continental margin environments, *in* Bennett, R.H., Bryant, W.R., and Hulbert, M.H., eds., Microstructure of Fine-Grained Sediments: New York, Springer-Verlag, p. 33–45.

Kuehl, S.A., Levy, B.M., Moore, W.S., and Allison, M.A., 1997, Subaqueous delta of the Ganges–Brahmaputra river system: Marine Geology, v. 144, p. 81–96.

Martin, T.C., and Hart, T.C., 1997, Time series analysis of erosion and accretion in the Meghna Estuary: Meghna Estuary Study Internal Report, Bangladesh Ministry of Water Resources Dhaka, Bangladesh, 20 p.

Michels, K.H., Kudrass, H.R., Hubscher, C., Suckow, A., and Wiedicke, M., 1998, The submarine delta of the Ganges–Brahmaputra: cyclone-dominated sedimentation patterns: Marine Geology, v. 149, p. 133–154.

Michels, K.H., Suckow, A., Breitzke, M., Kudrass, H.-R., and Kottke, B., 2003, Sediment transport in the shelf canyon "Swatch of No Ground" (Bay of Bengal): Deep-Sea Research II, v. 50, p. 1003–1022

Morgan, J.P., and McIntire, W.G., 1959, Quaternary geology of the Bengal basin, East Pakistan and India: Geological Society of America, Bulletin, v. 70, p. 319–342.

Paul, D.D., and Lian, H.M., 1975, Offshore Tertiary basins of southeast Asia: Bay of Bengal to South China Sea: 9th World Petroleum Congress, Proceedings, v. 3, p. 107–121.

Penland, S., Ramsey, K.E., McBride, R.A., Moslow, T.F., and Westphal, K.A., 1989, Relative sea level rise and subsidence in Louisiana and the Gulf of Mexico: Louisiana Geological Survey, Coastal Geology, Technical Report 3, 65 p.

Penland, S., Wayne, L., Britsch, L.D., Williams, S.J., Beall, A.D., and Butterworth, V.C., 2000, Process classification of coastal land loss between 1932 and 1990 in the Mississippi River deltaic plain: U.S. Geological Survey, Open File Report 00-418.

Prell, W.L., and Kutzbach, J.E., 1987, Monsoon variability over the past 150,000 years: Journal of Geophysical Research, v. 92, p. 8411–8425.

Raghavan, S., and Rajesh, S., 2003, Trends in tropical cyclone impact: A study in Andhra Pradesh, India: American Meteorological Society, Bulletin, v. 84, p. 635–644.

Reimann, K.U., and Hiller, K., 1993, Geology of Bangladesh: Berlin, Gebrüder Bornträger, Beiträge zur Regionalen Geologie der Erde, 20, 160 p.

Sarin, M.M., Krishnaswami, S., Dilli, K., Somayajulu, B.L.K., and Moore, W.S., 1989, Major ion chemistry of the Ganges–Brahmaputra river system: weathering processes and fluxes to the Bay of Bengal: Geochimica et Cosmochimica Acta, v. 53, p. 997–1009.

Segall, M.P., and Kuehl, S.A., 1992, Sedimentary processes on the Bengal continental shelf as revealed by clay-size mineralogy: Continental Shelf Research, v. 12, p. 517–541.

Segall, M.P., and Kuehl, S.A., 1994, Sedimentary structures on the Bengal shelf: A multi-scale approach to sedimentary fabric interpretation: Sedimentary Geology, v. 93, p. 165–180.

Sengupta, S., 1966, Geological and geophysical studies in the western part of the Bengal Basin, India: American Association of Petroleum Geologists, Bulletin, v. 50, p. 1001–1017.

Sengupta, R., Basu, P.C., Bandyopadhyay, A., Rakshit, S., and Sharma, B., 1992, Sediments in the continental shelf in and around the Swatch of No Ground: Geological Survey of India, Special Publication Series, v. 29, p. 201–207.

Sheyte, S.R., Shenoi, S.S.C., Gouveia, A.D., Michael, G.S., Sundar, D., and Nampoothiri, G., 1991, Wind-driven coastal upwelling along the western boundary of the Bay of Bengal during the southwest monsoon: Continental Shelf Research, v. 11, p. 1397–1408.

Singh, O.P., Ali Khan, T.M., and Rahman, Md.S., 2000, Changes in the frequency of tropical cyclones over the North Indian Ocean: Meteorology and Atmospheric Physics, v. 75, p. 11–20.

Stanley, D.J., and Warne, A.G., 1994, Worldwide initiation of Holocene marine deltas by deceleration of sea-level rise: Science, v. 265, p. 228–231.

Subramanian, V., 1978, Input by Indian rivers into the world oceans: Indian Academy of Sciences, Proceedings, v. 87, p. 77–88.

Subramanian, V., and Ramanathan, A.L., 1996, Nature of sediment load in the Ganges–Brahmaputra river systems in India, *in* Milliman, J.D., and Haq, B.U., Sea-Level Rise and Coastal Subsidence: Dordrecht, The Netherlands, Kluwer Academic Publishers, p. 151–168.

Suckow, A., Morgenstern, U., and Kudrass, H.R., 2001, Absolute dating of recent sediments in the cyclone-influenced shelf area off Bangladesh: comparison of gamma spectrometric (^{137}Cs, ^{210}Pb, ^{228}Ra), radiocarbon, and ^{32}Si ages: Radiocarbon, v. 43, p. 917–927.

Tomczak, M., and Godfrey, J.S., 1994, Regional Oceanography; An Introduction: Oxford, U.K., Pergamon Press, 422 p.

Umitsu, M., 1993, Late Quaternary sedimentary environments and landforms in the Ganges delta: Sedimentary Geology, v. 83, p. 177–186.

UNGER, D., ITTEKKOT, V., SCHAEFER, P., TIEMANN, J., AND RESCHKE, S., 2003, Seaonality and interannual variability of particle fluxes to the deep Bay of Bengal: influence of riverine input and oceanographic processes: Deep-Sea Research II, v. 50, p. 897–923.

WALKER, H.J., COLEMAN, J.M., ROBERTS, H.H., AND TYE, R.S., 1987, Wetland loss in Louisiana: Geografiska Annaler, v. 69, p. 189–200.

WEBER, M.E., WIEDICKE, M., KUDRASS, H.R., HÜBSCHER, C., AND ERLENKEUSER, H., 1997, Active growth of the Bengal Fan during sea-level rise and highstand: Geology, v. 25, p. 315 –318.

WIEDICKE, M., KUDRASS, H.R., AND HÜBSCHER, C., 1999, Oolithic beach barriers of the last sea-level lowstand at the outer Bengal shelf: Marine Geology, v. 157, p. 7–18.

Annex B72

Joseph R. Curray, "Tectonics and history of the Andaman Sea region", *Journal of Asian Earth Sciences,* Vol. 25, No. 1 (2005)

Available online at www.sciencedirect.com
SCIENCE DIRECT
Journal of Asian Earth Sciences 25 (2005) 187–232
Journal of Asian Earth Sciences
www.elsevier.com/locate/jaes

Tectonics and history of the Andaman Sea region

Joseph R. Curray*

Scripps Institution of Oceanography, La Jolla, CA 92093-0220, USA

Received 20 May 2004; revised 25 August 2004; accepted 1 September 2004

Abstract

The Andaman Sea is an active backarc basin lying above and behind the Sunda subduction zone where convergence between the overriding Southeast Asian plate and the subducting Australian plate is highly oblique. The effect of the oblique convergence has been formation of a sliver plate between the subduction zone and a complex right-lateral fault system. The late Paleocene collision of Greater India and Asia with approximately normal convergence started clockwise rotation and bending of the northern and western Sunda Arc. The initial sliver fault, which probably started in the Eocene, extended through the outer arc ridge offshore from Sumatra, through the present region of the Andaman Sea into the Sagaing Fault. With more oblique convergence due to the rotation, the rate of strike-slip motion increased and a series of extensional basins opened obliquely by the combination of backarc extension and the strike-slip motion. These basins in sequence are the Mergui Basin starting at ~32 Ma, the conjoined Alcock and Sewell Rises starting at ~23 Ma, East Basin separating the rises from the foot of the continental slope starting at ~15 Ma; and finally at ~4 Ma, the present plate edge was formed, Alcock and Sewell Rises were separated by formation of the Central Andaman Basin, and the faulting moved onshore from the Mentawai Fault to the Sumatra Fault System bisecting Sumatra.

Keywords: Andaman Sea; Backarc Basin; Oblique Convergence; Subduction; Myanmar; Sumatra

1. Introduction

The Andaman Sea (Figs. 1 and 2) is a complex backarc extensional basin that differs from most other such basins in that it is west facing and that it was formed by transtension. The Andaman Sea lies along a highly oblique convergent margin between the northeastern moving Australian and/or Indian plate and the nearly stationary Eurasian or Southeast Asian plate. As the Greater Indian continental mass converged on the southeastern Asian margin, it caused clockwise rotation of the subduction zone and increase in the obliquity to the point that transtension along a sliver fault has resulted in oblique rhombochasm-like opening of the Andaman Sea during the Neogene.

The tectonics and geological history of the Andaman Sea cannot be separated from the tectonics and geological histories of Myanmar (Burma) on the north, the Andaman and Nicobar Islands part of the accretionary prism on the western side of the Andaman Sea, and Sumatra on the south. The descriptions and discussion to follow will, therefore, include consideration of Sumatra and western and central Myanmar. The continental crust and pre-Neogene rocks of the Malay Peninsula and the Shan Plateau of Myanmar are directly involved in the tectonics where they have been rifted and thinned to form the Mergui Basin in the southeastern part of the Andaman Sea.

1.1. Previous exploration and investigation

An early sighting of the Andaman and Nicobar Islands by a western explorer is attributed to Marco Polo in 1298, allegedly on his return to Europe by sea. He wrote 'Angamanain is a very long island…', and then went on to describe the unsavory nature of the aboriginal inhabitants of both the Andaman Islands (Angamanain) and Nicobar Islands (Necuveran), descriptions that were subsequently shown to be untrue or greatly exaggerated (Mukerjee, 2003).

* Tel.: +1 858 534 3299; fax: +1 858 534 0784.
E-mail address: jcurray@ucsd.edu.

1367-9120/$ - see front matter © 2005 Elsevier Ltd. All rights reserved.
doi:10.1016/j.jseaes.2004.09.001

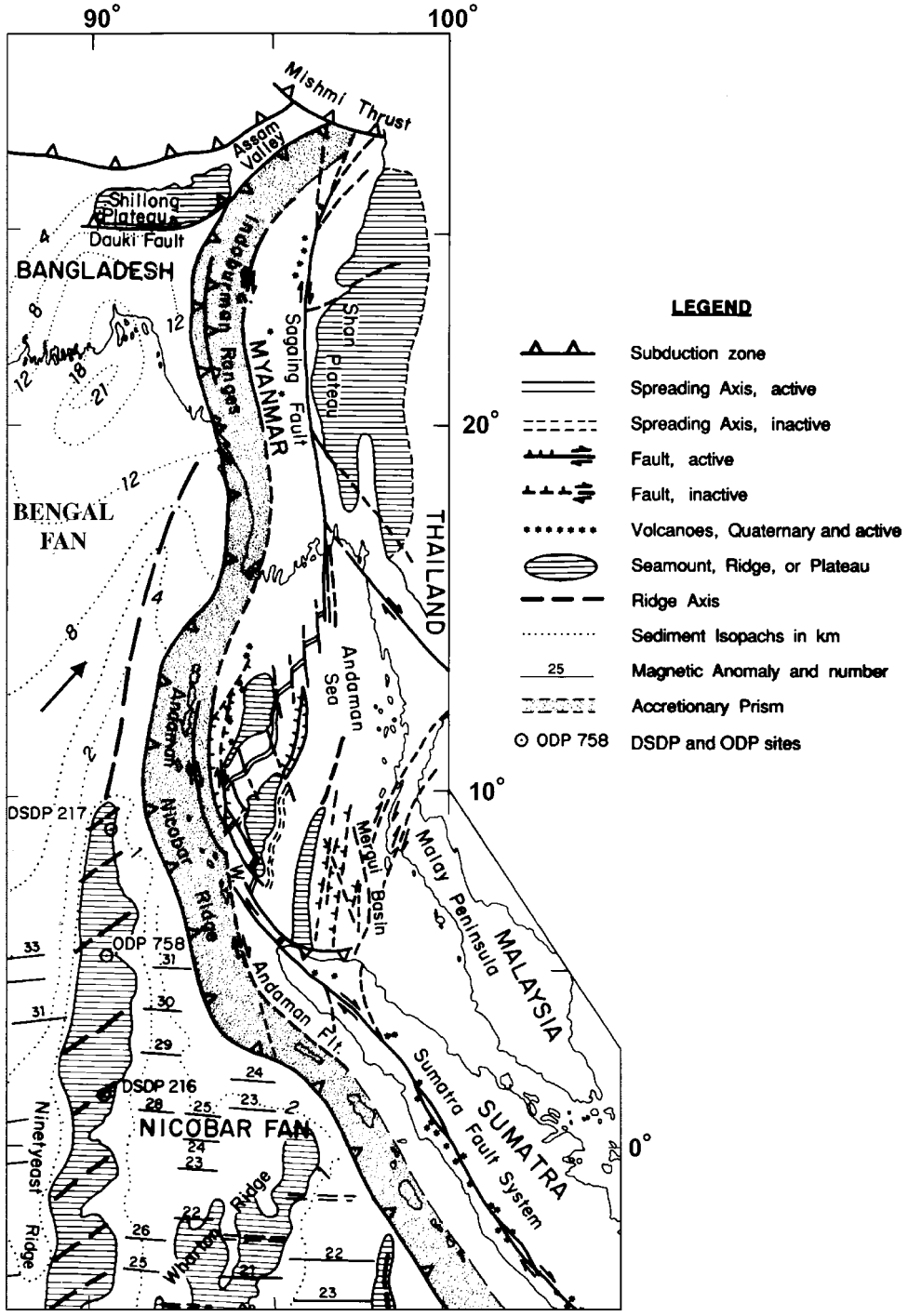

Fig. 1. Tectonic map of part of the northeastern Indian Ocean. Modified from Curray (1991).

Whether these comments were from his personal observations or taken from earlier Persian accounts, Marco Polo brought them to Europe.

The first organized oceanographic and marine biological investigations of the Andaman Sea were by Alcock (1902). Sewell (1925), Director of the Zoological Survey of India, did further oceanographic and geographic surveys. Rodolfo (1969a,b) named Alcock and Sewell Seamounts, later designated rises, after these two pioneers. Earlier workers had, however, made observations of Barren Island (about 12°N, Figs. 1, 2 and 4), the only active subaerial volcano and on the adjacent Andaman and Nicobar Islands and the Malay Peninsula. The first recorded observation of Barren Island by a western explorer was by Van Linschoten (1595). Mallet (1895) reviewed the history of observations of eruption of Barren Island, and reported that the first known landing on the island by a westerner was by Captain Archibald Blair in 1789, after whom Port Blair on South

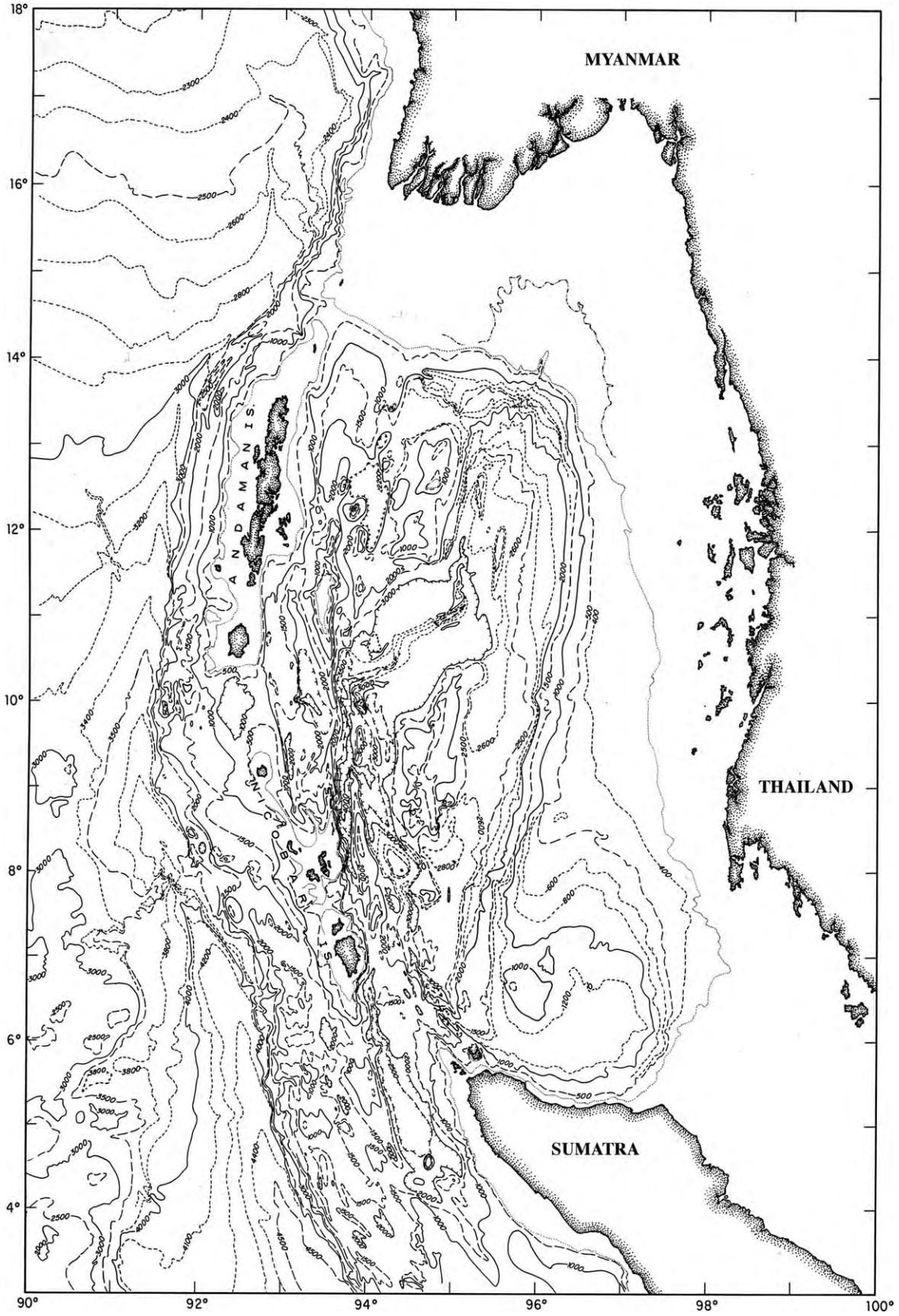

Fig. 2. Bathymetry of the Andaman Sea and part of the adjacent Indian Ocean, in corrected meters.

Andaman Island was named. The other subaerial volcano, Narcondam Island, is inactive or dormant.

The earliest known geological mention in the western literature of Myanmar (Burma) was by Fitch (1599) who traveled from Syria to Burma. Cox (1799a,b) described the hand-dug oil wells on the Yenangyaung anticline in the Central Burma basin, although there are reports of a Chinese traveler who reported oil workings at Yenangyaung in the 13th century. Suess (1904) divided Myanmar into three zones (Fig. 1): (1) The Western Indoburman Ranges; (2) The Central Tertiary Burma Basin; (3) The Eastern Zone Shan Plateau. Classic descriptions of the geology of Burma were published by Pascoe (1912), Chhibber (1934) and many other publications of the Geological Survey of India (GSI), as summarized by Goosens (1978).

Consideration of the geology and origin of the Andaman–Nicobar Ridge started with Rink (1847), who suggested that this ridge had been formed of sediments uplifted from the deep ocean floor, and consisted 'partly of those stratified deposits which occupied the level bottom of the sea', an early statement of the modern hypothesis of uplift and incorporation of sea floor deposits into an accretionary prism. Hochstetter (1869) pointed out that the same ridge extended southward as the outer arc ridge off Sumatra and Java. Sewell (1925) suggested that 'the Andaman–Nicobar Ridge has drifted toward the west away from the mainland, and has thus formed a pronounced curve with its apex in the region of Little Andaman Island'. Wegener was probably the first author to postulate a rift origin of the Andaman Sea in one of the early editions of his book 'Die Entstehung der Kontinente und Ozeane', starting in 1915. In the 1966 edition of the translation of his 1929 edition (Wegener, 1966), he compared Lawson's (1921) analysis of the San Andreas Fault of California and the opening of the Gulf of California with opening of the Andaman Sea. He says (p. 201) of the Andaman Sea 'We may perhaps assume here that the vast compression of the Himalaya put the Indochina chains in tension along their length, that under this stress the Sumatra chain was torn at the northern end of that island and that the northern part of the chain (Arakan) was, and still is, being pulled northwards like a rope's end into the great compression'.

Post-World War II work in the Andaman Sea, Burma and Sumatra which contributes to understanding the Andaman Sea includes important papers by Brunnschweiler (1966, 1974), Peter et al. (1966), Weeks et al. (1967), Aung Khin and Kyaw Win (1968, 1969), Rodolfo (1969a,b), Frerichs (1971), Mitchell and McKerrow (1975), Paul and Lian (1975), Mitchell (1976, 1981, 1985), Curray et al. (1979, 1982), Bender (1983), Chatterjee (1984), Roy and Chopra (1987), Mukhopadyay (1984, 1992), Polachan and Racey (1994), Acharyya (1994, 1997, 1998), Sieh and Natawidjaja (2000), Genrich et al. (2000) and many others. However, not all Indian syntheses agree with the plate tectonic interpretations presented in this paper. Rodolfo (1969a) was the first modern worker to fully understand the rifting and extensional opening of the Andaman Sea.

Newer information is gradually coming into public availability with excellent work in progress by Indian and French scientists and oil and gas exploration studies. Many of the irresolvable problems encountered in the present paper with the limited data available will eventually be resolved with these new sources of information, but many conclusions and interpretations in the present paper must for now remain speculation based on limited data.

My colleagues and I started publishing on the tectonics and history of the Andaman Sea in 1979 (Curray et al. 1979), including analysis of sea floor spreading magnetic anomalies for most of the Andaman Sea, which we had interpreted back to 11 Ma. Later, we extended that to 13 Ma. Several years ago, however, I carefully reviewed our anomaly interpretations and at first concluded that none prior to about 3 Ma were correct. More recently, we (S. Cande, personal communication, 2003) concluded that even those last 3 my anomaly identifications were not valid. We then concluded that anomalies could be identified back to 4 Ma for the Central Andaman Basin (Fig. 4).

While in the final stages of preparation of this manuscript, a long-awaited analysis of excellent closely spaced swath mapping and magnetic surveys of the Central Andaman Basin (Fig. 4) was published by Raju et al. (2004). I have now revised my discussion of our limited magnetic data in the Central Andaman Basin and have accepted their interpretation of the magnetic anomalies. Raju et al. (2004) agreed with our conclusion that the Central Andaman Basin has opened 118 km in about the last 4 my. Unfortunately, those authors misread our earlier publications that stated that the entire Andaman Sea had opened up to 460 km in the last 11 my. Instead they attributed our 11 my time to just the central most recent 118 km of opening. This opening history will be reviewed in Sections 6 and 7 in this paper.

1.2. Sources of data

Most of the ship tracks (Fig. 3) on which this study is based are from ships of the Scripps Institution of Oceanography, run between 1968 and 1979. In addition, some useful information has come from the cruises of R/V Pioneer and R/V Oceanographer from the US Coast and Geodetic Survey in 1964 and 1967, a few lines of the Lamont-Doherty Geological Observatory and several lines to which I was given access by oil companies. The data utilized include magnetics, gravity, 3.5 kHz bottom-penetrating (~100 m maximum) echo sounder and airgun seismic reflection profiling, mainly analog, but with some multichannel digital seismic reflection data. For most of our analog seismic reflection surveys, data were collected with two different sweep times and filter settings: a slower sweep, generally five seconds, filtered to 20–60 Hz; and a faster sweep, generally 2 s, filtered to 50–150 Hz for higher

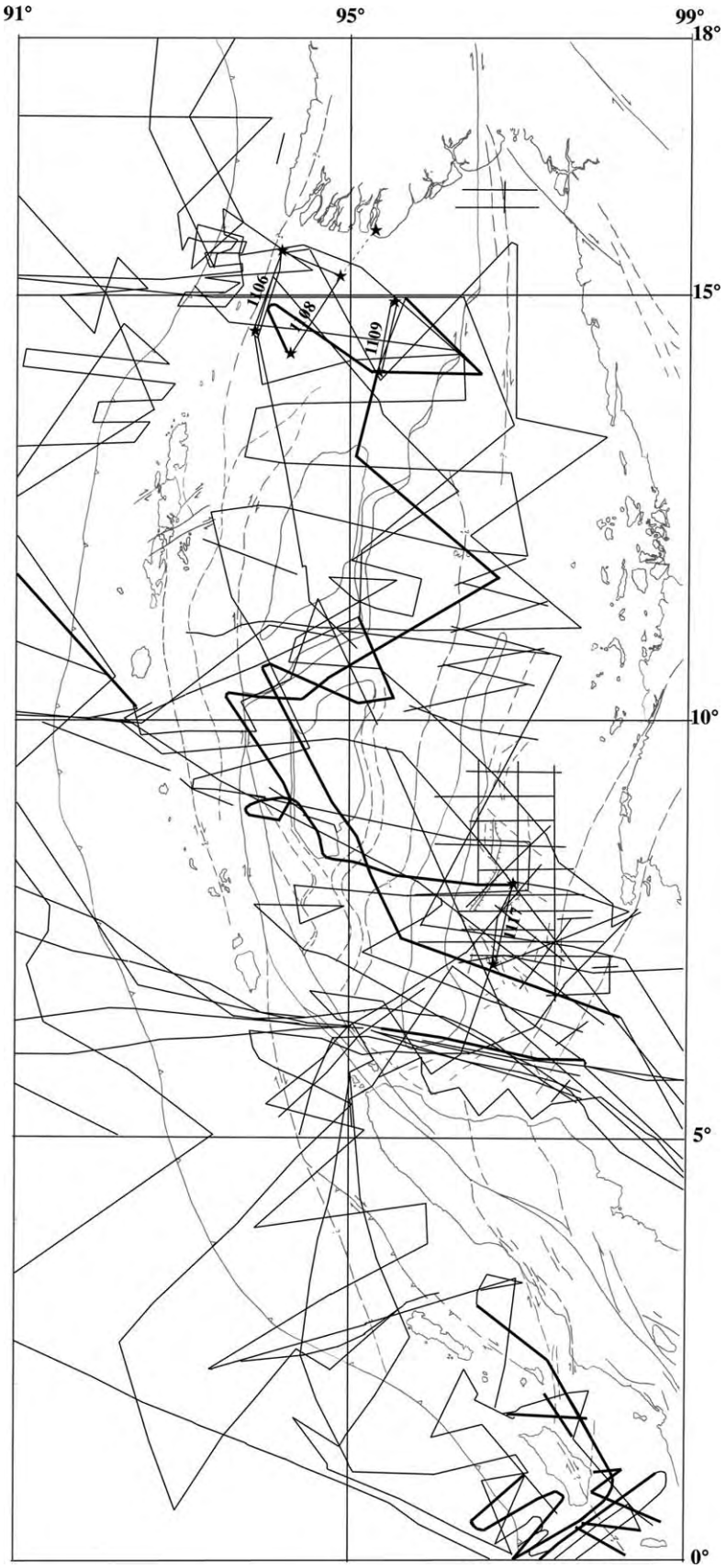

Fig. 3. Geophysical ship tracks available for this study, shown overlain on a partial tectonic map of Fig. 4. Bathymetry of Fig. 3 is based on many more tracks than shown here. Stars indicate ends of reversed seismic refraction lines. Heavy lines are SIO multichannel lines.

resolution. Swath-mapping bathymetry equipment was not available to us at the time of our surveys.

Some of the 134 seismic refraction and wide-angle seismic reflection stations involved single expendable sonobuoys; some were run with successive sonobuoys at intervals. All utilized air guns as a source, and about a third of the stations also utilized explosives as a source. Four of the refraction stations (Fig. 3) utilized moored telemetering hydrophones at each end of a reversed line as well as successively launched sonobuoys in between. The three lines on the Myanmar continental shelf were run in collaboration with geophysicists from the Myanma Oil Corporation, the Myanmar national petroleum company. A 24 channel analog receiving array was set up on the landward end. One of our technicians worked on shore with the oil company crew placing the geophones and synchronizing the shot timing by radio with our ship. A geophysicist from Myanma worked aboard our ship, which acted as both a shooting ship and receiving ship, while the time-synchronized signals were also received at the shore station. A geophysicist and a geologist from Myanma listed in the Acknowledgements at the end of this paper came to Scripps following the cruise to participate in analyzing the results.

Our bathymetric chart (Fig. 2) is based on many additional ship tracks, positions of which were adjusted to agree with the satellite-positioned lines of our own surveys. Our bathymetric and reflection profiles commonly exhibit a vertical exaggeration averaging about 10×. I have compared the bathymetry of Fig. 2 with bathymetry calculated from satellite altimetry (Smith and Sandwell, 1997) and conclude that while bathymetry from satellite measurements is useful for general trends, it is not satisfactory for understanding complex tectonic features.

2. Morphological and tectonic features of the Andaman Sea region

The major tectonic elements of the northeastern Bay of Bengal and the adjacent parts of Southeast Asia are shown in Fig. 1. The Indian and Australian plates are converging on the Eurasian or Southeast Asian plate in a northeasterly direction along the Himalayan front at the north and the Sunda Trench. The margin along the western Sunda Trench is an oblique convergence continental and arc margin. The sedimentary cover on the subducting plate is very thick because of the Bengal Fan (Curray et al., 2003), and sediments and ocean crust have been accreted and uplifted into the Indoburman Ranges, the Andaman–Nicobar Ridge and the outer arc ridge off Sumatra and Java. The sediments thin over the Ninetyeast Ridge, which is commonly interpreted as a hotspot trace (see, for example, Curray et al. (1982)), with NE–SW en echelon ridges on top. The bathymetric trench extends continuously from east of Java westward and northward to where it is overwhelmed by sediment of the Bengal Fan, and the surface trace of the subduction zone rises out of the depths onto land as the thrust faults of eastern Bangladesh, eastern India, western Myanmar and the southeastern edge of the Assam Valley (Fig. 1). The accretionary prism forms an entire mountain range, the Indoburman Ranges.

A tectonic map of the Andaman Sea region is shown in Fig. 4, extending from the Malay Peninsula on the east side to the Bay of Bengal sea floor on the west side, and from southern Myanmar in the north to northern Sumatra in the south. The free air gravity and seismicity for the same area are shown in Figs. 5 and 6, overlain on a simplified tectonic map. The overall basic structure, the tectonic elements, and the geology of the Andaman Sea region (Figs. 1 and 4) will be described in terms of extensions of the zones defined by Suess (1904) for Myanmar, consisting of: (1) The western zone extending from the Indoburman Ranges southward into the Andaman–Nicobar Ridge and to the outer arc ridge off Sumatra; (2) The Tertiary central Basin of Myanmar extending southward into the central basin of the Andaman Sea and the hydrocarbon rich backarc basins of Sumatra; (3) The Shan Plateau of Myanmar of mainly Mesozoic and Paleozoic continental rocks extending southward to the Malay Peninsula.

Fig. 4 shows the tectonic elements judged to be the most important, including topographic or subsurface highs, volcanoes, faults judged to be active, faults judged to be inactive, active and abandoned spreading axes and locations of important dredge or rock sampling sites. Discussion of most of these features follows.

3. Outer arc—Andaman–Nicobar Ridge

The Andaman–Nicobar Ridge is the part of the outer arc ridge of the northern segment of the Sunda subduction zone lying seaward of the Andaman Sea. As the accretionary prism of the subduction zone, its basic simplified structure is an imbricate stack of eastward-dipping fault slices and folds, with Cretaceous ophiolites and older deep sea sedimentary rocks lying generally at the top and on the eastern side of the pile, and progressively younger Neogene sedimentary rocks at the western side and bottom of the pile immediately above the trench. This imbricate stack is capped with Neogene sediments deposited on top and on the seaward face of the older rocks of the stack.

The stratigraphy of the Andaman Islands was first described in some detail by Oldham (1885), of the GSI, who mentions the fragmentary observations of others, including Rink (1847), Hochstetter (1869) and Ball (1870) in the Nicobar Islands, and some other early explorers in the Andaman Islands. Oldham divided the section into two basic formations, the Port Blair and the Archipelago Series. The Port Blair series consists principally of firm gray sandstone and interbedded gray shales, with minor amounts of coaly matter, conglomerate and limestone. The sandstone is the characteristic rock of the series. He also, however, noted the presence of some red and green jasper beds, serpentine and

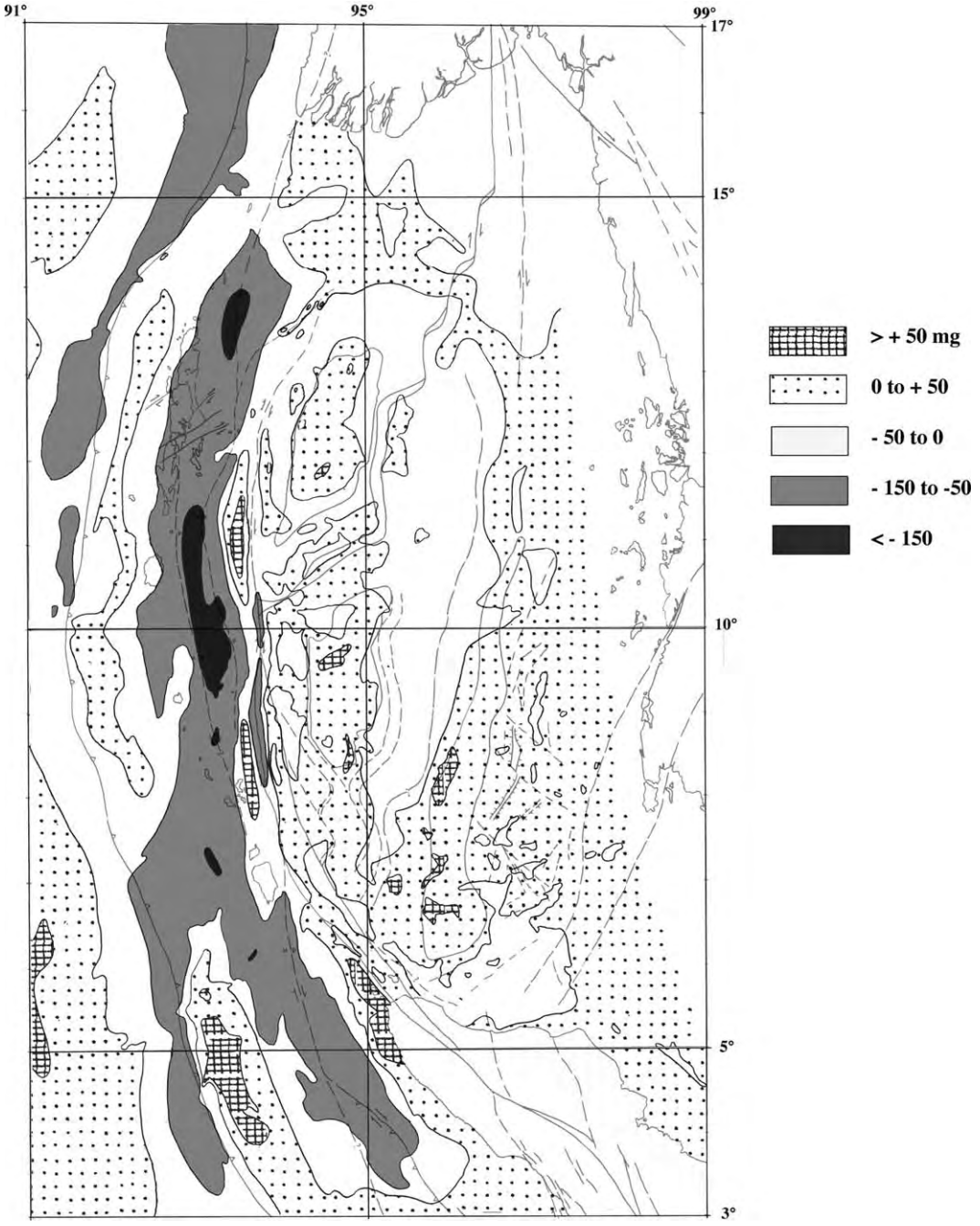

Fig. 5. Free air gravity, composite from shipboard measurements and satellite measurements, overlain on partial tectonic map.

volcanic beds, but he could not determine whether or not they were older than the sandstones and shales. The younger Archipelago Series, the capping on the imbricate stack, consist typically of soft limestones formed of coral and shell sand, soft calcareous sandstones and soft white clays.

Further contributions and more detailed work were done by other GSI geologists, e.g. Tipper (1911), Gee (1927) and Jacob (1954). The stratigraphy was revised and new names were given to some of the units in a series of papers by Karunakaran et al. (1964a,b,c, 1968a,b, 1975). For example, the Port Blair formation was redefined as the Andaman Flysch, and some other new formation names have been introduced. More recently, GSI geologists Chatterjee (1967, 1984), Parthasarathy (1984), Roy et al. (1988), Bandopadhyay and Ghosh (1998), Acharyya et al. (1990), Acharyya et al. (1997, 1998), Acharyya (1997), Chakraborty and Pal (2001) and Chakraborty et al. (1999, 2002) have published excellent new descriptions and facies interpretations, some of which I will follow in the subsequent discussions.

More recently, after much of this discussion had been written, a new paper by Pal et al. (2003) appeared in

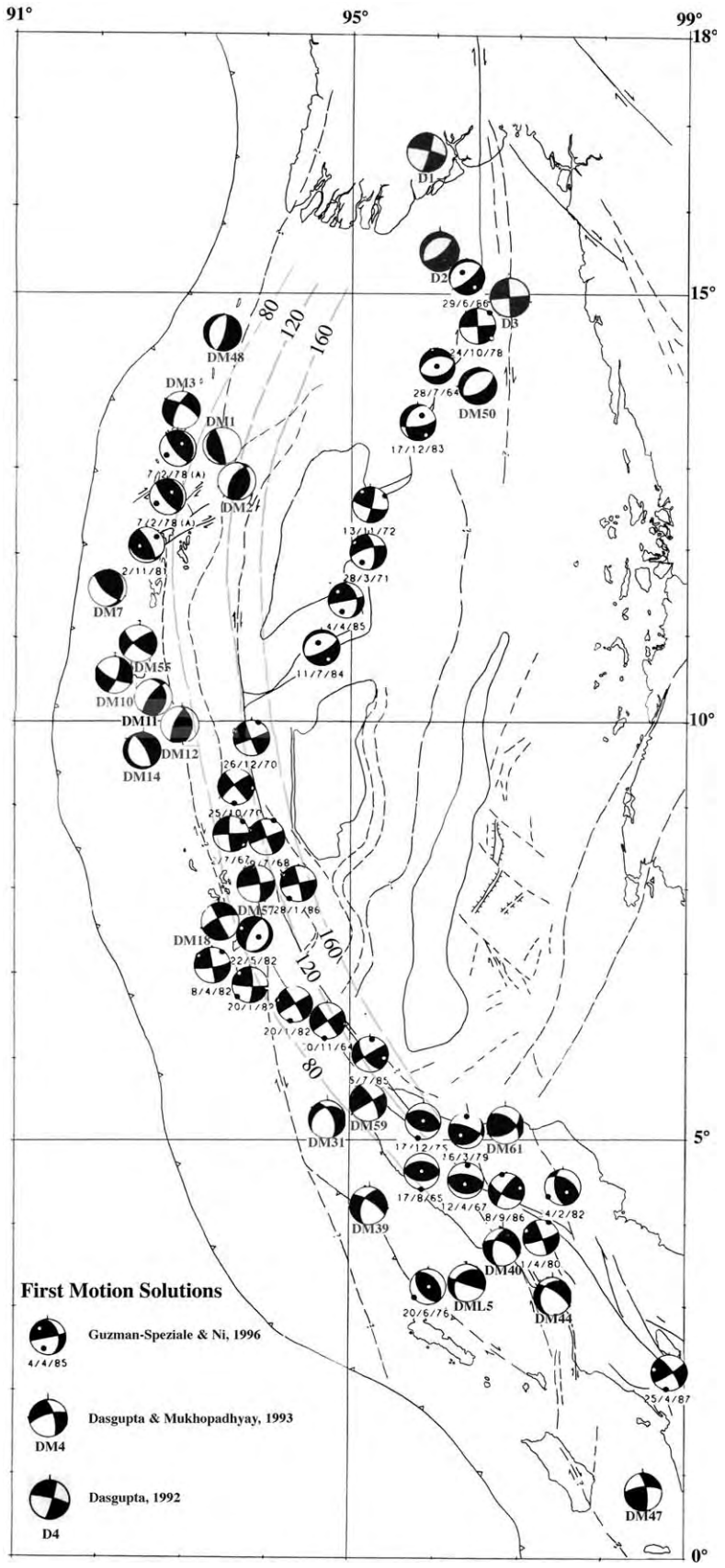

Fig. 6. Earthquake first motions solutions from the upper plate, from Guzmán–Speziale and Ni (1996) and Dasgupta (1992). Depth to Benioff, from Guzmán-Speziale and Ni (1996). Overlain on partial tectonic map.

the literature with excellent descriptions, analyses and interpretations. The following discussion is based in part on that newer paper.

Geologists from the Oil and Natural Gas Commission (ONGC) continued using the older GSI system of stratigraphy for their drilling and seismic work, with approximately the same units, with some of the original Oldham names for the formations. See, for example, Chatterjee (1967), Roy (1983, 1986), Misra and Roy (1984) and others. Ananthanarayanan et al. (1981) correlated the seismic, drilling and outcrop stratigraphy, by designating Seismic Sequences correlating with the formations. Subdivision of the Archipelago Group has been proposed by a series of papers by Srinivasan (see, for example, Srinivasan and Azmi (1979) and Srinivasan (1979, 1986)).

The generalized stratigraphy of the Andaman–Nicobar Ridge is shown in Table 1, with both the newer and older (in italics) formation and group names. The notations 'M Seismic Horizon?' and 'P Seismic Horizon?' in the right hand column refer to seismic horizons identified in the Bengal Fan sedimentary section, described in Curray et al. (2003).

In evaluating this stratigraphic column, it should be kept in mind that all observations have been made on either drill cores or cuttings or on outcrops of an accretionary complex, described by many of the authors as melange. The outcrops are furthermore only on the exposed island sections, much of which is described as humid jungle. Thus, the sections may be incompletely represented, and some of the rocks sampled in drilling do not crop out anywhere on land. And certainly, the facies shown in seismic reflection records from low on the western slope of the ridge do not crop out on land.

The final difficulty in attempting a general description of the stratigraphy and environments of deposition, the most difficult to reconcile, is very different interpretations of the environments of deposition. For example, the sedimentary rocks of the Archipelago Series have been interpreted by many to have been deposited mainly in shallow marine conditions, while others, including M.S. Srinivasan, of

Table 1
Stratigraphy of the Andaman–Nicobar Ridge

Age	Lithostratigraphic Units		Lithology	Facies	Seismic Units
Pleistocene 0 - 1.95 Ma	Nicobar Series	Shampenian	Shell limestone	Upper bathyal to shelf, to beach in Holocene, ca. 500 to 0 m or shallow marine?	SS 4
Late Pliocene 3.7 - 1.95 Ma		Taipian	Silty mudstone, limestone	Middle bathyal, ca. 500 - 2500 m or shallow marine?	SS 3
Early Pliocene 5-3.7 Ma		Sawaian	Mudstone, silty-mudstone, limestone	Lower bathyal to abyssal, ca. 2500 - 4000 m or shallow marine?	
Late Miocene 10 - 5 Ma	Archipelago Series	Neillian	Mudstone, silty-mudstone, limestone	Middle to lower bathyal, ca. 500 - 3500 m or shallow marine?	M Seismic Horizon?
Middle Miocene 16 - 10 Ma		Havelockian	Mudstone, silty-mudstone, limestone	Lower bathyal, ca. 2500 - 3000m or shallow marine?	
		Ongeian	Mudstone, limestone	Lower bathyal, ca. 2500 - 3000 m or shallow marine?	SS 2
		Inglisian	Creamish yellow calcareous chalk and marl	Lower bathyal, ca. 2500 - 3800 m or shallow marine?	
Early Miocene 25 - 16 Ma		Jarawaian	Creamish yellow calcareous chalk and limestone	Lower bathyal, ca. 3000 m or shallow marine?	
		Andamanian	Grey sandy limestone, white siliceous chalk and silt	Middle bathyal, ca. 500 - 3000 m or shallow marine?	
Upper Eocene to Oligocene ca. 45 - 25 Ma	Andaman Flysch Group *(Port Blair Group)*		Graded beds of sandstone and shale, with mainly southerly-directed flow.	Bengal Fan turbidites with some slope basin deposits	
Upper Cretaceous to Middle/Upper Eocene ca. 70 - 45 Ma	Mithakhari Group *(Baratang and Port Meadow Groups)*	Namunagarh Formation	Conglomerate, sandstone, siltstone, limestone and shale, grading upward into Andaman Flysch.	Small isolated trench-slope basins to paralic	SS 1
		Lipa Black Shale	Dark gray to black splintery shale, with local gypsum, pyrite, coal and mud cracks.	Shallow to sub-aerial	P Seismic Horizon?
Mesozoic to Eocene?	Ophiolite		Pillow basalts, serpentinites, ultramafic rocks, associated with radiolarian cherts and other sedimentary rocks.	Open ocean ophiolites	P Seismic Horizon?
Proterozoic ?	Older Sediments		Tectonic slices of deformed continental metamorphic rocks.	Fragments from pre-subduction continental margin	

Banaras Hindu University, interpret some of the same rocks as products of deposition in deep water (see Table 1). It would not be unreasonable, in view of the nature of the sampling, to conclude that both are present. For example, geologists who sampled the subaerially exposed sections of Archipelago rocks would have seen mainly the shallow water facies. These different facies should perhaps have been given different formation names, but they were not.

All of the rocks are the products of a subduction zone region. Possible environments of accumulation include the open ocean floor, the trench, slope basins on the landward slope of the trench and the top of an outer arc ridge. In addition, some of the older deposits could have originated on a pre-subduction passive continental margin, and olistostromes are common because the slopes above subduction zones are frequently steep and are disturbed by earthquakes. The consensus opinions of the environments and ages of the units are listed in Table 1.

Composites of line drawings of seismic reflection lines of portions of the outer arc ridge distributed southward down the Andaman–Nicobar Ridge from offshore Myanmar to northern Sumatra are illustrated in Figs. 8a–d. Tracks of seismic reflection records in the line drawings are shown in Fig. 7. Most of these sections do not cross the entire ridge of the Andaman and Nicobar Islands; they mainly show the landward trench slope from the floor of the Bay of Bengal to the top of the slope offshore from the islands. The principle passes through the ridge between the islands (Figs. 2, 4 and 7) are the 'Great Channel' north of Sumatra at about 6–7°N, the 'Ten Degree Channel' and 'Preparis Channels North and South', which lie south of the southwest tip of Myanmar. Several sections have been adapted from Roy (1983, 1992) and Roy and Chopra (1987).

Many of the sections clearly show folding of the sea floor Bengal Fan sediments, increasing from north to south, caused by convergence of the Australian (or Indian) Plate with the accretionary prism, especially in Fig. 8a, b and d in the central and southern parts of the area. The direction of plate convergence is much more oblique in the northern sector, Fig. 8a, and in fact is almost entirely transverse or strike slip. Where the direction of convergence is less oblique, sediments of the fan are wrinkled up into folds as they approach the base of the accretionary prism. These folds are then uplifted and progressively underthrust by new folds forming at the base of the slope. The folds form slope basins, some of which appear to be tilted landward (e.g. T 24–25. Fig. 8a; and T 55–56 and T 57–58, Fig. 8b). Eastward tilting of Car Nicobar has also been reported (Tipper, 1911).

Sections T 22–23 and T 24–25 (Fig. 8a) are adjacent to the location of a dredge sample, C-29, collected on our first cruise to the area on Circe Expedition in 1968. Frances Parker (personal communication, 1968) determined by micropaleontology that the shales in the sample are Miocene in age and of deep-water origin. This, stratigraphically, would be in the Archipelago Series. Younger rocks are being thrust into the slope below the level of this sample.

Several of the sections and parts of the area have mid-level plateaus, especially in the northern sector (Figs. 8a and b). The significance is not clear, but could possibly represent a change in rate or direction of convergence at some time in the Neogene.

The sections that cross over the top of the ridge are T 36–37,C–F–G in Fig. 8a, and all of the sections in Fig. 8c and d. Section T 36–37, C–F–G shows only a suggestion of folds over the ridge and eastward dips into the forearc basin. Sections Roy, S.K., Roy, T.K.-9, Roy and Chopra in Fig. 8c and Roy, T.K.-16 in Fig. 8d were interpreted to show eastward-dipping reverse or thrust faults all across the ridge and into the forearc basin lying to the east. In addition, they show the Neogene section, the Archipelago Series, both on the top of the ridge and starting westward down the landward slope of the trench. These sedimentary rocks were apparently deposited both in a shallow environment on top of the ridge and as deeper facies of the slope and slope basins, explaining the variation in interpretations of environment already mentioned.

Section Roy and Chopra in Fig. 8c and Sections M 8–9 and E 42–43 in Fig. 8d show the West Andaman Fault (WAF), which has also been called the Invisible Bank Fault. Sections AND-1 and Roy and Chopra in Fig. 8c and T 5–7 in Fig. 8d show the Eastern Margin Fault (EMF).

The 'Older Sediments', Table 1, are perhaps fragments derived from rocks of the continental margin that existed prior to the initiation of subduction in this sector of southern Asia. Offshore, ophiolites, i.e. ocean floor basalts and the associated pelagic sediments, formed as the floor of the Tethys Sea that lay between India and Asia. I believe that subduction along this margin started in the Cretaceous with the separation of India from its former Gondwana neighbors. The Lipa formation of shallow water to paralic sediments may have been deposited on the pre-subduction continental margin. The Namunagarh sediments appear to have been deposited in a range of environments that range from paralic to deeper trench slope basins.

Most authors agree that the Andaman Flysch or Port Blair Formation sandstones and shales are turbidities. We have interpreted them as sediments of the Bengal Fan (Curray et al., 1979; and subsequent papers). Newer work by Pal et al. (2003), however, attributes the Andaman Flysch mainly to a forearc basin environment, barred from deposition of turbidities from the Bengal Fan by the outer arc ridge. They suggest the possibility of the Irrawaddy (Ayeyarwady) Delta as a source of these sediments. They have described outcrops of Andaman Flysch on both sides of the top of the Andaman Islands in approximately the locations of some of the sections of Fig. 8c and d. To be forearc sediments from Myanmar, long distance transport down the axis of a forearc basin would be required. Also, if they are forearc deposits, the source of this thick (3000 m?) section could hardly have been from islands on the outer arc

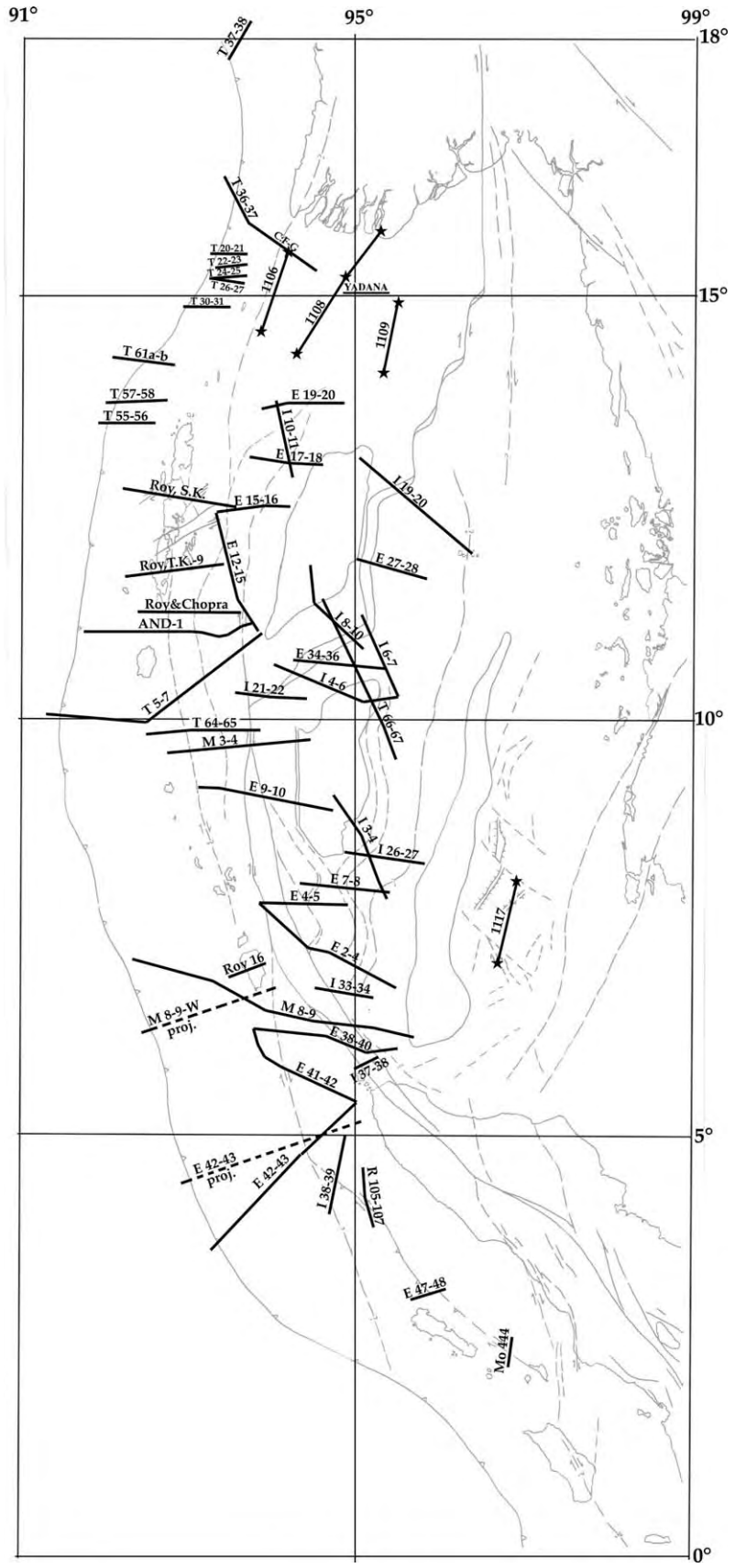

Fig. 7. Locations of line drawings of seismic reflection records in Figs. 8, 10, 11, and 12. Approximate location is shown for the Yadana line (Fig. 9), from Win Maw and Myint Kyi (1998).

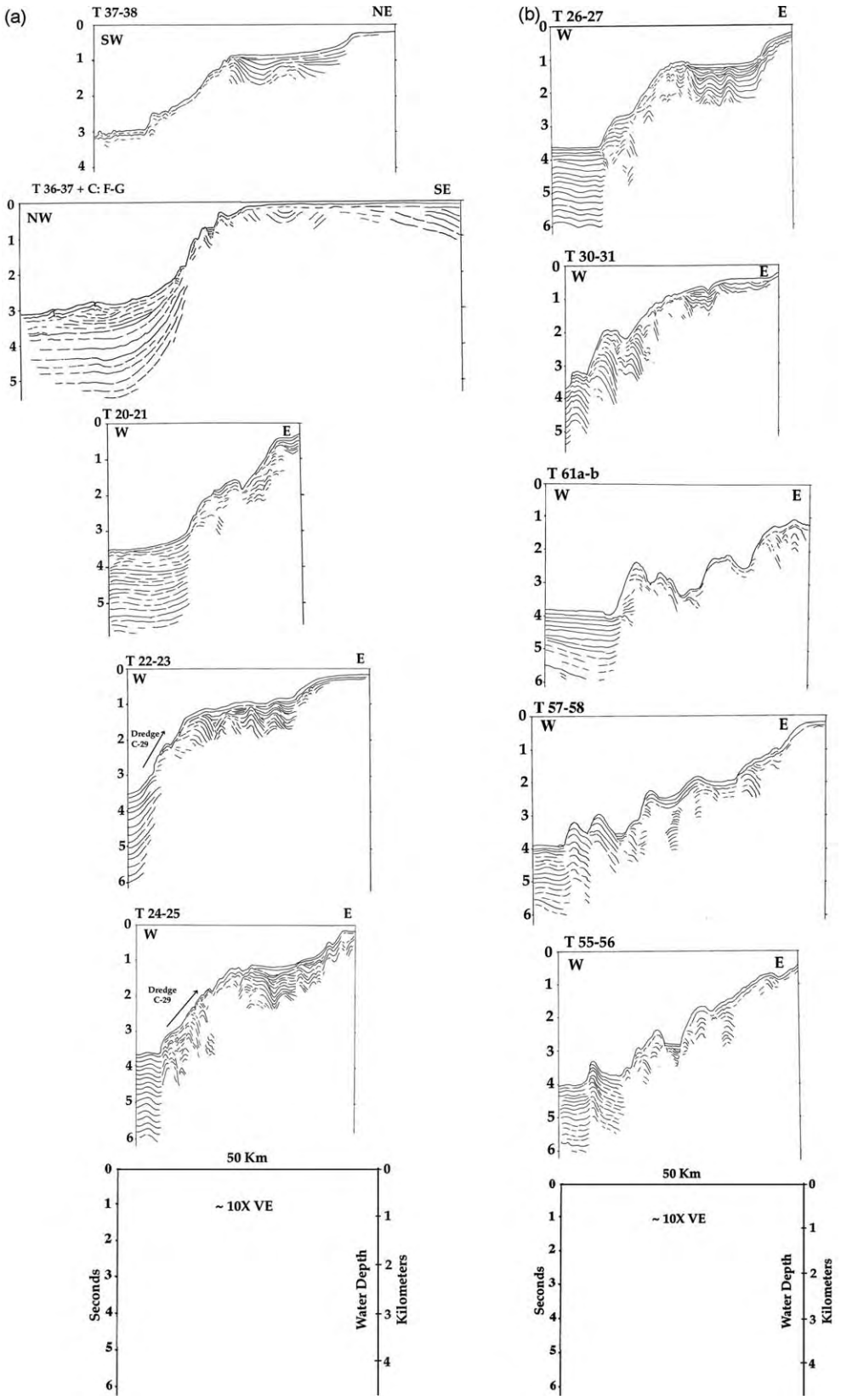

Fig. 8. (a–d) Line drawings of seismic reflection records of the Andaman–Nicobar Ridge and the Bay of Bengal continental slope. The base of the slope is within the Sunda Trench from T 30–31 southward. North of this point, about 15°N, the trench is filled with sediments of the Bengal Fan and from Myanmar. See Fig. 7 for locations. Sections M 8–9W and E 42–43 are compressed as if projected to lines normal to the structural trends, shown in Fig. 7 as dashed lines, to illustrate changes in width of the outer arc ridge.

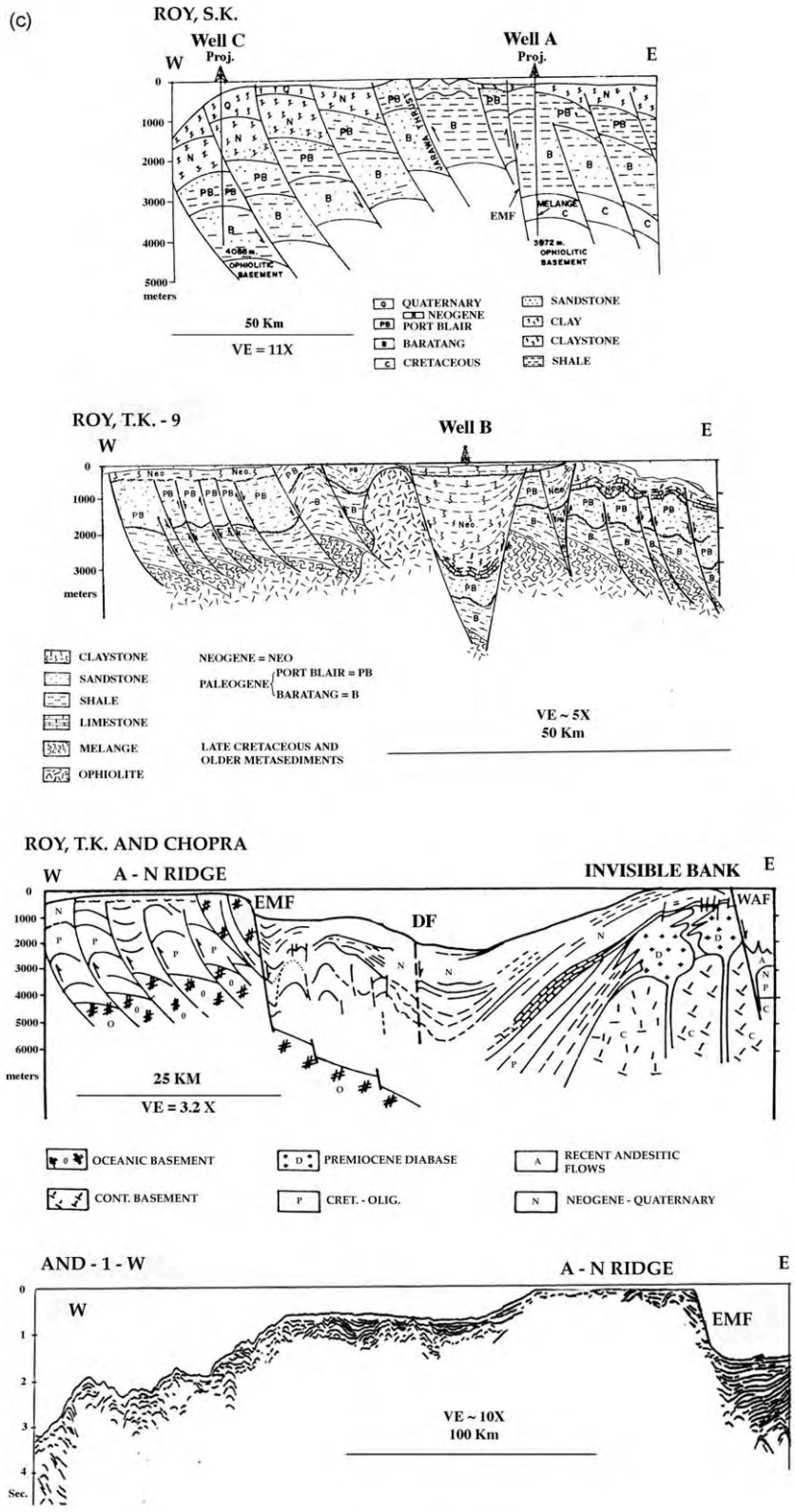

Fig. 8 (*continued*)

ridge that are very limited in size. The seismic sections of Fig. 8, moreover, show undeniable evidence of folding and uplift of Bengal Fan sediments at the base of this slope, so the interpretation that the Andaman Flysch is at least mainly Bengal Fan sediment will be used in this paper. Future provenance work of comparing Oligocene Andaman Flysch with Oligocene samples not yet recovered by drilling in the Bay of Bengal may resolve this problem.

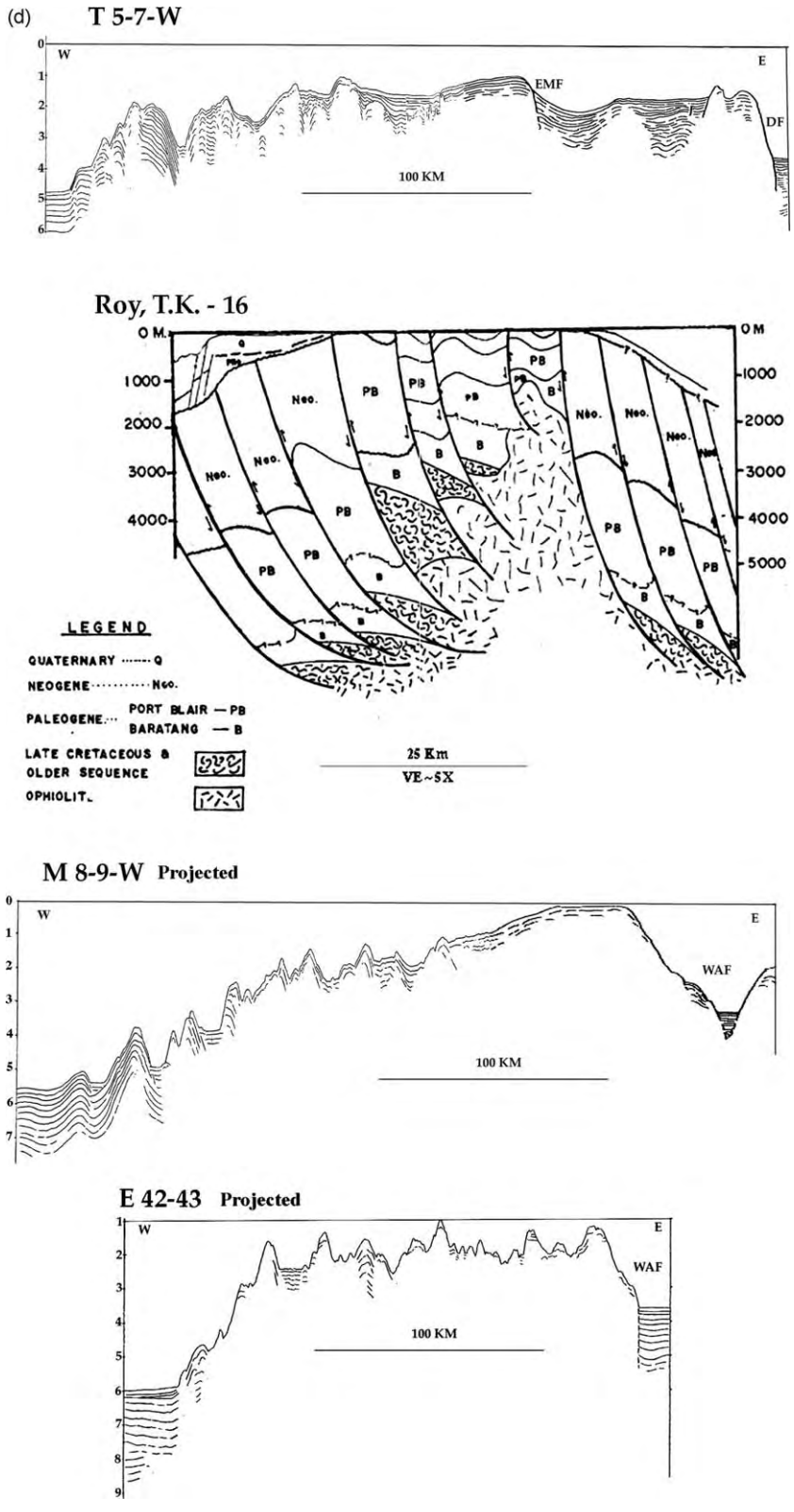

Fig. 8 (*continued*)

The Archipelago Series was interpreted as shallow marine, with water depths from 0 to 25 m by Roy (1983), and as deep water to neritic or outer neritic by Srinivasan (1986). In Table 1, the environmental interpretations of Srinivasan (1986) are shown first, followed by the alternative option. I conclude that the major part of the sedimentary rock is probably the facies as interpreted by Srinivasan, but suggest that shallow facies are also present,

considering the sampling problems discussed previously and the complexities of simultaneous deposition of sediments both on top of a accretionary prism and farther on down the slope and in slope basins.

The outer arc ridge is characterized by a strong negative free air gravity anomaly (Fig. 5), indicating an excess of relatively low-density sediment in the accretionary complex. Invisible Bank (~11°N, 93°E), part of the forearc basin, on the other hand, is a rather high positive anomaly (Fig. 5) because, as has been shown by Roy and Chopra (1987) (Fig. 8c), it is underlain by uplifted volcanics and/or intrusives. This may also explain the high positive anomaly at about 8°N, 93°E, east of Camorta Island (Fig. 4).

The first motion solutions for earthquakes on the upper Southeast Asia or Burma Plate within the Andaman–Nicobar Ridge (Fig. 6) are generally easily explained. Some, for example, suggest normal or reverse faults with a strike of about SE–ESE, as one might expect in this environment. A few suggest right-lateral strike-slip faulting approximately parallel to the arc and parallel to the similar solutions along the trend of the West Andaman Fault which lies within the central part of the Andaman Sea. Some of these may indicate continued strike-slip activity along the Eastern Margin or Diligent Faults, the boundary between the outer arc ridge and the central basin. A few others show 'nodal planes oriented NNW–SSE characterizing the deformation in the forearc region. The depths of these events suggest that they were located within the upper plate…and suggests that the sedimentary forearc is being deformed by the convergence [between the Indian and Southeast Asian plates]' (Guzmán-Speziale and Ni, 1996, p. 72). Normal faulting is occurring in the Central Andaman Basin and in the area of short spreading axes at about 14°N; and right-lateral strike-slip faulting is occurring along the transform segments east of Alcock Rise.

What is the nature of the crust underlying the outer arc ridge? Kieckhefer et al. (1981) concluded that the outer arc ridge off Sumatra is probably underlain by melange, including ultramafic rocks, or by continental crust. In Myanmar, in contrast, Mitchell (1989), Acharyya (1994, 1998) and Hutchison (1989) all conclude that the Indoburman Ranges are underlain by continental crust.

I have one reversed seismic refraction line over the Andaman–Nicobar Ridge, Line 1106, offshore from the Indoburman Ranges (Figs. 3, 7 and 9a). The section for Line 1106 had records from six buoy receivers. The thin water layer is ignored in these sections. A thick sedimentary rock section showed a range of velocities between about 2.8 and 3.3 km/s, but most of the solutions were not very good because of rather steep southerly dips, as shown in the reflection records. Some of this sedimentary section may be deltaic sediment from Ayeyarwady (Irrawaddy) River and other rivers, and some may be melange of uplifted sedimentary rocks. The variation in velocities in this thick layer shows somewhat more of the higher velocities of 3.5 km/s in the north, with the section of lower velocity 2.8 km/s thickening toward the continental slope to the south. The basement velocities of 6.3–6.9 km/s are suggestive of oceanic crust.

4. The central basin

This is the part of the Andaman Sea region where the action has occurred during the Neogene, where the strike-slip sliver faulting and transtensional extension have occurred. The major tectonic parts of this province are the forearc basin, the magmatic arc and the backarc basin. The forearc Basin in this discussion includes West Basin, Invisible Bank, and the other banks farther to the south. The magmatic arc discussion will be limited to the few known or suspected volcanic features in the Andaman Sea, the known volcanic line in Myanmar and the shelf lying in between. The backarc region will include Alcock and Sewell Rises, East Basin, the shelf and basins to the north and east and the small basin between the rises, the Central Andaman Basin (Fig. 4).

4.1. The forearc basin: West Basin, Invisible Bank and West Sewell Ridge

The dividing line between the outer arc ridge and the forearc basin is the Diligent Fault (DF) in the central and northern parts of the area (Fig. 4). It is shown in some of the sections in Fig. 8c and d, as are the Eastern Margin Fault (EMF; Roy, 1983) and the West Andaman Fault (WAF; Curray et al., 1979). The Eastern Margin and Diligent Faults are apparently normal faults, although there may both at times in the past and today possibly have been some dextral strike-slip motion (Fig. 6). No seismicity north of about 9° can convincingly be associated with these faults, but at about 7°N earthquake DM 18 (Dasgupta and Mukhopadhyay, 1993) and earthquakes 8/4/82 and 20/1/82 (Guzmán-Speziale and Ni, 1996) could possibly lie along these faults (Fig. 6). South of there the right-lateral strike-slip motions are probably associated with the West Andaman Fault. North of the Andaman Islands the Diligent Fault is shown questionably connected with the Kabaw Fault of Myanmar (Hla Maung, 1987) to form the eastern margin of the Indoburman Ranges. A splay may be the Cocos Fault (Fig. 4 and sections E 19–20 and I 10–11, Fig. 8a). To the south, the Diligent Fault can be traced questionably to the Nicobar Islands (Chatterjee, 1984). Off Northern Sumatra, the back of the outer arc ridge lies along the trace of the West Andaman Fault, behind Tuba Ridge, and in line with what has been called the Mentawei Fault (Diament et al., 1992) behind the islands off Sumatra. In this paper, the name West Andaman Fault will be applied to this fault to as far south as the apparent offset by the Battee Fault at 2°N, following the earlier definition (Curray et al., 1979; Curray, 1989, 1991). The name Mentawei Fault will be restricted to southeast of the Battee Fault.

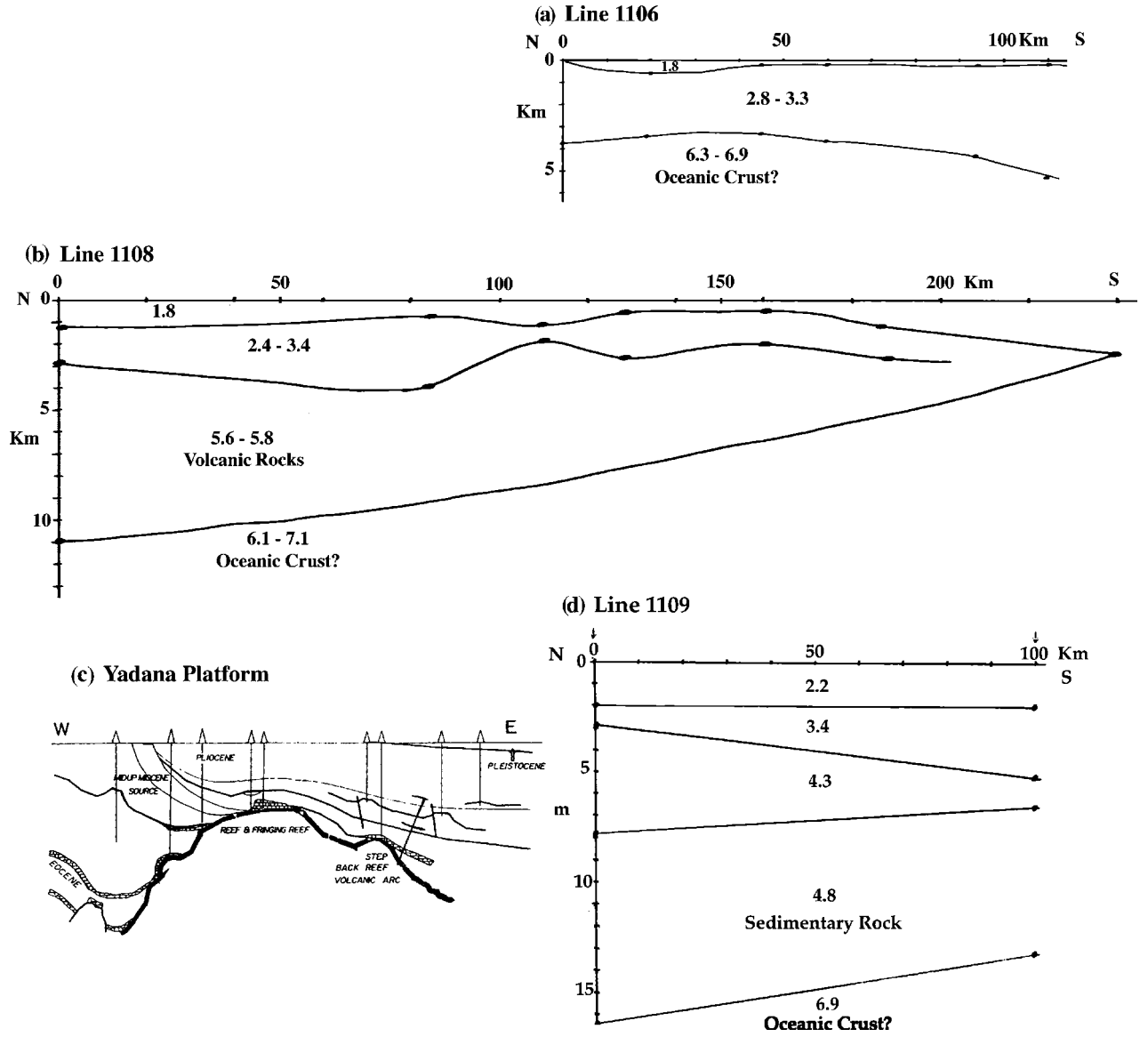

Fig. 9. Simplified plots of reversed refraction lines on the northern shelf off Myanmar (Figs. 3 and 7). Buoy stations indicated by small arrows. Buoys at ends of lines and some intermediate buoys and were anchored; other buoys were expendable. Northern station in line 1108 was land station with 24 channels (Ama Village, Fig. 4). The water layer, less than 200 m, is ignored in the sections. Line drawing of the Yadana line (Fig. 9c) is adapted from Win Maw and Myint Kyi (1998). The scales are unknown.

West Basin is a gently south-sloping plain of sediment from the continental slope at the north ponded against cuestas of the Cocos Fault, the volcanic seamounts of Barren and Narcondam Islands, some apparently volcanic seamounts and the northwest side of Alcock Rise. Unfortunately, I have no refraction data using explosives to establish the sediment thickness in this basin, but an airgun refraction line shows a velocity of only 2.14 km/s at a depth of 1.51 km beneath the sea floor. This is suggestive of young Tertiary sediment and a rather thick total section.

Invisible Bank is a cuesta formed by the West Andaman Fault (Figs. 4, 8c and d and 10). Fig. 10a–c shows section line drawings aligned along the WAF proceeding from north to south. It is not apparent where the WAF is in the northern section, E 19–20, and its northern end may be south of there. These two northern sections do, however, show a different cuesta behind a fault that I have named the Cocos Fault. The possible significance of this cuesta is discussed in Section 6.

Invisible Bank is a distinct cuesta formed by the WAF as far south as E 9–10, Fig. 10b at about 9°N. South of there the WAF forms the back of the outer arc ridge and the outside flank of the forearc basin. See M 8–9, Fig. 10b and the other sections farther south and east. Southeast of the bend in the WAF at about 4.5°N the right-lateral motion of the WAF has a component of convergence, that has formed Tuba Ridge (Figs. 4 and 10c). It cannot be definitively determined from the reflection records whether this convergence is still occurring today or is older.

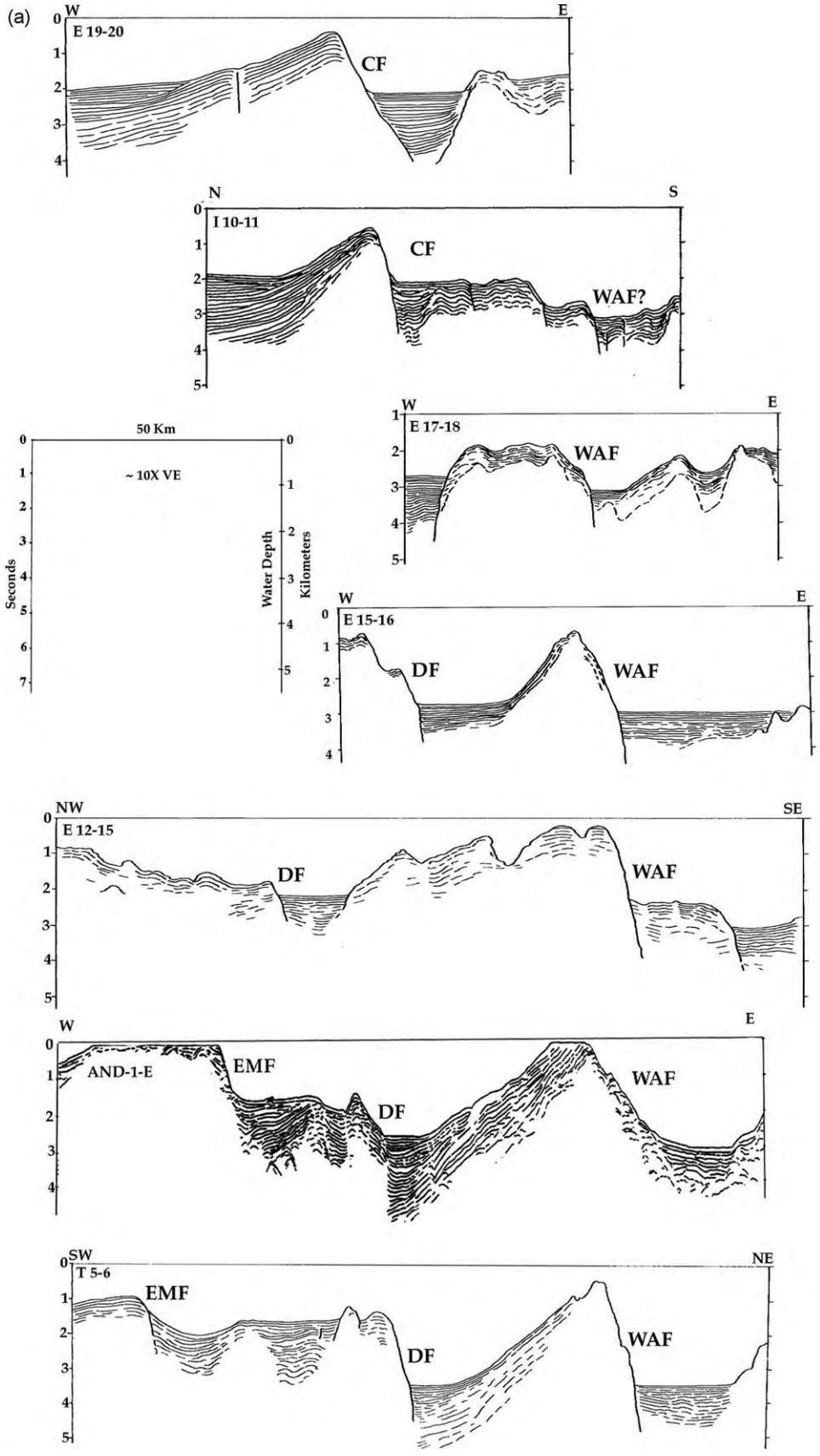

Fig. 10. (a–c) Line drawings of seismic reflection records aligned along the trace of the West Andaman Fault (WAF). See Fig. 7 for locations and caption Fig. 4 for abbreviations.

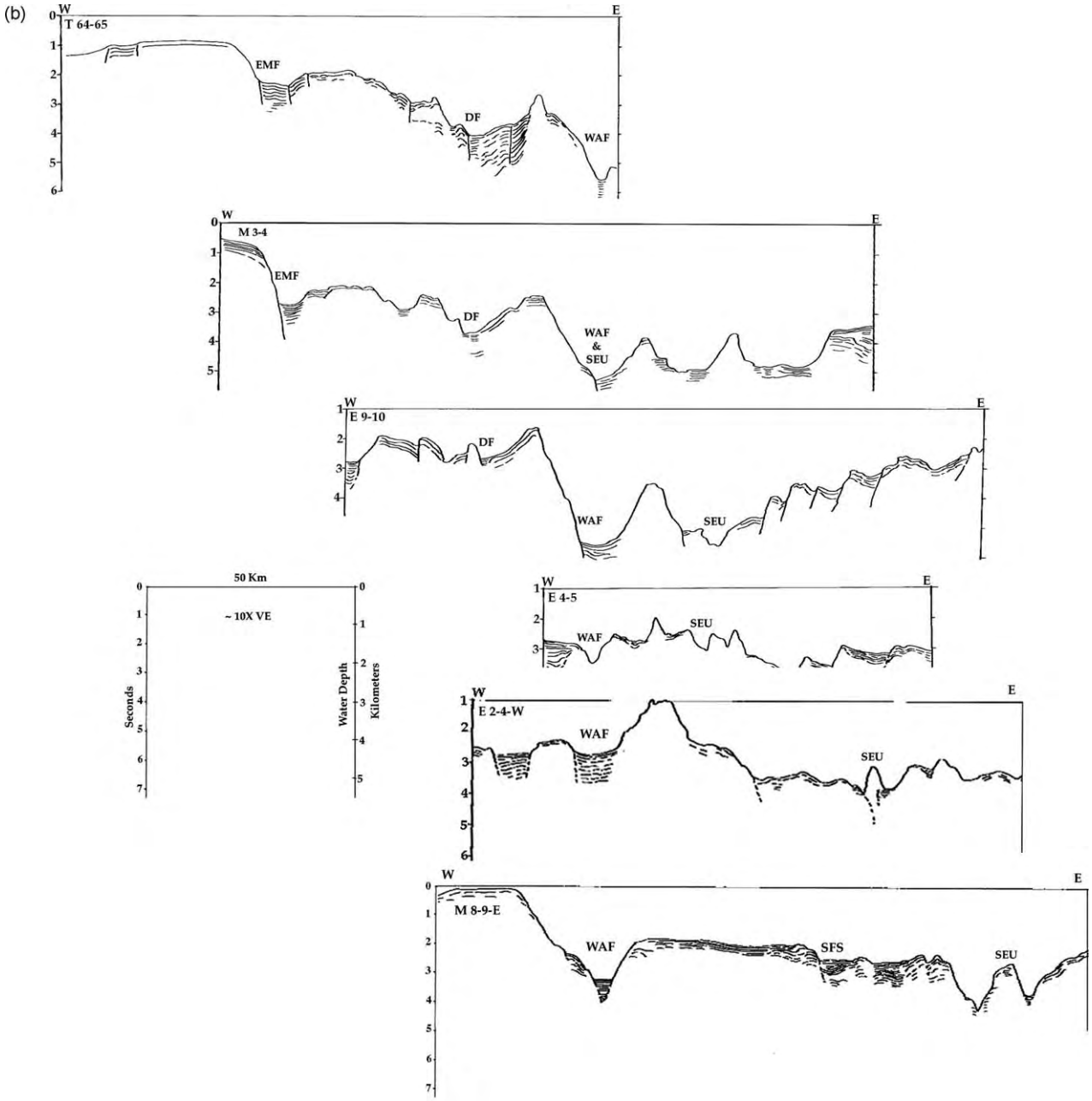

Fig. 10 (*continued*)

Roy and Chopra (1987) report that drilling near the crest of Invisible Ridge encountered thick lava flows below 1100 m of middle Miocene sedimentary rocks. Frerichs (1971) reports that dredge sample ***8*** (~9°N, Fig. 4) contained radiolarian shale of post-early late Miocene age, ~10 my, which was uplifted about 2000 m since deposition. Dredge sample ***12*** (~11.5°N) was late lower Miocene calcarenite and calcilutite, ~17 my, uplifted about 400 m since deposition; and dredge sample ***13*** (~12°N) was late upper Miocene, ~6 my, uplifted more than 500 m. These sediments are probably forearc basin sediments, and the West Andaman Fault probably formed the cuesta within the past 6 my.

The nature and rocks of the somewhat discontinuous West Sewell Ridge (WSR, Fig. 4) are not known. The North Sumatra Ridge (NSR, Fig. 4) is probably underlain by the continental crust of Sumatra.

4.2. The volcanic arc

The volcanic arc of the Andaman Sea lies between the active volcanic arc on Java and Sumatra and the extinct or dormant arc in Myanmar. The last volcanic activity of Mount Popa, Myanmar, ~21°N, is believed to have been sub-Recent (Chhibber, 1934; Bender, 1983; Stephenson and Marshall, 1984). Chhibber reported local legend of an

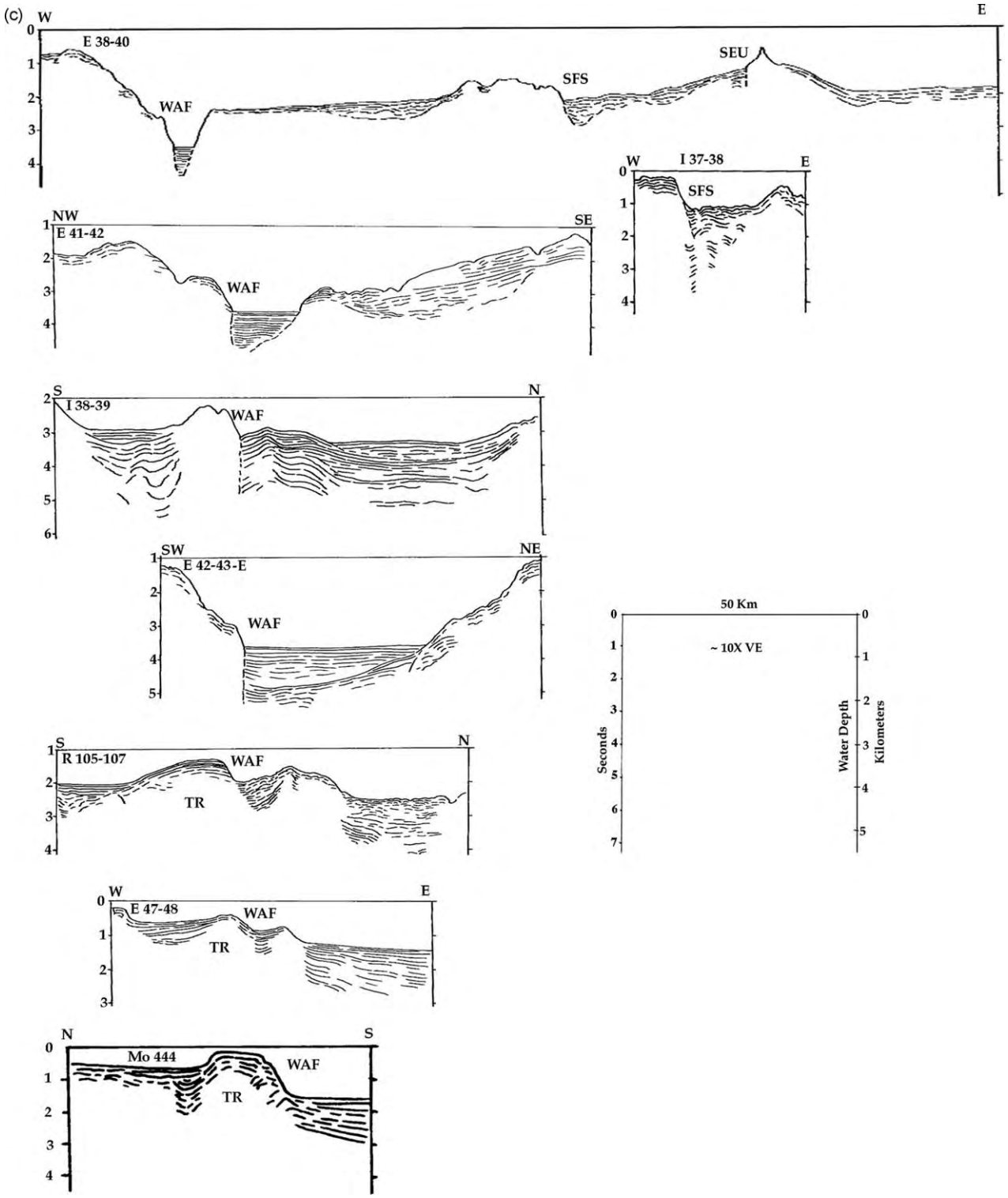

Fig. 10 (*continued*)

eruption about 2500 years ago, but could find no firm evidence. The other volcanic centers along this line in central Myanmar are also probably extinct or dormant. Stephenson and Marshall (1984) describe the volcanics at Popa as high K calcalkaline latites, rhyodacites and ignimbrites overlain by basalt and basaltic andesite.

The reversed refraction Line 1108 (Figs. 3, 7 and 9b) is in line with the volcanic arc between Narcondam and Barren volcanic islands and the volcanic area of Mount Popa near 21°N in Myanmar. The thin water layer is ignored in the sections. The thick section of velocity 5.6–5.8 km/s is interpreted as volcanic rock, overlying probable oceanic

crust of 6.1–7.1 km/s. Note that the northern end of the line lies at Ama Village on the Myanmar coastline.

Two volcanic islands (Bhattacharya et al., 1993) lie in the northern Andaman Sea (Fig. 4), Barren Island, which is still active, and Narcondam Island, which may be dormant. Barren showed some activity as recently as 1994. Andesite, dacite and basalt have been reported. Other sea floor features that may be volcanic in origin are shown in Fig. 4. The next definitely volcanic features are Wey and Brueh Islands off the north tip of Sumatra, approximately 400 km farther south, approximately the total amount of opening suggested for the entire Andaman Sea in Sections 6 and 7.

4.3. Backarc basin: Alcock and Sewell Rises, Central Andaman Basin and East Basin

The backarc region of the Andaman Sea (Fig. 4), a part of the central basin of the Andaman Basin, includes Alcock and Sewell Rises, the Central Andaman Basin between the two rises, East Basin and some other smaller topographic features of unknown character. It also includes part of the present plate edge between the Burma platelet and the Eurasian or Southeast Asian plate (Figs. 10a–c) and it includes a segment of what I interpret as an abandoned plate edge (Fig. 11).

Alcock and Sewell Rises were named Alcock and Sewell Seamounts by Rodolfo (1969a). They were renamed Alcock and Sewell Rises in the GEBCO Gazetteer of Undersea Features Names in November 2003, and will be referred to by those names in this paper. Neither feature is well surveyed bathymetrically, and they are shown with somewhat generalized contours in Fig. 2. The margins adjoining the Central Andaman Basin and spreading axis, Fig. 4, are however well enough known to suggest their reassembly (Section 6 of this paper) into a single rise prior to opening of this small basin. Both rises show a suggestion of northeast–southwest trending top surface features, approximately parallel to the trend of the spreading axis in the basin. The western margins of both rises appear to be faults, which align with each other in a reassembly.

The northern end of Alcock Rise is uncertain, as indicated in Fig. 4. Line drawing of a multichannel reflection line is shown in Fig. 9c, adapted from Win Maw and Myint Kyi (1998). Unfortunately, neither the scales nor the exact location were indicated in the original paper, so the location indicated in Fig. 7 is only approximate. The line does, however, show a ridge that might represent the northern end of Alcock Rise, or the connection with the Bago Yoma, as discussed later in Section 6.3.

Rodolfo (1969a) describes rocks from dredge sample ***14*** in the northern part of Alcock Rise (~13°N, Fig. 4) as 'large tabular slabs of massive unaltered intergranular augite basalt'. Unfortunately, the samples from this dredge haul collected from R/V Pioneer in 1964 are lost, and cannot be located for further analysis and dating. In 1977, my colleagues and I sampled rocks in dredge haul ***17*** from an escarpment at 900–1250 m from the southern part of Alcock (~11.5°N, Fig. 4). J.W. Hawkins (personal communication, 1982) described the rocks as 'moderately fractionated tholeitic basalts'. In 1993, two samples were dated by K–Ar as 19.8 ± 0.7 and 20.5 ± 1.0 my by Geochron Laboratories, Cambridge, MA.

Refraction/reflection Line 1109 (Figs. 3, 7 and 9d) lies north of the axis of thickest sediment accumulation in the Andaman Sea, and has a sedimentary rock section of high velocity between 14 and over 16 km thick. The high velocities are similar to deeply buried high sediment velocities beneath the Bengal Fan (Curray et al., 2003). Another possibility is that this section is mixed well-lithified sediments and volcanics. The basement velocity of 6.9 km/s is probably oceanic crust. The section could possibly be even thicker farther to the east in the center of the Gulf of Mottama (formerly the Gulf of Martaban) (Fig. 4).

East Basin has a section of flat ponded sediment at least 4.6 km thick. I have one especially good refraction line where the 'Oc' symbol is shown at about 9°10′N in Fig. 4. Basement is definitely oceanic, with a velocity of 6.7 km/s. The layers beneath the sea floor in this side solution, weighted least squares fit layer solution are: a sediment layer of 1.8 km/s, 1.0 km thick; a sediment layer of 3.4 km/s, 3.6 km thick; a layer of probable volcanic rock of 5.8 km/s and 2.7 km thick; all overlying oceanic basement of 6.7 km/s velocity.

The edge of continental crust is shown in Fig. 4 as interpreted from all available lines of evidence: gravity, magnetics, seismic reflection and refraction data and bathymetry. It is at best an approximation. The lower continental slope above this line is marked with listric block faulting down to the west or NW, as suggested in Fig. 11, Section I 19–20 and Fig. 12, sections I 3–4, I 26–27, E 7–8, E 2–4 and I 33–34.

The sliver plate between the Sunda subduction zone on the west and the Sagaing Fault in Myanmar, a plate edge in the Andaman Sea and the Sumatra Fault System (SFS) on the east was named the Burma Plate by Curray et al. (1979), but has been given various other names by later workers. The present plate edge (Fig. 4) is the Sagaing Fault in Myanmar, passing into the system of short spreading axes and transform faults down to the longer spreading axis at about 11°N, then southward on the WAF, SEU and SFS into the SFS which runs the length of Sumatra to the Sunda Strait.

Locations of major earthquakes in Myanmar were plotted by Chhibber (1934) along the now-known trend of the Sagaing Fault. The fault (Fig. 13) was recognized as separate from the Shan Scarp Fault which forms the edge of the Shan Plateau by Dey (1968). Win Swe (1972, 1981) recognized right-lateral offsets at Sagaing, near Mandalay. Mitchell (1977) referred to this fault as the Hninzee–Sagaing Fault and attributed in excess of 300 km of offset to it. Curray et al. (1982) suggested that the total offset might be as much as 460 km. Ba Than Haq (personal communication, 1986) observed offset of a Permo-Triassic limestone

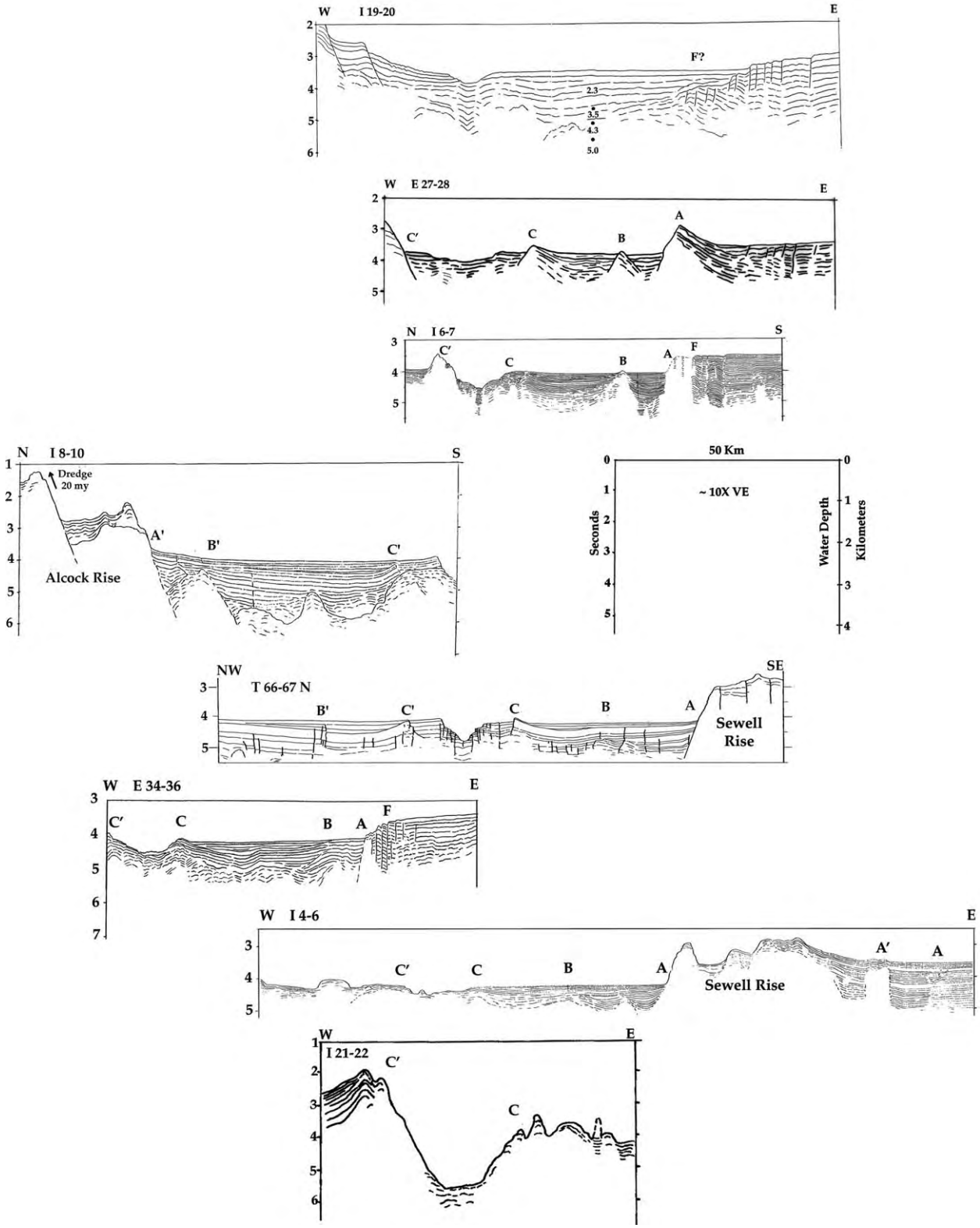

Fig. 11. Line drawings of seismic reflection records of the plate edge east of Alcock Rise and in the Central Andaman Basin.

of 444 km across the fault; and Hla Maung (1987) estimated between 425 and 460 km from river offsets. Another opinion was published by Myint Thein et al. (1981), stating that the Mayathein metamorphics 26 km north of Sagaing were continuous until late Oligocene or early Miocene and are now offset 203 km.

Guzmán-Speziale and Ni (1993) calculated rates of opening of the Central Andaman Basin and offset along

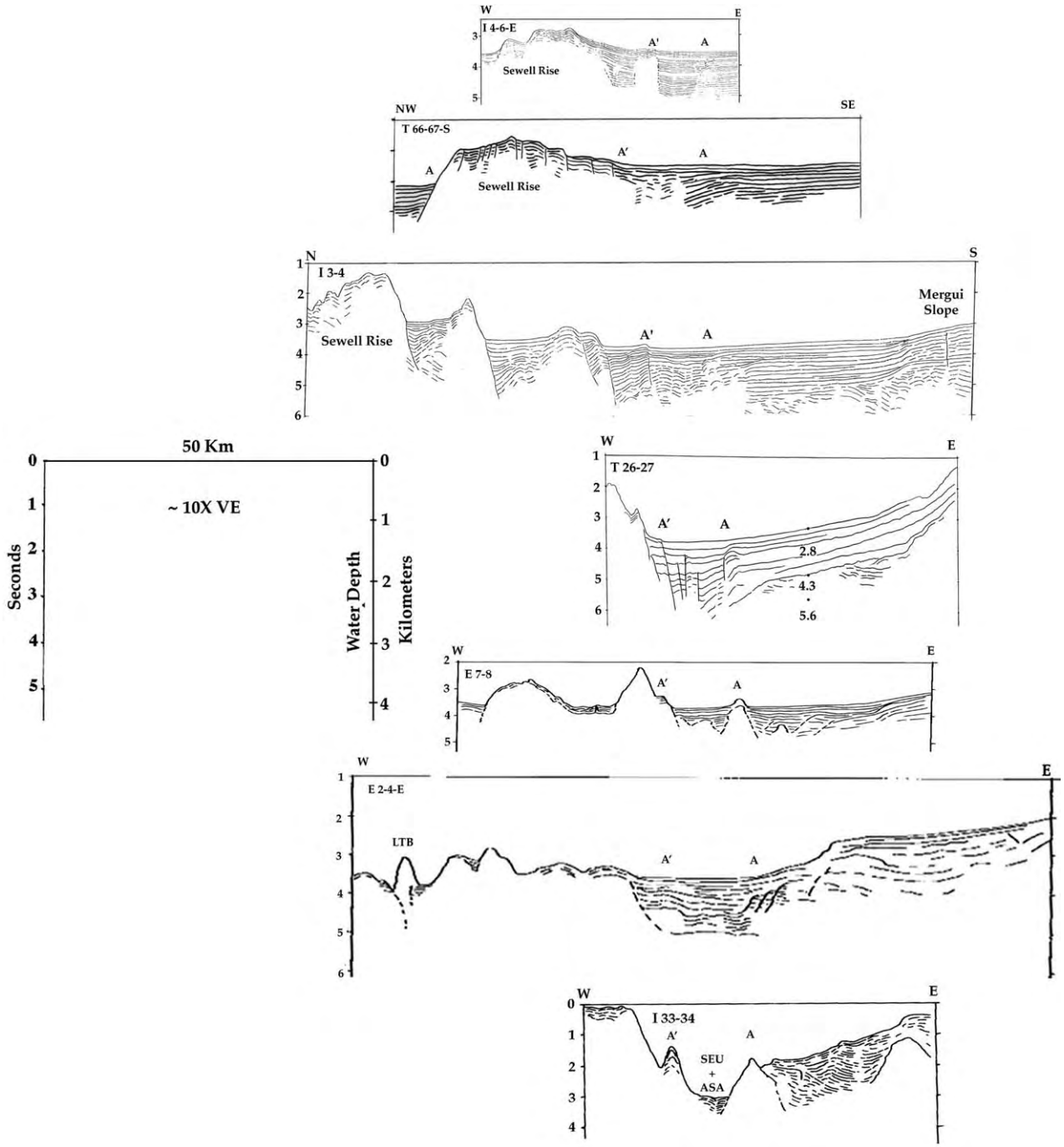

Fig. 12. Line drawings of seismic reflection records of the abandoned plate edge spreading axes and short segments of transform fault in the southern Andaman Sea east of Sewell Rise.

the Sagaing Fault from earthquake seismic moments. Using earthquakes from 1964 to 1986, they obtained rates of only 0.5 and 5 mm/yr, respectively. Using earthquakes back to 1908, they obtained a rate of 57 mm/yr for the Sagaing Fault. They suggested that opening of the Central Andaman Basin might be partly aseismic. Vigny et al. (2003) conducted field work in Myanmar and GPS surveys across the Sagaing Fault and Shan Scarp Fault zones and concluded that the Sagaing Fault motion today is <20 mm/yr of the total of 35 mm/yr of the India/Sundaland (Eurasia or Southeast Asia) strike-slip motion. The remainder of the motion is accommodated by distribution of deformation over a wide zone.

The Sagaing Fault appears to splay southward into two or three faults at about the point of intersection with the Three Pagodas Fault (TPF) at 17°N (Fig. 4). One of these trends may be the Shan Scarp Fault (SSF).

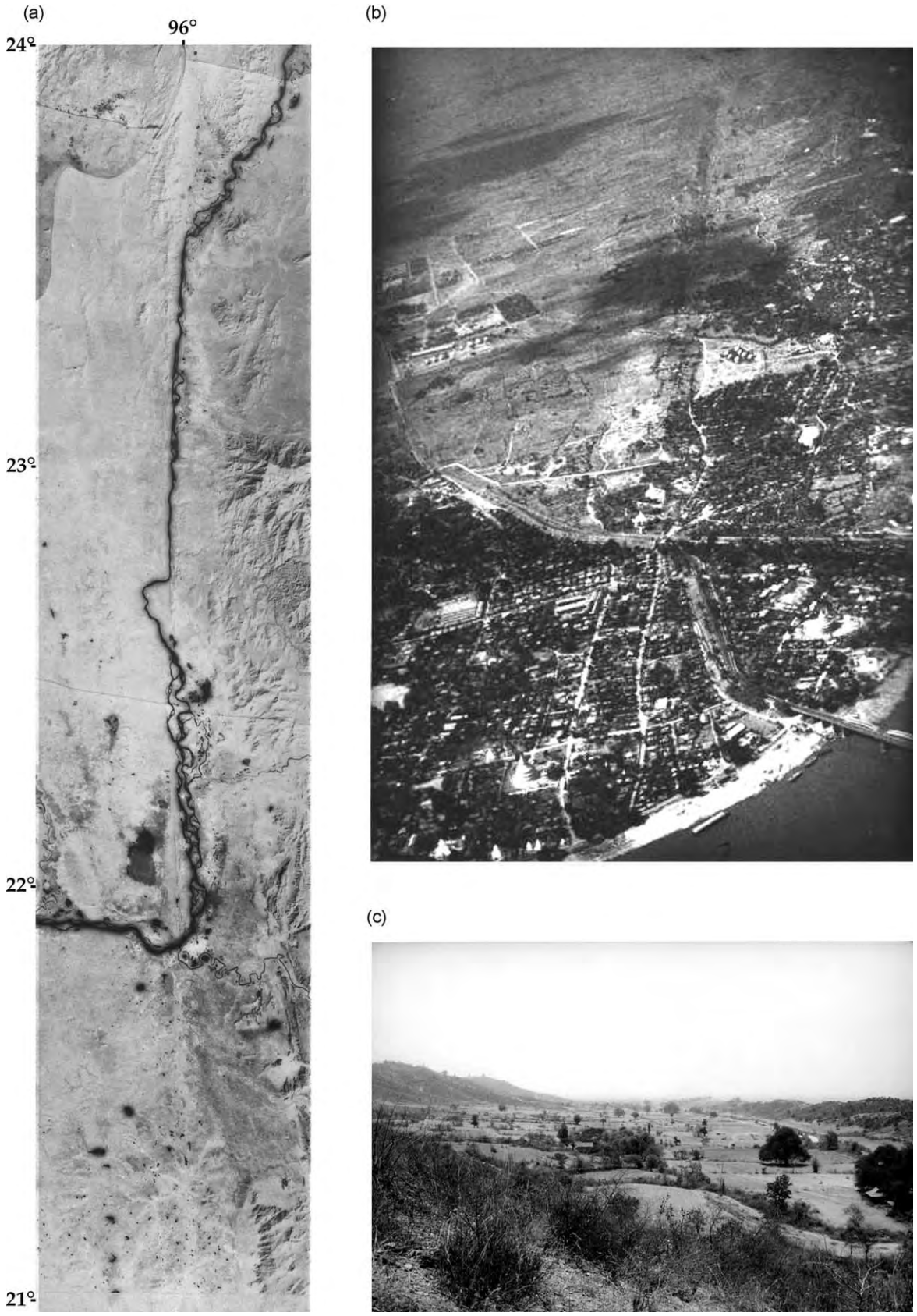

Fig. 13. Photographs of the Sagaing Fault. (a) Landsat photo mosaic. Ayeyawardy River joins the fault rift at 23°35′N and leaves it at 21°50′N at the town of Sagaing. (b) Low altitude oblique photo of Sagaing, the Sagaing Bridge and the fault rift. (c) Rift valley looking northward at Sagaing. Note temples on the ridge to the left.

A complex extensional fault system is seen in reflection surveys on the shelf. Fig. 4 shows an overly simplified pattern of short spreading axes and transform faults running off the continental slope into the Andaman Sea basin. This is based on seismicity (Fig. 6) as well as reflection evidence. The bathymetric and reflection record evidence is very good off the slope at the northernmost longer segment of spreading axis at about 13°N. Section I 19–20 (Fig. 11) shows a crossing of this spreading axis. This line shows the faulted eastern margin of Alcock Rise, it shows the present spreading axis, and it shows higher sediment velocities down to at least 2 km below the sea floor.

Section E 27–28 (Fig. 11) shows four upturned margins of the plate edge: C′, C, B and A. Edges C and C′ are arranged symmetrically outside of the present or youngest axis, as they are in other sections farther south and west. The older ridges, A and B are proportionately farther away from the present rift valley. These edges can be traced and correlated in the bathymetry and reflection records (Fig. 4) southward to the major NE–SW trending spreading axis in the Central Andaman Basin at 10.2–11°N (Fig. 11); and correlations of A and A′ are interpreted southward along the abandoned plate edge to as far as 7°N (Fig. 12).

These upturned edges were earlier interpreted as time lines in the opening of the central basin (Curray et al., 1979), and considered as indicating either episodic spreading or episodic deposition. We favored the latter explanation and suggested that a correlation should exist with fluctuations of sea level. See Section 6.

The plate edge delineated in Fig. 4, where it is a valley south of the continental slope, slopes continuously to the south and west to about 10°30′N and 94°25′E, indicating that during the last period of lowered sea level, turbidity currents flowed through this rift valley as a turbidity current channel until the river mouth supply had retreated too far across the shelf for much sediment to reach the canyon. Several other probable turbidity current channels are also indicated in Fig. 4 running down the slope to join this major channel. Thus, this valley is at the same time a rift valley of a spreading axis, in places a plate edge, which is mainly transform motion and a turbidity current channel. Again, analogous with the Bengal Fan, the valley below the submarine canyon cut into the Gulf of Mattama continental slope was filled during the decreased turbidity current activity of rising sea level. Just as in the Bengal Fan, the fan valleys farther down the fan are left open and inactive, and are relict conduits from the large turbidity currents of low stands of sea level.

The present rift valley in the Central Andaman Basin (Fig. 14) ranges from about 6 to almost 20 km in width and is typically 400–600 m deep. These are deeper and wider than fan valleys of the Bengal Fan, perhaps in part because of their dual role as spreading axes and in part because it is probably the only channel for all of the sediments coming from the combined Ayeyarwady (Irrawaddy), Sittoung (Sittang) and Thanlwin (Salween) Rivers.

It is not entirely clear why the former edges of the transform—spreading axis plate edge are upturned, but it is perhaps partly a subsidence effect and partly a result of natural levee deposition from the turbidity currents.

The oldest former plate edge delineated, F in sections I 6–7 and E 34–35, Fig. 11, and in Fig. 4, forms the western edge of the northern part of East Basin and the boundary between East Basin and the Central Andaman Basin. Typical crossings of F show a change of level of about 350–400 m. It lies very close to A, which appears to be the northwestern margin of Sewell Rise; A′ is the southeastern margin of Alcock Rise. If F represents the time of initiation of spreading in the Central Andaman Basin (CAB), it might be present in some of the faulting above the level of the CAB on the flanks of the rises and in some of the faulting on the east side of Alcock Rise. It may not represent much of a time hiatus. Difference in level across F is interpreted as differential subsidence of the younger sea floor.

Sediment thicknesses in the Central Andaman Basin range from essentially zero in the southwestern part of the basin to almost two km in the outer edges of the northeastern end near the bend in the plate edge to about

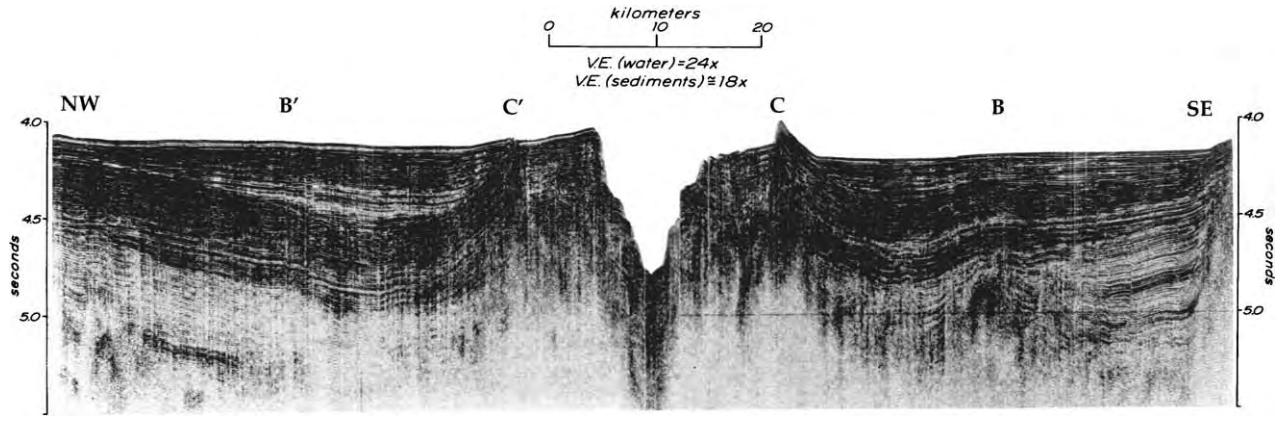

Fig. 14. Photograph of single-channel seismic reflection profile across the Central Andaman Basin spreading axis, line T 66–67. The older upturned edges are labeled.

north–south, as based on refraction data using both explosive and airgun sources and airgun wide-angle reflection data. Unfortunately, our data are insufficient to isopach the sediments.

Oceanic magnetic anomalies have been recognized in the southwestern part of the Central Andaman Basin where the sediment section is thin. These are discussed in Section 6.

Study of seismic reflection sections and seismicity suggests that the West Andaman Fault is inactive from its northern termination to where it intersects with the spreading axis at about 10.2°N (Fig. 4), south of line T 5–7 (Fig. 10a). From that point of intersection, it is active and constitutes the sliver plate edge to where the Seulimeum (SEU) Fault and/or the SFS then form the plate edge in Sumatra. The more active strand of the SFS in Aceh Province at the northwestern corner of Sumatra is what Sieh and Natawidjaja (2000) call the Seulimeum segment, abandoning the former name of Lam Teuba Baro (Bennett et al., 1981).

A possible abandoned plate edge is shown in Figs. 4 and 12 along the eastern margin of Sewell Rise. The margins of this spreading axis—transform system are correlated with plate margins A—A′ bordering the active plate edge farther north. This plate edge was presumably abandoned some millions of years ago, and the rift valley depression is filled. These are discussed in Section 6 of opening history, as are possible correlations of the old rift valley margins A–A′, B–B′, C–C′ with the chronology of sea level fluctuations.

5. Eastern zone of continental crust

Following the Suess (1904) subdivision, the eastern zone is the continental crust of the Shan Plateau in Myanmar and the Malay Peninsula and continental margin in the eastern Andaman Sea. This is basically the SIBUMASU Block of Metcalfe (1984) and Acharyya (1994). It includes Siam, Burma, Malaysia and Sumatra, and consists mainly of Paleozoic and Mesozoic rocks overlying continental crust.

The western margin of the Shan Plateau is generally interpreted to be an old suture, and is assumed to be along a fault known as the Shan Scarp Fault (Aung Khin et al., 1970; Mitchell, 1989) or the Central Burma Suture (Acharyya, 1998). The origin of the margin in the Andaman Sea is presumed to be an extensional margin formed by opening of the Andaman Sea along a back arc fault line, as outlined in Section 6 of this paper. Several of our reflection lines suggest down-to-basin listric faulting beneath this continental slope, as mentioned previously. Faulting on the shelf is also important in some of the areas of commercial wells drilled on this continental shelf, such as the Yetagun Field at about 13°N, 97°E and also in some of the seismic lines illustrated by Win Maw and Myint Kyi (1998).

The Mergui Basin (Fig. 4) is an offshore extension of the North Sumatra Basin. It is a backarc basin formed by rifting, transtension and thinning of continental crust, starting in Early Oligocene. The very simplified rifting structure is shown in Fig. 4. It is discussed and illustrated in much more detail in papers by Harding (1985), Polachan and Racey (1994) and Andreason et al. (1997). The basic simplified structure is a sag basin formed by graben and half-graben extensional faulting. The structural components (Fig. 4) are the Mergui Ridge, the West Mergui sub-basin, the Central Horst, the East Mergui sub-basin, the Ranong Ridge and the Ranong Trough. Extension was in an E–W to ESE–WNW direction, but dextral sliver faulting turns this extension direction to NW–SE, as explained in Section 7.

A simplified stratigraphy (Table 2) of the North Sumatra Basin and the Mergui Basin is adapted primarily from Polachan and Racey (1994) and Andreason et al. (1997). Lateral facies changes are important between the sub-basins of the Mergui Basin and the North Sumatra Basin, and both North Sumatra and Mergui Basin names are listed in Table 2. Fig. 15 shows profiles from reflection and refraction data, respectively, in a line in the East Mergui sub-basin (Figs. 3 and 7). The subsurface high at Well W9 B1 is the small horst located to the east and southeast of the Central Horst. My interpretation of these sections and velocities is that the 3.1–4.9 km/s velocity is Tertiary sedimentary rock, that the 4.9–5.7 km/s layer is probably Mesozoic or Paleozoic rock, that the 6.4 km/s layer (Fig. 15b) is continental intrusive and metamorphic rock, and that the 7.9 km/s horizon is the Moho.

The first marine incursion into the area was in Eocene, when early continent–continent hard collision was occurring between the Indian continental mass and Southeast Asia. Extension of continental crust occurred mainly during the Oligocene. This brought about rapid subsidence that continued through early Miocene. Subsidence slowed, and the grabens and half-grabens filled almost to sea level. The chronology of this extension and relationship to other opening events in the Andaman Sea are discussed in Sections 6.5 and 7.

The Ranong and Khlong Marui Faults (Fig. 4) may have been right lateral following early collision and reversed to left lateral during the Miocene with accelerated clockwise rotation of the region (Lee and Lawver, 1995).

6. Tectonic history of the Andaman Sea

Several scenarios and mechanisms of opening of the Andaman Sea have been published, including Wegener (1966), Rodolfo (1969a), Mitchell (1976), Curray et al. (1979, 1982), Hla Maung (1983), Bender (1983), Mukhopadyay (1984), Curray (1989), and many other papers. Some of these scenarios and chronologies were based in part on the erroneous interpretations previously mentioned of magnetic anomalies in the Central Andaman Basin. In this paper, a revised interpretation is presented of the opening history based on new interpretations of the magnetic anomalies, some dated rocks and the literature published on commercial drilling in the Mergui Basin and

Table 2
Mergui Basin and North Sumatra tectonics and deposition

Stratigraphic Age	Age my	Sequence Name	Thickness of Sediments m.	Environment of Deposition and Lithology	Tectonics and Deposition
Plio-Pleistocene	0 - 5	Takua Pa	300 to max. 3400	Outer Neritic (deep shelf) to Bathyal	Regression followed by transgression.
Late Miocene	5 - 11	Takua Pa Thalang Keutapang	to 1400	Estuarine/coastal from south to deep marine, including turbidites.	Transgression/subsidence.
Middle Miocene	11 - 15	Trang Surin Baong	to 800	Fluvial, deltaic and shallow marine from N and SE to bathyal mudstones.	Transgression/subsidence followed by regression.
Early Miocene	15 - 22	Tai Kantang Payang Peutu Belumai	to 2100	Maximum transgression. Patch and pinnacle reefs and deep marls and shales. Fluvial-deltaic sandstones from the N. Restricted marine to bathyal.	Rapid subsidence, sea level rise and transgression followed by regression and major unconformity.
Early Miocene Oligocene	22 - 36	Yala Ranong Bampo Bruksah	to 4600	Basal fanglomerates. deltas from the N. Restricted marine basins.	Sea level rise and subsidence during crustal extension.
Eocene	36 - 49			Shallow marine limestone and dolomite.	Stable with clockwise rotation.
Pre-Tertiary	> 49			Accreted melange of Permo-Carboniferous to Cretaceous schist, phyllite, quartzite, limestone, dolomite. Late Cretaceous granites.	

the Gulf of Mottama (see Fig. 4). Unfortunately, our seismic reflection records are not of sufficient power, penetration and resolution to enable much direct correlation with these exploration wells.

Simplified magnetic anomaly data adapted from Raju et al. (2004) in the Central Andaman Basin are shown in Fig. 16. Anomalies J, 2 and 2A are shown symmetrically arranged around a rift valley segment. These identifications are based on the Indian close spaced pattern of magnetic lines and on other data from NGDC, which are mainly our Scripps lines. The correlation we made from our limited data (S. Cande, personal communication, 2003) suggested a half-rate of 15 mm/yr, or opening of the Central Andaman Basin 118 km in 4 my, but it was not truly compelling. Raju et al. (2004) propose a half-rate of 8 mm/yr until sometime between anomalies 2 and 2A and then an increase in half-rate to 19 mm/yr. They tentatively identify anomaly 3 off the corner of Sewell Rise, but we were not able to identify this anomaly in our data. Their conclusion is the same as ours, that the Central Andaman Basin opened about 118 km in about 4 my.

Also shown in Fig. 16 are the locations of upturned edges A, A″, B, B″ C, C′ and F–F′. Lineation F probably lies along lineation A, within the escarpments bordering the Central Andaman Basin, and represents the time of initial rifting across the Alcock/Sewell combined Rises. Our explanation of these upturned edges (Curray et al., 1979) is that spreading was continuous and at an approximately constant rate, but that influx of sediment transported by turbidity currents into this basin was episodic with fluctuations in Plio-Pleistocene sea level. During periods of lowered sea level, sediments poured off the shelf down the canyons and gullies cut into the shelf edge and slope (Fig. 2) as massive turbidity currents. Then, during the rise of sea level as the river mouths retreated from the shelf edge, the sediment supply was greatly reduced and the fan valleys or turbidity current channels were filled. This is analogous to what happened with Quaternary sea level fluctuations on the Bengal Fan (Curray et al., 2003) and other submarine fans. This is the Andaman Submarine Fan, extending from the continental slope of the Gulf of Mattama southward to East Basin, with a more recently opened segment in the Central Andaman Basin (Fig. 4).

A and A′ and probably also the lineation F appear to be ~4 my. At a half-spreading rate of 19 mm/yr. B and B′ would be ~1.7 my; and C and C′ would be ~630,000 years. The outer edges of the rift valley (Fig. 14) would be about 260,000 years; the inner 'terrace' within the rift valley would be about 130,000 years and the narrow bottom of the inner rift would be about 66,000 years. The 66,000, 130,000, 260,000 and 630,000 year times very roughly occur in sea level lows in the climate curve by Imbrie et al. (1984) and Mitchell (1985) and the 1.7 my dates occurs very approximately during a low stand shown by Haq et al. (1987), but these correlations are not very good. This would imply that the large turbidity currents of lowered sea level scoured the channels and subsequent smaller turbidity currents have backfilled the open channels.

Several dredge samples of rocks and cores sampled during the 1964 Pioneer Expedition were dated

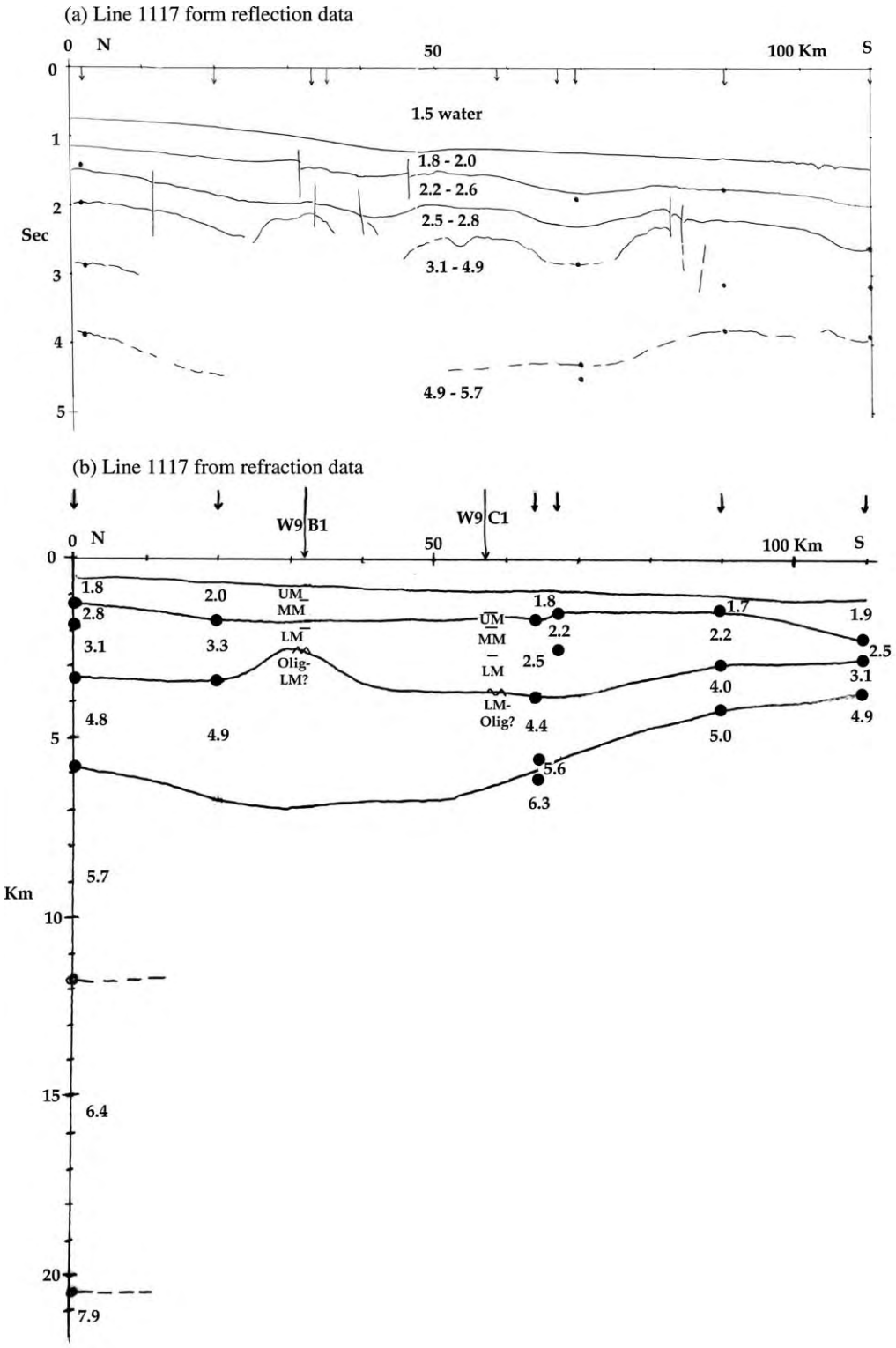

Fig. 15. North–south line 1117 in Mergui Basin (see Figs. 3 and 4). Buoy locations indicated by small arrows. (a) Section from reflection data, with velocity data from refraction and wide-angle reflection. (b) Section from refraction data.

stratigraphically by Frerichs (1971). These are located in Fig. 4 and are listed in the caption. Of especial value are some of the core samples of Neogene sediments with Frerichs' estimates of amount of uplift from their original depositional depth. Dredge sample ***17***, ~11°40′N, 94°3′E, from 950 to 1250 m is from an escarpment near the south flank of Alcock Rise. Two samples, described by J.W. Hawkins (personal communication, 1982) as moderately

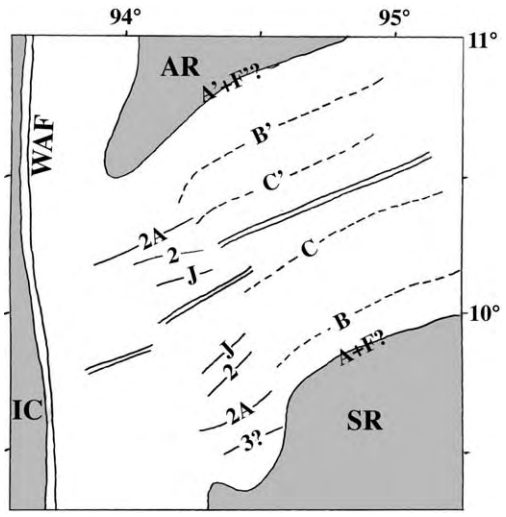

Fig. 16. Mergui Basin magnetic anomalies, simplified from Raju et al. (2004). Anomalies J, 2 and 2A are labeled. Rift margins B′, C′, C and B are shown, as are Alcock and Sewell Rises, Invisible Cuesta and the West Andaman Fault. Double lines indicate the three segments of spreading rift identified by Raju et al. (2004).

fractionated tholeitic basalts, dated by at 19.8 ± 0.7 and 20.5 ± 1.0 my.

Not all of the tectonic elements shown in Fig. 4 are active today, and an effort was made to distinguish between active and inactive elements. The elements judged to be active today are shown separately in Fig. 17. They include the two strands of the SFS, the main strand coming out of northwest Sumatra and the more active Seulimeum Fault (SEU) (Bennett et al., 1981; Sieh and Natawidjaja, 2000), the WAF from its intersection with the SFS to the western end of the Central Andaman Basin, the spreading axis in the Central Andaman Basin and the complex spreading axis-transform system extending northward from the eastern end of the Central Andaman Basin to where the Sagaing Fault comes offshore from Myanmar. The Eastern Margin and Diligent Faults (Fig. 4) are probably inactive, but this cannot be determined for sure.

As shown by the magnetic anomalies, the present full rate of spreading in the Central Andaman Basin (Raju et al., 2004) is about 38 mm/yr. This rate compares with the estimate of about 25 mm/yr for the SFS and SEU in northwestern Sumatra (Sieh and Natawidjaja, 2000; Genrich et al., 2000; Prawwirodirdjo et al., 2000). Sieh and Natawidjaja (2000) suggest that only the SEU at the northwest tip of Sumatra has been active for the last 100,000 years. The consensus of opinion of these workers in Sumatra is that the rate decreases to 10–20 mm/yr toward the southeast by either stretching of the sliver on the southwest side of the fault or by take-up of motion by other faults. These estimates of slip rate also compare with estimates for the Sagaing Fault. As mentioned previously, Vigny et al. (2003) have shown that less than 20 mm/yr of the total plate motion of 35 mm/yr occurs along the Sagaing Fault. They suggest that the remainder is accommodated by distribution of deformation over a wide zone. A wide zone of deformation must also exist along the SFS. These rates will be further compared in Sections 6.1 and 7.

The subduction zone of the Sunda Trench is active. Reflection records from the slope above the filled trench in Fig. 8a and b, sections T 24–25 and southward, show deformation of young sediments of the Bengal Fan low on the slope. North of T 24–25 the slope is depositional, probably from the large input of sediment from the Myanmar rivers and coastline, but a component of convergence probably still exists all the way up the Myanmar part of the arc, although this is controversial (see, for example, Satabala (1998) and Guzmán-Speziale and Ni (2000)).

Vectors are shown at several points along the trench axis (Fig. 17). The rate of convergence between the Indian and Eurasian (or Southeast Asian) plates is in dispute today. Estimates from GPS observations (Holt et al., 2000) differ from the earlier IN-EU-NUVEL-1A of DeMets et al. (1994). The vectors in Fig. 17 are therefore only approximate, and are shown only to illustrate that convergence appears to occur all along this segment of the trench because of the spreading in the Andaman Sea. Vectors AE represent the Australian plate with respect to the Eurasian or Southeast Asian plate; vectors AB represent Australia with respect to the Burma sliver plate; vectors AT represent the component of convergence normal to the trend of the trench, and vectors BE represent Burma with respect to Eurasia. Vectors are shown for the spreading across the Central Andaman Basin.

The vectors at 2°N are adapted from McCaffrey et al. (2000) who calculated vector AB as the slip vector from earthquakes. They found that vector BE is about 1/3 less than the total trench-parallel vector and interpreted this to mean that the additional strike-slip motion occurs between the SFS and the trench. This is analogous to Vigny et al. (2003) conclusion that some of the total plate motion occurs in a wide zone between the Sagaing Fault and the plate edge. This implies that there are many unmapped faults active within the Andaman and Nicobar accretionary complex.

I do not have access to slip vectors for the 7.5 and 15.5°N locations, so some assumptions have been made in attempting to show AB and BE. The rationalization behind these assumptions will be explained in Section 6.1, and at that time we will return to consideration of Fig. 17.

Opening of the Andaman Sea has occurred during the convergence of India and Asia since Paleogene time. The history of convergence and collision have been thoroughly discussed in the literature. This discussion will follow the chronology by Lee and Lawver (1995); an adaptation of their convergence curves is shown in Fig. 18. Some events in the Andaman Sea history appear to correlate with events in these convergence curves, while others do not. The stages of the opening of the Andaman Sea to be discussed below are summarized in Table 3.

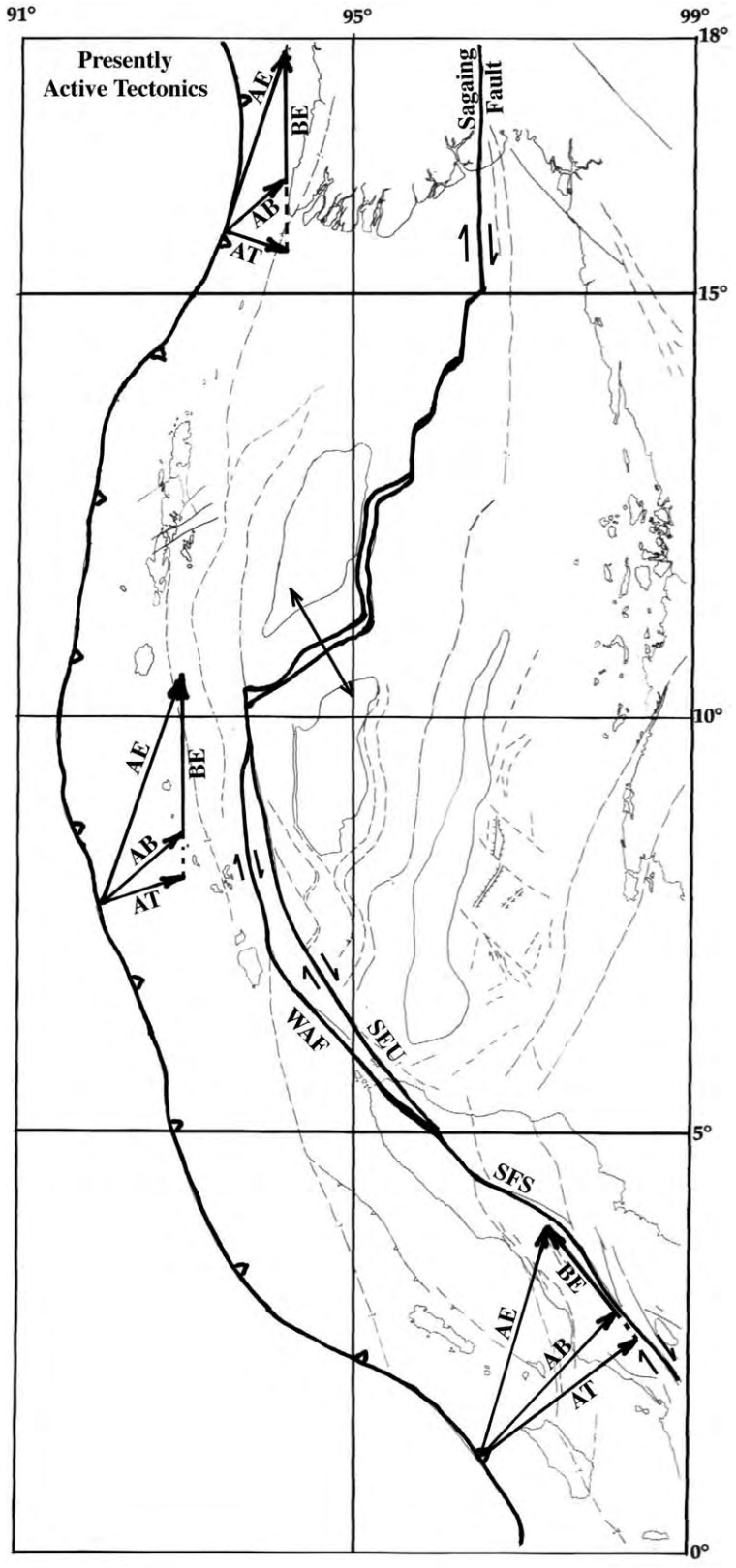

Fig. 17. Presently active tectonic elements. Edge between the Eurasian and the Burma sliver plate is the Sagaing Fault, the spreading axis in the Central Andaman Basin, the West Andaman (WAF) and Seuliman (SEU) Faults to the Sumatra Fault System (SFS). Vectors: AE, Australian plate with respect to Eurasia plate; AB, Australia with respect to Burma plate; BE, Burma plate with respect to Eurasia; AT, Australia with respect to the alignment of the trench or trace of the subduction zone, to demonstrate that while highly oblique, subduction is occurring all along this trench axis. Full rate of separation normal to the CAB spreading axis is currently about 38 mm/yr. Derivation of vectors explained in text.

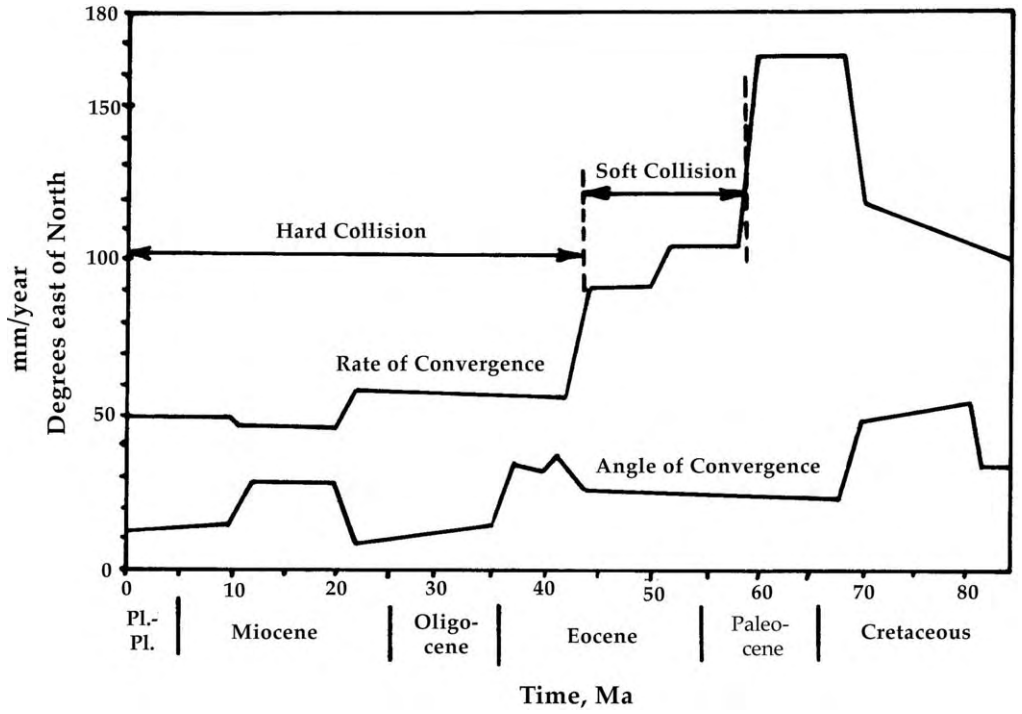

Fig. 18. Rate and direction of convergence between India and Asia. Modified from Lee and Lawver (1995).

Notice the reverse or thrust fault first motion solutions near the north coast of Sumatra in Fig. 6. In an earlier attempt at a history and tectonic scenario for the Andaman Sea (Curray et al., 1979), we suggested that a splay of the active West Andaman Fault might bend around the coastline with a component of convergence. Our seismic reflection lines do not show any such fault, nor does the land mapping, and those thrusting mechanisms remain a mystery.

No definitive paleomagnetic data have been collected in the Burma Block. Richter et al. (1993) and Richter and Fuller (1996) reported CW rotation of the Shan Plateau between Late Cretaceous and Late Oligocene, but Richter et al. (1999) reported 30–40° CCW rotation of peninsular Malaysia between late Eocene and late Miocene. The consensus of opinion based on tectonic considerations, however, is that CW rotation of the western Sunda Arc, the Burma Block to southwestern Sumatra, occurred during the Tertiary (e.g. Curray and Moore (1974), Ninkovich (1976), Tapponnier et al. (1982), Mitchell (1989), Lee and Lawver (1995), Varga (1997) and many others). The reconstructions in Figs. 19–23 show somewhat more rotation than Lee and Lawver (1995) showed, on the assumption of deep indentation by India into the Asian margin by the collision and extrusion of the Indochina block. Tapponnier et al. (1986) and Alam et al. (2003) suggested a linear pre-collision south Asian continental margin trending about 120–300° between the Gulf of Oman and Sumatra. Using this as the original alignment, I have assumed about 60° of rotation since initial 'soft collision' about 59–60 Ma, and rotation has been prorated in the reconstructions to follow: about 44° since 44 Ma, 32° since 32 Ma, etc.

The Andaman Sea has opened by extension in a series of stages that are reconstructed below, going backward in time. The process started some time after the collision of Greater India with the southeastern Asian margin, which was the locus of the zone beneath which the Tethys sea floor was subducted. This subduction zone is believed to have been active at least by Cretaceous time when the Gondwana continent was breaking up. Table 4 is a summary of the spreading history, as will be explained.

6.1. Reconstruction to 4 Ma (Fig. 19) and tectonics of 0–4 Ma

The tectonic action of the past 4 my was opening of the Central Andaman Basin across the spreading axis shown in Fig. 4 and comparable right-lateral offset along the transforms to the north and south, the Sagaing, West Andaman, Seuliman, and Sumatra Fault Systems. The opening of the CAB is estimated at 118 km in a direction of ca. 335° relative to the Eurasian, Southeast Asian or Sundaland block, at an average rate of about 30 mm/yr, starting at 16 mm/yr and then speeding up to 38 mm/yr at about 2–2.5 Ma (Raju et al., 2004). Although 4 Ma was a time of reorganization of the tectonics, with a plate edge jump from the east flank of Sewell Rise to the Central Andaman Basin and the West Andaman Fault, it shows no correlation with convergence between India and Asia and the overall tectonics of the Indian Ocean (Fig. 18).

The turbidity current channel occupying the plate edge rift is believed to have continued along the east side of Sewell Rise prior to opening of the CAB, to as far south

Table 3
Andaman Sea spreading history

Age	Event	Total Rotation*	Spreading Direction*	Spreading Amount km	Spreading Rate mm/yr.	North Component km	North Velocity mm/yr	West Component km	West Velocity mm/yr	Tectonics
ca. 4 to 0 Ma Early Pliocene to Present	Open Central Andaman Basin	4°	ca. 335°	ca.118	38 30 16	107	27	50	12	Plate edge jump from East Basin abandoned spreading axis to West Andaman Fault, central Andaman Rift, and SEU and SFS Faults.
ca. 15 to 4 Ma End Early Miocene to Early Pliocene	Open East Basin	16°	ca. 335°	ca. 100	9	91	8	42	4	Move contiguous Alcock and Sewell Rises away from edge of continental crust. Start jump from West Andaman and Mentawei Faults to Sumatra Fault System and Batee Fault.
ca. 23 to 15 Ma Early Miocene	Form Alcock and Sewell Rises	23°	ca. 322°	ca. 120	15	95	12	74	9	Backarc extension by creation of contiguous Alcock and Sewell Rises and Bago Yoma. Rapid subsidence of Mergui Basin and deposition of deep marine shale. Continuous Sagaing and West Andaman Faults. Ranong and Khlong Marui Faults change to left lateral.
ca. 32 to 23 Ma Early Oligocene to Early Miocene	Form Mergui Basin	32°	ca. 310°	ca. 60	7	39	4	46	5	Rift extension of continental crust, thinning it by $\beta \sim 1.5$. Deposition of fluvial, deltaic and shallow marine sediments. Continuous Sagaing, West Andaman and Old West Andaman sliver faults. Ranong and Khlong Marui Faults right lateral.
ca. 44 to 32 Ma Middle Eocene to Early Oligocene	"Hard" collision of India with Asia	44°								Rotate Burma, Sumatra and Sibumasu blocks. Form Sagaing-West Andaman splinter Fault at about end of period, ca. 32 Ma.
ca. 59 Ma	"Soft collision" India and Asia.	59°								Start of rotation of northern Sunda Arc.
Totals and Averages			327° Vector Sum	389 Vector Sum	12	332	10	212	7	

[a] Directions relative to present north.

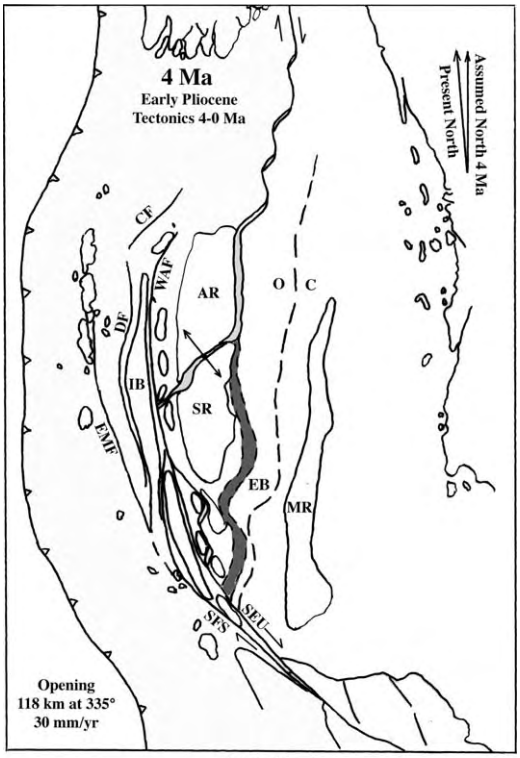

Fig. 19

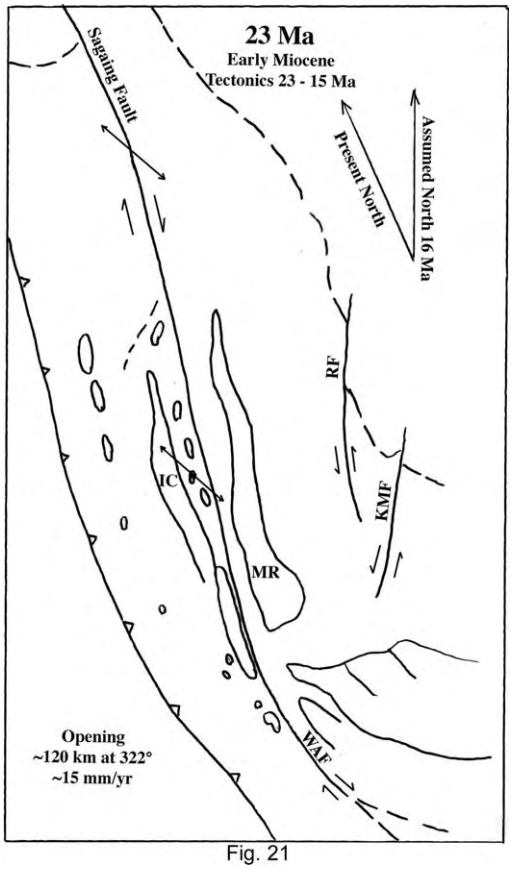

Fig. 21

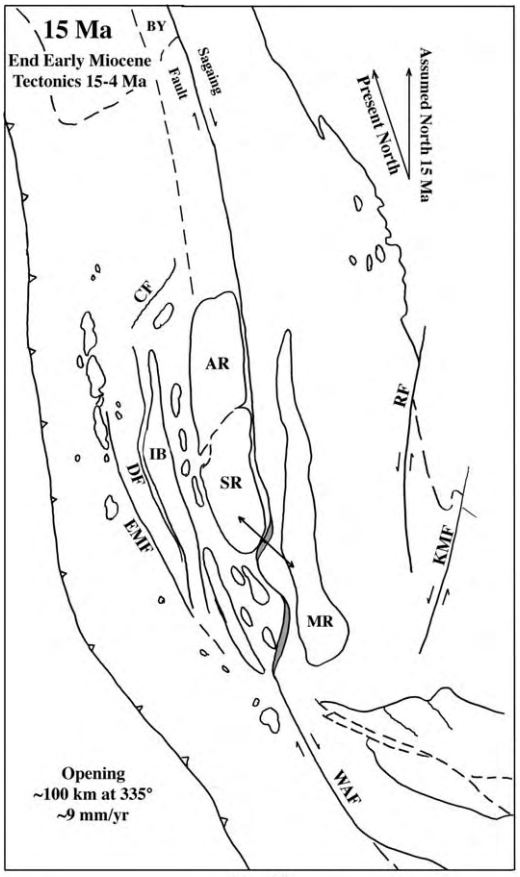

Fig. 20

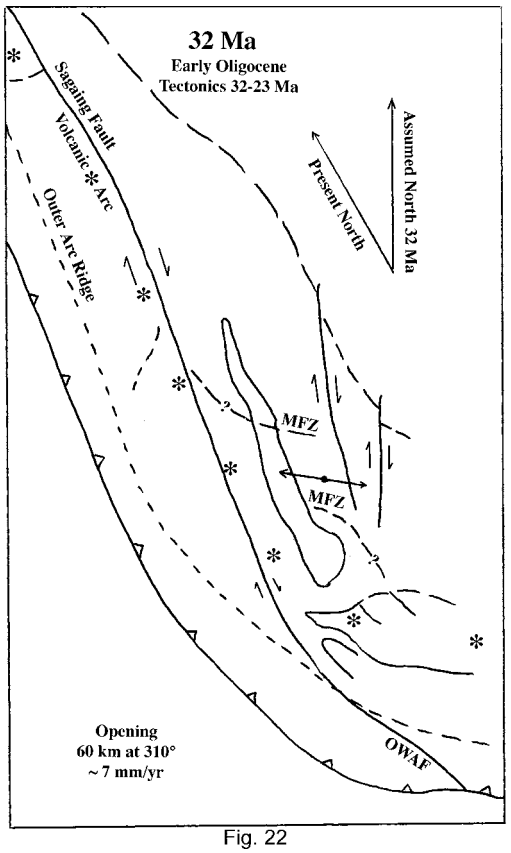

Fig. 22

as the intersection with the Seuliman Fault, although differential subsidence and later deposition have made the channel shoaler south of the northeast corner of Sewell Rise than it is farther north. The continuous gradient southward has not been preserved. The rifting of the CAB and the jump in the plate edge apparently initiated the subsidence now shown across lineation F of 350–400 m.

This reconstruction was made by fitting Alcock and Sewell Rises together along their margins, which are lines A′ and A, respectively, in Fig. 4. This brings the abandoned plate edge A–A′ from east of Sewell Rise approximately into line with the present rift valley A–A′ east of Alcock Rise. It also brings the western flanks of the two rises approximately into alignment, suggesting a fault or rift origin.

The West Andaman Fault was probably active all along its trend. From the west end of the Central Andaman Basin rift to its northern end, it may have been primarily a reverse fault forming the Invisible Bank Cuesta and uplifting older forearc basin sediments, while from this point south it also served as a strike-slip transform fault to northwest Sumatra. Dredged sediments (Fig. 4) were uplifted 400–2000 m above their depths of deposition in the forearc basin during this period (Frerichs, 1971; Rodolfo, 1969a). Invisible Bank continues as a cuesta to about the southern end of Sewell Rise (Line E 9–10, Fig. 10b). The Eastern Margin (EMF) and Diligent (DF) Faults were probably also active during this period.

The Cocos Fault (sections E 19–20 and I 10–11, Fig. 10a) created a cuesta, also suggesting a reverse fault. Since both the Cocos and West Andaman Faults were probably active during this period, a component of compression may have existed northwest of Alcock Rise as a result of the extension forming the rises, to be discussed in Section 6.2.

Fig. 19 shows faulting in northwestern Sumatra along both the Seuliman and Sumatra Fault System alignments although Sieh and Natawidjaja (2000) suggest that the Seuliman Fault did not start until about 2 Ma. They also suggest that the main strand of the fault (SFS in Fig. 19) has not been active for the past 100,000 years. Our offshore reflection records suggest that the SFS strand is currently inactive and that the SEU fault is the active strand (Fig. 10b, sections E 2–4W and M 8–9E; and Fig. 10c sections E 38–40 and I 37–38).

Sieh and Natawidjaja (2000) suggest that the Sumatra Fault System in northwestern Sumatra may be no older that 4 my and perhaps only 2 my in the remainder of Sumatra. They show a progressive shoreward or northeastward migration of the fault system with time, from offshore to onshore. This reinforces our belief that the West Andaman Fault represents an earlier sliver fault off northwest Sumatra running into the Mentawei Fault at the intersection with the Battee Fault. Our reflection lines off Sumatra suggest that the Mentawei Fault is not active today. Even earlier, from as early as Eocene until about early Miocene, we believe that the WAF ran across the outer arc ridge as the Old West Andaman Fault (OWAF; Fig. 4). Replumaz and Tapponnier (2003) speculated that a fault they named the Nicobar Fault runs where we had previously published the location of the West Andaman Fault and continuing across the accretionary prism where we show the OWAF, but they calculate that it has been active at a rate of 24 mm/yr during the past 5 my. We see no evidence for current activity of this fault, nor is its trend apparent in the seismicity, in the bathymetry or in the complex structures in the reflection profiles across the accretionary wedge.

Fitch (1972) introduced the concept of partitioning of motion in oblique subduction: that the lateral component is frequently taken up by an arc-parallel sliver fault and that the normal component represents subduction. Backarc extension can similarly be expressed as components, as in the case of the opening of the Central Andaman Basin with northward, arc-parallel sliver faulting by the Sagaing–West Andaman–Sumatra Fault System, and arc normal extension. In the CAB with spreading about 335° relative to present north at an average rate of 30 mm/yr, the northward component would be 27 mm/yr and the westward component relative to the eastern Andaman Sea would be about 12 mm/yr. In Table 3, each separate period of opening is expressed as an arc-normal and an arc-parallel component.

Fig. 19. Reconstruction at ca. 4 Ma. Plate edge after 4 Ma was same as Fig. 17, shown in light shading. Plate edge prior to the realignment of 4 Ma, shown in darker shading, was Sagaing Fault, abandoned spreading axis/transform complex east of Sewell Rise (SR), to SEU and SFS Faults in Sumatra. Farther southeast in Sumatra, Sieh and Natawidjaja (2000) suggest that the Sumatra Fault System did not move onshore until about 4 Ma, and that displacement was taken up by extension in the outer arc ridge seaward of the Battee Fault. AR, Alcock Rise; SR, Sewell Rise; EB, East Basin; MR, Mergui Ridge; IB, Invisible Bank. Other features are the same as in Fig. 4, but whether they were active cannot be established, e.g. Cocos Fault (CF), Eastern Margin Fault (EMF), Diligent Fault (DF) and West Andaman Fault west of Alcock Rise. Opening from 4 my to present was about 118 km at 335°.

Fig. 20. Reconstruction at about 15 Ma, made by closing East Basin and moving Alcock (AR) and Sewell (SR) Rises against the presumed edge of continental crust off the Mergui Ridge (MR) and continental slope to the north and rotating the region 15° CCW. BY, Bago Yoma. Other abbreviations as in Fig. 4. Opening during this period was about 100 km at 335° relative to present north.

Fig. 21. Reconstruction at about 23 Ma, made by closing Alcock and Sewell Rises and rotating region another 7° CCW. Opening during this period was about 120 km at 322°.

Fig. 22. Reconstruction at about 32 Ma, made by closing Mergui Basin and rotating region another 9° CCW. Opening during this period was about 60 km at 310°.

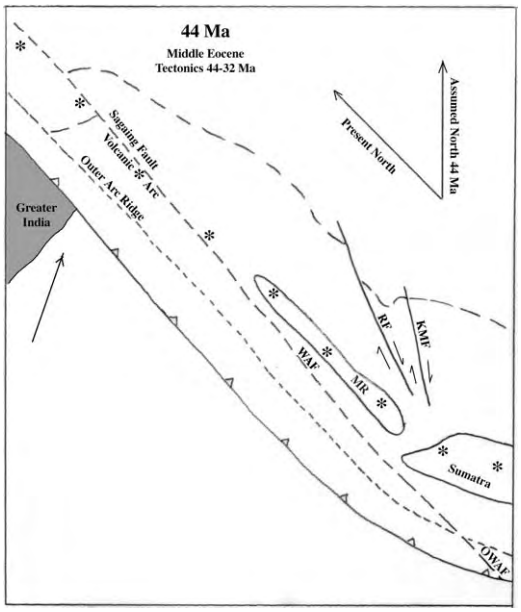

Fig. 23. Reconstruction at about 44 Ma, made by rotating region another 12° CCW and bending the arc at northwest Sumatra.

I had previously considered sliver faulting of the Burma Platelet in terms of rigid plate tectonics, with a pole of rotation at about 24°N, 125°E, assuming that the Sagaing and Sumatra Fault Systems are transforms and the Central Andaman Basin points toward this pole (Curray et al., 1979; Curray, 1989). It is clear now, as shown by McCaffrey (1991) and McCaffrey et al. (2000), that the sliver plate should not be considered to be rigid. By the Fitch concept (1972), the arc-parallel component of the oblique convergence is a function of the obliquity of convergence. Around the Sunda Arc, where convergence is normal to the arc, there is no arc-parallel component, and hence no sliver faulting. This point lies near the Sunda Strait between Sumatra and Java (Fig. 1), where the Sumatra Fault System terminates. Adjacent to the Andaman Sea, the convergence direction between the Australian and Eurasian (or Southeast Asian) plates is approximately parallel to the arc, and without the component of opening of the Andaman Sea there would be no subduction—only lateral motion.

In plotting the vectors for the 15.5 and 7.5°N locations in Fig. 17, it has been assumed that the vector BE, the motion of the Burma sliver plate relative to the Eurasian (or Southeast Asian) plate is N–S parallel to the Sagaing Fault, rather than oblique and parallel to opening of the Central Andaman Basin. Approximate vectors AB, Australia with respect to the Burma platelet, are estimated from the earlier calculations assuming a rigid Burma plate and by assuming that about 1/3 of the arc-parallel motion is absorbed in the forearc region, as McCaffrey et al. (2000) have shown. So magnitudes of strike-slip motion cannot therefore be calculated with any accuracy, but these vector plots demonstrate that a component of subduction exists normal to the arc. Our reflection and 3.5 kHz records also confirm that subduction is still occurring.

We have assumed that the sliver fault on the east side of the Burma sliver plate is the Sagaing Fault down to the Central Andaman Basin, the spreading axis in the Central Andaman Basin, the West Andaman Fault and the Sumatra Fault System. The rates of motion compare rather well. The plate motion is about 35 mm/yr in Myanmar, about 20 of which is on the fault itself. The northward component in the Central Andaman Basin is 27 mm/yr, and the estimates in Sumatra decrease from 25 mm/yr in the northwest to 10–20 mm/yr in the southeast, and may be greater if there is a wide zone of deformation between the fault and the trench axis.

6.2. Reconstruction to 15 Ma and tectonics of 15–4 Ma

Fig. 20 is a reconstruction of the Andaman Sea region at about 15 Ma. This was prepared by moving the contiguous Alcock and Sewell Rises against the edge of continental crust of Fig. 4, thus closing East Basin by about 100 km in direction 155°. The direction of motion to close East Basin is approximated by fitting the shapes of the rises and the shape of my estimate of the edge of continental crust. Seismic reflection records show some listric faulting of both the edge of the continental crust and the margins of the rises, but I cannot judge how much extension had occurred. Hence, I postulate opening during this period in direction 335° by spreading along two or more spreading axes, in a transform spreading axis connecting the Sagaing Fault with the West Andaman and Mentawei Faults offshore from Sumatra. An average rate of opening would have been only about 9 mm/yr. Starting at about 4 Ma, the rate apparently speeded up to about 16 mm/yr, and then speeded up again to 38 mm/yr after anomaly 2A, at about 2.0–2.5 Ma (Raju et al., 2004).

The Sumatra Fault System was probably not active yet, so the Burma sliver plate at this time probably included only western Myanmar and the western Andaman Sea region. The West Andaman Fault west of Alcock and Sewell Rises was probably not active during this period; the Eastern Margin and Diligent Faults may have been active; and the possible fault line along the western margin of the contiguous and joined rises may also have been active as a normal fault. The Ranong and Khlong Marui Faults were believed to have been left lateral during this period of time (Lee and Lawver, 1995; Andreason et al., 1997).

The beginning of this tectonic period, about 15–16 Ma was the end of early Miocene. This is an important time in the stratigraphy of the Mergui Basin, a time of rapid subsidence and deposition of bathyal shales in the center of the basin, following a maximum transgression (Polachan and Racey, 1994; Andreason et al., 1997). However, it shows no relationship to the convergence across the Indian Ocean (Fig. 18).

The Bago Yoma (formerly named Pegu Yoma) low mountains are shown in this figure, and are discussed in Section 6.3.

6.3. Reconstruction to 23 Ma and tectonics of 23–15 Ma

Fig. 21 is a reconstruction of the region at about 23 Ma. It was made by removing the contiguous Alcock and Sewell Rises and displacing the western sliver plate about 120 km toward 142°, relative to present north. The direction of motion to close up the space of the rises is judged by the structural grain of the tops of the rises. Hence, spreading during the formation of these volcanic piles was in a direction 322° relative to present north at an average rate of about 15 mm/yr.

Two rock dredge hauls have yielded information on the petrology of Alcock Rise. Pioneer dredge ***14*** at 13°N (Rodolfo, 1969a) is a 'tabular, massive unaltered intergranular augite basalt'. No dating has been done because the samples are lost. Dredge ***17*** is a moderately fractionated tholeitic basalt (J. W. Hawkins, personal communication, 1982). Two dates are 19.8 ± 0.7 and 20.5 ± 1.0 my. Thus, this part of Alcock Rise was formed about 20 Ma. Hawkins' analyses furthermore show that it is rather typical backarc basin basalt. This was the time of the earliest backarc basin sea floor spreading the Andaman Sea.

The northern limit of Alcock Rise is unknown; our seismic data are not adequate to resolve this, as is indicated in Fig. 4. Thus, the question is how far did the extension to form the rises continue to the north? The suggested solution shown in Figs. 20 and 21 is that it extended north about as far as the bulge in the Sunda subduction zone extends, or to at least 17°N, north of the present Myanmar shoreline. This assumes that the Sunda subduction zone and trench were approximately linear or a smooth curve between northern Sumatra and central Myanmar, rather than showing a pronounced bulge as it does today. A possibility is that this Alcock–Sewell extension continued into the Bago Yoma low mountain region in the southeastern part of the central basin of Myanmar (see Fig. 20) immediately west of the Sagaing Fault, to perhaps 19–20°N. The ridge in the Yadana section (Fig. 9c) might represent the connection between Alcock Rise and the Bago Yoma.

Rocks cropping out in the Bago Yoma are early to late Miocene. This region started subsiding in early Miocene and deposition in the Bago Yomas was in a long narrow north–south trough (Aung Khin and Kyaw Win, 1968, p. 246), compatible with the suggestion that this basin opened by rifting during this period. Pivnik et al. (1998) report that this area was subject to Miocene NNW-directed extension, followed by ENE-directed compression. This compression could be related to the suggested compression NW of Alcock Rise from 4 to 0 Ma, although the direction is wrong.

Seismic refraction line 1109 (Fig. 9d) shows a great thickness of sediment and high velocity sedimentary rock, over 16 km at its northern end, overlying apparent oceanic crust. These high velocity sediments are analogous with the deeply buried high velocity older sediments beneath the northern Bengal Fan, which have been interpreted by consideration of temperature and pressure conditions to be low grade greenschist facies metasediments (Curray, 1991). This is also compatible with the interpretation that extension occurred in this area while Alcock and Sewell Rises were forming. Volcanic filling of the extended backarc region occurred in the Alcock–Sewell region and the flood of sediment from the large rivers of Myanmar buried and filled the northern continuation in the Bago Yoma and shelf area.

Prior to 23 Ma, the Sagaing Fault apparently connected directly in line with the West Andaman Fault passing offshore west of the tip of Sumatra and perhaps connected southeastward with the Mentawei Fault. The Battee Fault, a splay of the Sumatra Fault System, was probably not active yet because the Sumatra Fault had not yet formed in Sumatra. The Samalanga Sipokok Fault in northern Sumatra (Fig. 4) became active in the Oligocene (Cameron et al., 1983; Keats et al., 1981) and might have continued as the Batee Fault, but the time of first activity of the Batee Fault is not known. The Ranong and Khlong Marui Faults were probably actively cutting the Malay Peninsula and are believed to have reversed from right lateral to left lateral at about this time (Lee and Lawver, 1995).

More rotation, 23°, is suggested than in the previous period. This time of 23 Ma was a time of change in convergence direction and rate between India and Asia (Fig. 18). The rate of convergence decreased from about 60 mm/yr to less than 50 mm/yr, and the direction of convergence turned more eastward, from about 010 to 025°. This was also perhaps the time of first emergence of the top of the Andaman–Nicobar Ridge above sea level, as documented by the shallow water facies of the Archipelago Series.

6.4. Reconstruction to 32 Ma and tectonics from 32 to 23 Ma

Fig. 22 is a reconstruction to early Oligocene, about 32 Ma. It was made by closing the extended continental crust in the Mergui Basin and the North Sumatra Basin. The direction of closing is determined by the trends of the normal faults in the basin. The pole of rotation for opening these basins is generally assumed to lie close to the north because the basin terminates in a point somewhere on the Myanmar shelf between about 12 and 14°N.

Fig. 15 shows the refraction line and a line drawing of the reflection line in the Mergui Basin with average velocities for each unit. The stratigraphy of two exploration wells is projected into the refraction line. At the north end of the line an arrival with 7.9 km/s velocity is interpreted as mantle at

Table 4
Correlation of chronology of events

India-Asia Convergence Fig. 18	Myanmar Irrawaddy Delta	Andaman Nicobar Ridge Table 1	Spreading History Table 3	Mergui N. Sumatra Basins Table 2	Sumatra Fault System	Geologic Time Scale
			Central		SFS on	Quater-
	Irrawaddy	Nicobar	Andaman	Takua Pa	Land	nary
~50 mm/yr	Group	Series	Basin			
~015°	Fluvial	----5 my----	---4 my---	----5 my----	---4 my---	---5 my---
	Delta					Late
			East Basin	Keutapang		Miocene
--10-12 my--	---~10 my--					--10 my--
		Archipelago			WAF &	Middle
	Upper	Series			Mentawei	Miocene
~50 mm/yr	Burman		--15 my---	----15 my---	Faults	--16 my--
~030°	Limestone		Alcock	Peutu		Early
			Sewell	Payang		Miocene
	--~20 my--		Rises			
--20-22 my--	Middle	---- 23 my---	--23 my---	----22 my---	-----?-----	--25 my--
	Burman		Mergui			
	Neritic to	Andaman	Basin	Ranong		
	Deltaic	Flysch	Opens	Bampo	OWAF	Oligocene
10-20 mm/yr	--~30 my---		---32 my--			
010°-030°	Lower		Sliver			
	Burman		Faulting	----36 my---		--36 my--
	Shallow		Arc			
	Marine		Rotation		-----?-----	
	Clastics &					Eocene
---44 my---	Tuff	----45 my----	--44 my---			
Hard				Shallow		
Collision		Mithakhari		Limestone		
90-100		Group				
mm/yr						--54 my--
025°						Paleocene
---59 my---			---59 my--			
Soft						
Collision						--66 my--
~165 mm/yr		----70 my---		----------		Cretaceous
~025°		Ophiolite				
		Mesozoic?		Pre-Tertiary		

		Proterozoic?				
		Sediment				

about 20 km depth. On the assumption that the original thickness of sedimentary rock plus continental crust was about 30 km, this suggests extension and $\beta = 1.5$, i.e. thinning from 30 to 20 km by extension and increasing the width of the basin to 1.5 times its original width (McKenzie, 1978).

Extension, and rapid subsidence in the Mergui Basin are postulated to have occurred in the Oligocene and early Miocene (Polachan and Racey, 1994; Andreason et al., 1997; Table 2). This was the first period of opening of the Andaman Sea, for approximately 60 km in a direction 310°, at a rate of about 7 mm/yr. The plate edge is believed to have been the Sagaing Fault, extending the length of the Andaman Sea at that time and connecting with the West Andaman Fault and what is called here the OWAF which crosses the outer arc ridge/accretionary prism to the Sunda Trench off Sumatra (Figs. 4 and 21).

6.5. Reconstruction to 44 Ma and tectonics from 44 to 32 Ma

Fig. 23 is a reconstruction to the end of middle Eocene, about 44 Ma. This was the time of hard continent–continent collision between India and continental Asia (Fig. 18). Initial collision occurred earlier, probably early Eocene, about 59 Ma, but convergence continued at about 100 mm/yr for about 15 my before the rate of convergence reduced to about 60 mm/yr (Fig. 18; Lee and Lawver, 1995). During all of this time clockwise rotation of this region continued, and perhaps some bending of the SIBUMASU block (Siam, Burma, Malay Peninsula, and Sumatra) between Sumatra and the southern Andaman Sea. Fig. 23 was drawn on this assumption, so the bend in the trend of the magmatic arc was decreased, and the Andaman Sea and Myanmar are shown more nearly in line with the trend of Sumatra.

The Greater Indian subcontinent had collided with the subduction zone and had started the clockwise bending of this northern part of the Sunda Arc. The sliver fault, the combined Sagaing and West Andaman Faults, perhaps started in middle to late Eocene, as suggested by Tankard et al. (1998) after some rotation had already occurred and the convergence direction was more oblique.

As shown in Table 3, the vector sum of the different periods of opening of the Andaman Sea is about 389 km in a direction 327° relative to present north.

7. Discussion of geological history and tectonics

Reconstructions of the several stages in the opening history of the Andaman Sea have been presented going backwards in time because that is the way the reconstructions were made. Let us now summarize that history moving forward in time (Table 4).

India separated from Australia and Antarctica in eastern Gondwanaland in the Cretaceous and started its spectacular flight northward. The precise time of this separation is irrelevant, but subduction along the eastern Asian margin had started by at least that time. Before the departure of India from Australia and Antarctica, the South Tibet, Burma and SIBUMASU Blocks had already spun off northward and had docked against Asia. Prior to initiation of the subduction system, this could have been a passive continental margin, the source of some of the older sediments found in Myanmar and the Andaman–Nicobar Ridge.

The northeastern corner of 'Greater India' hit this subduction zone at about 59 Ma (Klootwijk et al., 1992; Table 4), the so-called 'soft collision', and India underwent some counter clockwise rotation from about 59 to 55 Ma, at which time the suture was completely closed. During this time and until about 44 Ma, India was indenting the Asian margin and rotating the subduction zone in a clockwise direction. With this rotation the direction of convergence became increasingly more oblique. Finally, probably in the middle to late Eocene, about 44 Ma, a sliver fault formed, the forerunner of the Old West Andaman, West Andaman and Sagaing Fault systems (Fig. 23). Right-lateral motion started on the Khlong Marui and Ranong Faults at about this same time (Lee and Lawver, 1995) prior to the opening of the Mergui Basin during the Oligocene. Also active from the Late Oligocene were the Lhokseumawe-Lopok Kutacane Fault (Cameron et al., 1983) and the Samalanga Sipokok Fault (Keats et al., 1981; Cameron et al., 1983; Fig. 4). They could have been the southern ends of the Ranong and Khlong Marui Faults, respectively. With extension of the Mergui Basin starting in late Oligocene, the Mergui Faults, north and south (Fig. 4 and 22), could have terminated these connections. The northern strand of the Mergui Fault may have crossed the Mergui Ridge as a splay of the Sagaing Fault (Fig. 22). The Mergui Ridge was probably part of the original volcanic arc (Fig. 23).

By early Miocene, about 23 Ma (Fig. 21), the plate convergence was oblique enough that extension and backarc sea floor spreading moved westward to the sliver fault running approximately along the magmatic arc, which had by that time migrated westward. This sea floor spreading and creation of oceanic crust formed the rock masses comprising Alcock and Sewell Rises and possibly opened the southern Bago Yoma Basin. The dates on rocks from Alcock are early Miocene. With abandonment of extension in the Mergui Basin area, rapid subsidence occurred and the shallow water deposits of the late Oligocene were buried by deeper water facies.

With continuing rotation of the arc, the direction of extension relative to present north (Table 3 and Figs. 21 and 22) became more northerly, from 310 to 335°, between 32 and 15 Ma and stabilized thereafter at 335°.

At the end of early Miocene, about 15–16 Ma, a major change occurred in the Mergui Basin with an unconformity and deposition of dark gray to black shales of the Baong, Trang and Surin Formations over the carbonate sediments of the Peutu, Tai, Katang and Payang formations. At this time the conjoined Alcock and Sewell Rises started rifting away from the edge of continental crust forming East Basin (Fig. 4). And finally at about 4 Ma, the plate edge migrated again to cut Alcock and Sewell apart, and the present plate edge between the Southeast Asian and the Burma Sliver Blocks was formed.

The interpreted timing of tectonic events of the different parts of the system is compared in Table 4. We cannot determine whether these times of change were gradual and the tectonic events described overlapped, or whether these times were sharp events. Although some of the events appear to correlate from region to region within the Andaman Sea, we must bear in mind that the times in the spreading history, Table 3, and the middle column in Table 4, were estimated in part from the better-dated tectonic events in the Mergui Basin. Nevertheless, there are some apparent correlations. Major stratigraphic changes occurred on the Andaman–Nicobar Ridge and in the Mergui Basin at about 4–5 Ma, the time rifting began separating Alcock and Sewell Rises and the time the Sumatra Fault System moved onto land (Sieh and Natawidjaja, 2000). Compression and uplift of the older forearc basin had commenced approximately 6 Ma. Stratigraphic changes occurred at about 20–23 my in the Irrawaddy Delta, the Mergui Basin and in the sediments accreted on the Andaman–Nicobar Ridge. This is the time of a major unconformity in the Indoburman Ranges and on the Andaman–Nicobar Ridge (Acharyya et al., 1990). The time of 'hard' India–Asia collision, about 44 my, is about the age of the oldest Andaman Flysch on the A–N Ridge.

During this history of extension, northward motion of the sliver plate occurred as a result of the oblique convergence, and westward extension occurred, a result of the component of normal convergence like other backarc extensional basins. The relative northwest motion of the block west of

the sliver fault was oblique, a resultant vector of the normal extension and the north–south sliver faulting. Total offset of the Sagaing Fault during this spreading history should be just the northward component, 332 km, rather than the vector sum of the sliver block of 389 km toward 327°. These reconstructions, therefore, predict total offset of the Sagaing Fault as somewhere between the extremes previously published of 203 and 460 km.

The direction and magnitude of opening of each of these stages depends on an estimate of the direction of tectonic trends or opening lines within the basin or ridge. Each was explained during the descriptions of these stages. An error of a few degrees of direction in each could amount to tens of kilometers in amount of opening because of the shapes of the features. Thus, the possible error, although indeterminate, could amount to tens of kilometers.

The strike-slip fault rate, vector BE in Fig. 17, varies with the obliquity of plate convergence, from more oblique in the north to less oblique off Sumatra. Estimates of the rates of the Sagaing Fault and Sumatra Fault System appear to confirm this. Vigny et al. (2003) estimate total strike-slip plate motion in Myanmar as 35 mm/yr, with <20 mm/yr along the Sagaing Fault itself. Our estimate of N–S motion in the Central Andaman Basin is 27 mm/yr (Table 3). Sieh and Natawidjaja (2000) and Genrich et al. (2000) estimate 25 mm/yr at northwest Sumatra, decreasing to 10–20 mm/yr in southeast Sumatra.

The E–W component of opening of the Central Andaman Basin (Table 3) at the present time is 12 mm/yr. This compares with the rate of convergence between the Andaman Islands and mainland eastern India of 15 mm/yr reported by Paul et al. (2001) from GPS surveys.

The rates of spreading or opening in the Andaman Sea appear to range widely (Table 3) from Oligocene to the present from about 7 to 38 mm/yr. Fluctuations occur, and the apparent increase is not uniform. With increasing rotation of the trend of the arc from about 120–300° to N–S, the obliquity of the convergence increased, so the rate of sliver faulting should also increase. The reversals in spreading rate are undoubtedly misinterpretations in directions and amounts of opening during each stage and misinterpretations in the times.

The outer arc ridge, the combined Andaman–Nicobar and Mentawei Ridges, varies in width, as measured by the distance from the subduction zone to the islands or crest of the ridge. It ranges from 80 km at Preparis Island at 15°N, to 95 km off the Andaman Islands, to a maximum of 150 km at Great Nicobar, to 85 km at Similue and Nias (Figs. 1, 2 and 4). It thins rapidly southeast of where the OWAF crosses the ridge. If the OWAF has always been right lateral, one would expect the ridge to be a more constant width and one would not expect the sharp bend in the trench axis and subduction zone at 2°N. This bend suggests the interesting possibility that the OWAF was initially left lateral. Pivnik et al. (1998) have considered the possibility of initial left-lateral motion on the Sagaing Fault in Myanmar because of possible movement of the Burma Block during the collision process.

At about 42 Ma, the direction of convergence between India and Asia was about 38° (Fig. 18), and the perpendicular to the alignment of a straight linear arc would have been about 038° by the rate of rotation we have assumed. This would have been normal convergence. Furthermore, if the arc were bending, as we speculated in discussion of the period 44–32 Ma, east of that point the lateral component would have been left lateral; west and NW of that point would have been right lateral. Thus, the ancestral OWAF could possibly have been left lateral for a period of time.

As stated earlier, many of the interpretations and conclusions of this paper are speculative based on limited data. Much remains to be done within the Andaman Sea and in the adjacent land areas to resolve some of this speculation. We need more rock sampling, analysis, dating and stratigraphic analysis. Further definitive magnetic surveys are needed. More seismic refraction and/or deeper penetration multichannel seismic reflection are needed. Correlation of exploration seismic reflection data with hydrocarbon exploration wells is already possible, but needs to be expanded into the deeper water areas where such exploration drilling has not and will not be extended. The bathymetry is exceedingly complex, and detailed swath mapping and detailed high resolution seismic reflection surveys will be required to understand it and the tectonics.

Finally, a recent paper by Clark et al. (2004) considers river capture and changes in drainage patterns in eastern Asia as a result mainly of Miocene (?) uplift in eastern Tibet. They raise the possibility that the Salween (Thanlwin) River had captured drainage that previously had run into the South China Sea through the Red River. Subsequently, the Irrawaddy (Ayeyarwady) River captured drainage of the Tsangpo River, and even later the Brahmaputra River captured the Tsangpo drainage and the Irrawaddy (Ayeyarwady) drainage was limited to northern Myanmar. These drainage changes would be reflected in amount and provenance of sediment coming into the Andaman Sea in this late to post-Miocene time. It also raises the possibility that studies of provenance of the sedimentary record in cores from the Andaman Sea could help to establish the timing of these changes, if the source areas show differences in mineralogy.

8. Conclusions

1. The Andaman Sea is an active backarc extensional basin lying above and behind the Sunda subduction zone where convergence is highly oblique.
2. The Andaman Sea opened during the Cenozoic by a succession of extensional episodes.
3. During each extensional episode backarc extension normal to the trend of the subduction zone combined

with strike-slip faulting of a sliver plate, first formed probably in the Eocene, to result in oblique opening.
4. During the Cenozoic collision of India with Asia, the alignment of the Sunda subduction zone gradually rotated in a clockwise direction.
5. With this rotation, obliquity increased and the opening scenario shows an apparent increase in the rate of strike-slip motion.

Acknowledgements

I have many colleagues to thank for sharing in the collection, analysis and interpretation of the information in this paper. Dave Moore and Frans Emmel were my close colleagues who contributed especially significantly through the early years of this study, as did Larry Lawver (magnetics), Bob Kieckhefer, Russ Raitt and Marilee Henry (seismic refraction work), Perry Crampton, Paul ONeil, Aung Tin U, Hla Tin, Aung Min and our other colleagues who worked with us at sea. More recently, I have been especially assisted by Bob Kieckhefer, Steve Cande, Hla Maung and Kerry Sieh. Funding for the work at sea and early years of analysis was provided by the Office of Naval Research and the National Science Foundation. Dave Moore, Dick Murphy and Kelvin Rodolfo made careful, thoughtful reviews of an early version of this paper and made many excellent suggestions for improvement. Responsibility for all interpretations and opinions is mine.

References

Acharyya, S.K., 1994. Accretion of Indo-Australian Gondwanic blocks along Peri-Indian collision margins. Ninth International Gondwana Symposium, Hyderabad, India 1994, pp. 1029–1049.

Acharyya, S.K., 1997. Stratigraphy and tectonic history reconstruction of the India–Burma–Andaman mobile belt. Indian Journal of Geology 69, 211–234.

Acharyya, S.K., 1998. Break-up of the greater Indo-Australian continent and accretion of blocks framing south and east Asia. Journal of Geodynamics 26, 149–170.

Acharyya, S.K., Ray, K.K., Sengupta, S., 1990. Tectonics of the ophiolite belt from Naga Hills and Andaman Islands, India. Proceedings Indian Academy Science (Earth Planetary Science) 99, 187–199.

Alam, M., Alam, M.M., Curray, J.R., Chowdhury, M.L.R., Gani, M.R., 2003. An overview of the sedimentary geology of the Bengal Basin in relation to the regional tectonic framework and basin-fill history. Sedimentary Geology 155, 179–208.

Alcock, A.W., 1902. A Naturalist in Indian Seas. John Murray Publishing Company, London, p. 328.

Ananthanarayanan, P.V., Ramdev, C.M., Murti, K.V.S., 1981. Andaman Island Arc. Workshop on Geological Interpretation of Geophysical Data. Institute of Petroleum Exploration, Oil and Natural Gas Commission, Dehra Dun, India, p. 8

Andreason, M.W., Mudfor, B., St Onge, J.E., 1997. Geologic evolution and petroleum system of the Thailand Andaman Sea basins. Indonesian Petroleum Association. Proceedings of the Petroleum Systems of SE Asia and Australasia, May 1997, IPA97-OR-44 1997.

Aung Khin, Kyaw Win, 1968. Preliminary studies of the paleogeography of Burma during the Cenozoic. Union of Burma Journal of Science and Technology 1, 241–251.

Aung Khin, Kyaw Win, 1969. Geology and hydrocarbon prospects of the Burma Tertiary geosyncline. Union of Burma Journal of Science and Technology 2, 53–81.

Aung Khin, Aung Tin U., Aung Soe, Khin Han, 1970. A study on the gravity indication of the Shan Scarp fault. Union of Burma Journal of Science and Technology 3, 91–113.

Ball, V., 1870. Notes on the geology of the vicinity of Port Blair, Andaman Islands. Journal Asiatic Society of Bengal 39, 231–239.

Bandopadhyay, P.C., Ghosh, M., 1998. Facies, petrology and depositional environment of the Tertiary sedimentary rocks, around Port Blair, South Andaman. Journal Geological Society of India 52, 53–66.

Bhattacharya, A., Reddy, C.S.S., Srivastav, S.K., 1993. Remote sensing for active volcano monitoring in barren Island, India. Ninth Thematic Conference on Geologic Remote sensing, Pasadena, California, pp 993–1003.

Bender, F., 1983. Geology of Burma. Borntraeger, Berlin, p. 260.

Bennett, J.D., Bridge, D.McC., Cameron, N.R., Djunudden, A., Ghazali, S.A., Jeffery, D.H., Keats, W., Rock, N.M.S., Thompson, S.J., Whandoyo, R., 1981. Geologic Map of the Banda Aceh Quadrangle, North Sumatra. Geologic Map. Geological Research and Development Centre, Bandung, Indonesia, p. 19.

Brunnschweiler, R.O., 1966. On the geology of the Indoburman Ranges. Geological Society Australia Journal 13, 127–194.

Brunnschweiler, R.O., 1974. Indoburman Ranges. In: Spencer, A.M. (Ed.), Mesozoic–Cenozoic Orogenic Belts Geological Society London, Special Publication 4, pp. 279–299.

Cameron, N.R., Bennett, J.D., Bridge, D.McC., Clarke, M.C.G., Djunuddin, A., Ghazali, S.A., Harahap, H., Jeffery, D.H., Keats, W., Ngabito, H., Rocks, N.M.S., Thompson, S.J., 1983. The Geology of the Takengon Quadrangle, Sumatra. Geological Map. Geological Research and Development Centre, Bandung, Indonesia, p. 26.

Chakraborty, P.P., Pal, T., 2001. Anatomy of a forearc submarine fan: Upper Eocene–Oligocene Andaman Flysch Group, Andaman Islands, India. Gondwana Research 4, 477–486.

Chakraborty, P.P., Pal, T., Gupta, T.D., Gupta, K.S., 1999. Facies pattern and depositional motif in an immature trench-slope basin, Eocene Mithakhari Group, Middle Andaman Island, India. Journal Geological Society India 53, 271–284.

Chakraborty, P.P., Mukhopadhyay, B., Pal, T., Gupta, T.D., 2002. Statistical appraisal of bed thickness patterns in turbidite successions, Andaman Flysch Group, Andaman Islands, India. Journal of Asian Earth Sciences 21, 189–196.

Chatterjee, P.K., 1967. Geology of the main islands of the Andaman Sea. Proceedings Symposium on Upper Mantle Project, Geophysical Research Board, National Geophysical Research Institute, Hyderabad, India, pp. 348–360.

Chatterjee, P.K., 1984. The Invisible Bank fault and geotectonics of the Andaman Nicobar Islands. Quarterly Journal Geological Mineral Metallurgical Society India 56, 28–40.

Chhibber, H.L., 1934. The Geology of Burma. McMillan and Co, London, p. 530.

Clark, M.K., Schoenbohm, L.M., Royden, L.H., Whipple, K.X., Whipple, K.X., Burchfiel, B.C., Tang, W., Wang, E., Chen, L., 2004. Surface uplift, tectonics, and erosion of eastern Tibet from large-scale drainage patterns. Tectonics 23 (TC1006), 1–20.

Cox, H., 1799a. An account of the petroleum wells in the Burmha Dominions, extracted from a journal of a voyage from Ranghong up in the river Erai-wuddey to Amarapoorah to the present capital of the Burmha empire. Philosophical Magazine 9, 226–234.

Cox, H., 1799b. An account of the petroleum wells in the Burmha Dominions, extracted from a journal of a voyage from Ranghong up in the river Erai-wuddey to Amarapoorah to the present capital of the Burmha empire. Asiatic Research 6, 127–136.

Curray, J.R., 1989. The Sunda Arc: a model for oblique plate convergence, Netherlands. Journal of Sea Research 24, 131–140.

Curray, J.R., 1991. Possible greenschist metamorphism at the base of a 22 km sediment section, Bay of Bengal. Geology 19, 1097–1100.

Curray, J.R., Moore, D.G., 1974. Sedimentary and tectonic processes in Bengal deep-sea fan and geosyncline. In: Burk, C.A., Drake, C.L. (Eds.), The Geology of Continental Margins. Springer, New York, pp. 617–628.

Curray, J.R., Moore, D.G., Lawver, L.A., Emmel, F.J., Raitt, R.W., Henry, M., Kieckhefer, R., 1979. Tectonics of the Andaman Sea and Burma. In: Watkins, J., Montadert, L., Dickerson, P.W. (Eds.), Geological and Geophysical Investigations of Continental Margins American Association Petroleum Geologists, Memoir 29, pp. 189–198.

Curray, J.R., Emmel, F.J., Moore, D.G., Raitt, R.W., 1982. Structure, tectonics and geological history of the northeastern Indian Ocean. In: Nairn, A.E.M., Stehli, F.G. (Eds.), The Ocean Basins and Margins. The Indian Ocean, vol. 6. Plenum Press, New York, pp. 399–450.

Curray, J.R., Emmel, F.J., Moore, D.G., 2003. The Bengal Fan: morphology, geometry, stratigraphy, history and processes. Marine and Petroleum Geology 19, 1191–1223.

Dasgupta, S., 1992. Seismotectonics and stress distribution in the Andaman plate. Memoir Geological Society of India 23, 319–334.

Dasgupta, S., Mukhopadhyay, M., 1993. Seismicity and plate deformation below the Andaman arc, northeastern Indian Ocean. Tectonophysics 225, 529–542.

DeMets, C., Gordon, R.G., Argus, D.F., Stein, S., 1994. Effect of recent revisions to the geomagnetic reversal time scale on estimates of current plate motions. Geophysical Research Letters 21, 2191–2194.

Dey, B.P., 1968. Aerial photo interpretation of a major lineament in the Yamethin–Pyawbwe quadrangle. Union of Burma Journal Science and Technology 1, 431–443.

Diament, M., Harjono, H., Karta, K., Deplus, C., Dahrin, M., Zen Jr.., M.T., Gérard, M., Lassai, O., Martin, A., Malod, J., 1992. Mentawei fault zone off Sumatra: a new key to the geodynamics of western Indonesia. Geology 20, 259–262.

Fitch, R., 1599. The voyage of M. Ralph Fitch, marchant of London…. Hakluyt's Principal Navigation 2, 250–268.

Fitch, T.J., 1972. Plate convergence, transcurrent faults and internal deformation adjacent to Southeast Asia and the western Pacific. Journal Geophysical Research 77, 4432–4462.

Frerichs, W.E., 1971. Paleobathymetric trends of Neogene foraminiferal assemblages and sea floor tectonism in the Andaman Sea area. Marine Geology 11, 159–173.

Gee, F.R., 1927. The Geology of the Andaman and Nicobar Islands, with special reference to Middle Andaman Island. Records of the Geological Survey of India LIX, 208–232.

Genrich, J.F., Bock, Y., McCaffrey, R., Prawirodirjo, L., Stevens, C.W., Puntodewo, S.S.O., Subarya, C., Wdowinski, S., 2000. Distribution of slip at the northern Sumatran fault system. Journal of Geophysical Research 105, 28,327–28,341.

Goosens, P.J., 1978. Earth sciences bibliography of Burma, Yunan and Andaman Islands, Third Regional Conference on Geology and Mineral Resources of Southeast Asia, Bangkok, Thailand.

Guzmán-Speziale, M., Ni, J., 1993. The opening of the Andaman Sea. Geophysical Research Letters 20, 2949–2952.

Guzmán-Speziale, M., Ni, J., 1996. Seismicity and active tectonics of the western Sunda Arc. In: An Yin, Harrison, M.T. (Eds.), The Tectonic Evolution of Asia. Cambridge University Press, Cambridge, pp. 63–84.

Guzmán-Speziale, M., Ni, J., 2000. Comment on 'Subduction in the Indo-Burman region: is it still active?' by S.P. Satyabala. Geophysical Research Letters 27, 1065–1066.

Haq, B.U., Hardenbol, J., Vail, P.R., 1987. Chronology of fluctuating sea levels since the Triassic. Science 235, 1156–1167.

Harding, T.P., 1985. Seismic characteristics and identification of negative flower structures, positive flower structures, and positive structural inversion. American Association of Petroleum Geologists, Bulletin 69, 582–600.

Hla Maung, 1983. A new reconstruction of Southeast Asia and Gondwanaland: its relation to mantle plumes or hotspots. SEAPEX Proceedings VI, 66–70.

Hla Maung, 1987. Transcurrent movements in the Burma–Andaman Sea region. Geology 15, 911–912.

Hochstetter, F. von, 1869. Geology and physical geography of Nicobar Islands. Records Geological Survey of India 2 (Pt 3).

Holt, W.E., Chamot-Rooke, N., Le Pichon, X., Haines, A.J., Shen-Tu, B., Ren, J., 1918. Velocity field in Asia inferred from Quaternary fault slip rates and global positioning system observations. Journal of Geophysical Research 105, 19,185–19,209.

Hutchison, C.S., 1989. Geological Evolution of South-East Asia. Clarendon Press, London, p. 368.

Imbrie, J., Hays, J.D., Martinson, D.G., McIntyre, A., Mix, A.C., Morley, J.J., Pisias, N.G., Prell, W.L., Shackleton, N.J., 1984. The orbital theory of Pleistocene climate: support from a revised chronology of the marine $\delta^{18}O$ record. In: Berger, A., Imbrie, J., Hays, J., Kukla, G., Saltzman (Eds.), Milankovitch and Climate. D. Riedel, Boston, pp. 269–305.

Jacob, K., 1954. The occurrence of radiolarian cherts in association with ultrabasic intrusives in the Andaman Islands, and its significance in sedimentary tectonics. Records Geological Survey India 83 (Pt 2).

Karunakaran, C., Ray, K.K., Saha, S.S., 1964a. A new probe into the tectonic history of the Andaman and Nicobar Islands. Reports of the 22nd International Geologic Congress, New Delhi, India IV, 507–515.

Karunakaran, C., Pawde, M.B., Raina, V.K., Ray, K.K., Saha, S., 1964b. Geology of South Andaman Island, India. Reports of the 22nd International Geologic Congress, New Delhi, India. XI, 79–100.

Karunakaran, C., Ray, K.K., Saha, S.S., 1964c. Sedimentary environment of the formation of Andaman Flysch, Andaman Islands, India. Reports of the 22nd International Geologic Congress, New Delhi, India XV, 226–232.

Karunakaran, C., Ray, K.K., Saha, S.S., 1968a. A revision of the stratigraphy of Andaman and Nicobar Islands, India. Bulletin of the National Institute of Sciences of India 38, 436–441.

Karunakaran, C., Ray, K.K., Saha, S.S., 1968b. Tertiary sedimentation in the Andaman–Nicobar geosyncline. Journal Geological Society of India 9, 32–39.

Karunakaran, C., Ray, K.K., Sen, C.R., Saha, S.S., Sakar, S.K., 1975. Geology of Great Nicobar Island. Geological Society of India Journal 16, 135–142.

Keats, W., Cameron, N.R., Djunuddin, A., Ghazali, S.A., Harahap, H., Kartawa, W., Ngabito, H., Rock, N.M.S., Thompson, S.J., Whandoyo, R., 1981. The Geology of the Lhokseumawe Quadrangle, Sumatra, Geological Research and Development Centre, Bandung, Indonesia. Geological Map, p. 13.

Kieckhefer, R.M., Moore, G.F., Emmel, F.J., 1981. Crustal structure of the Sunda forearc region west of central Sumatra from gravity data. Journal of Geophysical Research 86, 7003–7012.

Klootwijk, C.T., Gec, J.S., Peirce, J.W., Smith, G.M., McFadden, P.L., 1992. An early India–Asia contact: Paleomagnetic constraints from Ninetyeast Ridge, ODP Leg 121. Geology 20, 395–398.

Lawson, A.C., 1921. The mobility of the Coast Ranges of California. University of California Publications in Geology 12, 431–473.

Lee, T.T., Lawver, L.A., 1995. Cenozoic plate reconstruction of Southeast Asia. Tectonophysics 251, 85–138.

Mallet, F.R., 1895. Some early allusions to Barren Island, with a few remarks thereon. Records Geologic Survey India 28, 22–34.

McCaffrey, R., 1991. Slip vectors and stretching of the Sumatran fore arc. Geology 19, 881–884.

McCaffrey, R., Zwick, P.C., Bock, Y., Prawirdirdjo, L., Genrich, J.F., Stevens, C.W., Puntodewo, S.S.O., Subarya, C., 2000. Journal of Geophysical Research 105, 28,363–28,376.

McKenzie, D., 1978. Some remarks on the development of basins. Earth and Planetary Science 40, 25–32.

Metcalfe, I., 1984. Late Paleozoic paleogeography of SE Asia: some stratigraphic paleontological and paleomagnetic constraints, Fifth Regional Congress Geology Mineral Resources. SE Asia, Kuala Lumpur Abstr. 20.

Misra, P.C., Roy, T.K., 1984. Exploration in Andaman forearc basin its evaluation, facies trend and prospects—a review. Fifth Offshore Southeast Asia, Singapore, 4.66–4.83.

Mitchell, A.H.G., 1977. Tectonic settings for emplacement of southeast Asian tin granites. Geological Society of Malaysia, Bulletin 6, 123–140.

Mitchell, A.H.G., 1981. Phanerozoic plate boundaries in mainland SE Asia, the Himalayas and Tibet. Journal Geologic Society London 138, 109–122.

Mitchell, A.H.G., 1985. Collision-related fore-arc and back-arc evolution of the northern Sunda Arc. Tectonophysics 116, 323–334.

Mitchell, A.H.G., 1989. The Shan Plateau and western Burma: Mesozoic–Cenozoic plate boundaries and correlations with Tibet. In: Sengor, A.M.C. (Ed.), Tectonic Evolution of the Tethyan Region. Kluwer Academic Publishers, Dordrecht, pp. 567–583.

Mitchell, A.H.G., McKerrow, W.S., 1975. Analogous evolution of the Burma orogen and the Scottish Caledonides. Geological Society of America Bulletin 86, 305–315.

Mukerjee, M., 2003. The Land of Naked People. Houghton Mifflin Company, Boston, New York, p. 268.

Mukhopadyay, M., 1984. Seismotectonics of subduction and back-arc rifting under the Andaman Sea. Tectonophysics 108, 229–239.

Mukhopadyay, M., 1992. On earthquake focal mechanism studies for the Burmese arc. Current Science 62, 72–85.

Myint Thein, Kyaw Tint, Aye Ko Aung, 1981. On the lateral displacement of the Sagaing Fault. Georeports 1, 1. University of Mandalay, Burma.

Ninkovich, D., 1976. Late Cenozoic clockwise rotation of Sumatra. Earth Planetary Science Letters 29, 269–275.

Oldham, R.D., 1885. Notes on the geology of the Andaman Islands. Records Geological Survey India 18 (Pt 3).

Pal, T., Chakraborty, P.P., Gupta, T.D., Singh, C.D., 2003. Geodynamic evolution of the outer-arc–forearc belt in the Andaman Islands, the central part of the Burma–Java subduction complex. Geological Magazine 140, 289–307.

Parthasarathy, T.N., 1984. The conglomerates of Middle Andaman and their geologic significance. Journal Geological Society India 25, 94–101.

Pascoe, E.H., 1912. The oil-fields of Burma. Memoirs of the Geological Survey of India, XL, 1, 1–269.

Paul, D.D., Lian, H.M., 1975. Offshore basins of southwest Asia—Bay of Bengal to South Sea. In: Proceedings of the Ninth World Petroleum Congress, Tokyo, vol. 3, pp. 1107–121.

Paul, J., Bürgemann, R., Gaur, V.K., Bilham, R., Larson, K.M., Ananda, M.B., Jade, S., Mukal, M., Anupama, T.S., Satyal, G., Kumar, D., 2001. The motion and active deformation of India. Geophysical Research Letters 28, 647–650.

Peter, G., Weeks, L.A., Burns, R.E., 1966. A reconnaissance geophysical survey in the Andaman Sea and across the Andaman–Nicobar Island arc. Journal of Geophysical Research 71, 495–509.

Pivnik, D.A., Nahm, J., Tucker, R.S., Smith, G.O., Nyein, K., Nyunt, N., Maung, P.H., 1998. Polyphase deformation in a fore-arc/back-arc basin, Salin subbasin, Myanmar (Burma). American Association of Petroleum Geologists Bulletin 82, 1837–1856.

Polachan, S., Racey, A., 1994. Stratigraphy of the Mergui Basin, Andaman Sea: implications for petroleum exploration. Journal of Petroleum Geology 17, 373–406.

Prawirodirdjo, L., Bock, Y., Genrich, J.F., 2000. One century of tectonic deformation along the Sumatran fault from triangulation and global positioning system surveys. Journal of Geophysical Research 105, 28,343–28,361.

Raju, K.A.K., Ramprasad, T., Rao, P.S., Rao, B.R., Varghese, J., 2004. New insights into the tectonic evolution of the Andaman basin, northeast Indian Ocean. Earth and Planetary Science Letters 221, 145–162.

Replumaz, A., Tapponnier, P., 2003. Reconstruction of the deformed collision zone between India and Asia by backward motion of lithospheric blocks. Journal of Geophysical Research 108, ETG 1-1-24.

Richter, B., Fuller, M., 1996. Paleomagnetism of the Sibumasu and Indochina blocks: implications for the extrusion tectonic model. In: Hall, R., Blundell, E. (Eds.), Tectonic Evolution for Southeast Asia Geological Society Special Publication No. 106, pp. 203–224.

Richter, B., Fuller, M., Schmidtke, E., Tin Myint, U., Tin Ngwe, U., Mya Win, U., Bunapas, S., 1993. Paleomagnetic results from Thailand and Myanmar: implications for the interpretation of tectonic rotations in Southeast Asia. Journal of Southeast Asian Earth Sciences 8, 247–255.

Richter, B., Schmidtke, E., Fuller, M., Harbury, N., Samsudin, A.R., 1999. Paleomagnetism of peninsular Malaysia. Journal of Asian Earth Sciences 17, 477–519.

Rink, P.H., 1847. Die Nikobar Inseln. Eine Geographische Skizze, mit speciieller Berüksichtigung der Geognosie, Kopenhagen. Translated Selections, Records Government India LXXVII, 540.

Rodolfo, K.S., 1969a. Bathymetry and marine geology of the Andaman basin, and tectonic implications for Southeast Asia. Geological Society of America Bulletin 80, 1203–1230.

Rodolfo, K.S., 1969b. Sediments of the Andaman basin, northeastern Indian Ocean. Marine Geology 7, 371–402.

Roy, T.K., 1983. Geology and hydrocarbon prospects of Andaman–Nicobar basin. In: Bhandari, L.L. (Ed.), Petroliferous Basins of India Petroleum Asia Journal, pp. 37–50.

Roy, T.K., 1986. Petroleum prospects of the frontal fold belt and subduction complex associated with the Indian plate boundary in the northeast. Proceedings of the Southeast Petroleum Exploration Society VII, 192–212.

Roy, S.K., 1992. Accretionary prism in Andaman forearc. Geological Survey India Special Publication 29, 273–278.

Roy, T.K., Chopra, N.N., 1987. Wrench faulting in Andaman forearc basin, India. Proceedings Offshore Technology Conference 19, 393–404.

Roy, D.K., Acharyya, S.K., Ray, K.K., Lahri, T.C., Sen, M.K., 1988. Nature of occurrence, age, and depositional environment of the oceanic pelagic sediments associated with the ophiolite assemblage, South Andaman Islands, India. Indian Minerals 42, 31–56.

Satabala, S.P., 1998. Subduction in the Indo-Burman region: is it still active?. Geophysical Research Letters 25, 3189–3192.

Sewell, R.B.S., 1925. The geography of the Andaman Sea basin. Asiatic Society of Bengal 9, 1–26.

Sieh, K., Natawidjaja, D., 2000. Neotectonics of the Sumatran fault, Indonesia. Journal of Geophysical Research 105, 28,295–28,326.

Smith, W.H.F., Sandwell, D.T., 1997. Global seafloor topography from satellite altimetry and ship depth soundings. Science 277, 1956–1962.

Srinivasan, M.S., 1979. Geology and mineral resources of the Andaman and Nicobar Islands, Andaman Nicobar Information 1978–1979. Government Printing Office, Port Blair.

Srinivasan, M.S., 1986. Neogene reference sections of Andaman–Nicobar: their bearing on volcanism, sea-floor tectonism and global sea-level changes. In: Ghose, N.C., Varadarajan, S. (Eds.), Ophiolites and Indian Plate Margin, pp. 295–308.

Srinivasan, M.S., Azmi, R.J., 1979. Correlation of late Cenozoic marine sections in Andaman–Nicobar, northern Indian Ocean and the equatorial Pacific. Journal of Paleontology 53, 1401–1415.

Stephenson, D., Marshall, T.R., 1984. The petrology and mineralogy of Mt. Popa and the nature of the late-Cenozoic Burma volcanic arc. Journal Geological Society of London 141, 747–762.

Suess, E., 1904. The Face of the Earth, vol. 5. Clarendon Press, Oxford.

Tankard, A.J., Balkwill, H.R., Mehra, A., Aung Din, 1998. Tertiary wrench fault tectonics and sedimentation in the central basin of Burma. American Association of Petroleum Geologists Bulletin 78, 1165, (Abstr.).

Tapponnier, P., Peltzer, G., Le Dain, A.Y., Armijo, R., Cobbold, P., 1982. Propagating extrusion tectonics in Asia: new insights from simple experiments with plasticine. Geology 10, 611–616.

Tapponnier, P., Peltzer, G., Armijo, R., 1986. On the mechanics of the collision between India and Asia, In: Coward, M., and Ries, A.C. (Eds), Collision Tectonics, Geological Special Publication No. 19, pp. 115–157

Tipper, G.H., 1911. The geology of the Andaman Islands. Memoir Geological Survey India 35, 195–216.

Van Linschoten, V.J.H., 1595. Itinerario Voyage ofte Schipvaert, Van Jan Huygen Van Lindschoten naer ooste ofte Portugaels Indien, Amstelredam.

Varga, R.J., 1997. Burma. In: Moores, E.M., Fairbridge, R.W. (Eds.), Encyclopedia of European and Asian Regional Geology. Chapman and Hall, London, pp. 109–121.

Vigny, C., Socquet, A., Rangin, C., Chamot-Rooke, N., Pubellier, M., Bouin, M.-N., Bertrand, G., Becker, M., 2003. Present-day crustal deformation around Sagaing Fault, Myanmar. Journal of Geophysical Research 108, ETG 6-1-10.

Weeks, L.A., Harbison, R.N., Peter, G., 1967. Island arc system in the Andaman Sea. American Association of Petroleum Geologists Bulletin 51, 1803–1815.

Wegener, A., 1966. The Origin of Continents and Oceans. Dover Publications, New York, p. 246.

Win Maw, Myint Kyi, 1998. Prospecting the Moattama/Tanintharyi Shelf of Myanmar, Proceedings, Gas Habitats of SE Asia and Australian Conference. Indonesian Petroleum Association.

Win Swe, 1972. Strike-slip faulting in central belt of Burma (abs). In: Haile, N.S. (Ed.), Regional Conference on the Geology of Southeast Asia, Kuala Lumpur, Malaysia Annex to Newsletter No. 34, p. 59.

Win Swe, 1981. A major strike-slip fault in Burma. Contributions to Burmese Geology 1, 63–72.

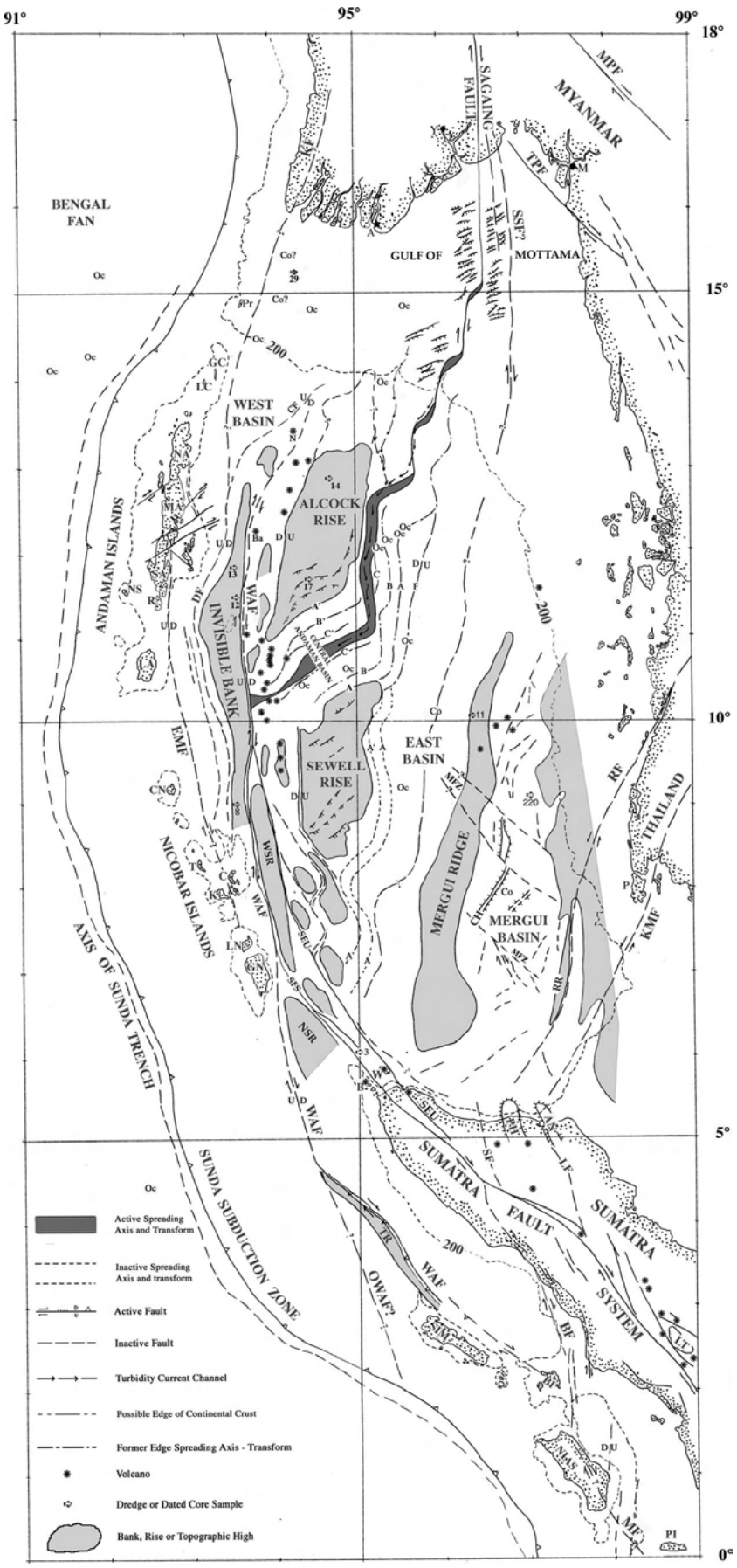

Fig. 4. Tectonic map of the Andaman Sea and adjacent southern Myanmar and northern Sumatra. Abbreviations for this and subsequent figures: A is Ama Village, AN is Arun High, B is Brueh Island, Ba is Barren Island, BF is Battee Fault, BI is Banyak Islands, C is Camorta Island, CF is Cocos Fault, CH is Central Horst, CN is Car Nicobar Island, Co is continental crust refraction determination, DF is Diligent Fault, EMF is Eastern Margin Fault, EP is Elephant Point, GC is Great Cocos Island, GN is Great Nicobar Island, K is Katchall Island, KF is Kabaw Fault, KMF is Khlong Marui Fault, LA is Little Andaman Island, LC is Little Cocos Island, LF is Lhokseumawe-Lopok Kutacane Fault, LN is Little Nicobar Island, LT is Lake Toba, M is Mawlamyine (Moulmein), MA is Middle Andaman Island, MF is Mentawei Fault, MFZ is Mergui Fault, MPF is Mae Ping Fault, N is Narcondam Island, NA is North Andaman Island, NS is North Sentinal Island, NSR is North Sumatra Ridge, Oc is oceanic crust refraction determination, OWAF is Old West Andaman Fault, P is Phuket Island, PH is Peusangan High, PI is Pini Island, Pr is Preparis Island, R is Rutland Island, RF is Ranong Fault, RR is Ranong Ridge, SA is South Andaman Island, SEU is Seulimeum strand of SFS, SF is Samalanga Sipokok Fault, SFS is Sumatra Fault System, SIM is Simeuleu Island, SSF is Shan Scarp Fault, T is Terressa Island, TPF is Three Pagodas Fault, TR is Tuba Ridge, W is Weh Island, WAF is West Andaman Fault, WSR is West Sewell Ridge, Y is Yangon (Rangoon). Dredge and dated core samples: ***17***, dredge I-17, moderately fractionated tholeitic basalt (J.W. Hawkins, personal communication ~11.5°N, deepth ~900–1250 m, dates 19.8±0.7, 20.5±1.0 my; ***29***, dredge C-29, Miocene deep-water shale (F.L. Parker, personal communication, 1968), depth ~1350–2100 m; The following from Frerichs (1967) and Rodolfo (1969a,b): ***3***, altered hypersthene augite basalt, ~11°N; ***8***, radiolarite shale, post-early late Miocene, ~10 my, uplifted >2000 m, plus altered extrusive rock ~9°N; ***11***, unaltered vesicular basalt from a 120 m pinnacle on the shelf, ~1.5–2 my, ~10°N; ***12***, late lower Miocene calcarenite and calcilutite, ~17 my, uplifted ~400 m, ~11.5°N; ***13***, late upper Miocene calcarenite and calcilutite, ~6 my, uplifted > 500 m, ~12°N; ***14***, tabular, massive unaltered intergranular augite basalt, undated; ***220***, core of early Pliocene shale, ~5 my, subsided >100 m, ~13°N.

Annex B73

C. Subrahmanyam & S. Chand, "Evolution of the Passive Continental Margins of India—A Geophysical Appraisal", *Gondwana Research*, Vol. 10, No. 1-2 (2006)

Available online at www.sciencedirect.com
SCIENCE DIRECT®
Gondwana Research 10 (2006) 167–178
www.elsevier.com/locate/gr

Evolution of the passive continental margins of India—a geophysical appraisal

C. Subrahmanyam [a,*], S. Chand [b]

[a] National Geophysical Research Institute, Hyderabad 500 007, India
[b] Geological Survey of Norway, Polarmiljøsenteret, NO-9296, Tromsø, Norway

Received 31 March 2005; accepted 7 November 2005

Abstract

The passive continental margins of India have evolved as India broke and drifted away from East Antarctica, Madagascar and Seychelles at various geological times. In this study, we have attempted to collate and re-examine gravity and topographic/bathymetry data over India and the adjoining oceans to understand the structure and tectonic evolution of these margins, including processes such as crustal/lithosphere extension, subsidence due to sedimentation, magmatic underplating and so on. The Eastern Continental Margin of India (ECMI) seems to have evolved in a complex rift and shear tectonic settings in its northern and southern segments, respectively, and bears similarities with its conjugate in East Antarctica. Crustal extension rates are uniform along the stretch of the ECMI in spite of the presence or absence of crustal underplated material, variability in lithospheric strength and tectonic style of evolution ranging from rifting to shearing. The Krishna-Godavari basin is underlain by a strong (~ 30 km) elastic lithosphere, while the Cauvery basin is underlain by a thin elastic lithosphere (~3 km). The coupling between the ocean and continent lithosphere along the rifted segment of the ECMI is across a stretched continental crust, while it is direct beneath the Cauvery basin. The Western Continental Margin of India (WCMI) seems to have developed in an oblique rift setting with a strike-slip component. Unlike the ECMI, the WCMI is in striking contrast with its conjugate in the eastern margin of Madagascar in respect of sedimentation processes and alignment of magnetic lineations and fracture zones. The break up between eastern India and East Antarctica seems to have been accommodated along a Proterozoic mobile belt, while that between western India and Madagascar is along a combination of both mobile belt and cratonic blocks.

Keywords: India; Passive margins; Tectonics; Gravity; Topography

1. Introduction

Passive margins develop at the trailing edges of continents when they break and drift away from one another. These margins mark the site of contact between old Precambrian land masses and young ocean basins and bear the imprint of the break up process between the continents as also the tectonic, magmatic and subsidence processes that have affected the margins. Therefore, a study of the passive continental margins is as important as the study of continental shields and ocean basins.

Passive margins evolve in a wide range of tectonic settings. Depending upon the tectonic and magmatic processes to which the passive margins were subjected, they have been categorized as: rifted vs. sheared margins, volcanic vs. non-volcanic (hot and cold) margins, sediment rich and sediment starved, wide and narrow, active vs. passive modes of rifting, and so on (e.g., Davison, 1997; Ruppel, 1995; White, 1992; White et al., 2003 and others). In the case of active rifting, a mantle plume impinges the overlying continental lithosphere resulting in the rifting of the landmasses. In contrast to this, there could be passive rifting where no plume activity is involved. There can also be normal rifting where the continents break and drift away from one another in which case the margins developed are classified as rifted margins. In contrast to these are the sheared or transform margins where continental blocks shear past one another. In case of the rifted margins, considerable extension of the continental crust takes place and a transitional or extended continental crust remains as a corridor between the continents and the oceans. However, in case of the transform margins, there is direct coupling between continental and oceanic crust.

* Corresponding author.
E-mail address: csmnyam@yahoo.com (C. Subrahmanyam).

1342-937X/$ - see front matter
doi:10.1016/j.gr.2005.11.024

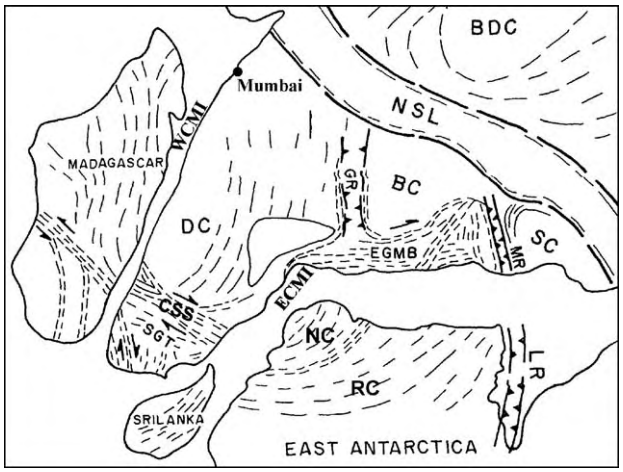

Fig. 1. Gondwana reassembly map showing structural grains in India, East Antarctica and Madagascar (compiled from Chetty, 1996; Yoshida et al., 1999). BC—Bastar craton, BDC—Bundelkhand craton, DC—Dharwar craton, EGMB—Eastern Ghats Mobile Belt, GR—Godavari rift, LR—Lambert rift, MR—Mahanadi rift, NC—Napier complex, NSL—Narmada-Son lineament, RC—Reiner complex, SC—Singhbhum craton, SGT—southern granulite terrain.

Passive margins display varied patterns of seismicity and this diversity is more pronounced in case of rifted and transform margins (Stein et al., 1989). These diverse characteristics arise from various reasons such as contrast in rheological character due to the nature of coupling between continental and oceanic lithospheres, sedimentation patterns and so on.

The Indian landmass is an important constituent of eastern Gondwanaland. The continental break-up processes between India–East Antarctica–Madagascar–Seychelles have left their imprints on the newly evolved continental margins of India as well as on the deep ocean floor surrounding them. The present study is oriented to examine the Indian passive continental margins in the light of the above geological and geophysical characterizations and aims at outlining the important future investigations that need to be carried out.

2. Geological setting

The Precambrian shield of India comprises Archean cratons and Proterozoic mobile belts (shown in Fig. 1 as a constituent of East Gondwana assembly) and surrounded by ocean basins of the Bay of Bengal and the Arabian Sea, which have started evolving since ca. 130 Ma and 90 Ma, respectively. The Precambrian continental rifts, viz., the Godavari, Mahanadi and the Narmada-Son rifts (Fig. 1), which traverse great lengths across the continent, are of significance as they were found to be closely linked to similar rifts in East Antarctica (e.g., Subrahmanyam et al., 1999). In the same context, the neoproterozoic shear zones and granulite terrains of south India are also important as they are found to be continuous with similar zones in Madagascar (Acharyya, 2000; Raval and Veeraswamy, 2003) and East Antarctica (Jandardhan, 1999; Yoshida et al., 1999).

The ECMI and WCMI are of the divergent type, both having evolved as a consequence of the break-up of East Gondwana. The ECMI is a mature margin, having come into existence about 130 Ma ago when India drifted away from East Antarctica. This margin is characterized by thick sedimentary basins (more than 5 km) some of which prograde into deltas (see Fig. 2). The shelf along the ECMI is narrow with the deep ocean floor encountered within 50–60 km distance from the coastline. Recent geophysical investigations indicate that the southern segment of the ECMI could represent a sheared margin while the northern segment appears to be rifted in nature (Subrahmanyam and

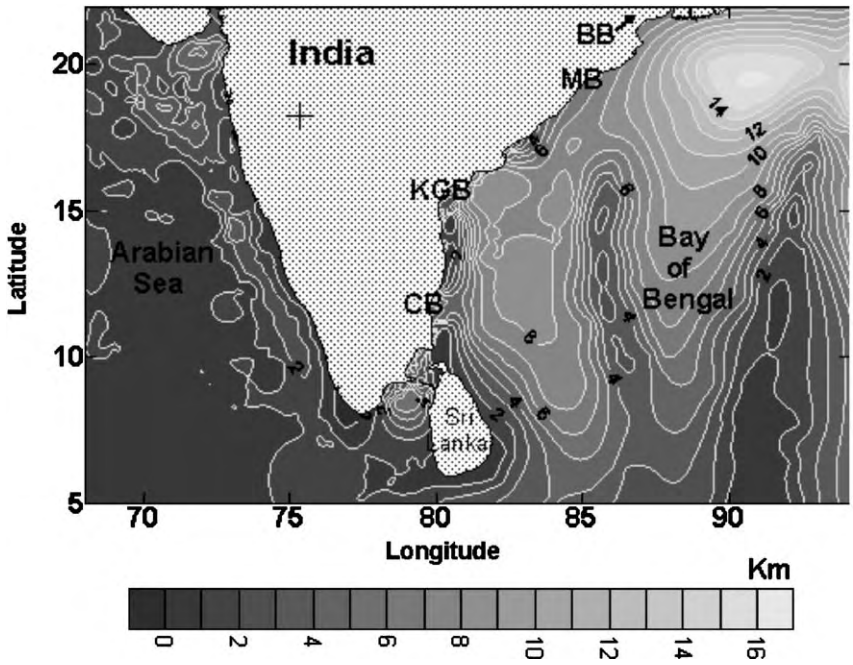

Fig. 2. Sediment distribution map for ECMI, WCMI, Bay of Bengal and Arabian Sea.

Singh, 1992; Gopala Rao et al., 1997; Subrahmanyam et al., 1999; Chand et al., 2001). In the deep-sea areas, the Bengal fan sediments are underlain by two hotspot traces, viz., the 85°E ridge, which runs in the central part of the fan and the Ninetyeast ridge farther east, close to the Andaman subduction zone (Subrahmanyam et al., 1999). Satellite-derived gravity images and seismic sections indicate that the 85°E ridge terminates at Mahanadi basin along the ECMI (Krishna, 2003) and its continuation further north on land, extending up to the Rajmahal traps, is indicated by the presence of dyke intrusions (Subrahmanyam et al., 1999). This study also revealed that the entire eastern region of India, including the Bengal basin represents a large volcanic province (Eastern Volcanic Province, EVP), somewhat similar to the Deccan Volcanic Province (DVP) along western India (Fig. 5).

The Western Continental Margin of India (WCMI) is relatively young, by about 40 myr compared to the ECMI, with Madagascar breaking away from India about 88 Ma ago (Storey, 1995; Storey et al., 1995). Further, the shelf, which is only about 50 km wide in the south, gradually widens progressing northward and attains a maximum width of nearly 300 km in Bombay offshore region. The thick sedimentary basins of the type observed along the ECMI are characteristically absent here and the sedimentation is moderate, usually not exceeding 3 km in thickness (Fig. 2) with the exception of Surat Depression where sediments are >6 km thick. The WCMI has several ridge-like features, which run parallel to the coast and also have significantly controlled the sedimentation pattern along the margin. Of these, the Chagos Laccadive Ridge (CLR) is the most significant topographic feature (Fig. 3), with several islands observed along its strike length. This ridge is recognized as a hot spot trace related to the Reunion plume (Duncan and Storey, 1992) whose magmatic activity has resulted in the emplacement of not only the ridge but also extensive continental flood basalt volcanism of the DVP, one of the large igneous provinces (LIPs) in the world (Coffin and Eldholm, 1994). However, Chaubey et al. (2002) suggest that the plume formed the structures on an already existing continental crust. Whether the CLR has formed on an oceanic crust or a continental crust needs to be resolved. The WCMI seems to be affected by plume activity at about 85 Ma and 65 Ma, respectively, the older Marion plume in the south and the younger Reunion in the north (Storey et al., 1995). Besides the CLR, several other ridges in the form of Laxmi ridge, Pannikkar ridge, Kori-Comorin high and the Prathap ridge complex (Naini and Talwani, 1983; Krishna et al., in press), and also groups of seamounts have been recorded along the WCMI in both bathymetry and seismic records. Thus, overall, the WCMI presents a complex picture of ridge-graben tectonic regime up to the western flank of the CLR, associated with intense mantle plume activity.

The ECMI, in its northern part, is marked by the Eastern Ghats Mobile Belt (EGMB) of Proterozoic age, which extends for over 1000 km along the east coast. The southern granulite terrain (SGT) of Precambrian age occupies the southern part. Overall, the break-up of eastern India from East Antarctica seems to have been accommodated along the Proterozoic

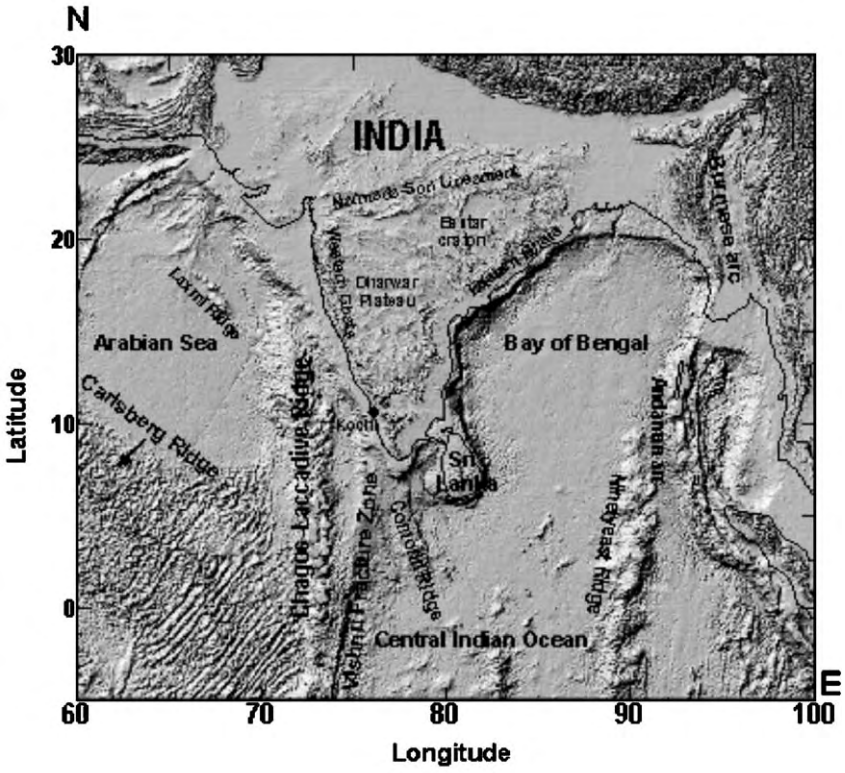

Fig. 3. Shaded relief map of topography for India and the surrounding seas (Source: GTOPO30 on land and ETOPO2 for the oceans).

EGMB. The rifting and associated magmatism can be related to hotspot activity beneath east Gondwanaland, at least in the northern parts of the ECMI, and these could be a reflection of Kerguelen plume activity (Kent, 1991; Kent et al., 1997; Anil Kumar et al., 2003).

The western margin is in striking contrast with the eastern margin. The break-up, with the exception of the granulite terrain of Kerala, seems to have been accommodated along the Dharwar craton of the Indian shield. The geology along the western margin varies dramatically, from granulites in the south to granite-greenstone country in the central parts to the Deccan trap volcanic flows in the north. As stated earlier, the volcanics relate to the Reunion plume activity and the break-up between western India and Seychelles. The evolution of the western margin seems to have been triggered by mantle plume activity in the form of the Marion and Reunion mantle plumes (e.g., Storey, 1995; Storey et al., 1995). Also, the break-up, to a major extent, seems to have occurred between the cratonic block of Dharwar and its conjugate in Madagascar (Raval and Veeraswamy, 2003).

3. Magnetic lineations, break-up and drift history

Existing ideas on the break-up of India from East Antarctica, Madagascar and Seychelles indicate that the events occurred at ca. 130 Ma, 88 Ma and 65 Ma, respectively. The inferences are more indirect in the sense that the dates have been fixed mainly on the basis of plate reconstructions, magmatic (plume activity) episodes and identification of sea floor spreading type magnetic lineations along the conjugate margins rather than direct identification of magnetic lineations along the ECMI and WCMI. About a decade ago, an attempt was made to identify Mesozoic magnetic lineations in the Bay of Bengal (Ramana et al., 1994), but conflicting views have been expressed, based on analysis of the marine magnetic data (e.g., Murthy et al., 1993; Gopala Rao et al., 1997). These interpretations suggest that the oldest anomalies along the ECMI can be as old as M11 (Ramana et al., 1994) or much younger at M0 (Gopala Rao et al., 1997). The recent findings of Nogi et al. (1992, 1996) and Gaina et al. (2003) bring out a fossil spreading ridge, marked by a positive gravity anomaly, in the Enderby basin (conjugate basin of the Bay of Bengal) flanked by magnetic lineations ranging from M2 to M9. If this interpretation holds good, then the younger magnetic lineations of M1 and M0 would probably exist in the Bay of Bengal. This points to the need for re-examination of the marine magnetic anomalies in the Bay of Bengal, particularly closer to the ECMI and keeping in mind the obliteration of the magnetic picture caused by the 85°E ridge. Such studies may accurately fix the ages for break-up along the east coast of India.

Ironically, the picture along the WCMI is not clear either. The first set back arises from the lack of identification of any magnetic lineations in the eastern basin of the Arabian Sea, between the west coast of India and the CLR–Laxmi ridge. In contrast to this, magnetic lineations up to anomaly 34 have been identified in the eastern offshore of Madagascar, with the fracture zones identified by offset of magnetic lineations (Norton and Sclater, 1979; Schlich, 1982) being confirmed by bathymetry and satellite-derived gravity signatures (e.g., Chand and Subrahmanyam, 2003). In the Mascarene basin, east of Madagascar, a fossil spreading ridge with both sets of magnetic lineations from anomaly 28 to 32 have been identified (see Fig. 4 of Bhattacharya and Chaubey, 2001). However, anomalies 33 and 34 were identified only towards the eastern margin of Madagascar and its conjugate towards north, near the Mascarene plateau, were found missing. Is it possible that these two magnetic lineations could still be found in the eastern basin between CLR and the west coast of India? East of Madagascar, the orientation of the magnetic lineations and the fracture zones indicates that the rifting is at a highly oblique angle and it is even suggested that there may be a strike-slip component associated with the rifting between western India and eastern Madagascar (Storey et al., 1995).

4. Topography and gravity shaded relief maps

The topography and gravity field over the Indian shield and the surrounding oceans are presented in Figs. 3 and 4 in the form of shaded relief maps and colour image, respectively.

4.1. Topography

The topographic shaded relief map, constructed using GTOPO30 data for land and ETOPO2 data for sea, displays strong features along the western margin and in the deep Arabian Sea. The wide shelf of nearly 300 km in the Bombay offshore region, which gradually narrows down to about 50–60 km in the Kochi offshore towards the southern parts of the WCMI, mentioned above, is well reflected in the topography map. The most prominent feature on the western margin is the CLR, which runs in a N–S direction displaying a strong topographic relief. At about 15°N, the ridge gets merged with the Prathap ridge complex and buried under the shelf sediments in the Bombay offshore region. This ridge is considered as the volcanic trace of the Reunion mantle plume, which resulted in the outpouring of the Deccan lavas at the time of break-up of Seychelles from India at about 65 Ma ago. East of the CLR, two more prominent topographic highs are observed with limited strike length. The ridge to the west of Sri Lanka is the Comorin ridge, which was investigated by Kahle et al. (1981). The topographic feature west of the Comorin ridge is probably related to the Vishnu fracture zone (e.g., Norton and Sclater, 1979). In the southwest corner of the map one can notice the short wavelength topographic features related to the fracture system of the slow-spreading Carlsberg ridge. In the northwest corner of the map is the Laxmi Ridge, which is associated with a strong negative gravity anomaly and the ridge is considered to be of continental origin (Miles et al., 1998; Talwani and Reif, 1998; Todal and Eldholm, 1998).

Over the Indian landmass, the strongest topographic feature is the relief of the western Ghats (see Fig. 3). From the gentle inland topography of the Karnataka plateau, the topography gradually rises towards the west coast, reaching a maximum of about 1.5 km about 50 km inland of the coast, where the great western Ghats escarpment is encountered. Here, the topography

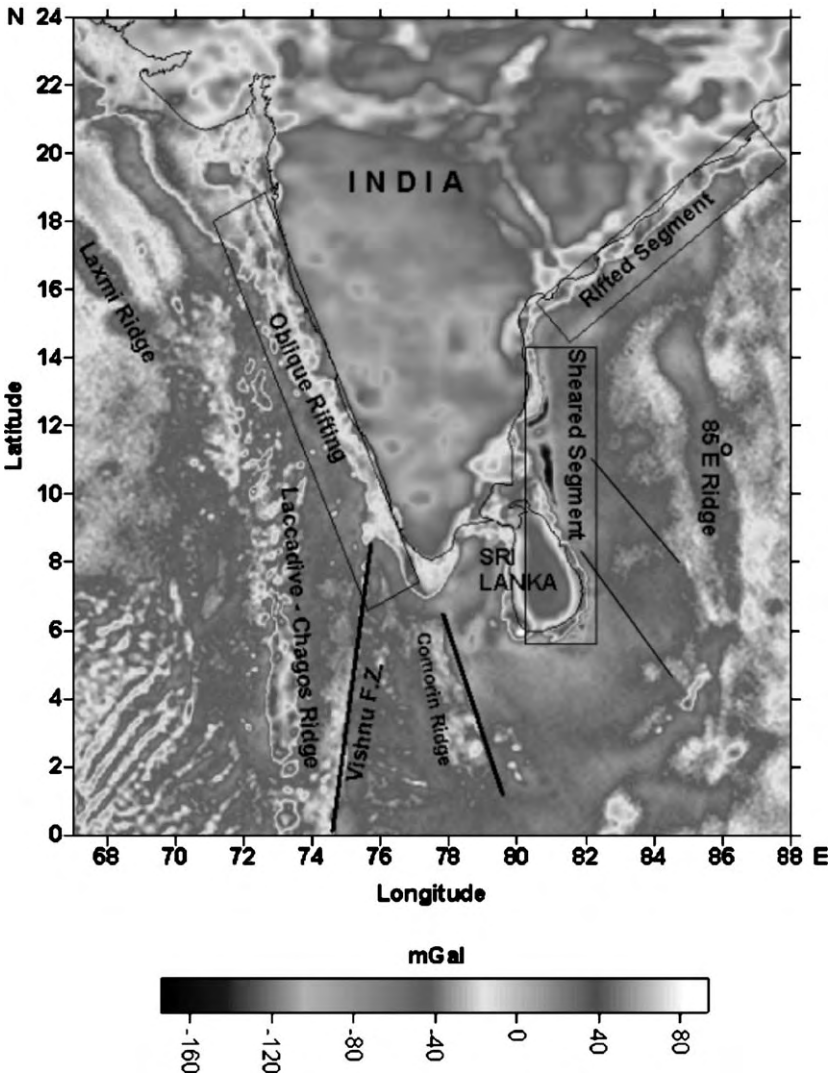

Fig. 4. Grey-scale image of gravity for India and surrounding oceans. Bouguer anomalies on land (NGRI, 1978) and satellite-derived free air anomalies (Sandwell and Smith, 1997) for the oceans. FZ—fracture zone.

suddenly drops to almost sea level and up to the west coast this low topography is maintained along what is known as the Coastal Plain, which has an average width of about 50 km. The Coastal Plain runs along almost the entire length of the west coast of India. This strong relief of the western Ghats topography is termed as a rift flank uplift and is compared to similar topographic signatures along several rifted margins in the world (e.g., Gallagher et al., 1998; Gunnell and Fleitout, 1998). This strong topography is explained by the process of denudation and flexural rebound, which results in the erosion of the western Ghats topography and subsequent sediment deposition in the depressed shelf regions of the western continental margin (Chand and Subrahmanyam, 2003).

The Bay of Bengal is devoid of any strong topographic expressions, with the exception of a few isolated, small topographic highs which may be reflective of seamount related volcanism in the distal Bengal fan region. The totally flat bathymetry in the east is due to the presence of the Bengal fan sediments, which stretch from the apex of the fan in the Bangladesh offshore to 7°40′S in the central Indian Ocean (Curray, 1991). The southern limit of fan sediments is clearly demarcated for the first time by Krishna et al. (2001).

The continental shelf along the ECMI is very narrow, particularly towards south, where the shelf width is hardly 40 km or so. It is the narrowest along the Sri Lanka margin.

4.2. Gravity

The grey-scale image of gravity field is shown in Fig. 4. The map was constructed using Bouguer anomalies on land (NGRI, 1978) and free air anomalies (Sandwell and Smith, 1997) over the ocean. The image displays tectonic features covering a wide span of geological times ranging from the Precambrian on land to the very young spreading related features of the Carlsberg ridge in the SW corner of the map. The image over land appears more subdued than that over the ocean mainly because of the type of anomalies used. The image generation has created some artifacts, particularly over the land, which may not be related to any geological feature and hence need to be ignored. One example of such an artifact is the perfectly E–W trending

feature at 20°N latitude. The gravity map brings out some major features such as those related to the spreading history between India, East Antarctica and Madagascar in the offshore and deep sea regions, and the lineaments over land related to older tectonic episodes, particularly the Precambrian continental rifts of Narmada-Son and Godavari.

Several lineaments both with NE–SW and NW–SE orientations can be noticed on the gravity map in the oceans surrounding India and Sri Lanka. The former reflect the spreading episodes between India and Madagascar, while the latter indicate the spreading between India and East Antarctica. Between CLR and Sri Lanka two prominent N–S trending gravity lineaments can be seen. The major one is along 75°E in the north–south direction and the NW–SE trending gravity high, which joins this feature at around 8°N. This is probably the trace of the Vishnu fracture zone that facilitated the movement of Madagascar away from India at around 85 Ma (Norton and Sclater, 1979). The N–S lineament joins the west coast at 10°N. Further north, the western margin is demarcated by the negative gravity of the Laxmi ridge and also the fracture zones related to the Tertiary rifting between India and Seychelles. The gravity lineaments related to the fracture zones along the Carlsberg ridge can be seen in the southwest corner of the map matching those noticed on the topography map.

The gravity map along the eastern margin of India has features related to the formation of the margin itself. The northern part of ECMI has a typical rifted margin characteristic like a gravity high along the shelf-break followed by a gently decreasing gravity anomaly towards the deep sea. However, the southern part of ECMI has a different character. Seaward of the gravity high at the shelf-break the gravity falls to a very low value of almost −120 mgal and this feature can be observed all along this segment and it continues southward to the eastern margin of the Sri Lanka also. Chand and Subrahmanyam (2001) have inferred that this gravity feature reflects the shearing between India–Sri Lanka from East Antarctica in the very early stages of the break-up history. Faint traces of lineaments can be seen in the Bay of Bengal extending from the western flank of the 85°E ridge to the east coast of India (not marked on Fig. 4) trending NW–SE and these are probably related to the rifting between India and East Antarctica with their counterparts shown in the offshore regions of East Antarctica (Ramana et al., 2001; Rotstein et al., 2001). It is noteworthy that Sandwell (1992) also identified several NW trending linear features in the gravity images of the offshore region of East Antarctica, which were inferred as representative of the spreading episodes between India and East Antarctica.

One important aspect to be noted here is that, with the exception of one fracture zone running N–S along longitude 75°E and abutting the west coast of India at latitude 10°N (see Fig. 4 and also Fig. 3b of Rotstein et al., 2001), all the fracture zones terminate at considerable distances ocean ward of the margin of India, particularly for the ECMI. Interestingly this is also the case with the fractures zones off East Antarctica (Chand et al., 2001). Only in the case of Madagascar the fracture zones seem to extend all the way up to the coast (Chand and Subrahmanyam, 2003).

5. Onshore–offshore tectonic links

In many cases, when continents break and drift apart, the structures onland were found to be extending into the offshore regions to considerable distances and seem to control the overall tectonics of the continental margins (Fichler et al., 1999). In the case of the Indian shield and its surrounding oceans, such onshore–offshore tectonic links have not been clearly established with the exception of one instance, where the Precambrian lineaments onland seem to have significantly controlled the movements of blocks in the western offshore regions (Subrahmanyam et al., 1995). Gravity and bathymetry data indicate the extension of several Precambrian lineaments into the offshore regions to considerable distances. Block movements in the offshore regions appears to be the response of ridge push forces emanating from the Carlsberg spreading ridge southwest of the WCMI (Subrahmanyam et al., 1995). These investigations indicate that Carlsberg spreading processes may be responsible for the reactivation of the Precambrian lineaments over western India. However, it is not clear whether these block movements are operational today or they took place at a time when the Carlsberg ridge was considerably closer to WCMI.

6. Mantle plume activity, hot spot traces and underplating

Volcanic provinces dot the Indian shield and their traces are found in the surrounding deep oceans (Curray and Munasinghe, 1991; Kent, 1991; Kent et al., 1997; Mueller et al., 1993; Storey, 1995, among others). In this scenario, it is of interest to examine whether the continental margins of India have experienced any underplating process because the emplacement of large underplated material at the base of the crust may strongly affect the ongoing sedimentation processes at the seafloor (Clift and Turner, 1998; Clift et al., 1998). Margins where post rift subsidence is going on, when subjected to such magmatic underplating processes, may experience uplift due to the passing of a mantle plume and such events can be traced in the subsidence history curves for the sedimentary basins along the margins. The underplated material is identified as a 7.5 km/s layer in the lower crustal levels on wide-angle seismic sections (e.g., White, 1992).

For the continental margins of India, there are at least two locations where such crustal underplating has been identified in seismic sections and both these occur along the northern ECMI. The first was in the Bengal basin where Mall et al. (1999) have identified a 7.5 km/s velocity zone at the base of the crust and interpreted this layer to be underplated material at the base of the continental crust underlying the Bengal basin. Mall et al. (1999) also observed a crustal upwarp in the eastern part of the Bengal basin, east of 87°E longitude demarcating the trace of a mantle plume in the continental region that gave rise to Rajmahal trap volcanism. However, they leave a question about the oceanward continuity of this plume trace.

More recently, Behera et al. (2004) also found evidence, from seismic and gravity data analyses, for crustal underplating beneath the Mahanadi basin. This basin is just southwest of the Bengal basin discussed above and is approximately located at

about 20°N latitude along the east coast of India. Three seismic crustal sections and gravity data indicate the presence of a high velocity 7.5 km/s and high density 3.05 gm/cm^3 layer at lower crustal levels beneath the Mahanadi basin. Behera et al. (2004) argue that these are related to the Kerguelen plume activity and the presence of similar volcanic rocks and structures in the conjugate East Antarctica indicates continuity of tectonic features from India to East Antarctica. Subrahmanyam et al. (1999) have earlier presented similar arguments favouring continuity of tectonic features between India and East Antarctica.

The Bengal and Mahanadi basin geophysical investigations (Behera et al., 2004; Mall et al., 1999) over the continent suggest underplating processes. If such underplating is a consequence of mantle plume activity, then it raises a question whether such plume activity has left any traces in the Bay of Bengal ocean floor. The Mahanadi basin on land is situated between 85° and 87°E longitude and the Bengal basin extends east of 88°E longitude. This geographic separation between the two basins raises another question whether they are located along the paths of two separate mantle plumes. Subrahmanyam et al. (1999) and Krishna (2003) have used gravity and single channel seismic analogue records to trace the path of the 85°E ridge from the Afanasy-Nikitin seamount in the central Indian Ocean towards the east coast of India and concluded that, beneath the Bengal fan sediments, it may extend up to the Mahanadi basin on the east coast. In contrast, the Ninetyeast ridge in the northern latitudes veers towards the Andaman subduction zone and shows NNE orientations shifting away from the direction of Rajmahal and Silhet traps. However, isotope geochemistry strongly favours links between the Rajmahal–Silhet traps, Ninetyeast ridge and the Kerguelen plateau (Anil Kumar et al., 2003). There is need to establish clearly the causal links between the surface occurrences of volcanic rocks (Rajmahal and Sylhet traps) in eastern India, the 85°E and Ninetyeast ridges in Bay of Bengal and the Kerguelen and Conrad Rise/Crozet hotspots in southern Indian Ocean.

For the WCMI, evidence for underplating comes from gravity modeling constrained by seismic data (Miles et al., 1998; Radhakrishna et al., 2002). The models indicate the presence of underplated material of density 3.0 g/cm^3 beneath the Laxmi and Laccadive ridges and the northwest portion of the Deccan Volcanic Province. The underplating process seems to be related to the passage of the lithosphere over the Reunion plume. These models have striking resemblance with those inferred for the southern Voring basin of the Norwegian margin inferred from gravity and wide-angle seismic data (Raum et al., 2002). It is noteworthy that seismic refraction work in the western offshore region of India (Naini and Talwani, 1983) has brought out a >7.0 km/s layer at several places in the lower crust and it is necessary to examine whether these layers are in anyway indicative of the top layer of an underplated material or they just reflect the top of the oceanic layer3.

7. Seismicity and neotectonics

Passive margins display earthquake activity for several reasons (Stein et al., 1989). Usually, these are related to the build up of stresses, both compressive and vertical, in the oceanic crust abutting a continental crust and both having diverse rheological characteristics. Margins, which have experienced excessive sedimentation with high rates of sedimentation, appear to be more vulnerable to earthquake activity (Stein et al., 1989). However, it has been recorded that, in general, seismicity characterizes more the rifted margins than the transform or sheared margins (Vogt et al., 1998). A seismicity map of India and the adjoining oceans is shown in Fig. 5 compiled from all the available data (Ramalingeswara Rao, 1998, 2000). Both the western margin and the southern segment of the ECMI are totally devoid of any seismic activity in their offshore regions. In contrast, the rifted segment of the ECMI north of latitude 15°N and also the Saurashtra offshore region along the western margin display moderate seismicity. Medium to large earthquakes are observed in these regions. Biswas and Majumdar (1997) attribute the eastern offshore and the Bay of Bengal seismicity to intraplate deformation experienced by the sea floor. Fault plane solutions for a majority of the events bring out pure thrust type faulting with some of the events having a small strike-slip component. It must be noted that the northern Bay of Bengal is a region of high rates of sedimentation. Following Stein et al. (1989), it can be argued that the seismicity in northern Bay of Bengal and also the Saurashtra offshore region is due to high rates of sediment deposition, particularly the northern parts of the eastern offshore regions of India and also that of Bangladesh. Obviously, there is need to resolve the cause of seismicity along northern ECMI.

8. Crustal extension and subsidence along the ECMI

When continents break and drift apart, a portion of the continental crust gets stretched and subsides along the newly evolving continental margin. Backstripping analysis helps in understanding the rates of extension and the subsidence history in the sedimentary basins along these passive continental margins. The ECMI is characterized by four major sedimentary basins, viz., Cauvery, Krishna-Godavari, Mahanadi and Bengal basins (Fig. 2), and subsidence models for all these basins, based on backstripping of well data and seismic stratigraphic sections, are available (Chari and Banerjee, 1993; Chari et al., 1995; Radhakrishna et al., 2000). In general, he tectonic subsidence in all the basins has a relatively low gradient during the Cretaceous, which reflects slow sedimentation rate as well as a low subsidence rate attributable to initial stages of slow denudation along the rift flanks. This points to the uplift of the rift flanks during the formation of margin due to the effect of the plume that caused rifting. From Paleocene to Eocene, all the ECMI basins have experienced high sedimentation as well as high subsidence rates. This may be due to the southeastward tilt of the Indian plate, caused by the uplift of western Peninsular India during the passage of India over the Reunion hotspot concomitant with the magmatic out pouring of Deccan traps (Subbarao and Sukheshwala, 1981). This eastward tilt caused a high rate of erosion by the rivers and deposition of large quantity of sediments in the sedimentary basins along the

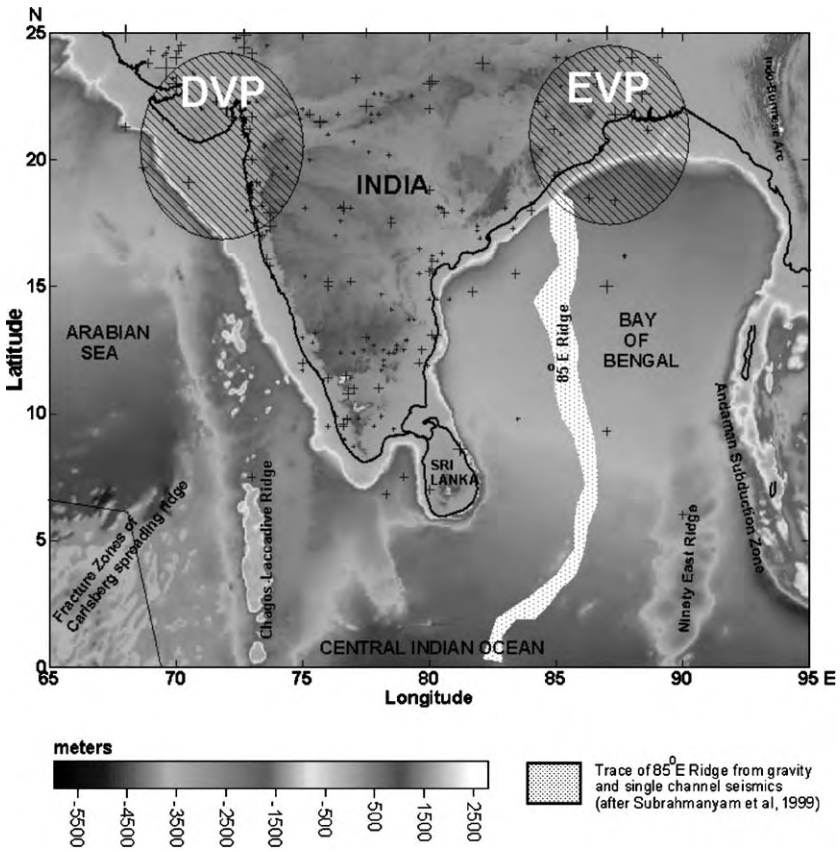

Fig. 5. Map showing earthquake epicenter distribution over India and surrounding oceans (Ramalingeswara Rao, 1998, 2000) with topography/bathymetry in the background. DVP—Deccan Volcanic Province, EVP—Eastern Volcanic Province.

ECMI. During the Oligocene and Miocene, subsidence was moderate due to marine transgression, which occurred during that period (Raju et al., 1999). From Pliocene to the Recent, the subsidence rates have again increased reflecting the high sedimentation caused by the erosion of the Himalaya and deposition of deltaic sediments in the Bengal, Mahanadi and Krishna-Godavari basins.

The tectonic parameters of the four basins of the Eastern Continental Margin of India are given in Table 1. By comparing the tectonic parameters such as crustal extension factor (β) from Bengal basin in the north to the Cauvery basin in the south, we can observe almost same values except in the case of Bengal basin where in Dhanajayapur well a high value is reported (Chari and Banerjee, 1993). As pointed out by many authors (e.g., Powell et al., 1988), the rifting between India and East Antarctica was initiated along the Bengal basin or north of it during the Jurassic period and continued southward. The rifting was asymmetrical with a maximum along the northern part as shown by reconstruction studies (Powell et al., 1988; Chand et al., 2001). The separation between the southern part of the ECMI and the East Antarctica was more like a transform type setting as pointed out from gravity and reconstruction studies (Powell et al., 1988; Subrahmanyam et al., 1999; Chand et al., 2001). In such a setting, the northern part of ECMI might have undergone more stretching compared to the southern part where stretching constrained by a transform-setting might have occurred (e.g., Chand and Subrahmanyam, 2001). But, the similarity in the results obtained along the basins situated in both the segments shows that, in spite of the shearing along the southern segment, crustal stretching experienced in all these basins is similar. The stretching in Cauvery basin located in the sheared segment was also in the general NW–SE rifting direction of the ECMI producing the rifting between India and Sri Lanka through wrench faulting. The wrench faulting took place along a series of wrench corridors, which might have allowed intrusion of water causing serpentinization (Gussinye and Reston, 2001; Reid and Jackson, 1997) and also the formation of a shear gouge weakening the lithosphere (Chand and Subrahmanyam, 2001). Vitrinite reflectance studies and other hydrocarbon maturation studies in Cauvery basin show that the sediments are inadequately mature for hydrocarbon generation in most part of the basin, pointing to the absence of any raising of thermal anomaly at the time of rifting (Rangaraju et al., 1993). The average geothermal gradient in the basin is 2.5–3.0 °C/100 m particularly in the area of wrench corridor (Rangaraju et al., 1993; Venkatarengan, 1988). The mature hydrocarbons are only seen along this corridor, which points to only a local enhancement in geothermal gradient. This is usually expected in areas of shear tectonics where the geothermal gradient is only slightly raised as the spreading centre migrates along the margin producing a weak suture (Verhoef and Jackson, 1991).

Table 1
Tectonic parameters for the four sedimentary basins along the ECMI

Basin	Well	Uniform stretching	Non-uniform stretching		
		Crustal stretching β_c	Crustal extension β	Sub-crustal extension δ	Total lithospheric attenuation β_L
Cauvery basin	ND-1		1.3	1.0	1.069
(Chari et al., 1995)	VG-2		1.4	1.1	1.170
	Y-3-2		1.4	1.8	1.667
	GT-1		1.3	1.0	1.069
	H-9-1		1.3	1.3	1.300
	H-3-1		1.3	1.1	1.150
	M-1		1.4	1.9	1.727
Krishna-Godavari basin	GS-5-1	1.68	Crustal stretching factor obtained assuming an effective elastic thickness T_e		
(Radhakrishna et al., 2000)	GS-12-1	1.82	of 30 km		
	G-13-1	1.88			
Krishna-Godavari basin	AMP-1	1.42	1.4	4.0	2.63
(Chand, 2001)	BMP-2	1.42	1.4	2.4	2.0
	BNT-2	1.18	1.3	10	3.48
	CTP-1	1.28	1.3	10	3.48
	DKSH-1	1.22	1.3	10	3.48
	DRK-1	1.16	1.2	2.9	2.08
	END-A	1.16	1.2	2.7	2.0
	END-B	1.17	1.2	2.7	2.0
	G-13-1	1.26	1.3	10.0	3.48
	GS-17-1	1.39	1.4	10.0	3.68
	GS-5-1	1.39	1.4	6.0	3.13
	KLR-1	1.14	1.2	4.8	2.61
	KMG-1	1.22	1.2	1.4	1.34
	KMK	1.28	1.3	2.1	1.79
	MDP-1	1.18	1.2	1.8	1.58
	MDP-4	1.16	1.2	2.3	1.83
Mahanadi basin	MND-1	1.09	1.1	1.4	1.301
(Chand, 2001)	MND-2	1.21	1.3	4.3	2.612
	MND-3	1.12	1.2	2.6	1.960
	MND-4	1.08	1.1	1.4	1.300
	MND-5	1.16	1.2	2.0	1.685
	MND-6	1.19	1.3	4.8	2.737
	MND-7	1.12	1.2	2.9	2.076
	MON-1	1.08	1.1	1.4	1.301
	MON-2	1.21	1.2	1.3	1.270
	MON-3	1.09	1.1	1.4	1.301
	MON-4	1.16	1.2	2.0	1.685
	NEC-1	1.17	1.3	8.2	3.298
Bengal basin	GALSI-3		1.0	1.7	1.421
(Chari et al., 1995)	JALANGI-1		1.06	8.5	2.867
	MEMARI-1		1.24	10.0	3.358
	DHANANJAYPUR-1		1.52	9.5	3.903

This points to a scenario where the rifting between India and Sri Lanka progressed very much during the shearing between India and the East Antarctica but was later aborted for reasons that are not yet clear.

The presence of a large igneous province underlying the Bengal basin, related to the exposed Rajmahal trap volcanism (Bakshi, 1995; Subrahmanyam et al., 1999) with possible extension up to the Mahanadi basin is already established. These volcanics are dated at 118–110 Ma. The presence of these volcanics (Biswas, 1996; Raju and Dave, 1993) confirms the earlier suggestion of the uplift of the lithosphere due to the incubation of a mantle plume head beneath the Bengal basin and adjoining areas prior to continental rifting (Kent, 1991). Admittance studies along the ECMI show that the northern part of it has a higher value of effective elastic thickness (T_e) of 10–25 km compared to a lower value of <5 km in the southern segment suggesting diverse types of formation mechanism these margins (Chand et al., 2001). 2-D subsidence analysis along K-G and Cauvery basins also indicated different T_e values of 30 km (Radhakrishna et al., 2000) and 3 km (Chand and Subrahmanyam, 2001), respectively. Though the Cauvery basin as well as the southern segment of ECMI are underlain by a low effective elastic thickness lithosphere, the Cauvery basin experienced similar amount of stretching in the same direction of spreading of the northern part of ECMI, and this rifting was later aborted and resulted in the formation of a sheared margin along the southern part of ECMI. Plume incubation seems to have affected the subsidence pattern of the Mahanadi basin. Similar study along the North Sea and Faeroe Shetland margin showed departures in subsidence curves due to the dynamic uplift brought by Iceland plume (Nadin et al., 1995).

9. Future perspectives and conclusions

The history of spreading between India and East Antarctica still remains enimagtic particularly with the identification of a fossil spreading ridge in Enderby basin and also both sets of magnetic lineations M2 to M9 (Gaina et al., 2003). Clearly, there is a need to re-examine the marine magnetic anomalies in the Bay of Bengal in the light of these new findings and also the possible linkages between the EVP, the 85°E and Ninetyeast ridges and Kerguelen plateau, Crozet and Conrad Rise in the Antarctic Plate.

Magnetic lineations 34 to younger ages were identified in the seafloor east of Madagascar but lineations of similar ages could not be identified from the eastern parts of the Arabian Sea. Both sets of magnetic lineations up to anomaly 32 were identified in Mascarene basin, but only one set of magnetic lineations 32 and 34 occur in the southern part near the east coast of Madagascar while their conjugate in the northern part of Mascarene basin are missing (see Fig. 4 of Bhattacharya and Chaubey, 2001). Does it imply that anomalies 33 and 34 still exist in the eastern basin of the Arabian Sea between CLR and west coast of India or is it possible that the younger Reunion plume activity has obliterated the signatures of such seafloor spreading magnetic anomalies? New geochronological and geochemical data (Anil Kumar et al., 2001) indicate that the magmatic/volcanic activity related to the Marion hotspot, situated between Madagascar and south-western India about 85 Ma ago, has been much more extensive than that envisaged earlier.

The passive margins of India seem to have evolved through a variety of tectonic processes, ranging from passive to active rifting and also strike-slip motion (the southern part of ECMI). If the seafloor spreading anomalies in the Bay of Bengal, particularly near the east coast of India, are properly identified and plate reconstruction models are established, the requirement for strike-slip motion along the southern segment of the ECMI may get resolved. The eastern margin, but for its northern most segment in the Bengal basin and possibly the Mahanadi basin, seems to have escaped association with any plume activity. In contrast, the western margin seems to have close affiliation with moderate to intense plume activity. It is necessary to establish the extent to which these activities have influenced the underplating processes along both the margins.

The break-up process between India and its erstwhile eastern Gondwanaland conjugate landmasses seems to have been accommodated both along Proterozoic orogenic belts and cratons. The eastern margin seems to have separated from East Antarctica along a Proterozoic orogenic belt, while the separation between India and Madagascar-Seychelles seems to have been accommodated to a large extent along cratonic blocks. Further, Storey et al. (1995) argue that the linear character of the east coast of Madagascar indicates strike-slip faulting (between India and Madagascar) before the Mascarene basin has started to evolve. From this, it can probably inferred that the style of rifting between India and Madagascar is highly oblique with a possible strike-slip component. Several aspects of the passive continental margins of India need further attention, such as their volcanic vs. non-volcanic character, active vs. passive rifting, the role of the Precambrian cratons and mobile in the processes of rifting, the nature of subsidence along the margins, oblique rifting vs. shearing, and so on. Well-focussed geophysical investigations are required to understand some of the above phenomena.

Acknowledgments

The authors are thankful to Dr. K.S. Krishna for critical and helpful reviews. This work is published with the permission of the Director, National Geophysical Research Institute, Hyderabad, India.

References

Acharyya, S.K., 2000. Break up of Australia–India–Madagascar block, opening of the Indian Ocean and continental accretion in southeast Asia with special reference to the characteristics of the peri-Indian collision zones. Gondwana Research 3, 425–443.

Kumar, Anil, Pande, K., Venkatesan, T.R., Bhaskara Rao, Y.J., 2001. The Karnataka Late Cretaceous dykes as products of the Marion hot spot at the Madagascar–India break-up event: evidence from ^{40}Ar–^{39}Ar geochronology and geochemistry. Geophysical Research Letters 28, 2715–2718.

Kumar, Anil, Dayal, A.M., Padmakumari, V.M., 2003. Kimberlite from Rajmahal magmatic province: Sr–Nd–Pb isotopic evidence for Kerguelen plume derived magmas. Geophysical Research Letters 30, doi:10.1029/2003GL018462.

Bakshi, A.K., 1995. Petrogenesis and timing of volcanism in the Rahmahal Flood Basalt Province, northeastern India. Chemical Geology 121, 73–90.

Behera, L., Sain, K., Reddy, P.R., 2004. Evidence for underplating from seismic and Gravity studies in the Mahanadi delta of eastern India and its tectonic significance. Journal of Geophysical Research 109, doi:10.1029/2003JB002764.

Bhattacharya, G.C., Chaubey, A.K., 2001. Western Indian Ocean—a glimpse of the tectonic scenario. In: Sen Gupta, R., Desa, E. (Eds.), The Indian Ocean—A Perspective, vol. 2. Oxford & IBH Publishing Co. Pvt. Ltd, India, pp. 691–730.

Biswas, S.K., 1996. Mesozoic volcanism in the east coast basins of India. Indian Journal of Geology 68, 237–254.

Biswas, S., Majumdar, R.K., 1997. Seismicity and tectonics of the Bay of Bengal: evidence for intraplate deformation of the northern Indian plate. Tectonophysics 269, 323–336.

Chand, S., 2001. Subsidence analysis along the continental margins of India. PhD thesis, Osmania University.

Chand, S., Subrahmanyam, C., 2001. Gravity and isostasy along a sheared margin—Cauvery basin, Eastern Continental Margin of India. Geophysical Research Letters 28, 2273–2276.

Chand, S., Subrahmanyam, C., 2003. Rifting between India and Madagascar —mechanism and isostasy. Earth & Planetary Science Letters 210, 317–332.

Chand, S., Radhakrishna, M., Subrahmanyam, C., 2001. India and East Antarctica conjugate margins: gravity and isostasy. Earth & Planetary Science Letters 185, 225–236.

Chari, M.V.N., Banerjee, B., 1993. Subsidence history of Bengal basin. Proc. Second Seminar on Petroliferous Basins of India. Indian Petroleum Publishers, Dehra Dun, India, pp. 47–59.

Chari, M.V.N., Sahu, J.N., Banerjee, B., Zutshi, P.L., Chandra, Kuldeep, 1995. Evolution of the Cauvery basin, India from subsidence modeling. Marine and Petroleum Geology 12, 667–675.

Chaubey, A.K., Gopala Rao, D., Srinivas, K., Ramprasad, T., Ramana, M.V., Subrahmanyam, V., 2002. Analyses of multichannel seismic reflection, gravity and magnetic data along a regional profile across the Central–Western Continental Margin of India. Marine Geology 182, 303–323.

Chetty, T.R.K., 1996. Proterozoic shear zones in southern granulite terrain, India. In: Santosh, M., Yoshida, M. (Eds.), The Archeaean and Proterozoic

Terrains of Southern India within East Gondwana. Gondwana Research Group Memoir, vol. 3, pp. 77–89.

Clift, P.D., Turner, J., 1998. Paleogene igneous underplating and subsidence anomalies in the Rockall–Faeroe–Shetland area. Marine and Petroleum Geology 15, 223–243.

Clift, P.D., Carter, A., Hurford, A.J., 1998. The erosional and uplift history of NE Atlantic passive margins: constraints on a passing plume. Journal of the Geological Society (London) 155, 787–800.

Coffin, M.F., Eldholm, O., 1994. Large igneous provinces: crustal structure, dimensions, and external consequences. Reviews of Geophysics 32, 1–36.

Curray, J.R., 1991. Possible greenschist metamorphism at the base of a 22-km sedimentary section, Bay of Bengal. Geology 19, 1097–1100.

Curray, J.R., Munasinghe, T., 1991. Origin of the Rajmahal traps and the 85°E ridge: preliminary reconstructions of the trace of the Crozet hotspot. Geology 19, 1237–1240.

Davison, I., 1997. Wide and narrow margins of the Brazilian South Atlantic. Journal of the Geological Society (London) 54, 471–476.

Duncan, R.A., Storey, M., 1992. The life cycle of Indian Ocean hot spots. In: Duncan, R.A. (Ed.), Synthesis of Results from Scientific Drilling in the Indian Ocean. American Geophysical Union Geophysical Monograph, vol. 70, pp. 91–103.

Fichler, C., Rundhovde, E., Olesen, O., Saether, B.M., Rueslatten, H., Lundin, E., Dore, A.G., 1999. Regional tectonic interpretation of image enhanced gravity and magnetic data covering the mid-Norwegian shelf and adjacent mainland. Tectonophysics 306, 183–197.

Gaina, G., Mueller, R.D., Brown, B., Ishihara, T., 2003. Microcontinent formation around Australia. Special Publication - Geological Society of Australia 22, 399–410.

Gallagher, K., Brown, R., Johnson, C.J., 1998. Geological applications of fission track analysis. Annual Review of Earth and Planetary Sciences 26, 519–572.

Gopala Rao, D., Krishna, K.S., Sar, D., 1997. Crustal evolution and sedimentation history of the Bay of Bengal since the Cretaceous. Journal of Geophysical Research 102, 17747–17768.

Gunnell, Y., Fleitout, L., 1998. Shoulder uplift of the western Ghats passive margin, India: a denudational model. Earth Surface Processes 23, 391–404.

Gussinye, M.P., Reston, T.J., 2001. Rheological evolution during extension at nonvolcanic rifted margins: onset of sepentinization and development of detachments leading to continental break-up. Journal of Geophysical Research 106, 3961–3975.

Jandardhan, A.S., 1999. Southern granulite terrain, south of the Palghat-Cauvery shear zone: implications for India–Madagascar connection. Gondwana Research 2, 463–469.

Kahle, H., Naini, B.R., Talwani, M., Eldholm, O., 1981. Marine geophysical study of the Comorin ridge, north central Indian basin. Journal of Geophysical Research 86, 3807–3814.

Kent, R., 1991. Lithospheric uplift in eastern Gondwana: evidence for a long-lived mantle plume system? Geology 19, 19–23.

Kent, W., Saunders, A.D., Kempton, P.D., Ghose, N., 1997. Rajmahal basalts, eastern India: mantle sources and melt distribution at a volcanic rifted margin. In: Mahoney, J.J., Coffin, M.F. (Eds.), Large Igneous Provinces. American Geophysical Union Geophysical Monograph, vol. 100, pp. 145–182.

Krishna, K.S., 2003. Structure and evolution of the Afanasy Nikitin seamount, buried hills and 85°E ridge in the northeastern Indian Ocean. Earth & Planetary Science Letters 209, 379–394.

Krishna, K.S., Bull, J.M., Scrutton, R.A., 2001. Evidence for multiple folding of the central Indian Ocean lithosphere. Geology 29, 715–718.

Krishna, K.S., Gopala Rao, D., Sar, D., in press. Nature of the crust in the Laxmi basin, Northwestern Continental Margin of India. Tectonics. doi:10.1029/2004TC001747.

Mall, D.M., Rao, V.K., Reddy, P.R., 1999. Deep sub-crustal features in the Bengal basin: seismic signatures for plume activity. Geophysical Research Letters 26, 2545–2548.

Miles, P.R., Munschy, M., Segoufin, J., 1998. Structure and evolution of the Arabian Sea and the eastern Somali basin. Geophysical Journal International 134, 876–888.

Mueller, R.D., Royer, J.Y., Lawver, L.A., 1993. Revised plate motions relative to the hotspots from combined Atlantic and Indian Ocean hotspot tracks. Geology 21, 275–278.

Murthy, K.S.R., Rao, T.C.S., Subrahmanyam, A.S., Malleswara Rao, M.M., Lakshminarayana, S., 1993. Structural lineaments from the magnetic anomaly maps of the eastern continental margin (ECMI) and NW Bengal Fan. Marine Geology 114, 171–183.

Nadin, P.A., Kuznir, N.J., Toth, J., 1995. Transient regional uplift in the early Tertiary of the northern North Sea and the development of the Iceland plume. Journal of the Geological Society (London) 152, 953–958.

Naini, B.R., Talwani, M., 1983. Structural framework and the evolutionary history of the continental margin of western India. In: Watkins, J.S., Drake, C.L. (Eds.), Studies in Continental Margin Geology. American Association of Petroleum Geologists Memoir, vol. 34, pp. 167–191.

NGRI, Gravity Map Series, GPH 1–6, 1978. Hyderabad, India.

Nogi, Y., Seama, N., Isezaki, N., 1992. The directions of magnetic anomaly lineations in Enderby basin off Antarctica. In: Yoshida, Y., Kaminuma, K., Shiraishi, K. (Eds.), Recent Progress in Antarctic Earth Science. Terra Scientific Publishing Co, Tokyo, pp. 649–654.

Nogi, Y., Seama, N., Isezaki, N., Fukuda, Y., 1996. Magnetic anomaly lineations and fracture zones deduced from vector magnetic anomalies in the west Enderby basin. In: Storey, B.C., King, E.C., Livermore, R.A. (Eds.), Weddell Sea Tectonics and Gondwana Breakup. Spec. Publ. - Geol. Soc. Lond., vol. 108, pp. 265–273.

Norton, I.O., Sclater, J.G., 1979. A model for the evolution of the Indian Ocean and the breakup of Gondwanaland. Journal of Geophysical Research 84, 6803–6830.

Powell, C.McA., Roots, S.R., Veevers, J.J., 1988. Pre-breakup continental extension in East Gondwanaland and the early opening of the eastern Indian Ocean. Tectonophysics 155, 261–283.

Radhakrishna, M., Chand, S., Subrahmanyam, C., 2000. Gravity anomalies, sediment loading and lithospheric flexure associated with the Krishna-Godavari basin, Eastern Continental Margin of India. Earth & Planetary Science Letters 175, 223–232.

Radhakrishna, M., Verma, R.K., Purushotham, A.K., 2002. Lithospheric structure below the eastern Arabian Sea and adjoining west coast of India based on Integrated analysis of gravity and seismic data. Marine Geophysical Researches 23, 25–42.

Raju, D.S.N., Bhandari, A., Ramesh, P., 1999. Relative sea level fluctuations during Cretaceous and Cenozoic in India. ONGC Bulletin 36, 185–202.

Raju, D.S.N., Dave, A., 1993. Foramaniferal events across the K/T boundary and Deccan volcanism in Krishna-Godavari basin, India. Proc. 2nd Seminar on Petroleferous Basins of India, pp. 315–329.

Ramalingeswara Rao, B., 1998. Seismicity and geodynamics of the low to high grade transition zone of Peninsular India. Tectonophysics 201, 175–185.

Ramalingeswara Rao, B., 2000. Historical seismicity and deformation rates in the Indian Peninsular shield. Journal of Seismology 4, 247–258.

Ramana, M.V., Nair, R.R., Sarma, K.V.L.N.S., Ramprasad, T., Krishna, K.S., Subrahmanyam, V., D'Cruz, M., Subrahmanyam, C., Paul, J., Subrahmanyam, A.S., Chandrasekhar, D.V., 1994. Mesozoic anomalies in the Bay of Bengal. Earth & Planetary Science Letters 121, 469–475.

Ramana, M.V., Ramprasad, T., Maria, Desa, 2001. Seafloor spreading magnetic anomalies in the Enderby basin, East Antarctica. Earth & Planetary Science Letters 191, 241–255.

Rangaraju, M.K., Agarwal, A., Prabhakar, K.N., 1993. Tectono-stratigraphy, structural styles, evolutionary model and hydrocarbon habitat, Cauvery and Palar basins. Proc. 2nd Seminar on Petroleferous Basins of India, pp. 371–388.

Raum, T., Mjelde, R., Digranes, P., Shimamura, H., Shiobara, H., Kodaira, S., Haatvedt, G., Sorenes, N., Thorbjornsen, T., 2002. Crustal structure of the southern part of the Voring basin, mid-Norway margin, from wide-angle seismic and gravity data. Tectonophysics 355, 99–126.

Raval, U., Veeraswamy, K., 2003. India–Madagascar separation: breakup along a pre-existing mobbing belt and chipping of the craton. Gondwana Research 6, 467–485.

Reid, I.D., Jackson, H.R., 1997. A review of three transform margins off eastern Canada. Geo-Marine Letters 17, 93–97.

Rotstein, Y., Munschy, M., Bernard, A., 2001. The Kerguelen province revisited: additional constraints on the development of the southeast Indian Ocean. Marine Geophysical Researches 22, 81–100.

Ruppel, C., 1995. Extensional processes in continental lithosphere. Journal of Geophysical Research 100, 24187–24215.

Sandwell, D.T., 1992. Antarctic marine gravity field from high-density satellite altimetry. Geophysical Journal International 109, 437–448.

Sandwell, D.T., Smith, W.H.F., 1997. Marine gravity anomaly from GEOSAT and ERS-1 satellite altimetry. Journal of Geophysical Research 102, 10039–10054.

Schlich, R., 1982. The Indian Ocean, aseismic ridges, spreading centers and basins. In: Nairn, E., Stehli, F.G. (Eds.), The Ocean Basins and Margins, The Indian Ocean. Plenum, New York, pp. 51–147.

Stein, S., Cloetingh, S., Sleep, N.H., Wortel, R., 1989. Passive margin earthquakes, stresses and rheology. In: Gregersen, S., Basham, P.W. (Eds.), Earthquakes at North-Atlantic Passive Margins: Neotectonics and Postglacial Rebound. Kluwer, pp. 231–259.

Storey, B.V., 1995. The role of mantle plumes in continental breakup: case histories from Gondwanaland. Nature 377, 301–308.

Storey, M., Mahoney, J.J., Saunders, A.D., Duncan, R.A., Kelley, S.P., Coffin, M.F., 1995. Timing of hot spot-related volcanism and the breakup of Madagascar and India. Science 267, 852–855.

Subbarao, K.V., Sukheshwala, R.N., 1981. Deccan volcanism and related basalt provinces in other parts of the world. Memoir - Geological Society of India 3, 374.

Subrahmanyam, C., Singh, R.N., 1992. Geotectonics of the Bay of Bengal. Indian Journal of Petroleum Geology 1, 161–180.

Subrahmanyam, V., Gopala Rao, D., Ramana, M.V., Krishna, K.S., Murthy, G.P. S., Gangadhara Rao, M., 1995. Structure and tectonics of the Southwestern Continental Margin of India. Tectonophysics 249, 267–282.

Subrahmanyam, C., Thakur, N.K., Gangadhara Rao, T., Ramana, M.V., Suhrahmanyam, V., 1999. Tectonics of the Bay of Bengal, northeastern Indian Ocean: new insights from satellite-derived gravity and shipborne geophysical data. Earth & Planetary Science Letters 171, 237–251.

Talwani, M., Reif, C., 1998. Laxmi ridge—a continental sliver in the Arabian Sea. Marine Geophysical Researches 20, 259–271.

Todal, A., Eldholm, O., 1998. Continental margin off western India and Deccan large igneous province. Marine Geophysical Researches 20, 273–291.

Venkatarengan, R., 1988. Depositional systems and thrust areas for exploration in Cauvery basin. ONGC Bulletin 63–66.

Verhoef, J., Jackson, H.R., 1991. Admittance signatures of rifted and transform margins: examples from eastern Canada. Geophysical Journal International 105, 229–239.

Vogt, P.R., Jung, Woo-Yeol, Brozena, J., 1998. Arctic margin gravity highs: deeper meaning for sediment depocentres? Marine Geophysical Researches 20, 459–477.

White, R.S., 1992. Magmatism during and after continental break-up. In: Storey, B.C., Albaster, T., Pankhurst, R.J. (Eds.), Magmatism and the causes of continental break-up. Geological Society London Special Publication, vol. 68, pp. 1–16.

White, N., Thompson, M., Barwise, T., 2003. Understanding the thermal evolution of deep-water continental margins. Nature 426, 334–343.

Yoshida, M., Rajesh, H.M., Santosh, M., 1999. Juxtaposition of India and Madagascar: a perspective. Gondwana Research 2, 449–462.

Annex B74

M. S. Steckler et al., "Collision of the Ganges-Brahmaputra Delta with the Burma Arc: Implications for Earthquake Hazard", *Earth and Planetary Science Letters*, Vol. 273 (2008)

Earth and Planetary Science Letters 273 (2008) 367–378

Contents lists available at ScienceDirect

Earth and Planetary Science Letters

journal homepage: www.elsevier.com/locate/epsl

Collision of the Ganges–Brahmaputra Delta with the Burma Arc: Implications for earthquake hazard

Michael S. Steckler [a,*], S. Humayun Akhter [b], Leonardo Seeber [a]

[a] Lamont-Doherty Earth Observatory of Columbia University, P.O. Box 1000, Palisades, NY 10964, USA
[b] Department of Geology, University of Dhaka, Dhaka 1000, Bangladesh

ARTICLE INFO

Article history:
Received 12 September 2007
Received in revised form 7 March 2008
Accepted 2 July 2008
Available online 15 July 2008

Editor: C.P. Jaupart

Keywords:
subduction
continental collision
accretionary prism
Ganges–Brahmaputra Delta
Bangladesh
tectonics
earthquake hazard

ABSTRACT

We take a fresh look at the topography, structure and seismicity of the Ganges–Brahmaputra Delta (GBD)–Burma Arc collision zone in order to reevaluate the nature of the accretionary prism and its seismic potential. The GBD, the world's largest delta, has been built from sediments eroded from the Himalayan collision. These sediments prograded the continental margin of the Indian subcontinent by ~400 km, forming a huge sediment pile that is now entering the Burma Arc subduction zone. Subduction of oceanic lithosphere with >20 km sediment thickness is fueling the growth of an active accretionary prism exposed on land. The prism starts at an apex south of the GBD shelf edge at ~18°N and widens northwards to form a broad triangle that may be up to 300 km wide at its northern limit. The front of the prism is blind, buried by the GBD sediments. Thus, the deformation front extends 100 km west of the surface fold belt beneath the Comilla Tract, which is uplifted by 3–4 m relative to the delta. This accretionary prism has the lowest surface slope of any active subduction zone. The gradient of the prism is only ~0.1°, rising to ~0.5° in the forearc region to the east. This low slope is consistent with the high level of overpressure found in the subsurface, and indicates a very weak detachment. Since its onset, the collision of the GBD and Burma Arc has expanded westward at ~2 cm/yr, and propagated southwards at ~5 cm/yr. Seismic hazard in the GBD is largely unknown. Intermediate-size earthquakes are associated with surface ruptures and fold growth in the external part of the prism. However, the possibility of large subduction ruptures has not been accounted for, and may be higher than generally believed. Although sediment-clogged systems are thought to not be able to sustain the stresses and strain-weakening behavior required for great earthquakes, some of the largest known earthquakes have occurred in heavily-sedimented subduction zones. A large earthquake in 1762 ruptured ~250 km of the southern part of the GBD, suggesting large earthquakes are possible there. A large, but poorly documented earthquake in 1548 damaged population centers at the northern and southern ends of the onshore prism, and is the only known candidate for a rupture of the plate boundary along the subaerial part of the GBD–Burma Arc collision zone.

1. Introduction

A reanalysis and reevaluation of new and existing data on the collision of the Ganges–Brahmaputra Delta (GBD) and the Burma Arc is warranted in order to gain to a new understanding of the nature of the accretionary prism and its seismic potential. The GBD and Fan is the largest depositional system in the world, containing >40% of the Cenozoic sediments from the Himalayan collision (Métivier et al., 1999). This huge sediment discharge of >1 GT/yr, 6–8% of the total world sediment flux (Milliman and Syvitski, 1992), has prograded the continental shelf edge over 400 km southwards since the Eocene (Figs. 1 and 2). This enormous sediment pile, likely resting on oceanic crust (Mitra et al., 2005), has entered the subduction zone of the Burma Arc. This is the beginning of a highly oblique collision of the Indian plate with the continental Burma Arc. In the northern Naga segment in Assam, the thick continental crust of India is colliding with the Burma Arc (Fig. 1). South of the Shillong Plateau, an uplifted block of continental basement, only the thick sediments of the GBD have entered the subduction zone. Here, the boundary exhibits typical oceanic subduction features including an accretionary prism, a forearc wedge, forearc basins, and a volcanic arc. However, because of the huge thickness of sediments entering the subduction zone, this is a rare occurrence of an 'oceanic' subduction zone where the deformation front is exposed on land. From ~18°N northwards, with the entrance of the GBD and Bengal Fan into the subduction zone, the accretionary prism begins widening, rising above sea level and broadening northwards into a large fold-and-thrust belt.

A general plate tectonic framework for the development of the GBD and its collision with the Burma Arc emerged by the 1980s (e.g., Graham et al., 1975; Hiller and Elahi, 1988; Murphy, 1988; Alam, 1989). Development of a detailed stratigraphic framework has been hampered by poorly fossiliferous strata in this region with overwhelming

* Corresponding author. Tel.: +1 845 365 8479; fax: +1 845 365 8179.
E-mail addresses: steckler@ldeo.columbia.edu (M.S. Steckler), shakhter@univdhaka.edu (S.H. Akhter), nano@ldeo.columbia.edu (L. Seeber).

0012-821X/$ – see front matter © 2008 Elsevier B.V. All rights reserved.
doi:10.1016/j.epsl.2008.07.009

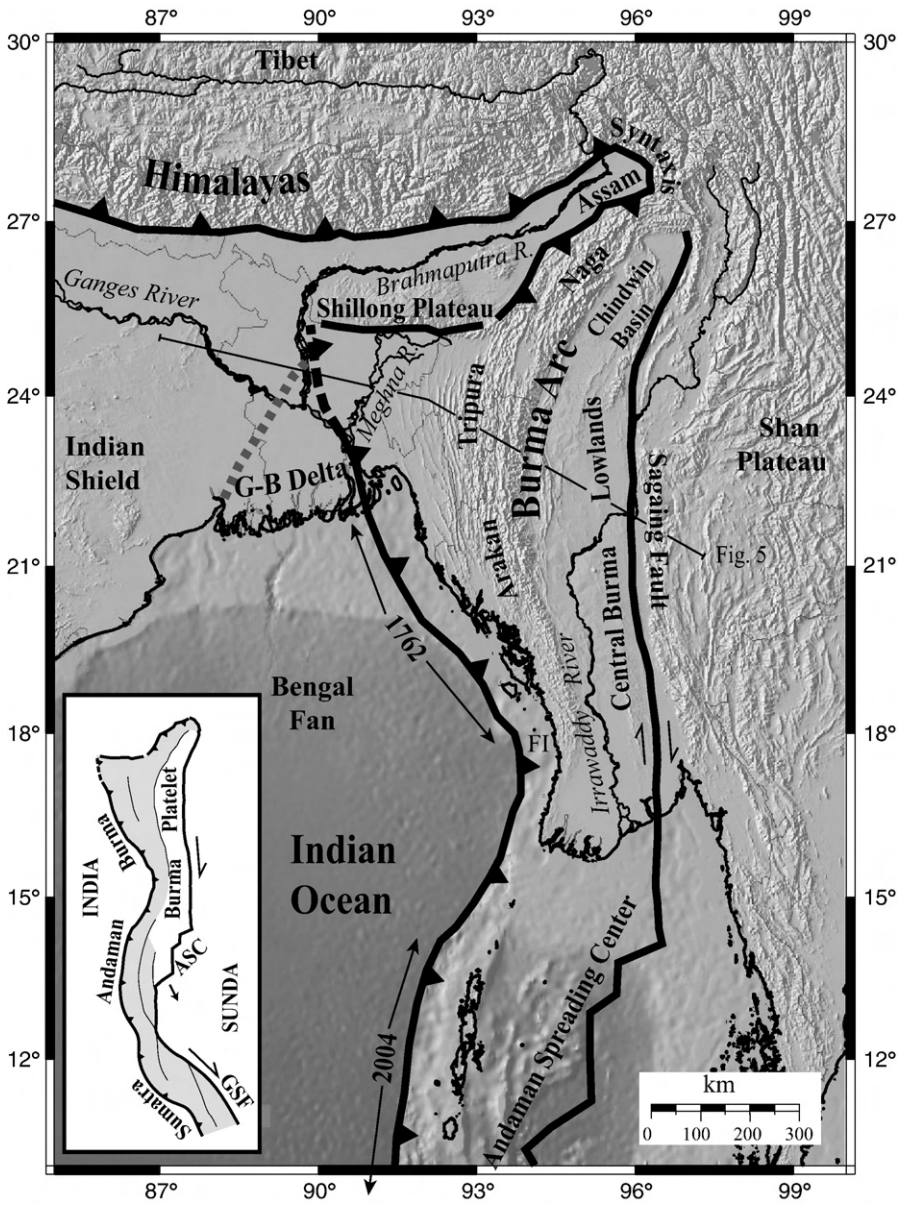

Fig. 1. Topographic map of Ganges–Brahmaputra Delta and Burma Arc region showing tectonic features. Major faults and tectonic boundaries are indicated by heavy black lines with thrusts barbed on the upper plate. Arrows indicate the source area of earthquakes that occurred in 1762 and 2004 FI = Foul Island. Inset map shows the outline of the Burma Platelet between the Sunda and Indian plates. The white area is the rigid core of the platelet, while the shaded region is the deforming forearc region. ASC = Andaman Spreading Center; GSF = Great Sumatran Fault.

clastic input. Thus, lithostratigraphy dominates despite the highly time-transgressive nature of sedimentation in the GBD, although sequence stratigraphic analyses are making inroads (e.g., Davies et al., 1999; Eliet et al., 1999; Gani and Alam, 1999; Partington et al., 2002). Seismic data are still primarily accessible only to industry, although more data are becoming publicly available. Thus, the tectonics of the delta and accretionary prism remain poorly known.

We investigate the topography, structure, geometry, and seismicity of the Burma Arc accretionary prism. The collision of the Burma Arc with the GBD exposes on land subduction/accretion structures that are usually submerged. The presence of a delta where subduction zones and continents meet is common (e.g., the Orinoco delta at the S. America–Caribbean boundary), but the size and sediment flux of the GBD are extreme. Other shallow-dipping accretionary prisms, such as the Mediterranean Ridge and Barbados (Davis et al., 1983), are submarine even where collision has begun. The GBD is also notorious for exposing a large vulnerable population to natural hazards, such as flooding, storm surges, coastal erosion, and earthquakes. The Tertiary sediment flux far exceeds the space created by subsidence and has built a vast delta that is only a few meters above sea level. Yearly flooding and sedimentation on the delta produces high fertility that permits a high population density, but also aggravates the effects of natural hazards. The GBD is traversed by an active plate boundary, yet we do not know how active it is and whether the motion is aseismic or is taken up by rare earthquakes, larger than any in the documented history. The unexpectedly large 2004 Sumatra–Andaman earthquake highlighted the uncertain seismic hazard along this plate boundary.

In this paper, we combine a variety of data to develop an updated understanding of the collision of the GBD and the Burma Arc, and of the tectonics of the accretionary prism. The huge width of the accretionary prism and of the implicit basal thrust fault raises the potential for very large earthquakes. As a result, earthquake hazard in Bangladesh may be higher than generally perceived. We first review published results on the GBD and the Burma Arc, then synthesize

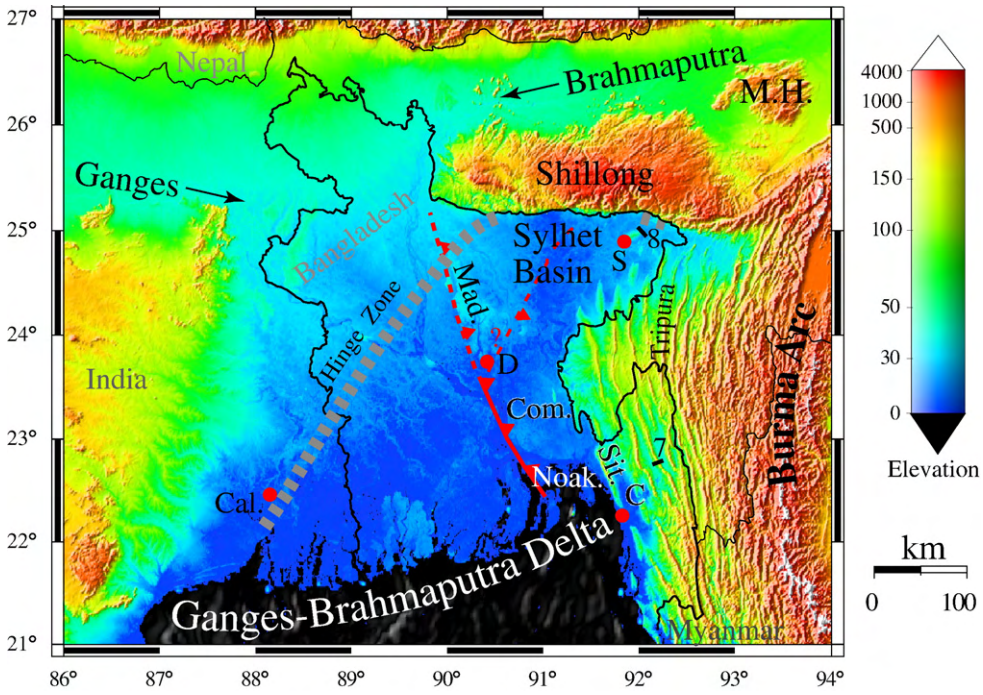

Fig. 2. Illuminated SRTM (Shuttle Radar Topography Mission) topographic map of Bangladesh and surrounding region showing main topographic, tectonic and geographic features. The Comilla Tract is an uplifted region (Brammer, 1996) of the delta underlain by buried folds. The Madhupur Tract is an uplifted Pleistocene interfluve that tilts toward the east and is possibly faulted in the west (Morgan and McIntire, 1959; Coates and Alam, 1990). Barbed line shows possible alignment of buried thrust front of the fold belt, dashed where uncertain. Alternative is thrust front continues to NE following trend of exposed anticlines. Dashed gray line shows position of Eocene shelf edge and marks the transition from thick continental crust to the NW and thinned continental and oceanic crust to the SE. The black bars labeled 7 and 8 indicate the location of the seismic lines shown in Figs. 7 and 8, respectively. C, D and S mark the locations of the cities of Chittagong, Dhaka and Sylhet. Cal. = Calcutta; Com. = Comilla Tract; Mad. = Madhupur Tract; M.K. = Mikir Hills; Noak. = Noakhali; Sit. = Sitakund Anticline.

them to reach new conclusions about the structure of the accretionary prism and the potential for large earthquakes in the region.

2. Ganges–Brahmaputra Delta

The GBD lies across the edge of the Indian craton, but the enormous sediment supply has prograded the delta far out over the continental margin. The edge of the pre-delta Eocene paleoshelf is marked by the shallow-water Sylhet Limestone, which runs NNE from near Calcutta to the edge of the Shillong Plateau (Fig. 2). The trend of this feature parallels the current shelf edge along the Indian continental margin to the south. The Sylhet Limestone drops by over 4 km across the 25-km wide hinge zone of the margin (Alam, 1989). NW of the hinge zone basement is relatively shallow (1–2 km; Lindsay et al., 1991; Alam et al., 2003), indicating the presence of thick continental crust. East of the hinge zone the great thickness of sediments indicates that the crust is greatly thinned or oceanic. At the Shillong Plateau, the Sylhet Limestone turns eastwards and is exposed in places along its southern margin. This suggests that the Shillong Plateau and the Dauki Fault, which forms its southern boundary, may have initiated along the edge of the continental margin. South of the plateau, the flexural loading from Shillong bends the Sylhet Limestone down to depths of 8 km or more. At the eastern end of the Shillong Plateau, the margin resumes a NE trend and continues into Naga, where it is involved in the NW-verging thrust belt (Fig. 3).

The enormous supply of sediments provided by the Himalayan collision fed the GBD and has produced ~400 km of progradation of the shelf edge since the Eocene. To the SE of the hinge zone, at least 5–6 km of post-Eocene sediments accumulated in a shallowing upwards sequence (Alam et al., 1990; Gani and Alam, 1999). Large clinoforms reflecting the progradation of the margin have been imaged beneath the delta (Lindsay et al., 1991). From the Middle Miocene onwards, the strata are extensively cut by large channels reflecting the development of the large river systems feeding the growing delta (Murphy, 1988; Eliet et al., 1999; Curiale et al., 2002). Formations reflecting the upward-shallowing transition from deep basin and base of slope to shelf and nonmarine strata are defined (e.g., Gani and Alam, 1999), but are not well dated and are likely highly time-transgressive, younging to the south. Sediment dilution and other factors make them poorly fossiliferous (Reimann, 1993; Worm et al., 1998).

Total sediment thickness beneath the GBD southeast of the hinge zone exceeds 16 km and the depth to basement may be as large as the 22 km estimated offshore (Curray, 1991). While the great sediment thickness implies thin crust, the position of the ocean/continent boundary is not known. It is often associated with a NE–SW trending gravity high that parallels the hinge zone. Mitra et al. (2005), using receiver functions at a station just over the Indian border in Tripura, detected the presence of a thin high-velocity layer interpreted to be oceanic crust. The Burma Arc thus appears to be underlain by subducting oceanic lithosphere.

3. Plate tectonic setting

The GBD lies near the cusp or syntaxis of two plate-convergence boundaries: the Himalayan and the Burma Arcs (Figs. 1 and 3). These arcs are convex toward the Indian plate and override it from the north and from the east, respectively. India, with the GBD, is thus the foreland of both Himalayan and Burma convergent boundaries with their broad advancing foredeeps and thrust–fold belts. Along the Himalayan arc, continents have been colliding since the Eocene. As the Himalayan collision progressed it extended around the Assam syntaxis (Fig. 1) and progressed from north to south along the Burma Arc (Lindsay et al., 1991; Lee and Lawver, 1995; Uddin and Lundberg, 1998). The first input of sediments to the GBD from Burma is in the Early Miocene (Uddin and Lundberg, 1998, 1999). At that time, before the uplift of the Shillong Plateau, the Brahmaputra discharged farther east (Johnson and Alam, 1991) into a deep-water embayment between the delta and the subduction zone (Gani and Alam, 2003). With time,

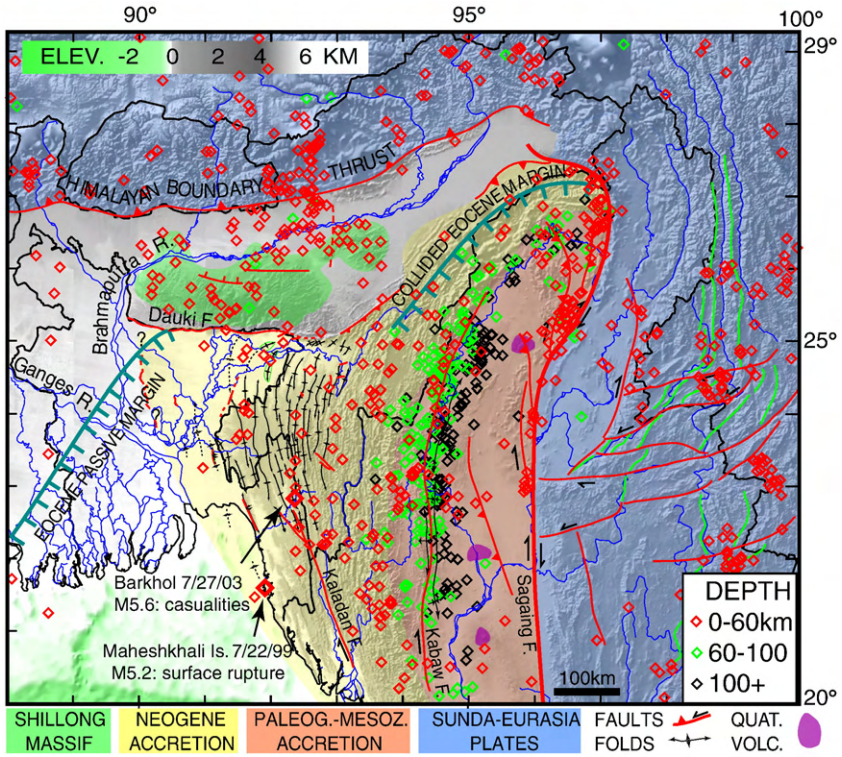

Fig. 3. Interpretive tectonic map of the Burma Arc. Topography in basemap shown in gray shade with color overlay for relevant tectonic units. Hypocenters from the relocated IASPE catalog. Subduction earthquakes extend to 200 km depth and Quaternary volcanoes are found in the Central Burmese Lowlands. Seismicity in the subducting slab (>60 km) is continuous except for a drop in activity north of the latitude of the Dauki Fault (25°N). The sharp drop in topography at the back of the fold-and-thrust belt into the Irrawaddy Lowlands (forearc basin) correlates with the 60 km depth contour (change from red to green hypocenters) on the slab (Ni et al., 1989). Shallow earthquakes are found throughout the wedge, widening with the wedge as it grows to the north. Fold axes interpreted from SPOT satellite images generally match topographic ridges. E–W shortening is confirmed by focal mechanisms and growth folds, but the rates are unknown. Two recent earthquakes of note in Bangladesh are indicated. PALEOG.–MESOZ. = Paleogene to Mesozoic; QUAT. VOLC. = Quaternary Volcanoes.

this embayment closed as the delta progressively collided with the Burma Arc.

The foredeeps of the Himalaya and Burma Arcs reflect bending of the subducting lithosphere under the load of overriding plates. Near the Assam syntaxis (Fig. 1) the two arcs are almost parallel and share the same foredeep, which is thus under a double load. The western part of this area exposes uplifted basement in the Shillong Plateau and Mikir Hills (Figs. 1–3). These cratonic blocks are believed to be fault bound and possibly decoupled from the rest of the continent (Mitra et al., 2005). Large historic earthquakes, such as the Great Indian earthquake of 1897, and modern seismicity (Fig. 3) in this area suggest that faults bounding these blocks are active (Bilham and England, 2001). The most prominent is the Dauki Fault, which marks the southern edge of the Shillong Plateau and probably a large dextral step-over of the continental margin (Figs. 1 and 2; Das Gupta and Biswas, 2000). This fault has been interpreted as a north dipping thrust related to the Himalayan front (e.g., Le Dain et al., 1984), as a steep dip–slip fault (e.g., Alam et al., 2003), or as a strike–slip tear fault associated with the Burma Arc. The latter is consistent with the drop of slab seismicity north 25°N, the latitude of the Dauki Fault (Fig. 3). These hypotheses are not mutually exclusive and oblique slip is also possible. It is clear that the Dauki Fault is a major active structure, yet its tectonic role and seismogenic potential are uncertain.

During the Neogene, the motion on the Dauki Fault created a huge south-facing scarp and offset in the basement (15 km: Hiller and Elahi, 1988; 8 km: Raman et al., 1990a; Johnson and Alam, 1991) and gravity field (130 mgals; Raman et al., 1990b). Uplift of the Shillong Plateau shifted the course of the Brahmaputra River westward around the uplift (Johnson and Alam, 1991). The Sylhet basin, immediately south of the Shillong Plateau is a low area that is flooded to 3–4 m depth every monsoon season. Holocene sedimentation rates exceed 7 mm/yr (Goodbred and Kuehl, 2000). Thus, the rapidly subsiding, swampy Sylhet basin (Figs. 2 and 3; Johnson and Alam, 1991) likely reflects flexural loading by the Shillong Plateau (Reimann, 1993).

The Burma Arc on the eastern side of the GBD displays all the characteristics of a subduction/convergence zone including a volcanic belt on the Burma overriding platelet (e.g., Le Dain et al., 1984) up to 25°N, the latitude of the Shillong Plateau (Fig. 3). A 150–200 km deep curtain of mantle seismicity defines a slab of subducted Indian plate lithosphere, which is traced as far north as the Assam syntaxis (Figs. 3 and 4; Ni et al., 1989; Chen and Molnar, 1990). There is a wide active fold–thrust belt verging westward toward the Indian foreland (Figs. 3 and 5; Le Dain et al., 1984; Ni et al., 1989). The topography rises gradually eastward across this belt forming the Indo–Burman ranges over the shallow-dipping portion of the subducting slab and then drops abruptly into the broad valley of the Irrawaddy River. Below this topographic break, the subducted slab steepens abruptly (Figs. 3 and 4; Ni et al., 1989). The Irrawaddy River valley, with the Chindwin and Central Burma lowlands, forms a relatively stable terrane floored by a Mesozoic/Paleogene arc complex. It is interpreted as a forearc basin of the current subduction system (Hamilton, 1979; Vigny et al., 2003). The dextral Sagaing Fault bounds it to the east.

The Sumatra–Andaman–Burma Arc (Fig. 1 inset) is also a classic area for partitioning of oblique convergence (Fitch, 1972). India–Sunda motion is partitioned between shortening in the frontal accretion zone and dextral motion along the Great Sumatran Fault and the Andaman Sea spreading center. Seafloor spreading in the Andaman basin (Raju et al., 2004) and the dextral Sagaing Fault (Vigny et al., 2003) separate a small Burma “platelet” between the Sunda and Indian plates. Gahalaut and Gahalaut (2007) consider this platelet as one unit with the Andaman and Sumatra forearc slivers further south. The motion of this Burma platelet and thus the convergence rate

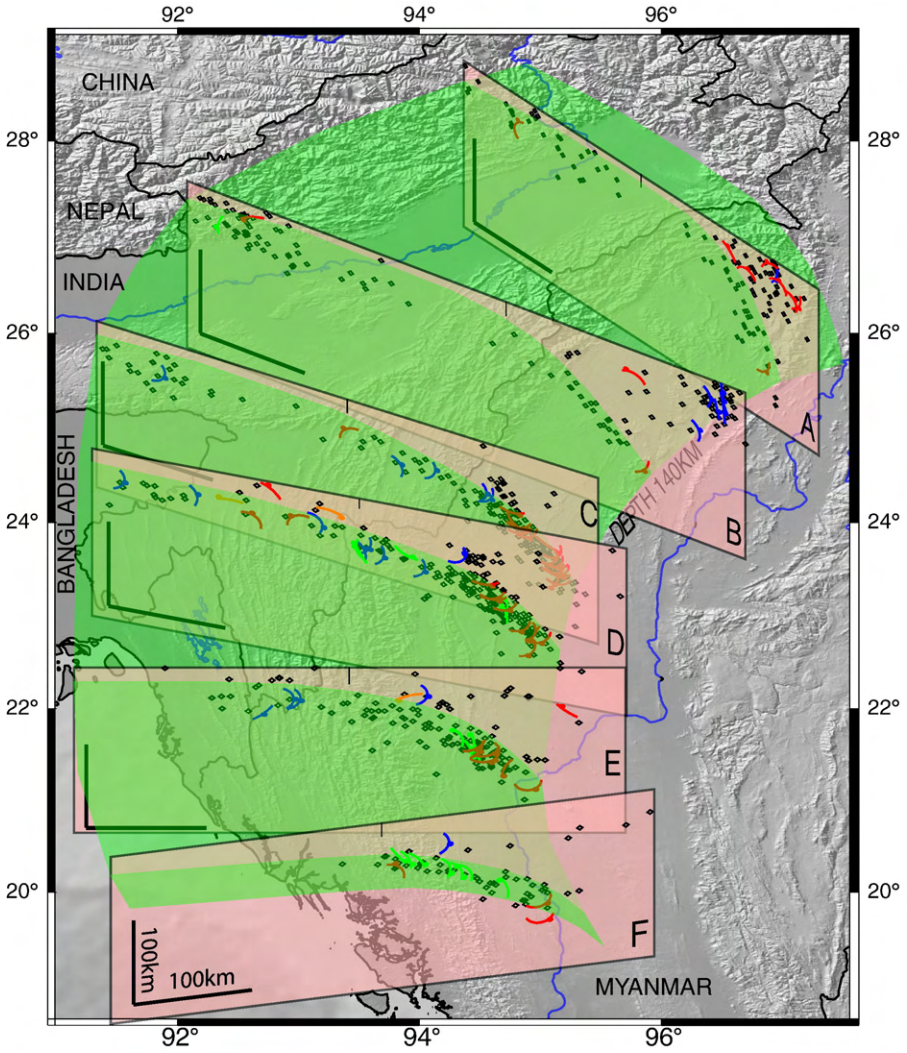

Fig. 4. Perspective view of subducting slab with vertical sections showing hypocenters and focal mechanisms along the Burma Arc. Earthquake data are projected onto sections for easier visualization of slab geometry. The coordinates of the center of the pink sections, their azimuth and the width over which hypocenters are projected is as follows: (A) 27.788°N 95.827°E, 140°, ±100 km; (B) 26.284°N 94.717°E, 120°, ±70 km; (C) 25.27°N 93.38°E, 115°, ±70 km; (D) 24.18°N 93.49°E, 105°, ±100 km; (E) 22.38°N 93.41°E, 90°, ±100 km; (F) 20.60°N 93.66°E, 80°, ±100 km. Horizontal and vertical bars in each section are 100 km long. The green surface is the plate interface interpreted from the seismicity.

across the India–Burma plate boundary is virtually unconstrained by global plate circuits (e.g., Bird, 2003). It has been proposed that the motion is pure strike–slip with no subduction (Guzman-Speciale and Ni, 1996; Rao and Kumar, 1999; Guzman-Speciale and Ni, 2000). Some plate-kinematic models (Lee and Lawver, 1995; Bird, 2003) predict separation between India and Burma at 1–4 cm/yr at the latitude of the GBD. Others (Satyabala, 1998, 2000, 2003; Nielsen et al., 2004) point to active folds, warped reference surfaces and seismicity along the fold belt and argue instead for current shortening as high as 1–2 cm/yr along the India–Burma boundary, in agreement with recent models constrained by GPS measurements in Myanmar (Vigny et al., 2003; Nielsen et al., 2004; Socquet et al., 2006). Shortening across the Burma Arc may also be increased by non-rigid flow of material from Tibet around the syntaxis and toward the Burma platelet, which is not accounted for in rigid plate models (Fig. 3).

At the latitude of Bangladesh there is about 35 mm/yr of oblique motion between the India and Sunda plates (Vigny et al., 2003; Socquet et al., 2006). The Sagaing Fault, separating the Burma and Sunda platelets (Fig. 1; Le Dain et al., 1984; Chen and Molnar, 1990), accomodates <20 mm/yr of right-lateral motion (Vigny et al., 2003). The rest must be accommodated by oblique subduction at the India–Burma boundary and internal deformation of the Burma platelet (Nielsen et al., 2004). GPS analysis by Socquet et al. (2006) found that the Central Burma Lowlands are rigid and the internal deformation of the Burma platelet must be limited to the fold belt west of the Kabaw fault (Figs. 1 and 5). Nielsen et al. (2004) suggests that the wide accretionary prism and forearc along the Burma segment contains strike–slip faults that accommodate the dextral motion, yielding more trench perpendicular subduction northwards.

4. Burma Arc fold belt and accretionary prism

The accretionary prism is small and steep offshore of Sumatra and Myanmar (Kopp and Kukowski, 2003; Nielsen et al., 2004). The profiles presented by Nielsen et al. (2004) off Myanmar at 16–18°N, just before the subduction zone hits the GBD, average 3–10°, while the break at the thrust front reaches 12–15°. When the Burma Arc subduction zone encounters the GBD, the width of the fold belt begins to increases dramatically. The outer accretionary prism emerges from the continental shelf at the south-facing Bengal margin, broadening and flattening northward to a maximum exposed width in Tripura (Figs. 1 and 3).

Topography along the Burma fold belt rises gently eastward from near sea level at the GBD (Fig. 6), reaching maximum elevations of 2500–3000 m at the eastern end of the fold belt. As the width of the fold belt increases northward along the Burma Arc, its average slope

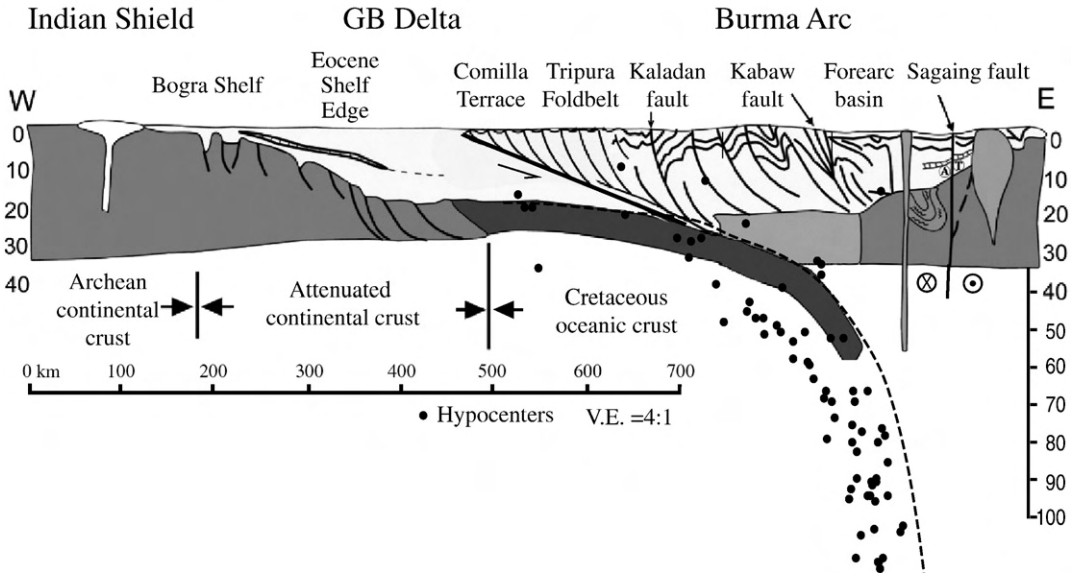

Fig. 5. Schematic cross-section of subduction zone from the Indian craton across the GBD and Burma Arc to the Sunda plate. Modified from http://www.auburn.edu/academic/science_math/geology/hrl/ew.htm based on figure from Murphy (1988). Added hypocenters (1960–2000 USGS) are used to tentatively interpret the top of basement in the downgoing slab and project the megathrust to the near surface.

decreases. Using SRTM topography, we calculate that the outer, western portion of the fold belt has the extremely low mean slope of ~0.1°. Even if the young sediments in the synclines were isostatically removed, the slope would not rise above ~0.2°. After a distinct break, the average slope in the older and higher eastern part of the fold belt steepens to ~0.5°. As the chain narrows southward, the average slope increases to almost 2°. In comparison, the lowest slopes at other prisms are the submarine Barbados prism with a slope of 1±0.5°, decreasing to 0.7±0.2° near the toe, and the Makran prism with a slope of 1.6±0.3° (Davis et al., 1983). Thus the average surface slope of the Burma thrust–fold belt is as much as an order of magnitude smaller than other subaerial fold-and-thrust belts or submarine accretionary prisms.

Early papers show the folded delta strata of the accretionary prism, but do not incorporate a basal detachment in their sections (e.g., Murphy, 1988; Alam, 1989). However, there is a low-velocity zone imaged at ~3 s two-way travel time (TWTT) in profiles across the westernmost exposed fold on the Comilla Terrace (Sikder and Alam, 2003). Thus we, like Alam et al. (2003) are guided by worldwide analogs to interpret the fold belt to be detached over a shallow-dipping basal megathrust (Fig. 5). Based on the distribution of teleseismic earthquake locations (Figs. 4 and 5), we speculate that the detachment dips on average 5–7° to the east. Applying a critical taper model to the prism (Davis et al., 1983; Dahlen, 1990), we note that as the pore pressure in the wedge and detachment approaches lithostatic, the surface slope approaches zero. If we assume that the wedge is at critical taper, then the low 0.1° slope in the wedge requires extremely high pore pressures that approach lithostatic. As in most sedimentary basins with high deposition rates, the Bengal Basin is overpressured (Imam and Hussain, 2002; Zahid and Uddin, 2005). Fluid pressures in a well in the Sitakund anticline north of Chittagong (Fig. 2) are 6927 psi (47.8 Mpa) at 2387 m and 7562 psi (52.1 Mpa) at 2616 m (BAPEX, pers. Comm., 2005). These pressures are over twice hydrostatic. Both depths yield pressures corresponding to 92% and 97% of lithostatic for assumed mean sediment densities of 2.2 and 2.1 g/cm^3, respectively. These are values comparable to Barbados and Makran, estimated at 97 and 98% (Davis et al., 1983). Higher slope wedges typically have pore pressure ratios (observed/lithostatic) of λ=0.7±0.2. Further evidence

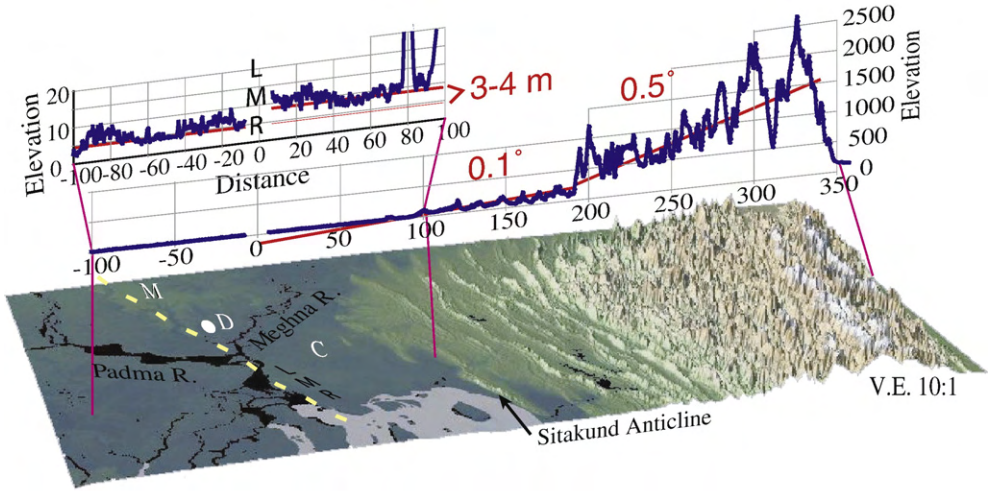

Fig. 6. Relief image of SRTM topography across the eastern GBD and Burma Arc fold belt. Profile shows the topographic slopes, including projection of the accretionary prism below the Comilla Terrace and uplift of Comilla (C). Detailed elevation shows uplift of Comilla Terrace relative to other parts of the GBD. Yellow dashed line is a possible location of thrust front. LMR = Lower Meghna River; M = Madhupur Terrace; D = Dhaka. (For interpretation of the references to color in this figure legend, the reader is referred to the web version of this article.)

of the high pore pressures in Bangladesh is that two mud volcanoes were reported on Sitakund anticline during the 1762 earthquake (Akhter, 1979). The depth to overpressure in this well is shallower (1100 m) than in others (3000 m) in Bangladesh. Zahid and Uddin (2005) show that there is a velocity decrease with depth below 3200 m reflecting increased overpressure. We suggest that this may be associated the detachment. Furthermore, in order to fit the low surface slope with the critical taper model, the coefficient of friction, μ, in the interior of the wedge must be much higher than the basal coefficient of friction, μ_b. For μ values in the range of 0.6–0.85, the basal coefficient of friction, μ_b, must be 0.26–0.47 for $\lambda \leq 0.95$. The detachment must be much weaker than the interior of the wedge.

The increase in slope of the eastern part of the fold belt corresponds to approximately where the depth of the detachment is ~20 km, roughly equal to the thickness of sediments in the Bengal Basin (Fig. 5). The low slope of the frontal thrust belt would then correspond to where it overrides and incorporates extremely overpressured sediments producing large input of fluids into the wedge. The higher, but still low slope, in the east would correspond to where the fold-and-thrust belt overrides oceanic basement after the bulk of sediments and fluids had been stripped off. We suggest that the lack of hydrological forcing combined with the older, more deformed and compacted sediments of the eastern fold belt results in the greater strength and slope of this region.

Field observations and seismic data (Fig. 7) show that many of the folds in the wedge have a box-like shape with a flat top (e.g., Mandal and Woobaidullah, 2006). For example, the exposed structure of the Sitakund anticline displays a broad flat at the culmination kinking abruptly into the back (east) limb. The broad sub-horizontal culminations typical of these folds is better accounted for by a fault-bend fold than by a fault-propagation fold interpretation (e.g., Sikder and Alam, 2003). Surface fractures from the 1999 Maheshkhali Island earthquake (Fig. 3), as reported by GSB scientists (Mir Fazlul Karim, pers. Comm., 2006), were extensional and followed the kink between the back limb and the flat on that anticline, suggesting coseismic slip on a blind ramp-flat fault with extension in the hangingwall block as it moved through the kink. Often, the vergence of the anticlines is toward the east (Fig. 7) indicating that the forward shear from the slight overall westward slope of the accretionary wedge is very weak compared to other factors that may control the local vergence. In sandbox models with overpressures (Mourgues and Cobbold (2006) bivergent box folds formed when the detachment was more overpressured and weaker than the wedge. Thus the fold geometry reinforces the conclusion that the basal detachment in Bangladesh is very weak. Farther east, the structures are tighter and more complex (Murphy, 1988; Alam, 1989). It is likely that these structures are detached from the overpressured shales below (Fig. 7).

The seismic profile in Fig. 7 and other profiles of anticlines in the Chittagong Hill Tracts show an extensive Miocene section of constant thickness that predates the growth of the anticline. Thinning of strata towards the crest of the structure is only visible above the shallowest green horizon (Fig. 7). The Miocene strata preserve shallowing upwards base of slope to neritic facies (Gani and Alam, 2003). Strata deposited during the deformation are primarily shelf to fluvial facies. We suggest that the shallowing upwards section represents the SE progradation of GBD and the syndepositional deformation of the shelf to fluvial sediments represents the advance of subduction onto the continental margin. The age of the start of deformation is uncertain and certainly time-transgressive. At the profile of Fig. 7, the accretionary prism climbed to shelf water depths probably by Late Miocene–Pliocene. The initial subduction of the GBD when the deformation front was still in deeper water slope and base of slope deposits may be exposed farther east in the more deformed parts of the fold belt. The post-Miocene section is thin due to the continued uplift of the advancing prism. In contrast, seismic profiles from the Sylhet basin (Fig. 8) show thick sedimentary sections that were

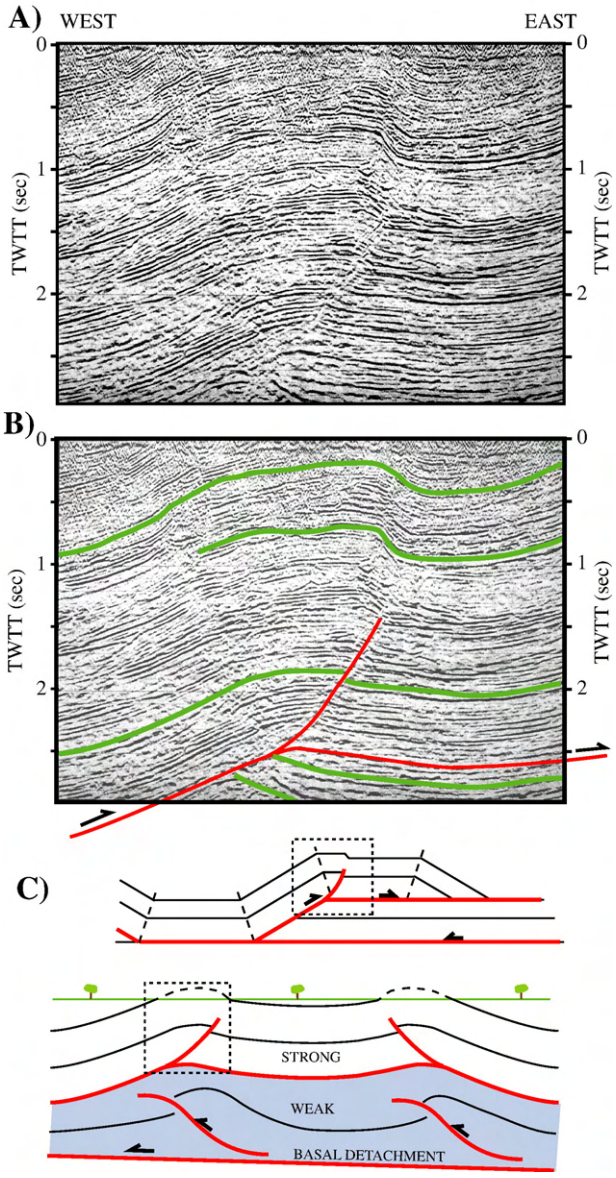

Fig. 7. Example of flat-topped "box" anticlines common throughout Chittagong–Tripura–Sylhet fold belt. Uninterpreted seismic section (A) showing the Gobamura anticline whose location is shown in Fig. 2. We interpret the structure as a fault-bend fold followed by a fault-propagation fold (B). In this example the vergence is toward the east indicating forward shear from the low slope of the accretionary wedge is weak compared to other local factors that may control vergence. Possible underlying geometries for the structure are shown in (C). Lack of a forelimb and broad synclines may be accounted for by two-layer tectonics. The Lower layer is mechanically weak (overpressured distal fine sediment?) and does not preserve bed thickness while the upper layer is strong (sandy slope to fluvial sediment) and shortens by kinks and thrust faults. Erosion unloads anticlines causing flow toward them in the lower layer. Anticline growth is younger than the upper green horizon because no growth is apparent below this level. Possible growth is seen in the upper 0.6 s on the flanks of the anticline.

deposited during fold growth. Some of the sections display the thrust faults at the root of the folds (e.g., Johnson and Alam, 1991; Sikder and Alam, 2003). We attribute this difference to the rapid subsidence and sedimentation in the Sylhet basin associated with the flexural load of the Shillong Plateau.

The outermost folds of the wedge are blind. At its western margin, the fold belt plunges beneath the slightly uplifted (3–4 m) Comilla Tract (Figs. 2 and 6). Here, the Holocene estuarine sediments form an oxidized horizon known as the Tippera Surface attesting to recent uplift and exposure of this area relative to the rest of the delta (Morgan and McIntire, 1959; Brammer, 1996). Folds are present in the subsurface

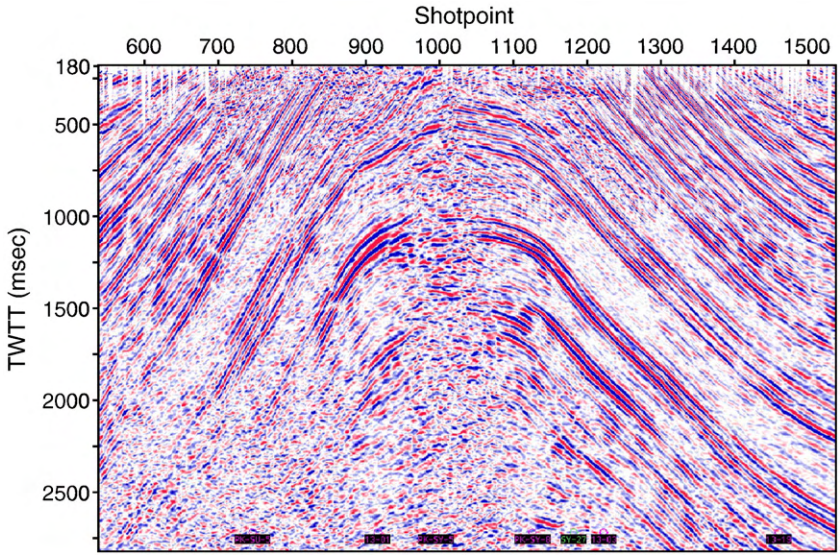

Fig. 8. Seismic line across the NE end of the Sylhet anticline. The position of the line is shown in Fig. 2. The Sylhet anticline also shows a flat top suggestive of fault–bend fold. Note the fanning of the reflectors on the flanks of the structure, most evident on the upper right. This growth indicates syntectonic sedimentation. The Sylhet basin is subsiding and being filled with sediment as the folding is occurring.

beneath the Comilla Tract and the Pleistocene exposure surface in tube wells is warped. Thus the fold belt continues farther west than its surface expression (Nielsen et al., 2004), to at least as far at the Lower Meghna River. Differential subsidence of the foredeep and eastward tilting of the delta west of the deformation front would be expected to attract the river toward the deformation front, which may thus be located at or near the Lower Meghna River (Figs. 2 and 6).

Whether the northward widening of the fold belt continues to the Dauki fault remains unresolved because the downflexing by the Shillong Plateau deeply buries the surface expression of compressional structures in the central Sylhet basin (Figs. 2 and 3). The folds rotate clockwise as they approach the Dauki Fault (Johnson and Alam, 1991), suggesting a narrowing of the belt. However, immediately to the west, the uplifted Madhupur Terrace, with hints of tectonic tilting and faulting along its western margin (Morgan and McIntire, 1959; Coates and Alam, 1990), may be the surface expression of the thrust front. If so, the accretionary prism continues to widen northwards to ~300 km. One possibility is that the thrust front jumped westward when the Shillong Plateau was uplifted.

The accretionary prism associated with the GBD thus covers a triangular area that is up to 300 km wide at 25° 10′N and extends southward to an apex at ~18°N, south of the continental shelf edge. The age of the initial collision of the GBD with the Burma Arc is uncertain. If we assume the prism growth started in the middle Miocene, then the average westward growth rate of the prism would be ~2 cm/yr. The current rate is likely much greater. If the first impact was near the Shillong Plateau and has been scissoring closed southwards, the rate is ~5 cm/yr. For a basal dip of 5–7°, we estimate that the total volume of the prism is comparable, given the uncertainties (within a factor of 2), to the amount of sediment entering the subduction zone for a convergence rate of 1–2 cm.

5. Earthquakes along the Burma Arc

A Wadati–Benioff zone of earthquakes illuminating the subducted oceanic lithosphere characterizes the entire India–Sunda boundary, including the northernmost onshore 800 km, from the Bay of Bengal to the eastern end of the Himalayan arc (Fig. 4). While earthquakes deeper than 60 km are concentrated in the slab, shallower epicenters may be on the boundary or on secondary faults above or below it (Figs. 3 and 4). Some of the plate-boundary earthquakes are huge. The Mw 9.3 on 26 December 2004 ruptured 1300 km of the boundary, including the southern part of the Burma platelet (Fig. 9). That event was not expected and has brought to the fore the potential for similar large ruptures along the rest of the Burma platelet. Lack of knowledge about these ruptures is critical for Bangladesh, with one of the highest population densities in the world (Fig. 9). Prior to 2004, the potential for mega-earthquakes along the subduction boundary north of Sumatra was overlooked (e.g., Pacheco and Sykes, 1992), in part because relative motion is highly oblique and is thus expected primarily on the dextral faults behind the arc (Figs. 1 and 9) and in part because no M≥8 earthquake was known in that portion of the boundary (Bilham, 2005). Similarly, the official earthquake hazard map for Bangladesh (Ali, 1998) is based on recent historical seismicity and neglects any hazard from large earthquakes on the detachment thrust. Important lessons are: 1) history may be short compared to repeat times for ruptures that have a very large slip; 2) Even slow slip rates can produce large earthquakes; and 3) The maximum intensity areas of M>8 Himalayan earthquakes tend to be displaced toward the foreland relative to the smaller earthquakes.

The easily accessible historic record of earthquakes in Bangladesh (e.g., Banglapedia, http://banglapedia.search.com.bd/HT/E_0002.htm) gives us only hints of the seismogenic behavior of the India–Sunda boundary north of the 2004 rupture (Fig. 1). A “great” earthquake in 1762 caused relative sea level changes along the Arakan coast up to Chittagong and fountaining of water and mud on the Sitakund anticline north of this city (Fig. 2). There was extensive flooding in the coastal Noakhali district (Fig. 2; Hunter, 1875). Whether this was due to subsidence or a tsunami in this low-lying area is unclear. The northernmost known damage by this earthquake is in Dhaka where 500 people died from seiches in the Buriganga river and overturned boats. The 1762 earthquake is thought to have ruptured the plate boundary up to but excluding the GBD (Tripura segment) (Cummins, 2007). The only candidate for a rupture of the Tripura segment is the earliest known earthquake in 1548. It damaged Sylhet and Chittagong, at both ends of the segment (Fig. 2), and “the earth opened in many places and threw up water and mud of a sulphurous smell”. The only other recorded comment is that it was a “terrible one”. This information is listed in the Banglapedia and is reputed to derive from Hunter (1875). However, Indian records report that a 1548 earthquake took place in Assam (Gait, 1906; Iyengar and Sharma, 1998; Rajendran et al., 2004), possibly on the Naga segment. Could these be a single event? Could the Assam event cause the damage in Chittagong, 580 km from the estimated epicenter? Might a rupture in Assam have

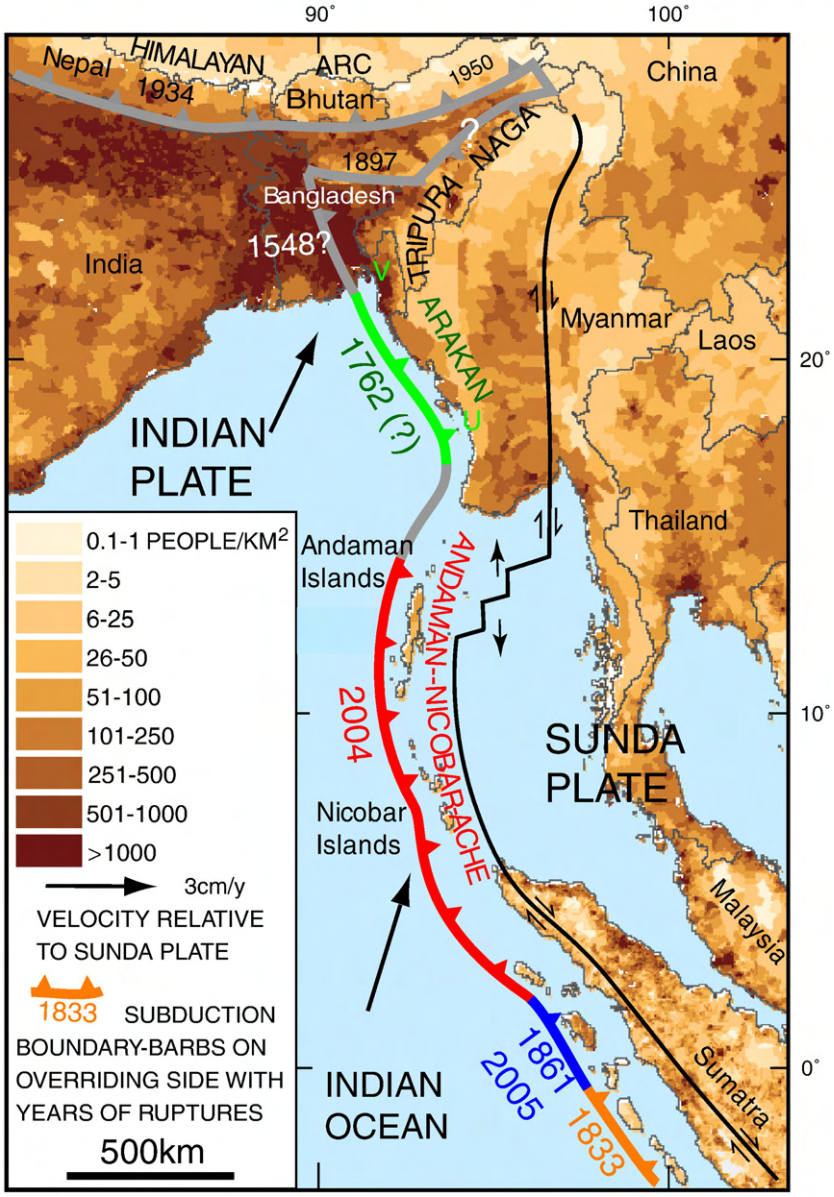

Fig. 9. The India–Burma–Sunda plate boundaries with historic ruptures superimposed on a population map (Balk et al., 2005). The U and V locate Uplifted shorelines on Foul Island and clastic Vents on the Sitakund anticline, respectively, that suggest the extent of the 1762 rupture. The Tripura segment traverses the Ganges–Brahmaputra Delta, one of the most densely populated regions of the world. The first recorded earthquake in Bangladesh, in 1548, "was a terrible one" that is the only possible historic rupture of this segment.

extended into or triggered a rupture of the Tripura segment? The most recent M≥7 earthquake on the Tripura segment was in 1918 in the Sylhet Basin, at the northern end of the segment. Given its size, Ms 7.5, the 1918 rupture is unlikely to be on a steep shallow fault because it apparently did not rupture the surface. If it was on a shallow-dipping thrust, it could not have ruptured a significant portion of this boundary because its large downdip extent would entail a large moment release per unit length. In summary, historic data clearly show that the southern half of the Burma Arc ruptured in a great earthquake 2.5 centuries ago (Richter, 1958). The southern extent of this rupture is unclear but it extended at least to Foul Island (18.1°N, 2.74 m uplift). Its northern extent reached at least 250 km beyond the edge of the Bengal shelf, thus rupturing a considerable area where the thick sediments of the GBD are being subducted. This suggests that the Tripura segment can also rupture in great subduction earthquakes, but is not conclusive.

Shallow seismogenesis close to the deformation front and the GBD is demonstrated by recent seismicity. A belt of crustal seismicity follows the Burma forearc and broadens northward with the fold belt (Fig. 3). Some of these earthquakes are in the lower crust of the subducting plate and may reflect typical bending failures near a plate boundary or high stress from the Himalayan continent–continent collision (Mitra et al., 2005). Other earthquakes are within the accretionary prism. The shallow 1999 M 5.2 earthquake in Maheshkhali Island is associated with one of the outermost folds (Fig. 3). Extensional fracturing along the crest of the Maheshkhali anticline (GSB data) suggests coseismic folding of the related blind ramp above the rupture. This earthquake indicates that these shallow faults, presumably imbricate thrusts rooted onto a basal detachment can be seismogenic, despite the high fluid pressures (Imam and Hussain, 2002; Zahid and Uddin, 2005).

Other recent thrust earthquakes (M 5.6 Barkhol, 2003, M 4.9 Barkhol, 2007) caused damage near the transition to the steeper part of the fold belt (Fig. 3). The 2003 event is associated with a 10-km long N–S striking surface rupture and caused relatively strong surface effects in Chittagong city, suggesting a shallow depth. In contrast, a M5 2004

thrust event near Sylhet was weakly felt and may have been in the lower crust, as other earthquakes in that area (Mitra et al., 2005). Thus, available instrumental data indicate seismogenesis on diverse structures over a range of crustal depths along the fold belt. In terms of both seismicity rate and complexity of seismogenic structure, the Tripura segment may be comparable to the sediment rich subduction system in Cascadia, where a great rupture is expected (Petersen et al., 2002).

6. Seismic vs. aseismic deformation

The 26 December 2004 earthquake off Sumatra focused world attention on the Sunda Arc subduction zone. The Tripura segment is part of this subduction zone, but whether it breaks in great earthquakes is unknown, but has huge societal implications (Fig. 9). Bangladesh is along strike of and within a rupture-distance from that enormous Mw 9.3 earthquake. Modified Mercalli (MM) intensities V–VI were widespread in the southern part of the country and caused damage, injuries, and panic (Martin, 2005). Lakes and ponds sloshed in seiches and wells were clouded and/or dried up. Most people felt the earthquake in Dhaka (MM IV). This event, as well as the 1897 earthquake from the north (Oldham, 1899), highlight the fact that the poorly consolidated sediments of the GBD are highly susceptible to strong ground motion and liquefaction.

Active convergence is manifested by recent M 5–6 earthquakes on blind thrusts associated with anticlines in the fold belt. These imbricate faults are probably rooted onto the subduction megathrust. How slip is taken up on this very large active fault is a critical issue for science and for hazard. Possibilities include continuous aseismic creep, discrete aseismic creep events or slow earthquakes, very large and relatively rare earthquakes, or all of the above on different portions of the megathrust. The lack of a clear historic precedent of a GBD-wide rupture and the thick and overpressured sediment being accreted have tended to sway speculations toward the aseismic end of the spectrum.

While the overpressured sediment in Bangladesh indicates weak mechanical conditions, whether this implies aseismic deformation is unclear. Counter examples include Cascadia and the eastern Aleutians–Gulf of Alaska where sediment rich accretion zones have produced some of the largest known earthquakes (Ruff, 1989; Oleskevich et al., 1999). Studies suggest the 100 °C isotherm and clay dehydration is the updip limit of the seismogenic zone (e.g., Hyndman and Wang, 1993; Oleskevich et al., 1999). However, there is evidence of seismic slipping and interseismic non-slip at subduction zones much shallower than would be expected from sediment conditions (e.g., Satake and Tanioka, 1999; Gagnon et al., 2005). The shallow part may not be locked, but may be buttressed by the deeper locked segment (Wang and Dixon, 2004) and still susceptible to seismic slip. Another factor is that the geothermal gradient in the overpressured sediments in SE Bangladesh is high (>40°/km, Zahid and Uddin, 2005), likely because of the low thermal conductivity of water, although rapid sedimentation decreases the gradient in the Sylhet Basin (Zahid and Uddin, 2005). Thus, the expected weakness of the sediments may be counterbalanced by higher temperatures that enable shallow stick–slip behavior.

The ability of the accretionary prism to support stresses and exhibit seismogenic strain-weakening behavior is believed to depend upon pressure, temperature, sediment type and fluid content (Moore and Saffer, 2001). The rapid sedimentation in the foredeep of the Tripura segment is responsible for the pervasive high pore pressure regime. As in most deltas, the sediment deposition rate is faster than fluids can escape (e.g., Gordon and Flemings, 1998). As the GBD progrades, coarser-grained deltaic sediments are deposited over finer-grained deep-water strata (Gani and Alam, 2003) with low permeability causing overpressures. Furthermore, the dynamic sedimentation regime of the delta with sandy channels, muddy overbanks, mixed clastics on the shelf, hemipelagic slope mud and basin-floor turbidites (Akhter et. al., 1998; Gani and Alam, 2003) yields a complex pattern of fine and coarse sediment, permeability and overpressure. The nature of sediments in this shallower (<40 km) portion of the subduction boundary may control how far updip towards the heavily populated lowlands a major rupture could propagate.

One factor that may influence this is the rapid Holocene deposition in the delta and synclines of the fold belt. This has buried the tip of the wedge in Comilla and likely contributed to a flattening of the wedge topography for the front 100 km. This would shift the wedge toward a subcritical state such that deformation should be concentrated within the wedge to thicken it. In this subcritical state, a rupture would be more likely to terminate updip into an imbricate fault in the wedge rather than propagate up to the deformation front. We note that the possible 1548 event is not reported to have damaged Dhaka or nearby Sonargaon, the capital at the time, but only Sylhet and Chittagong farther east. If a great subduction earthquake rupture were to terminate at an imbricate fault, it could spare the highly populated delta (Fig. 9) of the worst ground shaking.

7. Summary and conclusions

The Ganges–Brahmaputra Delta is the result of the huge amount of erosion of the Himalaya. The sediments built out the continental margin of the Indian subcontinent by over 400 km. The GBD, presumed to partly overlie oceanic crust, is now entering the Burma Arc subduction zone. Subduction of the >20 km thick sediment prism has fueled the growth of a broad accretionary prism. The accretionary prism is partly buried and deformed in the Sylhet area south of the Shillong Plateau, but may be as wide as 300 km there. The prism tapers southwards to an apex near the junction of the continental shelf edge of the GBD and the subduction zone at ~20°N. The Burma Arc fold belt in Bangladesh is a rare instance of an oceanic accretionary prism exposed on land. It also represents the earliest stage of continental collision when only the sediments of a continental margin have entered the subduction zone. This stage has lasted a long time because the GBD is so large and convergence is slow (3–400 km subducted at 1–2 cm/yr).

The front of the prism is blind, buried by the GBD sediments; the 100 km wide Comilla Tract, where the fold belt plunges beneath the surface, is uplifted by 3–4 m relative to the rest of the delta. The accretionary prism also has the lowest surface slope of any active subduction zone. The gradient of the prism is only ~0.1°, rising to ~0.5° in the forearc region to the east, the lowest of any prism. This low slope is consistent with the high level of overpressure found in the subsurface. It also implies a very weak detachment. The Tripura fold belt thus represents an extreme example of a wedge dominated by its sediment input and large hydrologic forcing (Saffer and Bekins, 2002). Fluids in the subducted sediments are underthrust faster than they can be expelled leading to high overpressure and a weak low-slope wedge. Wedges dominated by large sediment input, such as Makran and southern Barbados (Saffer and Bekins, 2002), are found where terrigenous sediment is transported onto the subducting plate. This situation is likely common at the early stages of continental collision as continental margins approach subduction zones.

Seismic hazard in the GBD is largely unconstrained, but may be higher than generally perceived because current estimates do not account for possible large subduction ruptures. It has been proposed that such a sediment-clogged system cannot sustain the stresses and strain-weakening behavior required for great earthquakes (Byrne et al., 1988; Pacheco et al., 1993). Yet, some of the largest known earthquakes have occurred in heavily-sedimented subduction zones (Ruff, 1989, 1992), such as the 1964 Alaska earthquake and the 1700 Cascadia earthquake. Most importantly, a large earthquake in 1762 ruptured the Arakan segment, south of the delta, including 250 km of the Bengal shelf, the offshore extension of the delta. A large, but sketchily known, earthquake in 1548 is reported to have damaged population centers at both ends of the Tripura segment and is the only known candidate for a rupture of this segment.

Knowledge about the GBD-BurmaArc system is limited, but growing rapidly. Field geologic work is ongoing and industry seismic data are starting to become accessible. Our ongoing efforts are contributing towards establishing and expanding GPS and seismic networks in the region. These are providing the first steps towards understanding this large dynamic system where subduction of the world's largest delta has created a broad, flat, subaerial accretionary prism.

Acknowledgements

This work was funded by NSF grants INT 99-00487 and EAR 06-36037 and NASA grant NNG04GA86G. We thank John Armbruster, the Geologic Survey of Bangladesh and PetroBangla for their assistance. We also thank two anonymous reviewers whose comments greatly improved the paper. Lamont-Doherty Earth Observatory publication number 7189.

References

Akhter, S.H., 1979. Structure, stratigraphy and sedimentology of the Upper Tertiary sediments of the central part of the Sitakund Hill Range, Chittagong, Bangladesh. M.Sc. thesis, Geology Department, Dhaka University, Bangladesh.

Akhter, S.H., Bhuiyan, M.A.H., Hussain, M., Imam, M.B., 1998. Turbidite sequence located in SE Bangladesh. Oil Gas J. 96 (51), 109–111.

Alam, M.K., Hasan, A.K.M.S., Khan, M.R., Whitney, J.W., 1990. Geological map of Bangladesh. Geological Survey of Bangladesh, Dhaka, scale 1:1,000,000.

Alam, M., 1989. Geology and depositional history of Cenozoic sediments of the Bengal Basin of Bangladesh. Palaeogeogr. Palaeoclimatol. Palaeoecol. 69, 125–139.

Alam, M., Alam, M.M., Curray, J.R., Chowdhury, M.L.R., Gani, M.R., 2003. An overview of the sedimentary geology of the Bengal Basin in relation to the regional tectonic framework and basin-fill history. Sediment. Geol. 155, 179–208.

Ali, M.H., 1998. Earthquake Database and Seismic Zoning of Bangladesh, INCEDE Report 11, Bangkok, pp. 59–73.

Balk, D., Gorokhovich, Y., Levy, M., 2005. Estimates of coastal population exposed to the 26 December 2004 tsunami. Note prepared for the Humanitarian Information Unit of the US Department of State, January 7, 2005. Also presented at "Tectonics, Politics and Ethics: The Tsunami and Its Aftermath," Columbia University School of International and Public Affairs, New York City, March 2005. 11 pp. http://www.ciesin.columbia.edu/tsunami2004.html.

Banglapedia, Asiatic Society of Bangladesh, 2006. http://banglapedia.search.com.bd/HT/E_0002.htm.

Bilham, R., 2005. A flying start, then a slow slip. Science 308, 1126–1127.

Bilham, R., England, P., 2001. Plateau pop-up in the great 1897 Assam earthquake. Nature 410, 806–809.

Bird, P., 2003. An updated digital model of plate boundaries. Geochem. Geophys. Geosyst. 4, 1027. doi:10.1029/2001GC000252.

Brammer, H., 1996. The Geography of the Soils of Bangladesh. University Press Ltd., Dhaka. 287 pp.

Byrne, D.E., Davis, D.M., Sykes, L.R., 1988. Loci and maximum size of thrust earthquakes and the mechanics of the shallow region of subduction zones. Tectonics 7, 833–857.

Chen, W.-P., Molnar, P., 1990. Source parameters of earthquakes and intraplate deformation beneath the Shillong Plateau and the northern Indoburman ranges. J. Geophys. Res. 95, 12,527–12,552.

Coates, D.A., Alam, A.K.M.K., 1990. The Mymensingh Terrace: evidence of Holocene deformation in the delta of the Brahmaputra river, central Bangladesh. Geol. Soc. Amer. Bull. 22, 310 Abstracts with Program.

Cummins, P.R., 2007. The potential for giant tsunamigenic earthquakes in the northern Bay of Bengal. Nature 449, 75–78. doi:10.1038/nature06088.

Curiale, J.A., Covington, G.H., Shamsuddin, A.H.M., Morelos, J.A., Shamsuddin, A.K.M., 2002. Origin of petroleum in Bangladesh. Am. Assoc. Petrol. Geol. Bull. 86, 625–652.

Curray, J.R., 1991. Geological history of the Bengal geosyncline. J. Assoc. Explor. Geophys. 12, 209–219.

Dahlen, F.A., 1990. Critical taper model of fold-and-thrust belts and accretionary wedges. Annu. Rev. Earth Planet. Sci. 18, 55–99.

Das Gupta, A.B., Biswas, A.K., 2000. Geology of Assam. Geological Society of India, Bangalore, 169 p.

Davies, C.E., Best, J., Collier, R., 1999. Plio-Pleistocene evolution of the Ganges Delta; studies of seismic, outcrop and core data. American Association of Petroleum Geologists Annual Meeting Expanded Abstracts, 1999, p. A30.

Davis, D., Suppe, J., Dahlen, F.A., 1983. Mechanics of fold-and-thrust belts and accretionary wedges. J. Geophys. Res. 88, 1153–1172.

Eliet, P.P., Willett, E.A.F., Mingard, H.F., McLeod, A., 1999. Forestepping progradational to aggradational sequence stacking geometries, offshore Bangladesh; implications for reservoir development. Amer. Assoc. Petrol. Geol. Annual Meeting Expanded Abstracts, p. A38.

Fitch, T.J., 1972. Plate convergence, transcurrent faults, and internal deformation adjacent to Southeast Asia and the Western Pacific. J. Geophys. Res. 77, 4432–4460.

Gagnon, K., Chadwell, C.D., Norabuena, E., 2005. Measuring the onset of locking in the Peru–Chile trench with GPS and acoustic measurements. Nature 434, 205–208.

Gahalaut, V.K., Gahalaut, K., 2007. Burma plate motion. J. Geophys. Res. 112, B10402. doi:10.1029/2007JB004928.

Gait, E.A., 1906. A History of Assam. Thacker, Spink and Co., Calcutta, p. 96.

Gani, M.R., Alam, M.M., 1999. Trench-slope controlled deep-sea clastics in the exposed lower Surma Group in south-eastern Fold Belt of the Bengal Basin, Bangladesh. Sediment. Geol. 127, 221–236.

Gani, M.R., Alam, M.M., 2003. Sedimentation and basin-fill history of the Neogene clastic succession exposed in the southeastern fold belt of the Bengal Basin, Bangladesh: a high-resolution sequence stratigraphic approach. Sediment. Geol. 155, 227–270.

Goodbred Jr., S.L., Kuehl, S.A., 2000. Enormous Ganges–Brahmaputra sediment load during strengthened early Holocene monsoon. Geology 28, 1083–1086.

Gordon, D.S., Flemings, P.B., 1998. Generation of overpressure and compaction-driven fluid flow in a Plio-Pleistocene growth-faulted basin, Eugene Island 330, offshore Louisiana. Basin Res. 10, 177–196.

Graham, S.A., Dickinson, W.R., Ingersoll, R.V., 1975. Himalayan–Bengal model for flysch dispersal in the Appalachian–Ouachita system. Geol. Soc. Amer. Bull. 86, 273–286.

Guzman-Speciale, M., Ni, J.F., 1996. Seismicity and active tectonics of the Western Sunda Arc. In: Yin, A., Harrison, T.M. (Eds.), Tectonic Evolution of Asia. Cambridge University Press, pp. 63–84.

Guzman-Speciale, M., Ni, J.F., 2000. Comment on "Subduction in the Indo–Burma region: is it still active?" by Satyabala, S.P.,. Geophys. Res. Lett. 27, 1065–1066.

Hamilton, W., 1979. Tectonics of the Indonesian region. US Geol. Surv. Prof. Pap. 1078. 345 pp.

Hiller, K., Elahi, M., 1988. Structural growth and hydrocarbon entrapment in the Surma basin, Bangladesh. In: Wagner, H.C., Wagner, L.C., Wang, F.F.H., Wong, F.L. (Eds.), Petroleum Resources of China and Related Subjects. Circum-Pacific Council for Energy and Mineral Resources Earth Sci. Series, vol. 10, pp. 657–669.

Hunter, W.W., 1875. A Statistical Account of Bengal, Volume 6 (H.M Kisch, Chittagong Hill Tracts, Chittagong, Noákhálí, Tipperah, Hill Tipperah). Trübner, London. D.K. Pub. House, Delhi, 550 p. 1973–6.

Hyndman, R.D., Wang, K., 1993. Thermal constraints on the zone of major thrust earthquake failure: The Cascadia subduction zone. J. Geophys. Res. 98, 2039–2060.

Imam, M.B., Hussain, M., 2002. A review of hydrocarbon habitats in Bangladesh. J. Petrol. Geol. 25, 31–52.

Iyengar, R.N., Sharma, S.D., 1998. Earthquake History of India in Medieval Times. Central Building Research Institute, Roorkee, 124 p. July 1998.

Johnson, S.Y., Alam, A.M.N., 1991. Sedimentation and tectonics of the Sylet trough, Bangladesh. Geol. Soc. Amer. Bull. 103, 1513–1527.

Kopp, H., Kukowski, N., 2003. Backstop geometry and accretionary mechanics. Tectonics 22, 1072. doi:10.1029/2002TC001420.

Le Dain, A.Y., Tapponnier, P., Molnar, P., 1984. Active faulting and tectonics of Burma and surrounding regions. J. Geophys. Res. 89, 453–472.

Lee, T.-Y., Lawver, L.A., 1995. Cenozoic plate reconstruction of Southeast Asia. Tectonophysics 251, 85–138.

Lindsay, J.F., Holliday, D.W., Hulbert, A.G., 1991. Sequence stratigraphy and the evolution of the Ganges–Brahmaputra delta complex. Am. Assoc. Pet. Geol. Bull. 75, 1233–1254.

Mandal, B.C., Woobaidullah, A.S.M., 2006. Sedimentary tectonics of the eastern fold belt of the Bengal Basin, Bangladesh. J. Geol. Soc. India 68, 115–128.

Martin, S.S., 2005. Intensity Assessment of the 2004 M9.0 Sumatra–Anadaman earthquake. Seismol. Res. Lett. 76, 321–330.

Métivier, F., Gaudemer, Y., Tapponnier, P., Klein, M., 1999. Mass accumulation rates in Asia, during the Cenozoic. Geophys. J. Int. 137, 280–318.

Milliman, J.D., Syvitski, J.P.M., 1992. Geomorphic/tectonic control of sediment discharge to the ocean: the importance of small mountainous rivers. J. Geol. 100, 525–544.

Mitra, S., Priestley, K., Bhattacharyya, A.Kr., Gaur, V.K., 2005. Crustal structure and earthquake focal depths beneath northeastern India and southern Tibet. Geophys. J. Int. 160, 227–248.

Moore, J.C., Saffer, D., 2001. Updip limit of the seismogenic zone beneath the accretionary prism of southwest Japan: an effect of diagenetic to low-grade metamorphic processes and increasing effective stress. Geology 29, 183–186.

Morgan, J.P., McIntire, W.G., 1959. Quaternary geology of the Bengal Basin, East Pakistan and India. Geol. Soc. Amer. Bull. 70, 319–342.

Mourgues, R., Cobbold, P.R., 2006. Thrust wedges and fluid overpressures: sandbox models involving pore fluids. J. Geophys. Res. 111, B05404. doi:10.1029/2004JB003441.

Murphy, R.W., 1988. Bangladesh enters the oil era. Oil Gas J. 86 (9), 76–82.

Ni, J.F., Guzman-Speziale, M., Bevis, M., Holt, W.E., Wallas, T.C., Seager, W.R., 1989. Accretionary tectonics of Burma and the three-dimensional geometry of the Burma subduction zone. Geology 17, 68–71.

Nielsen, C., Chamot-Rooke, N., Rangin, C., ANDAMAN Cruise Team, 2004. From partial to full strain partitioning along the Indo-Burmese hyper-oblique subduction. Mar. Geol. 209, 303–327.

Oldham, R.D., 1899. Report of the great earthquake of 12th June, 1897. Mem. Geological Society of India 1–379.

Oleskevich, D.A., Hyndman, R.D., Wang, K., 1999. The updip and downdip limits to great subduction earthquakes: thermal and structural models of Cascadia, South Alaska, SW Japan, and Chile. J. Geophys. Res. 104, 14965–14991.

Pacheco, J., Sykes, L.R., 1992. Seismic moment catalog of large shallow earthquakes, 1900 to 1989. Bull. Seismol. Soc. Am. 82, 1306–1349.

Pacheco, J.F., Sykes, L.R., Scholz, C.H., 1993. Nature of seismic coupling along simple plate boundaries of the subduction type. J. Geophys. Res. 98, 14133–14159.

Partington, M.A., Kabir, J., Eliet, P., Willett, E.A.F., Fowles, J.D., 2002. A sequence stratigraphic framework for Bangladesh. AAPG Annual Meeting Expanded Abstracts, pp. 136–137.

Petersen, M.D., Cramer, C.H., Frankel, A.D., 2002. Simulations of seismic hazard for the Pacific Northwest of the United States from earthquakes associated with the Cascadia subduction zone. Pure Appl. Geophys. 159, 2147–2168.

Rajendran, C.P., Rajendran, K., Duarah, B.P., Baruah, S., Earnest, A., 2004. Interpreting the style of faulting and paleoseismicity associated with the 1897 Shillong, northeast

India, earthquake: implications for regional tectonism. Tectonics 23, TC4009. doi:10.1029/2003TC001605.
Raju, K.A.K., Ramprasad, T., Rao, P.S., Rao, B.R., Varghese, J., 2004. New insights into the tectonic evolution of the Andaman basin, northeast Indian Ocean. Earth Planet. Sci. Lett. 221, 145–162.
Raman, M.A., Blank, H.R., Jr., Kleinkopf, M.D., Kucks, R.P., 1990a. Aeromagnetic anomaly map of Bangladesh, Geol. Surv. Bangladesh, scale 1:1,000,000.
Raman, M.A., Mannan, M.A., Blank, H.R., Jr., Kleinkopf, M.D., Kucks, R.P., 1990b. Bouguer gravity map of Bangladesh, Geol. Surv. Bangladesh, scale 1:1,000,000.
Rao, N.P., Kumar, M.R., 1999. Evidences for cessation of Indian Plate Subduction in the Burmese Arc Region. Geophys. Res. Lett. 26, 3149–3152.
Reimann, K.-U., 1993. Geology of Bangladesh. Borntraeger, Berlin, 160 p.
Richter, C.F., 1958. Elementary Seismology. W.H. Freeman & Co., San Francisco, 768 p.
Ruff, L.J., 1989. Do trench sediments affect great earthquake occurrence in subduction zones? Pure Appl. Geophys. 129, 263–282.
Ruff, L.J., 1992. Asperity distributions and large earthquake occurrence in subduction zones. Tectonophysics 211, 61–83.
Saffer, D.M., Bekins, B.A., 2002. Hydrologic controls on the morphology and mechanics of accretionary wedges. Geology 30, 271–274.
Satake, K., Tanioka, Y., 1999. Sources of tsunami and tsunamigenic earthquakes in subduction zones. Pure Appl. Geophys. 154, 467–483.
Satyabala, S.P., 1998. Subduction in the Indo-Burma region: is it still active? Geophys. Res. Lett. 25, 3189–3192.
Satyabala, S.P., 2000. Reply to comment on “Subduction in the Indo-Burma region: is it still active? Geophys. Res. Lett. 27, 1067–1068.
Satyabala, S.P., 2003. Oblique plate convergence in the Indo-Burma (Myanmar) subduction region. Pure Appl. Geophys. 160, 1611–1650. doi:10.1007/s00024-003-2378-0.
Sikder, A.M., Alam, M.M., 2003. 2-D modelling of the anticlinical structures and structural development of the eastern fold belt of the Bengal basin, Bangladesh. Sediment. Geol. 155, 209–226.
Socquet, A., Vigny, C., Chamot-Rooke, N., Simons, W., Rangin, C., Ambrosius, B., 2006. India and Sunda plates motion and deformation along their boundary in Myanmar determined by GPS. J. Geophys. Res. 111, B05406. doi:10.1029/2005JB003877.
Uddin, A., Lundberg, N., 1998. Cenozoic history of the Himalayan–Bengal system: sand composition in the Bengal Basin, Bangladesh:. Geol. Soc. Amer. Bull. 110, 497–511.
Uddin, A., Lundberg, N., 1999. A paleo-Brahmaputra? Subsurface lithofacies analysis of Miocene deltaic sediments in the Himalayan–Bengal system, Bangladesh. Sediment. Geol. 123, 239–254.
Vigny, C., Socquet, A., Rangin, C., Chamot-Rooke, N., Pubellier, M., Bouin, M.N., Bertrand, G., Becker, M., 2003. Present-day crustal deformation around Sagaing Fault, Myanmar. J. Geophys. Res. 108. doi:10.1029/2002JB001999.
Wang, K., Dixon, T., 2004. “Coupling” semantics and science in earthquake sesearch. Eos Trans. AGU 85 (18), 180–181.
Worm, H.-U., Ahmed, A.M.M., Ahmed, N.U., Islam, H.O., Huq, M.M., Lietz, J., 1998. Large sedimentation rate in the Bengal Delta: magnetostratigraphic dating of Cenozoic sediments from northeastern Bangladesh. Geology 26, 487–490.
Zahid, K.M., Uddin, A., 2005. Influence of overpressure on formation velocity evaluation of Neogene strata from the eastern Bengal Basin, Bangladesh. J. Asian Earth Sci. 25, 419–429.

Annex B75

A. Mukherjee et al., "Geologic, Geomorphic and Hydrologic Framework and Evolution of the Bengal Basin, India and Bangladesh", *Journal of Asian Earth Sciences*, Vol. 34, No. 3 (2009)

Journal of Asian Earth Sciences 34 (2009) 227–244

Contents lists available at ScienceDirect

Journal of Asian Earth Sciences

journal homepage: www.elsevier.com/locate/jaes

Geologic, geomorphic and hydrologic framework and evolution of the Bengal basin, India and Bangladesh

Abhijit Mukherjee [a,*], Alan E. Fryar [b], William A. Thomas [b]

[a] Bureau of Economic Geology, Jackson School of Geosciences, University of Texas at Austin, University Station, Box X, Austin, TX 78713-8924, USA
[b] Department of Earth and Environmental Sciences, University of Kentucky, KY 40506-0053, USA

ARTICLE INFO

Article history:
Received 7 June 2007
Received in revised form 9 May 2008
Accepted 22 May 2008

Keywords:
Ganges
Brahmaputra
Meghna
Fluvio-deltaic system
Holocene
Arsenic

ABSTRACT

The Bengal basin, the largest fluvio-deltaic sedimentary system on Earth, is located in Bangladesh and three eastern states of India. Sediment accumulates in the basin from the Ganges, Brahmaputra, and Meghna (GBM) river systems and is dispersed into the Bay of Bengal, forming the largest submarine fan in the world. The basin is located in the Himalayan foreland at the junction of the Indian, Eurasian, and Burmese plates. The basin is bounded by the Indian craton on the west and the Indo-Burmese fold belts on the east. It can be broadly divided into a stable shelf and a foredeep separated by a deep seismic hinge zone. Basin sediments overlie Gondwanan basement and vary in thickness from a few kilometers on the stable shelf to more than 16 km in the foredeep. The basin was initiated at the breakup of Gondwanaland in the late Mesozoic and evolved through the formation of the proto-GBM delta to the present delta starting around 10.5 Ma. The stratigraphy of the different parts of the basin differs considerably, because of contrast in depositional history within the several sub-basins that were produced by intra-plate tectonic activities associated with ongoing Himalayan orogeny. The present-day geomorphology is dominated by the extensive Holocene GBM floodplain and delta. The vertical succession of the deltaic plain can be classified into five units on the basis of differences in grain size, which reflect differing depositional environments. The initiation of the modern GBM delta at the onset of the Pleistocene glacial maximum and its evolution to the present configuration are intricately related to Holocene fluvio-dynamic processes, eustatic sea-level changes, and tectonic movements.

The sedimentology and mineralogy of the different parts of the basin reflect differences in sediment provenance. The mineralogy is dominated by detrital quartz, some feldspar, and minor amounts of carbonates; illite and kaolinite are the main clay minerals. The basin has profuse groundwater resources, but the architecture of the aquifers is not yet well resolved. Different classification schemes have been proposed on the basis of lithology. Regional groundwater flow follows a low hydraulic gradient from north to south, but pumping for irrigation during the past several decades appears to have severely distorted regional flow. Recharge occurs primarily during the monsoon season. Groundwater chemistry is dominated by anoxic, Ca–HCO_3-type water with relatively high concentrations of Fe, Mn, and As. Carbonate dissolution, silicate weathering, FeOOH reduction, and mixing with saline water are the primary processes controlling hydrochemistry.

Contents

* Corresponding author. Tel.: +1 512 232 1527.
E-mail addresses: abhijit.mukherjee@beg.utexas.edu (A. Mukherjee), alan.fryar@uky.edu (A.E. Fryar), geowat@uky.edu (W.A. Thomas).

1367-9120/$ - see front matter © 2008 Elsevier Ltd. All rights reserved.
doi:10.1016/j.jseaes.2008.05.011

1. Introduction

Of the more than 6 billion people worldwide, more than 2% (120 million) live in an area of ~200,000 km^2 (Alam et al., 2003) covering most of Bangladesh and parts of three eastern Indian states (mostly West Bengal, and some of Assam and Tripura). This includes two of the world's largest metropolitan areas: Calcutta, India (now Kolkata; estimated population 15.7 million, rank 12th), and Dhaka, Bangladesh (estimated population 12.6 million, rank 18th) (sources: Office of Registrar General and Census Commissioner, Government of India; Bureau of Statistics, Government of Bangladesh; Th. Brinkhoff, The Principal Agglomerations of the World, www.citypopulation.de, September 2007). This area, known as the Bengal basin, is the world's largest fluvio-deltaic system (Coleman, 1981; Alam et al., 2003).

The Bengal basin is drained by the rivers Ganges, Brahmaputra (also known as the Jamuna in Bangladesh), and Meghna, along with numerous tributaries and distributaries. Hence, the region is also known as the Ganges–Brahmaputra–Meghna (GBM) delta or basin. By discharge, the Brahmaputra and Ganges are the fourth and fifth largest rivers on Earth, respectively (www.waterencyclopedia.com, September 2006). The average discharge (1949–1973) of the River Ganges near the entrance to the Bengal basin (Farakka) was 12,037 m^3/s, while the average discharge (1969–1975) of the Brahmaputra in Bangladesh (Bahadurabad) was 19,673 m^3/s (www.sage.wisc.edu, September 2006). Cumulative riverine discharge through the Bengal basin to the ocean is the fourth largest in the world (Milliman and Meade, 1983). The Bengal basin also represents the world's largest sediment dispersal system (Kuehl et al., 1989; Milliman et al., 1995; Goodbred et al., 2003), with passage of an estimated 1060 million tons of sediment per year to the Bay of Bengal through a delta front of 380 km (Allison, 1998). Thus has formed the world's biggest submarine fan, the Bengal fan (Kuehl et al., 1989; Rea, 1992), with an area of 3×10^6 km^2.

The Ganges enters the basin from the northwest after draining the Himalayas and most of north India for about 2500 km (Fig. 1). The Ganges divides downstream into two distributaries. The main stem (River Padma) flows southeast toward the confluence with the River Brahmaputra in Bangladesh. The other part flows due south through West Bengal as the River Bhagirathi–Hoogly. For simplicity, both these distributaries are termed as the original stream, i.e., Ganges. The Ganges flows along a meandering course with very few braided reaches. The river channel is avulsing eastward for last ~250 years (Brammer, 1996). The Brahmaputra enters the basin from the northeast (Fig. 1) after draining Tibet and northeast India for about 2900 km. It has a paleochannel that bifurcated along the eastern edge of the Madhupur forest. In general, the Brahmaputra is a braided stream characterized by multiple thalwegs, mid-channel bars, and vegetated river islands. The channel belt shows a rapid lateral migration of as much as 800 m/year (Allison, 1998). The Meghna drains the Sylhet basin and part of the Tripura hills before flowing into the Brahmaputra (Fig. 1).

2. Boundaries of the basin

The Bengal basin is bounded (Figs. 1 and 2) on the west and northwest by the Rajmahal Hills (Trap), which are composed of lower Jurassic to Cretaceous trap basalts of the Upper Gondwana system (Ball, 1877). The northeast is bounded by the Garo, Khasi and Jayantia hills (west to east), which stretch for about 97 km from north to south and 240 km from east to west (Morgan and McIntire, 1959). In the far northeast, Shillong or Assam plateau acts as a boundary (Fig. 2). The hills and the plateaus are composed of intensely stressed Precambrian and early Paleozoic granite, gneiss, schist and quartzite overlain by the Eocene Nummilitic limestone (Wadia, 1949). The eastern limit of the Bengal basin is marked by the Tripura hills and Indo-Burmese fold belts to the north and Chittagong hills to the south (Fig. 2), which are composed of Paleocene–Pliocene age sediments of the Siwalik system (the Himalayan foredeep basin sediment system) (West, 1949). The Tripura hills include a train of plunging anticlines (Fig. 2), which die out under overlapping recent sediments of the Sylhet basin (Morgan and McIntire, 1959). The Bangladesh–India border follows the base of the hills.

3. Geologic framework and history

The Bengal basin is a classic example of a peripheral foreland basin formed via continent–continent collision. The basin is a result of the subduction of the Indian plate below the Eurasian (Tibetan) and Burmese plates. Although the direction of subsidence below the Eurasian plate is almost north–south, subduction occurs along a northeast–southwest trend below the Burmese plate (the Burmese–Andaman arc). The Moho has been estimated to be at a depth of about 15 km near the Bay of Bengal, and it deepens to about 36 km below the northern edge of the Bengal basin. Lithospheric flexure and subsidence of the basin are occurring at a rate of 2–4 mm/year (Goodbred et al., 2003). Recent seismic studies suggest that subduction has stopped below the Himalayan arc and is only partially continuing below the Burmese–Andaman arc (Biswas and Das Gupta, 1989; Biswas, 1991; Biswas et al., 1992; Biswas and Majumdar, 1997). The Cenozoic evolution of the eastern parts of the Bengal basin is related more to northeastward oblique subduction of the Indian plate beneath the Burmese plate, along with westward migration of accretionary prism complexes (Dasgupta and Nandy, 1995; Gani and Alam, 1999; Alam et al., 2003). As a result of the resistance to subduction below the Eurasian plate and plate convergence, intense deformation and seismic activity occur in the Indian intraplate region, including on the stable shelf in the western part of the Bengal basin (Fig. 2), resulting in folding of strata and brittle deformation via high-angle basement faults (Biswas and Majumdar, 1997). Tectonic loading to the north–northeast is accommodated along the Dauki fault zone (Alam et al., 2003), which consists of a set of near-vertical, deep-seated reverse faults.

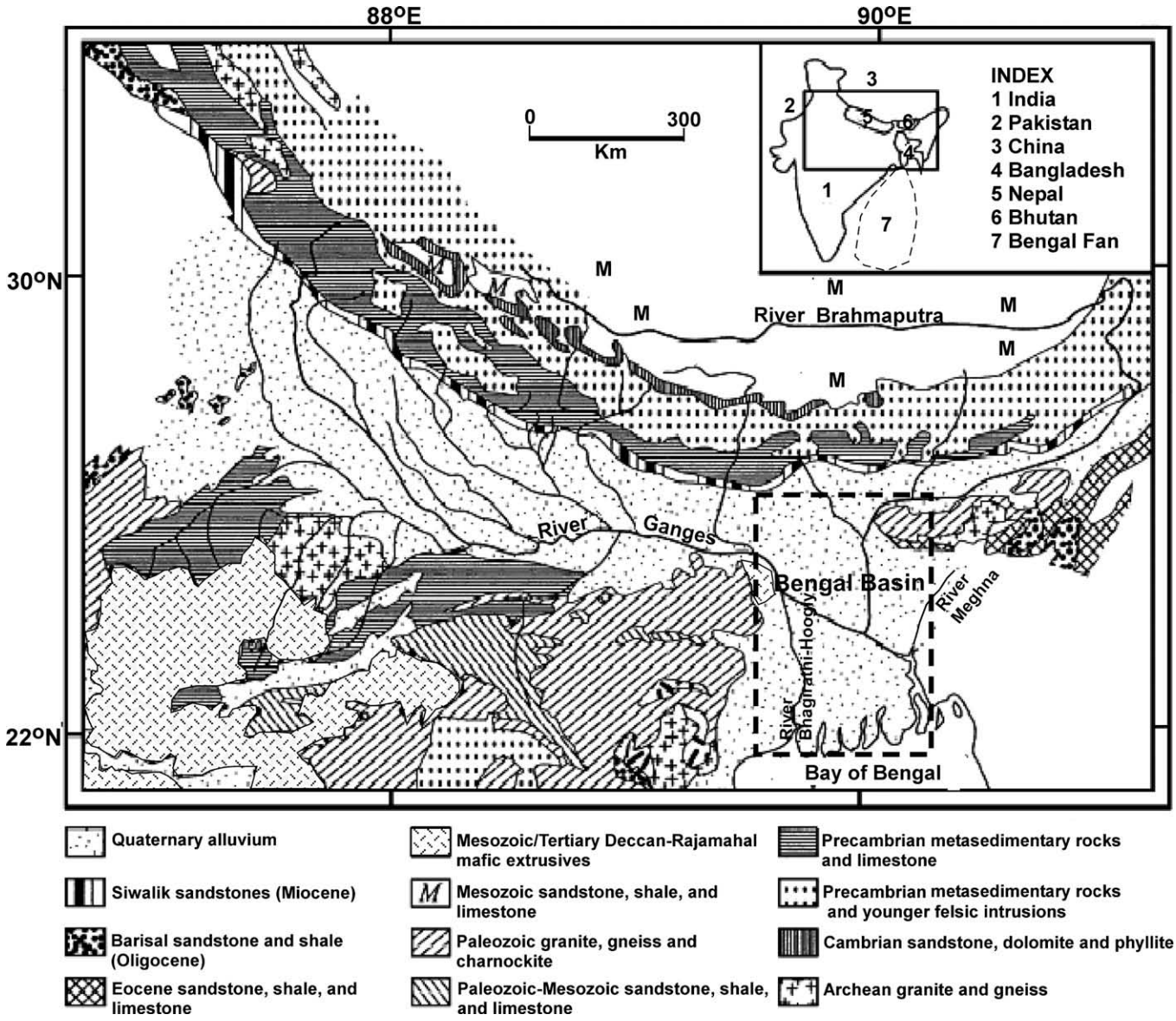

Fig. 1. Geologic map of the Indian subcontinent along with location of the Bengal basin (adapted from Heroy et al., 2003).

The Bengal basin is bounded on the west by the peninsular shield of India, which has a Precambrian basement of metasedimentary rocks with granitic, granophyric, and doleritic intrusions. These are covered by scattered, east–west trending intracratonic Gondwana deposits, such as in the Damodar basin with the Raniganj and Jharia coal basins, and some Tertiary deposits, such as the Baripada and Durgapur beds, as well as Mesozoic volcanics of the Rajmahal trap. On the east, the Naga–Lushai orogenic belt (Sengupta, 1966), also known as the Naga–Halflong–Disang thrust zone (Alam et al., 2003), bounds the basin. This belt consists of highly deformed Cretaceous-Tertiary strata and is bordered on the north and northeast by the Dauki fault zone (Evans, 1964) and on the east by the Naga thrust (Sengupta, 1966). The Shillong Plateau, which borders the basin on the north–northeast, is most probably the continuation of the Indian shield through the Garo–Rajmahal gap (Sengupta, 1966), which is a large depression with younger sedimentary fill between the Rajmahal and Garo hills. The boundary of the Indian plate below the Bengal basin is interpreted to be the Calcutta–Mymensingha hinge zone (CMHZ, discussed later) (Fig. 2), which also acts as a transitional zone between the stable shelf and Bengal foredeep (Alam, 1989). The shelf area in Bangladesh consists of three major features, the Dinajpur slope, Rangpur saddle, and Bogra slope, whereas the foredeep is formed by the Sylhet trough, Faridpur trough, and Hatia trough. About 1–8 km of Permian to Holocene clastic sediments rest on the stable shelf in the western part of the basin (Imam and Shaw, 1985), and as much as 16 km of Tertiary to Quaternary alluvial sediment fills the foredeep of the basin, which at present lies at the mouth of the Ganges and Brahmaputra rivers (Allison, 1998) (Fig. 2). The basin became a huge sink of the sediments eroded from the rising mountain range (Allison, 1998) by the mid-Miocene (Curray et al., 1982).

The ongoing orogeny along the Himalayan and Burmese front has kept the basin tectonically active, generating vertically displaced regional sedimentary blocks in the foredeep, and dividing the basin into numerous poorly connected sub-basins (e.g., Faridpur trough, Sylhet trough) (Goodbred et al., 2003). Also, sediment supply to the basin has varied over time (Fig. 2), including major provenances in the Indian shield, Himalayan foreland, and Burmese arc (Alam et al., 2003), thus causing conspicuous differences

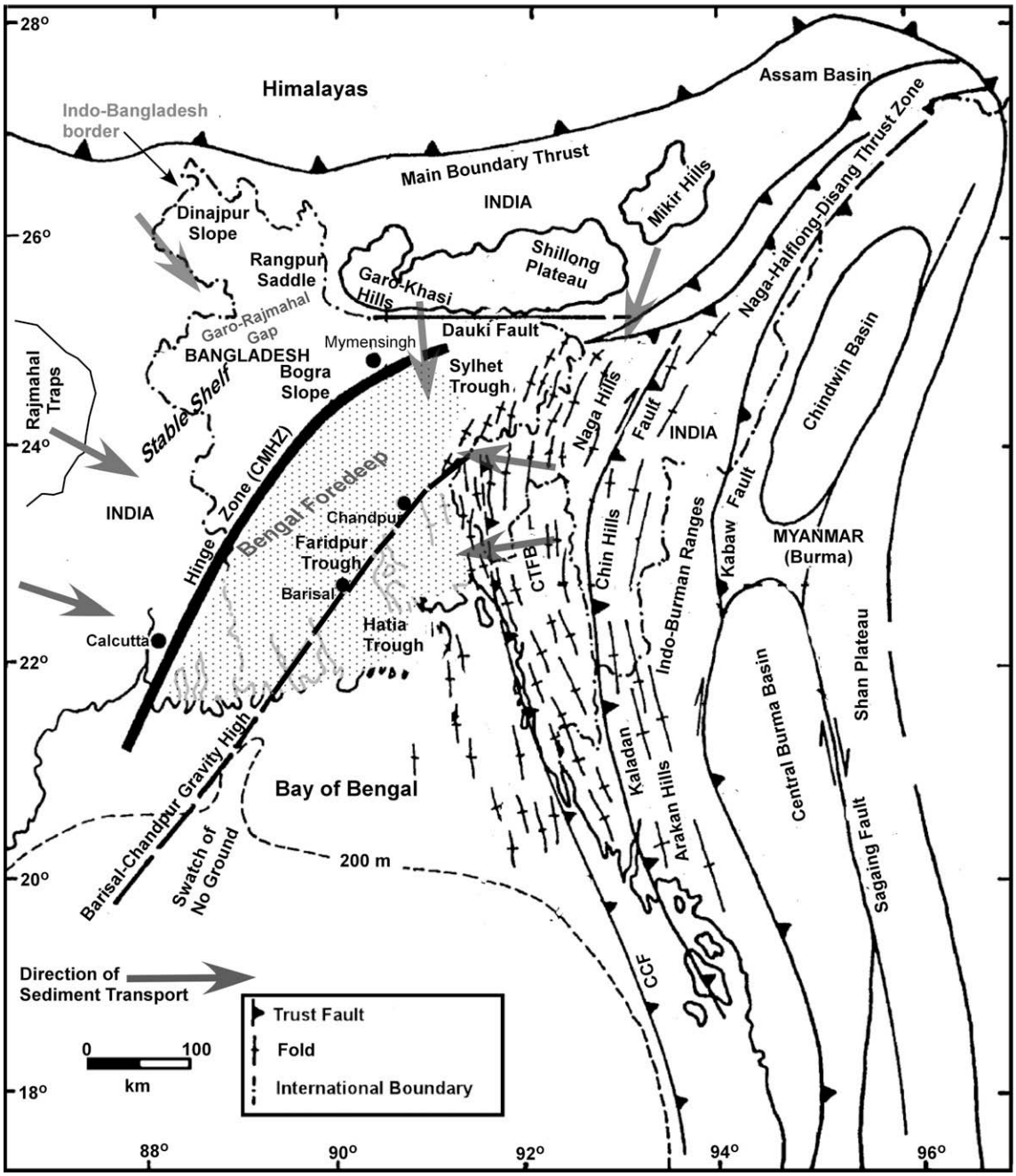

Fig. 2. Tectonic map of the Bengal basin and surrounding areas, showing the directions of sediment transport (modified from Uddin and Lundberg, 1999, and Alam et al., 2003). CCF: Chittagong-Cox Bazar fault; CTFB: Chittagong-Tripura fold belt.

in sedimentary environments, history, and lithology within the different parts of the basin (Goodbred et al., 2003). The basin has been viewed as divided into eastern (mostly foredeep) and western (mostly stable shelf) parts, which are separated by the CMHZ, as discussed earlier (Sengupta, 1966).

Stratigraphic comparison of the different areas of the Bengal basin shows that from the Cretaceous through the mid-Eocene, sedimentation patterns were similar throughout the basin (Fig. 3). The succession starts with the Gondwana sediments and volcanics, followed by a thick sequence of shallow-marine clastic and carbonate sediments in both the eastern and the western sub-basins. Arenaceous sediments dominate the clastic facies in both areas. A carbonate deposit, known as the nummilitic Sylhet Limestone, is found extensively throughout the basin. As a result of the basin configuration and nature of the submergence, the succession is thinner in the western sub-basin. After the deposition of the Sylhet Limestone, the sedimentation pattern of the basin changed to become more clay rich, as marked by the Kopili Formation. After deposition of the Kopili, some significant movement of the basin-basement and basin-margin fault systems led to completely different sets of depositional environments and stratigraphic successions in the two parts of the basin. Thick marine sediments continued to be deposited in the deeper eastern sub-basins (both stable shelf and Bengal foredeep), successively resulting in deposition of the Bogra or Barail, Jamalganj or Surma, and Tipam groups. In the western sub-basin representing the stable shelf, the Bhagirathi Group [consisting of the Memari–Burdwan, Pandua–Matla, and Debagram–Ranaghat formations (Biswas, 1963)] was deposited in

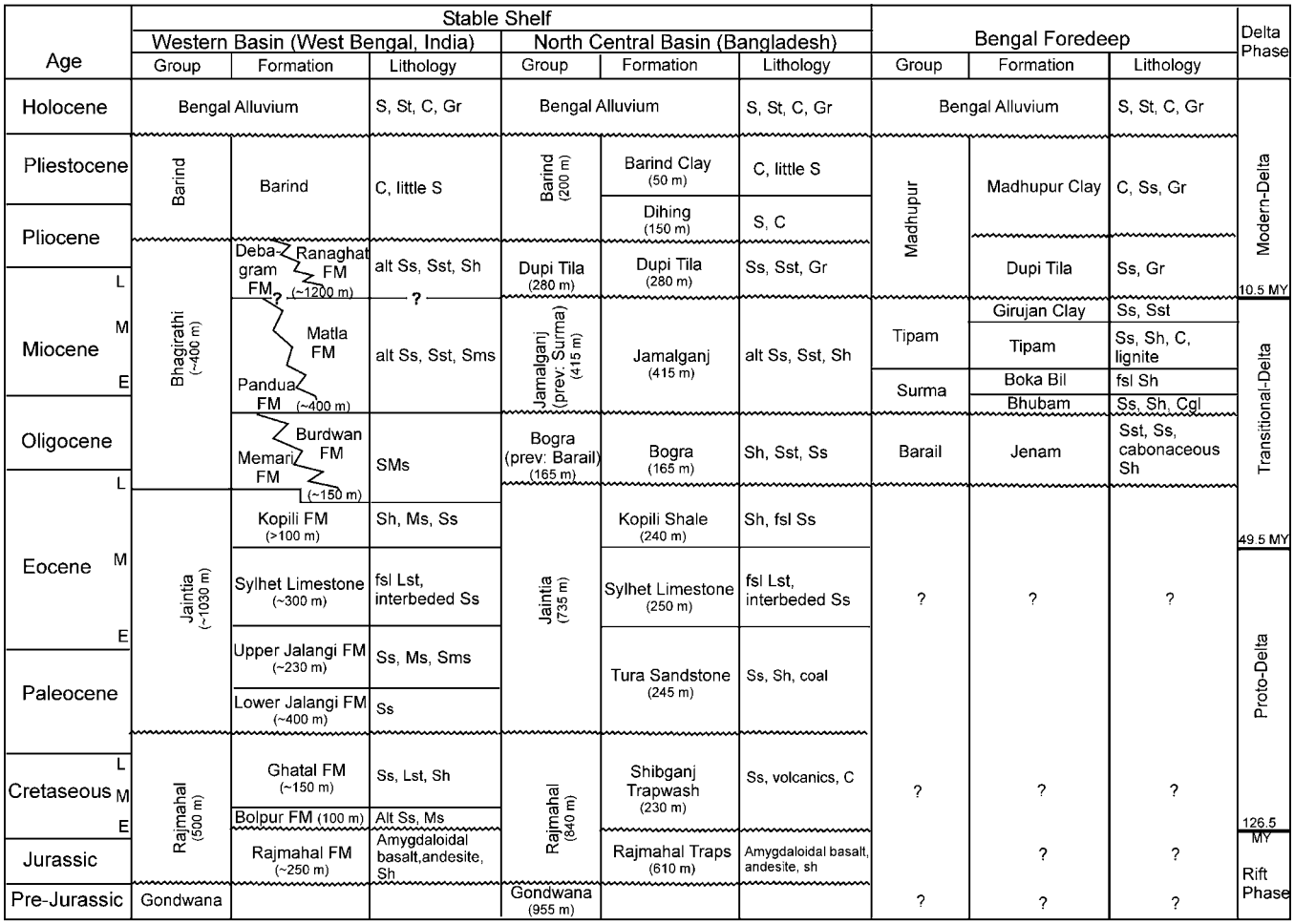

Fig. 3. Stratigraphic correlation diagram of the different parts of the Bengal basin. The stable-shelf succession has been further subdivided within Bangladesh and West Bengal (compiled from Biswas, 1963; Zaher and Rahman, 1980; Alam, 1989, 1997; Alam et al., 1990, 2003; Khan, 1991; Lindsay et al., 1991; Reimann, 1993; BOGMC, 1986).

a more near-shore environment. From the middle of the Pliocene, a similar style of sedimentation resumed throughout the basin, thereby depositing the Barind/Madhupur clay followed by the voluminous and extensive Bengal alluvium over all the previous lithotypes.

Sequence-stratigraphic and seismic studies have established that there is a narrow zone of flexure (the CHMZ) above the Sylhet Limestone in the southeastern part of the western basin. Because of bed instability and adjustment of movement, the post-Sylhet deposits have a broad synformal shape (Sengupta, 1966). The CMHZ acts as a seismic reflector and has been interpreted as a hinge zone or a zone of faults, which may be a shallow manifestation of a much more intense fault zone in the basement (Sengupta, 1966). The CMHZ passes from east of Calcutta (Fig. 2), where it is at a depth of about 4700 m, to the town of Mymensinhga in northern Bangladesh along a trend of N 30°E (Sengupta, 1966). Across this hinge zone, which can be visualized as an imaginary straight line drawn between Calcutta and Ranaghat, the depositional environment sharply changed from stable shelf to deeper-basin conditions (Sengupta, 1966) (Figs. 2–4). The area lying east of this zone has accumulated a great thickness (>8000 m) of argillaceous facies (Sengupta, 1966). The zone can be traced to where it is truncated by the Dauki fault zone in the Naga Hills of Assam (Sengupta, 1966). The location of the CMHZ is confirmed by an alignment of low-magnitude magnetic highs northwest of Calcutta and a steep gravity gradient in the west. Calcutta is flanked by broad gravity highs to the east, indicating the presence of a gravity divide in-between (Sengupta, 1966).

3.1. Basin evolution

The formation of the Bengal basin started with the break-up of Gondwanaland in the late Mesozoic, at about 126 Ma (Lindsay et al., 1991). Extrusion of basalt both in the Rajmahal areas and the south Shillong plateau (Banerjee, 1981) in the late Jurassic to early Cretaceous initiated the process of basin development. This was followed by the slow subsidence of the Bengal shelf in the late Cretaceous, leading to restricted marine transgression from the southeast in the proto-basin. The western part of the basin (mostly in West Bengal) records deposition of lagoonal argillaceous and arenaceous sediments, whereas the Assam front in the eastern and northeastern part was occupied by an open neritic sea (Sengupta, 1966). The proto-GBM delta started forming when sediments were deposited during repeated submergence and transgression over a planar erosional surface, which now is at about 2200 m depth in the central part of the basin, and dips toward the southeast (Lindsay et al., 1991).

During the middle Eocene, basin-wide subsidence initiated by movement along basin-margin faults caused an extensive marine transgression, which resulted in the deposition of the Sylhet

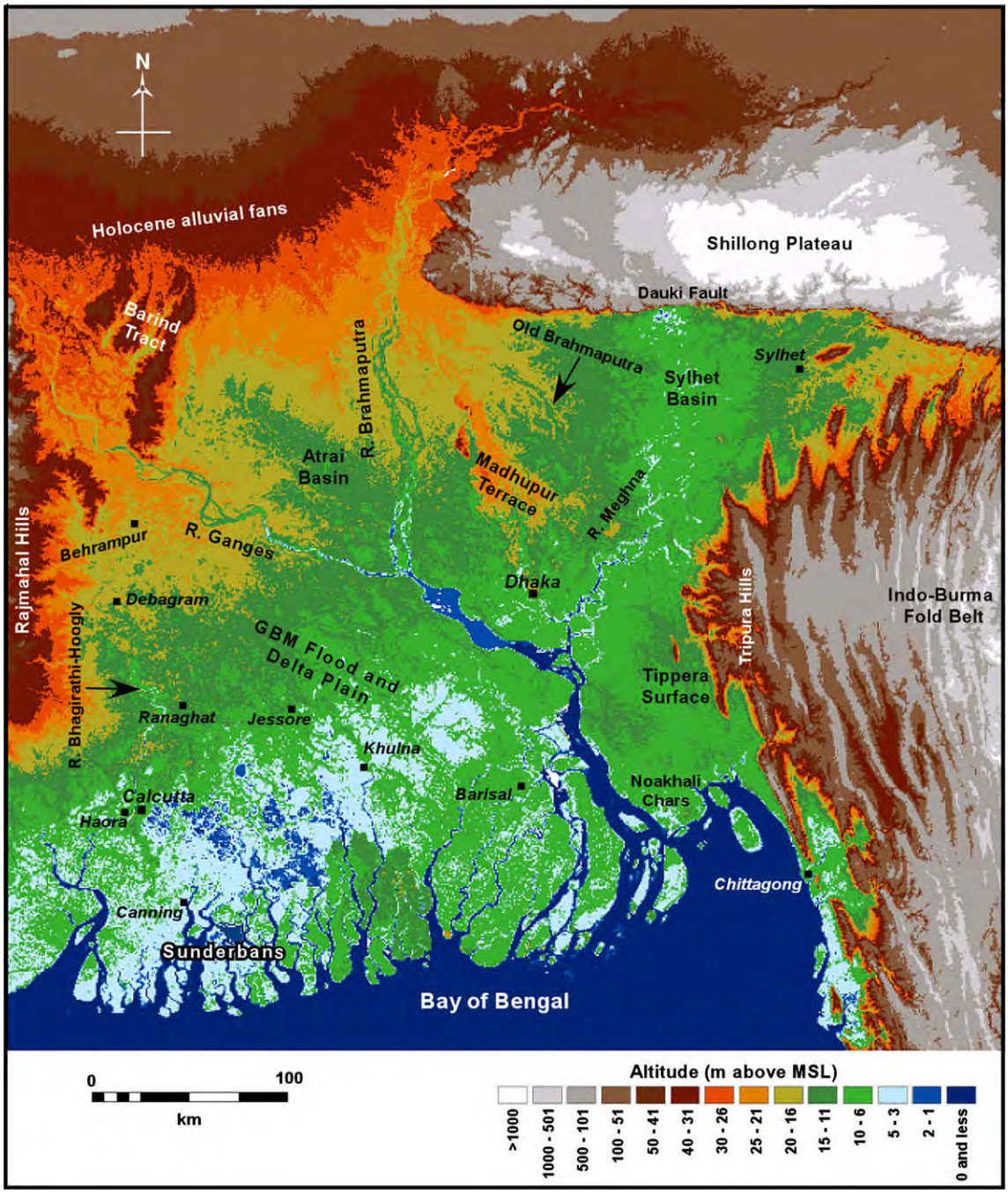

Fig. 4. Geomorphic map of the Bengal basin and surroundings superimposed on the SRTM-90 m digital elevation model (DEM) showing some of the important cities (italicized) and the important physiographic units of the basin: Pleistocene uplands (the Barind and Madhupur terrace) and Recent sediments (Holocene alluvial fans, Tippera surface, Sylhet basin, and GBM flood and delta plain).

Limestone. Basement fault movement probably imprinted the CMHZ on this limestone (Sengupta, 1966). This led to the beginning of separate evolutionary histories for the eastern and the western parts of the basin. Subsequently, the sea began receding from the Bengal basin. At about 49.5 Ma, a major shift in the sedimentation pattern began. The carbonate-clastic platform sedimentary sequence was replaced by a predominantly clastic deposit (Lindsay et al., 1991). The process became conspicuous at about 40 Ma, when the basin became dominated by fluvial clastic sediments and the transitional delta prograded rapidly with frequent lobe switching. The abrupt change in deltaic sedimentation and morphology was probably a manifestation of the collision of the Indian plate with the Eurasian plate and rising of the Himalayas. Comparison of stratigraphic records from the eastern and western parts of the basin shows a subsequent divergence in the sedimentary depositional history as a result of differential subsidence rate, tectonic movements, and eustatic sea-level changes. From the late Eocene–early Oligocene onward, the eastern part of the basin continued to experience marine conditions as marked by a thick arenaceous/argillaceous sequence, while the western part was under fresh water to estuarine conditions, leading to a thinner succession of dominantly argillaceous sediment (Sengupta, 1966). At about 10.5 Ma (Lindsay et al., 1991), in the middle to late Miocene, intense tectonic activity started along the Dauki fault zone and Naga thrust. The activity

became more intense in the Pliocene (Sengupta, 1966). The result was basin-wide regression with a major eustatic low. Thus all parts of the basin, including the eastern part, saw a shift from a marine-estuarine environment to a predominantly fluvial–tidal environment, which continues to the present. Deposition of the modern deltaic basin was thus initiated (Lindsay et al., 1991).

4. Physiography and Quaternary geomorphology

Physiographically, the Bengal basin can be divided into two major units, the Pleistocene uplands and deltaic lowlands (Morgan and McIntire, 1959). The divisions may be described as follows (Fig. 4).

4.1. Pleistocene uplands

The whole basin contains several Pleistocene units. There are four major terraces along with several small outliers (Morgan and McIntire, 1959). Two of these terraces flank the basin: east of the Cretaceous Rajmahal hills, and west of the early Tertiary Tripura Hills. The other two, Barind and Madhupur Jungle, lie within the basin.

These Pleistocene uplands are interpreted to be paleo-floodplains of the earlier GBM system. In terms of sediment characteristics and mineralogy, these deposits are very similar to their Holocene counterpart (Morgan and McIntire, 1959). For example, they have moderately well-sorted sand-size sediments. However, despite the similarities, there are some conspicuous differences. In contrast to the dark, loosely compacted, moist and organic-rich Holocene sediments, the Pleistocene sediments are reddish, brown or tan, mottled, ferruginous or calcareous-nodule rich, relatively dry and organic-poor (Morgan and McIntire, 1959). Moreover, there is a conspicuous difference in the geomorphic features formed by the Pleistocene and the Holocene sediments. The Pleistocene sediments form highlands, which are the manifestation of differential structural displacement between them and the Holocene deposits and also seaward subsidence and of lower areas' entrenchment during low-stand Pleistocene glaciation. Also, the upland is characterized by only a few prominent drainage systems, which flow through deeply scoured, well-defined meanders.

The Barind is the largest Pleistocene unit within the Bengal basin, with an areal extent of about 9400 km^2. It has been dissected into four separate units by recent fluvial systems, which include the north Bengal tributaries of the Ganges and Brahmaputra, namely the Mahananda, Karatoya, Atrai, Jamuna, and Purnabhaba. The area is actively affected by orogenic movements, which are indicated by earthquakes, tilting of the eastern part, river course switching, and visible major fault scarps.

The 4100 km^2 of the Madhupur terrace north of the city of Dhaka is the other important Pleistocene landform of the Bengal basin. The elevation of the upland rises from 6 m above mean sea-level (MSL) in the south to more than 30 m above MSL in the north. The western side has a higher average elevation, whereas the whole upland slopes toward the east, ultimately to be concealed under the thick Holocene alluvium. The western margin marks an abrupt separation between the low-lying, flat, Holocene flood plain in the west and the highly dissected older upland. The boundary is marked by six en-echelon faults ranging from 10 to 21 km in length and with the eastern side up-thrown by at least 6–18 m. It is thought by some workers that at least part of the uplift of the Madhupur terrace occurred during the 1762 catastrophic earthquake (Fergusson, 1863). The diversion of the Brahmaputra from its old course can be possibly attributed to the sudden uplift of the Madhupur terrace and gradual tilting toward the east, which also may have caused the sudden diversion of the Tista from being a tributary of the Ganges to that of the Brahmaputra in 1787. Moreover, the lowland between the en-echelon fault system of the Madhupur and the Karatoya River fault system (not shown in Fig. 4) of the northeast Barind indicates ongoing subsidence/uplift.

4.2. Holocene sediments

The other main physiographic division of the Bengal basin is the Holocene alluvial plain and delta of the GBM system (Morgan and McIntire, 1959), also known as the Holocene alluvial lowland of Bengal (Umitsu, 1987, 1993). These alluvial deposits are the most extensive part of the Bengal basin and cover almost the whole of the basin except the Pleistocene highlands.

Different workers have tried to classify this huge sedimentary basin in various ways. The classification described here is a combination of the two proposed by Morgan and McIntire (1959) and Umitsu (1987). According to this joint scheme, there are four physiographic subdivisions:

(a) *The alluvial fans:* These piedmont alluvial plains are in the foothills of the eastern Himalayas and are formed by deposition from the north Bengal tributaries of the Ganges and Brahmaputra such as the Tista, Atrai, Mahananda, and Purbabhaga (not shown in Fig. 4). These rivers also have dissected the Pleistocene upland of the Barind, as mentioned earlier. Coarse-grained sediments like cobbles and sand dominate these fans.

(b) *Tippera surface:* This 7800-km^2 area in the easternmost part of the basin, near the Tripura hills in the Tippera district, has been classified as a different subdivision on the basis of a characteristic drainage system (Morgan and McIntire, 1959). It is sometimes considered as a part of the GBM flood–delta plain (described later) (Umitsu, 1987). The rivers in this unit show a very well-defined rectangular pattern in contrast to the general braided or meandering pattern of the alluvial plains. The extent to which this distinct pattern has resulted from anthropogenic influence is debatable. The surface is delineated on the north by a northeast–southwest trending fault. The sedimentological characteristics of the deposit are very similar to those of other recent alluvial deposits except slightly more compacted and oxidized, but not as much as the strata in the Pleistocene uplands.

(c) *Sylhet basin:* This small basin is located in the extreme northeastern part of the main basin, surrounded by the Shillong plateau, Tripura hills, and the Madhupur terrace Pleistocene uplands. The south boundary is a major fault scarp. The basin has an average altitude of about 4.5 m above MSL at its center. It was earlier considered as a part of the Ganges–Brahmaputra delta. The Old Brahmaputra River (the original channel of the Brahmaputra) passes through the westernmost part. The present Brahmaputra course has an elevation of about 15 m above MSL, which shows that the Sylhet basin has subsided about 10.5–12 m during the last couple of hundred years. The cause is certainly tectonic, associated with movements of the fault systems. Holocene fossil wood fragments have been found at depths of 15–18 m below surface. The surface is inundated every year during monsoon season. The basin can be classified geomorphologically as having natural, continuously meandering levees with dendritic drainage (Umitsu, 1985). The sediment composition of the basin grades from sandy or silty near the surface to fine sand at a depth of about 12 m.

(d) *Ganges–Brahmaputra–Meghna flood and delta plain:* This is the principal unit of the Bengal basin. This unit is so vast that many studies, including this paper, refer to the Bengal basin

as virtually synonymous with the plain. It covers more than 10^5 km^2 of both Bangladesh and West Bengal, India, excluding the units that have already been mentioned.

The plain is bounded by the Pleistocene terraces on the west, the Barind and Madhupur terrace on the north, the Tippera surface on the east (Morgan and McIntire, 1959), and the Bay of Bengal in the south. Like many of the large alluvial systems of the world, the GBM plain is formed by overlapping of a number of sub-deltas (Morgan and McIntire, 1959) and alluvial flood plains. Moreover, avulsion of the major streams in the area within a time scale of 100 years has resulted in a Holocene sediment succession of about 100 m of overbank silts and clays incised by channel sands (Coleman, 1969; Umitsu, 1987; Goodbred and Kuehl, 2000; Allison et al., 2003). Evidence of subsidence of the Holocene sediments to accommodate depositional space has been reported (East, 1818; Smith, 1841; Hunter, 1875; Curtis, 1933; Morgan and McIntire, 1959) from various places, including Calcutta (as much as 12 m), Canning (~3 m), Khulna (~6 m) and the Sunderbans, which is the world's largest mangrove forest (as much as 9 m). The active delta area in the southernmost part of the plain, which supports the Sunderbans, can be demarcated from the flood plain by the farthest inland extent of water from the Bay of Bengal during the dry season of October to April (Allison et al., 2003).

The altitude of the GBM alluvial plain is about 15 to 20 m above MSL in the northwest, and decreases to 1 to 2 m above MSL to the south near the coast. According to physiographic characteristics, the plain can be divided into five distinct regions (Umitsu, 1987). These include (a) the area in and around the city of Calcutta; (b) the area of broad and indistinct natural levees (Umitsu, 1985) in the northwest part, also known as the moribund delta (Bagchi, 1944); (c) the central part of the plain, which includes areas with natural levees with dendritic distributary channels near the city of Khulna (Umitsu, 1985), along with meandering and distinct natural levees; (d) the Sunderbans; and (e) the mouth of the river Meghna (Umitsu, 1987).

The oldest surface sediments in the GBM flood plain are identified near Calcutta and near Commila in northeastern Bangladesh, very near the Tippera surface, whereas the youngest sediments are all located in the active floodplain and the delta. The sediments in all places are of Holocene age. The Ganges alluvial deposits are divided into an upper silty or clayey part and a lower sandy part to a depth of about 50 m. In the northwestern part of the plain, near the Tippera surface, the sediments in the upper horizons are slightly oxidized and light gray in color. In the central and southern parts of the plain, organic and peaty materials are locally visible in near-surface horizons. In the southernmost part, in and near the active delta region, silt and sand alternate within an upward fining sequence (Umitsu, 1987). The Brahmaputra-dominated alluvial plain extends between the Barind and the Madhupur terrace. This plain has a distinct basal gravel horizon overlain by a sequence of sandy sediments.

Umitsu (1987, 1993) classified the vertical sequence of the Holocene formations of the GBM plain into five units (lowest, lower, middle, upper, and uppermost). Each of these units is separated from the succeeding units by a difference in grain size, which is certainly a manifestation of differing depositional environments. The individual units can be differentiated as follows, after Umitsu (1987). The lowest unit, which has a thickness of about 10 m, is composed predominantly of gravel. In the northern part of the plain, the bed is at a depth of more than 70 m below the surface, indicating that sea-level at the time of deposition must have been about 100 m below the present level. Sediments from the Brahmaputra plain basal gravel at a depth of 101 m below MSL, in the south of the Barind, yield an approximate age of 28,320 ± 1550 years BP (Umitsu, 1987). The lower unit is dominated by sand-sized sediments with sparse gravel. The unit contains two relatively coarse zones near the middle and the top, reflecting a change in sediment size deposited by the rivers. Organic remains in the lower unit of the central GBM plain near the city of Khulna (Bangladesh), at a depth of 46 m below MSL, yield an age of 12,320 ± 240 years before present (BP) (Umitsu, 1993). Peat layers from the far western GBM plain (West Bengal, India) have been dated ~7100 to 9100 years BP at depths of 20 to 50 m in the coastal area (Hait et al., 1996). Sylhet basin organic materials at depths of 36.6 to 55 m below MSL yield ages of 6320 ± 70 years BP and 9390 ± 60 years BP, respectively (Goodbred and Kuehl, 2000). An unconformity, probably caused by temporary sea-level fall, separates the lower and the middle units; this is indicated by weathered and oxidized horizons at the top of the lower unit. The lower unit in some locations, mostly in the central plain, has sediments with some peat and organic material, indicating a swampy environment of deposition. The middle unit shows a coarsening upward sequence. Shell fragments and wood remains from the middle unit, at depths of 25–33 m below MSL, range from 7640 ± 100 to 8910 ± 150 years BP (Umitsu, 1993). At the active delta area near the main mouth of the GBM, radiocarbon dating of sediments from a depth of 25 to 30 m below surface records an age of 8400 years BP (Goodbred and Kuehl, 2000). Muddy sand about 50 m west of the aforementioned location and at a depth of 35 m below surface yields an age in the range of 7500–8000 years BP (Goodbred and Kuehl, 2000). The upper unit has a coarse-grained middle part, sandwiched between fine-grained upper and lower parts. This oscillation of sedimentation pattern is interpreted to have been caused by eustatic sea-level changes. Peat layer ages from the upper unit are 7060 ± 120 years BP at 18 m below MSL and 6490 ± 130 year BP at 14 m below MSL (Umitsu, 1993). Clay- and silt-sized sediments are characteristic of most of uppermost horizon, with some peaty sediments. The peaty materials in all these units are interpreted to have been deposited in mangrove swamps, which developed in the prograding delta over time (Vishnu-Mittre and Gupta, 1979; Umitsu, 1987; Islam and Tooley, 1999). Mangrove remains from Calcutta have been dated at ~7000 years BP (Sen and Banerjee, 1990). Peat fragments recovered in the older delta of the western basin yielded ages of 6500 to 7500 years BP at depths of 6 to 12 m and 2000 to 5000 years BP at depths <5 m (Banerjee and Sen, 1987). The sediments from a location near Calcutta have been dated as 5810 ± 120 years BP at 6.25 m below land surface to 2615 ± 100 years BP at 1.37 m below land surface (Vishnu-Mittre and Gupta, 1979). More dates from the basin are tabulated in Table 1.

5. Holocene landform evolution

As noted earlier, the main surficial lithostratigraphic and geomorphic units of the Bengal basin are mostly of Holocene age (Fig. 5). Hence understanding the Holocene fluvio-dynamic processes along with the effects of eustatic sea-level changes and tectonic impacts in this basin is critical for the study of present-day basin evolution. In the northeastern part of the basin, where tectonic processes are most active, fine-grained sediments dominate the stratigraphy. In the western part of the basin, near the stable shelf, the strong fluvio-dynamic processes have resulted in formation of extensive flood plains with a dominance of coarser grained sediments. The coastal region in the south has a mixture of fine-grained sand and mud deposits with peat layers, which have resulted from eustatic influence (Goodbred et al., 2003).

Deposition of the lowest unit of the modern GBM delta began at the onset of the Pleistocene glacial maximum in this part of the world (Fig. 6) (Islam and Tooley, 1999). This is documented by the fact that the lowest unit was deposited at a depth that is

Table 1
Reports of absolute age of sediments and peat layers from various locations of Bengal basin (after Uddin and Abdullah, 2003)

Location	Sample type	Depth (m bgl)	Age (years BP)	Source
Sirajganj	Wood fragments	NA	28,300	JICA (1976)
Between Madhupur and Barind	Upper coarse sand and micaceous silt	26	6400	Davies and Exley (1992)
		32	6290	
		62	>48,500	
Eastern Dhaka	Peat (from Bashabo formation)	NA	4040 ± 70–1270 ± 140	Monsur and Paepe (1994)
Fardipur	Micaceous silt	6.2	106.6 ± 0.58	BGS/DPHE (2001)
	Fine sand	9.8	960 ± 45	
	Fine sand	10.2	855 ± 45	
	Clay with peat	44.5	8260 ± 75	
	Medium sand	55.2	11,890 ± 80	
	Coarse sand	73.2	18,560 ± 130	
	Gravel	91.4	22,690 ± 190	
Laxmipur	Micaceous silt with peat	10.7	110 ± 0.58	BGS/DPHE (2001)
	Fine and medium sand	35	6920 ± 50	
	Sand	38.7	10,020 ± 85	
	Sand	46.3	9155 ± 70	
	Sand	73.2	8855 ± 70	
	Sand	91.7	11,320 ± 75	
	Sand with silt	137.5	12,585 ± 95	
Kharampur (Chandina deltaic plain)	Peat (top of bed) Peat (bottom of bed)	1–2	5580 ± 75	Uddin and Abdullah (2003)
			5620 ± 75	
Kachpur (Dhaka)	Peat	4	6390 ± 80	Uddin and Abdullah (2003)

now about 70 m below the present land surface, indicating that the glacial maximum sea-level and the base level of land erosion must have been at least 100 m below present MSL. Thus the rivers draining the plain during that time must have scoured through the earlier plains (Fig. 6A) and deposited the basal gravel at a depth analogous to the sea-level at that time (Umitsu, 1993). At that time, the "Swatch of no ground" submarine canyon (Fig. 2) now in the center of the Bay of Bengal most probably was the estuary of the GBM plain (Chowdhury et al., 1985). If this hypothesis is true, then most of the northern part of the Bay of Bengal was dry land during the Pleistocene glaciation (Islam and Tooley, 1999). The sediment supply at this time was low compared to the present (Milliman et al., 1995), and sediment inflow was low until the late Pleistocene, about 15,000 years BP (Weber et al., 1997).

Around 12,000–11,500 years BP, at the beginning of the Holocene, the southwest monsoon, which determines the climate-controlled processes in southeast Asia, became stronger than at present (Gasse et al., 1991), which led to a simultaneous increase in discharge and fluvial sedimentation. The sediment discharge has been estimated to be on the order of 2.5×10^9 t/year (Goodbred and Kuehl, 2000). The lower unit of the GBM plain was probably deposited at this time as an extensive flood plain in the central region (Umitsu, 1993). The coarsening upward of the lower unit may be correlated with increased discharge and aggravated erosion along the upper reaches of the main rivers.

The sedimentary record of 11,000–10,000 years BP contains both dissected flood plains (Umitsu, 1993) caused by fluvial erosion and also drastic fining of sediments and deposition of lower delta mud over lowstand oxidized sand units (Fig. 6B), which suggests sea-level rise (Goodbred and Kuehl, 2000). It has been hypothesized that the eustatic sea-level rose to about 45 m below present MSL (Fairbanks, 1989; Blanchon and Shaw, 1995), which caused extensive back-flooding and sedimentation (Goodbred and Kuehl, 2000) along with a temporary sea-level fall forming shallow valley plains (Umitsu, 1993). Various workers agree that the present GBM delta began to prograde into the Bay of Bengal at this time (Lindsay et al., 1991; Goodbred and Kuehl, 2000). The sharp decrease of sediment input to the submarine fan at this time (Weber et al., 1997) could be a manifestation of enhanced sediment trapping in the delta-plain system. The fine sediment thus deposited would constitute the middle unit of the GBM plain (Umitsu, 1993). Hence, most probably there was a short-lived but effective sea-level fall followed by a sea-level rise, which cumulatively initiated the modern delta-forming processes.

From about 10,000 to about 7000 years BP, in the mid-Holocene, a major and rapid transgression (Umitsu, 1993; Islam and Tooley, 1999; Goodbred and Kuehl, 2000) occurred probably as a result of glacial ice melting. Sea-level rise resulted in the deposition of fine sediments (the upper unit of the GBM plain) even in the north-central part of the basin (Fig. 6C). The coastline at that time transgressed up to the central delta north of Khulna (Umitsu, 1993). This continued transgression might also have included some short-lived regressions, which are indicated by increased fluvial activity (Islam and Tooley, 1999). During the latter part of this general transgression, the coastline probably receded slightly toward the south, causing the coarsening of the upper horizons of the upper unit. At this time, mangrove vegetation (Vishnu-Mittre and Gupta, 1979) spread over the central GBM plain and caused extensive deposition of peat.

After about 7000 years BP, the gradient of the sea-level rise curve decreased (Umitsu, 1993; Islam and Tooley, 1999; Goodbred and Kuehl, 2000). Nonetheless, the general trend of the eustatic sea-level curve shows continuous sea-level rise from the mid-Holocene onward (Fig. 7). The decreased rate of sea-level rise since 7000 years BP led to the deposition of the uppermost unit of the GBM plain, which contains clay, silt, and organic-rich layers throughout the southern Bengal basin (Fig. 6D). At about 5000 years BP (Fig. 6E), the main channels of both Ganges and Brahmaputra started draining the eastern part of the basin (Goodbred and Kuehl, 2000). The continuation of these processes resulted in the progradation of the active delta in the present-day configuration around 3500 to 3000 years BP (Goodbred and Kuehl, 2000) and the growth of the mangrove forests in the Sunderbans region (Fig. 6F).

Extensive peat layers in the upper and uppermost units throughout the southern Bengal basin have been reported by various workers, including Vishnu-Mittre and Gupta (1979), Sen and Banerjee (1990), Barui and Chanda (1992), Umitsu (1987, 1993) and Islam and Tooley (1999), who referred to the layers as the Bengal peat. Civil construction in Calcutta in the recent past, even at shallow depths, has yielded remnants of peaty material. The above-mentioned authors have claimed the peat as in-situ in origin and mostly formed from mangrove (or mangal) vegetation. Studies near the city of Khulna have yielded five well-developed and

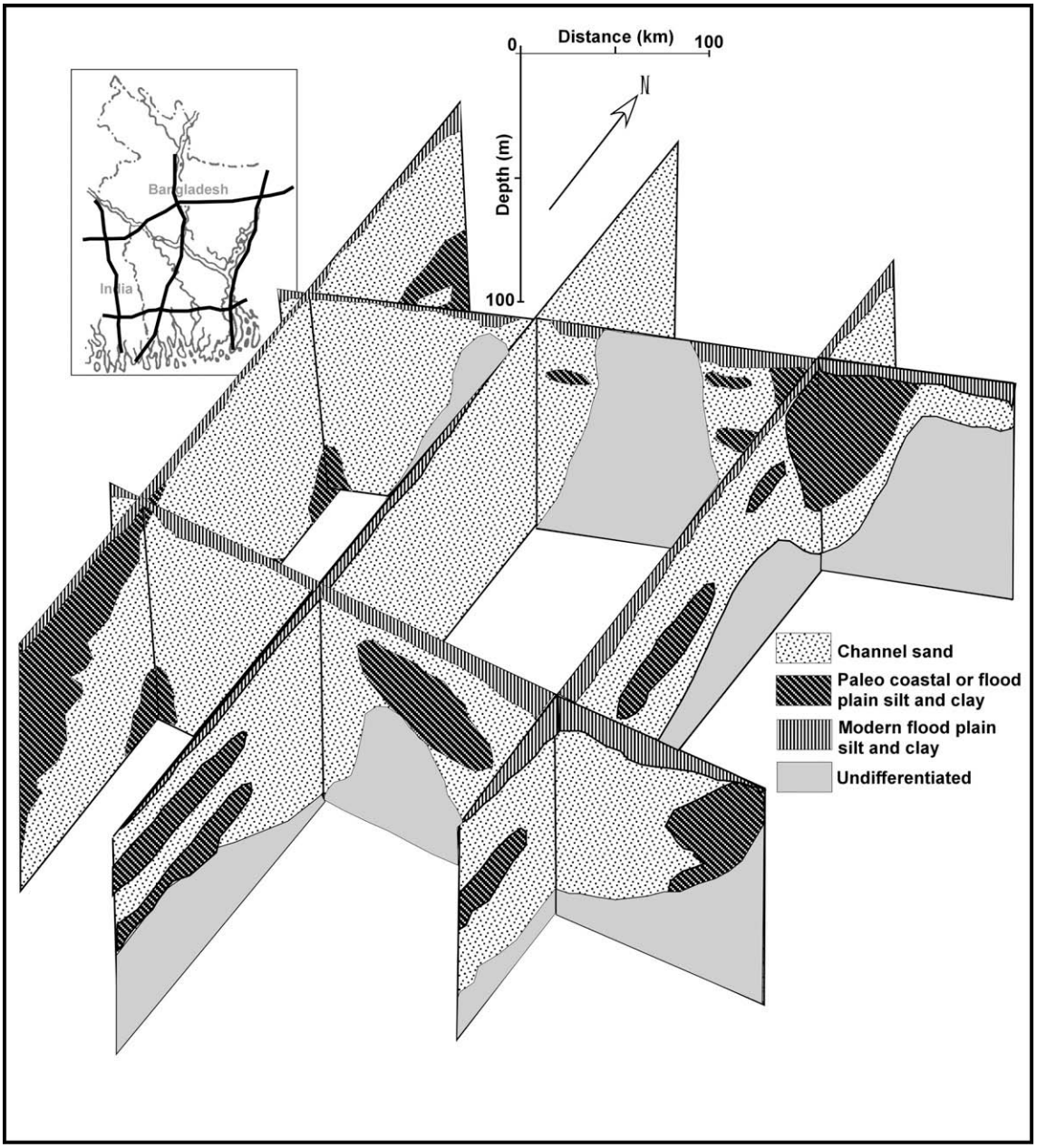

Fig. 5. Lithologic fence diagram of the most recent sediments in the Bengal basin (adapted from Goodbred et al., 2003, and Mukherjee, 2006).

generally thick layers of peat, each separated by inorganic layers (Islam and Tooley, 1999). The lowermost peat layer has been dated at 7000 to 6650 years old and contains remains of mangrove plants like *Acrostichum aureum*, *Heritiera* spp., and *Avicennia* spp. Parts of the uppermost layer have been dated at 5000–2000 years old and contain abundant remains of freshwater peat-forming plants. The intercalation of mangrove and fresh-water plants with mineral-rich layers has been interpreted to indicate deposition in a basin that was inundated by sea-level rise with intermediate temporary sea-level falls (Islam and Tooley, 1999).

6. Sedimentology, mineralogy, and elemental distribution

To a large extent, the sedimentology and mineralogy of the Bengal basin depend on the primary types of sediments eroded and transported by the Ganges, the Brahmaputra, and their northern tributaries like the Meghna, Tista, Rangeet, and Mahananda. Bank and floodplain sediments have been designated as major short-term river sediment sources (Meade and Parker, 1985). More than 76% of bed sediments from the GBM river system are fine to very fine sand, with a mean grain size of 2.5–4 Φ (1/6–1/16 mm) (Datta and Subramanian, 1997). The grain size decreases from upper to lower reaches, and 66% of the sediments are moderately to well sorted according to the scale of Folk and Ward (1957) (Datta and Subramanian, 1997). All bed sediments are positively skewed (Goswami, 1985; Datta and Subramanian, 1997), and 95% of the suspended sediments are more than 6Φ (0.01 mm) and are well sorted (Datta and Subramanian, 1997).

Because of differences in sediment provenance, the Brahmaputra and Ganges systems have quite distinctive mineralogies (Heroy et al., 2003). The Brahmaputra flows through various rock types, including Precambrian metamorphic rocks (high-grade schist, gneiss, quartzite, and marble), felsic intrusives, Paleozoic–Mesozoic sandstones, shales and limestones of the Himalayan terrain

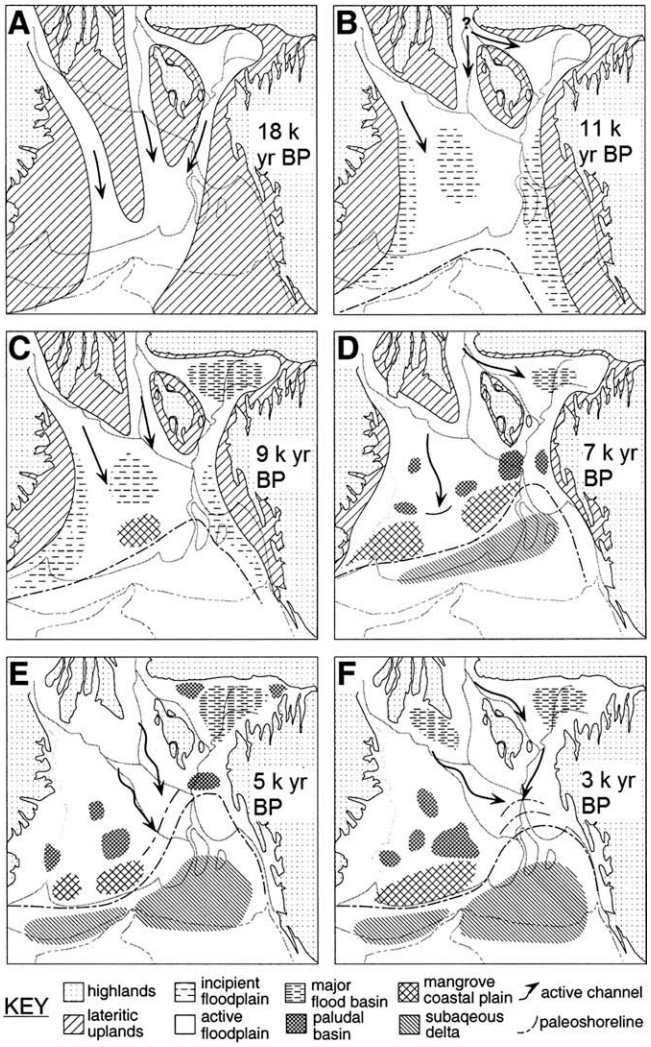

Fig. 6. Stages of Holocene landform evolution of the Bengal basin (see Section 6 of text for description). Reprinted from Sedimentary Geology, vol. 133, nos. 3–4, Goodbred, S.L., Kuehl, S.A., The significance of large sediment supply, active tectonism, and eustasy on margin sequence development: Late Quaternary stratigraphy and evolution of the Ganges–Brahmaputra delta, 227–248, copyright 2000, with permission from Elsevier.

(Huizing, 1971). The Ganges drains terrains with similar kinds of lithologies, but also receives lower course and lowland tributaries, which drain Mesozoic and Tertiary mafic extrusives and the Precambrian–Cambrian shield (Huizing, 1971). The tributaries of the lower Gangetic plain, in the upper reaches from the Bengal basin, produce a saline and alkaline soil, which contains calcareous concretions called "kankar" (Sarin et al., 1989). In contrast, the Brahmaputra alluvium has less calcareous matter than the Ganges (Wadia, 1981), and Brahmaputra and Meghna sediments are characterized typically by noncalcareous, acidic soil (Saheed, 1995).

The Bengal basin sediment mineralogy is dominated by detrital quartz and feldspar grains (Datta and Subramanian, 1997). The higher quartz content relative to feldspar is indicative of low-relief tropical weathering in the basin (Potter, 1978). Among the clay minerals, illite and kaolinite are profuse and are in nearly equal proportions, whereas chlorite and montmorillonite are insignificant (Datta and Subramanian, 1997). High illite and low chlorite content indicates the ongoing neotectonic activity around the basin (Morgan and McIntire, 1959) and the enrichment of the parent rocks in muscovite mica (Griffin et al., 1968). The large amount of kaolinite signifies the intense kaolinization of the parent minerals (e.g., feldspars). The Ganges system has a higher amount of smectite and a lower amount of kaolinite in comparison to the Brahmaputra (Sarin et al., 1989). Several studies have concluded that the kaolinite–smectite assemblage has been derived from the low-temperature alteration of the high-grade crystalline metasediments of the Himalayas by pedogenic processes within the Bengal basin, whereas the illite–chlorite suite has been derived from direct erosion of the Himalayas. Any component of these assemblages derived from the cratonic part of the Indian subcontinent is insignificant (France-Lanord et al., 1993; Heroy et al., 2003).

The heavy mineral assemblages in all three river systems of the Bengal basin are similar (Datta and Subramanian, 1997). Among the heavy minerals, amphibole is most prominent, followed by garnet and epidote. There is a slight enrichment of pyrope garnet in the Ganges system, while epidote and amphibole are slightly higher in the Brahmaputra system (Huizing, 1971; Datta and Subramanian, 1997). Unstable minerals in general dominate the heavy mineral assemblage (e.g., hornblende, garnet, magnetite, and ilmenite), followed by semistable minerals like apatite, epidote, staurolite, and kyanite. Stable and ultrastable heavy minerals are less common (Datta and Subramanian, 1997). The predominance of unstable heavy minerals is possibly a manifestation of lack of significant chemical alteration during transport (Kumar and Singh, 1978). The high-grade metamorphic terrains (see Fig. 1) are the provenance of 40–46% of the heavy minerals, followed by the igneous terrains with 21–29% (Huizing, 1971; Datta and Subramanian, 1997). Pyrite is rare but is found sometimes in the sediments of the basin (BGS/DPHE, 2001). This range of heavy minerals is comparable to that of Miocene and younger sediments eroded from various orogenic sources, including the Himalayas ophiolites (Uddin and Lundberg, 1998; Zheng, 2006).

The distributions of nitrogen and phosphorus in the sediments of the Ganges, Brahmaputra and Meghna river systems are similar and vary within a narrow range. The average total nitrogen (TN) of the three basins ranges from 0.1 to 0.6 mg/g (Datta et al., 1999). The average total phosphorus (TP) is about 0.7 ± 0.1 mg/g in the Meghna basin, 0.9 ± 0.2 mg/g in the Brahmaputra and 1.0 ± 0.4 mg/g in the Ganges (Datta et al., 1999). Total nitrogen in the basin may be controlled both by sources of organic matter and biogeochemical processes (Datta et al., 1999).

The total carbon (TC) content appreciably increases from the Meghna basin to the Ganges. The values are 1.8 ± 0.5 mg/g in the Meghna, 2.0 ± 1.7 mg/g in the Brahmaputra and 8.2 ± 2.8 mg/g in the Ganges (Datta et al., 1999). In the Meghna basin the total carbon consists primarily of TOC and there is little or no total inorganic carbon (TIC), but the Ganges basin contains appreciable amounts of both TIC and TOC. Sarin et al. (1989) reported higher concentrations of Na and Cl in Ganges sediments than in Brahmaputra sediments. In general, in the Bengal basin, there is a very good correlation between TN and total organic carbon (TOC) and between TOC and grain size of the sediments.

Common naturally occurring trace metal contaminants reported in the Bengal basin sediments include lead, arsenic, cadmium, mercury, and selenium (Aswathanarayana, 1995). The concentrations of trace elements like lead, arsenic, and mercury are lower in the Bengal basin than in typical shale and clay (Datta and Subramanian, 1997). The index of geoaccumulation (Müller, 1979) is negative for lead, arsenic, and mercury in the GBM system but is positive for cadmium in the Brahmaputra plains (Datta and Subramanian, 1997).

7. Hydrology

In recent years, groundwater in the Bengal basin has been the subject of attention because of water quality issues. In general,

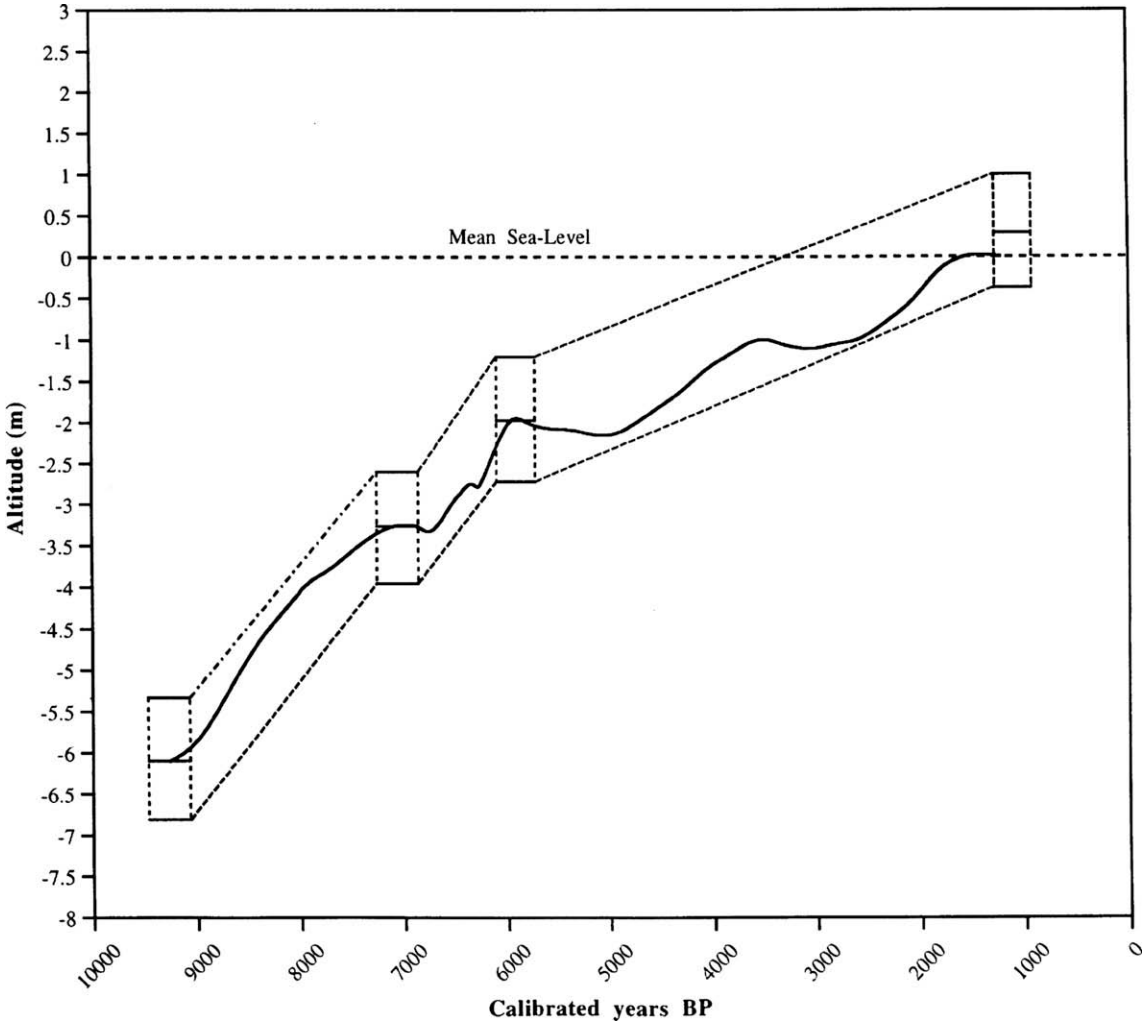

Fig. 7. Holocene sea-level curve (solid line) constructed for the Bengal basin from altitude and radiocarbon dating. The error margins are marked by the dashed lines beside the curve. Reprinted from Quaternary International, vol. 55, no. 1, Islam, M.S., Tooley, M.J., Coastal and sea-level changes during the Holocene in Bangladesh, 61–75, copyright 1999, with permission from Elsevier.

groundwater flow in the basin is strongly influenced by the heavy rainfall caused by the southeast monsoon wind from mid-June to mid-October originating from the Bay of Bengal. Annual rainfall ranges from about 125 cm in the west-central part of the basin to more than 500 cm near the Shillong plateau in the northeast and the Himalayas in the north. In the western Bengal basin, the average pre-monsoon rainfall (January–May) is 16.23% of annual rainfall, monsoon rainfall (June–October) is 82.21%, and post-monsoon (November–December) is 1.57% (Mukherjee et al., 2007a). The average temperature is about 30 °C in the summer and about 15 °C in the winter. Monsoonal rainfall and the water from Himalayan snowmelt carried by the Ganges and Brahmaputra cause extensive, damaging floods in the Bengal lowlands. BGS/DPHE (2001) reported as much as 56.9% of the total area of Bangladesh flooded annually between 1954 and 1988 [based on Miah (1988) and Brammer (1990a,b)].

7.1. Recharge

Everywhere on the delta plain, precipitation exceeds annual potential evapotranspiration (Allison, 1998). Recharge has been estimated to range from 0.3 to 5.5 mm/day (BGS/DPHE, 2001) and average 1.6 mm/day annually (Basu et al., 2001; Dowling et al., 2003) for the Bangladesh part of the basin. JICA (2002) calculated a potential recharge (PR) of 709 mm/year for western Bangladesh. For the West Bengal part, SWID (1998) estimated that absolute recharge is as much as 15% of total precipitation. On the basis of more than 100 years of historical climatological data, Mukherjee et al. (2007a) calculated the mean annual PR for western Bengal basin as 587 mm/year or 1.61 mm/day (range: 384–767 mm/year), which is 39% of the mean annual rainfall. Because of heavy monsoonal rainfall, most of the PR is during monsoon season (mean: 3.67 mm/day, range 2.41–4.86 mm/day), with little to no recharge during the pre-monsoon (mean: 0.18 mm/day, range 0.15–0.25 mm/day) and post-monsoon (mean: 0.06 mm/day, range 0.05–0.08 mm/day). The estimated annual absolute recharge from precipitation is 0.41–0.58 mm/m^2/day. However, a large part of the water that is abstracted for irrigation (annual mean: 1.2 mm/m^2/day) may return to the groundwater as recharge (annual mean: 0.75 mm/m^2/day) (Mukherjee et al., 2007a). Characterization of stable isotopic (δ^{18}O–δ^2H) composition of rainfall shows that the local meteoric water line is very similar to the global meteoric water line (Aggarwal et al., 2000; Mukherjee et al., 2007b); pre-monsoonal rainfall composition is much more isotopically enriched (heavier) than monsoonal rainfall, indicating a local moisture source rather than the Bay of Bengal (Mukherjee et al., 2007b).

7.2. Aquifer framework and groundwater flow

In various attempts to define the aquifer–aquitard structure of the Bengal basin, the aquifer systems have been classified by lithology and depth at the basin scale (e.g., UNDP, 1982; AIP/PHED, 1991, 1995; CGWB, 1994, 1997; SWID, 1998; Acharyya et al., 2000). However, stratigraphy has also sometimes been considered in smaller scale models (Ravenscroft, 2003). The difference in these processes of classification makes aquifer correlation across the basin challenging.

UNDP (1982) classified the aquifers in Bangladesh into three depth zones on the basis of lithological data to a depth of 137 m:

(i) *The shallower, upper aquifers:* These semi-confined aquifers consist of fine sands with thin medium sand interbeds and numerous, discontinuous clay layers below the surface soil. The thickness of these aquifers ranges from <10 m in the northwest of the basin to about 60 m in the south. In the coastal region, these aquifers contain brackish water, with some fresh water pockets.
(ii) *The main aquifers:* These semi-confined to locally unconfined aquifers act as the main drinking water source of the eastern part of the basin. They consist of medium- to coarse-grained sands, in part alternating with gravel layers. They vary in thickness from 5 m in the northwest to more than 75 m in the south, and are at a depth of about 140 to 150 m below ground level (bgl).
(iii) *The deeper aquifers:* These are confined aquifers at depths of 150 m to 200 m bgl, and are separated from the main aquifer by clay layers. They consist of medium to coarse sands with interbeds of silt and clay. These aquifers have very limited interaction with the overlying aquifers.

Besides classifying the aquifers by lithology, recent work has suggested divisions based on the apparent age of the groundwater. Aggarwal et al. (2000) considered groundwater recharged within the past 100 years to reside in the first (shallowest) aquifer (70 to 100 m deep). Groundwater about 3000 years old is inferred to reside in the second aquifer, which extends to 200–300 m bgl, whereas water about 20,000 years old resides in the third aquifer, below 200–300 m bgl. However, Aggarwal et al. (2000) noted that depth cannot be a dependable criterion for this classification of the aquifers.

In one of the most comprehensive groundwater studies of the Bengal basin, BGS/DPHE (2001) proposed five major aquifer systems. These are:

(a) Late Pleistocene to Holocene Tista mega-fanglomerate and Brahmaputra channel basal gravel aquifers composed of coarse sand, gravels, and cobbles.
(b) Late Pleistocene to Holocene Ganges, lower Brahmaputra and Meghna main-channel shallow aquifers composed of braided and meandering river sediments.
(c) Early to middle Pleistocene coastal and moribund Ganges delta deep aquifers composed of stacked, main-channel, medium to coarse sands at depths more than 130 m.
(d) Early to middle Pleistocene Old Brahmaputra and Chandina deep aquifers composed of red–brown medium to fine sands underlying Holocene gray medium to fine sands.
(e) Early to middle Pleistocene Madhupur terrace and Barind aquifers composed of coarse to fine fluvial sands, confined by near-surface clay residuum.

Islam and Udiin (2002) and Uddin and Abdullah (2003) proposed a four-layer, age-based classification of the aquifers, which from bottom to top are:

(1) *The Pliocene aquifers:* These are the Dupi Tila aquifers, composed of light grey to yellowish brown, medium to coarse sand, interbedded with gravels and pebbles.
(2) *The Late Pleistocene–Early Holocene aquifers:* These probably correspond to the deep aquifers of UNDP (1982), the third aquifer of Aggarwal et al. (2000), and the deep aquifer (c) of BGS/DPHE (2001) classification.
(3) *The Middle Holocene aquifers:* These aquifers may correspond to the main aquifer of UNDP (1982), the second aquifer of Aggarwal et al. (2000) or the lower shallow aquifer (b) of BGS/DPHE (2001) classification. These mostly exist in the GBM flood and deltaic plains of Bangladesh, and consist of upward coarsening sand layers, with some silt and peat at the top.
(4) *The Upper Holocene aquifers:* Corresponding to the upper shallow aquifers of UNDP (1982) and BGS/DPHE (2001), and the first aquifer of Aggarwal et al. (2000), these shallow aquifers are present all along the central and southern deltaic region of Bangladesh. They consist of vertically layered, interconnected sands, underlain by interbedded silts and clays.

For the western part of the Bengal basin, descriptions of the aquifers are based mostly on lithology, and few publications are available on the regional aquifer framework. Mukherjee et al. (2007a) delineated the regional hydrostratigraphy (down to 300 m below MSL), identifying a continuous, semi-confined sand aquifer (referred to as the main or *Sonar Bangla* aquifer), underlain by a thick, basal clay aquitard (referred to as the Murshidabad aquitard). The main aquifer thickens from the north (~80 m) toward the east (~150 m) and south (>200 m) (Fig. 8). In the southwestern part of the basin, near the modern delta, there are several intermediate-depth clayey aquitards, which divide the main aquifer into laterally connected, confined aquifers. Some isolated deeper aquifers are confined within the basal aquitards.

Transmissivity (T) values from Bangladesh range from ~3000 to 7000 m^2/day in BGS/DPHE (2001) aquifer systems (a) and (b) and from ~300 to 3000 m^2/day in aquifer systems (c)–(e) (BGS/DPHE, 2001). CGWB (1994) and SWID (1998) estimated T values in West Bengal from 3300 to 7000 m^2/day in Murshidabad, 5000–8800 m^2/day in North 24 Parganas, and 500–3000 m^2/day in South 24 Parganas. The mean T values in the four districts of the western Bengal basin are around 1000 m^2/day (Mukherjee and Fryar, unpublished data). Sikdar et al. (2001) reported a maximum value of 7774 m^2/day in the Sinthi neighborhood of Kolkata. Aquifer storage coefficients have been estimated to be within the range of 1.3×10^{-5}–6.7×10^{-3} for most of the aquifers of Bangladesh (BGS/DPHE, 2001). The hydraulic conductivity (K) of the young gray sediments has been estimated in the range of 0.4–100 m/day. The older red–brown sediments have K on the order of 0.2–50 m/day (BGS/DPHE, 2001).

On the basis of strontium isotope analyses, the groundwater flux to the Bay of Bengal has been estimated on the order of 2×10^{11} m^3/year, which is equal to about 19% of the total surface water flux (1.07×10^{12} m^3/year) (Basu et al., 2001). However, this estimate is controversial because a large groundwater flux is implausible in a flat terrain like the GBM plain, where in a distance of 100 km, the land surface elevation only decreases by about 10 m (Harvey, 2002). The hydraulic gradient decreases from about 1 m/km in the northern Bengal basin to about 0.01 m/km in the southern basin (BGS/DPHE, 2001). In general, the regional groundwater flow is from north to south with local variations in the vicinity of the river systems, which are mostly effluent. Modern continuation of such regional flow has been questioned by Harvey (2002) and Mukherjee (2006) in light of the large amount of

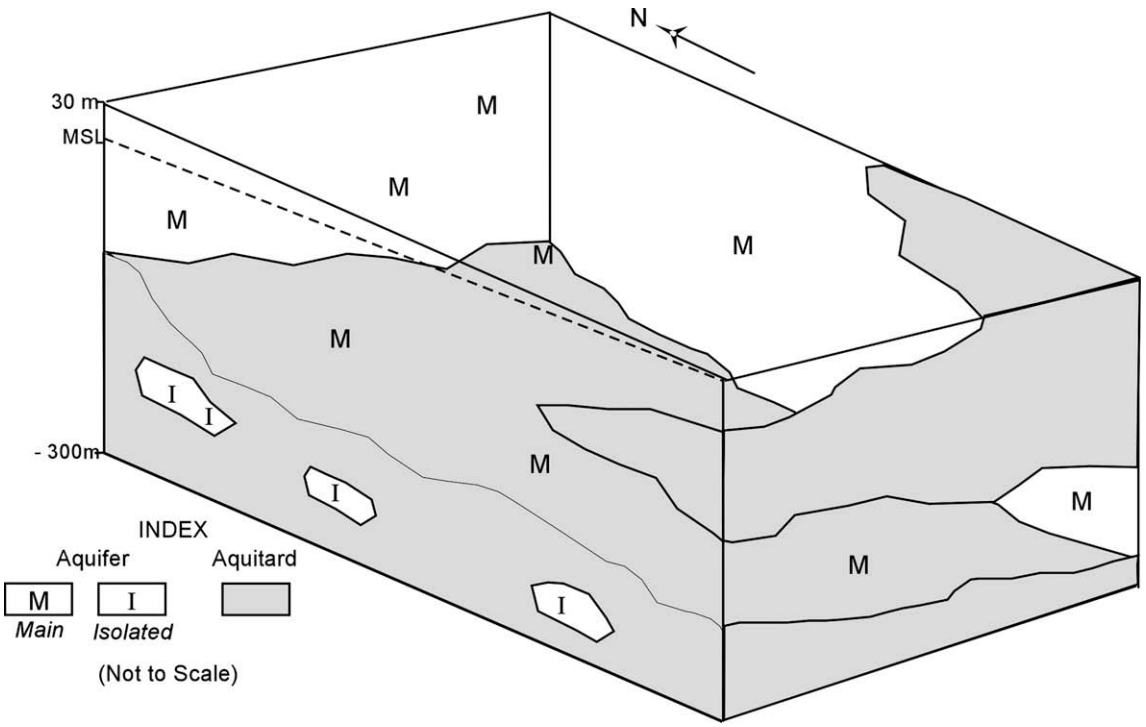

Fig. 8. A simplified, conceptual hydrostratigraphic model of the western part of the Bengal basin (adapted from Mukherjee, 2006). See text for discussion.

pumping, mostly for irrigation, within the basin. Sikdar et al. (2001) showed that there was a north–south regional flow in the vicinity of Calcutta, prior to the 1970s, which has since been disrupted as a consequence of urban pumping.

The low hydraulic gradient has led to a very slow flushing rate, which is thought to have had a significant effect on the chemistry of groundwater in the basin. Estimates show that Brahmaputra and Ganges basin sediments may have been flushed only once, if at all, since they have been deposited (BGS/DPHE, 2001). Using Darcy's law and volumetric calculations, BGS/DPHE (2001) estimated that the lower shallow aquifer would be flushed in ~20 to 71 ka under the present hydraulic gradient and in ~13 to 20 ka under an early Holocene hydraulic gradient. On the basis of ^{4}He accumulation, Dowling et al. (2003) calculated that groundwater at depths >200 m is >1 ka old. Klump et al. (2006) suggested that the groundwater is very young (<5 years) down to a depth of 10 m and may be about 40 years age within a depth of 15 to 30 m.

7.3. Source of groundwater

Using ^{18}O and ^{2}H analyses, Krishnamurthy and Bhattacharya (1991) and Mukherjee et al. (2007b) showed that groundwater of the western Bengal basin is mostly recharged by monsoonal precipitation. Moreover, the stable isotopic composition of groundwater demonstrates an continental depletion effect (Dansgaard, 1964) as the Indian southeastern monsoon wind moves from the Bay of Bengal west–northwest toward central India (Ananthakrishnan, 1977; Rao, 1981) and northward toward the eastern Himalayas. Dray (1983) inferred a lack of rapid interaction between River Ganges water and the groundwater of Bangladesh, while Shivanna et al. (1999) suggested that the depleted stable isotopic values of some shallow groundwater relative to local precipitation in Murshidabad district, West Bengal, are an artifact of interaction with the depleted Ganges water. Aggarwal et al. (2000) concluded that deep groundwater with δ^{18}O values >3‰ or <6‰ VSMOW represents recharge from precipitation during different climatic regimes from ~ 3 to 30 ka.

7.4. River water chemistry

The Ganges–Brahmaputra–Meghna river system is one of the global leaders in annual solute flux to the tropical seas. The river system contributes about 5% (152×10^{6} t/year) of annual global chemical flux to the world's ocean, which is about 68% of that of the Amazon river system (Datta and Subramanian, 1997b). The river system also contributes large proportions of the global fluxes of trace metals (e.g., F, Sr) (Datta et al., 2000; Basu et al., 2001). The river waters in the basin are circumneutral to slightly alkaline (Datta and Subramanian, 1997b; Mukherjee and Fryar, 2008), indicating chemical evolution associated with mineral weathering (Ollier, 1969). The cation loads are greatest in the Ganges river waters, followed by the Bramhaputra and the Meghna. Inland river waters are mostly Ca–HCO_3 type, with solute compositions in the lower range of the groundwater concentrations (Datta and Subramanian, 1997b; Mukherjee and Fryar, 2008). The chemistry suggests dominance of carbonate dissolution, with some input of calcic plagioclase and pyroxene weathering (Datta and Subramanian, 1997b). The weathering rate is two to three times that of the Amazon and Huang Ho river systems and three to four times the global average (Datta and Subramanian, 1997b). The local, groundwater-fed tributaries (e.g., Jalangi, Ichamati) of the major rivers generally have higher solute concentrations and greater ^{2}H and ^{18}O enrichment than the rivers, which originate at relatively high altitudes. The tidally influenced streams near the delta front are essentially Na–Cl type, with δ^{2}H and δ^{18}O compositions close to sea water (Mukherjee et al., 2007b; Mukherjee and Fryar, 2008). The river chemistry evolves with weathering during the pre-monsoon and is diluted during the monsoon (Sarin et al., 1989). Trace metal compositions in the river waters are generally much lower than in the adjacent groundwater, with no elevated dissolved As in the Himalayan rivers. However, high concentrations of As have been detected in local tributaries, probably reflecting the composition of base flow (Mukherjee and Fryar, 2008). Most of the As in the river solute load is associated with insoluble phases like crystalline Fe oxides (Stummeyer et al., 2002).

7.5. Groundwater chemistry

Although the chemistry of groundwater in the Bengal basin, like the stratigraphic framework, is heterogeneous, some generalizations can be made. Bengal basin groundwater tends to be Ca–HCO_3 dominated, with some Na–Cl dominated waters, relatively high As, Fe, and Mn, and low or undetectable SO_4 and NO_3 (e.g., Ahmed et al., 1998; BGS/DPHE/MML, 1999; Nickson et al., 1998, 2000; McArthur et al., 2001; Dowling et al., 2002). Mukherjee and Fryar (2008) noted that this description may be further typified in a hydrostratigraphic context in the western Bengal basin, where the main, semi-confined aquifer contains Ca–HCO_3 water and the isolated, deeper confined aquifers contain Na–Cl or HCO_3 waters, similar to descriptions provided by Handa (1972), Ahmed (1994), Sikdar et al. (2001), and Bhattacharya et al. (2002). Mukherjee and Fryar (2008) further noted that the main aquifer water may evolve to form the isolated waters by cation exchange with aquifer sediments and by mixing with connate water in various proportions. However, salinity caused by upward diffusion of connate water from very deep aquifers appears to be unlikely as predicted by geochemical modeling. Sikdar et al. (2001) attributed increasing salinization of groundwater in the Calcutta region, which has accompanied pumping, to mixing of fresh groundwater with modified connate water in low-permeability zones (Handa, 1972). Along the Bay of Bengal, relatively fresh groundwater underlies shallow saline groundwater (BGS/DPHE, 2001).

Galy and France-Lanord (1999) concluded that the water chemistry of the Bengal basin is controlled by the presence of carbonates, the composition of silicates, and the oxidation of sulfides. They suggested that weathering in the basin is dominated by H_2CO_3 liberated by degradation of organic matter in the soil, and <10% of the weathering of the Ganges basin is caused by H_2SO_4 derived from sulfide oxidation. The authors also suggested that, because Ca-plagioclase is not abundant in the Himalayas, weathering of the alkaline Himalayan silicates releases Na and K as the dominant cations. Mg found in the hydrobiotite, vermiculite, and smectite of the sediments derived from the Himalaya (Baumler and Zech, 1994; Grout, 1995) is probably introduced into the system from weathering of biotite, and to a lesser extent from chlorite, pyroxene, and garnet (Galy and France-Lanord, 1999). Dowling et al. (2003) found that the average $(Ca + Mg)/HCO_3$ molar ratio (0.9) and the correlation between Sr and HCO_3 are consistent with dissolution of detrital carbonates in the upper reaches of the river, and thus concluded that the Ganges and Brahmaputra flood plains have been dominated by carbonate weathering. Relatively high Ca and Mg concentrations in southwestern Bangladesh coincide with relatively calcareous sediments deposited by the Ganges (BGS/DPHE, 2001). The deposition of silt-dominated sediments in the foreland basin of the Himalayas (Burbank, 1992), however, probably favors silicate weathering (Derry and France-Lanord, 1996; Galy and France-Lanord, 1999).

Mukherjee and Fryar (2008) showed that groundwater of the western Bengal basin is influenced by both carbonate dissolution and silicate weathering. Hence, Na and K may enter the Bengal basin groundwater from incongruent dissolution of feldspars, micas, and pyroxenes, whereas Ca and Mg can be derived both from silicate and carbonate weathering. Other than carbonate and silicate weathering, HCO_3 in groundwater can originate from biogenic CO_2 gas dissolution in the vadose zone (Garrels, 1967).

Groundwater in the Bengal basin has been found to be anoxic (Mehta and Bhattacharya, 2000; Harvey et al., 2002; Swartz et al., 2004), with abundant detections of sulfide and CH_4 (e.g., Ahmed et al., 1998; Gavrieli et al., 2000; Nickson et al., 2000; McArthur et al., 2001, 2004) and very little dissolved O_2. Throughout Bangladesh, SO_4 concentrations are relatively low (median <1 mg/L) and Fe and Mn concentrations are relatively high, consistent with strongly reducing conditions (BGS/DPHE, 2001). Anomalously high SO_4 and NO_3 concentrations in Dhaka provide evidence of ground-water pollution by sewage (Ahmed et al., 1998). In West Bengal, SO_4 concentrations as high as 39.6 mg/L have been documented by Mukherjee and Fryar (2008), and those concentrations were found to vary with depth and distance from the coast.

Most of the recent studies of groundwater chemistry in the Bengal basin have advocated that the dominant redox process in the main aquifer is FeOOH reduction coupled to microbially mediated oxidation of natural organic matter (NOM) (Bhattacharya et al., 1997; Nickson et al., 1998, 2000; McArthur et al., 2001, 2004; Harvey et al., 2002, 2005; Zheng et al., 2004). NOM may be in forms of dissolved organic carbon or peat (McArthur et al., 2001, 2004; Ravenscroft et al., 2001, 2005; Harvey et al., 2002), and oxidation of NOM may result in elevated HCO_3 concentrations. On the basis of chemical and stable isotopic data, Zheng et al. (2004) and Mukherjee and Fryar (2008) suggested local-scale reoxidation of authigenic Fe sulfides, which indicates that Fe, S and C cycles within the subsurface are interrelated and complex.

In the past two decades, elevated concentrations of arsenic (As) have been found in groundwater of the Bengal basin. Prolonged ingestion of As contaminated water causes severe health effects, including cancer, and can be fatal (Smith et al., 2000). Arsenic concentrations vary widely in the basin, generally ranging from less than 0.005 to 3.2 mg/L (CGWB, 1999; BGS/DPHE, 2001), but concentrations as high as 4.1 mg/L have been identified (Ghosh and Mukherjee, 2002). The contaminated area is mostly restricted by the River Bhagirathi–Hoogly (distributary of River Ganges) in the west, the Rivers Ganges and Padma in the north, the flood plain of the River Meghna (tributary of the River Padma), and the River Jamuna in the northeast (Acharyya et al., 2000).

There has been much speculation about the primary source of As in this basin. It may have been transported by the River Ganges and its tributaries from the Gondwana coal seams in the Rajmahal trap area (Saha, 1991), by the north Bengal tributaries of the Ganges from near the Gorubathan base-metal deposits in the eastern Himalayas (Ray, 1999), or with other fluvial sediments derived from the Himalayas (e.g., McArthur et al., 2004). Arsenic may also have been biogenically deposited in the paleo-channels of the River Bhagirathi–Hoogly and the River Padma under euxinic conditions (P. Chakrabarty, West Bengal State Remote Sensing Board, 1999, personal communication).

Four main mechanisms have been identified by various workers to explain the mechanism of As mobilization in groundwater of the Bengal basin. These are:

(1) As is released by oxidation of As-bearing pyrite in the alluvial sediments (e.g., Mallick and Rajgopal, 1995).
(2) Arsenic anions sorbed to aquifer mineral grains are displaced into solution by competitive exchange of PO_4^{3-} available from fertilizers of surface soils (Acharyya et al., 2000).
(3) As sorbed to FeOOH (HFO) is released by reduction of solid-phase Fe(III) coupled to oxidation of peat (Bhattacharya et al., 1997; Nickson et al., 1998, 2000; McArthur et al., 2001, 2004; Ravenscroft et al., 2001) or of dissolved organic carbon (DOC) (Harvey et al., 2002, 2005).
(4) As is released from HFOs or other sediment phases by redox reactions related to Fe and S cycling (Zheng et al., 2004) and is retained in solution by partial redox equilibrium (Mukherjee et al., 2008). This proposed mechanism is a combination of mechanisms 1 (involving reoxidation of authigenic pyrite) and 3. In addition to these views, many workers have agreed

that indiscriminate agricultural and industrial pumpage may have facilitated the spread of As within groundwater (e.g., Harvey et al., 2005; Klump et al., 2006; Mukherjee et al., 2007a).

8. Summary

The Bengal basin in eastern India and Bangladesh is the largest fluvio-deltaic system of the world. It has been shaped by the rivers Ganges, Brahmaputra, Meghna and their tributaries and distributaries, which drain into the Bay of Bengal. The basin lies between the eastern Himalayas and the Bay of Bengal at the junction of the Indian plate with the Eurasian and Burmese plates. The basin was initiated as a subsiding foredeep basin beneath the uprising Himalayan front and the Indo-Burma range formed by the collision of the Eurasian, Indian, and Burmese plates starting in the late Mesozoic. By the mid-Miocene, the basin had become a huge sink for the sediments eroded from the rising mountain ranges. The basin can be broadly tectonically divided into a stable shelf, which mostly constitutes the extension of the Indian plate in the west, and the foredeep basin. These are separated by a deep-seated zone of flexure, known as the Calcutta–Mymensingha hinge zone. At present, about 1 to 8 km of Permian to Holocene clastic sediments rest on the stable shelf in the western part of the basin and as much as 16 km of Tertiary to Quaternary alluvial sediment fills the foredeep of the basin, which at present lies at the mouth of the Ganges and Brahmaputra rivers. The ongoing Himalayan orogeny has caused vertical uplift to divide the foredeep basin into numerous poorly connected sub-basins, which in turn has led to conspicuous differences in sedimentary environments and lithology.

The formation of the Bengal basin started with the break-up of Gondwanaland in the late Mesozoic, at about 126 Ma. During the middle Eocene, basin-wide subsidence caused an extensive marine transgression in the basin, which resulted in the deposition of a nummilitic limestone, the Sylhet Limestone. At about 49.5 Ma, a major shift in the sedimentation pattern began. The carbonate-clastic platform sedimentary sequence was succeeded by a predominantly clastic deposit. The western part of the basin saw deposition of lagoonal argillaceous and arenaceous sediments, whereas the eastern and northeastern parts were occupied by an open neritic sea. At about 10.5 Ma, intense tectonic activity began, resulting in basin-wide regression with a major eustatic low. This initiated the modern Bengal delta as a shift from a marine-estuarine environment to a predominantly fluvial–tidal dominated environment.

Physiographically, the Bengal basin can be divided into two major units, the Pleistocene uplands and Holocene sediments. The Pleistocene uplands include the Barind tract and the Madhupur terrace. The Holocene sediments include the alluvial fans in the foothills of the Himalayas, the uplands such as the Tippera surface, the deep tectonic basin (Sylhet basin), and the Ganges–Brahmaputra–Meghna flood and delta plain, the most extensive unit of the basin. The flood and delta plain consists of clastic fluvial deposits with elevations no more than 15 m above MSL in most areas. Radiocarbon dating of sediments from the plain yields an age of generally less than 10,000 years to a depth of 30 m below land surface in most areas.

Deposition of the lowest unit of the GBM delta began at the onset of the local Pleistocene glacial maximum. The rivers draining the previous plains during that time must have scoured through the earlier plains and deposited the basal gravel at a depth analogous to the sea-level at that time. The next unit of the GBM plain was probably deposited at about 12,000–11,500 years BP as an extensive flood plain in the central region. Major eustatic sea-level rise around 10,500 years BP caused extensive back-flooding and sedimentation, initiating the present GBM delta. From about 10,000 to 7000 years BP, a major and rapid transgression probably resulted in the deposition of fine sediments of the upper unit of the GBM plain.

The Bengal basin sediment is dominated by detrital quartz and feldspar grains. The clay minerals include illite and kaolinite, with minor chlorite and montmorillonite. The heavy mineral assemblages include amphibole, pyrope, and epidote. Some pyrite is also found in the basin sediments. In Ganges basin sediments, concentrations of both TIC and TOC are significant, and TOC is well-correlated to TN and grain size of the sediments.

There is a lack of consensus about the nature of groundwater flow and the stratigraphic framework of the aquifers in the basin. In general, three to five classes of aquifers have been proposed for Bangladesh, but only two to three for West Bengal. The gray Holocene sediments tend to have higher hydraulic conductivity than the brownish Pleistocene sediments. Regionally, groundwater tends to flow toward the coast with a very low hydraulic gradient, particularly in the south. The water is mostly of monsoonal origin with an isotopic composition consistent with the present-day climate. Groundwater chemistry is generally a Ca–HCO_3 type with some Na–Cl waters; the water also has high As, Fe, and Mn and is low in SO_4 and NO_3. Processes controlling groundwater chemistry include carbonate dissolution, silicate weathering, redox reactions (especially including Fe, C, and S), and mixing between fresh and saline waters.

Acknowledgements

The authors are grateful for the constructive reviews by Dr. Dilip Dutta, Khulna University, Bangladesh, and Dr. Steve Peters, Lehigh University, USA. The authors also thank Dr. Bridget R. Scanlon and the Bureau of Economic Geology, University of Texas at Austin, for support in preparation of this manuscript.

References

Acharyya, S.K., Lahiri, S., Raymahashay, B.C., Bhowmik, A., 2000. Arsenic toxicity of groundwater in parts of the Bengal basin in India and Bangladesh: the role of Quaternary stratigraphy and Holocene sea-level fluctuation. Environ. Geol. 39, 1127–1137.

Aggarwal, P.K., Basu, A.R., Kulkarni, K.M., Froehlich, K., Tarafdar, S.A., Ali, M., Hussain, A., 2000. A report on isotope hydrology of groundwater in Bangladesh: Implications for characterization and mitigation of arsenic in groundwater. International Atomic Energy Agency-TC Project BGD/8/016, 64 p.

Ahmed, K.M., 1994. Hydrogeology of the Dupi Tila aquifer of the Barind Tract, NW Bangladesh. Unpublished Ph.D. thesis, University of London, London.

Ahmed, K.M., Hoque, M., Hasan, M.K., Ravenscroft, P., Chowdhury, L.R., 1998. Occurrence and origin of water well CH_4 gas in Bangladesh. J. Geol. Soc. India 51, 697–708.

AIP/PHED, 1991. National drinking water mission submission project on arsenic pollution in groundwater in West Bengal. Final report, Steering Committee, Arsenic Investigation Project (AIP) and Public Health Engineering Directorate, Government of West Bengal, India, 58 p.

AIP/PHED, 1995. Prospective plan for arsenic affected districts of West Bengal. Arsenic Investigation Project (AIP) and Public Health Engineering Directorate (PHED), Government of West Bengal, Calcutta, India.

Alam, M., 1989. Geology and depositional history of Cenozoic sediments of the Bengal Basin of Bangladesh. Palaeogeogr. Palaeoclimatol. Palaeoecol. 69, 125–139.

Alam, M., 1997. Bangladesh. In: Moores, E.M., Fairbridge, R.W. (Eds.), Encyclopedia of European and Asian Regional Geology. Chapman & Hall, London, pp. 64–72.

Alam, M.M.K., Hassan, A.K.M.S., Khan, M.R., Whitney, J.W., 1990. Geological map of Bangladesh. Geol. Surv. Bangladesh.

Alam, M., Alam, M.M., Curray, J.R., Chowdhury, M.L.R., Gani, M.R., 2003. An overview of the sedimentary geology of the Bengal basin in relation to the regional tectonic framework and basin-fill history. Sediment. Geol. 155, 179–208.

Allison, M.A., 1998. Geologic framework and environmental status of the Ganges–Brahmaputra delta. J. Coastal Res. 14 (3), 826–836.

Allison, M.A., Khan, S.R., Goodbred, S.L., Kuehl, S.A., 2003. Stratigraphic evolution of the late Holocene Ganges–Brahmaputra lower delta plain. Sediment. Geol. 155, 317–342.

Ananthakrishnan, R., 1977. Some aspects of the monsoon circulation and monsoon rainfall. In: Krishnamurti, T.N. (Ed.), Monsoon Dynamics. Birkhauses-Verlag, Basel and Stuttgart.

Aswathanarayana, U., 1995. Geoenvironment: An Introduction. A.A. Balkema, Rotterdam. 270 p..
Bagchi, K., 1944. The Ganges Delta. University of Calcutta Press, Calcutta. 157 p..
Ball, F., 1877. Geology of the Rajmahal hills. Geol. Surv. Ind. Mem. 13, 1–94.
Banerjee, R.K., 1981. Cretaceous-Eocene sedimentation, tectonism and biofacies in the Bengal Basin, India. Palaeogeogr. Palaeoclimatol. Palaeoecol. 34, 57–85.
Banerjee, M., Sen, P.K., 1987. Palaeobiology in understanding the change in sea level and the coast line in Bengal basin during Holocene period. Indian J. Earth Sci. 14, 307–320.
Barui, N.C., Chanda, S., 1992. Late Quaternary pollen analysis in relation to palaeoecology, biostratigraphy and dating of Calcutta peat. Proc. Indian Natl. Sci. Acad. B54 (4), 191–200.
Basu, A.R., Jacobsen, S.B., Poreda, R.J., Dowling, C.B., Aggarwal, P.K., 2001. Large groundwater strontium flux to the oceans from the Bengal Basin and marine strontium isotope record. Science 293, 1470–1473.
Baumler, R., Zech, W., 1994. Soils of the high mountain region of Eastern Nepal: classification, distribution and soil forming processes. Catena 22, 85–103.
BGS/DPHE/MML, 1999. Groundwater studies for arsenic contamination in Bangladesh, Phase I: Rapid investigation phase. Department of Public Health Engineering, Government of Bangladesh, British Geological Survey and Mott MacDonald Ltd., UK.
BGS/DPHE, 2001. Arsenic contamination of groundwater in Bangladesh, vol. 2: final report. In: Kinniburgh, D.G., Smedley, P.L. (Eds.), British Geological Survey (BGS) Technical Report WC/00/19, Keyworth, 255 p.
Bhattacharya, P., Chatterjee, D., Jacks, G., 1997. Occurrence of arsenic-contaminated groundwater in alluvial aquifers from the Bengal Delta Plain, Eastern India: options for a safe drinking water supply. Water Resour. Dev. 13, 79–92.
Bhattacharya, P., Jacks, G., Ahmed, K.M., Khan, A.A., Routh, J., 2002. Arsenic in groundwater of the Bengal Delta Plain aquifers in Bangladesh. Bull. Environ. Contam. Toxicol. 69, 538–545.
Biswas, B., 1963. Results of exploration for petroleum in the western part of Bengal basin, India. Proc. Symp. Dev. Petrol. Res., Miner. Resour. Div. Serv. 18 (1), 241–250.
Biswas, S. 1991. Seismicity, earthquakes mechanism, tectonics and stress distribution in the Himalaya, Tibet, Burmese Arc and the Andaman Sea. Unpublished Ph.D. Thesis, Jadavpur University, Calcutta, 228 pp.
Biswas, S., Das Gupta, A., 1989. Distribution of stresses in the Himalayan and the Burmese Arcs. Gerlands Beitr. Geophys. 98, 223–239.
Biswas, S., Majumdar, R.K., 1997. Seismicity and tectonics of the Bay of Bengal: evidence for intraplate deformation of the northern Indian plate. Tectonophysics 269, 323–336.
Biswas, S., Majumdar, R.K., Das Gupta, A., 1992. Distribution of stress axes orientation in the Andaman-Nicobar island region: a possible stress model and its significance for extensional tectonics of the Andaman Sea. Phys. Earth Planet. Inter. 70 (1–2), 57–63.
Blanchon, P., Shaw, J., 1995. Reef drowning during the last deglaciation: evidence from catastrophic sea-level rise and ice sheet collapse. Geology 23 (1), 4–8.
BOGMC, 1986. The oil and gas seismic exploration project. The 'Hinge Zone' survey, Western Bangladesh. Interpretation Report, 1, 114 p.
Brammer, H., 1990a. Floods in Bangladesh. I. Geographical background to the 1987 and 1988 floods. Geograph. J. 156, 12–22.
Brammer, H., 1990b. Floods in Bangladesh. II. Flood mitigation and environmental aspects. Geograph. J. 156, 158–165.
Brammer, H., 1996. The Geography of Soils of Bangladesh. University Press Ltd., Dhaka. 287 p..
Burbank, D.W., 1992. Causes of recent Himalayan uplift deduced from deposited patterns in the Ganges basin. Nature 357, 680–683.
CGWB, 1994. Hydrogeological atlas of West Bengal, Scale 1:2,000,000. Central Ground Water Board (CGWB), Eastern Region, Government of India.
CGWB, 1997. High arsenic groundwater in West Bengal. Technical Report, series D, Central Ground Water Board (CGWB), Eastern Region, Calcutta, Government of India.
CGWB, 1999. High incidence of arsenic in groundwater in West Bengal. Central Ground Water Board, Ministry of Water Resources, Government of India.
Chowdhury, M.I., Hoque, M., Pramanik, A.H., 1985. Morphology and origin of swatch of no ground, Bay of Bengal. J. Natl. Oceanogr. Mar. Inst. 2, 19–29.
Coleman, J.M., 1969. Brahmaputra river: channel processes and sedimentation. Sediment. Geol. 3, 129–139.
Coleman, J.M., 1981. Deltas: Processes of Deposition and Models of Exploration, second ed. Burgess, Minneapolis.
Curray, J.R., Emmel, F.J., Moore, D.G., Raitt, R.W., 1982. Structure, tectonics and geological history of northern Indian Ocean. In: Nairn, A.E., Stehli, F.G. (Eds.), The Ocean Basins and Margins. Plenum, New York, pp. 107–112.
Curtis, S.J., 1933. Working Plan for the Forests of the Sunderbans Division, vol. 1. Bengal Government Press, Calcutta. parts 1 and 2, 7–22.
Dansgaard, W., 1964. Stable isotopes in precipitation. Tellus 16, 436–467.
Dasgupta, S., Nandy, D.R., 1995. Geological framework of the Indo-Burmese convergent margin with special reference to ophiolitic emplacement. Indian J. Geol. 67 (2), 110–125.
Datta, D.K., Subramanian, V., 1997a. Textures and mineralogy of sediments from the Ganges–Brahmaputra–Meghna river system in the Bengal basin, Bangladesh and their environmental implications. Environ. Geol. 30 (3), 181–188.
Datta, D.K., Subramanian, V., 1997b. Nature of solute loads in the rivers of the Bengal drainage basin, Bangladesh. J. Hydrol. 198, 196–208.
Datta, D.K., Gupta, L.P., Subramanian, V., 1999. Distribution of C, N, and P in the sediments of the Ganges–Brahmaputra–Meghna river system in the Bengal basin. Org. Geochem. 30, 75–82.
Datta, D.K., Gupta, L.P., Subramanian, V., 2000. Dissolved fluoride in the lower Ganges–Brahmaputra–Meghna system in the Bengal Basin, Bangladesh. Environ. Geol. 39 (10), 1163–1168.
Davies, J., Exley, C., 1992. Short term BGS pilot project to assess the "hydrochemical character of the main aquifers units of Central and North-eastern Bangladesh and possible toxicity of groundwater to fish and humans". Final report, British Geological Survey Technical Report WD/92/43R.
Derry, L.A., France-Lanord, C., 1996. Neogene Himalayan weathering history and river $^{87}Sr/^{86}Sr$: impact on the marine Sr record. Earth Planet. Sci. Lett. 142, 59–74.
Dowling, C.B., Poreda, R.J., Basu, A.R., Peters, S.L., 2002. Geochemical study of arsenic release mechanisms in the Bengal basin groundwater. Water Resour. Res. 38 (9), 1173–1191.
Dowling, C.B., Poreda, R.J., Basu, A.R., 2003. The groundwater geochemistry of the Bengal basin: weathering, chemosorption, and trace metal flux to the oceans. Geochim. Cosmochim. Acta 67, 2117–2136.
Dray, M., 1983. Contribution of isotopic techniques in the determination of the relationship of surface water/groundwater in Bangladesh (Ganges and Brahmaputra area). In: Proceedings of National Symposium on River Basin Development. Dacca, Bangladesh, pp. 158–170.
East, E.H., 1818. Abstract of an account, containing the particulars of a boring made near the river Hooghly, in the vicinity of Calcutta, from May to July 1814 inclusive in research of a spring of pure water. Asiatik Res. 12, 544–547.
Evans, P., 1964. The tectonic framework of Assam. J. Geol. Soc. Ind. 5, 80–96.
Fairbanks, R.G., 1989. A 17,000 glacio-eustatic sea-level record: influence of glacial melting rates on the Younger Dryas event and deep ocean circulation. Nature 342, 637–642.
Fergusson, J., 1863. On recent changes in the delta of the Ganges. Quarterly J. Geol. Soc. London 19, 321–354.
Folk, R.L., Ward, W.C., 1957. Brazos river bar: a study in the significance of grain size parameters. J. Sed. Petrol. 22, 125–145.
France-Lanord, C., Derry, L., Michard, A., 1993. Evolution of the Himalayas since Miocene time: isotopic and sedimentological evidence from the Bengal Fan. In: Treloar, P.J., Searle, M.P. (Eds.), Himalayan Tectonics, vol. 74. Geological Society Special Publication, pp. 603–621.
Galy, A., France-Lanord, C., 1999. Weathering processes in the Ganges–Brahmaputra basin and the riverine alkalinity budget. Chem. Geol. 159, 31–60.
Gani, M.R., Alam, M.M., 1999. Trench-slope controlled deep-sea clastics in the exposed lower Surma group in the southeastern fold belt of the Bengal Basin, Bangladesh. Sed. Geol. 127, 221–236.
Garrels, R.M., 1967. Genesis of some ground waters from igneous rocks. In: Abelson, P.H. (Ed.), Researches in Geochemistry. John Wiley & Sons, New York, pp. 405–421.
Gasse, F., Arnold, M., Fontes, J.C., Fort, M., Bingyan, L., Quinsang, Z., 1991. A 13,000 year record from western Tibet. Nature 353, 742–745.
Gavrieli, I., Zheng, Y., van Geen, A., Stute, M., Dhar, R., Ahmed, K.M., Simpson, J., Goldstein, S.L., 2000. Hydrogeochemical study of arsenic contamination in Bangladesh groundwater–role of redox condition. J. Conf. Abstract 5, 435.
Ghosh, A.R., Mukherjee, A., 2002. Arsenic contamination of groundwater and human health impacts in Burdwan District, West Bengal, India. Geol. Soc. Am. Abstracts with Programs 34 (2), 107.
Goodbred, S.L., Kuehl, S.A., 2000. The significance of large sediment supply, active tectonism, and eustasy of margin sequence development: Late Quaternary stratigraphy and evolution of the Ganges–Brahmaputra delta. Sed. Geol. 133, 227–248.
Goodbred, S.L., Kuehl, S.A., Steckler, M.S., Sarkar, M.H., 2003. Controls on facies distribution and stratigraphic preservation in the Ganges–Brahmaputra delta sequence. Sed. Geol. 155, 301–316.
Goswami, D.C., 1985. Brahmaputra river, Assam, India: physiography, basin denudation and channel aggradation. Water Resour. Res. 21 (7), 959–978.
Griffin, J.J., Windhom, H., Goldberg, E.D., 1968. The distribution of clay minerals in the world ocean. Deep Sea Research 15, 433–459.
Grout, H., 1995. Characterisation physique, mineralogique, chimique et signification de la charge particulaire et colloýdale derivieres de la zone subtropicale. Unpublished PhD thesis, Aix-Marseille, France.
Hait, A.K., Das, J.K., Ghosh, S., Ray, A.K., Saha, A.K., Chanda, S., 1996. New dates of Pleisto-Holocene subcrop samples from South Bengal, India. Indian J. Earth Sci. 23 (2), 79–82.
Handa, B.K., 1972, Geochemical characteristics and quality of groundwater in Gangetic West Bengal. Proc. Geohydrology and Geotechniques of the Lower Ganga Basin, IIT Kharagpur, West Bengal, B65–B81.
Harvey, C.F., 2002. Groundwater flow in the Ganges delta. Science 296, 1563.
Harvey, C.F., Swartz, C.H., Badruzzaman, A.B.M., Keon-Blute, N., Yu, W., Ali, M.A., Jay, J., Beckie, R., Niedan, V., Brabander, D., Oates, P.M., Ashfaque, K.N., Islam, S., Hemond, H.F., Ahmed, M.F., 2002. Arsenic mobility and groundwater extraction in Bangladesh. Science 298, 1602–1606.
Harvey, C.F., Swartz, C.H., Badruzzaman, A.B.M., Keon-Blute, N., Yu, W., Ali, M.A., Jay, J., Beckie, R., Niedan, V., Brabander, D., Oates, P.M., Ashfaque, K.N., Islam, S., Hemond, H.F., Ahmed, M.F., 2005. Groundwater arsenic contamination on the Ganges Delta: biogeochemistry, hydrology, human perturbations, and human suffering on a large scale. Compt. Rend. Geosci. 337, 285–296.
Heroy, D.C., Kuehl, S.A., Goodbred, S.L., 2003. Mineralogy of the Ganges and Brahmaputra Rivers: implications for river switching and Late Quaternary climate change. Sed. Geol. 155, 343–359.
Huizing, H.G.J., 1971. A reconnaissance study of the mineralogy of sand fractions from East Pakistan sediments and soils. Geoderma 6, 109–133.
Hunter, W.W., 1875. A Statistical Account of Bengal, vol. 1. Trubner and Co.. pp. 22–34.

Imam, M.B., Shaw, H.F., 1985. The diagenesis of Neogene clastic sediments from Bengal basin, Bangladesh. J. Sed. Petrol. 55, 665–671.
Islam, M.S., Tooley, M.J., 1999. Coastal and sea-level changes during the Holocene in Bangladesh. Quat. Int. 55, 61–75.
Islam, M.N., Uddin, M.N., 2002. Country paper on hydrogeology section. Proc. Int. Workshop on Arsenic Issue in Bangladesh, 23 p.
JICA, 1976. Feasibility Study Report for Jamuna River Bridge Construction Project, vol. VI: Geology and Stone Material. Japan International Cooperation Agency, Kokusai Kogyo Co. Ltd. and Mitsui Mineral Development Engineering Co. Ltd.
JICA, 2002. The study on the ground water development of deep aquifers for safe drinking water supply to arsenic affected areas in western Bangladesh. Draft final report, book 1–3. Japan International Cooperation Agency, Kokusai Kogyo Co. Ltd. and Mitsui Mineral Development Engineering Co. Ltd.
Khan, F.H., 1991. Geology of Bangladesh. The Univ. Press. 207 p.
Klump, S., Kipfer, R., Olaf, A.C., Harvey, C.F., Brennwald, M.S., Khandkar, N.A., Badruzzaman, A.B.M., Hug, S., Imboden, D.M., 2006. Groundwater dynamics and arsenic mobilization in Bangladesh assessed using noble gases and tritium. Environ. Sci. Technol. 40, 243–250.
Krishnamurthy, R.V., Bhattacharya, S.K., 1991. Stable oxygen and hydrogen isotope ratios in shallow groundwater from India and a study of the role of evapotranspiration in the Indian monsoon. In: Taylor, H.P., O'Neil, J.R., Kaplan, I.R. (Eds.), Stable Isotope Geochemistry. A Tribute to Samuel Epstein. Special Publication No. 3, The Geochemical Society, San Antonio, Texas, pp. 187–194.
Kuehl, S.A., Hairu, T.M., Moore, W.S., 1989. Shelf sedimentation off the Ganges–Brahmaputra river system: evidence of sediment bypassing to the Bengal fan. Geology 17, 1132–1135.
Kumar, S., Singh, I.B., 1978. Sedimentological study of Gomti river sediments, Uttar Pradesh, India: example of a river in alluvial plain. Senckenb Marit 10 (6), 145–211.
Lindsay, J.F., Holiday, D.W., Hulbert, A.G., 1991. Sequence stratigraphy and the evolution of the Ganges–Brahmaputra complex. Am. Assoc. Petrol. Geol. Bull. 75, 1233–1254.
Mallick, S., Rajgopal, N.R., 1995. Groundwater development in the arsenic affected alluvial belt of West Bengal–some questions. Curr. Sci. 70, 956–958.
McArthur, J.M., Ravenscroft, P., Safiullah, S., Thirlwall, M.F., 2001. Arsenic in groundwater: testing pollution mechanisms for aquifers in Bangladesh. Water Resour. Res. 37, 109–117.
McArthur, J.M., Banerjee, D.M., Hudson-Edwards, K.A., Mishra, R., Purohit, R., Ravenscroft, P., Cronin, A., Howarth, R.J., Chatterjee, A., Talukder, T., Lowry, D., Houghton, S., Chadha, D., 2004. Natural organic matter in sedimentary basins and its relation to arsenic in anoxic groundwater: the example of West Bengal and its worldwide implications. Appl. Geochem. 19, 1255–1293.
Meade, R.H., Parker, R.S., 1985. Sediments in rivers of the United States. National Water Summary, 1984. U.S. Geol. Surv. Water Sup. Paper 2275, 49–60.
Mehta, B.C., Bhattacharya, M., 2000. Hydrogeochemistry of mobilization of arsenic in groundwater of West Bengal, India. Central Ground Water Board, Calcutta.
Miah, M.M., 1988. Flood in Bangladesh: A hydromorphological study of the 1987 flood. Academic Publishers, Dhaka.
Milliman, J.D., Meade, R.H., 1983. World-wide delivery of river sediments to the oceans. J. Geol. 91, 1–22.
Milliman, J.D., Rutkowski, C., Meybeck, M., 1995., River discharge to sea: a global river index (GLORI). Texel, NIOZ, 125 p.
Monsur, M.H., Paepe, R., 1994. Quaternary stratigraphy of the Modhupur area of the Bengal Basin. Bangladesh. J. Sci. Res., 12.
Morgan, J.P., McIntire, W.G., 1959. Quaternary geology of Bengal Basin, East Pakistan and India. Geol. Soc. Am. Bull. 70, 319–342.
Mukherjee, A., 2006. Deeper groundwater chemistry and flow in the arsenic affected western Bengal basin, West Bengal, India. Unpublished Ph.D. dissertation, University of Kentucky, Lexington, 248 p.
Mukherjee, A., Fryar, A.E., 2008. Deeper groundwater chemistry and geochemical modeling of the arsenic affected western Bengal basin, West Bengal, India. Appl. Geochem. 23 (4), 863–892.
Mukherjee, A., Fryar, A.E., Howell, P., 2007a. Regional hydrostratigraphy and groundwater flow modeling of the arsenic contaminated aquifers of the western Bengal basin, West Bengal, India. Hydrogeol. J. 15, 1397–1418.
Mukherjee, A., Fryar, A.E., Rowe, H.D., 2007b. Regional scale stable isotopic signature and recharge of the deep water of the arsenic affected areas of West Bengal, India. J. Hydrol. 334 (1–2), 151–161.
Mukherjee, A., von Brömssen, M., Scanlon, B.R., Bhattacharya, P., Fryar, A.E., Hasan, M.A., Ahmed, K.M., Jacks, G., Chatterjee, D., Sracek, O., 2008. Hydrogeochemical comparison and effects of overlapping redox zones on groundwater arsenic near the western (Bhagirathi sub-basin, India) and eastern (Meghna sub-basin, Bangladesh) of the Bengal basin. J. Cont. Hydrol.. doi:10.1016/j.jconhyd.2007.10.005.
Müller, G., 1979. Schermetalle in den sedimenten des Rhines. Varenderungen seit 1971, Umaschau 79, 778–785.
Nickson, R., McArthur, J.M., Ravenscroft, P., Burgess, W.G., Rahman, M., 1998. Arsenic poisoning of groundwater in Bangladesh. Nature 395, 338.
Nickson, R., McArthur, J.M., Ravenscroft, P., Burgess, W.G., Ahmed, M., 2000. Mechanism of arsenic release to groundwater, Bangladesh and West Bengal. Appl. Geochem. 15, 403–411.
Ollier, C., 1969. Weathering. Oliver & Boyd, Edinburgh.
Potter, P.E., 1978. Petrology and chemistry of modern big river sands. J. Geol. 86, 423–449.
Rao, K.N., 1981. Tropical cyclones of the Indian Seas. In: Arakawa, H., Takahasi, K. (Eds.), World Survey of Climatology, 9. Elsevier, Amsterdam, pp. 257–281.
Ravenscroft, P., 2003. Overview of the hydrogeology of Bangladesh. In: Rahman, A.A., Ravenscroft, P. (Eds.), Groundwater resources and development in Bangladesh. The University Press Ltd., Dhaka, pp. 43–83.
Ravenscroft, P., McArthur, J.M., Hoque, B., 2001. Geochemical and palaeohydrological controls on pollution of groundwater by arsenic. In: Chappell, W.R., Abernathy, C.O., Calderon, R.L. (Eds.), Arsenic Exposure and Health Effects IV. Elsevier Science, Oxford, pp. 53–77.
Ravenscroft, P., Burgess, W.G., Ahmed, K.M., Burren, M., Perrin, J., 2005. Arsenic in groundwater of the Bengal basin, Bangladesh: Distribution, field relations, and hydrogeologic setting. Hydrogeol. J. 13, 727–751.
Ray, A.K., 1999. Chemistry of arsenic and arsenic minerals relevant to contamination of groundwater and soil from subterranean source. Everyman's Science 35 (1).
Rea, D.K., 1992. Delivery of the Himalayan sediments to the Northern Indian Ocean and its relation to global climate, sea-level, uplift and sea water strontium. In: Duncan, R.A. et al. (Eds.), Synthesis of Results from Scientific Drilling in the Indian Ocean. Am. Geophys. Un. Geophysical Monograph 70, pp. 387–402.
Reimann, K.U., 1993. The Geology of Bangladesh. Gebruder Borntraeger, Berlin.
Saha, A.K., 1991. Genesis of arsenic in groundwater in parts of West Bengal. Center for Studies on Man and Environment, Calcutta, annual volume.
Saheed, S.M., 1995. Bangladesh. In: Zink, J.A. (Ed.), Soil Survey: Perspective and Strategies of 21st Century. FAO, Rome, 51-56.
Sarin, M.M., Krisnaswami, S., Dilli, K., Somayajulu, B.L.K., Moore, W.S., 1989. Major ion chemistry of the Ganges–Brahmaputra river system: weathering processes and fluxes to the Bay of Bengal. Geochim. Cosmochim. Acta 54, 1387–1396.
Sen, P.K., Banerjee, M., 1990. Palyno-plankton stratigraphy and environmental changes during the Holocene in the Bengal Basin, India. Rev. Palaeobot. Palynol. 65, 25–35.
Sengupta, S., 1966. Geological and geophysical studies in the western part of the Bengal Basin, India. Am. Assoc. Petrol. Geol. Bull. 50, 1001–1017.
Shivanna, K., Sharma, S., Sinha, U.K., Nair, A.R., Navada, S.V., Ray, A., Talukdar, T., Mehta, B.C., Ghosh, A.K., 1999. Arsenic pollution in ground water of West Bengal. Proc. Workshop on Groundwater Pollution and Its Protection with Special Reference to Arsenic Contamination. Central Ground Water Board, Calcutta.
Sikdar, P.K., Sarkar, S.S., Palchoudhury, S., 2001. Geochemical evolution of groundwater in the Quaternary aquifer of Calcutta and Howrah, India. J. Asian Earth Sci. 19, 579–594.
Smith, R.B., 1841. On the structure of the delta of the Ganges as exhibited by the boring operations in Fort Williams, A.D. 1836–1840. J. Natural. Hist. 1, 324–343.
Smith, A.H., Lingas, E.O., Rahman, M., 2000. Contamination of drinking-water by arsenic in Bangladesh: a public health emergency. Bull. WHO 78 (9), 1093–1103.
Stummeyer, J., Marchig, V., Knabe, W., 2002. The composition of suspended matter from Ganges–Brahmaputra sediment dispersal system during low sediment transport season. Chem. Geol. 185, 125–147.
Swartz, C.H., Blute, N.K., Badruzzaman, B., Ali, A., Brabander, D., Jay, J., Besancon, J., Islam, S., Hemond, H.F., Harvey, C.F., 2004. Mobility of arsenic in a Bangladesh aquifer: Inferences from geochemical profiles, leaching data, and mineralogical characterization. Geochim. Cosmochim. Acta 66, 4539–4557.
SWID, 1998. A comprehensive hydrogeological information of Murshidabad district. Geologic Division No. III, State Water Investigation Directorate (SWID), Government of West Bengal, 43 p.
Uddin, M.N., Abdullah, S.K.M., 2003. Quaternary geology and aquifer systems in the Ganges–Brahmaputra–Meghna delta complex, Bangladesh. Proc. South Asian Geol. Cong., 20.
Uddin, A., Lundberg, N., 1998. Unroofing history of the eastern Himalayas and the Indo-Burma ranges: heavy mineral study of Cenozoic sediments from the Bengal Basin, Bangladesh. J. Sed. Res. 68 (3), 465–472.
Uddin, A., Lundberg, N., 1999. A paleo-Brahmaputra? Subsurface lithofacies analysis of Miocene deltaic sediments in the Himalayan–Bengal system, Bangladesh. Sed. Geol. 123, 239–254.
Umitsu, M., 1985. Natural levees and landform evolution in the Bengal lowland. Geograph. Rev. Jap. 58 (2), 149–164.
Umitsu, M., 1987. Late Quaternary sedimentary environment and landform evolution in the Bengal Lowland. Geograph. Rev. Jap. Series B 60, 164–178.
Umitsu, M., 1993. Late Quaternary sedimentary environments and landforms in the Ganges Delta. Sed. Geol. 83, 177–186.
UNDP, 1982. Groundwater survey: The hydrogeological conditions of Bangladesh. UNDP technical report DP/UN/BGD-74-009/1, 113 p.
Vishnu-Mittre, S., Gupta, H.P., 1979. Pollen analytical study of Quaternary deposits in the Bengal Basin. Paleobotanist 19, 297–306.
Wadia, D.N., 1949. Geology of India, 2nd edition. MacMillan and Co., Ltd., London. 460 p.
Wadia, D.N., 1981. Geology of India. Tata McGraw-Hill, New Delhi. 508 p.
Weber, M.E., Wiedicke, M.H., Kudgrass, H.R., Hubsher, C., Erienkeuser, H., 1997. Active growth of Bengal Fan during sea-level rise and highstand. Geology 25, 315–318.
West, W.D., 1949. Geological map of India. Geol. Surv. India Records 81 (1), 222.
Zaher, M.A., Rahman, A., 1980. Prospects and investigations for minerals in the northwestern part of Bangladesh. Petroleum and Mineral Resources of Bangladesh. Seminar and Exhibition, Dhaka, pp. 9–18.
Zheng, Y., 2006. The heterogeneity of arsenic in the crust: a linkage to occurrence in groundwater. Geol. Soc. Am. Abst. Progr. 38 (7), 179.
Zheng, Y., Stute, M., van Geen, A., Gavrieli, I., Dhar, R., Simpson, H.J., Schlosser, P., Ahmed, K.M., 2004. Redox control of arsenic mobilization in Bangladesh groundwater. Appl. Geochem. 19, 201–214.

Annex B76

T. Islam and Richard E. Peterson, "Climatology of landfalling tropical cyclones in Bangladesh 1877-2003", *Natural Hazards,* Vol. 48, No. 1 (2009), at pp. 115-16.

Nat Hazards (2009) 48:115–135
DOI 10.1007/s11069-008-9252-4

ORIGINAL PAPER

Climatology of landfalling tropical cyclones in Bangladesh 1877–2003

Tanveerul Islam · Richard E. Peterson

Received: 7 May 2007 / Accepted: 8 May 2008 / Published online: 30 May 2008

Abstract Bangladesh is highly susceptible to tropical cyclones. Unfortunately, there is a dearth of climatological studies on the tropical cyclones of Bangladesh. The Global Tropical Cyclone Climatic Atlas (GTCCA) lists historical storm track information for all the seven tropical cyclone ocean basins including the North Indian Ocean. Using GIS, tropical cyclones that made landfall in Bangladesh during 1877–2003 are identified and examined from the climatological perspective. For the convenience of study, the coast of Bangladesh is divided into five segments and comparisons are made among the coastal segments in terms of cyclone landfall and vulnerability. There is a large variability in the year-to-year occurrence of landfalling tropical cyclones in Bangladesh. Most of the tropical cyclones (70%) hit in the months of May–June and October–November generally show the well-known pattern of pre- and post-monsoon cyclone seasons in that region.

Keywords Tropical cyclones · Climatology · Landfall · Bay of Bengal · Bangladesh coast

1 Introduction

Tropical cyclones generally occur over some parts of tropical oceans in latitudes between 10° and 30° both sides of the equator, and they become severe when they are located between 20° and 30° latitude (Holmes 2001). Bangladesh lies between 20°34′ N and 26°38′ N latitude, and with a 440-mile long coastline is highly vulnerable to tropical cyclones and associated storm surges. In the past century, two of the world's deadliest tropical cyclones occurred in Bangladesh in 1970 and in 1991, killed about 300,000 and 140,000 people, respectively. In Bangladesh, even storms with low intensity can be very

T. Islam (✉)
Center for Texas Beaches & Shores, Texas A&M University-Galveston,
7400 Jones Dr. #3033, Galveston, TX 77551, USA
e-mail: islamt@tamug.edu

R. E. Peterson
Atmospheric Sciences Group, Texas Tech University, Lubbock, TX, USA

deadly at landfall because of the shallow bathymetry of the Bay of Bengal, funneling shape of the coastline with low-lying flat terrain, and very high population density (Ali 1979). Lack of effective early warning systems and poor housing conditions are also responsible for causing more damage during windstorms.

There have been numerous studies carried out on the Bay of Bengal cyclones, but only a few of them have focused on the Bangladesh coast in particular. Lot of modeling work on storm surges, e.g., Dube et al. (2004) is carried out for the Heady Bay region. Previously, climatological analyses on the Bay of Bengal cyclones are done by Rai Sircar (1956), Raghavendra (1973), Mooley (1980), and Mooley and Mohile (1983). In recent times, Alam et al. (2003) have done work on the frequency of landfalling Bay of Bengal cyclones with data from 1974 to 1999. The most comprehensive study on the landfalling Bay of Bengal cyclones has been done by the SAARC Meteorological Research Center (SMRC). In its study, the coast of Bangladesh is divided into four segments, where landfall locations are assigned for 82 cyclonic storms from 1582 to 1997 (Shrestha 1998). Tropical depressions are not included, which should be very important in terms of the Bangladesh coast. In most of the studies including the SMRC publication, landfall locations are assumed based on different sources such as newspapers and not judged from the actual storm track information.

This study aims to provide a comprehensive and reliable dataset on the landfalling tropical cyclones of Bangladesh with a climatological analysis for a 127-year period (1877–2003). Historical storm tracks for all the landfalling tropical cyclones in Bangladesh are shown including the tropical depressions.

2 Data sources

The hourly latitude/longitude storm track information is obtained from the Global Tropical Cyclone Climatic Atlas (GTCCA Version 1.0 and 2.0), which is prepared by the Fleet Numerical Meteorology and Oceanography Center (FNMOC). The database of GTCCA is a compilation of two historical digital tape deck data files (TD-9636 and TD-9697) archived at the National Climatic Data Center (NCDC), a Joint Typhoon Warning Center (JTWC) historical data file from Guam, and data forwarded to NCDC by the Regional and Specialized Meteorological Centers (RSMC) participating in the World Meteorological Organization's (WMO) Tropical Cyclone Program (FNMOC 1998). These data are validated by the hurricane database of the Unisys Corporation, which also uses the same JTWC source.

The Center for Research on the Epidemiology of Disasters (CRED), based in Belgium, has an online international disaster database, from which casualty and other damage records are collected.

3 Study area

In order to assign cyclone landfall locations, the coast of Bangladesh is divided into five segments following the old district lines. These are Khulna, Barisal, Noakhali, Chittagong, and Cox's Bazar (Fig. 1). The green area along the Khulna coast is the Bangladesh portion of the Sundarbans, which is the largest mangrove forest in the world.

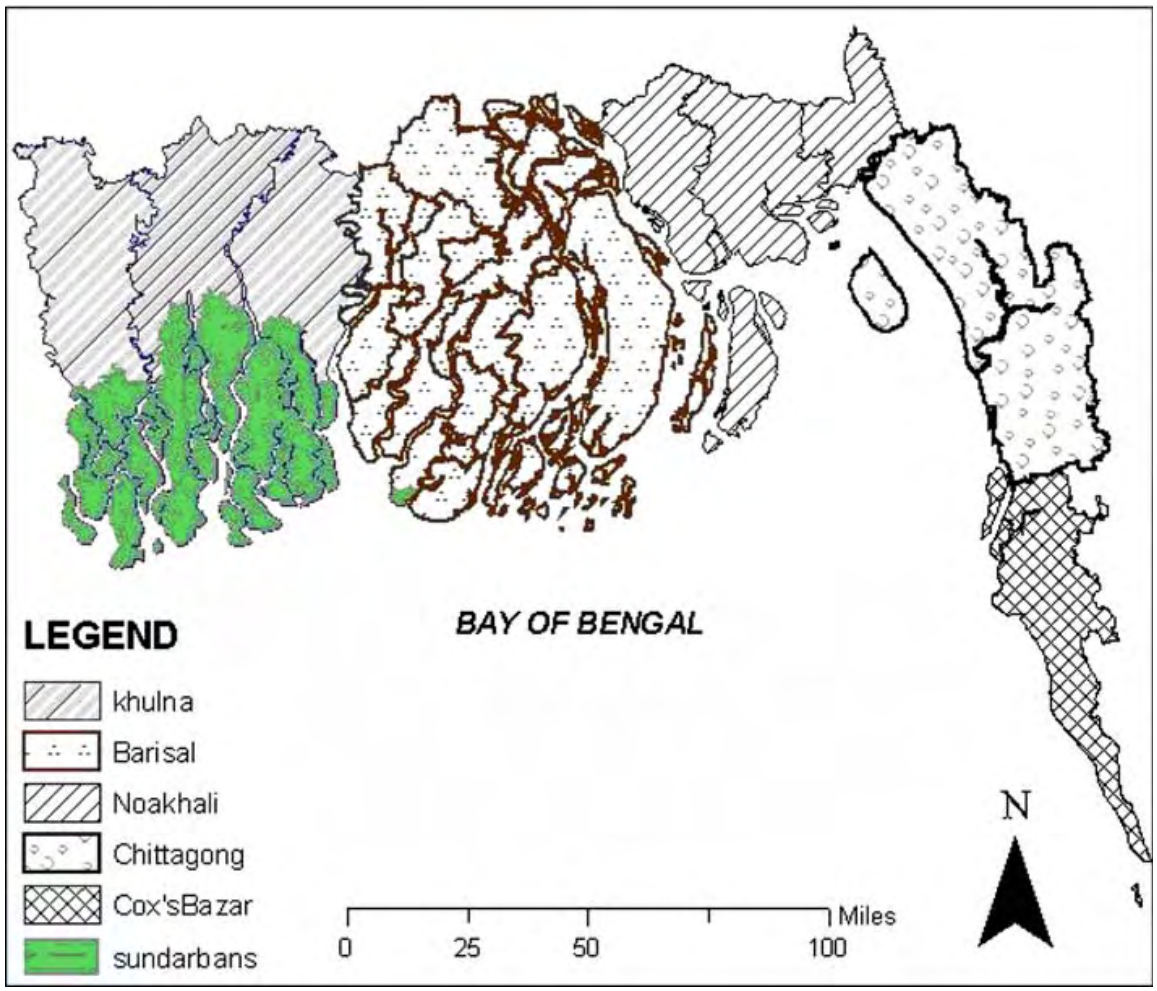

Fig. 1 Coast of Bangladesh with subdivisions

4 Organization of data

Tropical cyclones in the GTCCA database are classified by the following criteria (Table 1).

Based on this classification, the number of landfalling cyclones during the period 1877–2003 in Bangladesh is given in Table 2.

In the GTCCA database, for earlier storms many of the dates, positions, and intensities are deduced through estimates and compromise among various reports using synoptic and climatological judgment (FNMOC 1998). Thus, corresponding wind speeds are available only for 32 storms of the total 117 storms that hit during 1877–2003. According to the WMO classification (WMO 1986), these storms can be further categorized as follows (Table 3).

Table 1 GTCCA classification

Type	Category	Wind speed (knots)
Tropical depression	TD	<34
Tropical storm	TS	34–63
Hurricane		≥64

Table 2 Number of landfalling cyclones in Bangladesh (1877–2003)

Type	No. of storms
Tropical depression (TD)	39
Tropical storm (TS)	52
Hurricane	26
Total	117

Table 3 Number of landfalling cyclones in Bangladesh (1877–2003) by the WMO classification (only the storms with available wind speeds are considered)

Category	Wind speed (knots)	No. of storms
1. Low pressure area	<17	–
2. Depression	17–33	–
3. Cyclonic storm	34–47	5
4. Severe cyclonic storm	48–63	11
5. Severe cyclonic storm with a core of hurricane winds	≥64	(11 + 5) = 16
6. Very severe cyclonic storm	64–119	11
7. Super cyclonic storm	≥120	5
Total		32

In this study, the GTCCA classification is used to develop the historical storm dataset and climatology for Bangladesh.

5 Historical storm tracks of Bangladesh (1877–2003)

A list of tropical cyclones with year, month of occurrence, landfall location, wind speed, and category is given in Tables 4–15. For convenience, the list is break down in approximately 10-year period from 1877 to 2003. Corresponding storm tracks are shown in Figs. 2–13.

6 Climatology of landfalling tropical cyclones in Bangladesh (1877–2003)

A total of 117 tropical cyclones hit the coast of Bangladesh from 1877 to 2003 of which 39 are tropical depressions (TD), 52 are tropical storms (TS), and 26 reach hurricane intensity.

In the past century (1901–2000), the rate of tropical storms striking the coast is 10 storms/decade (Fig. 14), or one storm per year. Since 1950, the rate of landfalling tropical storms in this area has increased (Fig. 15), 1.18 per year for 1950–2000. Figure 14 shows that the rate has vacillated in the last century. The first rise is from 1920 up to 1939. The second is from 1959 up to 1969. Presently, there is an increasing trend again.

Based on the Saffir–Simpson Hurricane Scale (Simpson 2003) on potential damage, hurricanes that are found in this study can be further categorized in Table 16.

Based on the classification in Table 16, Fig. 16 shows the percentage of the frequency of major hurricanes during 1877–2003 for which wind speeds are available, i.e., for 16 hurricanes. Exactly half (50%) of the hurricanes are in Category 1, which means the

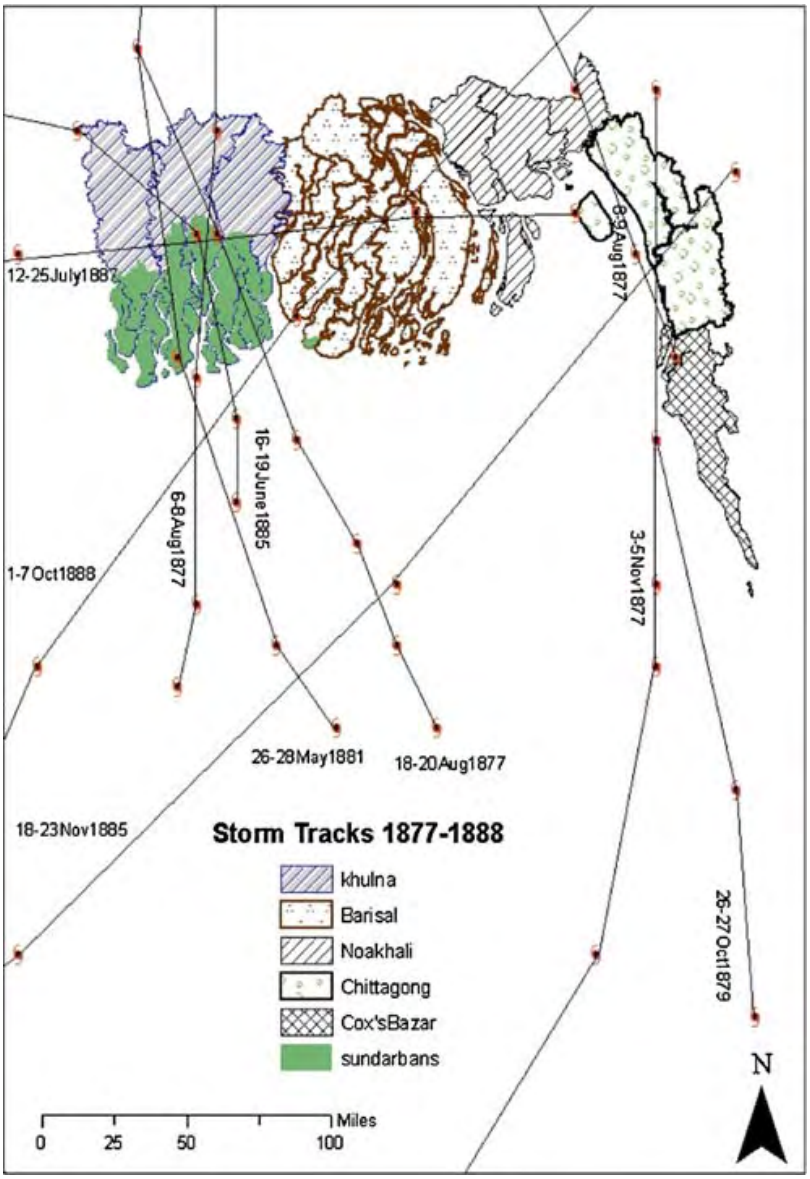

Fig. 2 Storm tracks 1877–1888

Table 4 Storm track information (1877–1888)

SL. no.	Year	No. of landfalling storms	Month of occurrence	Location of landfall	Reached hurricane intensity	Remarks
1	1877	4	6–8 August	Khulna	–	TD
2			8–9 August	Noakhali	–	TD
3			18–20 August	Khulna	–	TD
4			November	Cox's Bazar	–	TD
5	1879	1	October	Chittagong	–	TD
6	1881	1	May	Khulna	–	TD
7	1885	2	June	Khulna	–	TS
8			November	Chittagong	–	TS
9	1887	1	July	Barisal	–	TD
10	1888	1	October	Barisal	–	TS

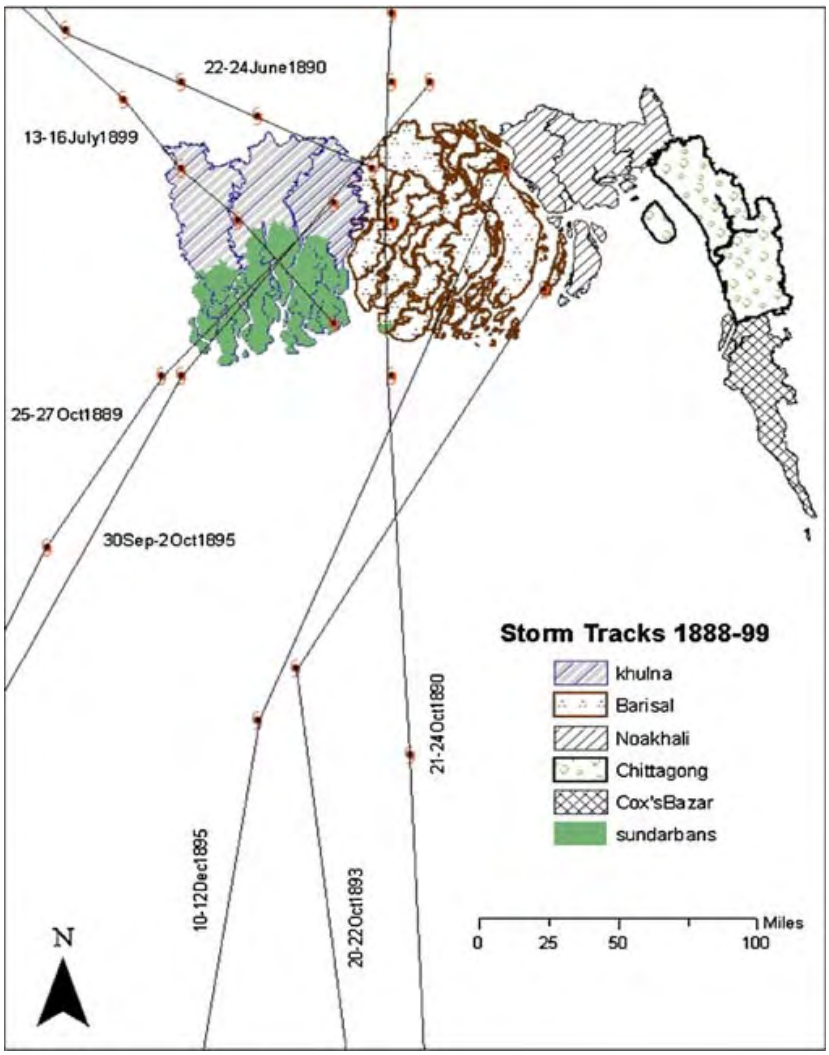

Fig. 3 Storm tracks 1888–1899

Table 5 Storm track information (1888–1899)

SL. no.	Year	No. of landfalling storms	Month of occurrence	Location of landfall	Reached hurricane intensity	Remarks
12	1890	2	June	Khulna	–	TD
13			October	Barisal	–	TS
14	1893	1	October	Barisal	Yes	Wind speed N/A
15	1895	2	September	Khulna	Yes	Wind speed N/A
16			December	Barisal	Yes	Wind speed N/A
17	1899	1	July	Khulna	–	TD

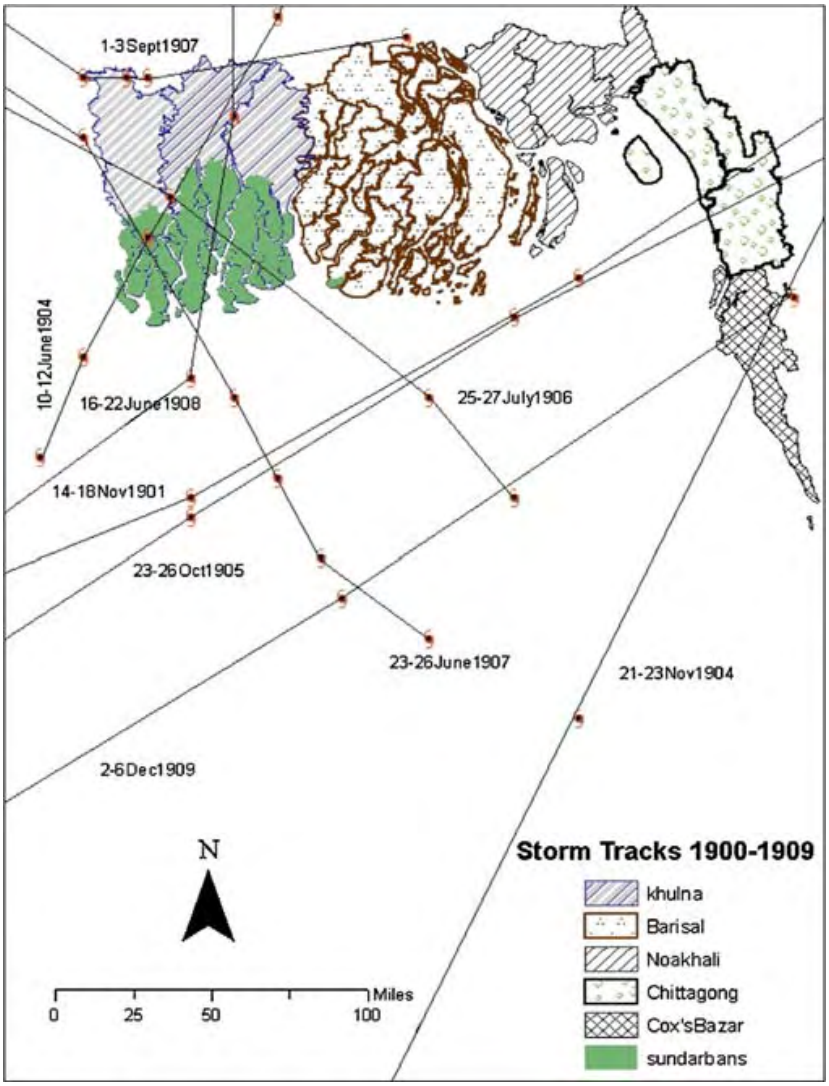

Fig. 4 Storm tracks 1900–1909

Table 6 Storm track information (1900–1909)

SL. no.	Year	No. of landfalling storms	Month of occurrence	Location of landfall	Reached hurricane intensity	Remarks
19	1904	2	June	Khulna	–	TD
20			November	Cox's Bazar	–	TS
21	1905	1	October	Chittagong	–	TS
22	1906	1	July	Khulna	–	TS
23	1907	2	June	Khulna	–	TS
24			September	Barisal	–	TD
25	1908	1	June	Khulna	–	TS
26	1909	1	December	Cox's Bazar	Yes	Wind speed N/A

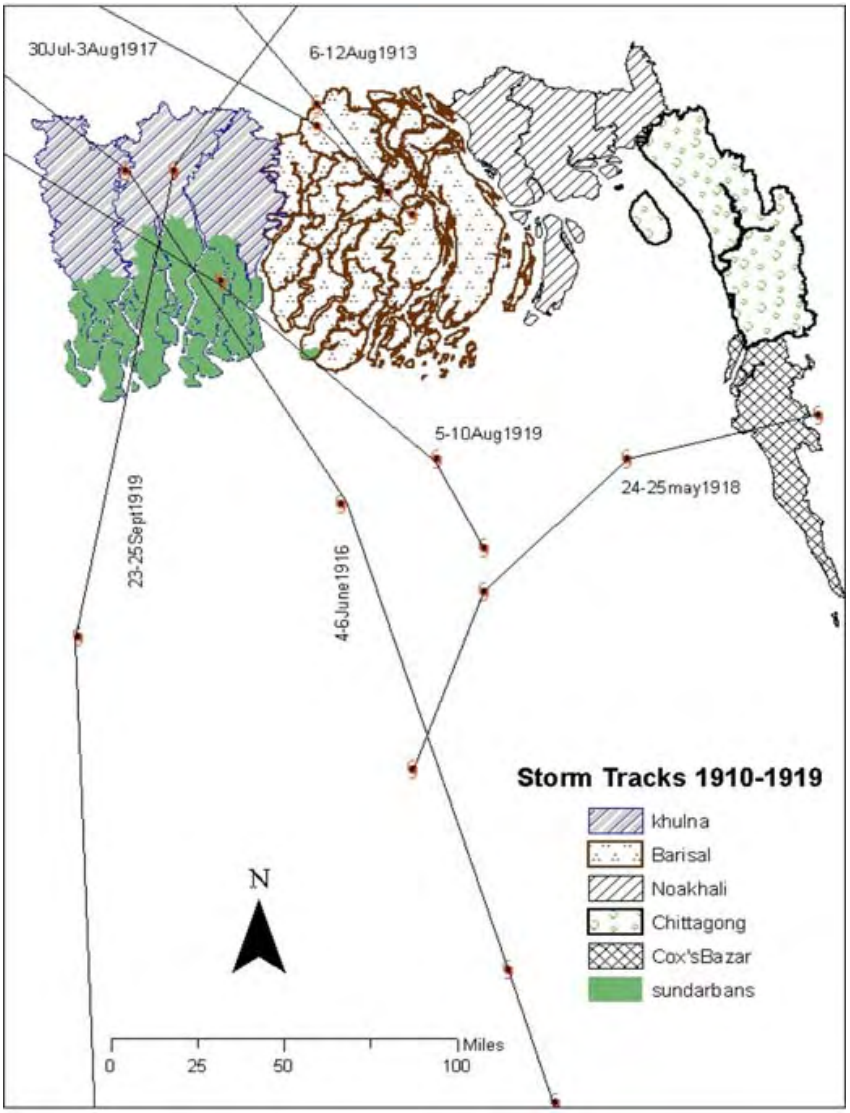

Fig. 5 Storm tracks 1910–1919

Table 7 Storm track information (1910–1919)

SL. no.	Year	No. of landfalling storms	Month of occurrence	Location of landfall	Reached hurricane intensity	Remarks
27	1913	1	August	Barisal	–	TD
28	1916	1	June	Khulna	–	TS
29	1917	1	July	Barisal	–	TD
30	1918	1	May	Cox's Bazar	–	TS
31	1919	2	August	Khulna	–	TD
32			September	Khulna	Yes	Wind speed N/A

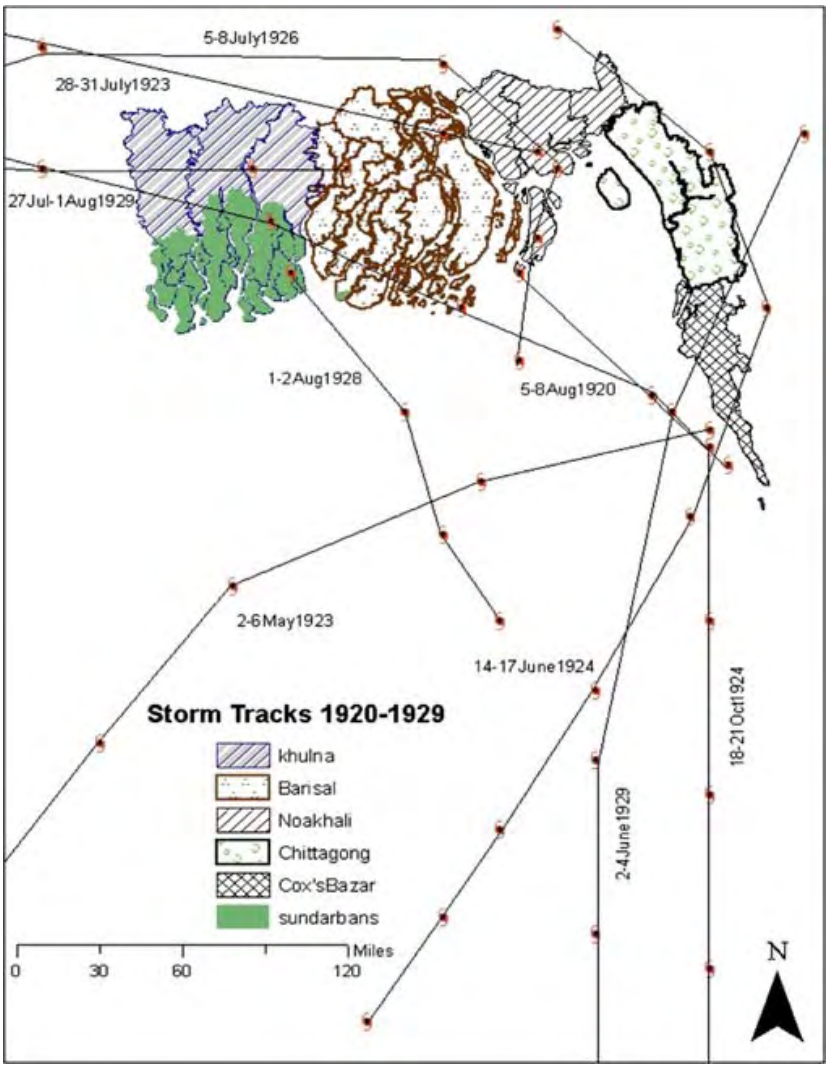

Fig. 6 Storm tracks 1920–1929

Table 8 Storm track information (1920–1929)

SL. no.	Year	No. of landfalling storms	Month of occurrence	Location of landfall	Reached hurricane intensity	Remarks
33	1920	1	August	Barisal	–	TD
34	1923	2	May	Cox's Bazar	Yes	Wind speed N/A
35			July	Barisal	–	TD
36	1924	2	June	Cox's Bazar	–	TS
37			October	Barisal	–	TD
38	1926	1	July	Noakhali	–	TS
39	1928	1	August	Khulna	–	TD
40	1929	2	June	Cox's Bazar	–	TS
41			July	Barisal	–	TD

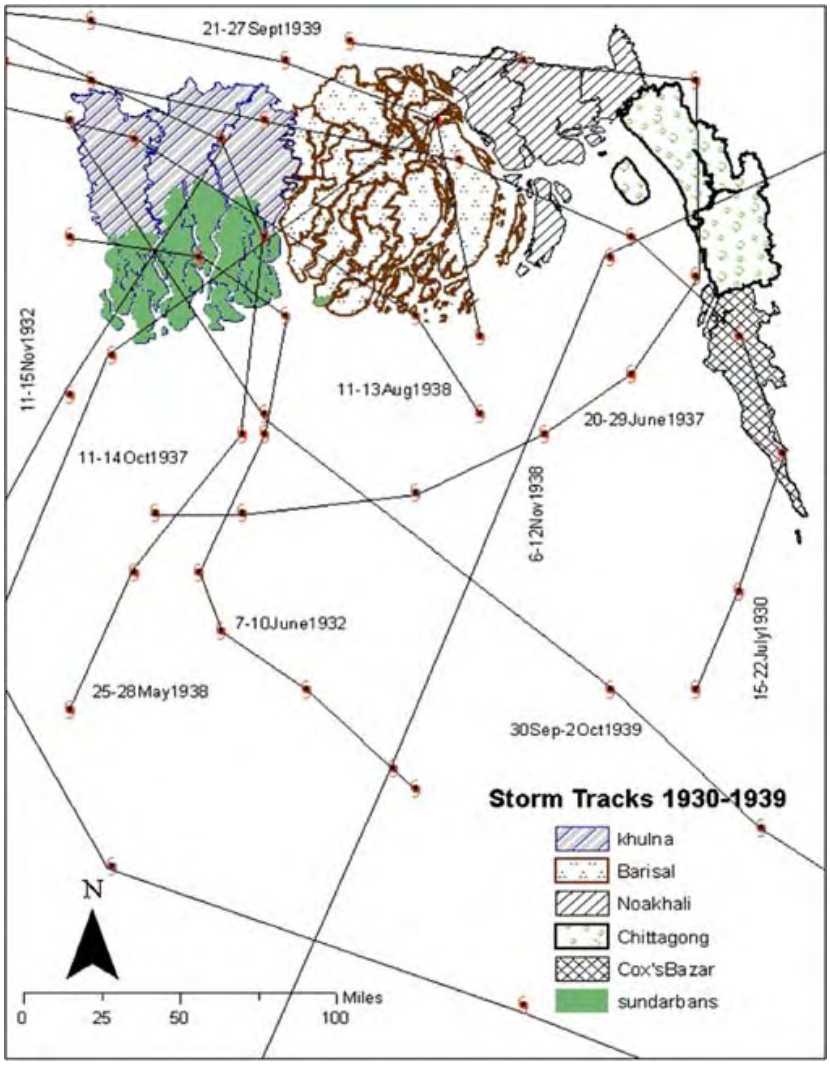

Fig. 7 Storm tracks 1930–1939

Table 9 Storm track information (1930–1939)

SL. no.	Year	No. of landfalling storms	Month of occurrence	Location of landfall	Reached hurricane intensity	Remarks
42	1930	1	July	Cox's Bazar	–	TS
43	1932	2	June	Khulna	–	TD
44			November	Khulna	–	TD
45	1937	2	June	Chittagong	–	TS
46			October	Khulna	–	TS
47	1938	3	May	Khulna	–	TD
48			August	Barisal	–	TD
49			November	Chittagong	Yes	Wind speed N/A
50	1939	2	September	Barisal	–	TD
51			September	Khulna	–	TD

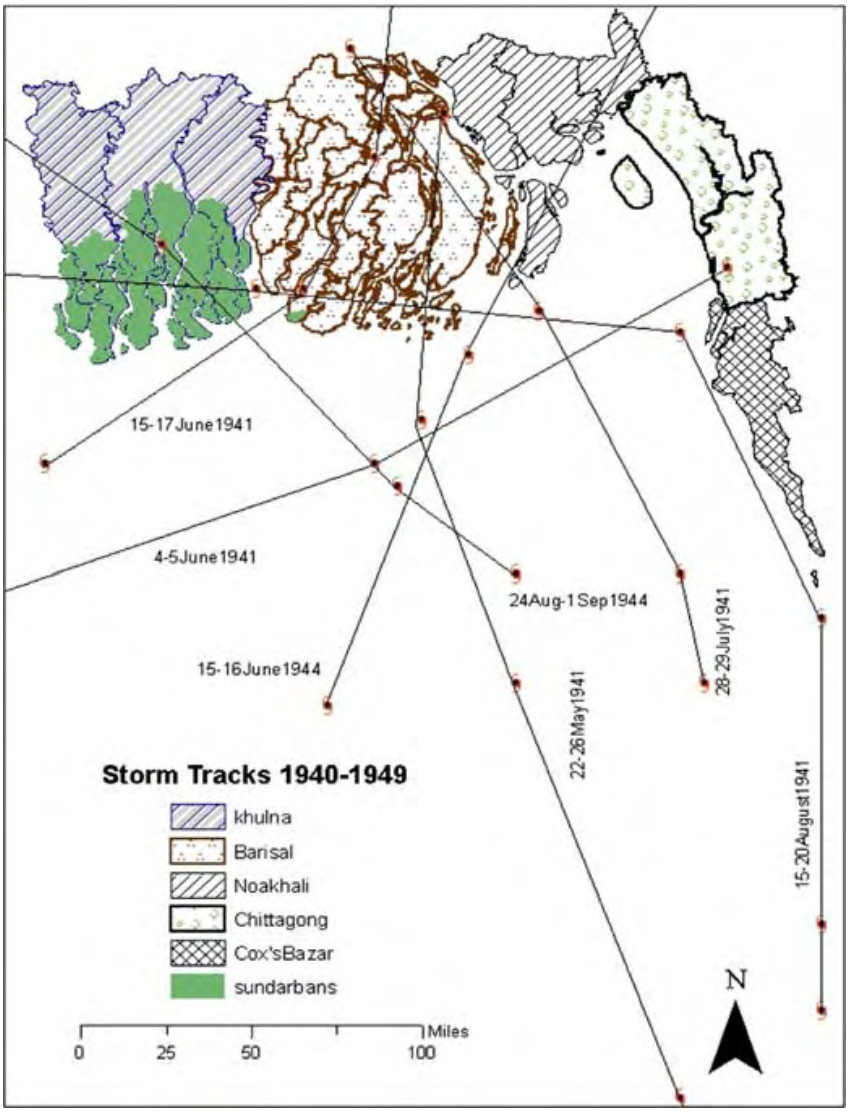

Fig. 8 Storm tracks 1940–1949

Table 10 Storm track information (1940–1949)

SL. no.	Year	No. of landfalling storms	Month of occurrence	Location of landfall	Reached hurricane intensity	Remarks
52	1941	5	May	Barisal	Yes	Wind speed N/A
53			4–5 June	Chittagong	–	TS
54			15–17 June	Barisal	–	TD
55			July	Barisal	–	TD
56			August	Barisal	–	TS
57	1944	2	June	Noakhali	–	TD
58			August	Khulna	–	TD

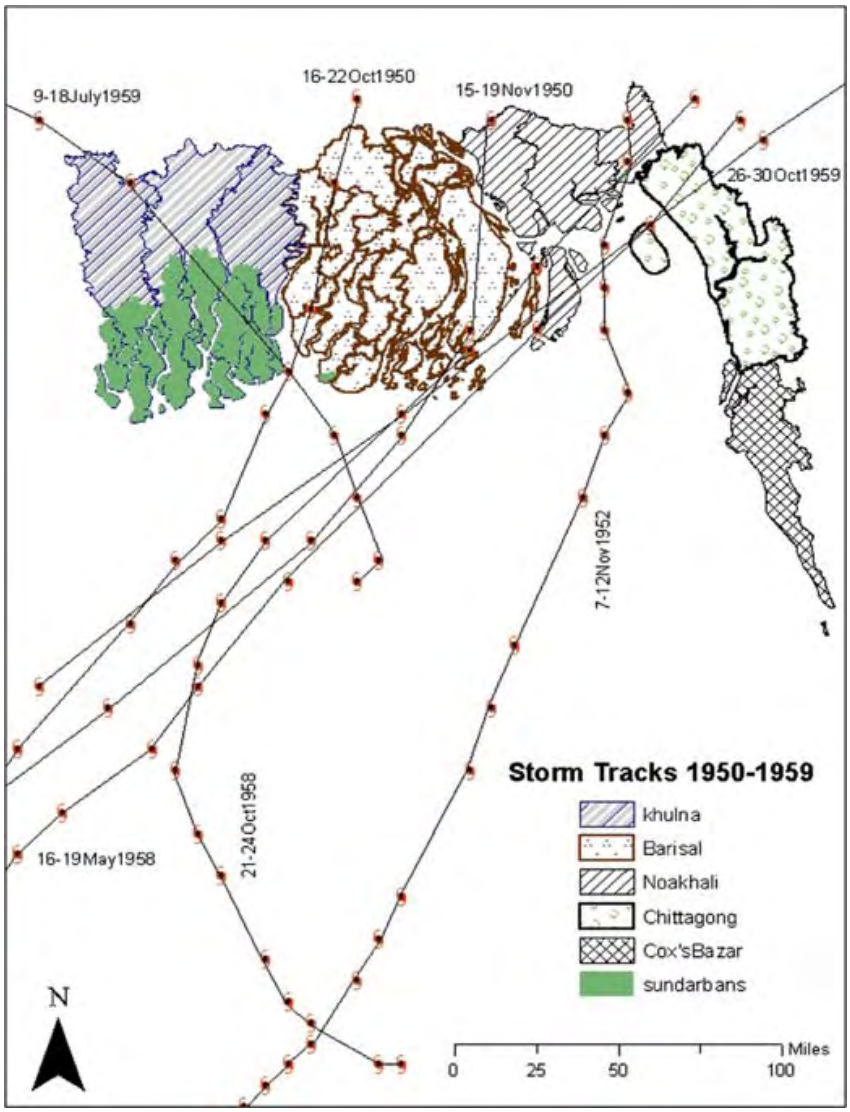

Fig. 9 Storm tracks 1950–1959

Table 11 Storm track information (1950–1959)

SL. no.	Year	No. of landfalling storms	Month of occurrence	Location of landfall	Reached hurricane intensity	Remarks
59	1950	2	October	Barisal	–	TD
60			November	Barisal	–	TS
61	1952	1	November	Noakhali	–	TD
62	1958	2	May	Noakhali	–	TS
63			October	Barisal	–	TD
64	1959	2	July	Khulna	–	TD
65			October	Chittagong	–	TD

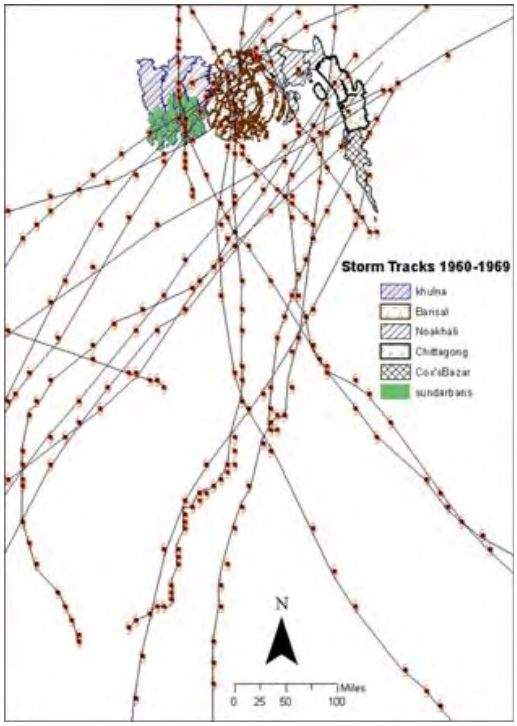

Fig. 10 Storm tracks 1960–1969

Table 12 Storm track information (1960–1969)

SL. no.	Year	No. of landfalling storms	Month of occurrence	Location of landfall	Reached hurricane intensity	Remarks
66[a]	1960	2	7–11 October	Noakhali	Yes	64 kt
67			27–31 October	Chittagong[b]	Yes	83 kt
68	1961	3	4–9 May	Barisal	–	TS (60 kt)
69			27–30 May	Chittagong	–	TS
70			October	Noakhali	–	TD
71	1962	1	October	Chittagong	–	TS
72	1963	2	May	Chittagong	Yes	130 kt
73			October	Khulna	–	TD
74	1964	1	October	Barisal	–	TD
75	1965	4	9–12 May	Khulna	–	TS
76			26–31 May	Barisal	Yes	Wind speed N/A
77			October	Cox's Bazar	–	TD
78			December	Cox's Bazar	Yes	120 kt
79	1966	2	September	Khulna	–	TS (50 kt)
80			December	Chittagong	–	TS
81	1967	2	7–11 October	Barisal	–	TS
82			19–23 October	Cox's Bazar	–	TS
83	1968	1	June	Khulna	–	TD
84	1969	2	June	Chittagong	–	TS
85			October	Khulna	–	TS

[a] Storm track is not shown in Fig. 10 as latitude/longitude coordinates are not available. Landfall location is assumed based on the UNISYS dataset and from the CRED disaster database

[b] Track data from the GTCCA is incomplete and suggests that the storm did not make landfall. But in CRED dataset, deaths, and damages were reported from Chittagong. So, it is assumed that the storm hit the coast of Chittagong

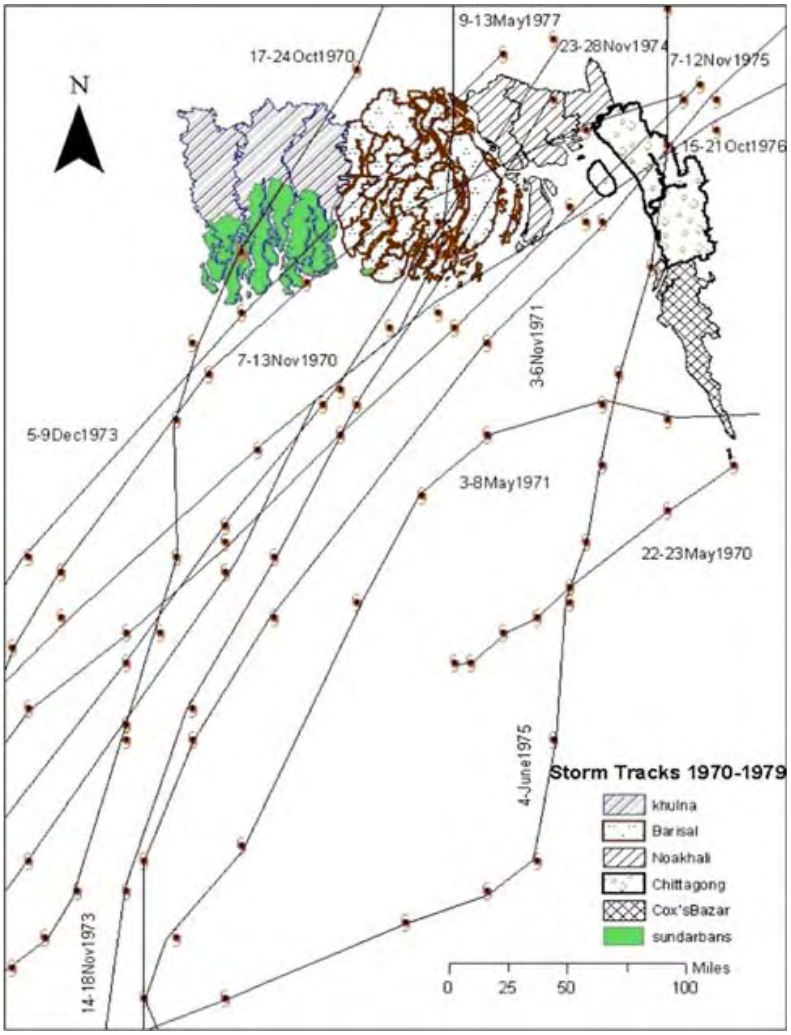

Fig. 11 Storm tracks 1970–1979

Table 13 Storm track information (1970–1979)

SL. no.	Year	No. of landfalling storms	Month of occurrence	Location of landfall	Reached hurricane intensity	Remarks
86	1970	3	May	Cox's Bazar	–	TS
87			October	Khulna	–	TS
88			November	Barisal	Yes	130 kt
89	1971	2	May	Cox's Bazar	–	TS
90			November	Chittagong	Yes	Wind speed N/A
91	1973	2	November	Barisal	–	TS (55 kt)
92			December	Khulna	Yes	70 kt
93	1974	1	November	Barisal	Yes	75 kt
94	1975	2	June	Chittagong	–	TS
95			November	Chittagong	–	TS (50 kt)
96	1976	1	October	Chittagong	–	TS (50 kt)
97	1977	1	May	Barisal	–	TS (60 kt)

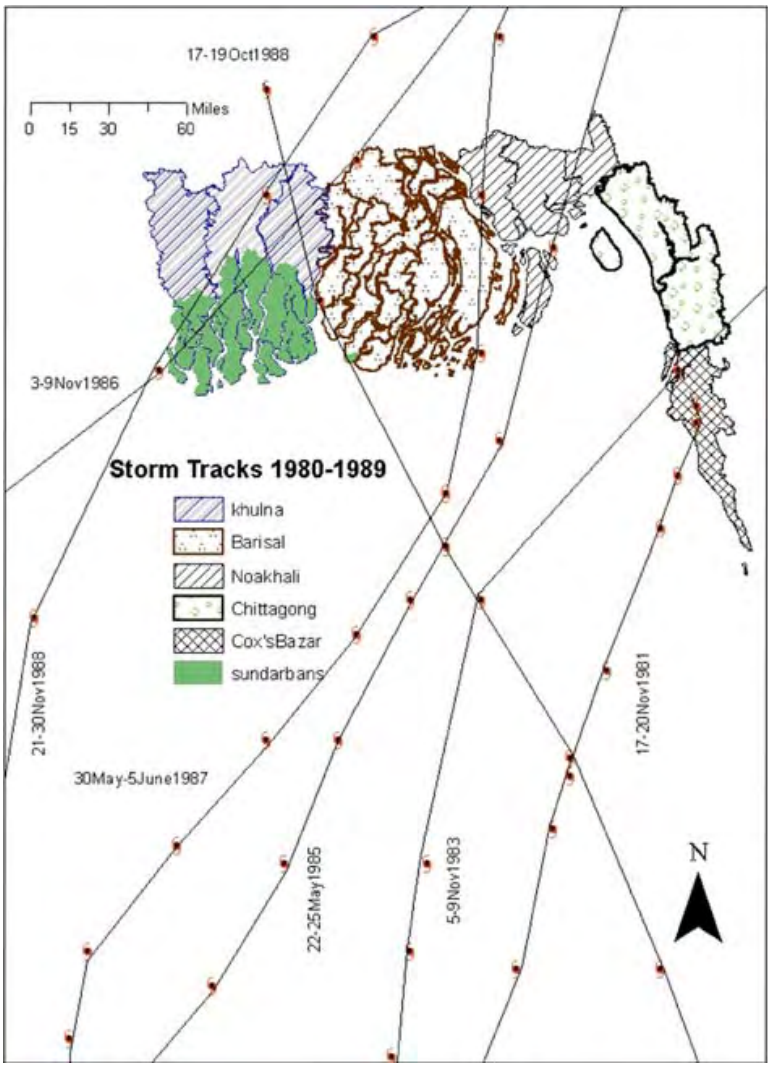

Fig. 12 Storm tracks 1980–1989

Table 14 Storm track information (1980–1989)

SL. no.	Year	No. of landfalling storms	Month of occurrence	Location of landfall	Reached hurricane intensity	Remarks
98	1981	1	November	Cox's Bazar	Yes	75 kt
99	1983	1	November	Cox's Bazar	–	TS (55 kt)
100	1985	1	May	Noakhali	–	TS (60 kt)
101	1986	1	November	Khulna	–	TS (50 kt)
102	1987	1	June	Barisal	–	TS (55 kt)
103	1988	2	October	Khulna	–	TS (35 kt)
104			November	Khulna	Yes	110 kt

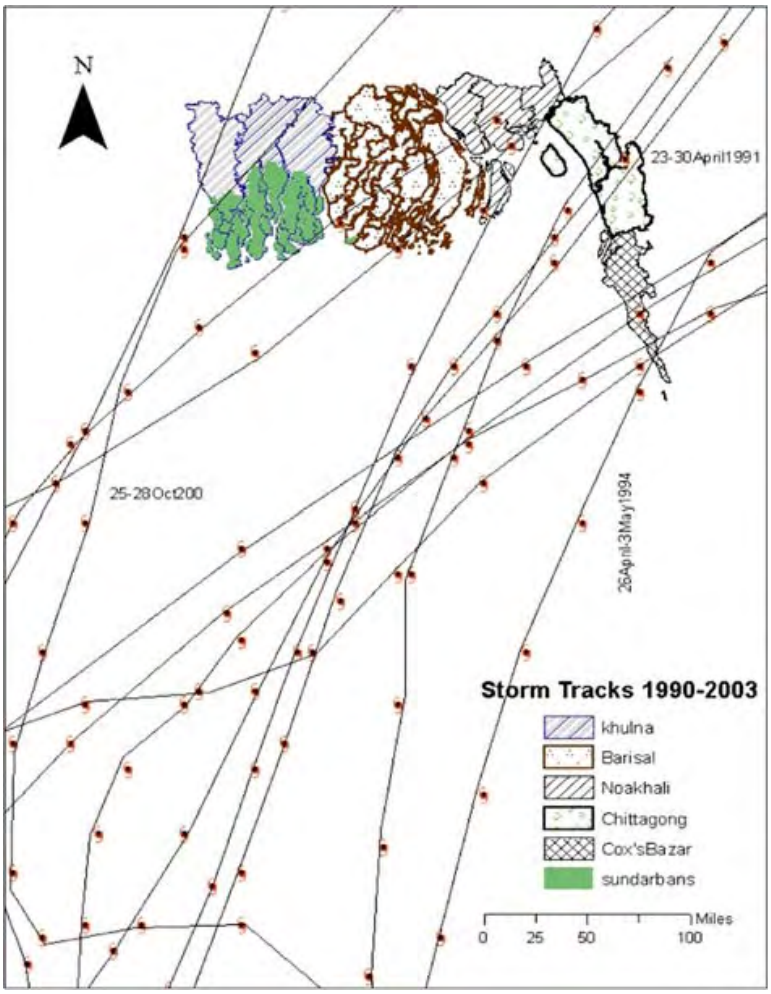

Fig. 13 Storm tracks 1990–2003

Table 15 Storm track information (1990–2003)

SL. no.	Year	No. of landfalling storms	Month of occurrence	Location of landfall	Reached hurricane intensity	Remarks
105	1990	1	December	Cox's Bazar	–	TS (45 kt)
106	1991	2	April	Chittagong	Yes	140 kt
107			May	Noakhali	–	TS (50 kt)
108	1992	1	October	Cox's Bazar	–	TS
109	1994	1	April	Cox's Bazar	Yes	125 kt
110	1995	1	November	Cox's Bazar	Yes	105 kt
111	1996	2	May	Cox's Bazar	–	TS (40 kt)
112			October	Khulna	–	TS (45 kt)
113	1997	2	May	Chittagong	Yes	115 kt
114			September	Barisal	Yes	65 kt
115	1998	2	May	Chittagong	Yes	70 kt
116			November	Khulna	Yes	75 kt
117	2000	1	October	Khulna	–	TS (35 kt)

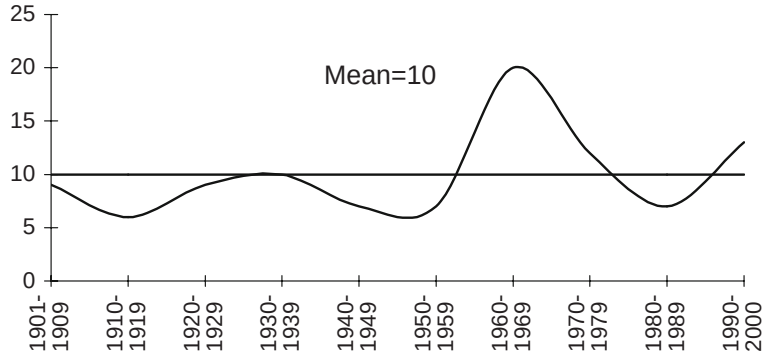

Fig. 14 Frequency of storms in 10-year period from 1901 to 2000

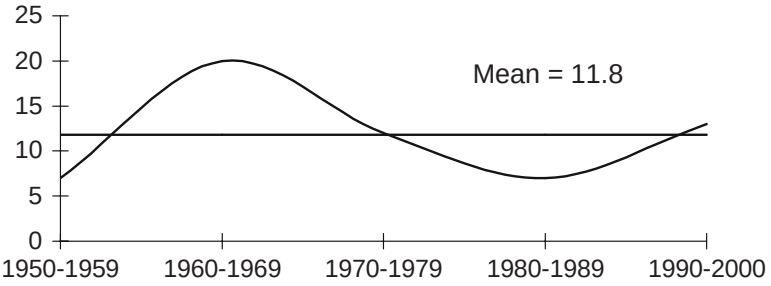

Fig. 15 Frequency of storms in 10-year period from 1950 to 2000

Table 16 Hurricanes by Saffir–Simpson intensity category

Category	Wind speed (knots)	Frequency
1	64–83	8
2	84–96	0
3	97–113	2
4	114–135	5
5	>135	1
	Wind speed not available	10

wind speed range is 64–83 kt according to the Saffir–Simpson Hurricane Scale. The next largest group is Category 4 hurricanes (wind speed 114–135 kt), which is 31% of the major hurricanes. The deadliest tropical cyclone in the world which killed more than 300,000 people in Bangladesh on 12 November 1970 was actually a Category 4 hurricane (130 kt). During 127-year period (1877–2003), only one tropical cyclone (6% of the major hurricanes) is found as a Category 5 hurricane (wind speed > 135 kt). This was the 1991 'Super Cyclone' (140 kt) that hit Bangladesh especially the Chittagong coast and killed 138,866 people (CRED database).

By landfall locations, Khulna coast located to the south-west corner of Bangladesh faced the highest number (36) of tropical cyclones in 1877–2003, which is 31% of the total storms. The next subdivision is Barisal, where 31 storms hit during 1877–2003, which is 26% of the total landfalling storms. Chittagong and Cox's Bazar are very close to each other by the number of hits, 21 and 20, which are 18% and 17%, respectively. The lowest number (9) of tropical cyclones hit the Noakhali coastal segment, which is only 8% of the total storms (Fig. 17).

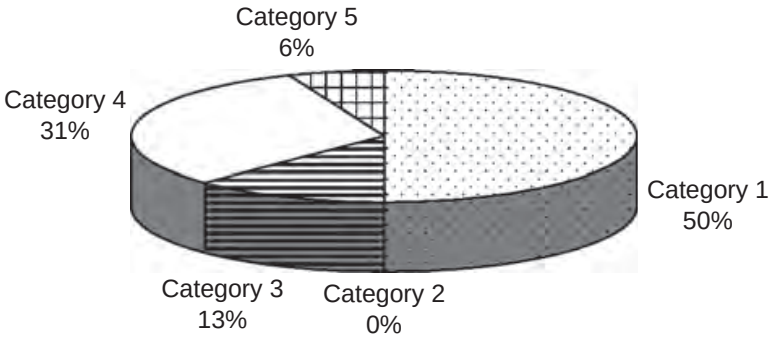

Fig. 16 Frequency distribution of major hurricanes 1877–2003

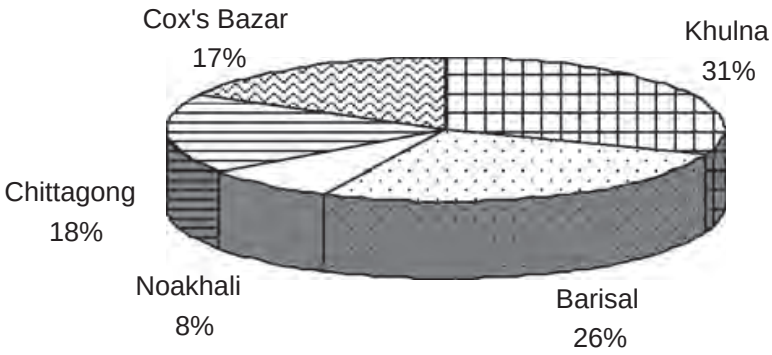

Fig. 17 Percentage of landfalling tropical cyclones in different coastal segments

Table 17 Number of cyclone deaths in Bangladesh 1904–2000

Coastal subdivision	Number of deaths
Khulna	5,267
Barisal	354,326
Noakhali	25,616
Chittagong	157,445
Cox's Bazar	413
Total	543,067

Table 17 shows the total number of deaths from cyclones in the five coastal segments of Bangladesh in 1904–2000. The International Disaster Database of CRED is the primary source of this information.

Barisal and Chittagong subdivisions experienced a large number of deaths compared to the other coastal segments mainly due to the 1970 and 1991 super cyclones. The former hit the Barisal coast and killed 300,000 people; the latter made landfall at Chittagong coast and caused 138,866 deaths. Ironically, Khulna coast experienced fewer deaths compared to its number of cyclone hits. The key mitigating factor is the location of the Sundarbans forest in this segment, which works as a shield against the wind and storm surge during tropical cyclones. Effective land-use is, therefore, very important to the reduction of cyclone damage. Cox's Bazar experienced the lowest number of deaths. Low population density in this segment might be one of the reasons for fewer casualties. A comparative picture of the number of storm hits and the number of cyclone deaths in different coastal segments is shown in Fig. 18 on a logarithmic scale.

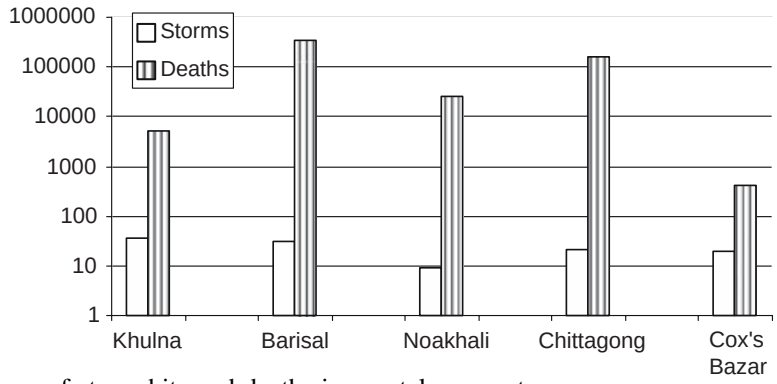

Fig. 18 Comparison of storm hits and deaths in coastal segments

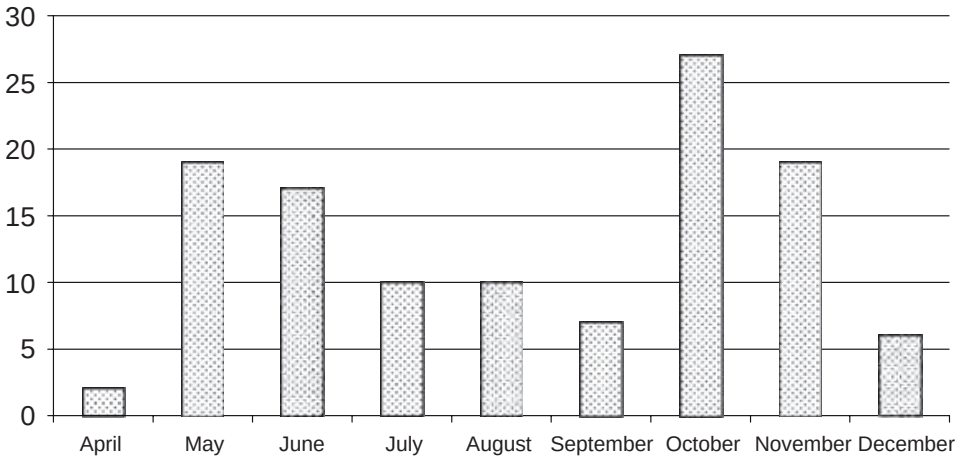

Fig. 19 Monthly distributions of landfalling tropical cyclones 1877–2003

Figure 19 shows the monthly distribution of cyclone landfall in Bangladesh from 1877 to 2003. Cyclonic disturbances are absent from January through March but frequently occur during the pre-monsoon (May–June) and post-monsoon (October–November) seasons, which match perfectly with the well-known general pattern of cyclone activities in this region.

Gray (1968) in his seminal article indicated the influence of the location of the Equatorial Trough for the two maxima of seasonal storm development (associated with the onset and retreat of monsoon) in the Bay of Bengal. He mentioned that frequency of development is largest when the Equatorial Trough is displaced farthest from the equator, i.e., in the months of May–June and October–November.

In the pre- and post-monsoon seasons, the average sea surface temperature in the Bay of Bengal region and associated weather conditions are ideal for the formation of tropical cyclones. Most of the tropical cyclones (70%) hit Bangladesh in the months of May–June and in October–November from 1877 to 2003. The seasons are also favorable for tropical cyclones with hurricane winds. During 1877–2003, 19 out of 26 hurricanes (73%) made landfall in these months.

The frequency of landfalling tropical cyclones and 5-year moving averages for different coastal segments are presented in Fig. 20. There is not much difference between the frequency and 5-year moving average for all the coastal segments.

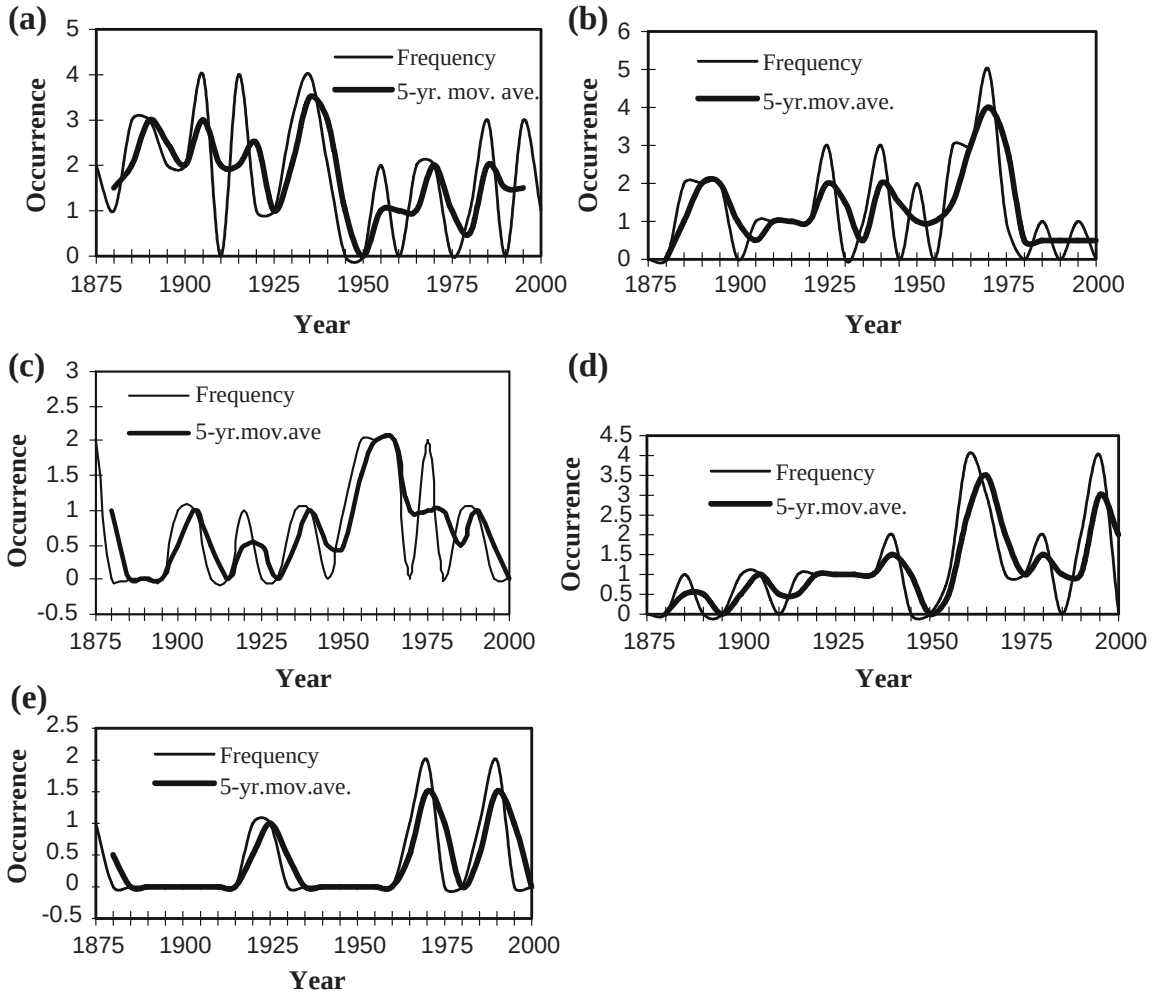

Fig. 20 Frequencies and 5-year moving average of landfalling tropical cyclones for different coastal segments (**a**) Khulna, (**b**) Barisal, (**c**) Noakhali, (**d**) Chittagong, (**e**) Cox's Bazar

7 Conclusion

A reliable and comprehensive landfalling tropical cyclone database and subsequent climatology have been established for the Bangladesh coast. The trend of tropical cyclones hitting the Bangladesh coast is not steady. It has vacillated in the past century. Presently, there is an increasing trend.

Among the coastal segments, Khulna is the most vulnerable in terms of cyclone landfall. Barisal and Chittagong coasts are highly vulnerable in terms of cyclone casualties. In Bangladesh, cyclonic disturbances are absent in January, February, and March. Most of the tropical cyclones including the ones in hurricane category strike the coast of Bangladesh in the pre- and post-monsoon seasons, thus, confirming two annual tropical cyclone seasons for the country.

References

Alam M et al (2003) Frequency of Bay of Bengal cyclonic storms and depressions crossing different coastal zones. Int J Climatol 23:1119–1125

Ali A (1979) Storm surges in the Bay of Bengal and some related problems. Dissertation, University of Reading

CRED/OFDA International Disaster Database (2006) Université Catholique de Louvain, Brussels. http://www.md.ucl.ac.be/cred/. Cited 3 Nov 2006

Dube SK, Chittibabau P, Sinha PC, Rao AD (2004) Numerical modelling of storm surge in the Head Bay of Bengal using location specific model. Nat Hazards 31:437–453

FNMOC (1998) Data base description for global tropical cyclone tracks (GTCT). Public release for distribution by Fleet Numerical Meteorology and Oceanography Detachment, Asheville

Global Tropical Cyclone Climatic Atlas (GTCCA), Version 1.0. Fleet Numerical Meteorology and Oceanography Detachment, Asheville, North Carolina. Internet version was available at http://navy.ncdc.noaa.gov/products/gtcca/gtccamain.html (now closed). Cited 15 Sept 2003

Global Tropical and Extra-tropical Cyclone Climatic Atlas (GTCCA), Version 2.0 (CD-ROM). Fleet Numerical Meteorology and Oceanography Detachment, Asheville

Gray WM (1968) A global view of the origin of tropical disturbances and storms. Mon Weather Rev 96:669–700

Holmes JD (2001) Wind loading of structures. Spon Press, London

Mooley DA (1980) Severe cyclonic storms in the Bay of Bengal, 1877–1977. Mon Weather Rev 108:1647–1655

Mooley DA, Mohile CM (1983) A study of the cyclonic storms incident on the different sections of the coast around the Bay of Bengal. Mausam 34:139–152

Raghavendra VK (1973) A statistical analysis of the number of tropical storms and depressions in the Bay of Bengal during 1890–1969. Indian J Meteorol Geophys 24:125–130

Rai Sircar NC (1956) A climatological study of storms and depressions in the Bay of Bengal. Indian J Meteorol Geophys 7:157–160

Shrestha ML (ed) (1998) SMRC-no.1—the impact of tropical cyclones on the coastal regions of SAARC countries and their influence in the region. SAARC Meteorological Research Center (SMRC), Dhaka

Simpson R (ed) (2003) Hurricane! Coping with disaster. AGU, Washington DC

UNISYS Hurricane Database (2006) UNISYS corporation. http://weather.unisys.com/hurricane/indian_oc/index.html. Cited 21 Dec 2006

WMO (1986) TCP-21: tropical cyclone operational plan for the Bay of Bengal and the Arabian Sea. WMO/TD-No.84, Geneva

Annex B77

Rodman E. Snead, "Bangladesh", in *Encyclopedia of the World's Coastal Landforms* (Eric C.F. Bird ed., 2010)

17.4 Bangladesh

Rodman E. Snead

1. Introduction

The coastline of Bangladesh, ignoring all the tidal channels and delta estuaries, is some 654 km long from the Indian border in the west to the Burmese border in the southeast (*Fig. 17.4.1*). The total length of coast, going around all the islands and up the estuaries, is estimated to be nearly 1,320 km. However, the width of the tidal channels, particularly in the Sundarbans, is impossible to measure with any precision, since the Bengal 1:250,000 scale maps are not very accurate. There is also the problem of how far inland the coastline should be considered to extend; tidal estuaries in places reach as far as 130 km inland, and storm surges may drive the Bay of Bengal waters up to 160 km inland.

The climate is tropical, with heavy rainfall during the monsoon (June–October). Cyclones occur, particularly before and toward the end of the monsoon. Chittagong has a mean monthly temperature of 19°C in January rising to 27.2°C in July, with an average annual rainfall of 2,831 mm.

The Bangladesh coast can be divided into four parts, each with its particular characteristics. In the west, partly in India but mostly in Bangladesh, is the old delta called the Sundarbans. Next, to the east, lies a section where the Sundarbans have been cleared and there is considerable farming. The third division is the delta of the Meghna, the easternmost branch of the Ganges, and the fourth is the Chittagong coast from the Feni River to the Naf River at the Burma border, a distance of about 274 km.

Except for the Chittagong section, the coastline is low, swampy, and rapidly changing. It comprises a large alluvial basin floored with Quaternary sediment deposited by two vast river systems, the Ganges and the Brahmaputra, with their numerous distributaries (Morgan and McIntire 1956). Discharge and sedimentary load figures are generally unavailable, but it can be said that the maximum flow of the Ganges River is 1.5 million cu. feet/s and the Brahmaputra some 2 million CCF/s. The geomorphological history of this huge deltaic plain is one of rivers that have continually shifted their courses back and forth as they fill in a large geosynclinal trough. In more recent times, the Ganges has shifted to the east, from a main outlet along the western margins (the Bhagirathi–Hooghly in India) to the present main course, the Padma–Meghna; streams such as the Kobadak, Pursur, Madhumati, and Tetulia represent intermediate, but not necessarily successive, positions of the main channel. There are several possible reasons for this shift, but the tectonic subsidence theory advanced by Morgan and McIntire (1956) appears to be the most plausible. They suggested deep faulting or structural subsidence along a trough running north-northwest from the active delta to the junction of the Ganges and the Brahmaputra, southeast of Padma. Their ideas are based on the apparent structural trends of the rivers and on the faulting that occurs along the western edge of the Madhupur Jungle. Subsidence is taking place in the Ganges–Brahmaputra delta (Alam 1996).

Whether any parts of the Bangladesh coast are prograding is a matter of debate.

There is certainly erosion locally. There seems to be little difference between the coastline shown on Rennell's map of 1770 and that of modern surveys, particularly in the western Sundarban region. However, the presence of old beach ridges in the western swamps points to earlier Holocene accretion. In the east, where large quantities of silt are brought down by the rivers in flood, stages in the process of land-building can be clearly seen from the air (Umitsu 1997). But no large delta appears to be extending into the Bay of Bengal, probably because of subsidence and a fairly narrow continental shelf. The rate of subsidence has evidently more than kept pace with the rate of sedimentary deposition (Morgan and McIntire 1956).

Tides along the Bangladesh coast are semidiurnal. Tidal heights vary with the season, being lower in February and March and higher during the monsoon, July through November. The mean spring tide range at the Pusur River mouth in the Sundarbans is 2.4 m, but tides here attain 7.0 m during monsoon storms (Sailing Directions 1978). At Chittagong mean spring tide range is 3.5 m and at Cox's Bazar 3.0 m.

Surface currents across the head of the Bay of Bengal are developed by the monsoon winds, and can be quite dangerous to small craft venturing into the bay.

Eric C.F. Bird (ed.), Encyclopedia of the World's Coastal Landforms, DOI 10.1007/ 978-1-4020-8639-7_17.4, © Springer Science+Business Media B.V. 2010 (Dordrecht)

Fig. 17.4.1
Predominant coastal landforms, Bangladesh.

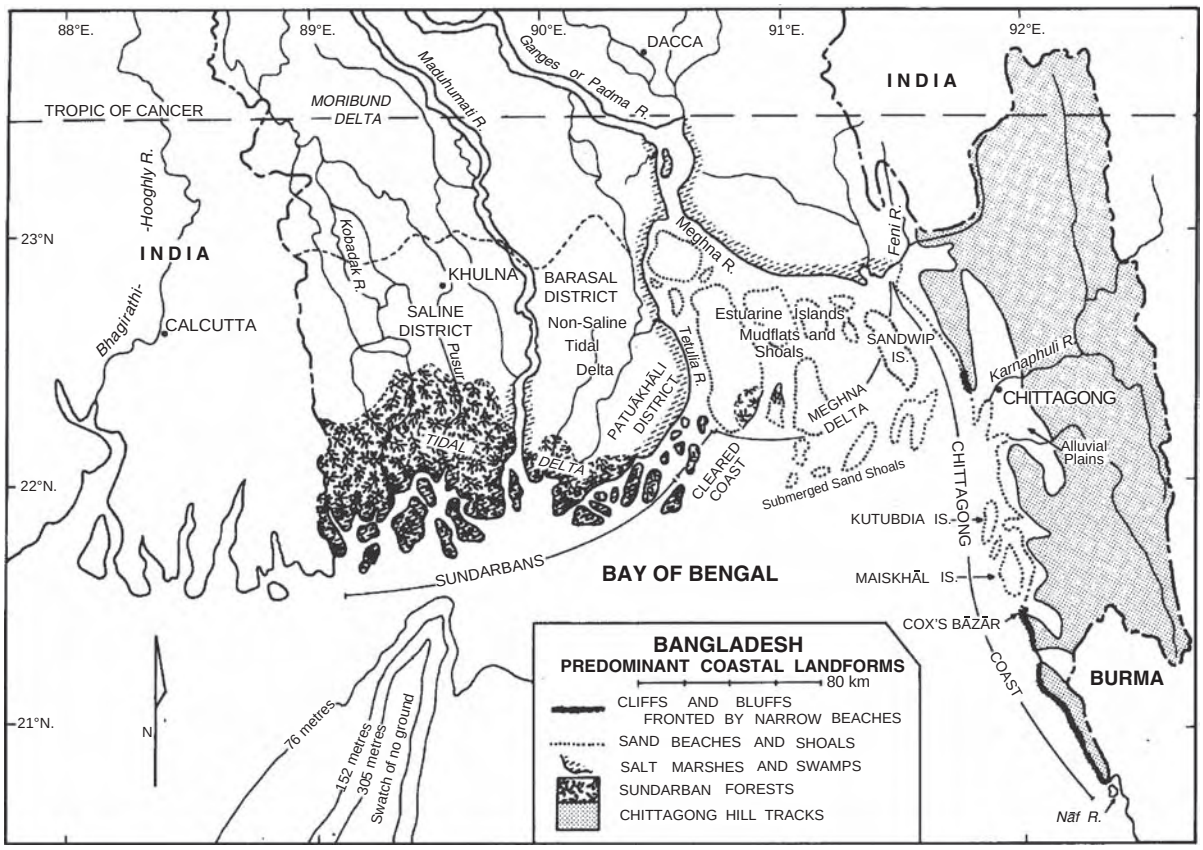

2. The Bangladesh Coastline

The Indian border crosses the Sundarbans, a heavily wooded mangrove and nipa palm swamp that extends from the Hooghly River in India eastward to the Tetulia River, a distance of about 280 km, of which nearly 193 km is in Bangladesh. The area covers about 6,000 sq km and represents the older deltaic plain of the Ganges River, with a seaward slope of about 0.076 m per mile. The largely uninhabited forest formerly extended northward to Khulna and eastward across the Barisal and Patuakha1i districts of Bangladesh, but with the encroachment of agricultural land and extensive cutting of the forests, the true mangrove and nipa jungles (*Fig. 17.4.2*) are now largely confined to the southern part of Khulna district. The seaward fringe consists of swamp forests fronted by mudflats exposed at low tide (*Fig. 17.4.3*).

The region is interlaced with a checkerboard pattern of tidal estuaries and tidal rivers. Many of these interconnecting channels are navigable. Interstream areas are shallow, saucerlike swamp depressions. Off the coast are a number of low, flat marshy islands. Navigation in the channels and estuaries is hazardous, especially during the "northeasters" in March, April, and May and the Bay of Bengal cyclonic storms from June to October. Tidal mangrove and sundri (*Heritiera littoralis*) forests predominate. The mangrove forest, mainly species of Rhizophora, with some Avicennia, is found along the waterways, the banks of which are composed of soft mud and clay that is under water at every high tide (*Fig. 17.4.3*). Many of the creeks and channels are fringed by nipa palms (*Phoenix paludosa*). Higher up is found the sundri forest, where the land is flooded with moderately brackish water at every high tide. The sundri tree reaches a height of about 16 m, and its red wood is of excellent quality. Close to the coast the high forest changes into lower species, separated in places by low sand dunes. The Sundarbans are the habitat of cobras, pythons, crocodiles, leopards, small deer, and the famous Bengal tiger, whose numbers are now being threatened by man.

Fig. 17.4.2
Nipa palms and mangroves in the Sundarbans.

Fig. 17.4.3
Mudflats and *Rhizophora* on the Tetulio River delta.

East of the Tetulia River, in the Barisal and Patuakhali districts of Bangladesh, over a distance of some 68 km, the Sundarban forest has been cleared (*Fig. 17.4.4*), and there is extensive farming (mainly paddy rice) on the drier and less saline interfluves of this part of the deltaic plain. Here population densities reach more than 2,900 per sq km. Along the coast lie scattered, partially cut mangrove forests.

The Ganges, Brahmaputra, and Meghna rivers all join into one main trunk stream in central Bangladesh before entering the Bay of Bengal through a single main channel called the Meghna River. Where it reaches the Bay of Bengal, it divides and spreads out around a series of extensive shoals called the Meghna Flats. These largely barren mud and sand shoals, at least ten of them of considerable size, extend from the Tetulia River on the west to the Feni River on the east, a distance of about 100 km. Wide, shallow channels separate the shoals, shifting so often that navigation is dangerous for large boats, especially during

Fig. 17.4.4
Cleared mangrove forest land in agricultural use, Patuakhali district, showing coastline erosion.

monsoon floods and severe cyclones. Only vessels with a draft of 3 m or less can proceed up the channels. The mud and sand shoals, with depths up to 5.5 m, extend southward for some 70 km to the Karnaphuli River. This is a drowned coastal region with no true delta building out into the Bay of Bengal (Singh 2002). During storms, waves cover these shoals and, in contrast to the Sundarbans, little vegetation survives on them.

The coast of the Chittagong district extends 274 km from the Feni River in the north to the Naf River on the Burmese boundary. The small Feni River empties into Sandwip Channel about 13 km above the northern end of Sandwip Island. Two other large islands, Kutubodia and Maiskhal, are found along this stretch of coast, as are several smaller islands and shoals. The coastal plain varies greatly in width here. Near the Karnaphuli River, it is from 48 to 64 km wide, but where the low Tertiary hills and cliffs rise immediately inland, it is virtually nonexistent. The Karnaphuli River, with its headwaters in Assam, is short but carries a large volume of water during the monsoon flood season. The land bordering the mouth of this river is low and flat, and the entrance would be difficult to find by ship but for the Norman's Point Lighthouse. Sand-covered mudflats, dry at low tide, extend about 1 km seaward of the mouth. Several small beaches and broad sand flats are found along the coast between the headlands, but in the south the coastal plain dwindles away before the uplifted and deeply eroded Chittagong Hills, which inland reach an elevation of 609 m. These hills are of stratified Tertiary marine and freshwater limestone and shale. At Cox's Bazar, there is a beach more than 152 m wide, but south of the town steep cliffs 9–15 m high front directly onto a narrow shore.

References

Alam M (1996) Subsidence of the Ganges-Brahmaputra delta of Bangladesh and associated drainage. Sedimentation and salinity problems, vol 2. Kluwer Academic Publications, the Netherlands, pp 169–192

Morgan JP, McIntire WG (1956) Quaternary geology of the Bengal Basin. Coastal studies Institute. Technical Report 9. Louisiana State University, Baton Rouge, LA

Singh OP (2002) Predictability of sea level in the Meghna estuary of Bangladesh. Water Energy Int (58):13–19

Umitsu M (1997) Landforms and floods in the Ganges Delta and coastal lowlands of Bangladesh. Mar Geod 20:77–87

Annex B78

Susmita Dasgupta et al., "Vulnerability of Bangladesh to Cyclones in a Changing Climate: Potential Damages and Adaptation Cost", World Bank Policy Research Working Paper No. 5280 (April 2010)

Annex B78
WPS5280

Policy Research Working Paper 5280

Vulnerability of Bangladesh to Cyclones in a Changing Climate

Potential Damages and Adaptation Cost

Susmita Dasgupta
Mainul Huq
Zahirul Huq Khan
Manjur Murshed Zahid Ahmed
Nandan Mukherjee
Malik Fida Khan
Kiran Pandey

The World Bank
Development Research Group
Environment and Energy Team
April 2010

Policy Research Working Paper 5280

Abstract

This paper integrates information on climate change, hydrodynamic models, and geographic overlays to assess the vulnerability of coastal areas in Bangladesh to larger storm surges and sea-level rise by 2050. The approach identifies polders (diked areas), coastal populations, settlements, infrastructure, and economic activity at risk of inundation, and estimates the cost of damage versus the cost of several adaptation measures. A 27-centimeter sea-level rise and 10 percent intensification of wind speed from global warming suggests the vulnerable zone increases in size by 69 percent given a +3-meter inundation depth and by 14 percent given a +1-meter inundation depth. At present, Bangladesh has 123 polders, an early warning and evacuation system, and more than 2,400 emergency shelters to protect coastal inhabitants from tidal waves and storm surges. However, in a changing climate, it is estimated that 59 of the 123 polders would be overtopped during storm surges and another 5,500 cyclone shelters (each with the capacity of 1,600 people) to safeguard the population would be needed. Investments including strengthening polders, foreshore afforestation, additional multi-purpose cyclone shelters, cyclone-resistant private housing, and further strengthening of the early warning and evacuation system would cost more than $2.4 billion with an annual recurrent cost of more than $50 million. However, a conservative damage estimate suggests that the incremental cost of adapting to these climate change related risks by 2050 is small compared with the potential damage in the absence of adaptation measures.

This paper—a product of the Environment and Energy Team, Development Research Group—is part of a larger effort in the World Bank to understand potential impacts of climate change and adaptation cost. Policy Research Working Papers are also posted on the Web at http://econ.worldbank.org. The author may be contacted at sdasgupta@worldbank.org.

Vulnerability of Bangladesh to Cyclones in a Changing Climate: Potential Damages and Adaptation Cost

Susmita Dasgupta[1]

Mainul Huq[2]

Zahirul Huq Khan[3]

Manjur Murshed Zahid Ahmed[4]

Nandan Mukherjee[5]

Malik Fida Khan[6]

Kiran Pandey[7]

Acknowledgements Financial support for this study was provided by the Economics of Adaptation to Climate Change study administered by the Environment Department of the World Bank. Funding for the Economics of Adaptation to Climate Change study has been provided by the governments of the United Kingdom, the Netherlands, and Switzerland.

We would like to extend our special thanks to Ms. Maria Sarraf, Dr. Ainun Nishat and Mr. Khawaja Minnatullah for their valuable guidance. We are thankful to Dr. Robert Mendelsohn and participants of the Economics of Adaptation to Climate Change country consultations for their useful comments and suggestions. We are also grateful to Ms. Roufa Khanam for her valuable help with the GIS and Mr. Brian Blankespoor for editorial help.

[1] Lead Environmental Economist, Development Research Group, The World Bank, Washington DC, USA.
[2] Development Policy Group, Dhaka, Bangladesh.
[3] Director, Institute of Water Modeling, Dhaka, Bangladesh.
[4] Senior Specialist, Institute of Water Modeling, Dhaka, Bangladesh.
[5] Adaptation Specialist, Climate Change Division, Center for Environmental and Geographic Information Services, Dhaka, Bangladesh.
[6] Director, Climate Change Division, Center for Environmental and Geographic Information Services, Dhaka, Bangladesh.
[7] Senior Economist, Environment Division, The World Bank, Washington, USA.

1. Introduction

An increase in sea surface temperature is strongly evident at all latitudes and in all oceans. The scientific evidence indicates that increased sea surface temperature will intensify cyclone activity and heighten storm surges.[8,9] These surges[10] will, in turn, create more damaging flood conditions in coastal zones and adjoining low-lying areas. The destructive impact will generally be greater when storm surges are accompanied by strong winds and large onshore waves. Tropical cyclone Sidr[11] in Bangladesh (November 2007) and cyclone Nargis[12] in the Irrawady delta of Myanmar (May 2008) provide recent examples of devastating storm-surge impacts in developing countries.

Some recent scientific studies suggest that increases in the frequency and intensity of tropical cyclones in the last 35 years can be attributed in part to global climate change (Emanuel 2005; Webster et al. 2005; Bengtsson, Rogers, and Roeckner 2006). Others have challenged this conclusion; citing problems with data reliability, regional variability, and appropriate measurement of sea-surface temperature and other climate variables (e.g., Landsea et al. 2006). Although the science is not yet conclusive (IWTC 2006: Pielke et al. 2005), the International Workshop on Tropical Cyclones (IWTC) has recently noted that "[i]f the projected rise in sea level due to global warming occurs, then the vulnerability to tropical

[8] A sea-surface temperature of 28° C is considered an important threshold for the development of major hurricanes of categories 3, 4 and 5 (Michaels, Knappenberger, and Davis 2005; Knutson and Tuleya 2004).

[9] A rising sea level as thermal expansion and ice cap melting continue will be another contributory factor. The most recent evidence suggests that sea-level rise could reach 1 meter or more during this century (Dasgupta, et al. 2009; Rahmstorf 2007), although the likelihood of that magnitude of increase remains uncertain.

[10] *Storm surge* refers to the temporary increase, at a particular locality, in the height of the sea due to extreme meteorological conditions: low atmospheric pressure and/or strong winds (IPCC AR4 2007).

[11] According to Bangladesh Disaster Management Information Centre (report dated Nov 26, 2007) 3,243 people were reported to have died and the livelihoods of 7 millions of people were affected by Sidr (http://www.reliefweb.int/rw/RWB.NSF/db900SID/EDIS-79BQ9Z?OpenDocument).

[12] In Mayanmar, 100,000 people were reported to have died and the livelihoods of 1.5 million people were affected by Nargis (http://www.dartmouth.edu/%7Efloods/Archives/2008sum.htm)

cyclone storm surge flooding would increase" and "[i]t is likely that some increase in tropical cyclone peak wind-speed and rainfall will occur if the climate continues to warm. Model studies and theory project a 3-5% increase in wind-speed per degree Celsius increase of tropical sea surface temperatures." The Intergovernmental Panel on Climate Change (IPCC AR4, 2007) using a range of model projections, also has asserted a probability greater than 66% that continued sea-surface warming will lead to tropical cyclones that are more intense, with higher peak wind speeds and heavier precipitation (IPCC 2007; see also Woodworth and Blackman 2004; Woth, Weisse, and von Storch 2006; and Emanuel et al. 2008).[13]

The historical evidence highlights the danger associated with storm surges. During the past 200 years, 2.6 million people may have drowned during surge events (Nicholls 2003). Although significant adaptation has occurred over time, and many lives have been saved by improved disaster forecasting, evacuation and emergency shelter procedures (Shultz, Russell, and Espinel 2005; Keim 2006); recent disasters in Bangladesh and Myanmar have demonstrated that storm-surge losses still remain huge in many areas. Allocating resources to increased disaster resilience along particularly vulnerable coastlines could reduce such losses. The need for disaster preparedness along vulnerable coastlines is especially pronounced in countries where concurrent scientific projections point towards more intense cyclones in a changing climate. However, setting a new course requires better understanding of expected changes in storm surge patterns in the future, associated damages and adaptation costs.

Currently, systematic studies of storm surge patterns in the future, location-specific potential damage and adaptation alternatives are scarce in developing countries. Analytical work to date has been confined to relatively limited sets of locations, impacts and adaptation measures (Ali 1999, Hoque 1994, Khalil, 1992). This paper is an attempt to

[13] Cyclones get their power from rising moisture which releases heat during condensation. As a result, cyclones depend on warm sea temperatures and the difference between temperatures at the ocean and in the upper atmosphere. If global warming increases temperatures at the earth's surface but not the upper atmosphere, it is likely to provide tropical cyclones with more power (Emmanuel et al. 2008).

narrow the gap by providing itemized estimates of potential damage and adaptation cost out to 2050 for Bangladesh- a tropical cyclone hotspot[14] in a changing climate.

The focus of this research is on 10-year return period cyclones -- cyclones with a 10% or greater probability of occurrence each year. In the computation of potential damage, this analysis concentrates on fatalities and injuries; and on housing, education, agriculture, non-agriculture productive sector, and infrastructure (roads, power, coastal protection), sectors experiencing serious damage in the most recent 10 year return period cyclone in Bangladesh (Sidr 2007). The primary objective of adaptation in this analysis is to avoid further damages associated with storm surge inundation as a result of climate change with a particular focus on various measures of adaptation to storm surges in Bangladesh. At the outset, we acknowledge several limitations in our analysis. This analysis has not addressed the likely problem of salinity intrusion nor has it addressed out-migration from the coastal zone that may be induced by sea level rise and more intense cyclones. We also have not attempted to estimate location-specific probability of 10-year return period cyclones.

The remainder of the paper is organized as follows. Section 2 presents the case of cyclones in Bangladesh. Our methodology and results are presented in Section 3, and Section 4 concludes the paper.

2. Cyclones in Bangladesh

Cyclones hit the coastal regions of Bangladesh almost every year, in early summer (April-May) or late rainy season (October-November). Between 1877 and 1995 Bangladesh was hit by 154 cyclones (including 43 severe cyclonic storms, 43 cyclonic storms, 68 tropical depressions)[15]. Since 1995, five severe cyclones hit coast of Bangladesh coast in May 1997, September 1997, May 1998, November 2007 and May 2009. On average, a severe cyclone strikes Bangladesh every three years (GoB, 2009).

Bangladesh is on the receiving end of about 40% of the impact of total storm surges in the

[14] See UNDP, 2004; Nicholls, 2003.

[15] The Indian Meteorological Department (IMD) is responsible for tracking tropical storms and cyclones in South Asia including the Bay of Bengal. Tropical storms are classified based on the observed maximum sustained surface wind measured at a height of 10m averaged over 3 minutes as follows: Super Cyclonic Storm (greater than 220 km/hour), very severe cyclonic storm (119-220 km /hour), severe cyclonic storms (90-119 km/hour), cyclonic storms (60-90 km/hour), Deep depression (51-59 km/hour), Depression (32-50 km/hour) (IMD, 2010).

world (Murty and El Sabh, 1992). The reasons for this disproportional large impact of storm surges on the coast of Bangladesh were reported[16] to be the following:

- The phenomenon of recurvature of tropical cyclones in the Bay of Bengal,
- Shallow continental shelf, especially in the eastern part of Bangladesh[17],
- High tidal range[18],
- Triangular shape at the head of the Bay of Bengal[19],
- Almost sea-level geography of the Bangladesh coastal land,
- High density of population and coastal protection system.

The Meghna estuarine region is the area where most of the surge amplifications occur. UNDP has identified Bangladesh to be the most vulnerable country in the world to tropical cyclones (UNDP, 2004).

Inundation due to storm surges generated by severe cyclones pose a threat to lives and (their) properties in the coastal region. Historical (time series) records of storm surge height are scarce in Bangladesh. However, existing literature indicates a range of 1.5 to 9.0 meter high storm surges during various severe cyclones. Storm surge heights in excess of 10 m or even more are also not uncommon with an occasional reference in the literature. For example, the Bakerganj cyclone had the greatest reported surge height of 13.6 m in 1876 and another cyclone had the height of 10 m in 1970 (SMRC, 2000).

A surge can be even more devastating if it makes a landfall during high tide. In general, it has been observed that the frequency of a wave (surge plus tide) along Bangladesh coast with a height of about 10 m is approximately once in 20 years, and the frequency of a wave with a height of about 7 m is approximately once in 5 years (MCSP, 1993).

In addition to these exceptional surges, waves caused by wind also occur; the dimensions of which depend on wind speed and direction, water depth, and duration of wind blowing over

[16] For example, see Ali, 1999 .
[17] The coast line of Bangladesh is characterized by a wide continental shelf, especially off the eastern part of Bangladesh. This wide shelf amplifies the storm surges as the tangential sea-level wind-stress field associated with the tropical cyclone pushes the sea water from the deep water side onto the shelf. Being pushed from the south by wind stress, the water has no place to go but upwards; which is the storm surge.
[18] Records indicate 7-8 m high tide in the Sandwip Channel.
[19] The triangular shape at the head of the Bay of Bengal helps to funnel the sea water pushed by the wind towards the coast and causes further amplification of the surge.

the bay. It has been observed that wind induced waves of up to 3.0 m height may occur under unfavorable conditions in the coastal regions (MCSP, 1993).Table 1 presents surge inundation characteristics for cyclones of varying strength in Bangladesh as documented by the MCSP (1993) (see Table 1).

According to the IPCC AR4, storm surges and related floods are likely to become more severe with increases in intense tropical cyclones in future (IPCC, 2007). For the Bay of Bengal, a study using dynamical models driven by RCM[20] simulations of current and future climates have shown large increases in the frequency of highest storm surges despite no significant change in the frequency of cyclones (Unnikrishnan et al, 2006).[21] Hence, from a practical perspective vulnerability of Bangladesh to cyclones/ storm surges may increase even more as a result of climate change.

3. Methodology and Estimates for Damage and Adaptation Cost

In order to estimate potential damage and cost of adaptation to potential intensification of storm surges, this analysis has followed a 5-step procedure:

1. Demarcation of potential vulnerable zone and projection of inundation depth from storm surges;
2. Identification of critical impact elements: assets and activities exposed to inundation risk;
3. Computation of potential damage and loss for a 10 year return period cyclone/ storm surges out to 2050;
4. Identification of existing adaptation measures and quantification of changes that will be required in a changing climate;
5. Costing of adaptation.

3.1 <u>Demarcation of vulnerable zone and storm surge height:</u>

This analysis has considered a sea level rise of 27cm[22], increased wind speed (10%)[23] and landfall during high tide[24] to approximate cyclones in a changing climate by 2050.

[20] Regional Climate Model
[21] For North Indian Ocean by 2100, a recent projection by Emanuel has indicated an increase in intensity of tropical storms, as measured by percent change in landfall power, for the Model for Interdisciplinary Research on Climate: MIROC (UN and World Bank, 2010).
[22] Source: UK DEFRA (2007).
[23] World Bank (2010).

The inundation effect of storm surges has been assessed using the two-dimensional Bay of Bengal Model recently updated and upgraded under the Comprehensive Disaster Management Program of Bangladesh (UK DEFRA 2007). The model is based on Mike 21 hydrodynamic modeling system, and its domain covers the coastal region of Bangladesh up to Chandpur and the Bay of Bengal up to 16º latitude. A detailed description of the model has been provided in Appendix 1.

For approximating a condition of cyclones in Bangladesh without climate change, cyclone tracks of all major 19 historical cyclones making landfall in Bangladesh during 1960 and 2009 (For details, see Appendix 2) have been used with corresponding observed wind and pressure fields. For simulating the storm surge and associated flooding, the Bay of Bengal model was then applied to generate the extent and depth of inundation without climate change. Resulting inundation map is based on the maximum level of inundation at every grid points of the model.

For approximating cyclones in a changing climate by 2050, potential cyclone tracks have been selected simulating 19 major cyclones making landfall in Bangladesh during 1960-2009, and the affected coastal regions. From the historical cyclone simulations, it has been observed that the Sunderban coast, the southwestern coast (Sunderban to Patuakhali), the Bhola and Noakhali coast in the Meghna Estuary and eastern coast (Shitakunda to Bashkhali) are covered by 1974, 1988, 1991 and 2007 cyclone tracks. In order to include the Sandwip coast and the part of the Noakhali and Chittagong coasts at the central region of the Meghna Estuary, an artificial track has been generated. Figure 1 shows the five cyclone tracks considered for the determination of inundation zones due to climate change induced storm surges (see Figure 1).

In order to determine potential future inundation zones in a changing climate by 2050, the storm surge model was run for the above mentioned five cyclone tracks covering the whole coastal area, incorporating a sea level rise of 27cm, 10% increase in wind speed, and landfall of the cyclones during high tide. Once again, inundation maps for 2050 with climate change have been generated based on the simulation results taking into potential intensification of cyclone induced inundation (See Figure 2).

[24] Since scientific evidence to date is pointing towards an increase in frequency of intense cyclones in Bay of Bengal, probability of a potential landfall during high tide will also increase.

Resulting area estimates indicate a potential 69% increase in the vulnerable zone with more than 3 m inundation depth and 14% increase in the vulnerable zone with more than 1 m inundation depth with climate change (See Table 2).

3.2 Identification of critical impact elements exposed to inundation risk:

In order to identify critical impact elements exposed to inundation risk, geographic Information System (GIS) software has been used to overlay the best available, spatially-disaggregated data on current assets and activities in the coastal zone of Bangladesh, with the inundation zones projected for 2050 - with and without climate change.

Impact elements considered in this analysis include: housing - by building material type, education institutions, growth centers, mills/ factories (large scale), national highways, regional highways, feeder roads-type A, feeder roads-type B, bridges, power plants, power transmission lines, deep tubewells, mosques, temples, historical places and tourist destinations. Relevant exposure surface dataset for land area, population, poverty map, and agriculture extent were also used. Exposure surface data were collected from various public sources, such as Bangladesh Railways, Bangladesh Water Development Board, Local Government Engineering Department (LGED), Center for Environmental and Geographic Information Services (CEGIS), Public Works Department, Roads and Highways Department, Water Resources Planning Organization and the World Bank. Estimates of exposure for each indicator were calculated by overlaying the inundation zone with the appropriate exposure surface dataset.

For the exposure grid surfaces, three GIS models were built for calculating the exposed value. Exposure indicators, such as land surface, agriculture extent, road infrastructure and railways were measured in square kilometers or kilometers. The values of the pixels in population surfaces represent number of people, therefore the exposure is calculated by multiplying the exposure surface[25] with the inundation zone and then summing up by multiplying grid count and value. Exposure estimates of other impact elements were counts.

[25] Population density of the lowest administrative unit, *Thana*, has been used in the computation.

Presently, our estimates indicate that 8.06 million inhabitants in coastal Bangladesh are vulnerable to storm surge related inundation depth of more than 1m; the number will increase 68% with population growth by 2050 even without climate change, and by 110 % by 2050 in a changing climate in the absence of further adaptation measures. Population exposed to inundation depth of more than 3m will increase by 67% from current trends to the 2050 scenario with climate change by 2050 (See table 3).

3.3 Potential Damage and loss from a 10 year return period cyclone/ storm surges in a changing climate by 2010:

Exposure estimates of critical impact elements derived from geographic overlays provide the basis for estimation of potential damage and loss from a 10 year return period cyclone induced storm surges in a changing climate by 2050. In addition, the assessment of exercise of potential damage and loss drew on the following:

a. Projection of growth in coastal population (1% per year) and GDP growth (6%-8% per year);

b. Experience of Bangladesh during the most recent devastating cyclone Sidr in 2007.[26] (The extent of storm surge inundation during Sidr was 8.7% more than an average inundated area of a historical 10 year return period cyclone of Bangladesh.[27] Accordingly, adjustment was made in computation of damage);

c. At present, average inundation area from one 10 year return period cyclone covers 26% of the total vulnerable area and inundation from one future 10 year return period cyclone (expected to be more intense) is likely to cover 43% of the total vulnerable area;

d. All estimates have been adjusted for 2009 price level as per 18% increase in the GDP deflator during 2007 and 2009.

In this analysis, *damages* include complete or partial destruction inflicted on assets (assets not portable as well as stock), and *losses* refer to the flows of goods and services that will

[26] It has been estimated that a cyclone like Sidr (wind speed of 223 km / hour) has a return period of 10 years in Bangladesh based on 21 major cyclone events from 1876 to 2009.
[27] The extent of inundation includes area with inundation depth of 1 m or more.

not be produced or rendered due to disasters. *Losses* also include disaster-induced increases in costs incurred for continuation of essential services.

Potential Human Casualty and Injury:

Approximately 3.45 million coastal inhabitants of Bangladesh were exposed to storm surge related inundation during Sidr, 2007. Post disaster assessments indicate 3,406 human casualties and 55,282 injuries. Although cyclone shelters saved thousands of lives, focus group interviews with the residents of cyclone-affected areas revealed that a large section of population was reluctant to move to cyclone shelters even during emergency. Distance from the homestead, difficult access to shelters, unwillingness to leave livestock behind unprotected, scarcity of sanitation facilities, lack of user friendly facilities for women, and overcrowded conditions in shelters are the primary reasons behind their reluctance. It has been estimated, under the assumptions of Bangladesh attaining replacement fertility rate by 2021 and an average 1.0% annual growth in coastal population per year between 2001 and 2050, a total of 5.34 million and 10.04 million coastal inhabitants will be exposed to the risk of a 10 year return period cyclone induced storm surge without and with climate change respectively by 2050. Extrapolation with the ratio of casualty to exposure (0.001), and the ratio of injury to exposure (0.016) experienced during Sidr indicates a risk of additional human casualties with an expected magnitude of 4,637, and an expected 75,268 injuries from a 10 year return period cyclone by 2050 as a consequence of climate change, in the absence of improved defensive measures.[28] Improved defensive measures would contribute to reduced fatality and injury risk from increased exposure without climate change, in addition to the additional risk engendered by climate change.

Attaching a monetary-equivalent value to these risks that can be combined with and compared to risks of financial damage and loss is enormously difficult. The most appropriate measure of the benefit from reduced risk of fatality is the "Value of Statistical Life" (VSL), which seeks to estimate the monetary equivalent of improved well-being for individuals from reduced mortality risk. In reality, VSL should reflect the context of the risk – for

[28] Estimated human casualty is 5,274 without climate change by 2050, and in a changing climate the estimate is 9,911. Estimated injury is 85,609 without climate change by 2050; and in a changing climate the estimate is 160,877.

example, the risk of sudden fatality from an accident would be different from the risk of reduced future life span from long-term pollutant exposure.

Unfortunately, VSL values are all but non-existent for developing countries, so it is necessary to make rough approximations based on VSL estimates for developed countries, in particular the USA. In this analysis a VSL of Taka 15.5 million (approximately $0.2 million) has been used. This estimate for Bangladesh has been computed by updating the central estimate of VSL of USA., $7.4 million ($2006) available from the EPA with price adjustment between 2006 and 2008 and GDP differential between USA and Bangladesh[29]. Multiplying this figure by the expected value of the increased number of lives at-risk from a 10 year return period cyclone under climate change, an increased economic damage of $1.03 billion from greater fatality risk has been estimated.

To calculate the economic damages from increased injury risk, a crude lower-bound estimate based on the WHO figure for cost per outpatient visit at a secondary hospital visit in Bangladesh, $4.86 (Cropper and Sahin, 2009) has been adopted. This yields a total economic damage from increased injury risk of $0.352 million. This estimate, however, does not include any value of lost production and income from injury, or the more subjective losses of well-being resulting from being injured or incapacitated.

The balance of this section focuses on sectors experiencing high monetary damage and loss during Sidr, 2007 – namely housing, education, agriculture, non agriculture productive sector and infrastructure: roads, power, coastal protection. (See Box 1).

Potential damage in housing:

The housing sector experienced maximum damage and loss during the Sidr cyclone in 2007 and accounting by housing/ dwelling type further indicates that "*semi-pucka*"[30] houses, "*kacha*"[31] houses and "*jhupris*"[32] were the predominant categories of damage.

[29] GDP Deflator 2008/ GDP Deflator 2006= 1.1; Per Capita USGDP ($ 2008, PPP) = 46,716 and Per Capita Bangladesh GDP ($ 2008, PPP) = 1,334 have been used in this computation.

[30] Housing with foundation made of earthen plinth or brick and concrete, walls made of bamboo mats, CI sheet and roof made of CI sheet with timber framing

[31] Housing with foundation made of earthen plinth with bamboo, walls made of organic materials and roof thatched made of straw, split bamboo etc.

Analysis of the 2001 census data in Bangladesh reveals only 2.23% of rural households with $470 per capita annual income[33] or more could afford a "*pucka*" house, a brick house with a concrete roof in 2001. However, Bangladesh is currently experiencing and expecting 6%-8% GDP growth per year for the coming decades. It is expected that approximately 98% of the households will be living in brick houses by 2050, even after accounting for inflation. This in turn implies a significant reduction in housing damages and a substantial increase in household asset damages during cyclones over time.

Projection of population in coastal regions by 2050 without and with climate change indicates that an additional 7.08 million inhabitants (i.e. an additional 1.45 million houses - under the assumption of an average family size of 4.89) will be exposed to significant damages from storm surges in a changing climate. Accounting for the larger areal extent of a cyclone under climate change an additional 1.6 million houses are projected to be damaged from a 10 year return period cyclone due to climate change.[34] The size of a standard house in Bangladesh is assumed to be 400 sq feet with 2,000 sq feet of brick wall surface and approximate value of household assets is $2,143 (Tk 150,000). Under the assumption that on average 50% of the walls and 50% of the household assets will be damaged during inundation, **re-plastering the houses will cost $229 million (at Tk 10/ sq. ft) and an estimate of household content damage is expected to be approximately $1.718 million**.

Potential damage in education infrastructure:

The population projection indicates that with an additional 7.08 million inhabitants in coastal Bangladesh exposed to storm surges in a changing climate by 2050; the expected exposure of primary school students will be 456,690 (in 2,283 primary schools) and that of secondary school students will be 312,957 (in 2,086 secondary schools).[35] Accounting for the larger

[32] In Jhupris, ceiling, which is less than four feet, is made of cheap construction materials straw, bamboo, grass, leaves, polythene, gunny bags, etc.
[33] Monthly income Tk 2,750 per capita.
[34] It has been assumed that inundation depth of 1m or less will have negligible impact.
[35] These estimates are based on the following assumptions: (a) ratio of children of primary school age to total population will be 6.45% and the ratio of secondary school children to total population will be 4.42% by 2050, (b) Bangladesh will attain 100% enrollment in primary schools and 70% enrollment in secondary schools by 2050, which is the current rate of school enrollment of Brazil, Lebanon, Malaysia, Uruguay –countries with per capita income similar to projected income for Bangladesh in 2050, (c) the standard capacity of a primary school is 200 students and a similar size school can accommodate up to 150 secondary students in Bangladesh.

areal extent of a cyclone under climate change an additional 4,840 primary and secondary schools are projected to be damaged in a 10 year return period cyclone. According to the standard specification of the LGED, the size of a standard school in Bangladesh is approximately 160 sq m and its contents are worth $2,857 (Tk 200,000). Under the assumption of expected average 50% damage to walls and contents during inundation, the **estimated** (total) **damage[36] in a changing climate is $8.96 million.**

The estimated total loss (cost of making alternative arrangements until the damaged facilities are ready for use again) **is $0.82 million**.

Potential damage in agriculture:

Computation of potential damage and loss in the agricultural sector focuses on likely impacts on crop production, livestock and fishery.

In the case of cereal production, this analysis is restricted to *Aman*, *Aus* and *Boro* variety of rice, which are the main cereal crops of Bangladesh. In a changing climate, these crops are expected to incur significant damage due to the expansion of storm surge inundation area. The following parameters have been used for their quantification of potential damage (See Table 4).

Historical records indicate the probability of Bangladesh being hit by a tropical cyclone in a post-monsoon season (67%) is higher than that in a pre-monsoon season (33%). The cropping calendar, planting - harvesting dates, of *Aman*, *Aus*, and *Boro* are different[37]. As a result, these crops are exposed to varying risk of storm surge inundation, and this difference has been taken into account in the damage estimation. Under the assumptions that cereal production will grow at the annual rate of 2.4% (observed annual growth rate during 2001-2007) in the future and there will be 50% damage in the yield if a 10 year return period cyclone strikes, the **estimated additional damage (primarily loss) for cereal is $788.83 million in a changing climate by 2050.**

Sidr (2007) has inflicted a damage of $19.3 million to livestock and losses and damages of $6.7 million to the fishery. Under the assumption that livestock and the fishery will grow at

[36] includes damage to the walls and therefore cost of re-plastering and damage of contents.
[37] *Aman* grows in monsoon, *Aus* grows in pre-monsoon and *Boro* grows in post-monsoon season.

the annual rate of 3% and 6% respectively (observed annual growth rate during 2001-2007) in the future, the **estimated additional damage and loss for the livestock and fishery are $55.62 million and $66.36 million, respectively, in a changing climate by 2050.** [38]

Potential damage in non- agricultural productive sector:

In 2007, Sidr triggered a total damage of $51.4 million to the non-agricultural productive sectors. In 2007, non-agricultural productive sectors (industries including small and medium size enterprises, commerce, tourism etc.) contributed to 82% of GDP of Bangladesh (World Bank, 2009). Economic structure of Brazil, Lebanon, Malaysia, Uruguay and South Africa - countries with present per capita income similar to the projected per capita income of Bangladesh indicates that the share of the non-agricultural productive sectors is likely to increase in Bangladesh by another 11% by 2050. GDP of Bangladesh is expected to increase 21.48 times between 2007 and 2050. Storm surge induced inundation area under Sidr, an average historical 10 year return period cyclone and a 10 year return period cyclone in a changing climate by 2050 are 588,512 hectares, 541,190 hectares and 1,017,008 hectares respectively. Combination of all the above implies **an additional potential damage of $87.9 million in a changing climate, by 2050**.[39]

The estimated potential additional loss is $1.084 billion.

Potential damage in road infrastructure:

In the case of storm surges, past experience suggests that roads are partially damaged when surge height/ depth of inundation is less than 1m, and fully damaged when the depth of inundation exceeds 1m. Under the assumption of 25% growth in road network between 2005 and 2050, geographic overlays of the road network and inundation zones indicate 3,998 km roads will be exposed to inundation depth of less than 1m and 8,972 km roads will be exposed to inundation depth of more than 1m by 2050 even without climate change. With climate change, the road exposure to less and more than 1m inundation depths will increase to 10,466 and 10,553 km respectively. Accounting for the larger areal extent of a

[38] Estimated damage to livestock is $63.26 million without climate change, and $ 118.88 million with climate change-by 2050. Estimated damage to fishery is $75.48 million without climate change, and $ 141.84 million with climate change-by 2050.

[39] Estimate of damage including loss but without climate change is $1.33 billion.

cyclone under climate change an additional 3,461 km of roads is projected to be partially damaged and 2,205 km fully damaged from a 10 year return period cyclone. Repair costs of Taka 1 million and Taka 2 million respectively in case of partial and full damage from the post damage loss assessment exercise of Sidr in 2007 have been applied in the computation. The post assessment of Sidr (2007) has further suggested that damages to bridges, culverts etc. were 1.13 times the damages to roads. The combination of all these damages indicates **an additional damage of $239.5 million to roads, bridges, culverts etc. in a changing climate by 2050**[40].

The estimated potential additional loss in a changing climate is $52.7 million.[41]

Potential Damage in power infrastructure:

In 2007, Sidr induced a damage of $8.2 million in the power sector of coastal Bangladesh. The projection of population indicates 1.53 times growth of coastal inhabitants in the coastal area between 2007 and 2050. The consumption of power in Brazil, Lebanon, Malaysia, Uruguay and South Africa -countries with the present per capita income similar to the projected per capita income of Bangladesh indicates per capita consumption of power is likely to increase 20 times in Bangladesh (and power infrastructure 5 times[42]) by 2050. Damages recorded during the Sidr (2007) coupled with the projection of the change in power infrastructure in the inundation areas (with and without climate change) indicates **an additional damage of $60.2 million.** [43]

The estimated potential additional loss is $150.0 million.

Potential damage in coastal protective infrastructure:

In the sixties, 123 polders and supporting infrastructure were constructed to protect low lying coastal areas against tidal flood and salinity intrusion in Bangladesh. In 2007, Sidr

[40] Estimate of potential damages to roads, bridges, culverts etc. is $173.6 million by 2050 even without climate change, and the corresponding estimate with climate change is $413.1 million.
[41] Loss estimates have been computed using 22% ratio between loss and damage in post Sidr assessment.
[42] Experts of the Asian Development Bank working on Bangladesh power sector suggested this adjustment factor.
[43] Estimates of potential total damage without and with climate change are $239.1 million and $449.3 million respectively.

induced a damage of $70.3 million in the polders and related water regulators in coastal Bangladesh. Past experience has identified "overtopping" of an embankment of a polder to be the most important factor responsible for polder's damage during cyclones.[44] Comparison of projected surge heights and heights of existing embankments of polders indicate an additional 15 polders are likely to be overtopped by 2050 in a changing climate,[45] and **the estimate of additional potential damage is $17.3 million**.

To sum up, Table 5 presents itemized additional potential damage and additional potential loss for an average 10 year return period cyclone induced inundation in a changing climate by 2050 without adaptation. **The estimates indicate if a 10 year return period cyclone (likely to be more intense than current cyclones with climate change) hits Bangladesh, additional potential damage is likely to be $2.437 billion and additional potential loss $2.123 billion** (See Table 5)**.**

3.4 Mapping existing Coastal Protection in Bangladesh and gap analysis:

Bangladesh has an extensive infrastructure such as polders, cyclone shelters, early warning and evacuation system to protect coastal regions.

a) *Coastal Polders*:

In the early sixties and seventies 123 polders, of which 49 polders are sea facing, were constructed to protect low lying coastal areas against tidal flood and salinity intrusion. Bangladesh Water Development Board (BWDB) maintains an extensive database of coastal polders, and it includes information on length, location, construction year and cost for each polder.[46] See Figure 3 for the lay out map of the costal polders (See Figure 3).

Geographic Information System (GIS) software has been used to overlay the best available spatially-disaggregated data on polders in the derived vulnerable coastal zone of

[44] When water surge overtops an embankment, rapid and deep scours start to form on the country side slope of the embankment. The process rapidly weakens the structure and leads to its collapse.

[45] Computation has been explained in details in the next section.

[46] In addition, information on riverbank and shoreline protection and re-sectioning of embankment works has been extracted from the Coastal Embankment Rehabilitation Project (CERP) and South-Eastern Zone-Chittagong, South-Western Zone-Faridpur, Southern zone-Barishal maintained by the BWDB. It includes information on the ongoing projects, construction period and cost.

Bangladesh. Differences between the crest level of embankment of each polder and the inundation depths projected for 2050 - with and without climate change have been computed to identify polders likely to be overtopped by intensified storm surges in a changing climate and to quantify the potential extent of overtopping. The result indicates 26 interior polders and 33 sea facing polders in the coastal region will be overtopped in a changing climate by 2050.

b) *Foreshore Afforestation*:

In the past, foreshore afforestation scheme proved to be cost effective in dissipating wave energy, and in reducing hydraulic load on the embankments during storm surges[47], but Bangladesh has inadequate foreshore forests. At present, the total length of embankment of 49 sea facing polders is 957 km, of which only 60 km has forest belts; and in many areas the existing forest belt is degraded. Officials of the Department of Forests and experts of the Institute of Water Modeling (IWM) have commented on the successes, failures and sustainability of past foreshore afforestation measures. According to their recommendation, a minimum of 500 meter width of mangrove forest is required for protection of sea facing polders. In this analysis, existing length of coastal afforestation, between the coastline and polders, has been estimated from Google Earth using GIS methodology; and the gap between recommended 500 m wide mangroves and area-specific existing ones has been computed.

c) *Cyclone Shelters*:

At present, cyclone shelters in the coastal region of Bangladesh play a very important role in protecting human lives and livestock during cyclones[48]. Although the need for and use of

[47] Benefit of foreshore afforestation was evident during the 1991 cyclone, Sidr (2007) and Aila (2009). It was reported that massive devastation to property and loss of lives during the 1991 cyclone, in Chokoria and areas around it, was primarily the result of virtual absence of mangrove forests along their coasts (BCAS). An in-depth study of the damages and losses inflicted by the Sidr (2007)has noted that even scattered and unplanned forestation on the foreshore of the embankments has substantially helped in breaking the velocity of storm surges (GoB, 2008).

[48] During the Sidr (2007), 15% of the affected population took refuge in cyclone shelters; and it has been estimated that cyclone shelters saved thousands of lives.

cyclone shelters is expected to decline if polders are raised adequately and maintained properly, cyclone shelters will still be needed in the following cases:

a) a number of smaller yet inhabited islands may turn out to be cost ineffective to be protected by polders. For those islanders, cyclone shelters will remain a vital necessity;

b) in localities where projected inundation depth exceeds 3 m and inhabitants of single storied houses would need evacuation.

The total number of additional cyclone shelters required will depend on, and have been calculated from the population likely to be exposed to inundation depth of more than 3m from accentuated storm surges in a changing climate and the capacity of existing cyclone shelters[49]. See figure 4 for location of existing cyclone shelters[50] (see Figure 4).

d) *Early Warning and evacuation System*:

In the past, the early warning and evacuation system of Bangladesh has played an important role in saving lives during cyclones. In general, Bangladesh Meteorological Department issues forewarning for any impending cyclone and storm surge; newspapers, television channels and radio stations broadcast the warning; and the local government administration and the local Cyclone Preparedness Program (CPP) volunteers run by the Red Crescent Society lead the evacuation of the people[51].

Although the overall quality of forecasting cyclones and storm surges has improved over the years, the general consensus is that there is scope for further improvement. At present, the forecast of an area likely to experience a storm surge is usually over-estimated and delineated over a large section of the coastal zone, which can lead to unnecessary repetitive evacuations and loss of popular faith in the early warning system. More precision in forecasting, especially in the landfall location and location-specific inundation depth, is

[49] Data and information on existing cyclone shelters are from the IWM and CEGIS, compiled from the Public Works Department (PWD), LGED, Education Engineering Department, Red Crescent Society, donor agencies, NGOs and local experts.

[50] Many of the existing cyclone shelters are in dilapidated condition. In a 2004 survey, CEGIS found that more than 65% of the shelters had no provision for the special needs of women; almost no facility was user friendly for people with disabilities; and 80% had no provision for livestock.

[51] Red Cross in Bangladesh

required. The Red Crescent Society officials, CPP volunteers and residents of major cyclone affected areas also pointed out the urgent need for broadcasting the warnings in the local dialects[52] and the need to raise awareness for the importance of timely evacuation. According to the CPP volunteers and residents of cyclone-affected areas, in the past, a significant number of fatalities could have been avoided had people not ignored/ resisted evacuation until the last minute.

Experts in the Meteorological Department and the Red Crescent Society were consulted on ways to improve the cyclone early warning and evacuation systems, and their recommendations on improvement of cyclone modeling, upgrading of equipment, training of personnel, and awareness raising programs have been considered for costing in this analysis.

3.5 Costing of Adaptation:

In this paper, focus of adaptation is to avoid further damage from storm surge inundation due to climate change. Hence, costing of adaptation relates to increase in inundation area and inundation depth for a 10 year return period cyclone in a changing climate. The cost of adaptation to an accentuated storm surge has been computed only for adaptation measures relevant to Bangladesh. Hence, the adaptation measures considered in this analysis are the following:

(i) Height enhancement of coastal polders;

(ii) Afforestation to protect sea-facing polders;

(iii) Multipurpose cyclone shelters;

(iv) Cyclone-resistant private housing;

(v) Strengthening the early warning and evacuation system;

Height enhancement of coastal polders:

For polders identified as “likely to be overtopped”, cost of height enhancement to avoid overtopping has been computed as follows:

[52] Illiterate poor people often experience difficulties in understanding sophisticated Bengali.

(a) Differences between the crest level of embankment of each polder and the storm surge level projected for 2050, with and without climate change have been computed to quantify the potential extent of overtopping of an embankment.

(b) The amount of earth needed for this purpose has been derived from engineering designs. Current local price for earthwork from the BWDB (Tk 109.96/ m^3 if collected from 300m to 1km distance; and Tk 133.44/ m^3 if collected from 1km to 5 km distance) has been used in the estimation. See appendix 4 for details.

(c) Compaction and turfing cost (Tk 7.07 per sq meter), used by the BWDB, have been used to derive total related costs.

(d) As "toe erosion" of the embankment of polders is a serious problem in Bangladesh, some sections of the polders would need hard protection. Cost of such hard protection has been computed using the rate for using cement concrete (CC) blocks with sand filters and geo-textile, Tk. 224,100/meter - the locally available technology, ranked as the best technology so far. [53]

(e) Height enhancement of embankments will require more land for strengthening the bases. For sea facing polders, foreshore land is usually government owned or *khas* land. For interior and marginal polders, however, neighboring land is often under private ownership. Hence, requisition of such land would involve compensating the landowners, and in some cases, their rehabilitation cost. This cost is included in the estimate.

(f) As per standard procedure of operation and maintenance (O&M) cost estimation, a fixed percentage (2%) of capital investment has been assumed to be the regular maintenance cost.

The result from this algorithm is in a projection of an adaptation cost of $892 million for coastal polders (26 interior polders and 33 sea facing polders) in a changing climate. Table 6 summarizes the projected cost(s) for "interior" and "sea facing polders" without and with climate change (See Table 6).

[53] In order to protect minor erosion, the use of vetivera grass is often recommended. However, past experience with the vetivera grass option is not very encouraging. The growth and survival rate has been poor along the Chittagong belt, apparently due to a combination of factors including high salinity of the soil. As the soil along the south-western coast is even more saline, it's not clear whether vetiver is the right option for Bangladesh. However, in other regions Vetivera grass may work, and cost of the vetivera plantation is Tk 70700/ ha.

See Appendix 5 for itemized cost estimates for sea facing and interior polders.

Coastal afforestation measures:

As mangrove forests exist along some segments of the coastline of Bangladesh, only the additional cost of further afforestation is computed. At present, estimation from Google Earth using GIS methodology indicates 897 km length[54] of existing sea polders would require mangrove forests for protection. This in turn implies that for a 500m wide protective forest belt, as recommended by the IWM officials, a foreshore area of 448.5 sq. km (= 897km x 0.5 km) would need afforestation. At the current cost of afforestation of $168,000 / sq km[55], the projected cost is US $ 75 million.[56]

Multipurpose Cyclone Shelters:

Current consensus is in favor of multipurpose cyclone shelters with elevated space for livestock and overhead water storage, which can serve as a primary school / office space at times other than an emergency.

In coastal Bangladesh, 8,059,185 people were exposed to storm surge related inundation depth of more than 3m in 2001. In 2050, with a projected growth of population[57], 13,571,667 inhabitants will be exposed to storm surge related inundation depth of more than 3m even without climate change. In a changing climate with the projected expansion of the inundation zone as well as an increase in inundation depth coupled with a projected population growth, an additional 9,122,762 inhabitants will be exposed to a similar inundation risk. In estimation of the costing of multipurpose cyclone shelters, current cost and capacity of cyclone shelters have been collected from the World Bank funded projects. At present, a World Bank-funded multipurpose cyclone shelter, under-construction, with provisions for 1,600 people costs $214,000. In order to accommodate 9,122,762 inhabitants

[54] At present, total length of 49 sea facing polders is 957 km, of which only 60 km has forest belts.
[55] The cost of afforestation per hectare used is from the CERP II project.
[56] With the addition of 500 m forest belt, requirement to enhance the elevation of embankments of sea polders may reduce by 30 cm in specific locations.
[57] Population for the coastal region in Bangladesh 2050 has been projected under the assumption that Bangladesh will attain replacement fertility rate by 2021, and 68.4% growth of coastal population between 2001 and 2050.

exposed to inundation risk due to climate change, additional 5,702 multipurpose shelters would be required at the estimated cost of $ 1.2 billion.[58]

Cyclone resistant private housing:

Inspection reveals that in the past cyclones, the housing sector has accounted for a significant portion of damage. For example, during the severe cyclone of 2007, Sidr, damage to the housing sector has been estimated to be $839 million accounting for 50% of total damages to the economy (GoB, 2008). In the coastal region, houses can be made cyclone resistant when suitable designs and building codes are followed. Upon consultation with local Architects and Civil Engineers, this analysis is recommending a revolving fund of $200million(for subsidizing construction material and extending subsidized housing credit)[59]to encourage the construction of brick-built houses with concrete roofs (on stilts, if necessary) in accordance with the proper building codes. It is expected that these houses, in turn, will serve as single/ multi-family cyclone shelters during storm surges.

Strengthening the early warning and evacuation system:

Focus group interviews were conducted with the experts of the IWM, Bangladesh Meteorological Department, the Red Crescent Society and residents of recent cyclone-affected areas on the requirements for strengthening the cyclone early warning and evacuation system in Bangladesh. Experts of the IWM emphasized the need for improved location-specific inundation projection; officials of the Bangladesh Meteorological Department emphasized the need for more accurate forecasting of cyclone landfall location and inundation depth; and the officials of the Red Crescent Society, CPP volunteers and residents of past cyclone affected areas emphasized the need for raising awareness to promote proper and timely evacuation.

[58] In construction of cyclone shelters, selection of sites and proper accessibility should be considered with caution. Some of the cyclone shelters in the past were sited and designed inappropriately.

[59] Subsidy systems should always be designed with caution so that misuse of subsidies can be avoided.

For improvement in location-specific inundation projections (basis of forecasting and adaptation planning), the IWM has pointed out the need for the following:

Items	Area	Per unit cost	Estimated Total Cost (in millionUS$)
Topographic Survey LIDAR & RTK GPS Survey	23,500 sq km	US$200/ sq km	5
Mathematical Modeling			3
Total			**8**

Officials of the Meteorology Department have identified the following requirements for strengthening the cyclone early warning system: a) modernization of existing 35 observatories, b) establishment of additional 30 observatories, c) establishment of 5 new radio stations, d) modernization of existing workshop and laboratory of the BMD, and e) development of a training institute. Approximate costs of these requirements are as follows:

	Items	Estimated Cost in MillionUS$
1.	Modernization of the existing 35 (thirty five) observatories of BMD	6.00
2.	Establishment of additional 30 (thirty) modern observatories of BMD at different locations of Bangladesh	12.00
3.	Establishment of 5 (five) new Radio Sonde[60] stations of BMD at different locations of Bangladesh	2.00

[60] The ***radiosonde*** is a balloon-borne ***instrument platform*** with radio transmitting capabilities. It contains instruments capable of making direct ***in-situ*** measurements of air temperature, humidity and pressure with height, typically to altitudes of approximately 30 km. These observed data are transmitted immediately to the ground station by a radio transmitter located within the instrument package. The ascent of a radiosonde provides an indirect measure of the wind speed and direction at various levels throughout the troposphere. Ground based radio direction finding antenna equipment track the motion of the radiosonde during its ascent through the air. The recorded elevation and azimuth information are converted to wind speed and direction at various levels by triangulation techniques.

4.	Modernization of existing workshop and laboratory of BMD	7.00
5.	Development of existing Training Institute facilities of BMD	3.00
Total		**30.00**

Operational & Maintenance cost:

	Items	**Estimated Cost in Million US$ per year**
1.	Operational cost of existing 3+additional 5 RS observatories for per year	2.00
2.	Operational cost and maintenance cost of existing 35+additional 30 observatories for per year	3.00
	Total	**5.00**

The current analysis has identified 19 coastal districts as vulnerable to accentuated storm surge related inundation. The Red Crescent Society has recommended an annual awareness promotion program of Tk 10 million (= US$ 142, 857) per district along with a Tk 20 million (= US $ 285,714) overhead cost for the Center, summing to a total cost of US$ 3 million.

On further Infrastructural Investment:

As strong structural protection measures, such as polders, are being suggested in this analysis, it reduces the need for making infrastructure (roads, bridges etc.) resilient to storm surge related inundation, except in regions where there will not be any full-scale structural protection, for example in islands which are not and will not be protected by polders. However, it should be noted that in these unprotected islands, there is not much infrastructure to protect.

To sum up, Table 7 presents the itemized estimated cost of adaptation for storm surge induced inundation in Bangladesh. The estimates indicate that an adaptation investment up to $2.462 billion by 2050 would be needed to implement the measures discussed, even without climate change. The estimate of the additional investment necessary to cope with

climate change is $2.407 billion with an annual recurrent cost of more than $50 million (See Table 7).

Bangladesh is a cyclone-prone country. Cyclones hit the coastal regions of Bangladesh every year. History of cyclones indicates that each year, probability of a Super Cyclonic Storm (wind speed greater than 220 km/hour), a very severe cyclonic storm (wind speed of 119-220 km /hour), and a severe cyclonic storms (wind speed of 90-119 km/hour) are at least 10%, 20% and 30% respectively. Current scientific projections point towards more intense cyclones in a changing climate. Projection of fatalities and injuries alone from one super cyclonic storm out to 2010 in a changing climate indicates a conservative benefit estimate of $1.03 billion. Hence, investment of $1.24 billion towards early warning & evacuation systems and emergency shelters is well worth considering as these will protect lives from all severe cyclones, which are typically frequent in Bangladesh, in addition to the super cyclones. Comparison of the financial damage and loss projection of $4.257 billion with the estimate of adaptation cost of $1.168 billion further reinforces the case for investment in embankment enhancement, foreshore afforestation and cyclone resistant housing in coastal Bangladesh.

4. Conclusion

The scientific evidence indicates that climate change will aggravate storm surge-related inundation for two reasons. First, surges will be elevated by a rising sea level as thermal expansion and ice cap(s) continue to melt. Second, a warmer ocean is likely to intensify cyclone activity and thus heighten storm surges. The destructive impact of storm surges will generally be greater when the surges are accompanied by strong winds and large onshore waves. Larger storm surges threaten greater future destruction, because they will increase the depth of inundation and will move further inland - threatening larger areas than in the past. This scientific evidence points to the need for greater disaster preparedness in countries vulnerable to storm surges.

At present, systematic studies of storm surge patterns in the future, location-specific potential damage and adaptation alternatives are scarce in developing countries; this research is an attempt to narrow this gap. In this analysis, the vulnerability of coastal areas in Bangladesh, a tropical cyclone hotspot, to larger storm surges and sea-level rise in a

changing climate by 2050 has been assessed. Hydrodynamic models have been used to delineate future inundation zones and location-specific inundation depths associated with 27 cm sea-level rise and 10 percent intensification of wind speed from global warming. After estimating future inundation, geographic overlays have been used to identify coastal populations, settlements, infrastructure and economic activity at risk of inundation. Potential damage from a 10 year return period severe cyclone has been estimated. Cyclones hit the coastal regions of Bangladesh almost every year and cyclone risk spans the entire coastline; as a result Bangladesh has developed an extensive infrastructure such as coastal polders, cyclone shelters, early warning and evacuation system to protect the coastal region. The changes in the protective infrastructure that will be required in a changing climate have been quantified and the cost of adaptation to the future climate (2050) as well as current adaptation deficit has been computed.

The storm surge-induced inundation area estimates indicate a potential 69% increase in the vulnerable zone with more than 3m inundation depth and 14% increase in the vulnerable zone with more than 1m inundation depth with climate change by 2050. At present, a 10-year return period cyclone with an average wind speed of 223 km/ hour (as recorded during the cyclone Sidr, 2007) covers 26% of the vulnerable zone; estimates of this study indicate that a similar cyclone will be more intense with global warming and is likely to cover 43% of the vulnerable zone by 2050. The post disaster damage and loss estimates revealed the most recent 10 year return period cyclone in Bangladesh (eg Sidr in 2007) caused a financial damage and loss of $1.67 billion. The projection of damage reported in this paper suggests a 10-year return period cyclone out to 2050 will result in an additional financial damage and loss of $4.560 billion[61] in a changing climate. In addition, a conservative estimate of monetized loss from additional deaths and injuries is $1.03 billion.

At present, Bangladesh has 123 polders, an early warning & evacuation system and more than 2,400 emergency shelters to protect coastal inhabitants from tidal waves and storm surges. Yet, estimates point out that currently Bangladesh has an adaptation deficit of $2.462 billion. It has been further estimated that in a changing climate by 2050, 59 polders will be overtopped during storm surges and another 5,500 cyclone shelters (each with the capacity of 1,600 people) will be needed. The estimate of additional investment necessary to

[61] of which damage is $2.437 billion and loss is $2.123 billion.

cope with climate change is $2.407 billion with an annual recurrent cost of more than $50 million. Among the adaptation alternatives, polders, foreshore afforestation, multi-purpose cyclone shelters, cyclone-resistant private housing and further strengthening of the early warning & evacuation system have been taken into consideration.

The UNDP has identified Bangladesh as a tropical cyclone hotspot. Cyclones hit the Bangladesh coast every year, and on average a severe cyclone (wind speed of 90 – 119 kmph) strikes Bangladesh every three years. The vulnerability of Bangladesh may increase even more as current scientific evidence points towards a probable increase in the frequency of intense tropical cyclones in the Bay of Bengal. The estimates reported in this paper indicate that the cost of addressing current cyclone/ storm surge hazards is significant in Bangladesh and compounded by the fact that the country has an outstanding adaptation deficit. The comparison of even a conservative damage estimate from a single 10-year return period cyclone with the adaptation cost indicates the incremental cost of adapting to climate change by 2050 is small compared to the potential damage[62], which strengthens the case for rapid adaptation. [63]

The climate is expected to change gradually; hence required investments for adaptation can be phased. The itemized adaptation cost estimates provided in this paper could help spur the Government of the People's Republic of Bangladesh to develop location-specific coastal adaptation plans now in order to avoid future losses. Ratios of location-specific potential damage[64] and adaptation cost can be of use for prioritizing investments and undertaking them sequentially, as resources permit.

For the international community, this paper presents a detailed bottom-up methodology to estimate potential damage and adaptation cost to intensified storm surges in a changing climate. The approach integrates information on climate change, assets and activities at risk, growth projections, likely damage and cost estimates.

---

[62] This comparison is a conservative one as damages from more frequent but less intense cyclones (nonetheless destructive) have not been considered.

[63] In addition, the large magnitudes of potential impacts on people and the economy provide strong evidence in support of rapid action from to reduce global warming by mitigating greenhouse gas emissions.

[64] Computation of location-specific damage estimates is subject of future research.

References:

Ali, A. (1999). Climate Change Impacts and Adaptation Assessment in Bangladesh. Climate Research, vol. 12, pp.109-116.

Bengtsson, L., K. I. Hodges, and E. Roeckner, 2006. Storm tracks and climate change. *Journal of Climate* 19: 3518-43.

Cropper M. and S. Sahin. 2009. Valuing Mortality and Morbidity in the Context of Disaster risks. The World Bank Policy Research Working Paper # 4832.

Dasgupta S., B. Laplante, C. Meisner, D. Wheeler and J. Yan. 2009. The impact of sea-level rise on developing countries: A comparative analysis. *Climatic Change,* Vol. 93, No. 3, 379-388.

Emanuel, K., 2005. Increasing destructiveness of tropical cyclones over the past 30 years. *Nature*: 436, 686-688.

Emanuel, K., R. Sundararajan, J. Williams. 2008. Hurricanes and Global warming: Results from Downscaling IPCC AR4 Simulations. Available at ftp://texmex.mit.edu/pub/emanuel/PAPERS/Emanuel_etal_2008.pdf

Government of the People's Republic of Bangladesh (2009): Bangladesh Climate Change Strategy and Action Plan 2009.

Government of the People's Republic of Bangladesh (2008): Cyclone Sidr in Bangladesh: Damage, Loss, and Needs Assessment for Disaster Recovery and Reconstruction.

Hoque, M. Mozzammel. "Strategies and Measures to Reduce Cyclone Damage." In Cyclone Disaster Management and Regional/Rural Development Planning: UNCRD-CIRDAP Seminar, Phase III, 27-29 January, 1992, Chittagong, Bangladesh, 25-45. Nagoya, Japan: UNCRD, 1992.

IMD 2010, http://www.imd.gov.in/section/nhac/dynamic/faq/FAQP.htm#q42 (accessed March 15, 2010)

International Workshop on Tropical Cyclones (IWTC). 2006. *Statement on tropical cyclones and climate change*. November, 2006, 13 pp. Available at: http://www.gfdl.noaa.gov/~tk/glob_warm_hurr.html

IPCC (2007). Climate Change 2007: Impacts, Adaptation and Vulnerability: Summary for Policymakers. Working Group II Contribution to the Intergovernmental Panel on Climate Change Fourth Assessment Report. IPCC, Geneva.

Keim, M. E. 2006. Cyclones, Tsunamis and Human Health. *Oceanography* 19(2): 40-49.

Khalil, G. 1992. Cyclones and Storm Surges in Bangladesh: Some Mitigative Measures. Natural Hazards. Vol. 6, pp 11-24

Knutson, T. R., and R. E. Tuleya. 2004. Impact of CO2-induced Warming on Simulated Hurricane Intensity and Precipitation Sensitivity to the Choice of Climate Model and Convective Parameterization. *Journal of Climate* 17: 3477-95.

Landsea, C.W., B.A. Harper, K. Hoarau, and J.A. Knaff. 2006. Climate Change: Can We Detect Trends in Extreme Tropical Cyclones? *Science*: 313(5786): 452-54.

Michaels, P. J., P. C. Knappenberger, and R. E. Davis. 2005. *Sea-Surface Temperatures and Tropical Cyclones: Breaking the Paradigm.* Presented at 15th Conference of Applied Climatology. Available at http://ams.confex.com/ams/15AppClimate/techprogram/paper_94127.htm

Ministry of Environment and Forest, Government of the People's Republic of Bangladesh (2005): National Adaptation Programme of Action

Multi-purpose Cyclone Shelter Project (MCSP) 1993. Summary Report, Bangladesh University of Engineering and Technology and Bangladesh Institute of Development Studies, Dhaka.

Murty, T.S., and El-Sabh, M.I. (1992). Mitigating the Effects of Storm Surges Generated by Tropical Cyclones: A proposal, Natural Hazards 6(3), 251-273.

Nicholls, R. J. 2003. *An Expert Assessment of Storm Surge "Hotspots".* Final Report (Draft Version) to Center for Hazards and Risk Research, Lamont-Dohert Observatory, Columbia University.

Pielke, R. A., C. Landsea, M. Mayfield, J. Laver, and R. Pasch. 2005. Hurricanes and Global Warming. *Bulletin of American Meteorological Society*, November, pp.1571-75.

Quadir, D. A. and Md. Anwar Iqbal. 2008. Tropical Cyclones: Impacts on Coastal Livelihoods, IUCN Working Paper.

Rahmstorf, Stefan. 2007. A semi-empirical approach to projecting future sea-level rise. Science, 315, 368-370. http://www.pik-potsdam.de/~stefan/Publications/Nature/rahmstorf_science_2007.pdf

Shultz, J. M., J. Russell, and Z. Espinel, 2005. Epidemiology of Tropical Cyclones: The Dynamics of Disaster, Disease, and Development. *Epidemiologic Reviews* 27: 21-35.

SMRC (2000). The Vulnerability Assessment of the SAARC Coastal Region due to Sea Level Rise: Bangladesh Case. SAARC Meteorological Research Centre, SMRC Publication.

UK DEFRA 2007,Investigating the Impact of Relative Sea-Level Rise on Coastal Communities and their Livelihoods in Bangladesh.

UNDP, 2004. A Global Report: Reducing Disaster Risk: A Challenge for Development. http://www.undp.org/bcpr

Unnikrishnan A.S., R. Kumar, S.E. Fernandez, G.S. Michael and S.K. Patwardhan, 2006. Sea Level Changes along the Indian Coast: Observations and Projections *Current Science India,* 90: 362-368.

United Nations and the World Bank, 2010. UnNatural Disasters: the Economics of Reducing Death and Destruction. Forthcomimg.

Webster, P. J., G .J. Holland, J.A. Curry, and H-R. Chang. 2005. Changes in tropical cyclone number, duration and intensity in a warming environment. *Science* 309: 1844-46.

Woodworth, P. L., and D. L. Blackman, 2004. Evidence for systematic changes in extreme high waters since the mid-1970s. *Journal of Climate* 17(6), 1190-97.

Woth, K., R. Weisse, and H. von Storch. 2006. Climate change and North Sea storm surge extremes: An ensemble study of storm surge extremes expected in a changed climate projected by four different regional climate models. *Ocean Dynamics* 56(1):

World Bank. 2010, "The Cost to Developing Countries of Adapting to Climate Change; New Methods and Estimates" , Washington DC.

Table 1: Typical storm surge characteristics for cyclones in Bangladesh

Wind Velocity (km/hr)	Storm-Surge Height (m)	Limit to inundation (km) from the coast
85	1.5	1
115	2.5	1
135	3	1.5
165	3.5	2
195	4.8	4
225	6	4.5
235	6.5	5
260	7.8	5.5

Source: MCSP, 1993

Table 2: Vulnerable Area Estimates (sq km)

Inundation Depth	2050 Without Climate Change	2050 with Climate Change	Percent Change
More than 1 m	20,876	23,764	+ 14%
More than 3 m	10,163	17,193	+ 69%

Table 3: Vulnerable Population Estimates (million)

Inundation Depth	(a) At Present	(b) 2050 Without Climate Change	Percent Change between (a) and (b)	(c) 2050 with Climate Change	Percent Change between (b) and (c)
More than 1 m	16.83	28.27	+ 68%	35.33	+25%
More than 3 m	8.06	13.54	+68%	22.64	+67%

Table 4: Parameters used for computation of Agricultural Loss

	Area exposed to storm surge inundation in 2050 without Climate Change (hectares)	Area exposed to storm surge inundation in 2050 with climate change (hectares)	Yield (ton/ hectare) in 2005
Aman	1,092,645	1,305,028	1.99
Aus	526,040	618,897	1.69
Boro	272,768	388,828	3.44

Table 5: Additional potential damage and loss from an average cyclone induced inundation in a changing climate by 2050

	Estimated Damage in $	Estimated Loss in S$
Housing	1,947.3 million	-
Education Infrastructure	9.0 million	0.8 million
Agriculture	75.4 million	835.4 million
Non-Agriculture Productive Sectors	87.9 million	1,084 million
Roads	239.5 million	52.7 million
Power	60.2 million	150.0 million
Coastal Protection	17.3 million	
Others	-	-
Total	2,436.6 million	2,122.9 million

Table 6: Estimated cost of height enhancement of coastal embankments

	Without Climate Change	Additional Cost with Climate Change
Interior polders	$ 317 million	$ 389 million
Sea facing polders	$ 2.145 billion	$ 503 million

Table 7: Cost of Adaptation (Investment cost and Recurrent Cost)

Adaptation Option	Without Climate Change	Additional Cost with Climate Change	
	Investment Cost	Investment Cost	Annual Recurrent Cost
Polders	2.462 billion	893 million	18 million
Foreshore afforestation		75 million	
Cyclone Shelters		1.2 billion	24 million
Cyclone Resistant Housing		200 million	
Strengthening of Early Warning & Evacuation System		39 million	8 + million
Total	2.462 billion	2.407 billion	50 million +

Figure 1: Cyclone tracks considered for demarcation of vulnerable zone in a changing climate

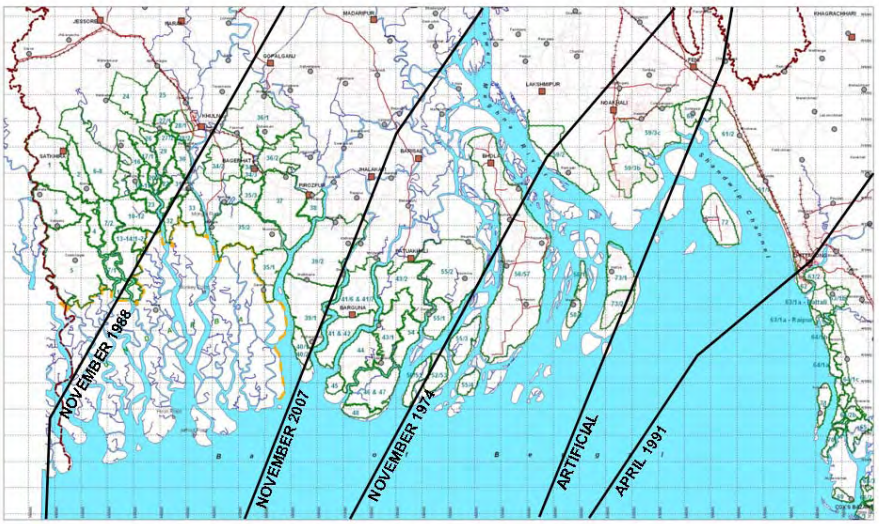

Figure 2: Projection of Storm Surge Inundation in a Changing Climate-2050

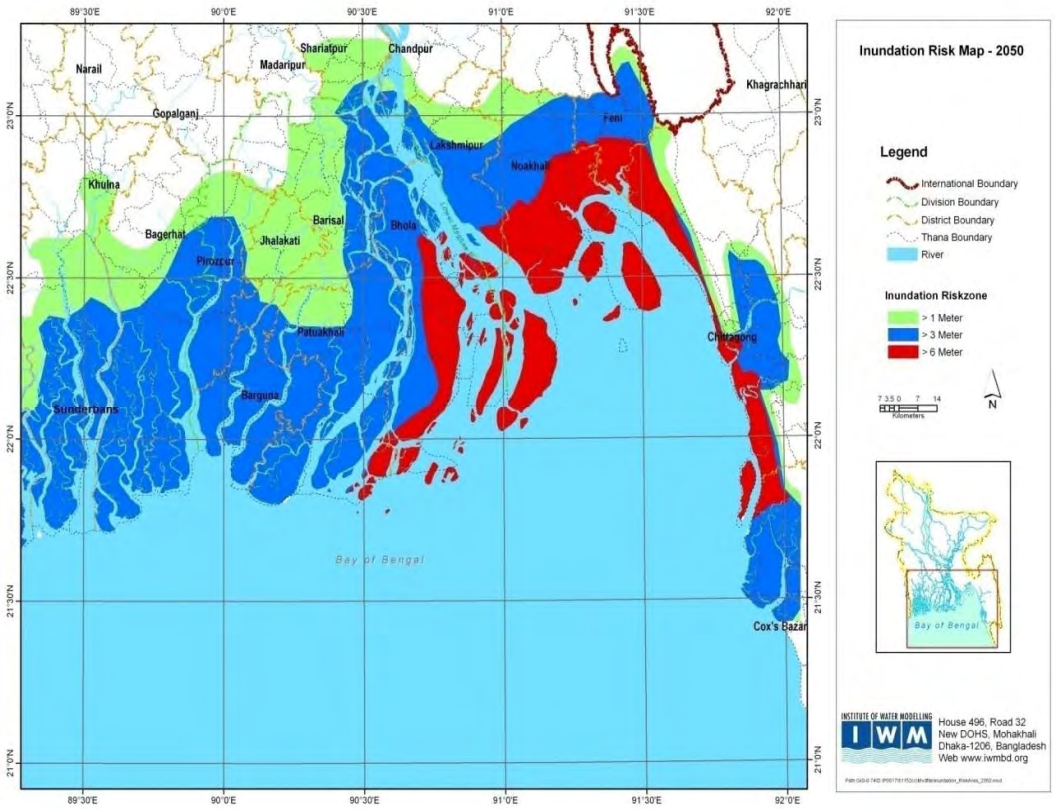

Figure 3 : Lay out map of coastal polders

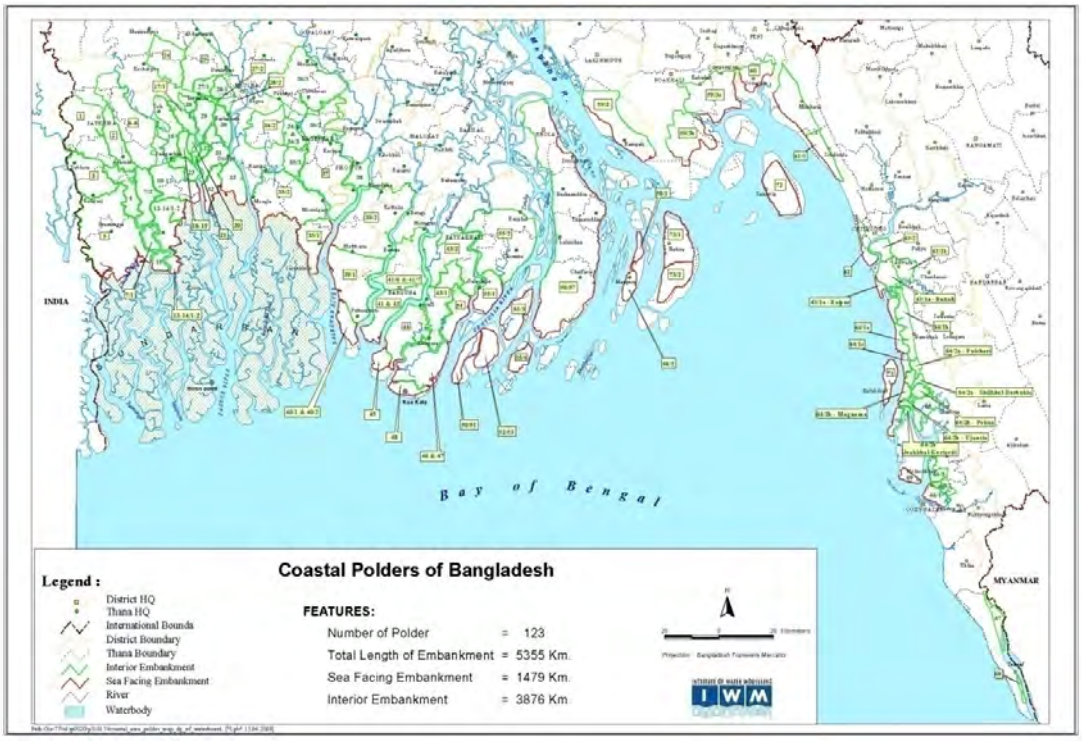

Figure 4: Spatial locations of existing cyclone shelters in the coastal area

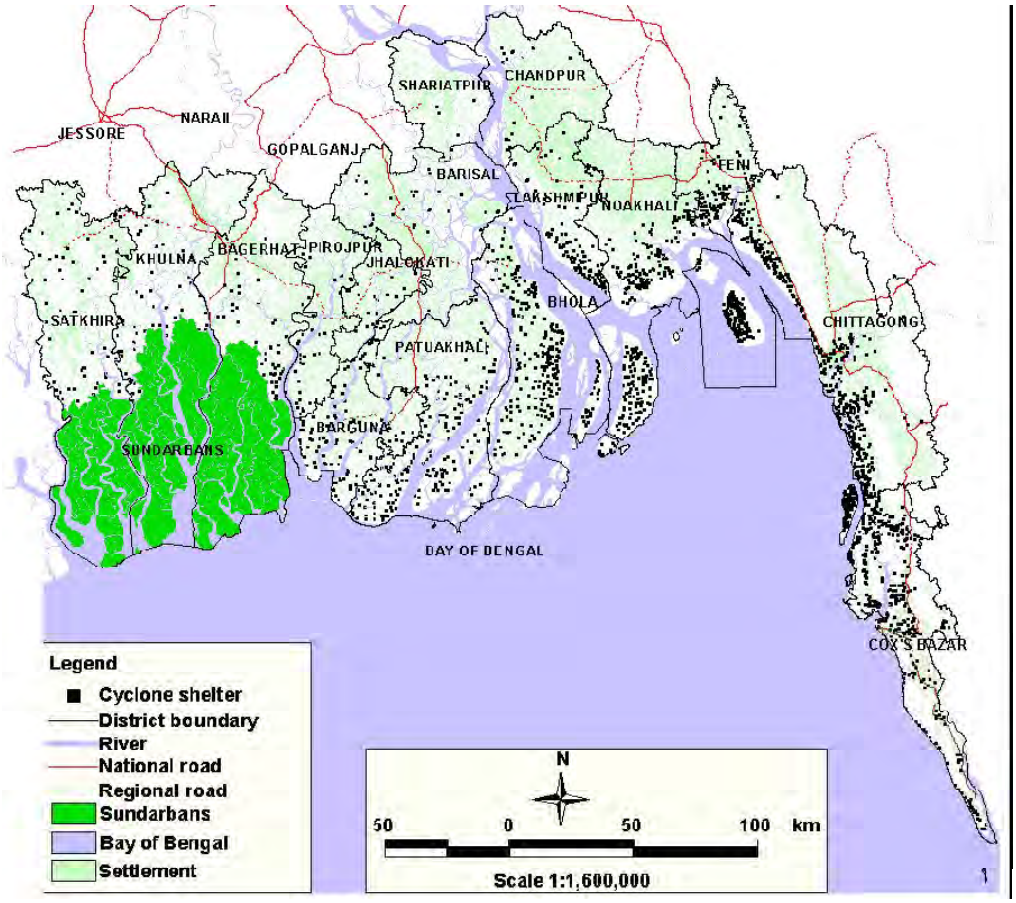

Source: CEGIS

Box 1: Sidr Damage to the Economy

Total damage including indirect loss: $1.67 billion

Of which,

- Housing damage & loss: $839 million (50%)
- Agricultural damage & loss: $438 million (26%)
- Transport-related damage & loss: $141 million (8.4%)
- Water Resource Control- related damage & loss: $71 million (4.3%)
- Education infrastructure-related damage & loss: $69 million (4%)
- Other sectors (industry, electricity, water and sanitation, urban and municipal, health, nutrition, commerce, tourism, environment, etc.): 7.3%

Source: GoB (2008)

Appendix 1

The storm surge model used in this analysis is a combination of a Cyclone model and a Hydrodynamic model.

The cyclone model simulated a cyclone based on the following parameters:

1. Radius of maximum winds;
2. Maximum wind speed;
3. Cyclone tracks, forward speed and direction;
4. Central pressure; and
5. Neutral pressure.

Then the simulated cyclone is run with the hydrodynamic model to generate cyclone-induced storm surge and associated coastal inundation. In this analysis, the Bay of Bengal model based on MIKE21 hydrodynamic modeling system has been used. It is a two way nested two-dimensional model and its domain extends from Chandpur to 16º latitude in north-south direction. The grid size of the model is 200m in the Meghna estuary and coastal region of Bangladesh. A description of the Bathymetry data used to develop the Bay of Bengal Model is as follows:

Bathymetry Data:

The main source of bathymetry data for the modeling is the C-Map (an Electronic Chart System Database), Meghna Estuary Study, Phase II (MES II, 1998-99), Mongla Port Study (2004), IPSWAM (2008) and other projects of Bangladesh Water Development Board (BWDB). Figure 2.2 shows the nested bathymetry of the Bay of Bengal Model.

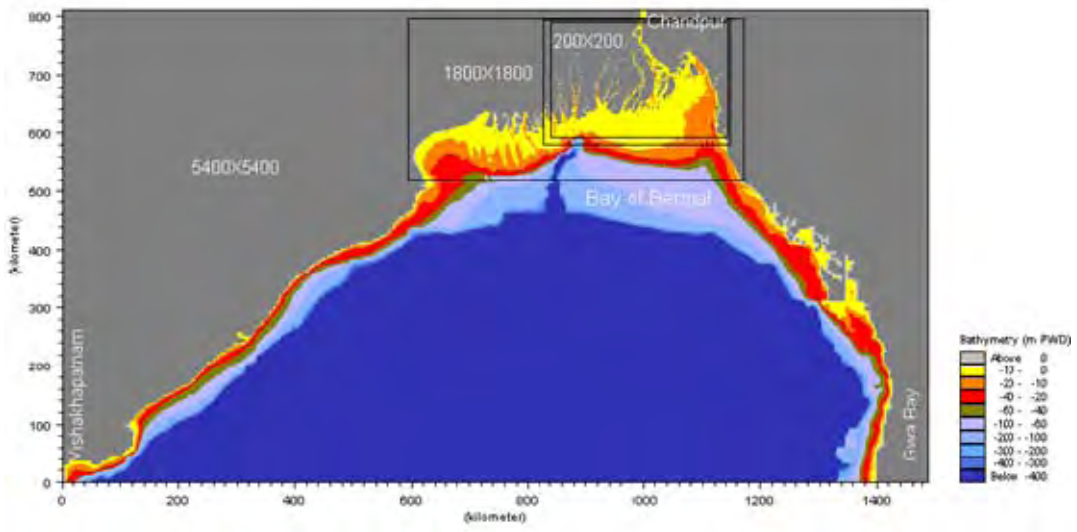

Figure 2.2: Nested bathymetry of Bay of Bengal Model

In order to simulate realistic flood depths, the following topographic data has been used in the analysis:

Topographic Data (Digital Elevation Model)

The main source of topographic elevation data for the coastal region of Bangladesh is the FINNMAP land survey, FAP 19- National DEM (1952-64) and projects of Bangladesh Water Development Board (i.e. Khulna Jessore Drainage Rehabilitation Project, 1997; Beel Kapalia project, 2008; and Beel Khuksia project, 2004). The FINNMAP topographic maps and other data were digitized to develop Digital Elevation Model (DEM) of the coastal region of Bangladesh. The grid size of the model is 50 m x 50 m. The DEM of the coastal region of Bangladesh is shown in Figure 2.3.

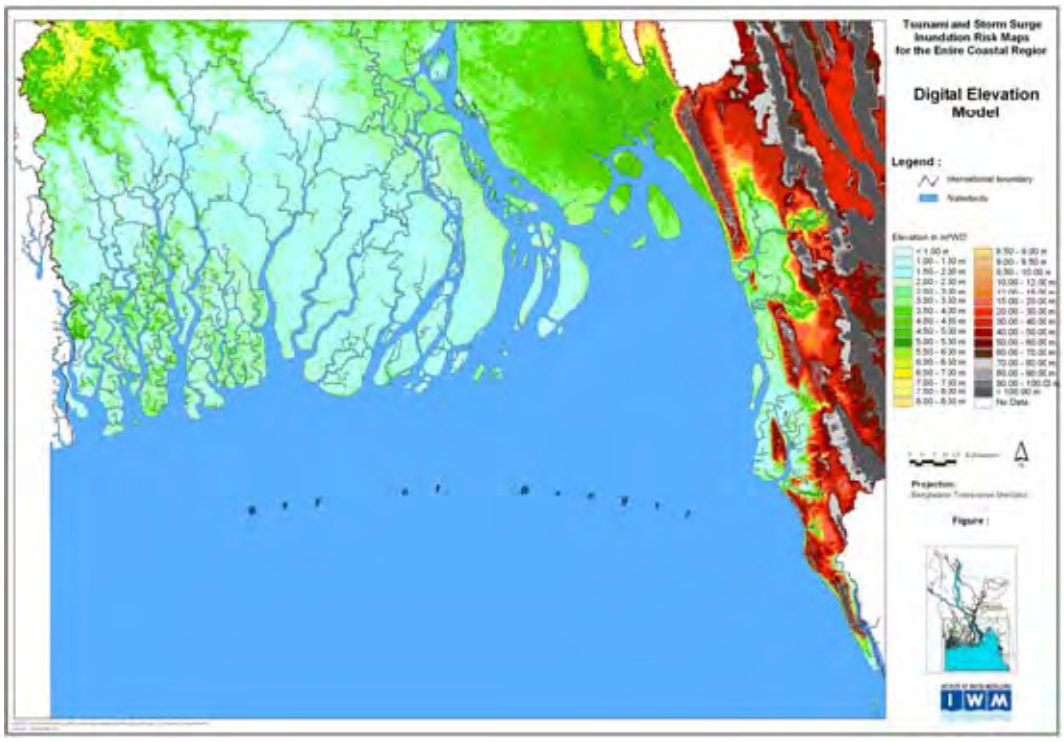

Figure 2.3: Digital Elevation Model of coastal region of Bangladesh

The MIKE 21 modeling system includes dynamic simulation of flooding and drying processes - important for a realistic simulation of flooding in the coastal area and inundation.

Appendix 2:

Tracks of major cyclones that crossed the coast of Bangladesh during the period 1960-2009

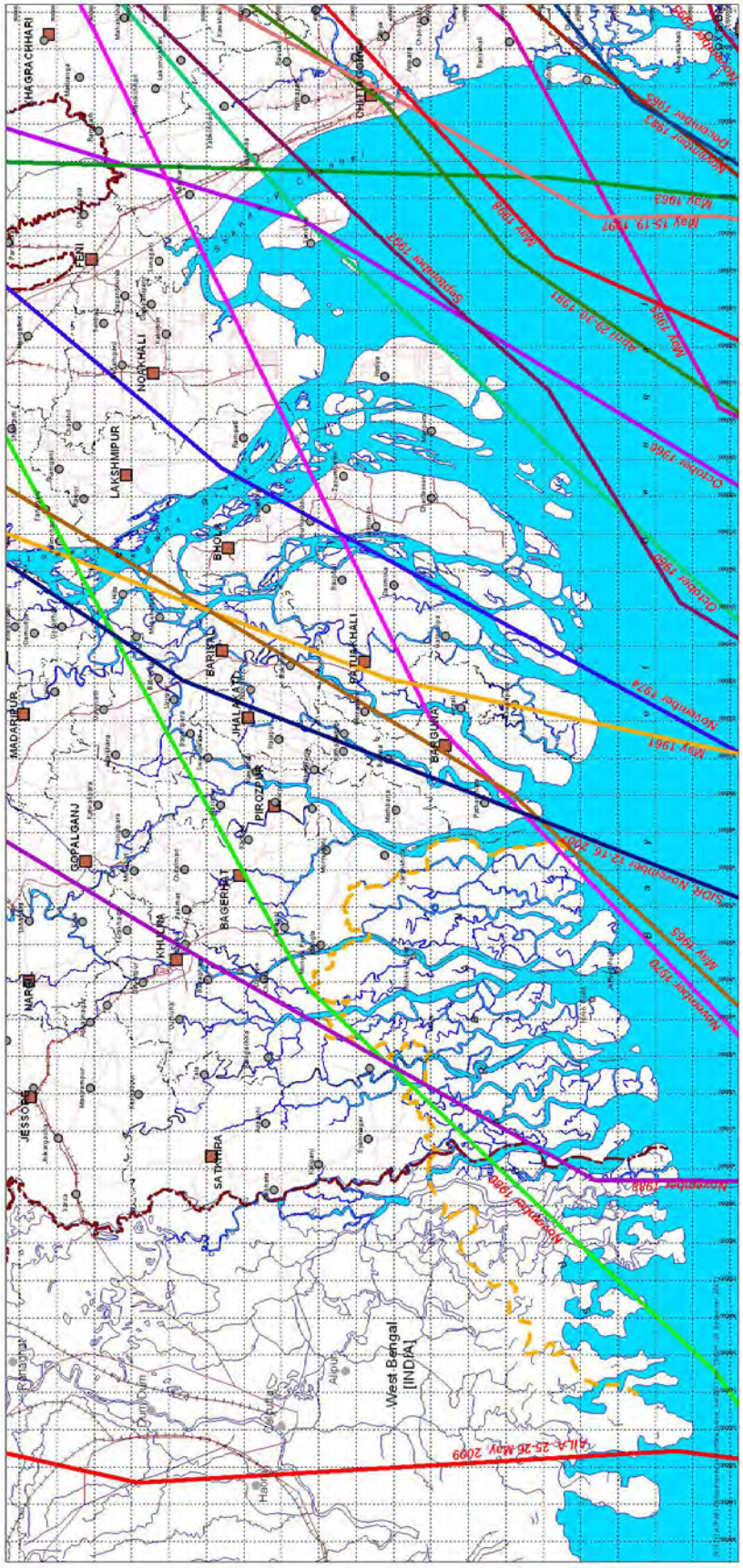

Appendix 3:

Major cyclones crossing Bangladesh Coast (1960—2009)

Year	Landfall date	Duration	Landfall Location	Wind speed (km/hr)	Storm Surges (m)	Human Casualties	Number of People Affected	Specific Economic Loss
1960	October, 31	October 30-31	Noakhali Chittagong	193	6.1	10000	200,000	Loss of livestock: 27,783, Destruction of Houses: 568,161, 5-7 Vessels capsized .
1961	May, 9	May 5-9	Meghna estuary	161	3.1	11468	NA	Estimated loss $11.9 billion. Loss of livestock: 25,000, Railway track between Noakhali and Harinarayanpur was damaged.
1963	May, 29	May 28-29	Noakhali Chittagong	202	6	11520	1,000,000	Estimated loss $46.5 billion. Loss of livestock: 32,617, Destruction of Houses: 376,332, 4787 boats were damaged
1965	May, 12	May9-12	Barisal-Noakhali	162	3.7	19279	15,600,000	Estimated loss $57.7 billion.

1965	December, 15	December 7-15	Cox's Bazar	184	3.6	873	60,000	Destruction of Houses: -35,636, Rice harvest loss 40-50%, Significant damage to fishing boats and nets.,40,000 salt beds were inundated
1966	October, 1	September 23-October 1	Noakhali	139	6.7	850	1,800,000	Estimated loss $22.4 billion. Loss of livestock: 65,000; Damage of poultry: 185,000, Destruction of Houses: 309000, damage of Food grains: 5,595 tons.
1970	November, 12	November 8-13	Bhola, Meghna estuary	224	10	300000	3,648,000	Estimated loss $86.4 billion.
1974	November, 28	November 24-28	Chittagong Cox's Bazar	161	5.1	50	NA	Loss of livestocks: 1,000, Destruction of Houses: 2,300 .
1983	November, 9	November 5-9	Chittagong Cox's Bazar near Kutubdia	135	1.5		NA	Destruction of Houses: 2,000, number of missing boats: 50, number of fishermen missing: 300.
1985	May, 25	May 22-25	Noakhali	154	4.5	4264	1,810,000	-

					5	(6805 missing)		
1986	November, 9	November 7-9	Patuakhali	110	0.61			-
1988	November, 18	November 16-18	Southeast coast of Teknaf	135			10,568,860	-
1991	April, 29	April 25-30	Noakhali Chittagong	235	7.6	133882	15,438,849	Estimated loss $1,780 billion.
1995	November, 25	November 25-15	Gulf of Bengal	110	3.6	172	250,000	-
1997	May, 19	May 15-19	Chittagong/ Sitakundu	200	4.6	155	3,052,738	Loss of livestocks: 3,118, Destruction of Houses: 211,717, damage of crops: 97,333 acres, damage to salt production: 2,232,000 acres.
1997	September 26	September 26-27		150	3	188	751,529	-
1998	May 20	May 17-20	Sitakundu	186			108,944	
2007	November 15	November 11-16	Sundarban Borguna	250	6-8	2388	8,978,541	Estimated Damage $ 2300 billion

2009	May 5	May 5-6	West Bengal, India	95	4	190	3,935,341	Estimated Damage $ 270 billion

Source: Quadir and Iqbal (2008) and EMDAT

Appendix 4

Earthwork Computation with an illustrative Example:

Sea facing Polders

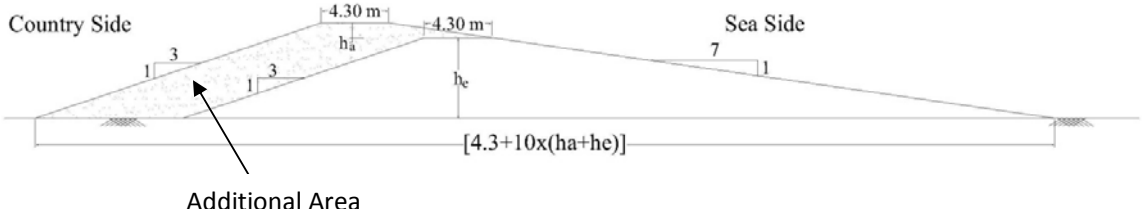

Additional unit volume of earthwork, A

$$= 0.5x\{4.3+4.3+10x(h_a+h_e)\}x(h_a+h_e)-0.5x\{4.3+4.3+10xh_e\}xh_e$$

$$= 5\ h_a^2+4.3\ h_a+10\ h_a\ h_e$$

Where,

h_e =Existing Height

h_a =Additional Height

Interior polders:

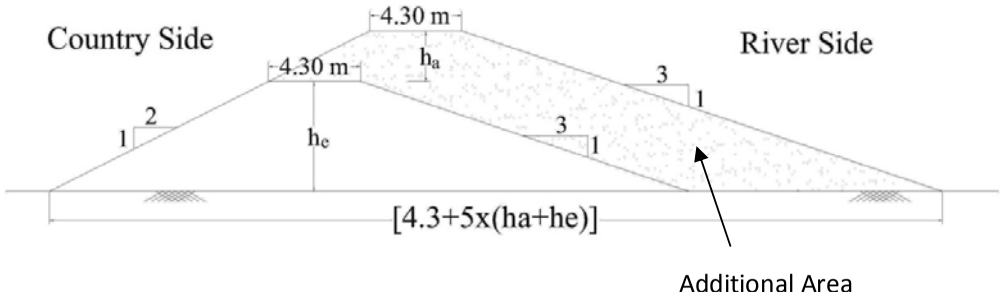

Additional unit volume of earthwork, A

$$= 0.5x\{4.3+4.3+5x(h_a+h_e)\}x(h_a+h_e)-0.5x\{4.3+4.3+5xh_e\}xh_e$$

$$= 2.5\ h_a^2+4.3\ h_a+5\ h_a\ h_e$$

Total earthwork volume is computed by multiplying the unit volume of earthwork with the affected length of polder.

Appendix 5

Table A: Estimated cost to prevent overtopping of interior polders by 2050 (even without climate change)

INTERIOR DYKE

_	Polder	Length	Existing Height	Height to be Raised	Cost (million US$)							
		(m)	(m)	(m)	Earthwork (300 m to 1.0 km)	Earthwork (1.0 km to 5.0 km)	Turfing	Plantation (Vetivera)	Land Acquisition	Major Protection Work	Toe Protection	**Total**
1	P10-12	67,400	4	2.5	8.1	0.9	0.1	0.0	1.4	42.9	0.0	**53.3**
2	P35/1	61,600	4.5	2.5	8.0	0.9	0.0	0.0	1.3	0.0	32.0	**42.2**
3	P35/2	104,600	3	2.5	10.5	1.1	0.1	0.1	2.2	0.0	0.0	**14.0**
4	P37	100,100	3.5	2.5	11.0	1.2	0.1	0.1	2.1	0.0	0.0	**14.5**
5	P38	39,500	3.5	3.5	6.6	0.7	0.0	0.1	1.2	0.0	0.0	**8.6**
6	P39/1	96,200	5	3.5	20.1	2.1	0.1	0.1	2.9	10.3	0.0	**35.6**
7	P39/2	109,200	3	3	13.8	1.5	0.1	0.0	2.8	0.0	0.0	**18.2**
8	P41/6-7	95,100	4.5	2.25	10.9	1.2	0.1	0.0	1.8	0.0	0.0	**14.0**
9	P42	28,000	4.5	3.5	5.5	0.6	0.0	0.0	0.8	5.1	0.0	**12.1**
10	P43/1	113,520	4.5	3.3	20.6	2.2	0.1	0.1	3.2	0.0	0.0	**26.2**
11	P43/2	120,600	4.5	3.3	21.9	2.3	0.1	0.1	3.4	0.0	0.0	**27.8**
12	P44	83,700	4.5	3	13.5	1.4	0.1	0.0	2.2	10.3	0.0	**27.5**
13	P55/2	109,100	0.75	3.4	9.6	1.0	0.1	0.0	3.2	0.0	0.0	**13.9**
14	P63/1A - Battali	38,000	5	3.25	7.3	0.8	0.0	0.0	1.1	0.0	0.0	**9.1**
												317.0

Table B: Estimated cost to prevent overtopping of interior polders by 2050, in a changing climate

INTERIOR DYKE

	Polder	Length	Existing Height	Height to be Raised	Cost (million US$)							
		(m)	(m)	(m)	Earthwork (300 m to 1.0 km)	Earthwork (1.0 km to 5.0 km)	Turfing	Plantation (Vetivera)	Land Acquisition	Major Protection Work	Toe Protection	**Total**
1	P07/1	31,800	4.5	2.5	4.1	0.4	0.0	0.0	0.7	21.4	0.0	**26.7**
2	P07/2	64,000	4	2.5	7.7	0.8	0.0	0.0	1.4	25.7	0.0	**35.6**
3	P10-12	67,400	4	2.5	8.1	0.9	0.1	0.0	1.4	42.9	0.0	**53.3**
4	P13-14/2	122,400	4.5	2.5	15.9	1.7	0.1	0.0	2.6	0.0	0.0	**20.3**
5	P23	36,700	4	3	5.5	0.6	0.0	0.0	0.9	21.4	0.0	**28.5**
6	P31	62,700	4	2.5	7.5	0.8	0.0	0.0	1.3	42.9	0.0	**52.6**
7	P32	48,800	4	2.5	5.9	0.6	0.0	0.0	1.0	25.7	0.0	**33.3**
8	P33	51,500	4	2.5	6.2	0.7	0.0	0.0	1.1	25.7	0.0	**33.7**
9	P35/1	61,600	4.5	4	14.2	1.5	0.1	0.0	2.1	0.0	32.0	**49.9**
10	P35/2	104,600	3	4	19.3	2.1	0.1	0.1	3.6	0.0	0.0	**25.0**
11	P35/3	39,700	3	3	5.0	0.5	0.0	0.0	1.0	0.0	0.0	**6.6**
12	P36/2	87,400	3	3	11.0	1.2	0.1	0.0	2.2	0.0	0.0	**14.5**
13	P37	100,100	3.5	4.25	21.7	2.3	0.1	0.1	3.6	0.0	0.0	**27.8**
14	P38	39,500	3.5	4.25	8.6	0.9	0.0	0.1	1.4	0.0	0.0	**11.0**
15	P39/1	96,200	5	4	23.8	2.5	0.1	0.1	3.3	10.3	0.0	**40.0**
16	P39/2	109,200	3	4.75	25.4	2.7	0.1	0.0	4.4	0.0	0.0	**32.7**
17	P41/6-7	95,100	4.5	2.5	12.3	1.3	0.1	0.0	2.0	0.0	0.0	**15.8**
18	P42	28,000	4.5	4.75	8.1	0.9	0.0	0.0	1.1	5.1	0.0	**15.3**
19	P43/1	113,520	4.5	3.5	22.2	2.4	0.1	0.1	3.4	0.0	0.0	**28.1**
20	P43/2	120,600	4.5	3.5	23.6	2.5	0.1	0.1	3.6	0.0	0.0	**29.9**
21	P44	83,700	4.5	3.7	17.5	1.9	0.1	0.0	2.7	10.3	0.0	**32.4**
22	P55/2	109,100	0.75	4.25	13.6	1.5	0.1	0.0	4.0	0.0	0.0	**19.1**
23	P63/1A -B	38,000	5	7.1	19.9	2.1	0.1	0.0	2.3	0.0	0.0	**24.4**
24	P64/2A	59,100	4.5	6.5	26.0	2.8	0.1	0.0	3.3	0.0	0.0	**32.1**
25	P64/2b-jo	17,000	4	4.5	4.3	0.5	0.0	0.0	0.7	0.0	0.0	**5.4**
26	P64/2b-Pe	30,000	4.5	5.25	9.9	1.1	0.0	0.0	1.4	0.0	0.0	**12.3**
												706.4

Table C: Estimated cost to prevent overtopping of sea-facing polders by 2050 (even without climate change

SEA DYKE												
	Polder	Length	Existing Height	Height to be Raised	Cost (million US$)							
		(m)	(m)	(m)	Earthwork (300 m to 1.0 km)	Earthwork (1.0 km to 5.0 km)	Turfing	Plantation (Vetivera)	Land Acquisition	Major Protection Work	Toe Protection	**Total**
1	P40/1-2	59,000	5	4	27.5	2.9	0.1	0.0	4.0	7.7	16.0	**58.3**
2	P41-42	80,500	4.5	3.5	29.6	3.2	0.1	0.0	4.8	7.7	16.0	**61.3**
3	P45	25,800	6	2.75	8.7	0.9	0.0	0.0	1.2	5.7	16.0	**32.6**
4	P46-47	79,600	5	3.25	28.7	3.1	0.1	0.0	4.4	14.7	0.0	**51.0**
5	P48	38,100	5.8	2.7	12.2	1.3	0.0	0.0	1.8	24.6	64.0	**104.0**
6	P50/51	48,300	5.18	3.3	18.2	1.9	0.0	0.0	2.7	0.0	0.0	**22.9**
7	P52/53	40,300	4.57	4	17.7	1.9	0.0	0.0	2.8	5.1	0.0	**27.6**
8	P54	60,000	4.5	3.3	20.5	2.2	0.1	0.0	3.4	10.3	0.0	**36.4**
9	P55/1	45,800	5	2.9	14.4	1.5	0.0	0.0	2.3	28.6	0.0	**46.8**
10	P55/3	52,700	5	2.75	15.5	1.7	0.0	0.0	2.5	25.7	0.0	**45.4**
11	P55/4	30,800	5.5	4.4	17.3	1.8	0.0	0.0	2.3	25.7	0.0	**47.2**
12	P56/57(E)	140,000	6.5	4	78.6	8.4	0.2	0.0	9.6	0.0	160.1	**256.8**
13	P56/57(W	90,000	5	3	29.4	3.1	0.1	0.0	4.6	0.0	0.0	**37.2**
14	P58/1	32,000	4.8	4.75	18.2	1.9	0.0	0.0	2.6	0.0	0.0	**22.7**
15	P58/2	28,000	4.8	4.8	16.1	1.7	0.0	0.0	2.3	0.0	32.0	**52.2**
16	P59/2	92,800	6	4.75	61.0	6.5	0.1	0.3	7.6	64.3	64.0	**203.8**
17	P59/3B	70,100	6	6	62.3	6.7	0.1	0.0	7.2	0.0	0.0	**76.3**
18	P59/3C	41,800	6	5.5	33.2	3.5	0.1	0.0	3.9	35.7	0.0	**76.4**
19	P60	44,900	7	5.75	41.8	4.5	0.1	0.0	4.4	0.0	0.0	**50.7**
20	P61/1	26,000	6	5	18.2	1.9	0.0	0.0	2.2	0.0	0.0	**22.4**
21	P61/2	45,100	6	2.5	13.6	1.5	0.0	0.0	1.9	0.0	0.0	**17.0**
22	P62	22,000	6	4	11.7	1.2	0.0	0.0	1.5	0.0	0.0	**14.4**
23	P63/1A-Ra	20,000	6	3	7.5	0.8	0.0	0.0	1.0	0.0	0.0	**9.3**
24	P64/1A	54,200	5.5	3.25	20.9	2.2	0.1	0.0	3.0	32.1	38.4	**96.8**
25	P64/2b-M	27,000	5	2.5	7.1	0.8	0.0	0.0	1.2	19.3	16.0	**44.3**
26	P70	29,200	6	2.5	8.8	0.9	0.0	0.0	1.3	30.0	0.0	**41.0**
27	P71	40,500	4.5	3.25	13.6	1.4	0.0	0.0	2.3	64.3	64.0	**145.6**
28	P72	61,700	5.5	5.5	46.3	4.9	0.1	0.0	5.8	75.7	128.1	**260.9**
29	P73/1AB	89,400	5.5	3.8	41.8	4.5	0.1	0.0	5.8	6.4	64.0	**122.6**
30	P73/2	47,600	5	4.1	22.9	2.4	0.1	0.0	3.3	32.1	0.0	**60.9**
												2144.9

Table D: Estimated cost to prevent overtopping of sea-facing polders by 2050 in a changing climate

SEA DYKE

	Polder	Length	Existing Height	Height to be Raised	Cost (million US$)							
		(m)	(m)	(m)	Earthwork (300 m to 1.0 km)	Earthwork (1.0 km to 5.0 km)	Turfing	Plantation (Vetivera)	Land Acquisition	Major Protection Work	Toe Protection	**Total**
1	P40/1-2	59,000	5	4.2	29.3	3.1	0.1	0.0	4.2	7.7	16.0	**60.5**
2	P41-42	80,500	4.5	4.75	43.9	4.7	0.1	0.0	6.6	7.7	16.0	**78.9**
3	P45	25,800	6	3	9.6	1.0	0.0	0.0	1.3	5.7	16.0	**33.7**
4	P46-47	79,600	5	3.5	31.4	3.4	0.1	0.0	4.8	14.7	0.0	**54.3**
5	P48	38,100	5.8	3.5	16.7	1.8	0.0	0.0	2.3	24.6	64.0	**109.4**
6	P50/51	48,300	5.18	3.75	21.3	2.3	0.1	0.0	3.1	0.0	0.0	**26.7**
7	P52/53	40,300	4.57	4.5	20.7	2.2	0.0	0.0	3.1	5.1	0.0	**31.2**
8	P54	60,000	4.5	3.75	24.1	2.6	0.1	0.0	3.9	10.3	0.0	**40.8**
9	P55/1	45,800	5	3.25	16.5	1.8	0.0	0.0	2.6	28.6	0.0	**49.4**
10	P55/3	52,700	5	3.5	20.8	2.2	0.1	0.0	3.2	25.7	0.0	**52.0**
11	P55/4	30,800	5.5	5.25	21.7	2.3	0.0	0.0	2.8	25.7	0.0	**52.6**
12	P56/57(E)	140,000	6.5	4.75	97.2	10.4	0.2	0.0	11.4	0.0	160.1	**279.2**
13	P56/57(W	90,000	5	4	42.0	4.5	0.1	0.0	6.2	0.0	0.0	**52.8**
14	P58/1	32,000	4.8	6.5	27.7	3.0	0.0	0.0	3.6	0.0	0.0	**34.3**
15	P58/2	28,000	4.8	5.75	20.5	2.2	0.0	0.0	2.8	0.0	32.0	**57.5**
16	P59/2	92,800	6	5.5	73.6	7.9	0.1	0.3	8.7	64.3	64.0	**218.9**
17	P59/3B	70,100	6	7.5	84.1	9.0	0.1	0.0	9.0	0.0	0.0	**102.2**
18	P59/3C	41,800	6	8	54.8	5.8	0.1	0.0	5.7	35.7	0.0	**102.1**
19	P60	44,900	7	8	64.5	6.9	0.1	0.0	6.2	0.0	0.0	**77.6**
20	P61/1	26,000	6	7.9	33.5	3.6	0.0	0.0	3.5	0.0	0.0	**40.6**
21	P61/2	45,100	6	8	59.1	6.3	0.1	0.0	6.2	0.0	0.0	**71.7**
22	P62	22,000	6	7	24.0	2.6	0.0	0.0	2.6	0.0	0.0	**29.3**
23	P63/1A-Ra	20,000	6	6	17.8	1.9	0.0	0.0	2.1	0.0	0.0	**21.8**
24	P64/1A	54,200	5.5	7.75	64.7	6.9	0.1	0.0	7.2	32.1	38.4	**149.4**
25	P64/2b-M	27,000	5	5	16.8	1.8	0.0	0.0	2.3	9.6	16.0	**46.6**
26	P64/2b-Uj	22,000	4	5	12.0	1.3	0.0	0.0	1.9	9.6	9.6	**34.4**
27	P66/3	36,600	6	2	8.5	0.9	0.0	0.0	1.3	0.0	0.0	**10.7**
28	P69	29,000	6	2.75	9.8	1.0	0.0	0.0	1.4	18.0	0.0	**30.2**
29	P70	29,200	6	3.25	12.0	1.3	0.0	0.0	1.6	30.0	0.0	**44.9**
30	P71	40,500	4.5	5.75	28.6	3.0	0.0	0.0	4.0	64.3	64.0	**164.0**
31	P72	61,700	5.5	7	64.0	6.8	0.1	0.0	7.4	75.7	128.1	**282.1**
32	P73/1	89,400	5.5	5	59.2	6.3	0.1	0.0	7.7	6.4	64.0	**143.7**
33	P73/2	47,600	5	4.5	25.8	2.8	0.1	0.0	3.7	32.1	0.0	**64.5**
												2648.2

Annex B79

Katherine J. Houghton et al., "Maritime boundaries in a rising sea", *Nature Geoscience*, Vol. 3, No. 12 (2010)

commentary

Maritime boundaries in a rising sea

Katherine J. Houghton, Athanasios T. Vafeidis, Barbara Neumann and Alexander Proelss

Sea-level rise is progressively changing coastlines. The legal implications for the seaward boundaries between neighbouring coastal states are neither straightforward nor foreseeable.

Sea-level rise is one of the certain consequences of climate change[1]. Global mean sea level has been rising throughout the twentieth and twenty-first centuries. Furthermore, because of the lag in the oceans' response to warming, it is expected to continue to rise for centuries, even under the most optimistic mitigation scenarios[2]. Projections of sea-level rise span a broad range. In its Fourth Assessment Report, the Intergovernmental Panel on Climate Change suggested 18–59 cm of global mean sea-level rise by 2100 compared with 1990 levels (plus an uncertain component from dynamic ice-sheet adjustment). Semi-empirical methods have since put forward values of 1.5 m and more[3,4]. Irrespective of the actual level of sea-level rise by 2100, future changes in the world's coastlines will pose fundamental new challenges, not least for international relations.

Sea-level rise will lead to increased coastal flooding, submergence and erosion, loss of wetlands and salinization of river deltas and coastal aquifers[2]. The associated socio-economic impacts that result are expected to be overwhelmingly negative[5], particularly in developing countries. But there are less obvious impacts, as well. One of the less-studied potential outcomes of sea-level rise is the effect of coastline retreat on the delimitation of the maritime areas in which individual states exercise sovereignty, sovereign rights or jurisdiction under the rules of the international law of the sea. The retreat of coastlines as a result of the submergence of low-lying areas, small islands and atolls, as well as coastal erosion, could significantly alter the reference line for the determination of a coastal state's legal zones in the ocean, termed the baseline[6].

Under the United Nations Convention on the Law of the Sea (UNCLOS)[7] and corresponding customary international law, this baseline constitutes the starting point for measuring the breadth of the coastal state's maritime zones. These include the territorial sea that is regarded as sovereign territory of the state, the contiguous zone where a state can exercise limited control to prevent infringements of certain laws, the exclusive economic zone where a state has exclusive economic rights over all resources, and the continental shelf where a state has exclusive economic rights over resources on or below the sea floor, but not in the water column. The baseline is also of crucial importance in the determination of the equidistance and median lines that can be drawn between adjacent or opposite coasts, respectively, to resolve overlapping maritime claims. The normal baseline is defined in Article 5 UNCLOS as the low-water line along the coast as marked on large-scale charts officially recognized by the coastal state. However, where the coastline is deeply indented and cut into, or where there is a fringe of islands along the coast in its immediate vicinity, the baseline can instead be drawn by joining appropriate points, and is then referred to as a 'straight baseline'.

International courts have indicated that changes in the actual coastline of a state will affect the location of the baseline as defined by the international law of the sea[8]. Sea-level rise may therefore profoundly affect the extent of a coastal state's maritime zones as well as maritime delimitations between states with opposite or adjacent coasts. As David D. Caron observes[9]: "[T]he outer boundary of the exclusive economic zone, the contiguous zone, and the territorial sea are ambulatory in that they will move with the baselines from which they are measured."

We explore the issues that would arise from coastline retreat associated with an illustrative projection of 1.5 m of sea-level rise (without consideration of adaptation measures, coastal erosion or land subsidence) and outline three possible legal scenarios: renegotiation of maritime boundary agreements based on the principle of equidistance to correspond with new geographic realities; re-evaluation of both equity and equidistance principles by international courts and tribunals in settling boundary disputes; or finally, reversion of highly disputed exclusive economic zone claims to the legal status of high seas. We argue that the legal implications of impending sea-level rise for the delimitation of coastal states' maritime boundaries need to be addressed preemptively by the affected countries, as an adaptation measure.

Territorial definitions

States may base their maritime claims not only on the baselines set in relation to their mainland coasts, but also on the baselines established in reference to islands that belong to their state territory (Article 121 (2) UNCLOS). However, rocks that cannot sustain human habitation or economic life have no exclusive economic zone or continental shelf (Article 121 (3) UNCLOS). The latter provision will, arguably, also apply to islands that, although not completely submerged, lose their ability to sustain human habitation or economic life owing to sea-level rise. Shifts in baselines that result from permanent submergence of small islands may therefore lead to new conflicts over natural resources, or intensify tensions in regions where maritime boundaries are already disputed.

Our projections for coastlines in response to 1.5 m of global mean sea-level rise are derived by combining elevation data from national and global digital elevation models[10–13] and assuming that all areas that are below 1.5 m and hydrologically connected to the sea will

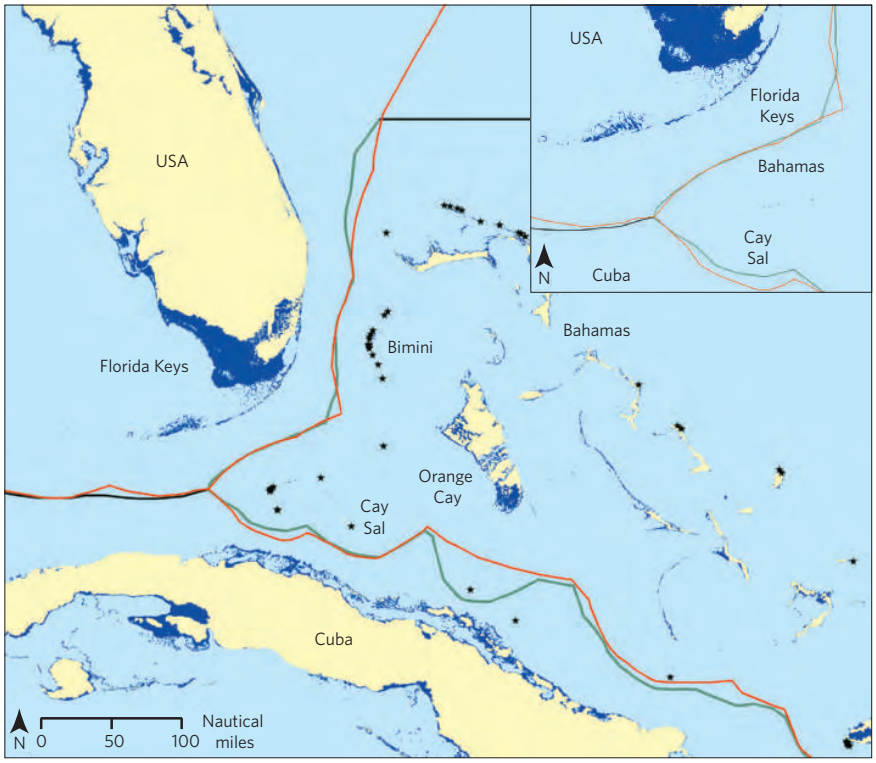

Figure 1 | Established boundaries called into question. With the projected submergence of low-lying coastal areas and islands, particularly the Florida coast and those forming Bahaman archipelagic baseline points, a sea-level rise of 1.5 m would shift the position of equidistance lines in the Caribbean. Should such a sea-level-rise scenario become manifest, the US is likely to insist on the geographic coordinates named in the US–Cuba Boundary Agreement (black line), the Bahamas are likely to insist on the continuing existence of their archipelagic baseline points (black stars) in relation to the US and Cuban baselines, whereas Cuba is likely to insist on the negotiation of new equidistance lines with the US and the Bahamas owing to the change in geographic circumstances after sea-level rise (red line).

be permanently submerged. The present maritime boundaries used in this case study were downloaded from the Flanders Marine Institute Maritime Boundaries Geodatabase (MARBOUND)[14]. We focus on three regions — the Caribbean, the Philippine Sea and the Bay of Bengal — that represent vulnerability hotspots for sea-level rise and illustrate the legal scenarios described here.

Renegotiation based on equidistance

As a first example, the maritime boundaries between the United States, Cuba and the Bahamas could be affected by 1.5 m of sea-level rise (Fig. 1). The present boundaries, according to the Maritime Boundary Agreement, between the United States of America and the Republic of Cuba[15,16] were identified based on the principle of equidistance in accordance with Article 1 of the agreement by determining two equidistant lines — one between both countries' respective normal baselines, and another between Cuba's straight baselines and a hypothetical equivalent baseline on the US coast — and then drawing a compromise line equidistant between these two lines[17].

In our sea-level rise scenario, the Florida coastline will recede so that the coordinates named in the agreement would no longer reflect the actual equidistance line. Cuba might argue in favour of a renegotiation of the treaty, as Cuba's maritime zones could be enlarged in a sea-level rise scenario, whereas the US are likely to insist on keeping the existing agreement, thereby rendering the concept of equidistance historical (or fictional) rather than factual. The Bahamas, which delimit their maritime boundaries using archipelagic baselines in line with Articles 47 and 48 UNCLOS, a special regime that reinforces the 'unitary nature' of island groups[18], would also experience a factual reduction of their exclusive economic zone, should existing archipelagic baseline points be submerged owing to sea-level rise. The vast majority of the world's boundary agreements have been concluded by, at least partially, taking the equidistance principle into account. Therefore, similar factual shifts in equidistance lines owing to the submergence of coastal areas and archipelagic baselines must be anticipated in many regions as a result of sea-level rise.

Re-evaluation of legal principles

A sea-level rise of 1.5 m may cause dramatic coastline recession in the Sundarbans in the Bay of Bengal, our second example. Such changes would substantially shift the exclusive economic zone boundaries that Bangladesh, India and Myanmar would be entitled to claim in accordance with UNCLOS if the equidistance principle were applied (Fig. 2). In 1974, Bangladesh established a system of straight, rather than normal, baselines on its unstable, highly indented and frequently shifting coastline, a practice that is hotly disputed by its neighbours and other states in the world.

With coastline retreat in India, Bangladesh's maritime zones may, contrary to previous projections, expand through sea-level rise, particularly if its practice of straight baselines is not found contrary to international law. Such an expansion would enhance Bangladesh's access to oil and gas reserves in the Bay of Bengal. Although a considerable amount of Bangladesh's territory will be so profoundly affected by flooding that it is likely to become uninhabitable, it cannot be ruled out that it will keep its capacity to generate baselines as it will not be completely, permanently submerged. It is accepted that loss of maritime area resulting from landward movements of the baseline can be prevented through the construction or reinforcement of sea defences[19].

India and Myanmar's exclusive economic zone claims in the Bay of Bengal would be maximized by pursuing

a settlement that discredits Bangladesh's straight baseline claims and fixes the present equidistance lines as the outer limits of the corresponding exclusive economic zones, measured from the respective low-water lines. Bangladesh has persistently pursued a settlement based on equity. Principles of equity take extenuating circumstances into account when the strict application of legal rules would lead to unduly harsh or unjust outcomes. Purely equidistant coordinates may, ironically, better secure Bangladesh's interests — particularly if they are calculated from straight baselines fixed without regard for progressive sea-level rise.

This highly complex dispute is being examined at present by the International Tribunal on the Law of the Sea. The decision of this tribunal created specifically by UNCLOS will be pivotal in determining future maritime boundary disputes, in particular, the adaptation of the delimitation practice developed in the jurisprudence of the International Court of Justice. This court is the United Nations' primary judicial organ, and has consistently moved away in such cases from a strict application of equidistance and towards the principle of equity anchored in Article 74 (1) UNCLOS[20]. A normative category of countries 'particularly vulnerable' to the adverse impacts of climate change is also currently emerging in the United Nations Framework Convention on Climate Change[21], which acknowledges the 'needs and special circumstances' of such countries. Bangladesh — already experiencing adverse impacts of climate change — falls into that category without a doubt.

It is questionable whether boundary delimitation is an appropriate forum to compensate or assist a vulnerable country in anticipation of foreseeable damages from sea-level rise. Nevertheless, maritime claims based on contentious mixtures of equity and equidistance are likely to increase and will be ever more difficult to resolve legally.

Reversion to a status of high seas

Finally, in the Okinotorishima atoll in the Philippine Sea, 1.5 m of sea-level rise may lead to the disappearance of low-lying islands on which Japan's claims for parts of its exclusive economic zone are based (Fig. 3). Territorial claims to Okinotorishima are highly contested because of the extensive natural resources contained in the corresponding exclusive economic zone, the strategic relevance of the location in the dispute between China and Taiwan, and the ever-escalating animosities between China and Japan. Japan's claim, based on the supposition that this land formation constitutes an island (in the sense of Article 121 UNCLOS), has been persistently challenged by China, who argues that Okinotorishima is merely a rock that cannot sustain human habitation or economic life and consequently cannot generate an exclusive economic zone. A sea-level rise of 1.5 m will fully submerge this area and could at first be seen as resolving a long-standing, seemingly intractable dispute between the two countries by simply removing the contested land formation from the map.

However, the reversion of this area to the status of high seas will open up an entirely new dimension to this dispute. Article 87 UNCLOS underlines the freedom of the high seas, which entitles all countries to explore and exploit the natural resources present there on a 'first come, first served' basis. This may ultimately trigger a 'tragedy of the commons' on a grand scale, when natural resources are exploited, unhampered by all but the comparatively general environmental protection obligations that apply to the high seas.

Should sea-level rise exceed 1.5 m, we may see similar circumstances emerge in other highly contested areas such as the Spratly and Paracel Islands in the South China Sea, which are variously claimed by China, Taiwan, Vietnam, Malaysia, the Philippines and Brunei, and are known to hold extensive oil and gas resources. If these islands keep their ability, at least to a certain extent, to sustain human habitation or economic life, the surrounding maritime areas will not lose their exclusive economic zone status. In such a situation, the states concerned are under a duty to cooperate (Art. 74 UNCLOS)

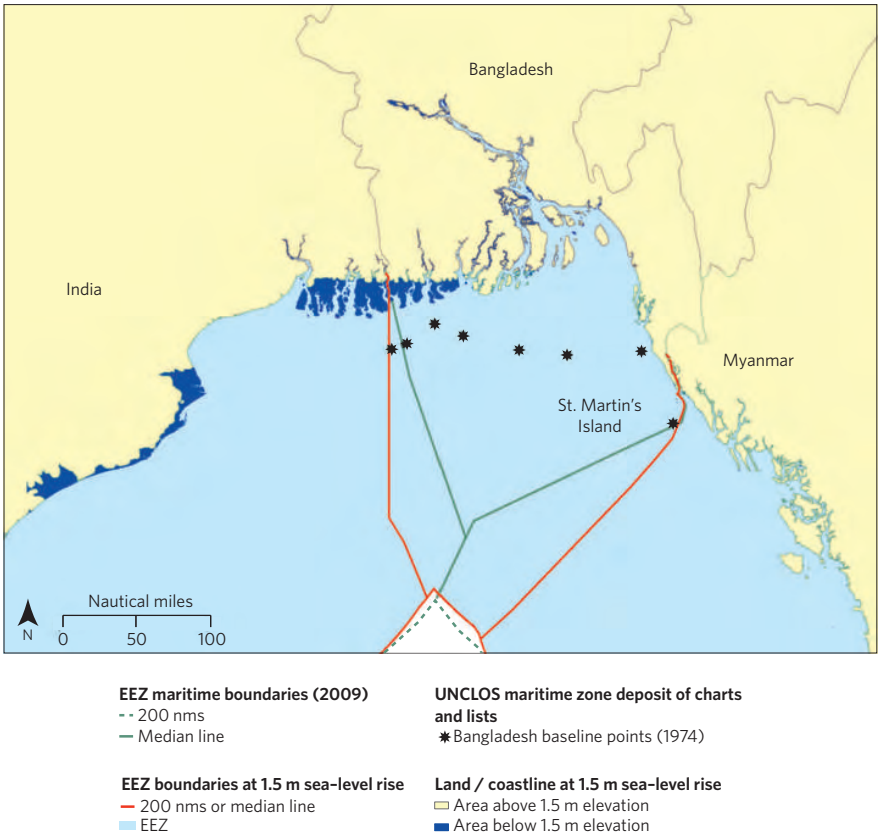

Figure 2 | Conflicting methods of boundary delimitation. The map shows potential consequences of a sea-level rise of 1.5 m in the Bay of Bengal, and in particular, on the highly indented coasts of Bangladesh and India. Grey lines indicate the respective countries' current claims for their exclusive economic zones if determined according to the equidistance principle, and red lines indicate potential exclusive economic zone claims after sea-level rise. Black stars indicate the geographical coordinates Bangladesh used to declare its straight baseline points in 1974.

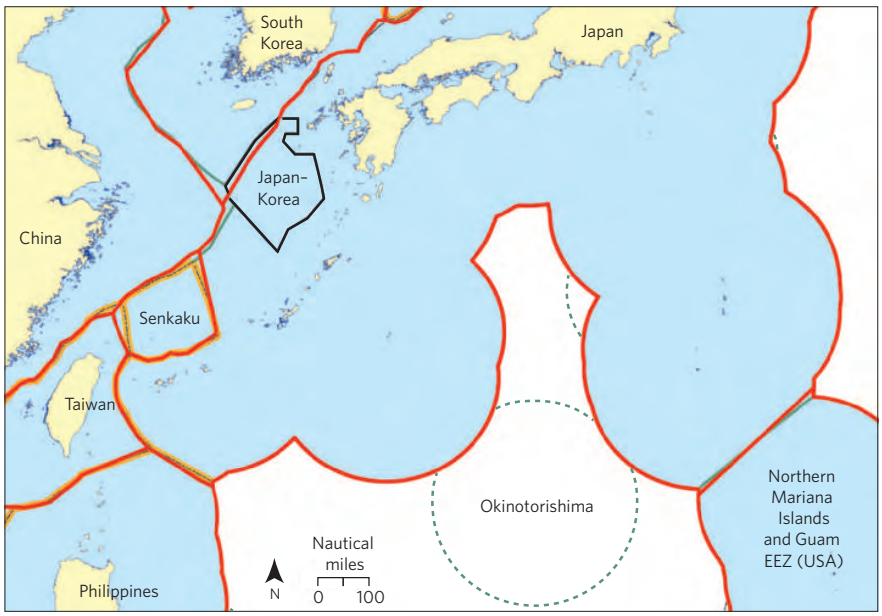

Figure 3 | Disappearing exclusive economic zones. The map shows the consequences of sea-level rise on a land formation claimed by Japan at present as an island, for the purpose of claiming the corresponding exclusive economic zone. The complete submergence of this land formation through sea-level rise would eliminate all existing baselines and lead to the reversion of a highly disputed exclusive economic zone claim to the status of high seas. White indicates a potential area of reversion to high seas.

with the aim to find provisional arrangements of a practical nature such as, for example, the establishment of joint development schemes.

International law for a rising sea

Sea-level rise is not only a question of scientific uncertainty — it also entails extreme legal uncertainty. Fundamental questions of law and international relations are at stake in prospective responses to sea-level rise. Coastline retreat brings with it potentially profound impacts on maritime boundary delimitation as well as rights and obligations with regard to natural resources located in the exclusive economic zones.

UNCLOS provisions on baselines will be subjected to two distinct and potentially conflicting interpretations in the future: normal baselines could either remain static, irrespective of changes in sea level, or they could become dynamic, in line with physical realities. The former strategy, which would posit the charted, historical low-water line as the legally binding baseline, would provide legal certainty for all states irrespective of the actual extent of sea-level rise, but would fail to reflect changing realities and may cement inequities in existing boundary regimes. The latter strategy, which would posit the actual low-water line as the legally binding baseline, would create a system of 'ambulatory baselines' — reflecting factual conditions but causing considerable legal uncertainty as to the state under whose sovereignty, or jurisdiction, the maritime territory in question would fall[22,23].

The conflict between those who argue for cementing twentieth-century baselines and those who demand dynamic adjustment will come to the fore all the more when low-lying coastal areas and islands become uninhabitable or completely submerged as a result of sea-level rise. Adaptation to climate change therefore has a significant legal component that will become increasingly relevant as sea-level rise proceeds. ❐

Katherine J. Houghton[1], Athanasios T. Vafeidis[2], Barbara Neumann[2] and Alexander Proelss[3] are at [1]Walther Schücking Institute for International Law, University of Kiel, Westring 400, D-24098 Kiel, Germany, [2]Institute of Geography, Coastal Risks and Sea-Level Rise Research Group, The Future Ocean Excellence Cluster, University of Kiel, Ludewig-Meyn-Str. 14, D-24098 Kiel, Germany, [3]Department of Law, University of Trier, D-54286 Trier, Germany.*
**e-mail: proelss@uni-trier.de*

References

1. Zhang, K. Q., Douglas, B. C. & Leatherman, S. P. *Climatic Change* **64,** 41–58 (2004).
2. Nicholls, R. J. *et al.* in *IPCC Climate Change 2007: Impacts, Adaptation and Vulnerability* (eds Parry, M. L. *et al.*) 315–356 (Cambridge Univ. Press, 2007).
3. Rahmstorf, S. *Nature Rep. Clim. Change* **4,** 44–45 (2010).
4. Vermeer, M. & Rahmstorf, S. *Proc. Natl Acad. Sci. USA* **106,** 21527–21532 (2009).
5. Nicholls, R. J. & Cazenave, A. *Science* **328,** 1517–1520 (2010).
6. Yamamoto, L. & Esteban, M. *Ocean Coast. Manage.* **53,** 1–9 (2010).
7. UNCLOS *Treaty Series* Vol. **1833,** 397 (United Nations, 1982).
8. Territorial and Maritime Dispute Between Nicaragua and Honduras in the Caribbean Sea Case (Nicaragua v. Honduras) *I C J Reports 2007,* 659–764 (2007).
9. Caron, D. D. *Ecol. Law Quart.* **17,** 621–653 (1990).
10. U S Geological Survey *Global 30 Arc Second Elevation Data Set* (Eros Data Center, 1996); available at http://go.nature.com/rRLoSz
11. Gesch, D. *et al. Photogramm. Eng. Rem. S.* **68,** 5–11 (2002).
12. Rabus, B., Eineder, M., Roth, A. & Bamler, R. *ISPRS J. Photogramm.* **57,** 241–262 (2003).
13. Abrams, M. *Int. J. Remote Sens.* **21,** 847–859 (2000).
14. Flanders Marine Institute *Maritime Boundaries Geodatabase, version 5*; available at http://www.vliz.be/vmdcdata/marbound
15. United States of America, Public Law No. 94–265 13 April 1976.
16. Government of the Republic of Cuba, Decree Law No. 2 24 February 1977.
17. Office of Ocean Law and Policy *Maritime Boundary: Cuba-United States* (Limits in the Seas No. 110, Bureau of Oceans and International Environmental and Scientific Affairs, 1990).
18. Churchill, R. R. & Lowe, A. V. *The Law of the Sea* 118–131(Manchester Univ. Press, 1999).
19. Soons, A. H. A. *Neth. Int. Law Rev.* **37,** 207–232 (1990).
20. Rothwell, D. R. & Stephens, T. *The International Law of the Sea* 393–408 (Hart, 2010).
21. United Nations Framework Convention on Climate Change *Treaty Series* Vol. 1771, 107 (United Nations, 1992).
22. Committee on Baselines Under the Law of the Sea *Internal Discussion Document* (International Law Association, 2008); available at http://www.ila-hq.org/en/committees/index.cfm/cid/1028
23. Schofield, C. *Carbon Clim. Law Rev.* **4,** 405–417 (2009).

Acknowledgements

This paper is supported by the Future Ocean Excellence Cluster, University of Kiel.

Annex B80

S. T. Sinha et al., "The Crustal Architecture and Continental Break Up of East India Passive Margin: An Integrated Study of Deep Reflection Seismic Interpretation and Gravity Modelling", *Search and Discovery,* Article #40611 (10 October 2010) (available at <http://www.searchanddiscovery.com/documents/2010/40611sinha/ndx_sinha.pdf>)

The Crustal Architecture and Continental Break Up of East India Passive Margin: An Integrated Study of Deep Reflection Seismic Interpretation and Gravity Modeling*

S. T. Sinha[1], M. Nemcok[2], M. Choudhuri[1], A.A. Misra [1], S. P. Sharma[1], N. Sinha[1], S. Venkatraman[3]

Search and Discovery Article #40611 (2010)
Posted October 14, 2010

* Adapted from an oral presentation at AAPG Annual Convention and Exhibition, New Orleans, Louisiana, USA, April 11-14, 2010

[1]Geology and Geophysics, Reliance Industries Ltd, Navi Mumbai, India. (Sudipta.Sinha@ril.com)
[2]Energy & Geoscience Institute at University of Utah, Salt Lake City, UT.
[3]GX Technology, Houston, TX.

Abstract

The East Indian passive margin was developed after the disintegration of eastern Gondwanaland by the break up from Antarctica in the Early Cretaceous. In accordance with other passive margins, the break-up involved stretching, thinning and a probable process of mantle exhumation prior to the sea floor spreading. To understand the continental break up and margin evolution; a combined study of gravity, magnetic and seismic data focuses on determining the crustal architecture and different crustal types, such as continental, proto-oceanic and oceanic crusts, and their boundaries. The data set comprises the latest India-Span deep reflection seismic profiles acquired by GX Technology along with gravity and magnetic data, and 2D seismic data from Reliance Industries Ltd.

Six major tectonic segments composing the East Indian margin played a pivotal role in the continental break up and passive margin development. The proto-oceanic crust corridor located oceanward of these segments indicates the role of different rifting processes and breakup mechanisms and can be kinematically linked to above-mentioned tectonic segments. The orthogonally rifted segments, e.g. the Krishna-Godavari and Cauvery rift zones, developed a hard linkage through a major dextral transfer fault called the Coromondal fault zone. The proto-oceanic corridor is narrow along the Coromondal segment and wide in segments, which were initiated by orthogonal rifting. The continental crust terminates abruptly along the Coromondal segment and thins considerably before it terminates in orthogonal-rifting segments. Outboard of proto-oceanic crust lies the oceanic crust. Outboard of proto-oceanic crust, the oceanic crust is present, where anomalies produced by geomagnetic isochrons are not yet identified due to the Late Cretaceous mantle plume activity that produced the 85E Ridge. This activity modified the thicknesses of all three crustal types in its influence zone.

Selected References

Geological Survey of India, 1993. Geological Map of India, Scale 1:5000000

Rao, G. N., 2001. Sedimentation, stratigraphy, and petroleum potential of Krishna-Godavari basin, East Coast of India. AAPG Bulletin, 85, 1623-1643.

Ray, D. K., 1963. Tectonic map of India. Geological Society of India, Calcutta, scale 1:2 000 000.

Reeves, C., & Wit, M. D., 2000. Making ends meet in Gondwana: retracing the transforms of the Indian Ocean and reconnecting continental shear zones, Terra Nova, 12, 6, 272-280

Sandwell, D.T. & Smith, W.H.F., 1997. Marine Gravity Anomaly from ERS-1, Geosat & Satellite Altimetry. Journal of Geophysical Research - Solid Earth, 102, 10,039-10,045.

The crustal architecture and continental break up of East India Passive margin: an integrated study of deep reflection seismic interpretation and gravity modeling

Sudipta Tapan Sinha[1, a], Michal Nemčok[2], Mainak Choudhuri[1], Achyuta Ayan Misra[1], Suraj P Sharma[1], Neeraj Sinha[1] & Sujata Venkatraman[3]

•Reliance Industries Ltd, Mumbai, India
•Energy & Geoscience Institute at University of Utah, Salt Lake City, UT, USA
•GX Technology, Houston, TX, USA
•Corresponding author, email: Sudipta.Sinha@ril.com

Abstract

The East Indian passive margin was developed after the disintegration of eastern Gondwanaland by the break up from Antarctica in Early Cretaceous. In accordance with other passive margins, the break-up involved stretching, thinning and a probable process of mantle exhumation prior to the sea floor spreading. To understand the continental break up and margin evolution; a combined study of gravity, magnetic and seismic data focuses on determining the crustal architecture and different crustal types, such as continental, proto-oceanic and oceanic crusts, and their boundaries. The data set comprises the latest India-Span deep reflection seismic profiles acquired by GX Technology along with gravity and magnetic data, and 2D seismic data from Reliance Industries Ltd.

Six major tectonic segments composing the East Indian margin played a pivotal role in the continental break up and passive margin development. The proto-oceanic crust corridor located oceanward of them indicates the role of different rifting processes and breakup mechanisms and can be kinematically linked to above mentioned tectonic segments. The orthogonally rifted segments, e.g. the Krishna-Godavari and Cauvery rift zones, developed a hard linkage through a major dextral transfer fault called the Coromondal fault zone. The proto-oceanic corridor is narrow along the Coromondal segment and wide in segments, which were initiated by orthogonal rifting. The continental crust terminates abruptly along the Coromondal segment and thins considerably before it terminates in orthogonal-rifting segments. Outboard of proto-oceanic crust lies the oceanic crust, Outboard of proto-oceanic crust, the oceanic crust is present, where anomalies produced by geomagnetic isochrons are not yet identified due to the Late Cretaceous mantle plume activity that produced the 85E Ridge. This activity modified the thicknesses of all three crustal types in its influence zone.

AAPG Annual Convention & Exhibition

The Crustal Architecture and Continental Break Up of East India Passive Margin: An Integrated Study of Deep Reflection Seismic Interpretation and Gravity Modeling

S. T. Sinha[1]; M. Nemcok[2]; M. Choudhuri[1]; A. A Misra[1]; S. P. Sharma[1]; N. Sinha[1] and S. Venkatraman[3]

1. Reliance Industries Ltd, Navi Mumbai, Maharasthra, India.
2. Energy & Geoscience Institute at University of Utah, Salt Lake City, UT, United States.
3. GX Technology, Houston, TX, United States.

Sudipta.Sinha@ril.com
+91 99 676 45 815

Key Questions

- What is the extent of continental crust in deepwater offshore East India?
- Is it possible to interpret mantle exhumation phenomenon in East India?
- Is it possible to identify kinematic linkage between rift zones and strike slip zones?

Break up History and Passive Margin Development of India

(from Reeves et.al. 2000)

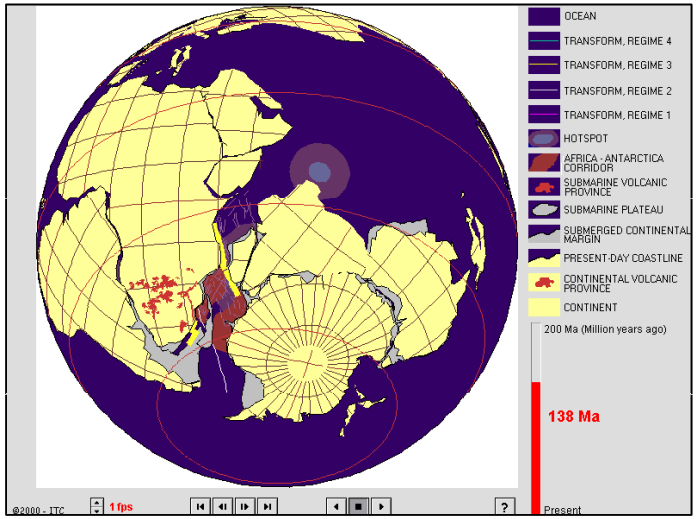

138 MA: Gondwana is an assembly of India-Antarctica and Australia

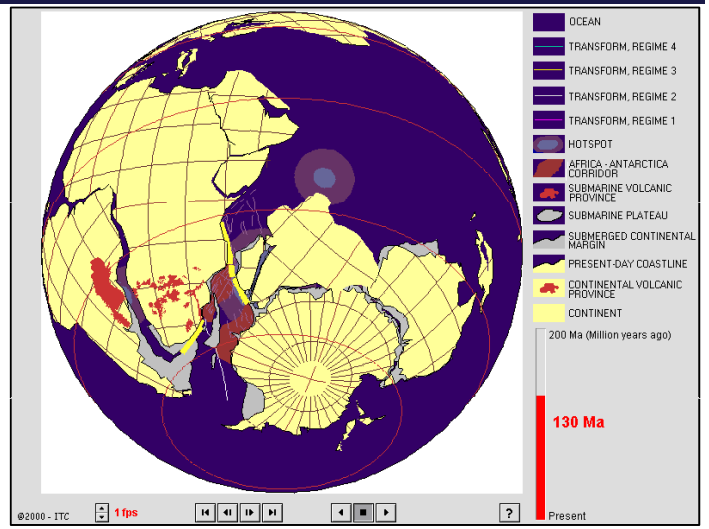

130 MA: Break up between India- Antarctica and Australia

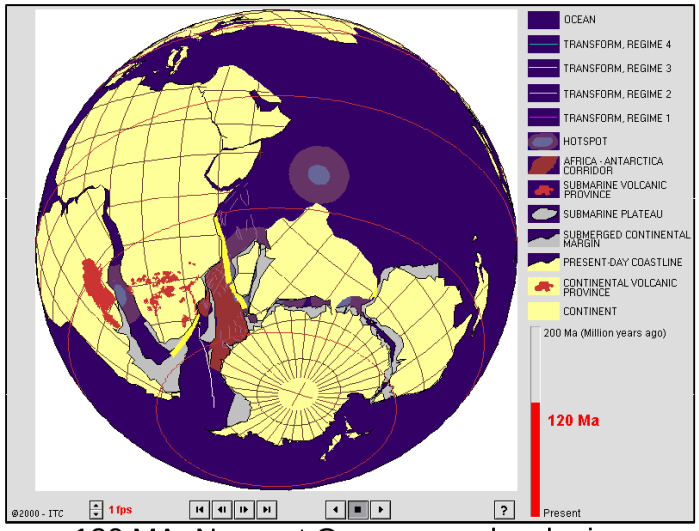

120 MA: Nascent Oceans are developing between India- Antarctica and Australia

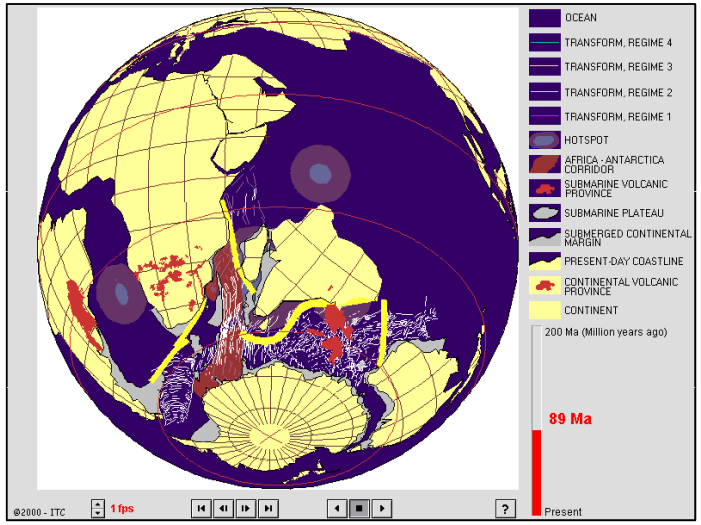

90 MA: India's rapid northward drift initiated

The Salient features of East India Passive Margins

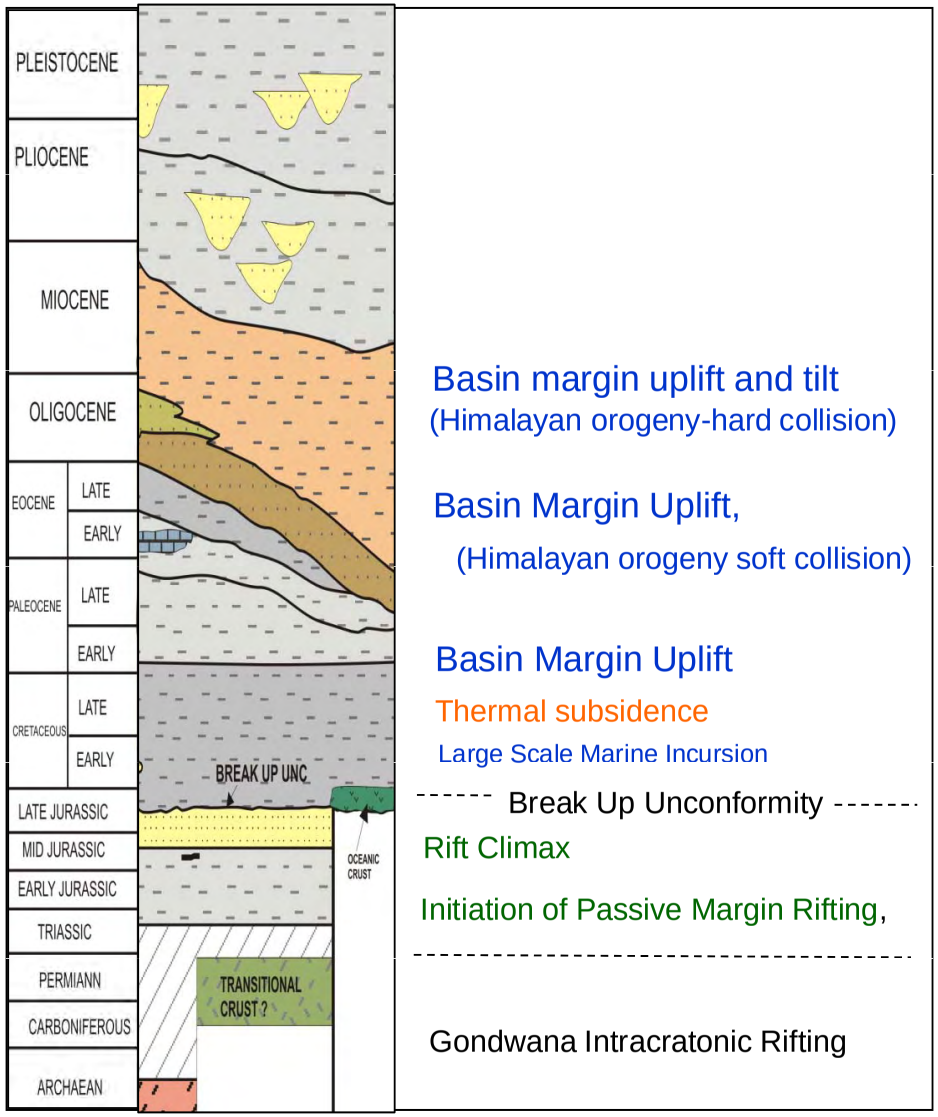

modified after Rao, G.N., 2001

- ✓ The passive margin of East India developed after India - Antarctica break up @136-132 Ma
- ✓ The Basement rock consists of Archean and Proterozoic mobile belts (Eastern Ghats)
- ✓ A interplay of orthogonal, oblique and strike slip segments are present all along passive margin
- ✓ Crustal architecture shows both non-volcanic and volcanic rifted margin
- ✓ Sedimentation history from Jurassic to Present

Study Area and Data Coverage

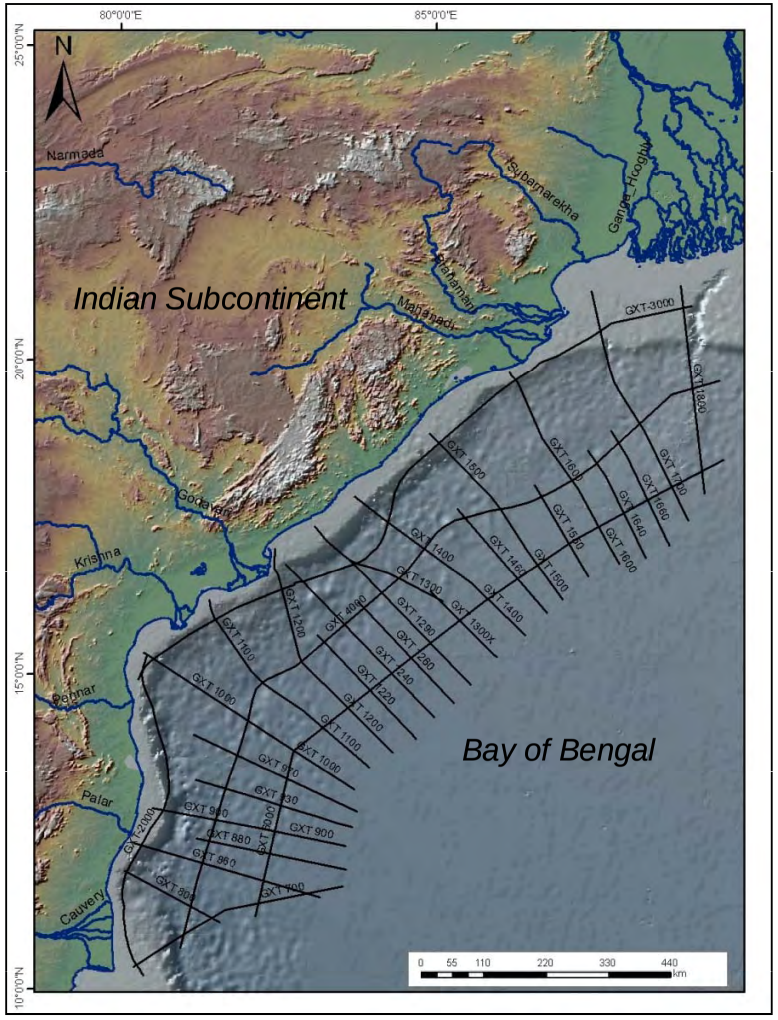

Map of the study area, offshore East India, showing

- IndiaSpan reflection seismic profiles (GX Technology)
- Onshore topography of Indian Subcontinent (Smith and Sandwell, 1997)
- Drainage system
- Offshore bathymetry of Bay of Bengal (Smith and Sandwell, 1997)

Additionally few key seismic profiles from Reliance Industries Ltd is also available for study

Note the narrow present day shelf all along passive margin

Sedimentary Basins along East Coast India

Source: Directorate General of Hydrocarbon in India, web: www.dgh.india.org

Proterozoic Basins

- Onshore Cuddapah Basin
- Onshore Vindhyan Basin

Permo-Triassic (Gondwana) Basins

- Onshore Pranhita-Godavari Basin
- Onshore Mahanadi Basin
- Onshore Damodar Valley Basins

Passive Margin Basins

- Onshore and offshore Cauvery basin
- Offshore Palar-Pennar Basin
- Onshore and Offshore Krishna- Godavari Basin
- Offshore Mahanadi Basin
- Onshore and offshore Bengal Basin

Geologic Setting and Basement Configuration

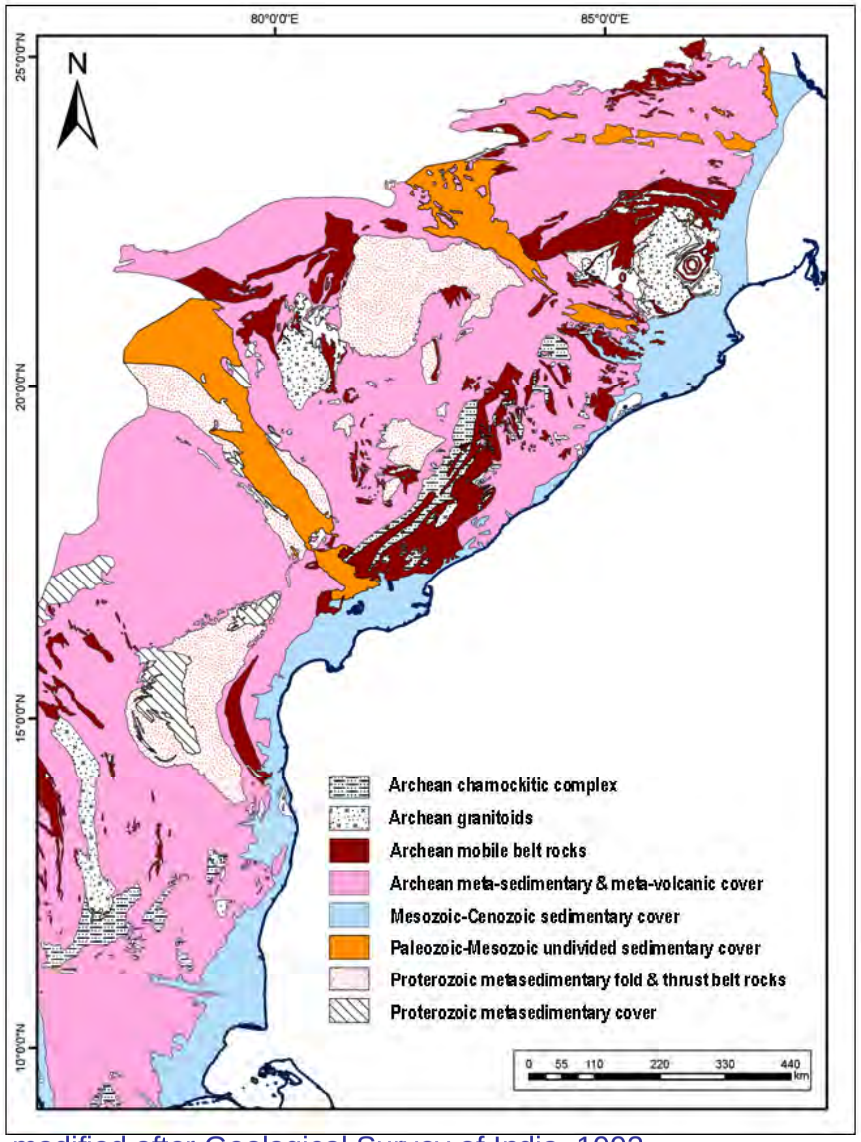

modified after Geological Survey of India, 1993

Primarlity dominated by Proterozoic mobile belts superimposed on top system of Achaean cratons. i.e. Southern Granulitic Terrain and the Eastern Ghat Mobile Belt.

The external onshore portion of the passive margin contains following basement rocks.

Remobilized basement with granitic gneisses adjacent to the Cauvery basin

mobile belt rocks with khondalite adjacent to the Krishna-Godavari basin

Remobilized basement with granitic gneisses adjacent to the rest of the Krishna-Godavari basin

Charnockite between Krishna-Godavari and Mahanadi basins

Singhbhum batholitic granites and some granodiorites adjacent to the Mahanadi basin

The Eastern Ghat mobile belt of India is supposedly the counter part of the Napier Complex in Enderby land in East Antarctica.

Isostatic Residual Anomaly Map

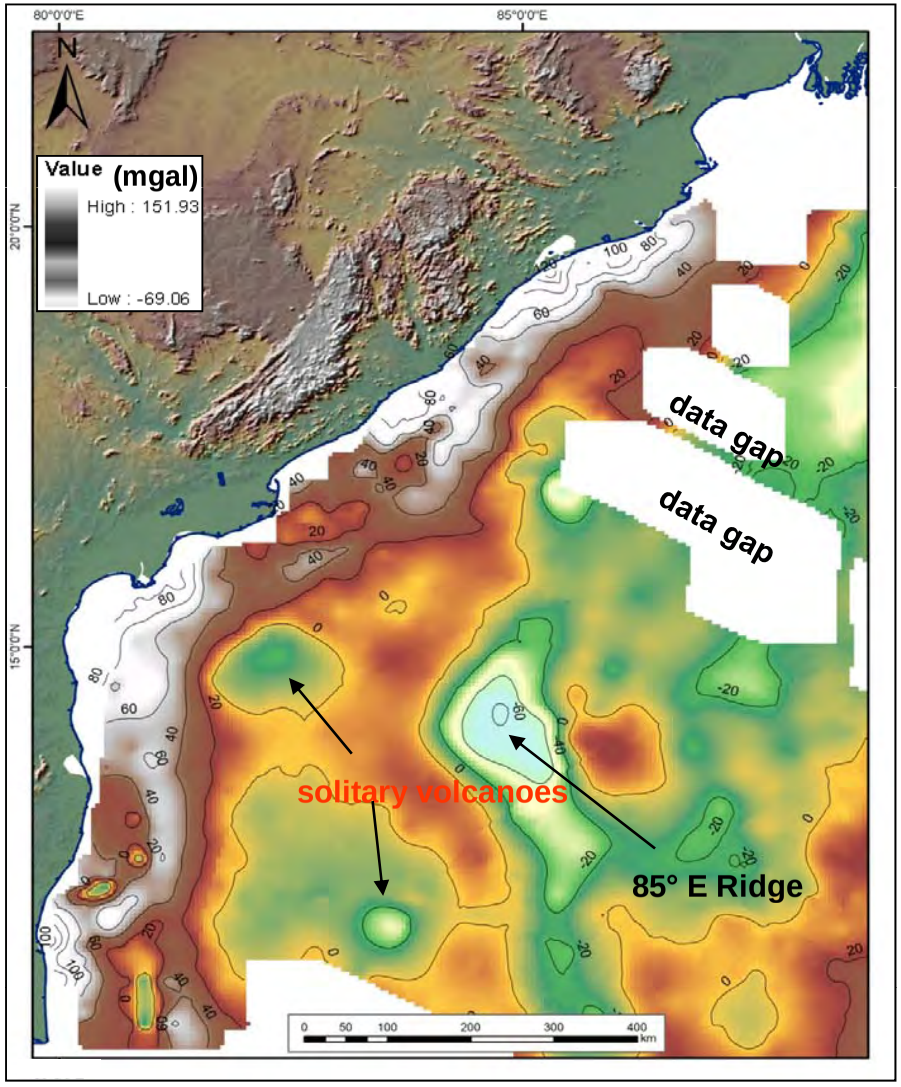

Courtesy: Reliance Industries Ltd, Fugro Robertson Inc., 2006

Isostatic residual anomaly map with 3*3 km resolution derived from interpolated ship-track gravity data (Fugro Robertson Inc., 2006).

The positive anomaly on continental side coupled with negative anomaly on oceanic side represents a good candidate for crustal boundary.

The 85^{o} E Ridge is a prominent gravity low representing crustal roots underneath a chain of volcanic loads.

Two isolated anomalies of similar origin to the W of the ridge in Krishna-Godavari and Cauvery basis are associated with hot-spot-related solitary volcanoes.

It is important to note that the Kerguelen hotspot activity closely after break up makes it difficult to indentify magnetic anomalies produced by geomagnetic isochrones in Bay of Bengal.

Tectonic Segments of Offshore India

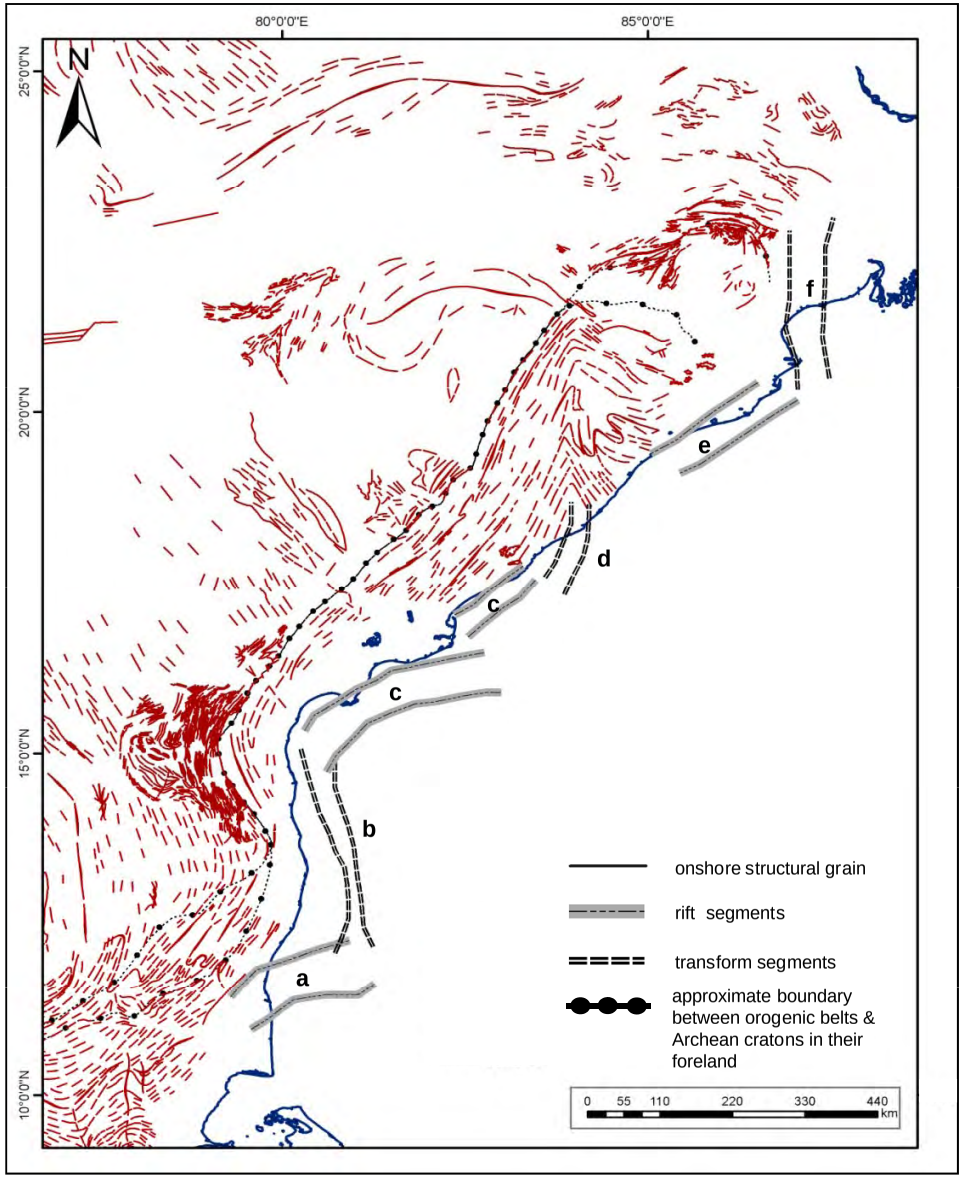

Map of major tectonic segments of the study area and structural features of the adjacent onshore

There are six major segments:

(a) The NE-SW trending Cauvery rift zone

(b) NNW-SSE trending dextral Coromondal transfer zone (Pennar-Palar Basin)

(c) NE-SW to ENE-WSW trending rift units of the Krishna-Godavari rift zone

(d) NNW-SSE trending North Vizag transfer zone between Krishna-Godavari and Mahanadi rift zones

(e) NE-SW trending Mahanadi rift zone

(f) NNW-SSE trending dextral Konark transfer zone.

modified from Ray, 1963; Geological Survey of India, 1993

Seismic Interpretation showing Break control along East India

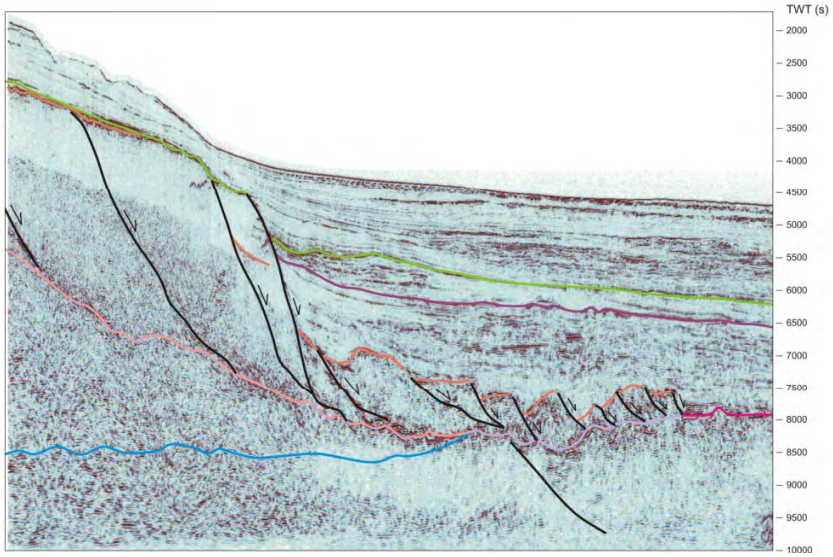

Break-up controlled by normal faulting (Easterly dipping) in the Cauvery basin region along dip oriented reflection seismic profile

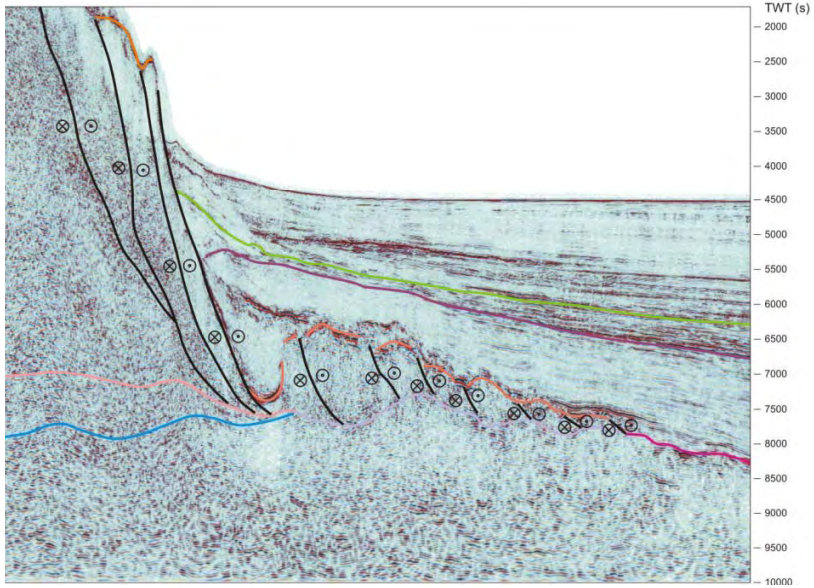

Break-up controlled by dextral strike-slip faulting (Coromondal Fault System) in the Pennar-Palar basin region along dip-oriented reflection seismic profile

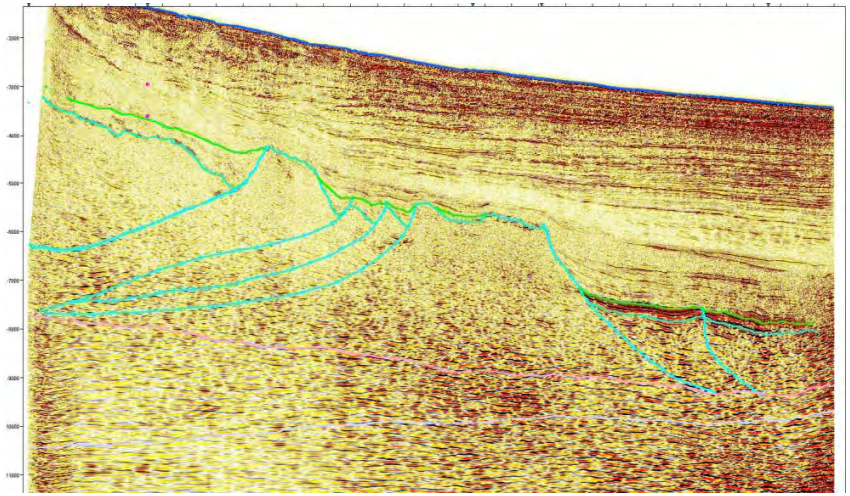

Break-up controlled by normal faulting (westerly dipping) in the Krishna-Godavari basin region along dip-oriented reflection seismic profile

Seismic Interpretation of GX 1000

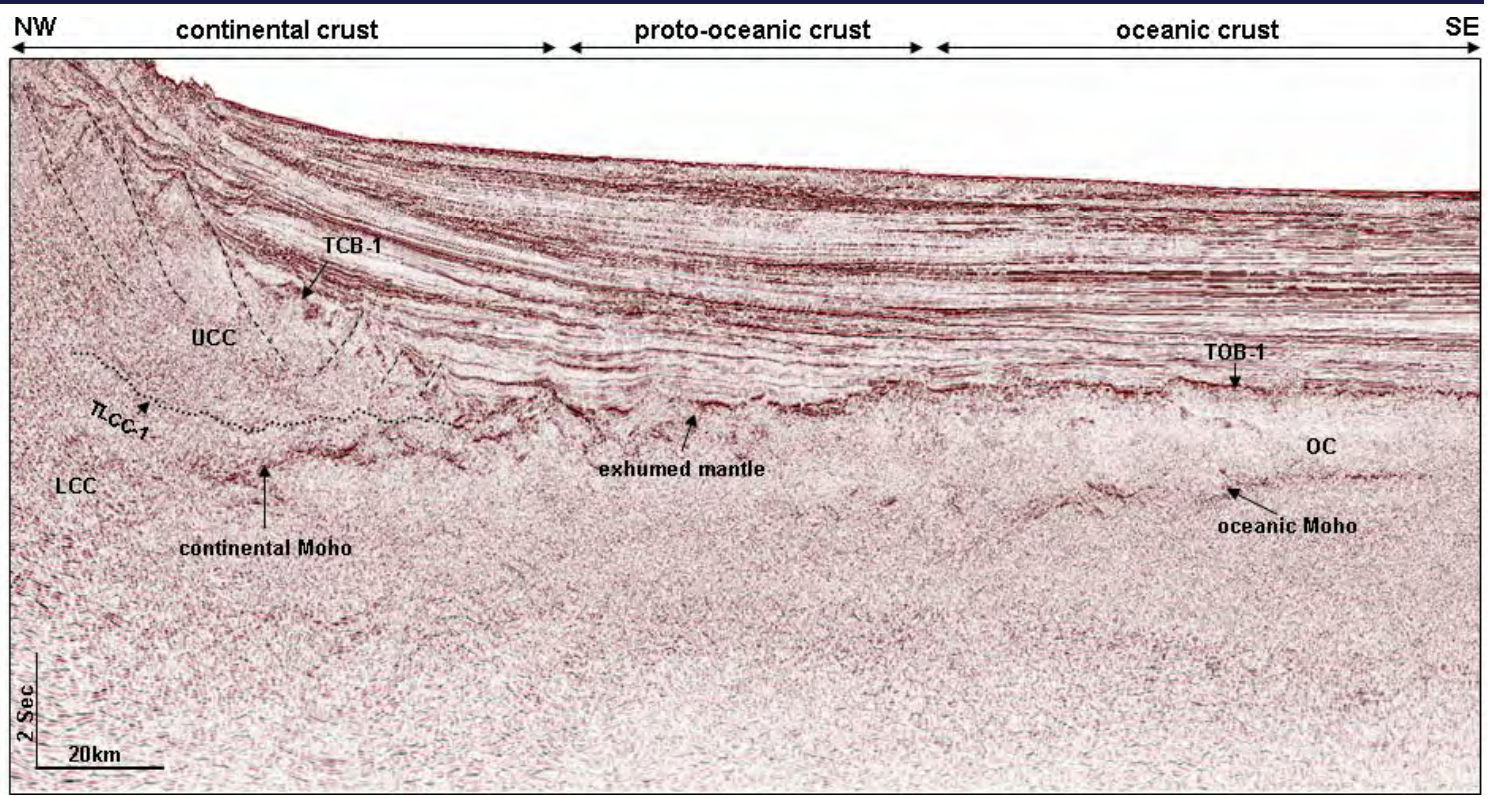

Profile GXT-1000 through the southern Krishna basin showing distribution of crustal types including thinned upper continental crust (UCC), thinned lower continental crust (LCC), proto-oceanic crust (exhumed mantle), and oceanic crust (OC), mapped as based on seismic signatures. Note the break-up initiated by normal faulting.

The continental Moho uprising towards NW is seismically very well imaged

Towards SE, the more organized layered normal oceanic crust with a prominent Moho resolution (oceanic Moho) can be observed. The top oceanic basement (TOB-1) is relatively flat and tectonically undisturbed

Seismic Interpretation of GX 1400

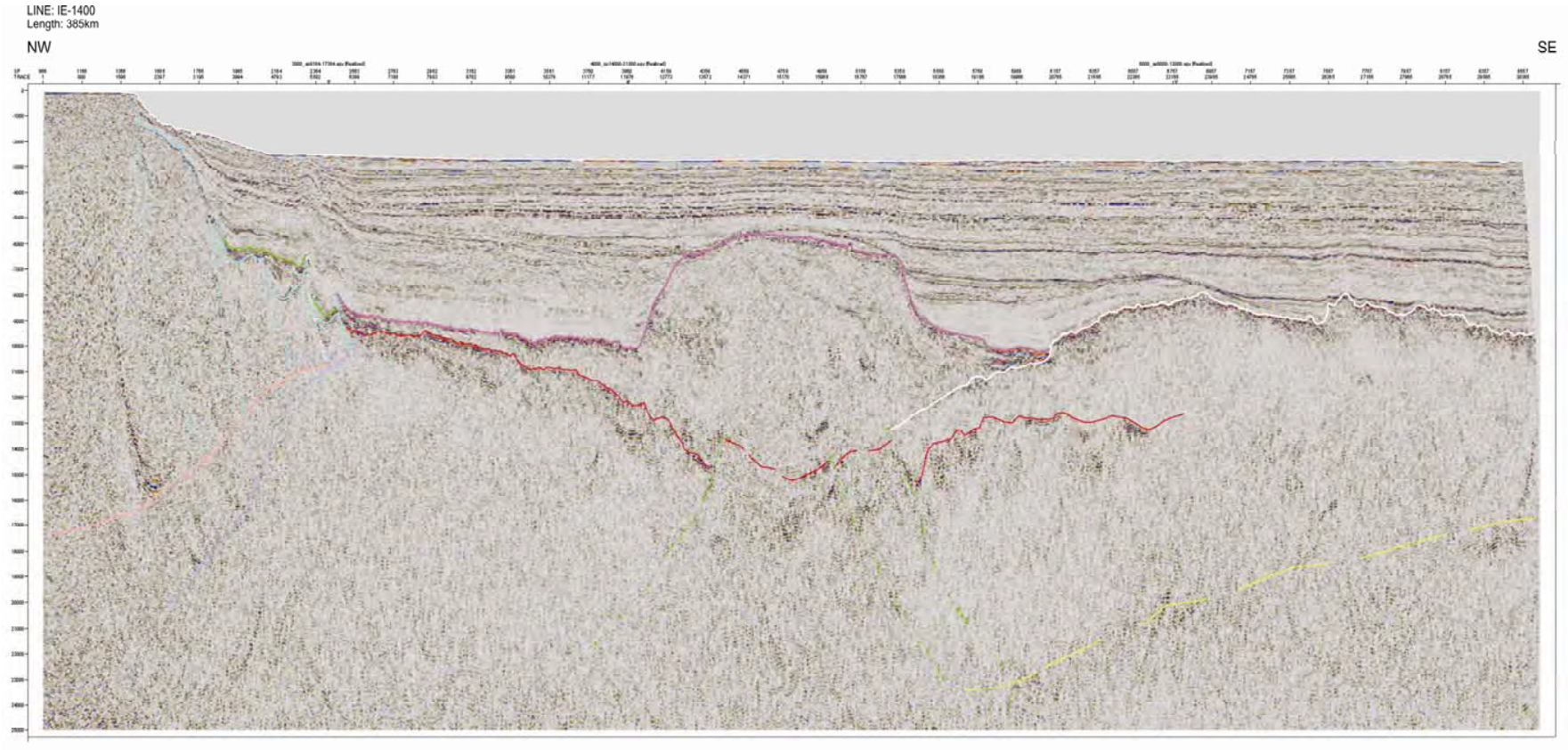

Depth-migrated seismic section of GX-1400. Note a hot spot-related volcanic load overlying the proto-oceanic crust. Due to the huge volcanic associated intrusions, geothermal fluid alteration and hot-spot associated deformation, it is practically impossible to determine the boundary between poc and oc underneath the load.

Seismic Interpretation of GX 1600

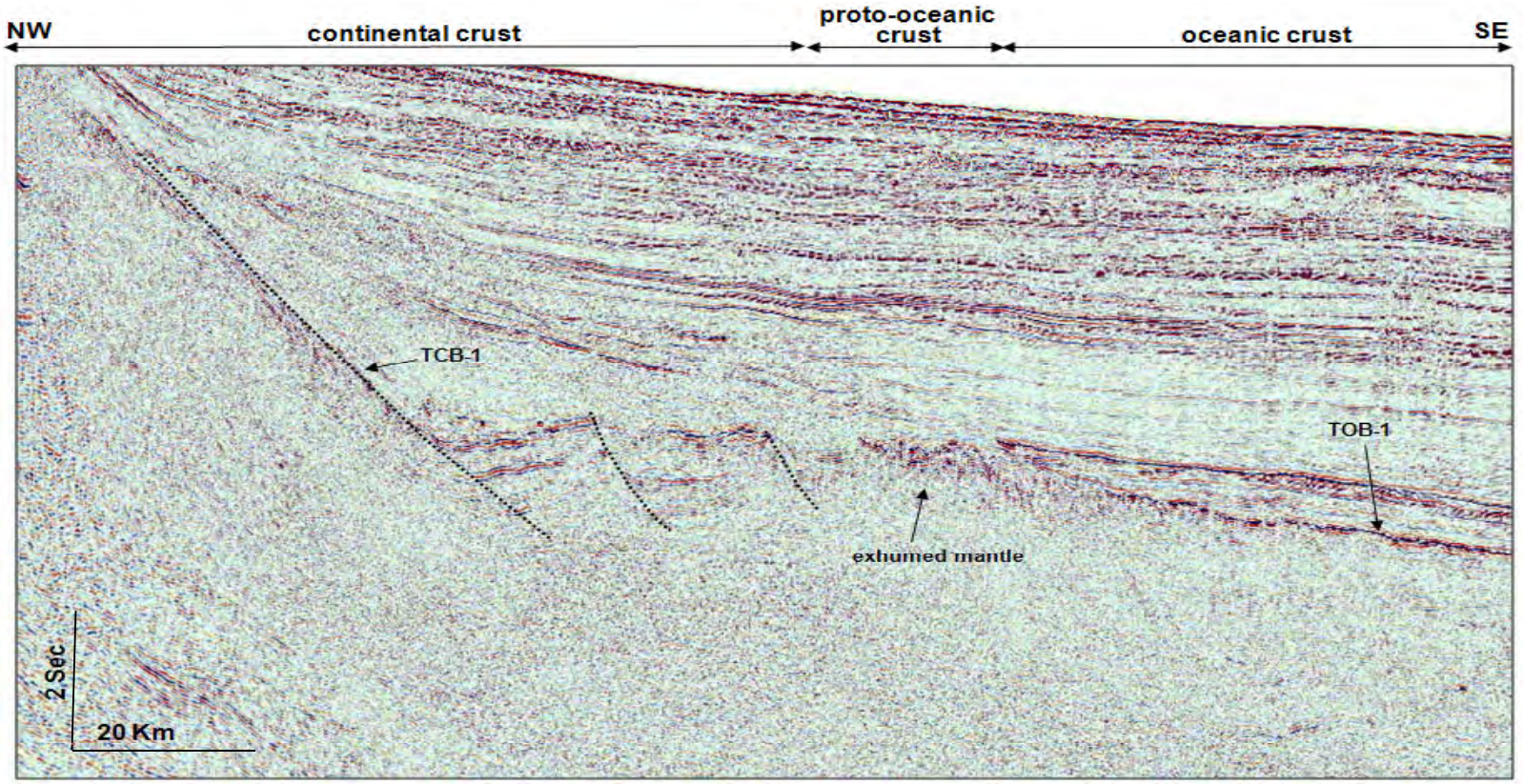

Profile GXT-1600 through the Mahanadi basin. The uprising continental Moho is not imaged well in this profile and the oceanic Moho is not very prominent. Two grabens can be seen on the continental margin. The oceanic crust is flat and strongly reflective with parallel-layered reflectors in its upper parts. Seismic image of the exhumed mantle is disturbed and characterized by wavy reflectors. Top of the continental basement (TCB-1) and top of oceanic basement (TOB-1) are interpreted on the basis of the last prominent continuous reflector in the continental and oceanic crust, respectively. The break-up was initiated with normal faulting

Differentiation of Upper and Lower Continental Crust from East India Seismic Data

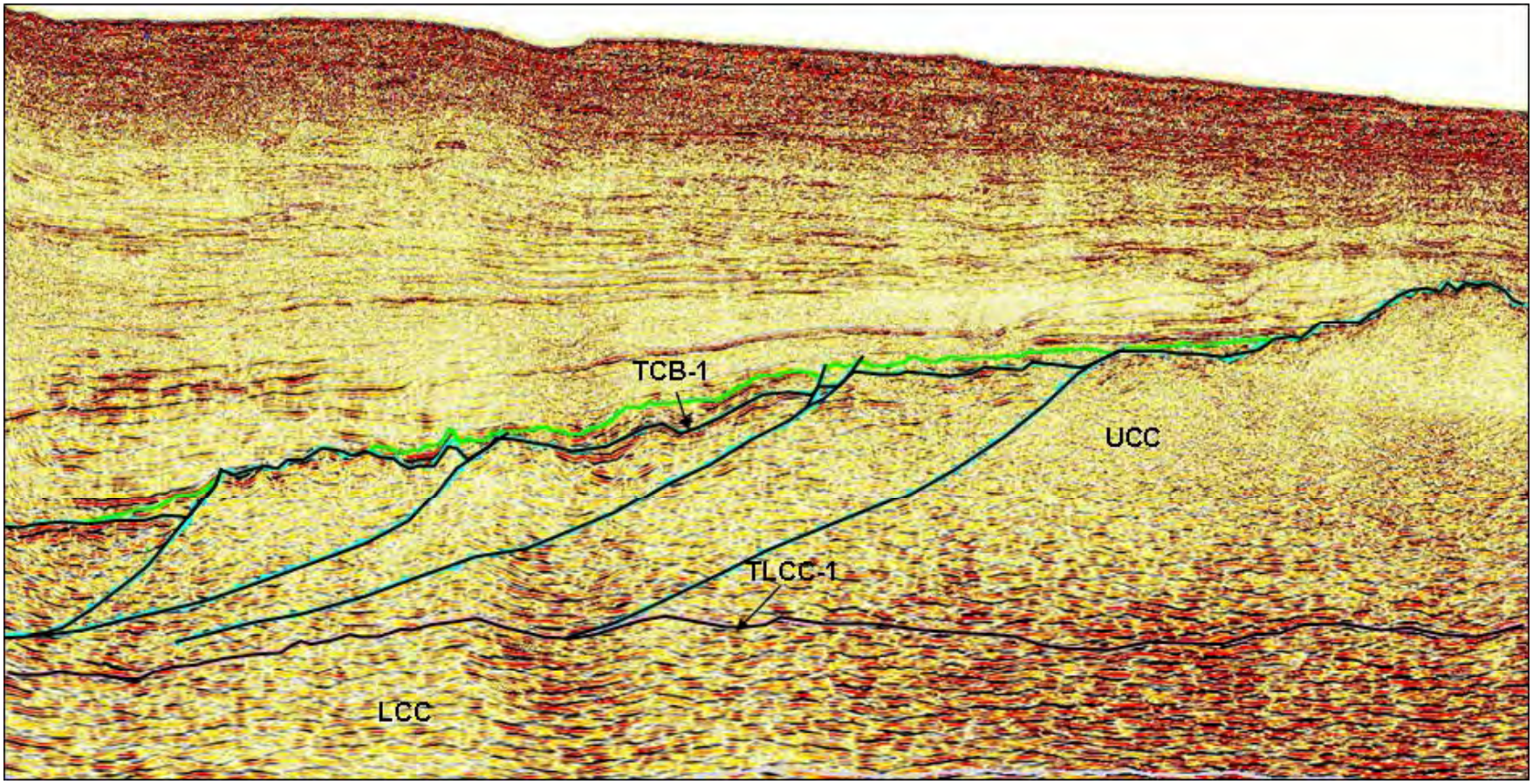

A strike-oriented seismic profile showing the continental crust in detail. Top of the continental basement (TCB-1) is faulted. The upper continental crust (UCC) is characterized by the presence of faults, shear zones and other pre-existing deformational features. It is relatively transparent in terms of reflectivity due to its brittle nature. The lower continental crust (LCC) is highly reflective with sub-horizontal reflector pattern due to its “flowable” ductile nature.

Gravity and Magnetic Modeling along GXT profile IE-1000

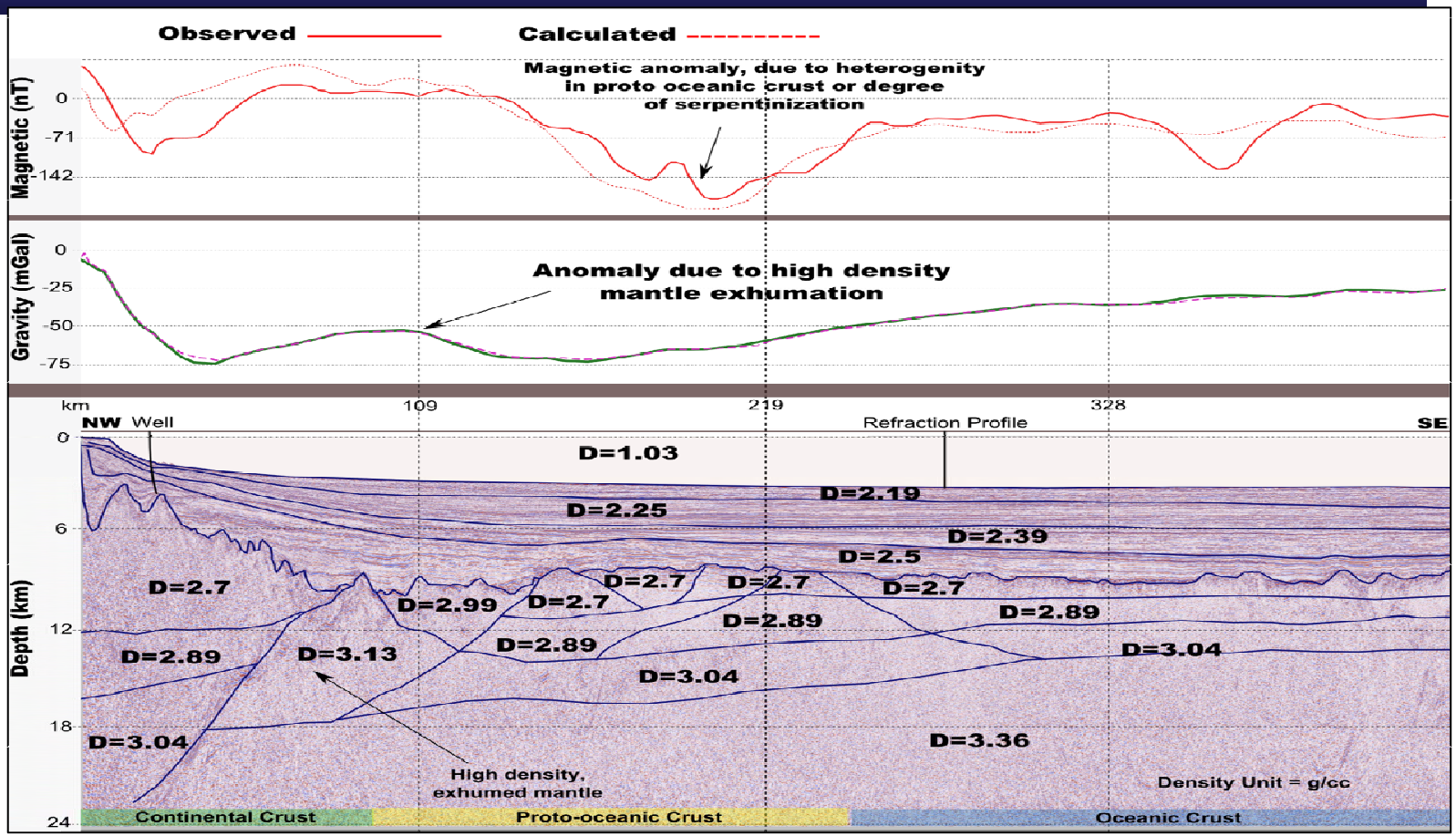

The gravity and magnetic models along depth migrated section GXT-1000 (Bird, 2008) showing a good match between observed and calculated gravity and magnetic data. The thick and thin lines show the calculated and observed curves, respectively. Profile shows a high density body with density of 3.13 gm/c3 as situated just east of the extended continental crust, indicating exhumed mantle. This is the best model for both curves for depth-migrated profile GXT 1000. The increased density of poc in sensitivity analysis does not seem to affect the model in any important way.

Gravity and Magnetic Modeling along GXT profile IE-1000

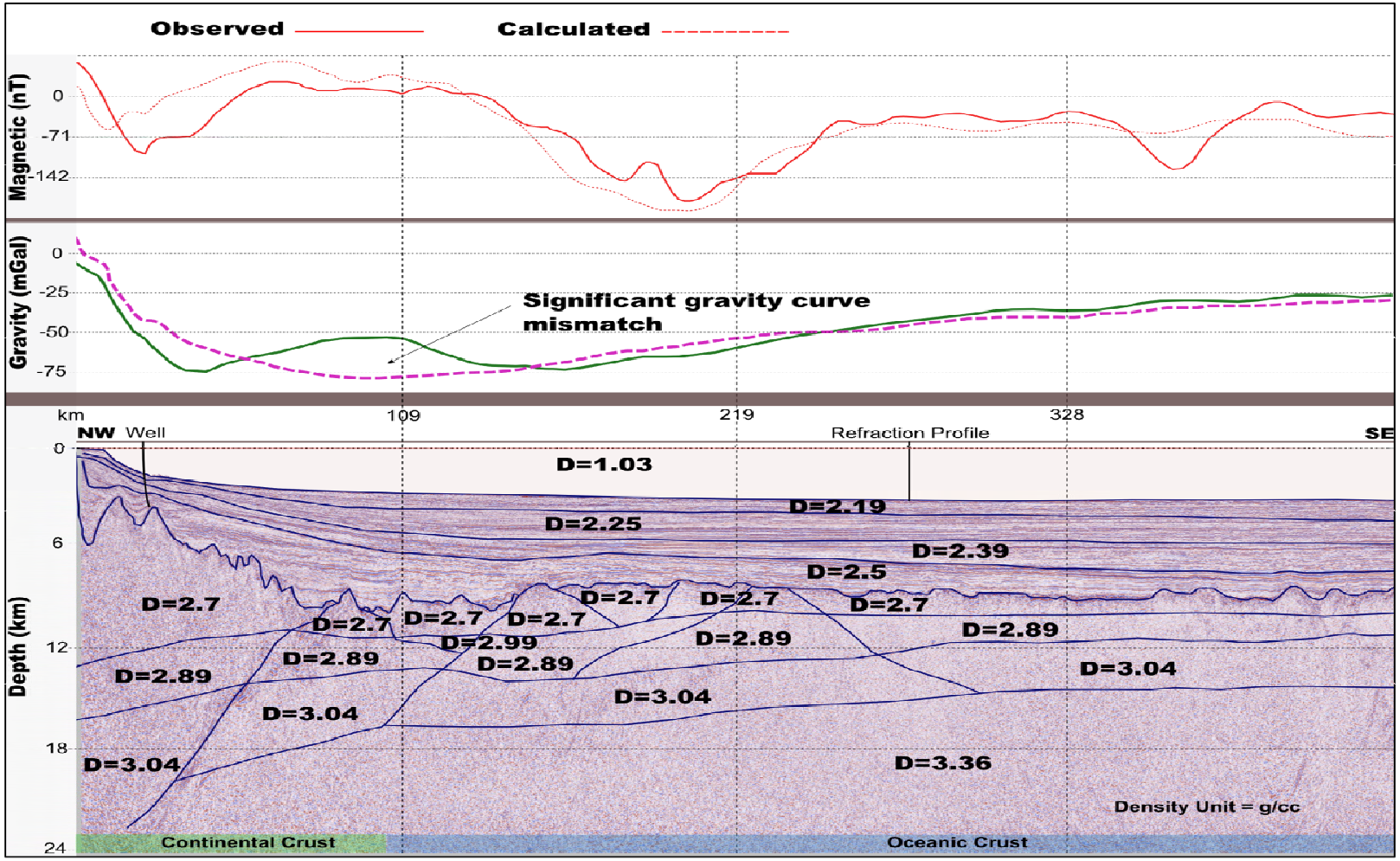

This time showing a classical continental-oceanic transition model. It shows a significant observed/modeled gravity curve mismatch at the continental-oceanic transition, indicating that the match can be achieved only with a model containing a high density material of the proto-oceanic crust formed by unroofed mantle.

Gravity and Magnetic Modeling along GXT profile IE-1200

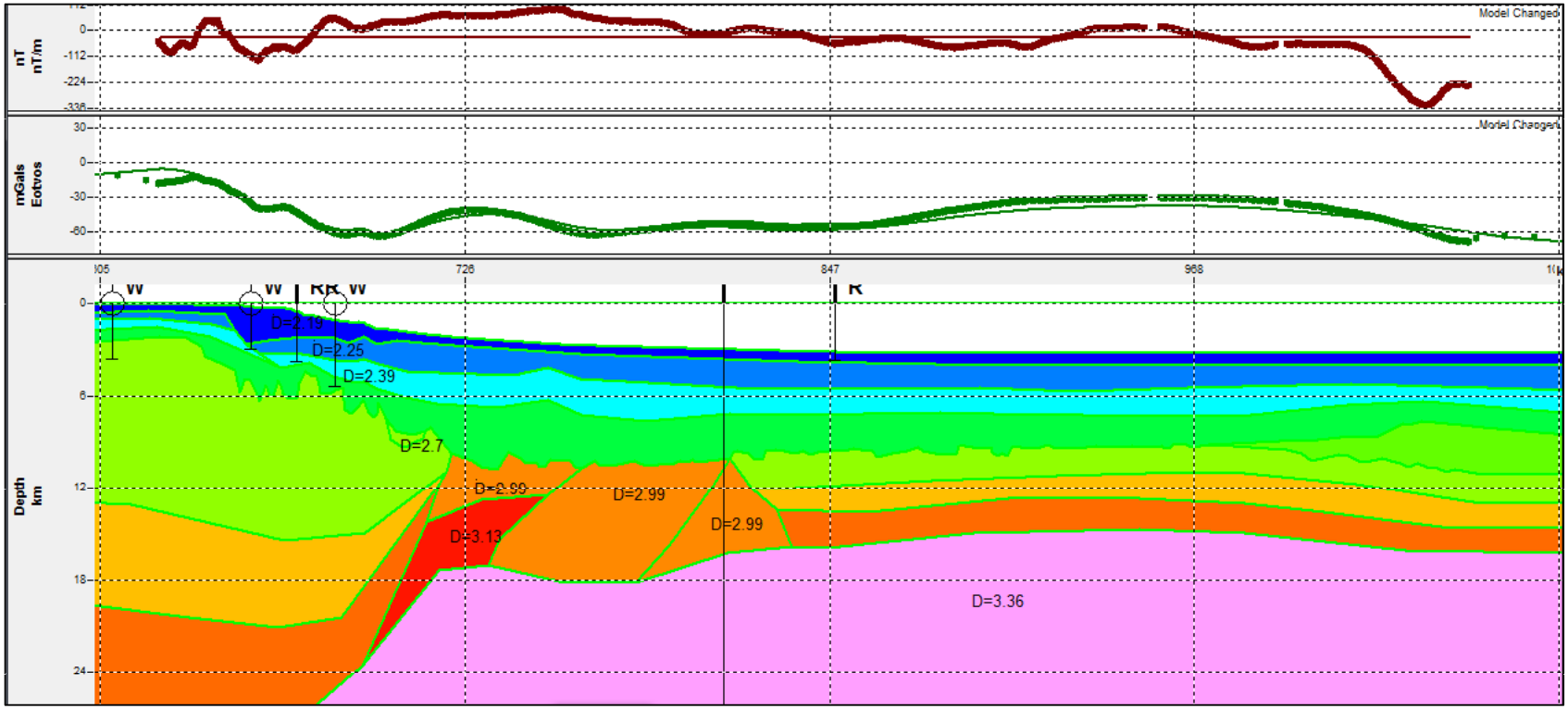

Profile GXT 1200, gravity/magnetic model. This is the best scenario with poc for the profile. Note lower densities in several blocks caused by serpentinization. Positive anomaly at poc/cc boundary needed correction for 3D effect of gravity field. Width of the poc corridor conforms to extent of poc interpreted from seismic imaging.

Crustal Boundary Interpretation

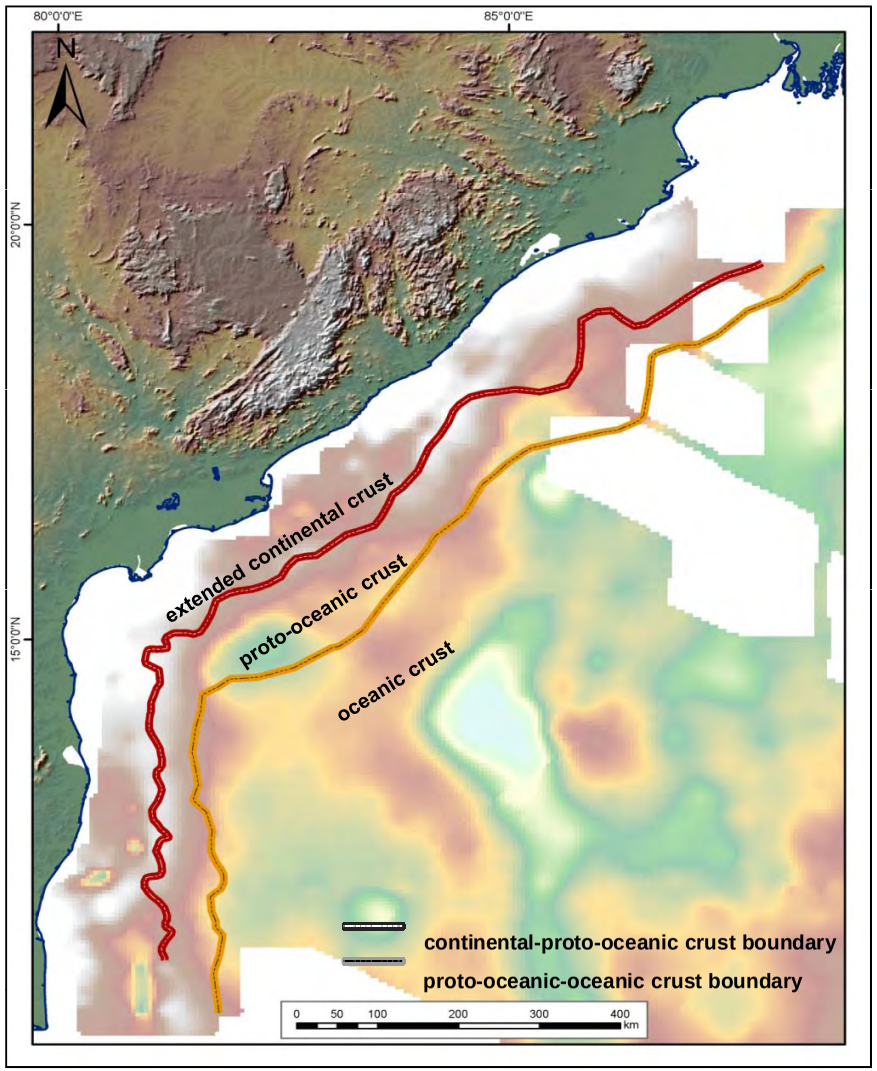

Map of the study area showing the extent of continental, proto-oceanic and oceanic crusts and their boundaries on top of the isostatic residual anomaly map.

Note that the width of proto-oceanic crust varies along the margin.

The width seems to depend upon the break up mechanism and extension rate.

It is narrow at strike-slip-controlled margin segments.

It is wide at normal fault-controlled segments.

Conclusions

- The ocean continent transition of East India was so far based on classical continental break up concept.
- The present study indicates possible mantle exhumation along East India margin.
- The break up is controlled by normal faulting in Cauvery, Krishna-Godavari and Mahanadi region, whereas the and Pennar-Palar Basin and north Vizag basin is mostly controlled by strike slip faulting.
- The Mantle exhumation is kinematically linked with break up control mechanisms.

Thank You

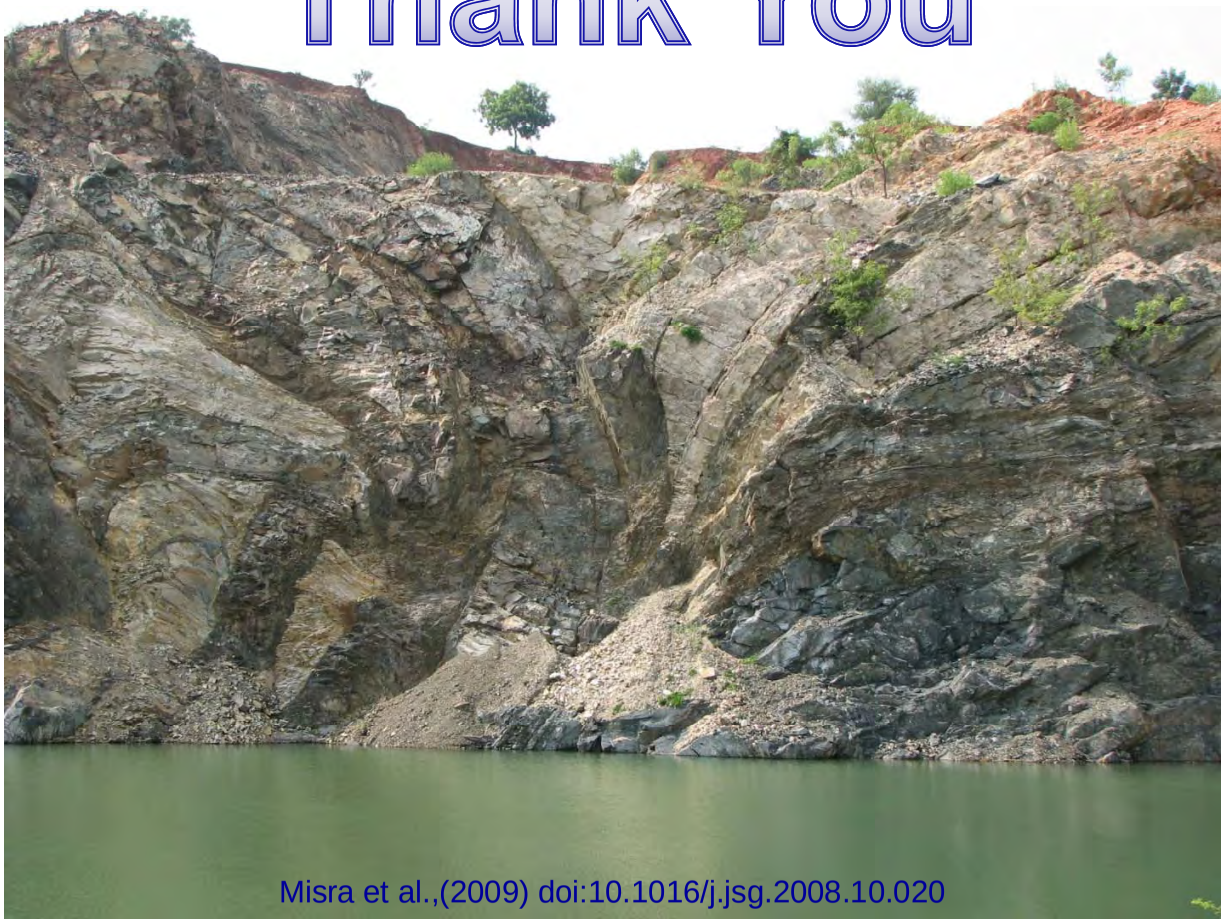

Misra et al.,(2009) doi:10.1016/j.jsg.2008.10.020

Sudipta T Sinha
Sudipta.Sinha@ril.com
Ph: +91 22 447 85926

Annex B80